Department of Applied Geology

Fluid Migration and Hydrocarbon Charge History of the Vulcan Sub-basin

Mark Lisk

This thesis is presented for the Degree of
Doctor of Philosophy
of
Curtin University

May 2012

Declaration

To the best of my knowledge and belief this thesis contains no material previously published by any other person except where due acknowledgment has been made.

This thesis contains no material which has been accepted for the award of any other degree or diploma in any university.

Signature: …….

Date: ……...

ABSTRACT

A comprehensive examination of the hydrocarbon charge and formation water history of the central Vulcan Sub-basin, Timor Sea has been completed and a model developed to describe the evolution of the region's petroleum systems. Reservoir horizons within the Mesozoic pre-, syn- and post-rift megasequences have been evaluated for their ability to host and retain oil and gas through a period of tectonic upheaval, associated with oblique plate collision in the Neogene. A coupled hydrocarbon-formation water model has been developed that describes two discrete formation water phases (W1 and W2) and three hydrocarbon phases (H1, H2, H3), with the timing of these events linked to important phases in the basin evolution.

The Vulcan Sub-basin contains the components required to produce an effective petroleum system. The principal clastic reservoirs generally exhibit good porosity and permeability and are capped by effective, regionally extensive, seal rocks. A consistent paragenetic sequence can be recognised for Mesozoic reservoirs with early glauconite and pyrite phases preceding clay authigenesis. These early phases are in turn enclosed by quartz overgrowths that are subsequently enclosed by ankerite cement and in more deeply buried samples, filamentous illite. Source rocks are suitably located adjacent to these reservoirs, are organically rich and have experienced sufficient burial to promote thermal maturation and expulsion of generated hydrocarbons.

The novel Grains with Oil Inclusions (GOI) fluid inclusion technique that allows the abundance of oil-filled fluid inclusions to be related to the maximum level of oil saturation experienced by a sandstone reservoir through time has been used to describe the charge history of a selection of wells from across the Vulcan Sub-basin. GOI data shows that the source rocks have been extremely productive, with three discernible hydrocarbon charge events recognised (H1, H2 and H3). An early gas charge (H1) appears to be widespread in the basin, but this may have been deleterious to regional prospectivity by reducing the volumetric capacity of traps that were well positioned to receive later oil charge.

Stable isotope data from early formed clay and carbonate cements indicate connate waters extant during the first phase of hydrocarbon migration (H1) had mixed with

meteoric water (W1) introduced into the reservoirs during periods of sub-aerial exposure associated with uplift related to rifting.

A regionally extensive oil charge (H2), derived from Upper Jurassic mudstones, produced numerous, volumetrically significant, oil columns. GOI data shows that many of the current oil fields were once much larger and that many reservoirs that are now gas or water bearing also previously contained oil accumulations.

Geochemical analysis of selected fluid inclusion oils (FIOs) show derivation from mixed marine and terrestrially derived source rocks of the Upper Jurassic Vulcan Formation. These oils form the first of two oil families that constitute the previously defined Jurassic Vulcan-Plover (!) petroleum system. In contrast the crude oils previously assigned to the second oil family and thought to have been derived from deltaic source rocks of the Middle Jurassic Plover Formation are not well represented in the FIOs. In addition a number of the FIOs are unlike either recognised oil family and show source rock characteristics that imply derivation from fully marine source rocks. These could represent either a previously unrecognised oil family or may reflect a true end member of the first family that has been mixed with the second family to produce an intermediate composition. The presence of the angiosperm marker Oleanane in some of the FIOs suggests a contribution from Cretaceous source rocks is also possible.

The GOI data indicate high charge rates to structurally valid traps with at least one in three valid traps showing clear evidence of oil accumulation. Fluid inclusion palaeotemperature data, integrated with one dimensional (1D) basin models, produce a similar prediction of the charge timing with oil charge mostly from Eocene time. This agrees well with subsidence curves, which show a period of increased subsidence in the Paleocene that is likely to have promoted oil generation and expulsion into carrier beds used to facilitate oil migration into traps.

Although an effective petroleum system can be demonstrated to have been present in the Tertiary, this has not been fully preserved due to events that post-dated hydrocarbon charge. The most significant of these has been the flexural bending of the lithospheric plate during oblique collision of the northwards moving Australian

Plate with the eastwards moving S.E. Asian Plate. This collision produced a net extensional stress field throughout the Vulcan Sub-basin, resulting in widespread reactivation of deeper rift fault systems, and the formation of extensive arrays of shallow Miocene-Pliocene faults. Interaction between these fault populations has, in many cases, increased net-vertical structural permeability and led to breaching of hydrocarbon traps and the attendant leakage of oil and gas.

Another major fluid-flow event that was controlled by the increase in structural permeability due to plate collision can also linked to the loss of hydrocarbons due to fault breach. A regionally extensive fluid-flow event, involving vertical, cross formation, migration of highly saline brine (W2) is indicated by fluid inclusion palaeo-salinity data. These palaeo-pore waters, with maximum salinities above 200,000 ppm NaCl equivalent, record the migration of high-salinity brines through Mesozoic and Tertiary sandstones. Fault controlled injection of brine from bedded salt at depths of up to 10 km is most likely the main source of this brine. Alternative salt sources in the drilled section are salt diapirs, but these are spatially restricted and their dissolution cannot reconcile the observed widespread distribution of these highly saline palaeo-fluids.

In samples taken from intact hydrocarbon columns the absence of hyper-saline fluid inclusions suggests brine flow occurred after initial hydrocarbon charge. Further, high salinities seen in samples from recognised residual oil zones suggests that trap breach facilitated the ingress of high-salinity brines. Numerical simulations, utilised to test this hypothesis, produce outcomes that broadly match the observed distribution of samples with high salinity fluid inclusions.

Brine flow from more deeply buried Palaeozoic strata also imparts a convective overprint on the conductive thermal background. Although not represented by the current geothermal conditions, thermal maturity data recording accumulated thermal stress, indicates localised heating of sediments immediately adjacent to faults bounding breached oil columns. The use of such anomalous maturity data when modelling hydrocarbon generation could lead to spurious conclusions if the restricted spatial extent of these convective effects is not considered.

Aside from Neogene fault reactivation at least four additional processes have modified the preservation potential of the Jurassic Vulcan-Plover (!) petroleum system since the initial hydrocarbon charge. Although generally second order effects on a regional scale, these can be extremely important at the local scale. The first involves passive leak zones formed by reactivation of long-lived fault intersections that appear to control the trap capacity of the Skua oil field and likely play an important role more widely. Subsequent structural tilting during the Late Tertiary altered the spill-points of some hydrocarbon traps resulting in further redistribution of hydrocarbons. Demonstrable evidence of modification to spill-points after initial oil charge is recorded in the Skua Field where the original OWC is inclined, and can be explained by the establishment of north-westerly tilting.

The third process to affect the system was a late stage gas charge (H3) that displaced oil from many of the traps that today contain gas. Considerable potential for down-dip or displaced oil legs in the Swan and Oliver fields respectively is inferred.

The final process to modify the petroleum system involved a significant increase in the magnitude of the horizontal stress component within the regional stress field, imparted by the jamming of the Banda Arc subduction zone by buoyant Australian Continental crust. The resultant reduction in observed extensional faulting likely led to an improvement in trap integrity such that heavily reactivated traps with access to charge could be successfully refilled.

Data acquired by this study provides a base map of the charge history in the Vulcan Sub-basin with which to test the applicability of models proposed to predict the retention of hydrocarbons in yet to be drilled traps. These data already have been used to test models that utilise a variety of seepage detection methodologies including airborne and satellite based direct detection as well as indirect methods such as hydrocarbon related diagenesis. In the future, rigorous integration of these data into numerical models of fault reactivation that describe the complex interplay between stress, fluid-flow and regional tectonics will contribute to a better understand the mechanisms controlling fault breach in this region and in sedimentary basins elsewhere.

ACKNOWLEDGEMENTS

This thesis represents the culmination of more than a decade of work aimed at applying a new set of methods to unravel the fluid history of the Vulcan Sub-basin. Punctuated by a new job and two beautiful children this thesis owes a debt of gratitude to many people but the support of my wife and family has been paramount to this work reaching completion. Initiated as a joint research project between CSIRO and the Australian Geological Survey Organisation (AGSO, now Geoscience Australia) the project and subsequent PhD thesis came about through the support and encouragement of Dr Geoffrey O'Brien at AGSO. The financial support provided initially by AGSO and subsequently by CSIRO is acknowledged together with the support of senior CSIRO staff, principally Dr Peter Eadington who conceived the original GOI method. Other colleagues within CSIRO are also thanked for their contributions to this project both in provision of data and discussion of results. I am particularly grateful to Dr Simon George (now at Macquarie Universitry) and Dr Herbert Volk for their contribution of MCI data that allowed my results to be more effectively placed within a petroleum systems framework and their review of chapters where the integration of these results is discussed. The assistance of Dr Anthony Gartrell is also acknowledged as making a significant contribution to the integrated models that seek to produce thematic outcomes for the Vulcan Sub-basin within the geological framework of the North West Shelf. Other colleagues at CSIRO during the duration of this study are thanked for their contribution to discussion including Mark Brincat, Wayne Bailey, Luke Johnson and Joesph Hamilton. This work has also benefited significantly from discussion with numerous staff at Geoscience Australia, in particular Dr John Kennard for contributions to the thermal history of the Vulcan Sub-basin and Dr Dianne Edwards for her tremendous insights into the geochemical charater of hydrocarbons within the basin. I would also like to recognise the many people within the oil and gas companies who have contributed to the development of the ideas presented in this thesis and importantly the practical application of the results. Finally I wish to acknowledge the ongoing support of my supervisors, Dr Peter Eadington at CSIRO and Dr Peter Collins at Curtin University. Their willingness to perservere throughout the extended time period taken to complete this work prevented the abandonment of this project and their support is gratefully acknowledged.

TABLE OF CONTENTS

LIST OF FIGURES

LIST OF TABLES

LIST OF APPENDICES

1. INTRODUCTION

1.1 SIGNIFICANCE

Migration of fluids is recognised as playing a fundamental role in virtually all geological processes (Bredehoeft and Norton, 1990; Torgerson, 1990; Parnell, 1998) making the movement of fluids through the sub-surface of importance for all those who seek to locate economic reserves of petroleum, mineral or water resources.

Sedimentary basins are complex multi-component systems that are constantly modified by a combination of fluid flow, heat transfer, mass transport and water-rock interactions of many types (Person and Baumgartner, 1995). Formation fluids extant during rock formation are altered by these processes or modified through the addition of new fluids that can derived anywhere from the surface to deep in the earths crust. Gradients in hydraulic potential that arise from topography, compaction, deformation, thermal disequilibrium, metamorphic dewatering and mantle degassing provide the major driving forces that promote basin-wide fluid migration (Torgerson, 1990; Sibson, 1994). Movement of fluid in the subsurface (Garven, 1995; Parnell, 1994, 1998; Al-Aasm et al., 1992) provides the opportunity to produce, transport and concentrate mineral (Bethke, 1986; Cathles, 1981; Hanor, 1979), hydrocarbon (Garven, 1989; Hubbert, 1953) and groundwater (Bethke, 1985) resources.

Current day fluids reflect the accumulated impact of these processes producing complex fluid mixtures that can be difficult to interpret without other reference points. Methods that provide detailed information on the constituent hydrocarbon fluids and associated formation waters, particularly at points in the geological past can reveal critical constraints on the processes that contributed to the current composition of these fluids (Lisk et al., 1998a). The challenge explorer's face relates to the presence of incomplete datasets requiring extrapolation or interpolation of data from the known into the unknown. Improved constraints allow for more accurate models that in turn produce a more refined working hypothesis that can be tested by future exploration.

The hydrocarbon exploration process involves running repeated trials (drilling wells) to address the chance of making future discoveries from a supply that is without replacement. As a finite resource each discovery reduces the overall inventory, making it progressively more difficult to be successful in future exploration. Pursuit of an increasingly elusive goal dictates that ongoing success will be governed by step changes in knowledge and technology.

Technology advances have clearly influenced the discovery rate for exploration on the North West Shelf of Australia. Longley et al (2002) describe four phases of activity since 1953. The years from 1953-1970, where relatively limited offshore drilling was undertaken, resulted in only limited discoveries but advances in 2D seismic imaging led to discovery of a number of very large gas fields during the nineteen seventies (Figure 1–1). Depletion of the inventory resulting from the largest, most obvious fields first led to a natural decline in the number and size of discoveries. More recently the advent of new 3D seismic technology helped to reverse this trend, although discovery size did not improved as dramatically (Figure 1–1). Technology and enhanced knowledge remain the two principal factors that can help to slow the inevitable decline in hydrocarbon resources and the work presented in this thesis seeks to contribute to both of these areas.

1.2 SCOPE OF RESEARCH

With crude oil production within Australia predicted to decline rapidly in coming years (Figure 1–2) delivery of technological solutions are needed to meet Australia and the worlds increasing demand for energy. Despite increased supply concerns due to the concept of Peak Oil (Campbell and Laherrere, 1998; Bureau of Transport and Regional Economics, 2005) and the impact of anthropogenic carbon emissions on global temperature and climate (IPCC, 2007), hydrocarbons are predicted to remain a key component of the Australian energy supply mix in the next two decades (Cuevas-Cubria and Riwoe, 2006; Powell, 2001; Figure 1–3).

Investigating suitable geological provinces, those where sufficient previous exploration allows a detailed retrospective application of new methods to be undertaken, enables an improvement of knowledge applicable to those basins but

also leads to the development of effective workflows that can be employed at earlier stage in less mature areas.

By restricting the investigation to a single discrete geological province the number of variables and degree of complexity is reduced and as a consequence there is a greater chance of highlighting the thematic processes that have controlled the distribution of hydrocarbons seen at the current day. The scope of investigation, however, must be large enough to capture the range of processes and encompass their region of influence if these processes are to be more fully understood.

In addition the spatial footprint of the study it is also important that the new types of data produced can be easily integrated into conventional methods for describing the accumulation of hydrocarbons in the sub-surface. For this objective the Petroleum Systems classification scheme introduced by Magoon and Dow (1994) provides a suitable genetic framework for this type of study and allows the scope of investigation to encompass all of the key elements needed to produce a working hydrocarbon system. This classification system recognises the geographic extent of petroleum accumulations that can be attributed to a single pod of genetically related source rock. This provides the boundaries within which to examine the other required components including reservoir, seal and trapping mechanisms needed to produce a hydrocarbon accumulation.

In order to build on, but not duplicate previous efforts, the application of new and emerging technology represents a critical part of this investigation. The goal is to deliver novel and unique information to supplement previous investigations by further reducing the fluid migration uncertainty of the petroleum system.

A more challenging aim of the research conducted in the current study is to move beyond the incremental addition of knowledge and look to deliver a fundamental step change in the way these key risks are addressed both in the geographic region of study, namely the Vulcan Sub-basin and more broadly across the petroleum exploration field of endeavor.

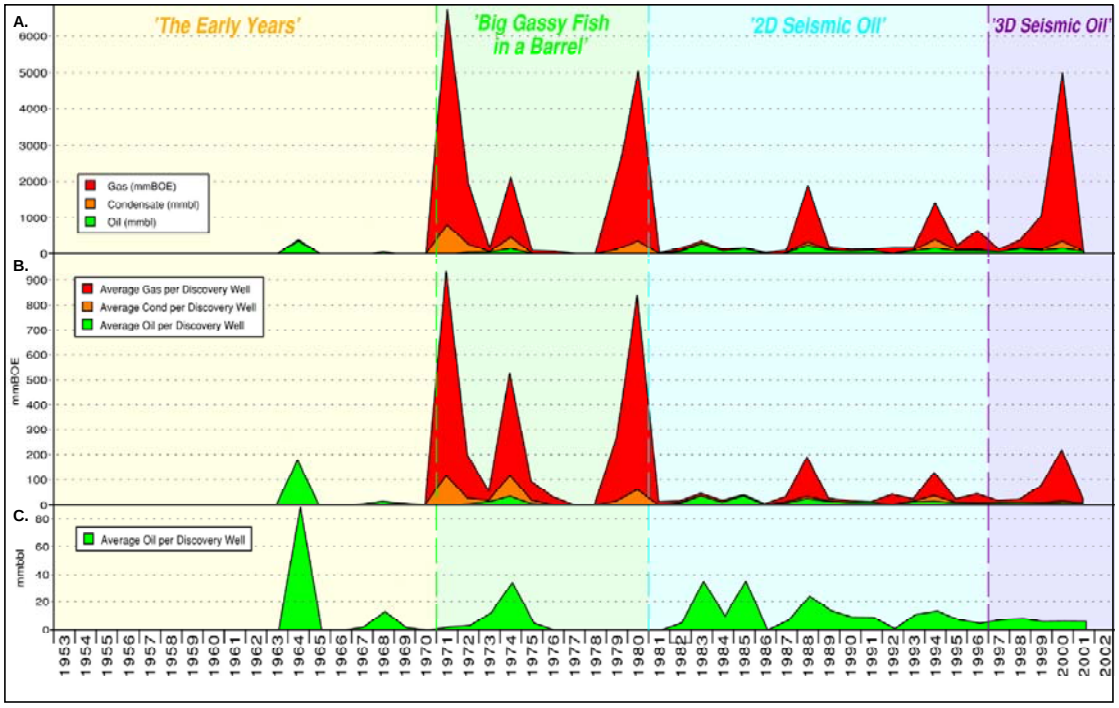

Figure 1-1: Historical summary of exploration along the Australian North West Shelf.

Shown by year for the period 1953-2001 are: a). Total oil condensate and gas volumes (by barrel of equivalent, BOE) discovered per year; b). The average discovery size per successful exploration well by oil, condensate and gas volumes (as boe); c). The average oil discovery volumes found in each exploration well (modified from Longley et al., 2002).

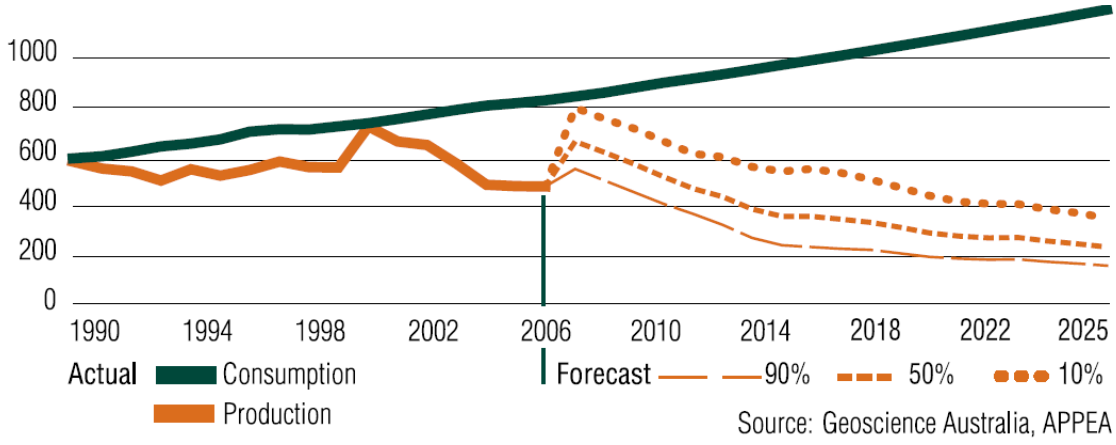

Figure 1-2: Australia's annual and predicted production of oil & condensate, 1990-2025.
Actual figures (in 000's of barrels) are quoted up until 2006 and forecast liquids supply is shown at 90%, 50% and 10% cumulative probability until 2025 shown in comparison to actual and predicted consumption (Source: Geoscience Australia, 2006a). Note: 90% represents Geoscience Australia's high probability case and 10% the low probability scenario.

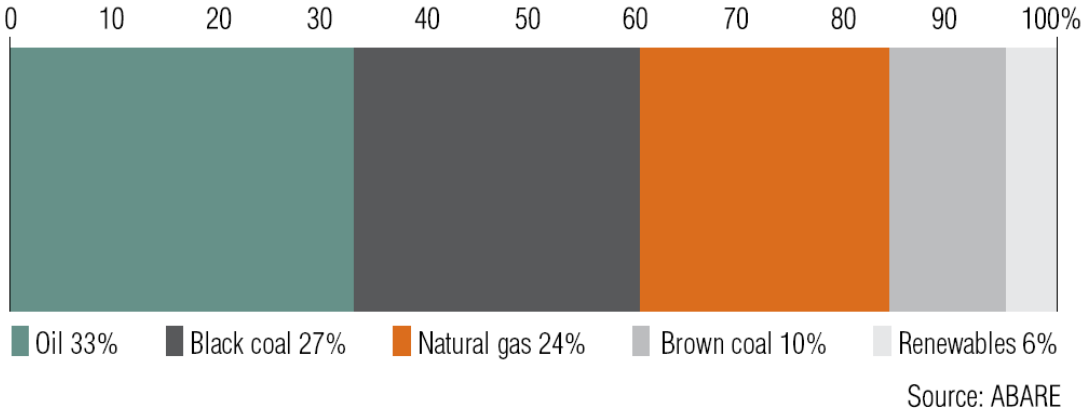

Figure 1-3: Predicted energy supply mix for Australia in the year 2020 (source: ABARE).
The graph shows that oil and natural gas are expected to provide nearly sixty percent of the energy supply by the year 2020 and illustrates the ongoing reliance on fossil fuels in the overall predicted energy mix (Cuevas-Cubria and Riwoe, 2006).

1.3 AIMS OF THE CURRENT STUDY

The Vulcan Sub-basin (VSB) represents an excellent candidate for the study of fluid migration and hydrocarbon accumulation through geological time. Located on the northern margin of the Australian Continental Shelf (Figure 1–4), this offshore region has experienced several phases of intense exploration effort for oil and gas, punctuated by periods of relative inactivity. Despite showing initial promise with the discovery of the Jabiru, Challis and Skua oil fields during the mid 1980s the success rate has been poor by accepted industry standards, particularly given an abundance of the required geological factors normally used to infer a high level of apparent hydrocarbon prospectivity.

In this regard the VSB contains the necessary combination of productive source rocks, high quality reservoir rocks and abundant petroleum traps that characterise the prolific basins that have secured the position of the greater North West Shelf as Australia's most important hydrocarbon province. Indeed compelling signs that oil and gas accumulations within the VSB were once more widespread and that a more successful petroleum system once existed were recorded prior to the onset of the current study. These observations included both direct observations of residual oil shows encountered during drilling and the application of a new technique that utilises hidden oil shows provided by oil-filled fluid inclusions to provide further evidence of widespread palaeo-oil charge (Lisk and Eadington, 1994).

The failure of the system is considered equally well understood; most workers attributing the absence of hydrocarbons at the current day to leakage associated with trap breach during Neogene plate margin collision (O'Brien and Woods, 1995; O'Brien et al., 1996a; 1998). Compelling indirect evidence provided by the widespread Neogene fault reactivation clearly evident on seismic data (e.g. Woods, 1992), coupled with the presence of Direct Hydrocarbon Indicators (DHIs) and observed sea-floor hydrocarbon seepage spatially related to shallow faults (O'Brien and Woods, 1995) provide prima facie evidence for fault-related trap breach.

The current investigation seeks to contribute to a greater understanding of these issues by reconstructing the fluid-flow history of the basin and in particular focusing

on the modifications produced by Neogene fault reactivation that appear to have so strongly controlled the preservation aspect of this hydrocarbon system.

This study will examine the current hydrocarbon distribution and combine conventional hydrocarbon shows with hidden oil shows provided by oil-filled fluid inclusions to address the palaeo-hydrocarbon charge history and attempt to elucidate the controls on retention of hydrocarbons.

A recently developed petrographic technique known as the Grains with Oil Inclusions (GOI; Lisk and Eadington 1994; Eadington et al., 1996) method provides the required step change in technology.

The challenge for the current study is to document the evidence, understand the key processes and most importantly provide improved mitigation strategies to maximise the chance of improved success in future exploration. For the purposes of a forensic investigation the VSB represents a rich natural laboratory. There is ample information, a clear causal effect and a suite of suitable tools available to analyse the events that have contributed to the poor record of prior exploration drilling.

The study of regional fluid migration and in particular the interplay between the charge and retention of hydrocarbons in the VSB provides a scientifically challenging and rewarding investigation for the following reasons:

1. A recognised issue, namely the retention of hydrocarbons during plate margin reactivation, provides a clear purpose for the study; an enhanced description of the petroleum system and the development of mitigation strategies needed to address the retention likelihood of yet to be drilled traps.

2. The basin has been extensively explored, and whilst exploration drilling density remains low compared to mature hydrocarbon provinces of the world there is a sufficient number of drill intersections and seismic coverage to enable an effective investigation of the hydrocarbon charge and retention history to be undertaken.

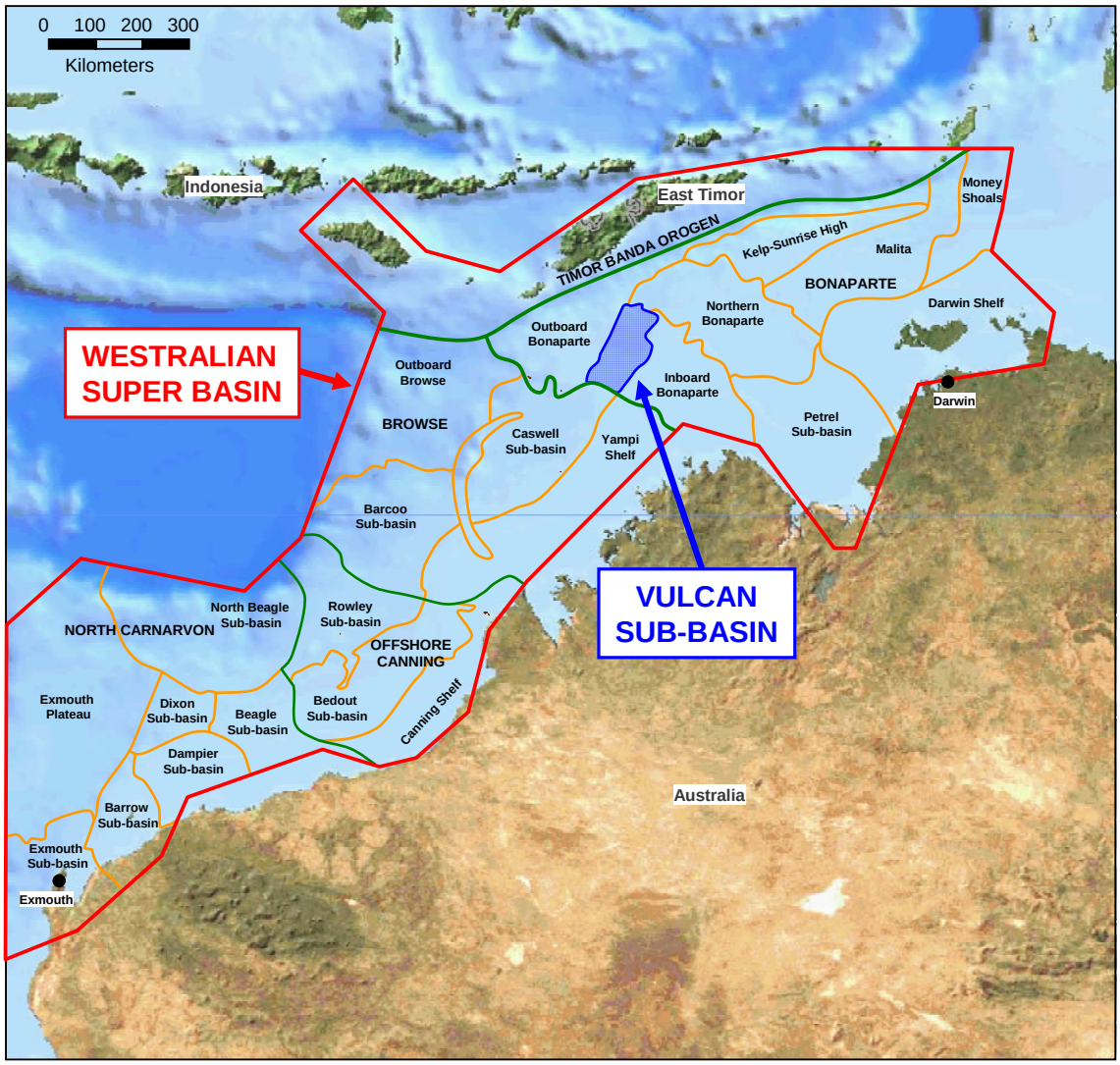

Figure 1-4: Location of the Vulcan Sub-basin relative to the greater North West Shelf.

The Westralian Superbasin consists of the series of sedimentary basins (shown in uppercase text) that make up the North West Shelf, with each basin having a number of discrete sub-basins or geological provinces (shown in lowercase text). The Vulcan Sub-basin lies at the western end of the Bonaparte Basin and adjoins the adjacent Browse Basin.

2. Complementary investigations have been completed during the period of this thesis, both by the industry and through other research organisations that contribute to a better understanding of the results generated in this study.

3. There remains an ongoing and increasing imperative to find more hydrocarbon reserves to replenish the ever dwindling Australian reserves.

1.4 SPECIFIC OBJECTIVES

The major aims of the study are:

1. To apply the new Grains with Oil Inclusions (GOI) method to further the technique and help to calibrate the method.

2. Identify and describe the episodes of hydrocarbon migration and accumulation within the VSB by describing the distribution of current and palaeo-hydrocarbon accumulations.

2. Establish the distribution of palaeo-hydrocarbon columns in the VSB and compare the size and extent of these with the distribution of current hydrocarbons to reveal the evolution of these accumulations through time.

3. Determine the evolution of palaeo-pore water composition for the VSB and examine the connection with the hydrocarbon system.

4. Use palaeotemperature data in conjunction with numerical basin modelling techniques to constrain the absolute timing of hydrocarbon migration, charge and subsequent partial leakage from the basin.

5. Contribute to an enhanced thematic model to compare and contrast against other predictive methodologies to aid the ranking of yet to be drilled traps in the VSB, highlighting those with the greatest likelihood of having received and retained economic volumes of hydrocarbons.

1.5 RESEARCH METHODOLOGY

A unique type of data are utilised in this study to provide additional constraints on the fluid flow history in this region and to complement the conventional methods of investigation normally employed by the exploration industry.

Fluid inclusions represent small samples of formation fluids that become entrained in the rocks during the process of burial diagenesis. These fluid inclusions capture and preserve minute, but representative samples, of fluids that moved through these rocks at various times in the geological past. Careful identification and analysis of these preserved fluids produces considerable information on their composition, source and timing of entrapment.

Whilst fluid inclusions trap all kinds of fluid this study utilises the relatively new (at the onset of the current study) fluid inclusion Grains with Oil Inclusions (GOI) technique that enables the relative oil saturation attained to be estimated and allows relict (or palaeo) hydrocarbon accumulations to be identified as well as providing information on the evolution of the presently intact hydrocarbon columns.

Combining GOI data with the more established measurements on fluid inclusions that help constrain the temperature of trapping and the salinity of associated formation waters will collectively provide a more comprehensive description of the fluid-flow history that when integrated with a conventional approach to play assessment should contribute more sophisticated risk reducing exploration models.

1.6 THESIS ORGANISATION AND OVERVIEW

The remainder of Chapter 1 provides information on the logistical details of samples and data utilised or produced by this study and introduces the reader to the issue of terminology that is unique to the subject matter being discussed.

Chapter 2 sets the scene by describing the geological context of the VSB within the greater Timor Sea region and the broader West Australian Superbasin. The

exploration history of the basin is reviewed to highlight the key risks that have adversely impacted the effectiveness of the petroleum systems.

Chapter 3 discusses the nature of reservoir rocks present in the VSB. Petrographic, core analysis, and flow test data are examined to elucidate the detrital composition and subsequent diagenetic history of key clastic reservoirs as well as to quantify porosity and permeability to provide an assessment of reservoir quality.

Chapter 4 reviews the conventional types of hydrocarbon show and introduces the GOI fluid inclusion technique that allows the maximum oil saturation experienced by a reservoir to be assessed, even where the rocks are currently water wet or gas saturated. These data are used to identify palaeo-hydrocarbon columns in water-wet or gas-saturated rocks as well as define the position of original hydrocarbon contacts in known oil fields. The initial distribution and size of residual hydrocarbon columns is determined and by comparison with the current hydrocarbon saturation, the filling history of each reservoir trap can be described and collectively on many traps to allow a regional charge history to be determined. The composition of hydrocarbons trapped within fluid inclusions is constrained from both petrological and geochemical data to describe the distribution of different oil families that have contributed to charge in the VSB.

Chapter 5 takes the results from individual wells presented in Chapter 4 and integrates these data with relevant geological data to demonstrate the value that can be gained by incorporating results from multiple wells on the same hydrocarbon structure, both in terms of advancing the knowledge of those traps but also by reconciling apparently disparate results. Detailed hydrocarbon charge history reconstructions are presented for a series of key fields in the Vulcan Sub-basin.

Chapter 6 addresses the thermal history of the Vulcan Sub-basin by integrating data on the current thermal state from reported temperature surveys with the palaeo-thermal conditions assessed directly by measured fluid inclusion palaeo-thermometric data and indirectly through organic maturity determination integrated with one dimension (1-D) numerical basin modelling.

Chapter 7 discusses the palaeo-hydrology of the Vulcan Sub-basin by comparing the salinity of palaeo-formation waters, derived from analysis of aqueous fluid inclusions, with the current pore water salinity determined from recovered formation waters and wireline log evaluation of each key reservoir sequence. Key processes controlling the observed changes are recognised and discussed and an important fluid-flow event with implications for predicting fault seal integrity is identified that challenges the validity of common assumptions about the thermal state of the basin.

Chapter 8 seeks to combine the data described in the previous chapters into a coupled hydrocarbon-formation water fluid flow model. This conceptual model covers the original hydrocarbon charge and the retention of that charge through time and demonstrates how fluid-flow events can act as markers for trap breach. This coupled model is compared against previously published trap integrity models for the VSB and broader Bonaparte Basin.

Chapter 9 provides conclusions to this study and looks at the types of future work needed if the results of this study are to provide the greatest support to on-going exploration activities.

1.7 LOCATION OF SAMPLES AND DATA

The samples prepared and the data produced from them reside with the Commonwealth Scientific and Industrial Research Organisation (CSIRO) at the headquarters of the Petroleum Division (now the Earth Science and Resource Engineering Division), located within the Australian Resources Research Centre at 26 Dick Perry Avenue in Kensington, Western Australia.

Preserved samples include any remaining rock material that was not utilised as well as the fluid inclusion petrographic thin sections prepared for this study. Data from analyses completed during this thesis either appear in this thesis or are electronically stored on Digital Video Disk (DVD) within CSIRO archives. A sample catalogue is provided in Appendix A.

Where required by law, results produced by this work have also been released to the appropriate regulatory authorities, in this instance to Geoscience Australia in Canberra and to the Northern Territory Mines Department in Darwin.

1.8 TERMINOLOGY

The petroleum industry relies heavily on terminology and somewhat unusual colloquial phrases that reflect the early origins of the oil and gas sector as an American dominated industry. This has also led to the persistent usage of imperial units of measurements in otherwise metric dominated countries such as Australia and a reliance on unique expressions, often with non-technical origins. As with most industries the plethora of technical terms are commonly shortened to a variety of acronyms made even more difficult by the practice of using company trade names (or acronyms) for the same process, tool or procedure. To assist the reader a list of the most commonly used terms, acronyms and measurement scales employed in this document are given in Appendix B.

2. GEOLOGIC OVERVIEW

2.1 REGIONAL GEOLOGICAL SETTING

The Vulcan Sub-basin is located on the northern margin of the Australian Continent within the eastern Bonaparte Basin (Figure 2–1) in a region known as the North West Shelf (Purcell & Purcell, 1988a). The area forms part of a greater geological province known as the West Australian Superbasin (WASB, Yeates et. al., 1987), which comprises a contiguous series of sedimentary basins that stretch more than 2400 km from the Arafura Sea between northern Australia and Irian Jaya in the east up to the Exmouth Plateau off the Northwest Cape in the west (Figure 1–4; Heine and Muller, 2005). The outboard limit of the North West Shelf is generally defined by the transition to oceanic crust except in the north where an accretionary wedge has developed due to Tertiary collision of the Australian Plate with the Banda Arc complex to the north (Figure 1–4). The inner margin is defined by sedimentary onlap onto basement rocks of the Proterozoic Kimberly block that define the Australian continental craton.

Longley et al. (2002) describe the North West Shelf as a composite rift margin, reflecting the multiple episodes of rifting that have shaped the geological evolution of the continental margin from the Palaeozoic until the current day. These key tectonic events formed the West Australian Super-basin (Yeates et. al., 1987) comprising four discrete sedimentary basins, the North Carnarvon, Offshore Canning (or Roebuck), Browse and Bonaparte basins.

The North West Shelf of Australia is a world class hydrocarbon province (Figure 2–2) with estimated reserves in 2002 of about 2.6 billion barrels (bbls) of oil, 2.6 billion bbls of associated condensate and 152 Trillion cubic feet (Tcf) of gas contained within a total of 233 hydrocarbon fields (Longley et al., 2002).

The geological evolution of the region has been well documented, with a wealth of descriptions of the regional geology, petroleum systems and significant discoveries provided in the published scientific literature.

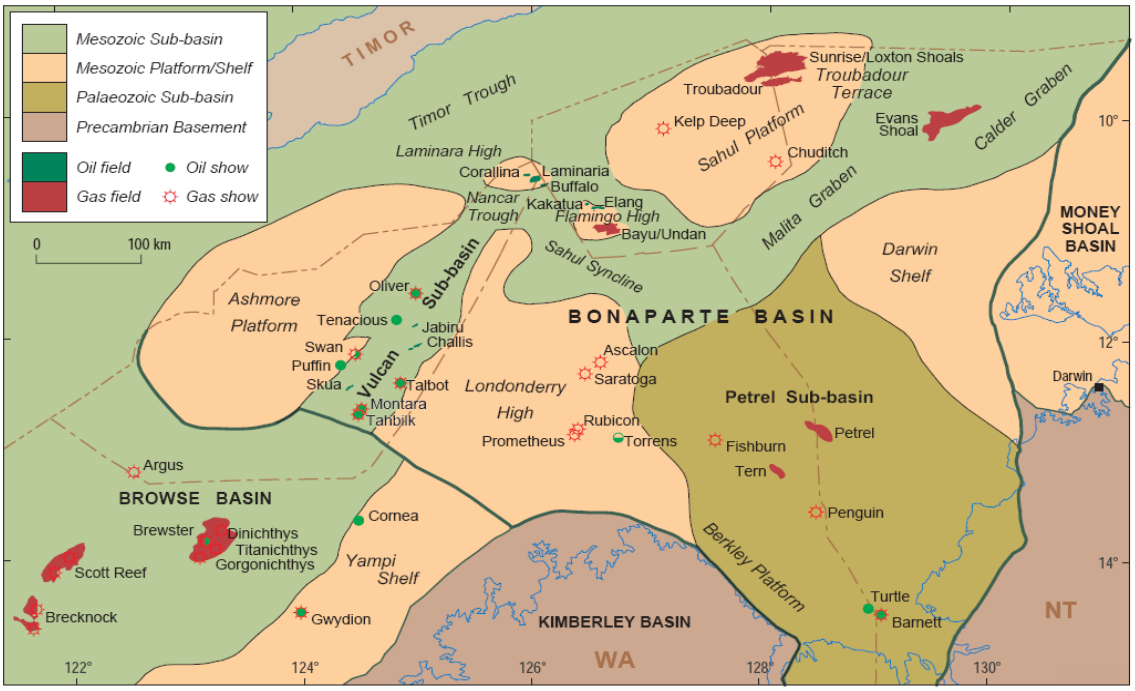

Figure 2-1: Location of Bonaparte Basin.

The Bonaparte Basin represents the mostly offshore region between the Australian Continent and the island of Timor, some 400km to the north. The Browse Basin adjoins the western edge of the basin with the Money Shoal Basin forming the eastern boundary. To the north the Timor Trough is a Neogene formed submarine trench and the island of Timor is a mix of obducted Australian crust and island arc terrains from across the Indonesian Archipelago. The Bonaparte Basin is sub-divided into two principal sub-basins; the Palaeozoic NW-SE orientated Petrel Sub-basin and the NE-SW trending Mesozoic Vulcan Sub-basin. Other major rift-related depocentres include the NE-SE trending, en-echelon Malita and Calder grabens and the NW-SE Flamingo and Sahul synclines. Large platform areas flank these sub-basins and preserve only the pre-rift and post-rift sequences. The Bonaparte Basin contains abundant hydrocarbon fields that are typically more gas-prone to the east and become more oil filled in the west including the Vulcan Sub-basin.

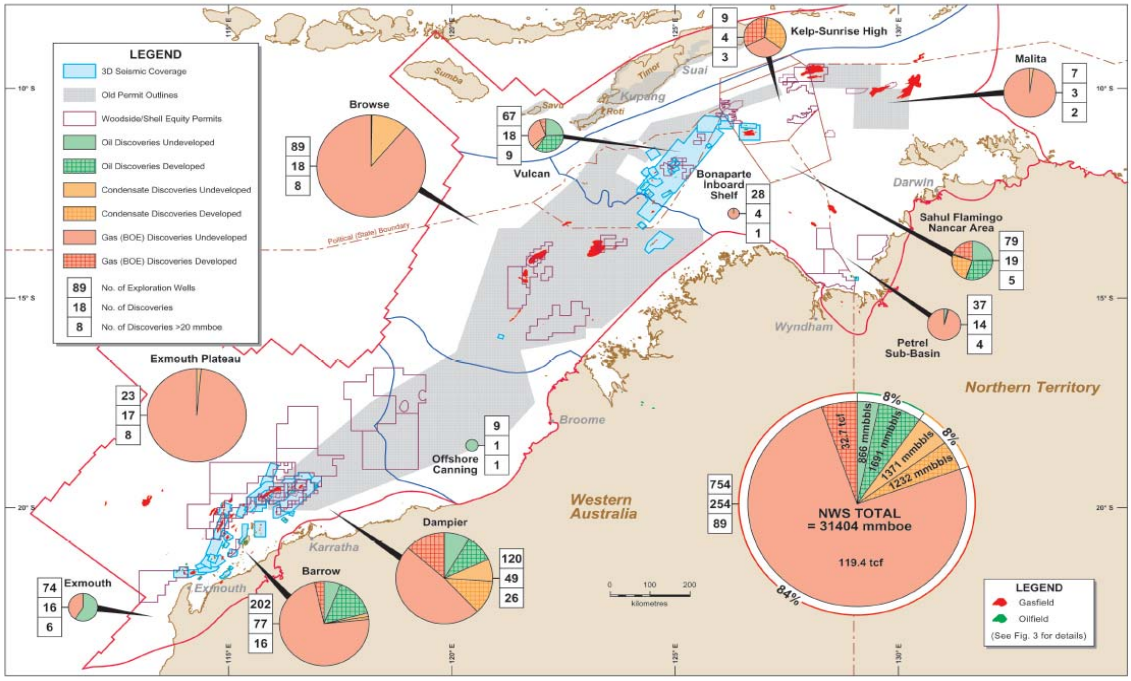

Figure 2-2: The North West Shelf hydrocarbon province.

A summary of estimated oil, condensate and gas reserves for the entire North West Shelf split into each of the principal sub-basin areas as at 2001 (from Longley et al., 2002). Overall the region has proven to be mostly gas prone with total hydrocarbon reserves of 31404 million barrels of oil equivalent (mmboe). The northern basins of the North West Shelf typically have much poorer success rates than the prolific regions of the Dampier and Barrow sub-basins and Exmouth Plateau to the south-east. Success rates in the Vulcan Sub-basin are particularly poor given the large amount of 3D seismic coverage that covers the area.

The published geological evolution and petroleum geology of the North West Shelf is well described in the proceedings of four Petroleum Exploration Society of Australia symposia edited by Purcell and Purcell (1988, 1994, and 1998) and Keep and Moss (2002). In addition a number of seminal papers can be found within the annual journals of the Australian Petroleum Production and Exploration Association (APPEA or APEA prior to 1996). By comparison a relatively limited number of papers on the North West Shelf region have been published within international peer reviewed journals and those that have are commonly modified versions of publications in the aforementioned symposia proceedings.

The most comprehensive summary of the region is provided by Longley et al. (2002) who provide a detailed description of the geological history compiling much of the previously published work on the region (Yeates et al., 1987; Gunn, 1988; Mory, 1998; AGSO, 1994; Baillie et al., 1994; Muller et al., 1998). This summary of the Vulcan Sub-basin and its position within the broader regional framework of the Bonaparte Basin and the greater North West Shelf draws significantly on this work, but also captures other influential work undertaken by Veevers (1988), Etheridge and O'Brien (1994), O'Brien (1993), O'Brien et al. (1999a) as well as more recent significant contributions (Keep et al., 2002; Edwards et al., 2004; Heine and Muller, 2005; Jablonski and Saitta, 2004).

2.2 TECTONO-STRATIGRAPHY OF THE NORTH WEST SHELF

The sedimentary sequence contained within the WASB comprises a thick (>12km) succession of late Palaeozoic, Mesozoic, and Cainozoic sediments (Figure 2–3) with a depositional history that is uniquely linked to the progressive rift fragmentation of the Tethyan margin of the Gondwana super-continent (Figure 2–4; Metcalfe, 1999; AGSO, 1994; Jablonski and Saitta, 2004).

Successive phases of uplift and subsequent erosion of Palaeozoic and Proterozoic hinterland on a continental scale provided the main sediment provenance to fill the depositional accommodation space created by the multiple rifting episodes that produced repeated episodes of break-up along the northern margin of Gondwana (Longley et al., 2002).

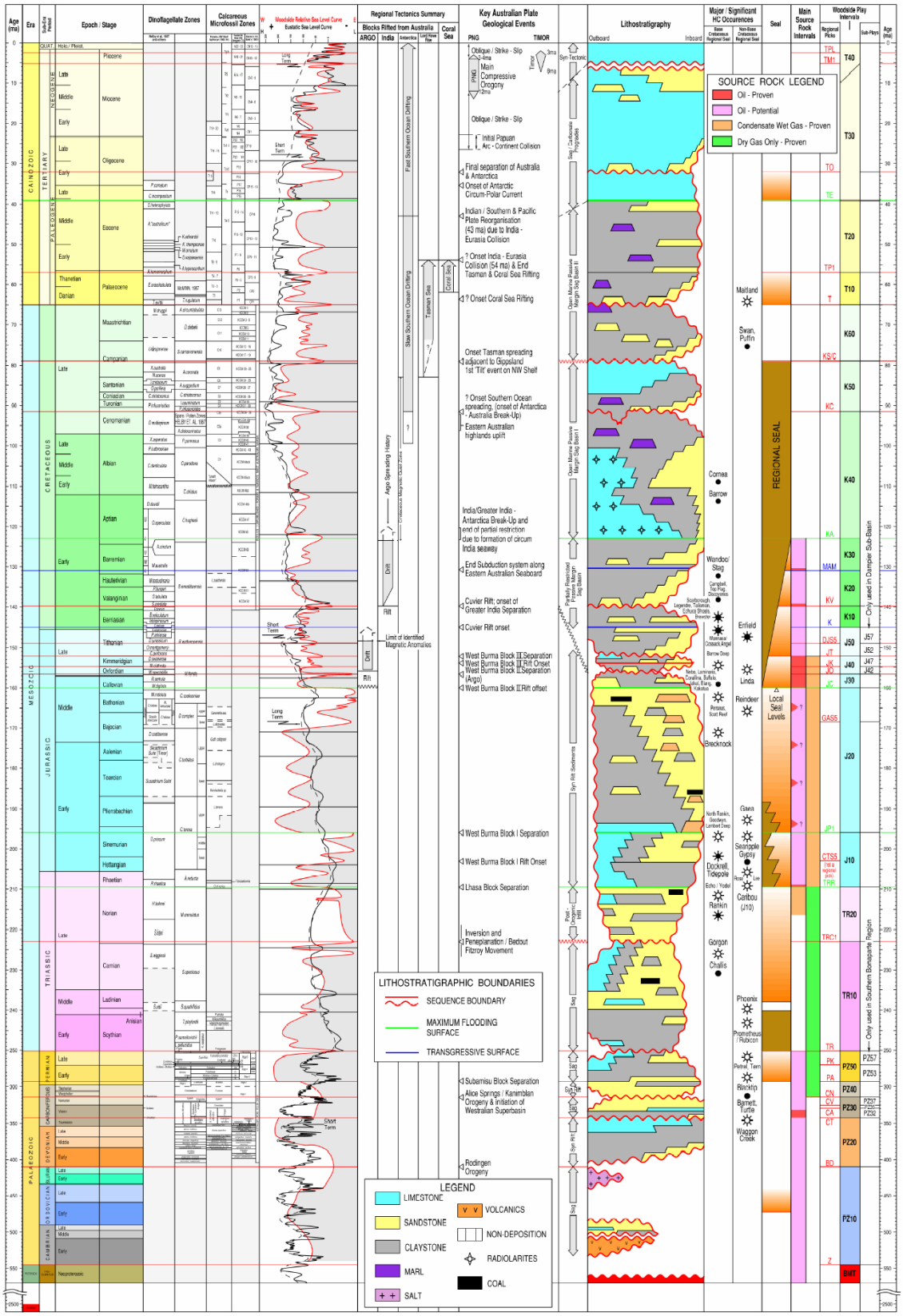

Figure 2-3: Chronostratigraphic summary of the North West Shelf

North West Shelf chronostratigraphy (from Longley et al., 2003) showing the principal biostratigraphic subdivisions, lithostratigraphy, relative sea-level curves, key tectonic and geological events, stratigraphic position of major discoveries, petroleum systems elements and play intervals.

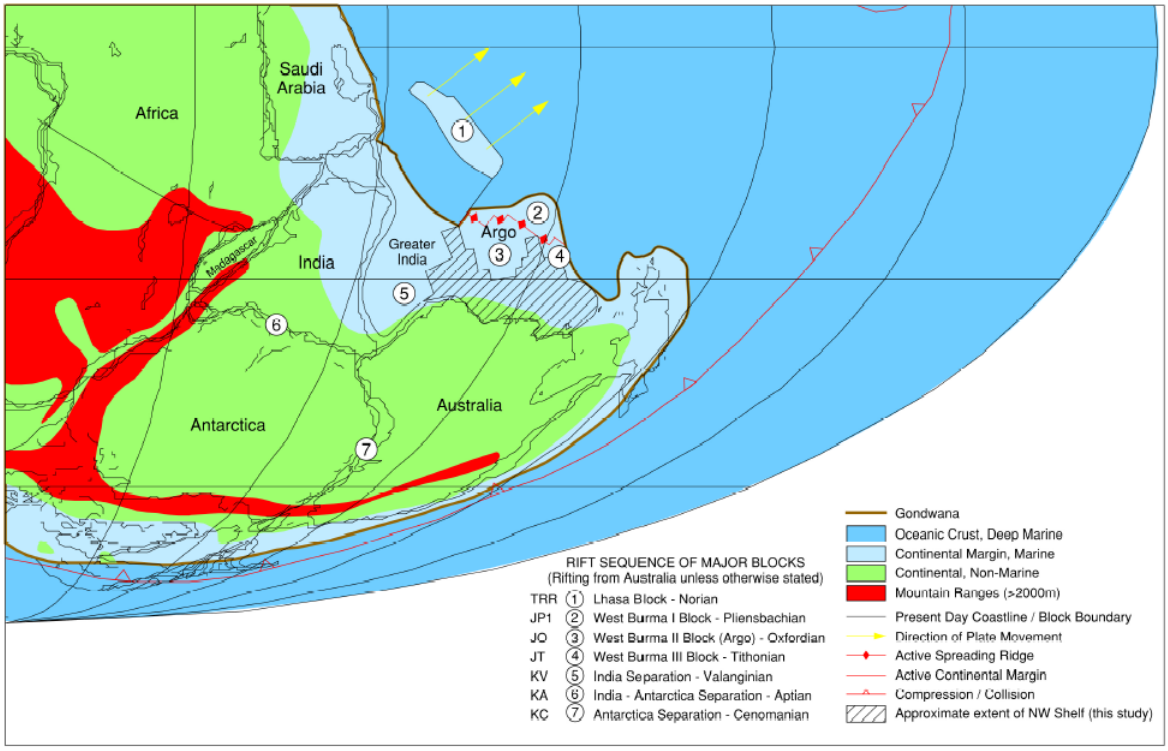

Figure 2-4: Simplified plate reconstruction at Early Jurassic time.

Simplified map showing a reconstruction of eastern Gondwana in Early Jurassic time (Pleinsbachian) and the sequence of major block rifting/separation events that affected the geological development of the North West Shelf (from Longley et al., 2002). The western margin of the Australian Continent faced the opening Tethyan Ocean in early Triassic time. Initially fragments of the Gondwanan Continent were progressively rifted away (events 1-4) prior to eventual break-up of Gondwana with the separation of Greater India, India and Antarctica from the Australian Continent (events 5-7). These events produced the principal control on the consistent chronostratigraphic and tectonostratigraphic record that is observed across the sedimentary basins of the North West Shelf region and continuing into the basins of Irian Jaya and Papua New Guinea.

From the Late Carboniferous until the Early Cretaceous the northern edge of Gondwana progressively broke into a series of microplates that drifted to the north across the proto-Tethyan ocean and were accreted into what are today the landmasses of China, Burma and Indonesia (Jablonski and Saitta, 1994).

The earliest sediments recognised on the NWS comprise isolated occurrences of early Palaeozoic Cambro-Ordovician rocks that are generally too deeply buried to contribute to the petroleum prospectivity of the area. These early Palaeozoic sediments are capped in places by thick salt deposits that locally have been re-mobilised to form salt-cored structures in the Bonaparte Basin (Gunn et al., 1988; McConachie et al., 1996), including the Vulcan Sub-basin (Smith & Sutherland, 1991). These poorly defined basal units are overlain by a more widespread Devonian to Permian section which was deposited during the first period of rifting associated with early Gondwanan breakup and dispersal (Bradshaw et al., 1994). During this first phase of rifting a montage of microplates (Simao, Indochina and South China) were separated from northern Gondwana (Jablonski and Saitta, 2004). Generally the distribution of the older section is poorly defined as most areas thick Mesozoic deposits overlie these units and make seismic imaging of the deep sediments more difficult, except where specifically designed deep seismic surveys provide an occasional window of information through the thick Mesozoic cover (e.g. Eastern Browse Basin, Struckmeyer et al., 1998). In the Canning Basin where the section is well preserved widespread glacial sediments within the Late Carboniferous to Early Permian Grant Group indicate high palaeolatitudes at this time (Playford, 2002).

The second of the two main Palaeozoic rift phases was initiated in the Late Carboniferous, and relates to the onset of the Sibamasu block separation (Veevers, 1988; Metcalfe, 1999). This rifting event created the northeast-southwest fault network that formed the framework of the WASB and allowed more than 10 km of continuous sediment fill to accumulate, comprising widespread Permian, Mesozoic and Tertiary strata (Bradshaw et al., 1988; AGSO, 1994). The presence of Late Permian intrusive and extrusive igneous rocks present in the Canning and Roebuck (Offshore Canning) basins (Reeckman and Mebberson, 1984) are used to infer a Late Permian age for final separation of the Sibamasu block (Jablonski and Saitta, 2004). Continental extension during this stage produced a wide rift basin (up to 500km wide

on the Exmouth Plateau) with deformation broadly distributed on an array of normal faults. This style of crustal extension has been interpreted to reflect deformation of a relatively warm and ductile crustal lithosphere (Gartrell, 2000).

The first significant period of terrane dispersion from the Gondwanan margin in the Mesozoic occurred in the period spanning the Late Triassic to Late Jurassic (Audrey-Charles et al., 1988), associated initially with the Norian drift of the Lhasa block (Block 1 in Figure 2–4) and subsequently separation of the West Burma and Woyla blocks into the Late Jurassic (Metcalfe, 1999; Blocks 2-4 in Figure 2–4).

Separation of the Lhasa block (Block 1 in Figure 2–4) was initiated during the Norian (Metcalfe, 1999). Initially erosion and uplift along the edges of the craton, commonly referred to as the "Fitzroy Movement" (Forman & Wales, 1981) led to the deposition of the Late Triassic Carnian to Norian succession. Jablonski and Saitta (2004) relate the Fitzroy Movement to thrusting and low grade metamorphism across eastern Australia associated with the Bowen Orogeny. Continental scale uplift and erosion produced thick deltaic successions that prograded some 500 km from the margin of the Onshore Canning basin, towards the Exmouth Plateau to the south, and into the marine embayment of the Wombat -Timor Trough (Nicoll & Foster, 1994) to the north. The Triassic sandstones of the Mungaroo Formation that provide the key reservoirs for the giant gas fields of the Rankin Platform in the Carnarvon Basin (Vincent and Tilbury, 1988) were deposited at this time. Time equivalent section in the Bonaparte Basin also provide an important reservoir section in the Vulcan Sub-basin, where sandstones of the Challis and Pollard formations host a number of small oil discoveries including the Challis-Cassini (Gorman, 1990) and Talbot (Bourne and Faehrmann, 1991) oilfields.

Following the drift of the Lhasa block, extension along the Gondwanan margin continued, culminating in a series of additional break-up phases throughout the Jurassic (Audrey-Charles et al., 1988). These events relate to the separation of the West Burma Block which rifted in at least three distinct stages during the Sinemurian, Oxfordian and Tithonian, respectively (Longley et al., 2002). A distinct change in the mode of continental extension from a wide rift basin to the development of a more narrow and steep sided rift basin occurred during the break-

up of the West Burma block. Gartrell (2000) suggest that this transition was the result of the cooling and associated strengthening of the lithosphere that occurred after the earlier phases of extension.

Preserved magnetic marine anomalies and potassium argon age constraints of samples from the Deep Sea Drilling Program (DSDP) suggest that the Oxfordian and Valanginian drift events formed the Argo and Cuvier oceanic basins respectively (Müller et al., 1998). These events did not always result in the blocks to be fully rifted and many failed rift arms are recognised and these played a key role in source rock distribution by sheltering these developing depocentres from open oceanic circulation (Longley et al., 2002).

In the model described by Longley et al (2002) the first West Burma segment (Block 2 in Figure 2–4) rifted in the latest Hettangian marking the onset of a major sand influx across the entire NWS. In the northern basins the oldest sections of the Plover Formation were deposited in a predominantly fluvial environment, whilst in the south, reservoirs of the North Rankin beds were deposited. This period of extension continued until break-up in the Sinemurian where subsidence caused by the emplacement of oceanic crust produced a regional flooding event (JP1 seismic marker in Figure 2–3) that extended from the North Carnarvon to the Browse Basin (Longley et al., 2002).

Accommodation space created by this rift event was infilled by a succession of prograding deltaic sediments (Longley et al., 2002). In the Carnarvon Basin these sediments are part of the massive Legendre delta that prograded from the north, providing key sandstone reservoir horizons for oil and gas accumulations in the Dampier Sub-basin (Vincent and Tilbury, 1988). To the south and west more distal conditions prevailed and the mud prone time equivalent section of the Athol Group was deposited. The basins to the north (Bonaparte Basin and parts of the Browse Basin) were beyond the limit of rift block rotation at this time and remained largely unaffected; sediments of the Plover Formation, a key reservoir within the Vulcan Sub-basin, continuing to be deposited as a broad delta in a predominantly fluvial depositional setting.

Longley et al (2002) place the onset of rifting from the margin of the second West Burma block (Block 3 in Figure 2–4) in the Callovian (JC seismic event in Figure 2–3) and suggest that rifting was complete by the Oxfordian (JO seismic event in Figure 2–3) in accordance with the radiogenic age dating of the Argo Abyssal Plain from the Ocean Drilling Program well 765 (Ludden, 1992).

Post-rift thermal collapse produced a major sea-level rise at the end of the Callovian that partially flooded the margin and largely terminated sand deposition in favour of the shales represented in the Carnarvon Basin by the Calypso Formation (Longley et al., 2002). The Bonaparte and Browse basins were again largely unaffected by this phase of tectonism due to the distance from the main rift axis and in these areas deposition continuing over a stable broad deltaic plain, but with an increased marine influence. This reflected the aforementioned sea-level rise and resulting transgressive sedimentation associated with deposition of the Elang (Laminaria) formations in the northern Bonaparte Basin and the Montara Formation in the Browse Basin and Vulcan Sub-basin. However, unlike the situation to the south this period of highstand resulted in the deposition of sandstones either as deep water fans in the Vulcan Sub-basin (Pattillo and Nicholls, 1990) or as shelfal sands across the northern Bonaparte Basin (Blevin et al., 1998a). These sandstones constitute the principal reservoir horizons for oil and gas fields in both areas, including the Elang (Young et al., 1995) and Laminaria (Smith et al., 1996) oilfields in the northern Bonaparte and the Montara oil and gas field in the Vulcan Sub-basin.

The third West Burma Block (Block 4 in Figure 2–4) is interpreted to have separated from the margin in the Tithonian, from a position outboard of the Bonaparte Basin, but details are limited as the oceanic crust and magnetic anomalies recording this event have subsequently been subducted or accreted (Longley et al., 2002). Direct evidence is, however, provided by the block rotation observed in wells from the northern Bonaparte and the associated significant unconformity near the base of the Tithonian (JT, top *D. swanense* biozone; Longley et al., 2002). The tectonic influence of the Tithonian rifting event on the southern portion of the margin was minimal, reflecting the distance of these depocentres from the main active rift area. This time period was nonetheless significant for the petroleum systems of the NWS as key source intervals were deposited where deep grabens and partially to fully

restricted oceanic conditions enabled high quality, liquid-prone mudstones to be deposited and preserved in an anoxic environment.

Creation of the Gascoyne Abyssal Plain occurred through the resumption of rifting in the southern end of the NWS in the Early Cretaceous (Berriasian) that has been attributed to the India-Australia breakup event (Stagg et al., 1999; Mihut and Muller, 1998). This created a long narrow rift basin running down the length of the current Perth Basin and produced a marine flooding event which is observed over the whole margin (Longley et al., 2002). More recent interpretation of the marine magnetic anomaly record suggests the formation of the Argo (West Burma blocks) and Gascoyne Abyssal plains started simultaneously in the Oxfordian before a rotation of the spreading ridge axis caused the northern spreading ridge to be abandoned in favour of plate motions along the Greater India Plate (Heine and Muller, 2005).

Uplift to the south of the Perth Basin shed a large volume of sediment into the southern part of the Northern Carnarvon Basin creating the northward prograding Barrow delta. These units provide key reservoir intervals for most of the hydrocarbon fields in the Barrow Sub-basin (McClure et al., 1988), but the delta failed to reach into the Dampier Sub-basin. Similar uplift of hinterland areas in the inboard areas of the Browse Basin also produced local progradational deltaic deposits in the Browse area, providing key reservoirs for the Ichthys area gas fields (Ban and Pitt, 2006).

Separation of Greater India (Block 5 in Figure 2–4) was complete by the Valanginian and post-rift thermal sag produced margin scale transgression that inundated the sand prone syn-rift section in all but the structural highest rift blocks (i.e. Rankin Trend in the Carnarvon Basin, Scott Reef high in the Browse Basin). Total inundation of the syn-rift section was not achieved until Aptian time when separation of Greater India from Antarctica (Block 6 in Figure 2–4 and Figure 2–5) led to the establishment of fully open oceanic conditions. This produced a change in climatic conditions that led to a switch from clastic dominated deposition to the carbonate systems that persist to the current day (Jablonski and Saitta, 2004). Whilst a range of intra-formation seals can be defined down into the Jurassic the regional flooding event marked by the KA seismic horizon (Figure 2–4) defines the ultimate regional top-seal for the North West Shelf (Longley et al., 2002).

Hinterland uplift in response to rift events along the Australian southern margin (Block 7 in Figure 2–4) occurred in the Campanian and produced a variety of inversion structures, particularly evident in the Exmouth Plateau and Exmouth Sub-basin areas (Tindale et al., 1998; Bradshaw et al., 1988). Transpressional reactivation and inversion of pre-existing rift related structures within the Barrow and Dampier sub-basins created traps of substantial size (e.g. Barrow Island). Further north in the Caswell Sub-basin, hinterland uplift resulted in a block rotation of the margin resulted in sediments inboard of the tilt line being eroded and redeposited as deep water fans (Blevin et al., 1998a). This regional tectonism is interpreted to be related to the far field plate movements, associated with the onset of Tasman Sea spreading (Bradshaw et al., 1988).

A significant change to sediment supply coincides with Tertiary onset of Coral Sea spreading, by which time the North West Shelf had drifted sufficiently northward to allow climatic conditions suitable for widespread carbonate deposition to be initiated. Rapid northwards movement of Australia in the middle Eocene occurred in response to a major plate re-organisation and carbonate deposition became dominant with massive carbonate progradation filling the remaining accommodation space provided by subsidence of the underlying rift basins (Baillie et al., 1994).

A final period of regional tectonism that occurred in the Neogene in response to plate collision along the Northern margin of Australia produced a range of both near and far field effects on the NWS hydrocarbon systems. The immediate near field impact was restricted to the Bonaparte Basin area, and was in response to the collision of the leading edge of the Australian plate with the Banda arc system located to the north (Audrey-Charles, 1988; Coblentz et al., 1998; Keep et al., 2002). Introduction of buoyant Australian continental crust jammed the subduction zone, producing a large array of neo-formed faults as well as reactivating pre-existing faults as the plate margin was increasingly flexed (Bradley and Kidd, 1991).

The impact of this collision was expressed as far field effects in the North Carnarvon and Browse basin areas, which have been attributed to changes in the regional stress field associated with the formation of the Irian-PNG Fold Belt (Hillis et al., 1997).

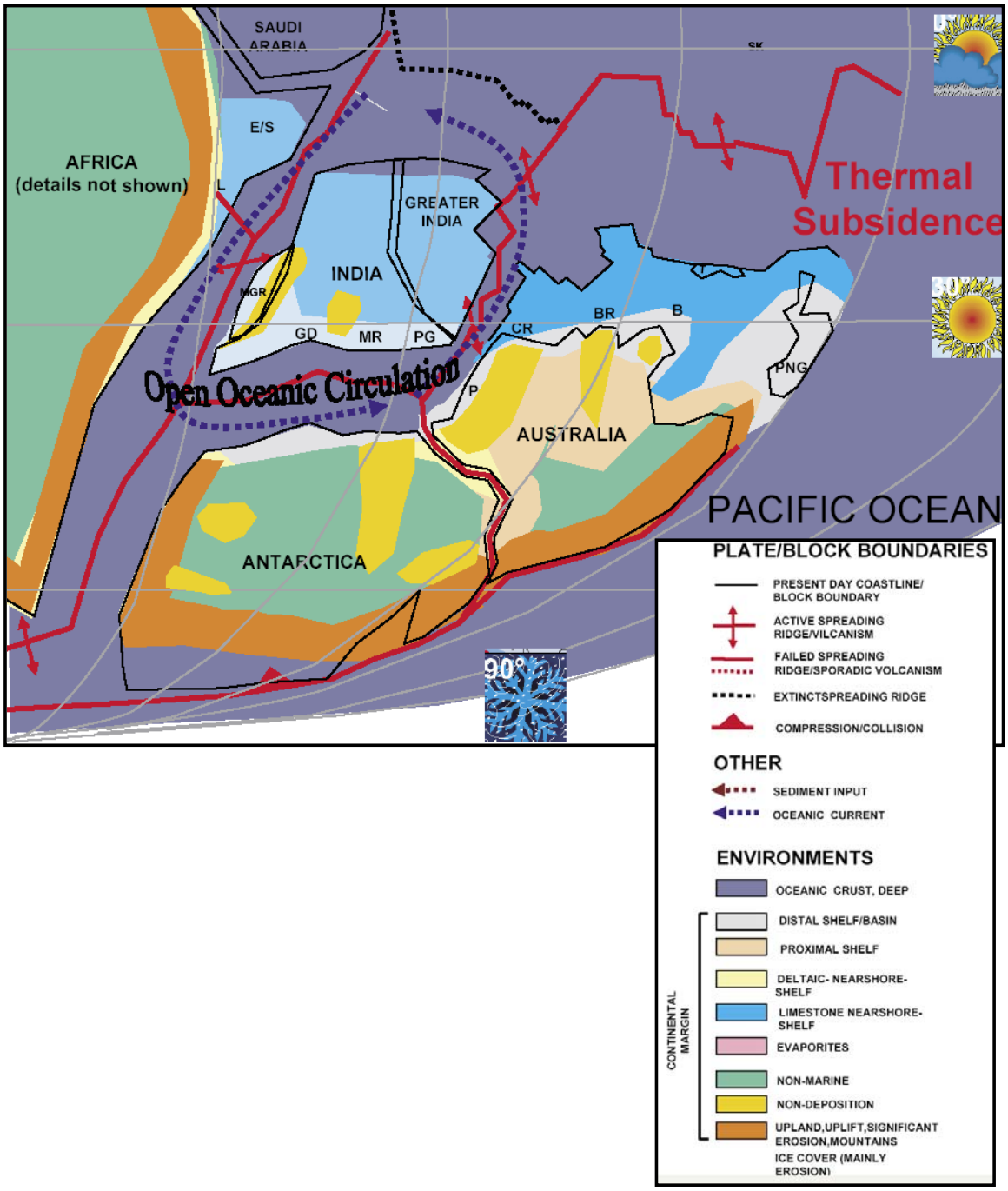

Figure 2-5: 123 My Aptian plate reconstruction.

Schematic diagram shows the establishment of open oceanic circulation that occurred in response to the separation of Greater India from the Australian and Antarctic continents in Aptian time (modified from Jablonski and Saitta, 2004). Australia and Antarctica remained joined until rifting along Australia's southern margin began in Cenomanian time. Capital letters refer to basin name (P = Perth, CR = Carnarvon, BR = Browse, B = Bonaparte, GD = Godavari) or geographic region PG = Panagarh, MR = Mahanadi Rift and MGR = Madagascar Rift).

2.3 PETROLEUM SYSTEMS OF THE NORTH WEST SHELF

The petroleum systems concept is appropriate to describe and classify the hydrocarbon fields of the NWS. Magoon (1987) describes a petroleum system as the recognition of any petroleum fluid that can be genetically linked to a discrete pod of hydrocarbon source rocks (Figure 2–6). A working petroleum system is one where all of the required elements ─ source, reservoir, seal, trap, overburden (required for maturation) as well as the processes required to facilitate (i.e. migration conduits) and preserve (e.g. suitable trap integrity and low biodegradation risk) the accumulation are present.

Systems where this genetic connection can be demonstrated are classified as "known" (!), whereas systems lacking evidence for either a demonstrated source rock or hydrocarbon fluid are referred to as "hypothetical" (.) and systems where evidence for both source rock and hydrocarbon fluids are lacking are labelled "speculative" (?) using the definitions of Magoon (1987). The speculative systems are, nevertheless, more than notional, typically being based on the presence of basin architecture that would be expected to produce conditions that can be considered analogous to known systems (Magoon and Dow, 1994). In all cases the intent of the petroleum systems approach is to determine the existence of the appropriate conditions to favour the generation and accumulation of hydrocarbons. The system operates successfully (i.e. hydrocarbons are accumulated and retained) when all the critical elements are present and occur in the correct time sequence (Bradshaw et al., 1994).

The petroleum systems concept as described in Magoon and Dow (1994) has been applied to the NWS by a variety of workers, but principally work done by geoscientists at Geoscience Australia (previously Australian Geological Survey Organisation and Bureau of Mineral Resources) has been instrumental in placing the bulk of the discovered hydrocarbon fields within a consistent petroleum systems framework (Bradshaw et al., 1988, 1994).

Bradshaw et al. (1994) described 3 Phanerozoic petroleum super-systems that are relevant to the stratigraphy of sedimentary basins across the NWS, namely the Larapintine, Gondwanan, and Westralian systems.

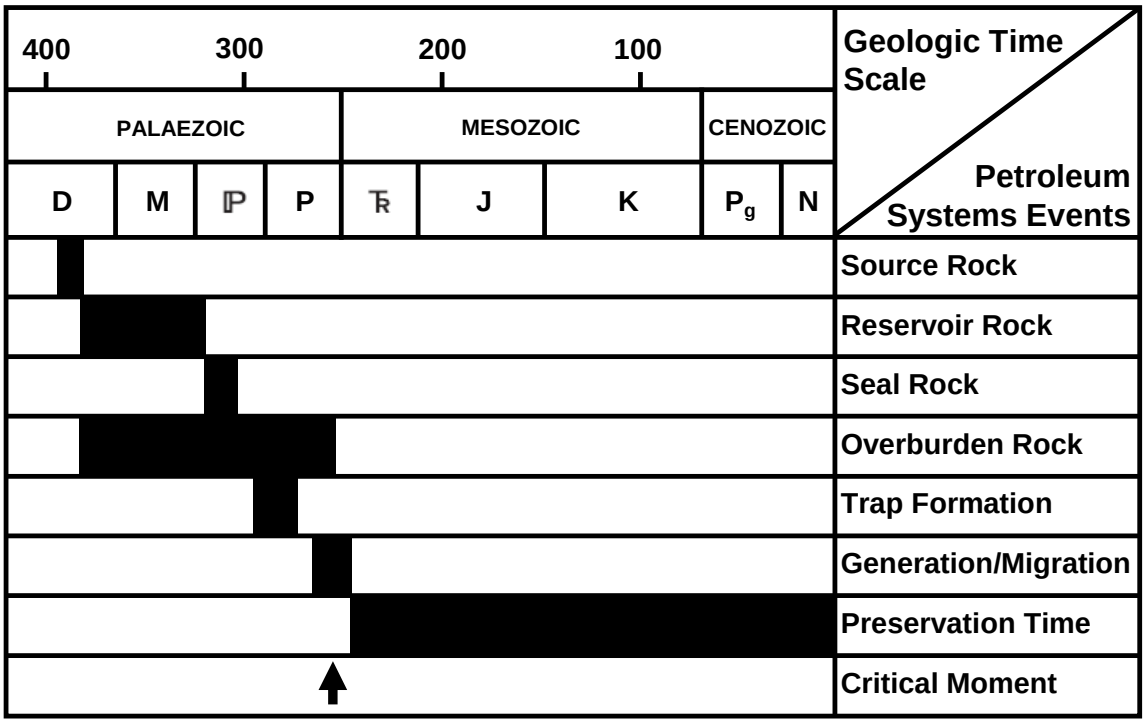

Figure 2-6: The Petroleum System concept

A generic petroleum systems 'event chart' (modified from Magoon and Dow, 1994) showing the relationship between the essential elements and processes needed for a petroleum system against geological time. The critical moment is the time, adjudged by the investigator that depicts the best opportunity for the generation migration-accumulation of hydrocarbons to successfully occur for that petroleum system. The preservation time represents the length of time that those criteria persisted for through geological time.

Detailed geochemical biomarker and isotope data collected on produced petroleum have enabled the various hydrocarbon fields and fluid recoveries to be assigned to the appropriate super-system (Edwards, et al., 1997, 2004; Summons et al., 1998). The Westralian System is recognised as by far the most important accounting for the greatest proportion of discovered hydrocarbons both in terms of number of discoveries and the largest hydrocarbon volumes.

As previously discussed an understanding of the Mesozoic break-up history of the NWS is a requisite for understanding the petroleum systems of the different basins that comprise the WASB. The break-up of Gondwana produced a complex spatial and temporal distribution of rift and post rift deposits, which strongly control not only the distribution of key reservoir units but also the potential for finding oil versus gas. On the whole the NWS is a strongly gas dominated system (84% by barrel oil equivalent [boe], Longley et al., 2002; Figure 2–2), controlled to some extent by depth of burial and associated thermal maturity levels, but more importantly by the palaeogeography prevailing during the deposition of source rocks.

As described previously, the Westralian Petroleum System (!) reflects three distinct rift phases that produced separation of the West Burma Block (Longley et al., 2002), linking a series of discrete basins stretching from the Carnarvon Basin in the southwest to the Papuan basin in the northeast through a common history of extension and eventual break-up in the Early Cretaceous.

Initially the broad rift margin created in the Early Jurassic was associated with the progradation of large deltas that produced source rocks with a high proportion of terrestrial organic matter (including coals) that favoured gas generation over oil. Condensates produced from the large gas fields of the NWS are assigned to a Westralian I classification reflecting a greater contribution from terrestrially dominated source rocks (Summons et al., 1998). Only where environments more suited to the preservation of oil prone organic matter on the delta-plain were developed (i.e. lacustrine environments) is it likely that significant liquids could have been produced. Geochemical vagrants such as the waxy oil found at Nebo-1 in the Beagle Sub-basin (Summons et al., 1998; Osborne, 1994) may represent the output from this type of source rock facies.

In parts of the WASB where narrow deep grabens formed as failed arms during the rifting of the second West Burma block in the Late Jurassic subsequent rising sea-level and associated transgressive encroachment resulted in these areas becoming isolated from open seaways producing environments with restricted marine circulation. Anoxic depositional conditions allowed organically rich source rocks with high oil generation capacity to be deposited and preserved from early oxidation. These key source rocks account for a large proportion of the oils present on the NWS that are grouped within the Westralian II classification (Summons et al., 1998).

An important consequence of the structural control imparted from the rifting events is a clustering of the greatest proportion of oil charged structures within only a few limited areas, namely the en-echelon grabens of the Dampier, Barrow and Exmouth sub-basins within the Carnarvon Basin, as well as the Sahul and Flamingo synclines and the Vulcan Graben, all within the Bonaparte Basin. These depocentres all contain a substantial thickness of Upper Jurassic marine shales that exhibit good generation potential for oil and gas (c.f. Edwards et al., 2004). Elsewhere the prevalence of open marine conditions or a more condensed (or absent) Upper Jurassic sequence precludes a liquid dominant contribution to the charge system. Instead, where successful, traps are filled predominately by gas derived mostly from Triassic or Lower to Middle Jurassic deltaic sedimentary sequences of the pre-rift Westralian I group.

In contrast to the prolific contribution from the pre- and syn-rift sediments the input from the post-rift sequence is not well represented in the hydrocarbon fluids discovered to date. This generally reflects inundation of the rift topography during sea-level rise driven by thermal subsidence associated with the cessation of rifting. The accompanying return to open oceanic circulation coupled with a reduction in sediment supply didn't favour deposition or accumulation of good source rocks.

Exceptions to this generalisation occur in the Browse and Bonaparte Basins where high quality source facies exist within organically rich mudstones of the Early Cretaceous Echuca Shoals Formation (Edwards et al., 2004). The productivity of these source rocks is largely driven by the level of thermal maturity attained at different parts of the basin.

In the Browse Basin, the continued emergence of the Buffon-Scott Reef high into the Early Cretaceous produced a large, partially restricted lagoonal embayment that allowed oil prone organic matter to be preserved. Transgressive onlap of the mid Valanginian seismic horizon (Kval) is observed across the Yampi Shelf and Prudhoe Terrace and a maximum flooding surface is interpreted at this time (Blevin et al., 1998a). Condensed sedimentation associated with this flooding surface has been shown to contain organic-rich intervals (Blevin et al., 1998b).

However, despite the favourable depositional conditions, a combination of a low impedance migration surface, allowing oil to reach the basin margins and be lost or biodegraded to produce heavy oil (Cornea and Gwydion oil fields), and deep burial of the source kitchen, pushing oil-prone source rocks into the gas window, resulted in minimal preservation and to date no economic hydrocarbon production sourced by the Echuca Shoals has been achieved. The oils encountered in the Gwydion (Spry and Ward, 1997) and Cornea (Stein et al., 1998; Ingram et al., 2000) discoveries together with oil from the Caswell-1 and Caswell-2 wells are sufficiently different in their composition from oils of the Westralian II group to form a new sub-group within the Westralian group, termed Westralian III (Blevin et al., 1998b).

The similar section within the Bonaparte Basin is also seen as having source potential (Preston and Edwards, 2000) and a contribution to the hydrocarbon charge from this source facies is recognised in the Bayu-Undan gas-condensate field (Brooks et al., 1996; George et al., 2002; 2004a). The environment of deposition is similar to the Browse Basin with remnant rift architecture acting to isolate areas prior to inundation by Late Cretaceous time. However, unlike the Browse Basin the contribution from the Echuca Shoals source rock in the Bonaparte Basin is more strongly controlled by maturity, the unit being immature except in the more deeply buried main grabens.

Despite the opportunities for a post-rift contribution, the overall importance of the petroleum system contained within the pre- and syn-rift megasequence can be demonstrated by the observation that almost all (97%) of the margins hydrocarbon resources are trapped below the Cretaceous regional seal (Longley et al., 2002). Similarly, the assignment of hydrocarbons to genetically similar oil families shows

an overwhelming dominance of the Westralian II oil family, defined as oils derived from Upper Jurassic source intervals (Bradshaw et al., 1994; Summons et al., 1998).

2.4 GEOLOGICAL EVOLUTION OF THE VULCAN SUB-BASIN

The Vulcan Sub-basin is a northeast-southwest trending Mesozoic extensional depocentre in the western Bonaparte Basin (Figure 1–4) and comprises a complex series of horsts, grabens and terraces (Figure 2–7). The major grabens are the Jurassic formed Swan and Paqualin grabens that die out to the northeast beneath the much younger (Neogene) depocentre of the Cartier Trough. The Montara Terrace flanks the Swan Graben to the east, and the Jabiru Terrace lies on the eastern margin of the Cartier Trough. The sub-basin abuts Permo-Triassic platforms, the Londonderry High to the southeast, and the Ashmore Platform to the northwest.

Most exploration wells in the region are sited on narrow intra-basin horst blocks, tilted fault blocks or major structural highs that form the margins of the basin-bounding terraces and flanking platforms.

The stratigraphic architecture of the Vulcan Sub-basin (VSB) has been well documented, initially based on a description of the lithostratigraphic observations (Mory, 1988) and subsequently using chronostratigraphic methods (Pattillo and Nicholls, 1990). The latter approach proved invaluable in providing a consistent set of time correlative markers with which to define the stratigraphic and structural development of the basin and helped to unify the previously disparate and largely informal stratigraphic nomenclature.

The tectonostratigraphic framework proposed by Pattillo and Nicholls (1990) sub-divides the Mesozoic sedimentary section of the VSB into three discrete megasequences (Figure 2–8), each linked to a key phase of basin development. More recent stratigraphic descriptions (e.g. Geoscience Australia) largely honour the sub-divisions of Pattillo and Nicholls (1990) but differ slightly in the timing of rift onset and recognise a distinction between cessation of rifting and the completion of thermal subsidence prior to the establishment of a true passive margin (Figure 2–9).

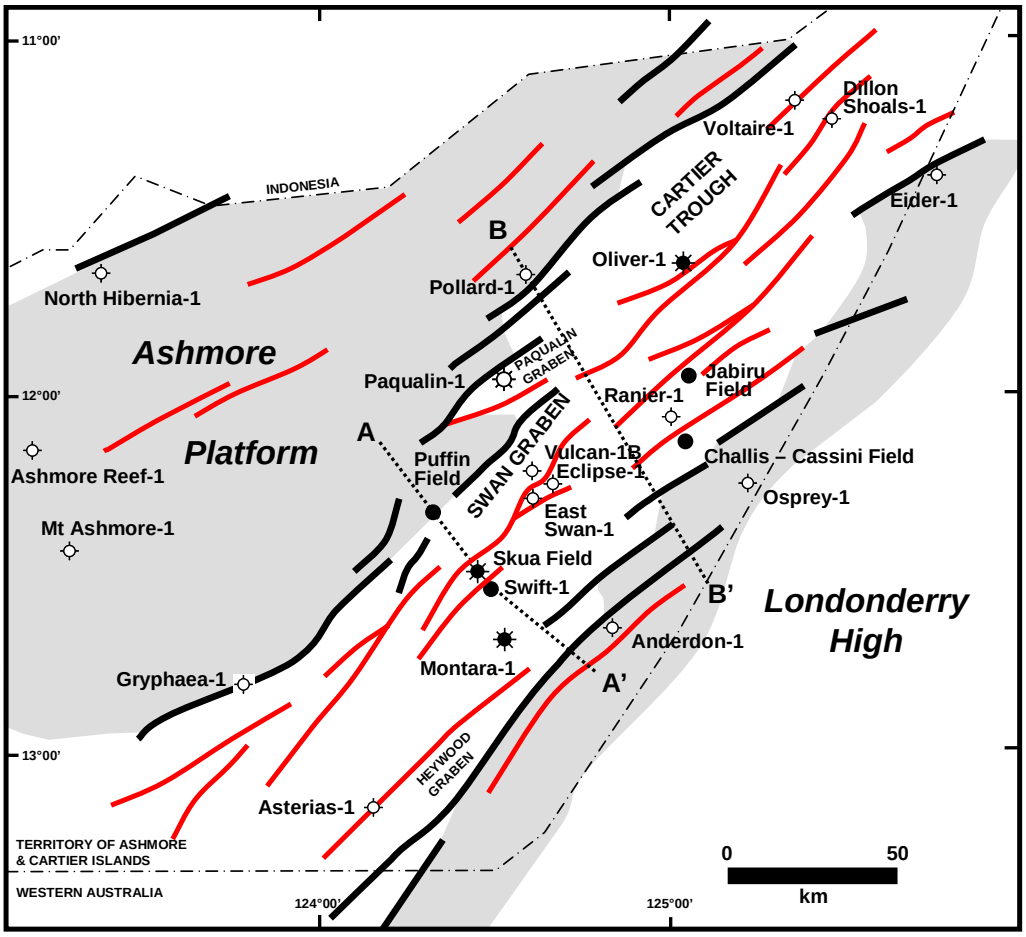

Figure 2-7: Location of key structural elements and wells within the Vulcan Sub-basin.

Map shows location of basin forming (black) and intra-basin (red) fault trends together with key wells and the important depocentres. The VSB is located within the Territory of Ashmore and Cartier Islands, an Australian territory that borders Indonesia to the North. Platform areas of the Ashmore Platform and Londonderry High flank the key depocentres and contain a condensed or absent Upper Jurassic sequence. Lines of section A-A' and B-B' show the location of cross sections that are shown in later diagrams.

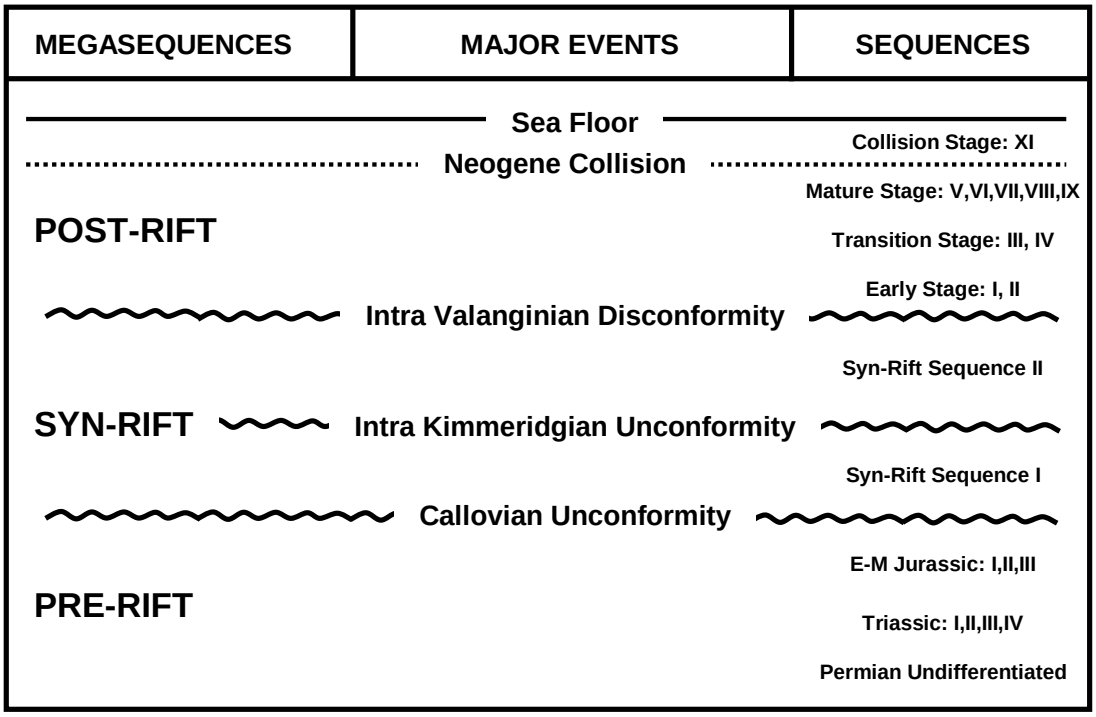

Figure 2-8: Chronostratigraphic sub-division of the stratigraphy of the Vulcan Sub-basin.

The sub-division of the basin sedimentary fill into three principal megasequences (from Pattillo and Nicholls, 1990) enables the tectonic elements that have shaped the basin development to be linked to the observed sedimentary fill and is useful for integrating information gained from wells with horizon surfaces interpreted from regional seismic data. The Pre-rift sequence is predominantly fluvio-deltaic and provides recognised reservoir sections within the Triassic and Jurassic sections as well as gas prone source rocks in the Early to Middle Jurassic sequence. The Callovian Unconformity marks the base or the syn-rift sequence and is clearer represented in the wells but is more subtle on seismic data. The syn-rift fill represents infill of accommodation space created by the rifting that led to separation of the West Burma block (Longley et al., 2002) and contains oil-prone Upper Jurassic shales as well as important reservoirs. The syn-rift section is punctuated by the Intra Kimmeridgian Unconformity, separating sandstones and restricted marine mudstones of the Montara and Lower Vulcan formations respectively from restricted marine mudstones and proximal fan sandstones of the Upper Vulcan Formation (Pattillo and Nicholls, 1990). The strongly erosional base of this section defines this unconformity within the main grabens but this merges with the Callovian Unconformity on the flanking platforms. The Post-rift megasequence marks the change to passive margin growth reflecting the cessation of rifting. This interval can be further divided into an early stage comprising sharply transgressive and increasingly deep (bathyal) water claystones, followed by a transition phase were deep water conditions prevailed and clastic deposition declined in favour of carbonates and finally into a mature stage where a thick carbonate wedge developed and prograded northwards during the Tertiary. The final stage of the Post-rift sequence involved rapidly increasing subsidence and carbonate aggradation in response to plate margin collision to the north.

In this study the tectonic elements of the tripartite system of Pattillo and Nicholls (1990) have been used as there is a lack of clear evidence in the VSB of the Early Jurassic rifting that is prominent elsewhere on the North West Shelf.

Irrespective of the tectonic framework that is used the stratigraphic sub-division reflects the complex and multi-phase structural history experienced by the VSB (O'Brien et al., 1993; O'Brien et al., 1996). Multiple episodes of rifting throughout the Palaeozoic and early Mesozoic culminated in a period of thermal subsidence as the basin developed into a tectonically quiescent passive margin.

A final phase of basin-wide structuring was produced in the Neogene in response to the collision of the northwards moving Australian Plate with a complex collection of smaller micro-plates that make up the southeastern end of the Indonesian Archipelago and the western part of the island of Papua New Guinea.

2.4.1 Pre-Rift Phase

The pre-rift phase (Figure 2–8) refers to sediments deposited prior to the Callovian Unconformity (Pattillo and Nicholls, 1990) and is somewhat of a misnomer as prior to the development of the Mesozoic rift phase that produced the Vulcan Graben the region experienced two earlier phases of Palaeozoic extension.

Initial rifting in the region first occurred in the Late Devonian and produced the northwest-trending Petrel Sub-basin in the eastern portion of the Bonaparte Basin (Figure 2–1) where a significant thick section of Palaeozoic and Mesozoic stratigraphy has been preserved (Colwell and Kennard, 1996).

This rift system was orthogonally overprinted in the Late Carboniferous to Early Permian by northeast-trending rift basins forming the proto-Malita and Calder Grabens in the east as well as the Browse Basin to the west of the Bonaparte Basin (O'Brien, 1993; Baxter, 1996; Struckmeyer et al, 1998; Shuster et al, 1998). A proto-Vulcan depocentre was initiated at this time (O'Brien, 1993), after which shallow marine to fluvio-deltaic Upper Permian–Triassic sediments was deposited on the northern margin of Gondwana facing the Tethyan ocean (Figure 2–4, 2–9).

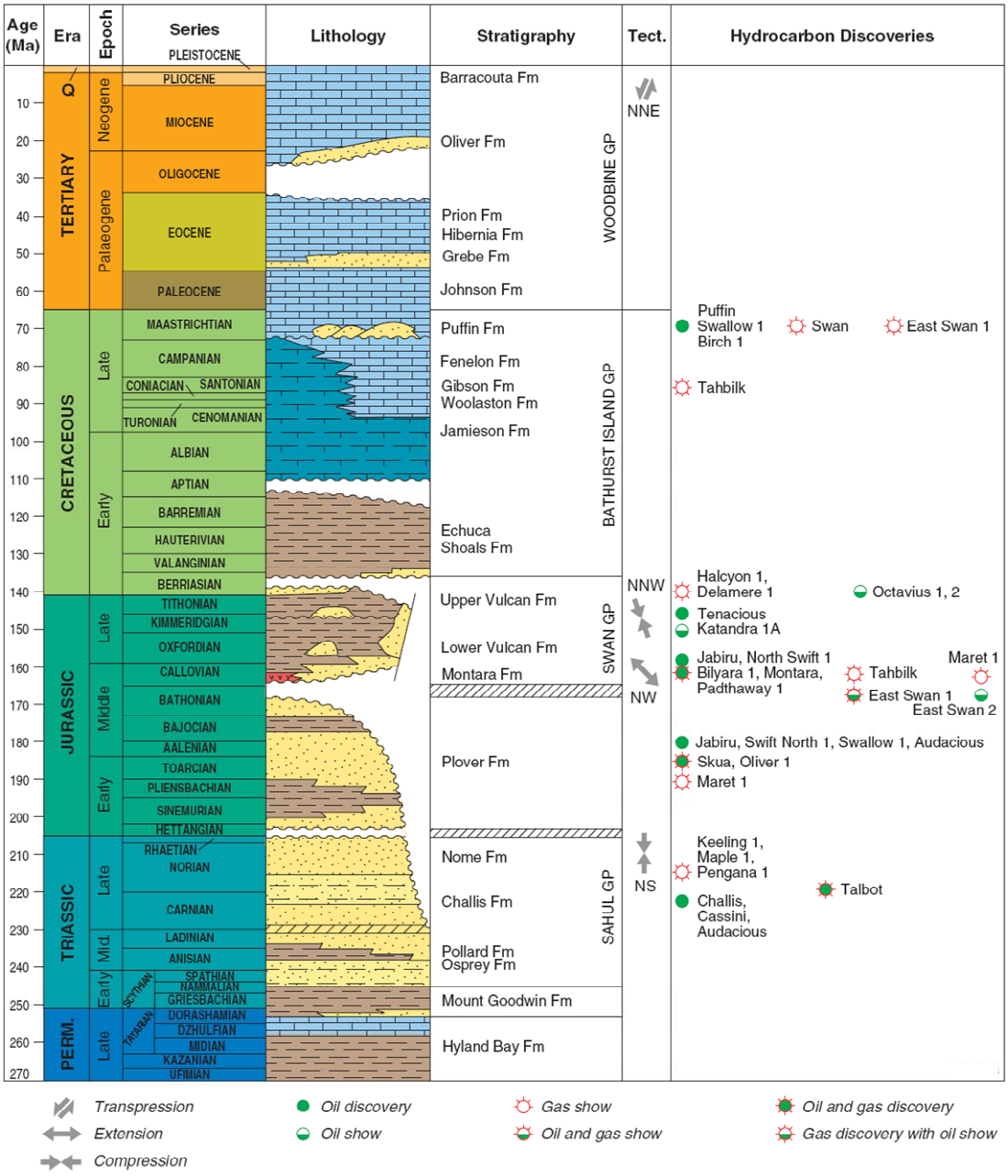

Figure 2-9: Generalised stratigraphy of the Vulcan Sub-basin from Triassic to Recent.

Stratigraphic position of the key hydrocarbon discoveries is shown and the principal tectonic events are also listed relative to the main unconformities (from Geoscience Australia, 2008). Lithostratigraphy column runs from west (right) to east (left) and demonstrates the fault controlled deposition of the syn-rift Swan Group as well as the deep erosion (non-deposition) of the pre-rift sequence and the missing section that defines the Callovian Unconformity.

Where penetrated in the VSB, the Upper Permian section comprises shallow marine carbonates and minor clastics of the Hyland Bay Formation (Figure 2–9). Reservoir properties are generally except where fracture porosity is developed and although the sequence is not hydrocarbon-bearing in the VSB, a number of sub-economic gas accumulations are present at this level across the greater Bonaparte Basin, most notably the Tern and Petrel gas fields (McConachie et al., 1996).

The overlying conformable Triassic stratigraphy comprise the Early Triassic transgressive sequence of marine shales and siltstones of the Mt Goodwin Group that are in turn conformably overlain by the Sahul Group, of Middle Triassic age and containing the Osprey, Pollard, Challis and Nome formations. These formations represent successive cycles of overall transgressive sedimentation with turbidites of the Osprey Formation grading upwards into more deltaic facies that are capped by shallow marine carbonates of the Pollard Formation (Mory, 1988).

Subsequent regression produced mixed clastic and carbonate deposition within the Challis Formation that was subsequently overlain by thick deltaics of the Nome Formation (Pattillo and Nicholls, 1990). The Challis Formation is the host of the Challis-Cassini and Talbot oil fields and together with the Nome Formation constitutes important reservoir targets for exploration in the VSB.

Late Triassic uplift produced significant erosion across the Ashmore Platform and Londonderry High. Regional uplift associated with the Fitzroy Movement eroded substantial volumes of sediment from the largely granitic Pilbara and Kimberly cratonic blocks. Erosion of these landmasses produced a large delta with Early to Middle Jurassic fluvio-deltaic sediments of the Plover Formation (Figure 2–9) prograding out across the Browse and Bonaparte basins.

In the VSB the Plover Formation is restricted to the area of the Vulcan Graben (Figure 2–9 and Figure 2–10) suggesting that it could represent either an erosional remnant of a previously more widespread unit or alternatively it may reflect filling of accommodation space created by some element of Early Jurassic rifting. Comparison with the adjacent Browse and Northern Bonaparte basins favours the unit initially being more widespread prior to a period of significant erosion.

The Plover Formation is made up of Early-Middle Jurassic deltaic sandstones, siltstones and coal. Three major sandstone sequences are recognised within an overall transgressive package. Braided stream and floodplain deposits characterise the Pleinsbachian to Early Bajocian aged lower sequence, overlain by a Bajocian-Callovian section comprising distributary channels and mouth bars interpreted to reflect increasing marine influence and capped by a shallow marine upper sequence of Late Callovian age (Pattillo and Nicholls, 1990).

The termination of deltaic sedimentation and the onset of shallow marine shelf deposition are interpreted to mark a phase of increased rifting leading into the breakup event along the Argo margin in the Callovian.

The Plover Formation forms the principal reservoir for the Jabiru (MacDaniel, 1988) and Skua (Osborne, 1990) oilfields and is hydrocarbon bearing in the Oliver discovery (Ambrose, 2004).

2.4.2 Mesozoic Syn-Rift Phase

The VSB developed as an intra-continental rift graben in the late Callovian, and extensional structuring continued until the end of the Tithonian (O'Brien et al., 1996b; Baxter et al., 1998) when final break-up occurred.

The Callovian unconformity separates the Middle Jurassic Plover Formation from the Upper Jurassic Swan group and marks the base of the Syn-Rift phase (Figure 2–8, 2–9, 2–11). Widespread marine conditions prevailed in the Vulcan Sub-basin during the syn-rift phase with shales of the Lower and Upper Vulcan formations being deposited, separated by the Kimmeridgian/Tithonian unconformity (Figure 2–8, 2–9, 2–11).

The Syn-rift stratigraphy is of critical importance to the VSB as it contains the source rocks that provide the majority of hydrocarbon charge to reservoirs above, below and within the syn-rift megasequence (Preston & Edwards, 2000; Edwards et al., 2004).

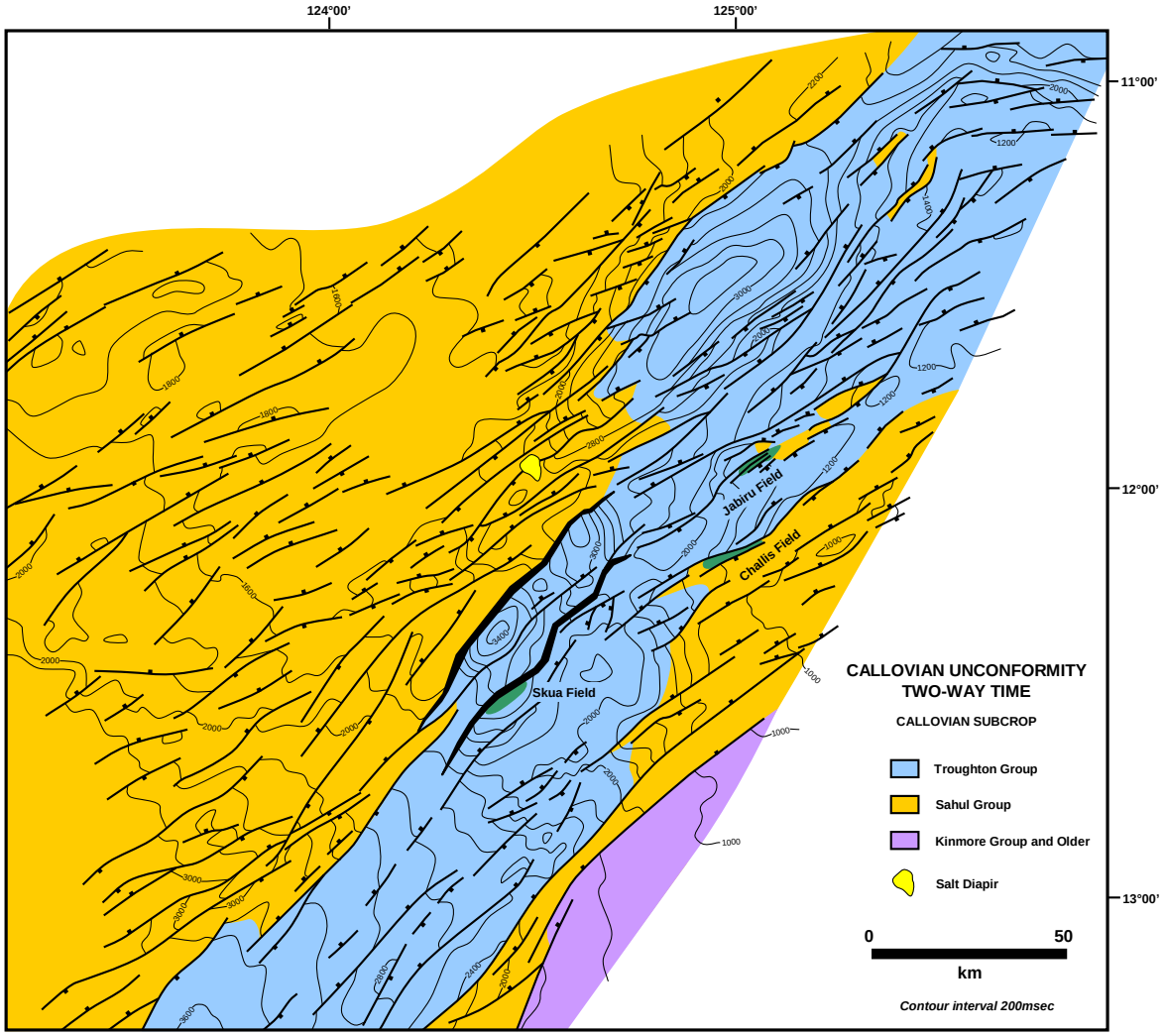

Figure 2-10: Callovian Unconformity two-way time structure map

This Callovian sub-crop depth-structure map shows the extent of the Troughton Group (Plover Formation) following Upper Jurassic extension and marks the end of the Pre-rift sequence (from Pattillo and Nicholls, 1990). Older sediments of the Triassic Sahul Group and Permian Kinmore Group sub-crop on the adjacent Ashmore Platform and Londonderry High where Plover Formation sediments have either been eroded, or represent a condensed section or were never deposited.

Extensional faulting during the mid-Oxfordian to early Kimmeridgian coincides with the commencement of sea floor spreading in the Argo Abyssal Plain to the west of the Browse Basin (Ludden, 1992), and was focused in the south western portion of the sub-basin where the deep and narrow Swan and Paqualin grabens were created (Figure 2–7). These narrow grabens were isolated from open marine circulation and thick Oxfordian (*W. spectabilis* palynozone) marine source rocks of the Lower Vulcan Formation (Figure 2–9) accumulated in anoxic conditions, with thinner interval also preserved on the adjoining Montara and Jabiru terraces (Figure 2–11).

The Jabiru, Challis and other intra-basinal horsts were partially to fully emergent at this time, and sand-rich lowstand fan deltas continued to be shed from the Londonderry High and exposed horsts into the adjacent depositional lows. Prograding fan-delta systems of the Montara Formation (Figure 2–9), resulting from localised footwall erosion of the exposed horsts and high-side rotated fault blocks form the basal part of the Swan Group and provide the principal reservoir interval for the small Montara, Bilyara and Tahbilk oil and gas fields.

Lower Oxfordian marine sediments of the Lower Vulcan Formation (*W. clathrata* palynozone; Figure 2–9) continued to accumulate within the grabens, but are generally thin or absent on the adjacent Montara and Jabiru terraces (Figure 2–11). Lower Kimmeridgian to Lower Tithonian marine sediments are also restricted to the main graben depocentres, but they probably extended across the adjoining terraces to the east prior to their subsequent uplift and erosion in the Tithonian.

Mid-Tithonian structuring produced the Kimmeridgian/Tithonian unconformity (Figure 2–9) associated with rifting of the West Burma III block (Figure 2–4). Associated footwall uplift resulted in sub-aerial exposure of the Montara Terrace and partial emergence of the Jabiru Terrace, whereas marine deposition continued in the Swan and Paqualin grabens where shales of the Upper Vulcan Formation were deposited. Exposure and local erosion by this unconformity provided an opportunity to shed coarse-grained clastics which were deposited as lowstand basin-floor fans in the central Vulcan Sub-basin and provide reservoir rocks for the small Tenacious oil field (Bint et al, 1998). Further to the north, the previous northeast Callovian fault trend was overprinted by east-west trending faults at this time (Woods, 1992).

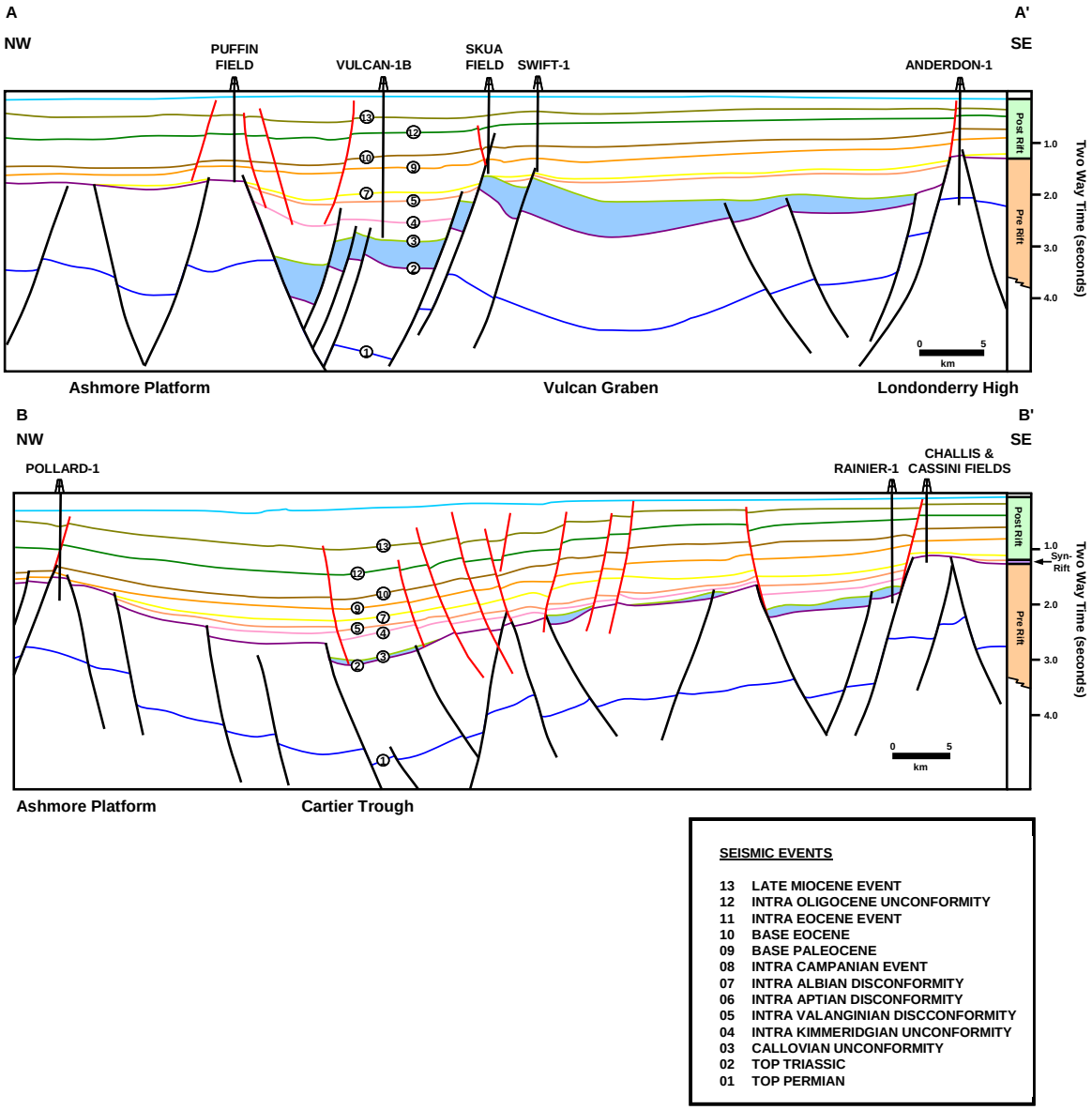

Figure 2-11: Key cross sections across the Vulcan Sub-basin

Seismically defined cross sections through the southern (A-A') and northern (B-B') depocentres of the VSB (see Figure 2-7 for location of sections). In the Southern part of the VSB significant Callovian tectonism produced deep grabens that were filled with thick packages of syn-rift sediment. In comparison, the Cartier Trough in the Northern VSB is a much more recent feature with syn-rift sediments being absent or only poorly developed (modified from Pattillo and Nicholls, 1990). The numbers refer to major seismic horizons and are specified in the table below.

2.4.3 Mesozoic Post-Rift Phase

Deposition of the Upper Vulcan Formation was terminated by the Valanginian unconformity, marking the end of the syn-rift phase (Figure 2–8) and a transition to passive margin conditions. Post-rift regional thermal subsidence commenced in the Valanginian and resulted in widespread flooding of the continental margin and deposition of the Valanginian to Maastrichtian aged Bathurst Island Group. The Valanginian-Aptian aged Echuca Shoals Formation (Figure 2–9) forms the base of this sequence and represents a transgressive condensed marine section that is confined largely to the grabens and adjoining terraces (Figure 2–11). With continuing subsidence, Aptian–Albian shaly and marly marine sediments of the Jamieson Formation (Figure 2–9) further transgressed the adjacent, previously emergent, areas of the Londonderry High and Ashmore Platform. A combination of restricted sediment supply and increasing water depth promoted the accumulation of Upper Cretaceous (Cenomanian–Santonian) fine-grained carbonates of the Woolaston and Gibson formations (Figure 2–9), and their progradation marks the transgressive peak of the post-rift succession.

Continued progradation of a fine-grained, mixed carbonate–clastic ramp continued until the Campanian (Fenelon Formation; Figure 2–9), before a sea-level fall led to the deposition of lowstand clastic fans (Puffin Formation; Mory, 1988; Figure 2–9) across the southern part of the VSB and adjacent Ashmore Platform in the Maastrichtian. These sandstones provide the reservoir for the Puffin oil field (Mory, 1988; De Boer, 2004) and the Swan gas discovery (BHP Petroleum Ltd, 1992).

Overlying the Bathurst Island Group is the Woodbine Group (Figure 2–9) representing progradation of a thick carbonate wedge across the outer Bonaparte Basin throughout the Tertiary. The Tertiary succession is characterised by the establishment of a sub-tropical carbonate platform as the Australian plate moved northward at an increasing rate, climatic warming culminated in the development of tropical carbonates and reefs. This carbonate deposition was interrupted in the Early Eocene and Miocene by glacio-eustatic sea level lowstands, allowing prograding sand-prone deltas of the Grebe and Oliver formations to be deposited.

A major Oligocene hiatus is recognised across the region (Figure 2–9) and, in the absence of evidence for structuring and major erosion, this event is attributed to eustatic and oceanographic factors (Quarles van Ufford and Cloos, 2004), associated with a global sea-level fall (Haq et al., 1987), rather than to a significant episode of uplift and erosion as previously proposed (Mory, 1988; Pigram and Symonds, 1991).

2.4.4 Neogene Collision Phase

In the Late Miocene to Early Pliocene, convergence of the Australian and Eurasian plates resulted in structural reactivation of many Mesozoic extensional faults as well as creating new faults (Figure 2–12; Woods, 1992; O'Brien and Woods, 1995; O'Brien et al., 1996b; Shuster et al., 1998). This event reflects the sum of a series of regional tectonic events beginning with the collision of Australian Continental crust and a northward facing subduction zone on the island of New Guinea at about 25Ma (Etheridge et al., 1991; Charlton, 2000). Shortening related to this collision created the New Guinea Fold Belt between about 12 Ma and 3 Ma (Hill and Raza, 1999, Etheridge et al., 1991) followed by the Sumba-Banda collision between 8 Ma and 3 Ma (Charlton et al., 1991; Woods, 1994, Keep et al., 2002).

The 8 Ma event probably coincides with the arrival of transitional Australian continental crust in the Timor area, whereas the 3 Ma tectonic event records the jamming of the subduction system as Australian continental crust was unable to be subducted beneath the Banda Arc (Figure 2–13). The 3 Ma tectonic event is also evident on areas of the Sunderland craton adjacent to Sumba (Keep et al., 2002) where massive structural inversion events occurred (Bransden and Matthews, 1992), and a synchronous change in relative plate motions also occurs in the Pacific at about this time (Pockalny et al., 1997). The northward movement of the Australian Continent was nevertheless able to continue, being accommodated by the initiation of a north-dipping subduction zone along the Wetar and Flores thrust system (McCaffrey, 1996; Genrich et al, 1996; Figure 2–13).

Regional Neogene tectonism also produced many new faults as well as widespread reactivation of existing faults and this faulting is widely seen as the cause of breach of many traps (O'Brien and Woods, 1995; O'Brien et al., 1998; Lisk et al., 1998b).

Leakage of hydrocarbons from syn and pre-rift hydrocarbon accumulations enabled seepage into the overlying section, to give hydrocarbon charge to shallower reservoirs such as the Maastrichtian Puffin sandstones of the Puffin Oil Field but the majority of leaking hydrocarbons likely reached the seabed and was lost.

Hovland et al. (1994) proposed that hydrocarbon seepage assisted in the formation of bioherms via the hydrocarbons providing nutrients for bacteria, which were, in turn, part of the food chain for organisms such as Halimeda codiacean algae. The association of leakage with surface biohermal mounds has also been noted by Bishop and O'Brien (1998) in the Nancar area and over the greater Timor Sea area by O'Brien et al. (2002a). However, whether all or just some of the Neogene to present-day reefs have been seeded from hydrocarbon leakage is not clear.

In addition to surface features that may be related to hydrocarbon leakage O'Brien and Woods (1995) and Cowley and O'Brien (2000) also describe seismic amplitude anomalies within the shallow sedimentary section that are interpreted to be seepage-related (called hydrocarbon related diagenetic zones, HRDZs). These features relate to pervasive carbonate cementation of shallow Tertiary sandstones that have highly depleted carbon isotope compositions suggesting a carbon source that was derived from the oxidation of migrating hydrocarbons (O'Brien and Woods, 1995).

Further evidence of ongoing hydrocarbon seepage has been documented by a variety of remote sensing techniques including water bottom geochemical sniffer surveys to detect hydrocarbons in the water column, water column sidescan sonar and seabed coring to identify active seepage, and sea-surface oil-seep detection methods such as the Airborne Laser Fluorosensor (ALF) method (Williams et al., 1995).

The importance of the reactivation phase in the development of the VSB cannot be overstated as these events are seen as the cause of poor hydrocarbon retention and the main reason that this region has failed to deliver the hydrocarbon reserves that were initially expected. Understanding the complex interplay between pervasive Neogene fault reactivation and attendant hydrocarbon leakage from Mesozoic fault blocks is of critical importance as is the interpretation of seepage indicators to the development of practical strategies to help mitigate the clear trap integrity risk.

2.5 PETROLEUM SYSTEMS OF THE VULCAN SUB-BASIN

The Vulcan Sub-basin is endowed with all of the critical elements needed to produce a successful petroleum system. The tectonic history produced a basin architecture ideally suited to accumulate and preserve organically rich Upper Jurassic source rocks capable of producing abundant hydrocarbon volumes once sufficient thermal maturity was attained.

Located immediately above high quality Middle to Lower Jurassic fluvio-deltaic sandstone reservoirs that are capped by regional extensive and highly effective capillary seals hydrocarbons generated from these source rocks were readily able to migrate into a variety of robust fault bound traps.

The region has similarities with the more prolific Carnarvon Basin where a similar combination of Jurassic rift architecture and an effective reservoir, source and seal configuration has resulted in a world class hydrocarbon province (Longley et al., 2002). The VSB contains a proven hydrocarbon system, with 19 technical discoveries from 75 exploration wells producing an overall technical success rate of 25%. Estimated reserves are about 725 million barrels oil equivalent (MMBOE) made of up 312 million barrels of oil and condensate and 2.4 Trillion Cubic Feet (TCF) of gas (Table 2–1).

Commercial discoveries occur within Late Triassic (Challis field), Early-Middle and Late Jurassic (Jabiru and Skua fields) and Late Cretaceous (Puffin field) clastic reservoirs. Other discoveries including Audacious, Bilyara, Birch, Delamere, East Swan, Eclipse, Halcyon, Keeling, Maple, Maret, Montara, Oliver, Padthaway, Pengana, Puffin, Swan, Swift, Tahbilk, Talbot and Tenacious are considered to be currently non-economic, principally reflecting the small size of these accumulations.

All of the discoveries made in the VSB have been assigned to a single petroleum system known as the proven Jurassic Vulcan-Plover petroleum system (Figure 2–14). The system is mostly restricted to an active source pod within the syn-rift zone but extends a short distance onto the Ashmore Platform to the west and the Londonderry High to the east (Figure 2–15).

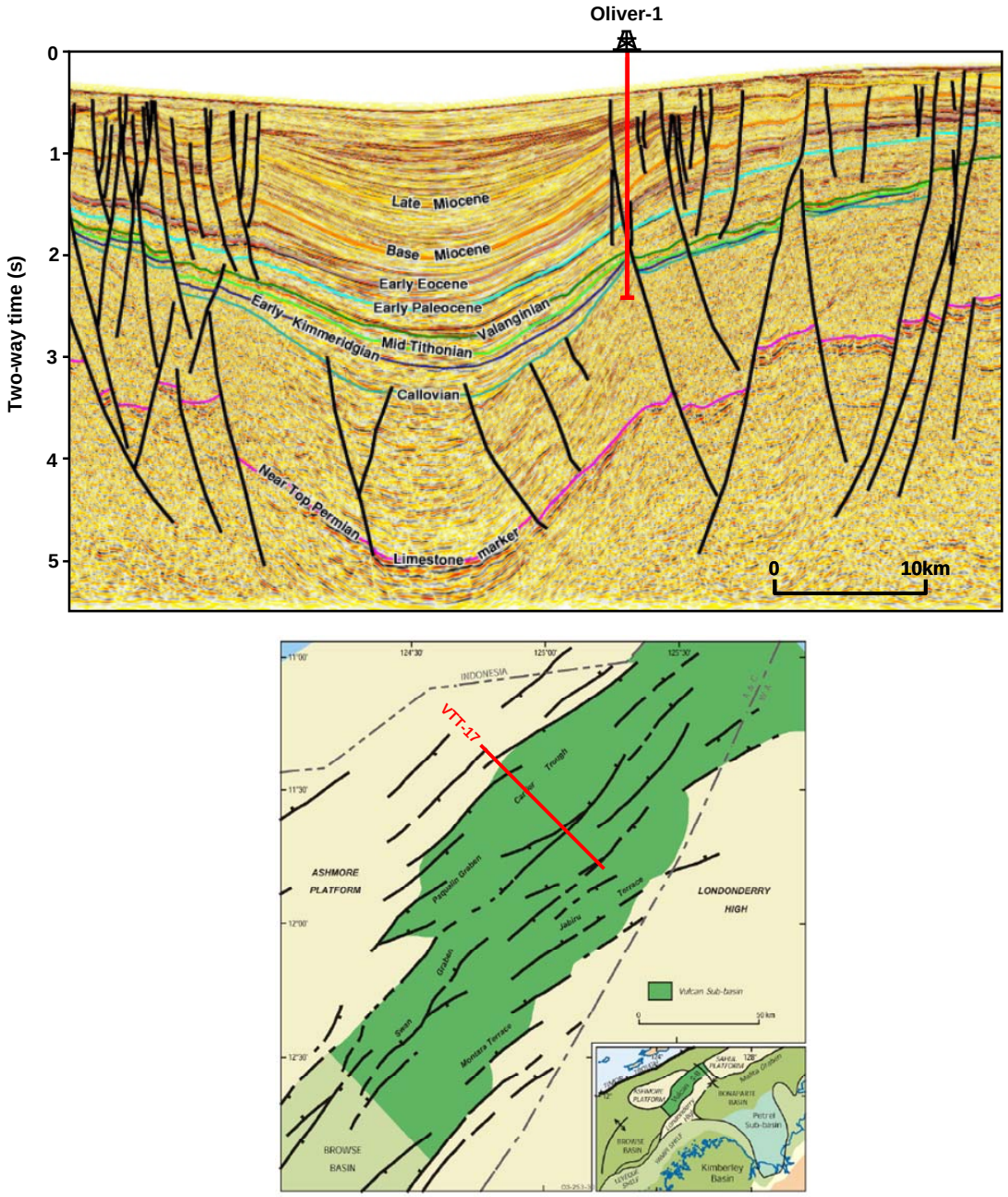

Figure 2-12: Seismic line showing typical pervasive Neogene fault reactivation.

Partial section of regional seismic line VTT-17 through the Oliver-1 well location showing a dense array of extensional faults on both sides of the recently formed Cartier Trough (Geoscience Australia, 2006b). These include both reactivation of pre-existing rift faults as well as creation of neoformed Tertiary aged faults during Neogene plate collision. Despite the widespread fault reactivation the impact on hydrocarbon trap integrity is not straightforward with wells like Oliver-1 testing an intact hydrocarbon column despite the obvious recent reactivation of the main trap bounding fault. Map below show location of section of VTT-17 shown in relation to the broader VSB.

The components required to produce the Jurassic Vulcan-Plover (!) petroleum system (Figure 2–16) include sandstone reservoirs, a mixed oil and gas mudstone source, and trap elements dominated by complex faulted structures that are capped by an effective regional seal.

Tertiary calcareous sequences provide the overburden to promote maturation with migration conduits aided by direct face loading or through a series of fault terraces and relay ramps. The successful preservation of the accumulations that formed represents the most critical risk to the effectiveness of the system.

2.5.1 Reservoirs

Clastic units within the pre-rift and syn-rift sequences host the majority of the petroleum accumulations identified to-date in the VSB (Figure 2–16). Sandstones of the Late Triassic Challis Formation (Challis and Cassini fields), the Middle Jurassic Plover Formation (Skua and Jabiru fields) and the Upper Cretaceous Puffin Formation (Puffin field) constitute the economically proven reservoirs. The key exploration targets in the VSB rely on these units as reservoir rocks well as sandstones of the Late Triassic Nome Formation, fan-delta sands of the Late Jurassic Montara Formation, and submarine gravity flow fans of the Late Jurassic Vulcan Formation (Figure 2–9).

Sandstones within the Cretaceous section are generally not considered to be widespread viable reservoir targets, but are locally important where the Puffin fan complex (De Boer, 2004) is present. The more significant and widespread sandstones within the Tertiary section lack a proven top seal and are not commonly targeted as a primary objective in exploration drilling.

A detailed examination of reservoir quality in the VSB is covered in Chapter 3 but typically the main reservoir targets exhibit good to excellent reservoir properties (high porosity, permeability and net to gross), except in the deepest parts of the main grabens where higher temperatures have resulted in advanced diagenesis that has occluded much of the primary depositional porosity.

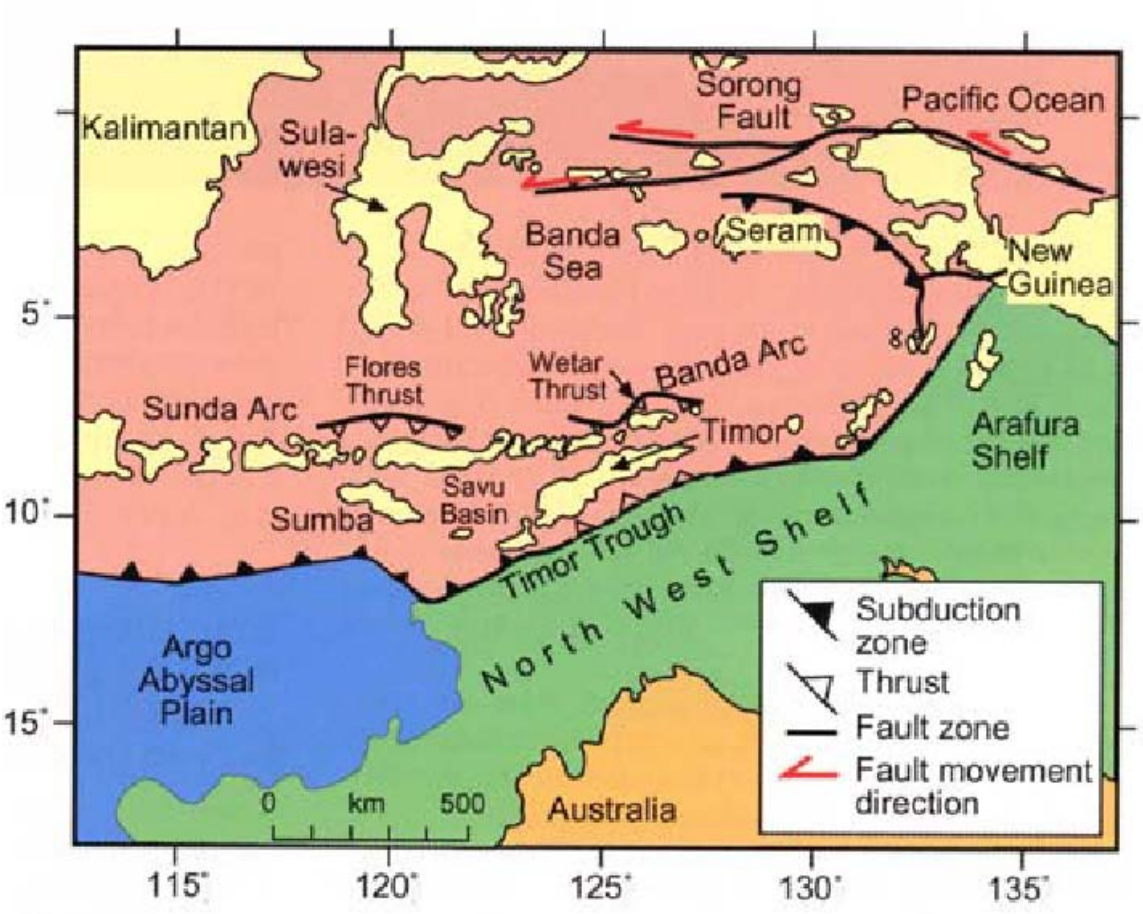

Figure 2-13: Tectonic elements of the Banda Arc.

The Banda Arc lies at the intersection of the Indo-Australian, Eurasian and Pacific plates with northwards movement of the Indo-Australian plates at about 70mm per year being accommodated by deformation across the leading edge at Timor and Sumba and the progressive consumption of ocean crust by the initiation of northwards facing subduction zones along the Wetar and Flores thrust systems. Subduction no longer occurs where continental crust (green) abuts the island of Timor but further to the west oceanic crust of the Argo Abyssal Plain (blue) continues to be subducted (from Keep et. al., 2002).

2.5.2 Source

Two main source rock intervals are recognised in the region; the marine dominated Late Jurassic Lower Vulcan Formation and the more terrestrial fluvio-deltaics of the Early-Middle Jurassic Plover Formation (Figure 2–16). The Lower Vulcan Formation is considered to be the dominant source rock interval for both the oil and gas generated in the region (Edwards et al., 2004). Collectively hydrocarbons that are derived from these source rocks constitute the proven Jurassic Vulcan-Plover (!) petroleum system.

Thick Jurassic sequences in the Swan and Paqualin Grabens (Figure 2–7) provide a petroleum charge for good quality, Jurassic clastic reservoirs in structural traps associated with intra-basin horst blocks and basin margin terraces. Extensive source rock evaluations have been completed in the VSB and are summarised in Edwards et al. (2004). Rock Eval pyrolysis data show that the Lower Vulcan and Montara formations contain organic-rich marine mudstones that have fair to very good source potential (Figure 2–18). The kerogen is predominantly Type II/III and comprises a mixture of marine algal material and bacterially reworked land-plant debris that would be expected to generate oil and gas (Edwards et al., 2004).

Source rocks within the Plover Formation are also organically rich with high Total Organic Carbon (TOC) levels (Figure 2–18), but are likely to be more gas prone due to a greater proportion of terrestrial organic matter including an abundance of coals. Carbonaceous shales, especially in wells on the Montara Terrace, have particularly high hydrogen indices that would normally be expected to generate significant liquids. However, such coaly source rocks are thought to require much higher Hydrogen Index (HI) values (~500) before they can be expected to generate and expel substantial liquids (Isaksen et al., 1998).

Rock-Eval data for the Upper Vulcan Formation and the Lower Cretaceous Echuca Shoals (Figure 2–18) is more limited, but these source rocks are not considered to contribute significantly to the hydrocarbons recovered in the basin (Edwards et al., 2004). The Upper Vulcan Formation has similar HI values to the prolific Lower Vulcan Formation, is a leaner source rock with TOC values mostly less than 1%.

Table 2-1: Reported volumes for VSB hydrocarbon discoveries

The notes provided indicate the basis of the estimates and the source of the information being the Department of Primary Industry, Fisheries and Mines, Northern Territory

Field	Petroleum System	Liquids (MMBBLS)	Gas (TCF)	Gas (MMBOE)	Date of Estimate	Source
Audacious	Vulcan-Plover (!)	3.1	0	0	Sep-05	DPIFM
Cash/Maple	Vulcan-Plover (!)	34.2	1.65	280.5	Jul-05	DPIFM
Challis and Cassini	Vulcan-Plover (!)	59.9	0	0	Dec-05	DPIFM
Jabiru	Vulcan-Plover (!)	112.4	0	0	Dec-05	DPIFM
Katandra	Vulcan-Plover (!)	1.2	0	0	Dec-04	DPIFM
MBTP	Vulcan-Plover (!)	20.8	0.36	61.76	Jun-03	DPIFM
Oliver	Vulcan-Plover (!)	20.4	0.35	58.67	Sep-03	DPIFM
Puffin	Vulcan-Plover (!)	14.3	0	0	Oct-05	DPIFM
Skua	Vulcan-Plover (!)	20.2	0	0	Dec-99	DPIFM
Swan	Vulcan-Plover (!)	5	0.07	11.9	Jan-00	DPIFM
Talbot	Vulcan-Plover (!)	1.8	0	0	Aug-05	DPIFM
Tenacious	Vulcan-Plover (!)	4.6	0	0	Apr-99	DPIFM
Vesta	Vulcan-Plover (!)	14.2	0	0	Sep-05	DPIFM

Notes:

All reserves are P50 probabilistic estimates

Conversion factor for gas (BCF) to MMBOE is 0.17

DPIFM – Department of Primary Industry, Fisheries and Mines, Northern Territory

MBTP – Montara, Bilyara, Tahbilk, Padthaway discoveries

Vulcan Sub-basin Petroleum Play Elements	
Source	Vulcan Formation (Middle Jurassic-Lower Cretaceous), Montara Formation (Middle Jurassic), Plover Formation (Lower to Middle Jurassic): oil and gas.
Reservoir	Puffin Formation (Upper Cretaceous), Vulcan Formation (Upper Jurassic-Lower Cretaceous), Montara Formation (Middle to Upper Jurassic), Plover Formation (Middle Jurassic), Challis Formation (Upper Triassic), Nome Formation (Upper Triassic).
Seal	Johnson Formation (Paleocene), Echuca Shoals Formation (Lower Cretaceous) regional seal, Vulcan Formation (Middle Jurassic to Lower Cretaceous) regional seal.
Traps	Detached rotated fault blocks, tilted fault blocks, hour glass horsts and anticlines.

Figure 2-14: Summary of the petroleum systems of the Vulcan Sub-basin

The four key elements required for a successful petroleum system are described in terms of the main stratigraphic units that deliver each of these elements in the VSB.

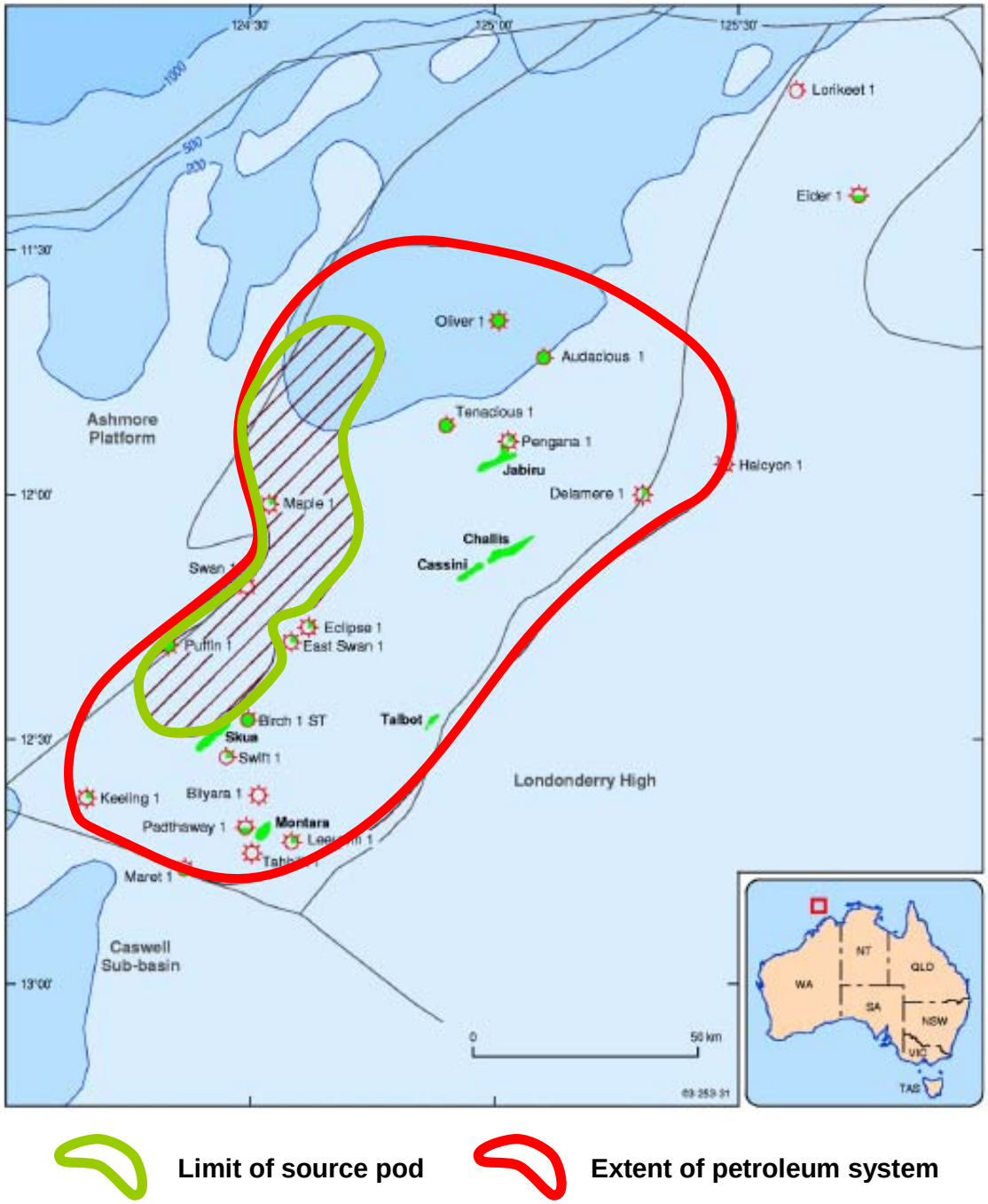

Figure 2-15: Spatial extent of the Jurassic Vulcan-Plover (!) petroleum system.

The petroleum system (red line) is restricted to the southern and central parts of the sub-basin with the limit of the source pod (green polygon) being defined by regional basin models of Kennard et al. (1999). The extent of the petroleum system encompasses all hydrocarbon occurrences that have been typed to a common source rock and indicates the likely extent of migration away from the recognised source pod where that source rock is presently mature for hydrocarbon generation.

The Lower Cretaceous, Echuca Shoals Formation also has significant source rock potential (Figure 2–18) but is probably thermally immature to marginally mature for petroleum generation over much of the VSB.

Further constraint can be placed on the efficacy of source rocks in the VSB by assessing the composition of the recovered hydrocarbons. In terms of their bulk physical properties the oils recovered from VSB are generally yellow to brown coloured, low gravity (39–51°API) fluids with typically low Gas Oil Ratios (GOR).

Recovered oils and condensates from the VSB mostly have a mixed marine and terrestrial geochemical signature, and can be divided into two distinct groups (A and B) on the basis of a combination of bulk oil characteristics, isotopic composition and detailed biomarker geochemistry (Edwards et al., 2004). Group A with the stronger marine source affinity is found at Audacious, Challis, Puffin, Jabiru, Skua, Talbot and Tenacious, which are sourced from the Late Jurassic Lower Vulcan Formation. Group B fluids with the stronger terrestrial source affinity are found at Bilyara, Montara and Padthaway, and were probably sourced from the Early-Middle Jurassic Plover Formation. The oil at Oliver-1 discovery appears to be a mixture of both groups (Edwards et al., 2004).

Most of the oils discovered in the VSB are typed to source rocks that are in direct contact with the reservoir horizon that hosts the accumulation (Figure 2–16) and migration pathways are relatively straightforward. In contrast, the Puffin oil field and the Swan gas discovery are contained in the overlying Upper Cretaceous and lack a direct stratigraphic juxtaposition with recognised Jurassic source rocks.

Both of these fluids, however, show strong affinity with the Group A family but show no evidence to support contribution from a younger source rock. They may, however, have an additional input from the Middle Jurassic Plover Formation, or older (Permo-Triassic?) sediments (Edwards et al., 2004). In either case migration of hydrocarbons up faults is required to charge these reservoirs.

Secondary alteration processes such as water washing and biodegradation have played a fairly minor role in influencing the nature of hydrocarbons in the VSB.

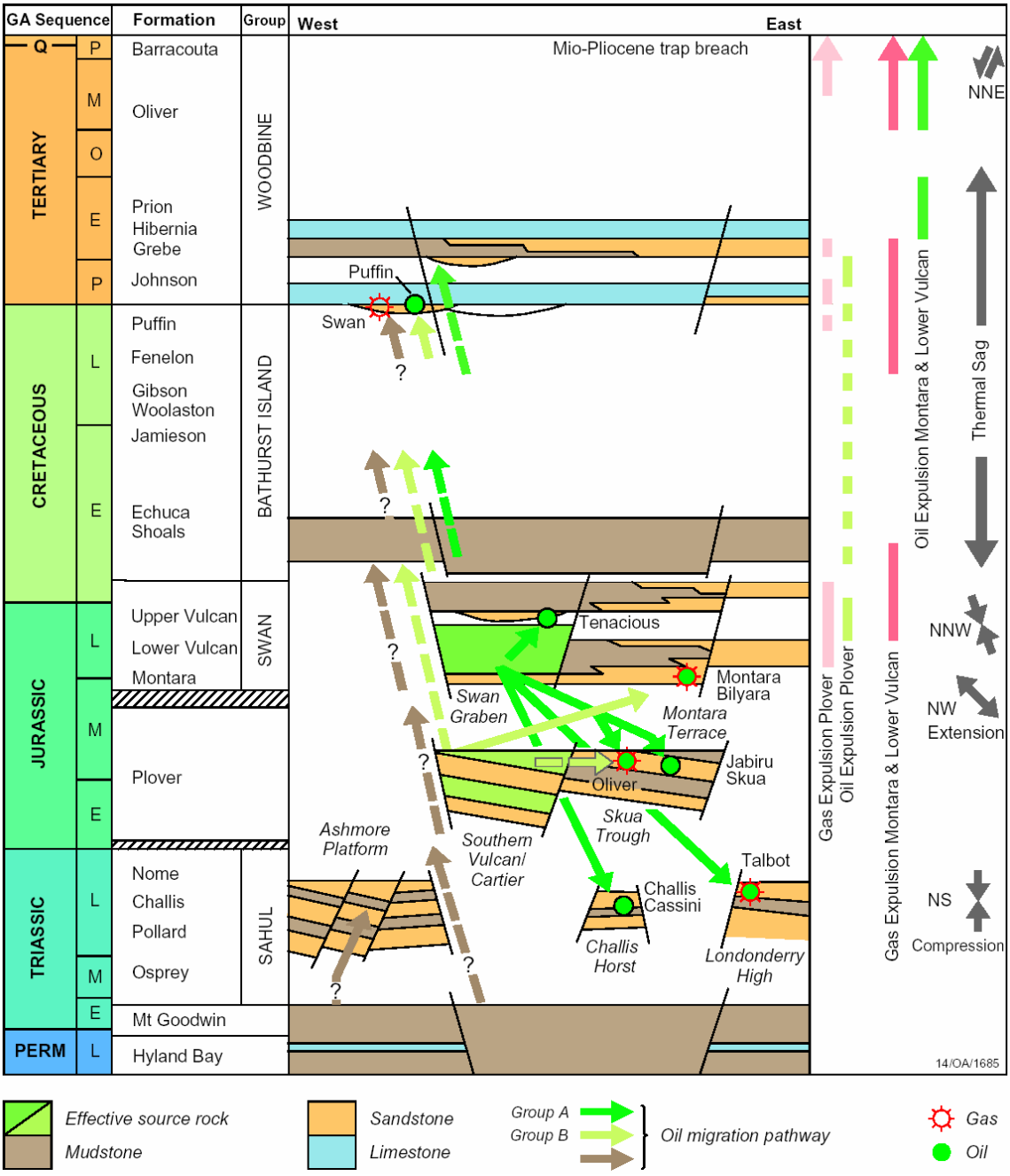

Figure 2-16: Schematic diagram of the Jurassic Vulcan-Plover (!) Petroleum System.

The stratigraphic position of the reservoir, source and seal units are shown relative to the key discoveries with inferred migration pathways shown for the discrete petroleum families. The timing of predicted hydrocarbon expulsion are also shown together with a summary of the important tectonic events (from Kennard et al., 1999).

Group A oils have been variably affected by water-washing through the selective removal of water soluble hydrocarbons such as benzene and toluene (Figure 2–19). The Group B oils are not water-washed but the composition of the low molecular weight hydrocarbons suggests that the oils are evaporative-fractionation (Thompson, 1987, 1988) residues, having separated from a gas during the migration process (Figure 2–19). Neither group of oils has been affected by biodegradation.

Stable isotope analysis of the recovered hydrocarbons adds further weight to the grouping of oils into two distinct groups. Group A oils show greater depletion (more negative values) in ^{13}C than the Group B oils (Figure 2–20) and as both groups were likely generated at similar maturity levels the more enriched Group B oils point to a greater terrestrial input to the source rock facies.

Hierarchical cluster analysis (HCA) techniques that integrate the molecular and isotopic parameters to produce the dendrogram or 'family tree', where the length of the branches reflects their relative degree of correlation (Summons et al., 1998) have been used to further assist accurate oil-oil correlation (Edwards et al., 2004). These data clearly split the hydrocarbons into two sub-groups of oils and condensates and three discrete gas families (Figure 2–21).

An important aspect of the grouping of the oils into two distinct oil families is that it implies that each group has migrated from a separate source rock depocentre with only limited evidence for mixing. Only at Oliver-1, on the edge of the Cartier Trough and in the Cretaceous reservoired Puffin Field can the oils be considered a mixture of the two groups (Edwards et al., 2004).

2.5.3 Seals

Effective seal rocks represent a critical element of any successful petroleum system. Unlike other key components that can remain effective even where they are unevenly distributed seal rocks will fail at their weakest point and therefore are most reliable when they are widespread and compositionally homogenous. Understanding the lateral and vertical distribution of suitable seal rocks and their ability to impede hydrocarbon movement is essential if this risk element is to be fully addressed.

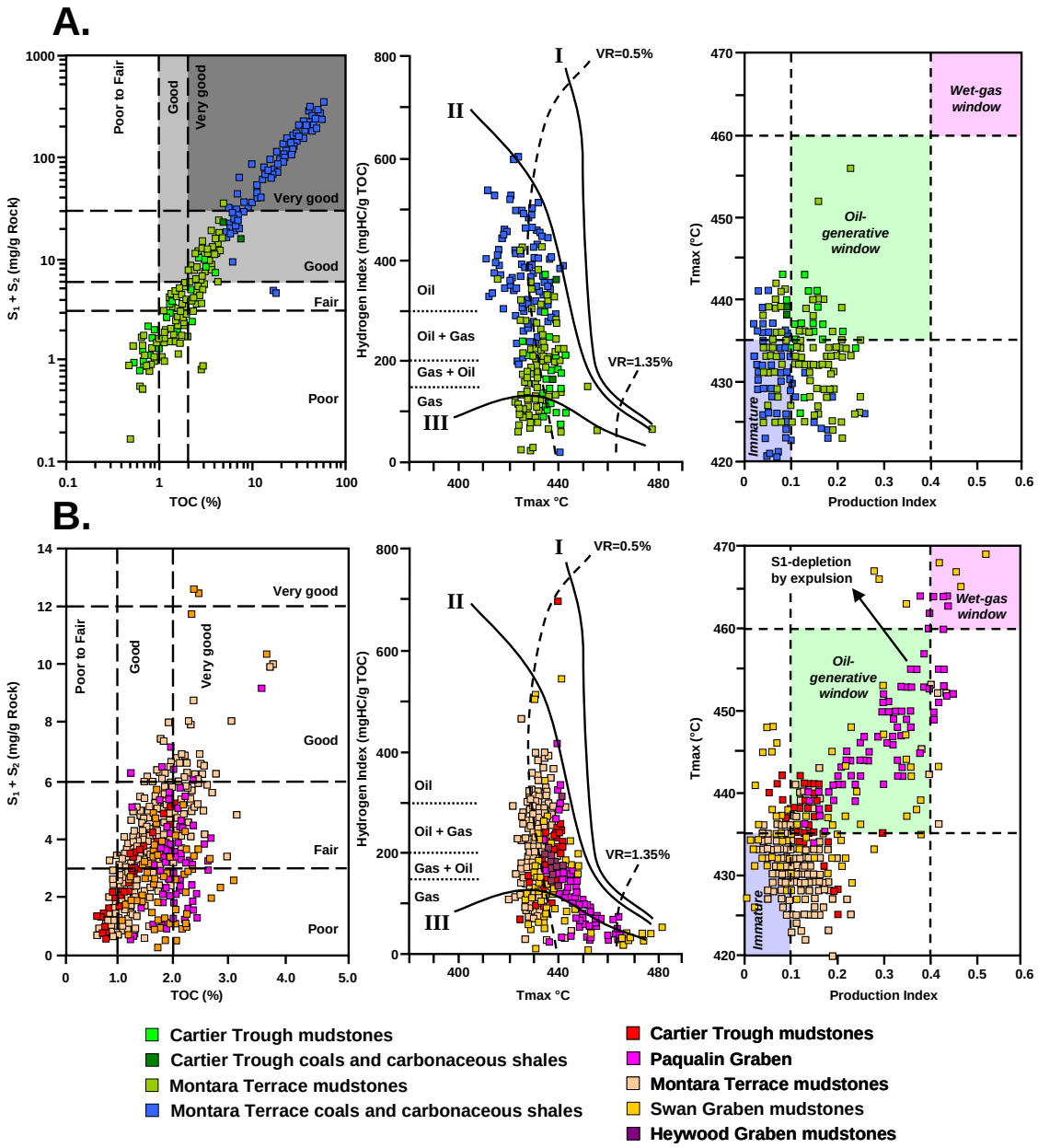

Figure 2-17: Rock-Eval pyrolysis plots for source rocks in the VSB.

Data shown are for samples from the Plover Formation (A) and the Lower Vulcan and Montara (B) formations and come from Edwards et al., 2004. The three plots for A and B show S1 + S2 (the amount of free hydrocarbons plus the amount of hydrocarbons generated by thermal cracking) plotted against the total organic carbon (TOC), the hydrogen index (the ratio of hydrogen to carbon) against Tmax (the temperature at which maximum release of hydrocarbons occurs during pyrolysis) and Tmax plotted against the production index (S1 divided by S1 + S2). The roman numerals on the hydrogen index versus Tmax plot define specific source rock types with type I being composed of marine organic matter, type II being mixed marine and terrestrial organic matter and type III being terrestrial organic matter.

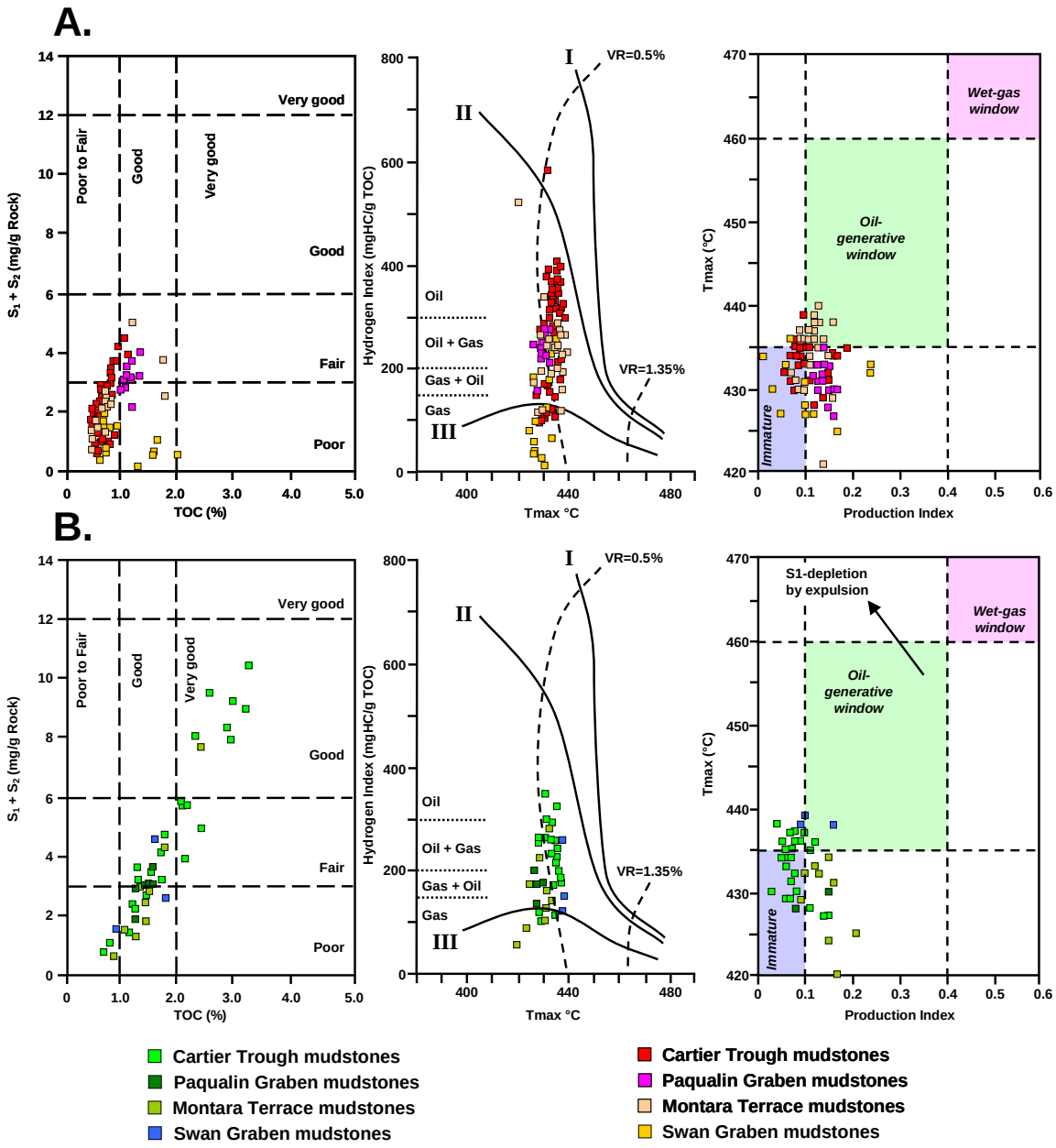

Figure 2-18: Rock-Eval pyrolysis plots for source rocks in the VSB.

Data shown are for samples from the Upper Vulcan Formation (A) and the Echuca Shoals (B) formations and come from Edwards et al., 2004. See caption for Figure 2–17 for description of plots.

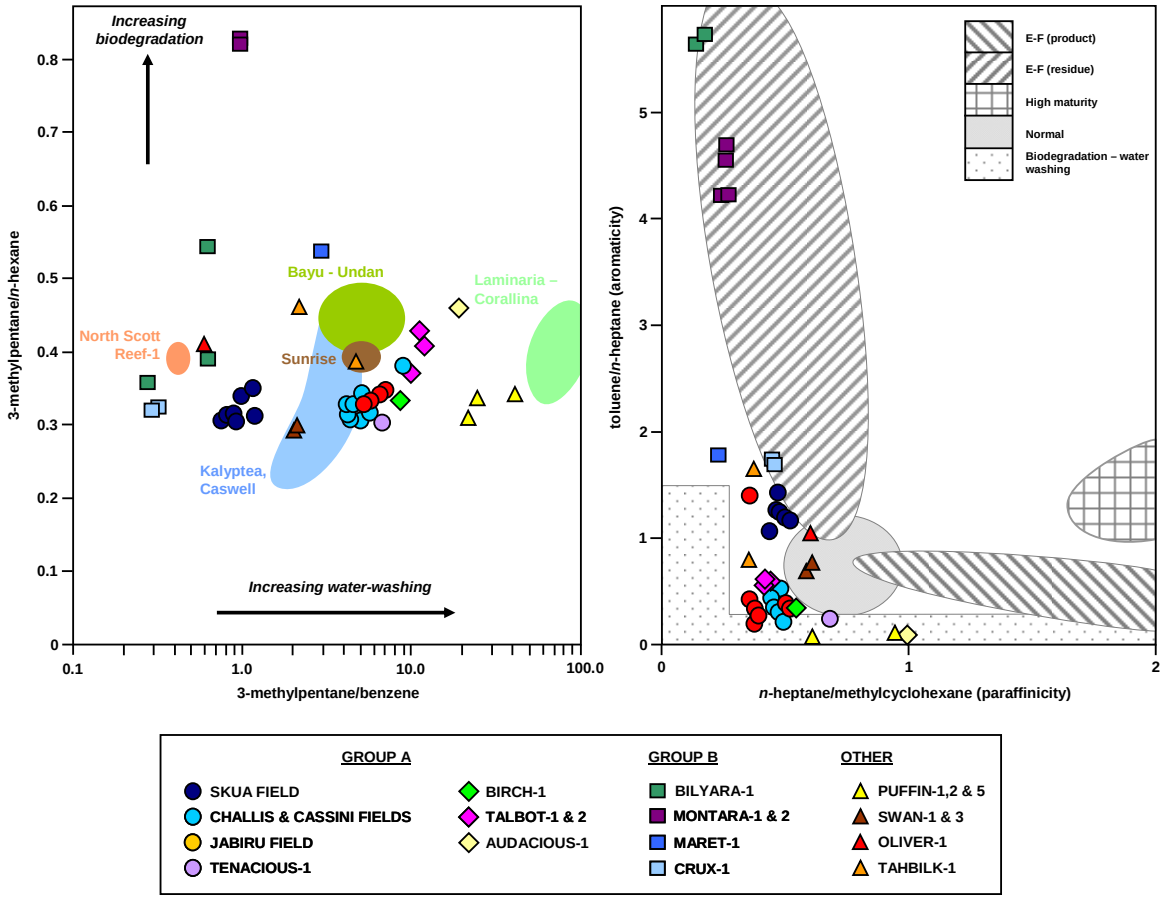

Figure 2-19: Effects of secondary processes on Vulcan Sub-basin hydrocarbons.

Cross plotting the ratios of low molecular weight (C_6 and C_7) hydrocarbons including 3-methylpentane/benzene against 3-methylpentane/*n*-hexane (left) and *n*-heptane/methylcyclohexane versus toluene/n-heptane (right, after Thompson 1987, 1988) allows the impact of secondary alteration processes to be evaluated (from Edwards et al., 2004). A selection of VSB oils from the two recognised oil families and a number of vagrant oils are shown as well as typical values for a range of hydrocarbon accumulations from the Bonaparte and Browse basins (coloured polygons). The VSB oils show varying degrees of influence from water washing but are largely unaffected by biodegradation (left). Several oils have compositions that indicate an origin through a process of evaporative fractionation (Thompson 1987, 1988) where a liquid residue separates from a gas phase due to a fall in pressure as hydrocarbons migrate up dip.

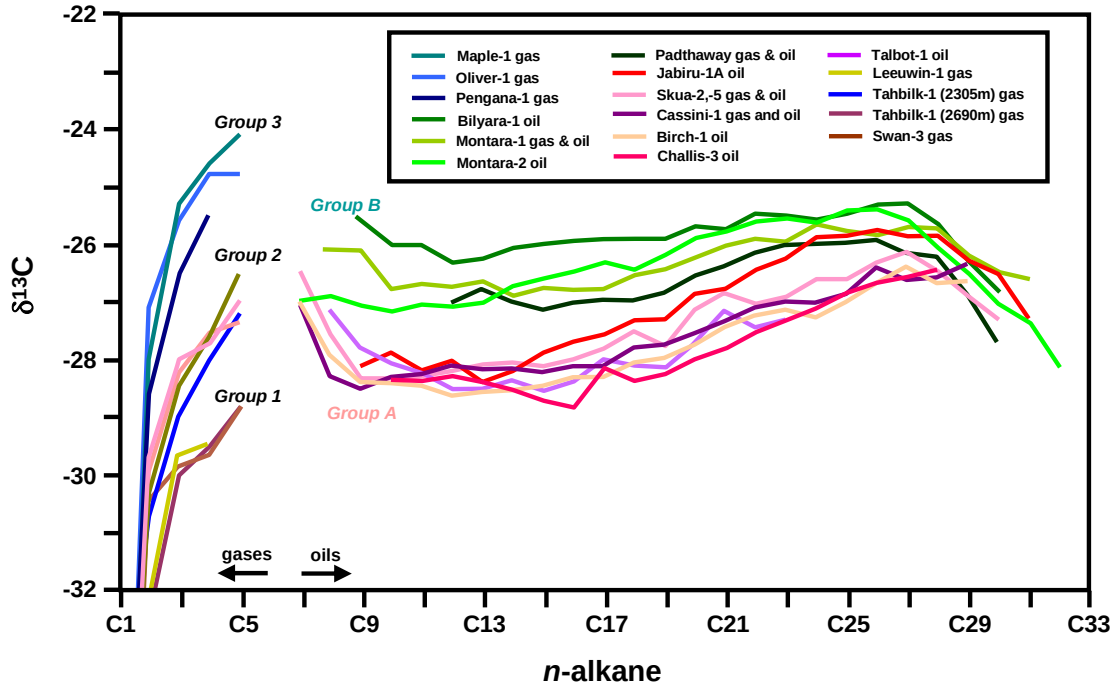

Figure 2-20: Carbon isotope composition for VSB hydrocarbons.

The carbon isotope composition ($\delta^{13}C$) of individual *n*-alkanes for VSB gases (C_1-C_5) and oils/condensates (C_{7+}) showing separation into two discrete groups of oils/condensates and three groups of gases (from Edwards et al., 2004).

A seal rock is broadly defined as any rock that prevents or impedes the movement of hydrocarbons by secondary migration processes (Schowalter, 1979). All seals will eventually fail when the pressure exerted by a growing hydrocarbon column reaches a critical threshold needed to establish capillary or mechanical breakthrough, but different lithologies will have widely variable thresholds.

Evaluating seal rocks typically involves establishing the extent and thickness of suitable seal facies, identifying areas where faults transect and potentially offset the seal against porous reservoir rocks or thief zones (collectively referred to as seal geometry) and analysing representative samples to determine the composition and capillary properties of potential seal rocks (seal capacity). Structural competency (seal integrity) is also critical and typically involves estimating the brittleness of the rocks either directly, commonly by conducting leak off tests (LOT) during drilling to artificially fracture the formation, or indirectly through an analysis of the sonic logs.

Evaluation of seal risk depends on the nature of the trap geometry. Structural traps rely on the presence of effective top and lateral seals, whilst stratigraphic trapping configurations also require a base seal. In the VSB the prevalence of fault bound traps requires top seals and cross-fault (juxtaposition) seals be addressed.

In structurally complex areas of the Vulcan Sub-basin, such as along the major northeast-trending horsts along its eastern flank, faulting is frequently difficult to image on seismic data and often the exact geometry of the sealing units has historically been difficult to determine. Recent advances in seismic acquisition and processing, however, are leading to more accurate imaging of trap geometries (Figure 2–22) and as a result improved seal predictions (Maxwell et al., 2004; Peresson et al., 2004).

Reservoir sections within the pre-rift and syn-rift megasequences are locally sealed by fine grained shales that reflect the overall transgressive nature of the syn-rift section and the early post-rift section (Figure 2–23). Within the main grabens the source-rich claystones of the Late Jurassic Lower and Upper Vulcan formations are ductile and would generally be favourable as effective capillary seals, except where they become interbedded with siltstone or sandstone (Kivior et al., 2002).

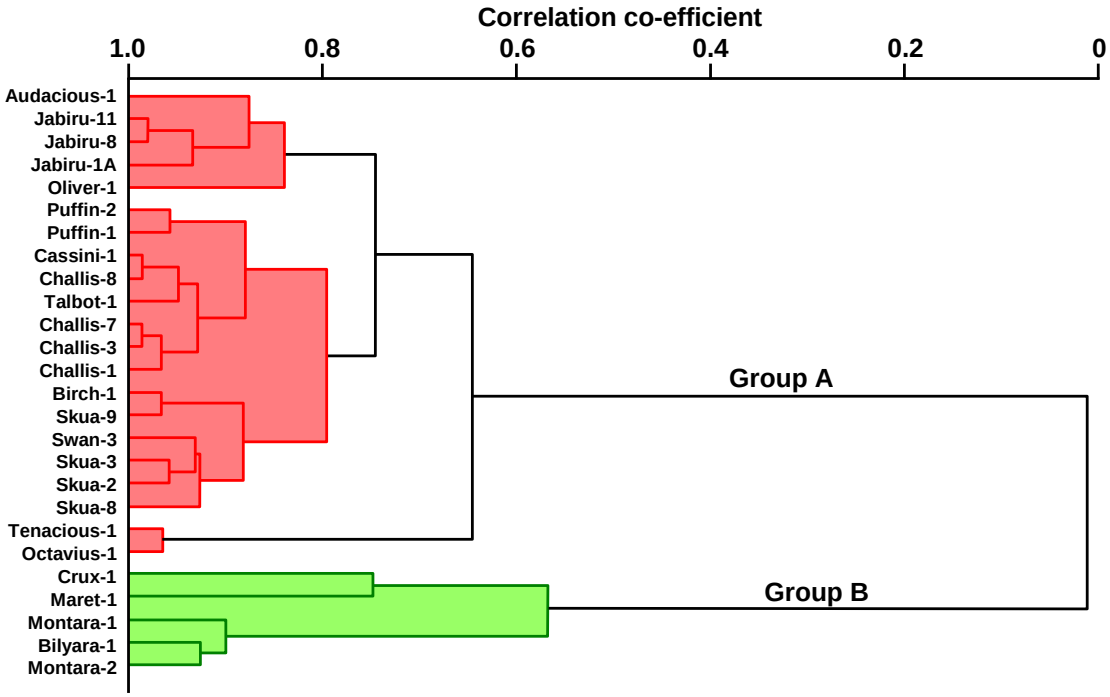

Figure 2-21: Compositional similarity of VSB hydrocarbons indicated by HCA.

The construction of a family tree (or dendrogram) using Hierarchical Cluster Analysis (HCA) demonstrates the two basic groups (A and B) that can be recognised in oils and condensates from the Vulcan Sub-basin (from Edwards et al., 2004). In HCA the distance between any two samples is a measure of their similarity (Edwards et al., 1997) with those samples that cluster together being the most closely related. Oils derived from different wells on the same field generally show correlations greater than 0.9%, whilst oils derived from the same petroleum system typically show correlation coefficients of 0.8 or higher (Summons et al., 1998). The geochemical variables that are used to correlate oils are various source dependant biomarker ratios and stable isotope compositions.

The restricted lateral extent of the syn-rift section (i.e. contained within the shoulders of the rift basin) coupled with the continuing periodic input of coarser grained clastic material from erosion of the bounding footwall blocks combine to restrict the effectiveness of these units as an effective regional seal.

With the cessation of rifting at the end of the Jurassic regional marine flooding of the margin in the Valanginian led to the deposition of predominantly fine grained sediments of the Cretaceous Bathurst Island group. At the base of this interval the shales of the Early Cretaceous Echuca Shoals Formation form a widespread and competent seal across the VSB but are thin or absent over the highest structural points and across the Ashmore Platform to the west (Figure 2–23). The Echuca Shoals Formation typically exhibits good sealing capacity and integrity but tends to be limited by the inconsistent thickness of this seal interval, particularly over the key structural highs that remained emergent at this time (Kivior et al., 2002).

Overlying the Echuca Shoals Formation, the calcareous shales of the Early to Middle Cretaceous Jamieson Formation represent the most effective regional seal in the VSB, extending across the Ashmore Platform and covering all of the previously emergent syn-rift structure with the exception of the Skua horst (Figure 2–24). These are highly ductile marine shales that have high measured capillary entry pressures capable of holding back significant hydrocarbon column heights (Kivior et al., 2002).

Deposition of fine grained hemipelagic marls and calcareous claystones of the Woolaston, Gibson and Fenelon formations coincide with the establishment of open marine conditions and completely cover the syn-rift architecture of the VSB (Figure 2–23). Compositional variations play a major role in the effectiveness of these units as seals with the claystones across the Londonderry High being rheologically more ductile and less prone to failure by brittle fracturing than the relatively brittle marls that prevail across the Ashmore Platform (Kivior et al., 2002). They nevertheless are important as seal rocks providing effective top seal for the Skua oil field.

Shallower reservoir units including the Eocene Grebe Formation sandstones rely on carbonates of the Hibernia Formation for seal, while those of the Oligocene-Miocene Oliver Formation depend on carbonates of the overlying Barracouta Formation.

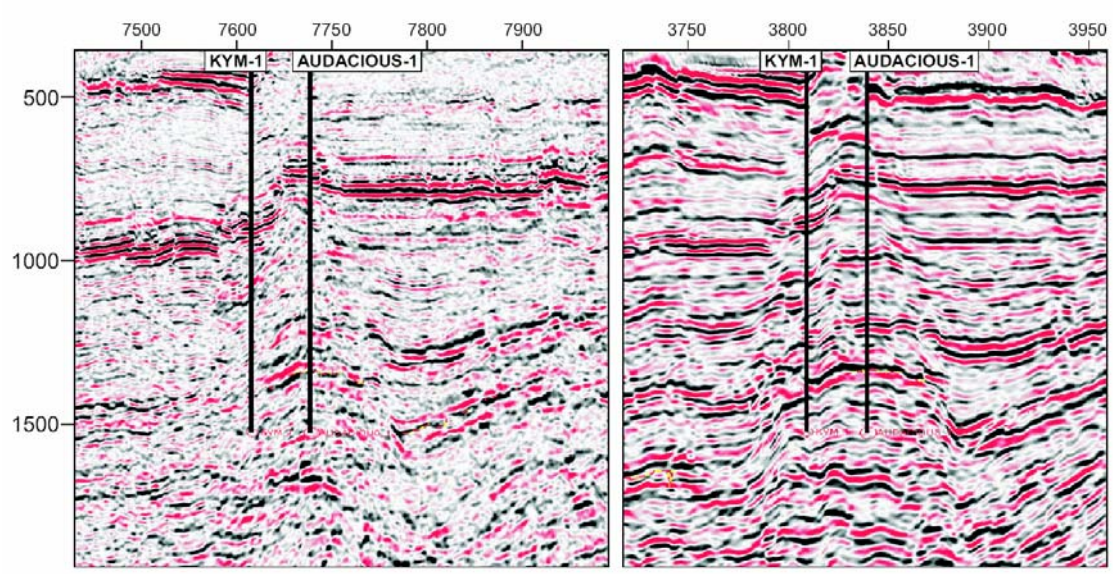

Figure 2-22: Example of the enhancement in trap delineation from improved seismic data.

Seismic lines from the Onnia 3D survey showing the improvements of the original data (left) gained by the utilisation of pre-stack depth migration (PSDM) in the processing sequence (from Maxwell et al., 2004). In addition to a substantial improvement in signal-noise ratio indicated by the more continuous reflections a dramatic improvement in fault definition has aided more accurate trap delineation. The Kym-1 well sited on poorer quality post-stack time migrated seismic data (PSTM) penetrated water bearing reservoir prior to the drilling of the Audacious-1 oil discovery located on the PSDM data.

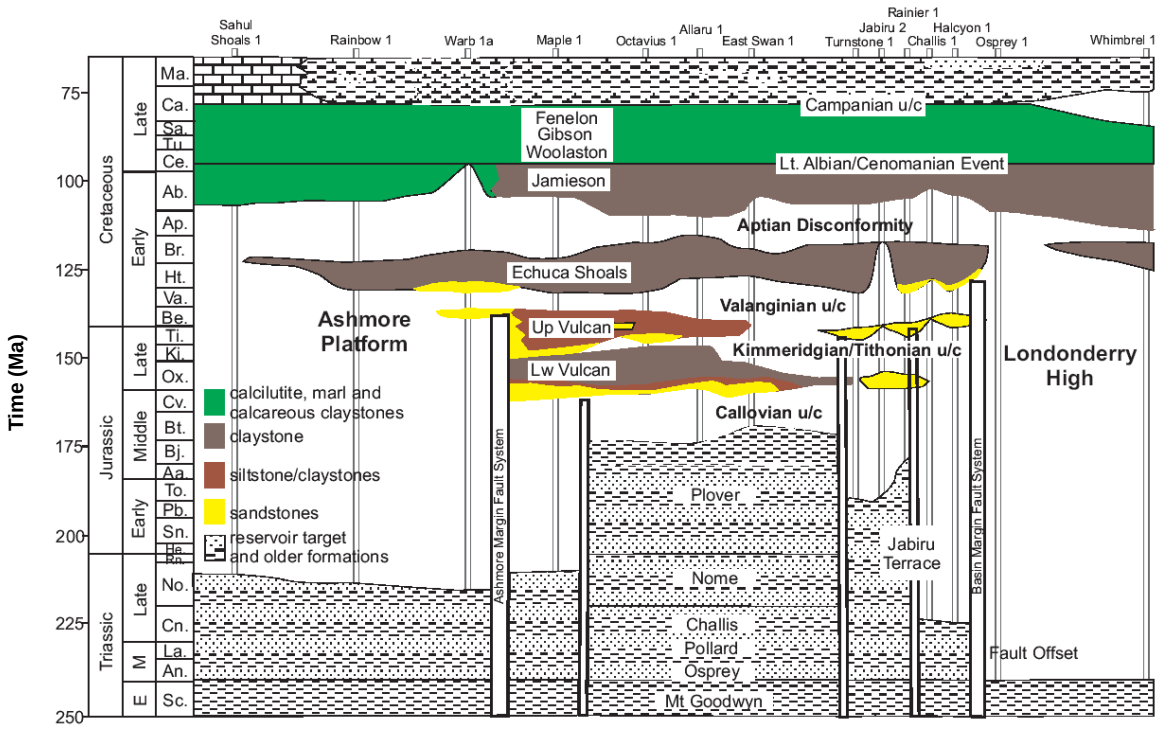

Figure 2-23: Chronostratigraphic diagram showing seal distribution within the VSB.

Composite region chronostratigraphic section, coloured by lithology, illustrating the distribution of reservoir-seal pairs across the VSB using 14 wells ranging from Sahul Shoals on the Ashmore Platform in the west to Whimbrel-1 on the Londonderry High in the east (from Kivior et al., 2002). The Late Jurassic and Cretaceous section is based on biostratigraphy and well log data whilst the general section below the Callovian Unconformity (pre-rift) is taken from Pattillo and Nicholls (1990). Note restriction of the syn-rift Late Jurassic sequence to wells located in the main grabens bounded by the Londonderry High and Ashmore Platform. These intervals can provide effective local seals, but the regional top seal for the VSB is provided by the widespread claystones of the Jamieson Formation or by the calcilutites of the overlying Fenelon, Gibson and Woolaston formations.

These units commonly contain abundant porosity and have not been demonstrated as effective seal rocks in the VSB.

2.5.4 Traps

Mesozoic rift related tectonism produced an abundance of structural traps including detached rotated fault blocks, tilted fault blocks and complex hour-glass horsts (Figure 2–25). Tilted horst blocks predominate in the south of the VSB with hour-glass structures being more prevalent in the north (Woods, 1992). A structural trap over a salt diapir was targeted at the Paqualin-1 well (Smith and Sutherland, 1991) and in the Swan-1 and -2 wells.

Tilted fault blocks and narrow heavily faulted horsts sealed by the Early Cretaceous Echuca Shoals Formation, have proved the most successful trap configuration resulting in discoveries reservoired within the Late Triassic Nome and Challis formations and the Jurassic Plover and Vulcan formations. At the Late Cretaceous (Maastrichtian) level the oil and gas accumulations hosted by the Puffin Formation at Puffin, Swan, East Swan 1 and Birch 1, usually involve four-way dip closure with a stratigraphic component possible in some cases (Swan for example against salt).

Historically accurate seismic definition of potential traps has been poor in the VSB resulting in many wells being drilled off structure (Figure 2–26) and hence failing to provide valid tests of the petroleum system. Increasingly 3D seismic data coupled with more sophisticated seismic acquisition and processing methods has contributed substantial improvements to the delineation of structural traps, particularly in the heavily faulted regions that were previously difficult to image (Figure 2–22).

Interpretations based on new 3D seismic data have highlighted the increased structural complexity of horsts block structures due to the oblique trends of the adjoining normal faults, with the intersection geometry of the two main sets of rift faults playing important roles in controlling trap definition (Peresson et al., 2004).

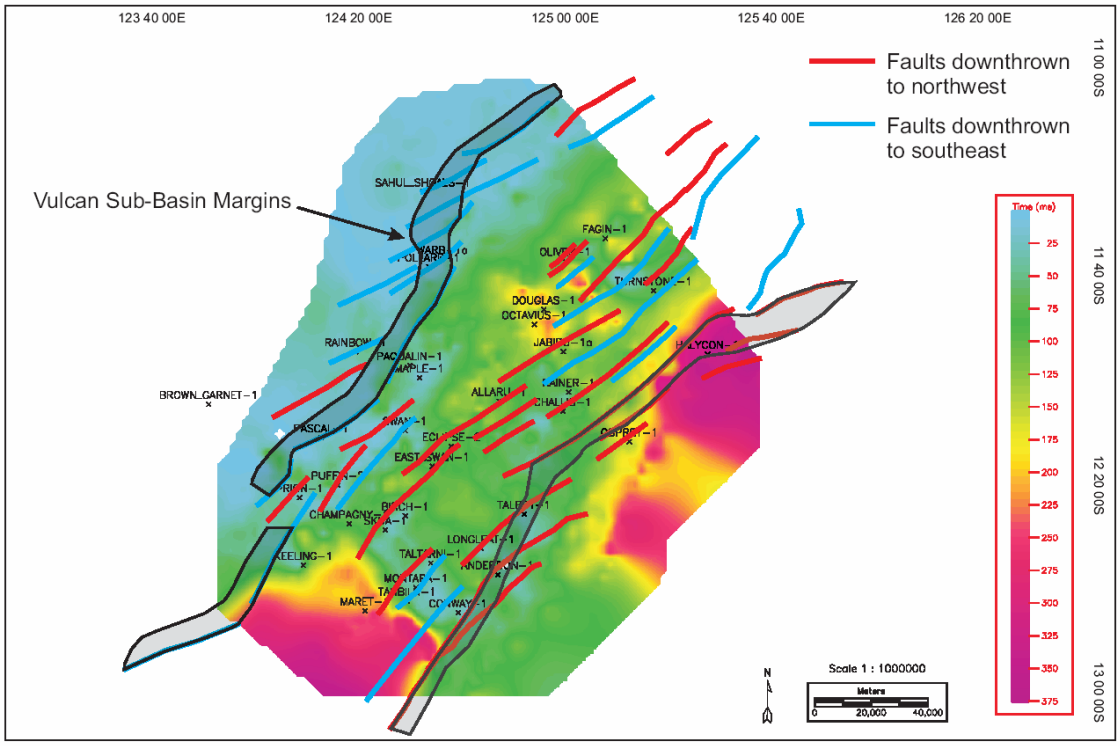

Figure 2-24: Isochron map of the Jamieson Formation.

The map describes thickness (in two-way time) and lateral extent of the regional seal for the Vulcan Sub-basin (from Kivior et al., 2002). Major fault offset directions mapped on the Valanginian horizon and the basin margins are shown for reference. Seal thickness is greatest in the Cartier Trough near the Douglas-1 well and thins appreciably over the Ashmore Platform to the west and towards the southern end of the VSB including across the Skua, Montara and Talbot oil and gas fields.

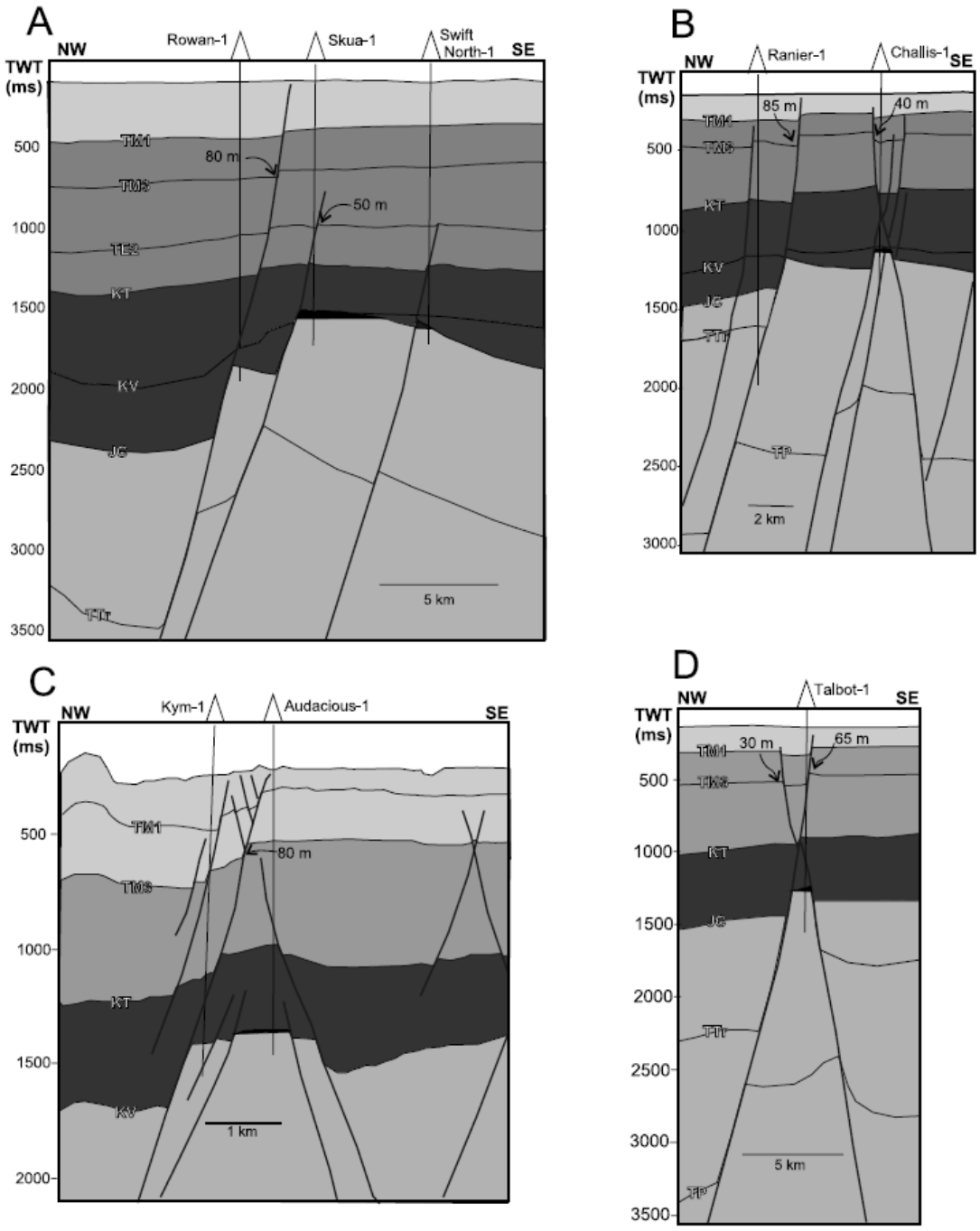

Figure 2-25: Representative examples of VSB trap types.

A series of schematic drawings showing the types of structural traps that have proven most successful in the VSB including the Skua oil field (simple tilted fault block, A), Challis, Audacious and Talbot oil fields (complex horst blocks, B-D) and that are typical of the traps targeted by exploration drilling (from Gartrell et al., 2006). Note the significant fault reactivation (indicated by the magnitude of fault offsets shown at the TM2, Miocene (or TE2), and Eocene regional seismic markers) that typify successful (i.e. Challis-1) and failed (i.e. Rowan-1) traps. The vertical scale is in two-way time (TWT), given in milliseconds (ms).

During the early part of the post-rift phase the VSB is tectonically quiescent until the Late Tertiary when widespread faulting associated with plate collision resulted in reactivation of many existing rift faults and the creation of new faults. High trap failure rates in the Timor Sea region have been attributed to leakage of hydrocarbons due to this period of post-rift fault reactivation (e.g. Lisk et al., 1998; O'Brien et al., 1999a; O'Brien and Woods, 1995).

2.5.5 Generation and Migration

Appropriate levels of thermal maturity required to promote generation and expulsion from the recognised source rocks to the available carrier beds are restricted to three discrete depocentres (Figure 2–27). The Swan and Paqualin grabens are related to Upper Jurassic subsidence associated with rifting, whilst the Cartier Trough is the product of flexural down-warping during Neogene plate collision.

Determining the extent of the source kitchens is made more difficult by the relatively poor quality of calibration data used to define the palaeo-thermal history. Vitrinite reflectance profiles from representative wells across the VSB (Figure 2–28) point to a complex thermal history in some wells whilst in others a more simple thermal history can be invoked to satisfactorily model the measured data.

These outcomes can be difficult to reconcile in basin models that only consider conductive heat transfer and ignore opportunities to have laterally varying thermal conditions such as those associated with fluid convection (e.g. Roberts, 2001).

Complications introduced by suppression effects reported for hydrogen rich (perhydrous) vitrinite (Wilkins et al., 1992) common to the marine source rocks of the area and variability in the degree of repeatability between different laboratories (Dembicki, 2009; Sentftle and Landis, 1991) make it difficult to satisfactorily produce well constrained basin models.

Basin modelling undertaken by Kennard et al. (1999) represented the most regionally inclusive examination of generation and expulsion from the recognised source rocks in the VSB to that date.

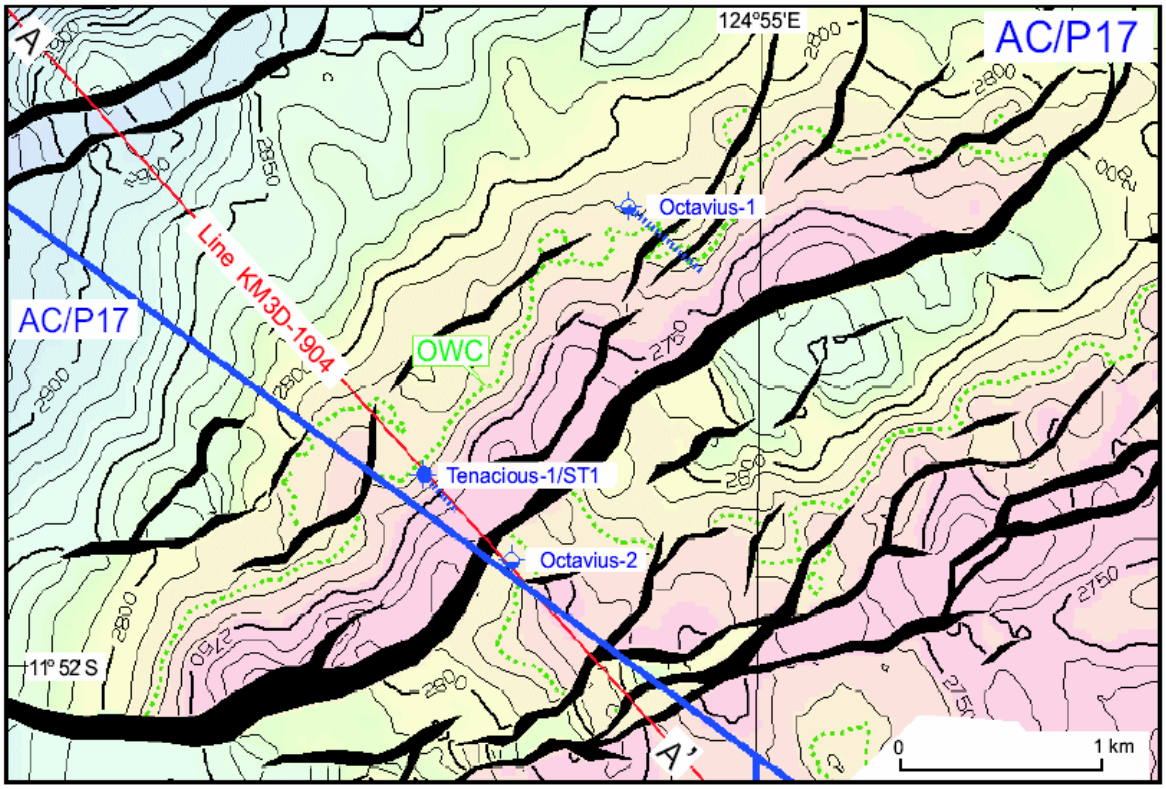

Figure 2-26: Exploration drilling needed to delineate the Tenacious oilfield.

Tithonian depth-structure map highlighting the value of good quality seismic imaging in accurately locating exploration wells as is well illustrated by the discovery of the Tenacious oilfield in the VSB. Discovered in 1995 utilising the Kym 3D marine seismic survey the field was narrowly missed by two previous exploration wells that were drilled on the previously available 2D seismic grid. The first Octavius well penetrated the Tithonian reservoir below the OWC and the Octavius-2 well drilled into the hanging wall side of the main bounding fault (from Woods et al., 2003). Note the width (<1km) of the narrow structural closure that makes accurate well placement extremely important.

In their models they invoke early generation of both oil and gas driven by rapid syn-rift burial and much higher heat flow during rifting, with an early phase of gas expulsion in the Jurassic but delayed expulsion of oil until a renewed period of rapid burial in the Late Tertiary. More sophisticated 3D modelling completed by Chen et al. (2001) and Fujii (2007) produced outcomes that were similar to the previous modelling efforts.

Irrespective of the accuracy of the basin models an important consequence of the restricted distribution of the thermally mature source pods within the VSB (Figure 2–15) is a need for migration pathways of up to 40km to account for the established oil and gas accumulations typed to these depocentres. Independent evidence to support relatively long migration distance comes from measurement of the abundance of key polar compounds (notably Carbzole concentration) that show a strong positive correlation with distance from possible source kitchens (Liu et al., 2003).

The pronounced NE-SW orientation of key structural lineaments in the VSB that can be clearly delineated on a Permian depth-structure map (Figure 2–29) shows the potential for expelled hydrocarbons to migrate long distances using fault relay ramps and along elongate fault terraces to provide charge to fault blocks located at the apex of these features and distal to source rock kitchens.

The Jabiru oil discovery demonstrates the effectiveness of this migration process to deliver hydrocarbon charge to traps that sit outside the pods of active source rock generation and where long distance migration is required for the observed hydrocarbon charge to be explained.

2.5.6 Retention

Aside from the aforementioned difficulty in correctly imaging the rift related traps on seismic data and the impact this has on accurately placing well locations the retention aspect of the VSB petroleum systems is widely seen as a major cause of exploration failure in many wells and a limitation on the effectiveness of the petroleum system.

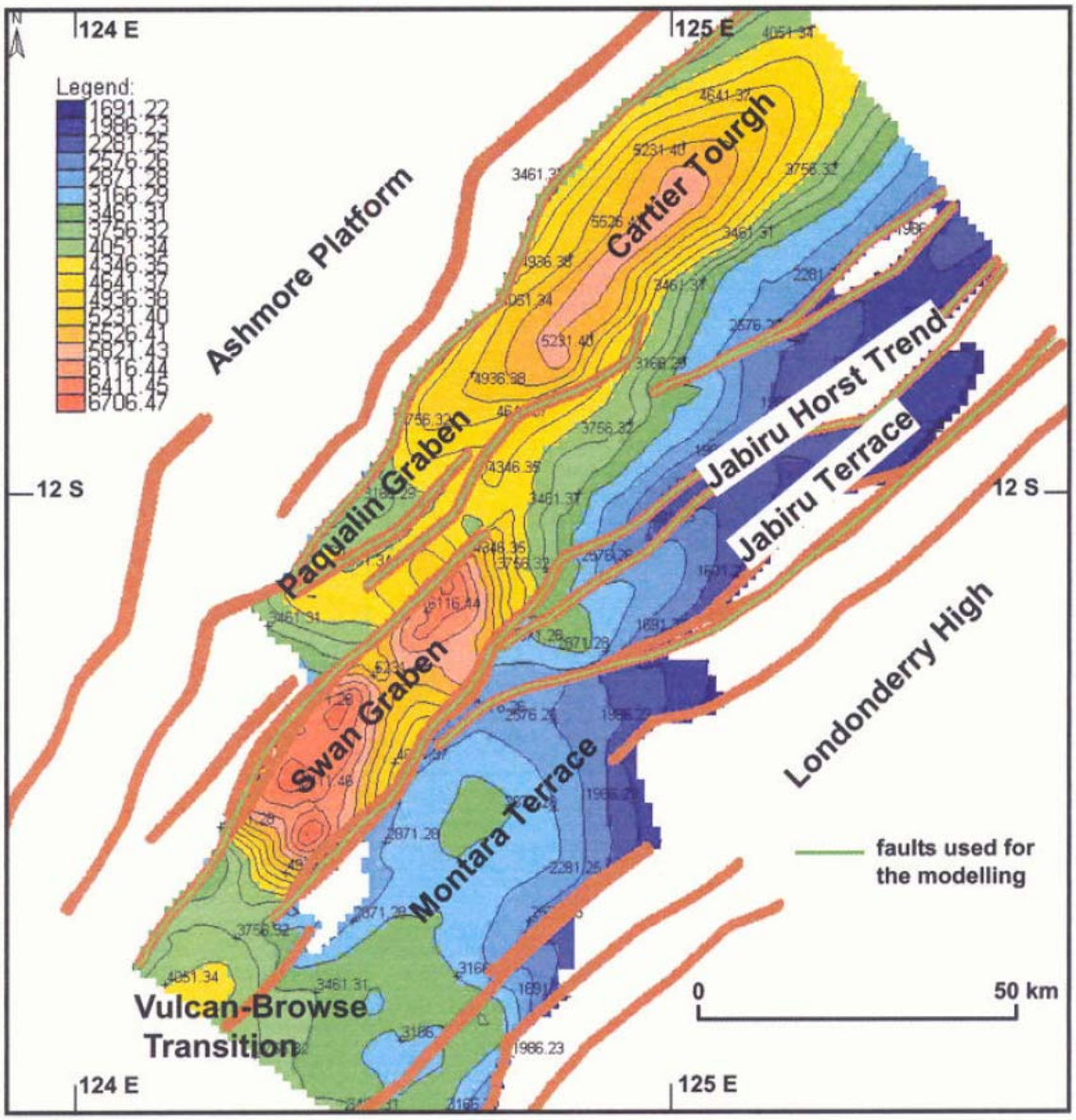

Figure 2-27: Top Plover depth-structure map showing position of key source kitchens.

Basin modelling results indicate that thermally mature source rocks are restricted to depths below about 3500m for oil and below about 4500m for dry gas indicating that current active generation is limited to the Swan and Paqualin grabens and the Cartier Trough for source rocks within the syn-rift megasequence (from Chen et al., 2002). Note the strong NE-SW orientation of the principal faults and the potential for fault relay ramps and terraces to focus the direction of hydrocarbon migration.

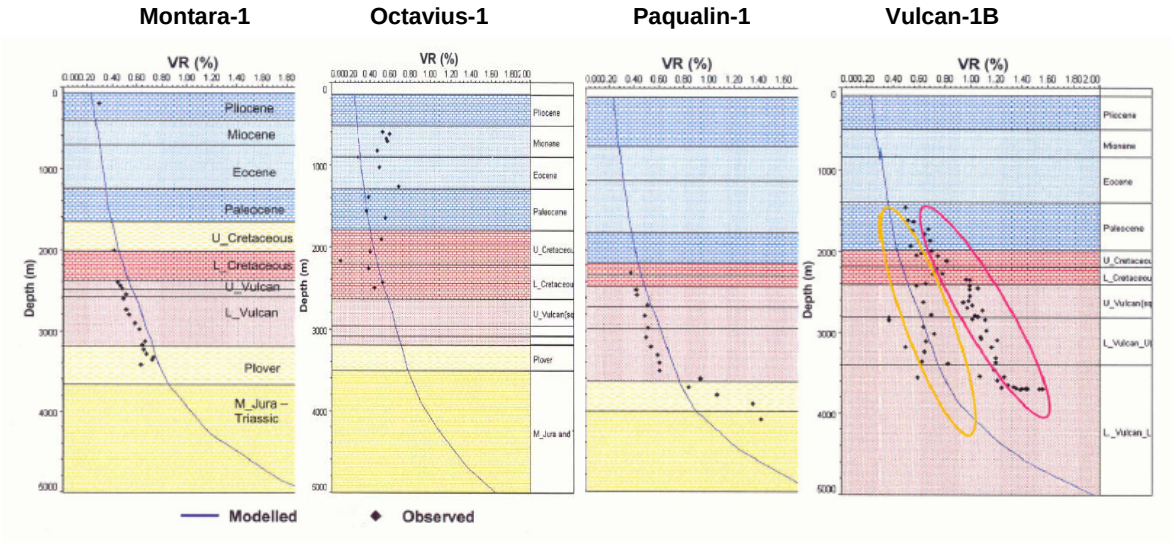

Figure 2-28: Vitrinite profiles from wells in the VSB.

Examples of key wells from the VSB showing some of the challenges faced when using conventional thermal maturity data to constrain temperature histories. The plots show measured vitrinite reflectance data (%VR observed, black diamonds) against depth compared against modelled VR curves (solid lines) produced from basin modelling software algorithms (from Fujii, 2007). In Montara-1 a reasonable fit is observed suggesting an accurate thermal history has been simulated. In contrast data from Octavius-1 shows only poor correlation. The measured data from Paqualin-1 display a sharp gradient change below the Plover Formation probably indicating a different heat-flow. In Vulcan-1B data provided from two separate analysts demonstrate the subjective nature of the measurement.

In the Miocene to Pliocene, the rapid convergence of the Australian plate and Southeast Asian microplates resulted in widespread reactivation of the previous Jurassic extensional fault systems, development of new shallow fault arrays that transect the regional seal and the rapid subsidence within the Cartier Trough due to foreland loading and associated flexure (e.g. Bradley and Kidd, 1991). This late faulting event is the major cause of trap breach in the VSB with many wells drilled in the area intersecting residual oil shows within fault dependent traps of Jurassic age.

Recognition that fault reactivation is the key issue controlling hydrocarbon retention has led to a major effort by workers in Industry and Academia alike to develop suitable mitigation strategies to address this specific element of the Vulcan-Plover (!) petroleum system and improve the success rates of drilling into the future. These studies have included detailed consideration of the geometric configuration of the trap bounding faults (O'Brien, 1993; O'Brien et al., 1996; Gartrell et al., 2005, 2006), in particular the importance of fault intersections zones (Gartrell et al., 2004) as well as the role of the contemporary regional stress field (Hillis, 1998; Mildren et al., 1994, 2002) and a variety of techniques for directly assessing the products of hydrocarbon leakage from Jurassic reservoirs into the shallow section and out into the overlying water column (O'Brien et al., 1998; 2000; 2002b).

The most comprehensive attempts to produce an integrated workflow to address the recognised trap integrity risks have been undertaken by O'Brien and various contributors (Table 2–2). Following on from initial work published in 1995 (O'Brien and Woods, 1995), O'Brien et al. (1996a) developed a tripartite trap classification for seal integrity that draws on the relationship between Hydrocarbon-related Diagenetic Zones (HRDZs) inferred from seismic data (O'Brien and Woods, 1995), the style of Late Tertiary faulting in relation to rift faults and a suite of direct and remotely sensed seep detection methods (O'Brien et al., 1998; 2000; 2002b).

Traps unaffected by fault reactivation and thus unlikely to have leaked are defined as High Integrity Traps (HITs), whilst Moderate Integrity Traps (MITs) have been reactivated but are likely to have retained some of the original hydrocarbon fill. Low Integrity Traps (LITs) are those that are heavily reactivated and exhibit multiple leakage indicators and are likely to have leaked completely (Table 2–2).

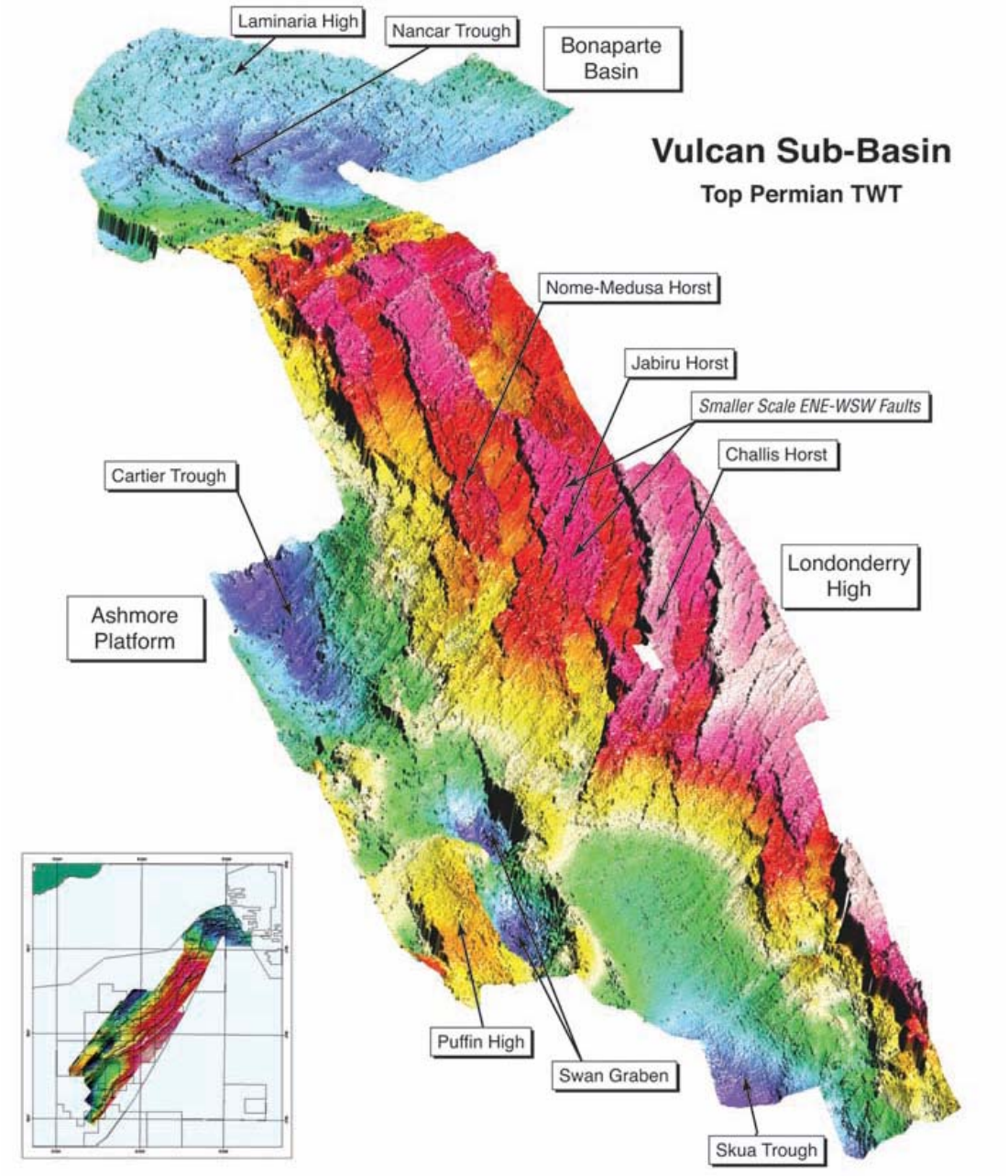

Figure 2-29: Top Permian time-structure map.

Regional two-way-time (TWT) structure map for the Top Permian seismic horizon (warm colours are highs and cold colours are lows) showing elongate N-S to NE-SW or NW-SE orientated fault relay ramps and fault terraces that dip down towards the key recognised source kitchens within the Swan (and Paqualin) Graben and Cartier Trough (from Edwards et al., 2005).

2.6 EXPLORATION HISTORY OF THE VULCAN SUB-BASIN

Exploration drilling in the Timor Sea region began in 1970 and despite a number of small oil and gas discoveries made in the first 4 wells drilled exploration drilling proceeded slowly, punctuated by periods with little or no drilling activity.

Success leading to commercial oil production in the VSB was not achieved until 1983 with the fifteenth well drilled, Jabiru-1A, defining a significant oil discovery, followed by three, more modest, commercial successes resulting in the Challis oil field in 1984, the Skua oil field in 1987 and finally the Cassini oil Field in 1988. This phase of drilling also produced a number of sub-economic oil and gas discoveries and led to increased exploration drilling over the period 1988-1992 (Figure 2–30), unfortunately without a comparable increase in the economic discovery rate.

A lack of further commercial success saw drilling activity drop to a low level with the small Tenacious oil discovery in 1997 (Woods and Maxwell, 2004) representing the only drilling success from 1990-2001. At the end of 2001, the VSB contained 18 new field discoveries from a total of 67 exploration wells. This represented a historical technical success rate of 27%, but a historical success rate for fields greater than 20 million barrels oil equivalent (mmboe) of only 13%. From these volumetrically more substantial discoveries only three commercial developments have been undertaken, reflecting a commercial success rate of less than 5%.

The VSB is estimated to contain reserves of 1.3 Trillion cubic feet (Tcf) of gas, 31 million barrels (mmbbls) of condensate and 357 mmbbls of oil (Longley et al., 2002). Of these discovered estimated (scope) reserves at the end of 2001 some 170 mmbbls of oil, 31 mmbbls of condensate and some 1.2 Tcf of gas remains undeveloped (Longley et al., 2002).

Table 2-2: Integration of predictive observations on trap integrity.

Tabulation of observations associated with particular fault styles and different levels of demonstrated trap integrity (from O'Brien et al., 2002a). Remote sensing data used in this study included geochemical sniffer where a hydrocarbon detector (fish) is towed close to the sea-floor, ALF, an aerial survey technique that detects oil seepage on the sea surface and Hydrocarbon Related Diagenetic Zones (HRDZ) that are observed on seismic data and relate to cementation that originates from the degradation of leaking hydrocarbons. Importantly, all of the constituent components of this approach are derived from datasets that can be acquired before the drilling on new prospects and represents, therefore, a genuinely predictive model that can be tested by future drilling.

Sniffer anomaly		*ALF anomaly*		*HRDZ*	*Fault style*	*Interpretation*
Size (m)	**Intensity (concentration)**	**Size (m)**	**Intensity (spectral response)**	**Size (m)**	**1. Fault displacement (ms) 2. Fault frequency 3. Relationship of Neogene and rift faults**	**Predicted type of trap**
Absent	Zero	Absent	Zero	Absent	1. None to small (<20) 2. None to rare 3. Parallel	HIT: Subcommercial gas with displaced oil leg
1000–2000	Strong	1000–3000	Strong	200–1500	1. Moderate (20–55) 2. Rare to common 3. Parallel to slightly oblique	MIT: Oil accumulation
Absent to 5000	Very weak	3000–6000	Weak	3000–5000	1. Strong (70–150) 2. Very common 3. Very oblique	LIT: Breached accumulation
Absent	Zero	Absent	Zero	Absent	1. Variable 2. Variable 3. Variable	If reactivated structurally: trap never charged, or in present-day migration shadow. If trap unreactivated structurally: possibly charged or uncharged HIT.

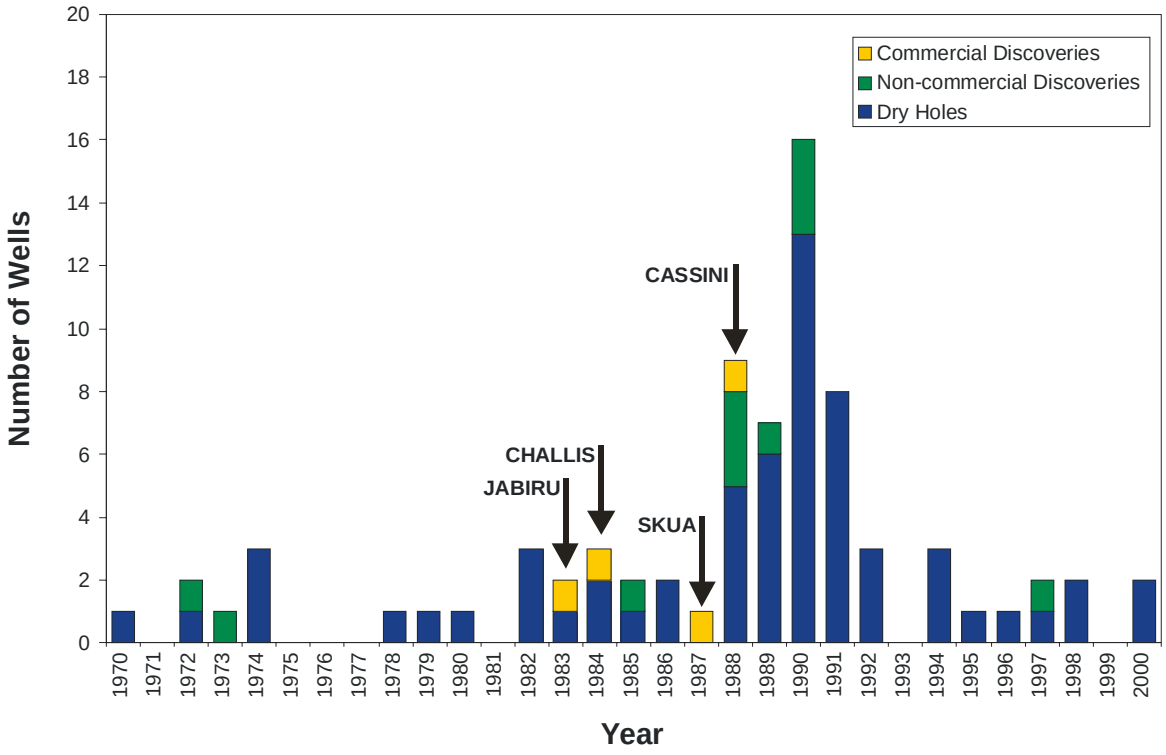

Figure 2-30: Drilling history of the Vulcan Sub-basin, 1970-2000.

Graph showing the number of exploration wells, excluding appraisal and development wells, drilled between 1970 and 2000. The discovery date for the four commercial fields is shown. Commercial discoveries represent those that have been put on production whilst non-commercial discoveries represent wells that recovered oil and/or gas to surface and where in-place hydrocarbons have been demonstrated on wireline logging and pressure data. The commercial success rate (1 in 19) is poor compared with global averages for offshore petroleum basins although the technical (commercial + non-commercial discoveries) success rate has been much higher (about 1 in 5).

3. RESERVOIR CHARACTERISATION

3.1 INTRODUCTION

Reservoir rocks in a petroleum setting comprise lithologies that contain sufficient porosity to store (reservoir) hydrocarbons either within the pore network or in fracture networks and enough permeability to allow those hydrocarbons to be extracted at economically viable rates. Potential hydrocarbon reservoirs generally consist of sedimentary rocks that can include clastic (sandstone) or carbonate facies and rely on either primary (intergranular) or secondary (mechanical fracture or chemical dissolution) porosity (Allen and Allen, 1990; Dandekar, 2006). Less commonly non-sedimentary rocks can act as effective reservoir rocks where sufficient secondary porosity has been created, normally through the development of fracture networks (Koning, 2003; P'an, 1982).

Characterisation of reservoir rocks is primarily undertaken in an effort to determine the likelihood that they would flow hydrocarbons to the surface at rates fast enough to be produced in an economically viable manner. In addition, characterisation of the reservoir can contribute information on the likelihood of formation damage that may inhibit the flow rate during production. Typical examples of formation damage that can restrict the pore network include the reaction of swelling clays with the drilling fluid or the physical breakdown of the reservoir and associated production of fines that can act to block flow paths to well perforations (Civan, 2007).

The rock properties (porosity, permeability, composition) of the reservoir and seal rocks constrain the productivity of any hydrocarbon system and their characteristics are usually described using a combination of petrographic and petrophysical techniques. The principal objectives of these investigations are to characterise the likely flow behaviour at the well location as well as to provide constraints on models used to predict reservoir properties away from the existing data points. The rock composition is also used to assess the provenance of the rocks (Weltje and von Eynatten, 2004), to determine susceptibility to diagenetic alteration as well as the

type and distribution of diagenetic minerals (Marshall, 1987) and can be used as a marker to correlate stratigraphic sequences between wells (Arribas et al., 2007).

A variety of data sets are routinely collected to evaluate petroleum reservoirs:

1. Porosity, permeability and saturation measurements made from routine (RCA) or special (SCAL) core analysis techniques (Monicard, 1980).

2. Permeability measurements made from fluid recovery tests using small scale wireline sampling tools (Repeat Formation Tester [RFT], Modular Dynamics Tool [MDT]) or more rarely by larger scale flow tests (Drill Stem Tests [DSTs] or Production tests) that produce larger hydrocarbon volumes over a longer timeframe (Chaudhry, 2003).

3. Porosity determination estimated from downhole logging tools that typically measure resistivity or other electrical properties. Increasingly Nuclear Magnetic Resonance (NMR) methods are employed to help better characterise petroleum reservoirs (Allen et al., 2000; Freedman and Heaton, 2004).

4. Rock composition and diagenetic sequence derived from petrographic (Scanning Electron or Plain Light microscopy) observations and point count data from core and cuttings samples (Tucker, 2001).

The types of data collected will depend on the objective of the well (exploration or appraisal), the well result (dry hole or discovery), the type of samples collected (Core, Sidewall Core, Cuttings), logging runs made (Formation Evaluation While Drilling, FEWD, or wireline logging tools) and the strategy of the company that commissions the well. Generally these datasets are acquired soon after completion of each well, normally through sub-contract to an oilfield services company.

A good understanding of the reservoir intervals sampled in the current study is an integral requirement if the fluid inclusion results are to be correctly interpreted and their significance to the fluid-flow history of the basin fully appreciated. Information on the porosity and permeability characteristics of the reservoir rocks are important

for this study as they constrain the likely level of hydrocarbon saturation that can be reached and define a vertical profiles of hydrocarbon saturation (Dake, 1978) that together with the electric log data can be used to interpret the significance of the observed fluid inclusion abundances (Eadington et al., 1996).

In Australia, data collected as part of routine post-well analysis are normally compiled within a well completion report that the operator is required to submit to both Federal and State/Territory agencies in order to comply with the terms of their exploration, retention or production license. The Australian Federal Government agency responsible for data archive, Geoscience Australia (GA), has compiled the basic petrophysical data from well completion reports into an online database system called RESFACS that can be freely accessed. These existing resources have been utilised as the principal data source to complete characterisation of the petrophysical and compositional properties of the key reservoir rocks investigated by this study. Information on the rock composition and diagenetic sequence has been obtained from available petrographic reports contained within the well completion reports and augments the petrophysical data taken from the RESFACS database.

Characterisation of the detrital and authigenic mineral composition using petrology techniques represents the first step in designing a fluid inclusion study (Goldstein and Reynolds, 1994; Goldstein, 2001; Munz et al., 2001). It enables the relative timing to be determined for the different fluid flow events recorded by the fluid inclusions that together with the palaeo-temperatures derived from fluid inclusions can be used to constrain an absolute time sequence.

However, as a consequence of the expansive availability of reservoir data from existing analyses and to avoid unnecessary duplication of effort only limited value was seen in acquiring new detailed petrology descriptions. Rather the petrographic work undertaken in the current study has been limited to qualitative observations aimed at confirming the veracity of the existing data sets and defining the petrographic sequence in those samples that were selected for detailed analysis such as palaeotemperature determinations.

3.2 COMPOSITION OF RESERVOIR ROCKS IN THE VSB

The composition of reservoir rocks is sub-divided into detrital and diagenetic mineral components. The detrital minerals represent constituents of the rocks introduced during the initial deposition of the sediments, whilst diagenetic minerals form subsequent to deposition through chemical and physical alteration of the detrital minerals and associated formation waters (Folk, 1974; Pettijohn et al., 1987). The detrital composition of the rocks provides insights into the provenance of the sediments (Arribas et al., 2007) to enable the depositional processes to be better constrained. This information can also infer the degree of diagenetic alteration likely to be induced by changes in temperature and fluid composition, which in turn allows more accurate predictions about reservoir quality to be made away from the location of the samples analysed (Burley and Worden, 2003).

The type and quantity of authigenic minerals crystallised is controlled by a complex interplay between reservoir composition, depositional environment, burial depth, temperature and time. The diagenetic mineral composition can involve dissolution of pre-existing minerals and redistribution as newly formed authigenic minerals or the creation of completely new minerals from materials introduced by fluid-flow in an open system (Burley and Worden, 2003).

Fluid flow can also result in the removal of existing minerals. Consequently, diagenetic processed can either enhance or degrade the quality of a reservoir by changing the original porosity and permeability (Scholle and Schluger, 1979).

The types of authigenic minerals present in a reservoir rock can provide constraints on the diagenetic environment, allowing reservoir quality away from the well intersection to be predicted (Bloch, 1991; Horbury and Robinson, 1993; Bloch and Helmold, 1995; Ajdukiewicz and Lander, 2010). In addition, the sequence of diagenetic mineralisation, commonly referred to as the paragenetic sequence (Larsen and Chilingar, 1979), allows the relative timing of each authigenic mineral to be determined. This information also enhances the ability to predict reservoir quality by establishing the stage that diagenesis has advanced to at different reservoir locations.

3.2.1 Detrital Composition of Reservoir Rocks from the VSB

As described in the preceding Chapter the important reservoir horizons in the Vulcan Sub-basin can be divided into three sub-types on the basis of depositional age and chronological position relative to the main episodes of Jurassic rifting, described in Pattillo and Nicholls (1990) as pre-, syn- and post-rift megasequences, separated by major unconformities (refer to Chapter 2 for a detailed description).

3.2.1.1 Detrital composition of Permo-Triassic reservoirs

Late Permian and Triassic units represent the upper portion of the pre-rift megasequence in the Vulcan Graben (Figure 2–8). Sandstones within the Late Permian and basal Triassic sequence are restricted to the Londonderry High and Ashmore Platform (Figure 2–9) and hence do not constitute important reservoir horizons within the Vulcan Graben, where they are too deeply buried to be prospective for hydrocarbons.

Thick deltaic sandstones of the Triassic Pollard Formation (Mory, 1988) represent excellent quality reservoirs, and host commercial hydrocarbon accumulations in the Challis-Cassini oil field (Wormald, 1988). The Pollard Formation grades upward into more shaly sands of the Triassic Challis Formation, which exhibits highly variable reservoir characteristics due to the complex facies assemblages that characterise the sequence (Pattillo and Nichols, 1990).

Sandstones of the Challis Formation provide the principal reservoir sequence in the Challis (Wormald, 1988) and Talbot oil fields (Bourne and Faehrmann, 1991). More predictable reservoir units occur in the overlying Nome Formation, where deltaic sandstones can produce excellent quality reservoirs. This formation is gas bearing in the Pengana-1 well (BHP Petroleum Ltd, 1988g) and also hosts the Crux gas field (Kaoru et al., 2003) in the adjacent Browse Basin.

The detrital composition of the Triassic reservoirs based on petrology from samples taken from the Pengana-1 well and in wells from the Challis Field is dominated by quartz, with feldspar and lithic fragments representing important, but less abundant constituents (Figure 3–1).

As a result the Triassic samples mostly plot in the sub-arkose to lithic sub-arkose fields using the Folk (1974) classification (Figure 3–2). The Triassic sandstones are mostly fine grained to occasionally medium grained and are typically well to moderately well sorted (Figure 3–3).

3.2.1.2 Detrital composition of Jurassic reservoirs

A regional unconformity separates the Triassic sequences from the overlying Early Jurassic sequence (Figure 2–8). Two principal periods of reservoir development are noted within the Jurassic section, pre-rift high-quality deltaic sandstones of the Early to Middle Jurassic Plover Formation and syn-rift, mostly marine fan deposits (deep water gravity flows) of Late Jurassic age (Lower Vulcan Formation).

The Plover Formation grades vertically and laterally from massive, medium to coarse-grained sandstones, with interpreted fluvial and deltaic environments, into more marine influenced sandstones and finally into thick sandstones that were deposited in high energy, delta front environments (Pattillo and Nichols, 1990).

The Plover Formation sandstones exhibit the best and most consistent reservoir characteristics within the pre-rift sequence and comprise the main reservoir intervals for the producing Skua oil-field (Osborne, 1990) and the sub-economic Oliver oil and gas accumulation (Ambrose, 2004).

The syn-rift megasequence directly overlies the Callovian Unconformity (Figure 2–7) and can be sub-divided into two discrete depositional sequences, punctuated by the intra-Kimmeridgian unconformity. The intra-Valanginian disconformity marks the upper boundary of the syn-rift megasequence (Pattillo and Nicholls, 1990). The Upper Jurassic syn-rift sequences provide important reservoir intervals as they contain excellent quality sandstones that are directly juxtaposed (face loaded) against the Late Jurassic mudstones that source the majority of oil discovered in the region to date (Summons et al., 1998).

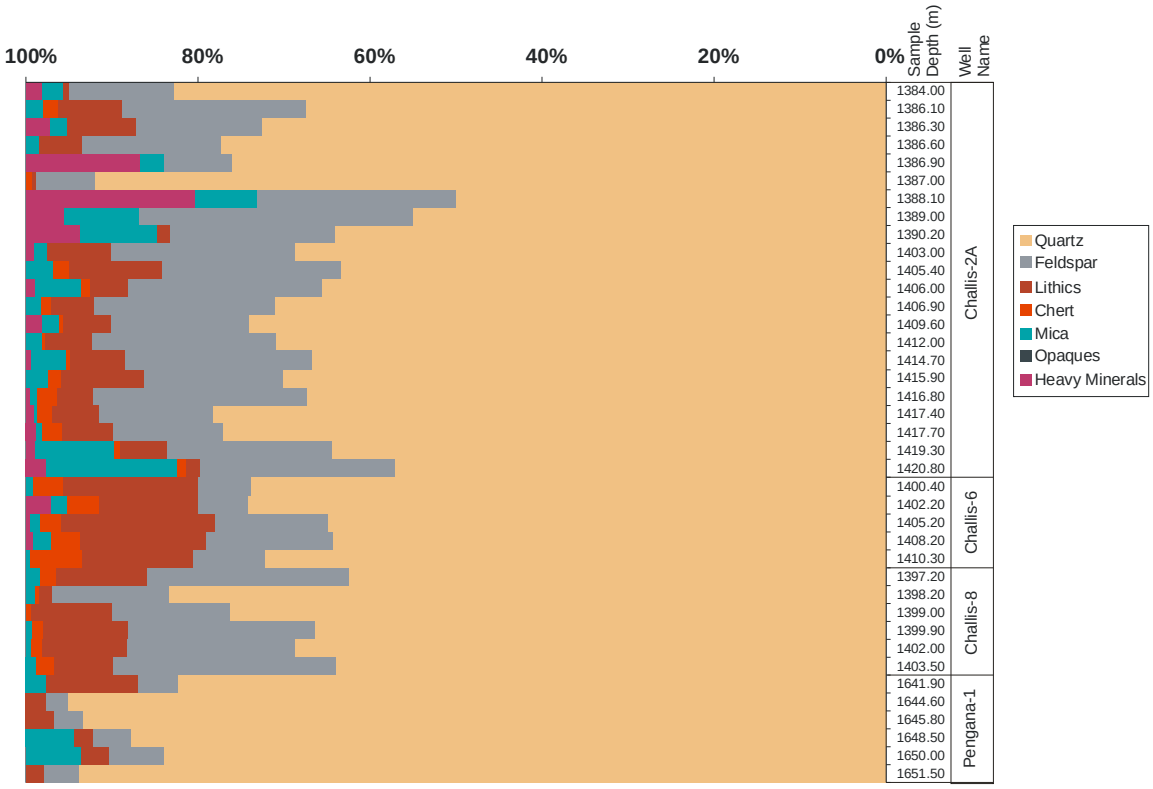

Figure 3-1: Detrital composition of Permo-Triassic reservoirs from the VSB

Graph showing the detrital composition of samples from Triassic reservoirs in the Challis-2A, Challis-6, Challis-8 (all Challis results from Martin, 1987) and Pengana-1 (Keene, J.B., 1988a) wells taken from the respective well completion reports. The samples are dominated by quartz but with significant proportions of feldspar and rock fragments also noted. Other accessory constituents are typically in low abundance and rarely exceed 10% of the total.

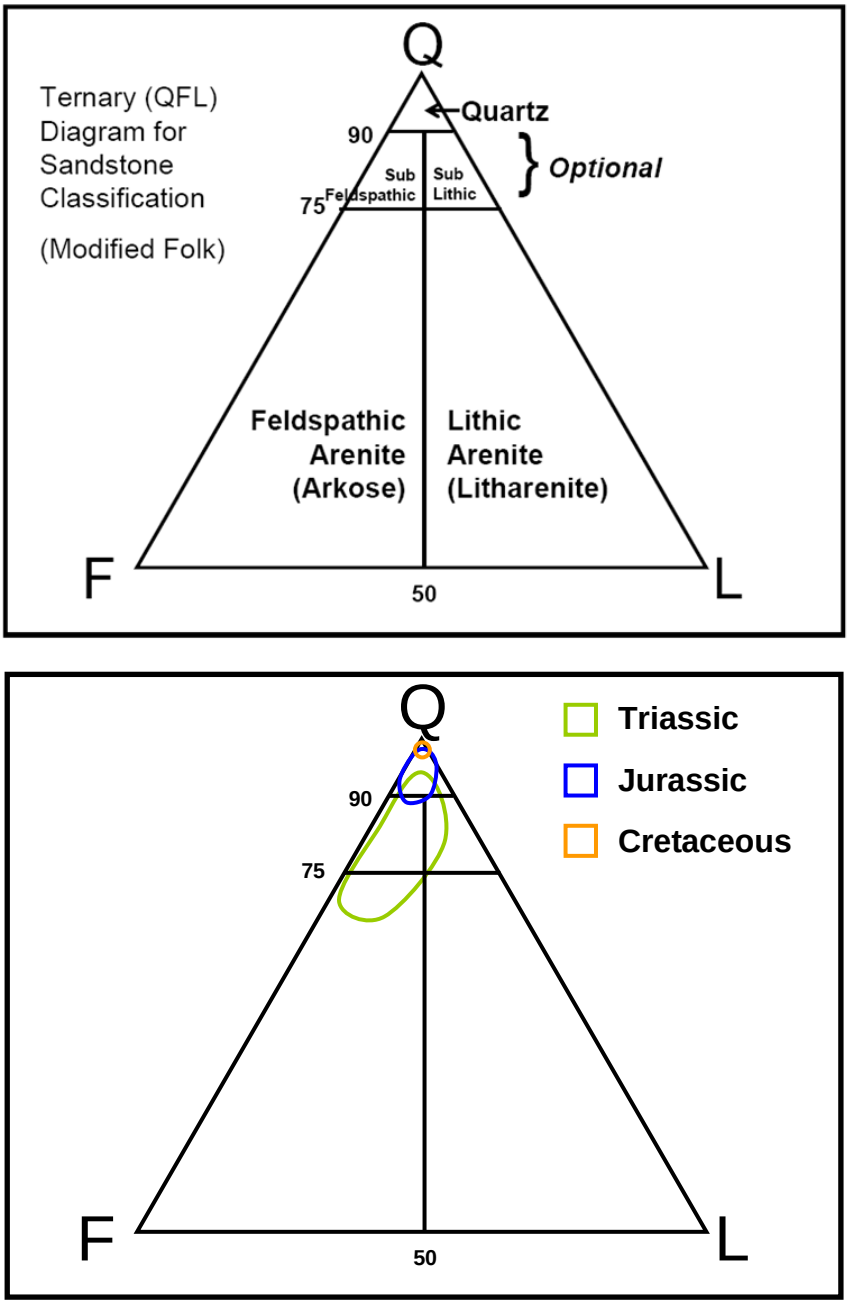

Figure 3-2: Ternary QFR plot

A ternary Quartz, Feldspar, Rock Fragments (QFR) plot (modified from Folk, 1974) for Cretaceous, Jurassic and Triassic reservoirs derived from petrology data sourced from well completion reports for VSB wells. The reservoir units typically become compositionally more variable and feldspar enriched (arkose) with increasing depositional age. This probably reflects a combination of repeated reworking increasing the sediment maturity as well as targeting of Triassic units on the flanks of the VSB where burial depths are lower and diagenesis less advanced, thereby preserving a greater quantity of the more labile feldspars.

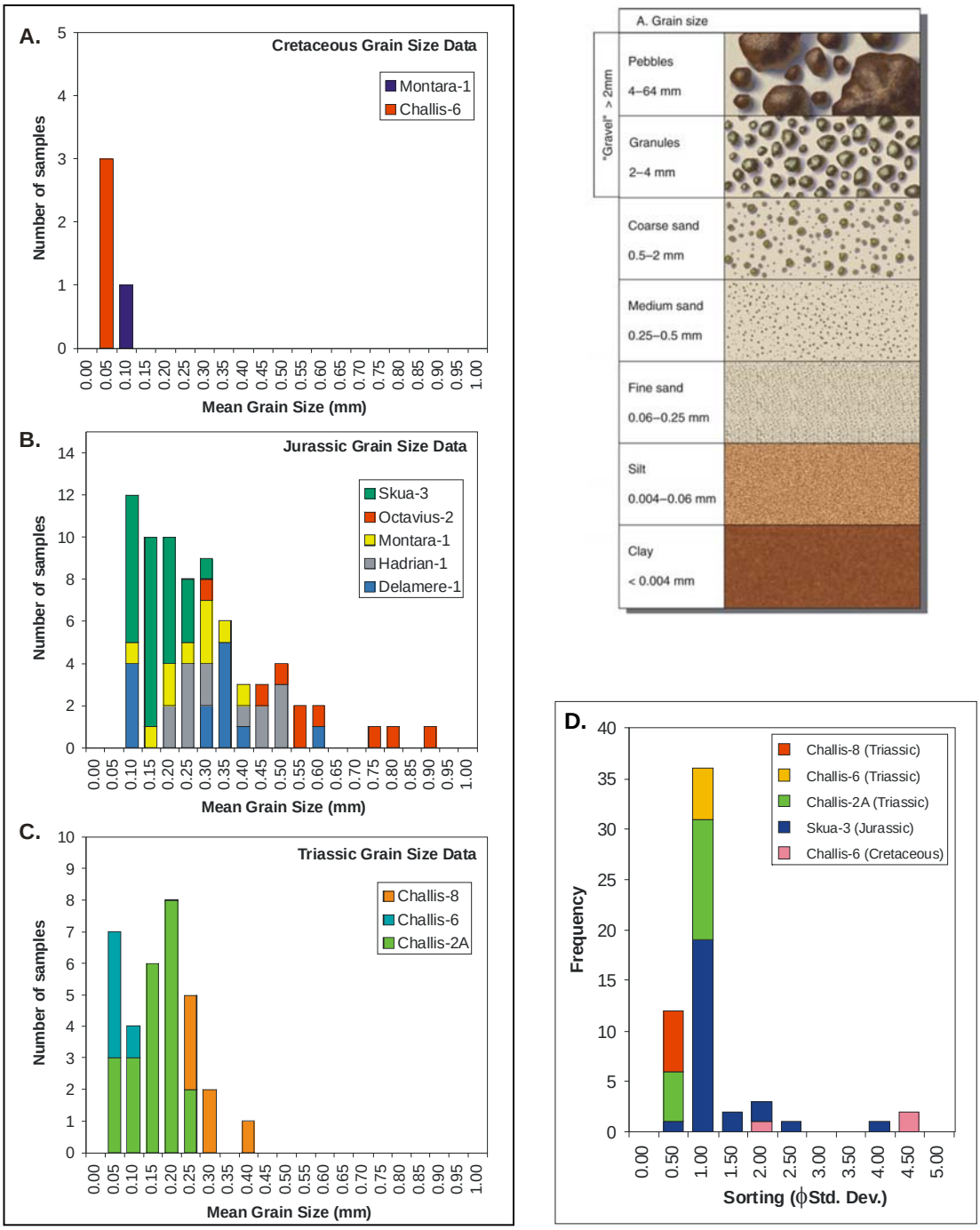

Figure 3-3: Summary of grain size and sorting variations in VSB reservoir rocks

Data are shown for Cretaceous, Jurassic and Triassic reservoirs (A-D) together with a standard grain size chart for comparison (based on the Wentworth Grade Scale, Wentworth, 1922). Cretaceous and Triassic sandstones are generally finer grained than the Jurassic sections and the Triassic samples typically are better sorted. Limited sample numbers precludes a more detailed assessment of these data. Data are derived from petrology reports contained in well completion reports (all Challis data from Martin, 1987; Skua-3 and Montara-1 data from BHP Petroleum Ltd., 1988a, f; Delamere-1, Hadrian-1 and Octavius-2 data from Martin, 1991a,b,c).

These sandstones represent reworking of older sediments during falls in sea level and periods of footwall uplift related to rifting. In the VSB they occur as submarine fans that were deposited immediately adjacent to eroded Middle Jurassic horst and tilted fault blocks (Pattillo and Nicholls, 1990).

The Oxfordian Montara Formation represents the principal reservoir horizon for the sub-economic Montara and Bilyara hydrocarbon fields at the southern end of the VSB, whilst the younger Tithonian sandstones have been shown to be oil bearing in the Tenacious oil-field (Woods and Maxwell, 2004) further to the northeast.

The detrital composition of the Jurassic reservoirs described in the petrology reports from wells across the VSB is strongly dominated by quartz, with only minor amounts of feldspar and lithic fragments (Figure 3–4). All samples plot in the quartz-arenite field using the Folk (1974) classification (Figure 3–2). The sandstones are mostly fine to medium grained and are well to moderately well sorted (Figure 3–3).

3.2.1.3 Detrital composition of Cretaceous and Tertiary reservoirs

The cessation of Jurassic rifting and the associated onset of thermal subsidence in the Valanginian resulted in a rapid regional transgression and the development of a passive margin sequence across the entire VSB (Post-rift megasequence; Pattillo and Nicholls, 1990). This event is of importance primarily because it led to the deposition of the regional seal facies comprising the Echuca Shoals and Jamieson formations.

A major depositional change from primarily siliciclastic to predominantly carbonate sedimentation occurs across the VSB above the KA (Aptian) seismic marker. Clastic sediment input periodically returned throughout the Late Cretaceous and into the Tertiary section when channelised submarine fan complexes (e.g. Maastrichtian Puffin Formation, Eocene Grebe Sandstone, Miocene Oliver Sandstone; Figure 2–8) were deposited during periods of regional low stand (Pattillo and Nicholls, 1990).

The Cretaceous and Tertiary sandstones are described in petrology reports from the Challis-6 and Montara-1 wells as quartz arenites (Figure 3–5) that are predominately fine grained and poorly sorted (Figure 3–2, Figure 3–3).

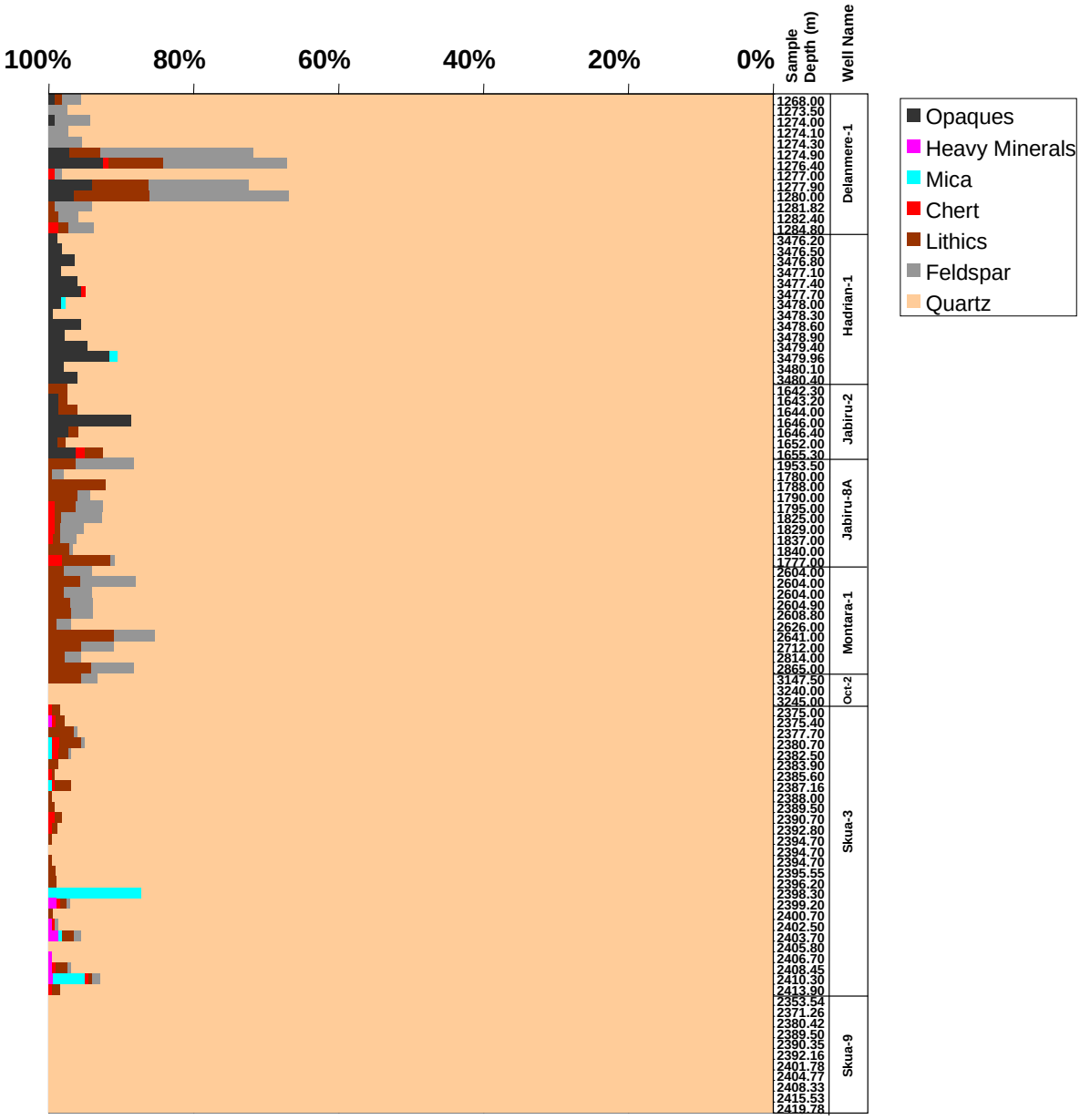

Figure 3-4: Detrital composition of Jurassic reservoirs from the VSB

Graph showing the detrital composition of samples from Jurassic reservoirs sampled in the Delamere-1, Hadrian-1, Octavius-2 (all from Martin, 1991a,b,c) Jabiru-2, Jabiru-8A, Montara-1, Skua-3 and Skua-9 (all from from BHP Petroleum Ltd., 1984b, 1988a, f, 1989e) wells showing a predominance of quartz with only minor amounts of feldspar and lithic fragments. Other accessory constituents are typically in low abundance and rarely exceed 10% of the total.

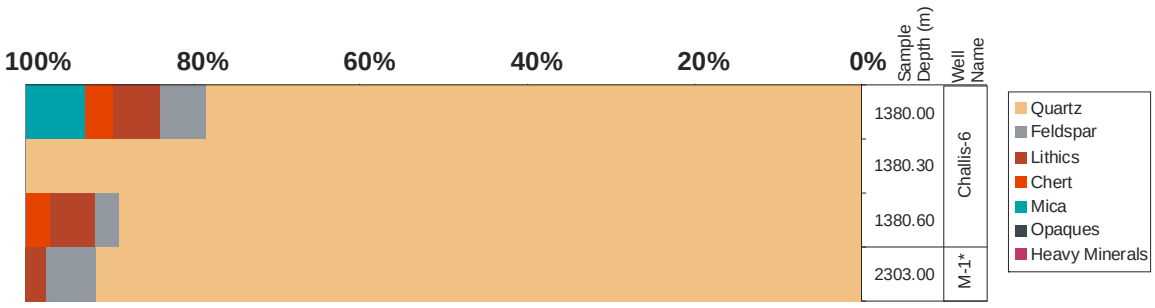

Figure 3-5: Detrital composition of Cretaceous reservoirs from the VSB

Graph showing the detrital composition of a small number of samples taken from Cretaceous reservoirs in the Challis-6 (Martin, 1987) and Montara-1 (M-1, BHP Petroleum Ltd., 1988f) wells showing a predominance of quartz with only minor amounts of feldspar and lithic fragments. Other accessory constituents are typically in low abundance and do not exceed 10% of the total.

Within the Cretaceous Post-Rift megasequence they represent viable reservoirs (e.g. Puffin Formation) with marls (calcilutites) providing an effective top seal. These reservoirs have proven hydrocarbon bearing in the Maastrichtian sandstones that host the Puffin (oil) and Swan (gas) fields. In contrast, the Tertiary reservoirs are less likely to be important for hydrocarbons as they generally lack an effective top seal.

3.2.2 Diagenetic composition of reservoir rocks from the VSB

As previously described the modification of the detrital composition of sediments through diagenesis begins during, and continues subsequent to deposition. New authigenic minerals are created, that are generally deleterious to reservoir quality, but the dissolution of the pre-existing detrital minerals to create secondary porosity, can enhance reservoir quality (Burley and Worden, 2003).

Petrological data contained in well completion reports for wells across the VSB together with observations made whilst undertaking the fluid inclusion analyses completed during this study have allowed the sequence that the diagenetic minerals crystallise, termed the paragenetic sequence, to be established. The paragenetic sequence is of interest to a fluid inclusion investigation because it allows minerals that are capable of trapping fluid inclusions, typically those with a framework structure such as quartz, feldspar and carbonates, to be placed in a relative time sequence (Goldstein and Reynolds, 1994). The different fluid inclusion populations represent unique fluid types (i.e. waters of different salinity, oil, gas) that allow a well-constrained fluid-flow history for the rocks being studied to be developed.

Diagenetic modification of the Mesozoic sandstone reservoirs within the Vulcan Sub-basin is generally relatively minor, except where burial depths exceed about 3 km. In sandstones above this depth reservoir quality is largely controlled by the detrital composition and lithologic facies with only a limited diagenetic overprint. The degree of diagenesis in the Tertiary sandstones is likely to be minimal given the relatively shallow burial depth, but quantitative point counting data are lacking for these intervals, due to a lack of core samples. The qualitative petrographic examination of ditch cuttings undertaken during this study on the Warb-1 and Pituri-1 wells, suggests diagenesis is dominated by poikilotopic carbonate cement with

variable reservoir quality to be expected where these cements are present. Conversely, good reservoir quality is likely where these cements are absent.

Diagenetic minerals that are of significance to reservoir quality in the Mesozoic sandstones include glauconite, pyrite, authigenic clays (mostly kaolinite), quartz overgrowths and several phases of carbonate cement including both early in the diagenetic sequence (e.g. siderite and calcite) that reflect the prevailing depositional environment as well as late formed phases (e.g. ankerite).

Quantitative petrographic point count data on the diagenetic phases taken from petrology reports for wells across the VSB show no significant differences in diagenetic composition between sandstones from the Triassic and Jurassic/Cretaceous sequences, despite substantial differences in detrital composition (Figure 3–1, Figure 3–4, Figure 3–5).

The greater abundance of feldspar in Triassic rocks provides more labile framework grains and should result in more pervasive diagenesis, particularly the crystallisation of authigenic clays, but this was not observed in the petrographic descriptions taken from the available well completion reports. This observation likely reflects the shallow burial depth of the Triassic reservoirs in the wells that have been sampled and in more deeply buried these sandstones will be more pervasively cemented.

3.2.2.1 Diagenetic composition of Triassic Reservoirs

As previously mentioned wells that have tested Triassic reservoirs in the VSB tend to have targeted prominent structural highs with relatively shallow burial (typically less than 2000m) and as a consequence rarely exhibit significant diagenetic alteration.

Carbonate cement volumetrically represents the most significant authigenic minerals in Triassic reservoirs although locally pyrite cement can also be pervasive (Figure 3–6). Quartz overgrowths and authigenic clay minerals (mostly kaolinite) are present in most samples (Figure 3–6) but generally are not volumetrically extensive enough to have a significant impact on reservoir quality.

Triassic sandstones within the Crux Field discovered in 2000 and located at the southwestern end of the VSB (Kaoru et al., 2003) have been extensively characterised (Nippon Oil Exploration (Vulcan) Pty. Ltd., 2000; Clews, 2000) and provide a useful type example for the Triassic reservoirs of the VSB.

High quality, massive to occasionally cross-bedded, sandstones (Figure 3–7A, B) make up the hydrocarbon bearing zone and exhibit high porosity and permeability. Quartz overgrowths and kaolinite represent the key authigenic phases (Figure 3–7C-F) and a clear paragenetic sequence can be defined with quartz overgrowths enclosing earlier formed kaolinite booklets (Figure 3–7F). Late stage ferroan dolomite cement completes the diagenetic record (Figure 3–7G).

Comparison of the well defined diagenetic sequence at the Crux Field with other petrographic studies of Triassic reservoirs in the VSB (Figure 3–8) typically show a similar paragenesis with an early carbonate cement (typically siderite) and pyrite followed by kaolinite cement that pre-dates quartz overgrowths.

3.2.2.2 Diagenetic composition of Jurassic Reservoirs

Wells targeting the Jurassic reservoirs are more frequent, test the greatest range in burial depths and consequently contain a more varied suite of authigenic minerals.

As was seen in the Triassic reservoirs authigenic clay, carbonate cement and quartz overgrowths represent the key porosity reducing diagenetic minerals (Figure 3–9) in the Jurassic section. Quartz overgrowths are the dominant authigenic phase in the deeper samples, reflecting the attainment of greater burial depths that allow for pressure solution processes (Houseknecht, 1984) to redistribute silica dissolved at the point of grain to grain contacts.

There is noticeable variability in the interpreted depositional environment as well as differences in both the degree of diagenesis and the types of authigenic minerals that occur in the different aged Jurassic reservoirs that make it important to consider these independently.

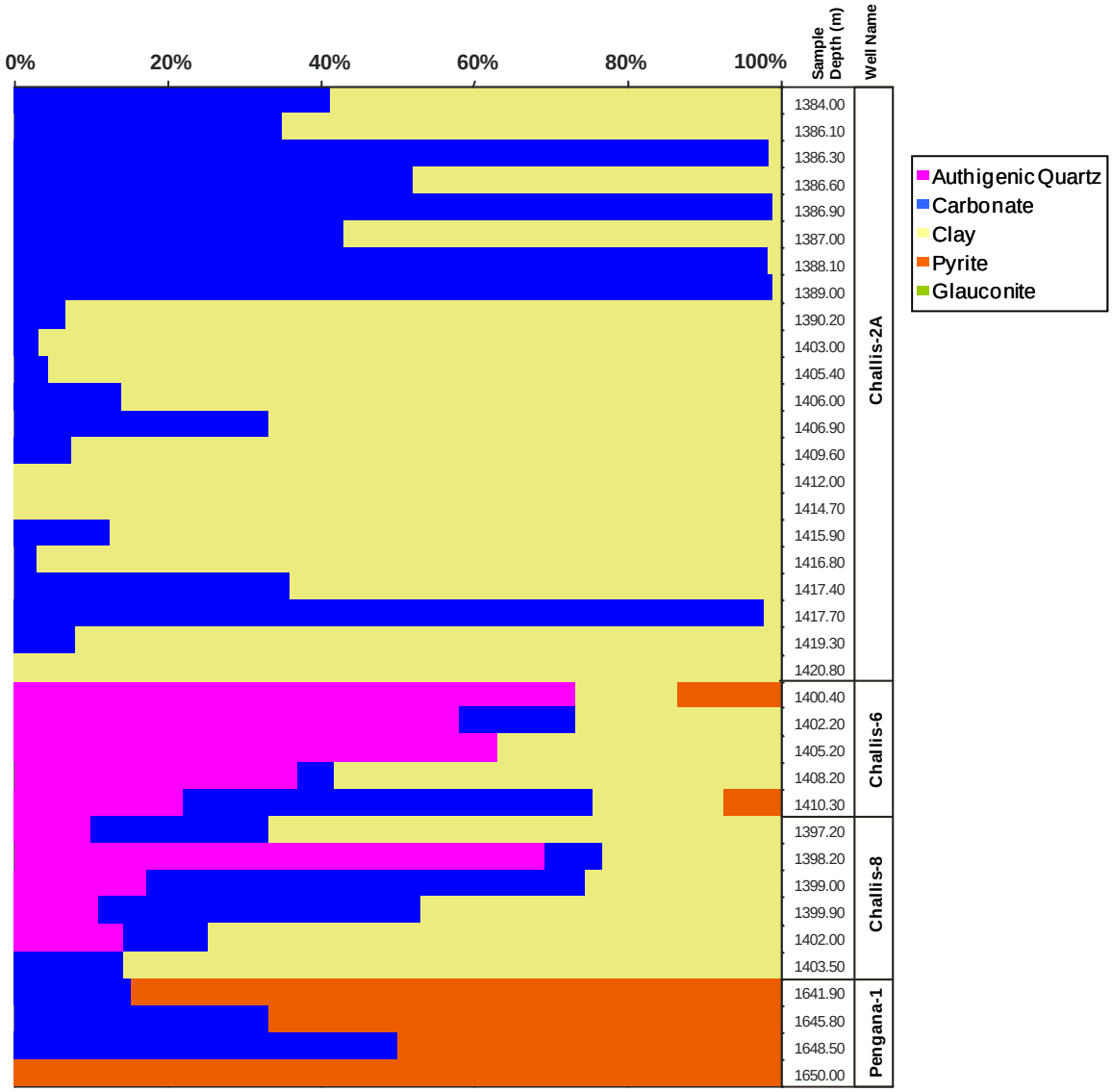

Figure 3-6: Diagenetic composition of Triassic reservoirs

Graph showing the relative proportion of different diagenetic minerals present in samples from Triassic reservoirs in the Challis 2A, Challis-6, Challis-8 (all Challis data from Martin, 1987) and Pengana-1 (Keene, J.B., 1988a) wells. A variety of diagenetic minerals are reported with no single mineral being dominant.

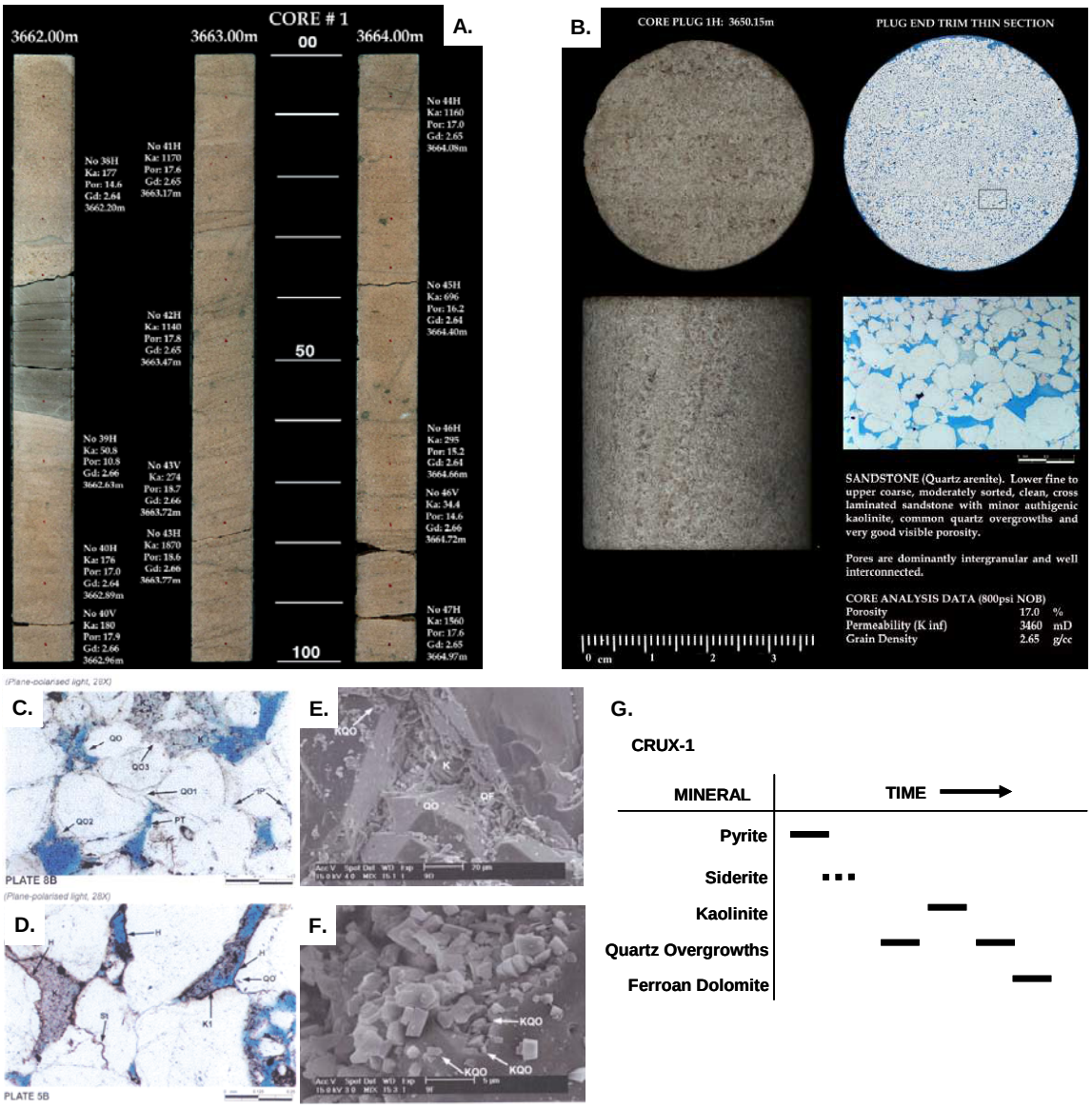

Figure 3-7: Triassic reservoir sandstones from the Crux Gas Field.

Composite diagram showing the nature of Triassic Nome Formation sandstones intersected in the Crux Field (data from Clews, 2000). **A.** Representative core photographs showing medium grained massive sandstone with some cross bedding, separated by a thin shale layer. Measured porosity and permeability values are from core analysis. Core 1 from 3662m to 3665m. **B.** Core Plug from 3650.15m showing medium grained, moderately sorted quartz arenite with abundant visual porosity (blue). **C-F.** Thin section photomicrographs (Crux-1 sidewall core CST10, 3810.18m [C] and CST16, 3658.0m [D]) and scanning electron photomicrographs (Crux-1 sidewall core CST6, 3855.4m [E,F]) showing of a high porosity medium grained quartz arenite with abundant authigenic quartz overgrowths that enclose earlier formed kaolinite cement. **G.** Inferred paragenetic sequence for the Crux reservoir sandstones.

CHALLIS-1, 2A, 3, 4

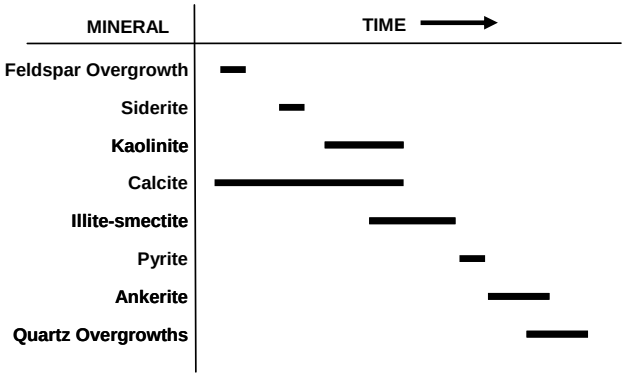

Martin, K.R., 1987. Diagenesis and reservoir quality in the Challis Field, Browse Basin, Northern Territory. Unpublished report to BHP Petroleum Ltd.

CRUX-1

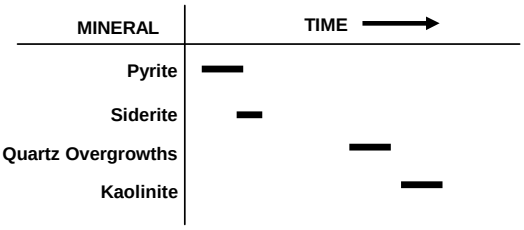

Clews, P., 2000. Crux-1, petrography of 15 CST samples from the interval 2657.3 – 3903.6m. Unpublished report to Nippon Oil Exploration Pty. Ltd.

TALBOT-1

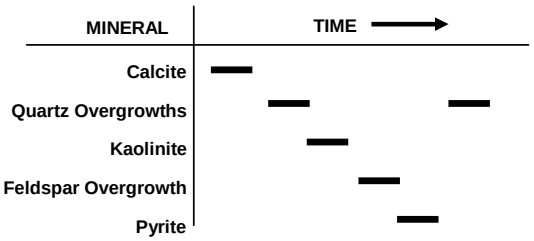

Lemon, N.M., 1990. Petrographic analysis report, Talbot-2. Unpublished report to Santos Ltd.

PENGANA-1

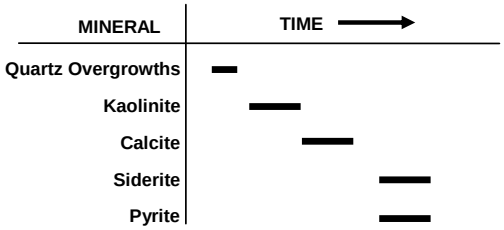

Keene, J.B., 1988. Petrology report, Pengana-1, Timor Sea. Unpublished report to BHP Petroleum Ltd.

DELAMERE-1

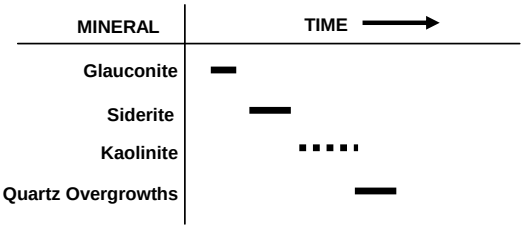

Martin, K.R., 1991. Petrography of core samples from Delamere No. 1, AC/P4, Northern Territory. Unpublished report to BHP Petroleum Ltd.

ANSON-1

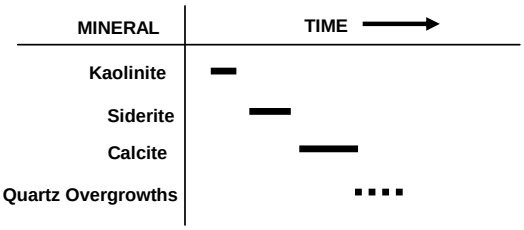

Santos Ltd., 1990. Anson-1 well completion report. Unpublished Santos Ltd report.

Figure 3-8: Paragenetic sequences reported for a selection of Triassic reservoirs

The variety in reported paragenetic sequences highlights the difficulty in arriving at unique interpretations from conventional petrological evaluations. The results from Martin (1987, 1991 a,b,c) are consistent with the observations recorded in the current study.

These differences reflect the variations in the prevailing depositional environment (particularly the increasing marine influence seen in the Upper Jurassic section) and the resultant facies types (including grain size and sorting) that have contributed to subtle differences in the diagenetic record.

The transition from a fluvio-deltaic depositional environment to one strongly influenced by tidal effects has a pronounced impact on the nature of the sediments deposited and the type of authigenic minerals that develop. In Lower to Middle Jurassic reservoirs of the Plover Formation a combination of granitic provenance (assumed to be the adjacent Proterozoic Kimberly Block) and the fluvio-deltaic depositional environment results in a high level of compositional and textural maturity that produces sediments dominated by quartz with little or no feldspar content (Figure 3–4). As a consequence diagenetic alteration in the Plover Formation is dominated by the formation of quartz overgrowths, with the formation of authigenic clay minerals being restricted mostly to kaolinite that is derived from the dissolution of the limited feldspar fraction.

Petrology results derived from well completion reports for the Jabiru-1A and Jabiru-10 wells typify the authigenic mineral assemblage commonly observed for Plover Formation reservoirs (Figure 3–10). Diagenesis is dominated by authigenic quartz and kaolinite formation, with variable levels of glauconite (Cloud, 1955) and pyrite reflecting the varying degrees of marine influence (providing sulphate required for pyrite formation from organic matter in reducing conditions; Berner, 1984) that are experienced across a delta plain depositional setting.

Petrology observations for the Jabiru Field (Figure 3–10) are compatible with the overall transgressive and increasingly marine influenced nature of the Plover Formation with time. Fluvial dominated sandstones (refer to the cross bedding in Figure 3–10D) represented in the early Plover section grade into marginal marine sediments at the top of the core (refer to the bioturbation obvious in Figure 3–10A).

Despite a relatively simple suite of authigenic minerals being observed, petrographic work undertaken by previous workers has produced markedly different views on the sequence of diagenesis in the Plover Formation (Figure 3–11).

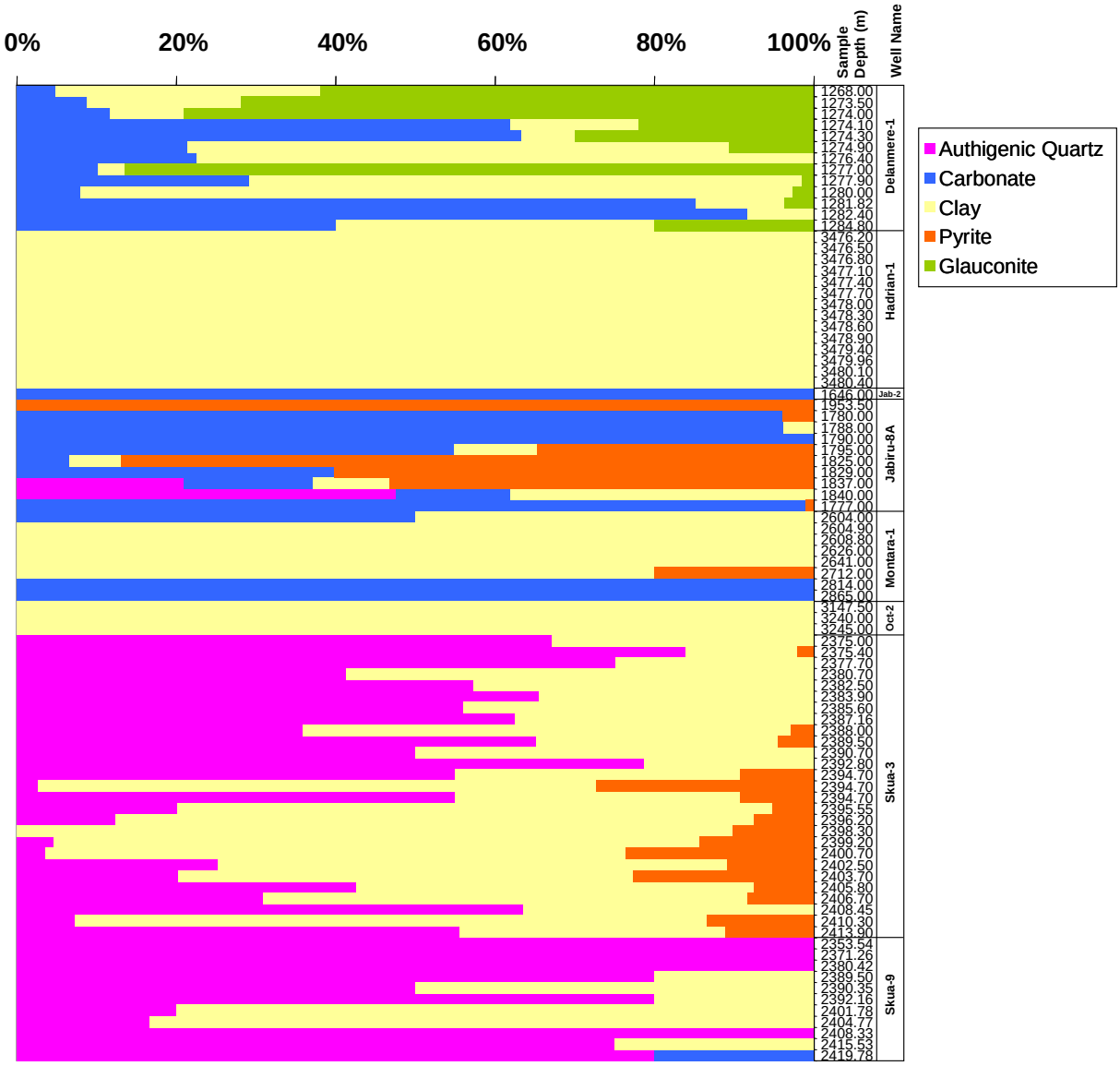

Figure 3-9: Diagenetic composition of Jurassic reservoirs

Graph showing the proportion of diagenetic minerals present in samples from Jurassic reservoirs in the Delamere-1, Hadrian-1, Octavius-2 (all from Martin, 1991a,b,c), Skua-3, Jabiru-8A, Montara-1, and Skua-9 (all from BHP Petroleum Ltd., 1988a, f,) wells. Note that in the samples where no quartz overgrowth cement recorded this reflects the difficulty in accurately estimating mineral overgrowths and in these samples no distinction is made between detrital and authigenic quartz. Data comes from petrology reports contained within the well completion reports for these wells.

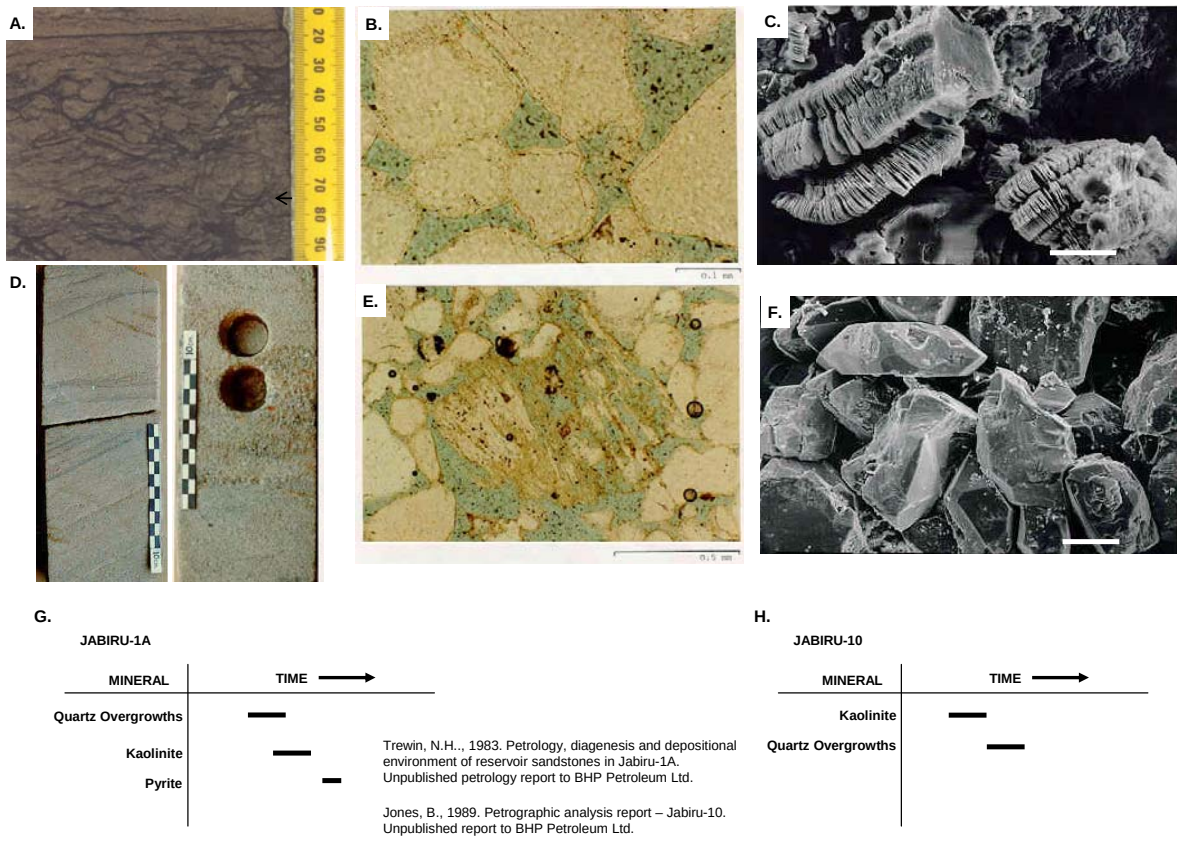

Figure 3-10: Summary of the Plover Formation in the Jabiru Field

Composite diagram showing the nature of Lower-Middle Jurassic Plover Formation sandstones intersected in the Jabiru Field. **A.** Core photograph of fine to medium grained bioturbated sandstone indicating a probable marine depositional setting. Trace fossil assemblage includes a large Thalassinoidees burrow (arrowed), Jabiru-12 core, 1641.41m. **B.** Core photographs of medium to coarse grained sandstone. Cross bedding seen in the left image indicates a degree of tidal influence, probably within a distributary channel on the delta plain. In the right hand image the graded bedding with coarser grains at the base is typical of fluvial channels with limited or no marine influence. **C-D.** Plain light photomicrographs showing moderately well sorted medium grained quartz arenite with common euhedral quartz overgrowths and abundant visual porosity (C) and a more poorly sorted example with the remnant of an altered detrital feldspar (E) with associated development of secondary porosity. **E-F.** Scanning Electron Micrographs showing the two dominant authigenic phases in Plover Formation reservoirs, with stacked kaolinite booklets (E) and well developed euhedral quartz overgrowths. **G-H.** Alternate paragenetic sequences reported for two wells from the Jabiru Field, highlighting the non-unique nature of the observations.

Whilst a unique solution for the petrological observations made in any one sample is lacking this study favours the work of Martin (1991a, b, c) as the interpreted paragenetic sequence is more consistent with the petrology results of the current study and the interpretation of the fluid inclusion data described later.

The authigenic mineral assemblages recorded in the first Upper Jurassic reservoir (Montara Formation) continues to reflect a change to a more marine depositional environment with an increased prevalence of glauconite and pyrite cement being noted in the petrology reports taken from well completion reports (Figure 3–12).

With further burial the diagenetic record resembles that of the Plover Formation with authigenic clay minerals, particularly kaolinite, and quartz overgrowths becoming common, the latter particularly prevalent within the cleaner sections of the reservoir interval. Visible porosity remains good even in samples with an advanced degree of diagenesis and this unit provides the principal reservoir unit in the Montara (BHP Petroleum Ltd, 1988b) and Tahbilk gas fields (BHP Petroleum Ltd, 1991).

As was noted for the underlying Plover Formation there is also considerable variation in the interpreted paragenetic sequence (Figure 3–12) described in the available petrology reports for samples from the Upper Jurassic Montara Formation.

Studies that invoke early quartz overgrowth precipitation and that consider pyrite to be a middle or late stage authigenic cement are inconsistent with the thermal and compositional requirements of these minerals and are likely to be the result of misleading petrographic relationships. The results of Jones (1989 a, b) are the most consistent with the observations of the current study and are used in the evaluation of the fluid inclusions results presented in subsequent chapters of this thesis.

Deposition in a fully marine setting is implied for the Tithonian reservoirs of the Lower Vulcan Formation that show a variety of interpreted environments ranging from shallow marine through storm wave base to offshore environments controlled by changes to relative sea-level. The sandstones show a wide degree of sorting implying relatively localised proximal sediment source, probably reflecting shedding from emergent Plover fault blocks.

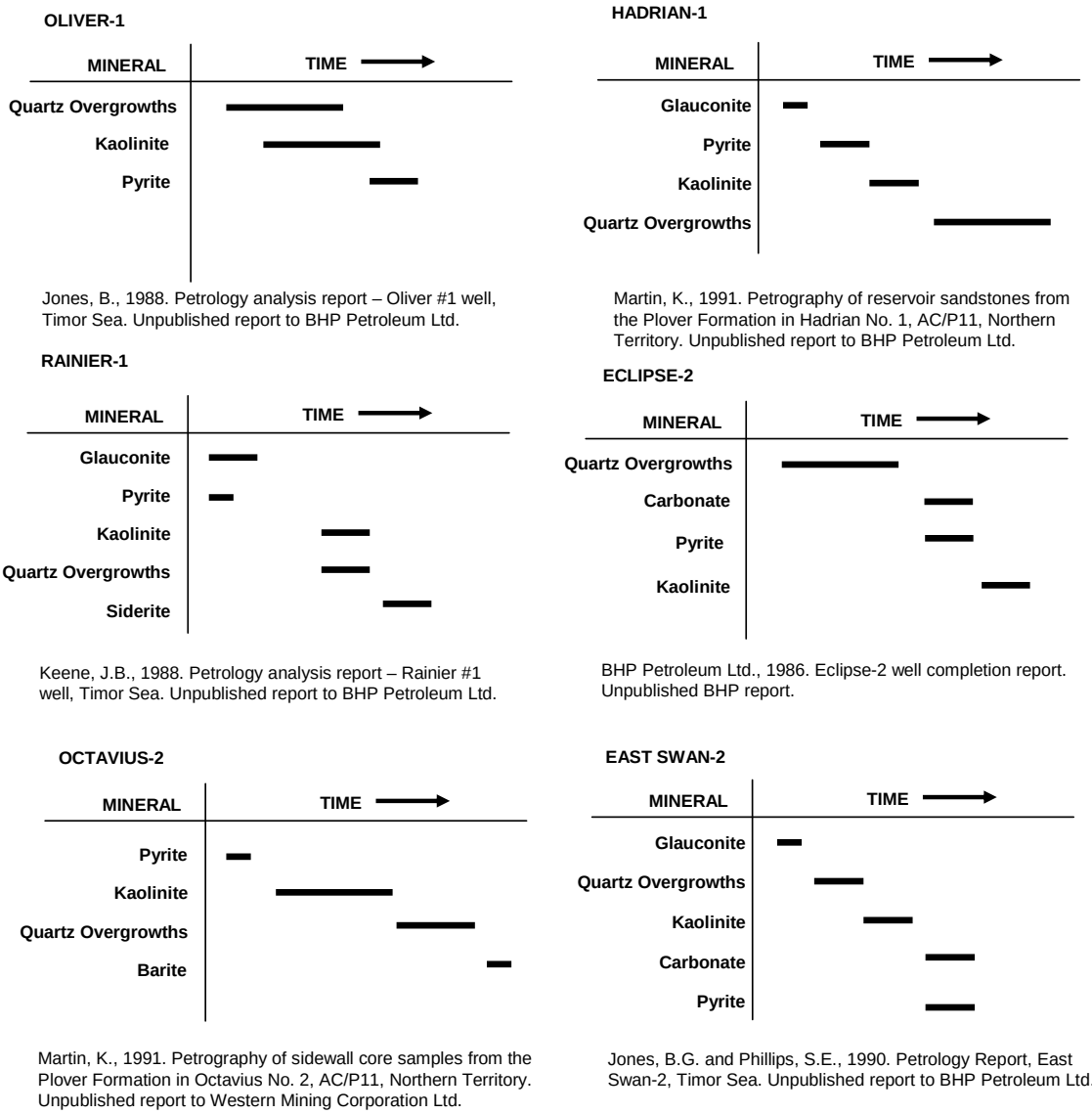

Figure 3-11: Reported diagenetic sequences for wells testing the Plover Formation

The variety in reported paragenetic sequences highlights the difficulty in arriving at unique interpretations from conventional petrological evaluations. Data come from petrology reports contained within well completion reports. The results from Martin (1991a, b, c) are the most consistent with the observations recorded in the current study.

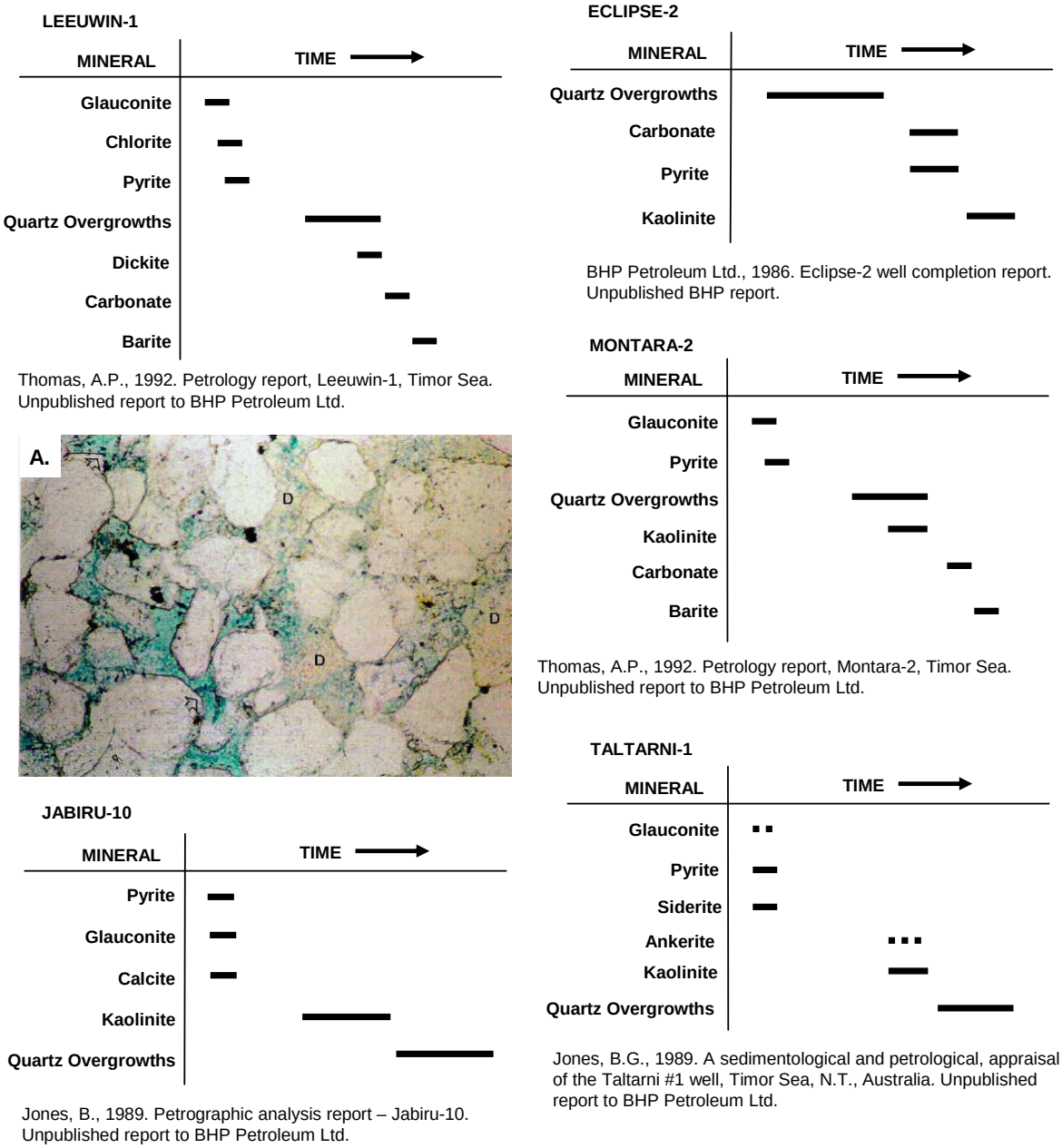

Figure 3-12: Petrology results from the Upper Jurassic Montara Formation.

Interpreted paragenetic sequences for the Montara Formation taken from previously reported petrographic studies for Vulcan Sub-basin wells. As with other reservoir levels there is considerable variation in the inferred sequence of diagenesis. An indicative example of a medium grained, moderately well sorted quartz arenite, typical of the Montara Formation, is shown in the photomicrograph (A.) and comes from the Leeuwin-1 well. Considerable intergranular porosity (blue) is present, except where in-filled by coarse grained kaolinite (Dickite, D) that is replacing altered detrital feldspar. Angular faces of euhedral quartz overgrowths are common with clear examples marked with the arrows. Leeuwin-1, sample no. 136, 3295.0m. Plain light. Field of view is 0.88mm.

Diagenetic mineral compositions in Tithonian sandstones samples (Figure 3–13) are similar to the Montara Formation with glauconite and pyrite representing early conditions with kaolinite and quartz overgrowths developing as burial proceeded. Several phases of carbonate cement are also recognised including early formed siderite and late stage carbonate cement (possibly Ankerite) that postdates all other diagenetic minerals.

3.2.2.3 Diagenetic composition of Cretaceous Reservoirs

Reservoir development in the Cretaceous section of the VSB is largely restricted to the Upper Cretaceous interval where high quality sandstones of the Puffin Formation constitute a viable exploration target being oil bearing in the Puffin oil field and gas charged in the three Swan wells (e.g. BHP Petroleum Ltd, 1992).

Post rift thermal subsidence following Jurassic rifting was typically too rapid to allow for preservation of early Cretaceous sandstones and aside from an isolated occurrence of gas in a glauconitic Santonian aged sandstone (Gibson Formation) at Tahbilk-1 (BHP Petroleum Ltd, 1991) and oil seen in an equivalent interval in Skua-2, the Early Cretaceous section is generally shale dominated.

Periods of major sea level fall at the end of the Cretaceous resulted in incision of the exposed shelf which allowed sand-rich sediment to be transported into deep water where it was deposited as a series of basin floor fans of the Puffin Formation during periods of lowstand (De Boer, 2004). The Maastrichtian aged Puffin sandstones are largely restricted to the southwestern end of the VSB, elsewhere in the basin this time interval is represented by deep water marls (Pattillo and Nicholls, 1990; De Boer, 2004) and effective reservoir development has not been demonstrated.

Sandstones of the Puffin Formation are loosely packed, well sorted quartz arenites reflecting their shallow depth of burial and textural maturity and are largely unaffected by diagenesis. The only authigenic mineral to have any significant impact of reservoir quality is are local patches of early formed calcite cement. The other authigenic minerals present include pyrite, kaolinite and limited quartz overgrowths, none of which have a significant impact on reservoir quality (Figure 3–14).

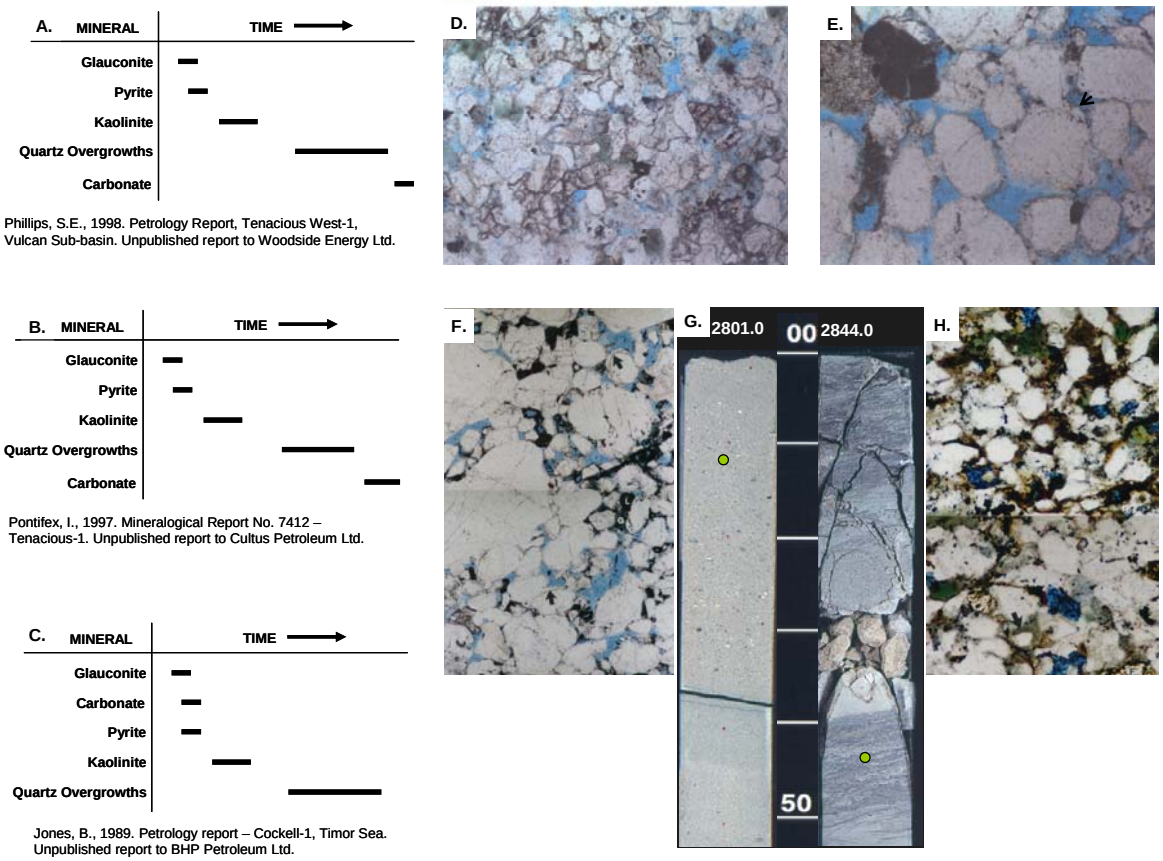

Figure 3-13: Summary of the Tithonian sandstones of the Lower Vulcan Fm.

Composite diagram summarising the nature of Tithonian sandstones seen in the Tenacious, Tenacious West and Cockell-1 wells taken from the relevant well completion reports. A fairly consistent paragenetic sequence has been reported (A-C) with only the timing of carbonate cement being in question (references shown). Photomicrographs shown in D-F illustrate a wide range in the degree of sorting probably reflecting a more proximal sediment source. The two core photographs shown in G are representative of the variability in reservoir facies ranging from massive (2801m) to argillaceous, highly bioturbated, sandstone (2844m). The argillaceous sandstone (H) is finer grained, has lower porosity and an increased proportion of detrital clay and glauconite reflecting a more quiescent lower shore face depositional environment. D. Fine grained, moderately well sorted quartz arenite showing some intergranular porosity (blue). Authigenic minerals include rare glauconite pellets (G), scattered carbonate cement (darker brown) and thin quartz overgrowths. Tenacious-1, Sidewall Core #34, 2806m. Plain light. Field of view approx 1.0mm. E. Medium grained, poorly consolidated quartz arenite showing considerable extensive intergranular porosity (blue). Authigenic minerals are limited to rare glauconite pellets (G) and thin quartz overgrowths (example marked with an arrow). Tenacious-1, Sidewall Core #31, 2839m. Plain light. Field of view approx 1.0mm. F. Coarse grained, poorly sorted quartz arenite showing considerable intergranular porosity (blue). Authigenic minerals include rare glauconite pellets (G), quartz overgrowths (example marked with an arrow) and minor carbonate spar (S). Tenacious West-1, Core plug 1H, 2801.11m. Plain light. Field of view approx 3.0mm. G. Slabbed core from Tenacious West-1 under plain light. H. Fine grained, moderately sorted lithic quartz arenite with minor feldspar (F) and limited porosity (pale blue). Common glauconite pellets (green) are associated with detrital clays (brown), whilst quartz overgrowths are restricted to areas of clean sandstone. Carbonate spar (bright blue) further occlude primary porosity. Tenacious West-1, Core plug 105H, 2844.44m. Plain light. Field of view approx 1.0mm.

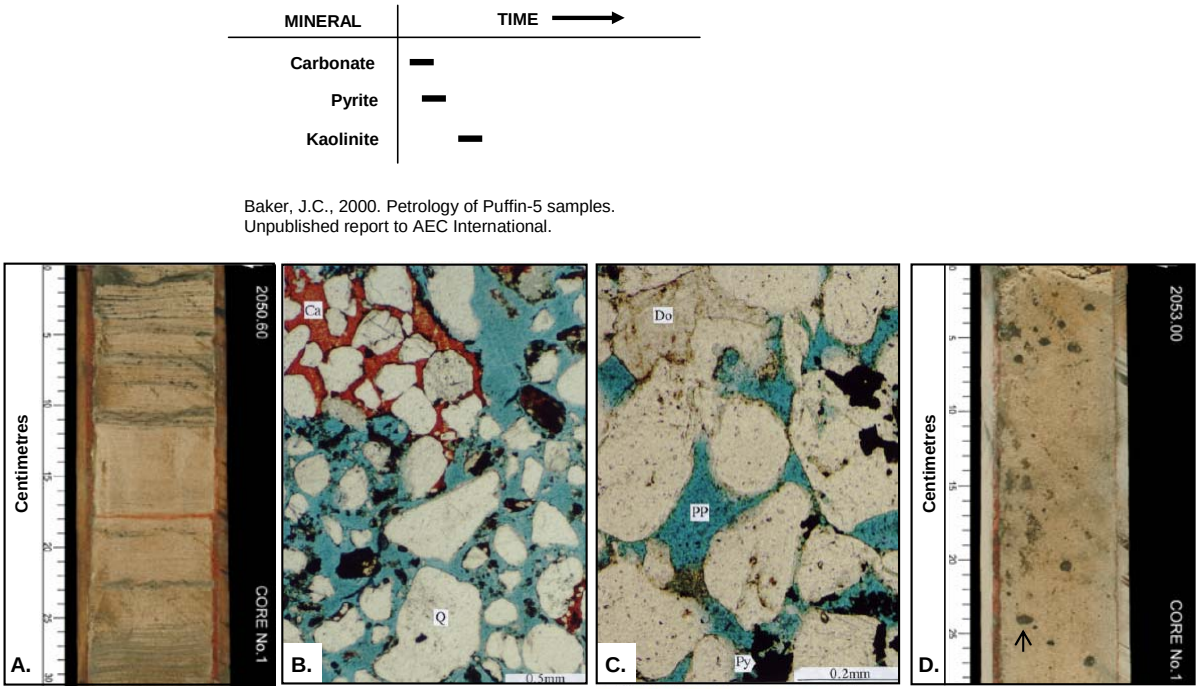

Figure 3-14: Summary of the Puffin Formation sandstone reservoirs.

Core and petrographic photomicrographs demonstrating the excellent quality of the Puffin Sandstone penetrated in Puffin-5 (from Baker, 2000). Diagenesis is limited to patches of isolated, early formed carbonate and pyrite cement with minor amounts of kaolinite cement. A. Core photograph of fine to medium grained high quality thinly laminated sandstone. Puffin-5, Core 1, 2050.6 – 2050.9m. B. Photomicrograph of a cuttings samples comprising disaggregated medium to fine grained quartz grains and isolated fragments of pyrite. A cluster of quartz grains are cemented by calcite (Ca, stained red). Puffin-5, cuttings sample, 2063-2066m. Plain light. Field of view 2.0mm. C. Photomicrograph showing loosely packed, moderately well sorted medium grained quartz arenite with abundant intergranular porosity (blue). Pyrite and isolated patches of dolomite cement locally reduce porosity. Puffin-5, off-cut 11S, 2053.25m. Plain light. Field of view 2.0mm. D. Core photograph of medium grained homogenous sandstone with isolated patches of nodular pyrite (example shown by arrow). Puffin-5, Core 1, 2053.0 – 2053.28mRT.

3.3 RESERVOIR QUALITY EVALUATION

Evaluating the quality of reservoir sections is important to define the flow characteristics of that reservoir both at that location (i.e. for field development planning) and in locations yet to be drilled. For the latter, porosity-depth trends are particularly useful as they help to define the depth to which viable levels of porosity are likely to be retained (the porosity floor). Plotting porosity against permeability is also useful to determine the viability of a reservoir sequence to flow hydrocarbons at an rates sufficient to warrant field development.

Petrophysical information, derived from core analysis, testing data (Repeat Formation Tester [RFT], Modular Dynamic Tester [MDT], Drill Stem Test [DST] and production tests) and interpretation of wire-line petrophysical logs, indicates a wide range in porosity (Figure 3–15 and 3–16) and permeability (Figure 3–17).

Porosity-depth trends for the Triassic and Jurassic rocks indicate that porosity values above 10% are likely to exist down to about 3.5km (Figure 3–15). The data in this section have not been filtered by facies type and therefore include data measured on shales and other non-reservoir rocks. Consequently it is likely that these mid-case estimates will underestimate the porosity that could be expected in purely reservoir facies at any particular depth.

The depth to the base of economically producible hydrocarbons will vary from basin to basin and is generally addressed by nominating a minimum permeability considered to constitute economic recovery. Cross plotting permeability against porosity allows an estimate of the equivalent porosity as normally porosity and permeability are somewhat related (Nelson, 2000).

Despite the notable difference in detrital composition (Figure 3–4, 3–5, 3–6), with the Triassic reservoirs typically having higher feldspar content, the observed decline in porosity with depth is similar between these groups suggesting that the rate of diagenetic alteration with depth is comparable for both the Triassic and the Jurassic reservoir sections (Figure 3–6, Figure 3–9, Figure 3–14).

Porosity-depth trends in the Cretaceous and Tertiary sections show wider scatter than the older reservoir units and consequently less pronounced porosity reduction trends with depth (Figure 3–16). For data that is derived from detailed core analysis and where a porosity and permeability measurement are made on each individual sample point these can be cross plotted to explore the degree of dependency between porosity and permeability values (Figure 3–17). For the VSB wells there is a moderately strong correlation between porosity and permeability that is fairly typical for a sedimentary basin.

The importance of understanding reservoir quality for the current study is relatively minor beyond establishing that normal burial trends exist and understanding the depths at which minerals that could host fluid inclusions begin to form. The migration of hydrocarbons is also directly controlled by the porosity of the carrier beds so recognising porosity depth trends has a direct relevance to understanding the saturation profiled that could be expected below significant capillary barriers.

The assessment of reservoir quality across the basin also provides value through excluding the presence of zones with anomalous porosity-depth relationships (Bloch et al., 2002) where the formation of fluid inclusions could be curtailed. Recognition of zones with anomalously low porosity-depth trends could imply inhibition of diagenetic cementation due to high pore pressure (i.e. Ramm and Bjørlykke, 1994; Taylor et al., 2010), widespread secondary porosity development (i.e. Bjørlykke, 1984; Giles et al., 1986) or the presence of grain coats (i.e. Ehrenberg, 1993; Aase et al., 1996; Taylor et al., 2010) that act to retard the crystallisation of authigenic minerals, including those that might contain fluid inclusions. Similarly zones that are anomalously cemented may act to preclude the entry of hydrocarbons where diagenetic cementation precedes the timing of hydrocarbon emplacement.

3.4 SUMMARY

The stratigraphy of the Vulcan Sub-basin can be effectively sub-divided into Pre-, Syn- and Post-rift megasequences and the composition of the sediments changes from dominantly clastics in the Pre- and Syn-rift section to predominantly carbonate in the Post-rift section.

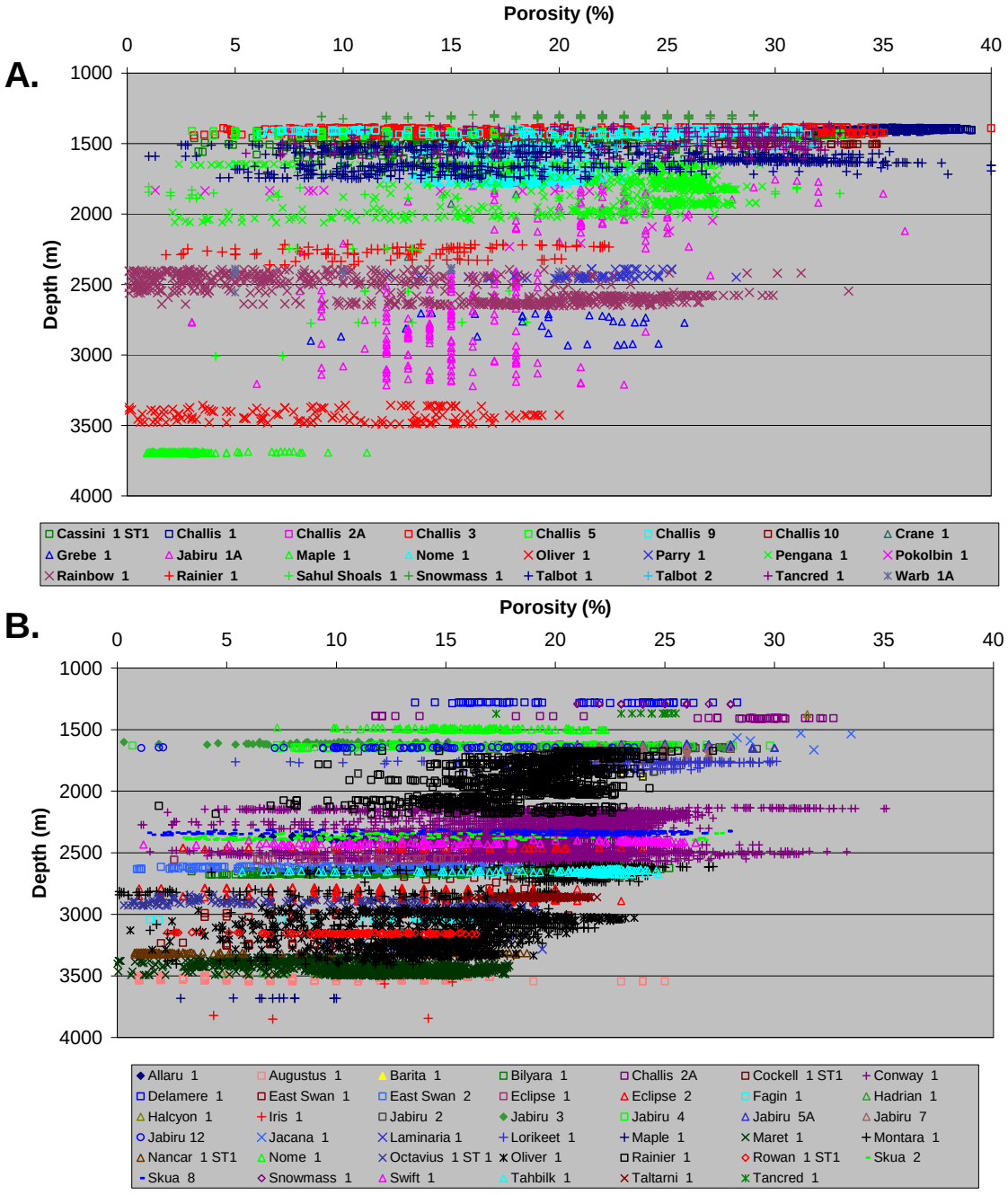

Figure 3-15: Porosity versus depth graph for Triassic (A) and Jurassic (B) reservoirs.

Data are shown for all VSB wells available in the RESFACS database as at 2004 and are displayed by well name. A clear trend of reducing porosity with depth can be observed with the large spread reflecting inclusion of both reservoir and non reservoir lithologies. Data derived from core analysis, testing data (RFT, MDT) and interpretation of wire-line petrophysical logs.

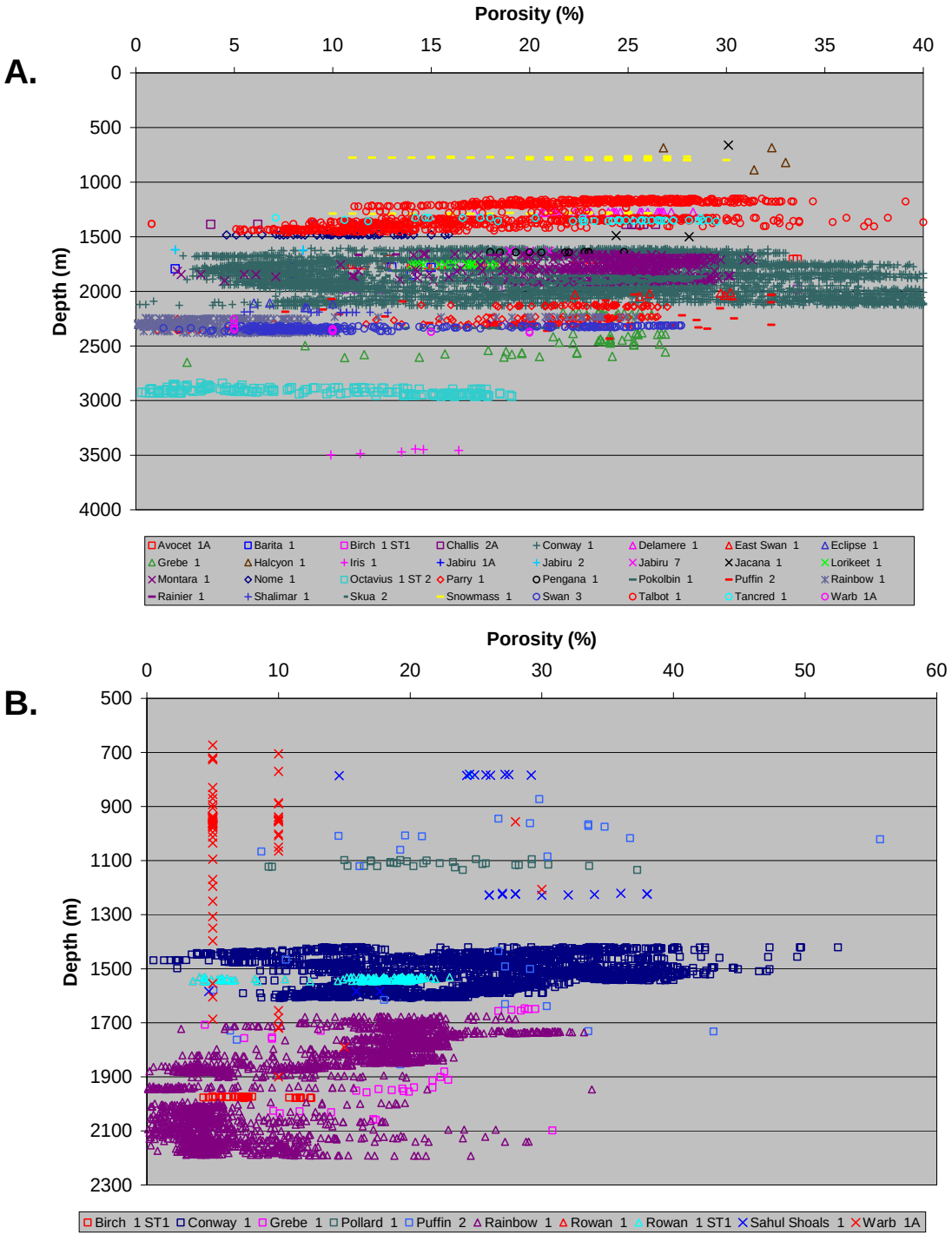

Figure 3-16: Porosity-depth graph for Cretaceous (A) and Tertiary (B) reservoirs in the VSB. Data are shown for all VSB wells available in the RESFACS database at 2004 and are colour-coded by well name. An overall decline in porosity with depth is apparent but less well defined that seen in the Triassic and Jurassic reservoirs shown in Figure 3–15. Data derived from core analysis, testing data (RFT, MDT) and interpretation of wire-line petrophysical logs.

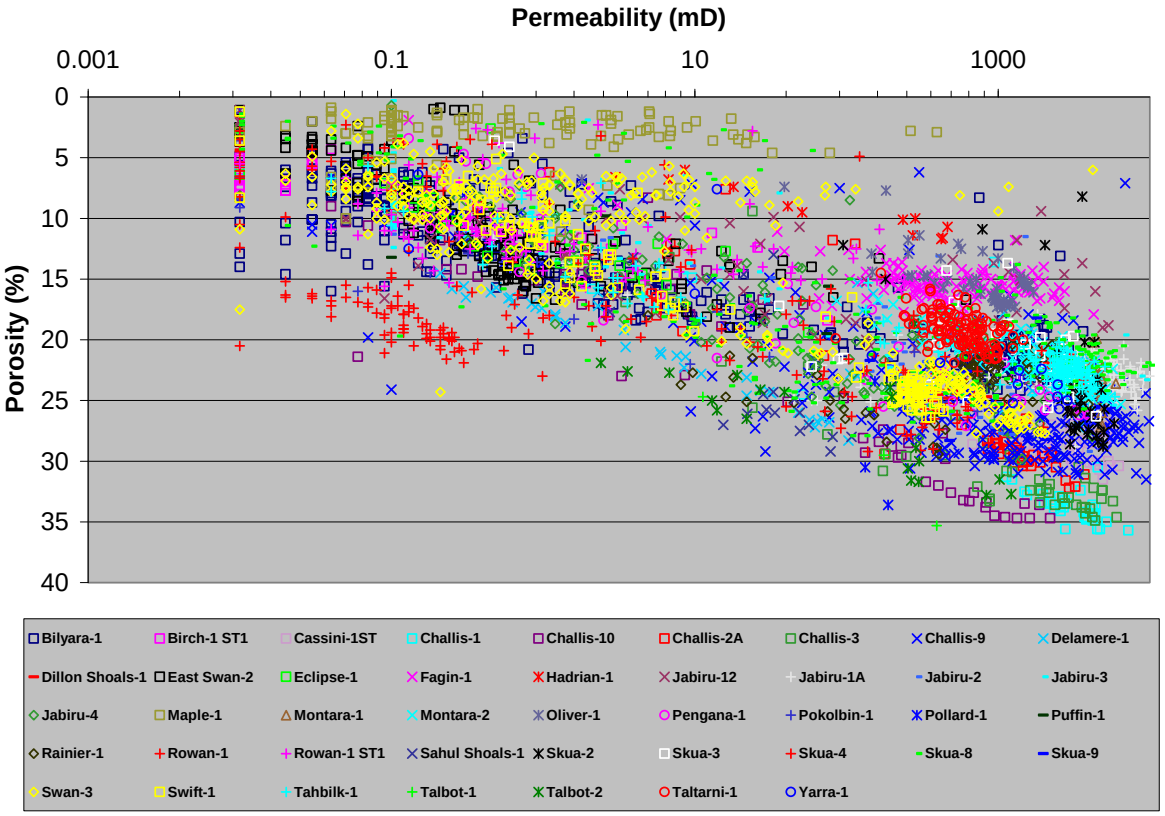

Figure 3-17: Porosity versus permeability graph for all core analysis data from the VSB.

Data are shown for all VSB wells available in the RESFACS database at 2004 and are colour-coded by well name. A good relationship between porosity and permeability is apparent and suggests that porosity data represents a reasonable proxy for the permeability range that could be expected at any particular depth.

Within the Pre- and Syn-rift section reservoir facies are exclusively comprised of clastics that vary in detrital composition from quartz arenites to sub-arkose sandstones. They are typically coarser grained and dominated by quartz in the Jurassic section, with finer grain sizes and increased feldspar content recorded in Triassic sediments. The Jurassic and Triassic rocks and moderately well sorted.

Reservoir units in the Post-Rift megasequence are dominantly quartz-rich and represent episodic returns to clastic sedimentation associated with periods of relative sea-level fall that allowed re-working of older sediments into deep water as slope channel or basin floor fans. The reservoir sediments show variable grain-size and are generally more poorly sorted than the Pre- and Syn-Rift units.

Diagenetic alteration of the sandstones is relatively minor, except below about 3km, and is dominated by clay authigenesis and quartz overgrowths in the Pre- and Syn-rift units and sporadic, but locally pervasive, carbonate cements in the Post-rift reservoirs. A relatively consistent paragenetic sequence can be recognised with early glauconite, carbonate and pyrite phases preceding clay authigenesis predominantly involving kaolinite, that are in turn enclosed by quartz overgrowths and subsequently overgrown by ankerite cement and in more deeply buried samples, filamentous illite. A review of the available petrographic reports taken from well completion reports do show some variability in their reported paragenetic sequence but largely these reflect difficulty in observing unique timing relationships. Preference has been given to the interpretations of those petrographers that consistently show agreement with the observations made on the samples analysed in this study and that suggest a similar approach has been taken in terms of the criteria used to assign the relative timing of authigenic mineral from petrographic observations.

Porosity and permeability data from the key reservoir horizons show similar trends of decreasing porosity with depth and a moderately strong correlation between porosity and permeability. Overall the data suggest that suitable porosity and permeability to reservoir hydrocarbons has been maintained within the depth range of the samples analysed and that overall diagenesis has played a relatively minor role in controlling reservoir quality. Instead reservoir quality is more strongly controlled by variations in detrital composition (i.e. percent shale and detrital clay content) than

from the effects of diagenesis. Consequently where clean sandstones exist they typically have retained effective porosity and permeability irrespective of the degree of diagenesis.

Despite the relatively limited diagenesis experienced by the majority of these samples diagenetic minerals with a suitable framework crystal structure needed to trap fluid inclusions occur in sufficient abundance to allow for a viable fluid inclusion study to be conducted. No evidence to support anomalous porosity preservation was observed suggesting these units have experienced normal depth-dependant porosity loss.

Fluid inclusions within the most recently formed minerals will be of greatest value to this study as their formation coincides with the likely timing for the introduction of hydrocarbons into the system. Also a consequence of studying late formed cements it that is more likely that the abundant core analysis data available to constrain reservoir quality observed at the current day will be representative of conditions prevailing when fluid inclusions were being trapped by these cements.

Overall the nature of the sediments available to this study are well suited to a detailed fluid inclusion investigation and will provide excellent constraints with which to place the fluid flow events recorded in the fluid inclusions in both a relative and absolute time sequence at multiple reservoir levels.

4. EVIDENCE FOR HYDROCARBON CHARGE

4.1 INTRODUCTION

The supply and accumulation of hydrocarbons within reservoir rocks is a process commonly referred to as hydrocarbon charge. This process is seldom fully understood, with considerable uncertainty about the timing, source, and phases of hydrocarbons involved, even where a discovery has been made. This reflects both a lack of suitable methods to unequivocally characterise the origin and timing of fluids contained in hydrocarbon-filled reservoirs and a paucity of tools to appraise palaeo hydrocarbon charge to reservoirs that are now water-bearing. This latter deficiency is particularly restrictive given that exploration drilling contributes many more failures than successes (typically a ratio of 10:1), making it imperative to fully evaluate all wells, not just those that were successful in delineating hydrocarbon accumulations.

In most cases information on one or several of the critical elements that control the supply and accumulation of hydrocarbons is incomplete and must be assigned a likelihood of being present. For the past 20 years petroleum exploration companies have commonly utilised probabilistic risking methods (Rose, 1987, 1999; Otis and Schneidermann, 1997), conditioned by available measurements, to assess the likelihood that each of these critical elements is present and effective. In reality, however, this approach is commonly much too simplistic to effectively characterise the variability of the natural system and as a result only poor control on many of these key issues is typically achieved by explorers.

Substantial advances in the numerical modelling of hydrocarbon migration, increasingly utilising sophisticated 3D computer simulations (Duppenbacker et al., 1998; Hantschel and Kauerauf, 2009), provide potentially accurate predictions, but the veracity of these outcomes is ultimately controlled by the quality and frequency of the control points that provide the hard data to calibrate these forward models.

An important consideration in the choice of suitable methods used to appraise hydrocarbon charge is the recognition that these events began in the geological past.

Whilst hydrocarbon charge may be continuing at the present day, the key elements needed to appraise the geographic extent and effectiveness of the process require integration of incomplete fragments of information that are retained in the geological record. Petroleum systems are continuously evolving. Hydrocarbons are commonly trapped and then lost and are constantly being modified by the surrounding environment and the geological history. Modifications can occur due to trap breach, in situ alteration through biodegradation or water-washing or changes in trap configuration due to structural movements.

The distribution of known oil and gas accumulations must be supplemented by considering the presence, frequency and significance of residual hydrocarbon shows. These residual hydrocarbons can reflect either migration of hydrocarbons without accumulation, the remnants of a prior accumulation that has subsequently been lost or even contamination from hydrocarbons used to facilitate the drilling of the well, particularly where oil-based drilling muds are employed (Hart and Fisher, 1998).

Differentiating between migration without accumulation and migration leading to accumulation is vital to appraise the significance of hydrocarbon shows detected during drilling or by subsequent analysis of recovered samples of rock or fluid. This has, however, been difficult due to the reliance on the qualitative methods that have routinely been used as the principal way of addressing this important question.

In this study an assessment of hydrocarbon shows, provided through an integration of residual oil and gas indications and non-conventional hydrocarbon shows provided by fluid inclusion data are used to provide a more complete record of the filling history of hydrocarbon traps in this region (Lisk et al., 1998a). A key delivery from this integrated approach is an enlarged footprint of investigation achieved by removing the reliance on assessment of intact hydrocarbon columns that are typically few in number compared with the total number of wells drilled. Instead, the hydrocarbon charge history of a much larger number of wells, comprising both hydrocarbon-bearing and water-wet reservoirs, has been completed and this enables a more robust assessment of the charge risk.

4.2 PREVIOUS STUDIES

Information on the hydrocarbon charge history of the Vulcan Sub-basin existing prior to the current study largely resides within well completion reports and is limited to interpretation of conventional oil and gas shows.

More detailed investigations (Lisk and Eadington, 1994; Whibley and Jacobsen, 1996) have recognised evidence of prior oil accumulation in some currently water-wet wells from the region and have attributed these indications to trap breach and hydrocarbon seepage. Studies by O'Brien et al. (1996a) incorporated these data and previously proprietary fluid inclusion data to produce a conceptual model to account for fault seal failure in the region.

Throughout the course of completing the current study a number of workers have contributed to the appraisal of charge and retention risks encountered in the region in both related (O'Brien et al., 1998; Brincat et al., 2001; Gartrell et al., 2002) and independent studies (Shuster et al., 1998; Newell, 1999; Cooper et al., 1998; Liu et al., 2003, 2004). These studies, with the exception of the work published by Newell (1999), cite trap breach through late stage fault reactivation as the most likely explanation for the presence of palaeo-hydrocarbon accumulations.

In a departure from the commonly reported trap breach model, Newell (1999) proposed hydrocarbon loss in the Laminaria High from the adjacent northern Bonaparte Basin could be explained through water-washing of initial gas-condensate accumulations alone and that fault seal breach was not required to describe the observed hydrocarbon distribution.

4.3 OBJECTIVES OF THIS CHAPTER

During the course of the current study data produced from the analysis of 74 wells from the Vulcan Sub-basin, combining existing information from fluid recoveries and conventional hydrocarbon shows with fluid inclusion petrographic observations made on 300 core and cuttings samples (Figure 4–1), was used to evaluate the level of palaeo-oil saturation attained as a means of constraining the hydrocarbon charge

history of key reservoirs within the Vulcan Sub-basin. The majority of fluid inclusion samples are new analyses although a small number of measurements were already within the public domain at the outset of this study and provided part of the incentive to initiate this regional investigation.

Documentation of fluid inclusion occurrences within these samples was supplemented by a careful review of well completion reports to obtain information on current fluids derived from conventional hydrocarbon recoveries and shows, fluid analyses, reservoir properties, source rock richness and thermal maturity.

The objective of this new and more comprehensive study has primarily been to increase the breadth of previous investigations (i.e. Lisk and Eadington, 1994; O'Brien et al., 1996a) through collection of a much larger regional dataset for interpretation. The previous studies and those completed throughout the duration of this study provide a variety of models that can be tested by the results obtained in the current investigation.

The specific objectives of the current study are:

- To calibrate the fluid inclusion methods on known hydrocarbon fields and explore the changes to these hydrocarbon columns through time.
- To assess the level of palaeo-oil saturation attained within key reservoir horizons to enable the identification and description of palaeo-oil columns in wells that are now either gas or water saturated.
- Where palaeo-oil columns are recognised, constrain the position of palaeo-hydrocarbon contacts (Palaeo-Gas-Oil Contacts [PGOC] and Palaeo-Oil-Water Contacts [POWC]) and to compare their position with any present day hydrocarbon fluid contacts (Gas-Water Contacts [GWC], Gas-Oil Contacts [GOC], Oil-Water Contacts [OWC]).
- Where data have been collected on multiple wells from the same hydrocarbon trap explore the relationship between wells to test the consistency of the method.

- To better constrain the timing of hydrocarbon charge relative to the history of diagenetic alteration.

- To evaluate the effectiveness of conventional hydrocarbon show data as an indicator of palaeo-hydrocarbon accumulation.

4.4 INDICATORS OF HYDROCARBON MIGRATION

4.4.1 Conventional Indicators

A compilation of direct hydrocarbon shows (ditch gas detection, observed direct or cut fluorescence), indirect petrophysical log evaluation, formation pressure data, physical (API gravity, pour point, viscosity) or geochemical (bulk composition, isotope and biomarker analysis) composition of fluids recovered by testing (RFT, DST, MDT), extraction or retorting commonly represent the conventional types of data that are typically available to allow an assessment to be made of hydrocarbon migration and/or any hydrocarbon accumulation (Schowalter and Hess, 1982).

These routine methods deliver important information to aid the evaluation of the drilling result and in particular to identify zones where high hydrocarbon saturation may exist. Decisions taken to engage in further operations to appraise these zones, such as coring or flow testing, generally rely on obtaining positive indications from the application of these basic techniques. Drilling systems, particularly those with the potential to add hydrocarbon based contamination or to obscure indigenous hydrocarbons through invasion of the reservoir with drilling fluid need also to be considered when interpreting conventional hydrocarbon shows to avoid drawing erroneous conclusions regarding the significance of these observations.

Continuous monitoring of the drilling mud to detect hydrocarbons derived from the formations being drilled (ditch or mud gas; ten Haven et al., 1999, Baker Hughes INTEQ, 1993) combined with regular examination of the rocks retrieved during drilling by the mud logger or well-site geologist represents the first line of available evaluation methods (Figure 4–2).

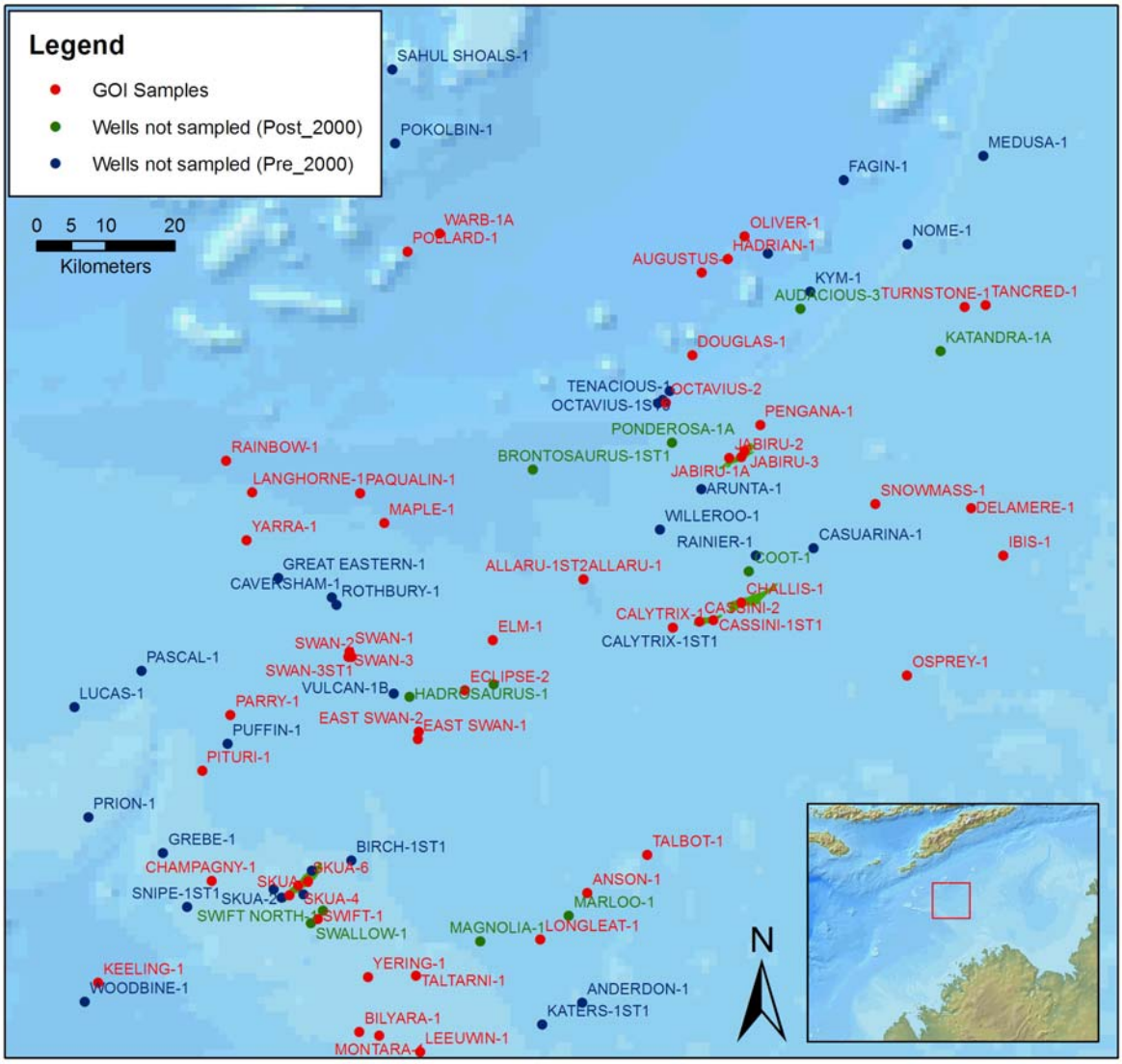

Figure 4-1: Location of wells analysed

Map of the Vulcan Sub-basin showing the location of exploration wells drilled up until 2005. Wells shown in red have been analysed as part of the current study. Wells shown in blue were available at the time samples were taken for this study but were not sampled. Wells shown in green were drilled after 2000 and were not available to this study.

Direct detection of hydrocarbons in the drilling mud is possible using a hot wire detector (mud gas), that together with a well-site chromatograph can provide a basic chemical breakdown of the fluid composition (Baker Hughes INTEQ, 1993).

A variety of petrophysical logs are routinely collected either by wireline logging programs run at the end of drilling or in more recent wells during drilling by Measurement Whilst Drilling (MWD) logs. Both methods provide more detailed evaluation with resistivity logs used to detect zones of more resistive hydrocarbons that contrast the less resistive water bearing rocks (Rider, 1996; Figure 4–3).

Where positive signs of hydrocarbons are encountered a series of additional down-hole wireline tools can then be run to collect information on the reservoir pressure to confirm the presence of a connected hydrocarbon phase, determine the density of reservoir fluids and help to locate the position of the hydrocarbon-water contact (Dake, 2001; Figure 4–3).

Samples of reservoir fluid can then be collected and in recent wells using modern equipment the fluids recovered and measurements made can be extremely representative of the down-hole fluid composition and the ambient reservoir conditions (Fujisawa and Mullins, 2007).

In addition to the disaggregated rock samples that are retrieved as a consequence of the drilling process (ditch cuttings) additional coring programs (conventional core, percussion sidewall core [PSWC] and rotary sidewall core [RSWC]) can be undertaken to retrieve more representative samples of the reservoir. These are examined at the well site for indications of visible hydrocarbons (Figure 4–4) and again under ultra-violet light to detect fluorescence derived from the aromatic fraction of oil that may coat the rock surfaces (Figure 4–5).

In addition to standard well-site methods, techniques that require some processing of samples or data are also widely used (Baker Hughes INTEQ, 1993). These include fluorescence response achieved by directly adding solvent to the rocks (termed cut fluorescence) or by chemical extraction of recovered samples to determine the presence of hydrocarbons that stain the rocks or are trapped within the pore network.

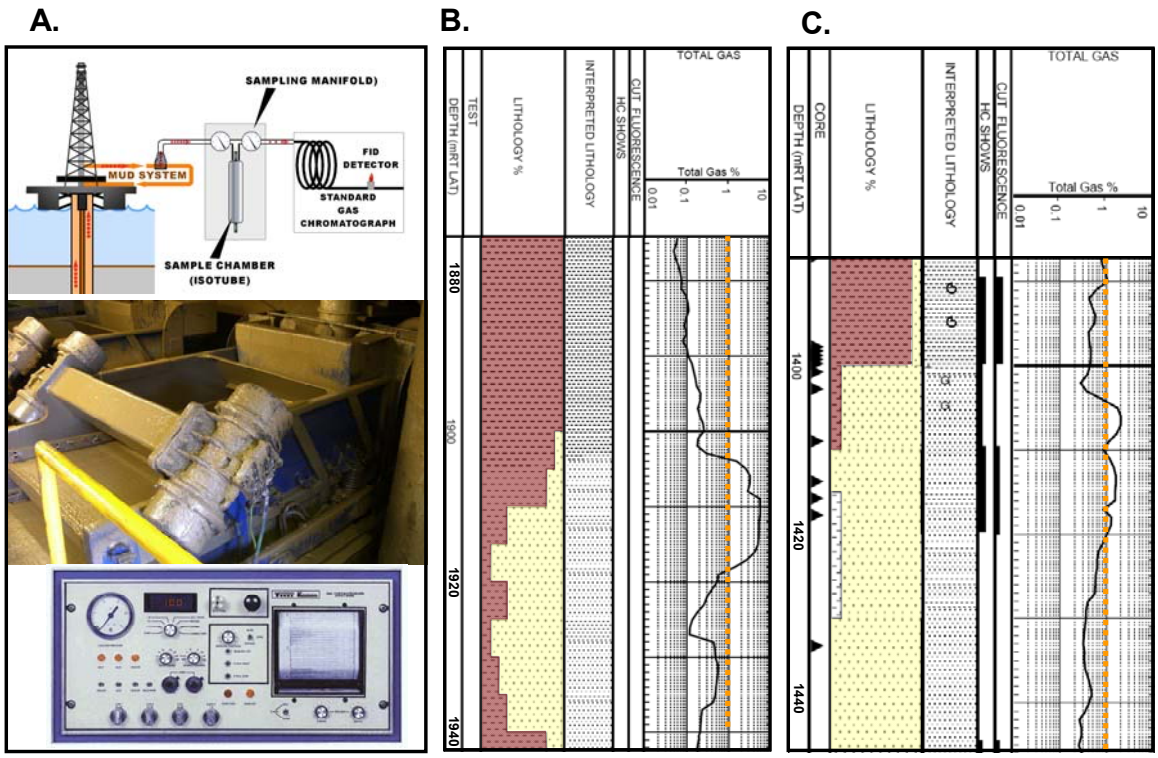

Figure 4-2: Summary of hydrocarbon indications recorded during drilling.

Mud-gas logs are routinely collected during the drilling of petroleum wells and involve placement of detection devices within the stream of circulating mud (A – top). Rock chips (cuttings) held in suspension are retrieved to the surface and can be examined for physical signs of oil as they pass across the shale shakers (A – middle). Hydrocarbons entrained by the mud are detected by a simple hot wire detector and can be analysed by real time chromatography or sampled for analysis back in the laboratory (A – bottom). Examples of a mud-gas profile from an oil discovery (B) and a dry hole (C) are shown to illustrate the increased levels of an oil column compared with a water-wet reservoir with minor hydrocarbon shows.

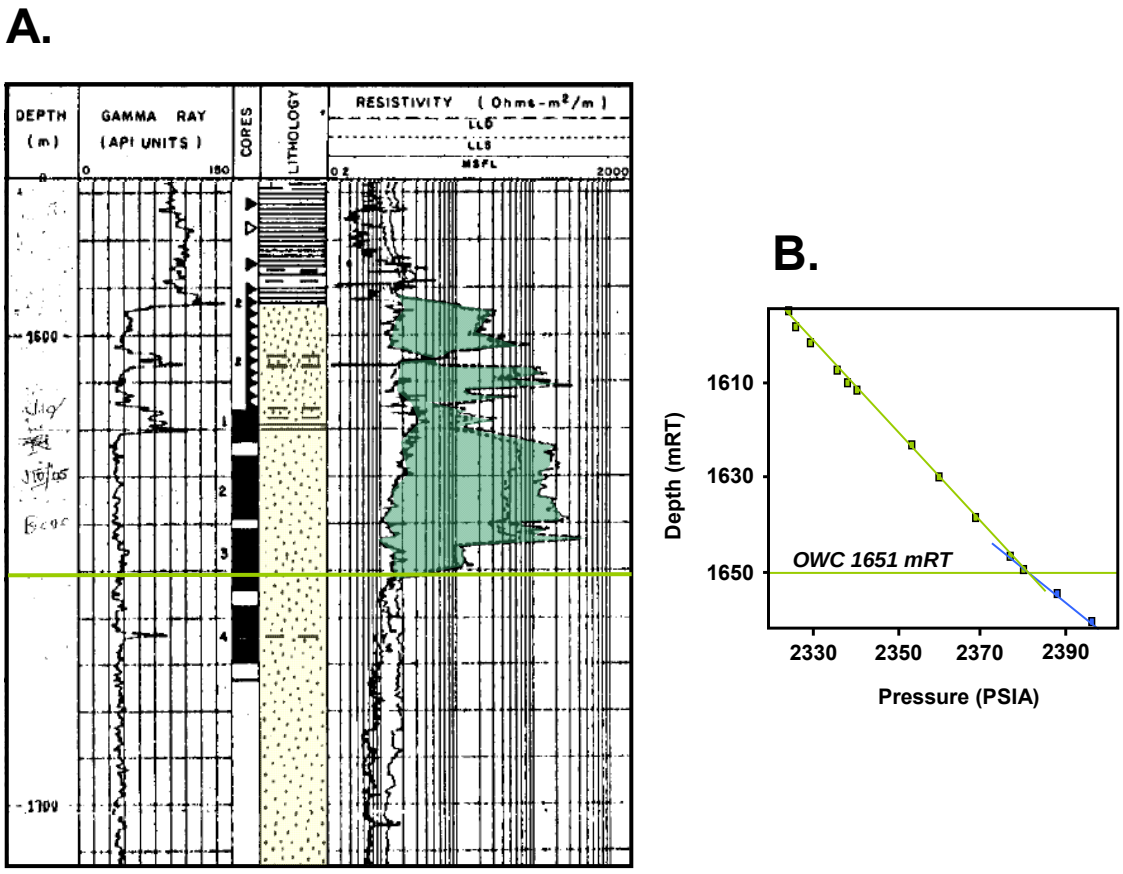

Figure 4-3: Example of resistivity logs and pressure data from an oil discovery.

The Jabiru-1A well shows a significant resistivity increase associated with the presence of an oil column (shaded green). Three resistivity logs, each with a different depth of investigation into the formation are recorded with hydrocarbon pay being recorded on the shallow (LLS) and deep (LLD) logs, whilst the micro-spherically focused log (MSFL) records the resistivity of the mud and filtrate close to the well-bore (A). Hydrocarbons are more resistive the formation waters and produce the separation of the MSFL log from the shallow and deep resistivity logs where water-based drilling fluids have been used. The position of the hydrocarbon-water contact can often be identified where the resistivity logs return to a baseline position in the water-leg below the hydrocarbon column. Down hole pressure measurements are taken to confirm the presence of a connected hydrocarbon zone and to define the location of the hydrocarbon water contact where the fluid gradients for less dense hydrocarbons (green line) intersect the more dense (blue line) formation waters (B).

Despite the value of these conventional methods, their basic nature invariably requires they be subject to assumptions that may not always be valid and hence the results from these methods can be inconclusive or misleading. False positives derived from fluorescence techniques can be related to the presence of thermally mature solid organic matter within the rocks (which may fluoresce on the addition of solvent) or to the presence of anthropogenic hydrocarbons used to facilitate the drilling process. Similarly, wireline logging tools, commonly utilising electrical methods (resistivity/conductivity) require thorough understanding of the properties of the fluids present (both natural and introduced by the drilling mud) and rely on several key assumptions if some of these fluid properties are unknown. Wireline logs also have a relatively limited depth of investigation away from the well-bore so can also be severely compromised if significant drilling fluid invasion has occurred.

Complications introduced by difficult drilling environments can also adversely influence the retention of conventional hydrocarbon shows. In the Vulcan Sub-basin significant geomechanical challenges have often been encountered during drilling that often created technical complications in preserving conventional shows. Poor well bore stability in response to the in situ stress field influencing the region (Hillis and Williams, 1993; Mildren et al., 1994) has proven to be a major impediment to successful drilling and completion operations.

In order to achieve safe and efficient operating conditions increased mud weights (higher specific gravity) have often been employed to stabilise the well-bore. These elevated drilling mud weights (termed overbalance), combined with the high rock permeabilities that typify the key reservoirs, result in significant fluid invasion into the rocks. Various chemical polymers to the water-based drilling muds, as well as the use of oil-based or fully synthetic mud systems are often utilised to combat specific drilling problems (Darley and Gray, 1988; Caenn and Chillingar, 1996).

Whilst these strategies can be effective for improved well control they are rarely ideal for achieving recovery of uncontaminated samples leading to a degradation of the conventional shows in the reservoir rocks due to flushing and produce equivocal fluid recoveries during subsequent testing.

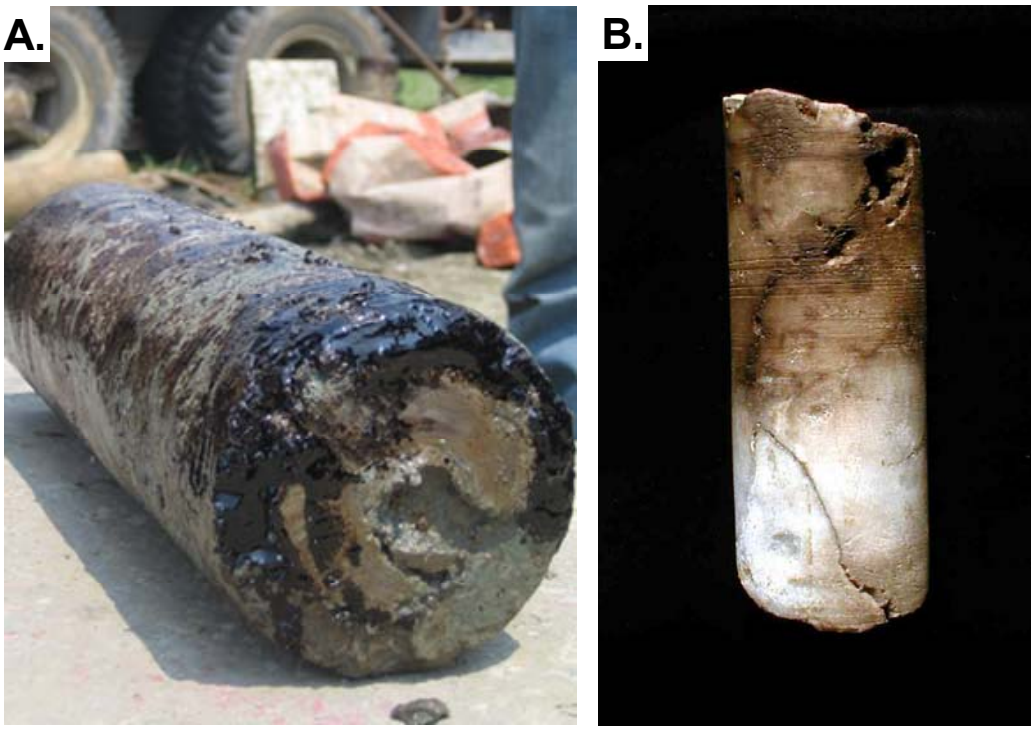

Figure 4-4: Generic examples of oil stained core samples.

Cores retrieved from the reservoir interval can show direct indications of hydrocarbons, in these examples oil bleeding from the core (A) and an oil stained natural fracture (B).

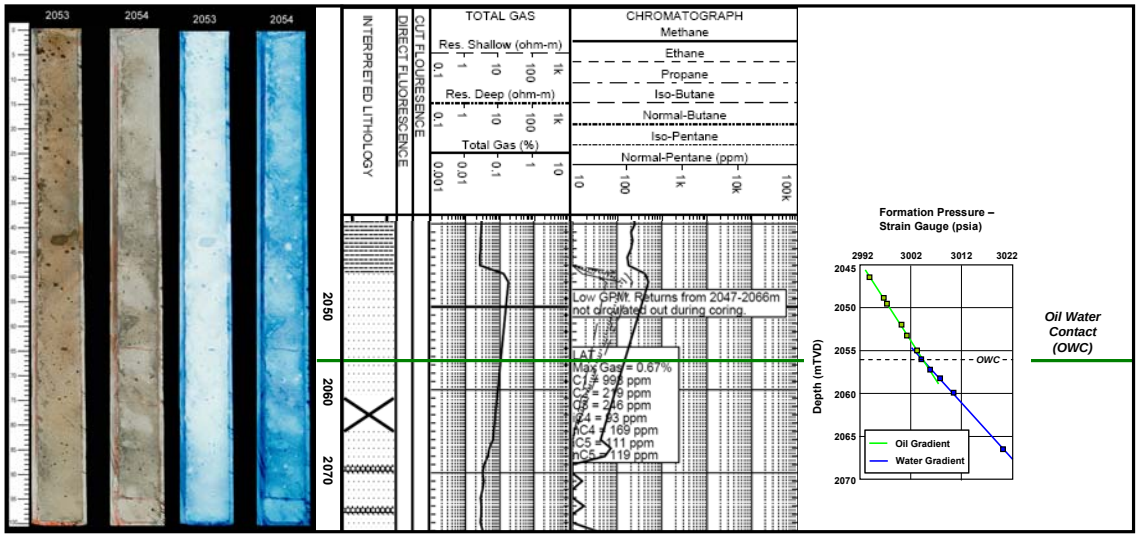

Figure 4-5: Composite diagram showing fluorescing core together with log and pressure data.

Core photographs from the Puffin-5 well showing very bright fluorescence down to 2054m before becoming patchier below 2054m. Pressure data places the Oil Water Contact (OWC) at 2056m. A combination of the patchy fluorescence below the OWC together with the slightly elevated mud-gas response is consistent with the presence of a residual oil column beneath the OWC.

Drilling pipe stuck in the well bore, numerous fishing exercises to recover lost drilling equipment and the frequent use of refined hydrocarbon products required to facilitate such engineering operations have further compounded problems with conventional evaluation methods.

In more recent wells, synthetic oil based mud (SOBM) systems have increasingly been employed to provide greater control on well-bore stability, primarily through improved lubrication and the prevention of clay swelling associated with the use of water-based mud systems. The positive impact on the completion of drilling objectives has, however, been offset by a substantial (or complete) loss of information from conventional hydrocarbon shows due to invasion of the SOBM and contamination of any naturally occurring hydrocarbons in situ within the reservoir.

For wells that fail to intersect a hydrocarbon column the conventional shows observed can often be difficult to interpret in a quantitative manner. Differentiating between wells that have intersected a migration pathway from those that have contained a hydrocarbon column in the geological past is often ambiguous (Figure 4–6). Similarly the lack of any hydrocarbon shows may be the result of the factors outlined above and conclusion about whether the reservoirs have been connected to an effective migration system can therefore be difficult to ascertain in all cases.

4.4.2 Non Conventional Indicators

The failure of conventional methods to provide reliable identification of hydrocarbon indications observed during drilling led to a variety of new techniques being developed to supplement the conventional data, both for application at the well site and for post well analysis in the laboratory. These techniques can augment the conventional data and alleviate uncertainty where an ambiguous result is obtained. Most of these supplementary methods utilise more sensitive detection equipment to identify and characterise residual hydrocarbons using either fluorescence based methods or through chemical extraction and analysis.

Fluorescence based methods utilise sophisticated fluorimeters and fluorescence spectrophotometers to evaluate oil shows during drilling and by laboratory analysis.

Zierfuss and Coumou (1956) developed the first reported commercial fluorimeter that was used to quantitatively characterise fluorescence intensity down hole in petroleum wells. More recently TEXACO has developed a patented proprietary Quantitative Grain Fluorescence (QFT II) technology designed to empirically estimate the attributes of residual oils (Supernaw, 1988).

Extraction based methods require chemical treatment of the samples with solvents to yield a sample for analysis. The Iatroscan thin layer chromatography and flame ionisation detection (TLC-FID) technique has been applied to detect residual hydrocarbons in petroleum reservoirs (Karlsen and Larter, 1989, 1991; Horstad et al., 1995; Bhuller et al., 1999). This method enables extracts to be separated into compound classes (saturated hydrocarbons, aromatic hydrocarbons and polar compounds) to provide a more detailed analysis of the residual oil. Sequential extraction methods that utilise multiple treatments with different solvents have also been utilised to unravel filling histories of petroleum reservoirs that received multiple phases of hydrocarbon (Wilhelms et al., 1996; Schwark et al., 1997).

A major limitation of the extraction-based methods is their requirement for core samples, which are much less common than the ubiquitous cuttings samples collected during drilling. This is particularly the case in exploration wells where conventional cores are rarely taken, and typically require the recognition of good hydrocarbon shows before such expensive operations are undertaken.

The detection and analysis of residual oil, irrespective of the method used, suffers from the need to retain hydrocarbons on the exterior surfaces of the reservoir rocks or within the pore network. Many factors ranging from the drilling method used to the length of storage time can all result in the loss of surface hydrocarbons.

The aforementioned degradation of shows that can accompany the drilling process or storage time is further exacerbated by difficulties in preserving such shows through geological time as signs of previous hydrocarbon migration and/or accumulation.

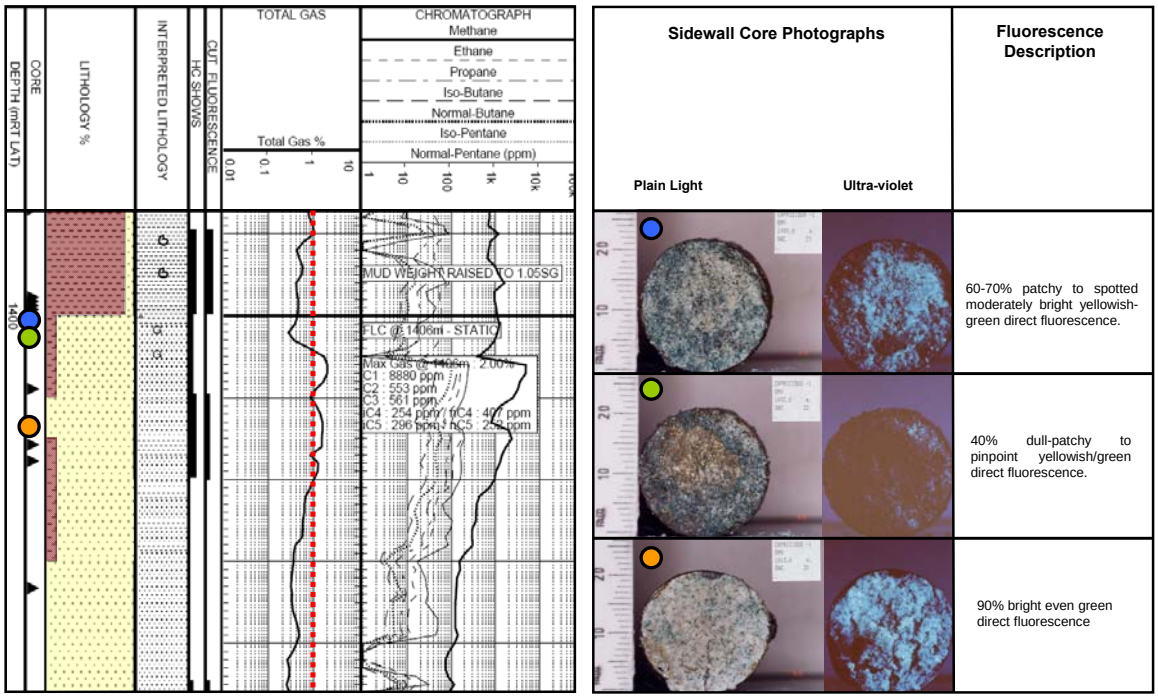

Figure 4-6: Hydrocarbon indications from the water-wet Capricious-1 well.

Hydrocarbon shows from mud-gas levels (left) and fluorescence from sidewall core samples (right) at the top of the targeted reservoir section in the Capricious-1 well from the VSB provide clear indications of hydrocarbons. However, is not obvious whether these relate to migration of hydrocarbons at relatively low saturation or are the residual remnants of a prior oil column that has been breached. Permeability increases encountered as the reservoir section is penetrated can also lead to invasion by drilling fluids that can be mistaken for natural hydrocarbons if oil-based mud has been used to drill the well.

4.4.2.1 Fluid inclusion methods

An alternative type of hydrocarbon show that is impervious to these influences is provided by fluid inclusions that are sealed from the pore network (Murray, 1957; Burruss, 1981; McLimans, 1987; Goldstein, 2001).

Fluid inclusions are small volumes of palaeo-formation fluid encapsulated in crystallising cement (Figure 4–7). Framework silicates and carbonate minerals such as quartz, feldspar and calcite may contain fluid inclusions. Fluid inclusions can contain samples of any fluid that has come in contact with the rock constituents throughout their geological evolution.

In diagenetic minerals they commonly range in size from 5-40 microns but are mostly range from 5-10 microns corresponding to ~3 picolitres of preserved fluid in each inclusion.

Hydrocarbons trapped within fluid inclusions represent a direct sample of reservoir fluids that are time-specific to the migration event (Eadington et al., 1991). Unlike other types of hydrocarbon show, preservation of these unconventional (or hidden) shows is generally excellent, since they are sealed from the pore network and cannot be easily removed or contaminated by subsequent changes in the reservoir fluid that occur naturally, or by the drilling process and/or subsequent storage conditions.

Fluid inclusions in sedimentary rocks may be formed in either of two ways:

1. The formation of a diagenetic mineral with a framework lattice allows samples of fluid in the adjacent pore space to be entrained during the crystallisation of the host mineral.

2. The propagation and healing of fractures in detrital or pre-existing diagenetic minerals in response to simple burial compaction.

For the first mechanism to be useful for hydrocarbon evaluation these fluids need to be present in the adjacent pore space at the same time as the host mineral is

crystallising. A common misconception is that oil inclusions are only trapped by the contemporaneous growth of suitable authigenic mineral cement within the pore space containing the oil. As a consequence it is often presumed that the fluid inclusion record is fortuitous in nature and hence only useful in limited circumstances.

However, the propagation and healing of fractures caused by burial compaction (either in detrital or pre-existing diagenetic minerals) provides an additional mechanism that is more likely to occur repeatedly over a longer time period.

This is a dynamic process, in which fracturing creates a large pressure draw down between the open fracture (at low pressure) and the adjacent pore space (at reservoir pressure). Draining of fluid from the pore space into the fracture plane is actively driven by this large pressure differential making this process an efficient mechanism for the sampling of reservoir fluids by the formation of fluid inclusions and provides a more continuous record of hydrocarbon migration.

Once fluid is drawn into the fracture plane localised (pore scale) pressure solution provides sufficient solute to facilitate healing (cementation) of these micro-fractures and allow hydrocarbons to be sealed from the pore network. Trails of fluid inclusions marking the position of these sealed microfractures in these detrital and authigenic minerals (Figure 4–7), provide evidence of fluid being drawn into fractures from the surrounding pore space. These observations demonstrate that the pressure differential produced when a fracture is first propagated exceeds the high capillary forces acting to inhibit ingress of fluid into such small fractures.

Investigation of fluid inclusions has historically involved petrographic methods (Burruss, 1981; Roedder, 1981; Goldstein and Reynolds, 1994). Inclusions that trap oil are easily identified in petrographic thin section by the fluorescence emitted from the aromatic fraction of the oil under violet and ultra-violet fluorescence illumination (McLimans, 1987).

More detailed examination of the emission spectra of fluid inclusion oils (e.g. Kihle, 1996) has been used to constrain the properties of the trapped oil, particularly the maturity (Tsui, 1990) or API gravity (Hagemann and Hollerbach, 1985).

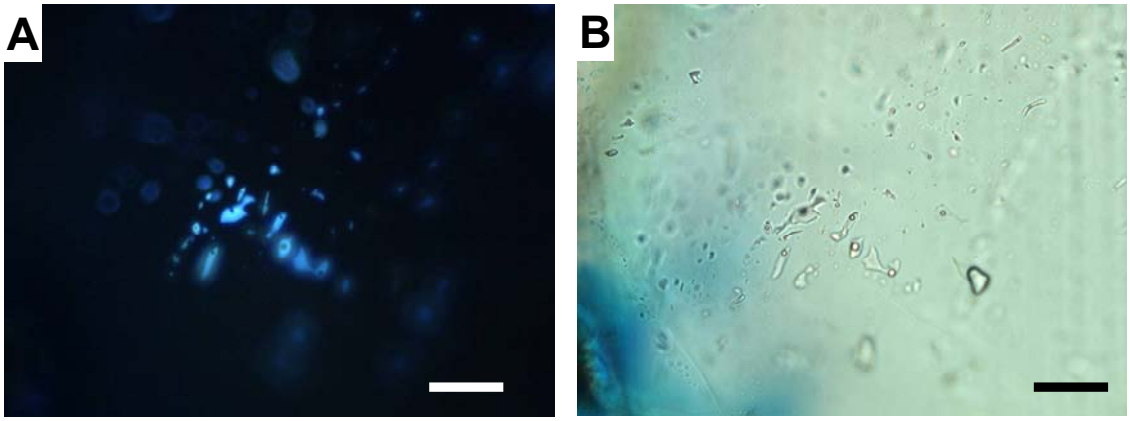

Figure 4-7: Photomicrographs of oil filled fluid inclusions from the VSB

Typical examples of two-phase fluid inclusions trapped on along the trace of a healed fracture plane within a detrital quartz grain. The individual inclusions have irregular shapes and mostly contain a circular contraction bubble that forms in response to a fall in pressure as the sample is retrieved to the surface. The two images are of the same sample, taken under UV fluorescence (A) and plain polarising light (B), with the fluorescence derived from excitation of aromatic compounds within the oil. Scale bars indicate 25 microns. Eclipse-1 2733-36m cuttings sample.

Inclusions that trap gaseous hydrocarbons are more difficult to identify by optical methods that rely on subtle differences in refractive index to differentiate a gas phase from the epoxy resin. Bubbles trapped in the epoxy during the manufacture of the thin section can be easily mistaken as genuine fluid inclusions by the novice. The identification of hydrocarbon gas inclusions is further complication by the variety of non-hydrocarbon gases that can be present in fluid inclusions that are inherited from the provenance of the detrital grains. Typically spectroscopic methods such as Raman spectroscopy (e.g. Burke, 2001) or Fourier Transform Infrared Spectrometry (e.g. Pironon, 1992) are required for *in situ* analysis of gas-filled fluid inclusions as these can reveal compositional information not easily obtained by other methods.

This study primarily utilises petrographic based fluid inclusion methods, however, the extraction and chemical analysis of fluid inclusions using chromatographic and mass spectrometry techniques are increasingly being used to more fully evaluate fluid inclusions (Karlsen et al., 1993; George, et al., 1997; Hall et al, 1997; Barclay et al., 2000). A disadvantage of the bulk inclusion extraction nature of these methods relates to the inability of such methods to distinguish multiple fluid inclusion assemblages and therefore they typically represent 'blind' geochemical techniques that invariably average the different populations present in any one sample. Nevertheless, these methods often provide a different type of information that can be readily incorporated with conventional petrography data to produce a more comprehensive examination of the fluids contained within the inclusions.

The detailed compositional analysis of single fluid inclusions remains more difficult (Barker and Smith, 1986) and although not routinely attempted methods to derive both molecular compositional data (Greenwood et al., 1998; Hode et al., 2006; Volk et al., 2010; Siljestrom et al., 2010) as well as PVT conditions existing at the time of entrapment (Thiery et al., 2002; Dubessy et al., 2001; Pironon et al., 1998; Munz et al. 2004; Teinturier et al., 2002) have been developed for individual inclusions.

These more sophisticated methods augment the relatively simple information that can be gained from standard fluid inclusion thermometric methods (Roedder, 1984) that utilise phase change observations to identify the type of fluid trapped and in the

case of aqueous fluids the bulk salinity can be determined from measuring the depression of ice melting point (discussed later).

The fluid inclusion methods utilised in the current study include two new methods; the Grains with Oil Inclusions (GOI) technique (Eadington et al., 1996) and the Molecular Composition of Inclusions (MCI) technique (George et al., 1996). These are incipient techniques that have continued to be developed since the inception of this project, itself representing one of the first regional applications of these new tools to the assessment of hydrocarbon charge and retention history.

4.5 PALAEO-OIL SATURATION FROM FLUID INCLUSIONS

The observation of oil inclusions in rock samples has previously been used to identify the presence of migration pathways for oil and to constrain the timing and phases of oil migration relative to the formation of authigenic minerals (Burruss, 1981, 1984; Roedder, 1981; Goldstein and Reynolds, 1994).

That the abundance of oil-filled fluid inclusions can reflect the relative oil saturation obtained in sandstones is a relatively new observation (Lisk et al., 1993, Nedkvitne et al., 1993) and represents a significant advance in the application of fluid inclusion data to studies of hydrocarbon charge.

At least two quantitative methods for measuring oil inclusion abundance have been published. These are:

1. Grains with oil inclusions (GOI) method (Lisk and Eadington, 1994)

2. Absolute abundance method (Oxtoby et al., 1995)

Whilst seeking to reveal the same information these methods differ fundamentally in the manner in which they measure oil inclusion abundance. The absolute abundance method, whilst not fully described in the literature, produces estimates of the total number of oil inclusions in each sample, whereas the Grains with Oil Inclusions (GOI) method estimates the percentage of quartz and feldspar grains that contain oil

inclusions. In this study, the patented GOI technique (fully described in Eadington et al., 1996 and below) has been used.

4.5.1 The GOI technique

The GOI method is a simple petrographic technique used to describe the frequency of oil inclusions within sandstones and relate this abundance to the level of oil saturation attained by comparison with an empirical database of such numbers from known oil fields. This patented method (Eadington et al., 1996), whilst straightforward in nature, is fundamentally different to other fluid inclusion based techniques (both petrographic and chromatographic) in how inclusion abundance can be linked with fluid saturation.

4.5.1.1 Theory

In sandstones the presence of oil inclusions within framework minerals indicates that at least one of the adjacent pore spaces once contained oil. Migrating oil that enters a heterogeneous sandstone flows preferentially through the largest pore throats due to differential capillary entry pressures (Schowalter, 1979; England et al., 1987; 1993). If there is no barrier to flow, capillary pressure will confine the oil to the largest interconnected pore network and only a relatively small number of pores will be exposed to oil.

Modelling studies (Dembicki and Anderson, 1989; Hirsch and Thompson, 1995; Thomas and Clouse, 1995; Sylta, 2008) suggest that oil saturations (S_o) on migration paths through heterogeneous porous media rarely exceed 1-2% and that migration stringers are focused within 1-2 metres of an overlying capillary barrier (Dembicki and Anderson, 1989; Sylta, 2008). A consequence of these observations is that only a small number of grains (i.e. those that intersect the migration stringer) have the opportunity to trap oil as fluid inclusions (Figure 4–8) resulting in a much lower GOI value (0-1%). These results also suggest that samples that are not located immediately below capillary barriers are unlikely to contain any oil-filled fluid inclusions. In addition samples located directly beneath oil columns are also unlikely to contain significant numbers of grains with oil inclusions as migration stringers that

fed the accumulation will be located on the flanks of the trap and not in most cases directly below the oil water contact (Schowalter, 1979; Dembicki and Anderson, 1989) unless vertical migration is anticipated.

The higher oil pressures achieved within an oil column, compared with a migration pathway, overcome the capillary pressure opposing oil flow into the smaller pore throats and allow the oil saturation to increase (So = 30-90%). Under conditions of high oil saturation (Figure 4–8) found in a stable oil column, most pores are exposed to oil and correspondingly a high proportion of grains have the opportunity to trap oil as fluid inclusions allowing the GOI value to significantly increase.

Confinement also results in high oil saturation developing over a depth interval as an oil column accumulates. In this instance elevated GOI values should occur over a greater depth interval than the 1-2m anticipated for a migration pathway (Schowalter, 1979; Dembicki and Anderson, 1989; McAuliffe, 1979). The attainment of high GOI values is difficult to envisage in circumstances where the oil saturation is at the level anticipated for a migration pathway as not enough of the pore network ever becomes oil saturated. One exception to this could occur where core samples intersect a migration pathway where minor ponding of oil has occurred. Essentially this occurrence still represents the accumulation of oil, albeit on a small scale, but this possibility should be considered in cases where high GOI values are restricted to a single high GOI sample.

The method of counting grains containing oil inclusions has advantages over methods that record the total number of oil inclusions (Oxtoby et al., 1995) in a specific area or that measure the volume of hydrocarbon fluid that is liberated by crushing a whole rock sample (Barclay et al., 2000; Liu et al., 2003, 2005a) or a subset comprising an isolated mineral concentrate (George et al., 2001a).

Oil saturation measures the number of pore spaces filled with oil. In sandstones the framework grains that border these pore spaces provide sites for samples of the pore fluids to be trapped as fluid inclusions. In this manner, the grains represent proxies for the number of oil filled pore spaced within the pore network, a feature not shared in such a direct way by any other technique.

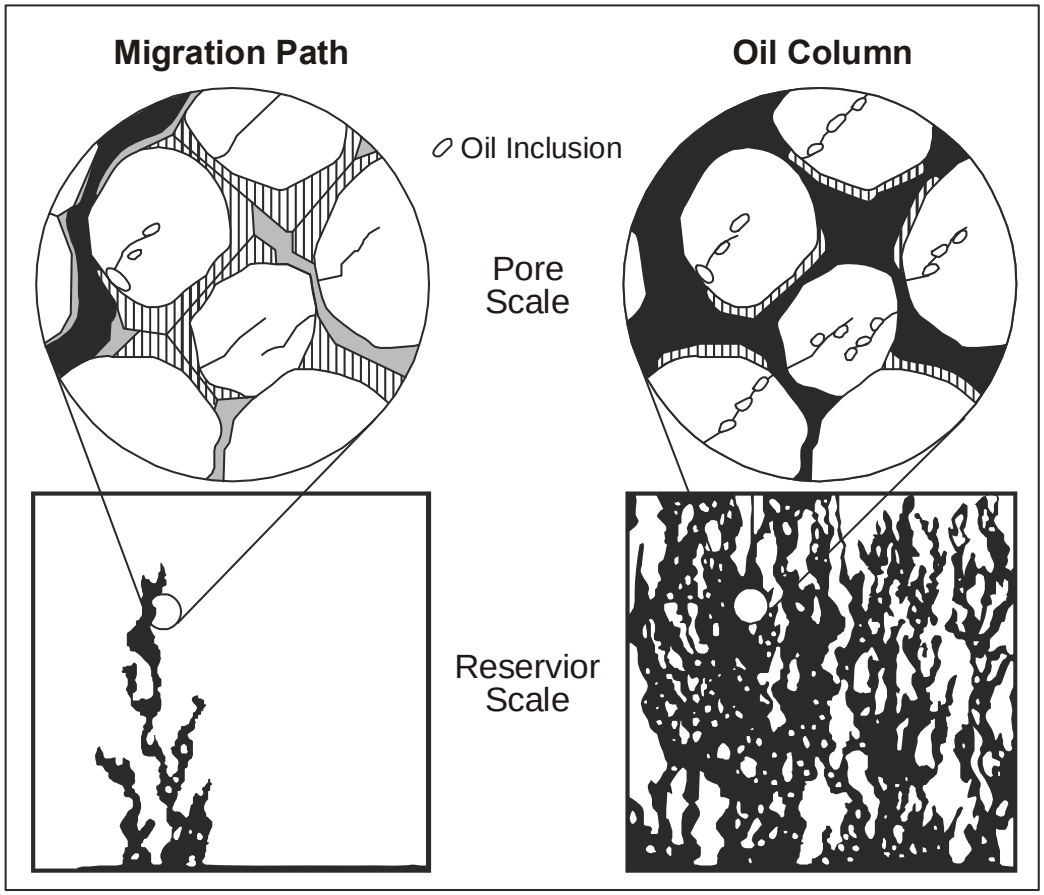

Figure 4-8: Oil saturation attained in a migration pathway compared with an oil column.

The schematic diagram illustrates the role of buoyancy and capillarity forces on controlling oil saturation at the pore scale (from Oxtoby et al., 2005) and the effect this has on the number of grains that have the opportunity to trap oil as a fluid inclusion(s). Where confinement is lacking the oil is restricted to a stringer that is defined by the largest interconnected pore throats and will form a thin (1-2m) migration zone (carrier bed) directly below an impermeable barrier. In this case only a very small proportion (if any) of the grains in a reservoir sample will ever be located close to an oil filled pore and will therefore likely be denied the opportunity to trap an oil inclusion. In contrast, in an oil column confinement (an impermeable top seal coupled with a structural or stratigraphic closure) allows the oil pressure to rise progressively enabling increasingly smaller pore throats to be overcome and the oil saturation increases accordingly. This provides a much greater opportunity for grains that contact an oil filled pore space to trap oil as a fluid inclusion(s). As a consequence GOI numbers are typically an order of magnitude higher in current oil zones compared to current water zones.

The advantage of a grain counting technique over an inclusion counting method can be further demonstrated by the degree of variation in inclusion number and size that is commonly observed. Considerable variability can be observed in the size and abundance of oil-filled fluid inclusions can be seen between different quartz grains. The number of oil inclusions in each quartz grain can be highly variable as can be the size of the individual inclusions (Figure 4–9).

The GOI method treats these different outcomes as the same, indicating that at least one of the pore spaces adjacent to the grain has been oil saturated, irrespective of the number or size of inclusions contained in each grain. In contrast, the volume of oil trapped within each grain can be quite different if there are different numbers of inclusions in each grain. Inclusion size exerts a strong control on the volume of contained fluid; the cube root relationship means that an inclusion with twice the diameter does not equate to twice as much fluid, but rather eight times the volume (George et al., 2001a). Interpreting the significance of these different volume responses is likely to be highly equivocal, but is more probably a reflection of different inclusion trapping efficiencies rather than different levels of oil saturation.

Trapping efficiency will also influence the number of grains containing oil inclusions with some grains being exposed to oil without having suitable conditions (i.e. fractures forming or overgrowths crystallising) to be able to form an oil inclusion. Whilst this effect will also reduce the efficacy of a grain counting method the impact is, however, likely to be less significant for the GOI method than for methods that rely on total inclusion abundance and are hence more sensitive to the effectiveness of the inclusion trapping processes.

4.5.1.2 Oil Inclusion Identification method

A standard Olympus petrographic microscope fitted with a dark field fluorescence attachment (mercury burner) was used to identify oil inclusions in thin section by the fluorescence emitted from the aromatic fraction of the oil under violet and ultraviolet fluorescence illumination (Burruss, 1981).

Excitation was achieved using a fluorescence light with constant wavelengths of about <365 nm (ultraviolet) and <410 nm (violet) with visually observed oil fluorescence (emission spectra) in the fluid inclusions (Figure 4–9) ranging from yellow (peaking at about 550 nm) through to blue (peaking at about 440 nm).

The identification of oil inclusions is relatively straightforward provided that the operator is aware of other fluorescing material that may be present in the sample. This can include diffuse mineral fluorescence, particularly from carbonate minerals or strong bright fluorescence from contaminants such as cellulose fibres or mineral oils that are used in the section preparation process.

Initial observations, considering the location of the fluorescence, enable fluorescing objects that occurs within the epoxy resin or on the surface of the grains to be excluded. Apparent fluorescence can be observed where there is reflection from other fluorescing objects, such as cellulose fibres. Reduction in the iris diaphragm on the microscope and observation at greater magnification are effective ways of distinguishing such effects. It is obviously important to exclude all of these responses to avoid spurious interpretations about oil migration in the examined samples.

Oil-filled fluid inclusions can be identified by a series of characteristic features. The most compelling observation is the combination of bright fluorescence with a moving vapour bubble within the inclusion. Fluid inclusions represent sealed vessels and a vapour bubble forms in response to pressure changes experienced as the sample is retrieved to the surface. In simple terms the fluid contained inside the inclusion shrinks more than the relatively rigid mineral host, with a vapour bubble forming to accommodate the differential contraction.

The observation of an internal vapour bubble is a critical piece of evidence to confirm that the fluorescing object is indeed a sealed capsule. Further confirmation is provided by the occurrence of a moving vapour bubble within the inclusion. The movement relates to Brownian motion caused by surface tension effects inside the inclusion that are related to small thermal gradients produced by the microscope light source (Roedder, 1984).

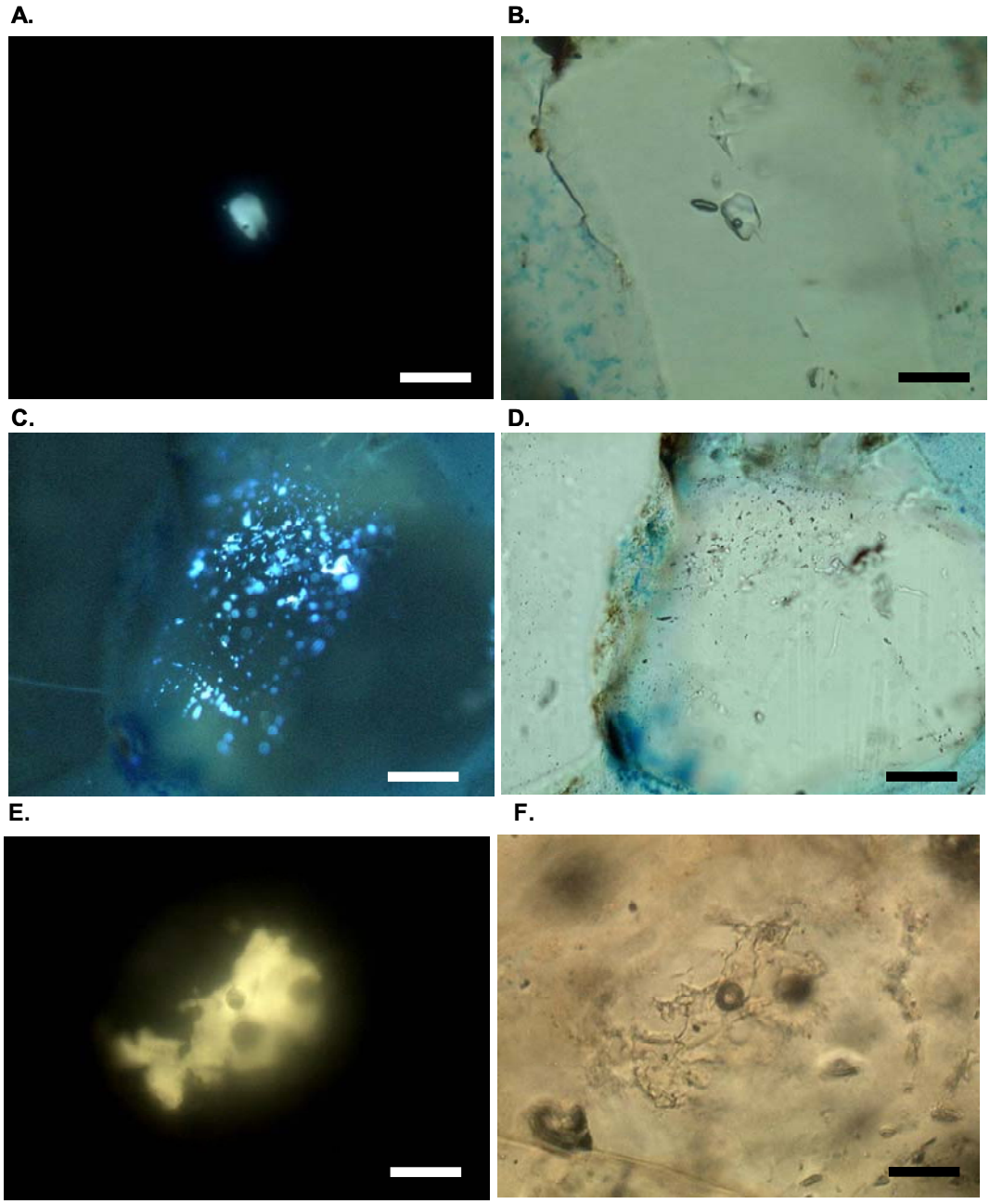

Figure 4-9: Size, frequency and fluorescence colour variations seen in fluid inclusions

A-B. A solitary two-phase oil filled fluid inclusion under UV (A) and plain light (B) showing a pale white fluorescence within a healed fracture cutting a detrital quartz grain (scale bar = 20 microns). Skua-8, 2424-2427 m cuttings sample. C-D. A cluster of two-phase blue fluorescing oil inclusions on healed fractures through detrital quartz (scale bar = 50 microns) under UV (C) and plain light (D). Eclipse-1 2733-36 m cuttings sample. E-F. Large solitary fluid orange fluorescing inclusion on a headed fracture in detrital quartz (scale bar = 20 microns) under UV (E) and plain light (F). Parry-1, 2097-2100m cuttings sample.

Unfortunately not all possible inclusions exhibit such definitive behaviour and other less robust criteria must be considered. A qualitative ranking system has been developed to describe the degree of certainty that can be attached to each observation. As the author has acquired the vast majority of the fluid inclusion petrographic data documented in this thesis, complications that arise when different operators are used (inter-operator variations) have not been considered in this study, but can be overcome by use of standard procedures and calibration samples.

The oil inclusion identification ranking system uses five levels of certainty (highest = 1 and lowest = 5) and relies on a combination of observations in order to attribute a rank to each grain containing oil inclusions observed. The criteria for each rank are:

1. Inclusions show bright fluorescence, a clearly defined moving vapour bubble, distinct outer edge and a lack of birefringence under cross polars.

2. Inclusions show bright fluorescence, a clearly defined stationery vapour bubble, distinct outer edge and a lack of birefringence under cross polars.

3. Inclusions show bright fluorescence, a less well-defined vapour bubble or outer edge and a lack of birefringence under cross polars

4. Inclusions show moderate to weak fluorescence with poorly defined bubble and outer edge with no associated birefringence

5. Inclusions show weak fluorescence with poorly defined bubble and outer edge with associated birefringence.

Inclusions with a ranking of 1 through 3 are including in the final GOI count. Inclusions with a ranking of 4 or 5 are not deemed sufficiently convincing to be clearly attributed to oil-bearing fluid inclusions and as a consequence they are not included in the GOI count. Recording such possible inclusions provides an opportunity to review these occurrences after each analysis (and with a different operator), and if necessary adjust the result.

One feature of the fluorescence observations that results in exclusion of a possible oil inclusion is the observation of birefringence within the inclusion as this indicates the likely presence of mineral matter. The fluorescence in these instances could reflect absorption of oil into clay micro-porosity but may equally be attributed to other factors such as mineral fluorescence. These occurrences could represent evidence of hydrocarbon migration, but due to the significant uncertainty in discerning the source of the fluorescence such indications are also excluded from the GOI count.

4.5.1.3 Counting Method

The GOI method utilises a motorised microscope stage controlled via a computer. A purpose written software program is used to grid the petrographic thin section into individual fields of view with each field of view covering an area of 500x500µm when using a 20x objective lens. This provides about 2000-3000 fields of view for a typical fluid inclusion thin section.

One of two counting protocols are utilised depending on the apparent frequency of oil inclusions observed by cursory examination of the sample under the microscope.

1. In samples with abundant oil inclusions 100 of the total fields of view are selected at random with a count made of the total number of quartz and feldspar grains and the total number of quartz and feldspar grains containing oil inclusions (random scan method). The percentage of quartz and feldspar grains with oil inclusions is the reported GOI value (Eadington et al., 1996).

2. In samples where oil inclusions are uncommon or the abundance remains unclear after cursory examination the thin sections are screened completely with a count made of the number of quartz and feldspar grains containing oil inclusions in the total slide (complete scan method). In samples covered by a complete scan the total number of quartz and feldspar grains was estimated by extrapolating counts of the number of quartz grains in seen in thirty, randomly selected, fields of view. The resultant percentage of quartz grains that contain oil inclusions in each sample is reported as the GOI value (Eadington et al., 1996).

In both counting protocols quartz and feldspar "grains" are taken to be the entire grain, including any overgrowth that is associated with that grain. Other cements that could contain fluid inclusions, principally carbonate minerals, generally lack discrete boundaries and hence are not easily related to the pore network. These minerals are not considered in the GOI count, irrespective of whether they contain oil-filled fluid inclusions or not, but occurrences of this type are recorded in a comments field. In samples where the presence of oil-filled fluid inclusions in these cements represents the dominant occurrence an alternative method that involves recording the presence of absence of inclusions in each field with no reference to a grain count can be employed (i.e. Lisk et al., 1996a). This more simplistic method provides a basic proxy for the GOI method, but lacks the robustness of a grain counting approach. In samples from the Vulcan Sub-basin analysed in this study only a small number of samples contain other suitable inclusion-bearing minerals and in no cases is the reported GOI result affected by the presence of such minerals.

4.5.1.4 Error Determination

The GOI method is applied to core and cuttings samples taken from drill holes that in themselves represent sub-samples of a much larger rock volume. From these samples a further sub-sampling is required to produce a thin section and finally to extract a region of investigation, either as complete or random scans.

The use of random sampling and extrapolation inherent in the GOI method introduces questions about the representativeness of the selection and the impact this has on accuracy of the measurement made on those samples. It is, therefore, important to consider the likely errors that relate to the statistical nature of a partial sample measurement as well as the potential errors introduced by equipment or operator variations. Collectively, these factors can be classified into two general categories: (i) random errors, and (ii) systematic errors (Taylor, 1997).

Random errors are the kinds of errors caused by natural variations. For GOI analyses these are likely to reflect the natural variability of the samples as well as the subjective decisions made by the operator. The significance of random errors can be addressed either by the application of standard statistical tools or through the

completion of repeatability (the ability to replicate a test result using the same materials, personnel and test equipment on the same product in the same test laboratory) or reproducibility (the ability to replicate a test result using the different materials, personnel and test equipment on the same product) experiments.

Two statistical tools are used to partially address random error in GOI analyses. Error relating to the use of a partial sample and extrapolation to achieve a total grain count is given by the *Poisson* distribution:

Error (95CL) = 1.96*SQRT ((TG in AOI)*(TF in AOI)/(TF counted)).

Where CL = Confidence Limit; TG = Total Grains; AOI = Area of Interest; TF = Total Fields of view.

Statistical variance associated with the GOI number, resulting from increases in the total grain count and the number of grains containing oil inclusions is addressed using a binomial function that has the following expression:

Error (95CI) = 1.96*SQRT(GOI*(1-GOI)/TG counted).

The GOI number lies in the interval GOI ±error with a 95% confidence, which approximates to ±2 standard deviations.

The application of these statistical tools to address error is restricted to the assessment of variability introduced by the use of a sub-sampling method. They ignore potential errors relating to factors such as recognition error (incorrect counts of grains or grains with oil inclusions) and detection errors (associated with the operator and the equipment). These can only be addressed through the use of repeatability or reproducibility experiments.

In contrast to random error, systematic errors are errors that relate to bias introduced either by the equipment or analytical method utilised by the operator (Taylor, 1997). Importantly these errors are not addressed by the statistical error functions described above and require the completion of reproducibility experiments to enable their significance to be addressed. For the current study, however, these errors can largely

be ignored due to the use of standard equipment and procedures by a single operator. This does not detract from the value of reproducibility experiment, but these are more vital where comparison of the results against those produced by other operators and using alternate equipment is attempted.

4.5.1.5 Interpretation of GOI data

GOI data are interpreted by consideration of the theoretical saturation profile expected for oil accumulation compared with that predicted for oil migration (Hirsch and Thompson, 1994) and through comparison against an empirical database of GOI data collected from known oil fields (Figure 4–10). As discussed in section (section 4.5.1.1) saturation levels expected for oil migration pathways are likely to be substantially lower than that encountered within a stable oil column. Proportionally this leads to major differences in the GOI numbers recorded in samples from intervals that are (or have been) oil saturated compared with those from migration pathways where only a small fraction of the pore network is exposed to oil.

Sampling of current day oil-fields provides one opportunity to assess the likely differences in GOI numbers from rocks that are presently oil-saturated from those beneath the Oil-Water Contact (OWC) where the oil saturation is currently low. GOI data reported for 23 producing oil fields from Australian sedimentary basins (Lisk and Eadington, 1994; Eadington et al., 1996; Lisk et al., 1998a) reveal at least one order of magnitude difference between samples taken from within current oil zones and samples with demonstrably low oil saturation from beneath the OWC (Figure 4–10). This observation is consistent with the results of analogue reservoir models, which suggest oil migration occurs at low oil saturation (relative to accumulation) and is restricted to isolated pathways which contact as little as 1% of the rock volume (Carruthers and Ringrose, 1997; Sylta et al., 1997; Hirsch and Thompson, 1995).

Eadington et al. (1996) suggested that a GOI value of 5% be taken as an empirical threshold for samples that have been exposed to high oil saturation, whereas values below 1% were likely to indicate zones of oil migration at much lower oil saturation. This threshold captures more than 95% of the GOI values determined for the oil zone samples within this published database. With the completion of a larger GOI sample

set it is likely that further segregation of the oil zone data will become possible. New thresholds (both higher and lower) may for example become necessary to interpret different rock types or other factors such as burial depth, oil chemistry or residence time, but these will likely represent refinements rather than a replacement of the existing interpretation procedure.

The current empirical threshold (GOI = 5%) established from the published oil field GOI data (Figure 4–10) can be used to assess gross palaeo-oil saturation in currently gas or water saturated sandstones as oil inclusions are retained even when oil is subsequently lost from the pore spaces of the rock.

High oil saturation (S_w less than 70%) is inferred for any sample where the measured GOI number exceeds the 5% threshold, whilst GOI values below 1% are attributed low oil saturation (S_w more than 90%) related to oil migration without accumulation.

Where the attainment of high oil saturation is indicated by the GOI data, the position of the palaeo-OWC is defined by a sharp fall in GOI values from above the 5% empirical threshold to values below 1%.

Intermediate GOI values between 1 and 5% occasionally occur, but these can generally be attributed to localised reduction in oil saturation caused by reservoir quality issues, such as advanced diagenesis or lower net to gross levels.

Where cuttings samples are utilised an intermediate GOI value can also reflect bracketing of a hydrocarbon contact with dilution by material from above (palaeo-Gas Oil Contact) or below (palaeo-OWC or) the palaeo-oil zone.

More subtle changes within the oil column, such as variable buoyancy pressure (and hence variable oil saturation profile) within the oil column (i.e. lower at the OWC compared with crest of column) or variations related to different depth of burial, compositional effects (rock and fluid) or other factors such as residence time for oil in the reservoir undoubtedly influence the GOI value, but these are not seen as the first order controls.

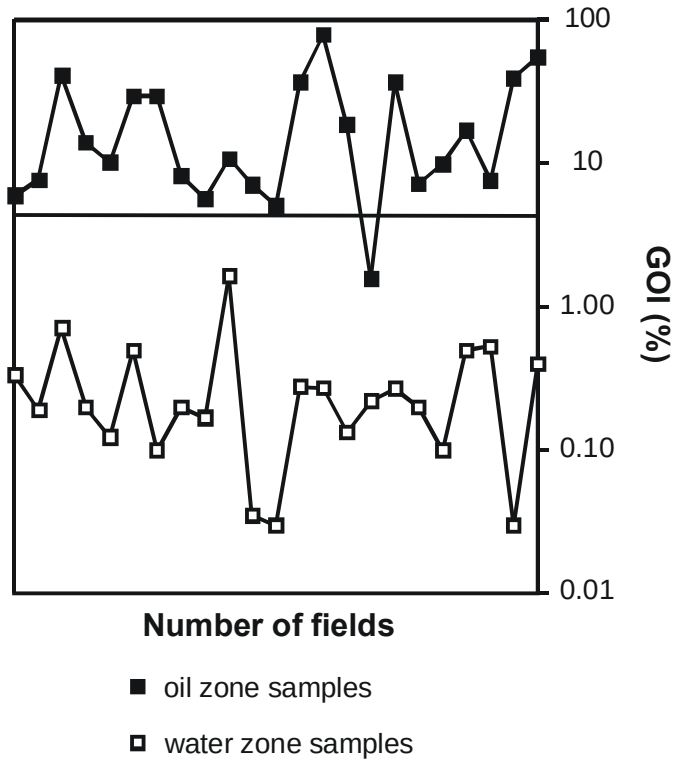

Figure 4-10: Database of GOI data from known oil fields

The graph shows average GOI values for samples from the oil and water legs for 23 oil fields that represented the number of fields analysed as at the completion of the collection of analytical data (ca. 2000). An empirical threshold for high oil saturation is placed at 5%, whilst samples that have experienced low oil saturation mostly fall below 1%.

These secondary factors are, however, likely to represent the principal causes of the significant variations that are recorded in GOI values for samples taken within an oil zone (GOI values 5-95%, Figure 4–10).

Another important aspect of the procedures used to interpret GOI values is the principle that values above the 5% threshold represent positive evidence that high oil saturation was attained, whilst values below this threshold are not considered to be positive evidence that high oil saturation was never attained. Theoretical considerations of anticipated saturation profiles discussed previously make it unlikely that the method would return a false positive result, but many factors have the potential to produce false negative results. Consequently adopting an approach that favours giving relatively more weight to the significance of high GOI values over the low GOI values reduces the likelihood of drawing erroneous conclusions. Equally the interpretation of the GOI results should not be a purely blind process, rather needs to draw on all appropriate sources of information to allow robust geological conclusions to be reached.

4.6 GOI RESULTS

The breadth (73 wells) and scope (300+ samples) of GOI data collected in this study produces challenges for how best to organise the results. A number of possible organisation schemes were considered to best categorise the GOI results obtained, each with some merit and, often equally, problems.

1. Group wells based on access to different source depocentres (oil families).

A genetic classification scheme, based on the recognition of geochemically distinct signatures has previously been proposed as a method to categorise conventional oil shows into discrete oil families (Summons et al., 1998). This 'families' approach could be used for the fluid inclusion results but has limitations for the Vulcan Sub-basin as nearly all of the oils recovered in the area form part of the same petroleum system and this similarity makes it difficult to correctly and unequivocally assign each well to an appropriate sub-set. This problem is further compounded by the

occurrence of oils at different stratigraphic horizons, but that appear to share derivation from a common source rock interval.

2. Sub-divide wells based on litho-, chrono- or tectonostratigraphic position.

Classification schemes based on the location of the samples within genetically related sequences of rock have proved useful in categorising sediment distribution within the Vulcan Sub-basin (Pattillo and Nicholls, 1990), but the application of a similar assignment for the hydrocarbon fluids is compromised by the presence of a common petroleum system and clear evidence for migration and accumulation of compositionally similar oils at multiple stratigraphic horizons.

3. Classify data on the basis of well drilling result.

The assignment of GOI results based on the published well result provides a simple classification system that avoids contentious debate. This approach bypasses conflicting opinion related to assignment of fluids to certain genetic families and biostratigraphic uncertainties that cloud stratigraphically or geochemically aligned classification systems. Option three was deemed the most suitable classification scheme for the GOI results obtained in this study.

From the list of possible drilling results four discrete categories have been used to categorise the GOI results obtained from each well.

These are:

1. Oil Fields

2. Oil fields with a defined gas cap (or gas fields with a defined oil rim)

3. Gas fields with no oil rim

4. Water-wet wells with no confirmed hydrocarbon column

4.6.1 Oil Fields

At the onset of this study in 1998, eight oil fields were known in the Vulcan Sub-basin (Figure 4–11). Three of these fields, Challis, Jabiru and Skua, are economic discoveries that have been producing hydrocarbons since the late 1980s to early 1990s (Northern Territory Department of Regional Development, Primary industry, Fisheries and Resources, 2009). The remainder represent more marginal discoveries that are currently considered sub-economic, due principally to the relatively small oil volume. Six of these eight fields have been sampled in the current study, only the Puffin and Tenacious oil fields have not been investigated.

Much can be learned from these discoveries to better understand the petroleum system and highlight the deficiencies that can be implied from the unsuccessful exploration wells. Firstly, the oil fields of the Vulcan Sub-basin provide key control points for this study, by establishing the applicability of GOI data as indicators of oil saturation where the level of saturation is known. A second, equally important objective is to describe the filling history of each field to understand common controls on oil charge and to investigate how these oil columns have been modified in size and geometry since that initial charge.

4.6.1.1 The Jabiru Oilfield

The Jabiru Field (Figure 4–12), the first commercial oil field in the Vulcan Sub-basin, was discovered in September 1983 by BHP Petroleum Ltd. The discovery well, Jabiru-1A intersected a 57m thick gross oil column that flowed 42.5° API oil from Lower and Upper Jurassic sandstones at flow rates of 6000 STB/D and 3466 STB/D respectively (MacDaniel, 1988).

Fourteen wells have been drilled on the Jabiru field over the period 1983-2000 (Figure 4–12). Initial oil reserves at Jabiru were estimated at 107.2 mmbbls (Cadman and Temple, 2003). Commercial oil production from Jabiru commenced in 1986 and at the end of 2008 cumulative oil production was estimated at 111.3 mmbbls (Northern Territory Department of Regional Development, Primary industry, Fisheries and Resources, 2009).

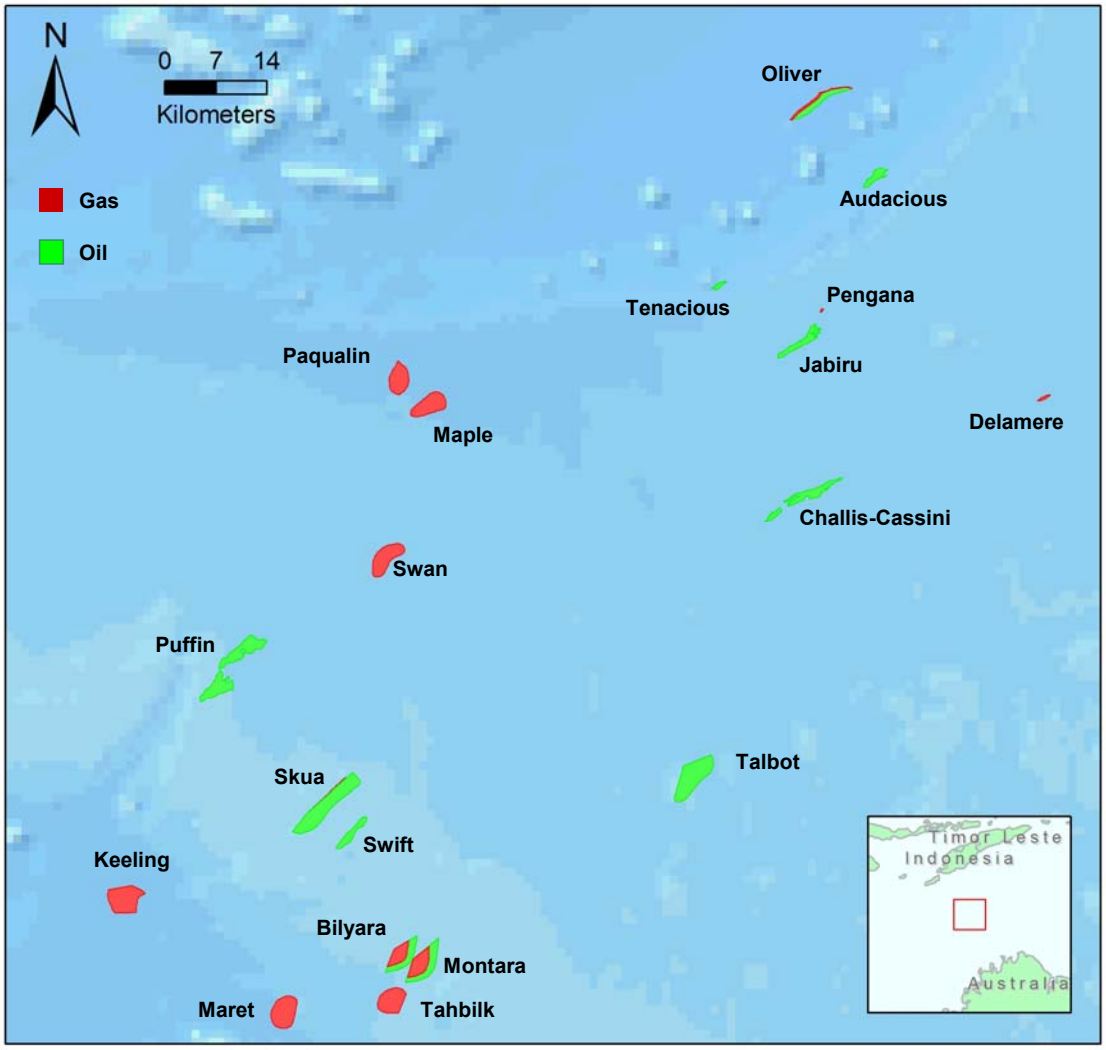

Figure 4-11: Hydrocarbon Fields within the Vulcan Sub-basin.

The map shows the location of oil and gas fields discovered in the VSB up until 2004. The background fill show the general current day bathymetry.

Three wells from the Jabiru field (Jabiru-1A, 2 and 3) have been sampled in the current study. These new GOI results augment previously reported values completed by the author on Jabiru-1 and Jabiru-2 and described in O'Brien et al. (1996a).

The aim of obtaining new analyses was to refine the location of the palaeo-OWC established in Jabiru-1A (O'Brien et al., 1996a). Additionally, the palaeo-OWC was also determined from GOI data in two offset appraisal wells that penetrate the reservoir close to the present field-wide OWC (Jabiru-2 immediately below and Jabiru-3 just above the OWC, Figure 4–12) in order to explore the geometry of the original oil column.

In Jabiru-1A a total of 18 samples were taken ranging from the top of the Jurassic reservoir to about 80m below the current OWC (Figure 4–13). GOI values recorded on samples from within the current oil column range from 3.2% to 68.9%, and with the exception of the lowest GOI value (3.2%, Table 4–1) all values significantly exceed the threshold for oil accumulation (Eadington et al., 1996). The 3.2% value recorded in the 1620.4m core sample (Figure 4–13) falls below the empirical threshold, but this core sample has reduced porosity and permeability compared to the surrounding rocks due to pervasive clay minerals. The reduced GOI value recorded in this sample reflects a zone of non-pay within the oil column due to less permeable rock at this depth, which in turn results in higher capillary entry pressure and a consequent reduction in the level of oil saturation attained at that depth (Lisk and Eadington, 1994).

GOI values above the threshold for oil accumulation continue in samples from Jabiru-1A below the current OWC, over the interval 1665.9m to 1700m, with values ranging from 12.9% to 66.9% (Figure 4–13). A sharp reduction in GOI values from 19.4% in the 1697-1700m sample to 0.4% in the 1712-15m sample (about 50 times lower) is interpreted to reflect a significant fall in oil saturation, consistent with the crossing of an original OWC.

GOI values consistently less than 1% occur in samples taken from 1715-1736 m, consistent with GOI values expected for water zone samples, either taken below an OWC or in samples from an inferred oil migration pathway (Eadington et al., 1996).

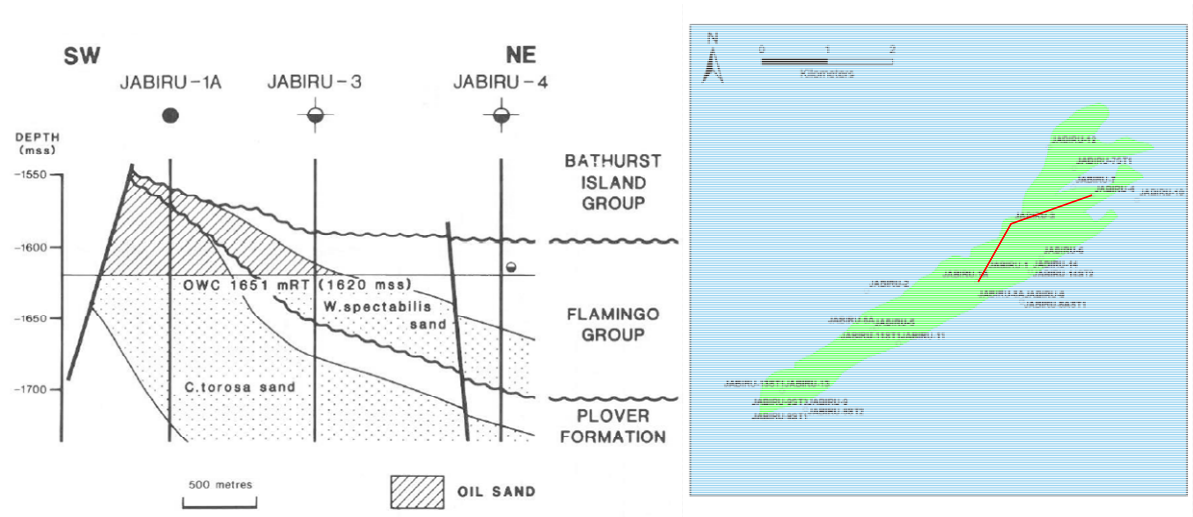

Figure 4-12: Cross section and map of the Jabiru Oilfield.

A cross section (left) of the Jabiru field (from MacDaniel, 1988) with the location of wells indicated by the red line on the adjacent map (right). Position of other wells on the field is shown for reference. The reservoir interval sampled includes the main Plover Formation reservoir (C. torosa biozone) and the younger, poorer quality Upper Jurassic, W.spectabilis (Oxfordian) secondary reservoir interval. Depth shown is in metres sub-sea (mss).

A palaeo-OWC is arbitrarily placed at a mid-point between the deepest high GOI sample and the shallowest low GOI samples (Figure 4–13), defining a palaeo-oil zone, at the Jabiru-1A well intersection, of between 50m and 62m and a total original (palaeo-) oil column height of about 113m.

The conventional oil show, log analysis and mud-gas responses recorded in Jabiru-1A are consistent with the presence of a residual hydrocarbon zone below the current OWC but collectively these data would place the original OWC slightly above that indicated by the GOI data. Percussion SWC samples recovered from Jabiru-1A show patchy dull to moderately bright white to yellow fluorescence down to 1615m with fluorescence being absent in the next deepest SWC sample at 1725m and in all samples from the Jurassic reservoir below this depth. Across the intervening cored section (1615-1673m) uniform bright to dull white to green fluorescence was noted.

Log derived water saturation calculations below the present OWC concur with the oil show data, with calculated water saturation ranging from 74 to 91% down to 1685m and 100% water saturation calculated below 1708.5m (BHP Petroleum Ltd., 1983a).

Total mud gas levels are also consistent with the other hydrocarbon indications, showing a sharp increase at the top of the oil zone and representing the first intersection with the reservoir before falling back to baseline levels near 1675m.

GOI analyses have been completed on 7 samples from the offset Jabiru-2 appraisal well, which intersected the main reservoir horizon deep to pre-drill prognosis and below the current OWC established in Jabiru-1A (BHP Petroleum Ltd., 1983b). Despite the reservoir currently being water-wet GOI values recorded on two of these samples are above the threshold for oil accumulation with values of 6.8% and 6.3% recorded in the 1661-64m and 1679-82m cuttings intervals respectively. A palaeo-oil column of at least 21 m is interpreted on the basis of these results (Figure 4–14).

A significant reduction in GOI values from 6.3% at 1679-82m to 0.8% in the underlying 1689-92m cuttings sample is interpreted to reflect a palaeo-OWC somewhere between these two samples. The next cuttings sample from 1715m returned a low GOI value (<0.1%) and confirms the transition to a palaeo-water leg.

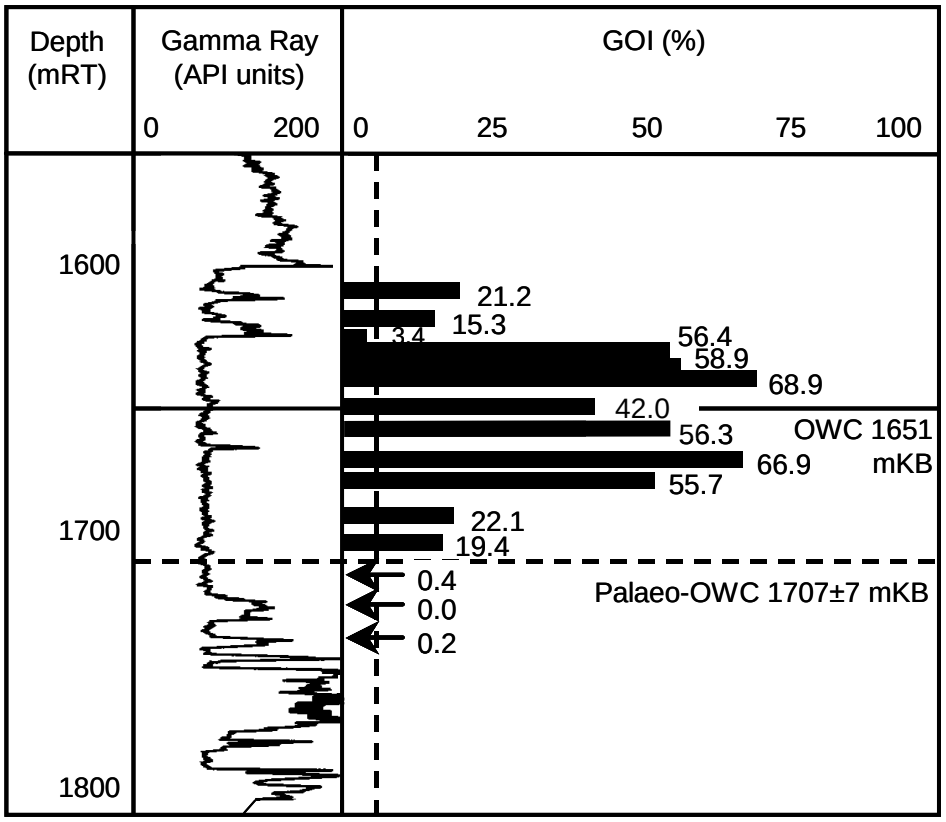

Figure 4-13: GOI results for Jabiru-1A.

Consistently high GOI numbers that are above the empirical threshold for oil accumulation (vertical dashed line at 5% GOI) are recorded in samples from the current oil zone except where reduced reservoir properties are indicated by the gamma ray log. In these intervals lower oil saturation occurs and translates into lower GOI values. High GOI numbers continue below the current OWC before falling sharply from 19.4 at 1700m to 0.4% at 1715m. The position of the palaeo-OWC is placed at the mid-point between these two samples. Depths are shown in metres from the rotary table (mRT).

Table 4-1 GOI Results from the Jabiru Field

Table shows all relevant data for the analysed samples, including depth, sample number and method employed. Abbreviations shown in the location of oil inclusions column refer to Fractures Cutting Detrital Minerals (FCDM) and Quartz Overgrowth Boundary. GOI Error was defined using the method outlined in the text. Numbers shown in the 7 right most columns refer to numbers of grains containing oil inclusions of specific colour or location. Where numbers are absent no measurement was made.

											Fluorescence Colours of Oil Inclusions			Location of Oil Inclusions	
Well Name	Start Depth (mRT)	End Depth (mRT)	CSIRO Number	Sample Type	Counting Method	Number of fields examined	GOI (%)	GOI Error (%)	Total Grains	Grains With Oil Inclusions	Blue	White	Yellow and Orange	FCDM	QOB
Jabiru-1A	1604		122400	cuttings	Random	100	21.25	3.79	447	95	31	55	9	48	47
Jabiru-1A	1613		122401	cuttings	Random	100	15.34	3.84	339	52	40	10	2	24	28
Jabiru-1A	1620.4		75867	core	Random		3.22	1.79	373	12	11	0	1		
Jabiru-1A	1627.7		122192	core	Random	100	56.40	4.61	445	251	232	19	0	99	152
Jabiru-1A	1632.2		122218	core	Random	50	58.88	4.10	552	325	319	6	0		
Jabiru-1A	1637.1		122219	core	Random	100	68.92	4.31	444	306	299	3	4		
Jabiru-1A	1646.4		75868	core	Random		29.68	4.81	347	103	97	4	2		
Jabiru-1A	1650		75869	core	Random	61	42.00	4.73	419	176	164	12	0		
Jabiru-1A	1665.9		122220	core	Random	100	56.25	4.77	416	234	226	6	2		
Jabiru-1A	1676		122221	core	Random	50	66.93	5.75	257	172	158	12	2		
Jabiru-1A	1685	1688	123173	cuttings	Random	100	55.70	10.95	79	44	40	2	2	23	21
Jabiru-1A	1688	1691	122332	cuttings	Random	100	12.93	3.53	348	45	36	4	5	15	30
Jabiru-1A	1688	1691	122222	cuttings	Random	50	22.08	5.25	240	53	41	10	2		
Jabiru-1A	1697	1700	122402	cuttings	Random	100	19.43	3.95	386	75	57	8	10	21	54
Jabiru-1A	1712	1715	122403	cuttings	Complete	1120	0.37	0.30	1605	6	3	3	0	2	4
Jabiru-1A	1712	1715	122418	cuttings	Complete	1628	0.49	0.28	2442	12	4	8	0	9	3
Jabiru-1A	1721	1724	122333	cuttings	Complete	650	0.00	0.00	607	0	0	0	0	0	0
Jabiru-1A	1733	1736	122419	cuttings	Complete	1936	0.18	0.25	1097	2	0	0	0	2	0
Jabiru-2	790	800	122399	cuttings	Complete	1518	0.00	0.00	2277	0	0	0	0	0	0
Jabiru-2	1642		122361	core	Complete	1032	0.14	0.09	6330	9	8	1	0	9	0
Jabiru-2	1655.21		122362	core	Complete	880	0.08	0.08	4723	4	4	0	0	4	0
Jabiru-2	1661	1664	122352	cuttings	Random	100	6.81	2.75	323	22	18	3	1	19	3
Jabiru-2	1679	1682	122353	cuttings	Random	100	6.33	2.03	553	35	14	10	11	28	7
Jabiru-2	1689	1692	122354	cuttings	Complete	682	0.84	0.29	3706	31	12	16	3	31	0
Jabiru-2	1712	1715	122355	cuttings	Complete	1575	0.03	0.05	3990	1	1	0	0	1	0
Jabiru-3	1625		123132	core	Complete	1026	0.05	0.05	8516	4	4	0	0	0	4
Jabiru-3	1637.7		123133	core	Random	99	12.64	3.12	435	55	53	1	1	13	42
Jabiru-3	1647	1650	123100	cuttings	Random	100	9.22	4.78	141	13	11	2	0	10	3
Jabiru-3	1659	1662	123244	cuttings	Complete	1665	0.47	0.22	3608	17	12	0	5	3	14
Jabiru-3	1662	1665	123101	cuttings	Complete	1575	1.14	0.27	6038	69	20	17	32	23	46
Jabiru-3	1680	1683	123102	cuttings	Complete	1548	0.05	0.05	7482	4	2	1	1	2	2
Jabiru-3	1704	1707	123103	cuttings	Complete	1656	0.02	0.03	10212	2	0	2	0	0	2

A second discrete zone of low GOI values is recorded in Jabiru-2, over the interval 1642-1655.2m, where GOI values of ≤0.1% were measured in rotary core samples taken from 1642m and 1655.2m (Figure 4–14). This zone of low GOI values overlies the interpreted palaeo-oil zone and is interpreted to reflect a zone of low palaeo-oil saturation above the recognised palaeo-oil column. In the absence of an intervening capillary barrier (such as sealing shale) that would impede vertical fluid communication and the generally good reservoir quality (Figure 4–14) it is not possible to attribute these low GOI values to an isolated (perched) water zone.

Instead, these low GOI values are interpreted to reflect a zone of low oil saturation caused by the presence of high gas saturation related to a palaeo-gas cap above the palaeo-oil column. This implies that some gas charge filled the crest of the trap prior to the arrival of a later oil charge, with the presence of high gas saturation preventing oil from accessing these parts of the reservoir.

Similar results, comprising zones of consistently low GOI values overlying zones of consistently high GOI values are observed in other wells from the Vulcan Sub-basin (described in the following sections). Whilst it remains possible that these zones reflect the absence of a suitable trapping mechanism for fluid inclusions the interpretation of a palaeo-gas zone is supported by the consistently low GOI values recorded in these zones. Changing trapping conditions are more likely to produce variable GOI profiles and these are not observed at Jabiru-2 or in other wells with similar results.

Collectively the GOI data from samples taken in Jabiru-2 define a palaeo-hydrocarbon column within presently water bearing reservoir of up to 52 m, comprising an oil rim spanning as much as 34 m (1655-1689 m) , overlain by a gas-cap of up to 24 m (Figure 4–14).

Conventional shows recorded in Jabiru-2 are fairly limited, but increase noticeably across the inferred palaeo-hydrocarbon zone. Trace to <5% spotty pale white fluorescence was noted near the top of the cored section at about 1640m, 40-80% dull yellow-white fluorescence at 1643.5m, 20-30% bright white fluorescence at about 1651m and 70% dull uniform fluorescence at about 1655m.

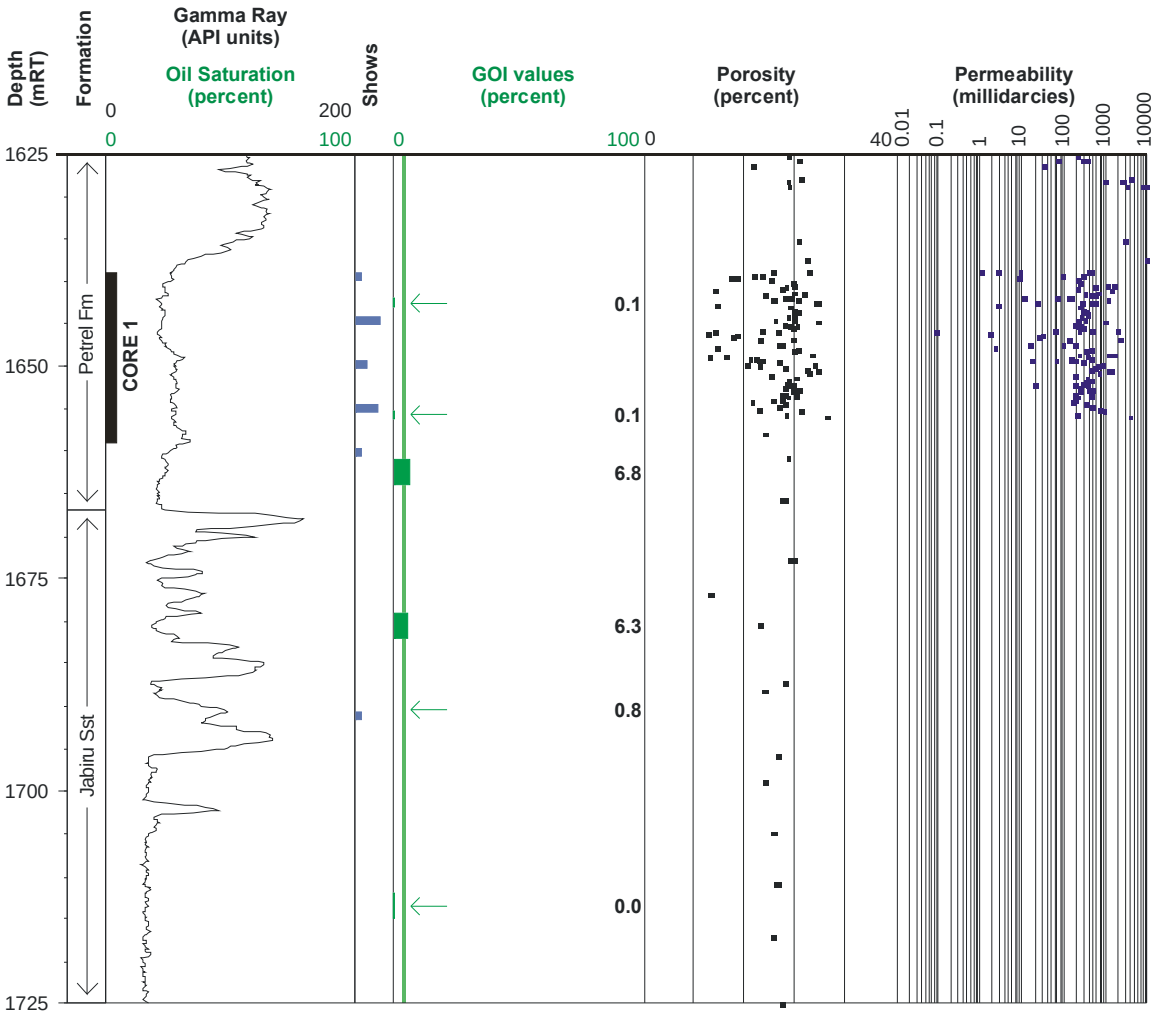

Figure 4-14: GOI results from Jabiru-2

GOI results displayed against to the gamma ray log with recorded porosity and permeability from core analysis data and where available oil saturation values derived from electric log analysis. Geological formation names and the location of cores taken are also shown. On the GOI log the green vertical line marks the position of the empirical threshold for oil accumulation with the width of the horizontal green lines showing the position and magnitude of the recorded GOI value (actual values shown to the right). Samples with low GOI values are marked with an arrow. Conventional shows reported in the well completion report are also shown with the width of the bar being proportional to the intensity of the show. Depth axis is in metres below the rotary table.

Less intense, patchy dull yellow fluorescence was also recorded in SWC samples at 1670m and 1690m but is absent in all samples below 1690m. Log analysis also indicates some residual oil saturation from 1637m to 1667m with small mud-gas peaks noted on the mud-log. BHP Petroleum Ltd. (1984) implied the presence of a residual oil zone in Jabiru-2, similar to that interpreted for the Jabiru-1A well (BHP, 1983a), and the GOI data reported here are consistent with this conclusion.

In Jabiru-3, a second offset appraisal well that intersected the main oil zone just above the field-wide current OWC (Figure 4–12), seven samples have been analysed, comprising one sample from within the current oil zone (1625 m) and six samples from below the current OWC (Table 4–1). High GOI values occur in two samples and define a zone of elevated palaeo-oil saturation over the interval 1637.7-1650m located within the current water-bearing section of the reservoir (Figure 4–15).

The single sample from the current oil zone at 1625m has a low GOI value (<0.1%) that is consistent with low oil saturation in this part of the reservoir when the oil inclusions were trapped. The absence of an intervening capillary barrier between this sample and the underlying high GOI values is similar to the Jabiru-2 well and once again is interpreted to reflect the presence of a palaeo-gas cap.

An important consequence of the observations made in the Jabiru samples and elsewhere in this study is the proposition that oil inclusions preferentially trap samples of the initial hydrocarbon charge, but do not provide a complete record of the oil saturation history experienced by each reservoir.

The reasons behind such observations remain speculative, but it maybe that the rate of inclusion formation increases dramatically during the initial influx of oil (perhaps reflecting chemical disequilibrium within the reservoir) then subsides (as equilibrium is re-established) making the marker relatively insensitive to changes in fluid composition or the trap geometry that occur after the trap was initially charged.

Conventional oil shows recorded in Jabiru-3 included dull yellow-white fluorescence in a SWC at 1651mRT and moderately bright white fluorescence in SWC samples from 1677-1684mRT. Recovered core showed similar fluorescence characteristics in

the upper part of the core (1599-1602mRT) and bright spotty blue to white fluorescence from 1604mRT down to the base of the core (~1638mRT) with a distinct decrease in intensity of fluorescence down the core (Figure 4–15).

Log analysis conducted on Jabiru-3 interpreted 7.6m of oil pay in the Upper Jurassic sandstones (BHP Petroleum Ltd., 1984b) with an OWC (1621mSS) and oil pressure gradient that are common (within error) to that defined in the earlier Jabiru-1A well (BHP Petroleum Ltd., 1983a). Calculated water saturation immediately below the current OWC was 100% and no residual oil zone was inferred (BHP Petroleum Ltd., 1984b). However, mud-gas levels increased significantly at the top of the current oil column with elevated responses that are well above baseline levels are noted down to 1665mRT, some 35m below the current OWC.

On the fluorescence data alone it is difficult to define any residual OWC and despite 100% calculated water saturation inferred from log analysis the depth at which mud-gas levels return to a baseline response (1665m) is broadly similar to the position of the palaeo-OWC defined by the GOI data (1650-1659m).

4.6.1.2 The Skua Oilfield

Initial exploration drilling on the Skua Jurassic tilted fault block structure produced equivocal results. Skua-1 tested the target Plover Formation reservoir within structural closure but below the OWC subsequently defined in Skua-3 (Figure 4–16).

The Skua-2 well, which was drilled close to the bounding fault, failed to penetrate a complete Jurassic reservoir sequence, but did flow oil from stratigraphically younger Santonian age sandstones intersected on the hanging wall side of the fault and juxtaposed against the Plover Formation reservoir in the footwall (Osborne, 1990).

The Skua-2 result prompted a third well to be drilled and in 1987 the Skua-3 well successfully delineated a 46.5m thick oil column in permeable Lower-Middle Jurassic sandstones of the Plover Formation (Osborne, 1990). A clear OWC was defined from pressure data at 2420mRT in the Skua-3 well.

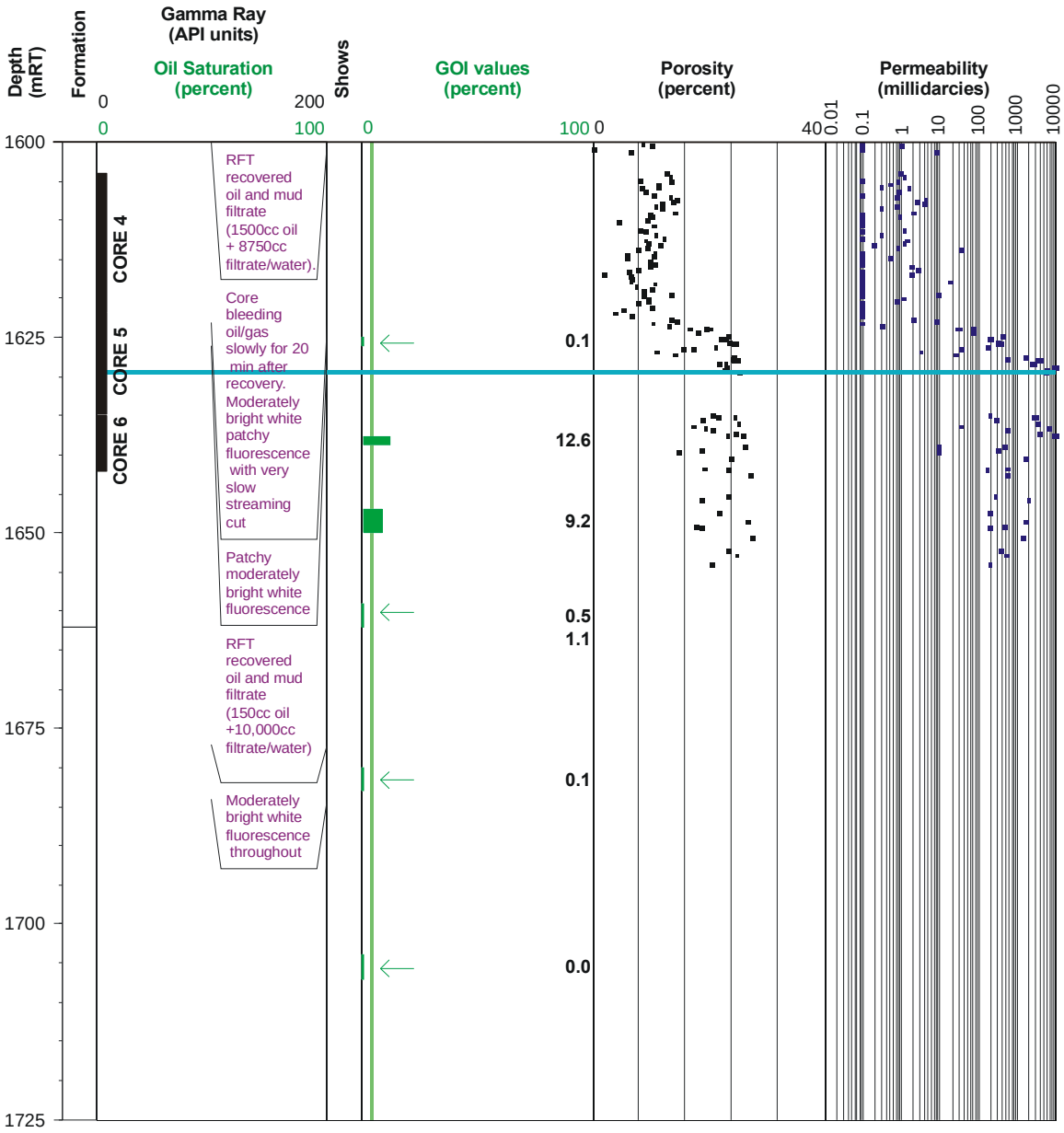

Figure 4-15: GOI results from Jabiru-3

GOI results displayed against recorded porosity and permeability from core analysis data. Geological formation names and the location of cores taken are also shown. On the GOI log the green vertical line marks the position of the empirical threshold for oil accumulation with the width of the horizontal green lines showing the position and magnitude of the recorded GOI value (actual values shown to the right). Samples with low GOI values are marked with an arrow. The blue horizontal line records the position of the current OWC. Conventional shows were reported from core taken in the well and are annotated. Depth axis is in metres below the rotary table.

The Plover Formation reservoir interval penetrated in the Skua Field consists of multiple stacked sandstone horizons of Early to Middle Jurassic age; these sands sub-crop the Callovian Unconformity and are sealed vertically and laterally by basal claystones and marls of the Cretaceous Bathurst Island Group (Figure 4–16).

Further appraisal drilling on the Skua structure subsequently confirmed a substantial oil accumulation, consisting of a 28m gas cap above a 46.5m oil-rim. Twelve appraisal and development wells have been drilled on the Skua Field. The field was brought on production in 1991 and continued to produce oil and associated gas for more than five years, with cumulative oil production of 0.2 million barrels prior to the field decommissioning and abandonment in 1997 (Cadman and Temple, 2003).

Three of the Skua wells (Skua-3, -4 and -6; Figure 4–16) have been sampled in this study, with a GOI values determined for 17 samples (Table 4–2). In Skua-3, GOI results from nine samples, covering the present oil and water legs, were produced by the author as part of an earlier study reported in O'Brien et al. (1996a). These results, which were reviewed as part of the current study, yielded GOI values for all samples within the current oil column that are above the threshold for oil accumulation.

In Skua-3 GOI values ranged from 93.5% in samples near the top of the Plover Formation to 17.3% in samples near the position of the current OWC (Figure 4–17). The first sample from below the current OWC also has an elevated GOI value (9% at 2425-28mRT) and supports the presence of a palaeo-oil column extending below the current oil zone. Three cuttings samples taken below this point (2434-2452 m) all have GOI values consistently less than 0.5% and indicate the presence of a palaeo-OWC at about 2431 m (mid point between 2425-28m high sample and 2434-37m low sample). Based on current sample spacing the GOI results from Skua-3 indicate that a small (Min 7 m and Max 13 m) palaeo-oil zone exists below the current position of the OWC.

Conventional oil shows recorded in Skua-3 comprised 10-80% faint to moderate green patchy fluorescence in cuttings between 2416mRT and 2470mRT, whilst the cored interval from 2375mRT to 2414mRT was typically 80-100% bright green to white fluorescence (BHP Petroleum, 1988a).

Table 4-2: GOI Results from the Skua Oilfield

Table shows all relevant data for the analysed samples, including depth, sample number and method employed. Abbreviations shown in the location of oil inclusions column refer to Fractures Cutting Detrital Minerals (FCDM) and Quartz Overgrowth Boundary. GOI Error was defined using the method outlined in the text. Numbers shown in the 7 right most columns refer to numbers of grains containing oil inclusions of specific colour or location. Where numbers are absent no measurement was made.

Well Name	Start Depth (mRT)	End Depth (mRT)	CSIRO Number	Sample Type	Counting Method	Number of fields examined	GOI (%)	GOI Error (%)	Total Grains	Grains With Oil Inclusions	Fluorescence Colours of Oil Inclusions			Location of Oil Inclusions	
											Blue	White	Yellow and Orange	FCDM	QOB
Skua-3	2378.1		122334	core	Random	100	93.50	1.78	738	690	683	0	7		
Skua-3	2389.9		122335	core	Random	100	92.70	2.44	438	406	404	0	2		
Skua-3	2409.2		122336	core	Random	100	51.60	3.29	887	458	453	4	0		
Skua-3	2416	2419	122422	cuttings	Random	100	17.30	2.63	797	138	126	10	2	103	35
Skua-3	2416	2419	122337	cuttings	Random	100	19.90	3.02	672	134	119	14	1	111	23
Skua-3	2425	2428	122423	cuttings	Random	100	9.00	1.96	815	73	67	0	6	45	28
Skua-3	2434	2437	122424	cuttings	Complete	924	0.08	0.03	31108	24	21	2	1	24	0
Skua-3	2440	2443	122425	cuttings	Complete	1088	0.24	0.05	42106	99	94	5	0	99	0
Skua-3	2449	2452	122426	cuttings	Complete	1332	0.50	0.19	5372	28	12	15	1	7	21
Skua-4	2349.8		123117	core	Random	100	30.24	2.97	916	277	267	9	1	114	163
Skua-4	2353	2356	123118	cuttings	Complete	588	1.90	0.31	7311	139	136	3	0		
Skua-4	2361	2364	123119	cuttings	Complete	1014	2.14	0.27	10647	228	225	3	0	192	36
Skua-4	2391	2394	123120	cuttings	Complete	1620	0.01	0.02	9774	1	0	0	1	1	0
Skua-6	1875	1878	123121	cuttings	Complete	1530	0.00	0.00	1581	0	0	0	0	0	0
Skua-6	2388	2391	123123	cuttings	Complete	1591	0.00	0.00	2758	0	0	0	0	0	0
Skua-6	2394	2397	123124	cuttings	Complete	1462	0.03	0.05	3996	1	0	1	0	1	0
Skua-6	2706	2709	123125	cuttings	Complete	784	0.00	0.00	5462	0	0	0	0	0	0

No obvious relationship between the conventional oil shows and the position of the palaeo-OWC from the GOI data can be discerned. Log analysis defined high water saturation below the OWC (defined at 2423mRT in Skua-3) of between 77 and 100% down to the base of the interpretation at 2429mRT (BHP Petroleum Ltd., 1988a).

In Skua 4, where four samples were analysed in the current study, a single sample taken within the current oil zone has a high GOI value (30.2%), whereas the three samples taken from below the current OWC (defined at 2353mRT in Skua-4, BHP Petroleum Ltd., 1988b) have much lower GOI values (Figure 4–18) ranging from <0.1% to 2.1% (2356-2394 m). This sharp reduction in GOI values is interpreted to reflect the crossing of a palaeo-OWC somewhere between 2349.8 m and 2356 m.

The GOI values recorded in two samples from immediately below the current OWC have slightly elevated values (1.9% at 2353-56 m and 2.1% at 2361-64) compared with GOI values typically seen within palaeo-water zones where GOI values are generally less than 1% (Eadington et al., 1996). These higher values come from disaggregated cuttings samples and probably reflect a degree of caving of sand, rich in grains containing oil inclusions, from the overlying oil zone.

Unlike the result at Skua-3 the position of the palaeo-OWC recorded in Skua-4 from the fluid inclusion data is at a similar depth as the current OWC. The significance of these different observations is discussed in the next chapter where the GOI data are integrated with other information on the structural history of the Skua trap.

Conventional oil shows recorded in Skua-4 included isolated zones of trace to 10% fluorescence in cuttings samples (1659-65mRT, 1716-25m) as well as faint to bright yellow pinpoint fluorescence in the cuttings samples from 2367mRT to 2385mRT (BHP Petroleum Ltd., 1988b).

SWC recovery was fairly poor in Skua-4 with only minor oil shows recorded in the upper reservoir section (2306-2308mRT) increasing to 100% moderately bright white fluorescence in the 2322mRT, 2323mRT, 2324mRT, and 2339mRT SWCs samples before falling to 70-80% patchy yellow fluorescence in SWCs at 2370mRT and 2383mRT.

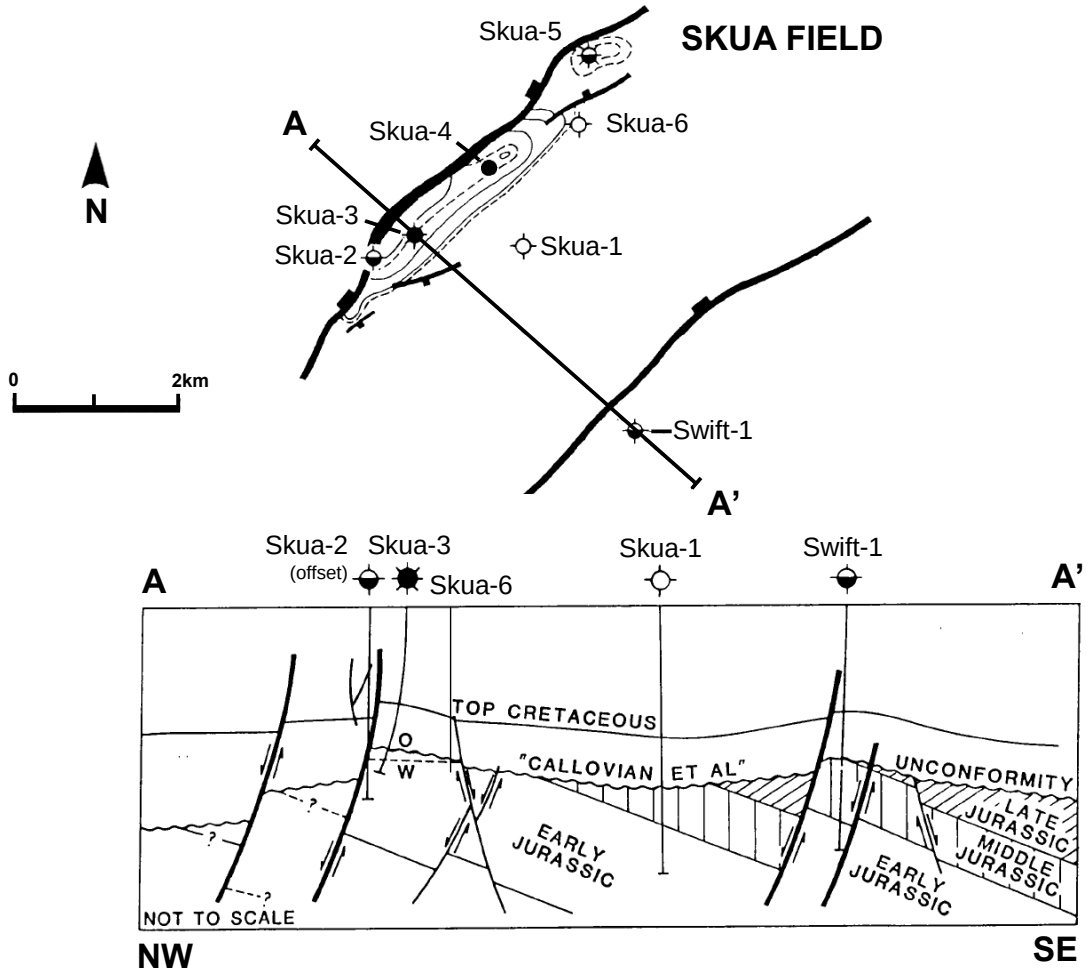

Figure 4-16: Map and cross section for the Skua Oilfield and the adjacent Swift Field.

Location of wells Skua-1 through Skua-6 and Swift-1 is shown relative to simplified depth-structure map and a cross section running from A to A'. Pre and Syn-Rift sediments of the Early to Middle Jurassic Plover Formation and the Late Jurassic Swan Group sub-crop at the Callovian Unconformity where they are onlapped by Cretaceous Post-Rift sediments. Note the location of Skua-6 that penetrates the reservoir section near the current OWC, whilst Skua-3 and -4 lie within the main part of the accumulation (modified from BHP Petroleum Ltd., 1989a).

Sandstones within the cored sections displayed up to 100% fluorescence, with a general decline towards the base of the core. Cuttings samples from below the current OWC showed minor fluorescence.

Log analysis defined an OWC in Skua-4 at 2352mRT, similar to the OWC defined by RFT pressures. Residual oil saturations of 10-20% are interpreted down to 2388m with 100% water saturation below 2399mRT (BHP Petroleum Ltd., 1988b).

GOI values measured in 4 samples from the presently water-wet Jurassic reservoir in Skua-6 (Figure 4–16, Figure 4–19) are all <0.1% suggesting oil saturation has always been low. Skua-6 intersected the reservoir horizon about 3.5m below the field-wide current OWC that had previously been defined by Skua-3 and Skua-4 (Figure 4–19). On a common depth datum (metres sub-sea) the samples from Skua-6 lie below the palaeo-OWC defined in Skua-4, but above the palaeo-OWC seen in Skua-3.

Conventional oil shows in Skua-6 are fairly limited in the cuttings, comprising trace to 5% over the interval 2358-2383mRT but SWCs from across the reservoir section recorded more significant fluorescence. Samples from near the top of the reservoir section showed 30-50% pale yellow-white fluorescence (2363mRT, 2361.5mRT, and 2370.2), whilst 50-80% patchy to even white-yellow fluorescence was noted deeper (2377mRT, 2379.5mRT, 2381.5mRT) in the well (BHP Petroleum Ltd., 1989a).

Log analysis interprets the entire reservoir section to be water-bearing with a residual hydrocarbon saturation ranging from 4-12% seen down to 2390m that is thought to indicate a former hydrocarbon saturated zone (BHP Petroleum Ltd., 1989a). However, accurate measurement of residual saturation was difficult to due to large errors that occur at low resistivity when using this type of resistivity log (BHP Petroleum Ltd., 1989a) and the interpretation is reliant on support from the fluorescence observations and increased mud-gas levels. For the latter the fast drilling rate related to the drilling bit used on this section is thought to have resulted in high gas levels across the last 500m of drilled section so it is unclear if the mud-gas values genuinely reflect increased residual hydrocarbons or are simply an artifact of the drilling system used for this hole section (BHP Petroleum Ltd., 1989a).

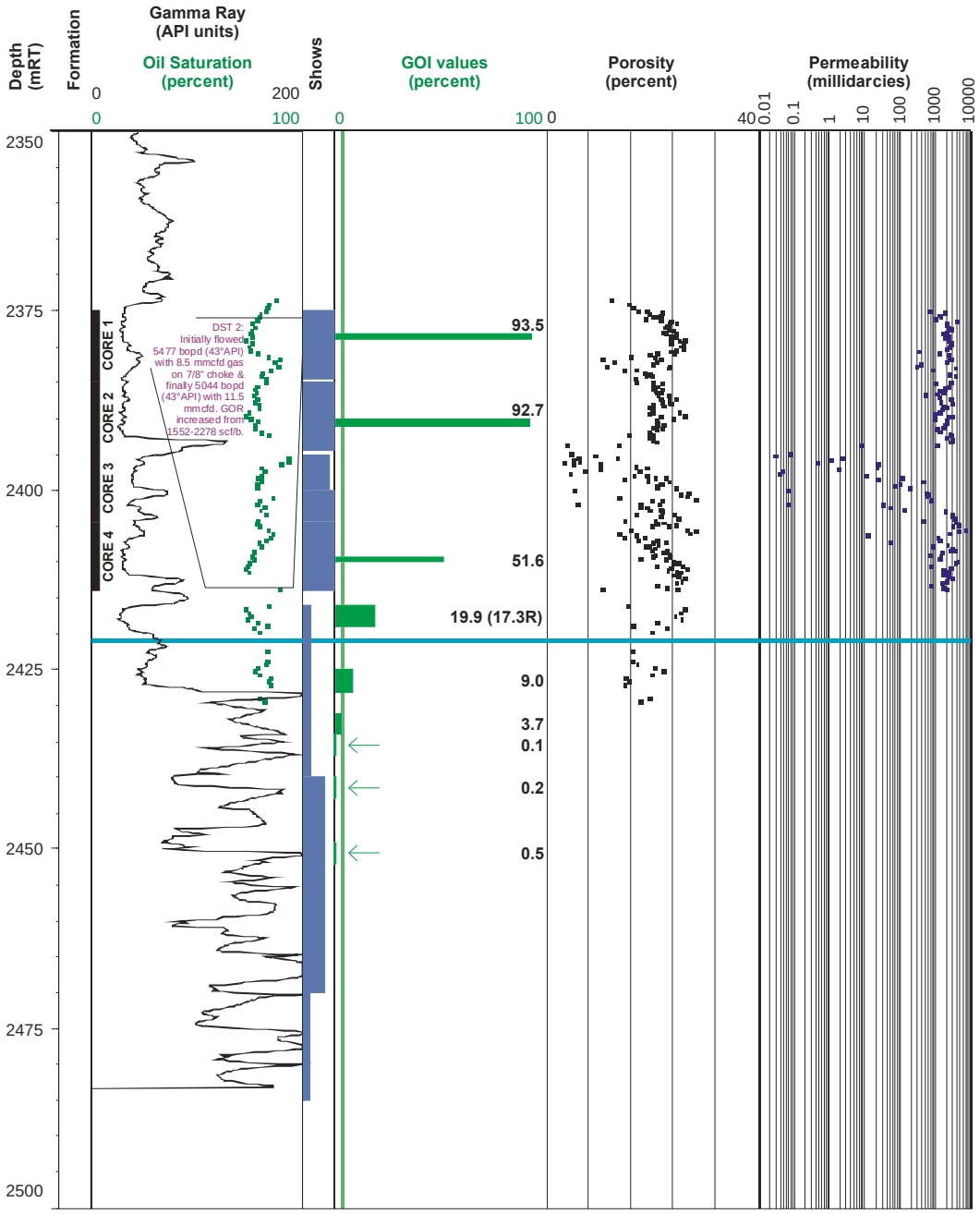

Figure 4-17: GOI results from Skua-3.

GOI results displayed against the gamma ray log with recorded porosity and permeability from core analysis data and where available oil saturation values derived from electric log analysis. Geological formations, the location of cores taken and production tests made are shown. On the GOI log the green vertical line marks the position of the empirical threshold for oil accumulation with the width of the horizontal green lines showing the position and magnitude of the recorded GOI value (actual values shown to the right). Samples where GOI is <1% are marked with an arrow. Conventional shows from the well completion report are shown with the thickness of the bar proportional to the intensity of the show.

The possible disparity between the recorded shows that have been interpreted by the operator to reflect a residual oil zone and the low GOI values completed in this study that infer migration, but without accumulation will be discussed in the next chapter where the charge history of the Skua Field is examined in more detail.

4.6.1.3 The Challis Oilfield

The Challis Oil Field (Figure 4–20) was discovered in 1984 when BHP Petroleum Ltd. drilled the Challis-1 well to test a narrow Triassic horst block. The well encountered a 29m thick oil column within stacked Triassic sandstones of the Challis Formation (Gorman, 1990). The reservoir sub-crops the Valanginian unconformity being sealed laterally and vertically by claystones, marls and carbonates of the Bathurst Island Group (Wormald, 1988; Gorman, 1990; Figure 4–20).

Subsequent appraisal drilling confirmed the economic viability of the Challis Field (Gorman, 1990), defining oil pay within stacked sandstone reservoirs that share a common OWC at 1410.5 m TVSS. The Challis and nearby Cassini oil fields were brought on production in December 1989, with combined initial oil reserves estimated at 56.6 million barrels (Cadman and Temple, 2003).

Only one well was sampled from the Challis Field in the current study, with three samples taken from the Challis-1 well (Table 4–3). GOI values recorded in two samples from the present oil zone are lower than is typical for samples from a zone of high oil saturation (Figure 4–21), although they are still above those values expected for samples from a migration path, where GOI rarely exceeds 1%. The only sample from the current water-leg is significantly lower (0.2% at 1447.15m) than recorded in the oil zone samples (1.5% at 1399.2m and 1.7% at 1405.1m) and hence the variation in GOI values in Challis-1 does appear to be internally consistent, with higher values recorded in the oil zone compared with the underlying water-leg. The depression of GOI values within these samples could reflect a combination of the shallow burial (~1400m) depth and the associated poorly consolidated nature of the reservoir sandstones. Compaction related fracturing, a key mechanism for inclusion formation, is likely to be less effective where there is minimal overburden loading and this could subdue the GOI values.

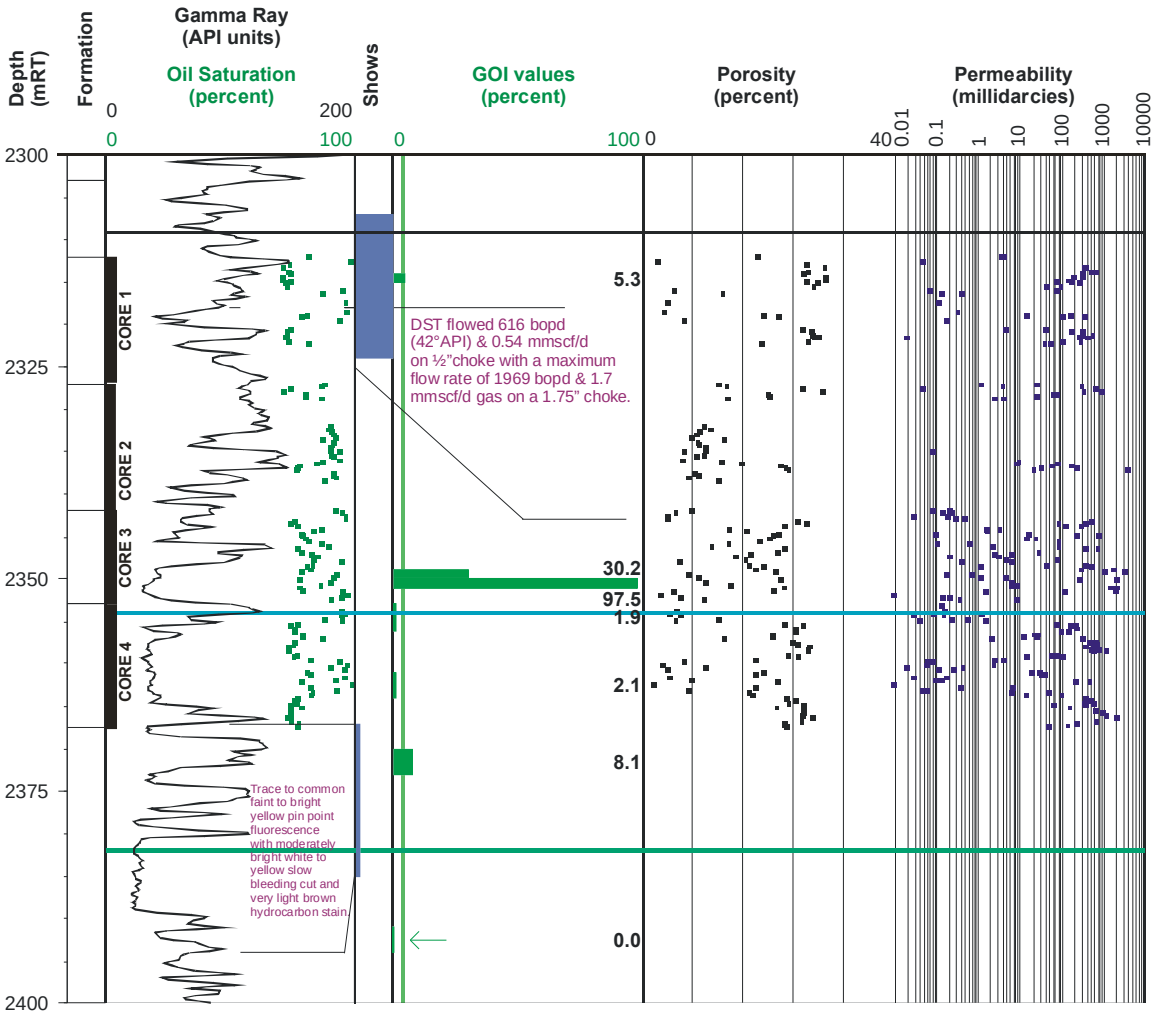

Figure 4-18: GOI results from Skua-4.

GOI results displayed against to the gamma ray log with recorded porosity and permeability from core analysis data and where available oil saturation values derived from electric log analysis. Geological formation names, the location of cores taken and drillstem tests made are also shown. On the GOI log the green vertical line marks the position of the empirical threshold for oil accumulation with the width of the horizontal green lines showing the position and magnitude of the recorded GOI value (actual values shown to the right). Samples where GOI is <1% are marked with an arrow. The position of the current OWC is shown by the horizontal blue line and is defined by log and RFT pressure data. Conventional shows reported in the well completion report are also shown with the thickness of the bar being proportional to the intensity of the show.

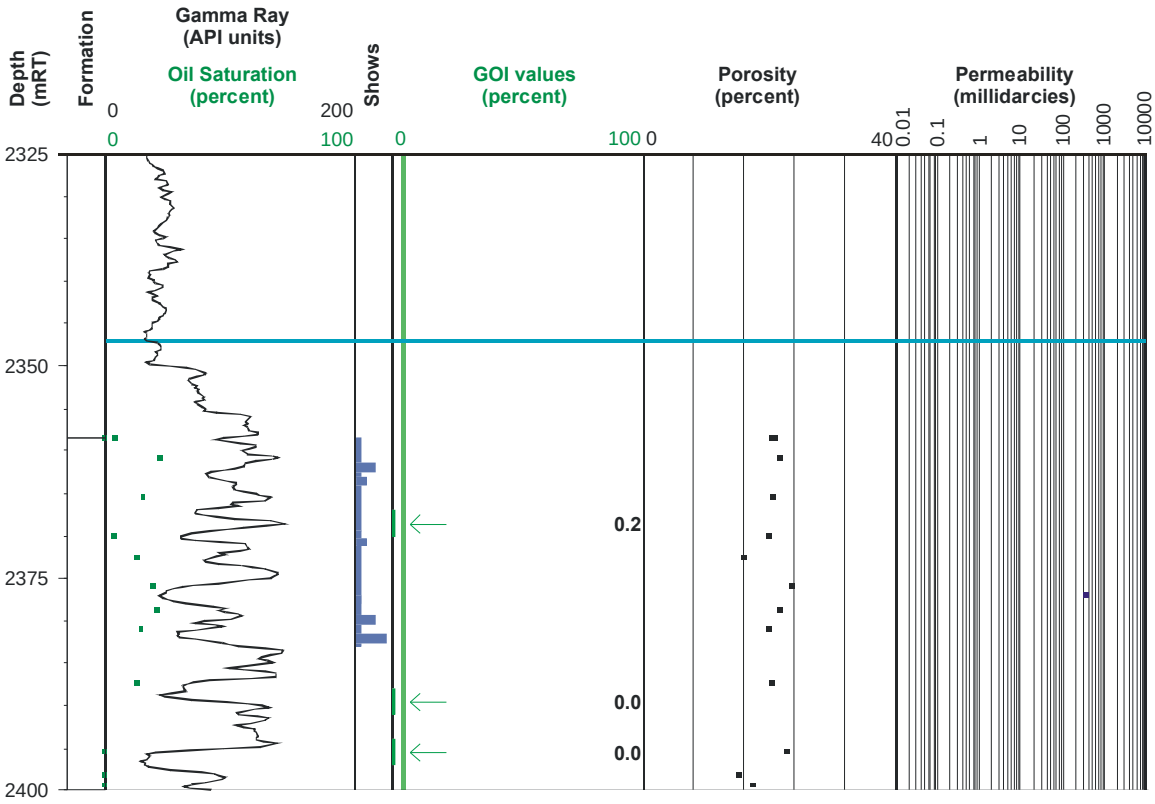

Figure 4-19: GOI results from Skua-6.

GOI results displayed against the gamma ray log with recorded porosity and permeability from core analysis data and where available oil saturation values derived from electric log analysis. Geological formation names, the location of cores taken and production tests made are also shown. On the GOI log the green vertical line marks the position of the empirical threshold for oil accumulation with the width of the horizontal green lines showing the position and magnitude of the recorded GOI value (actual values shown to the right). Samples where GOI is <1% are marked with an arrow. The position of the current OWC is shown by the horizontal blue line but this level lies above the top of the reservoir section in Skua-6. Conventional shows reported in the well completion report are also shown with the thickness of the bar being proportional to their intensity.

Conventional shows recorded in the Challis-1 well are not quantified but cuttings from the reservoir interval exhibit bright yellow-white fluorescence from 1387-1399mRT above the cored interval and from 1414-62mRT below the cored zone. In SWC samples fluorescence is first observed at 1388.1mRT with moderate to good white fluorescence recorded in all samples down to 1413.8mRT before becoming more variable, but overall less intense, in SWC from 1413.8mRT to 1442.5m. Below 1442.5 the SWC samples are devoid of fluorescence. Across the cored interval from 1399-1447mRT fluorescence is strongest in Core 1 down to 1408.25mRT, becoming more variable down to the base of Core 3 (1447.7mRT; BHP Petroleum Ltd., 1985).

The current OWC is not well defined from log analysis but the RFT pressure data indicates a fluid contact at 1418mRT, which is consistent with the 100% water saturation calculated below this depth (BHP Petroleum Ltd., 1985).

4.6.1.4 The Cassini Oilfield

The Cassini Field was discovered during an appraisal drilling program aimed at defining the extent of the nearby Challis Field (Figure 4–20). Cassini-1, drilled in 1988, tested a separate culmination within the same horst structure, being separated from the Challis closure by a small intervening saddle.

The well needed to be sidetracked in order to reach the reservoir target and was completed as Cassini-1ST. This successful well intersected a 13m net oil column within Triassic sandstones, with an OWC about 7m lower than in the adjacent Challis Field, confirming a separate oil accumulation. Cassini-1 was production tested and flowed at rates of up to 7500 BOPD. Further appraisal of the discovery followed with the drilling of the Cassini-2 well, located some 2 kilometres to the southwest of Cassini-1.

This Cassini-2 well penetrated the reservoir section low to prognosis at 1462mRT, some 19m below the OWC intersected at Cassini-1 thus limiting the south western extent of the Cassini field (Gorman, 1990).

A total of 12 samples were collected for GOI analysis, comprising 10 samples from the Cassini-1ST well and 2 samples from the Cassini-2 well (Table 4–3). In Cassini 1ST, samples taken from within the present day oil zone have low GOI values of between 0.2% and 0.7% that initially appear contrary to the high oil saturation observed in this interval at the current day (Figure 4–22).

However, a zone of high GOI values (4.9%-11.4%) is recorded in samples immediately below the current OWC, suggesting a zone of high palaeo-oil saturation underlies the current oil zone in rocks that are now water bearing. The occurrence of a continuous zone of high GOI values overlain by a series of low GOI values without an intervening capillary barrier is consistent with the presence of a palaeo-gas cap. This interpretation is not based on any petrographic characteristic (such as the presence of gas-filled fluid inclusions); rather it assumes that buoyancy pressure would result in accumulation of oil (and associated high GOI values) at the top of the reservoir if no capillary barrier or fluid barrier (provided by prior accumulation of more buoyant gas) prevented oil from entering this zone.

Conventional oil shows recorded in Cassini-1ST across the interval 1431-1449mRT comprise 100% bright pale yellow fluorescence in core with dull fluorescence noted in associated cuttings. Minor fluorescence is noted in cuttings down to 1500mRT. Below 1450mRT the fluorescence seen in the core is variable but remains significant down to the base of the core at 1473m (BHP Petroleum Ltd., 1988c).

SWC samples from across the reservoir section show good correspondence with the core and cuttings samples with trace patchy dull yellow fluorescence observed in the 1500mRT SWC representing the deepest occurrence of fluorescence. Above this depth fluorescence is noted in SWCs from all sandstone intervals where >50% patchy fluorescence is recorded up to 1475m with 100% bright pale yellow fluorescence observed in SWC from 1434-1432mRT (BHP Petroleum Ltd., 1988c).

Log analysis indicates a current OWC in Cassini-1ST occurs at 1444mRT, with minor hydrocarbon saturation (>90% S_w) calculated down to 1455mRT, below which water saturation is consistently indicated to be 100% (BHP Petroleum Ltd., 1988c).

Table 4-3: GOI results from the Challis-Cassini Oilfields

Table shows all relevant data for the analysed samples, including depth, sample number and method employed. Abbreviations shown in the location of oil inclusions column refer to Fractures Cutting Detrital Minerals (FCDM) and Quartz Overgrowth Boundary. GOI Error was defined using the method outlined in the text. Numbers shown in the 7 right most columns refer to numbers of grains containing oil inclusions of specific colour or location. Where numbers are absent no measurement was made.

Well Name	Start Depth (mRT)	End Depth (mRT)	CSIRO Number	Sample Type	Counting Method	Number of fields examined	GOI (%)	GOI Error (%)	Total Grains	Grains With Oil Inclusions	Fluorescence Colours of Oil Inclusions			Location of Oil Inclusions	
											Blue	White	Yellow and Orange	FCDM	QOB
Cassini-1ST	1434	1437	123138	cuttings	Complete	1540	0.22	0.14	4517	10	1	9	0	10	0
Cassini-1ST	1439.43		123134	core	Complete	1462	0.67	0.18	7602	51	5	41	5	51	0
Cassini-1ST	1443.9		123135	core	Random	115	4.91	2.00	448	22	6	15	1	21	1
Cassini-1ST	1447.45		123136	core	Random	100	8.63	2.22	614	53	5	34	14	48	5
Cassini-1ST	1460.25		123137	core	Random	100	11.42	1.96	1007	115	5	82	28	105	10
Cassini-1ST	1476	1479	123140	cuttings	Random	100	6.27	1.91	622	39	1	33	5	39	
Cassini-1ST	1485	1488	123286	cuttings	Random	100	6.92	1.75	809	56	1	54	1	56	0
Cassini-1ST	1566	1569	123542	cuttings	Complete	2376	0.00	0.00	9029	0	0	0	0	0	0
Cassini-1ST	1581	1584	123543	cuttings	Complete	1665	0.02	0.05	4052	1	0	1	0	0	1
Cassini-1ST	1596	1599	123544	cuttings	Complete	1702	0.00	0.00	6695	0	0	0	0	0	0
Cassini-2	1464	1467	123290	cuttings	Complete	870	0.55	0.26	3248	18	15	3	0	18	0
Cassini-2	1470	1473	123291	cuttings	Random	100	5.10	1.65	686	35	10	25	0	35	0
Challis-1	1399.2		122502	core	Complete	100	1.68	0.64	1550	26	7	18	1		
Challis-1	1405.05		122503	core	Complete	100	1.48	0.56	1760	26	9	17	0		
Challis-1	1447.15		122504	core	Complete	72	0.22	0.24	1385	3	3	0	0		

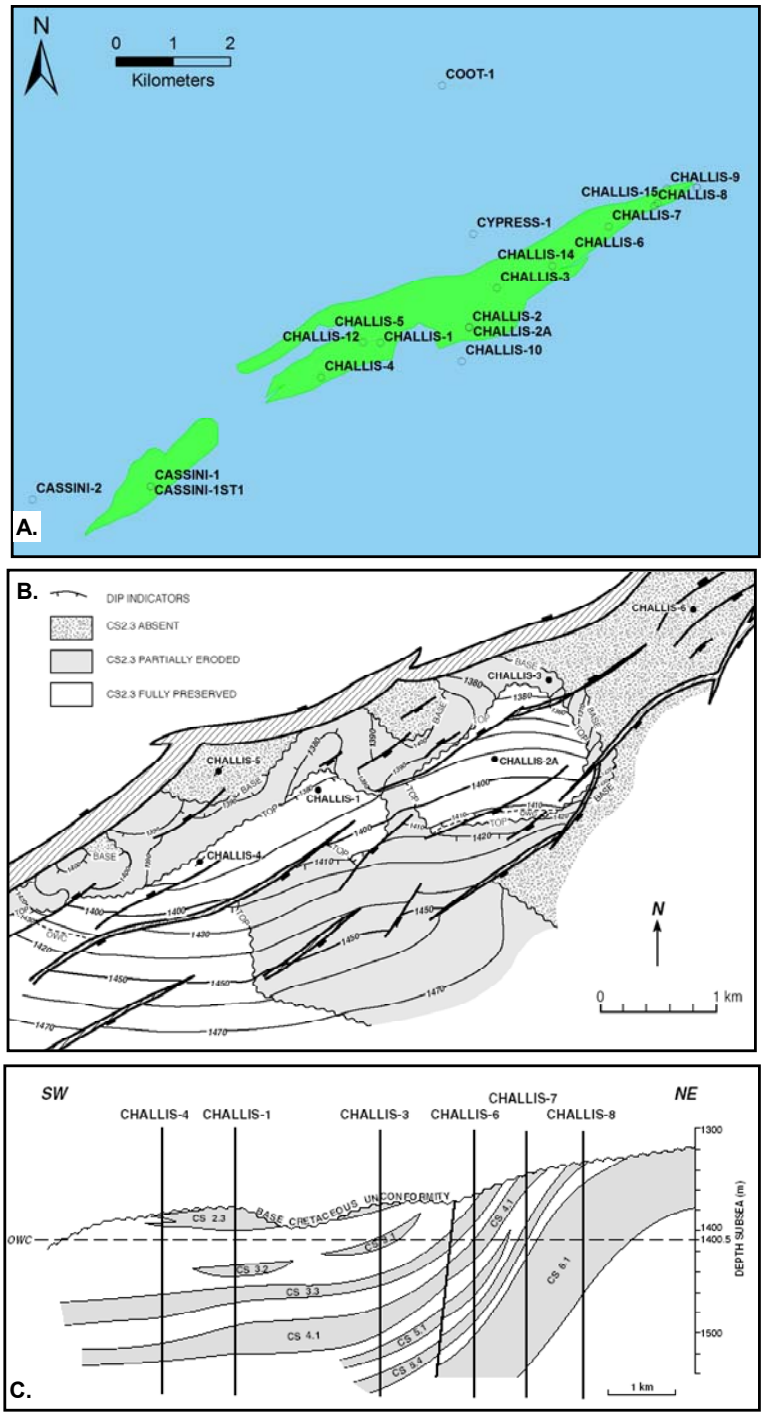

Figure 4-20: Location of wells within the Challis and Cassini oilfields.

The maps show: A. a simple location map for wells drilled on the Challis and Cassini oilfields and B. a more detailed sub-crop map at top porosity level and C. cross section for the Challis Field. The Challis Field is contained in an eroded horst and the map and cross section shows the position of sub-cropping chronostratigraphically defined units within the Challis Formation reservoir (modified from Gorman, 1990).

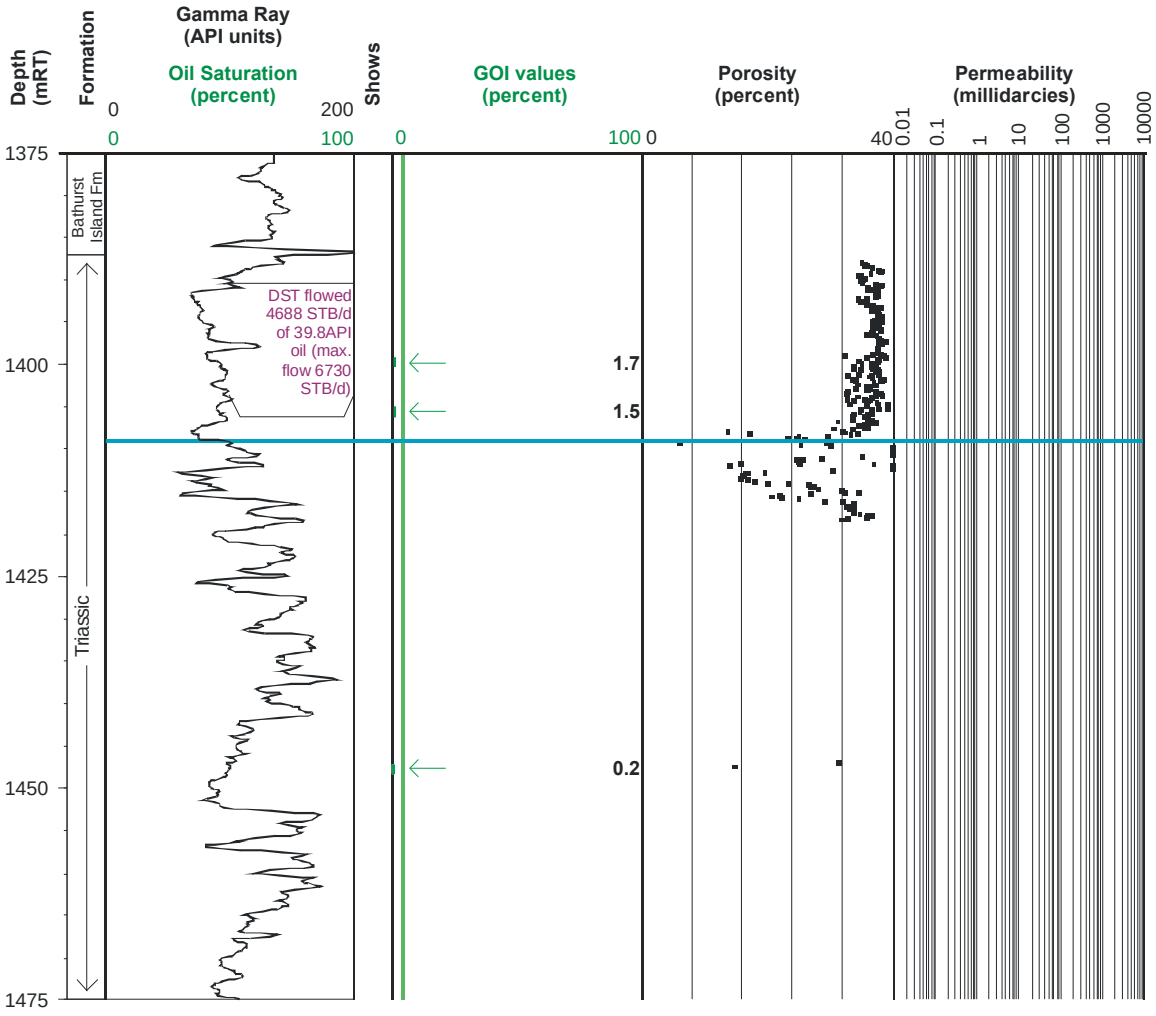

Figure 4-21: GOI results from the Challis-1 well.

GOI results displayed against the gamma ray log with recorded porosity and permeability from core analysis data and where available oil saturation values derived from electric log analysis. Geological formation names, the location of cores taken and drillstem tests conducted are also shown. On the GOI log the green vertical line marks the position of the empirical threshold for oil accumulation, with the width of the horizontal green lines showing the position and magnitude of the recorded GOI value (values shown to the right). Samples where GOI is <1% are marked with an arrow. The position of the current OWC is shown by the horizontal blue line. Conventional shows were not reported in the well.

Collectively, the GOI results from Cassini-1ST are interpreted to represent a 44-58 m palaeo-oil column overlain by an 8-16 m palaeo-gas cap. The position of the palaeo-fluid contacts is relatively poorly constrained by the spacing of the available samples and further infill sampling would be needed to address this more fully.

A palaeo-GOC is placed at about 1442 m, the mid-point between the deepest low GOI sample at 1439.43 m (0.7%) and the first high GOI sample at 1443.9 m (4.9%). Similarly, the position of the palaeo-OWC is arbitrarily taken as the mid-point between the deepest high GOI sample (1485-88 m) and the shallowest low GOI sample (1566-69 m). For the position of the palaeo-OWC the deepest sample with high GOI occurs above the base of the conventional shows and based on these shows the position of the palaeo-OWC likely lies closer to 1488mRT than 1566mRT.

GOI results for 2 samples taken from Cassini-2 (Figure 4–23) are consistent with the interpretation applied to Cassini-1ST. In Cassini-2 a low GOI value recorded in the 1464-67 m cuttings sample overlies a much higher value in the underlying 1470-73 m cuttings sample, consistent with a palaeo-gas over oil column. The extent of the palaeo-hydrocarbon zone in Cassini-2 is not constrained by the limited sampling; rather a palaeo-oil down to 1473mRT is indicated.

A palaeo-gas column of up to about 10 m is possible at the Cassini-2 well intersection, constrained by the top of the reservoir at 1460 m and the position of the high GOI value at 1470-73 m (Figure 4–23). In contrast, the position of the palaeo-OWC is unconstrained and it remains unclear if the two Cassini wells share a common palaeo-OWC. The position of the palaeo-GOC is, however, well constrained by the current sampling to be at 1468.5±1.5 m and can be directly compared with the palaeo-GOC defined for Cassini-1ST at 1442±2.5 m. This difference implies different palaeo-accumulations or that the position of the contact was modified by post charge tilting or increased fault offsets during reactivation.

Conventional oil shows in Cassini-2 comprise dull to occasionally bright yellow to yellow-white fluorescence in cuttings that decreases with depth from 1462mRT to nil below 1527mRT (BHP Petroleum Ltd., 1989b). In SWC samples 95% fluorescence is noted at 1515mRT, with no florescence recorded in SWC deeper in the well.

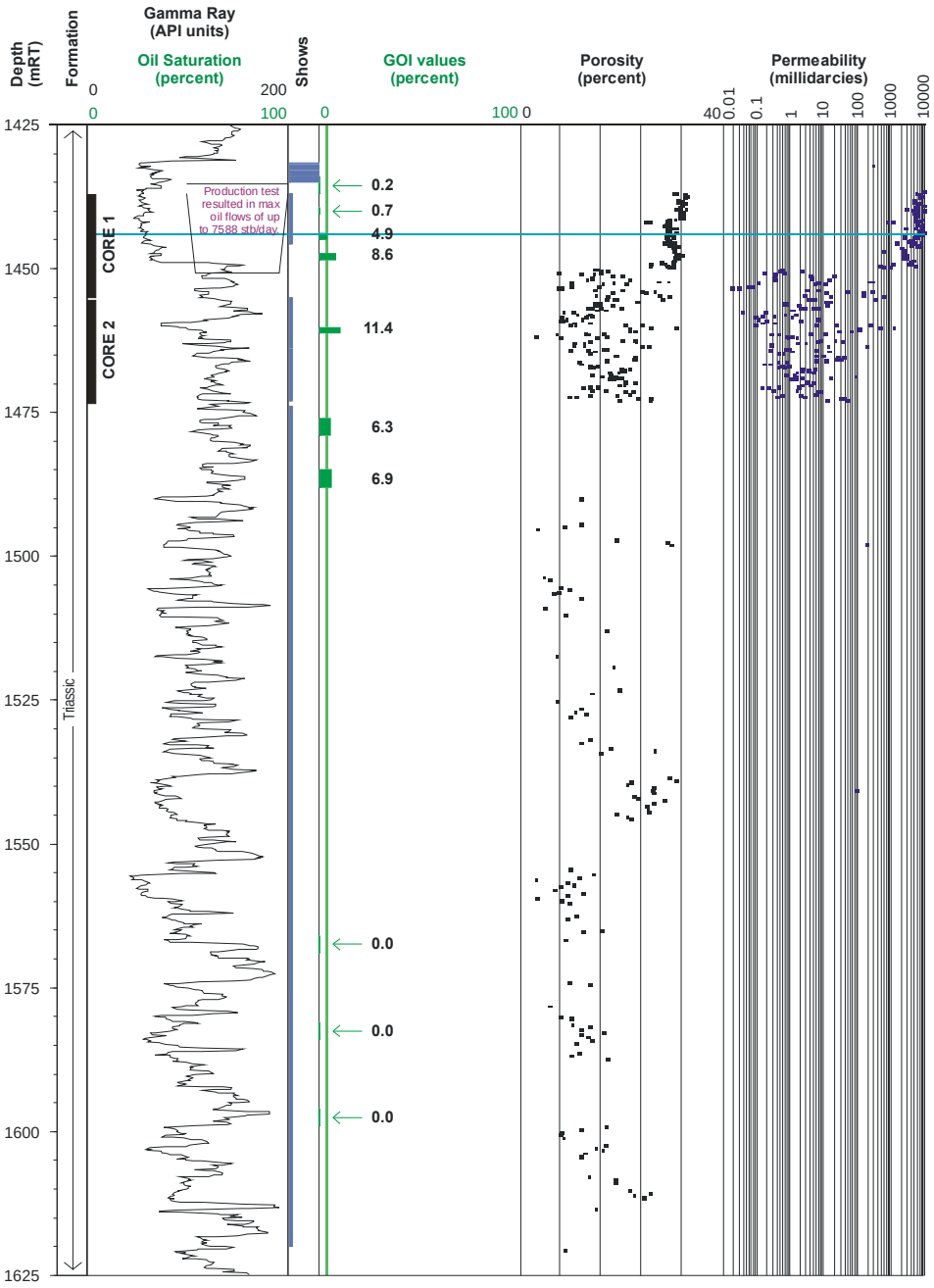

Figure 4-22: GOI results from Cassini-1ST.

GOI results displayed against the gamma ray log with recorded porosity and permeability from core analysis data and where available oil saturation values derived from electric log analysis. Geological formation names, the location of cores taken and production tests conducted are also shown. On the GOI log the green vertical line marks the position of the empirical threshold for oil accumulation, with the width of the horizontal green lines showing the position and magnitude of the recorded GOI value (actual values shown to the right). Samples where GOI is <1% are marked with an arrow. The position of the current OWC is shown by the horizontal blue line. Conventional shows reported in the well completion report are also shown with the thickness of the bar being proportional to their intensity.

Above 1515mRT the SWC samples show highly variable (5-95%) fluorescence levels, but become consistently strong in nearly every sample up to 1460mRT near the top of the reservoir section.

Quantitative log analysis (BHP Petroleum Ltd., 1989b) indicated that the reservoir interval down to 1527mRT is entirely water saturated with residual hydrocarbon saturations calculated to be <20%. Water saturation is commonly <90% down to near the base of the well at 1898mRT, which suggests the inputs to the analysis are inaccurate due to incorrect assumptions regarding the water resistivity values.

Collectively the conventional hydrocarbon show and GOI data collected on samples from the Cassini wells reflect a more complex charge history than is indicated by the present oil zone. A hydrocarbon column that originally extended below the current OWC is supported by these data but integration with information on the trap geometry and reservoir distribution is needed to fully evaluate these results.

Whilst this is discussed in the following chapter the limited sampling make it difficult to reach clear conclusions and further sampling is needed if a robust assessment of the history experienced by this trap is to be produced.

4.6.1.5 The Swift Oilfield

The presently sub-economic Swift oil discovery (Figure 4–16) was made with the drilling of Swift-1 in 1984. The well was drilled to test Middle Jurassic sandstones sealed by Upper Jurassic shales that sub-crop the base Cretaceous unconformity (BHP Petroleum Ltd., 1984b). A 44m gross oil column was defined within poor quality Upper Jurassic sandstones and was underlain by an interval of strong oil shows, interpreted to be residual in nature (BHP Petroleum Ltd., 1984b).

Four samples taken for GOI analysis are all were taken from below the current OWC at 2401m (Table 4–4). In these samples high GOI values of 4.2% at 2402.5 m and 7.1% 2417.7 m are consistent with high palaeo-oil saturation over this interval, whilst GOI values of <0.1% and 0% recorded in the 2431.6 m core sample and the 2441-44 m sample define a zone of low palaeo-oil saturation (Figure 4–24).

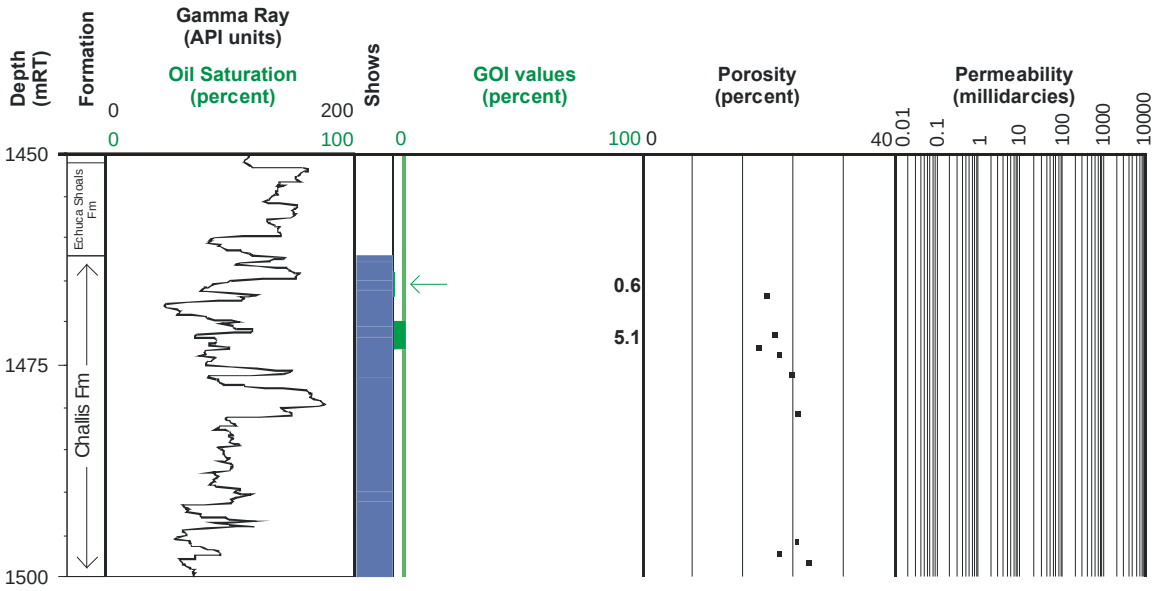

Figure 4-23: GOI results from the Cassini-2 well.

GOI results displayed against the gamma ray log with recorded porosity and permeability from core analysis data and where available oil saturation values derived from electric log analysis. On the GOI log the green vertical line marks the position of the empirical threshold for oil accumulation, with the width of the horizontal green lines showing the position and magnitude of the recorded GOI value (actual values shown to the right). Samples where GOI is <1% are marked with an arrow. Conventional shows reported in the well completion report are shown with the thickness of the bar being proportional to their intensity.

The position of the palaeo-OWC is poorly defined by the current sparse sample spacing and the increasing shale content below about 2425mRT that precludes taking samples of reservoir at regular intervals. The two samples with low GOI values come from within these shaly sections and are probably not part of the net reservoir. These sections could be isolated from the main reservoir by higher capillary entry pressures in these siltstones and mudstones.

Under these circumstances the low GOI values might not be considered genuine water zone samples and a clear palaeo-OWC may not have been defined. In this instance the lowest high GOI sample (2417.7m) could represent the position of a palaeo-Oil Down To (Palaeo-ODT) with a palaeo-OWC being located down-dip, away from the well intersection. In either case, the GOI data collected on Swift 1 indicate the presence palaeo-oil column, with high palaeo-oil saturation extending at least as deep as 2417.7 m or a minimum of about 17 m below the current OWC.

Conventional oil shows recorded in the Swift-1 well occur in SWC samples from the top of the reservoir (2392.4mRT) where 20-80% dull to bright white fluorescence is observed, generally remaining above 40% down to 2402.9 mRT. The intensity of fluorescence response declines markedly below this depth and is typically less than 20% down to about 1411mRT.

Conventional core cut from 2402-2420mRT exhibits 100% bright blue-white fluorescence falling in intensity below 2420mRT before becoming absent in core below a depth of about 2432mRT (BHP Petroleum Ltd., 1984b).

Log analysis identified 4.6m of net oil sand between 2392.5 mRT and 2401mRT with some residual hydrocarbon saturation calculated down to 2460mRT (BHP Petroleum Ltd., 1984b). RFT data indicate a current OWC at 2400.3mRT that is broadly consistent with the log interpretation.

There is good coincidence between the base of the conventional shows and the position of the palaeo-OWC indicated by the GOI data, with both datasets being consistent with the original OWC being deeper that observed at the current day.

4.6.1.6 The Talbot Oilfield

The Talbot oil field was discovered in 1989 with the drilling of Talbot-1. A 30m oil zone was defined within a variable quality sandstone section of Triassic age (Challis Formation) within a narrow horst block. The primary reservoir porosity is strongly influenced by the degree of authigenic carbonate cementation that is locally pervasive in distribution (Bourne and Faehrmann, 1991). Despite the observed reservoir variability the well flowed oil on test from two perforated intervals at a maximum unstabilised rate of 4981 BOPD, demonstrating effective reservoir deliverability (Bourne and Faehrmann, 1991).

An appraisal well confirmed the lateral extent of the Talbot oil field but in the current study samples have only been taken from the Talbot-1 well. GOI analyses have been completed on five samples, including two samples from the current hydrocarbon column (Figure 4–25, Table 4–5).

The maximum GOI value recorded is 0.2% from the 1558-61m sample below the current OWC. The two samples from the hydrocarbon zone both have GOI values less than 0.1%, although one of these is from within the current gas cap and may not be expected to have elevated GOI values.

The reason for the low values is unclear, but as only a single sample has been taken from the oil zone and the reservoir has highly variable net-gross distribution due to the authigenic carbonate cement the current sampling may not be from rocks that have been exposed to high oil saturation. Alternatively, the extensive carbonate cement, which is interpreted to be an early authigenic mineral, may have inhibited fracturing during later burial, thus removing an important mechanism for trapping oil as fluid inclusions. Additional sampling of the Talbot-1 well, together with sampling of the Talbot-2 well is needed in order to evaluate these options.

Conventional oil shows recorded in Talbot-1 comprise fairly poor shows in cuttings over the interval 1507-1542mRT. Fluorescence is noted SWC samples, typically recorded as greater than 20% up to 1557mRT, increasing to 80-100% in sandstones up to 1523mRT. Above this depth fluorescence is more variable up to the top of the reservoir section (Santos, 1990a).

Table 4-4: GOI results from the Swift-1 well.

Tables 4-4, 4-5 and 4-6 show all relevant data for the analysed samples, including depth, sample number and method employed. Abbreviations shown in the location of oil inclusions column refer to Fractures Cutting Detrital Minerals (FCDM) and Quartz Overgrowth Boundary. GOI Error was defined using the method outlined in the text. Numbers shown in the 7 right most columns refer to numbers of grains containing oil inclusions of specific colour or location. Where numbers are absent no measurement was made.

Well Name	Start Depth (mRT)	End Depth (mRT)	CSIRO Number	Sample Type	Counting Method	Number of fields examined	GOI (%)	GOI Error (%)	Total Grains	Grains With Oil Inclusions	Fluorescence Colours of Oil Inclusions			Location of Oil Inclusions	
											Blue	White	Yellow and Orange	FCDM	QOB
Swift-1	2402.5		123470	core	Random	100	4.21	0.75	2734	115	112	3	0	87	28
Swift-1	2417.65		123471	core	Random	100	7.12	1.68	899	64	63	1	0	39	25
Swift-1	2431.6		123472	core	Complete	891	0.01	0.02	11286	1	0	1	0	1	0
Swift-1	2441	2444	123473	cuttings	Complete	1404	0.00	0.00	11747	0	0	0	0	0	0

Table 4-5: GOI results from the Talbot-1 well.

Well Name	Start Depth (mRT)	End Depth (mRT)	CSIRO Number	Sample Type	Counting Method	Number of fields examined	GOI (%)	GOI Error (%)	Total Grains	Grains With Oil Inclusions	Fluorescence Colours of Oil Inclusions			Location of Oil Inclusions	
											Blue	White	Yellow and Orange	FCDM	QOB
Talbot-1	1507	1510	123126	cuttings	Complete	735	0.03	0.06	3234	1	1	0	0	1	0
Talbot-1	1525	1528	123127	cuttings	Complete	1188	0.03	0.04	7602	2	1	1	0	2	0
Talbot-1	1540	1543	123361	cuttings	Complete	1440	0.00	0.00	7248	0	0	0	0	0	0
Talbot-1	1558	1561	123128	cuttings	Complete	990	0.19	0.07	16137	31	8	23	0	30	1
Talbot-1	1597	1600	123129	cuttings	Complete	1628	0.01	0.01	16177	1	0	1	0	1	0

Table 4-6: GOI results from the Oliver-1 well.

Well Name	Start Depth (mRT)	End Depth (mRT)	CSIRO Number	Sample Type	Counting Method	Number of fields examined	GOI (%)	GOI Error (%)	Total Grains	Grains With Oil Inclusions	Fluorescence Colours of Oil Inclusions			Location of Oil Inclusions	
											Blue	White	Yellow and Orange	FCDM	QOB
Oliver-1	2946	2949	122223	cuttings	Random		6.30	1.67	809	51	36	15	0		
Oliver-1	2967	2970	122224	cuttings	Random		3.67	1.04	1255	46	45	1	0		
Oliver-1	2974.38		122407	core	Random		13.46	1.84	1322	178	177	1	0		
Oliver-1	2982	2985	122225	cuttings	Random		31.20	3.28	766	239	239	0	0		
Oliver-1	3006	3009	122226	cuttings	Random		9.47	1.86	950	90	73	10	7		
Oliver-1	3042	3045	122227	cuttings	Random		5.65	1.52	885	50	17	18	15		
Oliver-1	3078	3081	122228	cuttings	Complete		0.01	0.01	30713	3	1	1	1		
Oliver-1	3114	3117	122229	cuttings	Complete		0.05	0.04	13138	6	1	0	5		
Oliver-1	3147	3150	122230	cuttings	Complete		0.01	0.02	14715	2	0	1	1		

Table 4-7: GOI results from the Bilyara-1 well

Tables 4-7 and 4-8 show all relevant data for the analysed samples, including depth, sample number and method employed. Abbreviations shown in the location of oil inclusions column refer to Fractures Cutting Detrital Minerals (FCDM) and Quartz Overgrowth Boundary. GOI Error was defined using the method outlined in the text. Numbers shown in the 7 right most columns refer to numbers of grains containing oil inclusions of specific colour or location. Where numbers are absent no measurement was made.

Well Name	Start Depth (mRT)	End Depth (mRT)	CSIRO Number	Sample Type	Counting Method	Number of fields examined	GOI (%)	GOI Error (%)	Total Grains	Grains With Oil Inclusions	Fluorescence Colours of Oil Inclusions			Location of Oil Inclusions	
											Blue	White	Yellow and Orange	FCDM	QOB
Bilyara-1	2608.4		123282	core	Complete	1392	0.00	0.00	6589	0	0	0	0	0	0
Bilyara-1	2619.8		123279	core	Complete	1287	0.00	0.00	8323	0	0	0	0	0	0
Bilyara-1	2635.6		123280	core	Complete	1224	0.04	0.04	10894	4	3	0	1	4	0
Bilyara-1	2642.1		123468	core	Random	100	4.21	1.81	475	20	18	2	0	20	0
Bilyara-1	2643.2		123469	core	Complete	1125	0.02	0.02	17550	4	3	1	0	4	0
Bilyara-1	2651.9		123281	core	Complete	1496	0.00	0.00	28125	0	0	0	0	0	0
Bilyara-1	2694	2697	123283	cuttings	Complete	2405	0.01	0.02	8818	1	0	1	0	1	0
Bilyara-1	2703	2706	123284	cuttings	Complete	1628	0.02	0.03	6295	1	0	1	0	1	0
Bilyara-1	2712	2715	123285	cuttings	Complete	1628	0.03	0.04	6946	2	0	0	2	2	0

Table 4-8: GOI results from the Montara-1 well.

Refer to previous caption for a description of the abbreviations.

Well Name	Start Depth (mRT)	End Depth (mRT)	CSIRO Number	Sample Type	Counting Method	Number of fields examined	GOI (%)	GOI Error (%)	Total Grains	Grains With Oil Inclusions	Fluorescence Colours of Oil Inclusions			Location of Oil Inclusions	
											Blue	White	Yellow and Orange	FCDM	QOB
Montara-1	2604.4		122410	core	Complete	1344	0.32	0.13	7123	23	20	1	2	20	3
Montara-1	2610.05		122411	core	Complete	2144	0.04	0.03	13971	6	1	2	3	6	0
Montara-1	2616	2619	122412	cuttings	Complete	1368	0.00	0.00	5153	0	0	0	0	0	0
Montara-1	2622	2625	122413	cuttings	Complete	1512	0.01	0.02	10937	1	1	0	0	1	0
Montara-1	2625	2628	123357	cuttings	Complete	1665	0.01	0.02	6272	1	1	0	0	1	0
Montara-1	2628	2631	123358	cuttings	Complete	1575	0.01	0.02	14333	1	0	1	0	1	0
Montara-1	2631	2634	122414	cuttings	Complete	1512	0.01	0.02	9677	1	0	0	1	1	0
Montara-1	2634	2637	123359	cuttings	Complete	1548	0.01	0.02	7792	1	0	1	1	1	0
Montara-1	2640	2643	122415	cuttings	Complete	1554	0.00	0.00	5802	0	0	0	0	0	0
Montara-1	2643	2646	122416	cuttings	Complete	1628	0.04	0.05	5698	2	0	0	2	2	0
Montara-1	2649	2652	122417	cuttings	Complete	1620	0.07	0.07	5886	4	0	2	2	4	0

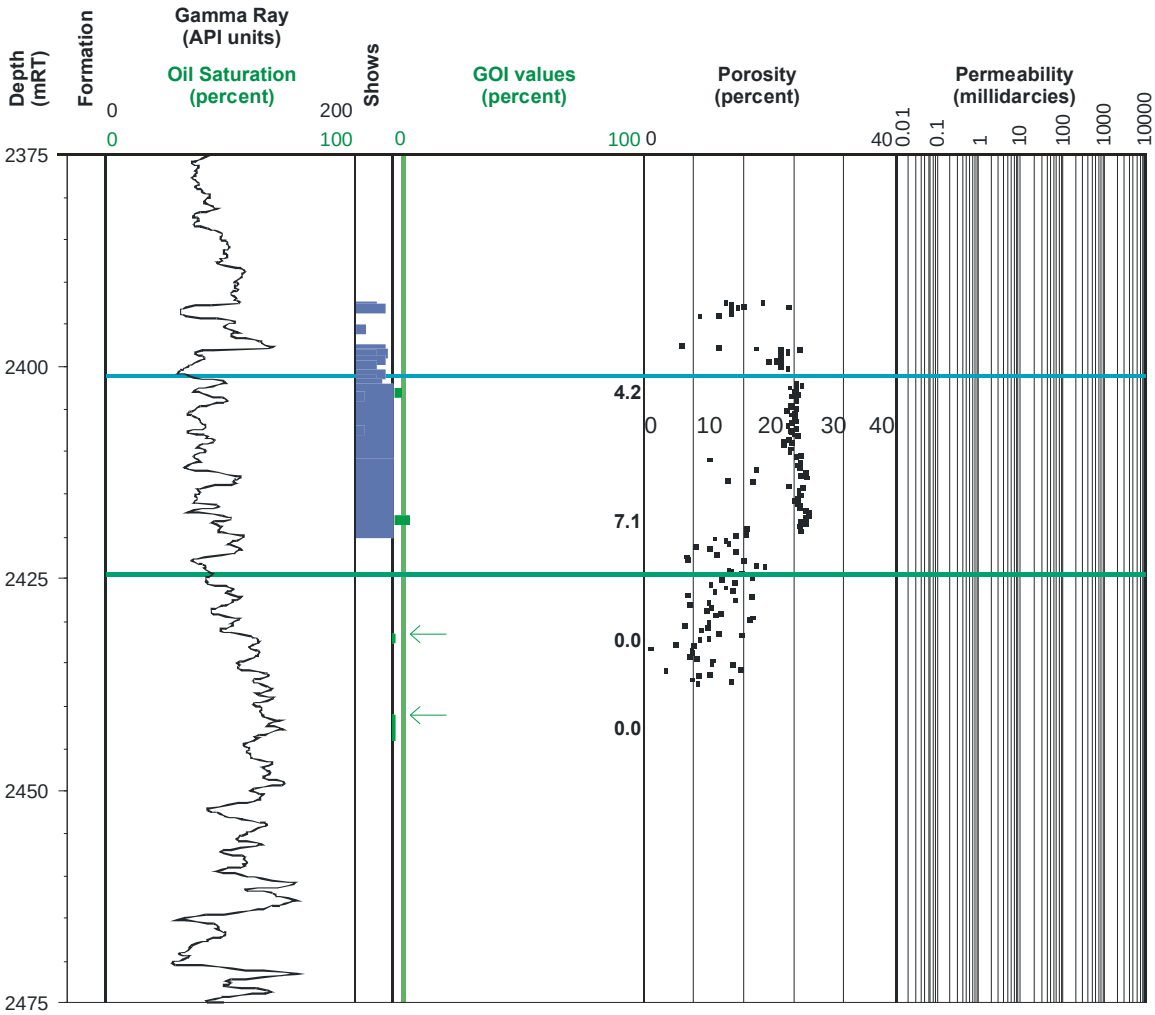

Figure 4-24: GOI results from Swift-1.

GOI results are displayed against to the gamma ray log with recorded porosity data and conventional oil shows also shown. On the GOI log the green vertical line marks the position of the empirical threshold for oil accumulation, with the width of the horizontal green lines showing the position and magnitude of the recorded GOI value (actual values shown to the right). Samples where GOI is <1% are marked with an arrow. Conventional shows come from the well completion report, with the thickness of the bar being proportional to their intensity.

Log analysis indicates 15.7m of net pay over the interval 1507.7mRT to 1541.7mRT with all sands below the OWC defined from the RFT data (1541.7mRT) being 100% water saturated. The mud log shows a rapid increase in total gas readings at the top of the reservoir returning to background levels at about 1575mRT (Santos, 1990a).

4.6.2 Oil and Gas Fields

Fields containing mostly gas, but with an associated oil leg, are represented in the VSB by the Montara, Bilyara and Oliver fields (Figure 4–11), all of which contain thick gas-legs underlain by thin oil rims. The presence of mostly gas rather than oil and the relatively small trap volume makes these fields currently non-economic although future development is planned for some of these accumulations.

The main objective to be addressed in these traps is to ascertain if the oil-legs were larger in the past. The traps are interpreted to be currently filled to structural spill points, hence understanding the filling history of these fields has significant exploration implications if it can be demonstrated that they once contained more substantial oil-legs as this is likely to have been spilled from the trap and could provide oil charge to satellite structures nearby (Lisk et al., 2002). Typically, the gas fields lack direct evidence for leakage (O'Brien et al., 1996a) and the inferred high integrity of these traps supports the attractiveness of displaced oil-leg plays.

4.6.2.1 The Oliver Field

The Oliver oil and gas field located in the north-eastern VSB (Figure 4–11) was discovered in 1988 by the drilling of Oliver-1, which encountered a 162.3m gas column underlain by a 13-16.8m oil rim (BHP Petroleum Ltd., 1988d).

The discovery is reservoired within sandstones of the Middle Jurassic Plover Formation directly below the Callovian Unconformity and is trapped within a simple tilted fault block. The field is currently considered sub-economic and although suspended as a potential oil and gas producer, the relatively small hydrocarbon volume, the relatively poor quality reservoir and thin oil rim all provide substantial challenges to any future development plan. The GOI results for Oliver-1 from the

current study augment the previously reported GOI values that were completed by the author and described in a broader study (O'Brien et al., 1996a).

A total of nine GOI analyses have been completed on samples from the Oliver-1 reservoir section, with GOI values ranging from less than 0.1% to a maximum of 31.2% (Figure 4–26, Table 4–6). A zone of elevated GOI values occurs at the top of the sampled interval where values of between 3.7 and 31.2% were recorded over the interval 2946-3045mRT. Except for the 2967-70mRT sample all of these values are above the threshold for oil accumulation and are consistent with prior oil accumulation within this currently gas-bearing reservoir. The 3.7% value recorded in the 2967-70m sample corresponds to a zone of poor reservoir quality and correspondingly lower oil saturation, resulting in a reduced GOI value relative to the remainder of the high GOI samples. Collectively, the data define a palaeo-oil column within presently gas-bearing sandstones of at least 99 m.

Using a range in palaeo-oil column heights based on the GOI numbers, O'Brien et al. (1996a) calculated an original volume of oil in place of between 166 and 220 MBBL. The current oil rim is considered to contain about 45 MBBL, leaving more than 120 MBBL unaccounted for and potentially available for remigration to traps located up-dip from the Oliver structure (Lisk et al., 1997; 2002). Significantly the excess oil could spill from the Oliver structure to potentially provide oil charge to structures that are shielded from the main source kitchen and would otherwise carry a much higher risk of receiving hydrocarbon charge.

The lack of high GOI values in samples from the current oil rim at Oliver-1 is a feature of many fields of this type (i.e. gas over oil) and has implications for the interpretation of GOI values in these cases and more broadly.

The absence of significant oil inclusions in rocks that are currently oil saturated is thought to indicate that the formation of oil inclusions occurs during initial oil charge and that subsequent modifications to fluid contacts, such as those introduced by tilting or gas displacement, are not recorded in GOI data (Lisk et al., 1998a).

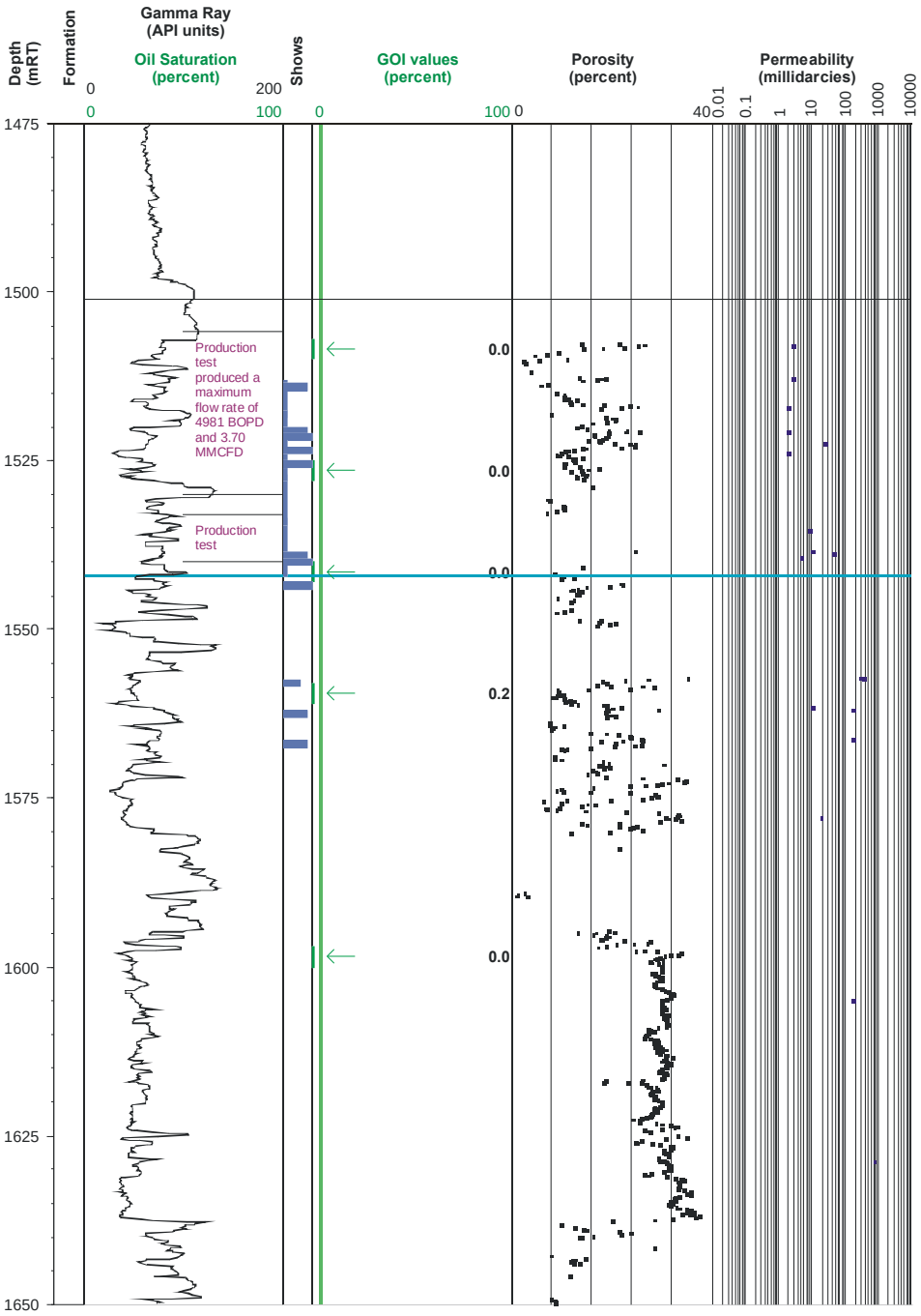

Figure 4-25: GOI results from Talbot-1.

GOI results displayed against the gamma ray log with recorded porosity and permeability data from core analysis. Production test intervals and conventional oil shows also shown. On the GOI log the green vertical line marks the position of the empirical threshold for oil accumulation with the width of the horizontal green lines showing the position and magnitude of the recorded GOI value (values shown to the right). Samples where GOI is <1% are marked with an arrow. Conventional shows are from the well completion report, with the thickness of the bar being proportional to their intensity.

This assertion is consistent with results from the geochemical analysis of fluid inclusion oils, which commonly show lower maturity for palaeo-oils than for the equivalent reservoired crude oils (George et al., 1997; 1998, Isaksen et al., 1998).

In the few examples where high GOI values are recorded in oil-leg samples, there is either no evidence for an early oil charge at the top of the structure or any early oil charge is geochemically unrelated to the currently reservoired oil (Lisk et al., 1996a). In these instances oil charge occurred after initial gas charge or separate pulses of oil charge can be attributed to different source rocks by geochemical composition.

Conventional oil shows recorded in the Oliver-1 well are limited to traces of fluorescence in cuttings from the reservoir section with no mention made of fluorescence in recovered SWC samples (BHP Petroleum Ltd., 1988d).

Conventional core taken from 2972-2981mRT from within the current gas zone also lacked fluorescence. Log analysis completed over the reservoir interval defined 99.9m of net pay over the interval from 2947-3117.1mRT with a GOC identified at 3111.4mRT and an OWC at 3125mRT, the latter derived from RFT pressure measurements. The interval of increased mud-gas levels corresponds reasonably well with the extent of the hydrocarbon column.

4.6.2.2 The Bilyara Field

The drilling of Bilyara-1 well in 1988 resulted in the discovery of the Bilyara oil and gas column reservoired within sandstones of the Oxfordian Montara Formation (BHP Petroleum Ltd., 1988e). After proving hydrocarbons the well became stuck in the hole at 2749m, and the Bilyara-1 well was plugged back and sidetracked, with Bilyara-1ST then drilled to a total depth of 2836m.

Gas bearing sands in the Bilyara-1 well are interpreted over the interval 2598.3-2638.6mRT, from log responses and from the recovery of gas by RFT. Pressure data from RFT defined clear gas and water gradients, with an intersection at 2639.4mRT (2611.9mSS) indicating an apparent GWC.

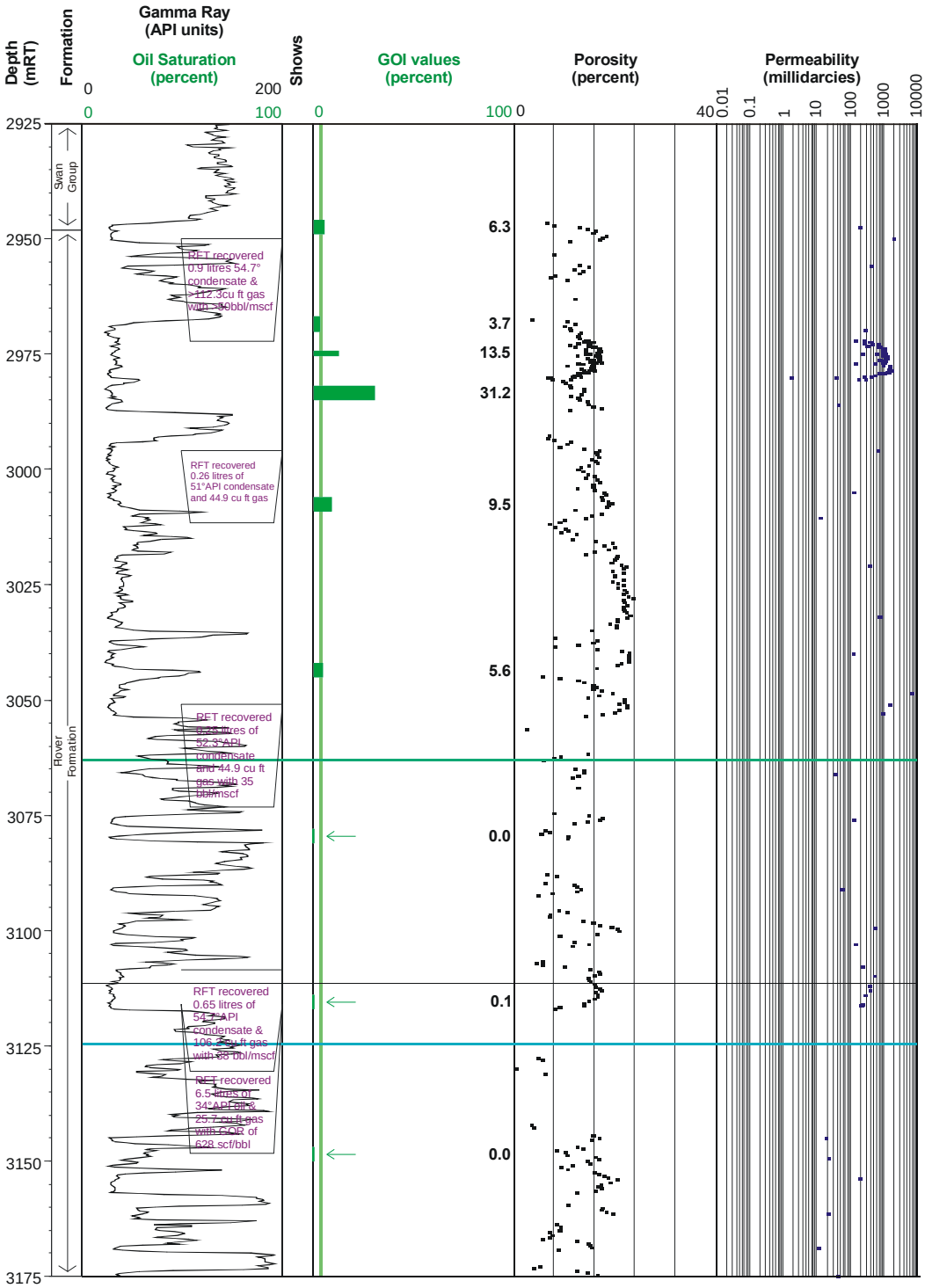

Figure 4-26: GOI results from the Oliver-1 well.

GOI results displayed against the gamma ray log with recorded porosity and permeability from core analysis data and where available oil saturation values derived from electric log analysis. On the GOI log the green vertical line marks the position of the empirical threshold for oil accumulation, with the width of the horizontal green lines showing the position and magnitude of the recorded GOI value (actual values shown to the right). Samples where GOI is <1% are marked with an arrow. Conventional shows reported in the well completion report are shown with the thickness of the bar being proportional to their intensity.

On log data the gas effect on the neutron-density logs decreases markedly below 2838.6mRT and is interpreted to reflect the position of a gas-oil contact at this depth (BHP Petroleum Ltd., 1988e).

Further appraisal drilling by Bilyara-1ST, which penetrated the reservoir 24.5m structurally lower, supported the presence of an oil rim and with the aid of RFT pressure data a GOC was placed at 2611.5mSS and an OWC could be defined at 2615.1mSS. The oil saturations measured from subsequent core analysis also provides evidence for an oil-leg over the interval 2638.6-2641.4mRT. Collectively, the drilling results from the Bilyara-1 and Bilyara-1ST wells defined a 43.1m zone of hydrocarbons, comprising a 2.8m oil rim overlain by a 40.3m gas cap.

A total of nine samples were analysed from Bilyara-1 and returned GOI values of between 0 and 4.2%. Except for the 2642.1mRT core sample (GOI=4.2%), all other samples have GOI values of less than 0.1% (Figure 4–27, Table 4–7).

A single high GOI value of 4.2% encountered in Bilyara 1 at 2642.1mRT (2614.3mSS) is consistent with the location of this sample within the current oil leg (GOC at 2611.5mSS and OWC at 2615.1mSS). The maximum vertical extent of this (palaeo-) oil column, based on the available sample spacing, is about 7.5 m, similar to the extent of the present oil rim as defined by RFT and log data (4.6m). Significantly, the lack of high GOI values in samples directly below the top seal does not support oil charge prior to gas. Charging of the reservoir with gas, and then with oil, or simultaneously is the preferred charge history in this instance.

This interpretation is consistent with the sediment extract geochemistry (BHP Petroleum Ltd., 1988e), which show high extract yields (average 3400 ppm) in samples that are restricted to the current oil-leg. The accumulation of gas prior to oil is predicted by regional basin modelling studies reported in Kennard et al. (2001).

The upper part of the reservoir section did not show any fluorescence in either the straight hole or the sidetrack whilst conventional shows in SWC samples are restricted to minor bright orange to pale green pinpoint fluorescence in a single sample at 260mRT (BHP Petroleum Ltd., 1988e).

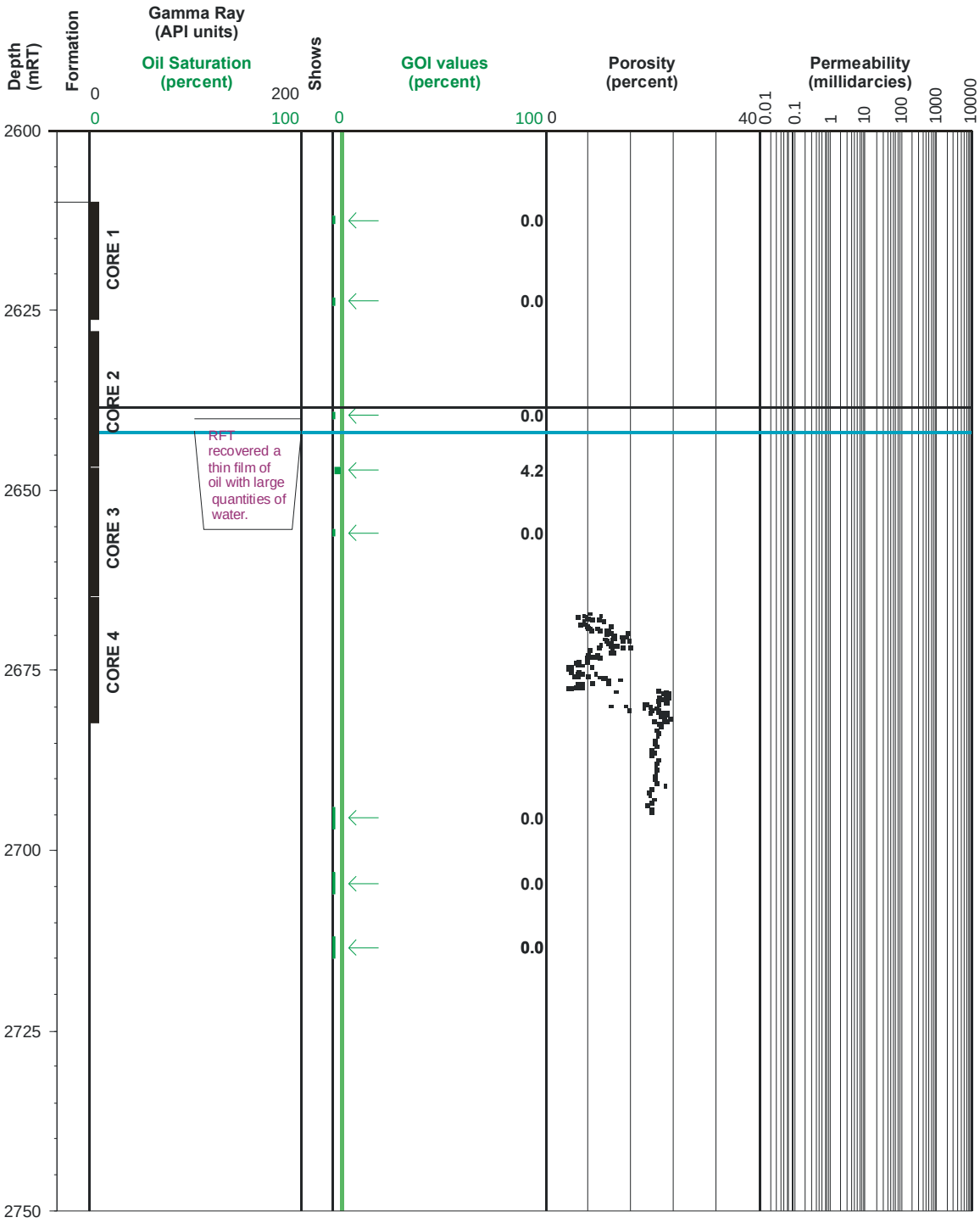

Figure 4-27: GOI results from Bilyara-1.

GOI results displayed against the gamma ray log with recorded porosity and permeability from core analysis and where available oil saturation values derived from electric log analysis. On the GOI log the green vertical line marks the position of the empirical threshold for oil accumulation, with the width of the horizontal green lines showing the position and magnitude of the GOI value (actual values shown to the right). Samples where GOI is <1% are marked with an arrow. Conventional shows reported in the well completion report are also shown with the thickness of the bar being proportional to their intensity.

SWC samples from the sidetrack well showed similar fluorescence from 2727-2758mRT increasing to moderate to strong white-yellow spotty fluorescence in SWC from 2711-2726mRT. In the conventional core only minor fluorescence is noted from 2606mRT down to 2611mRT before becoming more common from 2612-2615mRT where pinpoint yellow-orange fluorescence was reported, returning to trace levels below 2616mRT then increasing again from 2633mRT. Fluorescence increased markedly below this depth, described as 60-100% bright pale yellow fluorescence from 2636mRT to the base of Core 2 (2642.82mRT). Below this depth the intensity of fluorescence declined sharply with only minor fluorescence observed down to the base of the cored section at 2678.3mRT.

Log analysis from Bilyara-1 calculated residual oil saturations of 10-15% down to 2651mRT which corresponds to the base of an inferred residual oil zone in the sidetrack well. Increased mud-gas levels correspond to the current hydrocarbon zone but are not conclusive with respect to the inferred residual oil zone.

4.6.2.3 The Montara Field

The Montara oil and gas field was discovered by the drilling of Montara-1 in 1989, which encountered a 35m hydrocarbon column within Oxfordian sandstones, subsequently named as the type section for the Montara Formation (BHP Petroleum Ltd., 1988f). A 25m net gas pay and at least 10m of oil pay is interpreted over the interval 2599-2634m. A GOC is clearly defined at 2623.8m but the position of the OWC is less certain due to the heavily bioturbated and argillaceous nature of the reservoir near the contact.

GOI values recorded in the 11 samples analysed from Montara-1 are all between 0 and 0.3%, including nine samples that were taken from within the current hydrocarbon zone (Figure 4–28, Table 4–8). The four samples from the current oil-leg all have GOI values less than 0.1%. The cause of this discrepancy is poorly understood. The very low GOI values resemble baseline water-zone values rather than the intermediate values (between 1 and 5%) commonly seen in zones of reduced reservoir quality. This suggests that suitable conditions for the trapping of oil inclusions did not coincide with the attainment of high oil saturation.

Conventional oil shows recorded in the Montara-1 well included trace bright yellow fluorescence in ditch cuttings from 3405-08mRT. Recovered SWC samples showed up to 60-70% moderately bright yellow-green fluorescence at 2302mrt, 2303mRT and 2304mRT with 40-50% bright white to light blue fluorescence seen in all SWC from 2624mRT to 2636mRT.

Log analysis defined 34.2m of hydrocarbon pay (2599-2633mRT) with a GOC identified at 2624mRT underlain by an oil-leg, although the OWC lies within shale and the position of this contact was hard to constrain (BHP Petroleum Ltd., 1988f).

Based on log data and the results of a drill stem test the OWC is placed at 2642.5m, which corresponds well with a sharp reduction in total mud-gas levels. Subsequent drilling of two appraisal wells confirmed the free water level to be at 2620.5mTVDSS (corresponds to approximately 2637mRT in Montara-1).

The low GOI numbers recorded in the samples from the Montara-1 current oil zone may be analogous with those obtained in the Oliver-1 well (refer to section 4.6.2.1), where the GOI values are low (GOI <1%) in samples from the current oil zone, but instead record an initial oil charge as a high GOI zone at the top of the reservoir. The position of the well intersection becomes important in interpreting the significance of the results in these circumstances.

If sufficient remaining closure is present up-dip from the well intersection to accommodate the volume of oil present within the current oil rim then this oil could have been initially reservoired at the crest of the structure. If the palaeo-OWC is located structurally above the highest point of the reservoir sampled in Montara-1 then no high GOI zone would be detected (i.e. the current oil zone is located within the original palaeo-water leg).

Present day structure maps for the Montara trap, however, show that Montara-1 penetrated the reservoir section near the crest and is unlikely to have missed an up-dip palaeo-oil column (Figure 4–29) unless the depth conversion is incorrect. The results observed at the nearby Bilyara Field where an elevated GOI value is recorded within the current oil rim also discount this likelihood.

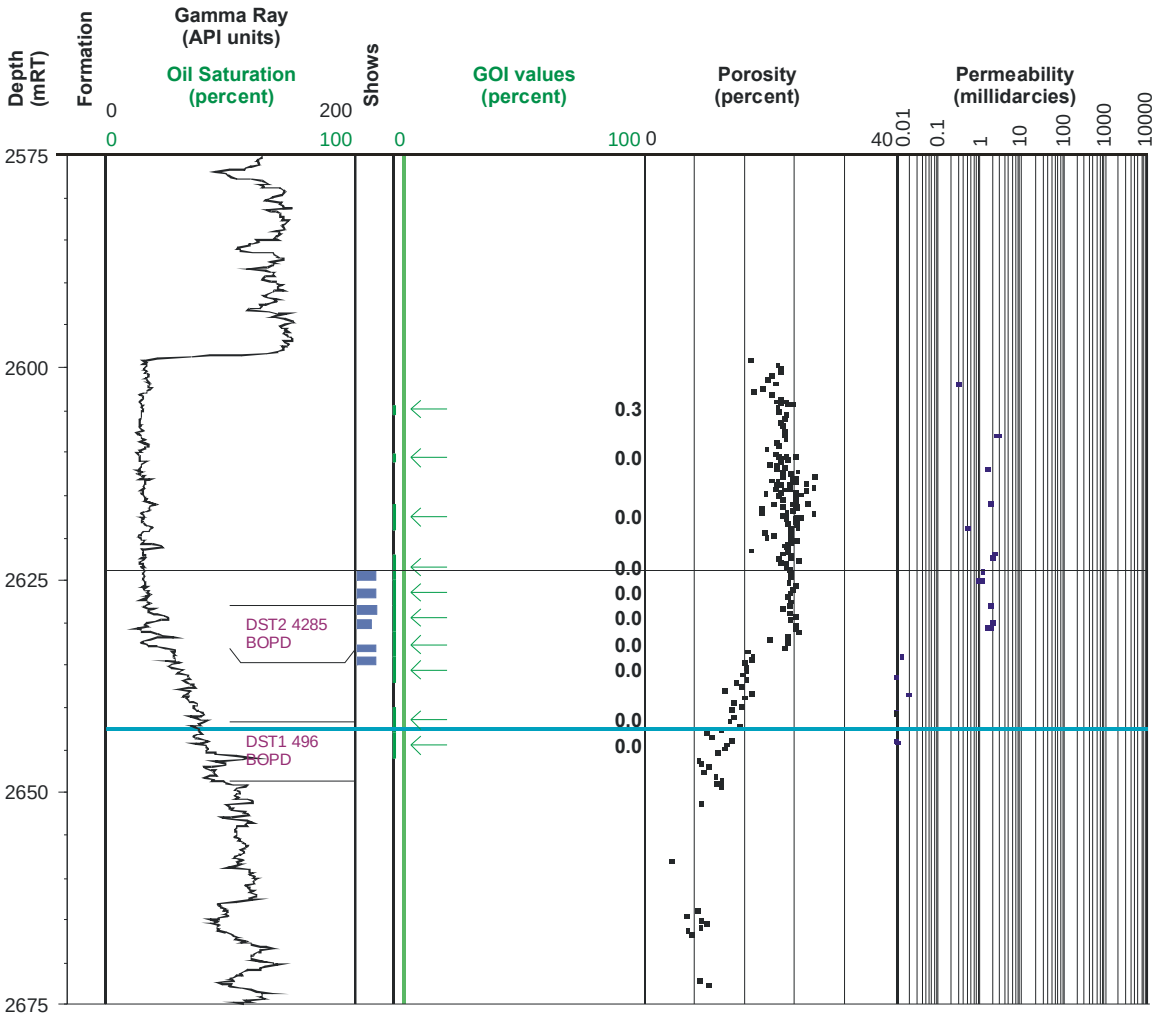

Figure 4-28: GOI results from Montara-1.

GOI results displayed against the gamma ray log with recorded porosity and permeability from core analysis data and where available oil saturation values derived from electric log analysis. Results of drill stem testing conducted on the reservoir are also shown. On the GOI log the green vertical line marks the position of the empirical threshold for oil accumulation, with the width of the horizontal green lines showing the position and magnitude of the recorded GOI value (actual values shown to the right). Samples where GOI is <1% are marked with an arrow. Conventional shows from the well completion report are also shown with the thickness of the bar being proportional to their intensity.

The low GOI values indicate that either the oil saturation was low when the inclusions were trapped or that oil inclusions were not formed due to the absence of a valid trapping mechanism.

An alternative explanation for the low GOI values seen in the Montara-1 well is suggested by the geochemical composition of the recovered hydrocarbons. Oil from the Montara-1 and -2 wells has a composition of low molecular weight hydrocarbons that indicate modification by a process known as evaporative fractionation. This process results in the light hydrocarbons contained in the oil being selectively retained within a separated gas phase that migrates away leaving behind an altered, residual oil that is deficient in low-molecular-weight straight-chain alkanes (Thompson, 1987, 1988). Although this process is normally considered to occur on the migration pathway it is possible that preferential loss of gas from a trap by partial trap breach could also produce such an outcome. This raises the possibility that the original charge to the Montara structure was single phase wet gas rather than discrete oil and gas phases. Partial trap breach and loss of some gas would have the effect of lowering reservoir pressure and could have caused the current oil-leg to dissolve out from the remaining gas to form the oil-leg. Under this scenario the original charge would not have resulted in the trapping of any oil inclusions and could explain the very low GOI values recorded across the Montara-1 hydrocarbon zones.

Preferential gas loss has been proposed to explain substantial variations in the Gas Oil Ratio (GOR) of VSB oil fields. O'Brien et al. (1996a, 1999a) noted that traps with a current gas cap in the VSB generally have much higher GOR than those traps that contain only oil surmising that preferential gas leakage had lowered the GOR of the retained oil. They highlighted the GOR of the Skua field that contains a gas cap (2,126 SCF/STB) and compared with that of the Jabiru (390 SCF/STB) and Challis (197 SCF/STB) oil fields that lack a gas cap to support this hypothesis. Whilst the Montara field still has a gas cap the oil is unusually under-saturated, with GOR values of 597-1426 SCF/STB. Partial gas leakage represents a feasible explanation for observed reduction in the GOR levels and could also support the proposition that charge to Montara may initially have consisted of single phase wet gas.

4.6.3 Gas Fields

Gas columns, without an associated oil-leg have been delineated within the Vulcan Sub-basin in traps tested by the Delamere-1, Keeling-1, Pengana-1, Tahbilk-1 and the Swan-1, -2 and -3 wells (Figure 4–11). Due to the small trap sizes and economic requirements for gas being prohibitive at the time of drilling these features were targeted as oil filled reservoirs where the volumetric capacity of a trap needed to produce an economic oil field are much smaller than is typically required for an equivalent gas discovery.

A consequence of incorrectly predicting fluid phase is that the small gas volumes and lack of an underlying oil-leg have prevented these discoveries from being commercialised and will likely remain as stranded gas for the foreseeable future.

As with the gas and oil discoveries a more complete understanding of the charge history provides useful information to improve the future prediction of hydrocarbon phase but also to appraise the likelihood of an oil-leg being displaced to nearby un-drilled structures. However, unlike gas over oil discoveries where the presence of an oil rim confirms that only oil has been spilled the risk in purely gas discoveries is that gas has also been spilled and that nearby traps may also be gas flushed. Small satellite structures that are oil-bearing constitute viable exploration targets if the oil charge risk can be successfully managed by constraining the likely volumes of remigrated oil.

GOI data have been obtained from gas and water-bearing reservoirs in the Keeling-1, Pengana-1 and Swan-1, -2 and 3 wells. As all of these gas accumulations lack conventional indications of a prior liquids charge, the key objectives was to determine if oil migrated into these traps in sufficient volumes to produce an oil accumulation that has subsequently been displaced.

4.6.3.1 The Keeling Field

The small Keeling gas discovery was made in 1990 with the drilling of Keeling-1 that targeted Middle Triassic sandstones within a faulted anticline (Norcen, 1990).

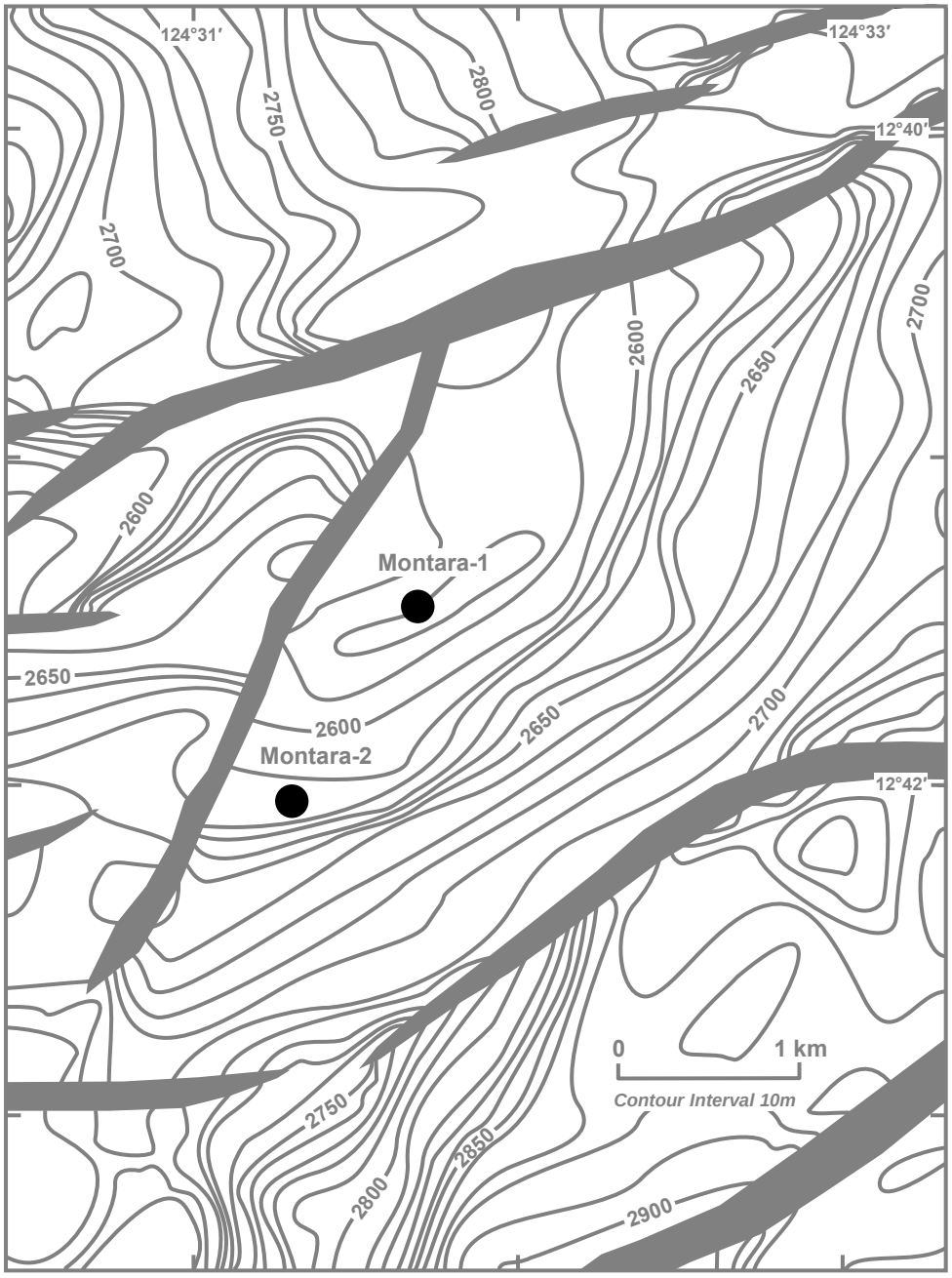

Figure 4-29: Depth structure map for the top Oxfordian reservoir, Montara Field.

Depth contour map showing depth to top porosity for the Oxfordian Montara Formation, major faults and the location of the Montara-1 and Montara-2 wells (modified from Cadman and Temple, 2003). Note the near crestal location of the Montara-1 well that suggests there is little up-dip reservoir that hasn't been tested by the well.

The well intersected a 25-30m gross gas column in both Lower Cretaceous and Triassic sandstones with reserves calculated at about 24 billion cubic feet (BCF) of gas initially in place (GIIP, Norcen, 1990). Commercial gas fields in this region typically require a minimum economic field size of more than 1000 BCF, making it unlikely for such a small gas column to be developed in the immediate future.

In this study the samples taken from across the gas and water legs in Keeling-1 have provided evidence for palaeo-oil accumulation, with high GOI values, of 3.7% to 8.4% recorded in four cuttings samples over the interval 3036-66 mRT (Figure 4–30; O'Brien et al., 1996a; Lisk et al., 1996b).

Conventional oil shows were absent in the Lower Cretaceous and Triassic reservoir interval in Keeling-1, although a pronounced gas peak from 3035mRT-3068mRT corresponds with top porosity (Norcen, 1990). Log interpretation is consistent with increased gas saturation from 3035mRT down to at least 3055mRT. RFT pressures show a GWC occurs at 3059mRT at the base of a shale (Norcen, 1990).

Significantly, this palaeo-OWC defined by the GOI data at 3067mRT±3m extends below the current gas water contact (GWC). Post-drill depth structure maps show the trap not to be filled to spill (Figure 4–31) so the change to the present configuration cannot be ascribed to a purely gas displacement mechanism, where an oil-rim is anticipated to have been retained in closure below the gas zone. Rather, partial or complete, loss of oil from the trap due to fault reactivation is consistent with published trap integrity predictions (O'Brien et al., 1996a, 1998; Lisk et al., 1997) and the presence of oil in basal Miocene sands (Norcen Ltd., 1990).

Consequently, displacement of this oil across the lateral spill-point of the trap is not anticipated unless the current trap configuration was different in the geological past.

4.6.3.2 The Swan Field

The Swan gas accumulation is defined by 3 wells drilled in the period, 1973-1991. The discovery well, Swan-1, targeted a Cretaceous clastic fan against an interpreted salt diapir, encountering gas in thin calcareous Upper Cretaceous sandstones.

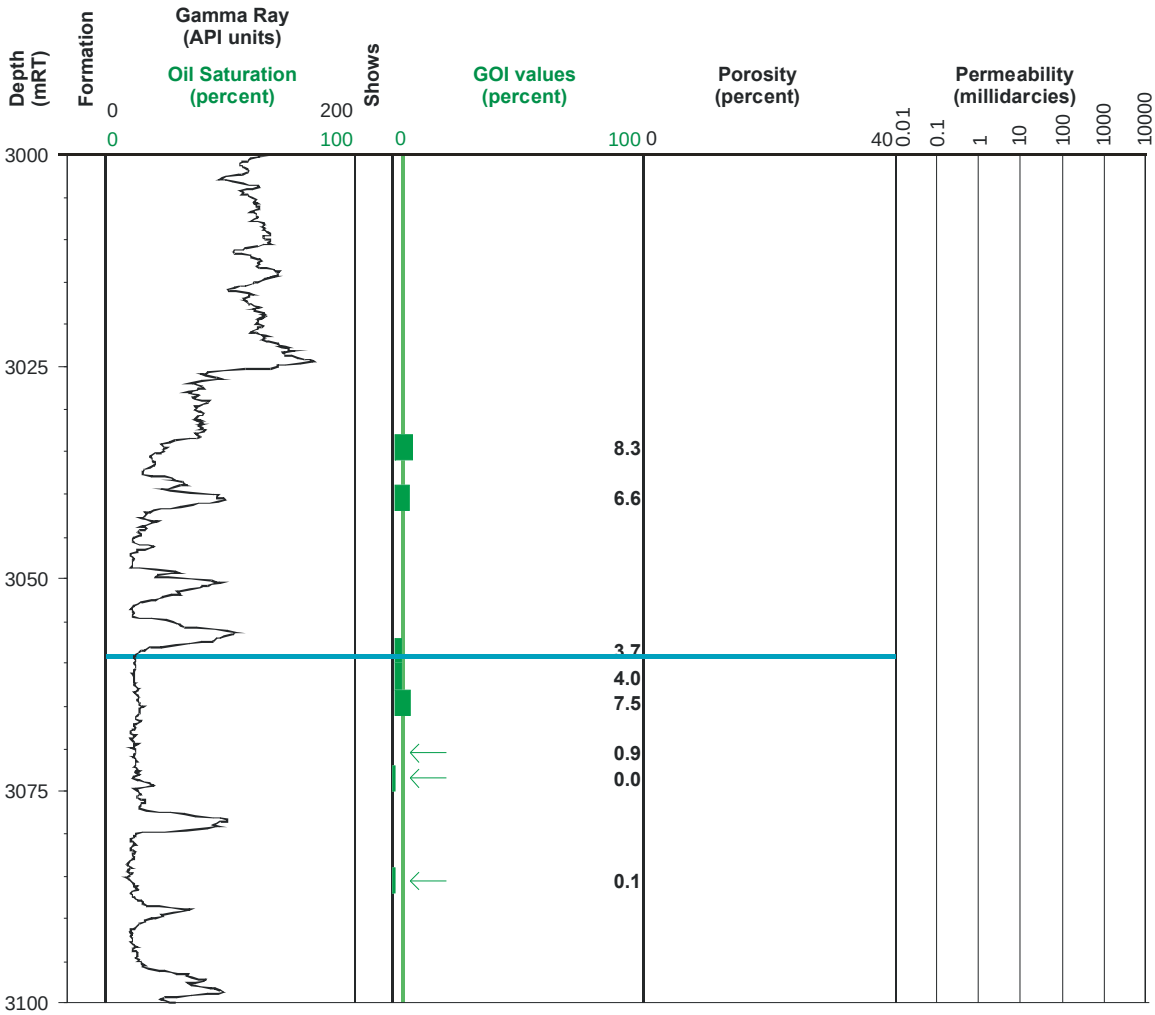

Figure 4-30: GOI results from the Keeling-1 gas discovery.

GOI results displayed against the gamma ray log with recorded porosity and permeability from core analysis data and where available oil saturation values derived from electric log analysis. On the GOI log the green vertical line marks the position of the empirical threshold for oil accumulation, with the width of the horizontal green lines showing the position and magnitude of the recorded GOI value (actual values shown to the right). Samples where GOI is <1% are marked with an arrow. Conventional shows from the well completion report are also shown with the thickness of the bar being proportional to their intensity.

The Swan-2 well was drilled in 1980 to test Middle Jurassic sandstones within a structurally complex zone interpreted to be a salt structure. The well failed to penetrate the Jurassic section but Cretaceous sandstones, constituting a secondary drilling objective, were gas-bearing as indicated by high mud gas levels and elevated resistivity responses on the wireline logs (CITCO Australia Petroleum Ltd., 1980).

Significant gas readings were also noted in thin Lower Cretaceous sandstones, but electric logging was compromised by drilling problems associated with elevated formation pressure and detailed log analysis was not possible for this interval (CITCO Australia Petroleum Ltd., 1980). Drill Stem Testing conducted over both sections failed to recover any significant hydrocarbons, which was also attributed to the recognised overpressure problems.

Swan-3 was then drilled by BHP Petroleum Ltd. in 1991 to further appraise the Swan 1 and 2 gas discoveries. Three discrete sand bodies, informally referred to as the P1, P2 and P3 sands of the Puffin Formation were targeted by Swan-3 within a complex combined structural-stratigraphic trap.

19.4m of net gas pay was defined in the P1 and P2 sands with direct and cut fluorescence noted, particularly towards the base of the section (BHP Petroleum Ltd., 1992). The P3 sand was not encountered so the well was sidetracked 250m south of the original location to successfully intersect the P3 sand. RFT pressure data indicated the P3 sand was also fully gas bearing. The Swan-3 and Swan-3/ST1 wells proved a significant, yet sub-economic, gas column within the Puffin Sandstone but no proven fluid contacts were identified and it remains unclear if these gas sands are connected to those seen in the Swan-1 and Swan-2 wells.

GOI analyses have been completed on a total of 19 samples from the Puffin Formation, comprising three samples from Swan-1, eight samples from Swan-2, three samples from Swan-3 and five samples from Swan-3/ST1 (Table 4–10).

In Swan-1, oil inclusions are restricted to the uppermost of the three samples with a GOI value of 0.2% being recorded at 2359-65mRT (Figure 4–32).

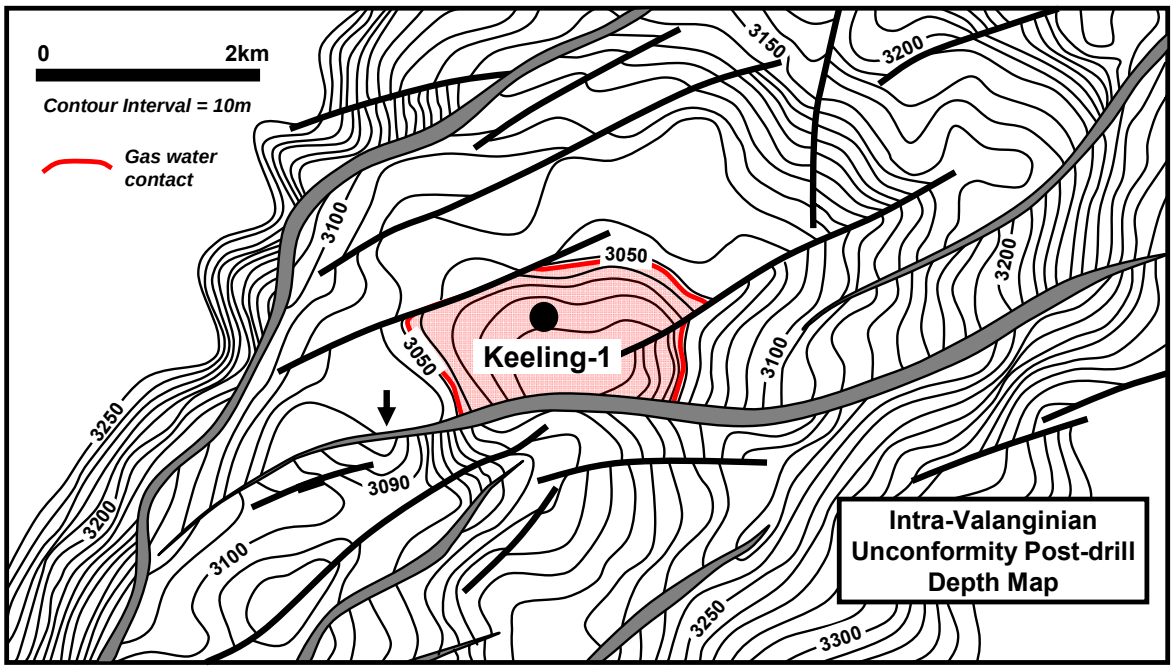

Figure 4-31: Top porosity post-drill depth-structure map, Keeling-1.

Intra-Valanginian depth map taken from the Keeling-1 well completion report (Norcen Ltd., 1990) showing the extent of the proven gas accumulation. The arrow marks the approximate position of the current spill point where fault throw falls below the thickness of the gas column and cross juxtaposition of reservoir section would occur (modified from Cadman and Temple, 2003).

This low GOI value in the upper sand together with the absence of oil inclusions in the two additional samples from the lower sand is consistent with focusing of migration pathways in the interval immediately below a regional top seal and indicates oil migration without any accumulation at this well location.

No conventional oil shows were observed during the drilling of Swan-1 but significant gas peaks were recorded across the two reservoir sands and log analysis and gas recovery by Formation Interval Test (FIT) confirmed the presence of two 5m thick gas zones (ARCO Australia Ltd., 1973).

In samples from Swan-2, a zone of high GOI values, ranging from 5.1% to 19.3% in five samples over the interval 2253-2322 (Figure 4–33) is above the threshold for oil accumulation and is interpreted to reflect a palaeo-oil column. A fall in GOI values to 1.3% at 2325-28m, 0.5% at 2328-31m and 1.7% at 3437-40m is consistent with a sharp fall in oil saturation and in the absence of an intervening capillary barrier is interpreted to reflect the crossing of a palaeo-OWC.

A net palaeo-oil column of about 20m over four discrete sandstone beds can be discerned, however, it is unclear if these represent a single continuous oil column or 4 discrete oil zones separated by intervening shales.

Conventional oil shows recorded in the Swan-2 well were limited to occasional SWC samples that displayed minor fluorescence described as pale white to yellow fluorescence noted in SWC at 2250mRT, 2254mRT and 2277mRT and pale blue fluorescence reported from a SWC at 2330mRT. As previously mentioned drilling problems encountered in the well prevented the completion of wireline logging so no petrophysical assessment was possible but strong mud-gas peaks corresponded with each sandstone unit over the interval 2250mRT-2330mRT with about 35m of net gas-bearing sand being recognised.

Samples taken from the presently gas-bearing Swan 3ST well support prior oil accumulation, with high GOI values of 6.1% at 2340-46 m and 8.4% at 2349-52 m defining an 11-15 m palaeo-oil column within the P1 and P2 sands (Figure 4–34).

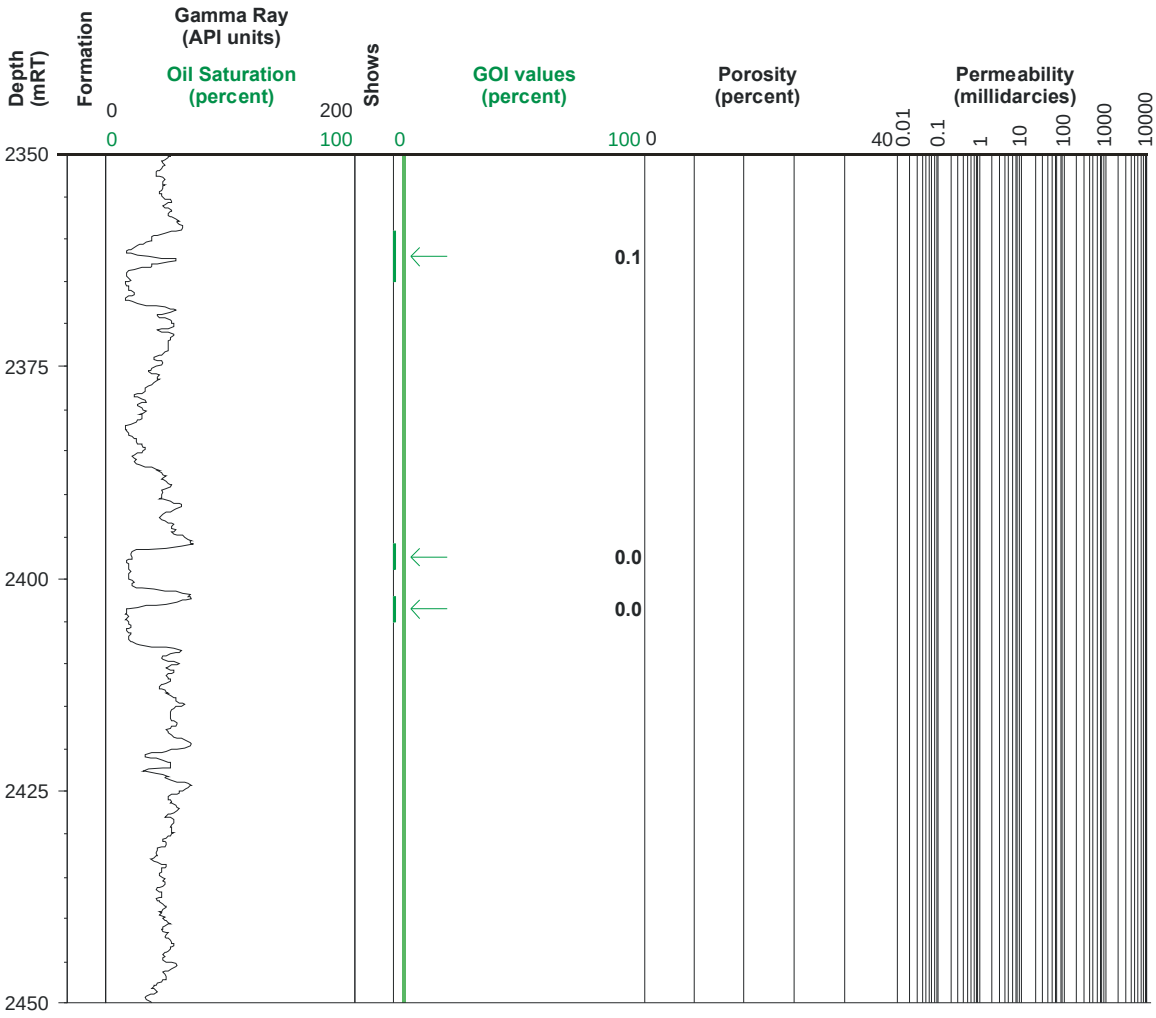

Figure 4-32: GOI results for the Swan-1 well.

GOI results displayed against the gamma ray log with recorded porosity and permeability from core analysis data and where available oil saturation values derived from electric log analysis. On the GOI log the green vertical line marks the position of the empirical threshold for oil accumulation, with the width of the horizontal green lines showing the position and magnitude of the recorded GOI value (actual values shown to the right). Samples with a GOI value of <1% are marked with a green arrow. Conventional shows reported in the well completion report are also shown with the thickness of the bar being proportional to their intensity.

Conventional oil shows are restricted to the base of the gas zone where 100% bright white fluorescence was recorded from 2466mRT to 2468mRT. Prominent mud-gas peaks were noted within the three sandstone intervals at 2341-52mRT, 2366-72mRT and 2445-2466mRT with resistivity logs indicating these zones are gas-bearing.

4.6.3.3 The Pengana Field

Pengana-1 defined a small gas discovery within Triassic sandstones. Combined RFT and electric log analysis showed the reservoir contained a 5m gross gas column between 1639-1644m with a GWC in the interval 1644-1647m (BHP Petroleum Ltd., 1988g). The small column height reflects differences between the pre-drill prediction and the actual formation tops due to uncertainties in depth conversion caused by a variable velocity field and an incorrect seismic pick (BHP Petroleum Ltd., 1988g).

Consequently a much smaller closure was encountered than was expected and is filled to spill with gas rather than the prognosed oil. The small trap size coupled with a gas rather than a liquids charge has resulted in a non-economic discovery.

Two samples were taken from Pengana-1 for GOI analyses, one from within the current gas zone and one from within the water-leg. Both of these samples are devoid of oil bearing fluid inclusions (Figure 4–35) and there were no conventional oil shows noted in the well (BHP Petroleum Ltd., 1988g). The absence of high GOI values in this trap could reflect the isolation of these fields from oil migration fairways, with the charge coming from gas-prone source rocks. Alternatively, the gas in these traps could be analogous to the early gas charge inferred in several other fields, including Cassini (section 4.6.1.4) and Bilyara (section 4.6.2.2). Filling of these traps to spill point with gas prior to the oil-prone source becoming mature would explain the absence of oil, without having to invoke an oil migration failure.

4.6.4 Plugged and Abandoned Wells

The results in previous sections of this chapter focused on currently hydrocarbon filled traps where the primary aim of the analyses has been to calibrate the application of the GOI method to samples with known hydrocarbon saturation.

Table 4-9: GOI results from the Keeling-1 well.

Tables 4-9, 4-10 and 4-11 show all relevant data for the analysed samples, including depth, sample number and method employed. Abbreviations shown in the location of oil inclusions column refer to Fractures Cutting Detrital Minerals (FCDM) and Quartz Overgrowth Boundary. GOI Error was defined using the method outlined in the text. Numbers shown in the 7 right most columns refer to numbers of grains containing oil inclusions of specific colour or location.

Well Name	Start Depth (mRT)	End Depth (mRT)	CSIRO Number	Sample Type	Counting Method	Number of fields examined	GOI (%)	GOI Error (%)	Total Grains	Grains With Oil Inclusions	Fluorescence Colours of Oil Inclusions			Location of Oil Inclusions	
											Blue	White	Yellow and Orange	FCDM	QOB
Keeling-1	3033	3036	111286	cuttings	Random		8.35	2.24	587	49	30	16	3	49	
Keeling-1	3039	3042	111290	cuttings	Random		5.24	1.34	1068	56	29	22	5		
Keeling-1	3039	3042	122385	cuttings	Random	100	6.58	1.76	760	50	31	15	4	50	0
Keeling-1	3057	3060	111287	cuttings	Random		3.68	1.34	761	28	14	10	4		
Keeling-1	3060	3063	111288	cuttings	Random		3.96	1.39	757	30	21	9	0		
Keeling-1	3063	3066	122359	cuttings	Random	100	7.50	2.13	587	44	36	6	2	19	25
Keeling-1	3069	3072	122406	cuttings	Complete	1120	0.92	0.30	3920	36	21	9	6	22	14
Keeling-1	3072	3075	111289	cuttings	Complete		0.00	0.00	8580	0	0	0	0		
Keeling-1	3084	3087	122360	cuttings	Complete	1295	0.05	0.10	1900	1	0	1	0	1	0

Table 4-10: GOI results from the Swan wells.

Refer to caption for Table 4-9 for details of abbreviations.

Well Name	Start Depth (mRT)	End Depth (mRT)	CSIRO Number	Sample Type	Counting Method	Number of fields examined	GOI (%)	GOI Error (%)	Total Grains	Grains With Oil Inclusions	Fluorescence Colours of Oil Inclusions			Location of Oil Inclusions	
											Blue	White	Yellow and Orange	FCDM	QOB
Swan-1	2359	2365	123325	cuttings	Complete	1020	0.15	0.12	3910	6	0	6	0	6	0
Swan-1	2396	2399	123326	cuttings	Complete	1530	0.00	0.00	816	0	0	0	0	0	0
Swan-1	2402	2405	123327	cuttings	Complete	1564	0.00	0.00	782	0	0	0	0	0	0
Swan-2	2253	2256	123360	cuttings	Random	100	19.26	4.70	270	52	22	28	2	47	5
Swan-2	2265	2268	123328	cuttings	Random	100	16.10	4.22	292	47	21	26	0	37	10
Swan-2	2277	2280	123329	cuttings	Random	100	9.15	3.29	295	27	16	11	0	15	12
Swan-2	2316	2319	123548	cuttings	Random	100	17.32	4.65	254	44	43	1	0	25	19
Swan-2	2319	2322	123549	cuttings	Random	100	5.14	2.25	370	19	17	2	0	9	10
Swan-2	2325	2328	123330	cuttings	Complete	1548	1.25	0.32	4644	58	39	19	0	47	11
Swan-2	2328	2331	123550	cuttings	Complete	1408	0.52	0.26	2863	15	14	1	0	11	4
Swan-2	2337	2340	123551	cuttings	Complete	1575	1.71	0.36	5093	87	74	13	0	82	5
Swan-3	2312.1		123141	core	Complete	729	0.44	0.17	5929	26	9	17	0	26	0
Swan-3	2325.35		123142	core	Complete	1026	1.81	0.28	8995	163	140	23	0	163	0
Swan-3	2415	2418	123143	cuttings	Complete	1496	0.02	0.03	6533	1	0	1	0	1	0
Swan-3ST1	2340	2346	123144	cuttings	Random	100	6.13	1.58	881	54	10	41	3	45	9
Swan-3ST1	2349	2352	123465	cuttings	Random	100	8.44	2.22	604	51	36	15	0	39	12
Swan-3ST1	2355	2358	123130	cuttings	Complete	1656	1.40	0.35	4416	62	33	29	0	51	11
Swan-3ST1	2370	2373	123131	cuttings	Complete	1656	0.33	0.12	8170	27	20	7	0	11	16
Swan-3ST1	2445	2448	123145	cuttings	Complete	1020	0.05	0.05	7922	4	1	2	1	4	0

Table 4-11: GOI results from the Pengana-1 well.

Refer to caption for Table 4-9 for details of abbreviations.

Well Name	Start Depth (mRT)	End Depth (mRT)	CSIRO Number	Sample Type	Counting Method	Number of fields examined	GOI (%)	GOI Error (%)	Total Grains	Grains With Oil Inclusions	Fluorescence Colours of Oil Inclusions			Location of Oil Inclusions	
											Blue	White	Yellow and Orange	FCDM	QOB
Pengana-1	1641.15		122461	core	Complete	1221	0.00	0.00	18478	0	0	0	0	0	0
Pengana-1	1651.09		122462	core	Complete	870	0.00	0.00	5510	0	0	0	0	0	0

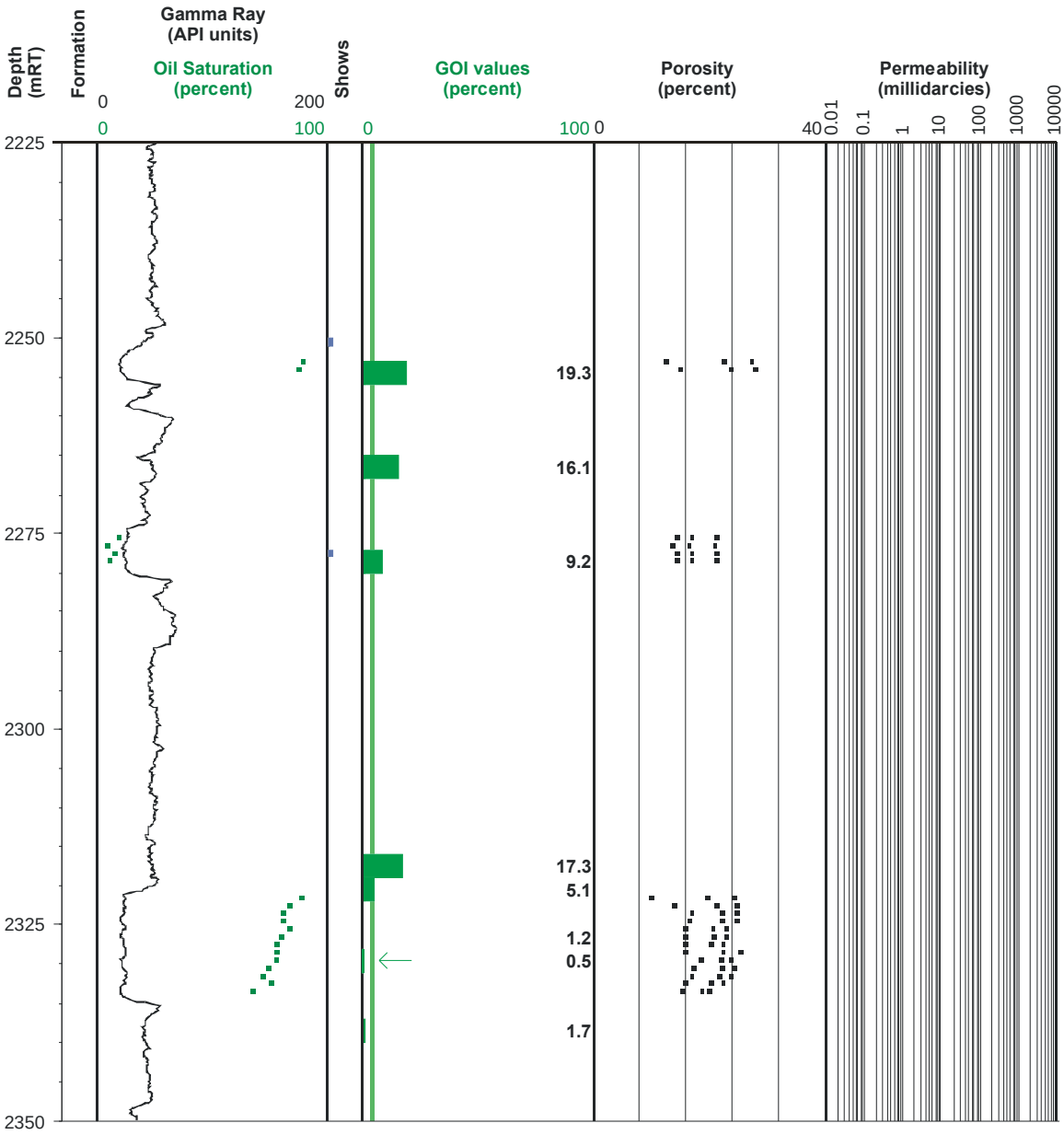

Figure 4-33: GOI results for the Swan-2 well.

GOI results displayed against the gamma ray log with recorded porosity and permeability from core analysis data and where available oil saturation values derived from electric log analysis. On the GOI log the green vertical line marks the position of the empirical threshold for oil accumulation, with the width of the horizontal green lines showing the position and magnitude of the recorded GOI value (actual values shown to the right). Samples with a GOI of <1% are marked with a green arrow. Conventional shows reported in the well completion report are also shown with the thickness of the bar being proportional to their intensity.

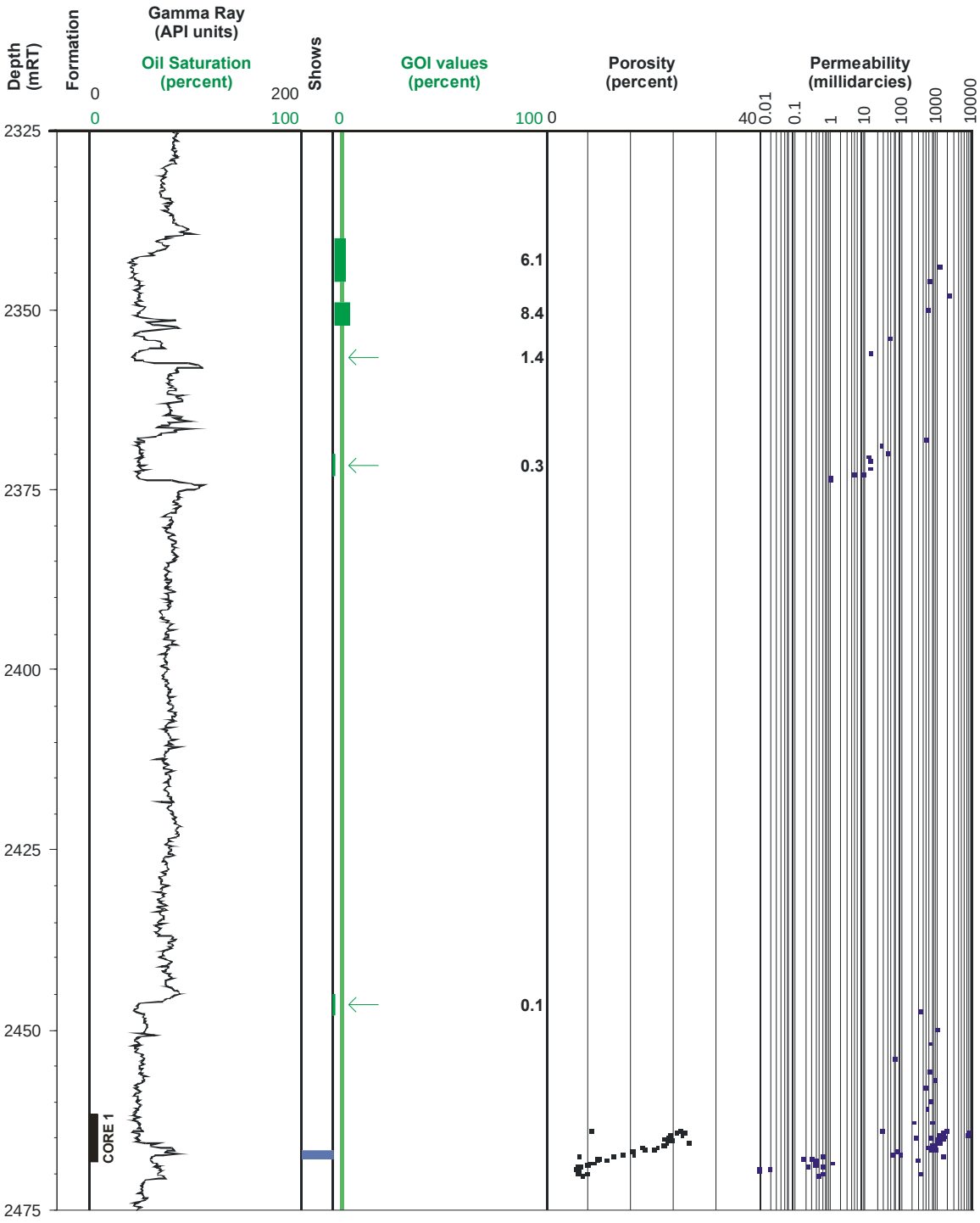

Figure 4-34: GOI results from the Swan-3ST well.

GOI results displayed against the gamma ray log with recorded porosity and permeability from core analysis data and where available oil saturation values derived from electric log analysis. On the GOI log the green vertical line marks the position of the empirical threshold for oil accumulation, with the width of the horizontal green lines showing the position and magnitude of the recorded GOI value (actual values shown to the right). Samples where GOI is <1% are marked with an arrow. Conventional shows from the well completion report are also shown with the thickness of the bar being proportional to their intensity.

Generally the fluid inclusion results show good agreement with the contemporary fluids with high GOI values in current oil zones where the trap fill is predominantly oil. In contrast those traps that contain gas or gas with a thin oil-leg typically show more complex GOI profiles. The results show that hydrocarbon traps are complex features that experience dynamic fluid histories and that the collection of GOI data can greatly assist in improving the understanding of how traps evolve with time.

In this section, the focus moves to the evaluation of wells that failed to prove the presence of hydrocarbons in the reservoir being tested. Analysis of these plugged and abandoned wells is undertaken to identify deficiencies in the prospect components or the broader play concept and to help to improve the chance of future success through improved awareness of the petroleum system.

Recognition that structures have received an oil charge is one important component of these post-drill reviews. The reliable identification of palaeo-oil accumulation is particularly significant as it demonstrates that all components required for a successful petroleum system were achieved, compromised only by retention failure.

The collection of GOI data from a large number of dry holes from the same basin enables an accurate charge map to be constructed, which can be used to more effectively scrutinise the source, trap, migration and retention elements of the various play types. Where a specific reason for failure is identified strategies can be developed to mitigate the risk of these factors and contribute to more successful drilling in subsequent drilling programs.

GOI data are not intended to replace conventional types of data, but when used in combination they can significantly augment the information derived from conventional shows and log analysis. They also provide for a more reliable observation where the interpretation of conventional hydrocarbon shows has been compromised by the hydrocarbon-based drilling mud systems or mud additives that have been used to facilitate the drilling process.

The recognition of palaeo-oil columns is seen as the most valuable contribution that GOI data can make to the post-mortem analysis of dry hole drilling results.

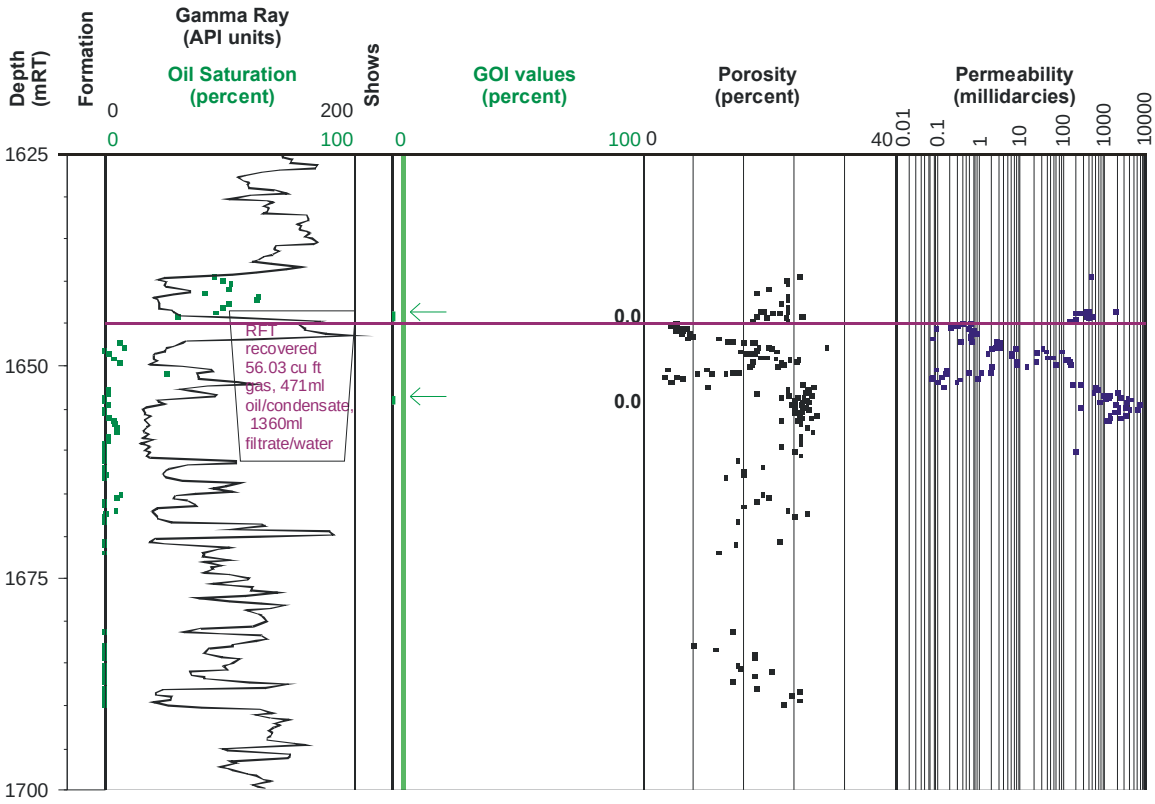

Figure 4-35: GOI results from the Pengana-1.

GOI results displayed against the gamma ray log with recorded porosity and permeability data and the position of an RFT sample point also shown. On the GOI log the green vertical line marks the position of the empirical threshold for oil accumulation, with the width of the horizontal green lines showing the position and magnitude of the recorded GOI value (actual values shown to the right). Samples where GOI is <1% are marked with an arrow. Conventional shows reported in the well completion report are also shown with the thickness of the bar being proportional to their intensity. The horizontal purple line shows the position of the current day GWC.

Wells with exclusively low GOI values, however, also provide important information for this review process. Evidence of hydrocarbon migration in a well that fails to test a valid closure can be considered to be positive encouragement for a potential oil charge to any valid traps located within closure immediately up-dip of the dry hole.

In contrast, the presence of low GOI values in a valid trap suggests that either migration occurred prior to the trap was created or alternatively that the volume of migrating oil reaching the trap was too small to allow an oil column to form. These data, when combined with conventional hydrocarbon shows produce a more accurate shows map that can be used to validate migration and charge predictions, be they based on simple migration maps or sophisticated numerical modelling techniques.

Plugged and abandoned wells with recognised palaeo-oil columns (Figure 4–36) will be examined individually and the remaining wells where the results indicate migration without accumulation will considered as a single group.

4.6.4.1 The Octavius-2 well

The Octavious-2 exploration well was drilled to test a Jurassic tilted fault block. The well was a follow-up to the Octavius-1 well, which was abandoned due to well-bore stability problems and failed to reach the main reservoir objective, sandstones of the Jurassic Plover Formation. The Octavius-2 well successfully penetrated the Plover Formation but found it to be water-wet (WMC Petroleum Ltd., 1992).

Sampling of the Plover Formation tested by Octavius-2 comprises two samples from a previous investigation (Lisk and Eadington, 1994), which have been added to with a single sample from the current study. All three samples have high GOI values ranging from 10.8% to 27.6% over a 60 m interval in clean, Middle Jurassic, Plover Formation sandstones (Table 4–12; Figure 4–37). The continuous nature of this sandstone together with the absence of any low GOI values supports the presence of a single palaeo-oil column with palaeo-oil down to at least 3260mRT. These observations concur with fluorescence and oil staining encountered during drilling, and interpreted as a residual hydrocarbon column (WMC Petroleum Ltd., 1992).

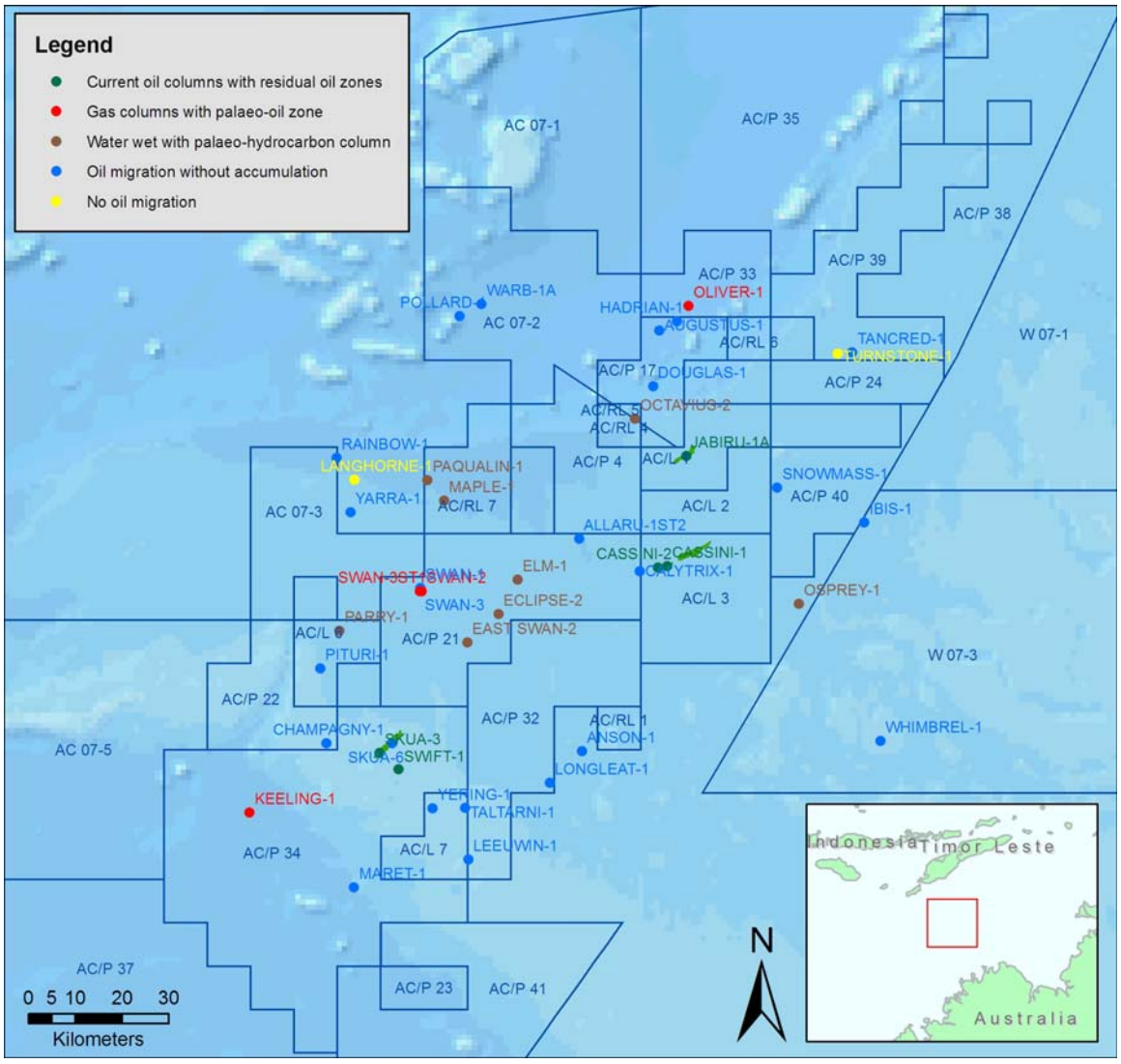

Figure 4-36: Map showing VSB well results.

Map summarises the GOI results obtained in this study, colour coded by interpreted charge history that combines the GOI observations with the current fluid fill. Note the small number of wells where all samples are devoid of oil inclusions and no evidence for oil migration can be inferred. This observation indicates that oil migration was widespread and effective in nearly all instances.

Cuttings across the Plover Formation reservoir section exhibit trace to 70% dull to occasionally bright white fluorescence. SWC samples taken near the top of the reservoir (3190-3215mRT) show 5-30% dull yellow-green fluorescence rising to 10-80% bright yellow-white fluorescence in samples from 3230-3262mRT. Below 2363mRT no fluorescence was noted in either cuttings or SWC.

Log analysis of the Plover Formation showed the section was fully water-saturated and mud-gas levels over this interval remained lower than the overlying shale. RFT pressure data confirmed the section was water-bearing with formation pressures falling on a hydrostatic water gradient (WMC Petroleum Ltd., 1992).

4.6.4.2 The East Swan-2 well

GOI results obtained for the East Swan-2 (Figure 4–38) were collected by the author during a previous investigation (O'Brien et al., 1996a). High GOI values of 3.3%-15.5% recorded over the interval 2630.58-2721mRT (Table 4–13) were interpreted to reflect high oil saturation over at least 90 m in Middle to Upper Jurassic sandstones (Figure 4–38). A reduction in GOI values to 1.2% at 2751-54mRT is interpreted to reflect the crossing of an original OWC, and a gross palaeo-hydrocarbon column height of 127±15 m is inferred from the current sample spacing.

A zone of low GOI values is seen near the top of the reservoir, where GOI values of 0.2% and 0% are recorded at 2609.4 mRT and 2620.7 mRT respectively. Given the relatively clean nature of the sandstone between these low values and the underlying high GOI samples, and considerations of the difference in gas and oil density, these low values are interpreted to indicate a palaeo-gas cap; the original charge to the East Swan structure comprising a 16m gas cap overlying a 111m oil column.

Conventional oil shows in the East Swan-2 well included 15-60% dull orange to moderately bright yellow-white direct fluorescence from cuttings over the interval 2606mRT-2619mRT with minor (10-20%) dull patchy orange recorded from 2643mRT to 2691mRT. A more significant oil show was noted from 2781mRT to 2787mRT with 30-60% pale yellow fluorescence seen in cuttings with up to 40% pale yellow-green fluorescence down to 2814mRT (BHP Petroleum Ltd., 1989c).

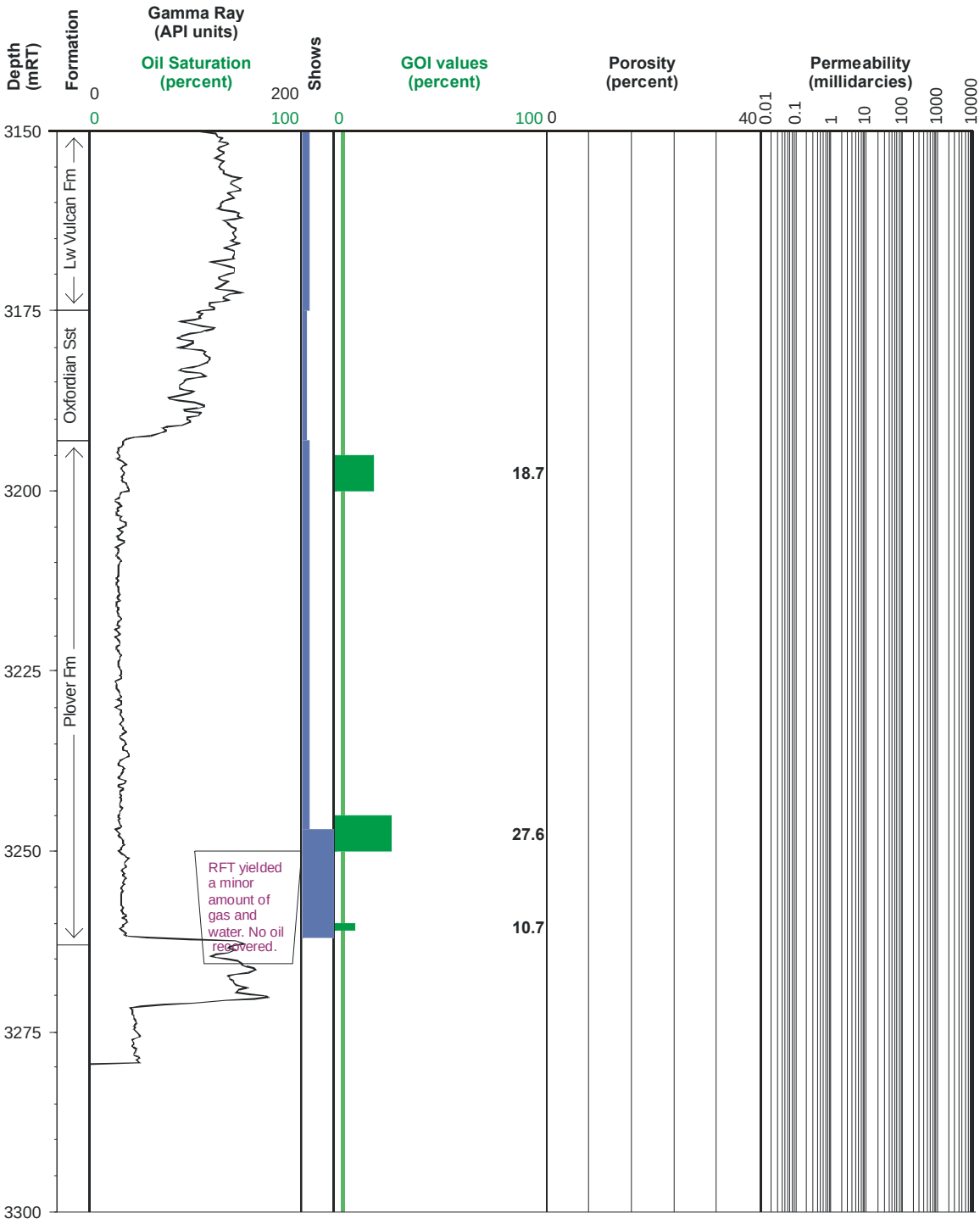

Figure 4-37: GOI results from the Octavius-2 well.

GOI results displayed against the gamma ray log with recorded conventional oil shows and the position of an RFT sample point also shown. On the GOI log the green vertical line marks the position of the empirical threshold for oil accumulation, with the width of the horizontal green lines showing the position and magnitude of the recorded GOI value (actual values shown to the right). Samples where GOI is <1% are marked with an arrow. Conventional shows reported in the well completion report are also shown with the thickness of the bar being proportional to their intensity.

Table 4-12: GOI results from the Octavius-2 well.

Refer to Table 4-4 for a detailed description of the set-up of tables 4-12, 4-13 and 4-14.

Well Name	Start Depth (mRT)	End Depth (mRT)	CSIRO Number	Sample Type	Counting Method	Number of fields examined	GOI (%)	GOI Error (%)	Total Grains	Grains With Oil Inclusions	Fluorescence Colours of Oil Inclusions			Location of Oil Inclusions	
											Blue	White	Yellow and Orange	FCDM	QOB
Octavius-2	3195	3200	75907	cuttings	Random	99	18.68	2.72	787	147	146	0	1	116	30
Octavius-2	3245	3250	125564	cuttings	Random	100	27.60	4.99	308	85	78	7	0		
Octavius-2	3260		75909	swc	Random	100	10.71	2.25	728	78	77	1	0		

Table 4-13: GOI results from the East Swan-1 and -2 wells.

Well Name	Start Depth (mRT)	End Depth (mRT)	CSIRO Number	Sample Type	Counting Method	Number of fields examined	GOI (%)	GOI Error (%)	Total Grains	Grains With Oil Inclusions	Fluorescence Colours of Oil Inclusions			Location of Oil Inclusions	
											Blue	White	Yellow and Orange	FCDM	QOB
East Swan-1	2726	2729	124130	cuttings	Complete	624	0.00	0.00	1726	0	0	0	0	0	0
East Swan-1	2750	2753	124131	cuttings	Complete	506	0.00	0.00	5262	0	0	0	0	0	0
East Swan-1	2765	2768	124132	cuttings	Complete	930	0.24	0.13	5797	14	14	0	0	14	0
East Swan-1	2814	2817	124135	cuttings	Complete	546	0.00	0.00	1001	0	0	0	0	0	0
East Swan-2	2609.4		122408	core	Complete	1394	0.22	0.05	38846	85	30	40	15		
East Swan-2	2620.7		122366	core	Complete	1628	0.00	0.00	29520	0	0	0	0		
East Swan-2	2630.08		122409	core	Random	100	15.49	2.75	665	103	64	37	2		
East Swan-2	2658	2661	122339	cuttings	Random		10.85	2.42	636	69	9	40	20		
East Swan-2	2679	2682	122340	cuttings	Random		4.57	1.13	1313	60	11	31	18		
East Swan-2	2700	2703	122341	cuttings	Random		7.09	1.86	733	52	16	17	19		
East Swan-2	2718	2721	122342	cuttings	Complete		3.30	0.59	3520	116	30	36	50		
East Swan-2	2751	2754	122343	cuttings	Complete		1.20	0.43	2509	30	23	3	4		
East Swan-2	2778	2781	122344	cuttings	Complete		0.31	0.14	5566	17	4	7	6		

Table 4-14: GOI results from the Eclipse-1 and 2 wells.

Well Name	Start Depth (mRT)	End Depth (mRT)	CSIRO Number	Sample Type	Counting Method	Number of fields examined	GOI (%)	GOI Error (%)	Total Grains	Grains With Oil Inclusions	Fluorescence Colours of Oil Inclusions			Location of Oil Inclusions	
											Blue	White	Yellow and Orange	FCDM	QOB
Eclipse-1	2547.9		122459	core	Random	100	3.19	0.65	2822	90	23	53	14	85	5
Eclipse-1	2554.5		122460	core	Random	100	4.98	0.71	3613	180	8	92	80	163	16
Eclipse-1	2565	2568	122491	cuttings	Random	110	3.52	1.38	681	24	9	15	0	21	3
Eclipse-1	2574	2577	122492	cuttings	Random	100	6.77	1.58	975	66	61	3	2	52	14
Eclipse-1	2586	2589	122856	cuttings	Random	100	6.56	6.21	61	4	2	2	0	4	0
Eclipse-1	2604	2607	122857	cuttings	Random	100	20.38	5.44	211	43	43	0	0	23	20
Eclipse-1	2607	2610	122494	cuttings	Random	100	35.19	6.37	216	76	75	1	0	42	34
Eclipse-1	2616	2619	122858	cuttings	Random	100	15.20	3.88	329	50	49	1	0	35	15
Eclipse-1	2622	2625	123104	cuttings	Random	100	26.25	2.36	1337	351	343	8	0	165	185
Eclipse-1	2634	2637	123105	cuttings	Random	100	15.27	3.86	334	51	30	19	2	39	12
Eclipse-1	2649	2652	123106	cuttings	Random	100	10.50	2.23	724	76	68	7	1	61	15
Eclipse-1	2679	2682	123347	cuttings	Random	100	32.25	5.51	276	89	86	3	0	41	48
Eclipse-1	2690	2693	123348	cuttings	Random	100	12.21	2.23	827	101	99	2	0	44	57
Eclipse-1	2703	2706	123349	cuttings	Random	100	4.62	0.81	2574	119	119	0	0	60	59
Eclipse-1	2733	2736	123350	cuttings	Random	100	40.98	6.73	205	84	81	1	2	48	36
Eclipse-1	2760	2763	123487	cuttings	Random	100	4.39	1.98	410	18	17	1	0	14	4
Eclipse-1	2787	2790	123488	cuttings	Complete	1702	0.07	0.05	12481	9	5	4	0	6	3
Eclipse-1	2808	2811	123489	cuttings	Complete	1554	0.03	0.02	25796	7	2	4	1	5	2
Eclipse-2	2454	2457	123351	cuttings	Random		30.61	4.64	379	116	34	76	6	24	91
Eclipse-2	2781	2784	123491	cuttings	Random		11.24	2.96	436	49	6	43	0	8	41
Eclipse-2	2784	2787	123107	cuttings	Complete		2.07	0.43	4209	87	1	86	0	34	53
Eclipse-2	2793	2796	123108	cuttings	Complete		0.46	0.12	11340	52	6	46	0	14	38
Eclipse-2	2805	2808	123109	cuttings	Complete		0.00	0.00	2333	0	0	0	0	0	0
Eclipse-2	2823	2826	123110	cuttings	Complete		0.03	0.04	7838	2	0	0	2	0	2
Eclipse-2	2838	2841	123111	cuttings	Complete		0.49	0.13	10304	50	2	48	0	17	33
Eclipse-2	2871	2874	123112	cuttings	Complete		0.02	0.04	5504	1	0	1	0	0	1

In SWC samples the fluorescence levels were highly variable ranging from being completely absent to up to the 100% dull yellow fluorescence that was noted in the 2683mRT sample (Figure 4–38).

Conventional core recovered from 2609-2627mRT exhibited good shows between the top of the core and 2613m, with this zone interpreted to reflect a residual oil column (BHP Petroleum Ltd., 1989c). Intermittent, but generally greater than 40% fluorescence was noted over the remainder of this core and across most of core 2 taken from 2627-2633.75mRT.

Log interpretation interpreted residual hydrocarbons, whilst mud-gas levels were variable through the reservoir interval but rarely above baseline values established in the overlying shale. RFT samples at 2610mRT recovered water and the pressure data is also consistent with a hydrostatic water gradient (BHP Petroleum Ltd., 1989c).

4.6.4.3 The Eclipse-1 and 2 wells

The 18 samples taken from the Middle Jurassic section in Eclipse-1 have GOI values ranging from 0 to 41% over the interval 2547.9-2811mRT (Table 4–14). GOI values consistent with a palaeo-oil accumulation occur over the interval 2547.9-2763mRT, with a palaeo-OWC, based on current sample spacing, placed at 2777±14 m (Figure 4–39 and Figure 4–40). A 229±14 m palaeo-oil column is inferred despite the lack of any conventional oil shows throughout most of this entire section.

Four samples from within this palaeo-oil zone have GOI values that are below the 5% empirical threshold for oil accumulation, but well above the GOI values considered to be indicative of migration without accumulation (GOI <1%). These values are likely to be a reflection of variable reservoir conditions, with the reduced GOI values corresponding with zones of reduced reservoir quality. These samples correspond with increased gamma ray response, indicating increasing shale content. This observation is most striking at the top of the reservoir where the reduction in reservoir quality associated with the increased gamma ray response is confirmed by core analysis data that show low porosity and permeability (Figure 4–39).

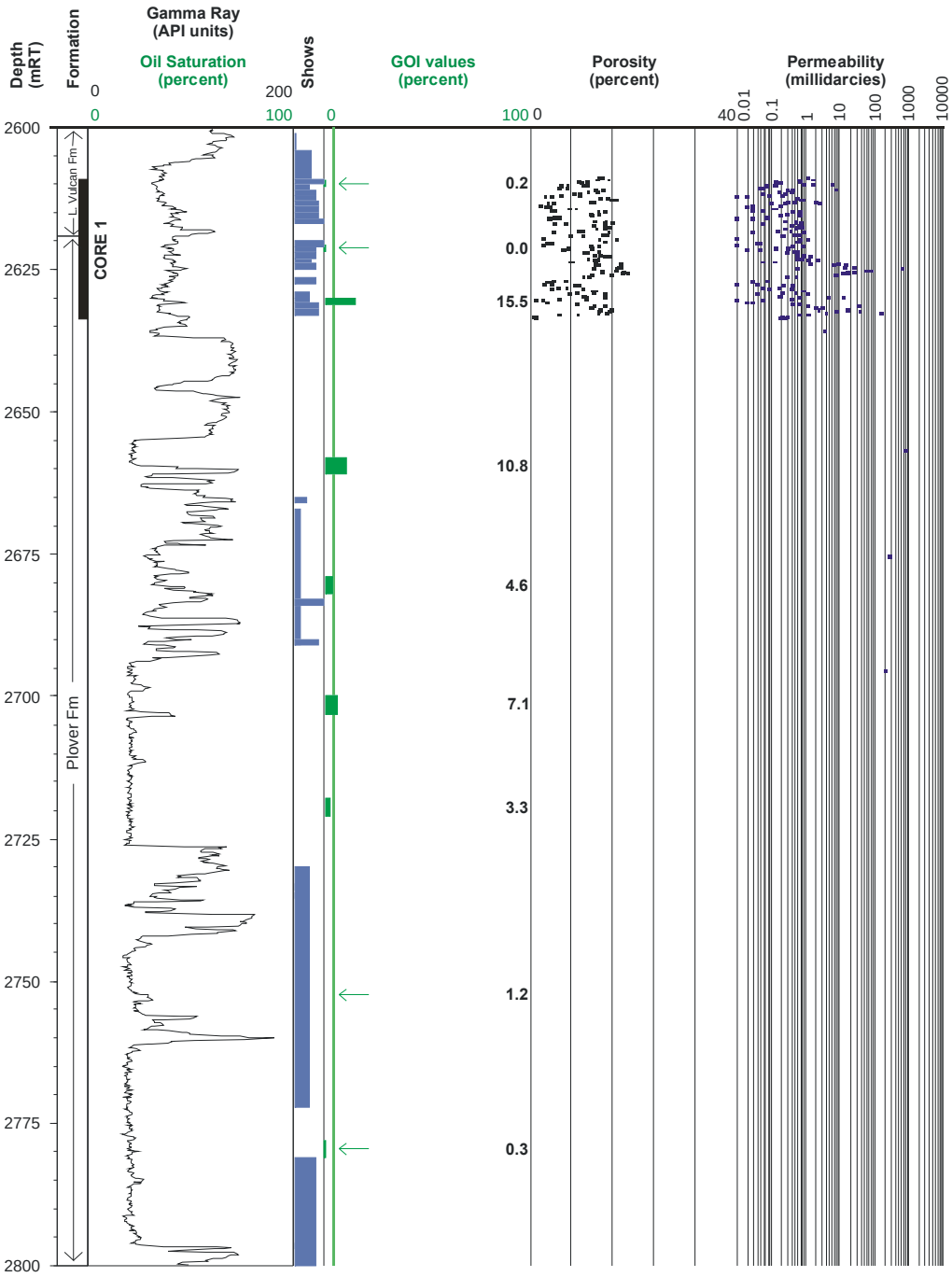

Figure 4-38: GOI results from East Swan-2.

GOI results displayed against the gamma ray log with recorded porosity and permeability, conventional oil shows and the position of core samples also shown. On the GOI log the green vertical line marks the position of the empirical threshold for oil accumulation, with the width of the horizontal green lines showing the position and magnitude of the recorded GOI value (actual values shown to the right). Samples where GOI is <1% are marked with an arrow. Conventional shows reported in the well completion report are also shown with the thickness of the bar being proportional to their intensity.

Conventional oil shows recorded in the Eclipse-1 (BHP Petroleum Ltd., 1984c) well included yellow fluorescence in cuttings from 2546-51mRT and again at 2649mRT. In SWC samples very dull pale white fluorescence was noted at 2566.5mRT and 2570.6mRT, but the absence of any cut fluorescence upon addition of solvent raises questions about the veracity of these shows.

In conventional core cut from 2547-2559.5mRT strong yellow fluorescence was noted near the top of the core (2547-2550.8mRT) declining to patchy spotty fluorescence below this depth down to 2553.4mRT. Log interpretation identified a potential oil zone between 2547mRT and 2567mRT but the calculated water saturation was high (57-80%) and it was concluded to be residual in nature (BHP Petroleum Ltd., 1984c). Mud-gas levels are of little value due to the core being cut over the main reservoir with bottoms up not being circulated during this operation, but below the cored interval they show levels lower that seen in the overlying shale and decrease with depth. All valid RFT points come from below the log-derived zone of interest and characterise a water gradient from 2577mRT to 2758mRT (BHP Petroleum Ltd., 1984c).

In Eclipse-2, GOI samples were taken from two discrete reservoir horizons, with a single sample from the Upper Jurassic section (Figure 4–41) and seven samples analysed from the Lower Jurassic section (Figure 4–42; Table 4–14). A high GOI value (11.2%) recorded in the Lower Jurassic sample from immediately below the Middle Jurassic top seal is consistent with high palaeo-oil saturation in this currently water-wet sand. The sample immediately below this high GOI value also has an elevated value (2.1%), but is well below the threshold for an oil column. As this is a cuttings sample it is likely that this intermediate GOI value represents bracketing of the palaeo-OWC and consists of a mixture of palaeo-oil and palaeo-water zone material. The remaining samples below this point have consistently low GOI values (ranging from 0-0.5%) and confirm a palaeo-water leg. At the well intersection these results define a thin palaeo-oil zone of no more than a few metres thickness.

The single sample from the Upper Jurassic section in Eclipse 2 returned a high GOI value of 30.2% and corresponds to oil shows and oil recovery, where a thin (2 m) gas column is underlain by a 0.5 m oil column (BHP Petroleum Ltd., 1986; Figure 4–41).

The location of the sample within the present gas zone suggests oil charged the structure prior to gas, before being displaced.

Conventional oil shows seen in Eclipse-2 (BHP Petroleum Ltd., 1986) were observed in cuttings over the interval 2450mRT to 2645mRT where trace to 70% yellow-green fluorescence was recorded. In SWC samples 80-100% yellow-green fluorescence was noted at 2460mRT and 2461mRT declining to less than 20% in the overlying samples at 2458.5mRT and 2459mRT. More extensive fluorescence was observed in SWC from 2787mRT to 2798.5 where sandstones showed 50-100% yellow-green to yellow-white fluorescence. Conventional core cut from 2459-2466mRT showed dull green-yellow fluorescence but the intensity was not reported.

Log interpretation defined a 2m hydrocarbon zone in the Late Jurassic section with a GOC at 2459.7mRT and an OWC at 2460.2mRT. A residual oil zone was interpreted from 2791-2800mRT in Middle Jurassic sandstones (BHP Petroleum Ltd., 1986).

A notable mud-gas peak coincides with the Upper Jurassic oil zone but across the Middle Jurassic sandstones total mud gas was barely above background levels. Hydrocarbons were successfully recovered from the Upper Jurassic section by RFT and an approximate hydrocarbon water contact established that is consistent with the log analysis. Reservoir pressure data from the Upper Jurassic water-leg showed a noticeable offset with the aquifer in the Middle Jurassic section inferring the upper sand is isolated from the Middle Jurassic section (BHP Petroleum Ltd., 1986).

The Eclipse-2 well penetrated an equivalent reservoir interval and within the same structural closure as Eclipse-1 well and the significance of the thin palaeo-oil zone seen in the Eclipse-2 result assumes greater significance when compared with the location of the palaeo-OWC defined from GOI data in the Eclipse-1 well.

The close similarity in the palaeo-OWCs defined for the Eclipse-1 and Eclispe-2 wells (Figure 4–40 and Figure 4–42) raises the possibility that they may have tested the same palaeo-oil column.

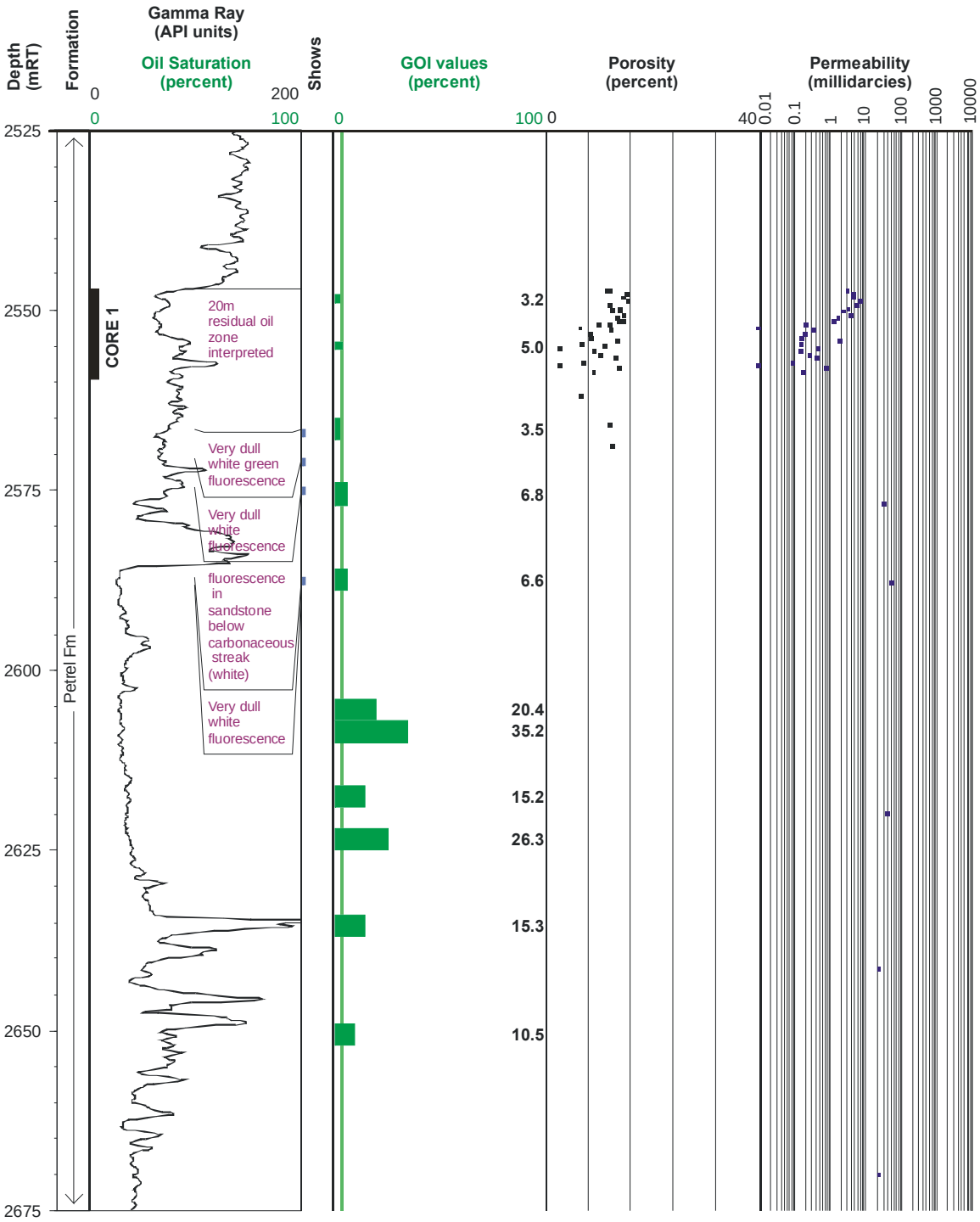

Figure 4-39: GOI results from the Eclipse-1 well (Upper Section).

GOI results for the upper reservoir section in Eclipse-1 displayed against the gamma ray log with recorded porosity and permeability, conventional oil shows and the position of core samples also shown. On the GOI log the green vertical line marks the position of the empirical threshold for oil accumulation, with the width of the horizontal green lines showing the position and magnitude of the recorded GOI value (actual values shown to the right). Samples where GOI is <1% are marked with an arrow. Conventional shows from the well completion report are shown with the thickness of the bar proportional to their intensity.

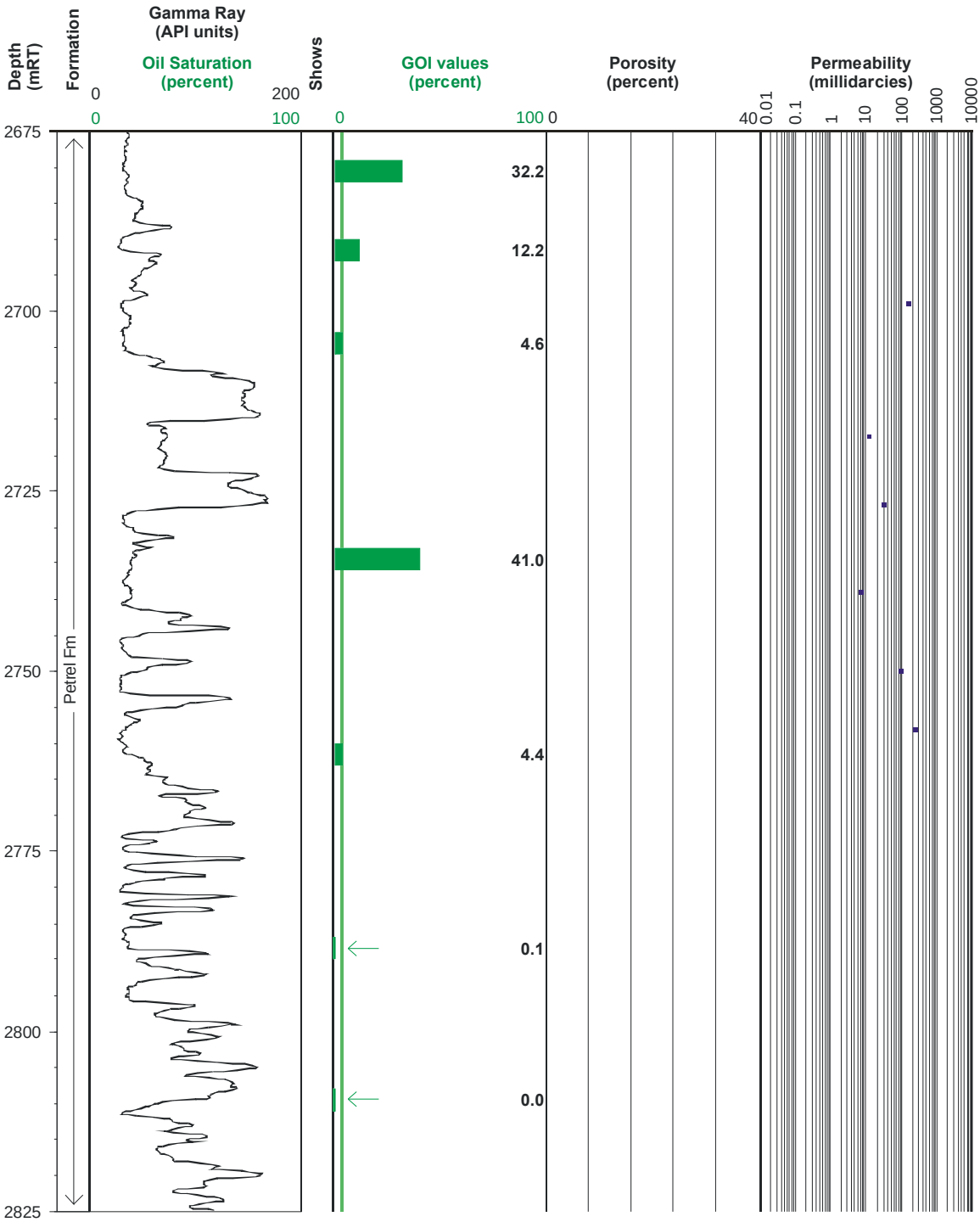

Figure 4-40: GOI results from the Eclipse-1 well (Lower Section).

GOI results displayed against the gamma ray log with available porosity and permeability and conventional oil shows data also shown. On the GOI log the green vertical line marks the position of the empirical threshold for oil accumulation, with the width of the horizontal green lines showing the position and magnitude of the recorded GOI value (actual values shown to the right). Samples where GOI is <1% are marked with an arrow. Conventional shows reported in the well completion report are also shown with the thickness of the bar being proportional to their intensity.

4.6.4.4 The Elm-1 Well

GOI values recorded in the four samples taken from upper part of the Lower Vulcan Formation in Elm-1 range from 1.1% to 16.8% over the interval 2778-2841 m (Table 4–15). The samples were taken from a series of thin sands so it is difficult to evaluate the significance of the samples collectively.

This is exacerbated by the failure to sample the thicker sands that constitute the top of reservoir porosity in the Lower Vulcan where significant conventional oil shows were recorded (BHP Petroleum Ltd., 1994).

The Elm-1 well completion report (BHP Petroleum Ltd., 1994) reports 30-100% moderately bright, yellow-white fluorescence in cuttings samples over 2742mRT-2772mRT. Fluorescence recorded as 100% solid bright yellow-white was observed in SWC samples from 2748mRT-2766mRT corresponding to a broad, but not particularly pronounced increase in total mud-gas. Log analysis calculated residual hydrocarbon saturations in each blocky sand of 25-60% with equivocal RFT data indicating a possible gas gradient in the upper sand. Samples of reservoir fluid recovered by RFT contained mostly filtrate and were not conclusive.

The high intensity of the conventional shows indicates that the upper clean sands are likely to have experienced high oil saturation down to at least the base of the 100% shows at 2766mRT. The high GOI sample at 2829-32m, with a GOI value of 16.8% that indicates high oil saturation, is overlain by two samples with intermediate GOI values of 3.1% at 2778-2781m and 2.1% at 2793-96m (Figure 4–43).

These intermediate GOI values are higher than would be typically expected for oil migration without accumulation (GOI < 1%) and come from sandstones that log analysis indicate have low porosity.

Collectively the reported conventional oil show data, combined with the GOI results and the electric log interpretation all point to a prior oil accumulation existing within the Elm structure.

The position of the palaeo-OWC is not consistent, with the conventional oil shows and the calculated residual hydrocarbon saturations indicating high oil saturation probably extended as low as 2767m. In contrast if the intermediate GOI values are attributed to poor reservoir quality then a palaeo-oil column extending as deep as 2832m is implied from the fluid inclusion results.

Unlike the upper reservoir sections the basal part of the Lower Vulcan Formation and the underlying Middle Jurassic Plover Formation contain only small numbers of oil inclusions with recorded GOI numbers all being less than 0.2%. In contrast to these very low GOI values conventional oil shows of up to 80% dull yellow fluorescence were reported in cuttings from the interval 2973-2991m (Figure 4–44).

Although SWC samples taken through this zone were largely devoid of shows elevated mud-gas levels do occur over this zone. Consequently, whilst the fluid inclusion results indicate migration of oil without accumulation the conventional shows are more equivocal.

4.6.4.5 The Paqualin-1 Well

Samples from two sands within the Upper Vulcan Formation in Paqualin-1 exhibited high GOI values of between 70% and 84.5% over the interval 2835-2883mRT (Table 4–16; Figure 4–45). A gross palaeo-oil column of nearly 50m is implied across a low net to gross reservoir section. The lack of any low GOI samples precludes the determination of a palaeo-oil water contact and it remains uncertain whether the series of high GOI values across two discrete blocky sands represents one continuous palaeo-oil zone (50m+) or reflects a series of stacked accumulations, each with their own separate palaeo-oil water contact and where the total column height can be defined only by the thickness of the palaeo-oil down to levels indicated for each sand (i.e. about 13m+ combined).

Conventional oil shows across the Upper Vulcan sands are in agreement with the high palaeo-oil saturations inferred from the GOI data. Cuttings and SWCs retrieved from these zones all exhibit 100% bright to pale yellow direct fluorescence and fairly prominent increases in mud-gas levels were noted on the mud-log.

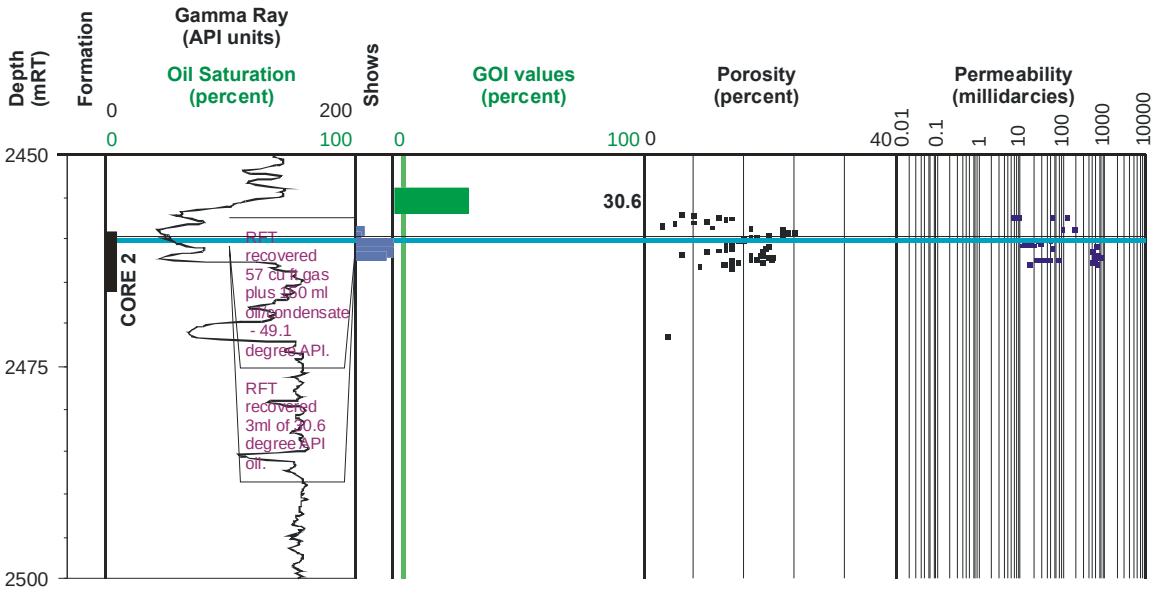

Figure 4-41: GOI results from the Upper Jurassic reservoir in the Eclipse-2 well.

GOI results displayed against the gamma ray log with available porosity and permeability, conventional oil show and RFT data also shown. On the GOI log the green vertical line marks the position of the empirical threshold for oil accumulation, with the width of the horizontal green lines showing the position and magnitude of the recorded GOI value (actual values shown to the right). Samples where GOI is <1% are marked with an arrow. Conventional shows reported in the well completion report are also shown with the thickness of the bar being proportional to their intensity.

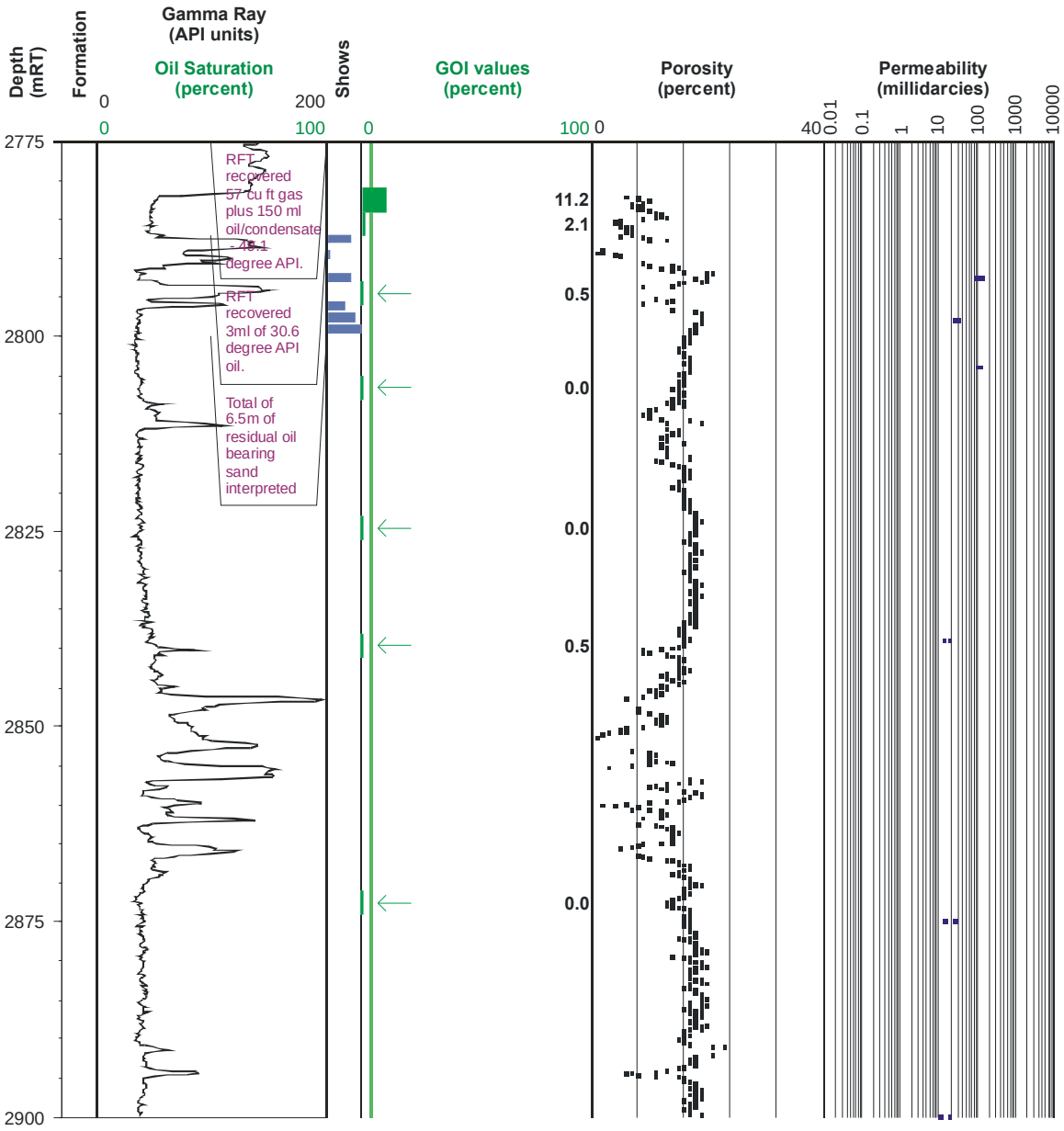

Figure 4-42: GOI results from the Middle Jurassic reservoir in the Eclipse-2 well.

GOI results displayed against the gamma ray log with available porosity and permeability, conventional oil show and RFT data also shown. On the GOI log the green vertical line marks the position of the empirical threshold for oil accumulation, with the width of the horizontal green lines showing the position and magnitude of the recorded GOI value (actual values shown to the right). Samples where GOI is <1% are marked with an arrow. Conventional shows reported in the well completion report are also shown with the thickness of the bar being proportional to their intensity.

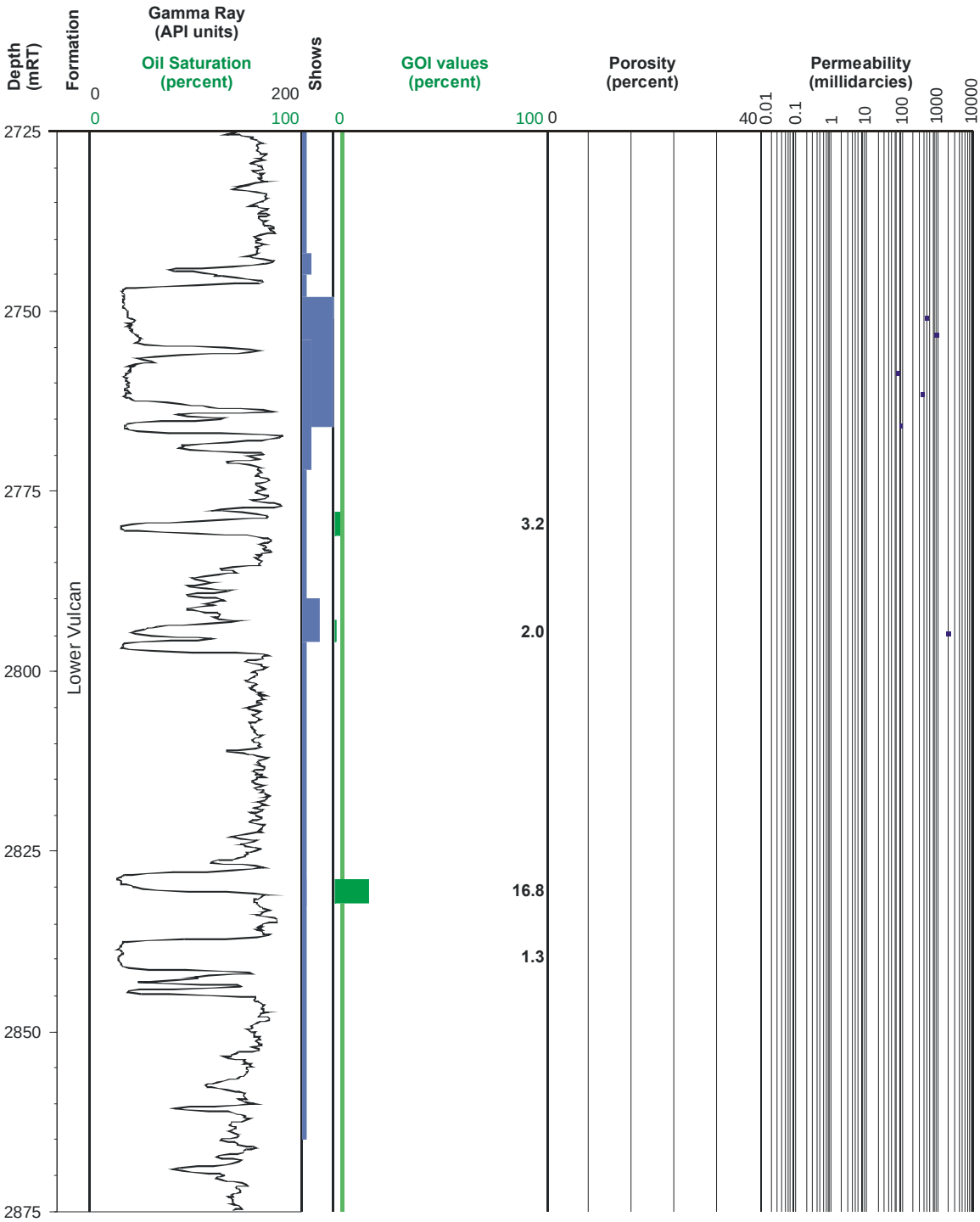

Figure 4-43: GOI results from the Upper Jurassic section in the Elm-1 well.

GOI results displayed against the gamma ray log with available porosity and permeability and conventional oil show data also shown. On the GOI log the green vertical line marks the position of the empirical threshold for oil accumulation, with the width of the horizontal green lines showing the position and magnitude of the recorded GOI value (actual values shown to the right). Samples where GOI is <1% are marked with an arrow. Conventional shows reported in the well completion report are also shown with the thickness of the bar being proportional to their intensity.

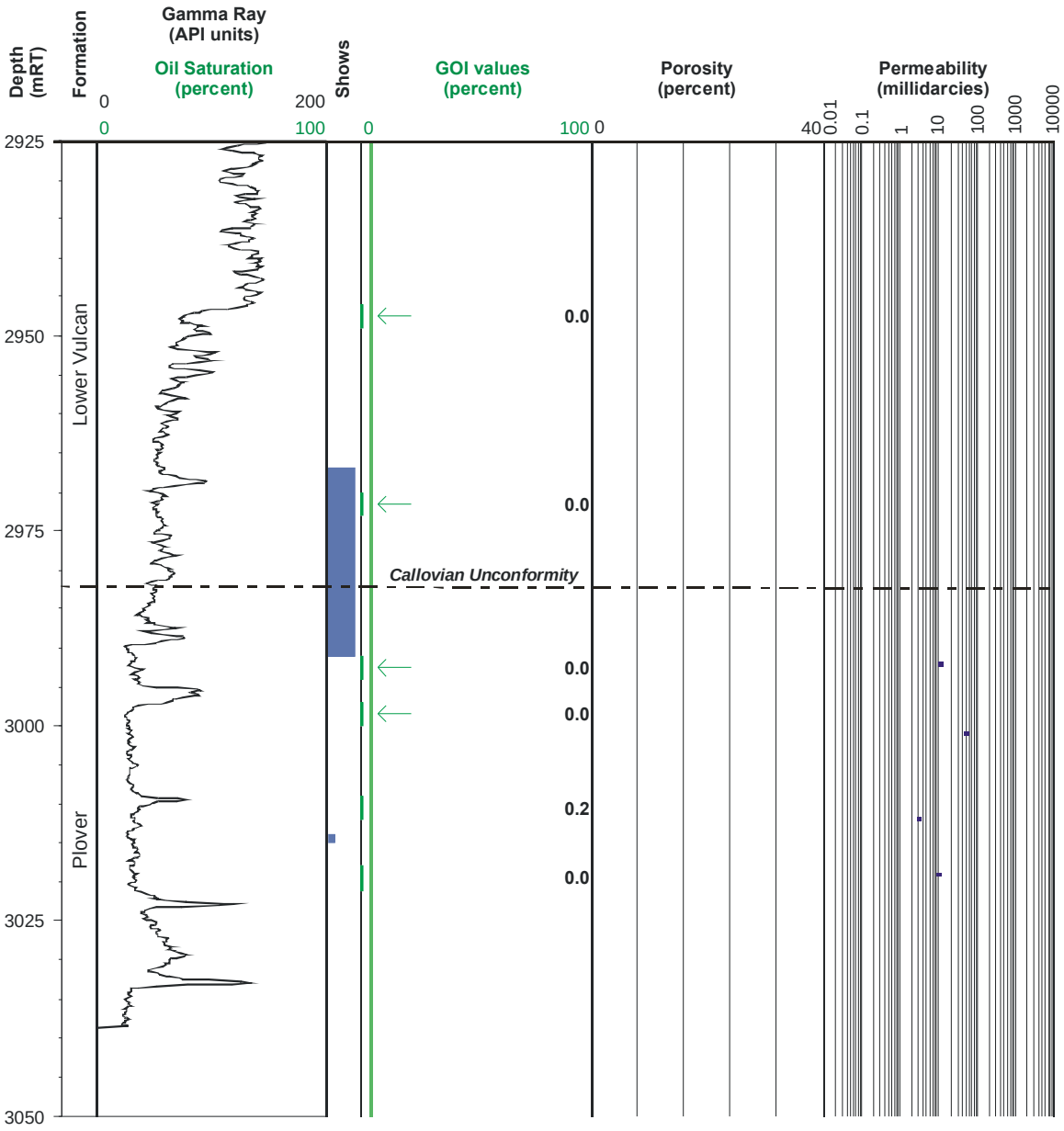

Figure 4-44: GOI results from across the Callovian Unconformity in the Elm-1 well.

GOI results displayed against the gamma ray log with available porosity and permeability and conventional oil show data also shown. On the GOI log the green vertical line marks the position of the empirical threshold for oil accumulation, with the width of the horizontal green lines showing the position and magnitude of the recorded GOI value (actual values shown to the right). Samples where GOI is <1% are marked with an arrow. Conventional shows reported in the well completion report are also shown with the thickness of the bar being proportional to their intensity.

Log analysis indicated that the upper sand was water-bearing with only low residual saturations, whilst the lower sand has calculated saturations of >80% and has been interpreted as a current hydrocarbon accumulation (BHP Petroleum Ltd., 1989d).

The RFT runs failed to recover any significant hydrocarbon fluids and although gas is thought to be present in the upper most part of the lower sand this was not confirmed by either sampling or pressure data, the latter defined clear water gradients in both sands (BHP Petroleum Ltd., 1989d). A pressure offset of about 40psi separates the water gradients measured in each of the sands and both sands are overpressured relative to an expected hydrostatic water gradient.

Whilst the contemporary pressure data may not be representative of conditions in the geological past the degree of compartmentalisation indicated by the RFT data makes it more likely that each of the sands have always been hydraulically isolated. As a consequence estimates of palaeo-oil column heights drawn from the GOI data would be at the lower ends of the ranges indicated (i.e. 13-50m) than would be the case if pressure communication was assumed.

Samples taken from across the Callovian Unconformity in Paqualin-1 where transgressive sandstones of the Upper Vulcan Formation directly overlie a shaly Plover Formation section that produced more variable GOI results. High GOI values, above the empirical threshold for oil accumulation, are recorded in the uppermost and lowermost samples, with the intervening samples having GOI values of less than 1% (Table 4–16; Figure 4–46).

When compared against the gamma ray log the GOI data can be interpreted as reflecting two discrete palaeo-oil columns separated by a capillary barrier represented by a thin shale. In the upper zone a palaeo-OWC could be delineated at 4141.5mRT ± 1.5m within the Upper Vulcan Formation by a sharp reduction in GOI values (Figure 4–46) whilst the lowermost sample lies within the Plover Formation and the high GOI value recorded in this sample implies the presence of a second palaeo-oil zone below the Callovian Unconformity (Figure 4–46). A lack of deeper samples precludes the recognition of any palaeo-OWC for this deepest sample and only a palaeo-ODT can be defined.

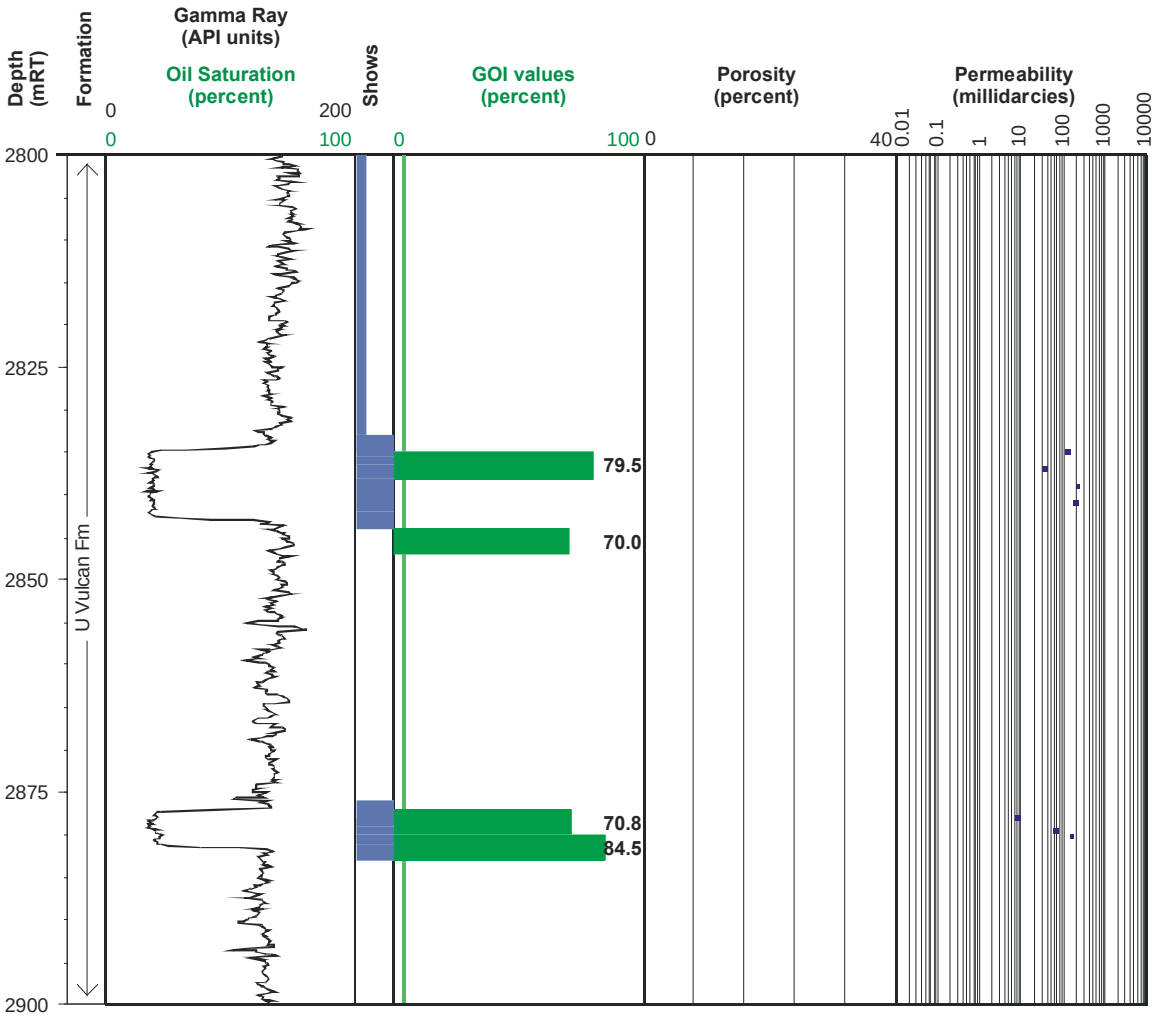

Figure 4-45: GOI results from the Upper Vulcan Formation in Paqualin-1.

GOI results displayed against the gamma ray log with available porosity and permeability and conventional oil show data also shown. On the GOI log the green vertical line marks the position of the empirical threshold for oil accumulation, with the width of the horizontal green lines showing the position and magnitude of the recorded GOI value (actual values shown to the right). Samples where GOI is <1% are marked with an arrow. Conventional shows reported in the well completion report are also shown with the thickness of the bar being proportional to their intensity.

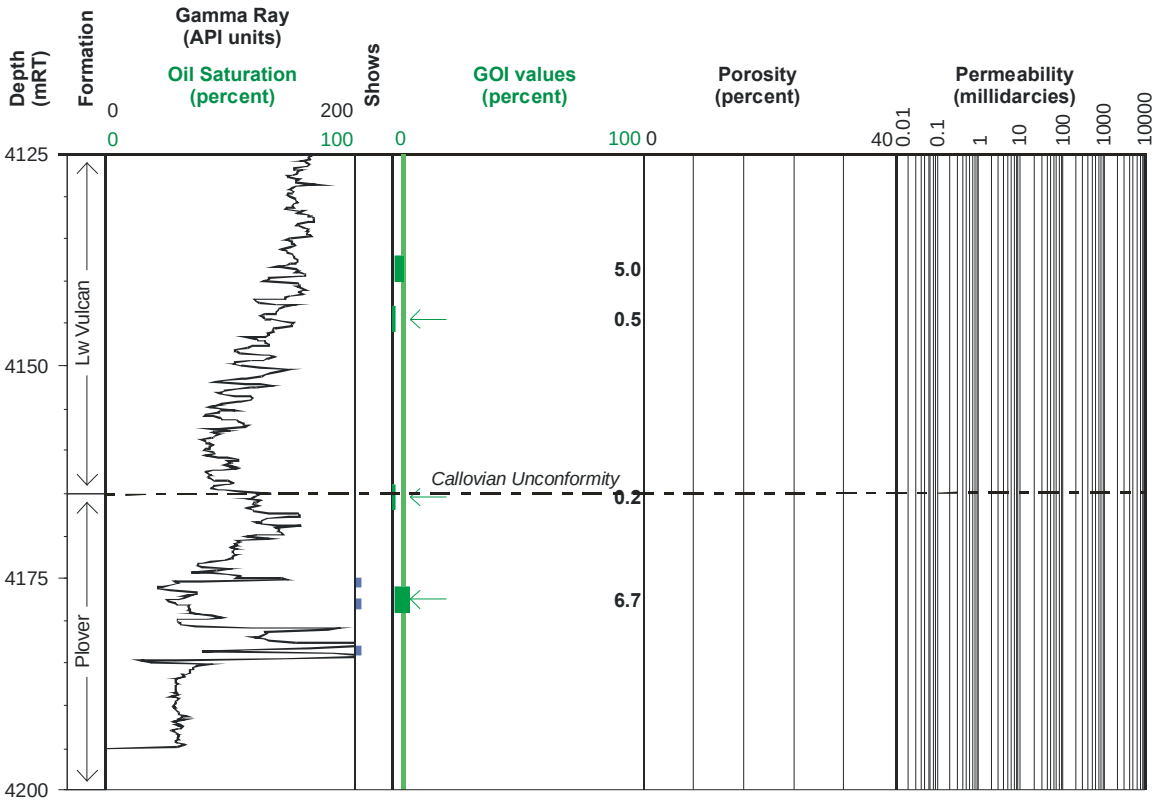

Figure 4-46: GOI results from across the Callovian Unconformity in the Paqualin-1 well.

GOI results displayed against the gamma ray log with available porosity and permeability and conventional oil show data also shown. On the GOI log the green vertical line marks the position of the empirical threshold for oil accumulation, with the width of the horizontal green lines showing the position and magnitude of the recorded GOI value (actual values shown to the right). Samples where GOI is <1% are marked with an arrow. Conventional shows reported in the well completion report are also shown with the thickness of the bar being proportional to their intensity.

Conventional oil shows reported from sands either side of the Callovian Unconformity (BHP Petroleum Ltd., 1989d) are limited to solvent cut fluorescence with mud-gas levels being lower than in the overlying shales. Log analysis also interprets the section to be water-wet although the argillaceous nature of the sediments makes it difficult to define a clean water line and this hampers the estimate of formation water resistivity for hydrocarbon saturation calculations.

4.6.4.6 The Osprey-1 Well

Presently water-saturated sandstones at the top of the Permian Hyland Bay Formation in the Osprey 1 well have high GOI values of 6.4%-10.8% over the interval 2476-82 m (Figure 4–47; Table 4–17). GOI values of 1.5%-1.8% encountered below this zone are higher than are normally encountered in rocks, which have not been exposed to high oil saturation, but as these are cuttings the slightly elevated values are attributed to caving from the overlying palaeo-oil zone. A palaeo-OWC is placed at 2486±1.5 m, giving a maximum hydrocarbon column of about 17 m at the well intersection.

Conventional shows in the Osprey-1 well were limited to several significant gas shows within the Permian Hyland Bay Formation (ARCO Australia Ltd., 1972). No oil indications were indicated in the mud-gas and no fluorescence was noted in the samples collected. A Drill Stem Test (DST) of the Permian section produced water.

The Osprey-1 well represents the only Palaeozoic interval tested in this study and the result can be interpreted in a number of ways. The oil originally reservoired at Osprey may have been sourced from Palaeozoic rocks outside of the Vulcan Sub-basin and could represent long distance migration from the Petrel Sub-basin to the south east. Alternatively, if the oil in Osprey is from Jurassic source rocks, then it has probably been generated within the Skua Trough in the Vulcan Sub-basin and migrated north-east, via the basin margin relay ramp up-dip from the Talbot oil field.

4.6.4.7 The Parry-1 Well

The uppermost of the three cuttings samples taken from water-wet Maastrichtian sandstones in Parry 1 has a high GOI value of 14.4% (2097-2100mRT) and is underlain by two samples with GOI values of less than 0.1%. The sharp reduction in GOI to <0.1% at 2104 mRT constrains the palaeo-OWC to lie at about 2102±2 mRT, defining a 6 m palaeo-oil column at the well intersection (Figure 4–48, Table 4–18).

Log analysis calculated slightly elevated hydrocarbon saturations from 2097-2112mRT but these are generally <15% and were not considered to be significant (BHP Petroleum Ltd., 1988h).

Following drilling, poor seismic control, coupled with limited oil shows, resulted in uncertainty about the validity of the Parry 1 test and the absence of hydrocarbons in the well was primarily attributed to a lack of closure (BHP Petroleum Ltd., 1988h).

In contrast, the GOI results are quite conclusive, providing evidence of prior oil accumulation that in turn implies the existence of an effective closure when the oil inclusions were formed. The trap is part of the fault dependant Puffin horst complex and, as such, a loss of fault seal integrity may explain the loss of this oil column. The nearby Puffin Field demonstrates retention of seal integrity so a detailed analysis of the reasons for loss of the accumulation from the Parry structure is needed.

No GOI samples were taken from the underlying Triassic reservoir at Parry 1, making it difficult to ascertain whether the Cretaceous palaeo-oil column is the product of lateral migration or localised vertical re-migration from a breached Triassic oil accumulation. However, aside from some minor hydrocarbon saturation indicated by the log analysis the lack of any shows and the subdued mud-gas profile provide little evidence for prior oil accumulation within the Triassic section.

4.6.4.8 The Pituri-1 well

In Pituri 1, a small one metre live oil column, interpreted within the Tertiary Grebe Sandstone (BHP Petroleum Ltd., 1995), was not adequately tested in this study.

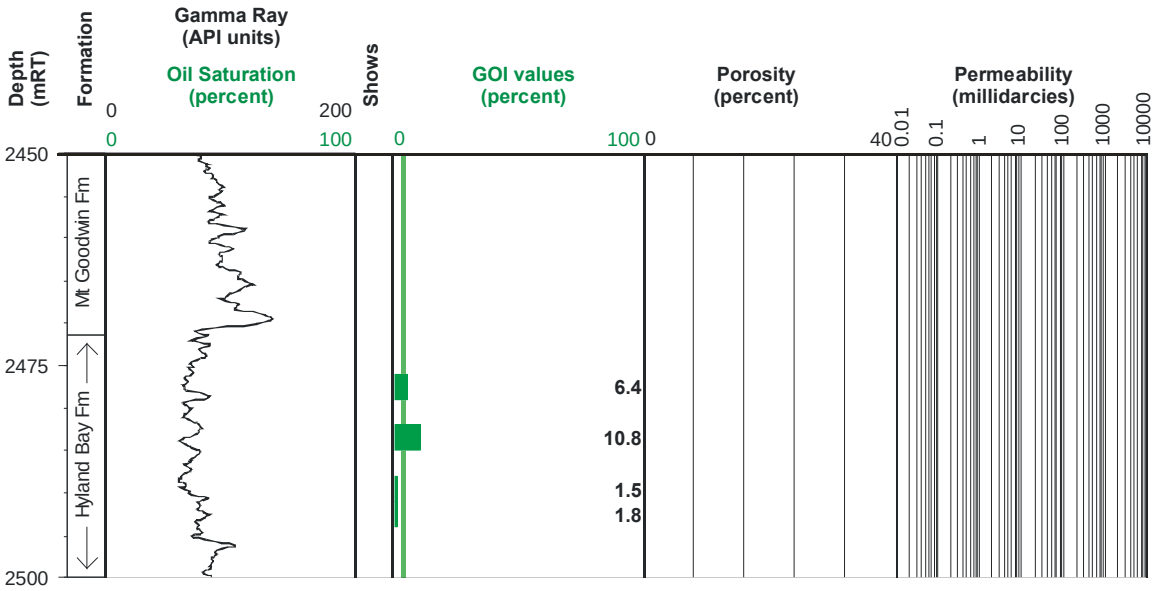

Figure 4-47: GOI results from the Osprey-1 well.

GOI results displayed against the gamma ray log with available porosity and permeability and conventional oil show data also shown. On the GOI log the green vertical line marks the position of the empirical threshold for oil accumulation, with the width of the horizontal green lines showing the position and magnitude of the recorded GOI value (actual values shown to the right). Samples where GOI is <1% are marked with an arrow. Conventional shows reported in the well completion report are also shown with the thickness of the bar being proportional to their intensity.

However, an anomalous GOI value of 2.3% at 1708-14 mRT is consistent with proximity to a zone of high (palaeo-) oil saturation (Figure 4–49, Table 4–19). The reduced value could reflect abundant caving in this poorly consolidated section from the overlying oil zone, or alternatively, the bracketing of a palaeo-OWC by this relatively widely spaced cuttings interval. The fall in GOI to 1.3% in the 1723-26mRT sample is more consistent with high water saturation and would allow for a poorly constrained palaeo-oil column of up to 10 metres.

Cuttings samples taken across the Tertiary section in Pituri-1 show trace spotty dull yellow-orange fluorescence in cuttings from 961mRT, increasing to 10% to 50% spotty bright yellow fluorescence in samples from 991-1018mRT. Further trace fluorescence, ranging from spotty to pinpoint moderately bright yellow to dull pale yellow, was also noted from 1714mRT to 1726mRT increasing to up to 10% dull yellow-green fluorescence from 2083mRT to 2107mRT.

SWC samples confirmed this deeper zone showing similar fluorescence results but no samples were taken across the shallower zones. A small conventional core acquired over 1018-1032mRT, which showed up to 30% dull yellow-orange fluorescence across the top 2m of the core and trace fluorescence down to 1021mRT (BHP Petroleum Ltd., 1995).

Mud-gas peaks were not recorded across the most of the Tertiary section but a prominent total gas peak was recorded in the Eocene Grebe Formation from 1710-1730mRT and corresponds to the 1m net oil zone that is interpreted over the interval 1706-10mRT (BHP Petroleum Ltd., 1995).

An RFT sampling conducted over the shallower Oliver Formation sandstone recovered only mud-filtrate and pressure data indicated a consistent water gradient from 1010-1042mRT.

4.6.4.9 Water wet wells with low GOI values

The GOI results from the remaining 16, water-wet, exploration wells examined in this study are summarised in Figure 4–11 and presented as GOI logs in Appendix C.

With the exception of samples from the Turnstone 1 and Langhorne-1 wells, all wells contained some samples with oil inclusions and except for Tancred 1, GOI values are all less than 1% (Table 4–20). In Tancred 1, a single sample returned a GOI value of 1.7%, which is higher than anticipated for samples from an oil migration pathway and may indicate proximity to an up-dip palaeo- or intact oil column.

In general, however, the significance that can be assigned to the low GOI values is subject to a number of important caveats described in section 4.5.1.1, which effectively limit the utility of the method as a reliable indicator of oil migration events when used in isolation. These can produce a range of plausible interpretations that limit the ability to reach a unique solution and/or require an impractical number of samples to reach even a most probable solution.

One option is to consider that oil inclusions represent direct samples of oil present, at some point in time, in the adjacent pore space and that the presence of low GOI values (above zero) confirms oil migration. In this instance, the presence of even a single oil inclusion could be taken as confirmation of oil migration, with low GOI values indicating that either oil migration occurred prior to the formation of a valid trap, or that the volume of oil charge was insufficient to form an oil column.

A more robust approach to assessing the significance of oil inclusions being present in low abundance is to consider their magnitude, represented by the measured GOI value, and evaluate this against the theory of two-phase hydrocarbon-water flow (Schowalter, 1979). Two factors need to be considered when interpreting the GOI values in this way, the level of oil saturation expected for a migration pathway and the position of samples relative to the location of the migration pathway anticipated from theoretical considerations.

The level of GOI response expected for a migration pathway (the first factor) can be estimated either empirically or by consideration of oil saturations expected for a migration pathway. In the first instance, the level of GOI response for palaeo-water legs beneath palaeo-oil zones where GOI values are generally less than 1% can be taken as an empirical indication of GOI values expected for a migration pathway.

The analysis of 83 samples from the 16 wells included in this section where only one sample exceeded 1% supports this baseline estimate.

An alternative is to rely on oil saturation levels predicted for migration pathways by scaled physical models (Thomas and Clouse, 1995; Hirsch and Thompson, 1995) and mass-balance considerations, both of which suggest that migration pathways are unlikely to have oil saturations of more than a few percent. GOI values of <1% are in reasonable agreement with these published values, given that not all oil-filled pore spaces will be sampled by fluid inclusion trapping.

The second factor can be addressed by considering the interplay between the buoyancy forces driving oil flow and the capillary forces opposing the entry of oil into the available pore spaces (Schowalter, 1979; Dembicki and Anderson, 1989; Carruthers, 2003). The sum of these opposing forces represents a migration vector, with migration focussed immediately below an overlying capillary barrier. Migration profiles anticipated for sandstones with sharp tops will be relatively thin (less than a few metres), whereas sandstones with gradually fining upwards sequences will have much broader potential migration zones. Sample selection procedures for GOI analysis seeks to exploit these forces by preferentially favouring samples from below obvious capillary barriers, such as shales, that act to focus migrating hydrocarbons.

In sandstones with well-defined sharp tops the number of samples needed to evaluate each discrete bed is less than sandstone sections with gradually fining upwards sequences where choosing where the reservoir ends and where the capillary barrier begins is difficult thus requiring a large number of samples to properly evaluate. The requirement for large numbers of samples is also encountered in strongly intercalated sand-shale sequences (e.g. fluvial channels or turbidite sequences) that contain many potential migration pathways, requiring a large number of samples to properly assess.

The requirement for large numbers of samples severely impedes the applicability of techniques such as GOI that utilise user intensive point-counting petrographic methods and will often prevent the collection of datasets sufficiently large to meaningfully interpret the results in terms of predicted migration profiles.

Table 4-15: GOI results from the Elm-1 well.

Refer to Table 4-4 for a detailed description of the set-up of tables 4-15, 4-16, 4-17, 4-18 and 4-19.

Well Name	Start Depth (mRT)	End Depth (mRT)	CSIRO Number	Sample Type	Counting Method	Number of fields examined	GOI (%)	GOI Error (%)	Total Grains	Grains With Oil Inclusions	Fluorescence Colours of Oil Inclusions			Location of Oil Inclusions	
											Blue	White	Yellow and Orange	FCDM	QOB
Elm-1	2778	2781	124150	cuttings	Random	100	3.21	1.17	871	28	22	6	0	25	3
Elm-1	2793	2796	124151	cuttings	Complete	1665	2.05	0.36	6105	125	10	105	10	125	0
Elm-1	2829	2832	124152	cuttings	Random	100	16.81	4.88	226	38	12	26	0	24	14
Elm-1	2838	2841	124148	cuttings	Random	101	1.25	0.92	558	7	5	2	0	6	1
Elm-1	2946	2949	124153	cuttings	Complete	1672	0.01	0.01	31489	2	1	0	1	2	0
Elm-1	2970	2973	124154	cuttings	Complete	1656	0.02	0.02	21142	5	5	0	0	5	0
Elm-1	2991	2994	124155	cuttings	Complete	1692	0.00	0.00	7896	0	0	0	0	0	0
Elm-1	2997	3000	124156	cuttings	Complete	1610	0.00	0.00	10089	0	0	0	0	0	0
Elm-1	3009	3012	124157	cuttings	Complete	1517	0.16	0.07	11327	18	5	1	12	14	4
Elm-1	3018	3021	124158	cuttings	Complete	1656	0.02	0.02	18437	3	2	1	0	3	0

Table 4-16: GOI results from the Paqualin-1 well.

Well Name	Start Depth (mRT)	End Depth (mRT)	CSIRO Number	Sample Type	Counting Method	Number of fields examined	GOI (%)	GOI Error (%)	Total Grains	Grains With Oil Inclusions	Fluorescence Colours of Oil Inclusions			Location of Oil Inclusions	
											Blue	White	Yellow and Orange	FCDM	QOB
Paqualin-1	2067	2070	124988	cuttings	Complete	1596	0.03	0.03	10906	3	1	2	0	3	0
Paqualin-1	2835	2838	124990	cuttings	Random	100	79.46	4.93	258	205	109	73	23	165	40
Paqualin-1	2844	2847	124991	cuttings	Random	100	70.05	6.09	217	152	78	65	9	114	38
Paqualin-1	2877	2880	124992	cuttings	Random	100	70.80	3.99	500	354	272	79	3	310	44
Paqualin-1	2880	2883	124993	cuttings	Random	100	84.51	3.63	381	322	172	149	1	275	47
Paqualin-1	4137	4140	124994	cuttings	Random	100	4.96	3.59	141	7	1	5	1	5	2
Paqualin-1	4143	4146	124995	cuttings	Complete	374	0.46	0.63	436	2	0	1	1	2	0
Paqualin-1	4164	4167	124996	cuttings	Complete	150	0.17	0.24	1145	2	2	0	0	2	0
Paqualin-1	4176	4179	124997	cuttings	Random	100	6.67	5.15	90	6	5	1	0	6	0

Table 4-17: GOI results from the Osprey-1 well.

Well Name	Start Depth (mRT)	End Depth (mRT)	CSIRO Number	Sample Type	Counting Method	Number of fields examined	GOI (%)	GOI Error (%)	Total Grains	Grains With Oil Inclusions	Fluorescence Colours of Oil Inclusions			Location of Oil Inclusions	
											Blue	White	Yellow and Orange	FCDM	QOB
Osprey-1	2476	2479	75964	cuttings	Random	125	6.38	1.68	815	52	52	0	0	52	0
Osprey-1	2482	2485	75966	cuttings	Random	125	10.80	2.07	861	93	92	1	0	93	0
Osprey-1	2488	2491	75968	cuttings	Complete	1102	1.48	0.27	7824	116	33	83	0	116	0
Osprey-1	2491	2494	75969	cuttings	Complete	1632	1.81	0.33	6256	113	27	86	0	113	0

Table 4-18: GOI results from the Parry-1 well.

Well Name	Start Depth (mRT)	End Depth (mRT)	CSIRO Number	Sample Type	Counting Method	Number of fields examined	GOI (%)	GOI Error (%)	Total Grains	Grains With Oil Inclusions	Fluorescence Colours of Oil Inclusions			Location of Oil Inclusions	
											Blue	White	Yellow and Orange	FCDM	QOB
Parry-1	2097	2100	123482	cuttings	Random	100	14.38	5.56	153	22	0	6	16	22	0
Parry-1	2103	2106	123483	cuttings	Complete	2484	0.05	0.04	13248	7	1	0	6	7	0
Parry-1	2119	2121	123294	cuttings	Complete	1645	0.03	0.03	9815	3	0	0	3	3	0

Table 4-19: GOI results from the Pitiri-1 well.

Well Name	Start Depth (mRT)	End Depth (mRT)	CSIRO Number	Sample Type	Counting Method	Number of fields examined	GOI (%)	GOI Error (%)	Total Grains	Grains With Oil Inclusions	Fluorescence Colours of Oil Inclusions			Location of Oil Inclusions	
											Blue	White	Yellow and Orange	FCDM	QOB
Pituri-1	1708	1714	123318	cuttings	Random	100	2.30	1.34	478	11	1	9	1	11	0
Pituri-1	1720	1726	123319	cuttings	Complete	1665	1.13	0.69	888	10	1	8	1	10	0

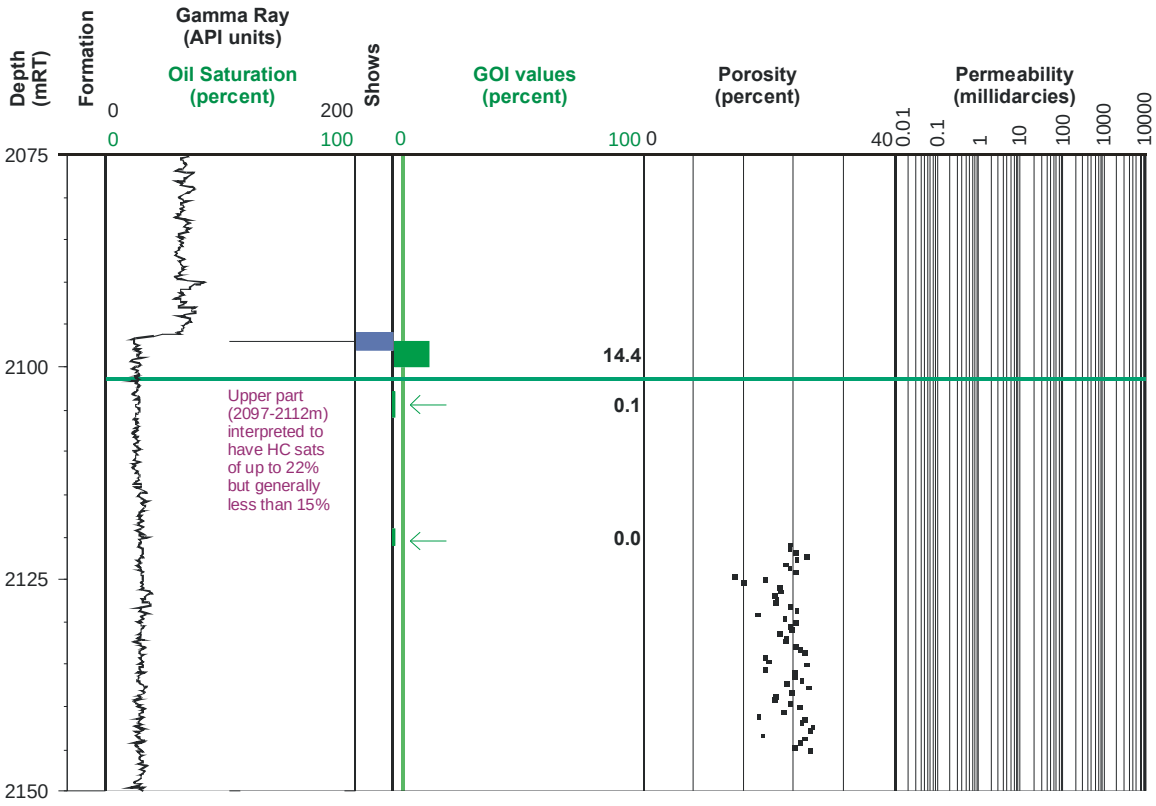

Figure 4-48: GOI results from the Parry-1 well.

GOI results displayed against the gamma ray log with available porosity and permeability and conventional oil show data also shown. On the GOI log the green vertical line marks the position of the empirical threshold for oil accumulation, with the width of the horizontal green lines showing the position and magnitude of the recorded GOI value (actual values shown to the right). Samples where GOI is <1% are marked with an arrow. Conventional shows reported in the well completion report are also shown with the thickness of the bar being proportional to their intensity.

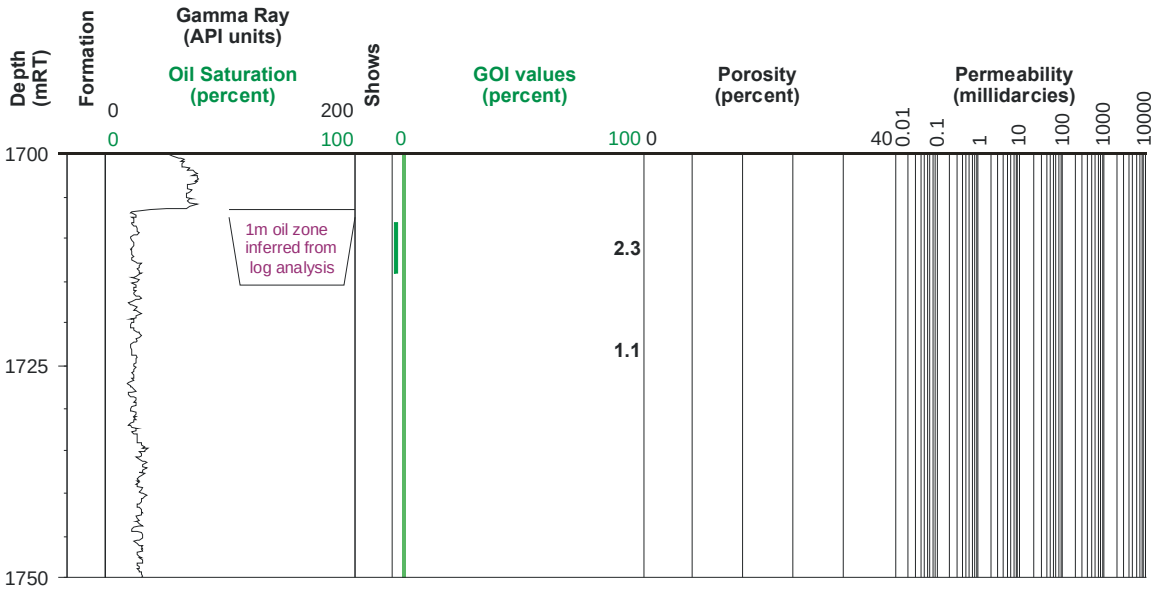

Figure 4-49: GOI results from the Pituri-1 well.

GOI results displayed against the gamma ray log with available porosity and permeability and conventional oil show data also shown. On the GOI log the green vertical line marks the position of the empirical threshold for oil accumulation, with the width of the horizontal green lines showing the position and magnitude of the recorded GOI value (actual values shown to the right). Samples where GOI is <1% are marked with an arrow. Conventional shows reported in the well completion report are also shown with the thickness of the bar being proportional to their intensity.

This requirement has not been met for a significant number of the water-wet wells examined in this study and utilisation of these results for regional migration analysis has not been attempted.

The importance of the low GOI values recorded in this study is further compromised by other factors that question whether the oil inclusions, where present in low abundance, can reliably be used as indicators of oil migration. The most important of these factors is the assumption that the oil inclusions are not inherited from an older petroleum system subsequently reworked by erosion. This possibility applies only to samples with very low GOI values as there is no conceivable process whereby grains with oil inclusions that have been eroded from an older formation should be sufficiently focused during re-deposition to produce a sample with a high GOI value. Indeed the chances of even a single grain with oil inclusions being reworked is remote given the huge sediment volume that is reworked compared with the small proportion of that volume that have come into contact with migrating oil.

In samples with low GOI, this chance can be further discounted where the oil inclusions occur within authigenic quartz overgrowths that display well preserved crystal faces, which are unlikely to be retained if the grains have been transported. In the water-wet wells sampled, however, only three of the 16 wells contain any oil inclusions within authigenic quartz overgrowths, in the remainder the oil inclusions observed occur exclusively on fractures in detrital quartz and the likelihood of reworking cannot be addressed.

The inferred provenance for the main reservoir intervals in the Vulcan Sub-basin includes a possible contribution of sediments derived from erosion of older sandstone horizons, so it would, therefore, be capricious to use these data as evidence for oil migration without raising the possibility of a reworked contribution. Conversely, interpreting samples with an absence of oil inclusions as negative evidence to support a lack of oil migration should also not be considered as a unique conclusion.

Another factor that could produce erroneous conclusions when using oil inclusions to constrain oil migration is the presence of oil inclusions within shaly reservoirs or sandstones in close contact with source horizons that are thermally mature and could

be generating oil *in situ*. In these instances, the oil seen in inclusions could be derived from a local source and may not be indicative of connection to a regionally effective migration network with sufficient volumes of oil to achieve an oil accumulation. Thermal maturity information, such as vitrinite reflectance measurements combined with pyrolysis or organic petrological data could, however, be used to filter out samples of this type.

Given the factors which could compromise the interpretation of the migration system and the difficulty in addressing the likelihood of these alternatives, the preferred approach to interpreting wells with exclusively low GOI values is to consider GOI values above zero to be permissive of oil migration. Similarly, for samples without oil inclusions deem it a possible that these wells may be in a migration shadow. Integration of GOI data with other oil migration indicators such as conventional oil shows is a crucial part of the evaluation process. Ultimately, the validity of other possibilities should be tested by other geological data, but interpreting low GOI values in isolation is to be avoided to prevent erroneous conclusions.

4.7 GOI CALIBRATION STUDY

Whilst the overall statistical robustness of the GOI numbers produced in this study has been addressed using the binomial and *Poisson* distribution functions outlined in section 4.5.1.4 it is recognised that these approaches do not address the potential errors that are introduced by the subjective nature of the GOI analysis method. To address these factors a replication study was completed using a selection of randomly chosen samples to assess the level of repeatability for the GOI numbers reported in this study. This allows the total error associated with this type of analysis to be estimated allowing more robust geologic interpretations of the numbers collected.

4.7.1 Method

To avoid potential bias and provide a representative, yet manageable, group of sample repeats taken from a large sample pool the samples chosen for the repeatability study were selected at random, with a single sample taken from each of seven bin ranges (i.e. seven samples in total).

Table 4-20: GOI results from the other water wet wells.

Refer to next page for detailed description of the layout of this table.

Well Name	Start Depth (mRT)	End Depth (mRT)	CSIRO Number	Sample Type	Counting Method	Number of fields examined	GOI (%)	GOI Error (%)	Total Grains	Grains With Oil Inclusions	Fluorescence Colours of Oil Inclusions			Location of Oil Inclusions	
											Blue	White	Yellow and Orange	FCDM	QOB
Allaru-1	2376	2379	124137	cuttings	Complete	1554	0.01	0.01	26055	3	2	0	1	3	0
Allaru-1	2388	2391	124138	cuttings	Complete	1620	0.00	0.00	21114	0	0	0	0	0	0
Allaru-1	2547	2550	124140	cuttings	Complete	1188	0.05	0.07	3802	2	1	0	1	2	0
Allaru-1	2892	2895	124141	cuttings	Complete	1665	0.00	0.00	11711	0	0	0	0	0	0
Allaru-1	2931	2934	124142	cuttings	Complete	1551	0.00	0.00	8531	0	0	0	0	0	0
Allaru-1ST2	2538	2541	124143	cuttings	Complete	930	0.02	0.03	8928	2	1	1	0	2	0
Allaru-1ST2	2871	2874	124144	cuttings	Complete	1122	0.00	0.00	18064	0	0	0	0	0	0
Allaru-1ST2	2910	2913	124145	cuttings	Complete	1575	0.00	0.00	14070	0	0	0	0	0	0
Allaru-1ST2	2955	2958	124146	cuttings	Complete	1665	0.00	0.00	8547	0	0	0	0	0	0
Anson-1	1707	1710	123354	cuttings	Complete	1554	0.01	0.03	7252	1	0	0	1	1	0
Anson-1	1716	1719	123355	cuttings	Complete	1628	0.08	0.06	7869	6	0	2	4	6	0
Anson-1	1725	1728	123356	cuttings	Complete	1591	0.03	0.04	6947	2	0	1	1	2	0
Augustus-1	3500	3515	75874	cuttings	Complete		0.84	0.38	2250	19	7	9	3	19	0
Augustus-1	3515	3530	75876	cuttings	Complete	100	0.12	0.23	887	1	0	1	0	1	0
Calytrix-1	1565	1570	124159	cuttings	Complete	870	0.00	0.00	10875	0	0	0	0	0	0
Calytrix-1	1570	1575	124160	cuttings	Complete	1610	0.04	0.05	5689	2	1	1	0	2	0
Calytrix-1	1575	1580	124161	cuttings	Complete	1140	0.00	0.00	4560	0	0	0	0	0	0
Calytrix-1	1580	1585	124162	cuttings	Complete	1485	0.00	0.00	8267	0	0	0	0	0	0
Calytrix-1	1585	1590	124163	cuttings	Complete	80	0.00	0.00	4904	0	0	0	0	0	0
Calytrix-1	1590	1595	124164	cuttings	Complete	1584	0.02	0.04	4594	1	0	1	0	1	0
Champagny-1	3210	3215	123409	cuttings	Complete	1656	0.42	0.09	21638	91	20	51	20	61	30
Champagny-1	3225	3230	123410	cuttings	Complete	1591	0.04	0.03	20842	9	4	3	2	9	0
Champagny-1	3350	3355	123411	cuttings	Complete	2520	0.17	0.04	34860	60	15	37	8	60	0
Champagny-1	3402	3405	123412	cuttings	Complete	1656	0.03	0.04	7894	2	1	1	0	1	1
Douglas-1	2515	2520	75872	cuttings	Random	102	0.20	0.39	496	1	1	0	0	1	0
East Swan-1	2726	2729	124130	cuttings	Complete	624	0.00	0.00	1726	0	0	0	0	0	0
East Swan-1	2750	2753	124131	cuttings	Complete	506	0.00	0.00	5262	0	0	0	0	0	0
East Swan-1	2765	2768	124132	cuttings	Complete	930	0.24	0.13	5797	14	14	0	0	14	0
East Swan-1	2814	2817	124135	cuttings	Complete	546	0.00	0.00	1001	0	0	0	0	0	0
Hadrian-1	3476.5						0.37	0.51	536	2	0	0	2	2	0
Ibis-1	1275	1280	123457	cuttings	Complete	1505	0.00	0.00	2308	0	0	0	0	0	0
Ibis-1	1285	1290	123458	cuttings	Complete	1665	0.05	0.10	2054	1	0	1	0	1	0
Ibis-1	1300	1305	123459	cuttings	Complete	1462	0.00	0.00	1754	0	0	0	0	0	0
Ibis-1	1350	1355	123460	cuttings	Complete	1628	0.05	0.07	4179	2	1	0	1	1	1
Langhorne-1	2511	2514	124971	cuttings	Complete	1404	0.00	0.00	5850	0	0	0	0	0	0
Langhorne-1	2526	2529	124972	cuttings	Complete	1440	0.00	0.00	4752	0	0	0	0	0	0
Langhorne-1	2541	2544	124973	cuttings	Complete	1505	0.00	0.00	4314	0	0	0	0	0	0
Leeuwin-1	1653	1656	123508	cuttings	Complete	1584	0.01	0.03	7234	1	0	1	0	1	0
Leeuwin-1	1674	1677	123510	cuttings	Complete	1656	0.01	0.02	10212	1	1	0	0	1	0
Leeuwin-1	1749	1752	123511	cuttings	Complete	1672	0.03	0.04	9642	3	0	3	0	3	0
Leeuwin-1	1761	1764	123512	cuttings	Complete	1665	0.01	0.03	7548	1	0	1	0	1	0
Leeuwin-1	1869	1872	123513	cuttings	Complete	1628	0.00	0.00	7706	0	0	0	0	0	0
Leeuwin-1	2469	2472	123515	cuttings	Complete	1120	0.02	0.02	12357	2	0	2	0	2	0
Longleat-1	1938	1941	124974	cuttings	Complete	1435	0.00	0.00	10380	0	0	0	0	0	0
Longleat-1	1974	1980	124975	cuttings	Complete	1505	0.01	0.01	13595	1	0	0	1	1	0
Longleat-1	2016	2022	124976	cuttings	Complete	1551	0.00	0.00	10702	0	0	0	0	0	0
Longleat-1	2064	2070	124977	cuttings	Complete	1320	0.00	0.00	6952	0	0	0	0	0	0
Longleat-1	2115	2118	124978	cuttings	Complete	1406	0.02	0.03	9561	2	0	2	0	2	0
Longleat-1	2154	2157	124979	cuttings	Complete	1620	0.00	0.00	7668	0	0	0	0	0	0

Table 4-20: GOI results from the other water wet wells continued.

Table shows all relevant data for the analysed samples, including depth, sample number and method employed. Abbreviations shown in the location of oil inclusions column refer to Fractures Cutting Detrital Minerals (FCDM) and Quartz Overgrowth Boundary. GOI Error was defined using the method outlined in the text. Numbers shown in the 7 right most columns refer to numbers of grains containing oil inclusions of specific colour or location. Where numbers are absent no measurement was made.

											Fluorescence Colours of Oil Inclusions			Location of Oil Inclusions	
Well Name	Start Depth (mRT)	End Depth (mRT)	CSIRO Number	Sample Type	Counting Method	Number of fields examined	GOI (%)	GOI Error (%)	Total Grains	Grains With Oil Inclusions	Blue	White	Yellow and Orange	FCDM	QOB
Maple-1	3666	3669	124980	cuttings	Complete	1505	0.01	0.01	17157	1	1	0	0	1	0
Maple-1	3681	3684	124981	cuttings	Complete	1540	0.00	0.00	11139	0	0	0	0	0	0
Maple-1	3684	3687	124983	cuttings	Random	100	3.46	1.36	693	24	15	9	0	24	0
Maple-1	3720	3723	124982	cuttings	Complete	1904	0.05	0.10	1904	1	1	0	0	1	0
Maple-1	3903	3906	124985	cuttings	Complete	300	0.00	0.00	1060	0	0	0	0	0	0
Maple-1	3975	3978	124986	cuttings	Complete	759	0.00	0.00	5389	0	0	0	0	0	0
Maple-1	4101	4105	124987	cuttings	Complete	1332	0.00	0.00	11899	0	0	0	0	0	0
Pollard-1	2040	2043	124998	cuttings	Complete	1554	0.00	0.00	13157	0	0	0	0	0	0
Pollard-1	2048	2052	124999	cuttings	Complete	1665	0.02	0.03	10212	2	1	1	0	2	0
Pollard-1	2100	2103	125000	cuttings	Complete	1591	0.00	0.00	5356	0	0	0	0	0	0
Rainbow-1	2573	2576	125001	cuttings	Complete	1548	0.01	0.02	9391	1	0	1	0	1	0
Rainbow-1	2591	2594	125002	cuttings	Complete	1634	0.00	0.00	15904	0	0	0	0	0	0
Rainbow-1	2621	2624	125003	cuttings	Complete	1050	0.00	0.00	7315	0	0	0	0	0	0
Snowmass-1	1294	1297	122477	cuttings	Complete	305	0.41	0.40	986	4	2	0	2	4	0
Snowmass-1	1318	1321	122478	cuttings	Complete	2183	0.25	0.12	6913	17	14	3	0	17	0
Snowmass-1	1345	1348	122479	cuttings	Complete	2160	0.02	0.03	5760	1	1	0	0	1	0
Snowmass-1	1417	1420	122480	cuttings	Complete	2304	0.06	0.06	6221	4	0	4	0	4	0
Taltarni-1	2853.9		123413	core	Complete	704	0.00	0.00	2652	0	0	0	0	0	0
Taltarni-1	2865.1		123414	core	Complete	1457	0.00	0.00	2652	0	0	0	0	0	0
Taltarni-1	2870		123415	core	Complete	1800	0.01	0.02	15060	2	0	1	1	2	0
Taltarni-1	3009	3012	123416	cuttings	Complete	2412	0.00	0.00	5869	0	0	0	0	0	0
Tancred-1	1344	1347	123484	cuttings	Complete		0.31	0.18	3835	12	7	2	3	6	6
Tancred-1	1365	1368	122471	cuttings	Complete	2210	1.69	0.55	2136	36	17	3	16		
Tancred-1	1386	1389	122472	cuttings	Complete	1961	0.16	0.11	5556	9	4	3	2		
Tancred-1	1419	1422	122473	cuttings	Complete	2346	0.11	0.11	3754	4	2	2	0		
Tancred-1	1455	1458	122474	cuttings	Complete	2310	0.00	0.00	2079	0	0	0	0		
Tancred-1	1479	1482	122475	cuttings	Complete	1995	0.02	0.04	4655	1	0	1	0		
Warb-1	1735	1740	125005	cuttings	Complete	1568	0.00	0.00	1411	0	0	0	0	0	0
Warb-1	2365	2370	125006	cuttings	Complete	1715	0.00	0.00	9433	0	0	0	0	0	0
Warb-1	2380	2380	125007	cuttings	Complete	1620	0.02	0.03	9234	2	2	0	0	2	0
Warb-1	2400	2400	125008	cuttings	Complete	1575	0.01	0.02	9345	1	0	0	0	1	0
Warb-1	2405	2410	125009	cuttings	Complete	1628	0.00	0.00	9877	0	0	0	0	0	0
Warb-1	2430	2435	125010	cuttings	Complete	1598	0.01	0.02	14382	2	0	1	0	2	0
Yarra-1	2557	2560	125011	cuttings	Complete	1645	0.00	0.00	4387	0	0	0	0	0	0
Yarra-1	2638	2641	125013	cuttings	Complete	1036	0.00	0.00	5905	0	0	0	0	0	0
Yarra-1	2698	2701	125014	cuttings	Complete	918	0.18	0.24	1132	2	0	2	0	2	0
Yarra-1	2812	2815	125015	cuttings	Complete	1188	0.00	0.00	2772	0	0	0	0	0	0
Yering-1	2812	2815	123406	cuttings	Complete	1575	0.02	0.03	8925	2	1	1	0	2	0
Yering-1	2923	2926	123407	cuttings	Complete	2448	0.00	0.00	5794	0	0	0	0	0	0
Yering-1	2959	2962	123408	cuttings	Complete	2520	0.05	0.05	8148	4	0	4	0	4	0

These bins cover the range of GOI values collected on samples using the random scan technique. The seven bins used were for GOI values 1-5%, 5-10%, 10-20%, 30-40%, 40-50% and >50%. GOI data collected by the continuous scan method (GOI values generally <1%) were not included in the replication study due to the high likelihood that a "memory" bias would be difficult to avoid in samples with very low numbers of grains containing oil inclusions.

For each sample, the GOI analysis was repeated five times (including the original value); with each repeat representing a different randomly selected 100 fields of view (FOV) from the same thin section. Repetition of the same 100 FOV was not attempted due to mechanical limitations of the stepping stage equipment that prevents exact relocation of the same fields. Each discrete 100 FOV equates to about 10% of the total sample so using a different set of fields for each repeat also greatly reduces the risk of a memory bias affecting the veracity of the results.

The series of repeats were conducted over a six month period, whilst the original analysis was completed up to 8 years prior to the completion of the first repeat and includes a number of samples that were first analysed prior to the start of this study.

4.7.2 Calibration Study Results

The results of the repeatability study are summarised in Table 4–21 and illustrated graphically in Figure 4–50. The greatest observed variation from the mean GOI value reaches a maximum of 31% in the 5-10% and 10-20% bin ranges, but the average variation from the mean for each bin range is no greater than 25% (e.g. A GOI number of 20% had an average error of ±5%).

Comparison of the error range produced in the repeatability experiment with that estimated by the binomial function shows fairly close agreement (Figure 4–51). Both the repeatability and binomial errors show an overall reduction as the GOI value increases, reflecting a reduced statistical error as the proportion of grains with oil inclusions increases.

Table 4-21: Results of the GOI replication study.

The table collates GOI repeats obtained on seven samples, each drawn randomly from samples with GOI values in each of the specific bin range listed. A GOI determination was made for each sample four times over an extended period of time, typically a few months to more than a year. The table gives the original GOI value and the GOI value recorded for each repeat as well as the binomial error associated with each measurement.

Well Name	CSIRO #	Depth (mRT)	Bin Range	Original Value	Binomial Error	Repeat 1	Binomial Error	Repeat 2	Binomial Error	Repeat 3	Binomial Error	Repeat 4	Binomial Error
Oliver-1	122224	2967-70	1 to 5	3.65	1.02	3.00	1.26	2.58	1.21	2.60	1.15	3.15	1.75
Oliver-1	122226	3006-09	5 to 10	9.48	2.87	7.20	2.62	6.32	2.56	7.32	2.66	6.42	2.54
Eclipse-1	122858	2616-19	10 to 20	15.20	3.88	10.34	3.20	15.82	4.15	17.25	4.39	16.40	4.59
Skua-2	126820	2340-43	20-30	22.73	6.19	22.67	6.26	17.59	5.29	20.86	5.82	18.13	5.77
Eclipse-1	122494	2607-10	30 to 40	35.19	6.37	37.35	7.36	31.91	7.69	31.76	7.50	26.51	6.71
Eclipse-1	123350	2733-36	40 to 50	40.98	6.73	39.44	8.04	40.68	8.86	42.31	8.49	37.07	8.79
Jabiru-1A	122218	1632	>50	58.88	4.10	62.72	4.71	63.37	4.33	67.84	4.44	68.69	4.57

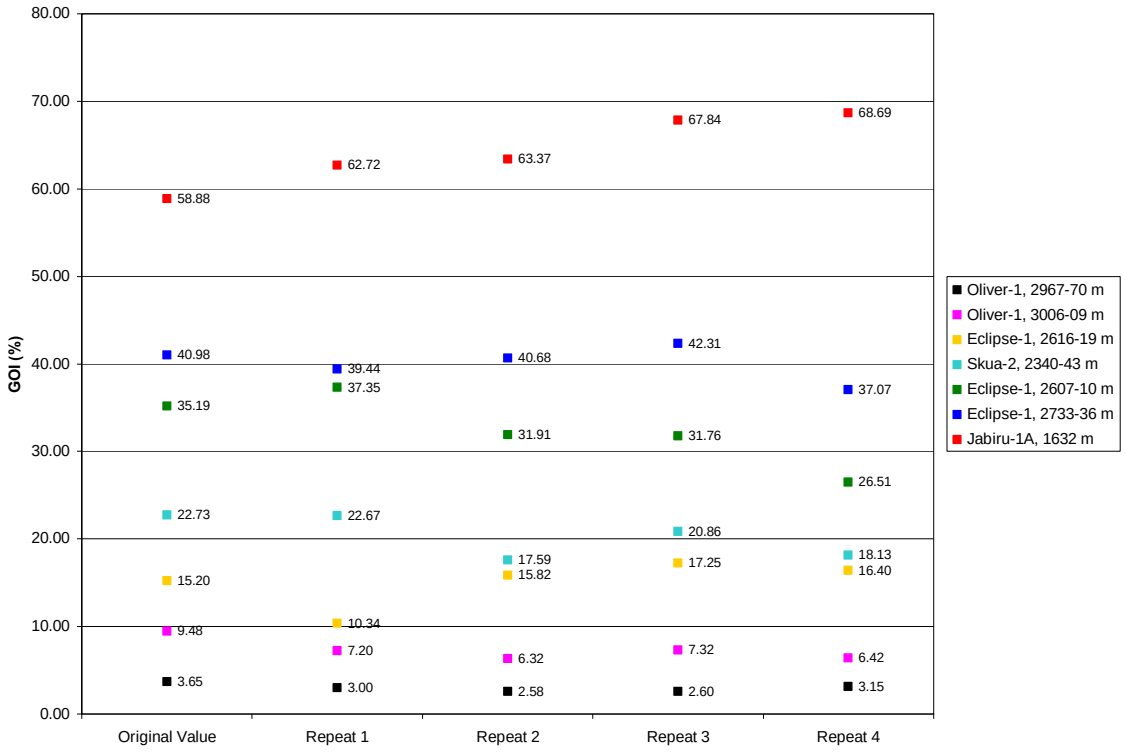

Figure 4-50: Graphical display of the result of the GOI replication study

The graph shows the measured GOI value produced for the original analysis of seven samples and the GOI values produced by four subsequent repetitions on each sample arranged in chronological order of the analysis date. The greatest variation in repeatability occurs in the highest GOI range. Note that repeatability of the lower GOI bin ranges is good and that the spread of values consistently provides an outcome that would support a common interpretation of the palaeo-oil saturation (i.e. values constantly greater than the empirical threshold) using the standard GOI interpretation procedures.

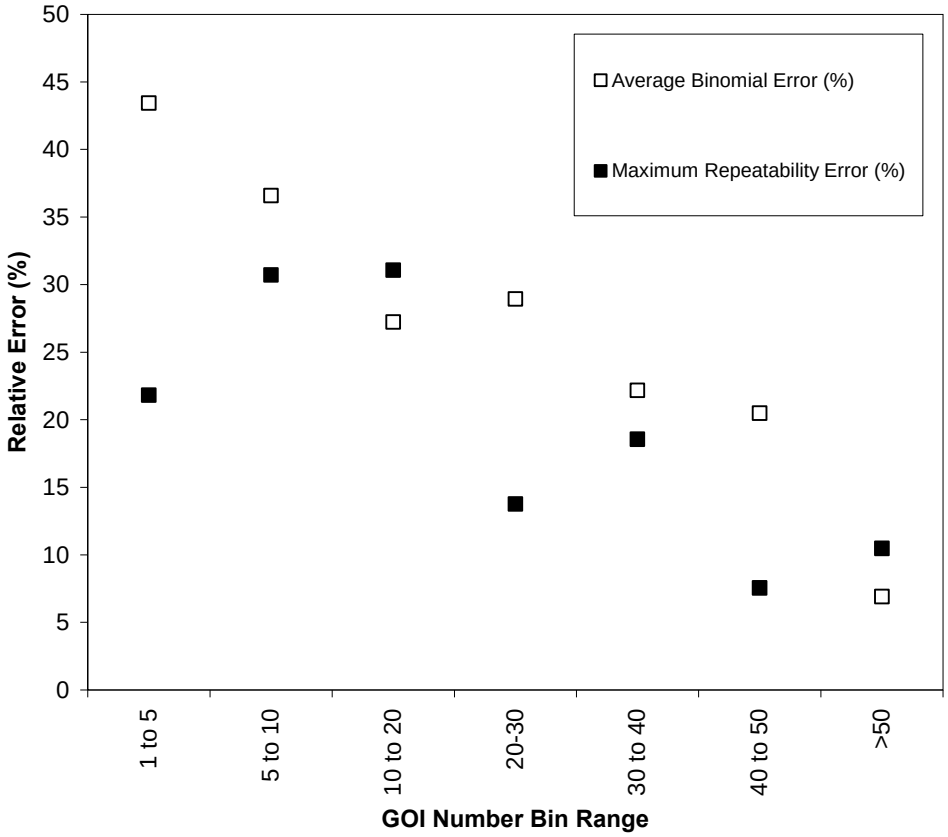

Figure 4-51: Repeatability error compared with binomial error.

This graph compares the statistically derived average Binomial Error against the deterministically derived Repeatability Error and shows that the true error is well captured by the binomial approximation that is used to routinely assess the validity of individual GOI numbers. The Repeatability Error is the maximum deviation away from the mean GOI value for each bin range produced by the repeated calibration analyses completed for each bin range.

The average replication error encountered in each bin range was less than the equivalent binomial estimate, strongly suggesting that the binomial function provides an effective, if conservative, estimate of the total error associated with GOI analyses. This provides confidence that the binomial function is a suitable statistical measure to evaluate both the random error as well as any systematic errors providing a suitably trained and experienced analyst undertakes the analyses.

This outcome supports the use of the binomial error function described in section 4.5.1.4 as a routine check to highlight samples where the accuracy of the GOI measurement is in question (i.e. where the outcome of the interpretation is altered).

Figure 4–52, describing the variation in GOI values against the date of the analysis, shows good repeatability even where the sample was first analysed up to 8 years ago. This suggests that improvements related to other factors such as equipment or analytical procedures played no significant role in influencing the ability to reproduce GOI data over this time period.

4.7.2.1 Significance of Calibration Results

The calibration study demonstrates GOI data within acceptable accuracy of the original value across a range of different GOI values is feasible, even where significant time has elapsed between completing the individual analyses.

The consistent over-estimation of the repeatability error by the binomial function provides good support for the use of this function as a conservative indication of the likely error associated with the bulk of the GOI values produced in the main study and in any future applications of the method.

Whilst the level of repeatability achieved remains relatively inaccurate this needs to be considered in light of the coarse interpretation protocols employed. In any sample where the recorded GOI value, less a relative error defined by the binomial function exceeds the empirical threshold for oil accumulation (GOI value >5%) this value is likely to represent a result unaffected by operator variability or the natural statistical variability that reflects the partial sampling nature of the GOI method.

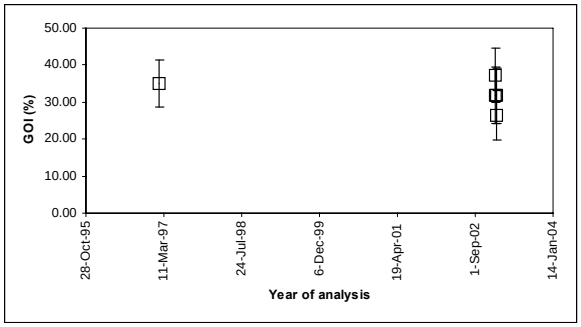

Eclipse-1_2607-10m sample

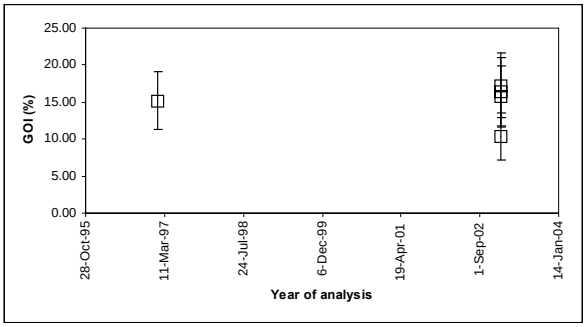

Eclipse-1_2616-19m sample

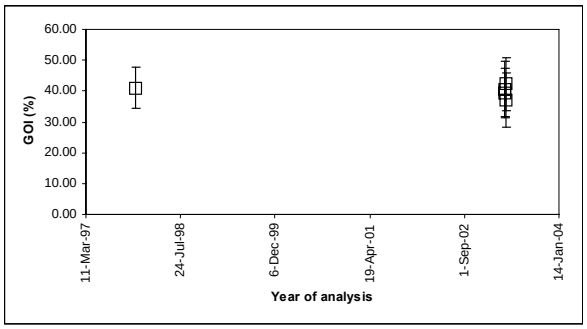

Eclipse-1_2733-36m sample

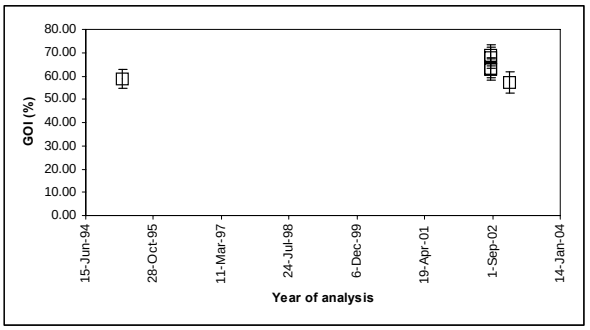

Jabiru-1A_1632m sample

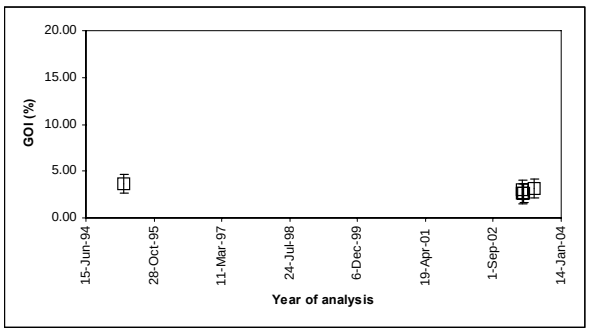

Oliver-1_2967-70m sample

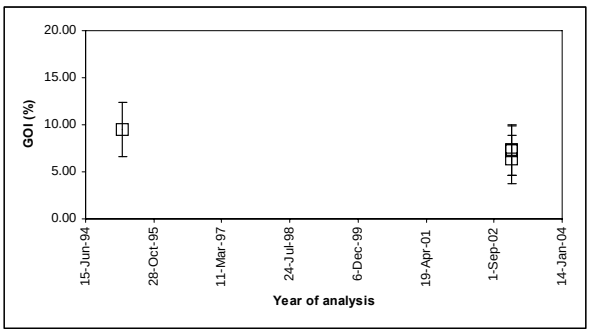

Oliver-1_3006-09m sample

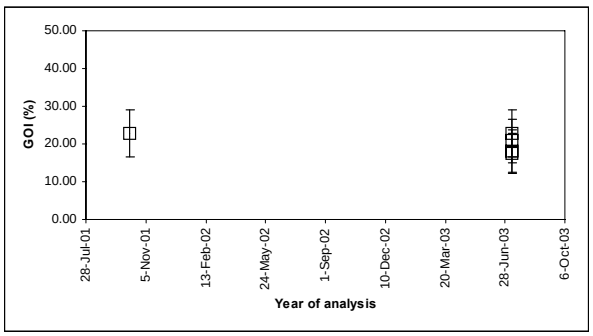

Skua-2_2340-43m sample

Figure 4-52: Variation in the GOI values with time.

Chronological plots showing the time period elapsed between the date of measurement of the original GOI values and the date of completion of each of the subsequent repeat analyses for all of the samples included in the replication study.

Variations in GOI values in the higher bins ranges have no impact on the conclusions drawn regarding palaeo-oil saturation (i.e. the values always exceed the empirical threshold and a robust conclusion regarding the attainment of a palaeo-oil column can be made). The binomial function is, however, an extremely helpful tool that allows potential errors in the lower bin ranges to be systematically evaluated before a conclusion regarding the level of palaeo-oil saturation is reached.

The results achieved in this calibration study describe the level of reproducibility possible for a single operator and do not address the ability of multiple operators to achieve comparable results. The value of the technique more broadly than the current study ultimately rests with future studies that confirm the inter-operator error associated with this method, but this goal is beyond the scope of the current investigation. Further development of the GOI method, in particular greater automation of the analysis, would reduce the reliance on human decisions and greatly improve the opportunity for this formation evaluation technique to be applied more widely in the future and through a greater number of laboratories.

4.8 RELATIVE TIMING OF HYDROCARBON MIGRATION

The position of oil inclusions within different authigenic minerals coupled with knowledge of the paragenetic sequence described in Chapter 3 and illustrated in Figures 4–53 and 4–54 allows relative constraints to be placed on the timing of hydrocarbon migration into these reservoirs. Fluid inclusions can be trapped during the crystallisation of the host mineral or by fracturing of pre-existing detrital minerals that become annealed by localised cementation. Not all minerals have a suitable framework crystal structure to enable fluid inclusions to be formed but understanding the diagenetic sequence allows the relationships between porosity loss due to diagenesis and the timing of fluid migration events to be explored.

Information on the diagenetic sequence can be obtained from individual samples but rarely are all of these phases present in any one sample. Consequently, the interpreted diagenetic sequence (Figure 4–54) is arrived at by petrographic observations (Figure 4–53) taken from a combination of samples and the likely controls on crystallisation of certain mineral types. Glauconite for example rarely

shows definitive timing relationships but this cement commonly forms directly below the sediment-water interface and often show Rb/Sr ages that coincide with the depositional ages (e.g. Morton and Long, 1984). Pyrite, commonly exhibiting a framboidal habit that is considered to be indicative of syn-depositional origin occurs is some samples. In contrast, more crystalline pyrite also occurs and has been interpreted as a late diagenetic cement (Figure 4–53).

Authigenic clays are a common, but not particularly abundant constituent of the diagenetic minerals observed in these samples. Kaolinite represents the principal clay type with subordinate amount of mixed layer illite-smectite clays, typically as grain replacement for detrital mica and less commonly feldspar.

Quartz overgrowths, which enclose and therefore clearly postdate the kaolinite, also represent an abundant diagenetic mineral, becoming more prevalent with depth. Filamentous illite, seen nucleating from the surface of authigenic quartz and hence post-dating quartz overgrowths is reported from some, more deeply buried, samples (Eadington et al., 1991), but it is generally rare.

Carbonate cements seen within some samples appear to represent either very early or very late diagenetic phases. Iron-stained siderite rhombs occur in some samples and probably represent an early diagenetic product as it fills pore space and has floating detrital quartz grains that indicate crystallisation prior to compaction (Figure 4–53). Siderite crystals are also sometimes enclosed by later formed quartz overgrowths.

Micritic carbonate cement occurs in some samples and based on crystallisation before substantial sediment compaction appears to be an early phase. A much later phase of carbonate cement that occurs in some samples and has a poikilotopic habit clearly encloses earlier formed quartz overgrowths (Figure 4–53).

From this collection of authigenic minerals only the carbonate cements and the quartz overgrowths have crystal structures that would enable fluid inclusions to be trapped. Fractures present in suitable detrital minerals (quartz and feldspar) can also provide constraint on the timing of inclusion entrapment if these fractures can be shown to clearly pre- or post-date an authigenic mineral (Figure 4–55).

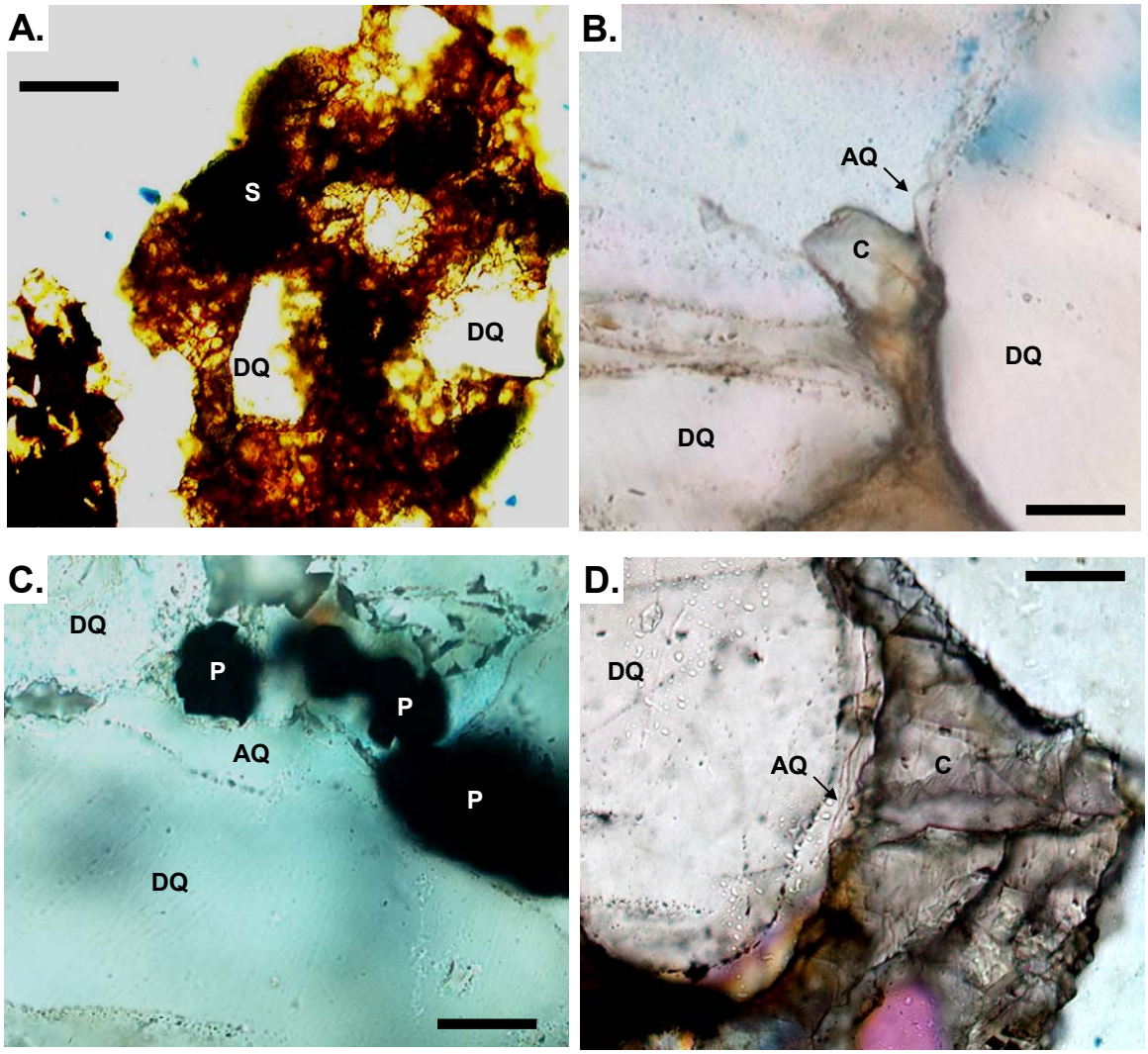

Figure 4-53: Examples of key petrographic relationships.

Plain light photomicrographs showing examples of petrographic relationships that have been observed in the current study and have been used to corroborate petrology observations undertaken on behalf of the operating companies and reported within the well completion reports. A. Iron stained siderite cement filling pore spaces with floating detrital quartz grains indicating crystallisation of siderite prior to significant burial compaction, Ibis-1, CSIRO sample 123458, 1285-90mRT cuttings sample, 10x objective. B. Thin quartz overgrowth partially enclosing earlier formed carbonate cement, Ibis-1 CSIRO sample 123458, 1285-90mRT cuttings sample, 50x objective. C Quartz overgrowth enclosing earlier formed pyrite cement, Skua-8, CSIRO sample 126829, 2320.7mRT core sample, 50x objective. D. Late carbonate cement enclosing earlier formed authigenic quartz overgrowths, Yarra-1, CSIRO sample 125011, 2557-60mRT, cuttings sample 50x objective. Scale bar shows 100µm in A and 20µm in B, C and D

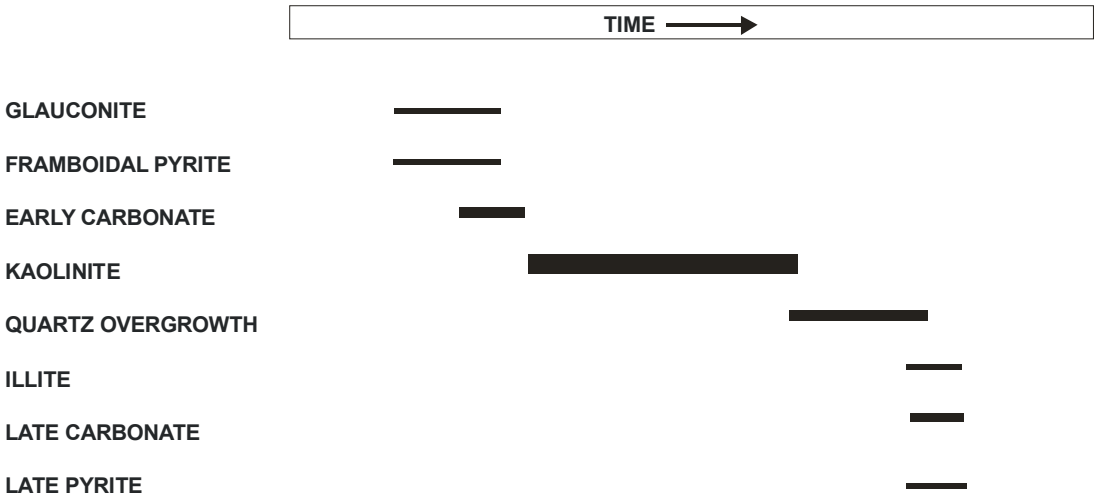

Figure 4-54: Implied paragenetic sequence common to wells in the VSB.

Composite paragenetic sequence for wells examined in this study with the thickness of the bars indicating the relative abundance whilst the length of the bar relates to the relative time period that each cement phase is likely to have been contributing to porosity reduction. Where these bars overlap there is petrographic evidence (such as variable timing relationships) that supports contemporaneous crystallisation, but in most instances there is no constraint on the duration of time that separates one phase from another. Not all of these minerals are present in each sample examined but the sequence is consistent between different samples and different wells.

In this study three discrete populations of oil inclusions are recognised:

1. Oil inclusions on fractures cutting detrital quartz (dominant).

2. Oil inclusions within quartz overgrowths (common).

3. Oil inclusions within authigenic carbonate (rare).

For the first two categories information on the proportion of inclusions trapped at each of these locations was recorded in the data tables but both the occurrence of carbonate cement and examples of inclusions within carbonate were so rare that this information was not routinely recorded.

Oil inclusions on fractures cutting detrital minerals (Figures 4–55, 4-56) represent the dominant location of oil inclusions in most samples (Figure 4–57) but provide no constraint on the timing of oil migration, except where such fractures abut the boundary with an enclosing authigenic mineral, indicating entrapment of oil inclusions prior to the formation of that mineral (Figure 4–55, Figure 4–56).

Quartz is the most common detrital mineral host, with a much smaller number of detrital feldspar grains also containing oil inclusions.

The greater propensity for oil inclusions to be located on fractures within detrital minerals compared with authigenic minerals (Figure 4–58) demonstrates the important role fracturing plays in trapping formation fluids. This observation dispels a widely held, but incorrect, assumption that the timing of hydrocarbon migration and the formation of suitable authigenic cements must coincide if these events are to be recorded in the fluid inclusion record.

The presence of oil inclusions within quartz overgrowths in many samples, particularly those with high GOI values suggests that oil migration and the crystallisation of quartz overgrowths were, at least in part, coincident events. Given the high proportion of oil inclusions within quartz overgrowths in samples with high GOI values (Figure 4-55), the formation of quartz overgrowths likely continued even when high oil saturation was attained (Lisk et al., 2000a).

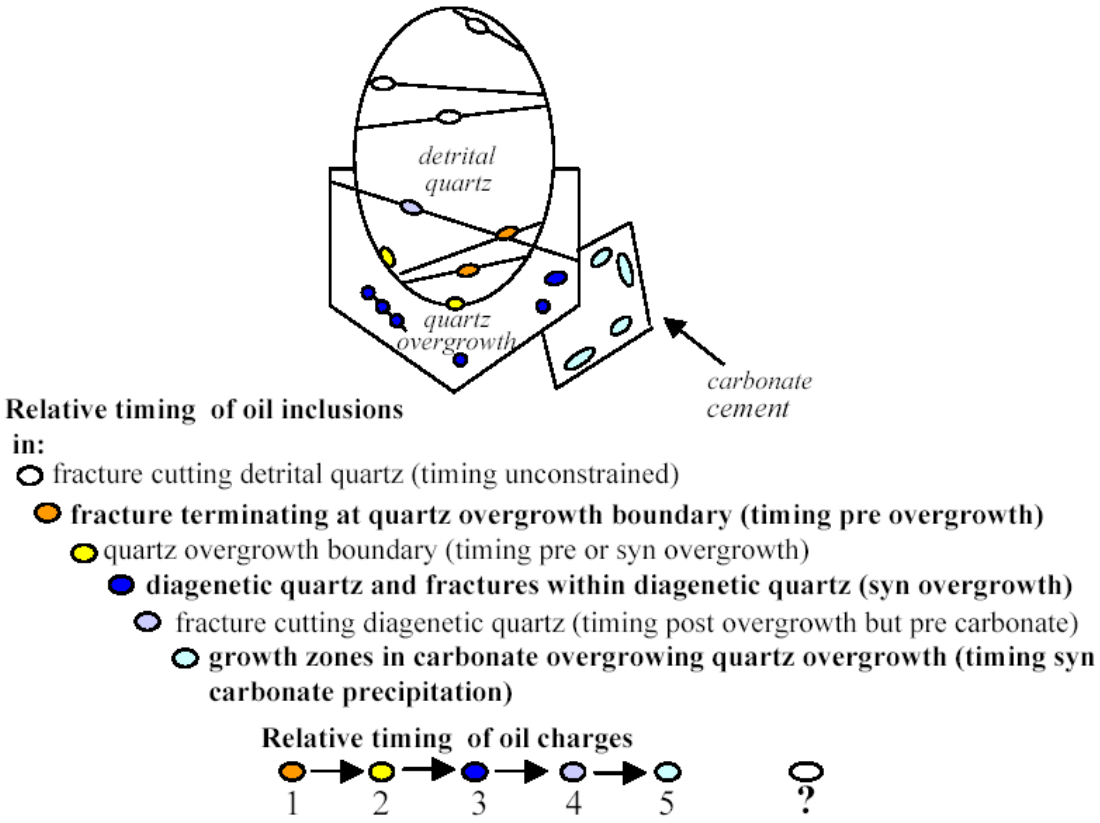

Figure 4-55 Cartoon showing relative timing relationship discernible from petrography.

The position of the fluid inclusions coupled with timing relationships derived from the superposition of different fluid inclusion assemblages and the sequence of authigenic minerals allows the timing of fluid migration events to be determined in a relative time sense. The colour scheme highlights the different types of observation that allow the timing of various fluid events to be constrained or where inclusions are solely within detrital minerals no timing relationship can be discerned.

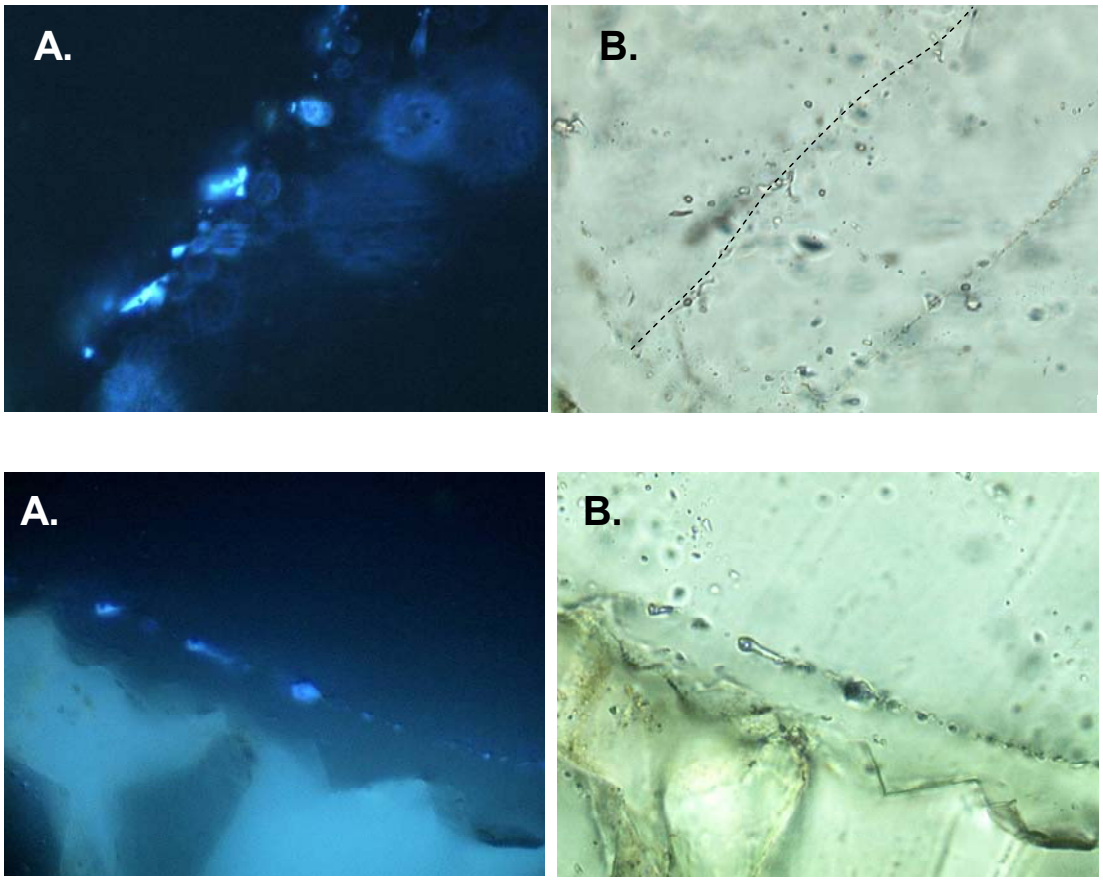

Figure 4-56: Photomicrographs showing fluid inclusions with different timing relationships

Generic examples of how the position of oil filled fluid inclusions relative to authigenic quartz overgrowths can be used to constrain the relative timing of fluid migration. In photomicrographs A and B the blue fluorescing oil inclusions are located on a healed fracture plain in detrital quartz that clearly terminates against the boundary of a subsequent quartz overgrowth and implies migration prior to the crystallisation of that quartz overgrowth. In photomicrographs C and D the blue fluorescing oil inclusions are located on the boundary between the detrital quartz and the diagenetic overgrowth indicating that the migration of oil and crystallisation quartz overgrowths was likely to be contemporaneous.

Linking oil migration with the formation of quartz overgrowths is important for several reasons. Quartz overgrowths are the last volumetrically significant diagenetic phase to form and aside from isolated occurrences of late carbonate cement and small amounts of illite and pyrite in a few samples the degradation of reservoir quality by diagenesis was largely complete by the time oil migration occurred.

Accurate reservoir quality prediction in undrilled traps, therefore, can be achieved by considering porosity-depth trends from both hydrocarbon-filled and water-wet wells as only minimal diagenesis has occurred in the period since oil charge began.

A second significant factor arising from the recognition that oil migration and quartz overgrowth crystallisation occurred contemporaneously is the opportunity to use fluid inclusion palaeo-temperatures measured on coeval aqueous inclusions within quartz overgrowths to further constrain the timing of oil migration. Unlike the petrographic observations that provide only a relative time constraint, information on the formation temperatures prevailing when the overgrowths crystallised can be integrated with basin modelling techniques to provide an absolute timing estimate. This integration is covered in Chapter 7.

4.9 COMPOSITION OF HYDROCARBON CHARGE

The data presented hitherto has not provided any detailed constraint on the composition of oil that migrated through these reservoir intervals. At the onset of this study, methods that address the composition of hydrocarbon fluids trapped within inclusions have largely been restricted to non-destructive qualitative techniques such as variations in observed fluorescence colour (Hagemann and Hollerbach, 1985; Tsui, 1990; Li and Mai, 1992).

The application of more sophisticated *in situ* techniques such as Raman spectrometry and Fourier Transform Infrared (FT-IR) spectroscopy (Barres et al., 1987; O'Grady et al., 1989) has been used to provide additional information on the bulk composition of entrapped fluids, but initially this technique required individual inclusions to be larger than is typically encountered in the diagenetic realm.

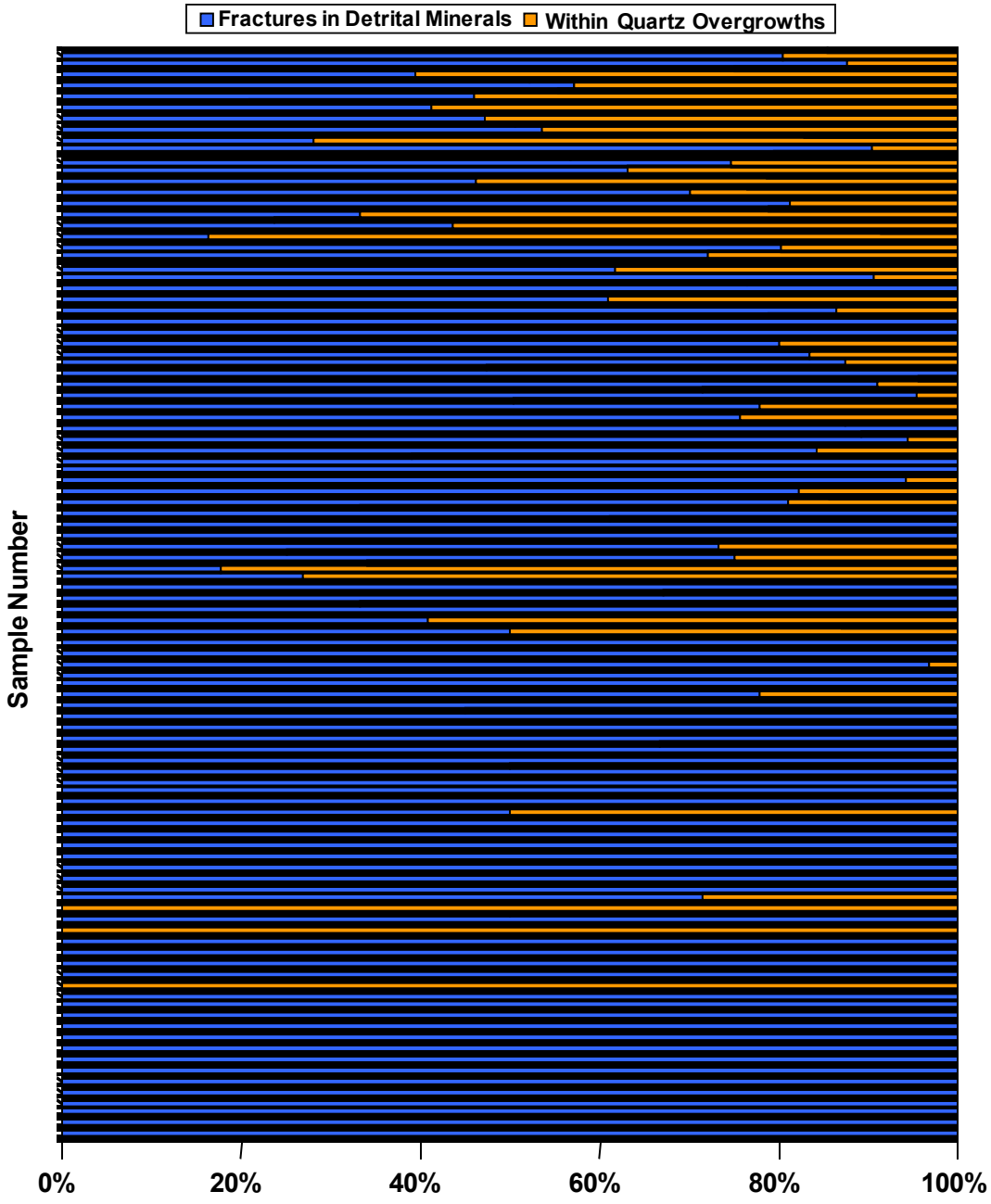

Figure 4-57: Location of oil inclusions.

Graph showing the location of oil inclusions for 194 samples (sample number axis) where GOI values were greater than zero and the location of inclusions was recorded. Some archived GOI analyses from earlier work did not have this type of information collected. Inclusion within quartz overgrowths refer to all inclusions at that location whether they are of a primary, secondary or pseudo-secondary nature. In most samples oil inclusions are predominantly within healed fractures that transect detrital quartz or feldspar grains (Fractures in detrital minerals). The graph favours oil inclusions within quartz overgrowths as the majority of these grains also contain some oil inclusions within the associated detrital grain.

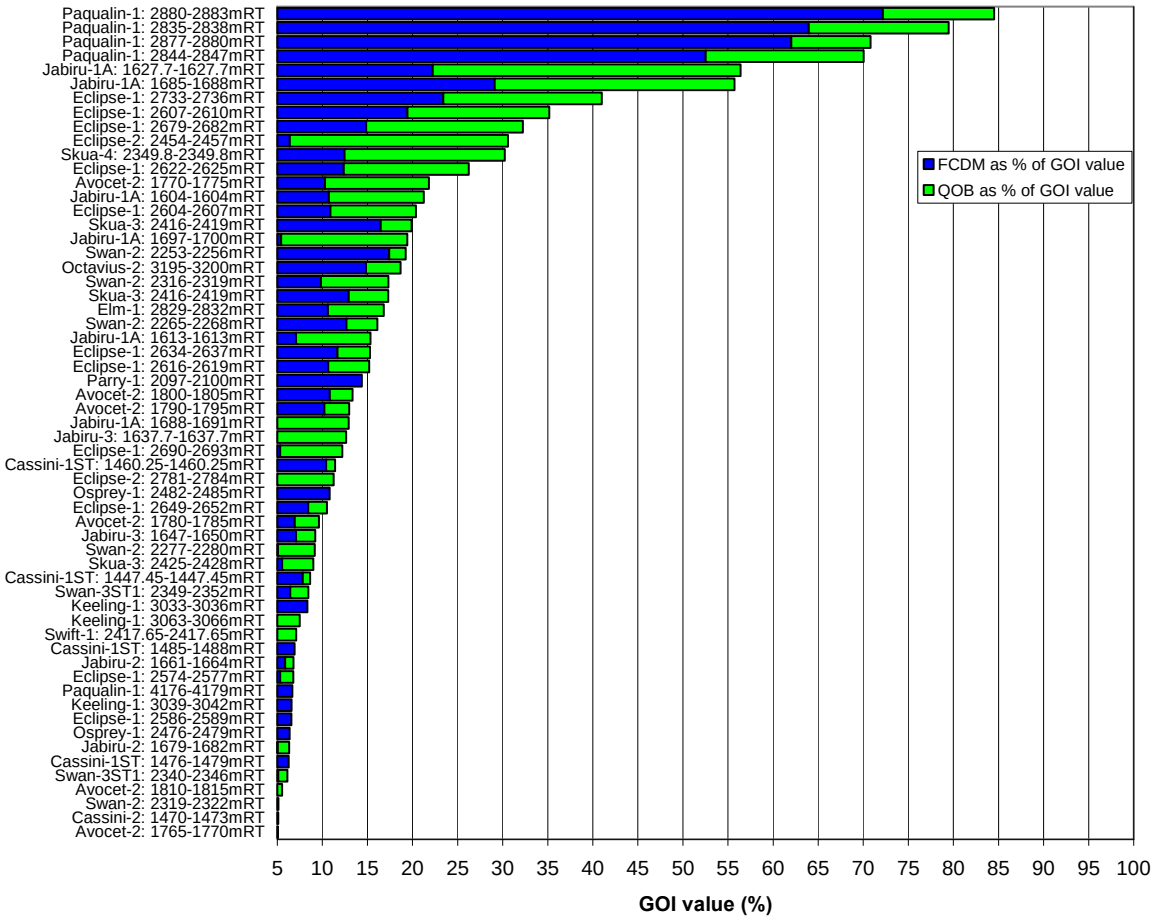

Figure 4-58: Oil inclusion location data for high (>5%) GOI samples

Same plot as shown in Figure 4-57, but excluding all samples with GOI values less than 5%. Samples with high GOI values (>5%) show a similar dominance of grains with inclusions on fractures cutting detrital minerals (FCDM) over grains with inclusions within the quartz overgrowths (QOB). As with Figure 4-57 the graph favours oil inclusions within quartz overgrowths as the majority of these grains also contain some oil inclusions within the associated detrital grain.

Pioneering efforts to extract the contents of hydrocarbon-bearing fluid inclusions for analysis by gas chromatography (GC) were increasingly being used to provide limited control on the composition of migrating hydrocarbons (Horsfield and McLimans, 1984; Burruss, 1981). Initially, these methods were severely limited by the sensitivity of the recording equipment and were only applicable where very large inclusions or a very high abundance of inclusions were present to allow sufficient volumes of oil to be recovered for analysis.

These limitations have largely been overcome by ongoing refinements of extraction procedures and by the substantial improvements in the sensitivity of the analytical instruments. It is now possible to routinely collect detailed molecular information on fluid inclusion oils using gas chromatography-mass spectrometry (GC-MS) equipment that enables source and maturity assessment of the fluid inclusion oil comparable to that routinely generated for produced oils (Karlsen et al., 1993; Lisk et al., 1996a; George et al., 1997).

When this study was conceived, the techniques needed to attain detailed compositional information on fluid inclusion oils were not sufficiently advanced to be considered for use in this project and information pertinent to the composition of oils contained within the inclusions was restricted to a qualitative assessment of visual observed fluorescence colours.

Throughout the duration of this study a number of related research projects, aimed at discerning the molecular composition of fluid inclusion oils, enabled a small number of fluid inclusion oils to be analysed from wells in the Vulcan Sub-basin and results from this work are also discussed.

4.9.1 Significance of Oil Inclusions Fluorescence Colour

Oil fluoresces under ultra-violet (UV) light due to excitation of the polycyclic aromatic compounds contained in the oil (Ryder, 2005). Illumination of rock samples with UV light is routinely used at the well site to identify rocks stained with oil (Ryder, 2005) and the same principal is used to identify oil filled fluid inclusions under the microscope (Figure 4–59; Blamey and Ryder, 2007).

The significance of variations in visually observed fluorescence colour of oils is contentious, particularly in regard to fluid inclusion oils. Published studies have produced correlations between fluorescence colour and oil composition, reflected in either API gravity or geochemically based maturity parameters.

Variations in fluorescence colours exhibited by oils can reflect changing API gravity as the maturity of the oil increases (Hagemann and Hollerbach, 1985) or where the oil gravity is reduced by alteration through biodegradation (Stasiuk and Snowdon, 1997) or presumably also by water-washing. Published studies related to fluorescence shown by fluid inclusion oils suggest that the yellow and orange fluorescence colours are indicative of oil derived from source rocks at the onset of oil generation while blue and white fluorescence can be attributed to oil derived from source rocks under peak oil generation conditions (Li and Mai, 1992; Tsui, 1990; McLimans, 1987).

Due to the subjective nature of direct colour observation some studies have used spectral methods to quantify the visually observed fluid inclusion fluorescence. Eadington and Kempton (2008) reported fluorescence colours of selected inclusions from the Jabiru-1A well in the VSB that were quantified by measuring fluorescence spectra and plotting these as CIE (1932) chromaticity diagrams (Figure 4–59). This approach confirmed that the visual distinction of blue and white fluorescing oil inclusions could not be purely assigned to difference in brightness (luminance) but did reflect different chromaticity values. This outcome could be significant for the interpretation of samples rich in white fluorescing versus blue fluorescing inclusions if end member samples could independently be shown to be geochemically different.

The use of spectroscopic methods to characterise the fluorescence spectra of fluid inclusion oils, mostly utilise different forms of Fluorescence Emission Micro-spectroscopy (Blamey and Ryder, 2007). In the VSB Liu et al. (2005) utilised the Total Scanning Fluorescence method of Brookes et al. (1983) to characterise the excitation-emission spectra of a selection of inclusion oils from wells, including some examined in this study. Liu et al. (2005) suggested that crude oils derived from the same geochemically defined family (defined in Edwards et al., 2004) could be identified on the basis of similar shaped excitation-emission spectra and the relative

level of fluorescence intensity (Figure 4–60). In turn this observation was extended to suggest that fluorescence spectra measured on fluid inclusion oils could be used as a correlation tool to relate fluid inclusion oils with crude oils using the same parameters (Figure 4–60).

Alternative approaches to the recording of spectral intensity have also been developed such as the Fluorescence Lifetime Microscopy (FLM) method. The FLM method characterises fluid inclusion oils by measuring the time a molecule remains in the excited state (the fluorescence lifetime) after absorbing a photon of light (Blamey and Ryder, 2007). On average heavier oils (low API gravity) have shorter average fluorescence lifetimes than lighter (high API gravity) oils (Ryder, 2004).

The assertion that fluorescence colour correlates with API gravity is relatively well demonstrated (Hagemann and Hollerbach, 1985; Stasiuk and Snowdon, 1997) compared to the claims that fluorescence colour variations can be attributed to differences in oil source or maturity. The advent of detailed molecular geochemical data for fluid inclusion oils has begun to allow these concepts to be more fully tested.

George et al. (2001c) reported examples from the Australian North West Shelf where maturity estimates based on geochemical biomarkers showed that fluid inclusion oils with blue fluorescence colours could have maturities anywhere in the oil window and consequently concluded that fluorescence colour was not a reliable indicator of oil maturity in fluid inclusions.

4.9.2 Fluorescence Colour Variations in VSB Fluid Inclusion Oils

Despite some controversy existing regarding the significance of fluorescence colour variations the collection of an extensive database of visually observed fluorescence colours in the current study warrants some review in order to determine if obvious patterns can be recognised. The fluorescence colours reported in this study were entirely visually observed (Figure 4–61) and no attempt was made to quantify these determinations using spectral analysis or utilising RGB or chromaticity data. However, they have been collected exclusively by the author so observed variations are not the result of variability between different operators.

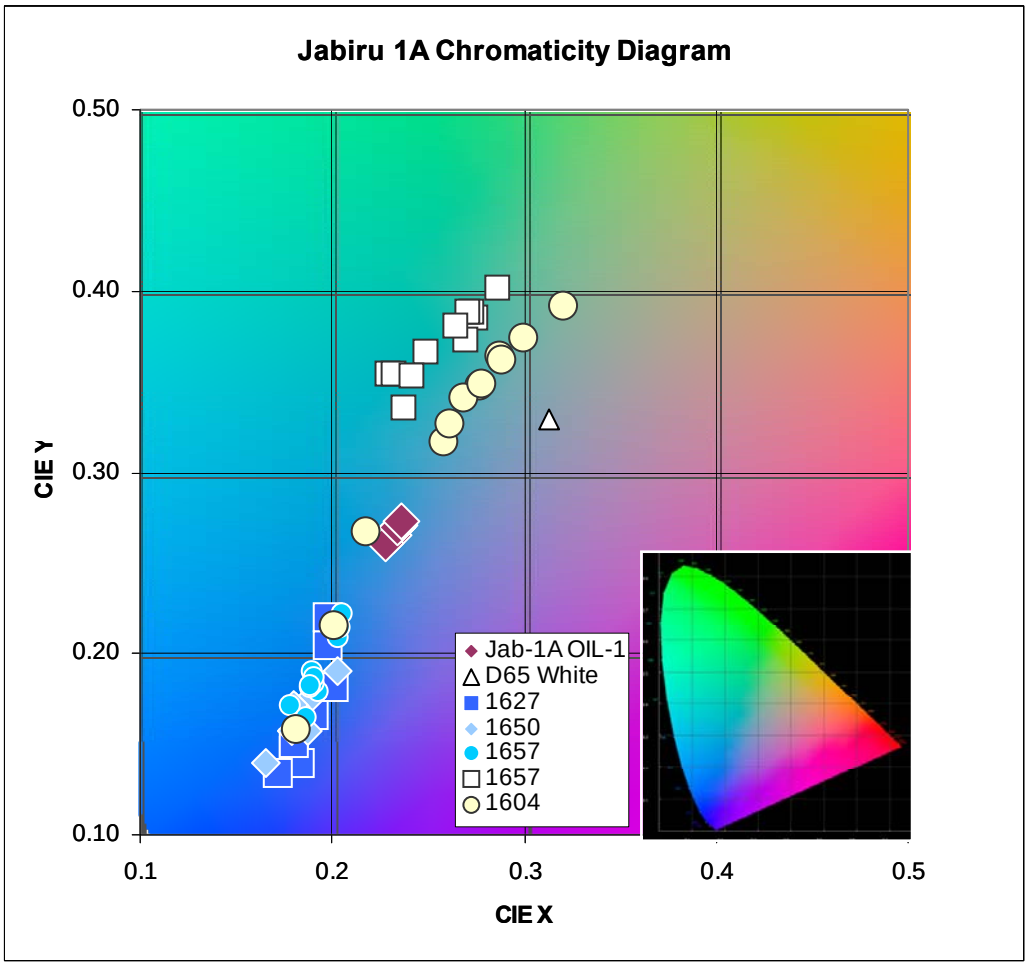

Figure 4-59: Chromaticity diagram showing fluorescence colour variation.

Fluorescence colours derived visually have been quantified by measuring fluorescence spectra plotted as CIE (1932) chromaticity diagrams. Results are shown for oil inclusions from a series of samples from Jabiru-1A (numbers shown represent the sample depth and the colour reflects the colour visually observed) and compared against crude oil (colour shown is not significant) recovered from the Jabiru-1A well (from Eadington and Kempton, 2008). CIE chromaticity plots allow the transformation of X, Y and Z tristimulus values (the relative proportion of each of the three primary colours that combine to form the observed colour) from 3D colour space into an X-Y two dimensional plot that allows all possible sets of tristimulus values to be represented (the full chromaticity range is shown in the inset diagram). The results suggest that the visually observed blue and white fluorescence colours do represent genuine colour differences that mostly plot at different XY positions on the chromaticity diagram. Increased brightness (luminance) probably accounts for the few visually observed white fluorescing inclusions that plot in the same space as the inclusions with the consistently visually observed blue fluorescing inclusions. White fluorescing inclusions plot within the overlap zone where proportions of the primary colours are broadly similar.

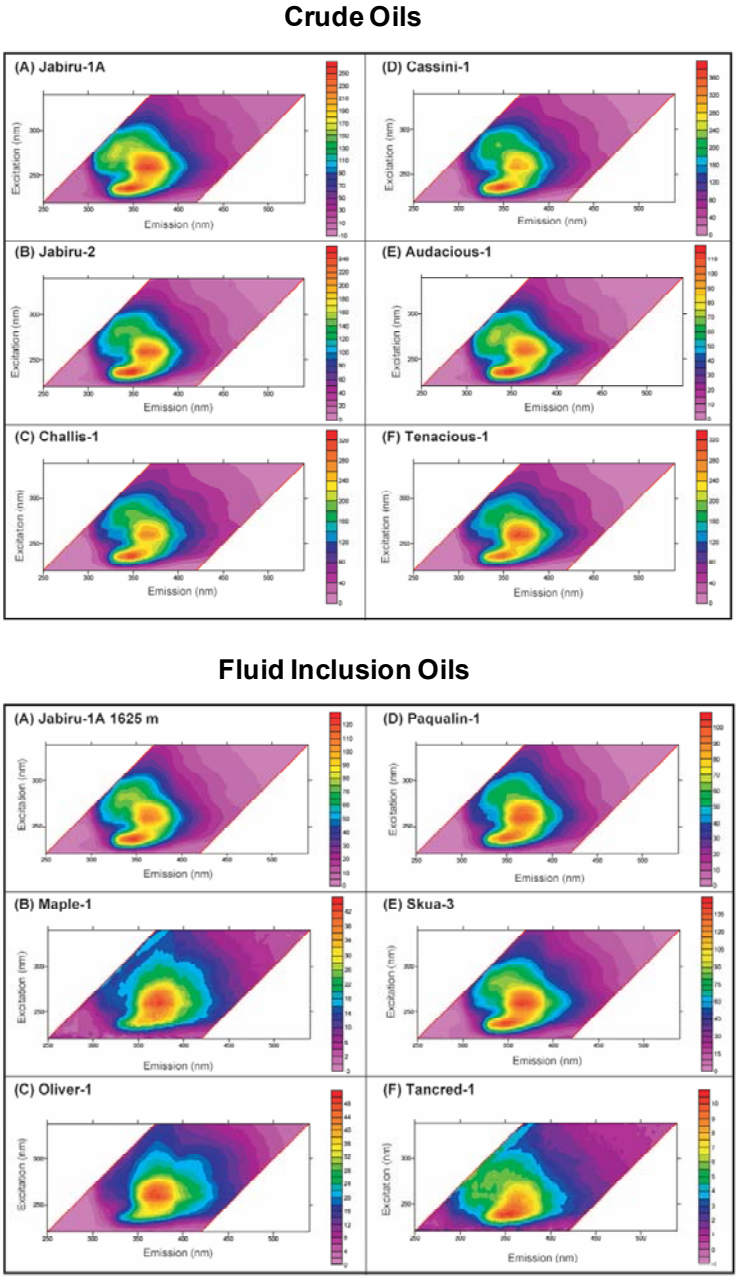

Figure 4-60: TSF plots showing variation in VSB inclusion oils.

Total Scanning Fluorescence (TSF, Brooks et al., 1983) excitation-emission contour plots are shown for crude oils from the Group A oils of Edwards et al., 2004 and a series of inclusion oils from the VSB. The plots record the maximum intensity of emission (recorded in photometer counts and displayed as the colour bar) along with the emission wavelength and the excitation wavelength that caused the emission (see Liu et al., 2005b for details). The crude oils show similar responses characterised by distinct dual peaks that cluster in a similar emission-excitation position. The fluid inclusion oils show general similarity in emission-excitation position and intensity, albeit with less well defined dual peaks. This similarity is interpreted to be consistent with derivation from the same oil family (From Liu et al., 2005b).

The most common fluorescence colour displayed by oil inclusions in samples from the VSB examined in this study is blue, but there is considerable scatter in the data (Figure 4–62) making it difficult to draw any meaningful conclusions.

The proportion of inclusions exhibiting blue fluorescence is also variable when compared across samples with different GOI values, but blue colours are generally dominant, particularly where the GOI values exceed 20% (Figure 4–63). The observed fluorescence colours are more variable in samples where GOI values fall below 20% with orange fluorescing oil inclusions becoming proportionally more abundant in samples with GOI values less than 1% (Figure 4–63).

The observed variation in fluorescence colour against the GOI value is not entirely inconsistent with a maturity influence neither does it provide strong direct support for this proposition. The proportion of inclusions with blue fluorescence broadly increases as the GOI values get higher and this could reflect a maturity control with higher maturity levels needed in order to generate the larger volumes of oil needed to allow a significant accumulations to form.

Indeed nearly all oils recovered from the Vulcan Sub-basin have relatively high maturity with equivalent vitrinite reflectance values of between 0.75 and 1.0% (Edwards et al., 2004), so the predominance of blue fluorescing oil inclusions in high GOI samples could be indicative of a maturity control. In contrast, the higher proportion of yellow-orange fluorescing oil inclusions recorded in samples with low GOI values, particularly where GOI values are less than 1%, could reflect the trapping of low maturity oil that represent early migrated oils or could reflect the in situ generation of low maturity oil where thermal maturity levels are high enough to support local generation.

Overall the significance of the variations in oil inclusion fluorescence colours observed for VSB samples remains to be demonstrated. The utilisation of more sophisticated spectral analysis techniques that enable the colour assignments made on individual fluid inclusions to be quantified is a clearly desirable objective to produce more informative results and to avoid issues of variability related to the comparison of visually assigned fluorescence colours by different microscopists.

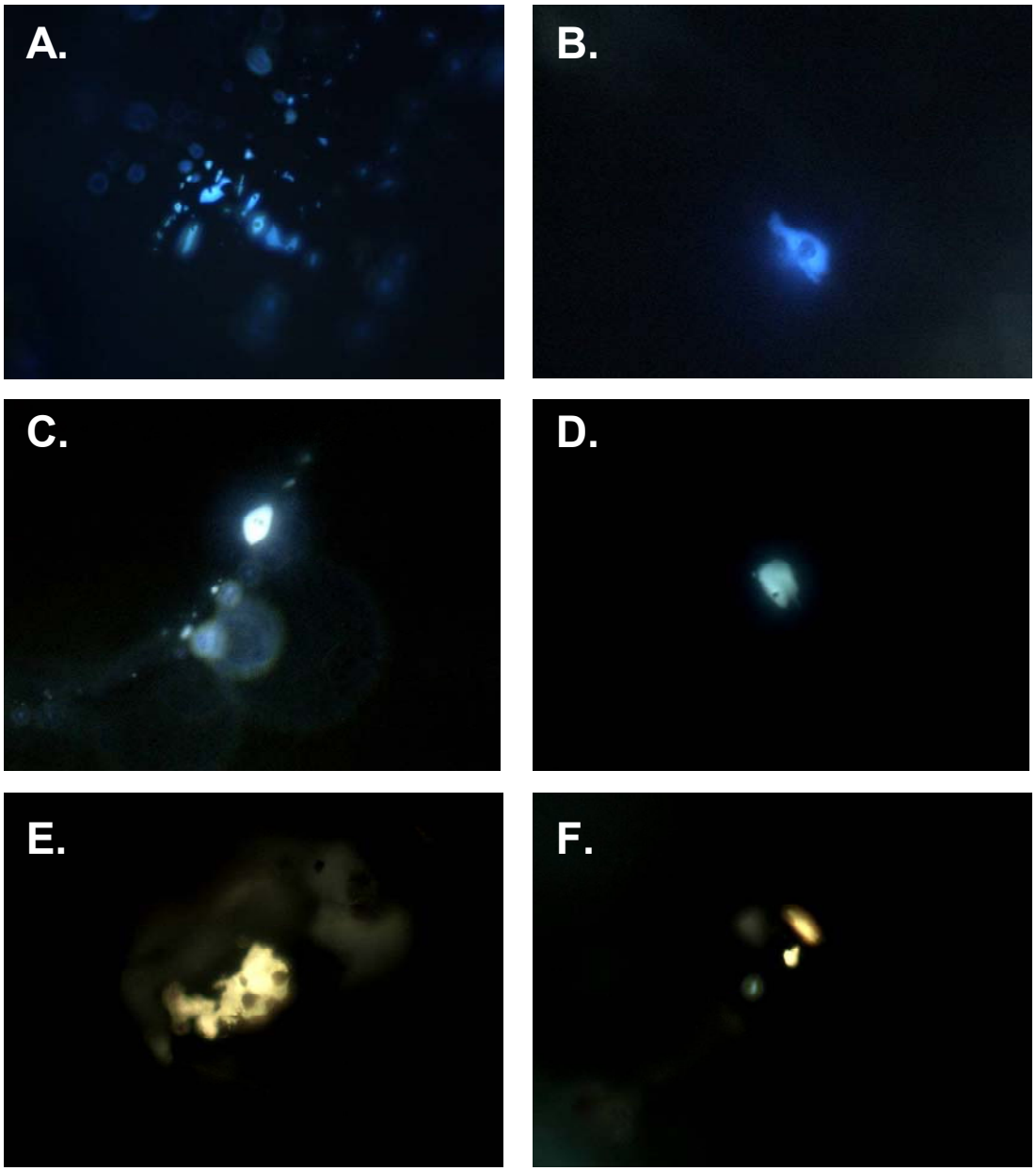

Figure 4-61: Typical fluorescence colours of fluid inclusions in samples from the VSB.

Range of typically observed fluorescence colours ranging from blue through white to orange-yellow.

The dataset produced by the current study, whilst not revealing strong conclusions regarding the significance of fluorescence colour nonetheless remains as a consistent and open file data set that could be re-examined when future studies are undertaken.

4.9.3 Molecular Composition of Fluid Inclusion Oils

Characterisation of fluid inclusion oils by geochemical methods has improved markedly in recent years (Karlsen et al., 1993; George et al., 1997, 1998). Routine collection of geochemical data comparable to that obtained for crude oils, including aliphatic and aromatic biomarker data, can now be obtained for most fluid inclusion oils (George et al., 2007). Only the isotopic composition of FIOs remains to be determined on a routine basis, although this can be obtained in ideal circumstances (George et al., 1997).

Defining the geochemical composition of FIOs allows a more refined understanding of both the charge history of individual traps and the relationships between different oil families that collectively contribute an improved understanding of the operating petroleum systems.

Understanding the chemistry of FIOs provides the opportunity to evaluate palaeo-fluids that can represent examples of end member compositions from which the current reservoir fluids represent a complex mixture with a composition that can be more difficult to unravel.

Throughout this study geochemical analyses have been completed independently on several fluid inclusion oils from the VSB (Figure 4–64), including samples from the Skua, Jabiru (George et al., 1997) and Oliver oil and gas fields, a palaeo-oil column at the currently water-wet Octavious-2 well (George et al., 1998) and more recently from oil migration pathways inferred from low GOI values in the Delamere gas column and the Champagny-1 dry hole (George et al., 2004b).

The additional constraint that these geochemical results provide on the charge history of the VSB is significant and relevant to the current study so a detailed review of the FIO data was warranted.

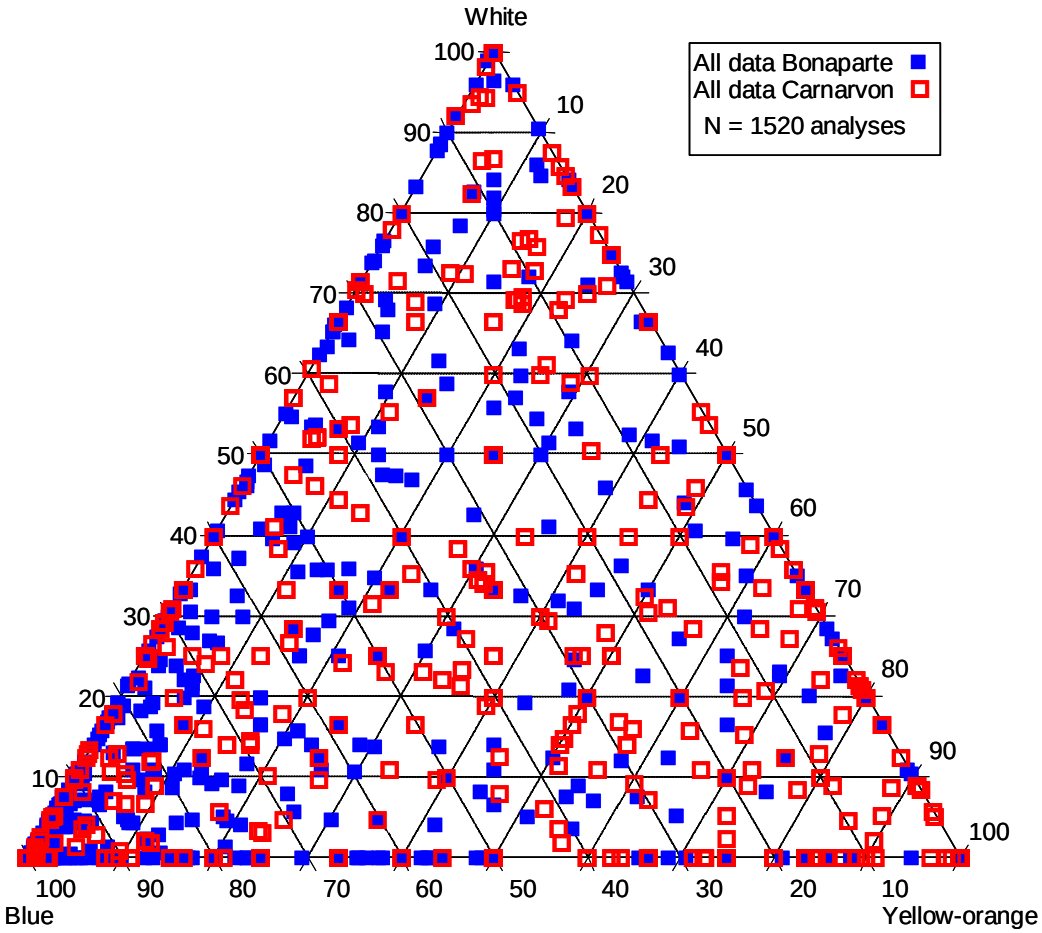

Figure 4-62: Variation in fluorescence colours for samples in the current study

This ternary plot denoting the abundance of the three primary end members colours (as used in this study) includes all GOI data acquired from the Bonaparte and Carnarvon basins by the year 2000 from a total of 1520 GOI analyses. The distributions show no overwhelming dominance of any one colour in either region except for a slight skew towards the blue end member.

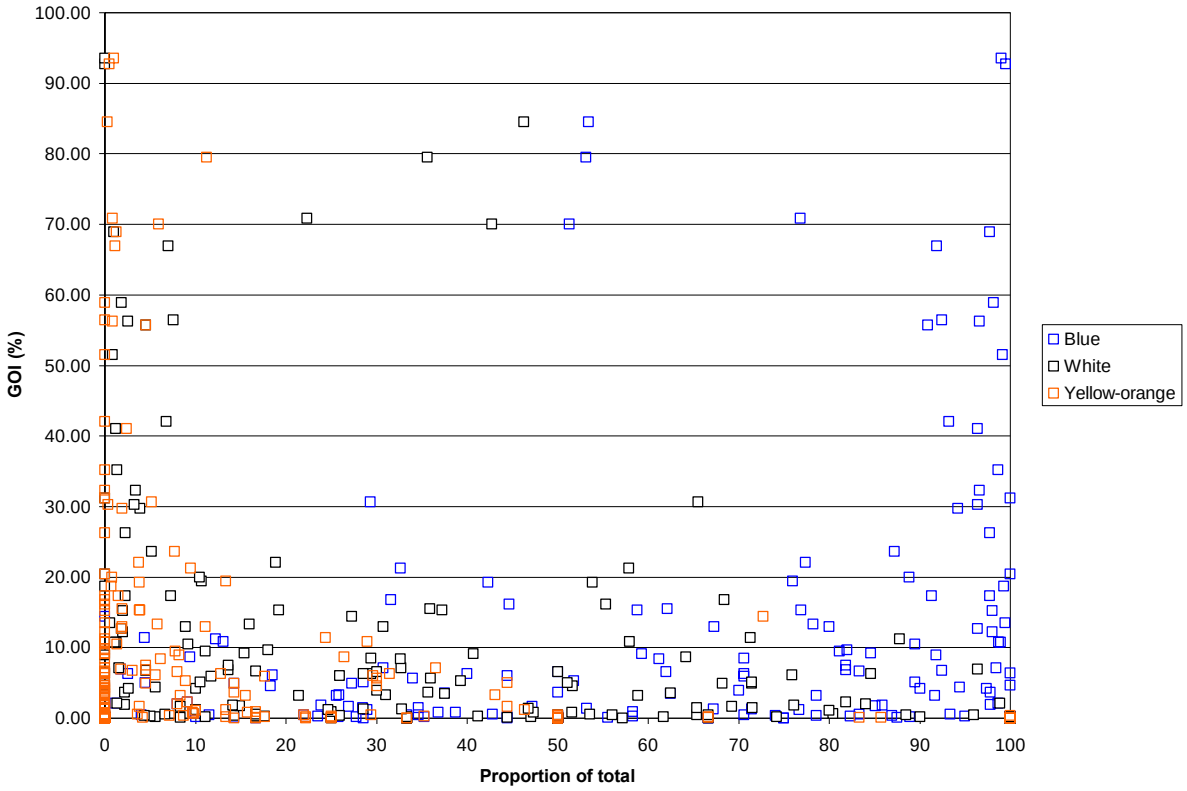

Figure 4-63: Fluorescence colour variations relative to GOI value of sample

This cross plot show the proportion of inclusions displaying each end member colour (blue, white, yellow-orange) against the total GOI number recorded for each of these samples. Overall the blue and white fluorescing inclusions are the more dominant population. At the lower end of the GOI range (0-20%) the three colours are more evenly distributed but blue fluorescing oil inclusions are clearly more dominant in the higher end (30-100%) range of the GOI values.

Extraction and analysis of the FIOs in all cases was undertaken using a procedure described fully in George et al (1998), with careful monitoring of system blanks to ensure cross contamination is eliminated or minimised. Recognition of any significant contamination also allowed any erroneous data to be selectively removed.

Overall the geochemical composition of the FIOs analysed from samples taken across the VSB generally reveal a close genetic similarity between the FIOs and produced oils in terms of both maturity levels and source affinity.

4.9.3.1 Source characteristics of VSB fluid inclusion oils

All of the VSB fluid inclusion oils (FIOs) are derived from marine source rocks varying principally in the relative amount of terrestrial organic matter. The majority of the FIOs show derivation from source rocks with a significant contribution from terrestrial organic matter, typically expressed by a slight odd predominance in the *n*-alkane profile and Carbon Preference Index (CPI) values consistently greater than one (i.e. George et al., 1997, 1998).

Increased abundances of retene and 1,7-dimethylphenanthrene noted in some FIOs (e.g. George et al., 1998) indicate source rocks with Araucariacean (coniferous) higher plant organic matter (Noble et al., 1985; Alexander et al., 1988).

The source rocks that generated the FIOs are interpreted to have been clay-rich and deposited in an oxic to sub-oxic environment (e.g. George et al., 1997, 1998). The relatively low abundance of high molecular weight *n*-alkanes makes them non-waxy in nature, whilst the low content of sulphur-containing hydrocarbons in most of the samples indicates derivation from a low-sulphur source rock. Biomarker characteristics such as low homohopanes, low Pr/Ph ratios, the abundance of diahopanes and diasteranes relative to hopanes and steranes and the sterane carbon number distributions all correlate well with recognised Jurassic source rocks in the Timor Sea region (George et al., 1998).

Previously two discrete oil families (Group A and B) have been identified from analysis of oils recovered from the VSB (Figure 4–65) using biomarker and isotope

data (Edwards et al., 2004; Dawson et al., 2007). Group A oils are considered to be sourced from Upper Jurassic marine mudstones of the lower Vulcan Formation, and Group B oils from fluvio-deltaic mudstones and coals, most probably from within the Lower to Middle Jurassic Plover Formation (Edwards et al., 2004).

Edwards et al. (2004) used selected biomarker ratios from Late Jurassic–Early Cretaceous sediment extracts in Vulcan-1B, together with higher-plant-specific aromatic ratios for Late Jurassic sediment extracts from Paqualin-1, to establish oil-source rock correlations for VSB crude oils (Figure 4–66). Tricyclic terpane and sterane data show that Group A oils correlate well with the lower Vulcan Formation extracts (Figure 4–66) whilst the Group B oils define a separate field that lacks correlation with these Upper Jurassic source rocks (Edwards et al., 2004).

Plotting the available data for the FIOs from the VSB broadly shows that the FIOs correlate more closely with the oils of Group A and are unlike the Group B oils. However, whilst broadly similar the FIOs are not close matches for either the Group A oils or putative source rocks and a number of the FIOs have low values that imply derivation from a more marine influenced source rock facies (Figure 4–66).

Use of the Higher Plant Index (HPI, van Aarssen et al., 1996) shows how the higher relative abundance of retene with respect to cadalene and iP-iHMN (66:29:5) shown by the Group A oils fit well with sediment extracts from Paqualin-1 (Figure 4–67) that age correlate with the *W. clathrata* dinoflagellate zone (Lower Vulcan Formation; Edwards et al., 2004). The FIOs, however, have Retene and Cadalene levels that imply derivation from older sections of the Lower Vulcan Formation with most plotting in the *W. spectabilis* biozone (Figure 4–67).

The implications of these two plots are that whilst the FIOs are more similar with the Group A than Group B oils there are consistent differences that would imply derivation from slightly different source rocks than the current day oils. It is unlikely that these differences represent fundamentally different source rocks but rather they reflect more subtle facies variations within the Lower Vulcan Formation Upper Jurassic source rock.

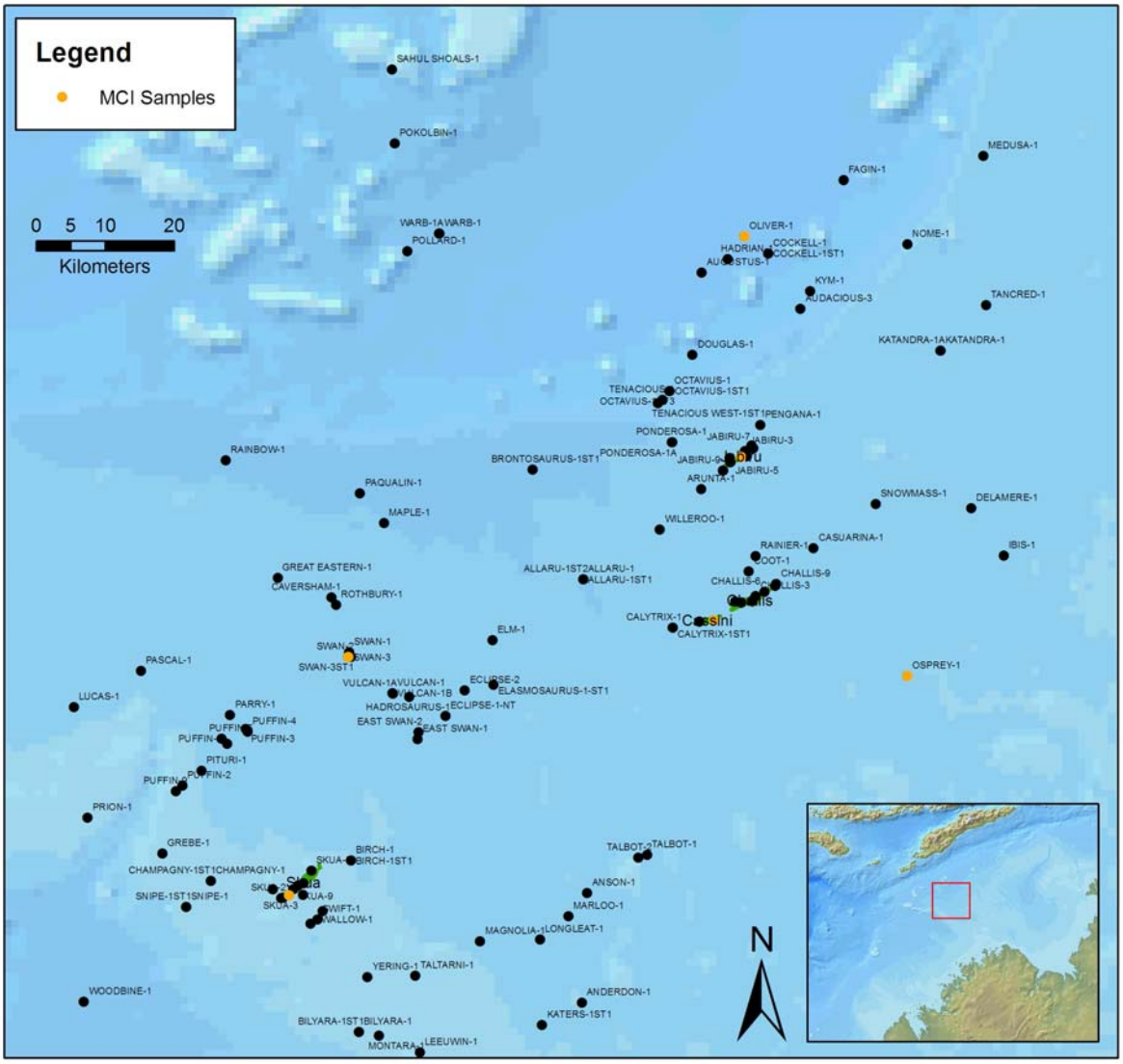

Figure 4-64: Location of wells with fluid inclusion geochemical (MCI) data

The highlighted wells contain at least one sample where the FIO composition has been analysed using the MCI technique. The Jabiru-1 (current oil zone), Octavius-2 (palaeo-oil zone) results were published in George et al., 1997, 1998 respectively, whilst results from Delamere-1 and Champagny-1 dealing with the characterisation of oil migration pathways are covered in George et al., 2004b. The remainder of samples have not been published and come from internal CSIRO research programs, the results from which reside in the public domain having been released to the relevant regulatory authority (State, Territory or Federal).

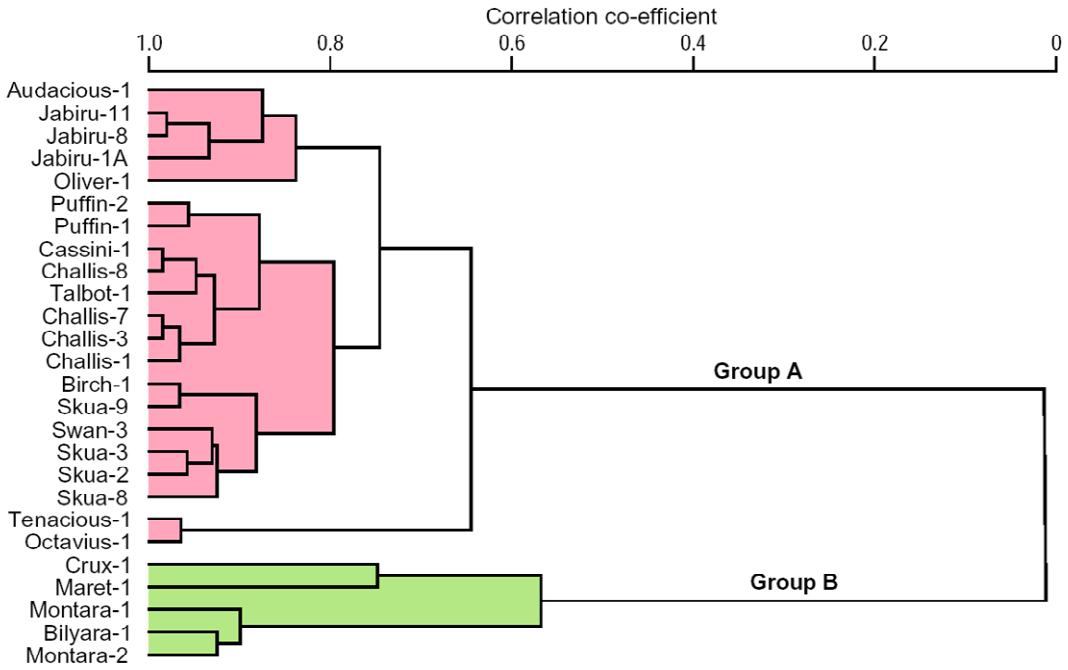

Figure 4-65: Dendrogram for the oils and condensates of the VSB.

Hierarchical Cluster Analysis (HCA) for a series of oils from the VSB has been used to evaluate the genetic associations of the different oil and condensate fractions, with the width of the bars indicating the degree of compositional similarity. Using this approach two discrete oil families have been identified from oil-oil correlations based on a combination of 16 molecular and isotopic parameters that were measured according to a reproducible protocol (from Edwards et al., 2004).

The exact reason for the observed differences remains speculative but it appears possible that these could represent the evolution of the generation process through time. Previous workers report a tendency for FIOs to exhibit compositions less mature and skewed towards the products of early oil generation where more labile organic matter makes a greater contribution to the early products that are generated and expelled (i.e. George et al., 1997).

With increasing thermal maturity more of the dispersed organic matter within these clay rich source rocks becomes generative as higher activation energies needed to promote the required chemical reactions are attained, causing the overall bulk composition of the generated hydrocarbons to be slightly modified.

The similarity between the majority the FIOs analysed by CSIRO from the VSB and the Group A crude oils identified by Edwards et al. (2004) is not unexpected given that they generally come from traps suitably located to receive hydrocarbons derived from source rocks thought responsible for the Group A family and in some cases migration from these depocentres can be demonstrated by the outcomes of regional three dimensional basin models (i.e. Fujii et al., 2004; Fujii, 2007).

The paucity of FIO analyses from traps containing Group B oil precludes the characterisation of this family, with only the Delamere-1 FIO being tentatively assigned to the Group B family (George et al., 2004b). There are, however, a number of FIOs that show only limited correlation with either recognised oil family and the FIOs in this category often coincide with outliers that are recognised from the composition of the equivalent produced oils (described below).

The Oliver-1 FIO and crude oils for example differ at first inspection from the majority of VSB oils by having an *n*-alkane distribution skewed towards the high molecular weight (maxima = n-C_{23}), indicating a more waxy composition (Figure 4–68). Initially, this observation together with the more enriched bulk isotope composition led to the Oliver-1 crude oil being assigned to the Group B family on the basis of being derived from source rocks with significant amounts of terrestrial organic matter (Edwards et al., 2004).

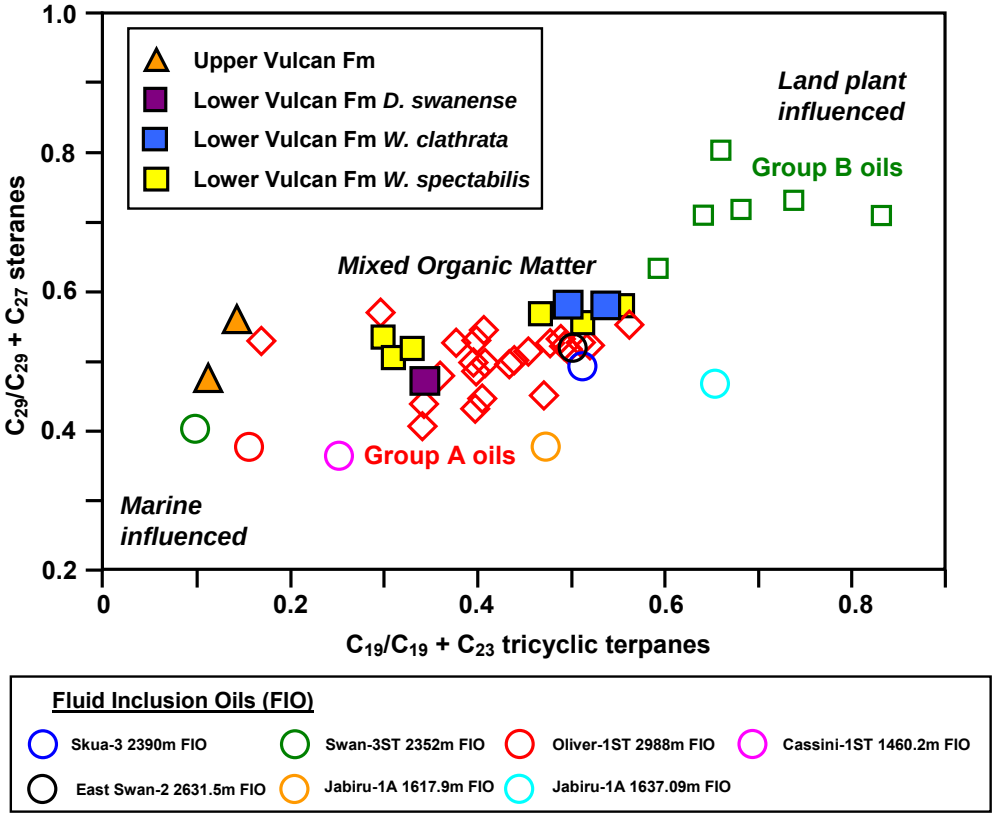

Figure 4-66: Source correlation plot from Edwards et al. (2004).

The plot has been modified to include data from available VSB fluid inclusion oils. $C_{19}/C_{19}+C_{23}$ tricyclic terpanes versus $C_{29}/C_{27}+C_{29}$ steranes are plotted to show source differences between the Upper and Lower Vulcan formations from Vulcan-1B and the similarity of representative oils from the Vulcan Sub-basin (modified from Edwards et al., 2004). Group A crude oils (red diamonds) closely correlate with Lower Vulcan Formation source rocks (filled squares) whilst Group B crude oils (open green squares) show no similarity with any of the analysed source rocks. Results obtained for the FIOs are plotted for comparison. The FIOs (open circles) correlate more closely with the Group A oils but include a number of oils that have low values and would appear to show derivation from a more marine influenced source rock. The Oliver-1 and Swan-3ST samples resemble the source rock extracts from the Upper Vulcan Formation.

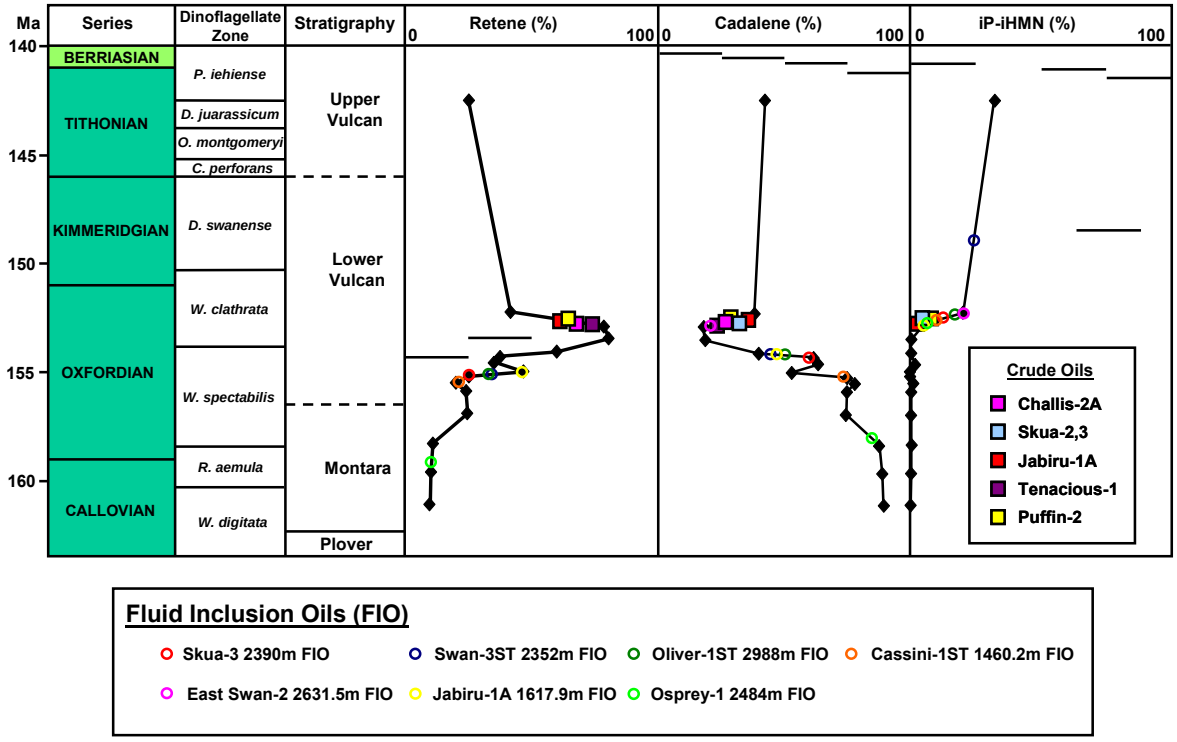

Figure 4-67: Higher plant fingerprint (HPF) of Vulcan Sub-basin crude oils and FIOs.

This plot, modified from Edwards at al. (2004), shows correlation of Vulcan Sub-basin crude oils (filled squares) and FIOs (open circles) against source rock extracts (black diamonds) from Paqualin-1, using AGSO Timescale and sequences defined in Kennard et al. (1999b). The HPF reflects the changing proportion of the land-plant contribution to the Middle-Late Jurassic marine sediments on the North West Shelf (van Aarssen et al., 1999) based on the relative abundance of the aromatic higher-plant-derived compounds retene, cadalene and 6-isopropyl-1-isohexyl-2-methylnaphthalene (iP-iHMN) in sediment extracts. The FIOs from the VSB typically indicate derivation from slightly older sections of the Lower Vulcan Formations within the *W. spectabilis* biozone on the basis of percentage of retene and cadalene, but are more consistent with iP-iHMN values expected for the younger *W. clathrata* biozone.

Subsequently, on the basis of the biomarker geochemistry, which indicates a greater overall affinity with the Group A oils (Edwards et al., 2004) the Oliver-1 oil was reassigned to the Group A oils. Compound Specific Isotope Analyses (CSIA) on oil and gas fractions provides a likely explanation for this confusion. These data show the gas fraction to be significantly more enriched in ^{13}C than the oil, implying that the oil and gas are not genetically associated (Edwards et al., 2004).

Collectively these geochemical observations led to the Oliver-1 crude oil being interpreted as most likely to be a Group A oil that had mixed with gas derived from more terrigenous source rocks, probably a Group B gas derived from the Plover Formation (Edwards et al., 2004).

Despite the Oliver-1 FIO showing similarity with the bulk composition of Oliver-1 crude oil other important differences also point to the FIO being derived from a marine source rock deposited under sub-oxic conditions with only limited input of higher plant organic matter. These include a low Pr/Ph ratio (1.4), the presence of a significant amount of 29,30-bisnorhopane, the high C_{29}/C_{30} hopane ratio and the low relative abundance of higher plant-derived biomarkers shown by the HPI values.

The Oliver-1 FIO could be interpreted as a true marine end-member of a continuum of oil compositions that spans the recognised oil families and perhaps oils within Group A are actually a mixture of a more marine oil corresponding to Upper Jurassic source rocks that has mixed with oils derived from the more strongly terrestrially influenced Middle Jurassic (Plover Formation) section?

Alternatively if the Oliver-1 FIO is considered to be distinct from the Group A oils then in it could be a genuine vagrant oil that would imply contribution from a third oil family. A contribution from a previously unrecognised oil source rock is not necessarily unexpected given that the Oliver trap is well positioned to receive local sourcing from the hitherto poorly calibrated Cartier Trough source kitchen. Edwards et al., (2004) speculated that the relatively isotopically enriched nature of oils from Octavius-1 and the Tenacious Oilfield could reflect sourcing from more marine source rocks in the adjacent Cartier Trough where facies variations could distinguish these oils from those produced by kitchens within the Swan and Paqualin grabens.

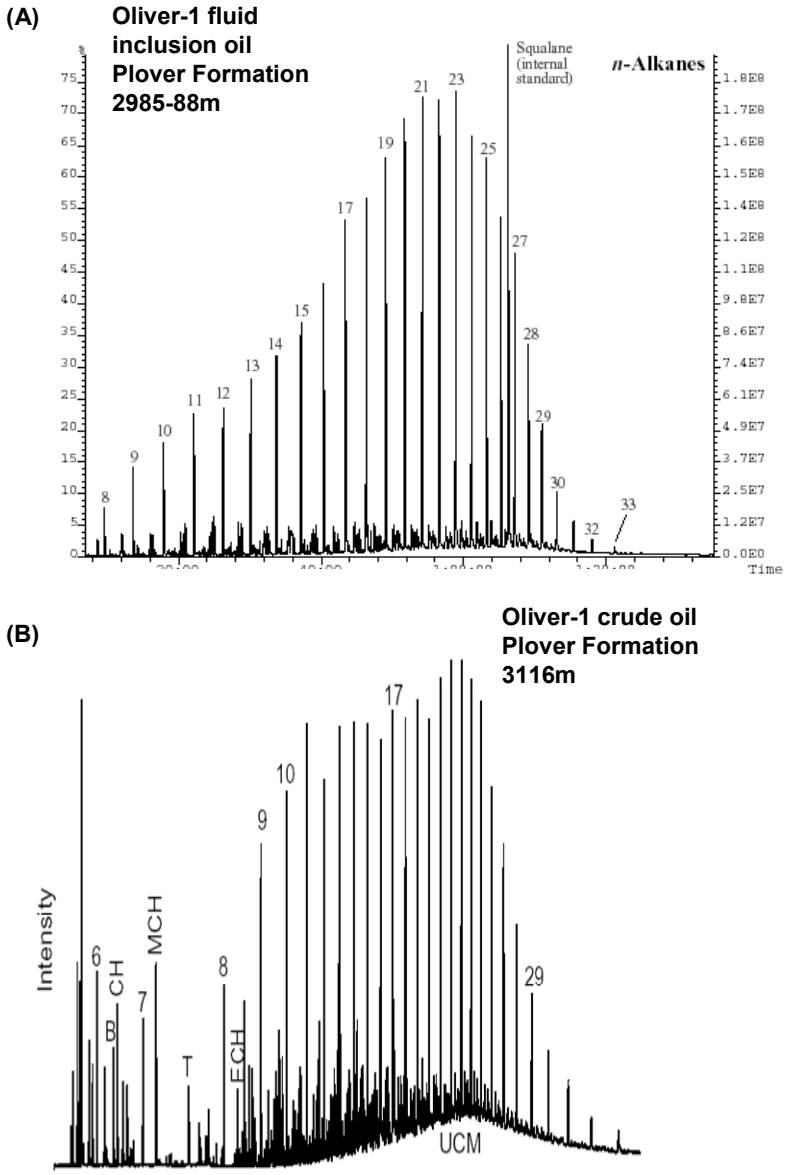

Figure 4-68: Comparison of whole oil gas chromatograms for the Oliver-1 FIO and crude oil.

The *n*-alkane distribution is skewed towards the high molecular weight (maxima = n-C_{23}), indicating a more waxy composition for both the palaeo-oil (FIO at 2985m) and the current crude oil. The Oliver crude oil chromatogram shows a small unresolved complex mixture (UCM) hump, considered indicative of biodegradation (Connan, 1984), but the retention of low molecular-weight hydrocarbons together with the absence of biomarkers diagnostic of biodegradation (e.g. 25-norhopanes) suggests biodegradation in this instance was only minimal.

A sub-group of the established Group A family was favoured over a discrete new oil family in this instance, but a new oil family remains possible. Potential present day analogues of the more marine influenced Oliver-1 FIO are identified by Edwards et al. (2004) with condensate from the Swan-3 showing the greatest marine influence (Figure 4–69) and showing possible correlation with Cretaceous shales of the Upper Vulcan Formation (Figure 4–66).

Paradoxically the FIO from the Swan-3ST1 well closely resembles the typical Group A oil family and is interpreted to be derived from a marine source rock containing a significant amount of terrestrial organic matter. Edwards et al. (2004) recognise that the Swan-1 and -3 condensates could have a similar source as the Group A family oils if they were generated at lower maturities and also entertain the possibility that the condensate has entrained hydrocarbons from Late Jurassic–Early Cretaceous marine sediments during its migration from the lower Vulcan Formation to the Puffin Formation reservoir.

Despite the opportunity to explain away the Swan-3 condensate composition as purely a maturity effect or one reflecting migration pick-up, other FIOs from the VSB also show evidence of derivation from a marine source rock that has received only limited input of terrestrial organic matter. The Osprey-1 FIO resembles the Oliver-1 FIO, being waxier with a relatively higher abundance of high molecular weight *n*-alkanes and a slight odd predominance in the *n*-alkane profile (Figure 4–70). Derivation of these FIOs from a marine source rock with limited terrestrial organic matter is implied.

Biomarker characteristics such as the high C_{29}/C_{30} hopane ratio, low Pr/Ph ratio (1.7), and the low diahopane content are similar to the Oliver-1 oil and serve to distinguish this FIO from the typical Group A oils from the Timor Sea. The low abundance of retene and 1,7-dimethylphenanthrene indicate only a limited contribution from Araucariacean higher plant organic matter (van Aarssen et al., 1999), further supporting a more marine influenced source rock facies being responsible for this FIO.

The Osprey-1 FIO also contains elevated levels of cadalene, 1,2,7-trimethylnaphthalene and a peak that is tentatively identified as being oleanane. These characteristics are typical of organic matter derived from Angiosperms (flowering plants) and collectively suggest a Cretaceous-or younger age constraint (Moldowan et al., 1994) for the source rock that generated the Osprey-1 FIO.

This result is surprising as unlike the majority of FIOs that are hosted in Jurassic reservoirs this Osprey sample comes from a Permian reservoir with what appears to be only limited access to potential Cretaceous source rocks.

Further evidence for a contribution from a Cretaceous source rock can be seen in the FIO from the palaeo-oil zone interpreted within the current water-leg of the Jabiru-1A well, which despite sharing biomarker characteristics that would be consistent with Jurassic source rocks from the VSB also contains a moderately high 29,30- and 28,30-bisnorhopane content (28,30-BNH/C30αβ hopane = 0.11), a tentatively-identified significant contribution of oleanane, low C_{24} tetracyclic terpane relative to tricyclic terpanes and high C_{23} tricyclic terpane contents. The Jabiru-1A water-leg FIO also has a moderate content of sulphur-containing hydrocarbons (P/DBT = 5), so may have been derived from a sulphur-rich source rock.

These anomalous results are not shared by the two FIOs from Jabiru-1A that lie above the current Jabiru Field OWC or by the produced oils from the field. Taken alone the results might be interpreted as possible contamination of the FIO but the similarities with some (but importantly not all) other FIO oils strengthens the conclusion that a non-Jurassic source rock is contributing hydrocarbons to the charge system operating in the VSB.

One highly important development in the analysis of FIOs is the recent attainment of high quality geochemical data from relatively inclusion poor (low GOI) samples that represent sampling of migration pathways rather than palaeo-oil accumulations (George et al., 2004b). Whereas most previously analysed fluid inclusion oils come from inclusion rich samples where extracted yields of fluid inclusion oil are greater than 100 ng *n*-alkanes per g of quartz crushed the samples in this new study produced only 8-16 ng *n*-alkanes per g of quartz crushed (George et al., 2004b).

Despite the much lower yield obtained from these samples the analysis of these FIOs show that the Delamere FIO correlates well with oils derived from the Late Jurassic Lower Vulcan Formation, whilst the results from the Champany-1 well show a much lower contribution from terrigenous organic matter that makes it unlike the major oil families (George et al., 2004b). The prospect of being able to obtain reliable geochemical data in samples where few inclusions get trapped highlights the potential to be able to geochemically map migration pathways across prospects or basins using information derived from fluid inclusion data.

Collectively the source data from the FIOs analysed in the VSB mostly correlate with oils assigned to the Group A oil family that are thought to be sourced from clay rich, terrestrially dominated marine source rocks of the Upper Jurassic Lower Vulcan Formation (Edwards et al., 2004) and indicate that the palaeo-oil zones in these wells most likely represent remnants of once larger oil columns rather than being products of other geochemically distinct source rocks.

The lack of FIO samples from traps that are currently filled with oils from the Group B family of Edwards et al. (2004) precludes any comment on how this family is represented within the palaeo-oils but a number of outliers in the FIOs exist that have characteristics that support derivation from non-Jurassic source rocks. Angiosperm-derived organic matter reflecting a Cretaceous or younger source rock is implied from the presence of Oleanane but this could reflect pick up from juxtaposed Cretaceous top and lateral seals. Notwithstanding this possibility this group of FIOs shows little correlation with either recognised oil family and could represent a third oil family. This is either not present in the current hydrocarbon fill or may be a true end-member composition with Group A oils being mixtures of terrestrially dominated Group B oils and this new oil family recognised in some FIOs.

4.9.3.2 Thermal maturity

Maturity assessment of the FIOs considers parameters derived from both the aliphatic and aromatic hydrocarbon fractions using interpretation procedures that are routinely applied to crude oil assessments (Peters and Moldowan, 1993) and can be used to determine the maturity of FIOs (e.g. George et al., 1997; 1998).

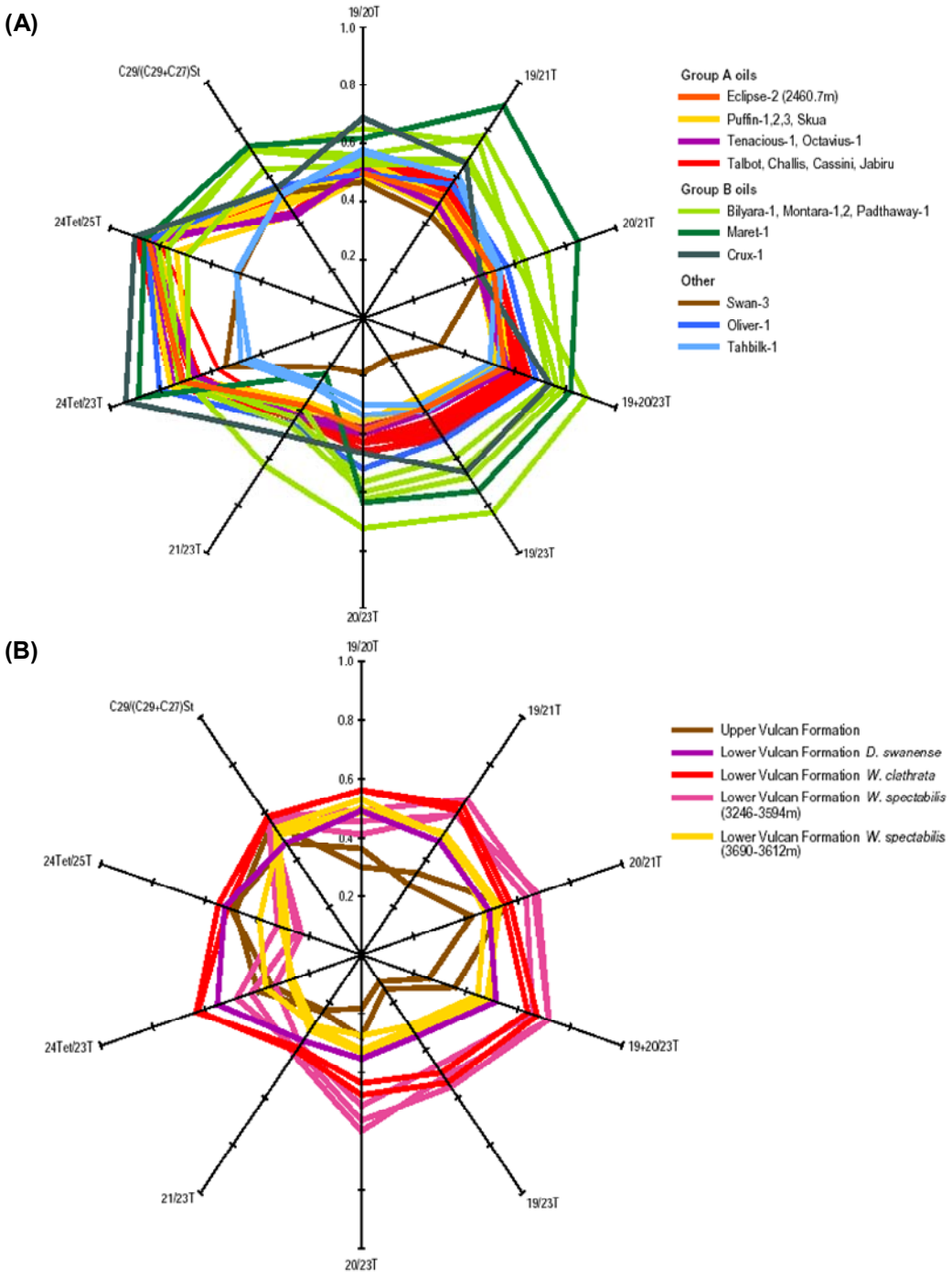

Figure 4-69: Spider diagram for a selection of VSB oils and source rocks.

The plot uses a selection of calculated biomarker parameters to demonstrate possible oil-oil (A) and oil-source rock (B) correlations for VSB crude oils and source rock extracts (From Edwards et al., 2004). The diagram is arranged so that those oils that show a stronger marine source rock influence plot closer to the centre of the diagram. The oils taken from the Swan-3, Oliver-1 and Tahbilk-1 wells (A.) all show greater marine influence as do source rock extracts from the Cretaceous Upper Vulcan Formation (B.).

A). Osprey-1 FIO

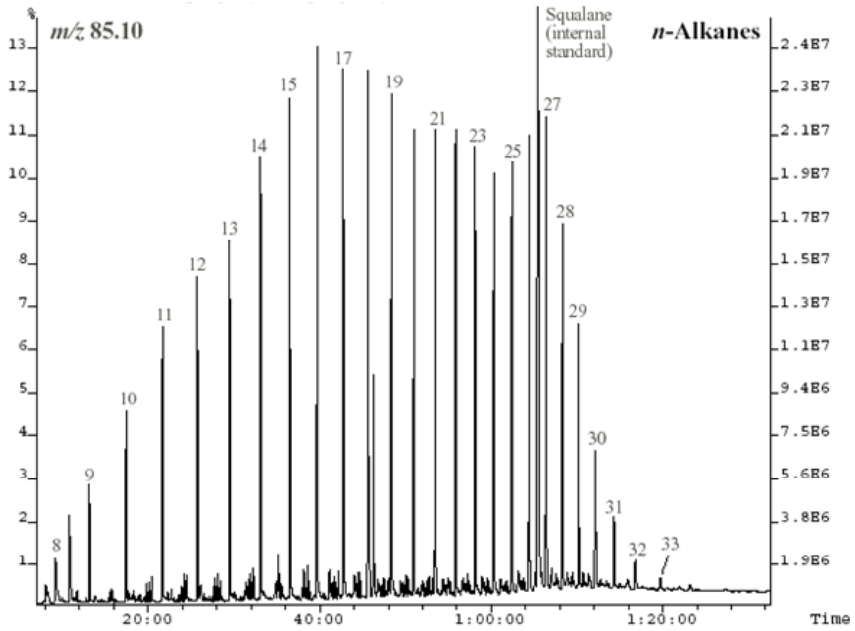

B). Oliver-1 FIO

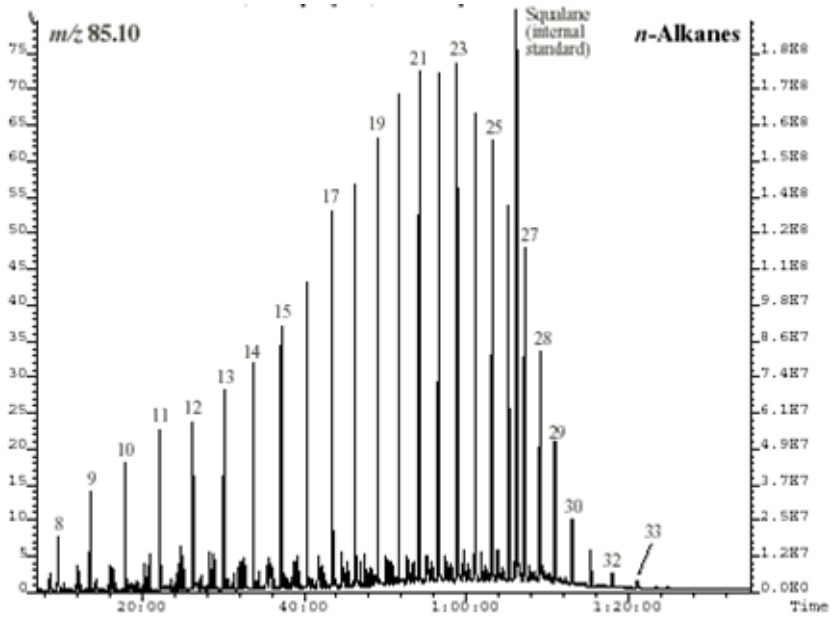

Figure 4-70: Comparison between the FIOs from Osprey-1 and Oliver-1.

Whole oil gas chromatograms are shown for the Osprey-1 FIO at 2484m (A.) and the Oliver-1 FIO at 2985m (B.). The n-alkane distribution is skewed towards the high molecular weight range (subordinate maxima at n-C_{26} in Osprey-1 [A.] and maxima of n-C_{23} in Oliver-1 [B]; indicating a more waxy composition for both of these FIOs.

Data presented in Edwards et al. (2004) using a range of maturation-sensitive biomarker (hopane and sterane) and aromatic ratios show that the VSB oils and the condensates recovered from the gas accumulations were generated from source rocks at a range of maturities within the conventional oil window. A plot of the ratios of C_{30} diahopane/C_{30} hopane versus C_{27} diasterane/C_{27} sterane highlight the maturity range shown by the two groups of VSB oils and condensates (Figure 4–71).

The Group A oils show a maturity trend, with the Talbot oils being the least mature (VR Equivalent of around 0.66%), and Audacious-1 being the most mature oil in the sub-basin (VR Equivalent = 1.1%). The FIOs from the VSB typically show mid oil window thermal maturity, with an equivalent vitrinite reflectance of about 0.7-0.8% (Figure 4–71). Aliphatic biomarker data indicate Hopane αβ/(αβ+βα) ratios that are at or just below equilibrium, Ts/Tm values are below three and C_{29} αββ/(αββ+ααα) sterane ratios are close to or at equilibrium. Low to moderate maturity is supported by the low abundance of tricyclic terpanes relative to hopanes, by the high isoprenoid/n-alkane ratios and by the short-over-long chain triaromatic steroid ratio.

Aromatic ratios from the FIOs supporting a mid oil window thermal maturity include dimethylnaphthalene ratios (DNR-1 ranging from 5 to 7), trimethylnaphthalene ratios (TMNr from 0.44 to 0.70), alkylbiphenyl ratios (e.g. methylbiphenyl ratios ranging from 10 to 21) and calculated vitrinite reflectances using the methylphenanthrene index (ranging from 0.66-0.84%).

When the FIO data from VSB oil fields are plotted in comparison with the equivalent crude oil from each field (Figure 4–72) it is notable that the maturity levels of the FIOs are consistently less than their associated crude oil, an observation that is in line with maturity estimated from the aforementioned biomarkers (Figure 4–72). These observations are consistent with the bulk of the fluid inclusions forming during the initial filling of the reservoir, with the lower maturity values reflecting either trapping of inclusions at an earlier point in time (i.e. coincident with charge) or could reflect oil inclusions forming more continuously with averaging effects acting to reduce the bulk maturity level below that currently observed.

Lower maturity in fluid inclusion oils compared with associated crude oils (Figure 4–72) is typical where the palaeo-oils (FIOs) and the crude oils are genetically related (George et al., 1997; Volk et al., 2001) and would suggest that the oils trapped within fluid inclusions are able to retain the maturity characteristics that existed at the point of entrapment and are not particularly sensitive to increases in reservoir temperature that occur after trapping. Indeed recent studies of FIOs extracted from Achaean rocks suggests that oil inclusions can endure temperatures of up to 300°C (Dutkiewicz et al., 2003; George et al., 2008) and still retain relatively pristine palaeo-compositions.

Within the FIO samples a number of outliers are recognised in terms of their inferred maturity level. The Jabiru-1A (1688-91m) FIO sample from the current water-leg has slightly lower maturity than the FIO or crude oil samples from the current oil rim, with aliphatic biomarker and aromatic hydrocarbon maturity-dependent ratios point to maturity levels of between 0.64 and 0.8% vitrinite reflectance equivalent compared with more than 0.8% reported for samples from the current oil zone. Hopane αβ/(αβ+βα) ratios and the C_{29} sterane ααα 20S/(20S+20R) ratio are at or just below equilibrium, Ts/Tm = 1.8 and the C_{29} αββ/(αββ+ααα) sterane ratio (0.53) is below equilibrium. Aromatic ratios supporting this level of thermal maturity include dimethylnaphthalene ratios (DNR-1 = 4.6) and trimethylnaphthalene ratios (TMNr = 0.68) whilst the calculated reflectance from the methylphenanthrene index (MPI) indicates an even lower maturity (0.64%), as do the isoprenoid/n-alkane ratios.

The slightly lower maturity in the Jabiru-1A water zone sample could reflect a contribution of non-Jurassic oil in this FIO oil with the data pointing to a less mature Cretaceous source rock. Other FIOs where the source characterisation indicated a Cretaceous source rock such as the Osprey-1 FIO are also relatively less mature than the main group with most of the aliphatic biomarker and aromatic hydrocarbon maturity-dependent ratios indicating an equivalent vitrinite reflectance of <0.7%.

As highlighted in the preceding section on source characterisation the implied Cretaceous origin of the low maturity FIOs could reflect biomarker pick up from Cretaceous rocks juxtaposed against Jurassic reservoirs. In this regard the Swan-3ST FIO from a Cretaceous reservoir also exhibits lower maturity and whilst migration of low maturity oil into the structure is possible it may indicate local contamination.

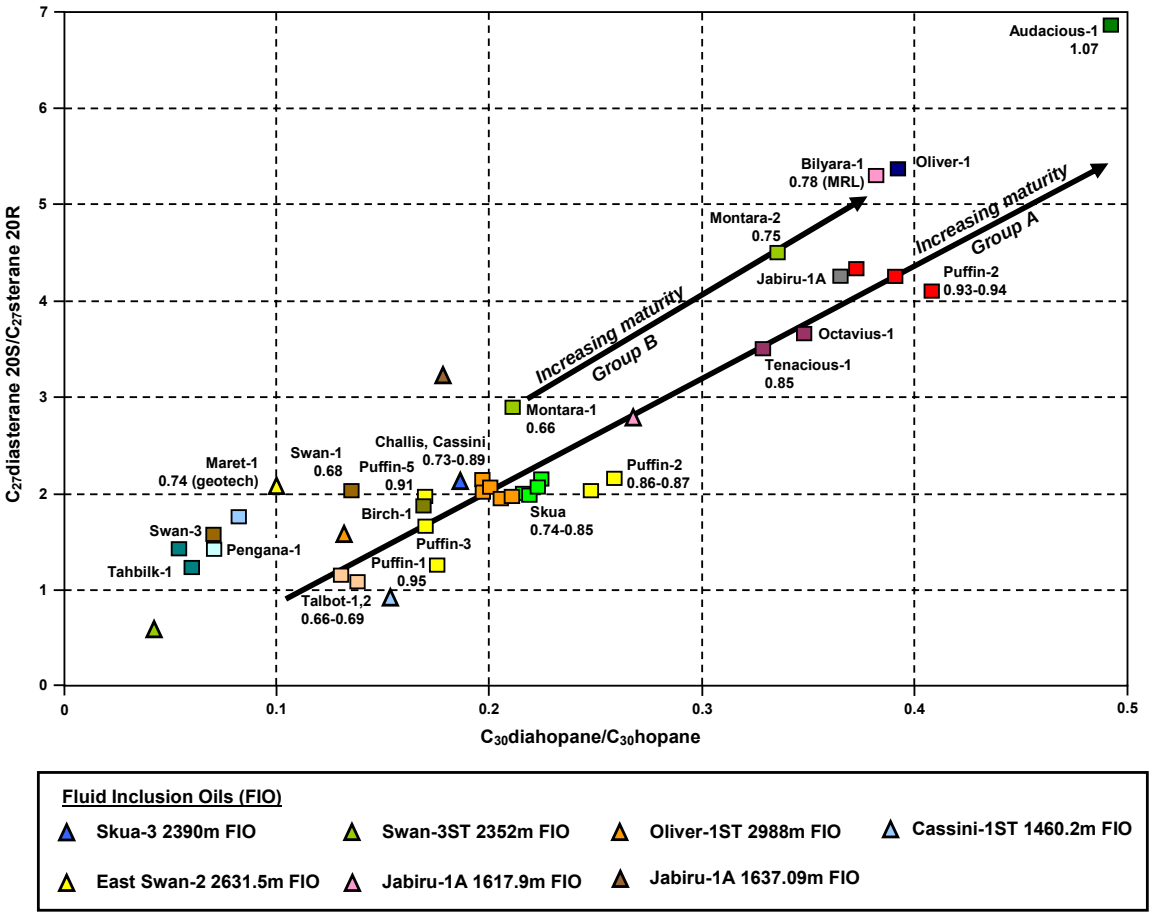

Figure 4-71: Plot showing the relative maturities of VSB oils, condensates and FIOs.

A plot of C_{30} diahopane/C_{30} hopane versus C_{27} diasteranes (20S)/C_{27} sterane (20R) is used to demonstrate the relative maturities of the Vulcan Sub-basin oils and condensates (filled squares; From Edwards et al., 2004) with data from available FIOs (filled triangles; Unpublished CSIRO data). The vitrinite reflectance equivalent values derived from the Methylphenanthrene Index (MPI-1; Radke and Welte, 1983) are given. MPI-1 = 1.5 x (2-MP+3-MP)/(P+1-MP+9-MP), where P = phenanthrene, MP = methylphenanthrene and % VRc = 0.6(MPI-1)+0.4 (after Radke et al., 1984). MPI values were determined by Geoscience Australia but where not available, values were obtained from well completion reports and the appropriate laboratory annotated. The FIOs from the VSB plot almost exclusively in the lower left of the diagram and are consistently associated with the crude oils that also have relatively low maturity.

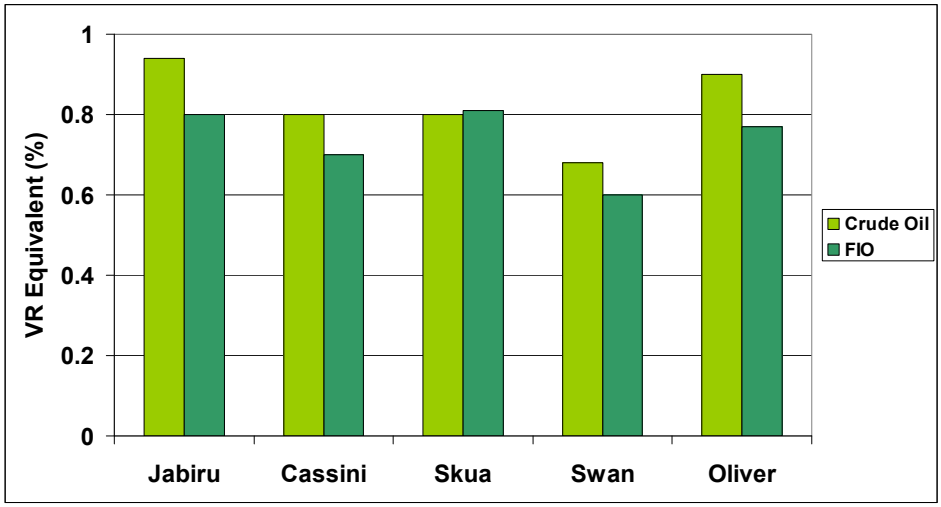

Figure 4-72: Maturity levels of FIOs compared with Crude Oils from the VSB.

The data represent Equivalent Vitrinite Reflectance values determined for the crude oils and FIOs using the Methylphenanthrene Index (Radke and Welte, 1983). FIOs consistently demonstrate lower maturity levels than the crude oils analysed from the same field.

Most of the aliphatic biomarker and aromatic hydrocarbon maturity-dependent ratios suggest that Swan-3ST fluid inclusion oil has an early oil window thermal maturity, at an equivalent vitrinite reflectance of about 0.6%. Hopane S/(S+R) ratios are at equilibrium, but αβ/(αβ+βα) ratios have not reached equilibrium and Ts/Tm = 0.7. Steranes and diasteranes indicate a lower maturity than the hopanes, with non-equilibrium sterane and diasterane S/(S+R) maturity ratios. The C_{29} αββ/(αββ+ααα) sterane ratio (0.39) is also well below equilibrium. Based on a calibration of C29 ααα 20S/20R to vitrinite reflectance equivalent, the Swan-3ST fluid inclusion oil has a maturity of 0.45%. Other aromatic ratios supporting a low level of thermal maturity include dimethylnaphthalene ratios (DNR-1 = 4.1), trimethylnaphthalene ratios (TMNr = 0.55), calculated reflectance from methylphenanthrene index (0.67%) and the alkylbiphenyl ratios (e.g. methylbiphenyl ratio = 7).

In contrast to the mid to low maturity range indicated for the other FIO samples the Octavius-2 FIO from an interpreted palaeo-oil zone has anomalously high maturity that is similar to the highest maturity levels reported for the crude oils (Audacious oil, Figure 4–71). Although the hopane biomarker ratios, which are at or close to equilibrium values, suggest a maturity at least in the mid oil window the maturity dependent aromatic hydrocarbon ratios have a greater dynamic range and record maturity levels up to peak oil generation and beyond. Alkylnaphthalene distributions of Octavius-2 FIOl contain relatively large amounts of the more thermally stable β-substituted isomers (e.g. 2-MN; 2,6- and 2,7-DMN; 2,3,6-TMN), indicating high maturity (George et al., 1998) and suggest a maturity in the range 1.0 to 1.3% vitrinite reflectance equivalent, which is consistent with the methylphenanthrene ratio, the alkylbiphenyl maturity ratios and the heptane and isoheptane parameters.

The higher maturity of the Octavius FIO suggests either that the reservoir was charged later in the burial history than the other wells sampled, or that the reservoir at Octavius-2 accessed higher maturity source rocks than other FIOs from the VSB.

A number of oils that have the potential to be sourced from the Cartier Trough also have higher maturity levels (i.e. Audacious, Tenacious, Oliver) that are consistent with a late charge derived from this source kitchen that underwent recent (Neogene) rapid burial.

4.9.3.3 Secondary Alteration

The VSB fluid inclusion oils are mostly unaltered with abundant low molecular weight *n*-alkanes and alkylcyclohexanes indicating they have not been subjected to water-washing (Lafargue and Barker, 1988). Some of the fluid inclusion oils (e.g. Jabiru-1A current oil zone at 1637.09m) have relatively reduced levels of low molecular weight aromatic hydrocarbons (benzene and toluene) suggesting that some degree of water washing occurred prior to trapping (Figure 4–73). The interpretation of water-washing can also be complicated for a FIO as a significant contribution of benzene and toluene can be derived from co-existing aqueous inclusions (Ruble et al., 1998) that could act to mask a partial water-washing signature.

Analysis of VSB crude oils shows varying degrees of water-washing has affected the Group A oils as determined by the selective removal of water-soluble benzene and toluene (Edwards et al., 2004). With the Skua oils taken as the completely unaltered end-member the Audacious-1 and Puffin oils are highly water-washed in comparison with the majority of the Group A oils being only slightly altered (Figure 4–73).

Edwards et al. (2004) suggest that the severity of water-washing evident in the Puffin oils could be caused by their vertical migration via faults through the regional seal into the Puffin reservoir as documented in more detail by O'Brien et al. (2002a). The degree of water-washing shown by the Puffin oils is almost comparable to that observed in the Laminaria and Corallina oil fields where hydrodynamic water flow is proposed as the mechanism causing the water washing (Newell, 1999; Preston and Edwards, 2000). Unlike the Laminaria Formation in the Northern Bonaparte Basin the Cretaceous reservoir sands of the Puffin Field are less likely to be connected to a dynamic aquifer making this process an unlikely explanation for this observation.

Up-fault flow represents an alternative mechanism to achieve water-washing rather than requiring lateral flow within the aquifer. The lack of significant water-washing in condensates the other Cretaceous hosted hydrocarbon discovery, the Swan gas field (Figure 4–73), does support a localised effect at Puffin that could reflect proximity to vertical fluid migration pathways such as faults.

Plotting of the FIO low molecular weight data onto Figure 4–73 illustrates the generally unaltered nature of the fluid inclusion oils from the VSB. On the plot of 3-methylpentane/benzene versus 3-methylpentane/n-hexane (Figure 4–73a) the FIO data are either similar to the equivalent crude oil composition or fall into the less water-washed quadrant of the diagram. As mentioned previously, a contribution to the FIO composition from any co-existing aqueous fluid inclusions could increase the level of water soluble low molecular weight hydrocarbons and could conceivably indicate a non-water washed oil.

However given the relative proportions being contributed from oil inclusions compared with water inclusions containing variable degrees of soluble hydrocarbons it is unlikely that the composition of a strongly water-washed oil trapped within inclusions could be shifted sufficiently by the content of the water inclusions to produce a composition that register as a non-water washed oil.

Despite showing limited evidence of water-washing some of the VSB FIOs and crude oils do exhibit signs of biodegradation. This is primarily indicated by elevated levels of the 25-norhopane biomarker that is considered to be an indicator of heavy biodegradation (Blanc and Connan, 1992). This diagnostic biomarker occurs in the Octavius-2, Osprey-1, and Jabiru-1A water zone FIOs despite the lack of any obvious humps showing unresolved complex mixtures (UCM) in the partial m/z 85 mass chromatograms (Figure 4–74C, I, and J), which would typically reveal loss of *n*-alkanes by biodegradation (Connan, 1984). In these particular samples the ratio of C_{29} 25-norhopane/C_{29} αβ hopane ranges from 0.15 in the water zone samples from Jabiru-1A to 0.22 in the Octavius-2 palaeo-oil zone sample (George et al., 1998).

In contrast the FIO from the Delamere-1 well is unusually depleted in low molecular weight *n*-alkanes relative to the higher molecular weight homologues and exhibits a prominent baseline hump of undifferentiated complex mixture (UCM) on the partial m/z 85 mass chromatogram (Figure 4–74L), which could be due to the presence of a biodegraded component. No other possible evidence of biodegradation was detected in this FI oil including an absence of the 25-norhopane biomarker and this would imply that any level of biodegradation experienced by this oil was relatively low.

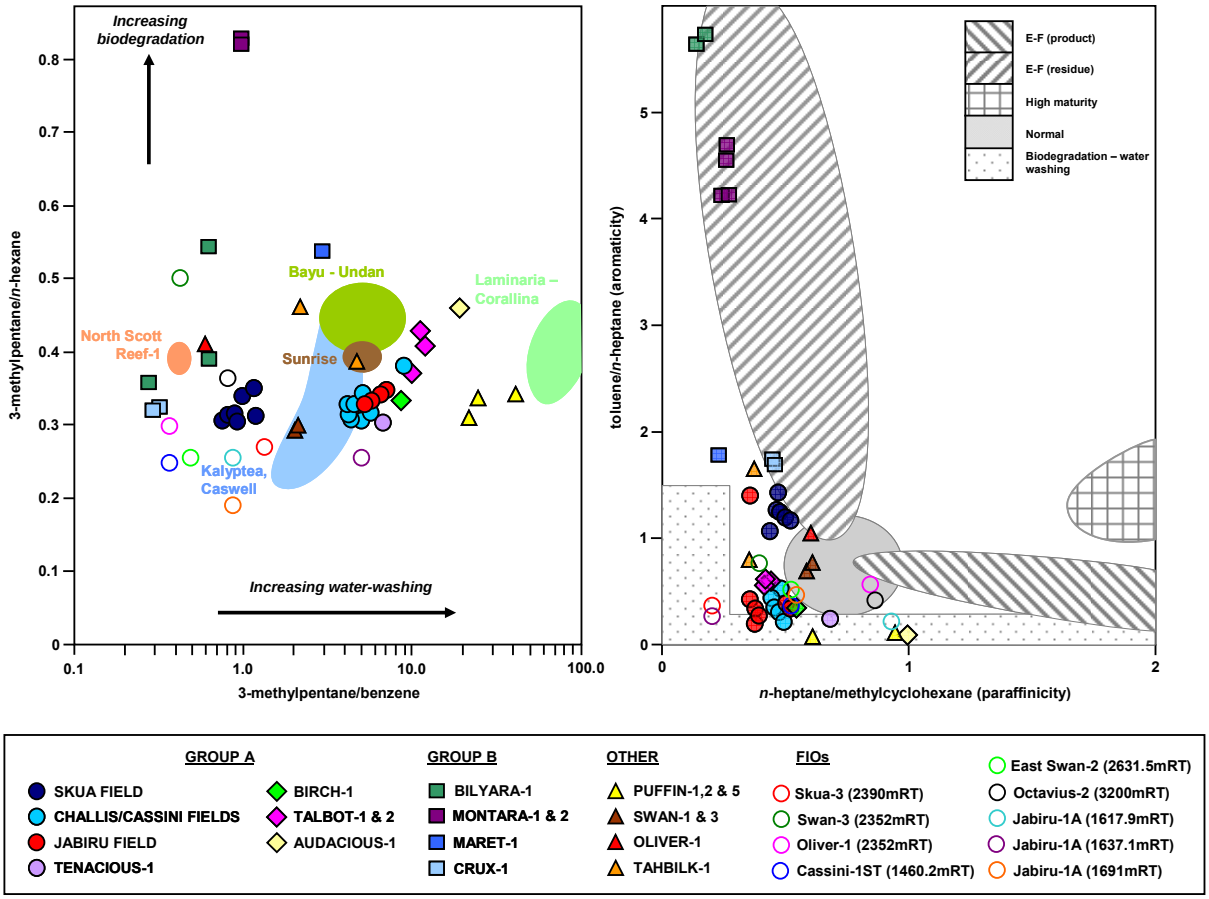

Figure 4-73: Secondary alteration of VSB crude oils, condensates and FIOs.

The impact of secondary alteration processes on hydrocarbon composition as shown by variations in the ratios of C_6 and C_7 hydrocarbons: a) 3-methylpentane/benzene versus 3-methylpentane/n-hexane, and b) n-heptane/methylcyclohexane versus toluene/n-heptane after Thompson (1987, 1988), E-F = Evaporative-Fractionation. Modified from Edwards et al. (2004) with compositions derived from the FIOs used to plot the samples analysed during the period of the current study. The FIOs show no evidence of significant water-washing or biodegradation, whilst there is some variation in the VSB crude oils in regards to water-washing, but not to the extent seen in the oils of the Laminaria-Corallina fields from the northern Bonaparte Basin that are severely water-washed (Preston and Edwards, 2000). Also note the position of crude oils from the Bilyara-1 and Montara-1, -2 wells that show evidence for evaporative fractionation using the definition of Thompson (1987, 1988).

Samples showing evidence of biodegradation either as a UCM hump or as elevated levels of the 25-norhopane biomarker in conjunction with an otherwise unaltered *n*-alkane profile can reflect a period of biodegradation that has been overprinted by later, pristine oil. For the FIOs that lack a UCM hump the presence of the 25-norhopane biomarker is taken to indicate a phase of severe biodegradation where the original oil has been almost totally destroyed.

Whilst indicators of biodegradation could point to a multi-phase charge history the significance of 25-norhopanes as an indicator of biodegradation remains contentious with some authors suggesting these biomarkers may have been inherited from the source rock (Bao, 1997) or have been entrained along the migration path.

Some of the currently reservoired crude oils from the VSB also show evidence of biodegradation. Gas chromatograms for the Montara-1 and -2, and Oliver-1 crude oils exhibit small unresolved complex mixtures (UCM), but as the low molecular-weight hydrocarbons remain and 25-norhopanes were not detected, biodegradation is regarded as minimal. Mixing of biodegraded with fresh oil would represent a valid mechanism to explain the geochemical observations from these oils.

4.9.3.4 Summary of the geochemical data

Analysed FIOs from the VSB provides additional insights into the evolution of the petroleum systems operating in this region. The samples mostly come from traps where charge is likely to be represented by oils of the Group A family of Edwards et al. (2004) that are derived from source rocks of the Upper Jurassic Lower Vulcan Formation. Source characteristics exhibited by the FIOs display a good correlation with crude oils representative of this family whilst lower maturity levels and the less altered composition indicate trapping through the geological past.

Crude oils forming part of the Group B family are not well represented in the FIOs analysed previously except for the Delamere-1 sample (George et al., 2004b) which correlates best with Group B oils that are thought to have been derived from the Middle Jurassic Plover Formation (Edwards et al., 2004).

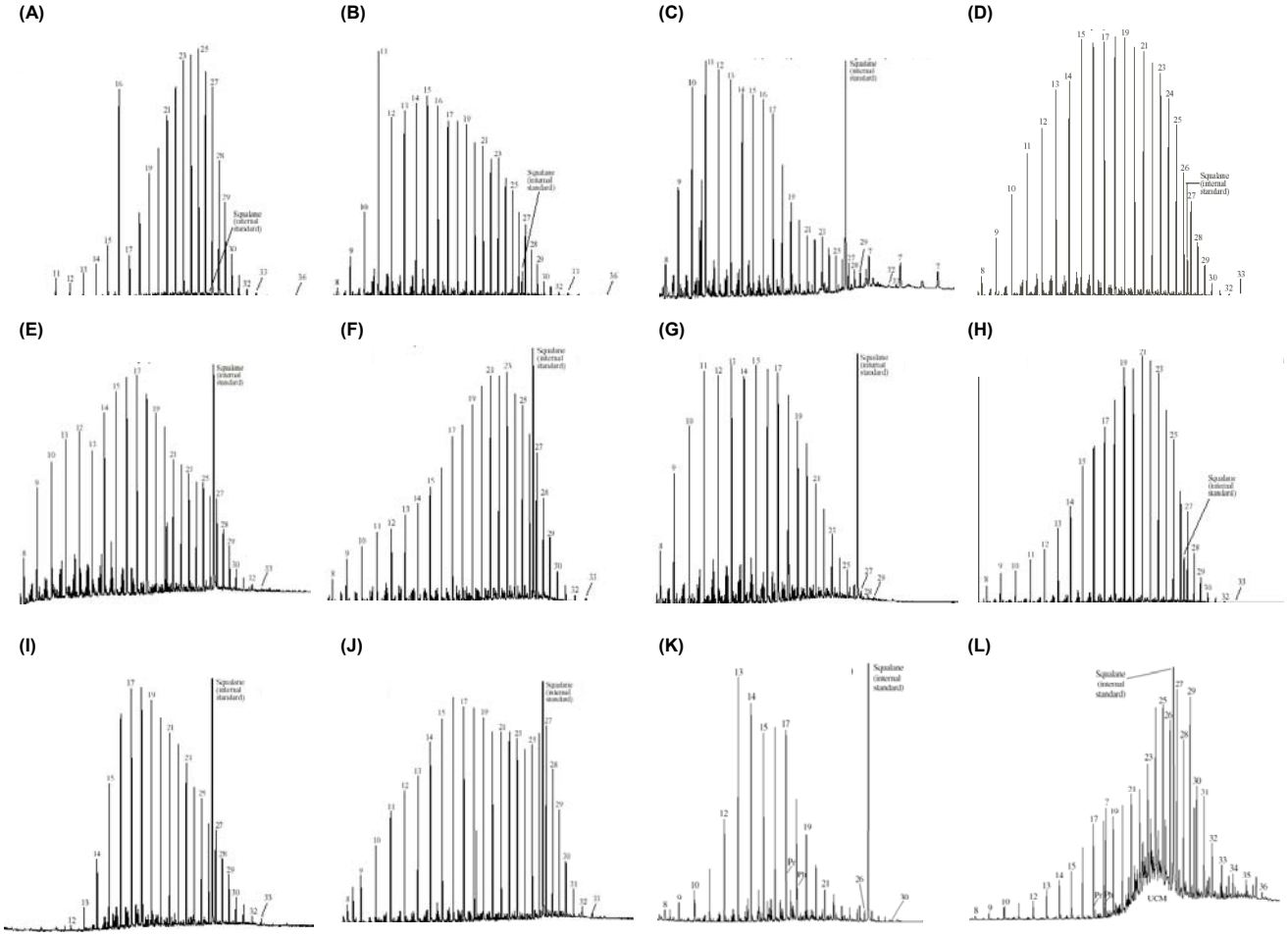

Figure 4-74: Distribution of n-alkanes and isoprenoids in VSB FIOs.

Detailed caption provided on next page.

Figure 4 74: Distribution of n-alkanes and isoprenoids in VSB FIOs.

Partial m/z 85 mass chromatograms for (A) Jabiru-1A, 1617m, (B) Jabiru-1A, 1637m, (C) Jabiru-1A, 1688-91m, (D) Skua-3, 2390m, (E) Cassini-1ST, 1460.2m, (F) Oliver-1, 2985-88m, (G) Swan-3ST, 2352m, (H) East Swan-2, 2631.5m, (I), Octavius-2, 3600m (J), Osprey-1, 2469-84m (K) Champagny-1, 3420-29m, (L) Delamere-1, 1336-54m. Numbers refer to n-alkane chain length, Pr = pristane, Ph = phytane, UCM = undifferentiated complex mixture. The squalane was added as an internal standard. All samples shown, with the exception of Delamere-1 (L) show relatively complete *n*-alkane profiles (aside from light end depletion that is a product of the work up procedure used for the FIOs, George et al., 1998) that show no evidence for biodegradation. In the Delamere-1 FIO the presence of a pronounced UCM hump, but relatively complete *n*-alkane profiles could indicate mixing of fresh unaltered oil with a strongly biodegraded residue.

Instead a number of FIOs show source characteristics that are unlike either recognised oil family and imply derivation from more marine dominated source rocks. These could be representatives from additional oil families that are yet to be confirmed, but are hinted at by the crude oil data.

Alternatively the more marine influenced nature of the FIOs could represent a true end-member of the Group A family that has subsequently mixed with terrestrially dominated hydrocarbons sourced from the underlying Plover Formation (Group B) to produce the current composition that is assigned as Group A. This possibility seems less likely given the apparent contribution from Cretaceous source rocks indicated by the presence of the angiosperm marker Oleanane is some of the FIOs, with the Upper Vulcan Formation seen as a likely option for the derivation of this oil.

Evidence of varying degrees of water-washing seen in some of the crude oils are generally not seen in the FIOs suggesting alteration by this process postdated inclusion oils being trapped. Evidence of biodegradation is limited in the crude oils and whilst the FIOs show complete *n*-alkane profiles, generally without a baseline hump of undifferentiated complex mixture, the presence of elevated levels of the 25-norhopane biomarker in some samples does imply that these may have experienced episodes of severe biodegradation before being replenished by a fresh oil charge to produce the observed bulk composition. A multi-stage charge history for the VSB represents an intriguing insight into the evolution of the petroleum system but the severity of biodegradation precludes any effective characterisation of these remnants.

4.10 SUMMARY

In this chapter a review of the various types of conventional oil indications have been discussed including the limitations in these techniques that have produced the incentive to develop alternate methods of describing oil saturation histories. Rather than providing a replacement for these historical techniques the application of new methods based on measuring oil inclusion abundances is aimed at augmenting the conventional data to provide a clearer and less ambiguous understanding of the hydrocarbon charge history.

The collection of a comprehensive basin-wide suite of analyses to describe the abundance, location and fluorescence colour characteristics of oil-bearing fluid inclusions preserved in samples of the key reservoir horizons has provided a unique insight into the history of hydrocarbon accumulation in traps from the VSB. In combination with the conventional oil shows a more complete picture of the filling of these traps with hydrocarbons can be discerned, including for the first time well defined palaeo-hydrocarbon-water contacts. The advent of novel new techniques to extract and analyse minute quantities of hydrocarbons trapped in fluid inclusions provides further invaluable constraint by allowing the fluid inclusion oils to be incorporated into the understanding of the petroleum systems operating in the basin.

Vertical profiles compiled from 320 GOI measurements collected on 74 wells from across the VSB allowed for the identification of eight palaeo-oil columns in currently water-wet traps, a further three palaeo-oil columns in now gas-filled structures and revealed a more complex charge history for the present day oil columns. These data substantially augmented the information available from conventional oil shows by delivering less ambiguous information on the level of oil saturation attained and enabling the position of palaeo-gas-oil and palaeo-oil-water contacts to be identified. In most instances these palaeo-fluid contacts were clearly expressed by large changes in the magnitude of GOI values recorded above and below these interpreted palaeo-fluid contacts.

Aside from those traps where evidence of palaeo-oil accumulation was detected the GOI results showed that all but two of the traps investigated showed some evidence of oil migration at some point in the geological past. These results point to widespread hydrocarbon generation and the presence of effective migration pathways linking source kitchens with traps that are in many instances located well outside the extent of the recognised kitchens.

A comprehensive calibration experiment provided the first detailed assessment of the reproducibility of the GOI method and highlighted that with the application of careful procedures it is possible to produce data that can be readily replicated within error limits that have no material impact on the interpretations drawn from the data.

Collectively the fluid inclusion GOI results and conventional oil show data indicate that a much larger number of traps have received oil charge and accumulated often substantial palaeo-hydrocarbon columns, both in traps where conventional shows would imply previous accumulation but importantly also in traps with only limited conventional indications of prior oil charge. Where good conventional oil shows are reported the GOI data recorded on these wells show good agreement with the conclusions that would be drawn from the oil show data alone. Often any disparity between the two data sets relates to a positioning offset, some of which can be explained by smearing of shows during drilling or lags associated with cuttings samples that can reduce the depth assignment accuracy. Rarely are good oil shows not represented in the GOI data, but some examples, in particular the Talbot and Montara fields as well as the Elm-1 well have produced apparently disparate results.

Ultimately complete agreement between these datasets are not anticipated as they measure different processes, the fluid inclusions related to palaeo-fluid events that become isolated from the pore network when sealed as inclusions and the conventional oil show is controlled by a complex interplay governing entrainment and preservation of hydrocarbon fluids in an open system. It is likely that each of these markers provide a different time window that when considered collectively have the effect of widening the footprint of the investigation of regional charge history thus contributing a overall more comprehensive evaluation of this key factor in the assessment of effectiveness of this petroleum system.

Despite the high proportion of traps that received volumetrically sufficient hydrocarbons to produce an accumulation the failure to retain these palaeo-columns highlights the adverse role of two processes, namely flushing by gas and loss of hydrocarbons due to trap breach by late stage fault reactivation.

Aside from the palaeo-saturation data the observational data collected allowed further constraint to be placed on the operation of the petroleum system by description of the location of oil inclusions relative to authigenic mineral cements and the fluorescence characteristics of the fluid inclusion assemblages. These data indicated that the migration of oil into these structures was often coincident in part with the formation of authigenic quartz overgrowths, an observation that is critical

for the application of fluid inclusion palaeothermometry data that will be used to place absolute constraints on the timing of hydrocarbon migration. The fluorescence observation proved to be less revealing with no clear pattern being observed that could be attributed to anticipated variations in oil maturity or composition.

The apparent randomness of the fluorescence colours would appear consistent with published geochemical data for fluid inclusion oils in VSB samples are more broadly that failed to distinguish a link with maturity of the contained oils (George et al., 2001b, c). The result highlighted the need to utilise all available techniques to fully describe the charge history or a sedimentary basin, rather than relying on poorly constrained or anecdotal evidence.

Of great benefit to the current study has been concomitant collection of detailed geochemical data from fluid inclusion oils taken from many of the palaeo-oil zones recognised from the VSB. These data provide invaluable constraints on the resultant charge history that clearly demonstrate that the fluid inclusion oils can largely be attributed to one of the two recognised oil families seen in the region from conventional geochemistry of recovered crude oils and condensates. These fluid inclusion oils are consistently less mature than the equivalent currently reservoired oils and confirm that entrapment of migrating hydrocarbons is a historical event and that the entrained fluid becomes isolated from the open system and are able to retain the characteristics of the oil at the time of trapping.

Whilst the majority of wells produced GOI profiles where the oil saturation could be readily interpreted using established protocols for GOI data a number of well results produced unexpectedly low GOI values given that the reservoir is presently oil-filled. Although not clearly understood these results highlight several key factors related to the interpretation of GOI data. Firstly they demonstrate that care should be taken to avoid overly dogmatic interpretation of the data, particularly where low GOI values are encountered, with false negatives being possible explanations. In contrast the saturation profile needed to produce high GOI values is more robust making it more difficult to envisage situations where a false positive may be produced. Secondly and in line with the observation from the geochemical data that shows fluid inclusion oils to be consistently lower in maturity than currently reservoired oils it is likely that oil

trapped within fluid inclusions is more representative of conditions in the geological past making it unnecessary that palaeo-saturation profiles should always be equivalent to the current level of oil saturation. Instead the GOI data provide a window to the geological past and integration with all hydrocarbon indications is needed if the charge history of individual traps and the petroleum systems as a whole are to be understood.

A final aspect that impacts on the interpretation of GOI data is the need to fully incorporate information on the geological history of the basin or trap being studied. In the next chapter of this thesis the results from individual wells are placed within geological context to demonstrate how robust hydrocarbon charge history reconstruction can be achieved and in doing so many of the apparent inconsistencies seen in GOI profiles from single wells can be more clearly reconciled.

5. HYDROCARBON CHARGE HISTORY RECONSTRUCTION

5.1 INTRODUCTION

The previous chapter introduced techniques for evaluating the level of oil saturation experienced by reservoir rocks throughout their geological history. This enabled those wells that had previously contained oil accumulations to be differentiated from those that were isolated from oil migration pathways or those which experienced oil migration but in insufficient volume to produce an accumulation or migrated prior to the existence of a viable trap. When integrated with the current fluid fill, be it oil, gas or water, together with conventional information from shows, log analysis and fluid sampling the data combine to produce an integrated charge history for that well. A key benefit of the fluid inclusion methods relates to the ability to define the position of palaeo-oil water and palaeo-gas oil contacts as these parameters produce physical constraints that allow the geometry of the palaeo-column to be assessed relative to the geometry of the trap confining them.

Whilst the information that can be gained from any one well can be significant the true value of such data lies in widening the footprint of investigation and this is most clearly demonstrated when data collected on individual wells, either from across a single field or collectively across a basin is integrated within a geological framework.

This chapter draws on the single well results presented in Chapter 4 to constrain reconstructions of the charge history experienced by the main oil and gas fields, by traps that once contained oil but are now water-wet and to identify valid traps that failed to receive hydrocarbon charge. These data combine to allow constraints to be placed on the petroleum systems that have operated within the VSB and provide a regional charge history that will enable the processes controlling charge and retention to be more clearly understood. Results from complementary studies that were undertaken during the duration of this study will also be drawn upon to augment the interpretation of the hydrocarbon charge history experienced by the VSB.

5.2 OIL FIELD CHARGE HISTORIES

Previous studies have left no doubt that the oil fields of the VSB have experienced complex charge and retention histories, with conventional oil shows often noted below the current oil water contacts and within the overburden section. Coupled with obvious evidence of Neogene fault reactivation it seems clear that partial or complete breach and attendant loss of hydrocarbons has frequently occurred.

GOI data collected on the three most significant oil discoveries have helped to more clearly define the architecture of these accumulations prior to episodes of breaching by the aforementioned Neogene faulting. Palaeo-OWCs that lie below the current OWC are commonly observed allowing detailed information on the geometry of palaeo-oil accumulations to be collected.

5.2.1 Skua Oilfield

The Skua oil field (Figure 5–1; Osborne, 1990) was discovered by BHP Petroleum in 1985 and is one of only three commercial hydrocarbon discoveries within the VSB. The hydrocarbons are reservoired within Early Jurassic sandstones of the Plover Formation with top and lateral seal provided by Early Cretaceous calcareous shales of the Bathurst Island Group (Figure 5–2).

The Skua trap is a simple tilted fault block structure related to Jurassic rifting with three-way dip closure (Figure 5–2). The principal reservoir section is the Plover Formation consisting of Early to Middle Jurassic fluvio-deltaic, excellent quality, stacked sandstone horizons that exhibit high porosity and permeability. The Skua Oilfield was discovered despite initial exploration drilling targeting the Skua structure producing equivocal results.

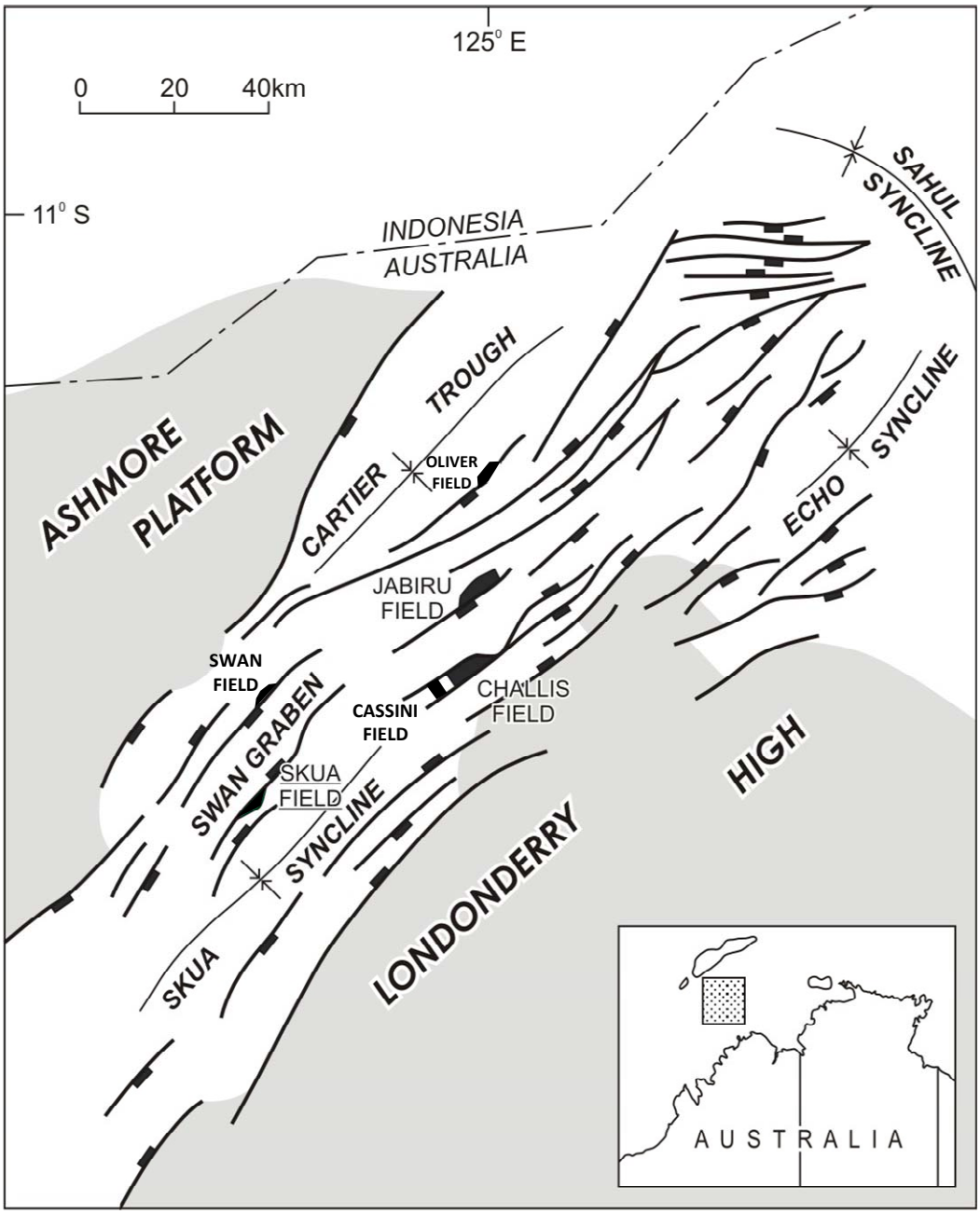

Figure 5-1: Location of the hydrocarbon fields discussed in this chapter.

Simplified Jurassic fault map for the Vulcan Sub-basin showing the main structural elements (modified from Pattillo and Nicholls, 1990) relative to the location of the hydrocarbon accumulations discussed in this chapter.

The exploration history of the Skua Field was described in the previous chapter, but briefly the field was discovered by the drilling of Skua-3 after the first two wells failed to penetrate the main footwall block or drilled below the OWC. Subsequent appraisal drilling confirmed a substantial hydrocarbon accumulation, consisting of a 28m gas cap above a 46.5m oil-rim.

5.2.1.1 Sampling Details

The Skua Field was first sampled by the author as part of an earlier study (O'Brien et al., 1996a) and this initial application of the GOI technique provided the early impetus to initiate the current investigation. Trap integrity issues had already been highlighted for the Skua Field during field appraisal drilling with residual oil shows seen below the current Oil-Water-Contact (OWC) in most wells and communication of oil across the main bounding fault observed from the Skua 2 result that inadvertently tested the hangingwall stratigraphy (Osborne, 1990).

GOI data collected on samples taken in the initial study and reported in O'Brien et al. (1996a) for Skua-3 delineated a small palaeo-oil column below the current OWC with a palaeo-OWC defined some 7-13m below the level of the present day contact. Based on this palaeo-OWC and assuming a horizontal fluid contact O'Brien et al. (1996a) estimated that as much as 20 million barrels of oil had been lost from the Skua trap after initial charge.

Integration of the fluid inclusion data, with a suite of remote sensing techniques that included hydrocarbon seepage detection using water-bottom geochemical sniffer and Airborne Laser Fluoresensor (ALF) data were combined with recognition of hydrocarbon-related diagenetic zones (HRDZs) in the shallow section were collectively used to demonstrate hydrocarbon leakage from the Skua trap (O'Brien and Woods, 1995; O'Brien et al., 1996a). Fault reactivation in the Mio-Pliocene was considered to be the most likely cause of seal breach.

Subsequent sampling undertaken in the current study produced results that indicated a more complex palaeo-oil accumulation than that implied by O'Brien et al. (1996a).

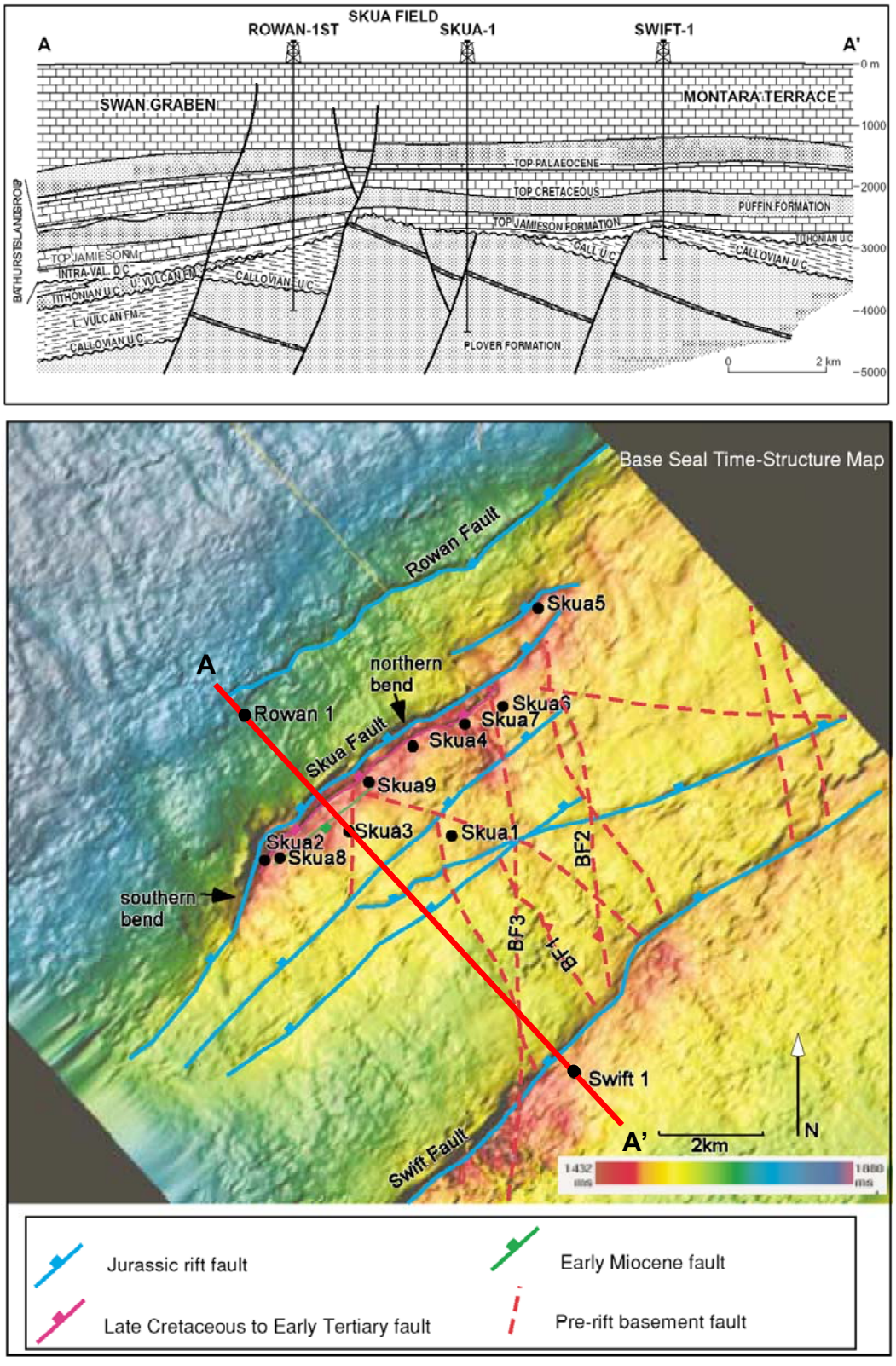

Figure 5-2: The Skua Oilfield

Structural cross-section through the Rowan, Skua and Swift fault blocks (after Fittall and Cowley, 1992) with the line of section (A-A') shown on a Base Seal time-structure map taken from Gartrell et al., 2002.

Based on analyses completed on samples from three wells along the strike of the Skua Field it is apparent that the position of the palaeo-OWC defined by the GOI data is deeper in the west and shallows to the east (Figure 5–3).

Unfortunately the samples taken in Skua-6 lay below the projected palaeo-OWC and the full geometry of the Skua palaeo-oil accumulation could not be fully described. Nevertheless the data pointed to a previous accumulation that was not necessarily any larger volumetrically than the current field, but rather existed within a trap geometry that was different to that seen at the current day.

The realisation that changes in trap geometry could significantly alter the conclusions drawn from one dimensional sampling prompted the initiation of new research efforts to study the use of GOI data to describe the geometry of palaeo-oil columns by sampling multiple wells from the same structure. Whilst this new investigation was not completed as part the current study the additional GOI data collected on further wells from the Skua Field was produced by the author and are therefore included here to demonstrate this application.

GOI results produced from this new study (Gartrell et al., 2002) provided a significant refinement of the understanding of the geometry of the Skua palaeo-oil column. The new GOI data collected on samples taken from the Skua-8 and -9 wells allowed the tilted palaeo-OWC to be more tightly defined and reinforced the observations of the earlier study showing the palaeo-OWC to be deeper on the western side of the field.

This observation suggested that the palaeo-OWC indicated by the GOI data has captured a previous geometric position of the OWC that had been frozen into the rocks before being tilting down to the west after initial hydrocarbon charge (Figure 5–4; Gartrell et al., 2002).

Significantly, the GOI data can largely accommodated by post-charge regional tilting during the Cretaceous with little or no volume change required and the results are not strongly supportive of vertical leakage from the Skua trap. This highlights the need to consider a range of alternatives when interpreting GOI results from a single well.

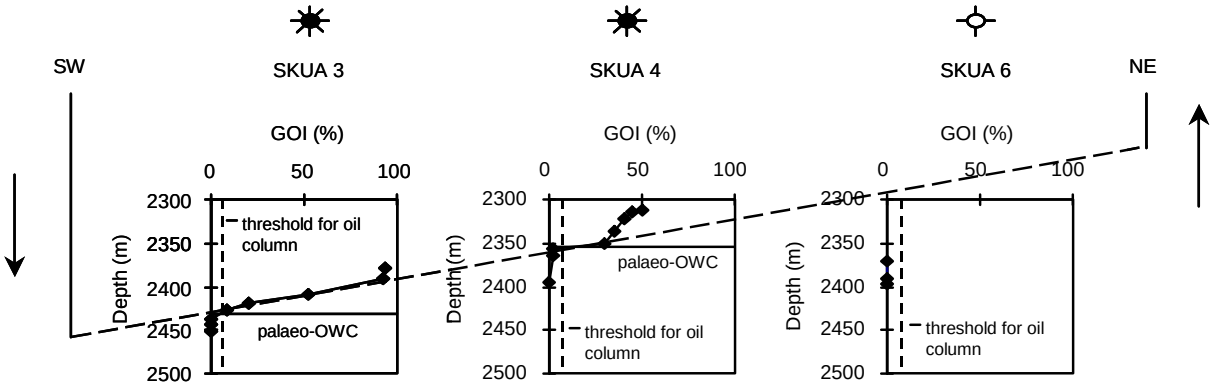

Figure 5-3: GOI results for the Skua Field.

Simplified GOI plots shown for Skua-3, -4 and -6 wells showing a deeper inferred palaeo-OWC in the southwestern Skua-3 well becoming shallower in the Skua-4 well to the northeast. Low GOI values recorded in the Skua-6 well show that high palaeo-oil saturation did not extend to this location despite the reservoir being penetrated above the lowest closing contour for the Skua trap. A tilting of the trap down towards the southwest provides a viable mechanism to explain the transition to the current horizontal OWC. Depths are shown on a consistent datum (metres sub-sea) and the 5% GOI threshold for oil accumulation is shown as the vertical dashed lines. The well symbols refer to the current reservoir fluid type; Skua-3 and Skua-4 contain oil with an overlying gas cap, whilst the Skua-6 well is water-wet. Refer to Figure 5–3 to locate the wells shown.

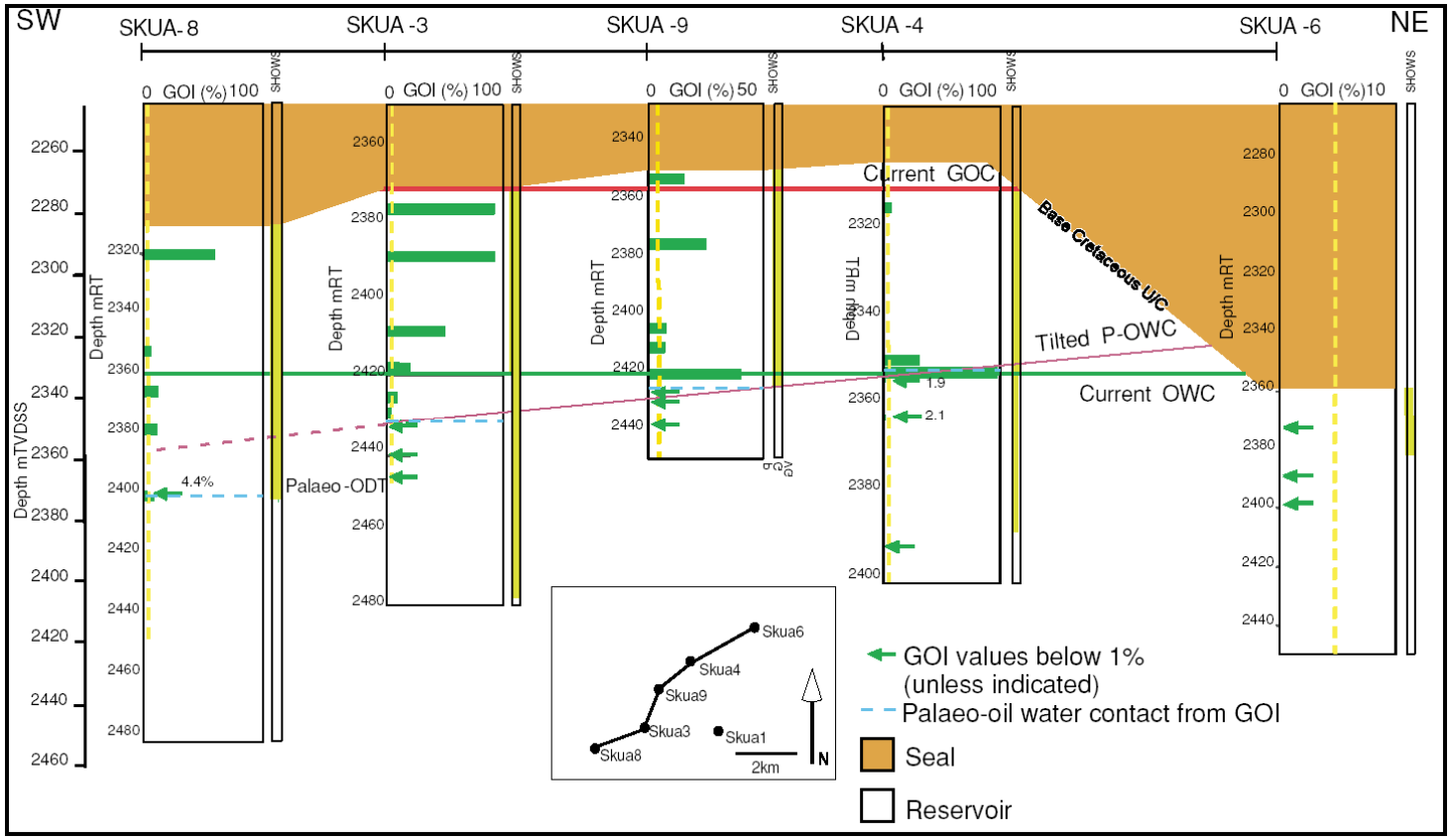

Figure 5-4: Summary of GOI data from Skua Field showing inferred palaeo-OWCs.

A cross-section of wells from the Skua Field (from Gartrell et al., 2002) showing the GOI results obtained for these wells and the position of the current GOC, OWC and the inferred palaeo-OWC. The GOI empirical threshold for oil accumulation is shown as the dashed yellow line whilst arrows indicate samples where GOI values were less than 1%. The top seal to the reservoir section is coloured orange, the base of which marks the position of the Base Cretaceous Unconformity. The extent of conventional oil shows are shown as vertical solid yellow bars. Refer to Figure 5–3 to locate the wells shown. An inclined palaeo-OWC, dipping down to the southwest is interpreted and is consistent with all samples except for the lowermost sample in Skua-8. The discrepancy at Skua 8 can be attributed to structural-hydrodynamic analyses that suggest that Skua 8 may not be in communication with the rest of the field (Gartrell et al., 2002).

5.2.1.2 Restoration of the Skua Palaeo-oil Column

To further investigate the evolution of the palaeo-oil column seen from the Skua wells Gartrell et al. (2002) employed three dimensional structural restoration methods to progressively restore the Skua trap back in time (Figure 5–5). The palaeo-oil water contacts, defined by the GOI data, provided a useful datum with restoration of the trap undertaken until the tilted palaeo-OWC was returned to a horizontal position. This represented the most likely orientation that would have existed when the field was first charged and represented a unique solution with respect to the time steps employed in the restoration. Indeed further restoration results in an increasing divergence of the datum points from this horizontal plane (Fig 5–6). This outcome places a direct constraint on the likely timing of initial charge and facilitated a comparison between the palaeo-field and present-day field structural closure that allows the evolution of the trap to be more clearly understood.

The restoration results suggest the palaeo-OWCs in Skua 3 and Skua 4 had the same depth (i.e. formed a horizontal plane) at sometime prior to the Early Miocene but after the end of the Paleocene (Gartrell et al., 2002). Hence, if the palaeo-OWC was initially flat and not tilted hydrodynamically, initial oil charge is constrained by the restoration to have occurred sometime in this time interval (Figure 5–6).

A comparison between the present-day field and palaeo-field at Skua (Figure 5–7) demonstrates that the restored field has some additional volume within the palaeo-oil column due to its greater structural relief. The gross rock volume in the palaeo-field is calculated to be about 8% larger (~5 MMBBL) than the present-day (Gartrell et al., 2002), and likely to have contained considerably less oil than the estimates of palaeo-oil in place volumes described by O'Brien et al. (1996a).

5.2.1.3 Revised Fill-Spill Model for the Skua Field

The integration of palaeo-OWC data provided by GOI results with a 3D structural restoration is a powerful method for describing the development of hydrocarbon columns through time (Lisk et al., 2005), helping to produce a revised fill-spill model for the Skua field (Gartrell et al., 2002).

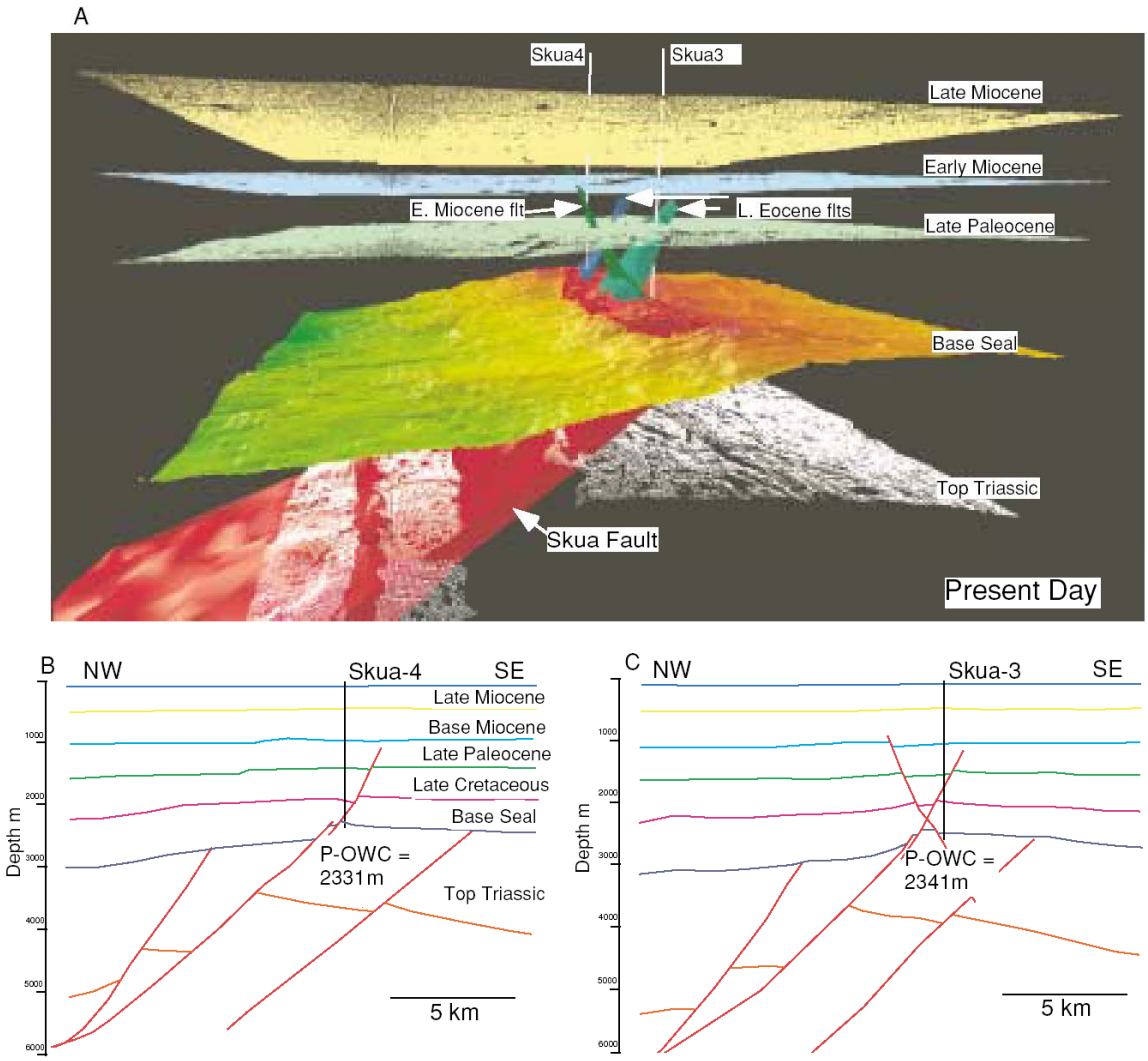

Figure 5-5: Skua 3D restoration – Late Miocene.

Diagram shows the configuration of the Skua trap at the current day representing the starting point for the 3D restoration (from Gartrell et al., 2002). The position of the Skua-3 and -4 wells are shown. Horizons for key seismic markers as well as faults come from interpretation of the HV11 3-D seismic survey. a). 3D model with for the present-day structure viewed looking towards the northeast. b). Cross-section through the 3D model at Skua 4. c). Cross-section through the 3D model at Skua 3. Initial palaeo-OWC at Skua 3 located 10 m deeper than palaeo-OWC at Skua 4.

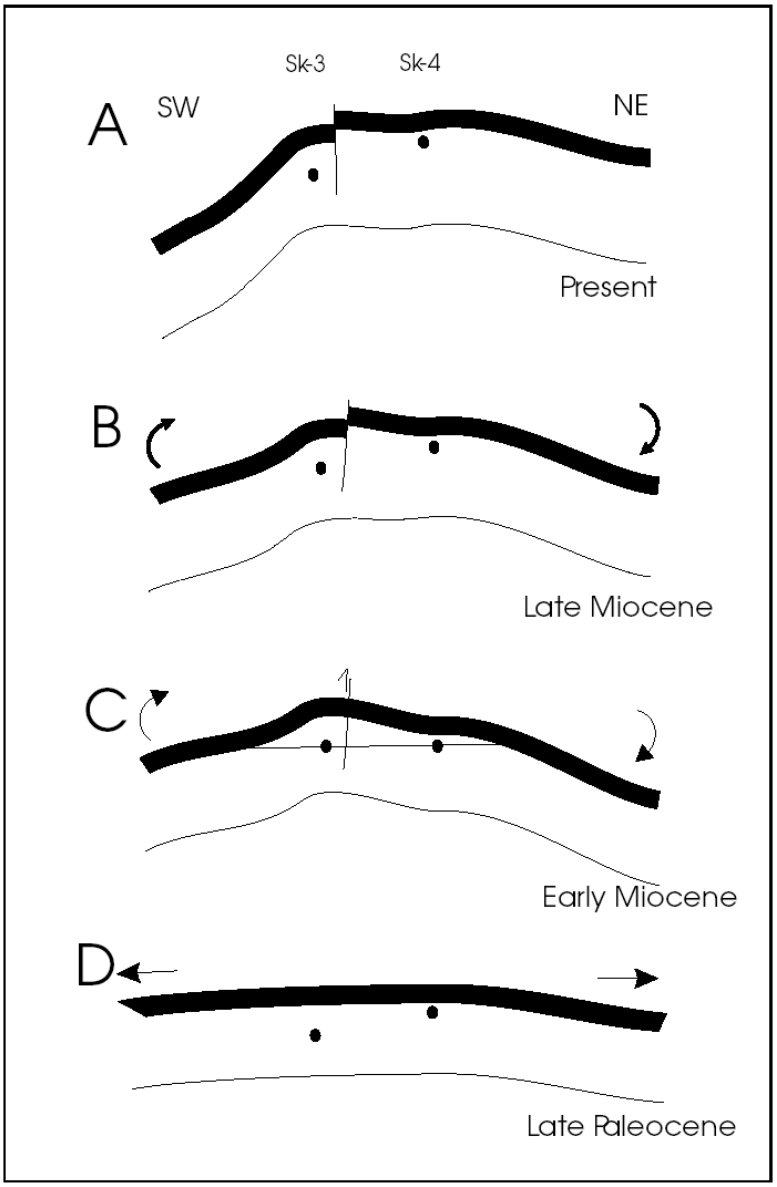

Figure 5-6: Schematic diagram illustrating the Skua structural restoration.

The effect of the 3D restoration on the trap geometry and the reference markers (black dots) provided by the position of the palaeo-OWCs seen in the Skua-3 and 4 wells is illustrated for four key time steps. a). Strike-section through the field at the present day. b). Restoration to Late Miocene horizon rotates the SW end of the trap upwards, which enhances the structural relief on the trap and decreases the depth difference of the palaeo-OWC markers. c). The palaeo-OWC markers are brought to equal depths (1699 mSS) as a result of a small amount of additional rotation and removal of fault displacement during restoration to the Early Miocene horizon. d). Restoration to the Late Paleocene flattens the trap, causing the palaeo-OWC markers to diverge indicating an over rotation of the datum provided by the palaeo-OWC. The thick and thin black lines represent the top and base of the reservoir respectively.

Whilst previous investigations into trap integrity of the Skua Field that highlighted zones of preferential fluid leakage at the intersection of NNW-SSE basement faults with younger fault systems (Cowley and O'Brien, 2000) based on the distribution of Hydrocarbon Related Diagenetic Zones (HRDZs, O'Brien and Woods, 1995) observed in seismic data the restoration work presented in Gartrell et al. (2002) allows for further refinement of the leakage mechanism.

In line with previous studies the Gartrell et al. (2002) study indicate that intersections of pre-rift basement faults with rift faults produced the primary control on hydrocarbon leakage from the Skua structure (Figure 5–8). However, unlike the previous studies Gartrell et al. (2002) locate the most likely leak point where a N-S trending basement fault (BF3 in Figure 5–8) intersects a secondary rift fault located to the east of the Skua Fault (Figure 5–8). The observed coincidence of this fault intersection with both the current OWC and the palaeo-OWC restored to the time of charge shows that it played a key role in controlling the size of the Skua Field through time (Figure 5–8). Support for the controlling role of this fault intersection is also provided by the position of the largest and most prominent of HRDZs observed over the field that is located directly above the identified intersection point.

Unlike previously published models that assign partial trap breach to Mio-Pliocene fault reactivation (O'Brien et al., 1996a; O'Brien and Woods, 1995) the more recent study implies that the initial failure zone was created prior to oil charge in the Early Tertiary. This model explains the absence of high GOI values in samples from the Skua-6 well, which although within structural closure lies below the depth where this key fault intersection penetrates the top of the reservoir.

Under-filling of the trap, reflecting a restricted oil charge, could also explain this observation, but the coincidence of both the palaeo- and current OWCs strongly suggests that the fill capacity of the trap was controlled by this leak point rather than the volume of charge the trap received.

Although less than the palaeo-oil in place previously reported, the decrease in trap capacity is unlikely to reflect the total volume of leaked hydrocarbons, as continued migration into the trap probably occurred over the long time period of leakage.

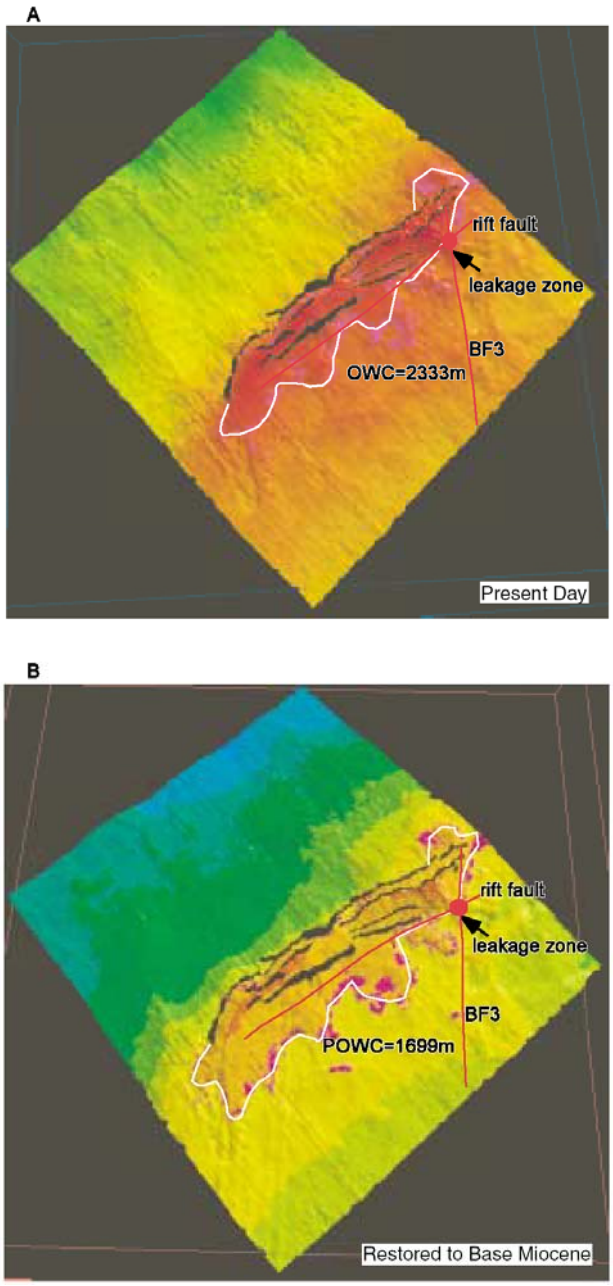

Figure 5-7: Comparison of present day and palaeo-spill points for the Skua Field.

Depth structure maps for the Skua Field are shown for a). Present day field extent determined by OWC depth contour on depth structure map of the base Cretaceous seal horizon (from Gartrell et al., 2002). b). Palaeo-field extent determined by palaeo-OWC depth contour on depth-structure map of the base Cretaceous seal horizon after restoration to Early Miocene (from Gartrell et al., 2002). Note that the position of the intersection point (marked as leakage zone) between the rift fault and the basement fracture (BF3) coincides with the position of the present OWC and the interpreted palaeo-OWC that has been restored to the Early Miocene.

In this situation large volumes may have been lost with modifications to trap size responsible for only a small proportion of total leakage. The apparent efficiency of the leak zone implies that the seal was intensely damaged at this location, highlighting the role of fault intersection points in creating enhanced structural permeability (Gartrell et al., 2004).

Water column geochemical sniffer surveys conducted across the Skua Field (O'Brien and Woods, 1995) demonstrate the hydrocarbon leakage continues to occur from the field with prominent ethane peaks seen in the water column overlying the Skua trap. Whilst these coincide with the fault intersection zone highlighted in the Gartrell et al. (2002) study the response across other faults across the field is also high and it seems likely that further fault reactivation during the Neogene further contributed to a further decrease in trap integrity at Skua. Contemporary leakage probably reflects the ongoing charge that the field is receiving from source kitchens located in grabens adjacent to the field.

An important consequence of the detailed work completed at Skua is the realisation that trap breach within the VSB is not strictly related to the widely reported Neogene fault episode but began with earlier structural modifications. The dynamic nature of traps is clearly demonstrated with traps such as Skua, first created by rifting in the Jurassic experiencing an extended period of ongoing and repeated trap modifications, the collective impact combining to control trap integrity and ultimately capacity.

5.2.2 Jabiru Field

The Jabiru Oilfield (Figure 5–1) represents the first and largest commercial oil field discovered in the Vulcan Sub-basin (Cadman and Temple, 2003). The discovery well, Jabiru-1A, was drilled in September 1983 and intersected a 57m thick gross oil column that flowed 42.5° API oil from Lower and Upper Jurassic sandstones at rates of 6000 STB/D and 3466 STB/D respectively (MacDaniel, 1988).

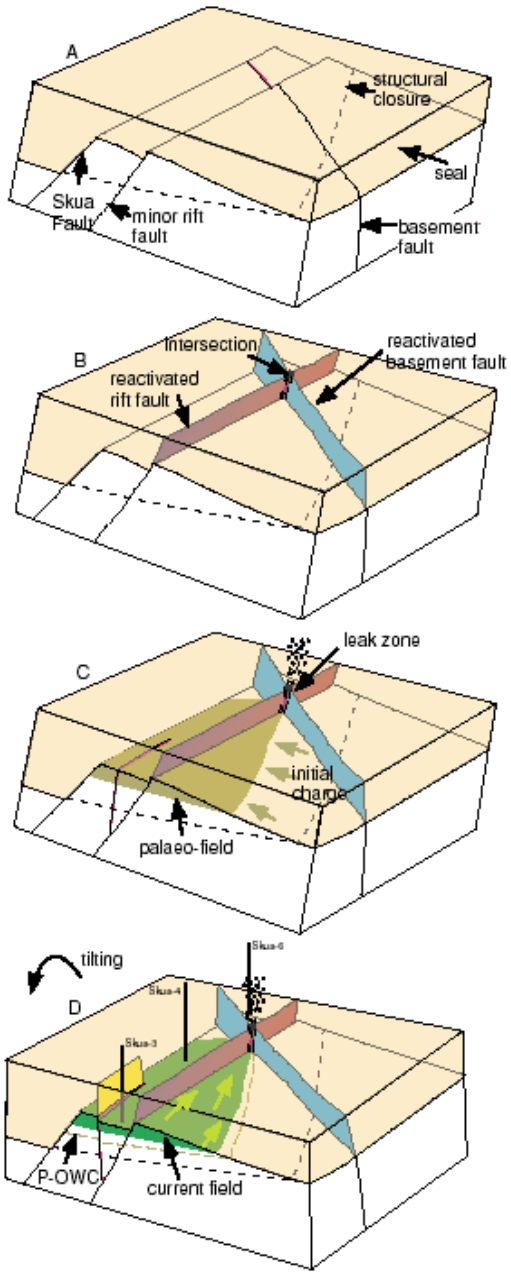

Figure 5-8: Revised model for charge and retention at Skua.

Integrated structural and charge history model for the Skua Field (from Gartrell et al., 2002). a). Prior to reactivation and hydrocarbon charge. b). Late Cretaceous to early Tertiary reactivation of basement fault and subordinate rift fault causes intense seal damage at the intersection of the faults. c). Initial oil charge around the Early Miocene. Extent of the palaeo-field is controlled by the location of the fault intersection (leak zone). d). Palaeo-OWC is tilted due to post rift subsidence and faulted due to Early Miocene deformation. Tilting of the trap also causes hydrocarbons to flow up-dip towards the NE to continually feed the leak zone. Note: leakage of hydrocarbons is into overlying strata and not directly to the seafloor.

Lower Cretaceous shales overlying the base-Cretaceous unconformity provide the top seal and combine with Upper Jurassic shales in the hangingwall to provide lateral seal. The reservoir for the field is provided by two excellent quality, high net/gross sandstone reservoirs, one within the *W. spectabilis* biozone of the Upper Jurassic Flamingo Group and the other comprising sandstones within the *C. torosa* biozone of the Lower Jurassic Plover Formation (MacDaniel, 1988). An intervening shale divides these two intervals, except on the field crest where the shale has been eroded allowing direct communication between these reservoir units and reservoir pressure data indicate the oil zone is well connected despite abundant intra-reservoir faults.

Mapping of the Jabiru structure has been hampered by the lack of a reliable seismic event near the reservoir horizon, intense and poorly imaged faulting and associated strong reservoir thickness variations resulting from syn-depositional fault-controlled subsidence. Early appraisal wells were not optimally located due to this combination of poor seismic data quality and depth conversion errors that are related to shallow velocity variations. As a consequence many of the appraisal and development wells had to be sidetracked in order to reach the reservoir in an optimal location.

Prior to the acquisition of better-quality 3D seismic data, the structure was interpreted as a horst-block formed initially during Jurassic extension and then inverted during Neogene tectonism (Figure 5–9). Strike-slip features which were not recognized on the early seismic data could be clearly mapped after several appraisal wells had been drilled and a higher quality 3D seismic survey had been shot and interpreted (Nelson, 1989).

Jabiru-2 (Figure 5–10), also drilled in 1983, penetrated the Intra-Valanginian unconformity deep to prognosis depths and below the OWC and was plugged and abandoned with no significant hydrocarbon shows. Jabiru-3 (BHP Petroleum Ltd., 1984a) and Jabiru-4 (BHP Petroleum Ltd., 1984b; Figure 5–10) successfully penetrated the oil column but encountered thin and sub-economic reservoir sections that led to a substantial reduction in the estimated in place oil volumes (Wallace and Balnaves, 1988).

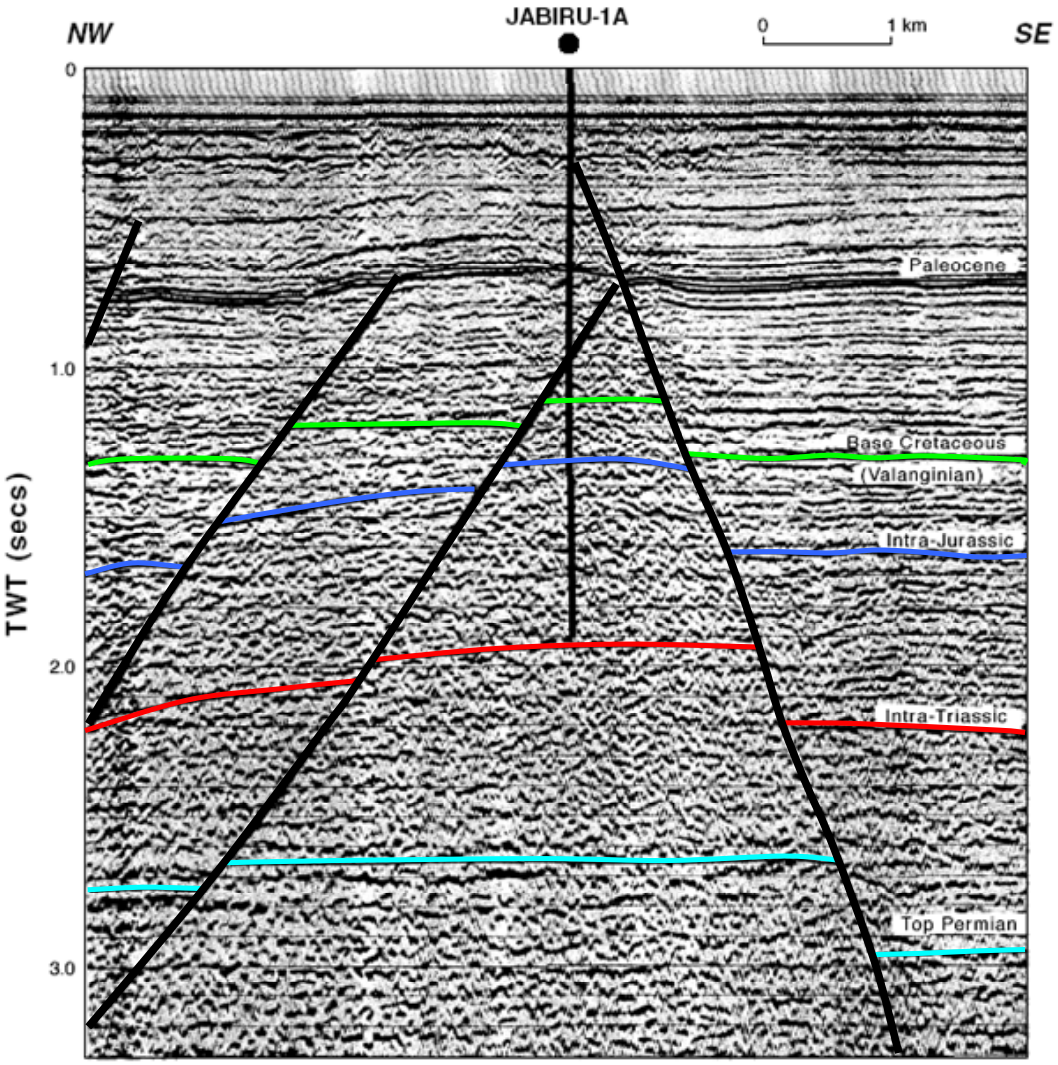

Figure 5-9: Seismic line across the Jabiru Field.

A NW-SE orientated seismic section across the Jabiru Field (from Nelson, 1989) and through the Jabiru-1A well location, showing the early interpretation of the structure as a reactivated horst-block (Nelson, 1989). Note the recent inversion of the footwall that is associated with Neogene tectonics responsible for the fault reactivation that also implies a degree of strike-slip motion. Vertical scale is given in seconds of two-way time (TWT) whilst a horizontal scale bar for one kilometre is also shown. Interpreted seismic horizons are labelled at the left margin of the line. The location of the seismic line is shown in Figure 5-11.

Despite these early set-backs the acquisition of a full 3D seismic grid over the field enabled the full extent of the field to be determined, although most of the subsequent successful appraisal wells proved to be challenging. A total of 15 appraisal and development wells have been drilled on the field over the period 1983-2000.

5.2.2.1 Sampling Details

GOI data have been collected on three wells from the Jabiru Field including the discovery well, Jabiru-1A and the first two appraisal wells drilled on the field. Each of these wells showed fluid inclusion evidence to support the presence of a palaeo-hydrocarbon column extending below the current OWC. However when compared on a common depth datum it becomes obvious that a complex interpretation is required as the implied palaeo-OWCs determined in each well occur at different depths. In addition the data appear to imply the presence of palaeo-gas zones in the Jabiru-2 and Jabiru-3 wells (Figure 5–11) that currently lie structurally lower than the palaeo-oil zone defined from the Jabiru-1A well.

The Palaeo-OWCs defined from GOI data in the Jabiru-1A and Jabiru-2 wells occur at about the same depth (within the error associated with sample spacing) but the palaeo-OWC in Jabiru-3 is about 20m shallower and is well constrained by the spacing of the available samples (Figure 5–11).

In addition the Jabiru-2 and Jabiru-3 wells both exhibit a zone of low GOI values near the top of the reservoir section that appear not the be a reflection of poor reservoir quality and instead have been interpreted to be possible palaeo-gas caps. The palaeo-gas zone seen in Jabiru-2 does not correspond in depth to a similar zone seen in Jabiru-3 and indications of high palaeo-oil saturation in Jabiru-1A extend higher than the palaeo-GOCs seen in either Jabiru-2 or Jabiru-3 (Figure 5–11).

Unlike the detailed analyses available for the Skua Field no additional GOI data were available for other wells from the Jabiru Field. As a result of the limited constraint provided by only three wells it is difficult to reach firm conclusions on the geometry of the palaeo-hydrocarbon columns in such a structurally complex field. Further sampling of key wells is needed for a more definitive solution to be reached.

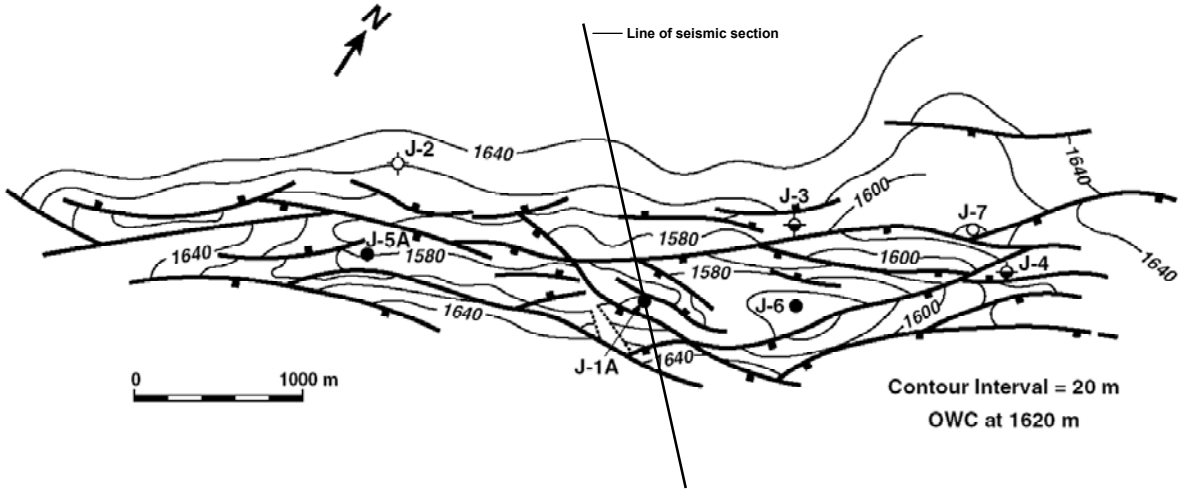

Figure 5-10: Structure map of the Jabiru Field.

Depth-structure map (depths given are in metres subsea, mSS) showing the location Jabiru well one through seven together with the major faults and depth contours on the top W. spectabilis level corresponding to top porosity for the main reservoir (from Wallace and Balnaves, 1988). The position of the seismic line shown in Figure 5–10 is also displayed. The Jabiru structure is a highly faulted elongate horst block with a field wide OWC at 1620mSS indicating that the trap as mapped is not currently filled to structural spill.

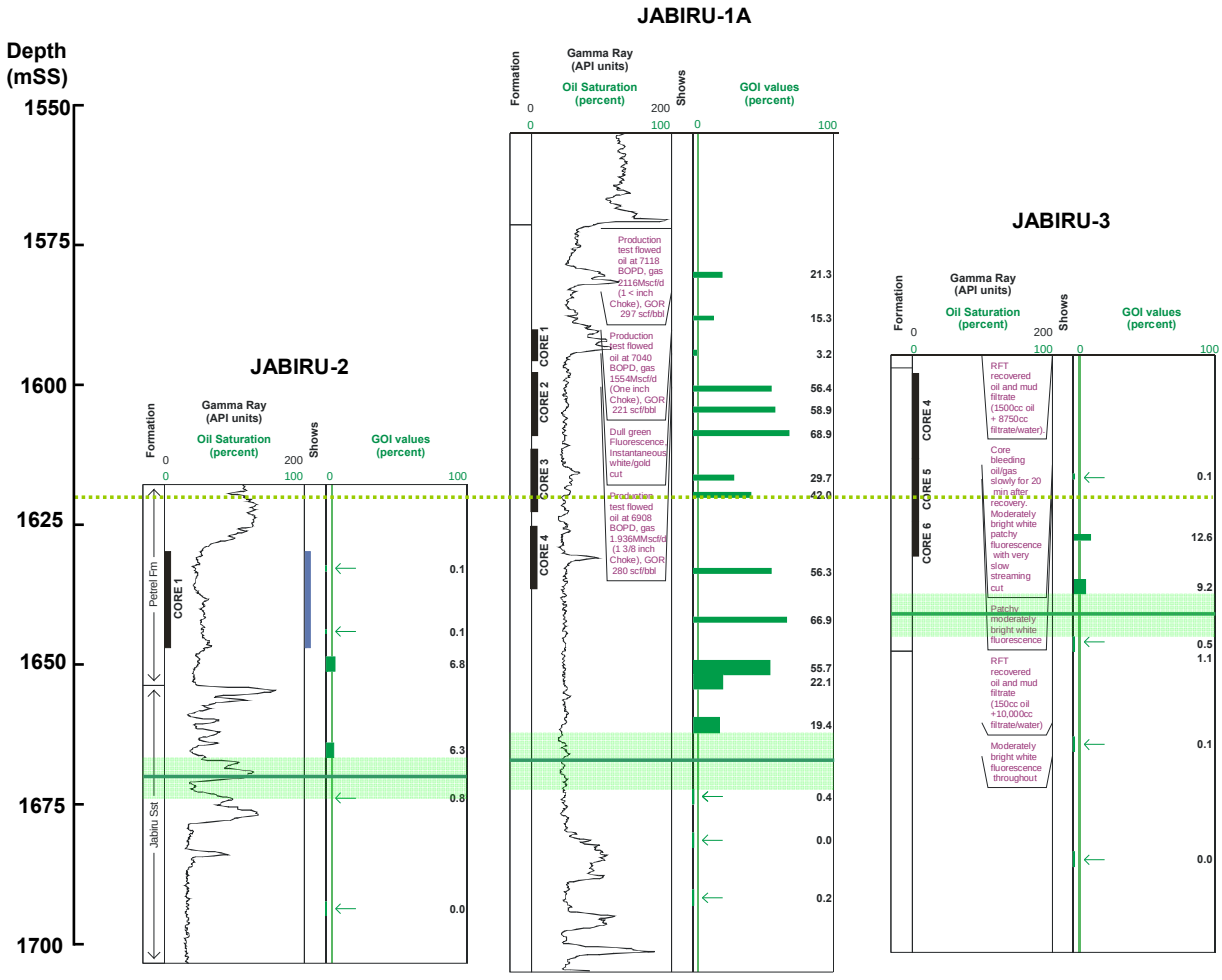

Figure 5-11: GOI results from the Jabiru Field.

GOI logs for the Jabiru-1A, -2 and -3 wells shown on a common datum (metres sub sea, mSS) to demonstrate the variable position of the palaeo-OWCs defined in each well. Each of the GOI logs records GOI data against the gamma ray log and where available information on conventional shows and fluid recoveries, the location of cores and the values of petrophysically defined oil saturation. The current OWC is shown by the dashed green line, whilst the palaeo-OWCs are shown as the solid green lines with the transparent shading indicating the range that is possible based on current sample density. Low GOI values seen in samples from the upper parts of Jabiru-2 and -3 are interpreted to represent palaeo-GOCs. Refer to Chapter 4 for individual GOI figures.

5.2.2.2 Charge Model for the Jabiru Field

The value of integrating the results from single wells with the available geological data becomes obvious when results from fields like Jabiru are considered. Whilst apparently reasonable interpretations can be made of the individual well results consideration of the GOI results between wells highlights obvious inconsistencies. The palaeo-gas zones implied for Jabiru-2 and -3 wells that penetrate hangingwall fault compartments are difficult to explain relative to the continuous palaeo-oil zone seen in the up-dip Jabiru-1A well that tests the adjacent footwall fault block. Similarly the palaeo-OWCs defined from the GOI data are within error of the sample spacing in Jabiru-1 and Jabiru-2 but about 20m shallower in the Jabiru-3 well.

Whilst it always remains possible that the absence of abundant fluid inclusions within rocks that have experienced high oil saturation can be attributed to the lack of a suitable trapping mechanism for the formation of inclusions this option is not well supported by the data from the VSB. Where high GOI values have been encountered it is extremely rare to see wildly variable values in the one contiguous section, rather sharp transition from consistently high values to consistently low values is observed, except where a clear reason for reduced oil saturation is present (i.e. reduced permeability due to reservoir quality decline). If inclusion trapping was highly sensitive to appropriate conditions then it would appear more likely that erratic GOI profiles would be the result, yet such profiles are not commonly observed in the VSB or elsewhere the technique has been applied.

Unfortunately a unique solution is not always available, particularly where there is limited well or sample control and this makes it necessary to carry a range of possible scenarios to capture the uncertainty. As was seen with the Skua Field the palaeo-contacts defined by the GOI data reflect the initial charge of the trap and are sensitive to subsequent changes in trap geometry produced by structural modifications that postdate initial filling of the trap.

At Jabiru the main episode of trap modification involved structural inversion and fault reactivation, which occurred during the Miocene-Holocene strike-slip phase. The principal fault throughout the structural evolution of the Jabiru Field is

interpreted to be a steep fault located along the southeastern margin of the field, which has a maximum throw at top-reservoir level of 100 m and extends into the basement. Inversion was asymmetric, occurring mainly along this fault (Nelson, 1989). This is likely to have produced significant changes to trap geometry with the crest of the structure migrating towards the southern side of the trap. The relative position of palaeo-fluid contacts will have been modified by these changes and palaeo-gas caps trapped in structural culminations on the northern side of the field downthrown to their current position.

Alternatively the high degree of structural complexity produced by the abundant faults that transect the reservoir implies a segmented structure with opportunities for pressure compartmentalisation. The palaeo-gas zones inferred for the Jabiru-2 and -3 wells could reflect isolation from the main field as these wells test separate fault blocks on the flanks of the field.

Although the numerous intra-field faults compartments that characterise the field are currently in pressure communication, based on the common oil and water pressure gradients shared by wells that test the different blocks, this does not preclude the possibility of that the field was compartmentalised in the geological past. Neogene fault reactivation resulted in revised cross-fault juxtaposition relationships that could have resulted in partial breaching of sealing faults that allowed the fluid contacts to equilibrate to the common OWC seen today.

Unfortunately the high level of structural complexity in the Jabiru Field coupled with the difficult nature of the seismic data make it difficult to arrive at a firm conclusion but this result serves to demonstrate the importance of drawing on all available information when attempting to reconstruct hydrocarbon charge histories.

5.2.3 Challis Field

The Challis Field (Figure 5–1) was discovered in 1984 when BHP Ltd. drilled Challis-1, to test an eroded Triassic horst block and encountered a 29m thick gross oil column in Triassic sandstones of the Challis Formation. This structure, referred to as the Cleghorn Horst, also hosts the smaller Cassini oil field and forms one of a

series of en echelon structures that create many of the hydrocarbon traps in the northern part of the VSB.

The reservoir sands sub-crop the Valanginian unconformity and are sealed by claystones, marls and fine-grained carbonates of the Cretaceous Bathurst Island Group (Wormald, 1988; Gorman, 1990). High quality reservoir sandstones of the Middle-Upper Triassic Sahul Group were deposited as laterally extensive sand sheets, consisting of amalgamated estuarine channel sand bodies (Gorman, 1990).

Subsequent appraisal wells (Gorman, 1990) intersected oil at various stratigraphic intervals defined by the Triassic sub-crop relationship (Figure 5–12), but with all reservoirs sharing a common OWC at about 1410.5 m TVDSS (Figure 5–12).

Appraisal of the field by Challis-2A, drilled in 1986 about 1.5 km east of the discovery well, added an additional 6 m of net oil pay in a younger Triassic sand (the CS2.2 reservoir) that was not seen in Challis-1. Subsequent drilling of further appraisal wells intersected oil within numerous Triassic reservoirs (informally named the CS2.2, CS2.3 and CS3.1 reservoir units) but Challis-4 found the CS2.3 reservoir to have virtually shaled-out, whilst the base-Cretaceous unconformity in Challis-5 came in 33 m low to prognosis and the CS2.3 reservoir was not penetrated. In contrast wells drilled to appraise the northeast extent of the field were successful, defining further reserves in three older Triassic reservoirs (CS4.1, CS5.4 and CS6.1).

While Challis-6 was being drilled in 1988, well Cassini-1 was drilled to the south-west of the Challis Field to test a structural culmination within the same horst structure, being separated from the Challis closure by a small intervening saddle (Figure 5–12). The well, sidetracked due to mechanical difficulties with the main hole, encountered 19 m of net oil-bearing sand, but with an OWC 7m deeper than then seen at Challis. An appraisal well, Cassini-2 intersected the base Cretaceous unconformity 37m low to prognosis and 19m below the OWC from Cassini-1.

Virtually all production is from only one reservoir unit (the CS2.3 unit, Figure 5–12), which has 15m of average net pay with an average permeability of 1320 mD.

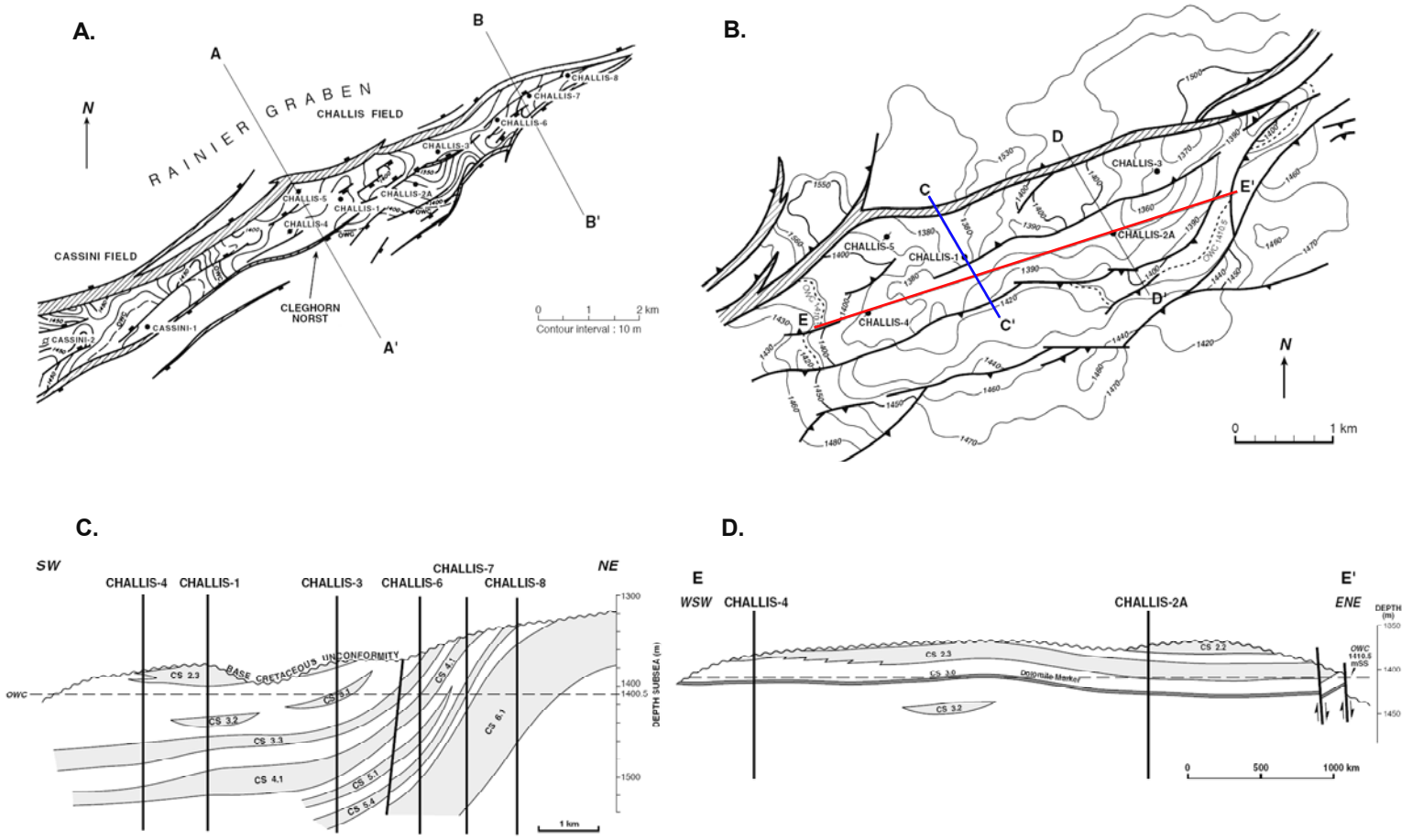

Figure 5-12: The Challis-Cassini Field

Top reservoir maps showing wells drilled across the Challis and Cassini fields and cross sections for the Challis Field. A. Structure map of the Cleghorn Horst, including the Challis and Cassini fields, at base-Cretaceous level (Gorman, 1990). B. Structure maps of the Challis Field at the top of the CS2.3 reservoir (the main reservoir). Blue and red lines indicate the position of cross sections shown in C. and D. respectively. C. and D., Schematic SW-NE and WSW-ENE structural-stratigraphic cross-sections of the Challis Field showing the nature of the sub-cropping reservoir units below the Base Cretaceous Unconformity (Gorman, 1990).

This reservoir shows good inter-well communication, which is not significantly impaired by the many intra-field faults or by major stratigraphic flow-barriers that relate to the complex sub-crop geometry (Figure 5–12).

5.2.3.1 Sampling Details

Three wells from the Challis-Cassini Field complex have been sampled in the current study with GOI data showing variable profiles (Figure 5–13). The GOI results from Challis-1 were difficult to interpret with values falling well below the empirical threshold for oil accumulation despite coming from an interval that is currently oil-bearing. This observation could be attributed to the shallow depth of burial, perhaps indicating there had been insufficient loading to generate fractures needed to trap oil inclusions or due to the paucity of authigenic quartz overgrowths in these samples.

However, the results from Cassini-1ST and -2 both showed samples with GOI values that exceeded the 5% empirical threshold. In Cassini-1 a zone of high GOI values was overlain by samples with low GOI values and in the presence of good reservoir has been interpreted to reflect the presence of a palaeo-gas cap (Figure 5–13).

A similar result, albeit based on only two samples, was recorded in Cassini-2 but in this instance the uppermost sample with a low GOI value occurred in poor quality reservoir and could have implied either a palaeo-gas cap or low oil saturation related to the presence of tight, low permeability rock. The latter interpretation was initially favoured as a comparison in TVD placed the possible palaeo-gas zone at an equivalent depth as the palaeo-oil zone seen in Cassini-1ST (Figure 5–13).

5.2.3.2 Charge Model for the Challis-Cassini Field

The integration of the GOI results from the Challis-Cassini wells with the reservoir framework defined by chronostratigraphic correlation of high resolution biostratigraphic data makes the interpretation of the data more straightforward and highlights the need to place GOI results in geological context.

Unlike the variable interpretations that are required to explain the results when considered individually a single explanation is possible when the data are considered collectively within a well constrained geological framework. Figure 5–13 showing the GOI results relative to the chronostratigraphic correlation of the field described by Gorman (1990) helps to unravel what initially appears to be conflicting results.

The lateral correlation of the upper CS2.3 sand demonstrates the generally westerly dipping orientation of Triassic sediments along the Cleghorn Horst. The low GOI values recorded in the CS2.3 sand in Challis-1 are interpreted to represent the upper part of an original gas zone in the Challis Field that extended down to the base of this sand at the well intersection (Figure 5–13).

The Cassini-1ST well tested the same reservoir sand in a down-dip position from the Challis-1 location and also records low GOI values at the top of this sand (Figure 5–13). Deeper samples from the same sand, however, show high GOI values and define the location of the palaeo-gas oil contact at the mid-point between the shallowest high GOI sample and the deepest low GOI (palaeo-gas zone) sample. The position of the palaeo-OWC in Cassini-1ST could be taken as a mid-point between the deepest high GOI sample and the shallowest low GOI sample, but as this occurs within a different sand this interpretation is poorly constrained and influenced by the thick low net to gross section that precludes the sampling of reservoir material from the intervening section (Figure 5–13).

A lack of samples from the chronostratigraphically equivalent sand in the down-dip Cassini-2 well further precludes an opportunity to determine the thickness of the palaeo-oil leg present in the CS2.3 sand sampled in Cassini-1ST (Figure 5–13).

Higher in the Cassini-2 well, a stratigraphically younger, shaly sand also appears to have tested a palaeo-gas zone with an underlying palaeo-oil zone (Figure 5–13), again a lack of deeper samples precludes any greater constraint on the thickness of the palaeo-oil zone or the position of the palaeo-OWC. Collectively with the GOI results from the Challis-1 and Cassini-1ST and -2 wells appear to define a stacked palaeo-hydrocarbon zone.

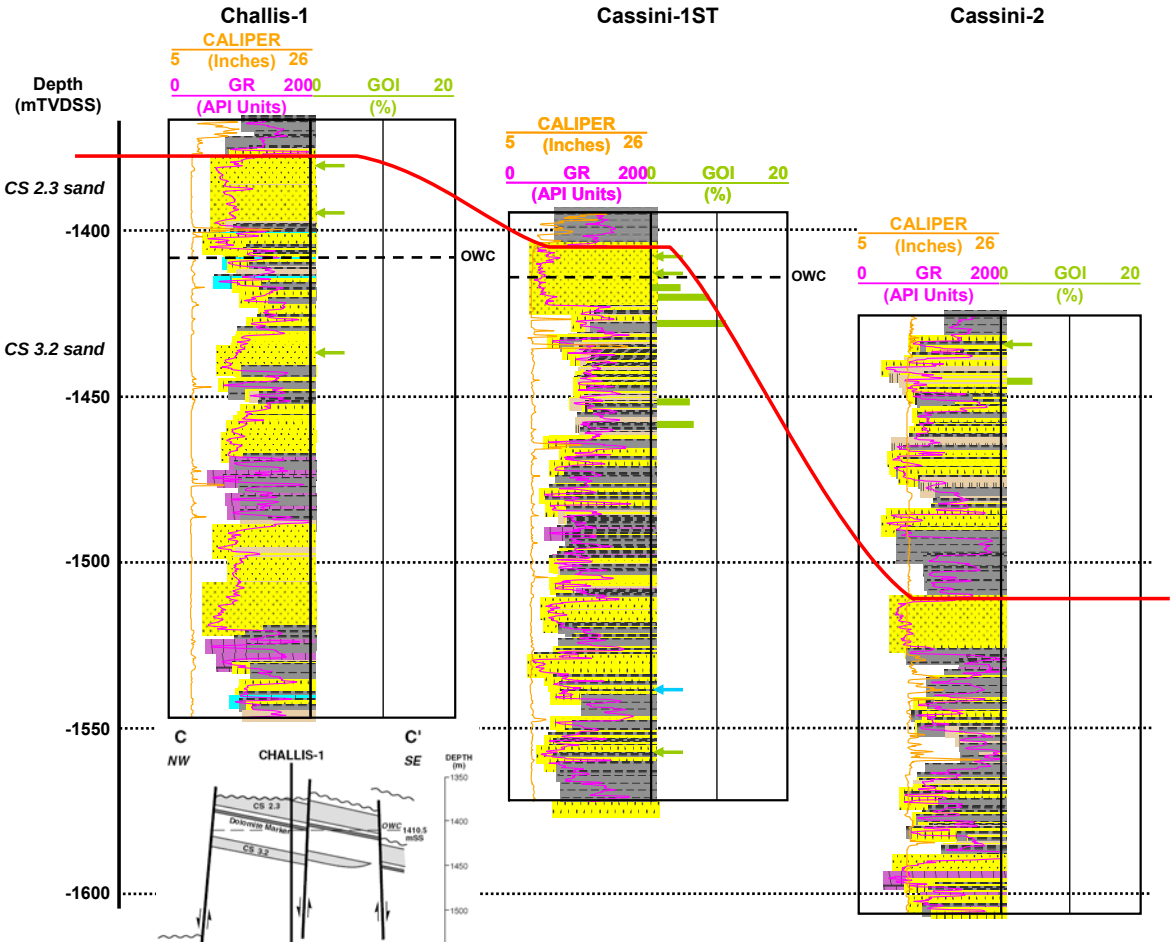

Figure 5-13: GOI results from the Challis-Cassini Field.

GOI results for Challis-1, Cassini-1ST and Cassini-2 displayed on a common depth datum (True Vertical Depth Sub Sea, TVDSS). GOI data are given relative to the gamma ray log with green arrows indicating samples where GOI values were less than 1% and blue arrows denoting samples that were devoid of oil inclusions. The top of the main CS 2.3 reservoir is shown as the red line. The palaeo-gas zone inferred at the top of Cassini-1ST is consistent with the palaeo-gas zone indicated by the low GOI values in the up-dip intersection of this sand in Challis-1. The base of the CS 2.3 reservoir lies above the palaeo-oil zone seen in Cassini-1ST so the lateral equivalent of this zone is not seen in the Challis-1 well. A second palaeo-oil and gas zone recorded in the Cassini-2 well occurs in a stratigraphically younger reservoir and is not a correlative for the Cassini-1ST well.

In Challis-1 the lowest sample comes from the stratigraphically older CS3.2 sand that is not represented in the Cassini-1ST well and presumably shales out. High GOI values seen in shaly sands at an equivalent depth in Cassini-1ST are within a stratigraphically younger section and are likely layer bound up-dip from the well.

Collectively the integration of the relevant datasets indicate hydrocarbon charge to the Challis-Cassini area involved both gas and oil with the initial fill comprising a gas cap that probably extended across much of the now oil-bearing Challis structure and that was underlain by an oil-leg. The original position of the palaeo-OWC for this oil-leg is not defined on the current data, instead only a palaeo-oil down to level can be described, but this lies below the current OWC in Cassini-1ST and suggests that the now separated fields were originally part of a single accumulation. A second palaeo-hydrocarbon column is seen in the younger Triassic section penetrated by the Cassini-2 well but this appears to have been isolated from the deeper palaeo-column and is interpreted to represent stacked palaeo-oil and gas columns.

The outcome from sampling individual wells across a single structural closure demonstrates that obtaining a good understanding of the nature of the trap is imperative if sensible and robust interpretations are to be reached. This example also shows the value of gaining this perspective prior to samples being taken rather than selecting a suite of samples based on an interpretation of the electric logs from each well independently and then convolving an integrated interpretation once the GOI results have been produced.

5.3 GAS FIELD CHARGE HISTORIES

The structural style in the VSB, favouring narrow horst blocks and traps that are heavily segmented by faults, often with relatively low amplitude structures, results in closures that are typically too small to be viable as gas fields on economic grounds. This situation is in stark contrast to oil fields where even relatively modest volumes can form the basis of viable commercial development.

Consequently where gas has been discovered it is important to ascertain if traps were previously filled with oil so that other un-drilled features can be assessed. Where

prior oil charge can be demonstrated this can provide tremendous incentive to drill for an oil-leg where a gas down to level has been defined and additional closure down-dip of that depth could contain a displaced oil-leg.

Fluid inclusion methods provide a useful may to determine the palaeo-charge history in currently gas-bearing traps initially be detecting the presence of palaeo-oil then by providing the ability to clearly differentiate migrated oil from a previous accumulation. Perhaps the most significant contribution from the fluid inclusion methods compared with standard techniques is the ability to accurately delineate the position of palaeo-fluid contacts.

This enables the volumes initially emplaced to be estimated thereby providing greater constraints to be placed on possible volume of oil that may reside down-dip, occupying the space between a gas down to level and the lowest closing contour that defines the spill point of the trap (Figure 5–14). Whilst it remains possible that gas charge has also flushed this untested zone of any oil it allows the volumetric potential of this zone to be evaluated and consequently decisions about the merits of appraisal drilling can be considered with more certainty. Displaced oil may also provide charge to nearby traps (Figure 5–14) so the risk of oil charge to these features is also lessened by the collection of this type of data.

Evaluating the hydrocarbon charge history in presently gas-filled traps also requires consideration of the complex interplay between the composition of the hydrocarbons and the PVT environment prevailing during and after the period of active hydrocarbon charge. The miscibility of liquid hydrocarbons into gaseous hydrocarbons is a critical factor in assessing oil-leg potential to avoid erroneous predictions from being made.

Where gas migration follows initial oil accumulation the formation of a gas cap will depend on the composition and volume of gas charging the trap, the composition of oil within the trap and the reservoir pressure and temperature at the time of charge. Initially gas reaching the trap will be absorbed into the oil until saturation is achieved (bubble point) and a discrete gas cap is formed under equilibrium conditions.

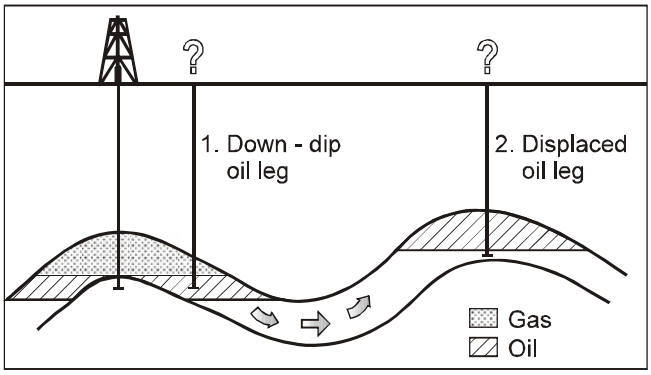

Figure 5-14: Oil-leg potential in gas fields

A summary cartoon showing the new play concepts that are created by the recognition of oil-leg potential in presently gas-bearing sands where no Gas-Oil-Contact has been defined. The drilled well tests an anticline that intersected a gas down to within a stratiform reservoir horizon, whilst the recognition of prior oil charge to that section promotes the opportunity for oil to have been displaced down-dip and eventually across the spill point to allow for further lateral migration. A follow up well could be drilled to test for a deeper oil-leg in the same structure or an up-dip satellite structure could be targeted.

Subsequent gas charge will not be entrained in the oil-leg but will bubble through the oil to increase the size of the gas cap and push the oil leg deeper in the structure. Equilibrium between oil and gas phases will also change with increasing temperature and pressure so the conditions will be dynamic.

The capacity for gas to absorb oil increases as temperature and pressure rise (Figure 5–15). Reservoired oil will also respond to additional burial of the trap as the gas becomes more able to absorb additional oil causing oil to increasingly partition into the gas phase. With sufficient pressure increase the complete loss of oil can occur once the dew point of the gas is reached. The amount of oil that can be lost into the gas is controlled by the composition of gas charging the trap and the greatest loss of oil will occur when the gas is composed purely of methane.

5.3.1 Swan Gas Field

The enigmatic Swan gas field, located about 20 km to the northeast of the Puffin oil field (Figure 5–1), has proven difficult to define. The proven gas column is layer bound within a number of discrete sandstone beds that collectively form part of a submarine fan complex (Maastrichtian Puffin Formation) and trapped against an interpreted salt diapir (BHP Petroleum Ltd., 1992). Despite an appraisal period covering 18 years (1973-1991) with 3 successful exploration wells the field remains uneconomic, due mostly to uncertainties regarding the lateral distribution of the reservoir and accurate depth conversion. These uncertainties in turn contribute to an ill-defined GWC and only limited constraint on the volume of gas currently trapped. The presence of gas down to levels rather than a GWC also leaves open the opportunity for an oil-leg to be present beneath the proven gas column, potentially providing a more lucrative exploration target.

The timing of hydrocarbon charge is significant for the understanding of the Swan gas accumulation. Detailed structural analysis of the growth of both the Swan and Paqualin salt structures and inferred from fault collapse features at the crest reveals that the salt began to move and form salt pillows in the Late Jurassic, but that salt diapirism responsible for the creation of the Swan trap, only occurred towards the end of the Miocene (Smith and Sutherland, 1991).

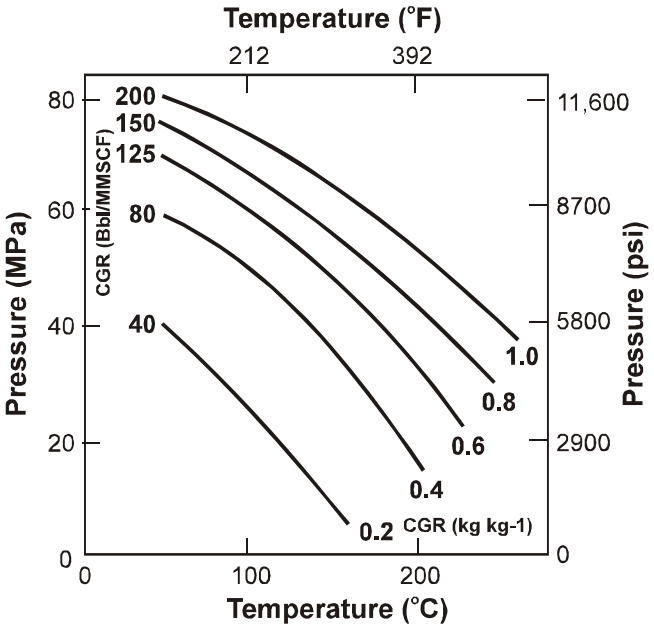

Figure 5-15: Changes in CGR of gas with changing pressure and temperature.

Graph showing the solubility of oil in methane with varying pressure and temperature, using experimental data from Price et al. (1976). With increasing temperature and pressure methane can progressively absorb a greater volume of oil leading to an increased Condensate-Gas-Ratio (CGR).

The discovery well, Swan-1, targeted a Cretaceous clastic fan sealed against the interpreted salt diapir and encountered gas in thin calcareous sandstones of Upper Cretaceous age. In addition to the electric log analysis, gas was confirmed by the formation interval tester (FIT) tool, which recovered 72.6 cubic feet of gas and 625 cubic centimetres of colourless condensate (ARCO Australia Ltd., 1973).

The Swan-2 well was drilled in 1980 to test Middle Jurassic sandstones with the Cretaceous sandstones, representing a secondary objective (CITCO Australia Petroleum Ltd., 1980). The Jurassic primary objective was not reached but the Upper Cretaceous sandstones were gas-bearing as indicated by high measured gas levels and resistivity log response.

Significant gas readings were also noted in thin Lower Cretaceous sandstones, but electric logging was compromised by drilling problems associated with elevated formation pressure. Testing of both Cretaceous sections failed to recover any hydrocarbons, which was attributed to overpressure problems. The well was subsequently plugged and abandoned.

A further 11 years passed before BHP Petroleum Ltd. drilled the Swan-3 well in 1991 to further evaluate the Upper Cretaceous sandstones that had been found to be gas bearing in the previous Swan-1 and -2 wells. Three discrete sand bodies, informally referred to as the P1, P2 and P3 sands of the Puffin Formation, were targeted within a closure considered to be a combined structural-stratigraphic trap associated with reservoir onlap against the interpreted salt diapir (BHP Petroleum Ltd., 1992). The well was technically successful with the P1 and P2 sands found to be entirely gas bearing and a total of 19.4m of net gas pay was interpreted. Associated direct and cut fluorescence, particularly towards the base of the drilled section was also noted, which could indicate proximity to a down-dip oil-leg.

The P3 sand was not encountered in the straight hole and the well was sidetracked (Swan-3ST1) 250m south of the original location to successfully intersect the P3 sand. RFT pressure data indicated the P3 sand was also fully gas saturated.

The Swan-3 and Swan-3/ST1 wells proved a significant, yet sub-economic, gas column within the Puffin Sandstone but no fluid contacts were identified and it remains unclear if these gas sands are connected to those seen in the Swan-1 and Swan-2 wells. Ultimately the discovery of gas was disappointing with insufficient reserves to justify development and the wells were plugged and abandoned without further flow testing.

Post-drill appraisal of the Swan-3 and 3ST wells provided indications of an associated oil-leg from reservoir pressure data and PVT measurements made on the recovered condensate fraction. This was supported by later sediment extract geochemical analysis the showed increased level of heavy hydrocarbons that were interpreted to reflect residual oil left over from an oil column that had been subsequently flushed by gas (BHP Petroleum Ltd., 1992).

Despite being sub-economic the Swan gas field is an ideal candidate for the application of the GOI technique to more definitively ascertain the charge history of the trap and in particular provide a constraint that enables the palaeo-oil volumes to be estimated. Given a significant volume of prior oil charge, incentive to conduct further exploration may be justified, particularly if improved seismic imaging of the trap could be achieved. In recent years seismic imaging close to salt has improved dramatically (Sava, 2006), both in terms of better processing (Etgen et al., 2009), but also in regard to the development of new acquisition techniques such as wide or multi-azimuth seismic (Long, 2010).

5.3.1.1 Collective Interpretation of the Swan Field GOI Data

The relationship between the GOI results from the different Swan wells sampled is displayed graphically in Figure 5–16. From this display the spatial position of the high GOI samples that define the palaeo-oil zones appear to reveal two separate palaeo-oil columns that have been sampled across multiple wells.

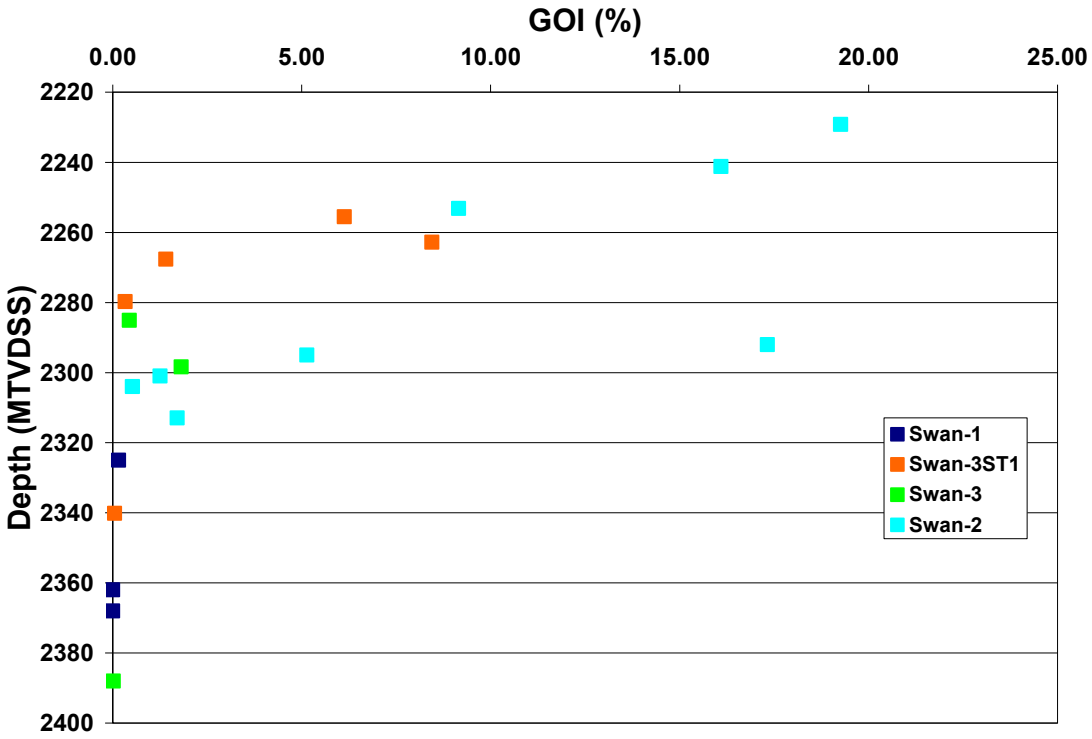

Figure 5-16: Initial assessment of GOI results from the Swan Gas Field.

Graph showing GOI values recorded in samples from the four Swan wells sampled plotted in Metres True Vertical Depth Sub Sea (TVDSS). Overall there is a reduction in GOI with depth consistent with a downwards decreasing hydrocarbon saturation profile. Two discrete palaeo-oil zones can be discerned, one that extends at least at deep as 2263mTVDSS and a second one from 2292-2295mTVDSS. Low GOI values seen between 2280-85mTVDSS define the first clear palaeo-water zone, whilst consistently low GOI values in samples from 2325mTVDSS and deeper define a second palaeo-water zone. In both cases a number of intermediate (>1% but <5%) values lie between the clear high (>5%) GOI values and the clear low GOI (<1%) values making it difficult to accurately locate the position of clear palaeo-OWCs.

The uppermost palaeo-oil zone extends from the shallowest sample at 2229mTVDSS to at least at deep as the 2263mTVDSS sample before GOI values reduce sharply in the samples from 2268-85mTVDSS where GOI numbers range from 1.4 to 0.3%. The uppermost of these three samples has a GOI value slightly higher than is typical for water zone samples where GOI values of <1% are expected. This could imply close proximity to the palaeo-OWC suggesting the contact lies closer to 2268mTVDSS than 2263mTVDSS, where the last high (>5%) GOI value was seen.

A second palaeo-oil zone is inferred from samples taken across 2292-2295mTVDSS. Below 2295mTVDSS a number of intermediate (>1% but <5%) make it difficult to locate a clear palaeo-OWC based on standard protocols for interpreting GOI data (i.e. <1% = migration without accumulation and >5% = palaeo-oil accumulation). As discussed for the upper zone these intermediate GOI values often occur close to the palaeo-OWC and where cuttings samples are involved can represent bracketing of the palaeo-OWC. Alternatively, if reservoir properties degrade near the base of the inferred palaeo-oil column then these intermediate GOI values can simply reflect lower oil saturation, possibly indicating a transition zone.

The simple relationship between the Swan wells illustrated in Figure 5–16 can be further interpreted by incorporating the results into their geological context, where the samples from the four wells analysed are displayed against a gamma ray log, are placed on a common depth datum (metres below sea-level) and proportionally spaced to reflect their geographic spacing (Figure 5–17). This projection allows the different GOI data from each sandstone horizon to be compared in true vertical depth and against a biostratigraphically constrained chrono-stratigraphic correlation.

Figure 5–17 shows at least two possible ways to interpret the observed GOI values depending on whether the P1 and P2 sandstones are in communication. If the P1 sand is isolated from the deeper sands then the high GOI values seen in samples from the P1 sand in Swan-2 and Swan-3ST wells could define a strata bound palaeo-oil column. The low GOI value (1.4%) seen in the lowermost P1 sample from Swan-3ST could indicate crossing of the palaeo-OWC or, given the high gamma ray response, could reflect poor reservoir quality.

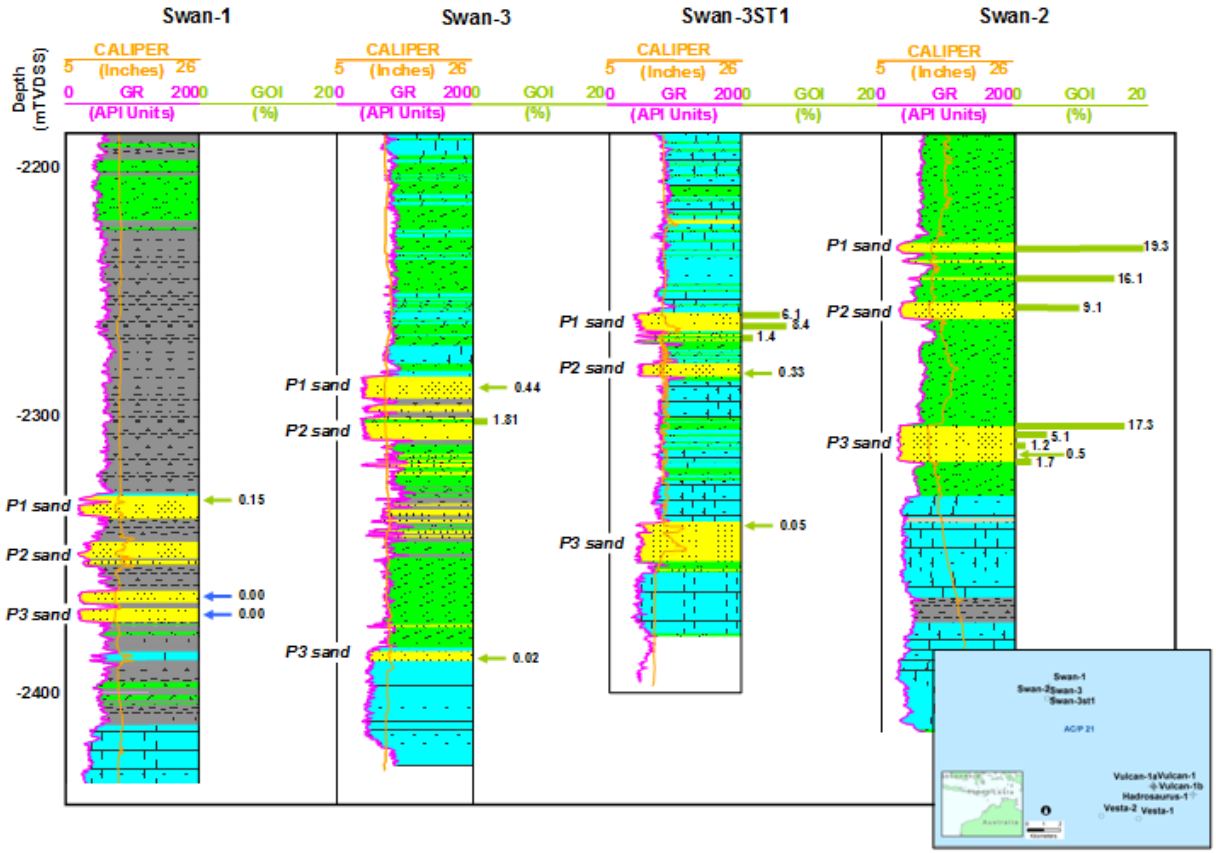

Figure 5-17: Stratigraphic correlation of GOI results from the Swan Gas Field.

Correlation panel for the four wells sampled from the Swan gas field showing GOI results against a gamma ray log and interpreted lithology. The three informally named sands are labelled with GOI values shown. Arrows denote samples where the GOI value was less than 1% (green) or where no oil inclusions were observed (blue). The logs are datumed on True Vertical Depth Sub-Sea (TVDSS) allowing the zones of high GOI to be correlated between wells. High GOI values seen in the P1 and P2 sands from the stratigraphically highest Swan-2 well can be correlated with high GOI values seen in the stratigraphically lower P1 sand in Swan-3ST where a potential palaeo-OWC can be defined by the low GOI at the base of the P1 sand. Samples from the stratigraphically deepest wells (Swan-3 and Swan-1) confirm a transition to low GOI values in the P1 sand in both of these wells. A second zone of high GOI values is recorded in the P3 sand in Swan-2 where a palaeo-OWC that is deeper than that seen for the P1 and P2 sands can be discerned where GOI values fall sharply. Low GOI values in the samples from the P3 sand analysed in the other wells confirms this transition to a palaeo-water zone.

However the low GOI values seen in the P1 sand from the down-dip Swan-3 and Swan-1 wells confirm the position of the palaeo-water leg with a palaeo-water up to of 2285mTVDSS (Swan-3). The deepest high GOI sample from Swan-3ST provides a palaeo-oil down to 2263mTVDSS (i.e. excluding the 1.4% GOI value on the basis of poor reservoir). Collectively these observations allow for a palaeo-oil column height of at least 34m and potentially more than 56m.

In the P2 sand the high GOI value recorded in the single high GOI sample from Swan-2 coupled with the single low GOI sample in the down-dip Swan-3ST well is consistent with a common palaeo-OWC for the P1 and P2 sands or could indicate a slightly shallower palaeo-OWC in the P2 sand.

A palaeo-OWC can be confirmed for the P3 sand in the Swan-2 well based on the sharp reduction in GOI values (Figure 5–17) and although the low values are slightly higher (up to 1.7%) than that typically seen in water-wet sands (<1%) the friable nature of these sandstones is conducive to caving that is likely to have contaminated these samples with material caved from the palaeo-oil zone above.

Significantly, the high GOI values seen in the P3 sand in Swan-2 define a palaeo-oil zone that extends below the highest palaeo-water up to seen in both the P1 (Swan-3) and P2 (Swan-3ST) sands so indicates a deeper palaeo-OWC in the P3 sand that is consistent with the presence of stacked palaeo-oil zones (Figure 5–17).

An alternative interpretation of the collective GOI data can be made if the P1 and P2 sands are assumed to have been in communication. The potential for a common palaeo-OWC represents one indication that this was the case and this is supported by the downwards decreasing trend in GOI values from the P1 and P2 sands (Figure 5–17). This observation is consistent with the type of saturation profile expected due to buoyancy pressures that will be higher nearer the top of the column than at the base due to the greater column height (Eadington et al., 1996). The impact of this alternate interpretation is not particularly significant as the data allow for a common palaeo-OWC for the P1 and P2 sands in both cases and has no impact on the interpretation of stacked palaeo-oil zones indicated by the GOI results from the P3 sand.

5.3.1.2 Revised Charge Model for the Swan Gas Field

Collectively the GOI results measured on the Swan wells, when integrated with the geological framework, suggest that the currently gas filled Swan structure once contained at least two discrete palaeo-oil zones, a more significant column within the P1 and P2 sandstones underlain by a thinner palaeo-oil column in the P3 sandstone. The deeper palaeo-OWC is significant as it suggests that the two palaeo-oils zones were probably not in communication at the time of initial oil charge.

Palaeo-oil columns of at least 34m in the P1 and P2 sands and at least 3-5m in the P3 sand are indicated for the interval sampled by the wells (Figure 5–17). However, when the uppermost palaeo-oil column is placed on a depth-structure map for the P1 sand the extent and significance of this palaeo-oil column can be more fully illustrated (Figure 5–18). The data enable a palaeo-oil column height of up to about 150m to be defined for the P1 and P2 sandstone and potentially as much as 115m for the P3 sands assuming the sands extend to the crest of the mapped closure and were in fluid communication.

Detailed palaeo-volumetric calculations are beyond the scope of the current investigation but given there is only about 25 m of vertical closure existing between the current Gas Down To (GDT) and the base of the mapped lowest closing contour on the trap some spillage of oil from the Swan trap due to gas flushing seems likely. Nevertheless, on an early vintage, albeit poor quality seismic line the dip of the interpreted P1 sand horizon reduces on the flanks of the structure (Figure 5–18) and consequently a greater volume of oil could be contained within a 25m thick zone at this depth than an equivalent thickness at the crest of the structure.

A set of volumetric calculations could easily be attempted if suitable maps were produced and the lateral changes in sand thickness could be constrained. Comparison between the palaeo-oil volume and the volumetric capacity of the untested part of the closure could be used to determine the proportion of the oil that potentially could have been retained in the trap compared with that lost across the spill point.

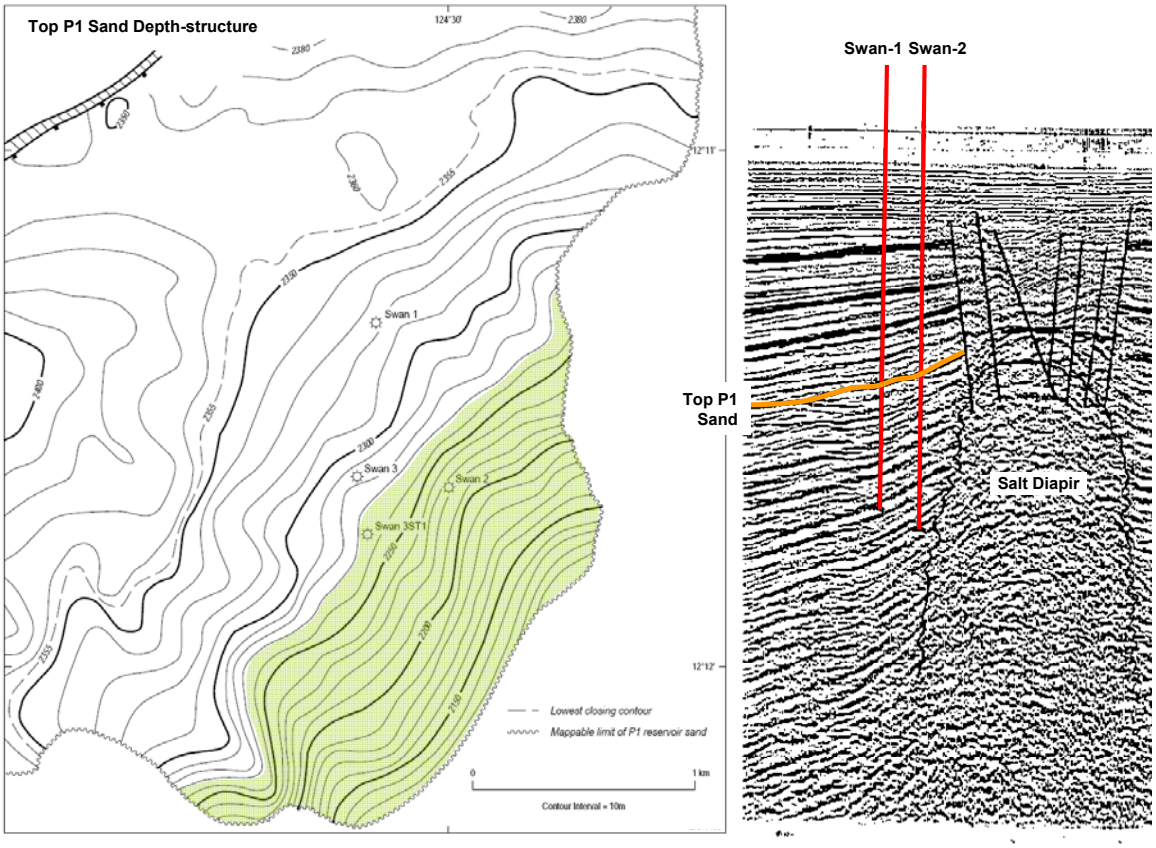

Figure 5-18: Depth-structure map and seismic line showing the P1 Sand in the Swan Gas Field.

The depth-structure map for the top of the P1 sand with the yellow shading showing the approximate extent of the palaeo-oil zone defined by the GOI results from the sampled wells, assuming the structure has remained structural unchanged since the time of initial oil charge. The Swan-3 well has a gas down to (GDT) at the P1 level whilst the result from Swan-1 is ambiguous. An untested reservoir section of about 60m lies between the clear GDT in Swan-3 and the lowest closing contour for the trap interpreted by BHP Petroleum (1992) to be at 2355m sub-sea. Displacement of a palaeo-oil column into this untested section of the reservoir could provide an attractive target for a future down-dip appraisal well.

5.3.2 Oliver Gas Field

The Oliver oil and gas field was discovered in 1988 by the drilling of Oliver-1, which encountered a 162.3m gross gas column underlain by a 13-16.8m oil rim (BHP Petroleum Ltd., 1988d). The field lies on the margin of the Cartier Trough, a Neogene formed depocentre about 30 km to the north of the Jabiru oilfield (Figure 5–1). The gas is reservoired within variable quality sandstones of the Middle Jurassic Plover Formation.

The Oliver trap is an elongate northeast-southwest trending tilted fault block formed during Late Jurassic rifting (BHP Petroleum Ltd., 1988d) and subsequently reactivated during Neogene oblique collision of the Australian continental plate with the Banda Arc to the north.

The structure is fault dependent with juxtaposition of the reservoir against the argillaceous Swan Group providing top and lateral seal in combination with shales of the overlying Bathurst Island Group (Figure 5–19). No production testing was conducted and the well was suspended as a sub-commercial oil and gas discovery.

Despite being suspended as a potential oil and gas producer, the small volume of hydrocarbons, the relatively poor quality reservoir, the thin nature of the oil rim and remoteness from existing infrastructure all provide substantial challenges to the viability any future development of the Oliver Field as a stand alone project.

The presence of oil beneath gas at Oliver-1 provides an obvious indicator that the oil and gas may be related although only trace fluorescence was recorded within the gas-leg. The lack of fluorescence from the gas cap makes it difficult to determine if the volume of oil present in the oil rim represents the total volume of oil that has migrated into the trap or if an initial oil charge was volumetrically more significant.

In the latter case, constraints on the size of a displaced oil volume would allow the likelihood of oil charge to nearby satellite structures or traps located further along the spill chain to be addressed. This could also include features that are in the shadow of direct migration paths from the main kitchen.

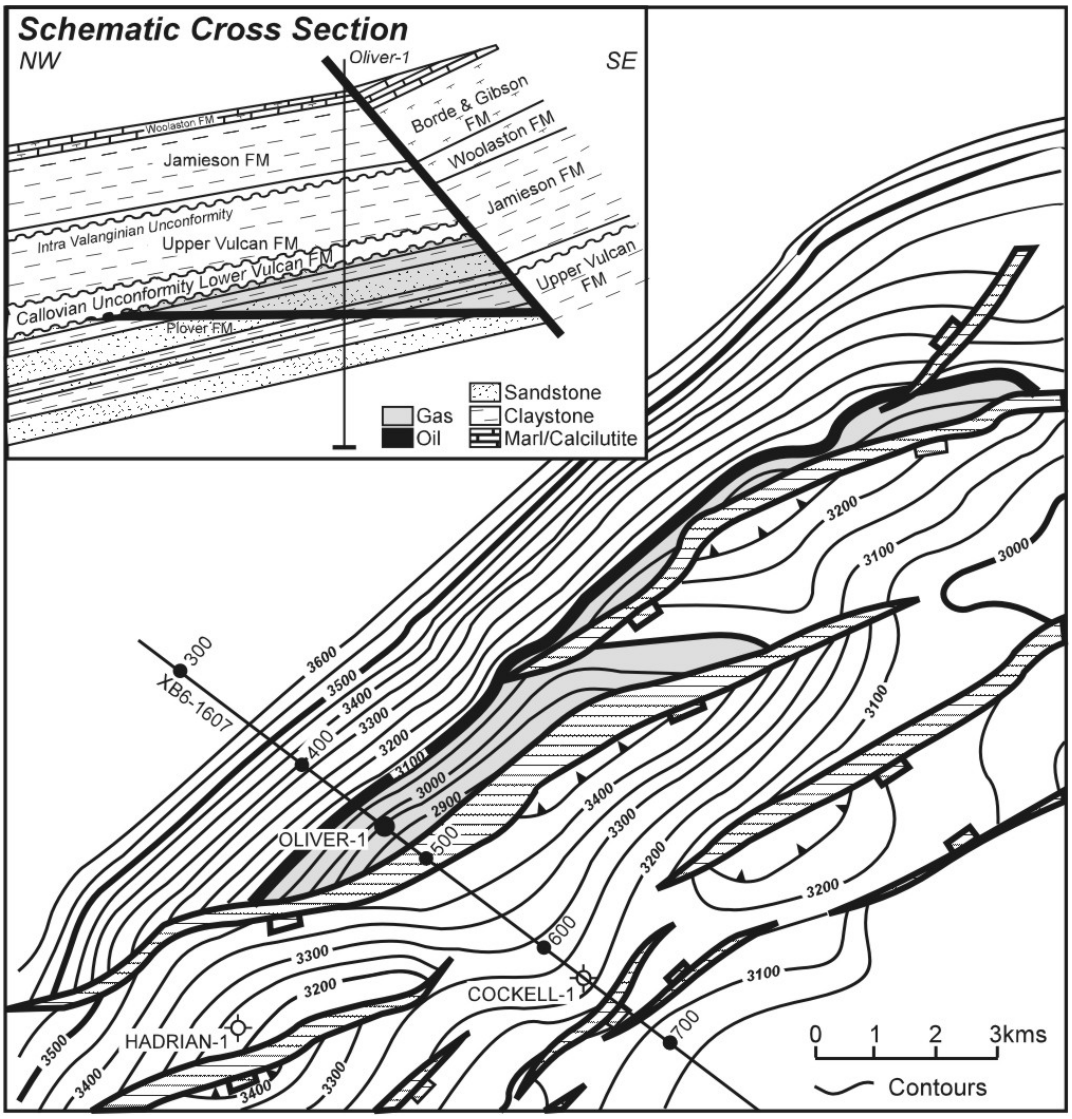

Figure 5-19: Cartoon showing the Oliver structure.

Depth structure map at top Plover Formation level (main picture) and a schematic cross section through the well location, showing juxtaposition of the Plover Formation reservoir against shales of the Jamieson and Upper Vulcan formations in the hangingwall. Gas is shown as a light grey shading with the oil rim represented by the horizontal black line. The nearby Cockell-1 and Hadrian-1 wells were both dry holes. Contour interval is 50m.

PVT analyses conducted on gas recovered by repeat formation tester (BHP Petroleum Ltd., 1988d) from the Oliver Field show that calculated dew point pressure of the gas coincides with the measured reservoir pressure (Figure 5–20) indicating the gas is in equilibrium with an underlying oil-leg and therefore likely to be related fluids. This is further supported by the coincidence of the intersection of the bubble point curve for the associated oil phase (Figure 5–20).

5.3.2.1 Sampling Details

GOI results for the Oliver-1 well were outlined in the previous chapter but in summary samples from 2946 m to 3045 m have GOI values ranging from 3.7 to 31.2%, indicating the presence of an oil column in Oliver-1 prior to gas charge. The position of the palaeo-OWC is defined by a sharp reduction in GOI values from 5.7% at 3045 m to <0.1% at 3078 m (Figure 5–21). Given that the top of the reservoir occurs at 2940 m these data delineate a palaeo-oil column of 99 m to 132 m.

The location of the palaeo-OWC within the present gas-leg and above the current GWC is significant as it suggests that the oil column was hydrodynamically static when the majority of oil inclusions were formed. This observation and similar observations in other fields (e.g. Lisk et al., 1996a and the Swan field discussed in the previous section) precludes a process of gradual smearing of an originally much smaller oil column during later emplacement of gas. For the latter process to occur high GOI values would be expected throughout both the gas and oil legs (Figure 5–22). Similarly, if oil inclusions were trapped more randomly then variable GOI profiles would be anticipated, but commonly (and in this instance) a zone of continuously high GOI values is observed that is underlain by a zone with continuously low GOI values (Figure 5–21).

The GOI data also indicate that high oil saturation originally extended to the top of the reservoir section and as a consequence a significant gas cap was absent from the original palaeo-hydrocarbon accumulation. The volume of oil present in the trap at the time of initial oil charge is likely to have been much larger than the volume contained today.

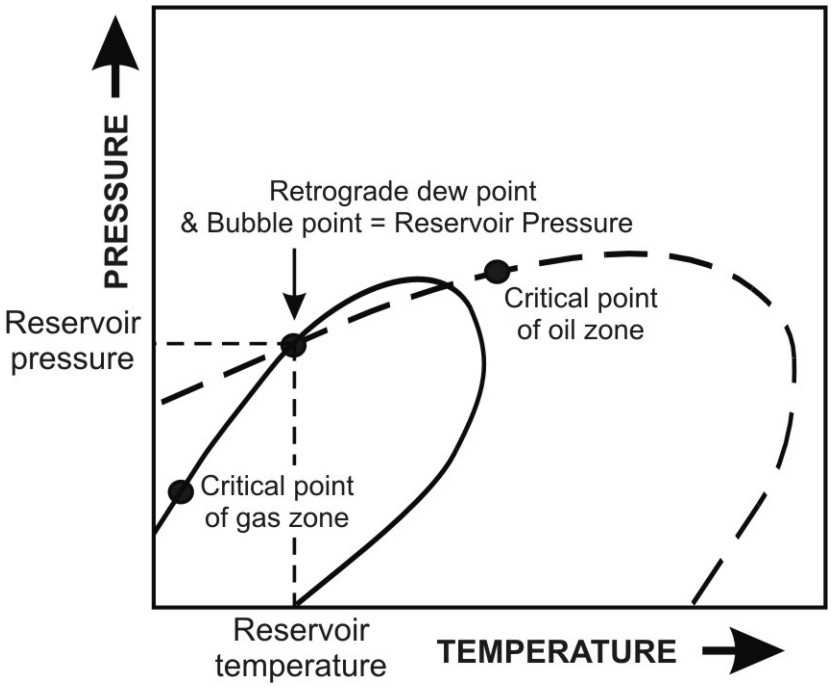

Figure 5-20: PVT data for the Oliver Field.

Simplified phase diagram showing bubble point and dew point curves for the Oliver Field. The measured reservoir pressure coincides with the intersection point of the curves indicating the fluids are in equilibrium.

The single sample taken from within the current oil-leg has a low GOI value (<0.1%) that is inconsistent with the presence of the current high oil saturation (Figure 5–21). This observation supports the proposition that the formation of oil inclusions mostly occurs during the initial stages of oil charge and that subsequent fluid movements resulting from later gas displacement do not promote further significant episodes of oil inclusion formation.

5.3.2.2 Palaeo-volumetric Calculations

Volumetric estimates of original oil in place for the Oliver trap were determined using the thickness of the palaeo-oil columns (as defined from the GOI data) integrated with relevant information on rock volumes and reservoir parameters, such as average porosity (Ø), water saturation (Sw), net/gross ratio and formation volume factor for oil (Bo'), all compiled from information contained in the Oliver-1 well completion report (BHP Petroleum, 1988d). These estimates use the presently mapped area of closure and assume that modification to the structure after oil charge has not made significant changes to the volumetric capacity of the trap.

Unlike other traps in the region where recent fault reactivation may have produced significant changes the Oliver trap is a product of Neogene fault reactivation with similar fault offsets recorded at the Callovian Unconformity (top reservoir) and the Base Miocene seismic horizon (BHP Petroleum Ltd, 1988d). Above this marker observed fault offsets decrease and the main bounding fault terminates before reaching the current sea-floor. This suggests ongoing, but reduced structural growth that may have subtly altered the volumetric capacity of the trap but given the relatively small fault displacements above the Base Miocene maker it is unlikely to have dramatically altered the volumetric capacity of the trap.

In addition to uncertainties related to structural modification of the trap after initial oil charge other factors also influence the accuracy of volumetric estimates. The Oliver structure is penetrated by a single intersection and difficulties in accurate conversion of time to depth due to velocity gradients produced by seismic amplitude anomalies in the Tertiary section create uncertainty in accurately mapping the extent of closure on the field.

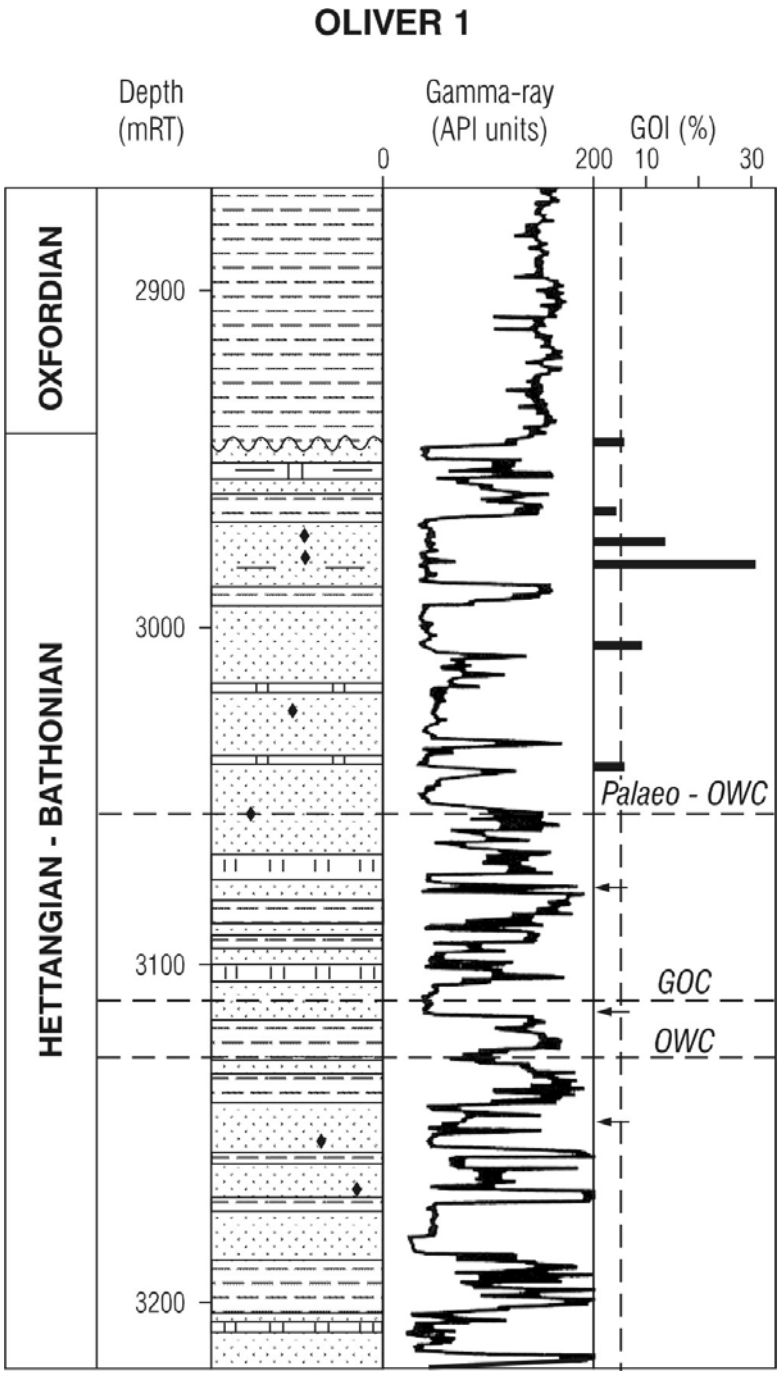

Figure 5-21: Summary of GOI data from Oliver-1.

The GOI log for Oliver-1 showing the position and magnitude of GOI data from across the current gas and water zones plotted against a gamma ray log to provide information on the reservoir lithology. A zone of continuously high GOI values within the current gas-leg defines the palaeo-oil zone, whilst the sharp fall in GOI values to less than 1% (samples shown by black arrows) indicates the position of the inferred palaeo-OWC. Note the absence of high GOI in the sample from the current oil rim.

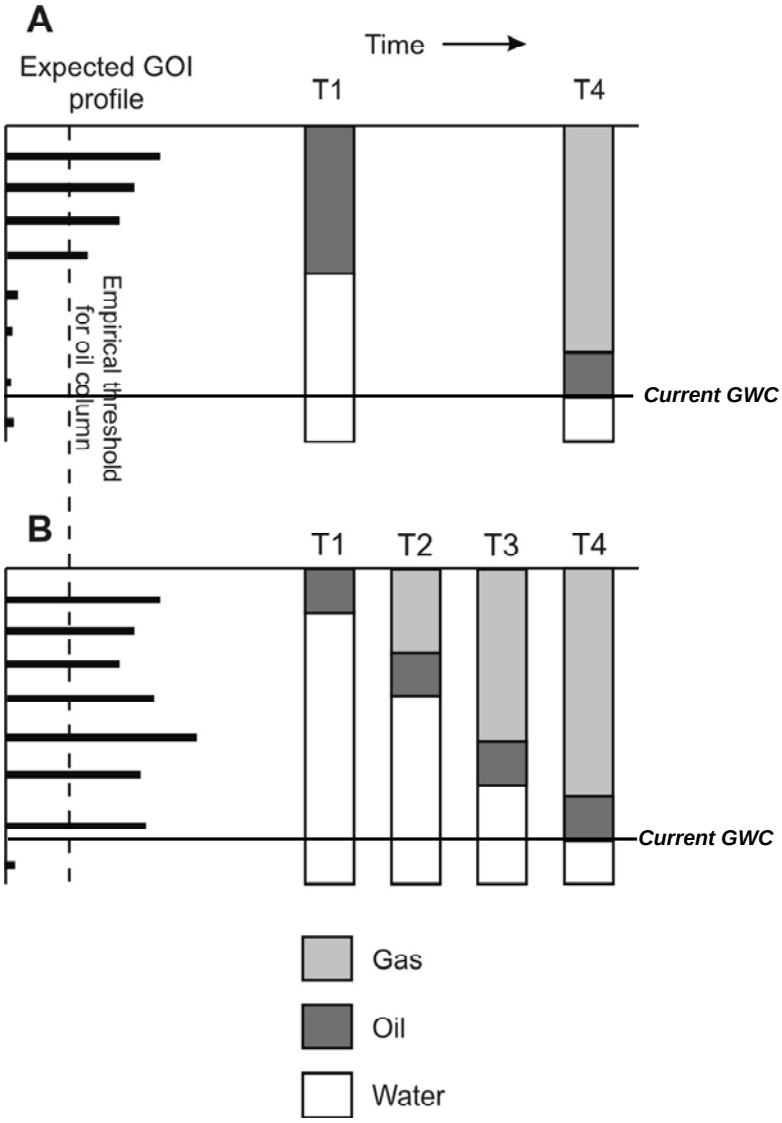

Figure 5-22: Possible GOI profiles produced by gas displacement.

Cartoon showing the type of GOI profile expected for A., a hydrodynamically stable palaeo-oil column with inclusions mostly trapped during initial oil charge (with a well defined palaeo-OWC; T1) and a paucity of oil inclusions in samples from the current oil rim (T4) and B., trapping of inclusions continuously through time with high GOI values produced as the oil is slowly displaced from the trap by gas charge (T1 through T4) resulting in high GOI values being recorded in samples taken throughout the current hydrocarbon column.

More recent work by Evans et al. (1995) also raised uncertainty in reserve estimation for Oliver by showing that previously mapped high angle faults are erroneous due to seismic imaging problems caused by ray-path distortion. Nonetheless, these uncertainties apply equally to volumetric calculations for both palaeo- and present hydrocarbon columns and are typical of the limited data available during the early stages of field appraisal.

Despite the various factors that can contribute to the accuracy of estimates regarding the palaeo-oil volume the exercise remains worthwhile as a way of assessing the economic incentive of chasing nearby satellite closures. In the case of the results from Oliver-1 a gross palaeo-oil column measuring between 99 m (2946-3045 m) and 132 m (2946-3078 m) within the gas leg (median = 115.5 m) is delineated by GOI mapping and when combined with the aforementioned information on rock volumes and reservoir parameters suggests that the trap contained 200 million barrels of oil prior to gas charge (Figure 5–23). Similar calculations completed for the present 14.5 m oil-leg equate to approximately 45 MMBBL suggesting that up to 155 MMBBL of oil has been lost from the Oliver trap by gas flushing (Lisk et al., 2002).

5.3.2.3 Mechanisms Controlling the Loss of Oil

Whilst a conclusion of oil being displaced from the trap seems the most likely the identification of a palaeo-oil column within presently gas bearing sands does not, by itself, confirm that oil was displaced by gas charge. Several other kinds of losses that occur after accumulation must be accounted for: in reservoir biodegradation or water washing; leakage of petroleum through a seal; and in situ phase change related to changing pressure and temperature conditions.

Detailed geochemical characterisation of oils and gas recovered from Oliver-1 (BHP Petroleum Ltd., 1988d) as well as analyses undertaken on the fluid inclusion oils (discussed in the previous chapter) show no evidence of significant biodegradation or water washing allowing this mechanism to be excluded from further consideration as a possible mechanism to explain the loss of the Oliver palaeo-oil column.

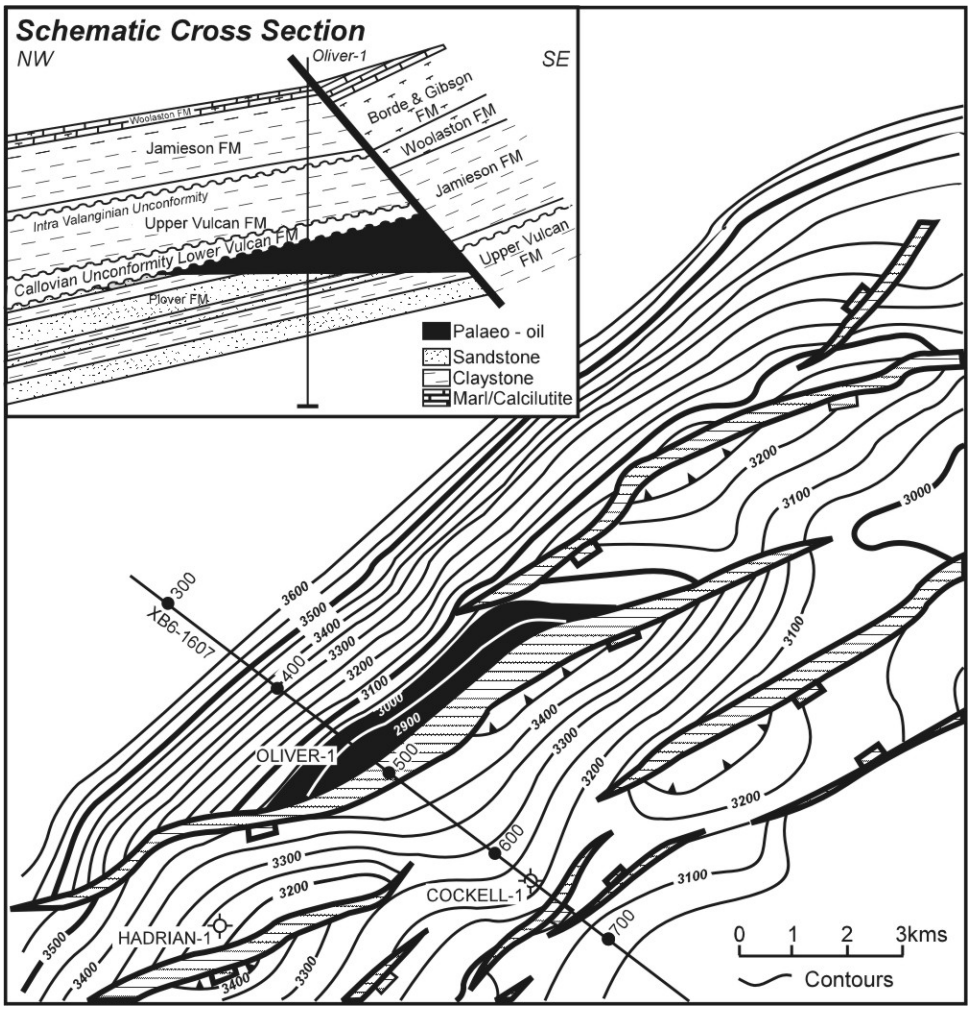

Figure 5-23: Extent of the palaeo-oil column.

Current depth structure map at top Plover Formation modified from Figure 5–24 and schematic cross section through the Oliver-1 location (inset) showing the extent of the palaeo-oil column (black fill) inferred from the GOI data collected on Oliver-1. This map has not been adjusted to accommodate for any structural changes that may have occurred since the assumed time of charge (trap formation by the Base Miocene), but the post Miocene fault offsets are small and any modifications are likely to have been minor.

A plausible explanation for the loss of oil from a tilted fault block structure such as Oliver may be leakage of oil due to breach on the closing fault. As this and other studies have demonstrated the Timor Sea is a region that is characterised by a high number of residual oil columns that are attributed to fault controlled leakage (Whibley and Jacobson, 1990; O'Brien and Woods, 1995; Lisk and Eadington, 1994; O'Brien et al., 1996a; Lisk et al., 1998b). However, the fact that the seal is sufficient to hold the presently reservoired gas column suggests that fault breach is unlikely. Further, recent studies of trap integrity in the Timor Sea by O'Brien et al. (1996a), O'Brien and Woods (1995) and O'Brien and Lisk (1995) have concluded that the Oliver structure is an example of a high integrity trap. Consequently it is unlikely that breach of fault seal was responsible for the loss of liquids and displacement of oil across the spill point of the Oliver structure by late gas charge, is considered to be a more likely outcome.

Another important mechanism for loss of an early oil charge needs to be considered before a conclusion of gas displacement can be reached. This relates to the very process that causes gas displacement, namely increased maturation and associated gas generation from over-mature source rocks. Formation of a gas cap will depend on the composition of gas charging the trap, the composition of oil within the trap and the reservoir pressure and temperature at the time of charge. Initially gas reaching the trap will be absorbed into the oil until saturation is achieved (bubble point) and a discrete gas cap is formed under equilibrium conditions. Subsequent gas charge will bubble through the oil to increase the size of the gas cap and push the oil leg deeper in the structure.

Equilibrium between oil and gas phases will change with increasing temperature and pressure. The capacity for gas to absorb oil increases as temperature and pressure rise (Figure 5–15). Reservoired oil is not immune to further maturation and with additional burial of the trap oil will increasingly partition into the gas phase and could ultimately result in the complete loss of oil once the dew point of the gas is exceeded. The amount of oil that can be lost into the gas is controlled by the composition of gas charging the trap and the greatest loss of oil will occur when the gas is composed purely of methane.

At Oliver-1 the presence of discrete oil and gas zones at the present day suggests that both fluids exist at saturation where reservoir pressure equals both the dew point of the gas and the bubble-point of the underlying oil (Figure 5–20). Loss of oil from the palaeo-oil column into the gas cap may have occurred if gas charging the trap was undersaturated with respect to oil. The maximum loss of oil by this mechanism can be crudely calculated from the condensate-gas ratios measured on gas recovered by repeat formation tester which range from 35 to 39 barrels per million standard cubic feet of gas (bbl/MSCF). When combined with estimates of gas in place at Oliver-1 of some 300 BCF and assuming later gas charge was comprised purely of methane then the maximum loss of oil is placed at about 11.7 million barrels and the net loss of oil from the Oliver trap could be reduced to about 143 million barrels. Cracking of oil to gas in situ can be excluded as vitrinite reflectance data indicates that the sampled section is immature for hydrocarbon generation (BHP Petroleum Ltd., 1988d).

In summary, processes other than gas displacement can result in the loss of an early oil charge and it is therefore prudent to consider other mechanisms. Fortunately none of these are particularly difficult to identify and providing that an integrated approach to prospect evaluation is employed then the potential for erroneous predictions can be minimised.

5.3.2.4 Regional Significance of the Displaced Oil

Petroleum exploration is governed by economics and the significance of the volume of oil displaced will vary depending on location of the field. This can be considered by comparing the magnitude of palaeo-oil columns with the size of commercial oilfields located nearby and in this way, taking into account obvious losses during remigration, their significance can be assessed.

Producing hydrocarbon fields in the Timor Sea have oil reserves ranging from 30 to 200 million barrels and fields while Oliver is thought to contain 45 million barrels in place (Cadman and Temple, 2003). Whilst this suggest Oliver could contain economically viable oil volumes these have been considered too marginal to warrant field development at this time, with gas breakthrough hindering effective completions for oil production in the thin oil-leg.

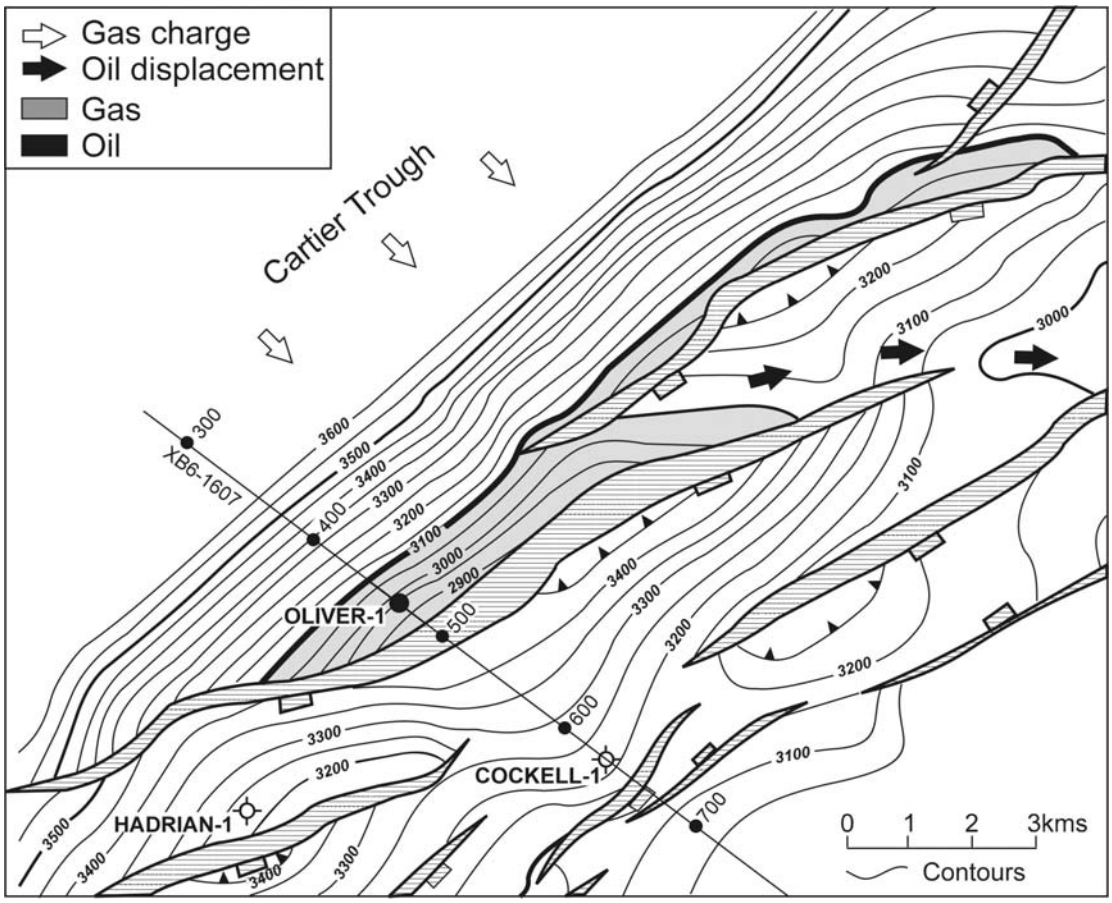

Figure 5-24: Possible remigration pathways for the Oliver structure.

Current depth structure map at top Plover Formation modified from Figure 5–24 showing the extent of the presently reservoired oil and gas legs with the open block arrows indicating the direction of gas migration from the adjacent source kitchen and the solid block arrows showing the anticipated spill pathways for oil displaced by this gas charge. Fault blocks located up-dip from the Oliver trap and potentially disregarded as being within a migration shadow can still receive the significant volume of oil inferred to have been displaced from the Oliver trap. Available maps do not cover a sufficient area to determine if any of these satellite features represent valid traps.

In contrast, the results of this study, indicating loss of oil from the Oliver structure of up to 155 million barrels, provide considerable incentive to map remigration pathways in an effort to locate structures that could have been well positioned to receive this displaced oil leg (Figure 5–24).

Indeed recent studies by Ambrose (2004) draw on the volume of palaeo-oil reported by Lisk et al. (2002) to have been lost from the Oliver trap to suggest that a larger oil volume may still be present in the Oliver structure. Ambrose (2004) suggests that an intra-formational seal at the base of the current oil zone could be acting as a seal and that the underlying water-wet sand may not be in communication with the oil bearing sands above. Ambrose (2004) argues that the water gradient used to define the position of the Oliver OWC and drawing on water pressures from the deeper sand is not an appropriate assumption if these sands are isolated.

Furthermore a difference in salinity recorded at the nearby Hadrian-1 well, where formation water salinity is interpreted to be 50,000ppm, fresher than the 78,000ppm interpreted at Oliver-1 is used to invoke a slightly different water gradient due to density differences. The outcome of using a different water gradient is a deepening in the inferred OWC and Ambrose (2004) reports an increase in column height from 13-17m to as much as 38m (Figure 5–25).

This deepening of the current OWC would greatly increase the oil volumes from the current levels, estimated by the Northern Territory Government to be 20.4 million barrels recoverable, to volumes of between 130-160 million barrels (Ambrose, 2004). The volumes previously calculated for the Oliver-1 palaeo-oil column (Lisk et al., 2002) were estimated to be about 200 million barrels in place, sufficient to provide the increased volumes of oil required to accommodate this alternate estimate of the OWC. In this manner, the Oliver-1 example clearly demonstrates the value that can be generated by more fully understanding the charge history of traps that are now filled with gas. This type of data play an important role in prompting development of new ideas and ultimately enabling a more comprehensive assessment of exploration risk for future appraisal drilling.

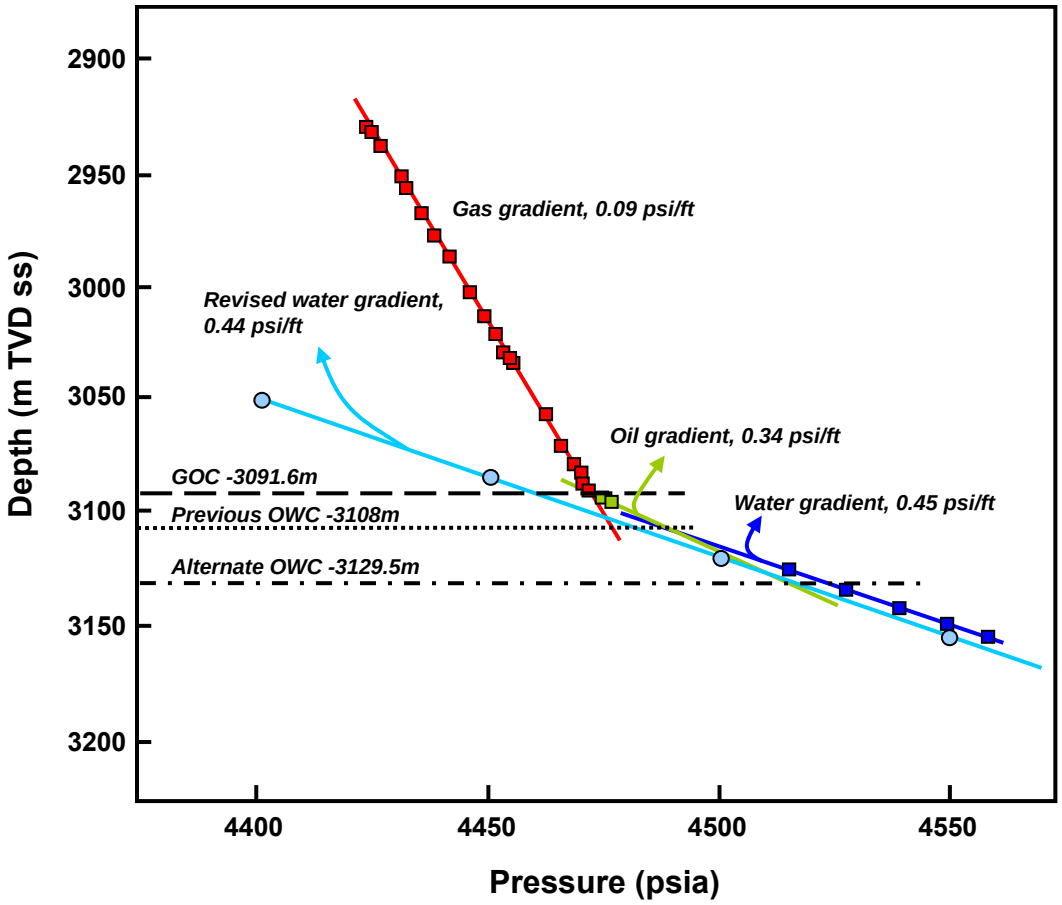

Figure 5-25: Possible OWCs for the Oliver Field

Pressure-depth plot for the Jurassic reservoir section in Oliver-1 showing interpreted gas, oil and water gradients used to define the location of current fluid contacts (GOC and OWC). A deepening of the OWC is demonstrated when a different water gradient (light blue line) is utilised that employs a less saline (lighter) formation water than that used in the initial (dark blue line) petrophysical assessment (Modified from Ambrose, 2004).

5.4 DRY HOLE CHARGE HISTORIES

Evaluating the charge history of unsuccessful wells is an important step in helping to constrain the properties of petroleum systems operating in the basin so that future wells can benefit from the learning's obtained from dry holes. Ascertaining whether a trap received a charge, experienced oil migration without accumulation or never was connected to a source kitchen represent possible outcomes that have substantial implications for identifying the deficiencies in the petroleum system.

Unlike wells that test reservoirs that are in contact with hydrocarbons and produce generally very obvious indications that oil or gas has been encountered the data coming from water-wet wells can be heavily compromised by both geological processes or by drilling strategies that seeks to suppress entry of hydrocarbons into the well bore to avoid the potential for a blow out. The value of using fluid inclusion "oil shows" as a piece of information that is retained to provide a representative sample of the reservoir fluid that can be recovered for analysis is even more significant in a dry hole situation.

5.4.1 Eclipse Palaeo-oil Column

Two exploration wells have been drilled to test the hydrocarbon potential of the Eclipse structure, both targeting a structural closure mapped at the Middle Jurassic level and located directly up-dip from the East Swan-1 well where traces of oil were previously encountered at this stratigraphic level (BHP Petroleum Ltd., 1989c).

The Eclipse structure is situated on the eastern side of the Swan Graben (Figure 5–26) along the elongate Eclipse-Skua Horst trend. It is mapped as a four way dip closed SW-NE trending anticlinal feature at the base upper Jurassic Level (BHP Petroleum Ltd., 1989c). The feature was augmented by tilting in the Neocomian, associated with movement on the faults bounding the adjacent Vulcan graben and was subsequently affected by minor fault movements through the Cretaceous and Tertiary that further enhanced the relief of the Eclipse-Skua structural high (BHP Petroleum Ltd., 1989c).

Despite poor seismic quality below the Base Cretaceous Unconformity the Eclipse 1 well is thought to have tested a valid closed structure. Wireline log, core examination and RFT testing indicated that only minor hydrocarbons were present (BHP Petroleum Ltd., 1989c). Failure of a prospect was considered to be due to trap integrity or inadequate migration paths. In this regard the exploration efforts directed at the Eclipse structure, like many traps in the VSB produced an equivocal outcome.

Seismic mapping completed after Eclipse-1 showed faults separated the Eclipse structure into three culminations, with a central crest interpreted to be up-dip from Eclipse-1 providing the target of the Eclipse-2 well. Prior to drilling the central crest was interpreted to be 215 m up-dip from Eclipse-1 with oil in place volumes of 440 million barrels (BHP Petroleum Ltd., 1989c).

Eclipse-2, drilled 4.5 km northeast of Eclipse-1, successfully encountered the prognosed reservoir intervals, but the Lower Jurassic objective was water-wet. Minor fluorescence was encountered in tight sandstones from 2787.0 to 2798.5 m in the Middle Jurassic. Log analysis identified a 6.5 m zone of residual oil from 2787 to 2800 mRT in the Lower Jurassic, with RFT pressures confirming a water gradient.

Fluorescence observed in the Upper Jurassic sandstones was more pronounced with 57 cubic feet of gas together with minor oil or condensate recovered by RFT from a 2.5 m zone of fluorescing porous sandstone from 2458.5 to 2461.0 m. RFT pressure data defined an OWC at 2460.2 mRT with a possible GOC interpreted at 2459.7 mRT (BHP Petroleum Ltd., 1989c).

5.4.1.1 Sampling Details

The Eclipse-1 reservoir section has been extensively sampled, covering both Upper Jurassic sandstones of the Lower Vulcan Formation as well as deeper sandstones from the Plover Formation. A smaller number of samples taken in the Eclipse-2 also test the same primary and secondary objectives but these intervals are separated by Lower Vulcan Formation shale (Figure 5–26).

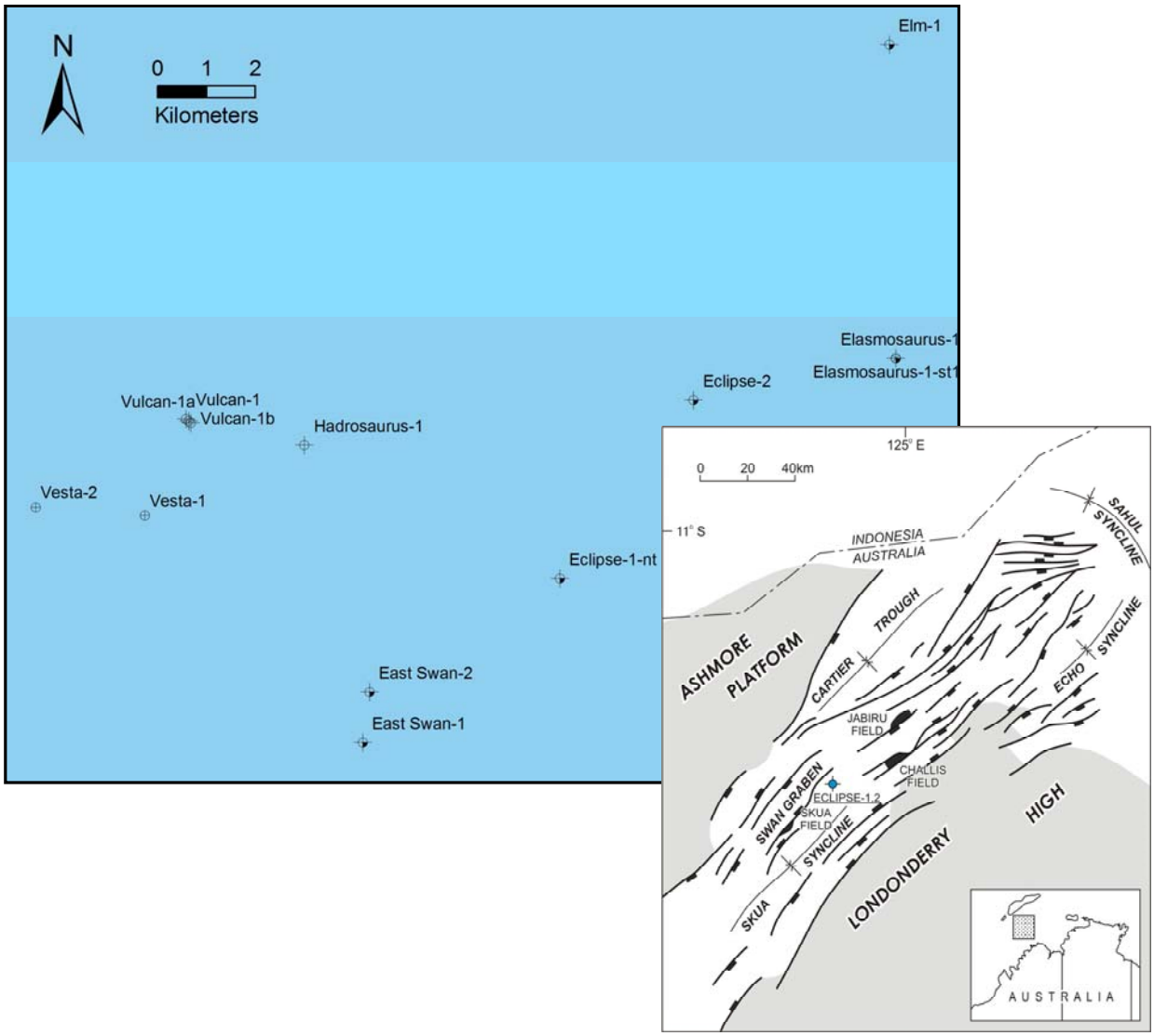

Figure 5-26: Location of the Eclipse wells

Close up location map showing the location of the Eclipse-1 and Eclipse-2 wells relative to nearby offset wells, with the inset map placing the well in the context of the broader Vulcan sub-basin. The Eclipse wells lie to the south of the Jabiru and Challis oil discoveries and immediately to the northwest of the recognised source kitchen with the Swan Graben where it is face loaded against Upper Jurassic oil prone source rocks.

GOI results from the Eclipse wells were described in the previous chapter with the results indicating a large palaeo-oil column of more than 225m at Eclipse-1 and two discrete high GOI zones in Eclipse-2, one within a currently hydrocarbon bearing thin Lower Vulcan Formation sandstone (<10m) and a second thin (<5m) palaeo-oil zone seen in the presently water-wet Middle Jurassic section (Figure 5–27).

5.4.1.2 Interpreted Charge History

The Eclipse wells are revisited to demonstrate the value that can be attained by integration of GOI results with information on the relevant geological setting in order to provide a more comprehensive evaluation of the charge history.

In Eclipse-2 a combination of poor seismic imaging and poor dip-meter data contributed to pre-drill difficulty in determining the degree of truncation below the base Cretaceous unconformity (BHP Petroleum Ltd., 1989c). Consequently, whilst the Eclipse-2 well intersected the top of porosity substantially up-dip of the base Cretaceous Unconformity intersected in Eclipse-1 only a thin Upper Jurassic sandstone section was encountered. Unlike Eclipse-1 where the Plover Formation sub-cropped immediately below this Upper Jurassic sandstone Eclipse-2 encountered a thick shale-prone Upper Jurassic section below this sand. As a result the prognosed primary objective represented by the Plover Formation was penetrated about 325m deep to prognosis (Figure 5–27). Whilst the current study had no access to seismic data from the Eclipse area the well based stratigraphy implies a significant growth section, probably associated with post-Plover Upper Jurassic faults (Figure 5–27).

Despite this stratigraphic uncertainty the GOI data reveal a close similarity in the position of the palaeo-OWCs interpreted in the Plover Formation of each wells when placed on a common depth datum. It seems reasonable to infer that the Upper Jurassic section in Eclipse-2 forms part of the same palaeo-oil column that was identified in the Eclipse-1 well.

Considered independently the results could fit a range of potential interpretations but where the results can be placed in geological context it is more likely that the three "discrete" palaeo-oil zones actually represent a common palaeo-oil column.

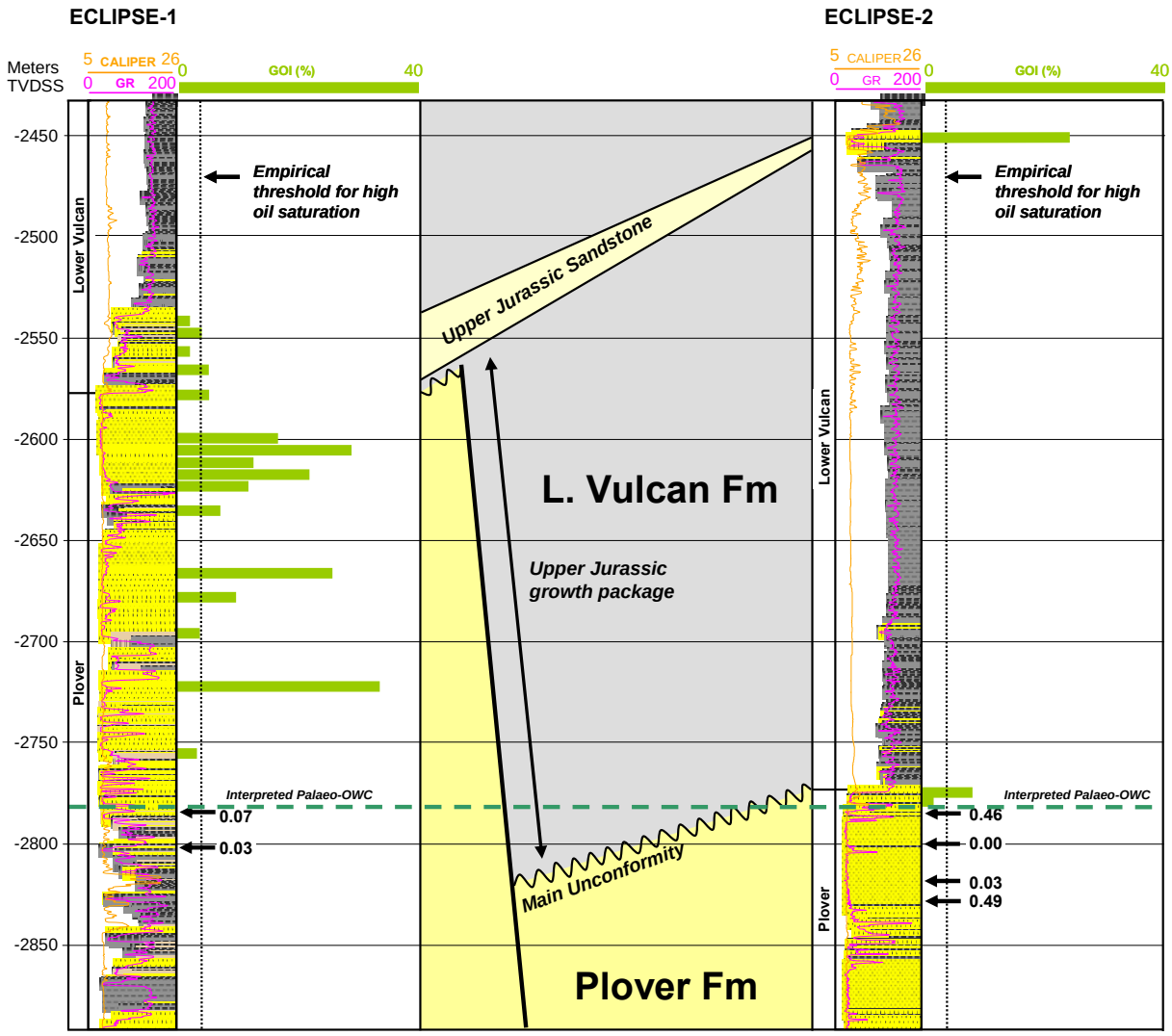

Figure 5-27: GOI results from the Eclipse-1 and Eclipse-2 wells.

Well correlation plot showing GOI results relative to the gamma ray log with an interpreted inter-well correlation. In Eclipse-1, Upper Jurassic (Lower Vulcan Formation) reservoir sandstones immediately overlie the Middle Jurassic Plover Formation unconformably, whilst in Eclipse-2 a thick shale section related to growth on an intervening fault separates the Upper Jurassic sandstones from the older Middle Jurassic reservoir. The thick palaeo-oil zone defined in the Eclipse-1 but a large number of samples appears to also be represented in the more lightly sampled Eclipse-2 well where discrete zones of high GOI values are seen in both sands, but are separated by the thick shale.

The degree of connectivity cannot be definitively confirmed but it seems probable that the Upper and Middle Jurassic reservoirs were in pressure communication at the time of charge with an original palaeo-oil column height exceeding 300m.

Whilst the Eclipse-2 well indicates that the base Cretaceous unconformity is a poor proxy for the top of the Plover Formation the seismic surface defining the top of porosity remains a valid representation of the trap geometry at the base of the Cretaceous section. Figure 5–28 shows that the mapped deepest closing contour at about 2800mSS provides sufficient closure to accommodate the palaeo-oil column defined by the GOI data. Together, the comparable palaeo-OWC and mapped trap geometry provide additional confirmation that the fluid contacts defined by the GOI data are genuinely reflecting the degree of trap fill prior to late stage breaching.

Despite indicating a single, connected palaeo-oil column at the time of initial charge, RFT pressure data recorded in each reservoir section shows slightly offset water gradients (21 psi) that would indicate a lack of pressure communication at the current day. This could suggest that these intervals were always isolated and an alternative interpretation of the GOI data would be discrete palaeo-oil zones in both wells.

5.4.2 Octavius Palaeo-oil Column

The result from the Octavius-2 well (Figure 5–29) typifies the challenges that have confronted exploration efforts undertaken in the VSB, but also provides a compelling example of the value that can be derived from application of the GOI method.

From the drilling of the Octavius-1 well testing Tithonian sandstones outside of closure to the delineation of a large palaeo-oil column in Octavius-2 it required a sustained effort using all available technologies to finally succeed in defining a significant, albeit presently sub-economic oil field with the Tenacious-1 discovery well in 1997.

The first test of the structure, Octavius-1 drilled in 1989, was a deviated well designed to test the entire Jurassic sequence through the leading edge of the footwall block of a northeast-trending tilted fault block.

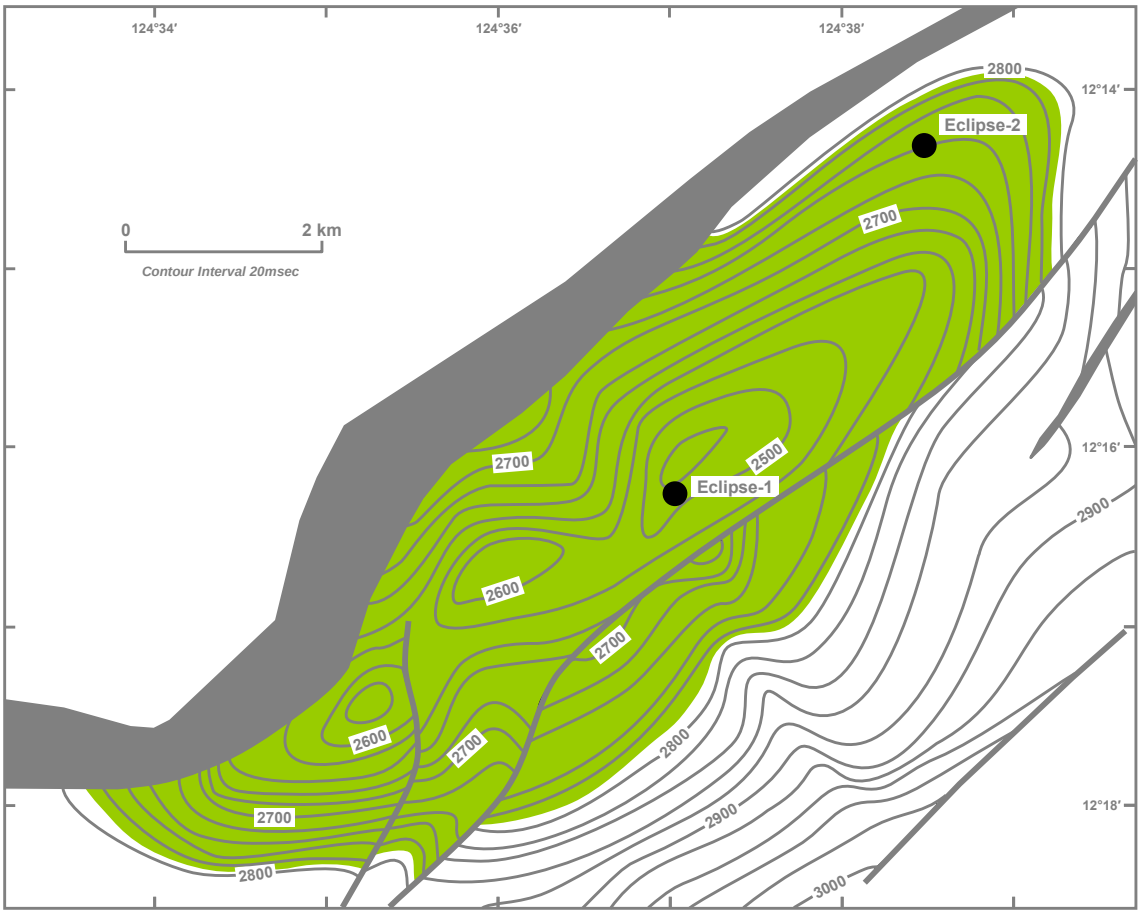

Figure 5-28: Depth-structure map for the Eclipse structure.

Depth-structure at the base Cretaceous Unconformity demonstrating a 3-way fault dependant structural closure likely to be sufficient in size to fully accommodate the maximum palaeo-oil column height (green shading; figure modified from Cadman and Temple, 2003). Note: The original figure from Cadman and Temple (2003) refers to this map as a two way time (TWT) structure map (contour interval is given in milliseconds rather than metres) but the close agreement in depth of the well ties and the shot point data from the wells suggest this is actually a depth-structure map.

Whilst drilling the siltstone section within the Upper Vulcan Formation Octavius-1 encountered oil shows in the mud, but failed to reach the primary objective Plover Formation due to bad hole conditions and was finally abandoned within the Lower Vulcan claystone section (WMC Petroleum Ltd., 1990).

A second well was drilled on the Octavius prospect in 1991 located some 1.75 km south-southwest of Octavius-1 (Figure 5–29) and successfully penetrated the Plover Formation reservoir section, but encountered only residual oil shows (WMC Petroleum Ltd., 1990). The shallower Tithonian sandstone reservoir was penetrated out of closure in the hanging-wall block and had only minor shows. Octavius-2 was declared a dry hole and was also plugged and abandoned.

Further reprocessing of Kym 3D seismic survey revealed untested up-dip closures at both the Tithonian sandstone and Plover Formation levels with sufficient volumetric potential to warrant a third well on the Octavius structure (Figure 5–30). The aptly named Tenacious-1 well was drilled in 1997 and penetrated the Tithonian sandstone up-dip from the Octavius-1 well and despite an absence of conventional oil shows in the cuttings a possible oil zone was seen on the wire-line logs. Moderate to very strong bright bluish-white fluorescence observed in sidewall cores taken across this zone supported the log interpretation with the Modular Formation Dynamics Tester (MDT) tool used to confirm an oil phase on pressure data and take samples of light oil (50.8°API at 15.6°C; Woods and Maxwell, 2004). Serendipitously, the interpreted oil–water contact at Tenacious-1 (2,776.3 m TVDSS) is interpreted to lie only 1.4 m above the Tithonian sandstone intersected in the dry Octavius-1 well.

Subsequent sidetracking of the Tenacious-1 well confirmed the structural prognosis, penetrating the Tithonian sandstone some 34 m higher than in Tenacious-1. A total of 22.9 m of net oil pay was delineated that flowed at a maximum rate of 7,667 BOPD (Woods and Maxwell, 2004). Further appraisal drilling at Tenacious West-1 in 2000 (OMV Australia Ltd. 2000) intersected Tithonian sandstones just below the OWC of the field. Currently the Tenacious oil field remains undeveloped and is classified as a sub-economic oil discovery.

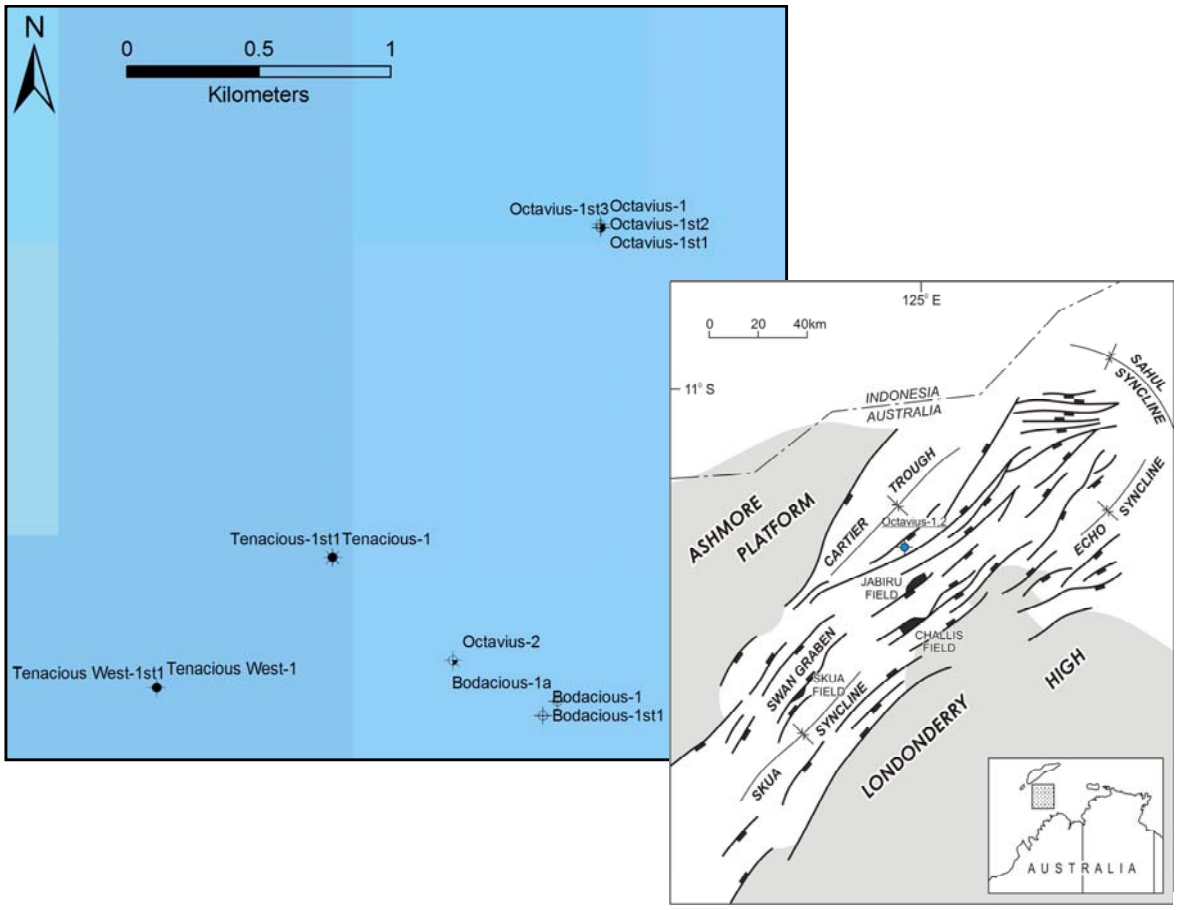

Figure 5-29: Location map showing position of the Octavius wells and the more recent wells.

Close up location map showing the location of the Octavius-1 and -2 wells relative to nearby offset wells, with the inset map placing the well in the context of the broader Vulcan sub-basin. The Tenacious-1 and 1ST and Tenacious West-1 and 1ST wells were oil discoveries, whilst the Octavius wells and the nearby Bodacious-1 and 1ST wells were all dry holes.

The requirement for multiple wells to fully test the potential of the Octavius structure highlights the difficulty in correctly defining traps in structurally complex settings where inaccuracies in the depth conversion and difficult fault imaging contribute to poor placement of the exploration wells (Figure 5–30).

Persistent improvement of the data quality through improved seismic reprocessing and better calibrated velocity models for more accurate depth conversion have allowed the potential of the trap to be fully evaluated. For this reason the full evaluation of unsuccessful wells is critical to recognition of remaining potential that may encourage the drilling of an additional well if trap definition can be improved.

5.4.2.1 Sampling Details

Only the Octavius-2 well was sampled in the current study, drawing on previous results presented for this well in Lisk and Eadington (1994). A previous investigation of the Octavius-1 well where oil inclusion abundance was only qualitatively described (Eadington et al., 1990) and subsequent GOI results from the Tenacious-1 and 1ST wells (Brincat and Dutkiewicz, 1998) were used to aid this evaluation.

As described in the previous chapter the GOI results from Octavius-2 define a substantial palaeo-oil accumulation of about 60m within the currently water-wet Plover Formation. No low GOI samples have been measured so the results only constrain a palaeo-oil down to level at about 3260 mRT. A significant shale interval near the base of the well limits the amount of further sampling that could be undertaken on the deeper reservoir section.

No depth-structure maps are available for the Plover Formation across the Octavius structure but a time-structure map (WMC Petroleum Ltd., 1992) reveals about 25 milliseconds of additional closure down-dip of the Octavius-2 well intersection (Figure 5–31). A detailed depth-conversion has not been attempted but the interval velocities for the Plover Formation derived using check-shot data taken from the well completion report (WMC Petroleum Ltd., 1992) can be used to construct a simplistic depth conversion model.

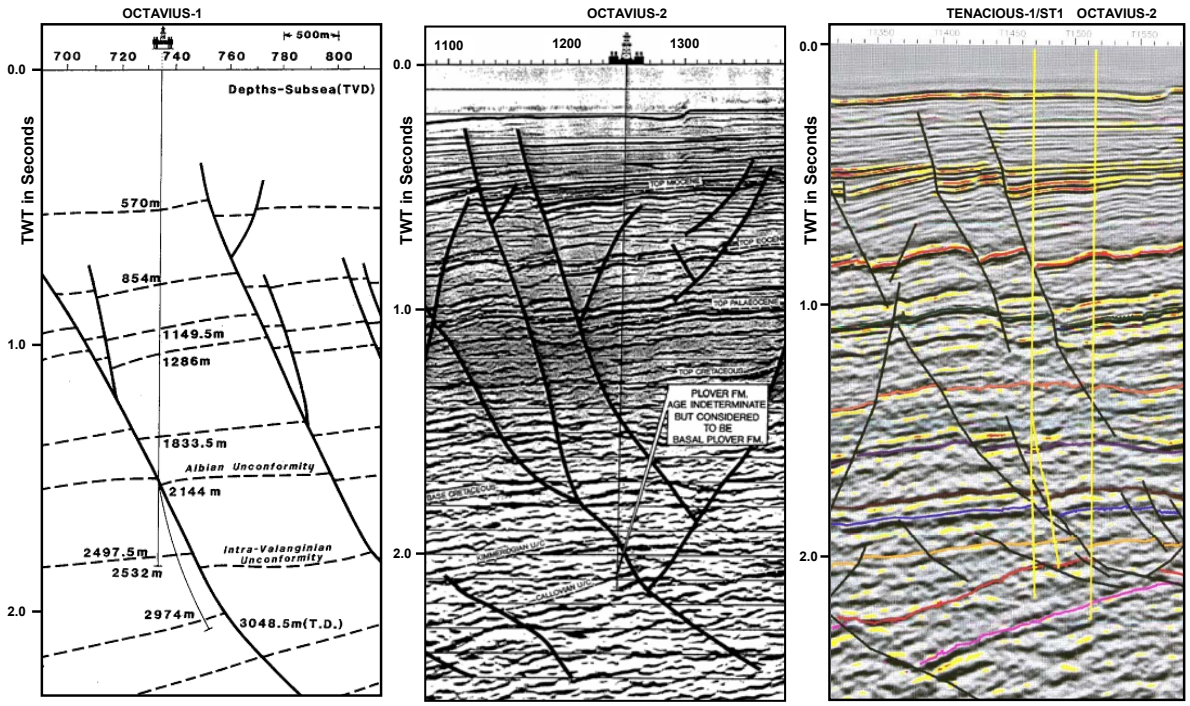

Figure 5-30: Imaging of the Octavius trap.

A composite of seismic interpretations covering the Octavius-1 (WMC Petroleum Ltd., 1990), Octavius-2 (WMC Petroleum Ltd., 1992) and Tenacious-1/ST1 wells that demonstrates the evolving interpretation that led to a successful discovery at Tenacious. The left hand panel is a pre-drill schematic diagram prior to Octavius-1 that shows the intent to target the footwall of a fault dependant structure but the well incorrectly drilled through the fault above the reservoir and reached TD within the hangingwall section. The middle panel describes the second attempt to drill the Plover Formation within closure with Octavius-2 successfully testing the Plover Formation reservoir within closure but being water-wet. Improved seismic data allowed for a third well (Tenacious-1) to be drilled to test a previously unrecognised closure at the Tithonian level (orange horizon) that was not tested by Octavius-2 which only targeted the Plover Formation (red horizon). The straight hole was a success and the well was subsequently sidetracked to penetrate a thicker section up-dip from Tenacious-1.

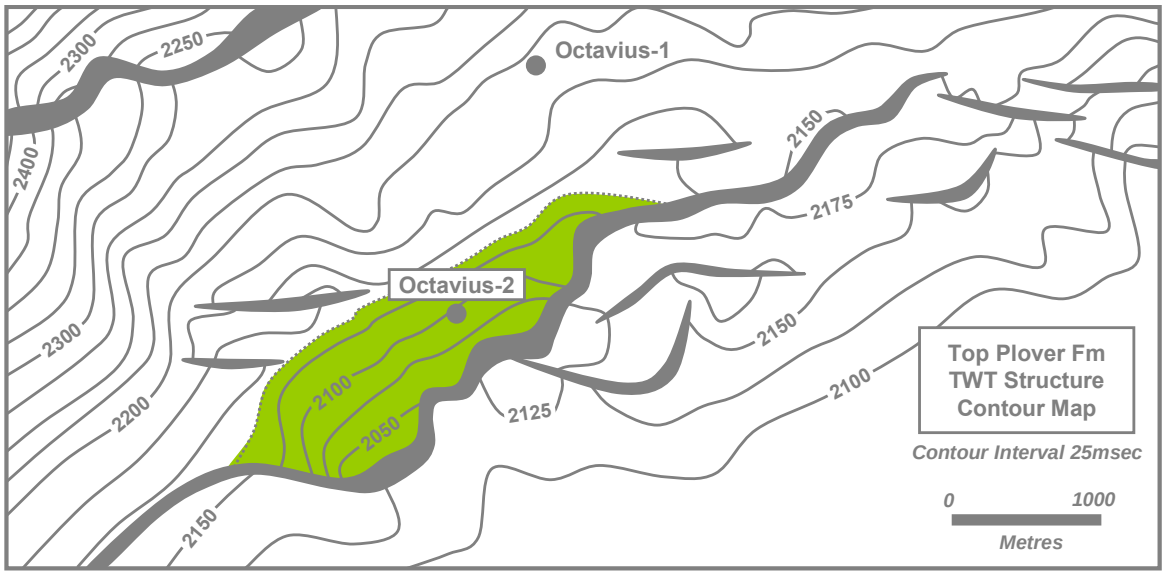

Figure 5-31: TWT structure map for the Octavius structure

Simplified time-structure map for the Top Plover Formation post Octavius-2 (modified from WMC Petroleum Ltd., 1992) showing the approximate extent of the palaeo-oil column delineated by the GOI data (green shading) relative to the mapped structural closure. The depth of the deepest high GOI sample (palaeo-ODT at 3260mRT) was converted into equivalent Two Way Time (TWT) using check shot data taken from the well completion report (WMC Petroleum Ltd., 1992) and marks the base of the green shaded area. Whilst the exact position of the spill-point is not well defined by the relatively broad contour interval the extent of the palaeo-oil zone on this map suggests that the Octavius trap was probably filled to spill before being breached by later fault reactivation.

Using these constraints the 25 milliseconds of mapped closure below the top of the Plover Formation at the Octavius-2 well location equates to about 65 metres of vertical closure using the lowest closing two-way-time contour. This estimate is similar to the height of the palaeo-oil column inferred from the GOI data in the Octavius-2 well. Consequently the trap has sufficient closure to accommodate to minimum palaeo-oil column height (Figure 5–31) further supporting the veracity of GOI data as a genuine indicator with which to detect the position of palaeo-OWCs.

Although the Octavius-1 well failed to reach the Plover Formation it seems likely using this interpretation of the depth conversion that it would have penetrated the Plover Formation outside of closure and below the palaeo-oil down to level defined from GOI data collected on Octavius-2.

The palaeo-oil zone detected in the Octavius-2 well (Lisk and Eadington, 1994) had important implications for later drilling by confirming effective oil charge to the Octavius structure and when combined with revised mapping (Woods and Maxwell, 2004) indicated remaining oil potential at the Plover Formation level, both as an up-dip "attic" zone as well as a separate culmination (Figure 5–32).

The Tenacious-1 and 1ST wells were drilled in 1997 to test the larger of these two Plover Formation closures (the separate culmination shown in Figure 5–32) but subsequently discovered oil in the overlying, Tithonian sandstones, that represented a secondary objective of the well. Tenacious-1 was drilled a further 207m but the Plover section was not penetrated in this well or the subsequent sidetrack well due to a combination of incorrect depth conversion, poor fault imaging and a much thicker than expected Lower Vulcan section (Cultus Timor Sea Ltd., 1997).

The resultant post-drill structural interpretation downgraded the remaining potential at the Plover Formation level (Woods and Maxwell, 2004), leaving only a small closure up-dip from the Octavius-2 well (Figure 5–33). A further well, Bodacious-1/1ST drilled in 2001 and designed to further test the remaining potential at the Plover level successfully penetrated the Plover Formation but was plugged and abandoned as a dry hole.

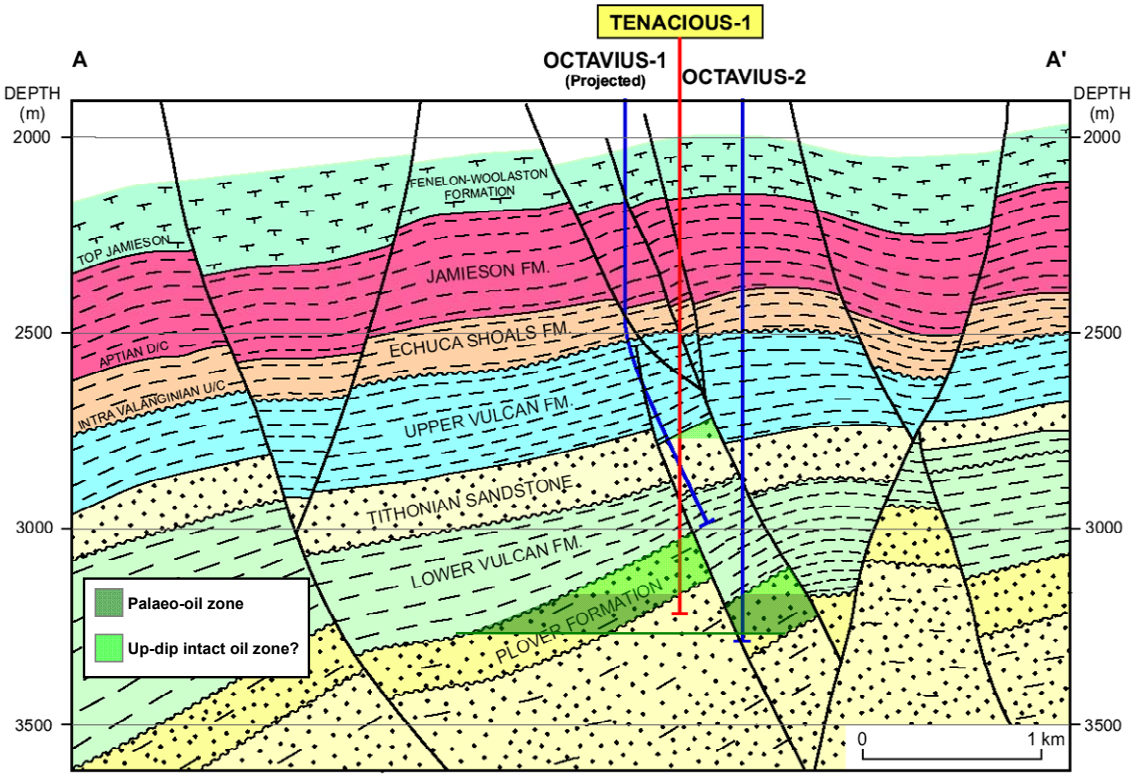

Figure 5-32: Pre-Tenacious-1 structural schematic for the Octavius-Tenacious structure

Cartoon showing the interpreted trap configuration prior to the drilling of Tenacious-1 showing untested up-dip "attic" oil potential constrained by the GOI results from Octavius-2. A separate culmination was interpreted within the same Plover closure and this formed the target of the projected Tenacious-1 well (from Woods and Maxwell, 2004).

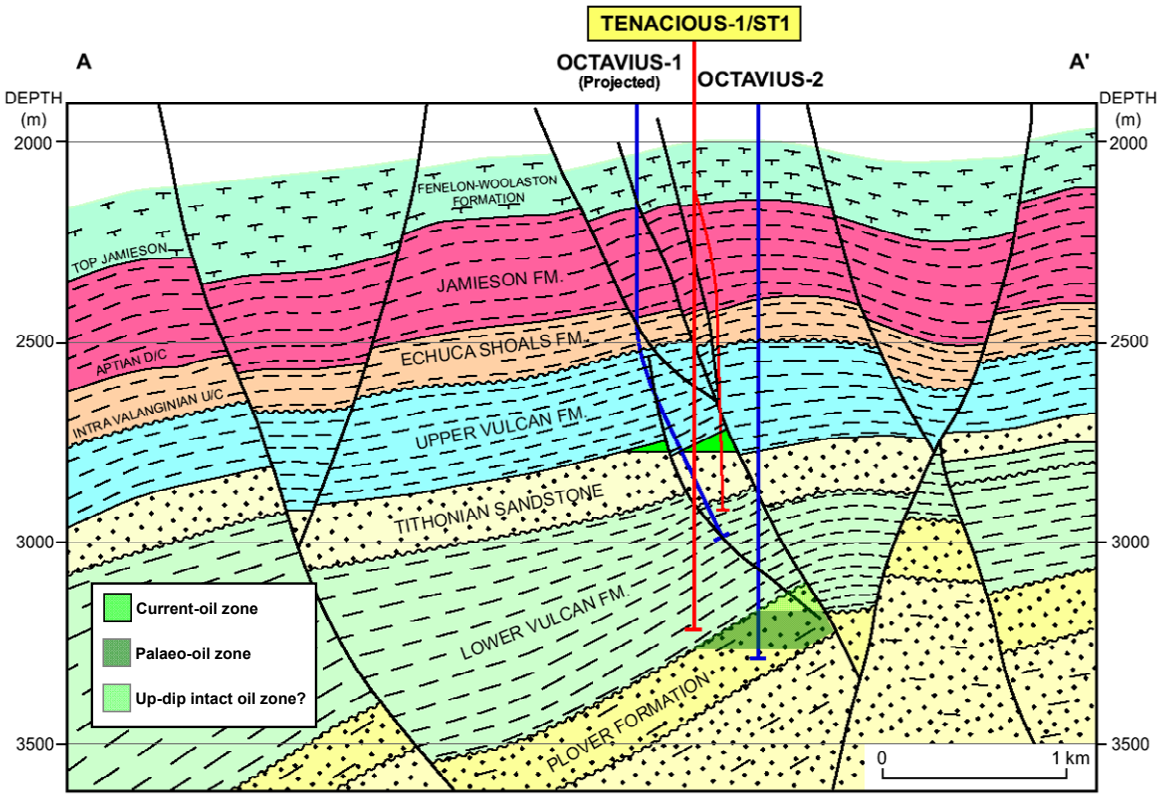

Figure 5-33: Post-drill structural schematic for the Octavius-Tenacious structure

The Tenacious-1/1ST well confirmed the presence of oil at the Tithonian sandstone level but failed to intersect the primary objective of the deeper Plover Formation target. The well was sidetracked to allow for a more optimal penetration of the Tithonian oil zone but was not deepened to test the Plover Formation. Post well remapping removed the larger Plover Formation culmination, leaving only the small "attic" volume immediately up-dip from Octavious-2 (from Woods and Maxwell, 2004).

5.4.2.2 Refined charge history for the Octavius-Tenacious structure

The GOI data from Octavius-2 well provides initial insights into the charge history of the well but further exploration effort conducted over the period of this study has provided additional information to further constrain the charge history (Woods and Maxwell, 2004).

Woods and Maxwell (2004) presented GOI results for the Tithonian sandstones penetrated in the Tenacious-1 and Tenacious-1ST1 wells (Brincat and Dutkiewicz, 1998). In spite of the presence of high oil saturation at the current day none of the samples analysed in that study produced GOI numbers above the threshold for oil accumulation. In Tenacious-1 GOI values ranged from 0.2–0.4%, whilst in Tenacious-1ST1 values ranged from 0.3–2.3% (Brincat and Dutkiewicz, 1998).

The reason for a lack of high GOI values in the oil zone tested by the Tenacious wells remains speculative. The lack of a suitable trapping mechanism for oil inclusions remains a possible explanation but is considered unlikely. Based on the results for other wells described in this chapter a geological explanation rather than a failure of the trapping process is favoured as the most likely cause.

As documented elsewhere, the presence of a palaeo-gas cap represents one possibility with the upwards movement of the oil-leg during partial trap breach producing the current oil column, without trapping significant numbers of new oil inclusions. In this scenario the palaeo-oil column recorded in the Plover Formation at Octavius-2 may have been part of a larger palaeo-hydrocarbon column spanning the Plover and Tithonian reservoirs.

The previous results from Octavius-1 (Eadington et al., 1990) provide some qualitative constraint with only small numbers of oil inclusions recorded in samples from the Tithonian sandstone implying low GOI values in the down-dip well. Based on post-drill depth maps (from Woods and Maxwell, 2004) there appears to be insufficient closure at the Tithonian Sandstone level between the position of the deepest Tenacious-1 sample and the shallowest Octavius-1 sample to accommodate a palaeo-oil zone of sufficient magnitude (Figure 5–34).

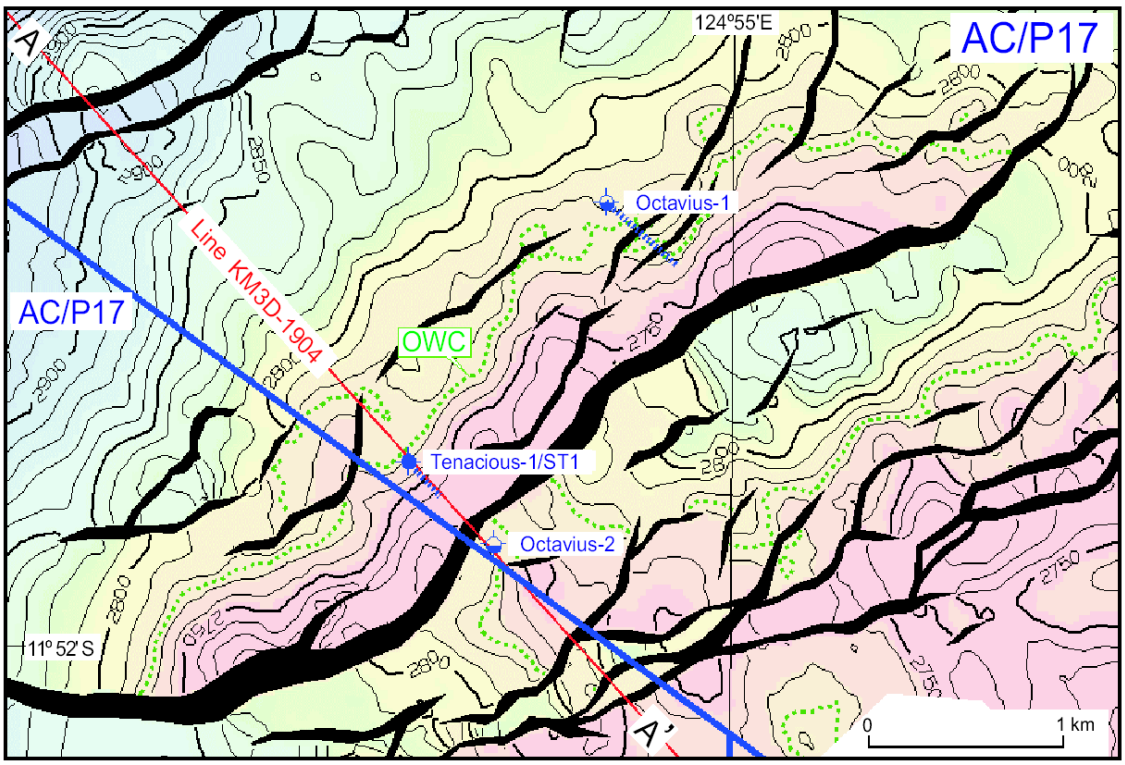

Figure 5-34: Post drill depth structure map for the Tithonian sandstone

Remapping of the Octavius/Tenacious structure after Tenacious-1ST1 showing that only limited closure lies below the oil-bearing Tenacious-1ST1 and above the water-bearing Octavius-1 well (from Woods and Maxwell, 2004). This observation, together with the limited oil inclusions seen in Octavius-1 (Eadington et al., 1990) makes it unlikely that a palaeo-oil zone exists below the current Tenacious oil zone.

More substantial closure is mapped below the Octavius-1 penetration and although not very thick the larger areal footprint could translate into a sufficient volume to account for the oil currently reservoired.

Woods and Maxwell (2004) introduced another possible explanation suggesting that there may have been insufficient residence time to trap oil inclusions due to oil charge occurring very recently to the Tenacious structure. The fault that produces the closure at the Tithonian sandstone level formed during Neogene structuring, involving the reactivation of a deeper Kimmeridgian–early Tithonian fault, providing evidence that supports a relatively short residence time for the Tenacious oil pool.

Additional support for a recent oil charge comes from the Brincat and Dutkiewicz (1998) report that used fluid inclusion palaeo-temperature data combined with basin modelling predictions to conclude that oil charge to the Tenacious pool occurred since about 8 Ma.

A further piece of pertinent information was subsequently provided by analysis of the fluid inclusion oil seen in the Octavius-2 well. George et al. (1998) demonstrated that although the fluid inclusion oil in Octavius-2 was, in many regards, similar to the Tenacious-1 crude oil, the maturity of the Tenacious oil was notably lower in maturity (by about 0.1–0.2 vitrinite reflectance equivalent) than the Octavius-2 inclusion oil (1.0–1.3 vitrinite reflectance equivalent), probably precluding the breaching and remigration concept. Instead, it seems more likely that the Tithonian and pre-Callovian petroleum systems are independent in the Tenacious area, accessing different source units and/or locations, and having independent migration pathways (Woods and Maxwell, 2004).

5.4.3 Summary

The selection of detailed charge history examples presented where sufficient data, both in terms of analytical results and access to general geological data, are available clearly demonstrates the value of high-resolution collection of GOI data as a tool in helping unravel complex charge histories. Whilst the results are not always conclusive nor do they necessarily lead to a more favourable view of the petroleum

system being studied they do provide valuable constraints on the possibilities that should be considered.

Similarly whereas high resolution studies involving many wells and detailed sampling can reveal important aspects of the charge system they can be equally valuable where collected in a more reconnaissance level sampling program as will be discussed in the next section. Ultimately the integration of high resolution studies on specific traps with more regional sampling helps to produce a more comprehensive understanding of the petroleum systems at work in sedimentary basins.

5.5 REGIONAL CHARGE HISTORY

Integration of the palaeo-hydrocarbon distribution determined from the fluid inclusion data with the present day hydrocarbon distribution derived from discoveries and conventional oil show data allows a detailed charge history to be discerned that draws on a larger footprint of investigation. Differences in the palaeo-fluid phase and the position of palaeo hydrocarbon–water contacts enables the mechanisms controlling these changes to be identified at the trap scale and together with the regional distribution of these features contributes to the formulation of improved models to predict likely charge and retention potential throughout the Vulcan Sub-basin and the region as a whole.

The observed current hydrocarbon distribution together with the GOI results presented in detail in the preceding chapter and as part of the integrated charge histories discussed in preceding sections of this chapter, indicate that at least three discrete pulses of hydrocarbon fluids (H1 to H3) contributed to the charge history experienced by the VSB (Figure 5–35). These include an early gas rich charge (H1), a widespread oil charge (H2) and a late gas flush (H3). Three key processes, namely gas displacement, fault seal breach and structural tilting have influenced the retention of these discrete hydrocarbon pulses. Understanding the relative contribution from each of these processes and the interplay between them provides an opportunity to be more predictive when considering the location of remaining hydrocarbon reserves.

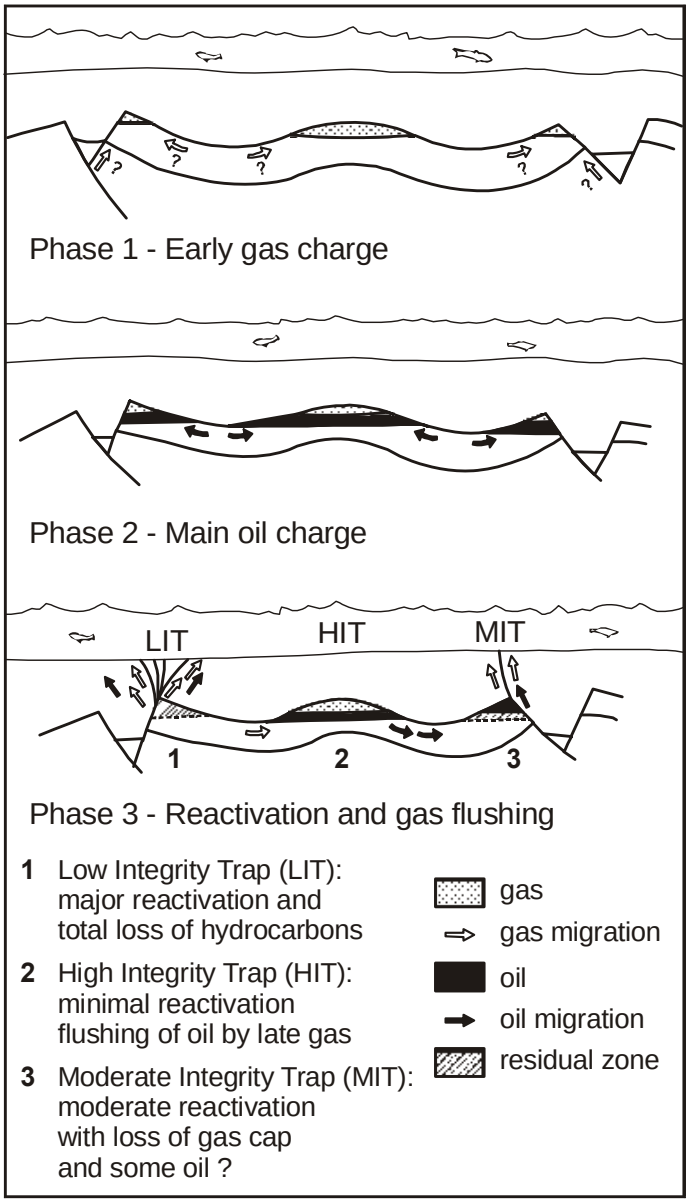

Figure 5-35: Cartoons showing proposed hydrocarbon charge history

A three phase charge history is implied for the VSB involving an early gas-charge phase followed by a more widespread oil charge and subsequently influenced by gas flushing and structural modification. In stage 1 a gas charge (H1) representing the early products from mixed oil and gas source rocks filled available closures. Oil generated from these source rocks was expelled during Phase 2 (H2) and produced many oil columns across the VSB. Further maturation of these source rocks produced a late gas charge (H3) that mixed with and displaced early oil charge from the crests of traps (Phase 2). In the final phase widespread fault reactivation and attendant trap breach allowed partial (Moderate Integrity Traps, MIT) or complete (Low Integrity Traps, LIT) loss of hydrocarbons except where traps where shielded from reactivation (High Integrity Traps, HIT; i.e. four way dip closed structures).

5.5.1 Phase 1 – Initial Gas Charge (H1)

Fluid inclusion results suggest that initial hydrocarbon charge to traps in the VSB involved a gaseous fluid (H1) that resulted in partial or total filling of the closures available at that time (Figure 5–36). The source of this fluid is uncertain, but regional basin modelling studies (Kennard et al., 1999) suggest that hydrocarbon generation from the key Upper Jurassic source kitchens occurred in two distinct episodes. The first of these involved gas generation and expulsion and is attributed to increased heat flow and a phase of rapid burial due to increased subsidence associated with the Jurassic rifting (Figure 5–37).

A subsequent period of tectonic quiescence produced a phase of slow burial and an associated waning in basin heat flow during the post-rift thermal relaxation ("drift") that contributed to a fall in formation temperatures and led to a quenching of widespread generation and expulsion in the Cretaceous (Figure 5–37).

Kennard et al. (1999) suggest that gas was preferentially expelled during this initial generation phase due to higher buoyancy, with oil being retained within the source interval until increased compaction associated with Tertiary burial allowed expulsion thresholds to be reached. The terrestrially dominated source rocks of the Jurassic section in the VSB is likely to have favoured this process both in terms of allowing for absorption of oil within the kerogen and a preference for generation of abundant gas from source rocks that are dominated by Type III organic matter.

The fluid inclusion record collected by the current study does not directly demonstrate an early gas charge as the existence of gas-filled inclusions was not rigorously documented either petrographically (optically) or through other suitable techniques such spectroscopic methods or chemical analysis of gas released from crush-leach samples. The evidence to support an early gas charge instead comes mostly from zones where low GOI values overlie interpreted palaeo-oil zones and that have been inferred to represent palaeo-gas caps where gas charge was prior to or contemporaneous with an associated oil charge.

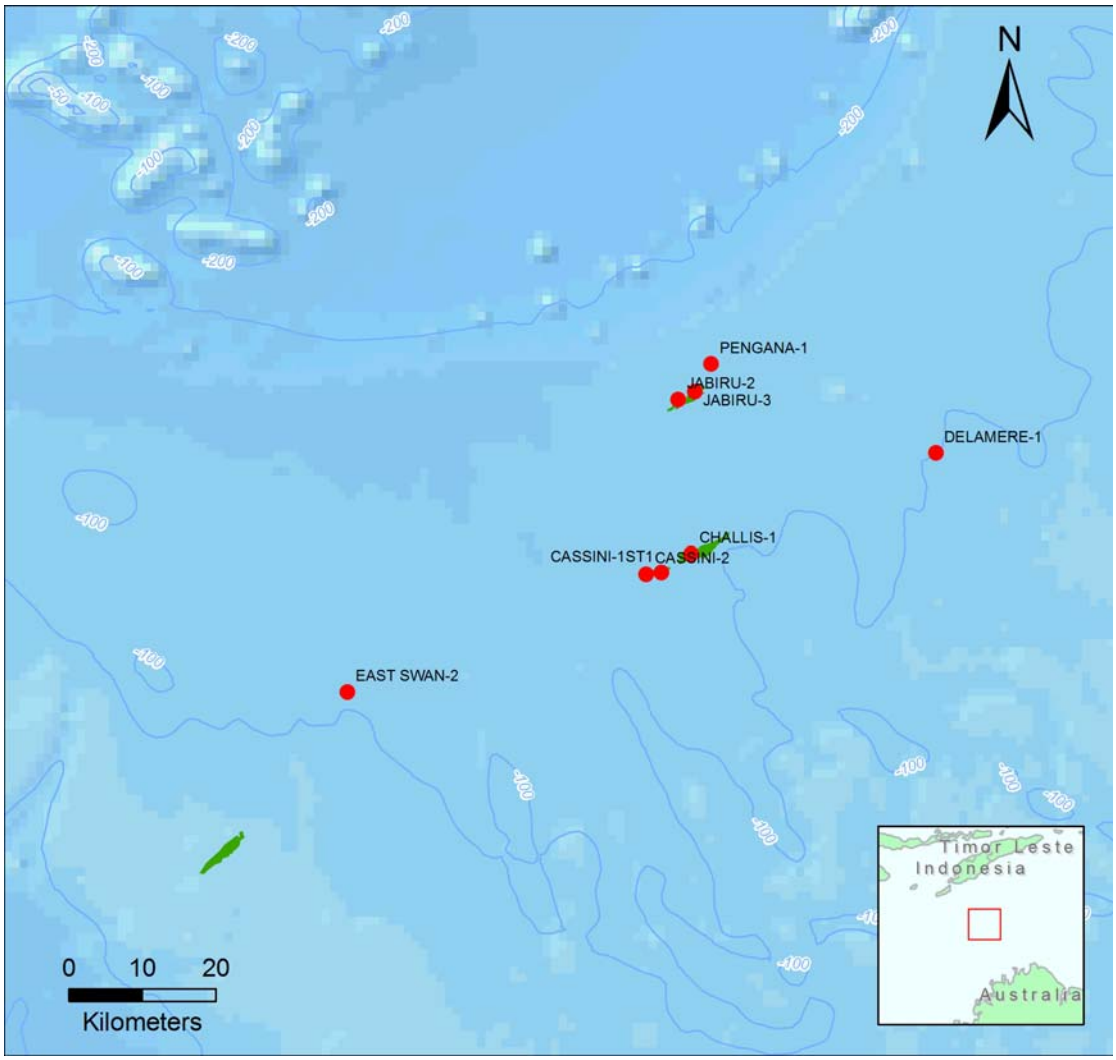

Figure 5-36: Distribution of wells with a palaeo-gas cap

Map highlights the location of wells where evidence to support an initial gas charge are observed, either as zones of low GOI values above interpreted palaeo-oil zones or where the absence of oil inclusions within traps that are currently filled to spill with gas has been inferred to indicate charge by gas prior to the onset of regional oil migration.

However, in the Pengana-1 and Delamere-1 traps samples taken from within the current gas zones are devoid of any oil-filled fluid inclusions, despite oil inclusions being noted in samples from below the current GWC. In the Delamere and Pengana wells this early gas charge appears to have completely filled the available closure, apparently preventing accumulation of the later oil charge, especially at Pengana-1 which is well positioned to receive a later oil charge.

Gaining an understanding of the distribution of this early gas charge is a critical factor in risking the likelihood that small structures have been gas filled prior to oil prone source rocks becoming mature. Such structures are likely to lack sufficient closure to contain large enough gas volumes to represent economically viable accumulations and should be avoided as potential drilling targets.

Examples of this early gas charge are also recorded as palaeo-gas caps in currently oil-filled traps such as the Jabiru, Swift and Challis-Cassini fields and in the presently water-wet trap tested by the East Swan-2 well (Figure 5–36). However, unlike Delamere and Pengana in these examples the presence of some oil inclusions in samples from the inferred palaeo-gas caps indicates both oil and gas fluids were migrating phases.

This raises the possibility that the oil and gas are co-generated rather than involving a discrete early gas-phase. Three dimensional basin modelling results (Fujii, 2007) show migration of early generated gas to some of these traps but others, such as Challis-Cassini are not connected to the recognised source kitchens at this time. In these instances later generation of large volumes of oil and gas during the second phase of generation is more likely and not unexpected for a Type III source rock.

5.5.2 Phase 2 – Main Oil Charge (H2)

Expulsion of oil generated from the principal source rock in the region, marine shales of the Upper Jurassic Vulcan Formation (Edwards et al., 2004), resulted in widespread oil charge (H2), mostly generated from the recognised Upper Jurassic source kitchens located in the Swan, Skua and Paqualin grabens (Figure 5–37).

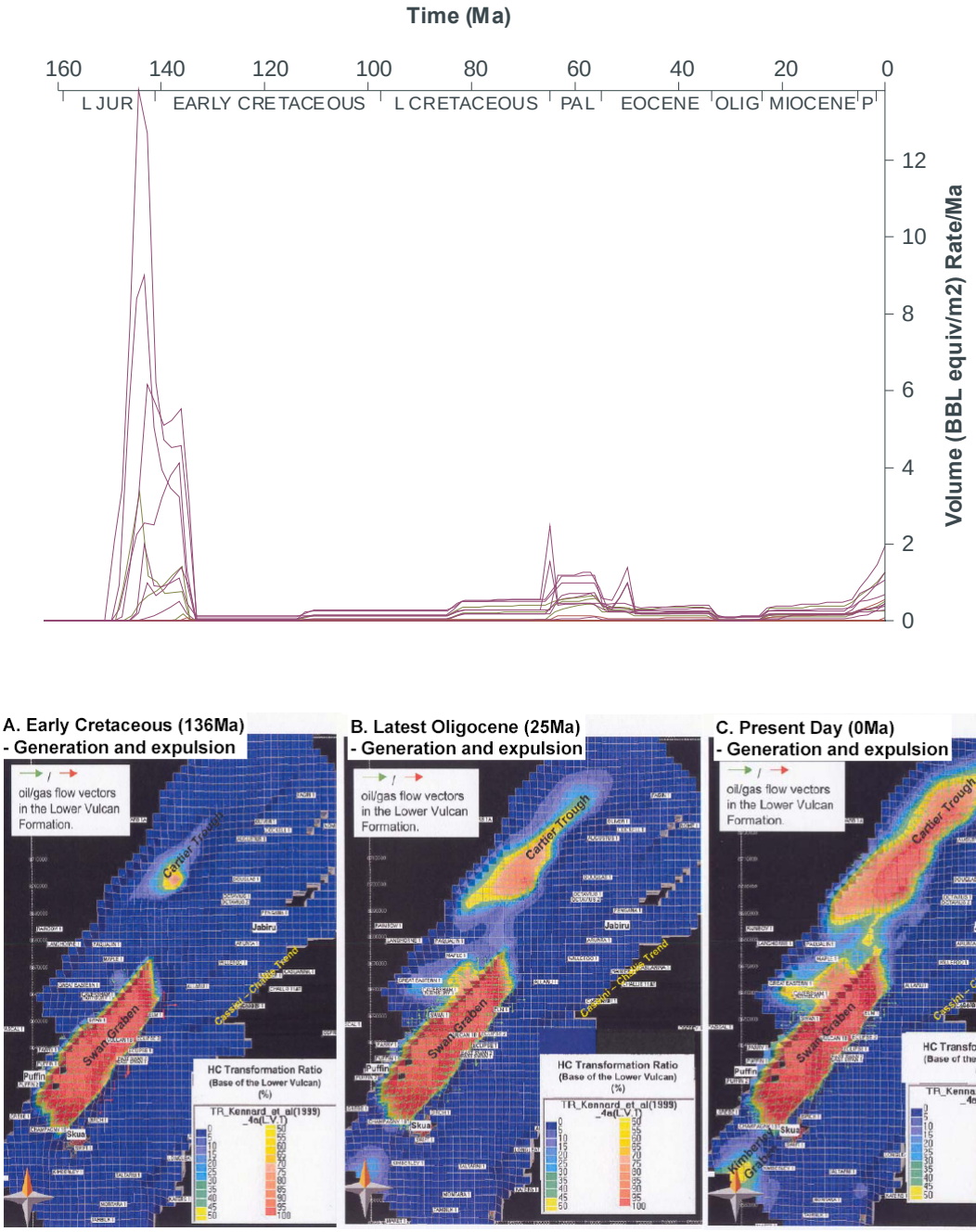

Figure 5-37: Models of source rock expulsion for the Lower Vulcan Formation in the VSB.

Upper diagram shows a hydrocarbon expulsion model for gas generated from the Lower Vulcan Formation through time (from Kennard et al., 1999), whilst the map views in the lower diagram (from Fujii, 2007) show predicted hydrocarbon generation and expulsion from the Lower Vulcan Formation at A., 126Ma immediately following rifting, B., at 25Ma representing the onset of plate collision and for the present day (C.). The models indicate substantial generation and expulsion of gas in the Late Jurassic, almost entirely derived from the Swan Graben. The Cartier Trough does not provide significant gas generation until the Late Tertiary and the predicted volumes expelled are much less than produced immediately after rifting.

These Upper Jurassic source kitchens are predicted to have become mature for oil expulsion by the Cretaceous (Kennard et al., 1999; Figure 5–37) and likely contributed much of the early oil charge with only limited contribution from the Cartier Trough kitchen due to a relative lack of burial and much leaner Upper Jurassic source rocks. However this kitchen may also have contributed hydrocarbon charge derived from the underlying Plover Formation, but given the much poorer source rock quality (low TOC and Low HI values) gas rather than oil would have been the dominant fluid.

In contrast the source rock quality within the Upper Jurassic section of the grabens to the southwest is typically good to occasionally excellent (Edwards et al., 2004) and the subsidence history (Kennard et al., 1999) suggests burial depths are likely to have been favourable for generating significant amounts of oil. These narrow depocentres formed during Jurassic rifting and provided ‘restricted circulation’ anoxic conditions to favour the deposition and preservation of high-quality oil-prone source rocks.

In contrast, the Cartier Trough was largely created by Tertiary down warping associated with plate margin collision from about 25Ma and particularly from between about 8 Ma and 3 Ma when collision at Sumba occurred (Keep et al., 1998). Here the subsidence history played no role in optimising the source rock potential, instead contributing the high temperatures to mature the source rocks. The more open marine and oxic depositional conditions make it unlikely that this depocentre was as prolific an Upper Jurassic source kitchen as the deep grabens in the south-western part of the VSB, but a contribution from coaly facies within the underlying Plover Formation deltaic sequences may have been significant, albeit more gas-prone.

The GOI results produced in this study confirm the efficacy of the Jurassic mudstones as an oil-prone source rock within the Swan and Paqualin grabens with a high proportion of wells positioned adjacent to these narrow grabens found to contain either significant palaeo-oil columns in traps that are currently water wet-well or as thick residual oil zones that lie beneath the OWCs of most of the intact oil columns (Figure 5–38).

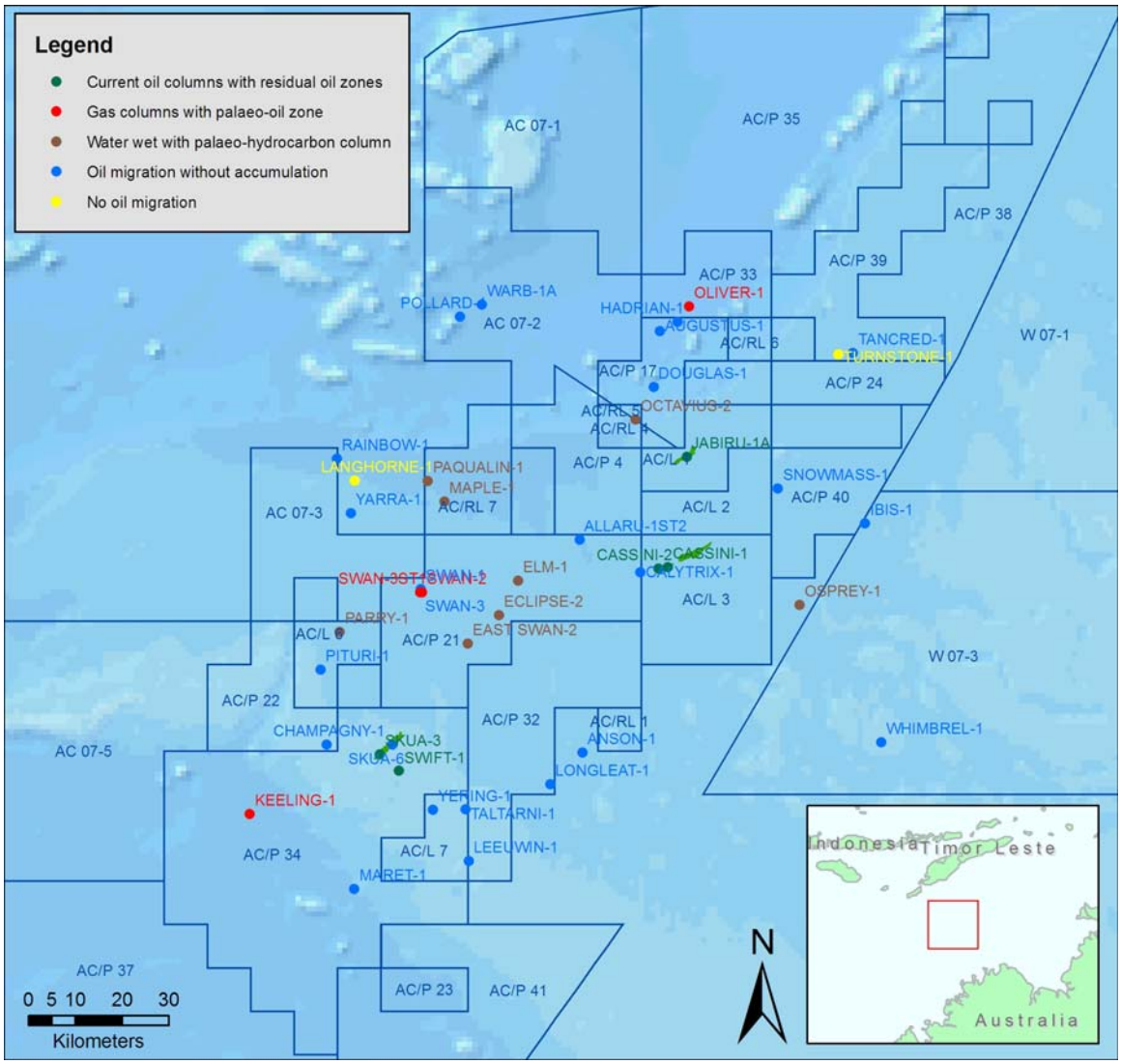

Figure 5-38: Distribution of wells with a palaeo-oil column.

Map showing the charge history of wells that has been interpreted from the GOI results produced in the current study, colour coded to describe the current fluid fill and to reflect the main process controlling the observed distribution. Note that only two wells of the 73 wells investigated show a complete absence of oil filled fluid inclusions in all samples analysed.

The GOI data concur with basin modelling predictions of charge dominated by oil, although evidence for an associated, but subordinate, gas charge is seen in some wells. More distal traps such as Jabiru are also likely to have been sourced from the Swan Graben; with these fields utilising NE-SW orientated fault bound terraces and relay ramps to facilitate long distance migration paths (Figure 5–39). Importantly this mechanism allowed charge to traps located outside the pod of active source rock.

In contrast to the limited information on the early gas-charge (H1) the main oil charge (H2) is more comprehensively described in the fluid inclusion record, both petrographically and geochemically. The presence and size of palaeo-oil zones is well defined and in traps where multiple wells have been sampled the geometry of these features can also be constrained. Geochemical analysis of fluid inclusion oils (FIOs) from the palaeo-oil columns seen in wells adjacent to the Swan and Paqualin grabens confirm a likely derivation from source rocks of the Upper Jurassic Lower Vulcan Formation and correlate well with the Group A family of Edwards et al. (2004) that are derived from the same source rock. The lower maturity levels and the less altered composition of the fluid inclusion oils is consistent with the main phase of trapping occurring in the geological past, an outcome that is well matched by the observation that the fluid inclusion appear to records palaeo-trap configurations that relate to the initial charge event.

The FIOs from traps that were well positioned to draw charge from the Swan and Paqualin grabens are typically derived from more marine dominated facies than the currently reservoired crude oils (Group A oils of Edwards et al., 2004) and whilst these could indicate a distinct third oil family it is more likely that these represent a true end-member of the Group A family that has subsequently mixed with terrestrially dominated hydrocarbons (Group B) to produce the composition that typifies Group A crude oils.

The presence of the angiosperm marker Oleanane is some of the FIOs indicates a contribution from Cretaceous source rocks, probably from the Upper Vulcan Formation, but could also represent contamination by hydrocarbons that are being leached from the Cretaceous cap rocks that seal these traps.

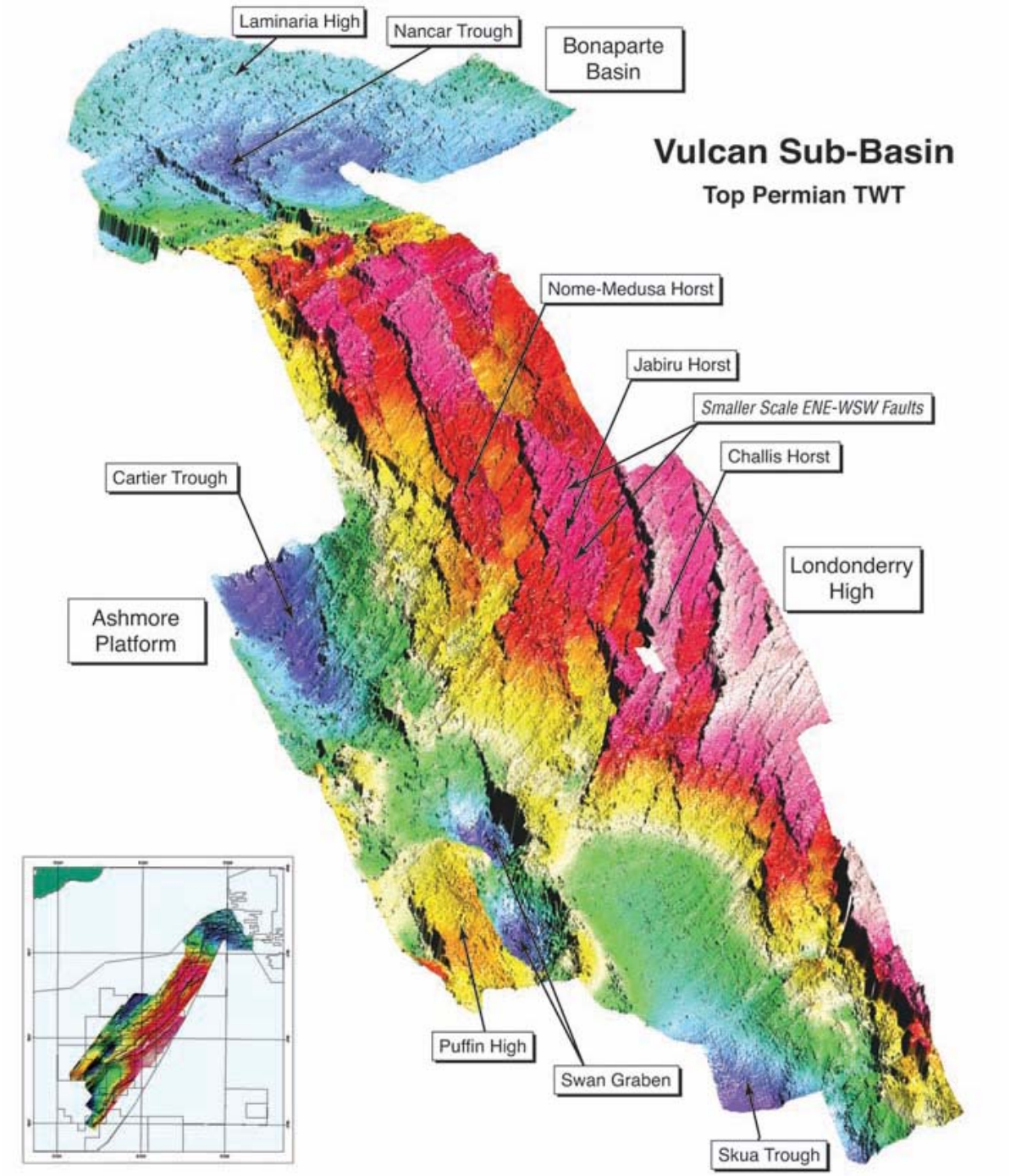

Figure 5-39: Influence of regional structure on migration pathways.

A regional TWT structure map at top Permian level derived from 3D seismic data (from Edwards et al., 2005) demonstrating the style of *en echelon* fault architecture that produces large relay ramps capable of facilitating long distance hydrocarbon migration. Oil generated in the key source kitchens within the Swan Graben is able to reach distant traps without needing to cross major structural barriers. Cool colours are deep and warm colours are shallow in TWT.

Traps relying on oil sourced from the Skua Trough are thought to include the Montara, Tahbilk, Bilyara, and Talbot oil and gas fields, while long distance migration along structural ramps (O'Brien et al., 1996b) may account for oil charge to the Challis-Cassini complex (Figure 5–39) and possibly the Osprey-1 palaeo-oil column. The charge history to these fields is poorly described by the GOI data and appears to be more complicated, with an overall greater propensity for gas indicating less oil-prone source facies or a complex maturation history.

The more subdued or absent GOI response in oil zone samples from many of the traps that likely derived hydrocarbon charge from the Skua Trough has a number of possible explanations. Firstly, where more detailed geological information is available traps that at first inspection appear to have anomalous GOI results can often be explained, such as the results seen in the Challis-Cassini area where the distribution of the high GOI samples is very consistent with the sub-cropping nature of the reservoir stratigraphy. The presence of a palaeo-gas cap that has subsequently been lost is well supported by the data and delivers a coherent charge history.

In other traps where sampling may not be sufficient to allow a complex charge history to be discerned an alternative or perhaps associated reason for the low GOI values recorded in traps drawing charge from the Skua Trough could also reflect the different nature of hydrocarbons being expelled from this source kitchen. At the Talbot Field, for example, where no high GOI values were seen in samples from the oil zone, Edwards et al. (2004) speculate that the oil trapped in this field may be the product of evaporative fractionation. This composition could have been produced by partial trap breach and gas loss from a hydrocarbon column that initially accumulated purely as a gas-condensate. In this instance, hydrocarbon fluid during initial charge may have been gas rather than oil and due to wettability issues less likely to be trapped as fluid inclusions. Suitable conditions for the trapping of oil inclusions may not have prevailed when a discrete oil phase was liberated by a fall in reservoir pressure associated with preferential gas leakage.

Further to the north-east the GOI results from this study provide improved constraints on the hydrocarbons produced from the more speculative source kitchen within the Cartier Trough at the north-eastern margin of the VSB. Rapid Neogene

subsidence experienced in this part of the basin, coupled with the uncertainties regarding the source potential within the trough previously resulted in an industry perception that the region has a higher tendency for gas-rich charge.

Aside from more recent discoveries such as Audacious and Tenacious that are well positioned to receive charge from the Cartier Trough the fluid inclusion results from Octavius-2 and Oliver-1 reveal that substantial palaeo-oil columns were able to accumulate. This provides demonstration that this source kitchen has the potential to produce large volume oil plays in this area, if the risk of flushing by late gas charge can be effectively mitigated pre-drill.

However, despite the relatively simple subsidence history of the Cartier Trough the well results indicate considerable complexity in the petroleum system operating in this part of the VSB. At Octavius-2 the analysis of the FIO reveal the accumulation of high maturity oil that is likely to reflect deviations from rapidly subsiding source rocks driven by Neogene plate collision. This contrasts lower maturity of the Tenacious and Audacious crude oils and the FIO from the Oliver-1 palaeo-oil zone, implying either earlier charge or different migration pathways. Similarly the Oliver-1 FIO was derived from a much more marine source rock quite unlike the significant terrestrial source rock input seen in the other Carter Trough oils.

The Cartier Trough is more lightly explored than other parts of the VSB so indications of large palaeo-oil volumes highlight significant liquids potential. Significantly, in all other dry holes drilled adjacent to the Cartier Trough, the well completion reports highlight concerns over the validity of the trap and consider it unlikely that a valid trap has been tested. If these questionable drilling results are excluded then the oil charge rate derived from this kitchen, based on demonstrably valid traps, is at or close to 100% (Lisk et al., 1998b). Enhanced imaging of prospective targets and improved data processing, epitomised by the successful use of pre-stack depth migrated processing (PSDM) of 3D seismic data that led to the drilling of the Audacious oil discovery (Maxwell et al., 2004), clearly could provide the key to future success in wells targeting the Cartier Trough.

Whilst the majority of effort in the current study has focused on traps that rely on migration of oil into Jurassic reservoir sections vertically or horizontally juxtaposed against the recognised source rock horizons some hydrocarbon migration into the shallower stratigraphy is also indicated. The Puffin oil accumulation, the Parry-1 and Swan Field palaeo-oil columns (Figure 5–38), in Maastrichtian sands, together with conventional oil shows commonly reported from the post-rift section are interpreted to represent oil sourced from the Swan Graben using faults as migration pathways from underlying breached Jurassic reservoirs (Edwards et al., 2004).

At the onset of this study the petroleum system that was viewed to by operating in the VSB was seen as involving charge to structures mostly during the passive margin phase of basin evolution and that these remained relatively static until late Tertiary fault reactivation caused widespread breaching of many of these traps. The results of the current study together with a number of published studies have challenged this view and are pertinent to the three stage model being outlined.

The inclined palaeo-OWC defined for the Skua Field (Gartrell et al., 2002) that implies a degree of modification of the trap after the initial oil charge is probably related to structural tilting that occurred in response to rapid progradation of the Tertiary overburden sequence. In the same field the benefit of high-resolution, multi-well, investigations is demonstrated by recognition of the role that pre-existing fault intersections play as passive leak points. At Skua these leak points appear to have existed prior to the onset of initial oil charge and have acted to control the trap capacity to a level less than the volumetric capacity of the mapped closure (Figure 5–40; Gartrell et al., 2004).

The wider role of these fault intersections can be alluded to from the occurrence of deep basin lineaments that reflect earlier Palaeozoic rifting in the VSB and that are orientated at a high angle to the later period of faulting associated with Jurassic rifting. The effectiveness of these fault intersection zones as points of enhanced fluid leakage is well supported by numerical geomechanical modelling experiments conducted for the Skua Field (Figure 5–40, Gartrell et al., 2004).

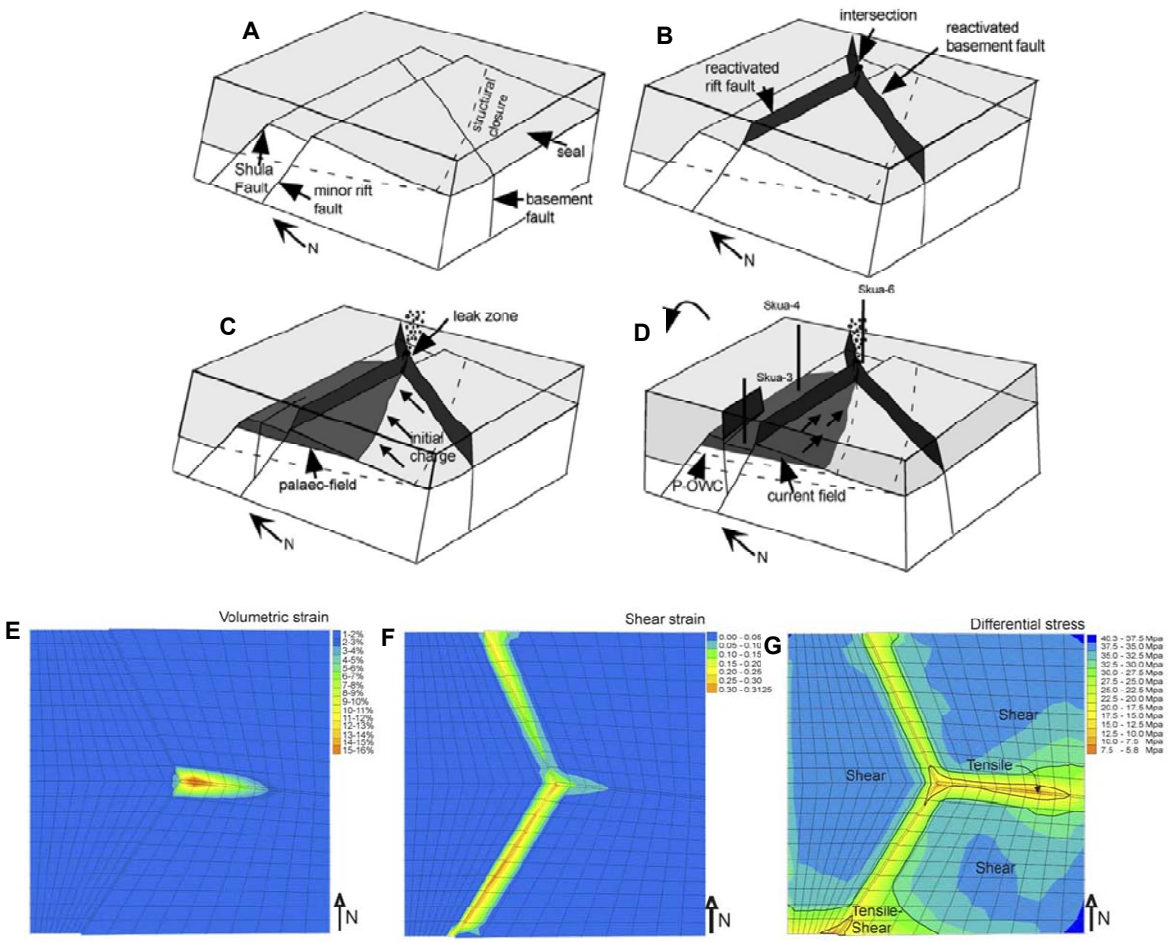

Figure 5-40: Role of fault intersections in controlling the Skua Field

Integrated structural and charge history schematic model for the Skua Field. (a) Prior to reactivation and hydrocarbon charge. (b) Late Cretaceous to early Tertiary reactivation of basement fault and subordinate rift fault causes damage at the intersection of the faults. (c) Initial oil charge with the extent of the palaeo-field is controlled by the location of the fault intersection (leak zone). (d) Palaeo-OWC is tilted due to post rift subsidence causing hydrocarbons to flow up-dip towards the leak zone. (e) Results from the simple fault model based on Skua showing after 1% contraction the volumetric strain increment (dilation, E) and (g) the shear strain increment and (f) the differential stress distribution (s1–s3) showing areas of tensile, hybrid tensile-shear and shear fracture mode (From Gartrell et al., 2004).

This modelling work also lends support to earlier proposed empirical models for trap integrity in the VSB that suggested the degree of obliquity between the orientation of Jurassic rift faults compared with the later Neogene faults was an important indicator of trap breach potential (O'Brien and Woods, 1995; O'Brien et al., 1996a).

5.5.3 Phase 3A – Late Gas Charge (H3)

A late gas charge (H3) represents a third phase of hydrocarbons to have contributed to the charge history (Figure 5–41), but is one that has generally been deleterious to the economic potential of traps within the VSB due to the limited value of small volume gas.

VSB source rocks have recognised gas potential reflecting the abundance of terrestrial organic matter and would be expected to generate significant gas volumes when mature. Gas generation comes from the over-maturation of the more oil prone Upper Jurassic source rocks as well as a contribution from terrestrially dominated facies within the underlying fluvio-deltaic Plover Formation.

The transition from a liquid rich to gas prone charge is driven by the higher temperatures produced by rapid subsidence in the Pliocene that was related to the flexure of the Australian Plate during the early stages of collision with the Eurasian Plates to the north. This accelerated the maturation of source rocks and promoted increased gas expulsion (Figure 5–37) that led to widespread gas charge and partial or complete associated flushing of oil from any pre-existing oil columns.

Palaeo-oil columns defined by GOI data within reservoirs currently filled with gas are recorded in the Keeling, Oliver, Swan and Skua fields (Figure 5–38). Late gas charge to these traps will have displaced these palaeo-oil columns by ‘Gussow’ type displacement (Gussow, 1954) and loss of some oil across the spill-point could have provided a remigrated oil charge to adjacent structures (Lisk et al., 1999).

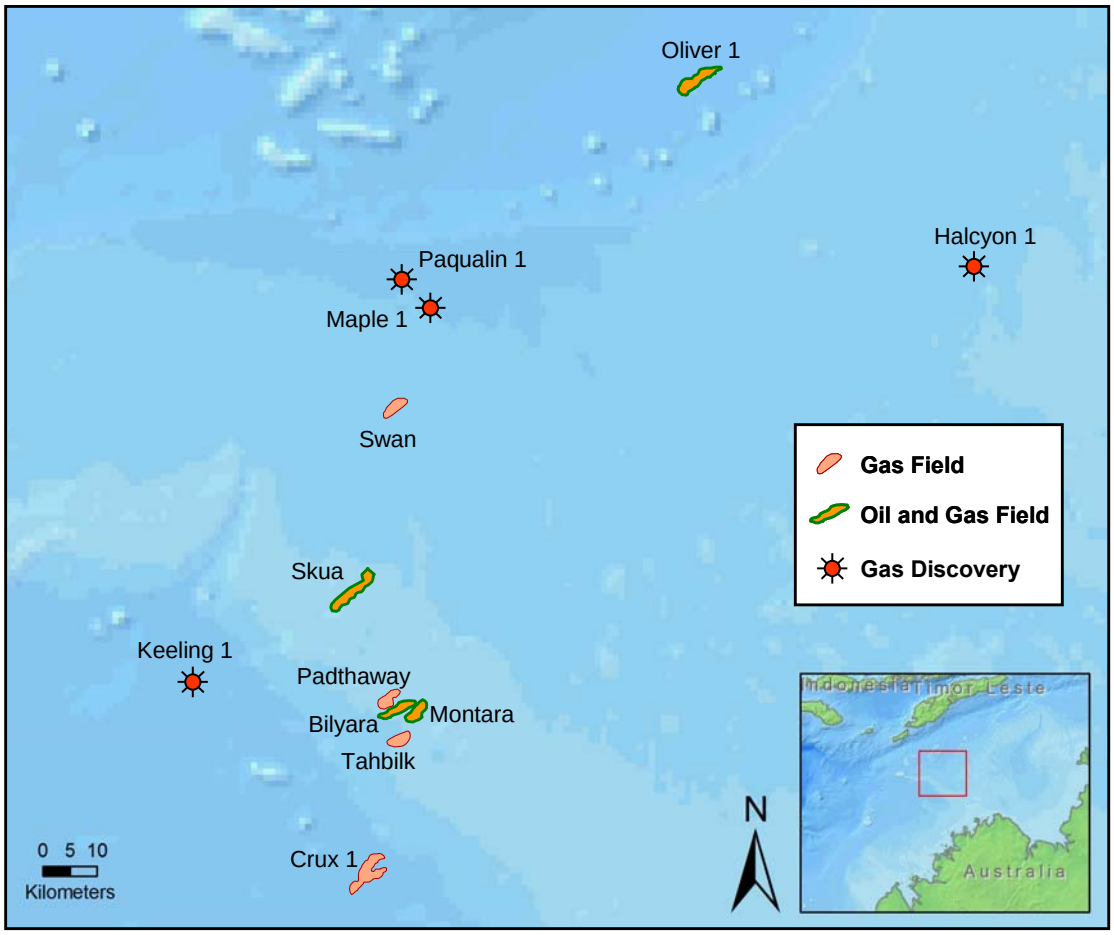

Figure 5-41: Distribution of wells with a current gas fill

Location of wells and fields that currently contain either gas or gas with an underlying oil rim from the VSB showing widespread influence of late gas charge to the region. None of the fields shown are currently economic but several have displaced potentially significant palaeo-oil volumes that may have charged satellite structures adjacent to these fields.

The propensity for oil to undergo 'Gussow' displacement (Gussow, 1954) is controlled not only by gas buoyancy but also by changing reservoir pressure, volume, temperature (PVT) conditions prevailing through time and the composition of migrating hydrocarbons both already resident in the trap as well as new fluids reaching the trap. These conditions will change dynamically as burial and heat flow change through time, adding additional complexity of the charge history experienced by individual traps.

Predicting the phase condition of hydrocarbons within the reservoir is obviously important when considering the likelihood of an oil-leg being located down-dip of a fully gas saturated reservoir (a gas down to level in the well rather than a clear GWC) and is a critical factor to be considered in order to properly risk the chance of success of such drilling efforts.

The amount of oil that can be lost into the gas phase is principally controlled by the liquids content of gas charging the trap (expressed by the Condensate Gas Ratio, CGR) and the greatest loss of oil will occur when this gas is composed purely of methane (CGR=0). These calculations are beyond the scope of the current investigation, but a description of the workflow for assessing the impact of these changes is described in the previous chapter and in Lisk et al. (2002) using the Oliver-1 results as an example.

5.5.4 Phase 3B – Neogene Fault Reactivation

The three principal phases of hydrocarbon charge (H1-H3) experienced by the Vulcan Sub-basin have played an important role in determining the distribution of hydrocarbons seen at the current day, but they are not the only control on the composition and retention of oil and gas. Integration of the fluid related processes with the structural history of the basin is needed to fully describe the hydrocarbon charge and retention history.

The impact of structural modifications on hydrocarbon preservation within the VSB has been widely documented, focussed primarily on the impact of Neogene collision (O'Brien et al., 1998; Lisk et al., 1998b; Cooper et al., 1998; Peresson et al., 2004).

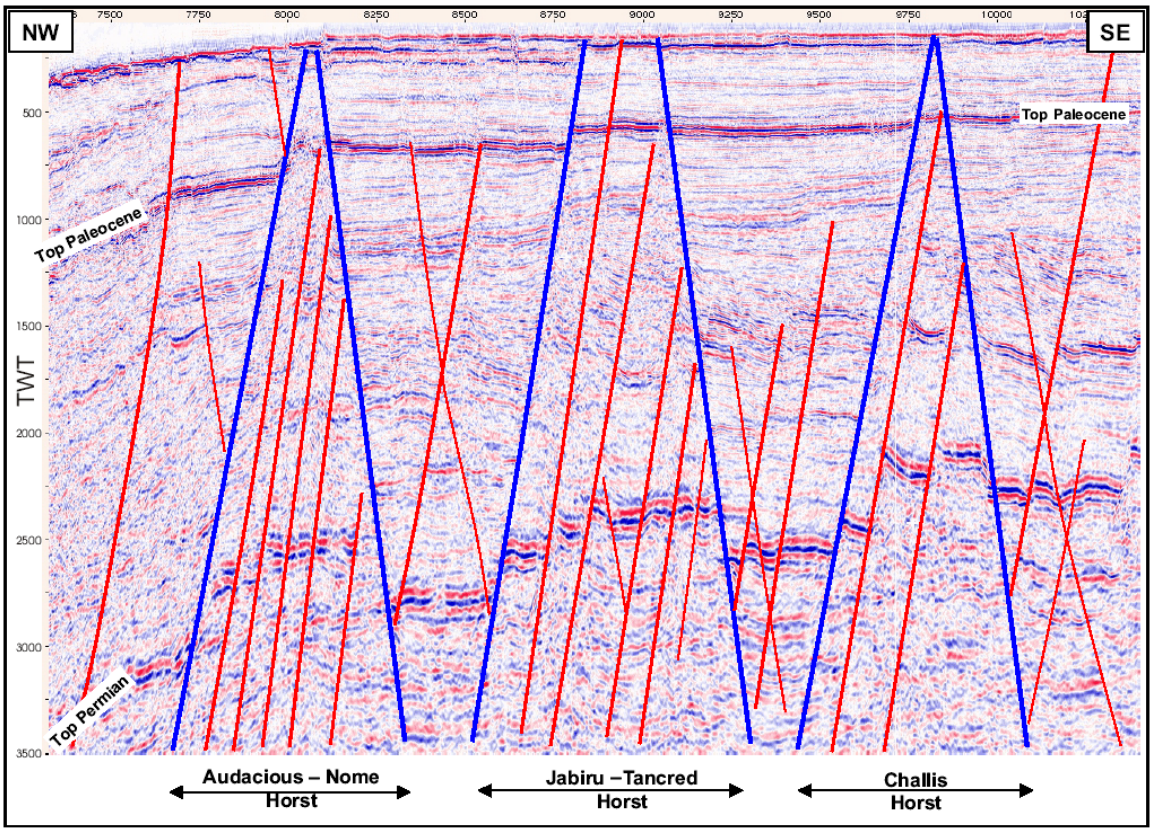

Figure 5-42: Representative examples of fault reactivation.

A representative seismic section from across the south eastern margin of the Cartier Trough showing the intense recent faulting that is characteristic of the VSB. The blue faults represent the main northeast rending horsts whilst the red faults are more minor faults that segment these horsts and are often only identified where 3D seismic data is available (from Peresson et al., 2004). Note the difference in fault offset at the Top Permian compared with the Top Paleocene levels indicating that these were pre-existing faults that have experienced episodes of later reactivation.

Fault reactivation produced by this event and attendant hydrocarbon leakage is seen as a major control on the retention of hydrocarbons, with many residual oil columns attributed to fault controlled leakage (Whibley and Jacobson, 1990; O'Brien and Woods, 1995; Lisk and Eadington, 1994; O'Brien et al., 1996a; Lisk et al., 1998b).

The pervasive nature of reactivation (Figure 5–42) throughout the VSB and across the entire northern margin of the Australian Plate (de Ruig et al., 2000; Castillo et al., 2000) suggests that fault reactivation could be a common cause of the widespread trap breaching. This phase of faulting involved both the reactivation of earlier formed Jurassic rift faults, often on multiple occasions, as well as the creation of new fault arrays generally with an orientation that is oblique to the early fault sets. Although pervasive, movement associated with the Neogene faults account for only 20% of the total extension with the remainder being attributed to the Jurassic faulting seen in the pre- and syn-rift sections (Peresson et al., 2004).

Two main stages of Neogene collision have been recognised on Timor Island (Charlton et al., 1991; Woods, 1994); the first stage occurred in the late Miocene (~8Ma), when the transitional Australian continental crust reached the subduction system; the second stage occurred when true Australian continental crust began to enter the subduction system in the middle Pliocene (~3Ma; Charlton et al., 1991) causing the system to lock.

The latter event coincides with a distinct pulse in fault growth occurring at 3–5 Ma in some areas of the VSB (Gartrell et al., 2006). Displacement rates subsequently decrease significantly after about 3 Ma, but faults that offset the sea floor are observed in the region indicating that a degree of ongoing reactivation has continued to recent times in some areas.

However, the low frequency of faults that offset the sea-floor suggests fault creation has slowed from an initial higher rate, an observation that is supported by other data sources. Earthquake frequency data collected over the last 30 years for example show the Bonaparte Basin to be relatively quiet seismically, with most of the current seismic activity being located in, and around the island of Timor (Figure 5–43).

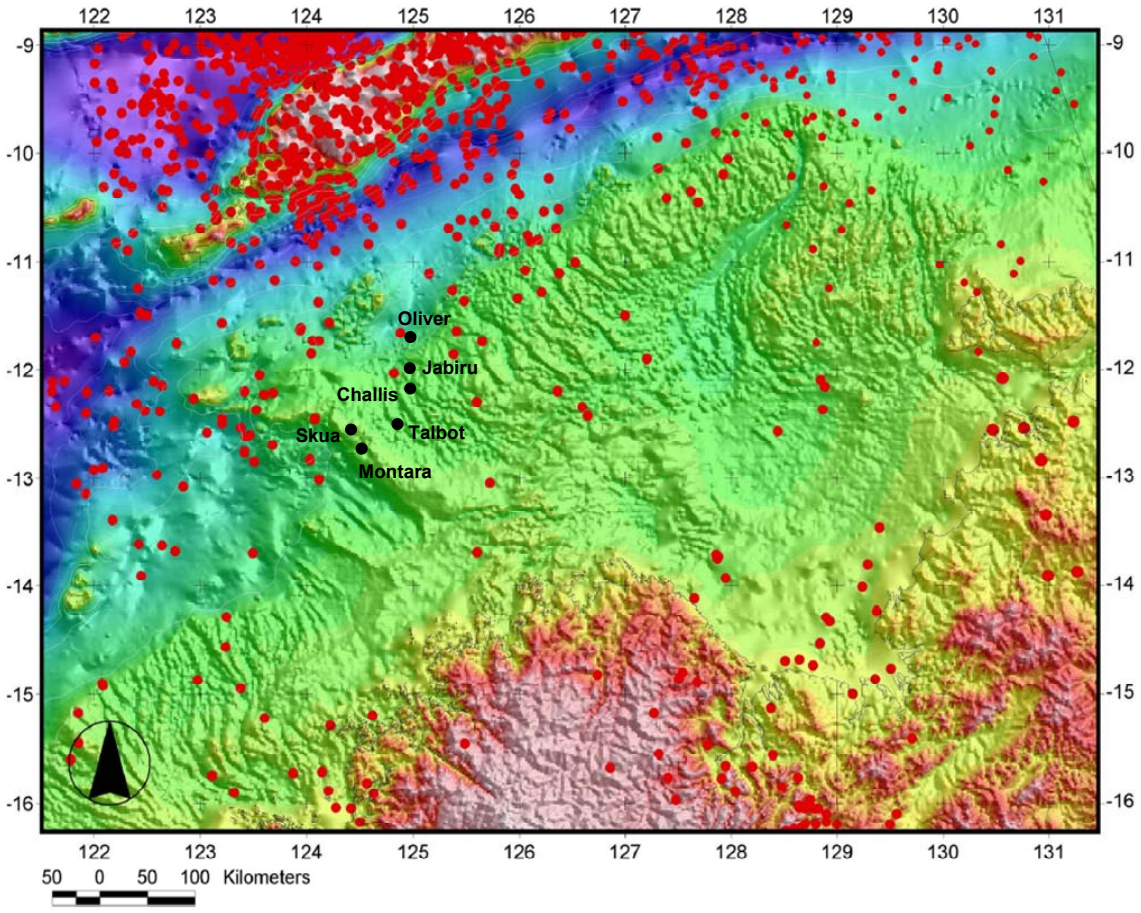

Figure 5-43: Earthquake epicenters from the Timor Sea.

Map showing the abundant earthquake loci that characterise the tectonically active nature of the northern margin of the Australian Continent. Location of key fields in the VSB shown for reference and the background is sea-floor bathymetry. Data from Geoscience Australia reproduced from O'Brien et al., 2002a. The data show focusing of earthquakes across Timor Island with relatively few events recoded across the VSB and greater Bonaparte Basin.

The most seismically active regions in the Bonaparte Basin lie on the flanks of Neogene depocentres and these coincide with the highest density of faults that offset the sea-floor (O'Brien et al., 2002a).

The nature of the contemporary stress field also points to a reduction in the propensity of the rock to fail by extension alone. Presently the stress regime in the area is transtensional, in which σ1 is horizontal and oriented ENE-WSW (067°-247°, Gartrell et al., 2006). Reactivation of existing Jurassic rift faults can occur within this stress regime due to pre-existing planes of weakness, but neo-formed normal faults are more difficult to explain when σ1 is horizontal (Gartrell et al., 2006).

Gartrell and Lisk (2005) utilised 3D restoration and fault slip inversion methods to show an extensional stress regime existed in the VSB at Late Miocene time, with σ1 vertically oriented. Mohr circles describing the contemporary stress and palaeo-stress tensors illustrate the practical importance of concluding that the stress field has changed in recent time. Although the differential stress (i.e. σ1-σ3) may have been similar at both times, the higher magnitudes for all of the principal stresses (i.e. higher mean stress) shifts the Mohr circle for the present day stress tensor to the right, away from the failure envelope (Gartrell and Lisk, 2005; Figure 5–44). Consequently as collision is initiated the initial response of increasing σ1 due to increased subsidence is widespread extensional failure, a prediction that is consistent with the observed extensional faults, most which die out before reaching the seafloor.

As collision proceeds and presumably in response to the entry of Australian continental crust acting to jam the subduction zone horizontal stresses progressively increase ultimately causing σ1 to flip and become horizontal. This change acts to progressively push faults away from the failure envelope and the frequency of extensional faulting correspondingly also subsides (Figure 5–44).

The intensity of seepage also points to a reduction in hydrocarbon leakage rates (Figure 5–45). Remote sensing programs using combinations of Synthetic Aperture Radar (SAR), water column detection of hydrocarbons (sniffer) and Airborne Laser Fluorosensor (ALF) have shown that seepage within the Bonaparte Basin is widespread, but generally at a low level (O'Brien et al., 1998; 2002a).

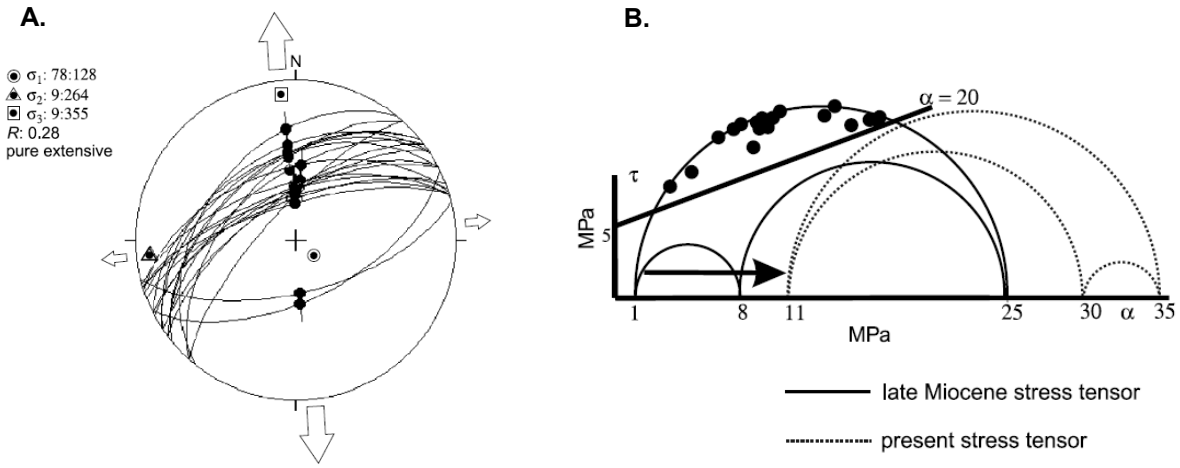

Figure 5-44: Palaeo-stress fields for the Skua Field

A. Results of the fault slip inversion plotted on a stereonet (Schmidt lower hemisphere projection). Fault plane and slip lines used for the inversion are described in Gartrell and Lisk, 2005. B. Mohr Circle construction showing a comparison between late Miocene and present-day stress tensors derived from the measured fault slip data shown in A. The Mohr Circle for the Late Miocene stress tensor as defined by the measured fault data is adjusted until the entire data set plots above the failure curve as these faults have already slipped. In contrast the Mohr Circle describing the present day stress tensor moves the right reflecting the higher mean stress and reduces the predicted propensity for extensional failure.

The areas with most intense present-day seepage cluster in regions with thin seals (which are more prone to fault seal failure) within and around Neogene depocentres where the combination of a reinvigorated petroleum system and faulting offsetting the sea-floor is most prevalent.

Integrating the fluid history with the structural history contributes an enhanced understanding of both processes. Widespread oil and gas charge during the Early Tertiary occurred when the region existed as a passive margin, but much of this was lost during a intense fault reactivation accompanying the onset of plate collision in the Miocene to Early Pliocene. Present day fault-related seepage detected in the region probably is volumetrically insignificant, at least in comparison to the probable rates of Late Miocene hydrocarbon leakage (O'Brien et al., 1999).

The interpretation of seepage data is evolving, with different tools better suited to different types of seeps. Seepage detected by the ALF method targets smoothing of the sea-surface by leaking oil whereas water column sniffer data more effectively detect wet gas that is actively leaking from the sea-bed (O'Brien et al., 2002b). Typically, intact, but leaking hydrocarbon fields will produce focused seepage whilst breached traps show more diffuse leakage signatures (O'Brien et al., 1998).

The type of hydrocarbons controls the type of seepage observed. In the Southern VSB published seepage data (O'Brien et al., 2002b) show oil leakage from a series of breached traps with the intact Skua oil field showing limited oil response but pronounced gas seepage (Figure 5–45). This observation probably reflecting leakage from the gas cap or the increased gaseous nature of hydrocarbons that are currently migrating into these traps (O'Brien et al., 1998).

Generally indications of palaeo-leakage are restricted to data coming from wells, typically as residual oil shows, either from within the reservoir section or observed in any porous rocks that occur in the shallow section. O'Brien and Woods (1994) reported seismically definable leakage indicators that reflect zones of localised cementation related to hydrocarbon leakage. These cements have highly depleted carbon isotope signatures that are attributed to a carbon source produced by the

biological alteration of leaking oil and gas and produce vertical areas of velocity pull-up and distortion on seismic data (Figure 5–46).

The impact of Neogene fault reactivation has largely been deleterious to the petroleum systems of the VSB through widespread trap breaching, but some advantages may have resulted. O'Brien et al. (1998) suggest that less intensely reactivated traps could have allowed substantial recent gas charge to be preferentially lost, preventing the flushing of pre-existing oil accumulations.

This proposition is consistent with the observed palaeo-gas caps seen in for many of the oil-fields of the VSB that have been investigated in the current study, which current lack gas caps or have only small gas caps above the oil column.

Another clear advantage of a change to a more quiescent tectonic environment as inferred by the changing stress field has been the opportunity for some traps to re-heal allowing trap integrity to improve and enabling even heavily reactivated structures to be capable of trapping more recent oil and gas charge.

The Tenacious oil discovery is one example where success has been achieved despite the trap showing a significant level of fault reactivation. In this instance the trap formation and oil charge appear to have both post-dated Neogene fault reactivation (Woods and Maxwell, 2004). This illustrates that reactivated traps should not automatically be considered as being non-prospective. Risking of individual traps should be done on a case by case basis utilising all of the available methods in order to fully understand the evolution of individual traps.

5.6 SUMMARY

The hydrocarbon charge history of the Vulcan Sub-basin has been investigated using a combination of conventional hydrocarbon show data and a new type of data provided by an assessment of oil-filled fluid inclusions known as GOI analysis. Careful application of a proven calibrated analytical procedure has enabled robust GOI data to be collected on 300 samples taken from 74 wells distributed throughout the Vulcan Sub-basin.

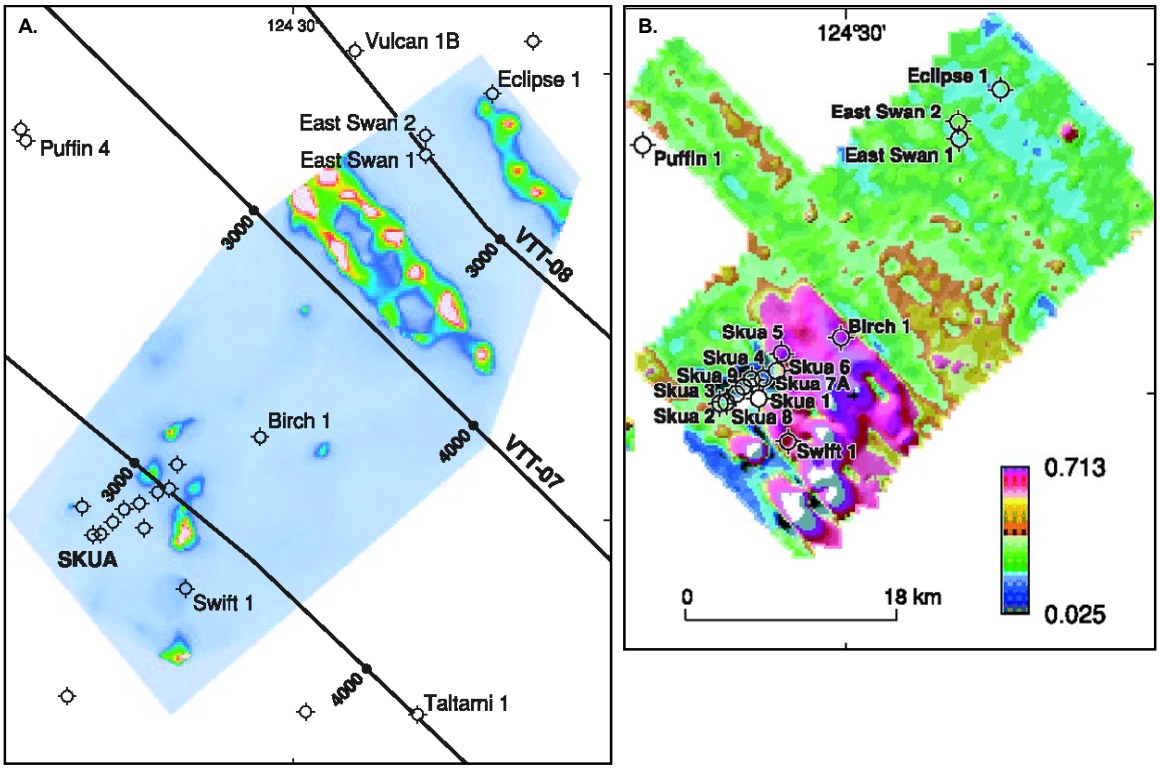

Figure 5-45: Example of contemporary seepage patterns from the VSB

Contrasting seepage responses from the Southern Vulcan Sub-basin (modified from O'Brien et al., 2002b). A. Airborne Laser Fluoresensor data (ALF) data showing detectable oil slicks above breached traps at Eclipse and East Swan that are largely absent from the Skua Oil-field. B. Water column geochemical sniffer data for the same area shown focused gas (ethane) seepage across the Skua Field but baseline values across the breached East Swan and Eclipse traps.

Using the currently oil bearing traps for calibration of the expected GOI response in samples from zones of high current day oil saturation has allowed the charge history of these traps to be revealed and underpins the successful application of the method to discern the hydrocarbon fill history of traps that are now either gas or water-filled. A calibration study conducted on a suite of randomly selected samples demonstrated that GOI values can routinely be repeated with precision of no poorer than ±25% variation from the mean GOI value for all but the highest GOI values.

In instances where GOI data have been collected on multiple wells from the same trap it becomes clear that the distribution of a palaeo-hydrocarbon column can be described in more detail and that palaeo-fluid contacts represent unique surfaces that can be mapped between wells. Often this appreciation allows apparently incongruous results from a single well to be reconciled in a geologically acceptable manner when viewed collectively with results from nearby wells.

The data reveal that hydrocarbon charge to the Vulcan Sub-basin involved at least three discernible hydrocarbon phases. An early gas charge (H1) was widespread in the basin and may have substantially reduced the volumetric capacity of traps that would have been well positioned to receive later oil charge. In volumetrically small traps, such as those tested by the Delamere-1 and Pengana-1 wells, the early gas charge completely fills the available closure and prevents the ingress of later generated oil. In larger traps, these early filled gas zones appear as intervals of low GOI values that overly zones of prior oil accumulation defined by consistently high GOI values.

Extensive oil charge (H2), derived from Upper Jurassic mudstones, produced numerous oil columns across the VSB, with a high proportion of valid traps receiving oil charge. Significant palaeo-oil zones have been recognised below the current OWCs of the Jabiru, Skua, Swift and Cassini oil fields with a further 9 palaeo-oil columns detected in the 28, currently water-wet, wells examined with palaeo-oil columns ranging from a few metres to more than two hundred metres. Stratigraphically, evidence for oil accumulation has been documented in sandstones ranging from Triassic to Tertiary in age.

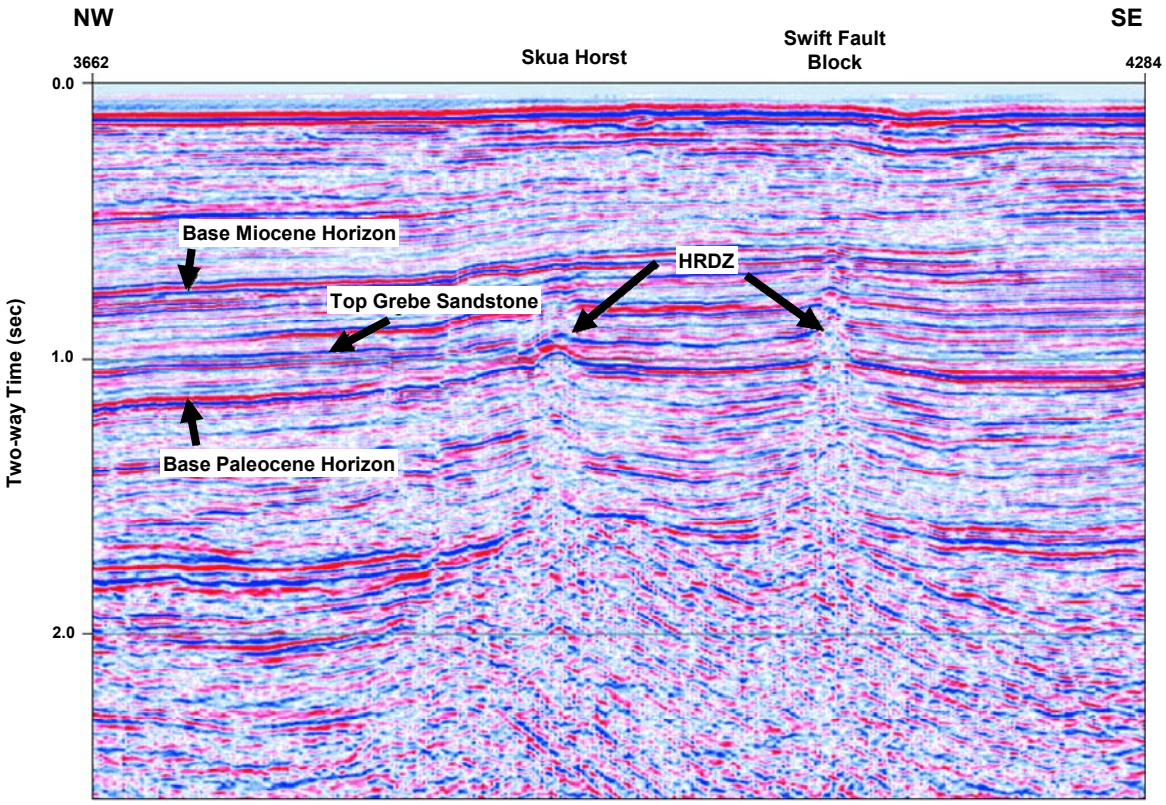

Figure 5-46: Seismically define Hydrocarbon Related Diagenetic Zones (HRDZs).

Regional 2D seismic line (AGSO 98R/8) from O'Brien et al., 1998, showing hydrocarbon-related diagenetic zones (HRDZs) developed over the Skua and Swift traps. These zones appear as sub-vertical zones of seismic pull-up and distortion that are caused by carbonate cemented sandstones in the shallow section (Grebe Sandstone), which produce localised zones of faster interval velocity. The cements have a very light carbonate isotope composition that is attributed to a carbon source produced by the biological degradation of hydrocarbons that are leaking into the shallow section (refer to O'Brien and Woods, 1995 and O'Brien et al., 1998 for details).

The presence of a high proportion of palaeo-oil columns (ca. one in three) identifies the retention of hydrocarbons as the critical risk in the Vulcan Sub-basin (Lisk et al., 1998a). This proportion is even more significant when one considers that the other key risk influencing exploration success in the basin has been trap validity with about half the dry holes drilled failing to penetrate a valid closure (Lisk at al., 1998). Combined, these observations indicate that any valid structure has a very high likelihood of having received hydrocarbon charge and consequently improvements made to the trap definition and retention elements of the play concepts offer considerable opportunity to increase the future exploration success rate.

The fluid inclusion oils present in samples with GOI values above the empirical threshold for oil accumulation are dominated by blue fluorescing oil inclusions, which could be indicative of the relatively high maturity and implied common putative source for the oils recovered from this basin. Geochemical analysis of these fluid inclusion oils undertaken by other workers provide evidence linking these palaeo-oils to one of the two oil families recognised in the VSB, although the fluid inclusions oils are typically less mature and often show variability that augments the conventional understanding of the petroleum systems at work in the basin. A more variable fluorescence range is recorded in samples with low GOI values reflecting the presence on migration pathways of oils generated across the maturity range.

A third phase of hydrocarbons (H3) is indicated by the currently reservoired hydrocarbons with gas columns often containing evidence for prior oil accumulation. This implies that pre-existing oil columns have been flushed or absorbed into a later gas phase, potentially providing opportunities for a down-dip oil leg in traps where no gas-water contact has been defined or a remigration of displaced oil into nearby satellite structures, including those that might otherwise lie in migration shadows.

At the onset of the late Tertiary a rich collection of oil and gas fields existed in the VSB reflecting abundant generation of oil and gas from mostly Upper Jurassic source rocks located in three deep grabens. A major tectonic episode coincided or immediately post-dated the H3 migration and charge event that would alter the petroleum system irrevocably and allow huge volumes of oil and gas to escape.

Many of these incipient oil fields have not been preserved or have been substantially reduced in size by subsequent leakage or flushing by late gas charge.

Widespread trap breaching that is linked to the pervasive Neogene Fault reactivation is widely recognised as the most likely mechanism for explaining the loss of these oil and gas columns. Combined with the flushing of H2 oils by a later gas charge (H3) these processes forever changed the fortunes of the VSB as a world class hydrocarbon province.

A massive flux of hydrocarbon fluids was released by the trap breaching that accompanied the Neogene reactivation event. Mostly this was deleterious to the retention of oil and gas, but in some instances positive outcomes were achieved by allowing remigration of oil into the shallower stratigraphy that produced new oil-fields or by preferentially allowing gas to be lost whilst retaining oil. Mostly the leaking hydrocarbons were lost to the sea-floor or biodegraded in the shallow section to produce hydrocarbon related diagenetic zones that are recognised on seismic.

Neogene fault reactivation severely compromised trap integrity, but appears to have produced a relatively short-lived pulse of major fluid loss that probably occurred as an episodic process. Plate collision along the northern Australian margin that initiated widespread fault reactivation in the Mio-Pliocene was halted when Australian Continental crust jammed the northward facing subduction zone and resulted in a switch in the stress regime from an extensional to more transtensional stress field. The frequency of faulting abated and previously leaky faults began to become less permeable and probably started to re-establish trap integrity, in some cases allowing very recent hydrocarbon charge to be trapped.

6. THERMAL HISTORY

6.1 INTRODUCTION

The thermal state of a sedimentary basin can be investigated either directly through evaluation of measured formation temperatures or indirectly through methods that measure thermal stress that has been accumulated through time. An understanding of the thermal history of a basin is critical to constraining models for hydrocarbon generation and the degree of diagenetic alteration experienced by reservoir rocks.

Measurement of formation temperatures is generally a routine operation conducted during drilling and wireline logging operations. Due to the cooling effects of the circulating mud system used to facilitate the drilling process temperature measurements made during drilling operations are highly inaccurate and of little value for assessing genuine reservoir temperatures. More reliable temperatures can be measured when mud circulation has stopped. When this occurs temperature near the well bore slowly return to an unperturbed state, but normally this requires a timeframe well beyond the period that circulation is stopped.

In order to remove the cooling thermal effects of mud circulation whilst drilling recorded bottom hole temperatures are extrapolated using a technique known as a Horner Plot correction (Horner, 1951; Hermanrud et. al., 1990). This approach uses a series of temperature measurements made at regular time intervals after circulation has been halted to extrapolate these to estimate the virgin reservoir temperature. This approach provides the most common type of reliable direct measurement of reservoir temperature, but limitations with this method have been recognised (Hermanrud et. al., 1990).

More accurate temperatures can be achieved from temperature surveys that are conducted during extended testing programs such as Drill Stem Tests (DST) or production tests where a large volume of fluid is produced and reservoir temperatures stabilise more readily.

Estimating formation temperatures in the geological past is more challenging. Current formation temperatures coupled with the conductivity of the various lithologies can be used to determine basal heat-flow and in combination with burial history reconstruction temperatures through time can be predicted with a degree of certainty that is directly controlled by the accuracy of the input data used.

A key uncertainty in this approach relates to variations in the basal heat flow that occur constantly through time, reflecting the contribution of heat from various basin forming processes (e.g. rifting). To better constrain the predictive models a variety of methods are available that indirectly assess thermal history. These include organic petrological methods such as vitrinite reflectance, organic geochemical assessment of recovered hydrocarbons, stable isotope and fission track analyses. All of these methods measure accumulated thermal stress and require a detailed knowledge of the kinetics controlling the impact of changing temperature on each of these parameters. These kinetic reactions are now well understood and algorithms are available that allow a calculated value to be determined that can be compared with the observed value to assess the accuracy of the proposed thermal model in an iterative manner.

Fluid inclusion palaeothermometry offers an advantage over these other methods by providing a unique opportunity to directly measure formation temperatures in the geological past. As with the indirect methods a number of assumptions remain but the controls on the measurements are well understood and with care accurate temperature estimates can be obtained. Importantly the ability to describe discrete populations of inclusions by the contents of the inclusions or by the superposition relationships with respect to other mineral cements offers the opportunity to describe temperature evolution through geological time.

In this study, a suite of fluid inclusion palaeotemperature data have been collected on wells (Figure 6–1) from across the VSB and integrated with available vitrinite reflectance data and other thermal maturity data to constrain a series of 1-D basin models that attempt to describe the thermal evolution of the basin.

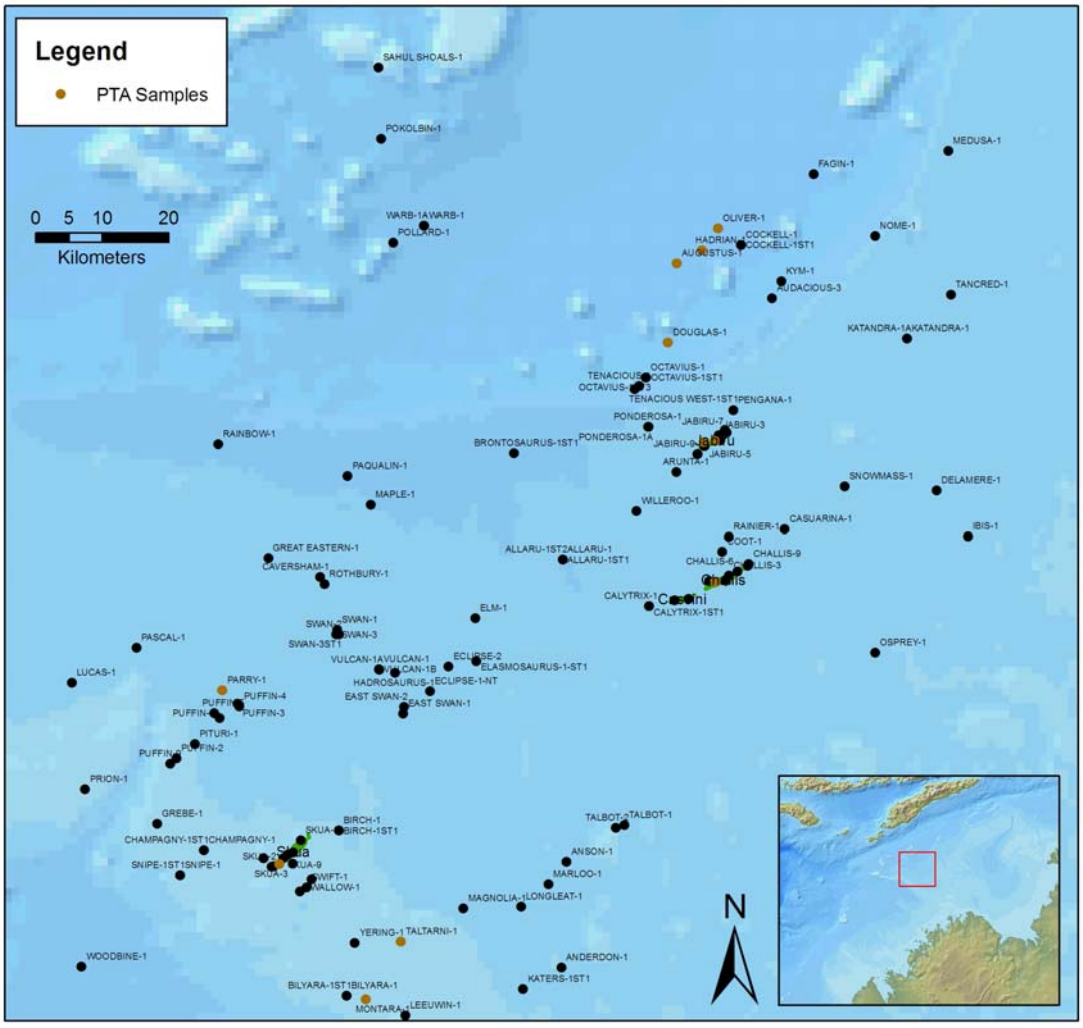

Figure 6-1: Wells with palaeotemperature (PTA) measurements.

Wells with samples used for PTA measurements are distributed across the VSB and allow for variations in geological processes that control reservoir temperatures to be described. A mixture of currently hydrocarbon bearing traps, water wet traps with evidence to support palaeo-oil accumulation and traps where oil migration occurred without accumulation have been sampled and allow for a comprehensive assessment of the thermal history of the basin.

6.2 CURRENT FORMATION TEMPERATURES

Basal heat flow in the Vulcan Sub-basin, as indicated by current formation temperatures, is relatively consistent with other old passive margin settings (Beardsmore, 2002; Allen and Allen, 1990). Geothermal gradients, derived from 48 wells across the region, range from about 20-36 °C/km, with an average value of about 30 °C/km (Table 6–1). Over much of the region the variation from the average is less than 3°C/km. Noticeable anomalies occur in wells on the Ashmore Platform where measured geothermal gradients are significantly cooler than the average and in the north eastern end of the Cartier Trough where gradients are considerably higher than the basin average.

6.3 FLUID INCLUSION PALAEOTEMEPARTURE ANALYSIS

Fluid inclusion palaeo-thermometry (thermometric analysis) is a well established technique for investigating the thermal history of most rock types and in many different environments ranging from low temperature sedimentary rocks to high temperature metamorphic rocks (Roedder, 1981, 1984; Burruss, 1981; Goldstein and Reynolds, 1994).

Homogenisation temperatures are measured on fluid inclusions to constrain the temperature of crystallisation of the host mineral. Where discrete populations of inclusions can be defined, termed fluid inclusion assemblages by Goldstein and Reynolds (1994), a series of temperature constraints can be obtained to describe changes in the thermal state of the basin through time. Inclusions that can be related in a time sequence through relative juxtaposition relationships observed either between different mineral phases or within individual minerals if fracture sets of different age or growth zones can be recognised.

A comprehensive description that contains general information on thermometric techniques can be found in Goldstein and Reynolds (1994), but a description of the method and the specific procedures for interpreting the homogenisation temperatures collected in the current study are discussed later in this chapter.

Table 6-1: Summary of geothermal gradients in wells from the Vulcan Sub-basin.

Data come from a selection of wells with gradients (°C per 100m) calculated using temperature data taken from well completion reports that where suitable information is available have been corrected for the effects of circulation (Extrapolated BHT) using the Horner plot method (Horner, 1951). Data that are uncorrected represent minimum estimates of the geothermal gradient and are likely to underestimate the true gradient. Temperatures derived from extended flow testing (Drill Stem Test, DST) or during long term production represent the most reliable indication of temperature but are generally a less common type of temperature measurement.

Well Name	Depth (m)	Seafloor Temp	BHT	Interval	Method	Gradient
Augustus-1	3554		127		Extrapolated BHT	3.01
Cartier-1	2635		98	Triassic		2.96
Challis-1	1400		56	Triassic	Extrapolated BHT	2.57
Challis-6	1399		68	Triassic	DST	3.43
East Swan-2	2850		95	Jurassic	Extrapolated BHT	2.63
Eclipse-1	2980		113	Jurassic	Extrapolated BHT	3.12
Eclipse-2	2930		95	Jurassic	Extrapolated BHT	2.56
Elm-1	3030	20	115.4	Plover		3.15
Hadrian-1	3517		120	Plover	Extrapolated BHT	2.84
Ibis-1	1440		68.9	Triassic	Uncorrected	3.40
Jabiru-1A	1600		72	Plover	Production Temperature	3.25
Montara-1	3440		119	Plover	Extrapolated BHT	2.88
Octavius-2	2976		107.5		Extrapolated BHT	2.94
Paqualin-1	4201	18	156	Plover	Extrapolated BHT	3.24
Pengana-1	2081		82.5	Triassic	Extrapolated BHT	3.00
Rainbow-1	2700		95		Extrapolated BHT	2.78
Skua-3	2442		98		Extrapolated BHT	3.19
Skua-6	2831		107	Plover	Extrapolated BHT	3.07
Swan-2	4063		159	L.Cretaceous		3.42
Swan-3	2430	18	87.5	Puffin	Extrapolated BHT	2.86
Swan-3ST1						
Swift-1	2800		108	Jurassic	DST	3.14
Talbot-1	1523	25	75	Triassic	DST	3.28

6.3.1 Theory

Fluid inclusions that trap a single-phase fluid at reservoir conditions separate into two phases (liquid + vapour) when pressures (P) and temperatures (T) fall below a critical level called the two phase boundary or ‘bubble point’ curve (as occurs when a sample is retrieved to surface). This is a reversible process that can be reproduced by heating the inclusion in the laboratory under controlled conditions to recreate this P-T path.

Thermometric measurements involve heating the inclusion and recording the temperature at which the two phases in the inclusion return to a single phase (homogenisation temperature). This temperature can be accurately measured in the laboratory and provides a minimum estimate of the temperature at which the fluid was trapped under the prevailing sub-surface conditions.

Homogenisation temperatures measured on fluid inclusion can be used to infer trapping conditions only if each inclusion measured satisfies several important criteria (Roedder 1984). The inclusion must have trapped a single, homogeneous phase, the inclusion must remain a constant volume system after trapping (excluding any reversible elastic volume changes) and nothing can be added to, or removed from the inclusion following initial trapping (Bodnar, 2003).

Following initial entrapment in the host phase, inclusions generally will change shape through a process referred to as "necking down" that involves dissolution and re-precipitation of the host phase to reduce the surface area and produce many smaller and more stable inclusions from the incipient larger inclusion (Figure 6–2). During this process, the shape of the inclusion tends to become more regular, ultimately forming spherical or negative-crystal shaped fluid inclusions if P-T conditions allow (Roedder, 1984). The lower temperatures and pressures of the diagenetic realm are not sufficient to allow this to happen and typically most inclusions trapped under these conditions retain a more irregular shape. Exceptions to this generalisation occur where the host mineral has well developed cleavage and the inclusions can mimic this shape (e.g. carbonates).

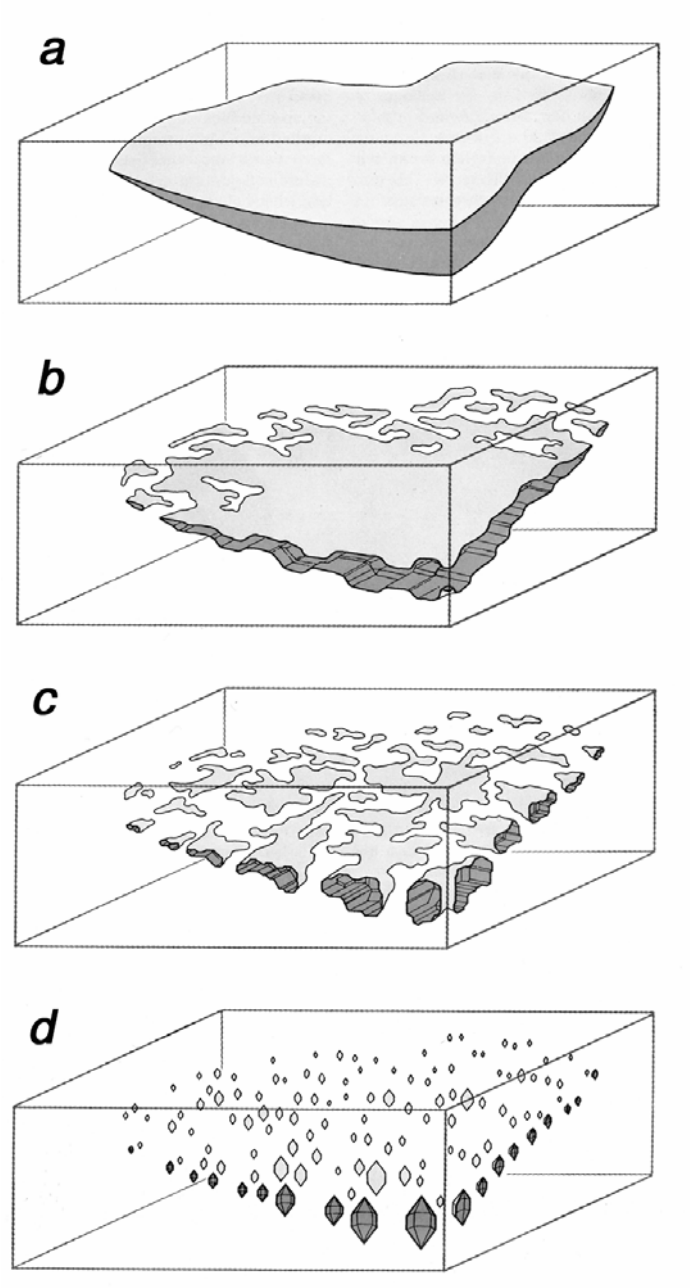

Figure 6-2: Cartoon showing the formation of secondary fluid inclusions through necking down. Fluid enters the open fracture (a) material from the walls is dissolved and re-precipitated to heal the fracture, isolating small pockets of fluid in the process (b). With continued healing the originally irregularly shaped fluid inclusions become more regular in shape (c) and eventually negative-crystal shaped fluid inclusions (d) are produced (from Bodnar, 2003).

Inclusions that undergo necking down at constant temperature and pressure, whilst still within the one-phase fluid field (i.e. above the bubble point curve) retain similar phase relations as well as thermometric behavior and therefore remain as reliable indicators of the pressure, temperature and composition (PTX) that existed at the trapping conditions.

In practical terms a population of necked inclusions that trapped samples of the same homogeneous liquid under single-phase trapping conditions should be distinguished by a symmetric frequency distribution of bulk-fluid density and the measured homogenisation temperatures, except in the immediate vicinity of the critical point (Loucks et al., 2000).

6.3.2 Fluid Inclusion Assemblages

Thermometric analysis of fluid inclusions requires petrographically identifying inclusions that formed at about the same time or during the same diagenetic event. Typically three types of inclusion may be present within each of these inclusion assemblages. Primary inclusions represent fluids trapped during the initial formation of the host mineral. In contrast, secondary inclusions occur within fractures in the mineral host and form subsequent to initial crystallisation. A third type of inclusion, termed pseudo-secondary, also occurs within fractures, but these form concomitantly with the crystallisation of the host mineral.

Inclusions measured in this study are two-phase water (water liquid and water vapour) and oil (liquid oil and gas) inclusions that typically show a broad range of liquid-vapour ratios. Measurements were made on two principal fluid inclusion assemblages (FIO):

1. Inclusions on the quartz overgrowth-detrital quartz grain boundary (QOB).

2. Inclusions on fractures through quartz overgrowths.

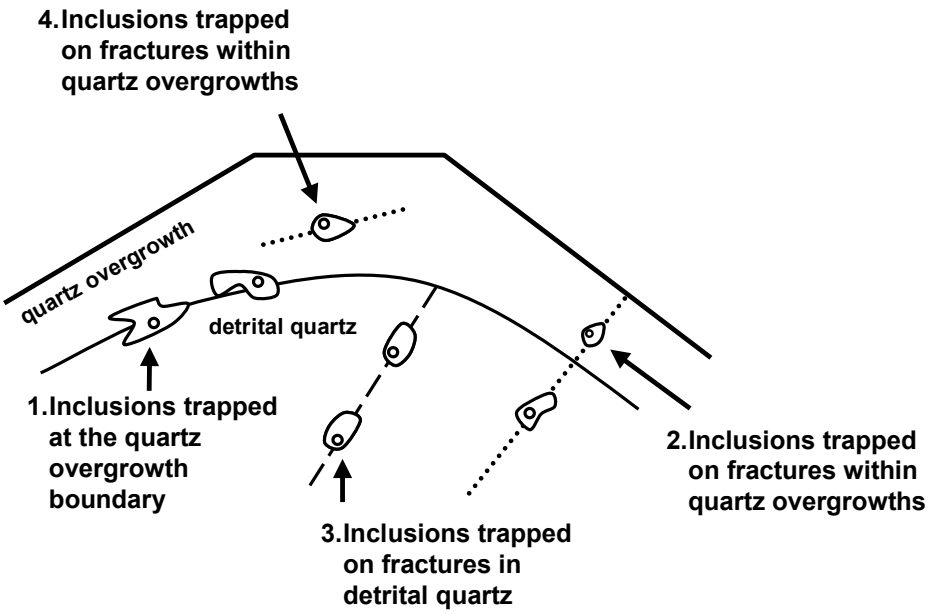

Figure 6-3: Fluid inclusion populations recognised in this study

Schematic diagram showing the types of inclusions recognised in samples from the VSB. Thermometric measurements have been made on inclusions trapped on the boundary between the detrital quartz grains and the authigenic quartz overgrowths (1) and on inclusions within healed fractures that are contained within the overgrowth (2). Inclusions trapped on fractures in detrital quartz (3) have not been measured even where the fracture plane cuts across the quartz overgrowth and no inclusions of sufficient size for measurement were seen on fractures that were wholly within the quartz overgrowth (4).

The QOB assemblage exclusively consists of primary inclusions located along the boundary between the detrital quartz grain and its diagenetic syntaxial overgrowth. These inclusions typically parallel the boundary and commonly range in size from 5-20 µm (long axis). Shapes can be highly irregular to equant with smaller inclusions showing a greater tendency to be regular in shape. Primary inclusions that lie fully within the quartz overgrowth are rare by comparison with those on the quartz overgrowth boundary and were excluded from this population due to the timing uncertainty associated with their origin (i.e. primary versus secondary inclusions).

The FQO population consists of inclusions interpreted to be secondary in nature. The inclusions occur in fractures that transect the detrital quartz grain and its syntaxial overgrowth (Figure 6–3), differentiating them from pseudo-secondary inclusions.

Inclusions in this population were only measured from the part of the fracture that transects the authigenic quartz overgrowth. Inclusions in this population are generally smaller and are more regular in shape. Inclusions located on the part of the fracture plane that transects the detrital grain were not measured due to concerns that these could be related to an existing fracture that has been reactivated.

6.3.3 Thermometric Analysis Method

Homogenisation temperatures are determined by heating, under controlled conditions, of inclusions that contain discrete liquid-vapour phases at room temperature to record the temperature at which these two phases homogenise to form a single-phase fluid. Increased temperature results in gradual shrinkage and eventual disappearance of the vapour phase at the point of homogenisation (T_{hom}). Measurements were made on a Linkam LM600 heating/freezing chamber mounted on an Olympus BX60 microscope.

Computer software provides temperature ramps to accurately control the heating rates to as low as 1°C per minute. As the inclusions are visually observed during measurement relatively fast heating rates are used (up to 50°C/minute) on the first ramp to reach temperatures within about 20°C of the homogenisation temperature.

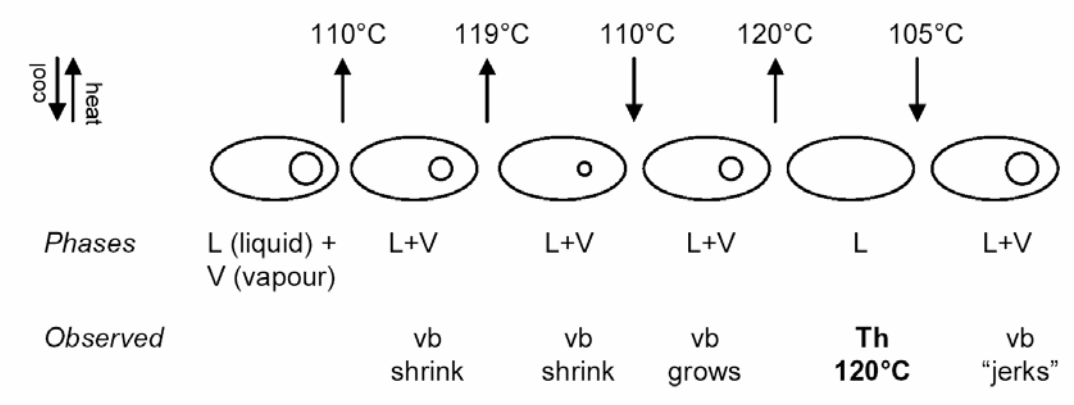

Figure 6-4: The thermometric cycling technique applied to homogenisation temperatures

Schematic representation of the "cycling" technique (Goldstein and Reynolds 1994) used for determining the homogenisation temperature using as an example an inclusion with a T_{hom} value of 120°. "vb" refers to vapour bubble. The process uses an ascending plateau method where the temperature is raised to a level where it becomes uncertain as to whether the inclusion still contains a liquid and vapour phase. The test for persistence of two phases involves cooling the inclusion from this temperature plateau until two-phases can be clearly resolved. Where the T_{hom} value has not been reached a reduction in temperature of less than 10°C is usually sufficient to achieve this outcome, whereas if the T_{hom} value has been passed then a greater amount of cooling is required and the return to two-phases generally occurs instantaneously with a jerking motion. Repeated cycles allow the T_{hom} value to be bracketed with increasing accuracy with the final measurement typically being accurate to within ±1°C.

To avoid large thermal gradients within the sample chamber, the heating rate is progressively slowed as the vapour bubble shrinks indicating proximity to the homogenisation temperature. Heating rates of between 1-4°C per minute were employed for the final ramp when the inclusion was deemed to be close to the homogenisation temperature (indicated by a small bubble size within the inclusion).

Reproducible homogenisation temperatures were obtained by using a temperature cycling method (Goldstein and Reynolds, 1994) near the homogenisation temperature phase change (Figure 6–4). This approach is required due to the small size of the vapour bubble near the point of homogenisation making it difficult to visually confirm the exact temperature of the phase change. This is particularly the case for very small inclusions, those that fail to demonstrate rapid movement of the vapour phase, or where the optical clarity is for some reason partially obscured.

Using this method rapid cooling (>20°C per minute) from temperatures just below this phase change results in the slow re-growth of the vapour phase, normally within 5-10°C and indicates that homogenisation of the liquid and vapour phases was not achieved (Figure 6–4). Conversely, cooling from temperatures slightly above the homogenisation temperature typically requires a larger reduction in temperature (>10°C) to re-nucleate the vapour bubble and generally involves visually observed instantaneous bubble reappearance (jerk). With repeated cycles the homogenisation temperature can be bracketed with increasing precision and accuracy.

6.3.4 Equipment Calibration

The veracity of the thermometric measurements reported in this study are dependant on the precision and accuracy of the equipment being utilised. The manufacturers (Linkam) claim precision and accuracy for the LM600 heating/freezing equipment of ±0.3°C. This can be tested by making multiple measurements on a suite of synthetic fluid inclusions that contain different types of fluid with known phase behaviour. These synthetic fluid inclusions used to calibrate the equipment are created in the laboratory from solutes of known composition. The standards used to perform the calibration on this equipment are listed in Table 6–2.

Table 6-2: Details of the Fluid Inclusion Standards

A summary of the synthetic fluid inclusion standards used to calibrate the Linkam LM600 heating/freezing chamber used to produce the thermometric measurements made in this study. The source of the standard is given together with the nature of the phase change being observed and the theoretical temperature at which this anticipated to occur. The range of temperatures covered by the standards covers the temperature ranges expected for most sedimentary environments.

Standard	Source	Phase Change	Anticipated Temperature (°C)
CO_2	Linkam	Univariant Triple Point	-56.6
Pure H_20	Bubbles Inc.	Critical Point	374.1
Pure H_20	Bubbles Inc.	Final ice melting	0.0
25wt% NaCl	Bubbles Inc.	Eutectic temperature	-21.2

Table 6-3: Calibration results

Results from measurements made on a suite of synthetic inclusions with known composition. Refer to Table 6–1 for details on the expected phase changes for each standard fluid.

Standard	Temperature	Analyst	Inclusion	Temperature	Precision (±)	Correction
Linkam CO_2 Triple Point	-56.6	Lisk	1.1	-56.8	0.1	-0.2
Linkam CO_2 Triple Point	-56.6	Lisk	2.1	-57.1	0.1	-0.5
Linkam CO_2 Triple Point	-56.6	Lisk	2.2	-57.2	0.1	-0.6
Linkam CO_2 Triple Point	-56.6	Lisk	2.3	-57.1	0.1	-0.5
Linkam CO_2 Triple Point	-56.6	Lisk	3.1	-57.1	0.1	-0.5
Linkam CO_2 Triple Point	-56.6	Lisk	3.2	-57.1	0.1	-0.5
Linkam CO_2 Triple Point	-56.6	Lisk	3.3	-57.1	0.1	-0.5
Linkam CO_2 Triple Point	-56.6	Lisk	4.1	-57.1	0.1	-0.5
Linkam CO_2 Triple Point	-56.6	Lisk	4.2	-57.2	0.1	-0.6
Linkam CO_2 Triple Point	-56.6	Lisk	4.3	-57.1	0.1	-0.5
Linkam CO_2 Triple Point	-56.6	Lisk	5.1	-57.1	0.1	-0.5
Linkam CO_2 Triple Point	-56.6	Lisk	5.2	-57.2	0.1	-0.6
Linkam CO_2 Triple Point	-56.6	Lisk	5.3	-57.1	0.1	-0.5
Bubbles Inc. Critical Point (pure water)	374.1	Lisk	1.1	377.6	0.5	3.5
Bubbles Inc. Critical Point (pure water)	374.1	Lisk	2.1	377.9	0.5	3.8
Bubbles Inc. Critical Point (pure water)	374.1	Lisk	3.1	377.9	0.5	3.8
Bubbles Inc. Critical Point (pure water)	374.1	Lisk	4.1	377.5	0.2	3.4
Bubbles Inc. Critical Point (pure water)	374.1	Lisk	5.1	377.6	0.4	3.5
Bubbles Inc. Critical Point (pure water)	374.1	Lisk	6.1	377.2	0.2	3.1
Bubbles Inc. Critical Point (pure water)	374.1	Lisk	7.1	377.6	0.4	3.5
Bubbles Inc. 0wt% NaCL final melting	0.0	Lisk	1.1	-0.1	0.1	-0.1
Bubbles Inc. 0wt% NaCL final melting	0.0	Lisk	1.2	0.0	0.1	0.0
Bubbles Inc. 0wt% NaCL final melting	0.0	Lisk	1.3	-0.1	0.1	-0.1
Bubbles Inc. 0wt% NaCL final melting	0.0	Lisk	1.4	-0.1	0.1	-0.1
Bubbles Inc. 0wt% NaCL final melting	0.0	Lisk	1.5	0.0	0.1	0.0
Bubbles Inc. 0wt% NaCL final melting	0.0	Lisk	2.1	-0.1	0.1	-0.1
Bubbles Inc. 0wt% NaCL final melting	0.0	Lisk	2.2	-0.1	0.1	-0.1
Bubbles Inc. 0wt% NaCL final melting	0.0	Lisk	2.3	-0.1	0.1	-0.1
Bubbles Inc. 0wt% NaCL final melting	0.0	Lisk	3.1	-0.1	0.1	-0.1
Bubbles Inc. 0wt% NaCL final melting	0.0	Lisk	3.2	-0.1	0.1	-0.1
Bubbles Inc. 0wt% NaCL final melting	0.0	Lisk	3.3	-0.1	0.1	-0.1
Bubbles Inc. 0wt% NaCL final melting	0.0	Lisk	4.1	0.0	0.1	0.0
Bubbles Inc. 0wt% NaCL final melting	0.0	Lisk	4.2	-0.1	0.1	-0.1
Bubbles Inc. 0wt% NaCL final melting	0.0	Lisk	4.3	0.0	0.1	0.0
Bubbles Inc. 0wt% NaCL final melting	0.0	Lisk	5.1	-0.1	0.1	-0.1
Bubbles Inc. 0wt% NaCL final melting	0.0	Lisk	5.2	-0.1	0.1	-0.1
Bubbles Inc. 0wt% NaCL final melting	0.0	Lisk	5.3	-0.1	0.1	-0.1
Bubbles Inc. 0wt% NaCL final melting	0.0	Lisk	6.1	-0.1	0.1	-0.1
Bubbles Inc. 0wt% NaCL final melting	0.0	Lisk	6.2	0.0	0.1	0.0
Bubbles Inc. 0wt% NaCL final melting	0.0	Lisk	6.3	0.0	0.1	0.0
Bubbles Inc. 25wt% NaCl eutectic	-21.2	Lisk	1.1	-21.2	0.1	0.0
Bubbles Inc. 25wt% NaCl eutectic	-21.2	Lisk	1.2	-21.2	0.1	0.0
Bubbles Inc. 25wt% NaCl eutectic	-21.2	Lisk	1.3	-21.3	0.1	-0.1
Bubbles Inc. 25wt% NaCl eutectic	-21.2	Lisk	1.4	-21.2	0.1	0.0
Bubbles Inc. 25wt% NaCl eutectic	-21.2	Lisk	2.1	-21.2	0.1	0.0
Bubbles Inc. 25wt% NaCl eutectic	-21.2	Lisk	2.2	-21.3	0.1	-0.1
Bubbles Inc. 25wt% NaCl eutectic	-21.2	Lisk	2.3	-21.3	0.1	-0.1
Bubbles Inc. 25wt% NaCl eutectic	-21.2	Lisk	3.1	-21.2	0.1	0.0
Bubbles Inc. 25wt% NaCl eutectic	-21.2	Lisk	3.2	-21.3	0.1	-0.1
Bubbles Inc. 25wt% NaCl eutectic	-21.2	Lisk	3.3	-21.3	0.1	-0.1
Bubbles Inc. 25wt% NaCl eutectic	-21.2	Lisk	4.1	-21.3	0.1	-0.1
Bubbles Inc. 25wt% NaCl eutectic	-21.2	Lisk	5.1	-21.6	0.1	-0.4
Bubbles Inc. 25wt% NaCl eutectic	-21.2	Lisk	5.2	-21.6	0.1	-0.4
Bubbles Inc. 25wt% NaCl eutectic	-21.2	Lisk	5.3	-21.7	0.1	-0.5

These standards provide control over temperature ranges that are appropriate for the homogenisation temperatures and ice melting temperatures (reported in a later section) collected in this study.

6.3.4.1 Method

For each synthetic fluid inclusion standard, each containing a large number of discrete inclusions, a series of measurements was made on at least five separate inclusions chosen at random. For each inclusion the measurement was repeated a number of times to ensure that a repeatable measurement had been made and to assess the precision of the measurement. The method used to make the measurements was identical to that used to collect the main data, including the type of temperature ramps (heating rates) employed.

6.3.4.2 Calibration Results

The lower end of the temperature range (0 to -60°C), defined by measurements on the pure water, 25wt% NaCl solution and the pure CO_2 inclusions (Table 6–3) yielded precision of ± 0.1°C and accuracy of at least ± 0.3°C, which is consistent with the specifications claimed by the manufacturer. At the high temperature end, represented by the critical point on pure water inclusions (Table 6–3) the precision of the measurements is very good (± 0.4°C), but the measurements made are less accurate (± 2.0°C).

In the absence of suitable fluid inclusion standards to evaluate the temperature range between 0°C and 374.1°C it is not possible to further characterise the deviation in accuracy seen at the high temperature end. However, in the context of this study measurement of homogenisation temperatures (T_{hom}) values, which are accurate to better than ± 2.0°C is considered to be acceptable for the purpose of defining the temperature of entrapment for this type of geological investigation.

6.4 FLUID INCLUSION PALAEOTEMEPARTURE RESULTS

In this study, fluid inclusion palaeotemperatures have been collected on 8 samples, taken from 6 wells (Figure 6–1). These results are discussed individually below. Results from a further 19 samples from 8 wells are taken from previous published investigations (Lisk et al., 1999) to augment these new data and allow a more refined regional interpretation to be constructed from the complete dataset.

6.4.1 Homogenisation Temperatures, Eclipse-1

In a single cuttings sample at 2679-82 mRT, taken from within the recognised palaeo-oil column, homogenisation temperatures for two discrete aqueous fluid inclusion assemblages have been measured (Table 6–4, Figure 6–5). Oil inclusions also occur within these assemblages but were not measured.

1. Primary aqueous inclusions on the quartz overgrowth boundary (n=19, where n = number of inclusions measured). Measured homogenisation temperatures range from 100 to >150°C (Table 6–4, Figure 6–5).

2. Secondary aqueous inclusions on fractures cutting quartz overgrowths. (n=4, where n = number of inclusions measured). Homogenisation temperatures range from 99 to 195°C (Table 6–4, Figure 6–5).

6.4.2 Homogenisation Temperatures, Jabiru-2

Measurements have been made on two cuttings samples, one from Tertiary sandstones at 790-800 mRT and one from a palaeo-oil column within the main Jurassic reservoir at 1661-64 mRT (Table 6–5, Figure 6–6). In each sample homogenisation temperatures were determined for inclusions from two discrete fluid inclusion assemblages.

1. Primary aqueous inclusions located on the quartz overgrowth boundary, 790-800 mRT sample (n = 25, where n = number of inclusions measured). Measured homogenisation temperatures range from 83 to >150°C (Table 6–5, Figure–6).

Table 6-4: Fluid inclusion homogenisation temperatures, Eclipse-1.

QOB = Quartz Overgrowth Boundary; FCO = Fractures Cutting Overgrowth. Inclusions marked as greater than did not reach homogenisation and could have much higher T_{hom}.

Well Name	Start Depth (mRT)	End Depth (mRT)	CSIRO Number	Sample Type	Mineral Type	Inclusion Type	Location	Th (°C)
Eclipse-1	2679	2682	123347	cuttings	quartz	aqueous	QOB	100
Eclipse-1	2679	2682	123347	cuttings	quartz	aqueous	QOB	100
Eclipse-1	2679	2682	123347	cuttings	quartz	aqueous	QOB	100
Eclipse-1	2679	2682	123347	cuttings	quartz	aqueous	QOB	102
Eclipse-1	2679	2682	123347	cuttings	quartz	aqueous	QOB	102
Eclipse-1	2679	2682	123347	cuttings	quartz	aqueous	QOB	103
Eclipse-1	2679	2682	123347	cuttings	quartz	aqueous	QOB	104
Eclipse-1	2679	2682	123347	cuttings	quartz	aqueous	QOB	104
Eclipse-1	2679	2682	123347	cuttings	quartz	aqueous	QOB	104
Eclipse-1	2679	2682	123347	cuttings	quartz	aqueous	QOB	105
Eclipse-1	2679	2682	123347	cuttings	quartz	aqueous	QOB	107
Eclipse-1	2679	2682	123347	cuttings	quartz	aqueous	QOB	108
Eclipse-1	2679	2682	123347	cuttings	quartz	aqueous	QOB	108
Eclipse-1	2679	2682	123347	cuttings	quartz	aqueous	QOB	113
Eclipse-1	2679	2682	123347	cuttings	quartz	aqueous	QOB	114
Eclipse-1	2679	2682	123347	cuttings	quartz	aqueous	QOB	141
Eclipse-1	2679	2682	123347	cuttings	quartz	aqueous	QOB	>150
Eclipse-1	2679	2682	123347	cuttings	quartz	aqueous	QOB	>150
Eclipse-1	2679	2682	123347	cuttings	quartz	aqueous	QOB	>150
Eclipse-1	2679	2682	123347	cuttings	quartz	aqueous	FCO	99
Eclipse-1	2679	2682	123347	cuttings	quartz	aqueous	FCO	101
Eclipse-1	2679	2682	123347	cuttings	quartz	aqueous	FCO	102
Eclipse-1	2679	2682	123347	cuttings	quartz	aqueous	FCO	195

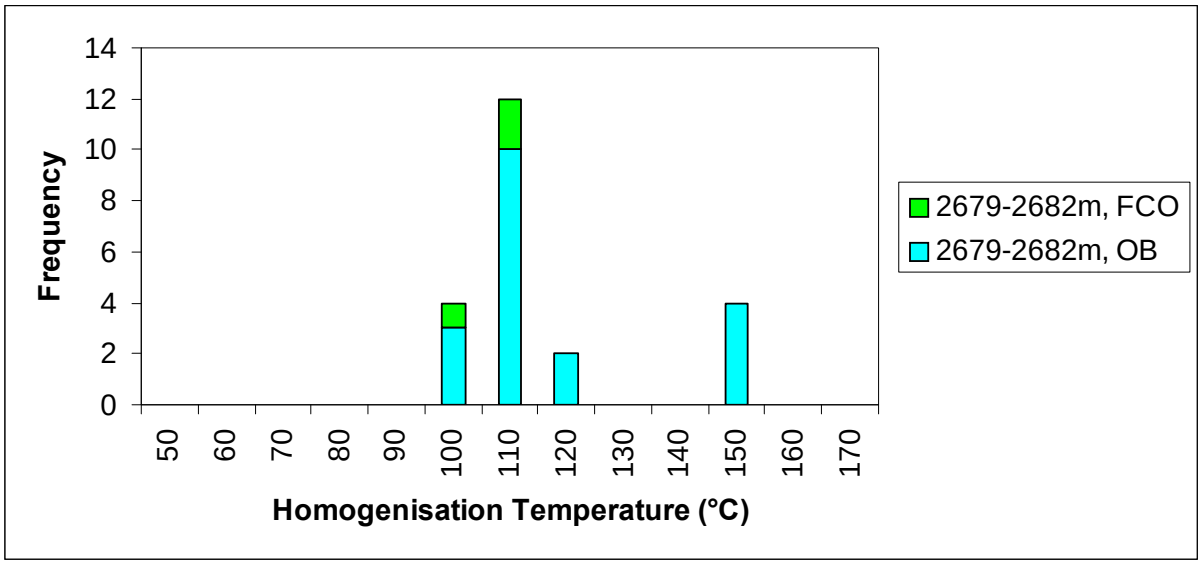

Figure 6-5: Histogram of homogenisation temperatures, Eclipse-1.

Homogenisation temperatures measured on aqueous fluid inclusions located on the quartz overgrowth boundary (OB) and on fractures cutting overgrowths (FCO) from the 2679-82m sample in Eclipse-1.

Table 6-5: Fluid inclusion homogenisation temperatures, Jabiru-2.

QOB = Quartz Overgrowth Boundary; FCO = Fractures Cutting Overgrowth. Inclusions marked as greater than did not reach homogenisation and could have much higher T_{hom}.

Well Name	Start Depth (mRT)	End Depth (mRT)	CSIRO Number	Sample Type	Mineral Type	Inclusion Type	Location	Th (°C)
Jabiru-2	790	800	122399	cuttings	quartz	aqueous	QOB	83
Jabiru-2	790	800	122399	cuttings	quartz	aqueous	QOB	85
Jabiru-2	790	800	122399	cuttings	quartz	aqueous	QOB	87
Jabiru-2	790	800	122399	cuttings	quartz	aqueous	QOB	89
Jabiru-2	790	800	122399	cuttings	quartz	aqueous	QOB	90
Jabiru-2	790	800	122399	cuttings	quartz	aqueous	QOB	94
Jabiru-2	790	800	122399	cuttings	quartz	aqueous	QOB	103
Jabiru-2	790	800	122399	cuttings	quartz	aqueous	QOB	107
Jabiru-2	790	800	122399	cuttings	quartz	aqueous	QOB	107
Jabiru-2	790	800	122399	cuttings	quartz	aqueous	QOB	109
Jabiru-2	790	800	122399	cuttings	quartz	aqueous	QOB	124
Jabiru-2	790	800	122399	cuttings	quartz	aqueous	QOB	125
Jabiru-2	790	800	122399	cuttings	quartz	aqueous	QOB	130
Jabiru-2	790	800	122399	cuttings	quartz	aqueous	QOB	139
Jabiru-2	790	800	122399	cuttings	quartz	aqueous	QOB	142
Jabiru-2	790	800	122399	cuttings	quartz	aqueous	QOB	144
Jabiru-2	790	800	122399	cuttings	quartz	aqueous	QOB	>150
Jabiru-2	790	800	122399	cuttings	quartz	aqueous	QOB	>150
Jabiru-2	790	800	122399	cuttings	quartz	aqueous	QOB	>150
Jabiru-2	790	800	122399	cuttings	quartz	aqueous	QOB	>150
Jabiru-2	790	800	122399	cuttings	quartz	aqueous	QOB	>150
Jabiru-2	790	800	122399	cuttings	quartz	aqueous	QOB	>150
Jabiru-2	790	800	122399	cuttings	quartz	aqueous	QOB	>150
Jabiru-2	790	800	122399	cuttings	quartz	aqueous	QOB	nd
Jabiru-2	790	800	122399	cuttings	quartz	aqueous	QOB	111
Jabiru-2	790	800	122399	cuttings	quartz	aqueous	QOB	123
Jabiru-2	790	800	122399	cuttings	quartz	aqueous	FCO	111
Jabiru-2	1661	1664	122352	cuttings	quartz	aqueous	QOB	68
Jabiru-2	1661	1664	122352	cuttings	quartz	aqueous	QOB	64
Jabiru-2	1661	1664	122352	cuttings	quartz	aqueous	QOB	66
Jabiru-2	1661	1664	122352	cuttings	quartz	aqueous	QOB	67
Jabiru-2	1661	1664	122352	cuttings	quartz	aqueous	QOB	67
Jabiru-2	1661	1664	122352	cuttings	quartz	aqueous	QOB	67
Jabiru-2	1661	1664	122352	cuttings	quartz	aqueous	QOB	68
Jabiru-2	1661	1664	122352	cuttings	quartz	aqueous	QOB	68
Jabiru-2	1661	1664	122352	cuttings	quartz	aqueous	QOB	68
Jabiru-2	1661	1664	122352	cuttings	quartz	aqueous	QOB	72
Jabiru-2	1661	1664	122352	cuttings	quartz	aqueous	QOB	76
Jabiru-2	1661	1664	122352	cuttings	quartz	aqueous	QOB	80
Jabiru-2	1661	1664	122352	cuttings	quartz	aqueous	QOB	89
Jabiru-2	1661	1664	122352	cuttings	quartz	aqueous	QOB	109
Jabiru-2	1661	1664	122352	cuttings	quartz	aqueous	QOB	111
Jabiru-2	1661	1664	122352	cuttings	quartz	aqueous	QOB	127
Jabiru-2	1661	1664	122352	cuttings	quartz	aqueous	QOB	135
Jabiru-2	1661	1664	122352	cuttings	quartz	aqueous	QOB	143
Jabiru-2	1661	1664	122352	cuttings	quartz	aqueous	QOB	150
Jabiru-2	1661	1664	122352	cuttings	quartz	aqueous	QOB	150
Jabiru-2	1661	1664	122352	cuttings	quartz	aqueous	QOB	150
Jabiru-2	1661	1664	122352	cuttings	quartz	aqueous	QOB	150
Jabiru-2	1661	1664	122352	cuttings	quartz	aqueous	QOB	150
Jabiru-2	1661	1664	122352	cuttings	quartz	aqueous	QOB	150
Jabiru-2	1661	1664	122352	cuttings	quartz	aqueous	QOB	150
Jabiru-2	1661	1664	122352	cuttings	quartz	aqueous	FCO	109
Jabiru-2	1661	1664	122352	cuttings	quartz	aqueous	FCO	120
Jabiru-2	1661	1664	122352	cuttings	quartz	aqueous	FCO	125
Jabiru-2	1661	1664	122352	cuttings	quartz	aqueous	FCO	125
Jabiru-2	1661	1664	122352	cuttings	quartz	aqueous	FCO	126
Jabiru-2	1661	1664	122352	cuttings	quartz	aqueous	FCO	131
Jabiru-2	1661	1664	122352	cuttings	quartz	aqueous	FCO	131
Jabiru-2	1661	1664	122352	cuttings	quartz	aqueous	FCO	133
Jabiru-2	1661	1664	122352	cuttings	quartz	aqueous	FCO	144
Jabiru-2	1661	1664	122352	cuttings	quartz	aqueous	FCO	146
Jabiru-2	1661	1664	122352	cuttings	quartz	aqueous	FCO	147
Jabiru-2	1661	1664	122352	cuttings	quartz	aqueous	FCO	150
Jabiru-2	1661	1664	122352	cuttings	quartz	aqueous	FCO	150
Jabiru-2	1661	1664	122352	cuttings	quartz	aqueous	FCO	150
Jabiru-2	1661	1664	122352	cuttings	quartz	aqueous	FCO	150
Jabiru-2	1661	1664	122352	cuttings	quartz	aqueous	FCO	150
Jabiru-2	1661	1664	122352	cuttings	quartz	aqueous	FCO	150
Jabiru-2	1661	1664	122352	cuttings	quartz	aqueous	FCO	150
Jabiru-2	1661	1664	122352	cuttings	quartz	aqueous	FCO	160

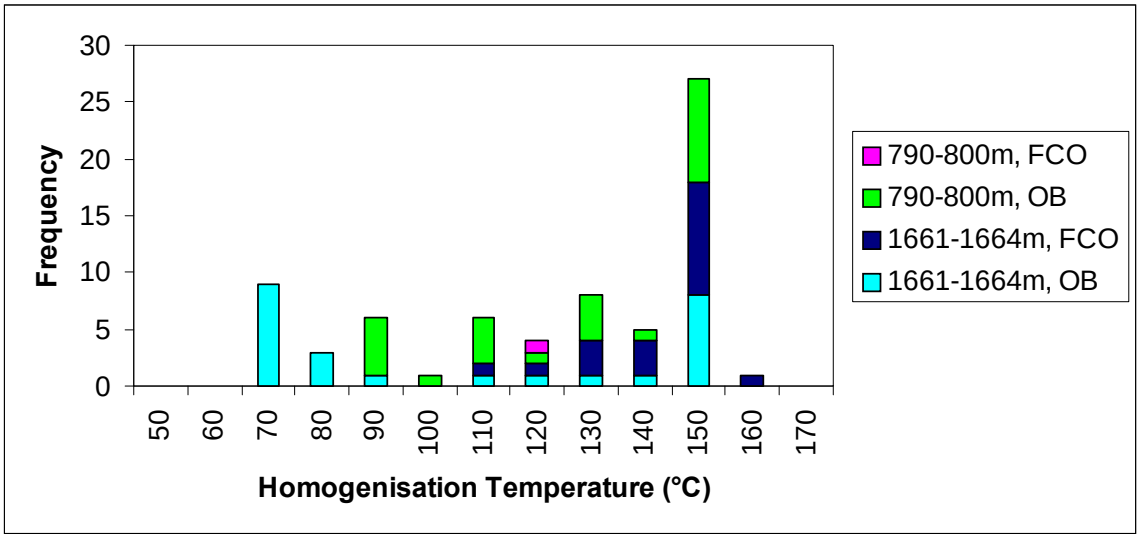

Figure 6-6: Histogram of homogenisation temperatures, Jabiru-2.

Homogenisation temperatures measured on aqueous fluid inclusions located on the quartz overgrowth boundary (OB) and on fractures cutting overgrowths (FCO) for cuttings samples in the Tertiary and Jurassic section from Jabiru-2. Note the abundance of T_{hom} values at the high end, many of which represent greater than values and these could be much higher than shown. This has the visual effect of compressing the length of the tail at the high temperature end.

2. Secondary aqueous inclusions located on healed fractures cutting quartz overgrowths, 790-800 mRT sample (n = 1, where n = number of inclusions measured). The only inclusion measured had a homogenisation temperature of 111°C (Table 6–5, Figure 6–6).

3. Primary aqueous inclusions on the quartz overgrowth boundary, 1661-64 mRT sample (n = 25, where n = number of inclusions measured). Measured homogenisation temperatures are from 64 to >150°C (Table 6–5, Figure 6–6).

4. Secondary aqueous inclusions are located on fractures that cut authigenic quartz overgrowths, 1661-64 mRT cuttings sample (n = 19, where n = number of inclusions measured). Measured homogenisation temperatures range from 109 to 160°C (Table 6–5, Figure 6–6).

6.4.3 Homogenisation Temperatures, Keeling-1

Measurements have been made on one cuttings sample within Triassic sandstones at 3039-42 mRT and the inclusions all fall in a single fluid inclusion assemblage, primary aqueous inclusions at the quartz overgrowth boundary (n = 40, where n = number of inclusions measured). The sample was chosen as it has a GOI value with oil inclusions also seen within quartz overgrowths. The measured homogenisation temperatures range from 90 to 130°C (Table 6–6, Figure 6–7).

6.4.4 Homogenisation Temperatures, Oliver-1

Measurements from the Oliver-1 well have been made on one core sample from a palaeo-oil column within presently gas saturated Jurassic sandstones of the Plover Formation at 2774.38 mRT. Oil inclusions also occur within quartz overgrowth in this sample. The inclusions all fall in a single fluid inclusion assemblage, consisting of primary two-phase aqueous inclusions located at the quartz overgrowth boundary (n = 20, where n = number of inclusions measured). The measured homogenisation temperatures range from 100 to >150°C (Table 6–7 Figure 6–8).

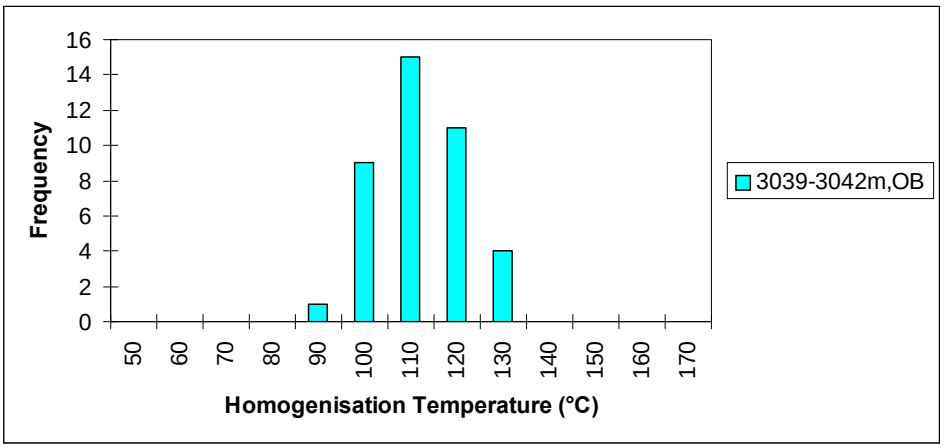

Figure 6-7: Histogram of homogenisation temperatures, Keeling-1.

Homogenisation temperatures measured on aqueous fluid inclusions located on the quartz overgrowth boundary (OB).

Table 6-6: Homogenisation temperatures, Keeling-1.

QOB = Quartz Overgrowth Boundary.

Well Name	Start Depth (mRT)	End Depth (mRT)	CSIRO Number	Sample Type	Mineral Type	Inclusion Type	Location	Th (°C)
Keeling-1	3039	3042	122385	cuttings	quartz	aqueous	QOB	90
Keeling-1	3039	3042	122385	cuttings	quartz	aqueous	QOB	92
Keeling-1	3039	3042	122385	cuttings	quartz	aqueous	QOB	92
Keeling-1	3039	3042	122385	cuttings	quartz	aqueous	QOB	92
Keeling-1	3039	3042	122385	cuttings	quartz	aqueous	QOB	93
Keeling-1	3039	3042	122385	cuttings	quartz	aqueous	QOB	98
Keeling-1	3039	3042	122385	cuttings	quartz	aqueous	QOB	99
Keeling-1	3039	3042	122385	cuttings	quartz	aqueous	QOB	99
Keeling-1	3039	3042	122385	cuttings	quartz	aqueous	QOB	99
Keeling-1	3039	3042	122385	cuttings	quartz	aqueous	QOB	100
Keeling-1	3039	3042	122385	cuttings	quartz	aqueous	QOB	101
Keeling-1	3039	3042	122385	cuttings	quartz	aqueous	QOB	103
Keeling-1	3039	3042	122385	cuttings	quartz	aqueous	QOB	105
Keeling-1	3039	3042	122385	cuttings	quartz	aqueous	QOB	105
Keeling-1	3039	3042	122385	cuttings	quartz	aqueous	QOB	106
Keeling-1	3039	3042	122385	cuttings	quartz	aqueous	QOB	106
Keeling-1	3039	3042	122385	cuttings	quartz	aqueous	QOB	107
Keeling-1	3039	3042	122385	cuttings	quartz	aqueous	QOB	107
Keeling-1	3039	3042	122385	cuttings	quartz	aqueous	QOB	107
Keeling-1	3039	3042	122385	cuttings	quartz	aqueous	QOB	107
Keeling-1	3039	3042	122385	cuttings	quartz	aqueous	QOB	108
Keeling-1	3039	3042	122385	cuttings	quartz	aqueous	QOB	108
Keeling-1	3039	3042	122385	cuttings	quartz	aqueous	QOB	109
Keeling-1	3039	3042	122385	cuttings	quartz	aqueous	QOB	110
Keeling-1	3039	3042	122385	cuttings	quartz	aqueous	QOB	110
Keeling-1	3039	3042	122385	cuttings	quartz	aqueous	QOB	111
Keeling-1	3039	3042	122385	cuttings	quartz	aqueous	QOB	112
Keeling-1	3039	3042	122385	cuttings	quartz	aqueous	QOB	113
Keeling-1	3039	3042	122385	cuttings	quartz	aqueous	QOB	115
Keeling-1	3039	3042	122385	cuttings	quartz	aqueous	QOB	115
Keeling-1	3039	3042	122385	cuttings	quartz	aqueous	QOB	117
Keeling-1	3039	3042	122385	cuttings	quartz	aqueous	QOB	117
Keeling-1	3039	3042	122385	cuttings	quartz	aqueous	QOB	118
Keeling-1	3039	3042	122385	cuttings	quartz	aqueous	QOB	118
Keeling-1	3039	3042	122385	cuttings	quartz	aqueous	QOB	119
Keeling-1	3039	3042	122385	cuttings	quartz	aqueous	QOB	120
Keeling-1	3039	3042	122385	cuttings	quartz	aqueous	QOB	121
Keeling-1	3039	3042	122385	cuttings	quartz	aqueous	QOB	121
Keeling-1	3039	3042	122385	cuttings	quartz	aqueous	QOB	130
Keeling-1	3039	3042	122385	cuttings	quartz	aqueous	QOB	130

6.4.5 Homogenisation Temperatures, Parry-1

Measurements have been made on one cuttings sample from a palaeo-oil column within water-wet Maastrichtian sandstones at 2094-97 mRT. The inclusions all fall in a single fluid inclusion assemblage, consisting of primary aqueous inclusions at the quartz overgrowth boundary (n = 20, where n = number of inclusions measured). Homogenisation temperatures range from 65 to >120°C (Table 6–8 Figure 6–9).

6.4.6 Homogenisation Temperatures, Skua-3

Measurements have been made on two cuttings samples, one from within the current oil column at 2425-2428 mRT and one from a palaeo-oil column below the current oil zone at 2434-37 mRT. In each sample homogenisation temperatures were determined for inclusions from two discrete assemblages (Table 6–9, Figure 6–10).

1. Primary aqueous inclusions located on the quartz overgrowth boundary, 2425-28 mRT sample (n = 30, where n = number of inclusions measured). Measured homogenisation temperatures range from 82 to >120°C (Table 6–9, Figure 6–10).

2. Secondary aqueous inclusions located on healed fractures cutting quartz overgrowths, 2425-28 mRT sample (n = 2, where n = number of inclusions measured). Homogenisation temperatures of 104°C and >130°C were recorded (Table 6–9, Figure 6–10).

3. Primary aqueous inclusions located on the quartz overgrowth boundary, 2434-37 mRT sample (n = 40, where n = number of inclusions measured). Measured homogenisation temperatures range from 78 to >130°C (Table 6–9, Figure 6–10).

4. Secondary aqueous inclusions located on fractures cutting quartz overgrowths, 2434-37 mRT sample (n = 10, where n = number of inclusions measured). Measured homogenisation temperatures range from 94 to 125°C (Table 6–9, Figure 6–10).

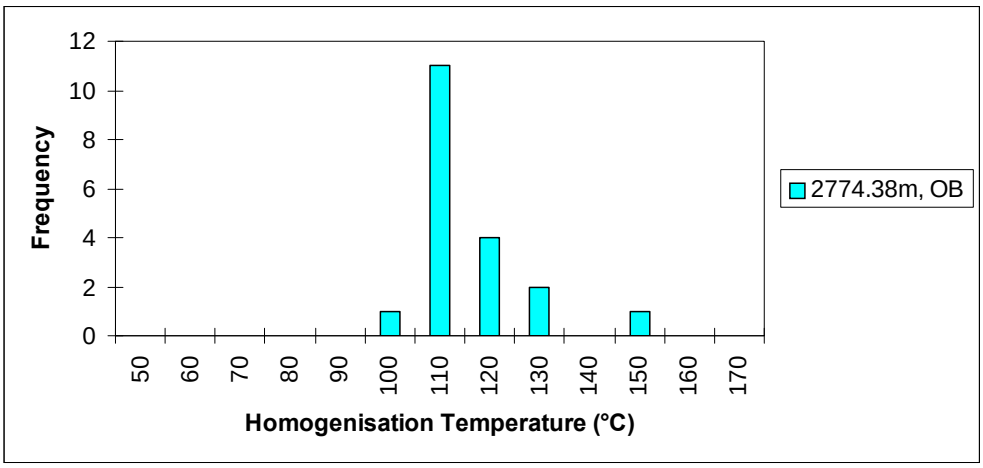

Figure 6-8: Histogram of homogenisation temperatures, Oliver-1.

Homogenisation temperatures measured on aqueous fluid inclusions located on the quartz overgrowth boundary (OB) from a core sample at 2774.38mRT.

Table 6-7: Homogenisation temperatures, Oliver-1

QOB = Quartz Overgrowth Boundary. Inclusions marked as greater than did not reach homogenisation and could have much higher T_{hom}.

Well Name	Start Depth (mRT)	End Depth (mRT)	CSIRO Number	Sample Type	Mineral Type	Inclusion Type	Location	Th (°C)
Oliver-1	2974		75959	core	quartz	aqueous	QOB	100
Oliver-1	2974		75959	core	quartz	aqueous	QOB	101
Oliver-1	2974		75959	core	quartz	aqueous	QOB	104
Oliver-1	2974		75959	core	quartz	aqueous	QOB	104
Oliver-1	2974		75959	core	quartz	aqueous	QOB	105
Oliver-1	2974		75959	core	quartz	aqueous	QOB	106
Oliver-1	2974		75959	core	quartz	aqueous	QOB	106
Oliver-1	2974		75959	core	quartz	aqueous	QOB	106
Oliver-1	2974		75959	core	quartz	aqueous	QOB	108
Oliver-1	2974		75959	core	quartz	aqueous	QOB	108
Oliver-1	2974		75959	core	quartz	aqueous	QOB	109
Oliver-1	2974		75959	core	quartz	aqueous	QOB	110
Oliver-1	2974		75959	core	quartz	aqueous	QOB	113
Oliver-1	2974		75959	core	quartz	aqueous	QOB	114
Oliver-1	2974		75959	core	quartz	aqueous	QOB	115
Oliver-1	2974		75959	core	quartz	aqueous	QOB	118
Oliver-1	2974		75959	core	quartz	aqueous	QOB	124
Oliver-1	2974		75959	core	quartz	aqueous	QOB	125
Oliver-1	2974		75959	core	quartz	aqueous	QOB	>150

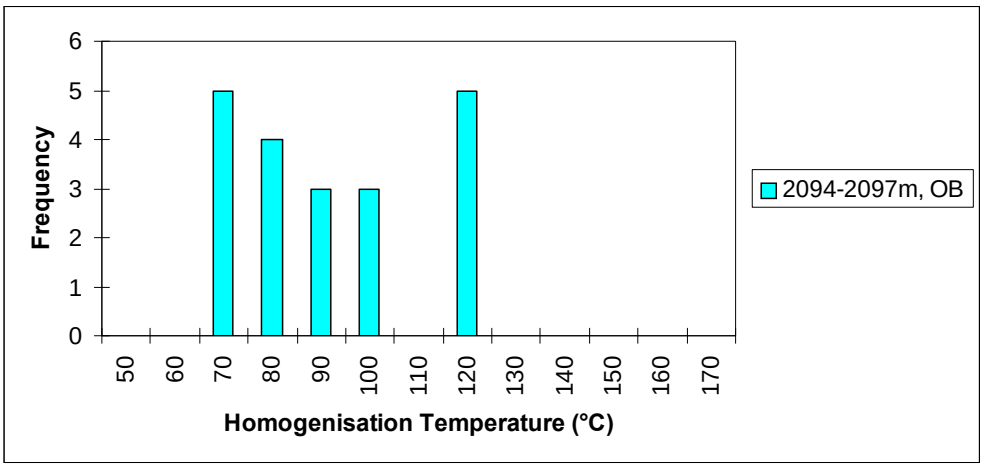

Figure 6-9: Histogram of homogenisation temperatures, Parry-1.

Homogenisation temperatures measured on aqueous fluid inclusions located on the quartz overgrowth boundary (OB) from a cuttings sample from 2094-97mRT.

Table 6-8: Homogenisation temperatures, Parry-1.

QOB = Quartz Overgrowth Boundary. Inclusions marked as greater than did not reach homogenisation and could have much higher T_{hom}.

Well Name	Start Depth (mRT)	End Depth (mRT)	CSIRO Number	Sample Type	Mineral Type	Inclusion Type	Location	Th (°C)
Parry-1	2094	2097	123481	cuttings	quartz	aqueous	QOB	65
Parry-1	2094	2097	123481	cuttings	quartz	aqueous	QOB	65
Parry-1	2094	2097	123481	cuttings	quartz	aqueous	QOB	68
Parry-1	2094	2097	123481	cuttings	quartz	aqueous	QOB	69
Parry-1	2094	2097	123481	cuttings	quartz	aqueous	QOB	70
Parry-1	2094	2097	123481	cuttings	quartz	aqueous	QOB	71
Parry-1	2094	2097	123481	cuttings	quartz	aqueous	QOB	75
Parry-1	2094	2097	123481	cuttings	quartz	aqueous	QOB	80
Parry-1	2094	2097	123481	cuttings	quartz	aqueous	QOB	80
Parry-1	2094	2097	123481	cuttings	quartz	aqueous	QOB	81
Parry-1	2094	2097	123481	cuttings	quartz	aqueous	QOB	90
Parry-1	2094	2097	123481	cuttings	quartz	aqueous	QOB	90
Parry-1	2094	2097	123481	cuttings	quartz	aqueous	QOB	92
Parry-1	2094	2097	123481	cuttings	quartz	aqueous	QOB	94
Parry-1	2094	2097	123481	cuttings	quartz	aqueous	QOB	98
Parry-1	2094	2097	123481	cuttings	quartz	aqueous	QOB	>120
Parry-1	2094	2097	123481	cuttings	quartz	aqueous	QOB	>120
Parry-1	2094	2097	123481	cuttings	quartz	aqueous	QOB	>120
Parry-1	2094	2097	123481	cuttings	quartz	aqueous	QOB	>120
Parry-1	2094	2097	123481	cuttings	quartz	aqueous	QOB	>120

6.4.7 Previous Homogenisation Temperature Data

To augment the new thermometric data collected in the current study additional homogenisation temperatures were collated from a further 19 samples (Figure 6–11) that come from previous investigations completed by the author and other workers including published (Lisk and Eadington, 1994) and unpublished reports (Eadington et al., 1991; Hamilton et. al., 1991).

These data, with the exception of the results from Bilyara-1 (Bone, 1990), come from the same CSIRO laboratory and were acquired using very similar analytical procedures as those utilised in the current study. The data from Bone (1990) are not directly comparable with these results having been recorded on different equipment and with different analytical protocols, but are included as they show general consistency with the data collected in this study.

The palaeotemperature data retrieved from these previous studies together with the new thermometric data of the current study provide a broad spatial coverage across the VSB and also across the different interpreted fluid zones inferred from the GOI data (Current hydrocarbon, palaeo-hydrocarbon and in currently water wet wells where consistently low GOI values are interpreted as migration pathways).

The occurrence of coeval oil inclusions in most of the fluid inclusion assemblages analysed provides good support to imply that the temperature conditions measured on the aqueous inclusions represent a valid proxy for the conditions prevailing when those co-formed oil inclusions were trapped.

The temperature ranges recorded in the fluid inclusions show that trapping of fluid inclusions by the formation of authigenic quartz overgrowths or the healing of fractures that transect those quartz overgrowths first started at about 64°C and ranged to more than 150°C, but that most of the inclusions measured appear to have been trapped between about 90°C and 120°C.

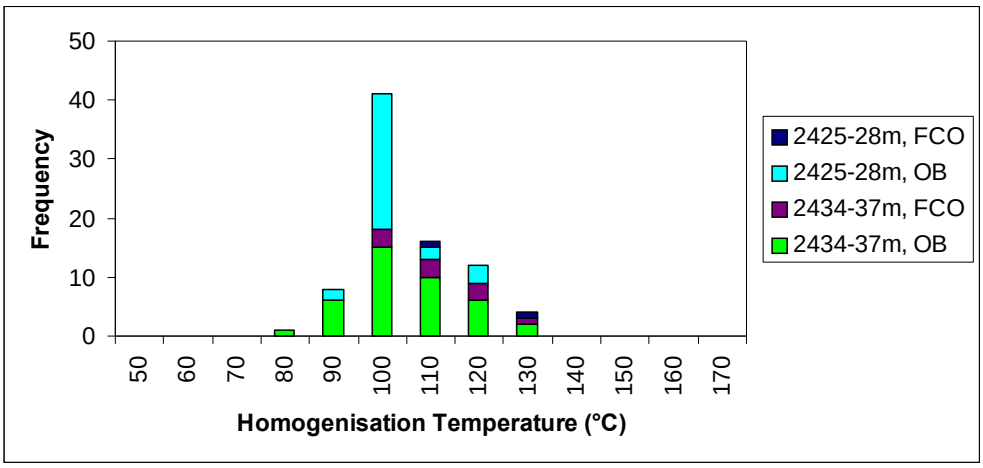

Figure 6-10: Histogram of homogenisation temperatures, Skua-3.

Homogenisation temperatures measured on aqueous fluid inclusions located on the quartz overgrowth boundary (OB) and on fractures cutting overgrowths (FCO) from two cutting samples from Skua-3.

Table 6-9: Homogenisation temperatures, Skua-3

QOB = Quartz Overgrowth Boundary; FCO = Fractures Cutting Overgrowth. Inclusions marked as greater than did not reach homogenisation and could have much higher T_{hom}.

Well Name	Start Depth (mRT)	End Depth (mRT)	CSIRO Number	Sample Type	Mineral Type	Inclusion Type	Location	Th (°C)
Skua-3	2425	2428	122423	cuttings	quartz	aqueous	FCO	104
Skua-3	2425	2428	122423	cuttings	quartz	aqueous	FCO	>130
Skua-3	2425	2428	122423	cuttings	quartz	aqueous	QOB	82
Skua-3	2425	2428	122423	cuttings	quartz	aqueous	QOB	90
Skua-3	2425	2428	122423	cuttings	quartz	aqueous	QOB	92
Skua-3	2425	2428	122423	cuttings	quartz	aqueous	QOB	94
Skua-3	2425	2428	122423	cuttings	quartz	aqueous	QOB	94
Skua-3	2425	2428	122423	cuttings	quartz	aqueous	QOB	94
Skua-3	2425	2428	122423	cuttings	quartz	aqueous	QOB	94
Skua-3	2425	2428	122423	cuttings	quartz	aqueous	QOB	95
Skua-3	2425	2428	122423	cuttings	quartz	aqueous	QOB	95
Skua-3	2425	2428	122423	cuttings	quartz	aqueous	QOB	95
Skua-3	2425	2428	122423	cuttings	quartz	aqueous	QOB	95
Skua-3	2425	2428	122423	cuttings	quartz	aqueous	QOB	96
Skua-3	2425	2428	122423	cuttings	quartz	aqueous	QOB	96
Skua-3	2425	2428	122423	cuttings	quartz	aqueous	QOB	96
Skua-3	2425	2428	122423	cuttings	quartz	aqueous	QOB	96
Skua-3	2425	2428	122423	cuttings	quartz	aqueous	QOB	96
Skua-3	2425	2428	122423	cuttings	quartz	aqueous	QOB	96
Skua-3	2425	2428	122423	cuttings	quartz	aqueous	QOB	97
Skua-3	2425	2428	122423	cuttings	quartz	aqueous	QOB	98
Skua-3	2425	2428	122423	cuttings	quartz	aqueous	QOB	98
Skua-3	2425	2428	122423	cuttings	quartz	aqueous	QOB	98
Skua-3	2425	2428	122423	cuttings	quartz	aqueous	QOB	98
Skua-3	2425	2428	122423	cuttings	quartz	aqueous	QOB	98
Skua-3	2425	2428	122423	cuttings	quartz	aqueous	QOB	98
Skua-3	2425	2428	122423	cuttings	quartz	aqueous	QOB	99
Skua-3	2425	2428	122423	cuttings	quartz	aqueous	QOB	103
Skua-3	2425	2428	122423	cuttings	quartz	aqueous	QOB	110
Skua-3	2425	2428	122423	cuttings	quartz	aqueous	QOB	112
Skua-3	2425	2428	122423	cuttings	quartz	aqueous	QOB	116
Skua-3	2425	2428	122423	cuttings	quartz	aqueous	QOB	>120

Table 6.9 continued: Homogenisation temperatures, Skua-3

Well Name	Start Depth (mRT)	End Depth (mRT)	CSIRO Number	Sample Type	Mineral Type	Inclusion Type	Location	Th (°C)
Skua-3	2434	2437	122424	cuttings	quartz	aqueous	FCO	94
Skua-3	2434	2437	122424	cuttings	quartz	aqueous	FCO	98
Skua-3	2434	2437	122424	cuttings	quartz	aqueous	FCO	99
Skua-3	2434	2437	122424	cuttings	quartz	aqueous	FCO	106
Skua-3	2434	2437	122424	cuttings	quartz	aqueous	FCO	106
Skua-3	2434	2437	122424	cuttings	quartz	aqueous	FCO	108
Skua-3	2434	2437	122424	cuttings	quartz	aqueous	FCO	111
Skua-3	2434	2437	122424	cuttings	quartz	aqueous	FCO	112
Skua-3	2434	2437	122424	cuttings	quartz	aqueous	FCO	114
Skua-3	2434	2437	122424	cuttings	quartz	aqueous	FCO	125
Skua-3	2434	2437	122424	cuttings	quartz	aqueous	QOB	78
Skua-3	2434	2437	122424	cuttings	quartz	aqueous	QOB	81
Skua-3	2434	2437	122424	cuttings	quartz	aqueous	QOB	84
Skua-3	2434	2437	122424	cuttings	quartz	aqueous	QOB	86
Skua-3	2434	2437	122424	cuttings	quartz	aqueous	QOB	87
Skua-3	2434	2437	122424	cuttings	quartz	aqueous	QOB	89
Skua-3	2434	2437	122424	cuttings	quartz	aqueous	QOB	89
Skua-3	2434	2437	122424	cuttings	quartz	aqueous	QOB	92
Skua-3	2434	2437	122424	cuttings	quartz	aqueous	QOB	93
Skua-3	2434	2437	122424	cuttings	quartz	aqueous	QOB	93
Skua-3	2434	2437	122424	cuttings	quartz	aqueous	QOB	94
Skua-3	2434	2437	122424	cuttings	quartz	aqueous	QOB	95
Skua-3	2434	2437	122424	cuttings	quartz	aqueous	QOB	95
Skua-3	2434	2437	122424	cuttings	quartz	aqueous	QOB	96
Skua-3	2434	2437	122424	cuttings	quartz	aqueous	QOB	97
Skua-3	2434	2437	122424	cuttings	quartz	aqueous	QOB	97
Skua-3	2434	2437	122424	cuttings	quartz	aqueous	QOB	97
Skua-3	2434	2437	122424	cuttings	quartz	aqueous	QOB	98
Skua-3	2434	2437	122424	cuttings	quartz	aqueous	QOB	98
Skua-3	2434	2437	122424	cuttings	quartz	aqueous	QOB	98
Skua-3	2434	2437	122424	cuttings	quartz	aqueous	QOB	99
Skua-3	2434	2437	122424	cuttings	quartz	aqueous	QOB	100
Skua-3	2434	2437	122424	cuttings	quartz	aqueous	QOB	101
Skua-3	2434	2437	122424	cuttings	quartz	aqueous	QOB	102
Skua-3	2434	2437	122424	cuttings	quartz	aqueous	QOB	103
Skua-3	2434	2437	122424	cuttings	quartz	aqueous	QOB	103
Skua-3	2434	2437	122424	cuttings	quartz	aqueous	QOB	104
Skua-3	2434	2437	122424	cuttings	quartz	aqueous	QOB	104
Skua-3	2434	2437	122424	cuttings	quartz	aqueous	QOB	106
Skua-3	2434	2437	122424	cuttings	quartz	aqueous	QOB	107
Skua-3	2434	2437	122424	cuttings	quartz	aqueous	QOB	108
Skua-3	2434	2437	122424	cuttings	quartz	aqueous	QOB	109
Skua-3	2434	2437	122424	cuttings	quartz	aqueous	QOB	113
Skua-3	2434	2437	122424	cuttings	quartz	aqueous	QOB	117
Skua-3	2434	2437	122424	cuttings	quartz	aqueous	QOB	117
Skua-3	2434	2437	122424	cuttings	quartz	aqueous	QOB	118
Skua-3	2434	2437	122424	cuttings	quartz	aqueous	QOB	118
Skua-3	2434	2437	122424	cuttings	quartz	aqueous	QOB	120
Skua-3	2434	2437	122424	cuttings	quartz	aqueous	QOB	>130
Skua-3	2434	2437	122424	cuttings	quartz	aqueous	QOB	>130

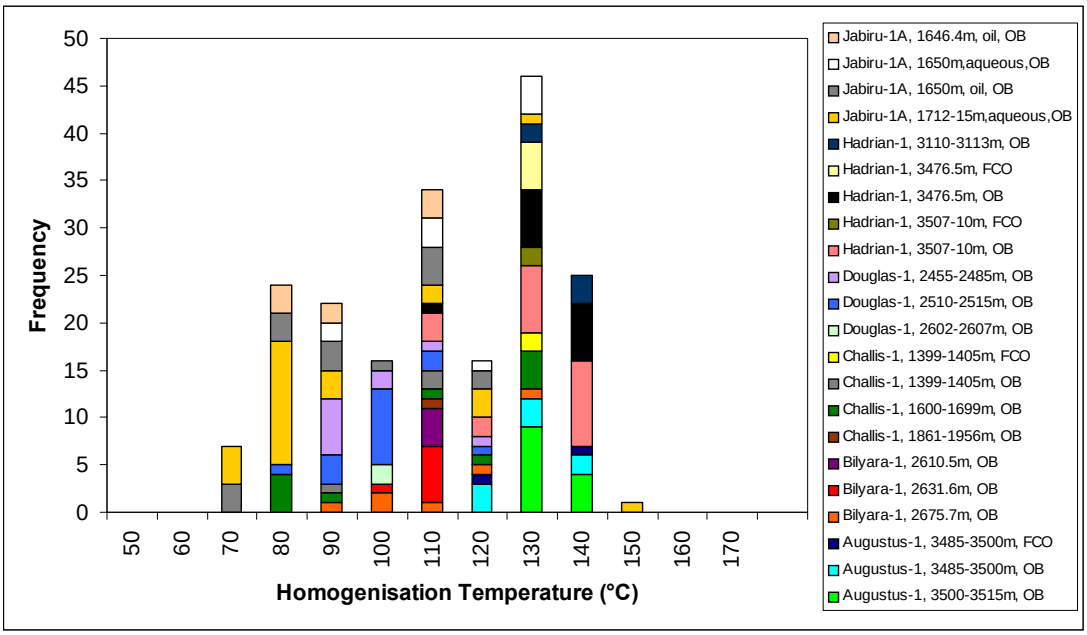

Figure 6-11: Histogram of previously reported homogenisation temperatures

Data comes from open file CSIRO reports (see text for references), published studies (Lisk and Eadington, 1994) or from Bone (1990) and cover 22 samples from 6 wells.

6.5 GEOLOGICAL TEMPERATURES FROM FLUID INCLUSIONS

The homogenisation temperatures measured on fluid inclusions represent precise and accurate determinations of the phase change from two-phase to single phase condition. To translate these measurements into temperatures that can be used to make geological interpretations relies on a number of important criteria that must be fully considered if valid assessments of true trapping temperature are to be obtained.

6.5.1 Homogenisation Temperature Interpretation

Homogenisation temperatures record the position on the bubble point curve of the entrapped fluid (Figure 6–12) and represent the conditions that existed when the sample crossed this phase boundary during sample retrieval from the sub-surface. As such, they provide a minimum estimate of the temperature at which the fluid contained within the inclusion was trapped.

The true trapping temperature, however, may have been higher than this and generally requires the homogenisation temperatures to be corrected to the likely pressure conditions existing at the time of trapping. This is achieved through use of experimentally derived lines (isochores) of constant density (Figure 6–12) that connect the point of intersection on the bubble point curve with the true trapping temperature and pressure in the single-phase field. The degree of correction that is required is therefore dependant on the density of the trapped fluid. Liquid hydrocarbon inclusions are, for example, more compressible than equivalent aqueous inclusions and hence require more substantial pressure corrections (Figure 6–12).

The pressure at which the inclusions were trapped is not known, but several approaches can be used to estimate this unknown parameter. In the simplest case, trapping pressure can be estimated by assuming hydrostatic conditions and using the sample depth to derive a likely trapping pressure. The assumption that reservoir conditions were hydrostatic is, however, not always valid and significant errors can result from this approach.

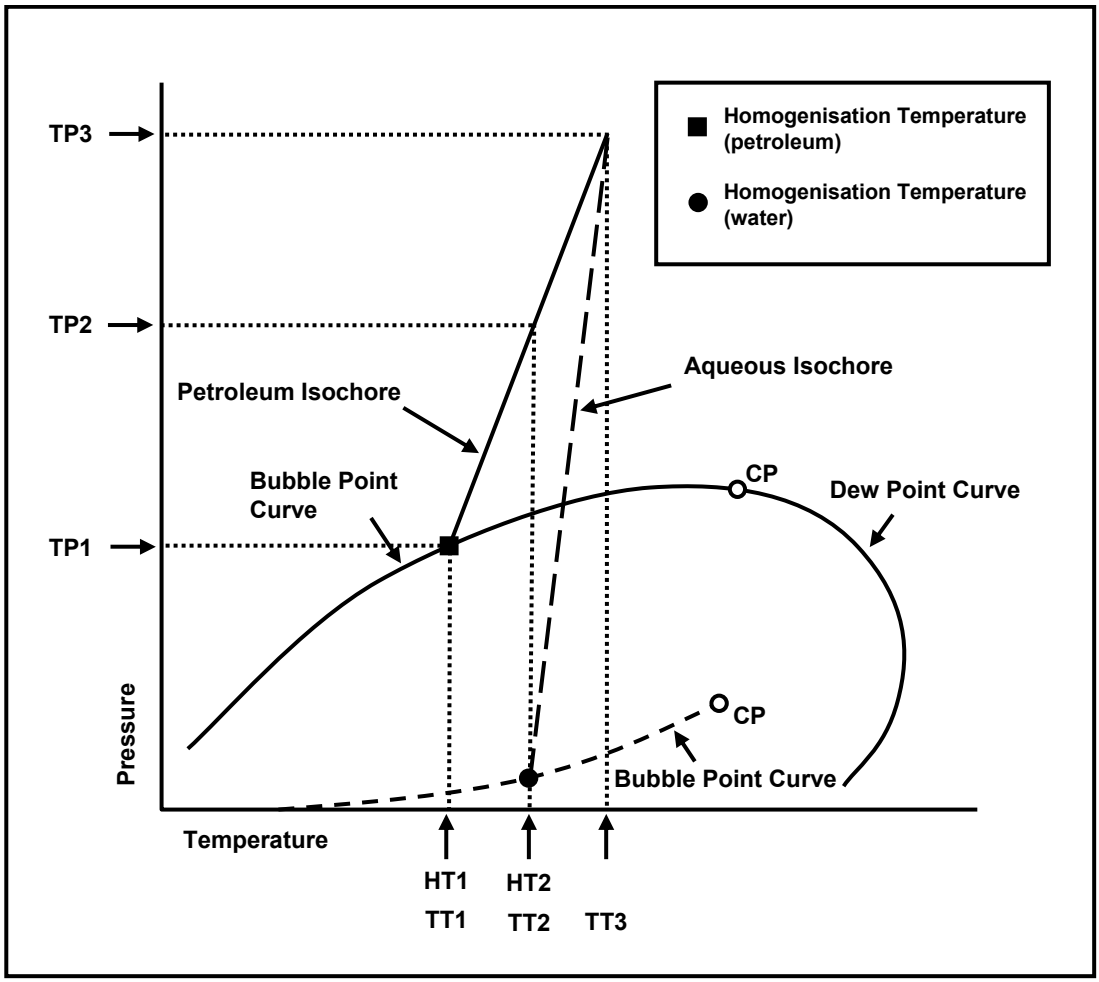

Figure 6-12: Pressure-Temperature plot showing phase envelopes for water and petroleum.

The display shows generic phase envelopes for water and petroleum with homogenisation temperatures shown for petroleum (HT1) and water bearing (HT2) inclusions. Also shown are possible interpretations of trapping temperatures (TT1-TT3) and pressures (TP1-TP3) depending on whether homogeneous or heterogeneous trapping has occurred. If trapped heterogeneously (2-phase) then the point of intersection with the relevant bubble point curve represents the true trapping temperature and the homogenisation temperature (HT) and the Trapping Temperature (TT) are the same. In contrast if trapped as homogeneous fluids (1-phase) then a pressure correction using an isochore is needed to determine the true trapping temperature. In this case the intersection point of the petroleum and water isochores defines the position of the Trapping Temperature (TT3) and Pressure (TP3). One additional possibility is that the petroleum phase was trapped as a single phase and the water phase was trapped heterogeneously in which case Trapping Temperature 2 (TT2) and Trapping Pressure 2 (TP2) would apply.

A more reliable alternative is available when pairs of petroleum and aqueous inclusion assemblages can be demonstrated from petrographic observations to be trapped coevally. In this instance the homogenisation temperatures derived from coexisting inclusions can be used to determine the true trapping temperature and pressure conditions prevailing in the in the subsurface by the intersection of isochores for the aqueous and hydrocarbon phases (Figure 6–12). The main limitation with this approach is the inherent uncertainty about the composition of the hydrocarbon phase and the effect this has on the shape of the phase envelope and isochores used to produce the intersecting isochore construction.

Analytical methods for determining the composition of hydrocarbon inclusions have improved dramatically in recent years for bulk samples (Karlsen et. al., 1993; George et al., 1997, 2001a, 2002) but the detailed description of individual inclusions remains difficult (Greenwood et al., 1998). An alternative that is increasingly being used to constrain the fluid-pressure history of sedimentary basins is the use of confocal laser scanning microscopy (CLSM) in combination with suitable P-V-T modeling software to approximate composition of the petroleum within individual fluid inclusions (Macleod et al., 1996; Pironon et al., 1998; Aplin et al., 1999).

This approach utilises accurate measurement of liquid-vapour ratios of individual fluid inclusions (Figure 6–13) together with conventional homogenisation temperatures as input data, to estimate the bulk composition of the included fluid through a series of iterative PVT simulations. A more constrained phase envelope (to determine the minimum saturation pressure) and isochore can then be constructed for the included oil thereby allowing the use of the intersecting isochores method with greater certainty.

6.5.2 Significance of Heterogeneous Trapping

The assumption that a single phase has been trapped within each of the individual fluid inclusions measured represents a key element in the interpretation of homogenisation temperatures, and in particular this factor determines if any pressure correction is required to convert the measured value into an estimate of the true trapping temperature of that inclusion.

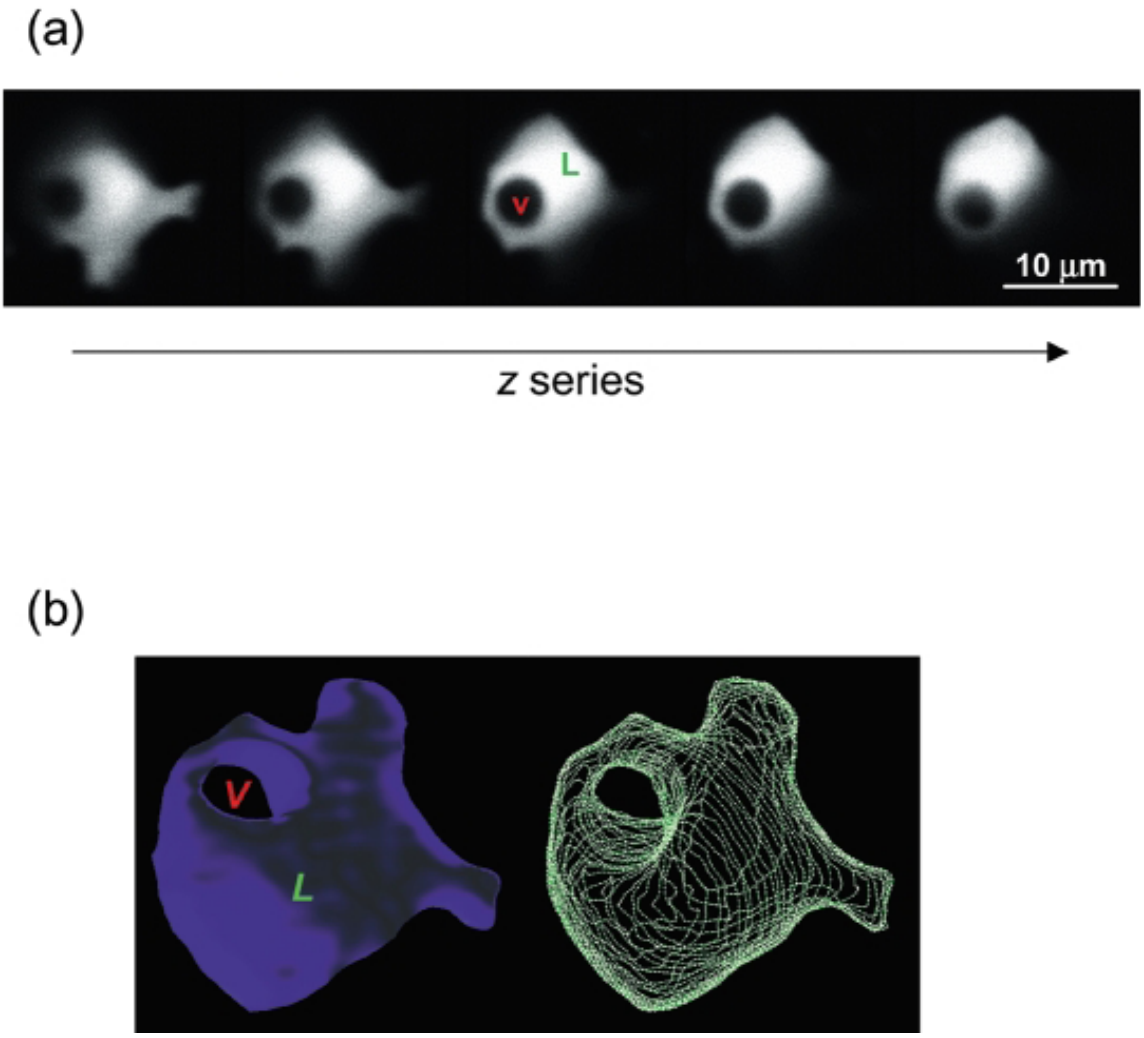

Figure 6-13: Imaging of liquid-vapour ratios for a petroleum inclusion in quartz.

Selected 2D images (a) from CSLM of a petroleum inclusion in a sample from the Ellon Field, East Shetland Basin together with 3D volume and contour images (b) of the sample inclusion constructed by the modified GOCAD program (from Tseng and Pottorf, 2002). These images allow the accurate measurement of the liquid and gas phases that provide constraints to be placed on the PVT conditions during trapping.

This assumption impacts all routinely used methods for estimating true trapping temperatures and pressures so is critically important to the correct interpretation of homogenisation temperature data. However, in petroliferous sedimentary environments gaseous products such as methane, and, or carbon dioxide are a common component of sub-surface fluids. These gases are readily dissolved in formation waters and in deeper sedimentary basins it is not unusual for formation water to be fully methane saturated (Hanor, 1980). Entrapment of mixtures of immiscible fluids within individual inclusions is more prevalent and problematic to accurate geothermometry than has generally been recognised (Loucks, 2000).

The presence of two fluids in the same inclusion requires that these fluids coexisted at the time of trapping. If the inclusions were trapped in an immiscible fluid system then a complete range of fluid compositions will be recorded from trapping variable mixtures of the two or more phases present (Bodnar, 2003). This situation results in populations of inclusions with scattered densities, variable percent vapour at room temperature, and therefore a wide range in measured homogenisation temperatures (Ramboz et al., 1982) with a characteristic skewed distribution towards the high temperature end (Loucks, 2000). In contrast, where fluids are trapped as a single phase constant liquid-vapour ratios are expected within individual fluid inclusion populations with a tighter and more uniform distribution of measured homogenisation temperatures (Bodnar, 2003).

For an inclusion where an infinitesimally small amount of an immiscible fluid is trapped heterogeneously (2-phase) then the point of intersection with the relevant bubble point curve will represent the true trapping temperature and the homogenisation temperature (HT) and the Trapping Temperature (TT) will be the same. In reality, however, inclusions that trap more than one phase will typically yield temperatures that are higher than the true geological temperature as the proportion of the second phase can vary widely. The trapping of a second phase always acts to increase the recorded homogenisation temperature so it follows that the minimum homogenisation temperatures will provide the best estimate of the true geological temperatures (Roedder, 1981; Burruss, 1992; Pichavant et al., 1982; Ramboz et al., 1982).

However, this does not preclude trapping of fluid inclusions at higher temperatures and this is likely to occur given that cementation is not generally an instantaneous event. However, the utilisation of homogenisation temperatures greater than the minimum must be consistent with other thermal indicators (e.g. vitrinite reflectance) and conclusions should not be based on the fluid inclusion data alone. Homogenisation temperatures that exceed maximum palaeotemperature indicated by other thermal indicators need to be considered cautiously and not used in isolation.

Visual petrographic observations of the range in percent vapour within individual inclusions allow fluid inclusions that trapped mixtures of fluids such as pore water and gas (increased percent vapour) to be identified. This alerts the analyst to the likelihood of heterogeneous trapping but is not a robust enough criteria to exclude all heterogeneously trapped inclusions as even a small proportion of a second phase can dramatically increase the true trapping temperature above the measured homogenisation temperature.

If an interpretation that assumes all measured inclusions trapped two-phases is adopted then a chance remains that inclusions genuinely trapped as a single-phase will not be pressure corrected and hence the true trapping temperature could be underestimated. The practical impact of this potential error is relatively minor for aqueous inclusions where the pressure correction is typically small (10-15°C) due to the steep gradient of the isochore but can lead to large errors for hydrocarbon inclusions that require large pressure corrections due to the increased compressibility of these fluids (Figure 6–12).

6.5.3 Basis for T_{hom} Interpretation adopted in the Current Study

In the interpretation of the homogenisation temperatures measured on samples from this study no pressure correction has been applied as petrographic observations provide clear evidence that more than one phase were trapped in at least some of the inclusions that were measured. Fluid inclusions within the QOB and FQO populations (Figure 6–3) fall into the highly variable liquid-vapour group of Goldstein and Reynolds (1994) with some inclusions (not measured) exhibiting liquid-vapour ratios that exceed 50% (Figure 6–14).

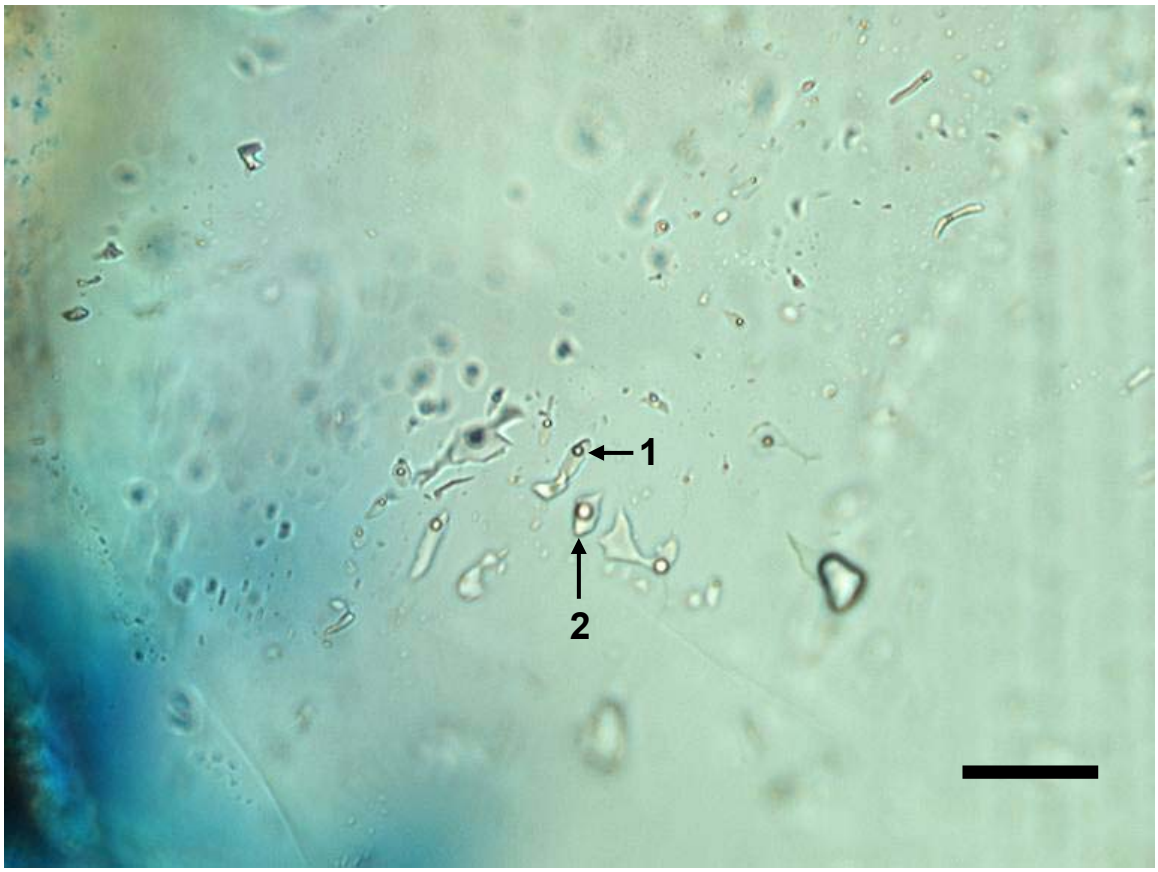

Figure 6-14: Representative example of the variation in liquid vapour ratios.

Plain light photomicrograph showing multiple fluid inclusions trapped within a fracture set. The size of the circular vapour bubble shows noticeable variation between different inclusions which can be used to indicate that these inclusions have trapped a combination of liquid and gas rather than a homogenous fluid. The inclusion marked 1 has for example a much lower percent vapour than the inclusion marked 2. Scale bar shows 20 microns.

A comparison against the current reservoir temperatures taken from corrected bottom hole temperatures also supports an interpretation of heterogeneous trapping with the maximum T_{hom} values and most of the modal T_{hom} values recorded in each well plotting above the current formation temperatures (Table 6–10). Current burial depths are likely represent the maximum depth experienced (see burial history analysis this chapter) so temperatures significantly above this level are unlikely to reflect genuine reservoir temperatures.

The main line of evidence that inclusions have trapped immiscible fluids, however, is that individual inclusions in a coeval population contain varied proportions of the immiscible fluids (Figure 6–14) and consequently have homogenisation temperatures (T_{hom}) that vary widely (Figure 6–10; Table 6–10). In addition, heterogeneous trapping should produce a distribution of homogenisation temperatures that are skewed to the high end (Loucks, 2000), such as that seen in most of the samples analysed in this study.

Figure 6–15 summarises homogenisation temperatures from selected samples that contain sufficient measurements to produce a meaningful plot. All of the samples show a range in measured T_{hom} values (Table 6–10) that is greater than would be anticipated for inclusions that trapped single phase fluids. The majority of samples also show a distribution that is skewed towards the high end (Figure 6–15, Table 6–10) although not always with a mode near the lower end of the range as would be theoretically expected for a population of heterogeneously trapped inclusions (Loucks, 2000).

The lack of strongly skewed distributions of T_{hom} values is also not particularly unexpected given the nature of the analytical method employed that gave a preference to selecting inclusions with low liquid-vapour ratios in order to minimise the effect of heterogeneous trapping once the risk of heterogeneous trapping had been recognised petrographically from the variable liquid-vapour ratios. The method favoured the reporting of a greater than value where the T_{hom} value was shown to exceed the current formation temperature by more than 50°C rather than heating all inclusions to homogenisation.

Table 6-10: Tabulated summary of T_{hom} measurements.

Table shows the current Bottom Hole Temperature (BHT) for each sample compared against the fluid inclusion homogenisation temperature data and the calculated skewness of the data.

Well	Depth (mRT)	BHT	Min Th	Min Th extrap	Max Th	Modal Th	Mean Th	Skewness
Augustus-1	3485	127	113	105	135	116	125	-0.07
Challis-1	1399	56	63	62	125		89	0.36
Challis-1	1600	56	75	63	125	75	92	0.84
Douglas-1	2455	96	83	73	113		94	1.21
Douglas-1	2510	96	74	74	113	89	95	-0.29
Eclipse-1	2679	113	99	93	195	100	111	3.46
Hadrian-1	3476.5	120	108	110	145	123	128	-0.60
Hadrian-1	3110	120	122	116	137		131	-0.76
Hadrian-1	3507	120	104	102	139	135	126	-0.67
Jabiru-1A	1646.4	72	71	56	101	73	82	0.67
Jabiru-1A	1650	72	74	65	112	96	93	-0.03
Jabiru-1A	1712	72	67	63	142	70	83	1.89
Keeling-1	3039	109	90	86	130	107	108	0.12
Octavius-2	3195	108	107	105	131	127	125	-1.71
Octavius-2	3260	108	128	126	134	131	131	-0.72
Oliver-1	2974	121	100	91	125	106	110	0.89
Parry-1	2094	93	65	50	98	65	79	0.28
Skua-3	2425	98	82	79	116	96	98	0.10
Skua-3	2434	98	78	78	125	98	101	1.00

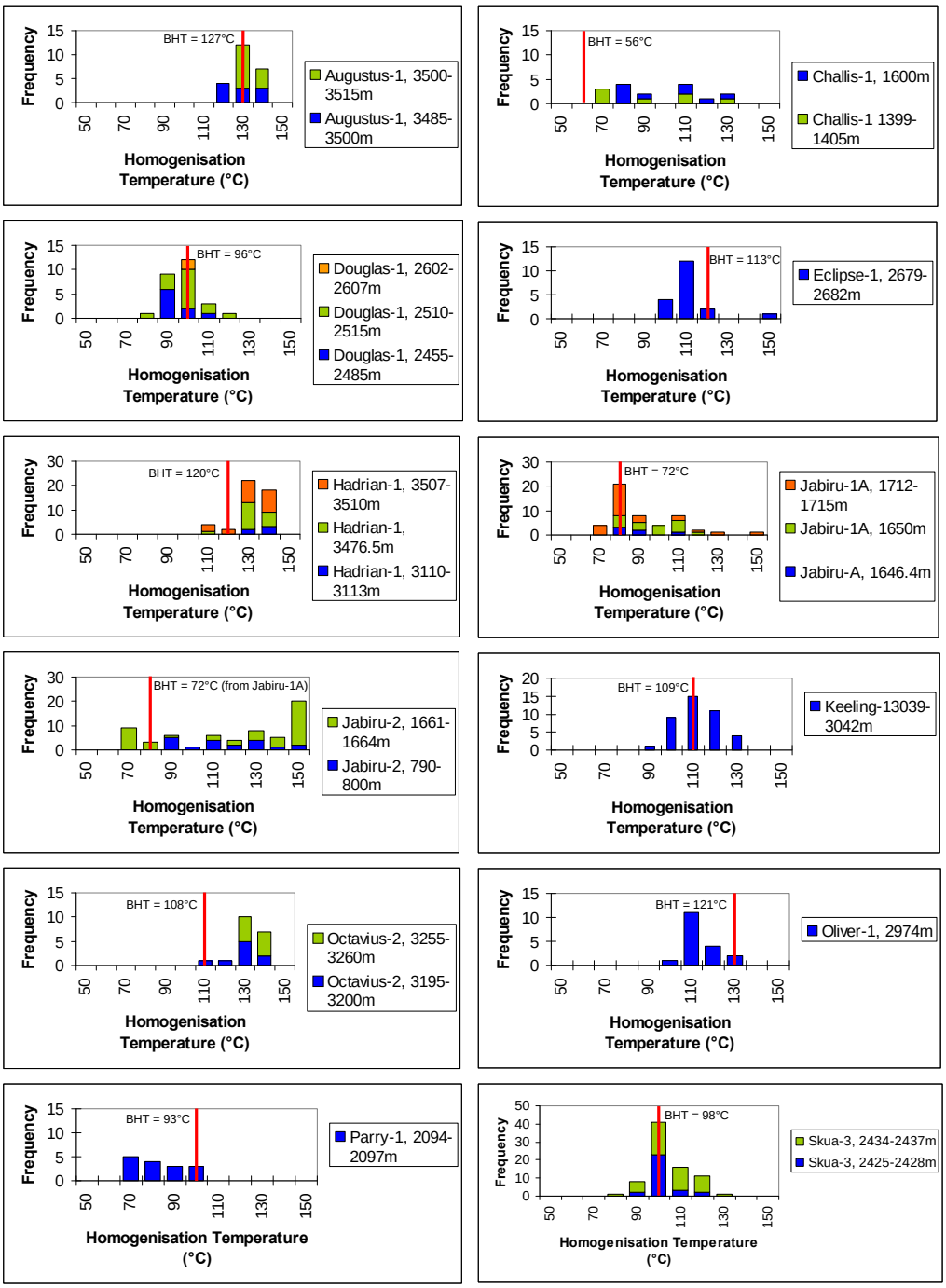

Figure 6-15: Selection of PTA samples showing histogram of T_{hom} values

Histograms of T_{hom} values are shown for samples with sufficient measurements together with the current formation temperature derived from extrapolated bottom hole temperatures. Note the wide spread and skewed distribution of T_{hom} values in many of the samples. Only the Keeling-1 and Douglas-1 samples show a spread of values that resemble a normal distribution Additionally in all samples there are T_{hom} values that exceed the current formation temperatures estimated from bottom hole temperatures.

This results in some of the histograms showing a mode at high temperature that acts to compress the tail (and degree of skewness) that would have likely otherwise resulted had these inclusions not been recorded as greater than T_{hom} values. Whilst this approach is likely to have limited the degree of skewness seen in the data the lack of consistent normal distributions indicates that this approach has not completely prevented the measurement of at least some heterogeneously trapped inclusions. This occurs because the addition of even a small proportion of a second phase can dramatically increase the measured homogenisation temperature well above the true trapping temperature above and as a consequence a degree of skewness occurs.

Consequently the application of a method for selecting suitable inclusions that is solely based on visually observed liquid-vapour ratios is alone unlikely to provide sufficiently robust criteria to completely exclude all of the heterogeneously trapped inclusions from the measured population.

A further approach has been used to provide support for heterogeneous trapping in the data recorded in this study, which draws on theoretical studies that predict any population of coeval fluid inclusions that sampled immiscible fluids should have an exponential frequency distribution of the fluid-phase proportions and hence homogenisation temperatures (Loucks, 2000).

To apply this concept to the current data set, the homogenisation temperature data recorded for each fluid inclusion assemblage in each sample has been plotted on log probit paper. The data from Douglas-1, for example, plot as a linear array that confirms that the data set has a numerically dominant sub-population that obeys an exponential probability function (Figure 6–16).

Most of the other samples analysed in this study show a similar observation result (Figure 6–17, 6–18 and 6–19) and as a result the conclusion that these samples have trapped immiscible fluids related to formation waters that are fully saturated with respect to methane or other soluble hydrocarbons can be further strengthened.

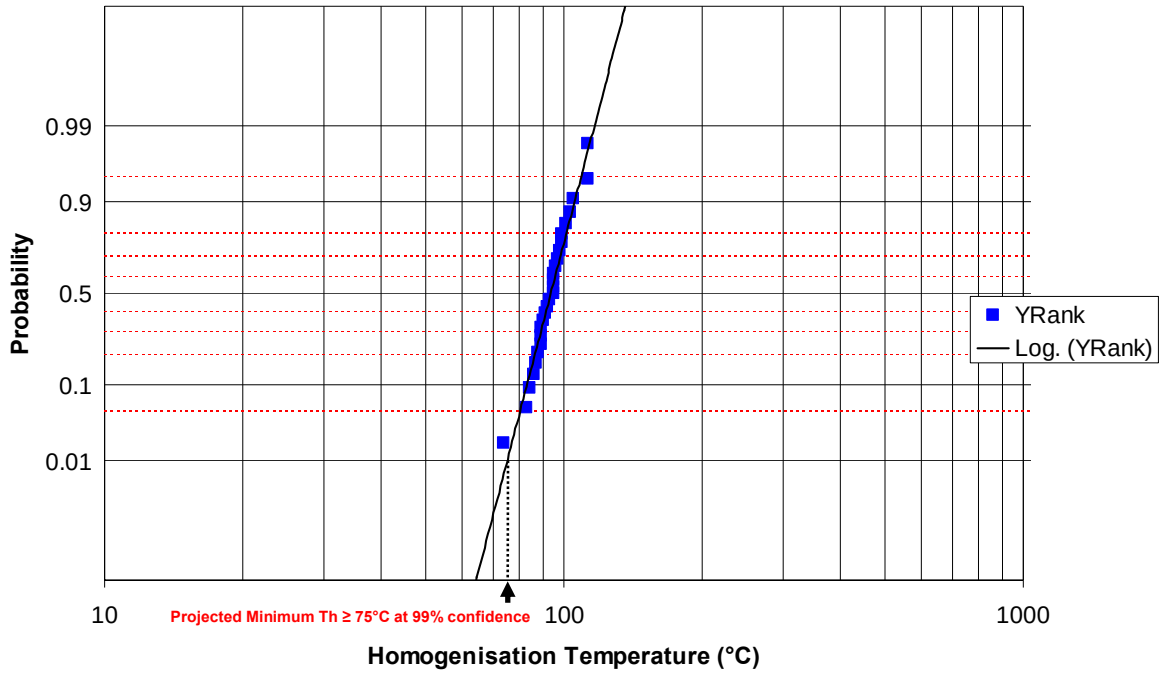

Figure 6-16: Distribution of T_{hom} values from Douglas-1 plotted on log probit paper.

The measured T_{hom} data from Douglas-1 plot as a linear array indicating that the data set has a numerically dominant sub-population that obeys an exponential probability function. In this example the projection of this regression line allows a minimum T_{hom} value to be estimated as greater than or equal to 75°C at the 99% confidence level.

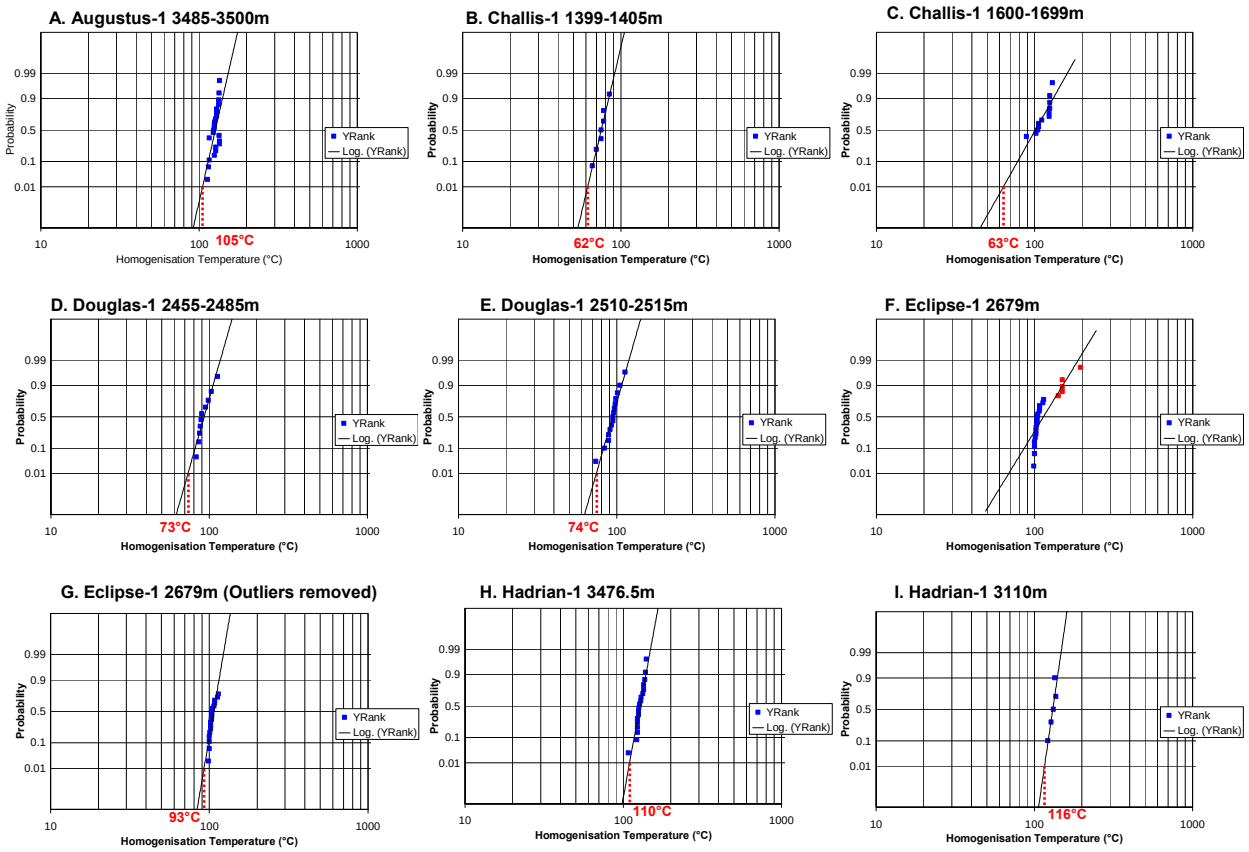

Figure 6-17: T_{hom} data for measured samples plotted on log probit paper (Part 1).

T_{hom} data from the samples analysed typically plot as a linear array indicating that the data set has a numerically dominant sub-population that obeys an exponential probability function. The red line and text shows the projected minimum T_{hom} value to be estimated as greater than or equal to at the 99% confidence level. In data from the Eclipse-1 well visual inspection suggests that more than one population is represented (F) so some data were omitted as outliers and the process repeated (G).

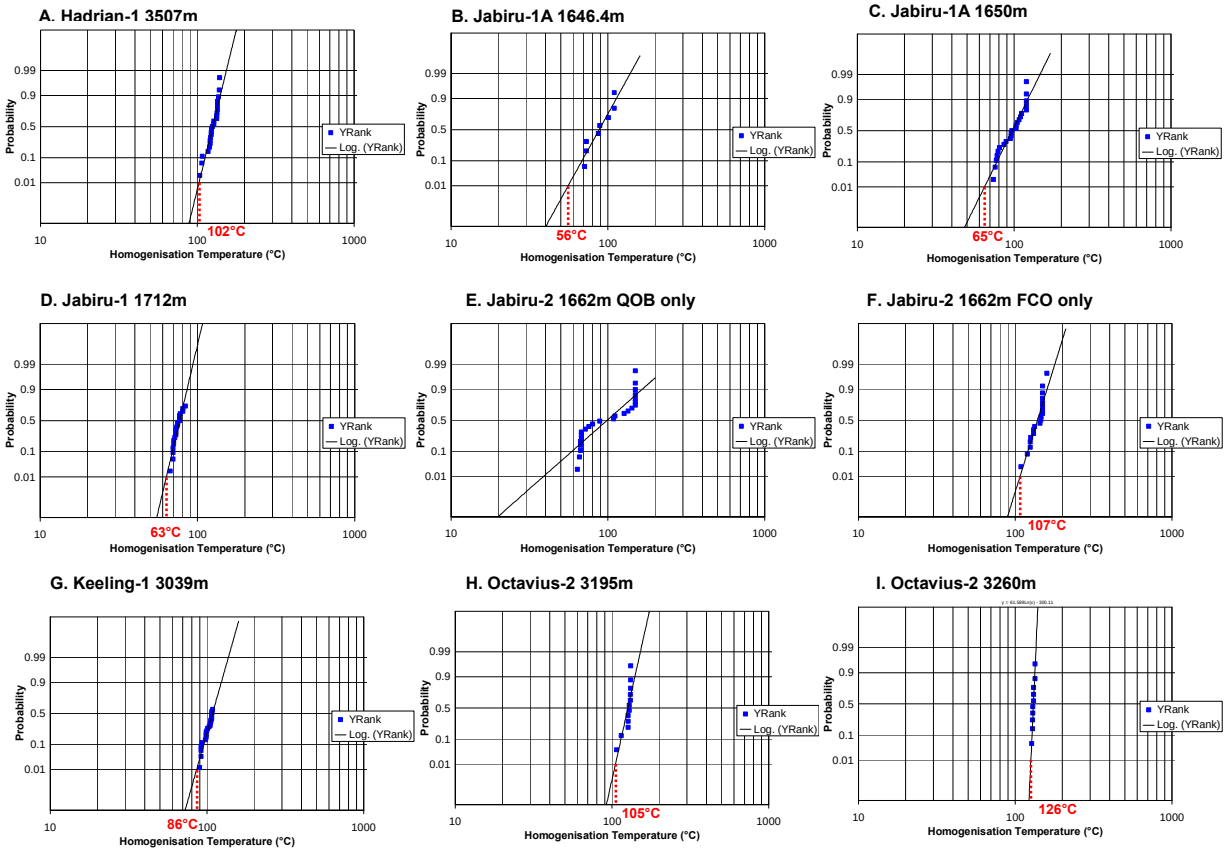

Figure 6-18: T_{hom} data for measured samples plotted on log probit paper (Part 2).

T_{hom} data from the samples analysed typically plot as a linear array indicating that the data set has a numerically dominant sub-population that obeys an exponential probability function. The red line and text shows the projected minimum T_{hom} value to be estimated as greater than or equal to at the 99% confidence level. Visual inspection of the Jabiru-2 Quartz Overgrowth (QOB) data suggests that more than one population is represented (E) particularly given the consistent nature if the data that come from Fracture Cutting Overgrowth population (F).

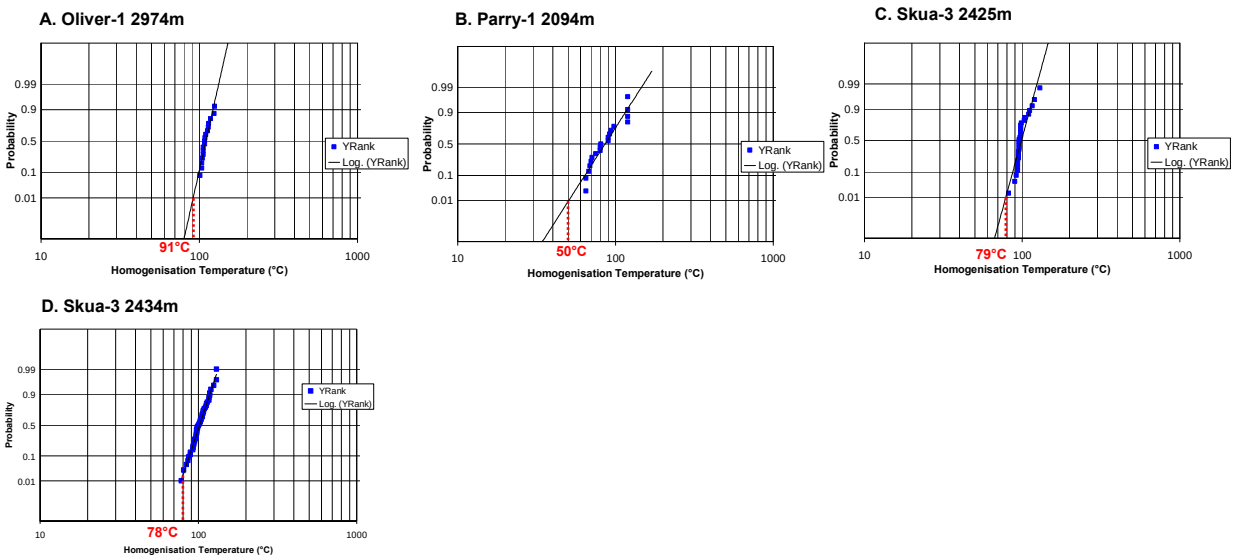

Figure 6-19: T_{hom} data for measured samples plotted on log probit paper (Part 3).

T_{hom} data from the samples analysed typically plot as a linear array indicating that the data set has a numerically dominant sub-population that obeys an exponential probability function. The red line and text shows the projected minimum T_{hom} value to be estimated as greater than or equal to at the 99% confidence level.

For those samples that do not show a linear distribution expected for an exponential probability function it is likely that the measurements come from more than one discrete fluid inclusion population or that insufficient measurements have been made to describe the data in a statistically meaningful manner.

Recognising the signs of heterogeneous entrapment has implications beyond the interpretation of the results and should be considered when determining the most appropriate analytical procedure to employ in making this type of measurement. Attempts to measure T_{hom} values on inclusions that contain heterogeneous trapping fluids has the potential for overheating inclusions to temperatures that greatly exceed the true geological trapping temperature and in doing so potentially cause stretching of other inclusions in that sample that are subsequently measured.

Stretching of inclusions, resulting from mechanical changes produced by increasing the internal pressure within the inclusion through overheating has been demonstrated for mechanical soft minerals such as calcite (e.g. Prezbindowski and Larese, 1987). This mechanism can invalidate the key assumption in the interpretation of homogenisation temperatures that the inclusion has not undergone inelastic deformation after initial formation (Roedder, 1984). Whilst the potential for inclusions in quartz to stretch in this manner has only rarely been proposed for the diagenetic environment (Haszeldine and Osborne, 1993; Osborne and Haszeldine, 1993) and remains contentious (Worden et al., 1995; Robinson et al., 1992), stretching of inclusions in quartz has only demonstrated in the laboratory using synthetic inclusions in quartz where very substantial overheating has occurred (Bodnar and Binns, 1986; Bodnar et al., 1989).

Results of experiments published by Bodnar et al. (1989) demonstrated that the degree of additional internal pressure to initiate stretching of inclusions in quartz was more than 500 bars (50 Megapascals), or equivalent to 5km of additional burial if a hydrostatic pressure gradient is assumed. The size of the inclusion is critically important with smaller inclusions requiring greater overheating to induce stretching (Bodnar et al., 1989). This type of thermal overprint would be easily recognised in independent thermal maturity indicators and would have destroyed the Jurassic petroleum system in the process.

Consequently whilst inelastic stretching was considered highly unlikely for quartz hosted inclusions the approach taken in the current study has intentionally avoided any significant overheating, instead recording a greater than value for any inclusion where T_{hom} was likely to greatly exceed the current measured formation temperature. This was achieved by not heating inclusions to more than 150°C or less where current formation temperatures were well constrained.

Given the multiple lines of evidence to support inadvertent measurement of at least some heterogeneously trapped inclusions the minimum temperature recorded for each individual fluid inclusion population is taken as providing the best estimate of the geological temperature at the onset of trapping of that population (Table 6–10).

6.5.4 Comparison with other Published Studies

The approach of taking minimum T_{hom} values for each fluid inclusion assemblage and largely ignoring the observed range, model or mean T_{hom} values is different to that adopted by the bulk of studies published in the literature that often fail to either make pressure corrections or make reference to the likelihood of heterogeneous entrapment (Schmid, et. al., 2004; Conliffe et al., 2010).

Only a limited number of published studies fully consider the impact of heterogeneous trapping on the interpretation of true trapping temperatures (e.g. Burley et. al., 1989). However, even where the likelihood of heterogeneous trapping has been recognised and invoked to argue against the need to make a pressure correction the full spread of T_{hom} values is still adopted as the most likely range of trapping temperatures (Burley et. al., 1989; Robinson and Gluyas, 1992; Girard et. al., 2001) with use of a mean or modal values commonly used as the most likely temperature of entrapment. These studies often allude to the steep slope of the isochore for aqueous fluids and the relatively small degree of pressure correction needed as being too small to significantly alter the interpreted geologic temperatures of host mineral formation.

However, this approach fails to recognise that the condition of heterogeneous trapping that allows T_{hom} to equal the true trapping temperature (i.e. no pressure

correction; Hanor, 1980) is only true for those inclusions that trap an infinitesimally small amount of the second phase and that further addition of a second phase only acts to progressively increase the recorded homogenisation temperature above the geologically valid trapping temperature (Roedder, 1981; Burruss, 1992; Pichavant et al., 1982; Ramboz et al., 1982). As a consequence the range in measured T_{hom} values measured for any discrete fluid inclusion assemblage may not have any geological significance unless the methane content of every inclusion measured is determined.

Analytical methods that determine the methane content of individual inclusions provide definitive evidence that high levels of dissolved methane are common (i.e. Guilhaumou et al., 1998). In time the routine application of such techniques will allow this issue of determining which temperatures to use will be effectively resolved, but for now those inclusions that have been trapped on the bubble point curve can never be unequivocally identified. It therefore becomes important to measure a sufficient number of inclusions that show low liquid-vapour ratios to ensure that at least some homogeneously trapped inclusions have been measured in any discrete fluid inclusion assemblage. Using this type of approach it also follows, and has been adopted for this study, that the minimum homogenisation temperature rather than the mean or modal T_{hom} provides the only reliable estimate of the true geological temperatures.

Indeed in the thermometric data collected in this study the mean and commonly the modal T_{hom} values both exceed the current formation temperature constrained from circulation corrected bottom hole temperatures (Figure 6–20) and would require a thermal history that produces higher temperature in the geological past. Often T_{hom} values that exceed the current formation temperature or that cannot be accommodated within a conductive heat transfer history are ascribed to flow of hot fluids (Parnell et. al., 2001; Conliffe et al., 2010) even where there is little other direct evidence to support such an interpretation. In these instances the determination of ice melting temperatures (Goldstein and Reynolds, 1994) to constrain the salinity of the included fluid becomes useful as a tool to support changes in fluid chemistry and when cross-plotted against T_{hom} values can be used to infer heat transfer by fluid migration (e.g. Wycherley et. al., 2003).

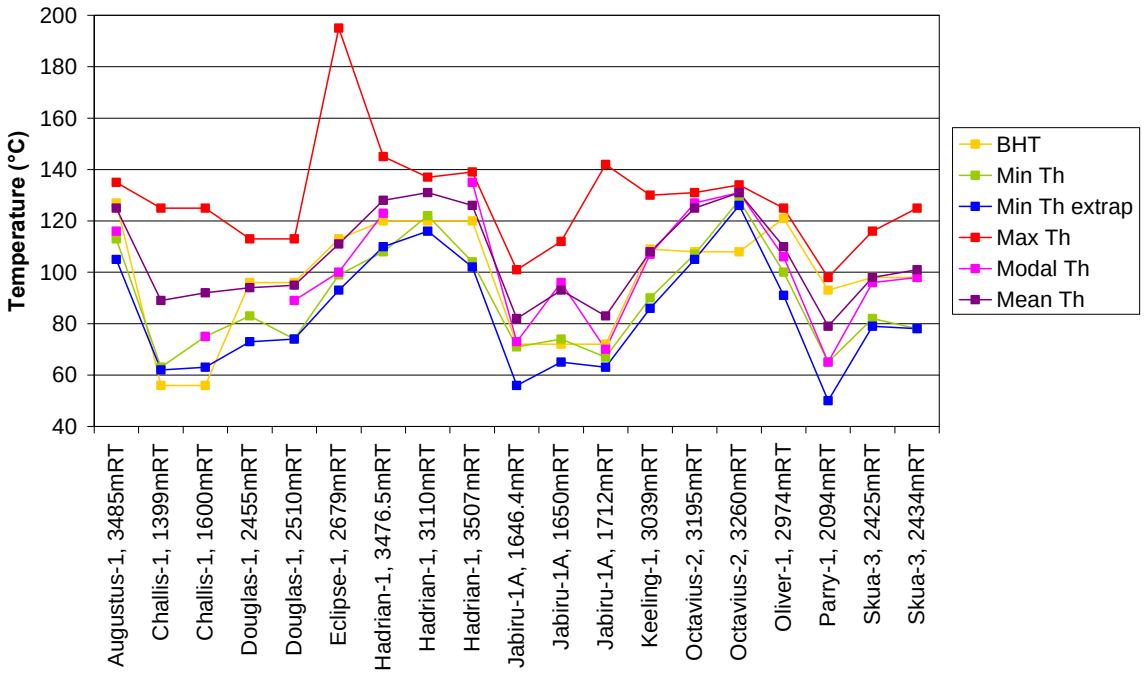

Figure 6-20: Summary of T_{hom} measurements in a graphical display.

Graph showing the relationship between the current formation temperature estimated from BHT data compared against the minimum, maximum, modal and mean T_{hom} values as well as a projected minimum value arrived at through a regression line approach described in the text.

For the current study, the ability to reconcile temperatures indicated by the fluid inclusion data that are greater than the current day will be discussed in the next section where basin modelling results allow the temperature history to be compared against other independent indicators commonly used to constrain thermal history.

As mentioned previously an interpretation that uses of the minimum T_{hom} value does not in any way preclude trapping of fluid inclusions at higher temperatures, rather it recognises that it is impossible to distinguish the inclusions that trapped exactly on the bubble point from those formed by heterogeneous trapping within the single phase field that is predicted for a purely water system. Where more than one discrete fluid inclusion population has been recognised then a series of minimum T_{hom} values could be used to describe the thermal history of the basin through time.

A potential danger with the use of minimum T_{hom} values (particularly in samples where a small number of measurements have been made) is the opportunity to overestimate the thermal conditions if a genuine (or close to) minimum value has not been recorded. In this regard a significant benefit of demonstrating that the measured T_{hom} data conform to an exponential probability function is the ability to use the measured data, especially where a smaller number of measurements have been made, to stochastically predict the minimum T_{hom} value associated with any coeval population of fluid inclusions.

The plotting of the data on log probit paper enables the T_{hom} data to be displayed in terms of probability. This allows any value to be assigned a probability value and by extending the regression line below the lowest measured T_{hom} a more accurate minimum T_{hom} value can be predicted to whatever probability level deemed necessary. For the purposes of this study the intersection of this extrapolated regression line at the 1% probability level is used to express the minimum T_{hom} that is equal to or greater than a 99% probability level (Figure 6–16 to Figure 6–19). This approach helps to reduce the uncertainty that arises from the use of minimum T_{hom} values, namely how certain it is that the minimum temperature that has been measured is actually a representative value?

As the projected minimum T_{hom} values represent predicted greater than or equal to values at a 99% confidence level they provide an even more conservative approach (than use of the measured minimum T_{hom} value) to the interpretation of geologically reliable temperatures marking the onset of inclusion formation by the crystallisation of quartz overgrowths or the host authigenic cement.

6.6 THERMAL MODELLING OF THE VULCAN SUB-BASIN

A simulation of the thermal history of the Vulcan Sub-basin using the one dimensional Basinmod© 5.0 modelling software (Platte River Associates, 1995.) has been used to constrain the timing of temperatures indicated by the fluid inclusions for the onset of quartz overgrowth crystallisation. Individual basin models have been constructed for the 14 wells with available fluid inclusion palaeotemperatures. An estimate on the absolute timing of hydrocarbon migration and accumulation is also derived from these models, by comparing the location of oil inclusions relative to the quartz overgrowths that contained the aqueous inclusions that palaeotemperatures were measured on. In most samples the presence of co-existing oil inclusions within the quartz overgrowths indicates contemporaneous trapping and therefore a direct link between time and temperature for these fluids.

6.6.1 Input Data

Construction of a basin model requires information on the burial and thermal history to be as well constrained as possible. Stratigraphic data including formation thickness, age and lithology have been obtained from the relevant well completion reports to constrain the burial history. Unconformities have been treated as hiatus due to the lack of control on the amount of eroded section.

Constraints on the thermal history come from formation temperatures and measured vitrinite reflectance data. Circulation corrected bottom hole temperatures have been used in conjunction with lithology generic, depth dependent, thermal conductivities to establish current day heat flows. Initially, a constant heat flow through time was used. Heat flow was probably higher during the Jurassic rift phase due to reduced

crustal thickness, however, shallow burial at this time means that within reasonable limits of heat flow values used, the timing of cementation is insensitive to these variations. Cooling of the lithosphere caused by under-plating during Neogene plate collision may also have occurred, however in the absence of empirical data to support this process a constant heat flow history based on the current heat flow has been adopted as the default condition.

A constant surface temperature history has been utilised in these models as the default setting. Palaeolatitude reconstructions (Veevers, 1984) indicate considerable variation in the position of the Australian Continent through the Mesozoic but throughout the Tertiary (when most burial occurred) the continent has been at relatively low palaeo-latitudes. Minor variations in surface temperature are unlikely to influence the validity of the simulations produced by these models.

Vitrinite reflectance (Ro) and Fluorescence Alteration of Multiple Macerals (FAMM, Wilkins et al., 1998) measurements taken from available well completion reports have been used to determine the likely maximum temperature experienced by these rocks and to independently cross check the validity of the models that have been produced. This has been achieved by comparing measured Ro (or FAMM) data with a kinetic simulation of maturity that is computed by the model in an iterative manner.

In many cases the default models that use a constant heat flow based on the current geothermal gradients fail to produce a good match between the measured and calculated maturity values. In some instances the calculated maturity profile plots above the measured values and probably reflects the influence of vitrinite suppression (Wilkins et al., 1998) rather than any variations in palaeo-surface temperature or heat flow. In situations where the calculated profile falls below the measured values a variable heat flow history was used in an attempt to obtain a better match with the measured values.

6.6.2 Constraining Absolute Timing Estimates

Outputs from the basin models are used to constrain the timing of the onset of fluid inclusion entrapment by reconciling the minimum fluid inclusion homogenisation

temperature for each sample with isotherms computed by the basin modelling software. Trapping of fluid inclusions by each mineral host is considered possible when the modelled formation temperatures at the sampled depth first exceeded the minimum fluid inclusion homogenisation temperature measured on fluid inclusions (or the stochastically predicted minimum T_{hom} value), for each respective host authigenic cement phase.

The accuracy of these timing estimates is governed by the validity of the input data used to constrain each model, the assumption that a minimum homogenisation temperature was measured and that this minimum temperature represents a true geological temperature for the crystallisation of the host mineral.

In an attempt to test the sensitivity of the model to these various assumptions, timings using temperatures that are derived from the stochastic prediction of minimum T_{hom} are also utilised. In addition, error bars showing ±10% variations from the measured homogenisation temperature are also employed to further explore the impact on the predicted timings if these assumptions were invalid.

6.6.3 Augustus-1, Basin Modelling Results

The default 1D basin model produced for the Augustus-1 well generates a timing estimate for the onset of trapping of fluid inclusions by quartz overgrowths of Oligocene time, but this timing prediction is relatively sensitive to the accuracy of the minimum temperature estimate (Figure 6–21A). Modifying this temperature by ±10°C results in a relatively wide range in predicted timings that vary from Paleocene to Pliocene time (Figure 6–21A).

The default thermal model also produces a poor agreement with the measured vitrinite reflectances available for this well (Figure 6–22). The maturity profile calculated by the model underestimates the measured vitrinite reflectances in the upper section, but overestimates maturity values measured in the lower section. The deviation in the deeper section is probably associated with vitrinite reflectance suppression (Wilkins et al., 1992) of the mostly marine deposited Lower Cretaceous and Upper Jurassic shale prone section.

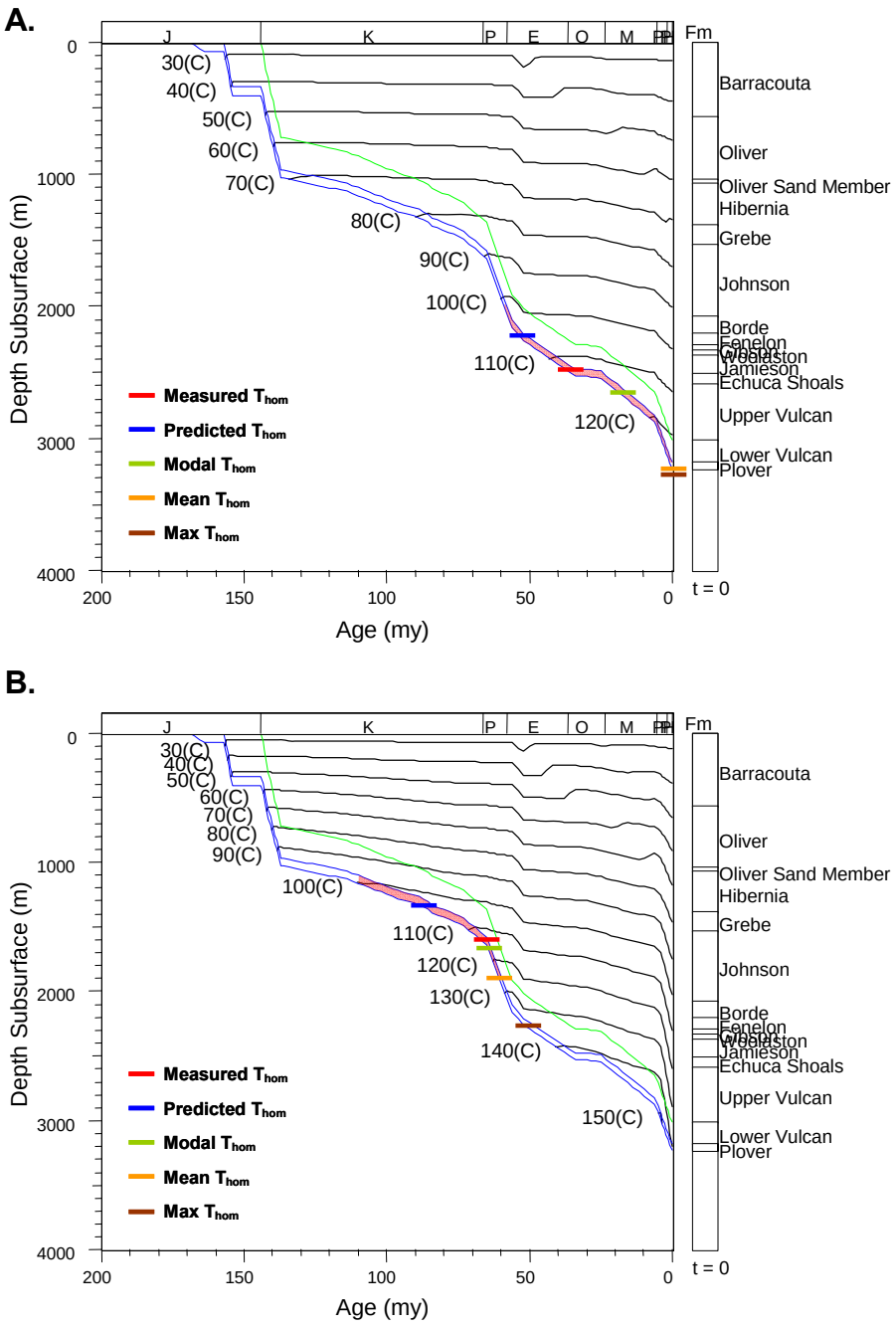

Figure 6-21: Basin models for the Augustus-1 well.

Burial history plots for the Plover and Lower Vulcan formations for the default model (A) and the variable heat flow model (B) are shown with calculated isotherms overlain. The minimum T_{hom} value recorded in samples from the Augustus-1 well of 113°C is shown as the solid red line, whilst the red shaded area represents a sensitivity envelope based on a ±10% variation in the recorded temperature. The other coloured lines are described in the legend and lines that plot to outside the main diagram represent values that exceed the maximum temperatures predicted by the model.

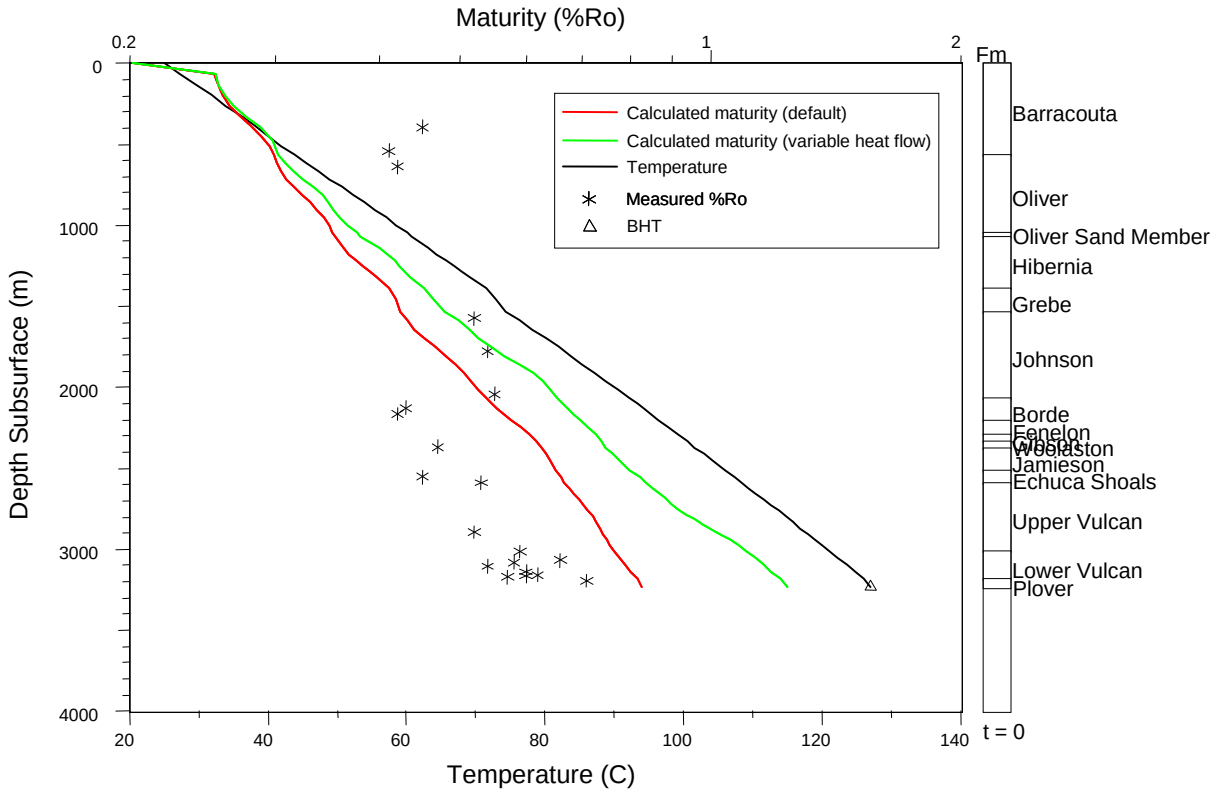

Figure 6-22: Calculated maturity compared with measured maturity data, Augustus-1.

Graph showing measured vitrinite reflectance values (%Ro) and temperature data as well as calculated profiles for temperature and two alternate calculated maturity profiles, one for a default thermal model and one for a variable heat flow model.

Further iterations using alternative thermal models are needed to produce a closer match with measured maturity data in the upper section (Figure 6–21B) require higher palaeo-heat flows that are about 20% higher than at present to persist into the Pliocene, before falling sharply to reach the current heat flow derived from the measured BHT. The fit with the measured vitrinite reflectance data remains poor and this model produces timing estimates for the initial trapping of fluids that are earlier than is predicted from the default model, ranging from Mid-Cretaceous to Late Paleocene (Figure 6–21B).

The narrow spread in measured vitrinite reflectance data coupled with the wide depth range (Figure 6–22) suggests these data are not providing a genuine indication of true thermal maturity levels and are likely compromised by a combination of caving and oxidation of the organic material. In this instance the preference is to consider the data to be unreliable and instead rely on the default thermal profile to constrain the most likely time of trapping for the fluid inclusions.

6.6.4 Challis-1 Basin Modelling Results

The default 1D basin model utilised for the Challis-1 well fails to generate predicted formation temperatures in the Triassic section that exceed the minimum temperature measured from the fluid inclusions sampled from this interval or the minimum temperature predicted probabilistically (Figure 6–23A).

The maturity profiles computed by the modelling algorithms within the software (Figure 6–24), however, consistently underestimate the measured vitrinite reflectance data and this constraint suggests that palaeo-heat flows at this location may have been higher in the geological past.

Alternative thermal models needed to produce a better match with measured maturity data require palaeo-heat flows that are about 75% higher than at present and that these need to persist into the Late Pliocene, before falling sharply to achieve the current heat flow derived from the measured BHT.

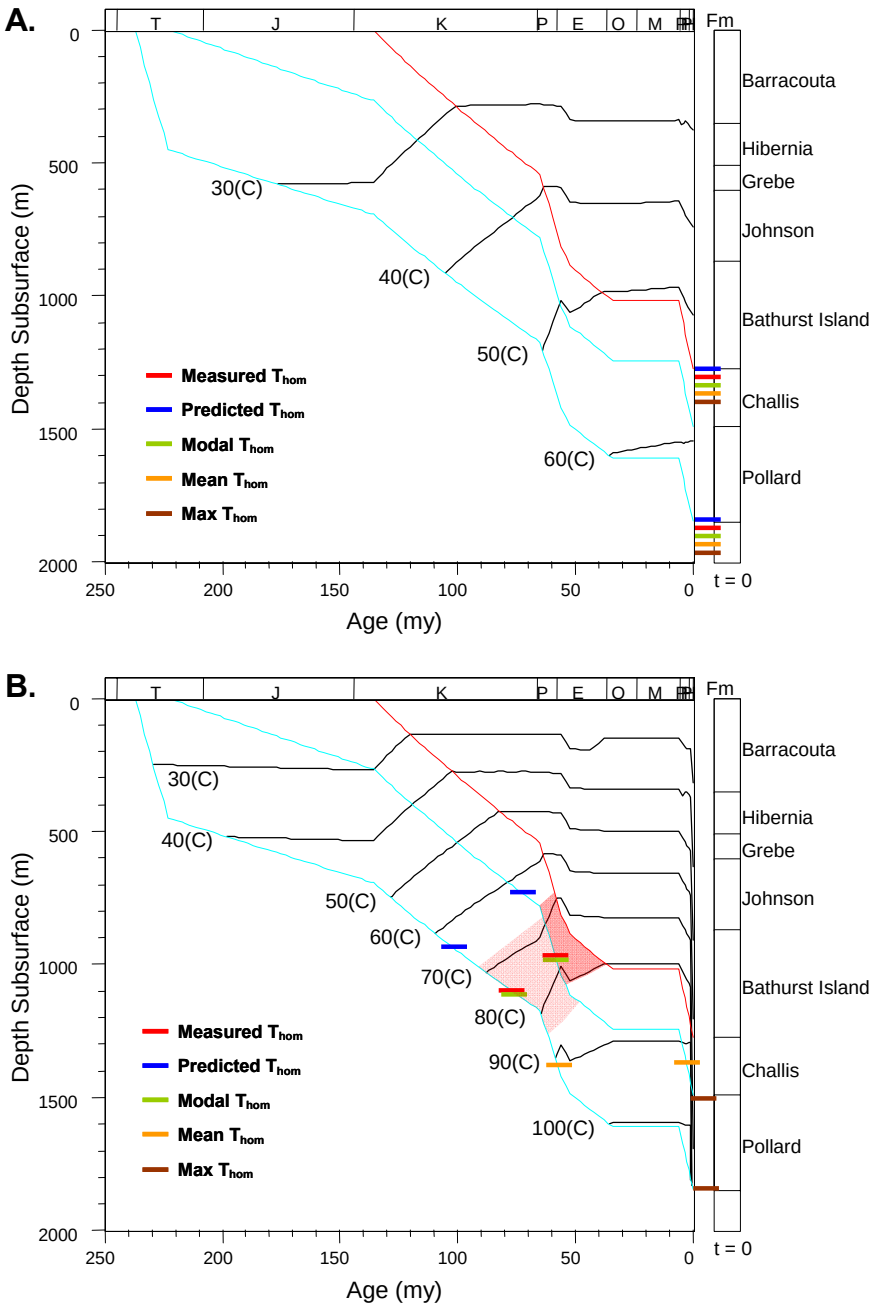

Figure 6-23: Basin models for the Challis-1 well.

Burial history plots for the Triassic Pollard (blue line) and Challis (red line) formations are shown with calculated isotherms overlain. The minimum T_{hom} value recorded in samples from the Challis-1 well of 75°C for the Pollard Formation and 63°C for the Challis Formation are shown as the solid red lines, whilst the red shaded areas represents a sensitivity envelope based on a ±10% variation in the recorded temperature. The other coloured lines are described in the legend and lines that plot to the right of the main diagram represent values that exceed the maximum temperatures predicted by the thermal model.

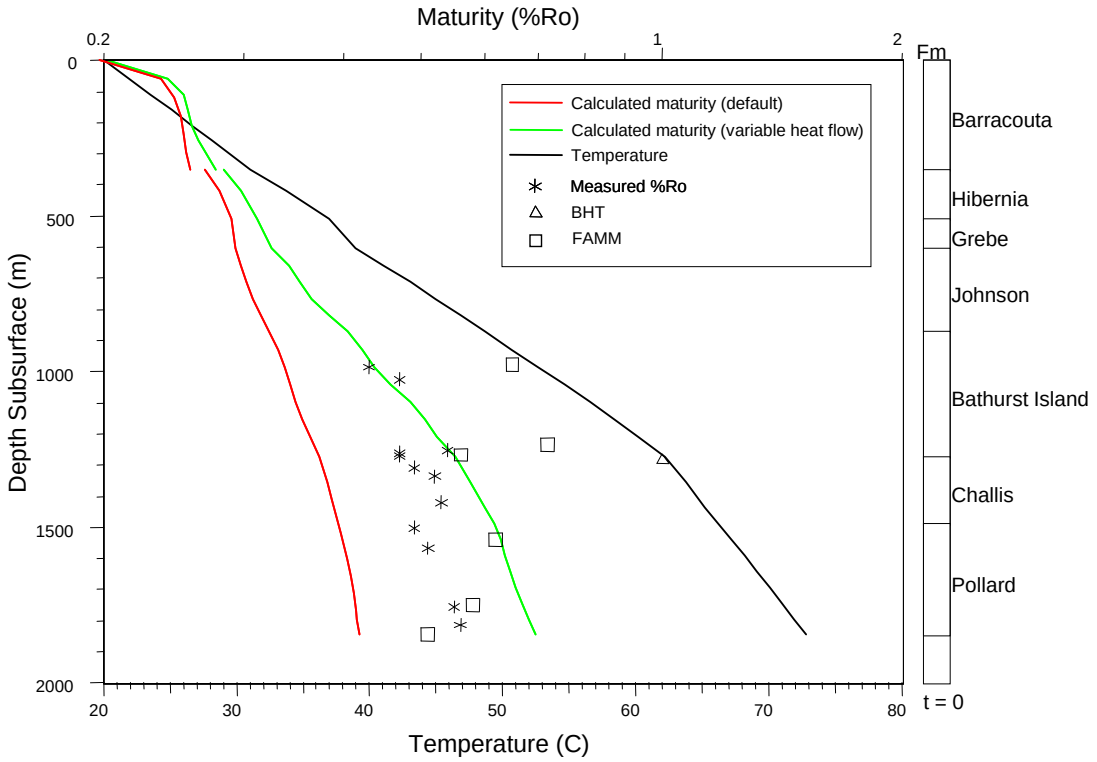

Figure 6-24: Calculated maturity compared with measured maturity data, Challis-1.

Graph showing measured vitrinite reflectance values (%Ro) and temperature data as well as calculated profiles for temperature and two alternate calculated maturity profiles, one for a default thermal model and one for a variable heat flow model.

This model produces a reasonable match with the measured vitrinite reflectance data in the upper section but a poor match with a group of lower values near the base of the well (Figure 6–24). The latter group can be attributed to possible caving in the well. In contrast the maturity estimates provided by the Fluorescence Alteration of Multiple Macerals (FAMM) technique cannot be adequately modelled by considering conductive heat transfer alone. This variable heat flow model, whilst seemingly implausible geologically, results in predicted timing of initial fluid inclusion entrapment by quartz overgrowths that range from the Mid-Cretaceous to the Early Eocene (Figure 6–23B).

6.6.5 Douglas-1, Basin Modelling Results

The default thermal model utilised for the Douglas-1 well produces a timing estimate for the onset of trapping of fluid inclusions by the crystallisation of quartz overgrowths (minimum T_{hom} of 115°C) of Mid Eocene time for the Plover Formation and more recently for the overlying Tithonian sandstone (Pliocene), but these predictions are relatively sensitive to the inferred accuracy of the minimum temperature estimate derived from the fluid inclusion results (Figure 6–25A).

Modifying the minimum temperature provided by the fluid inclusion data by ±10°C results in a relatively wide range in predicted timings that vary from Eocene to Pliocene time (Figure 6–25A). The default thermal model produces a calculated maturity profile that agrees well with measured values from within the Triassic section, but significantly underestimates the measured vitrinite reflectance data recorded in the overlying Mesozoic and Tertiary section (Figure 6–26).

Two alternative thermal histories were constructed to obtain a better match with the majority of the measured vitrinite reflectance data. The first assumes the measured BHT values have not been fully corrected to remove the effects of circulation during logging. A 20% increase in the measured BHTs results in a much better match with most data from the Lower Cretaceous and Jurassic section but produces a relatively poor match with the samples from the Triassic and mid-Cretaceous section. Onset of fluid inclusion entrapment predicted in this model is earlier than in the default model and ranges from Paleocene to Eocene.

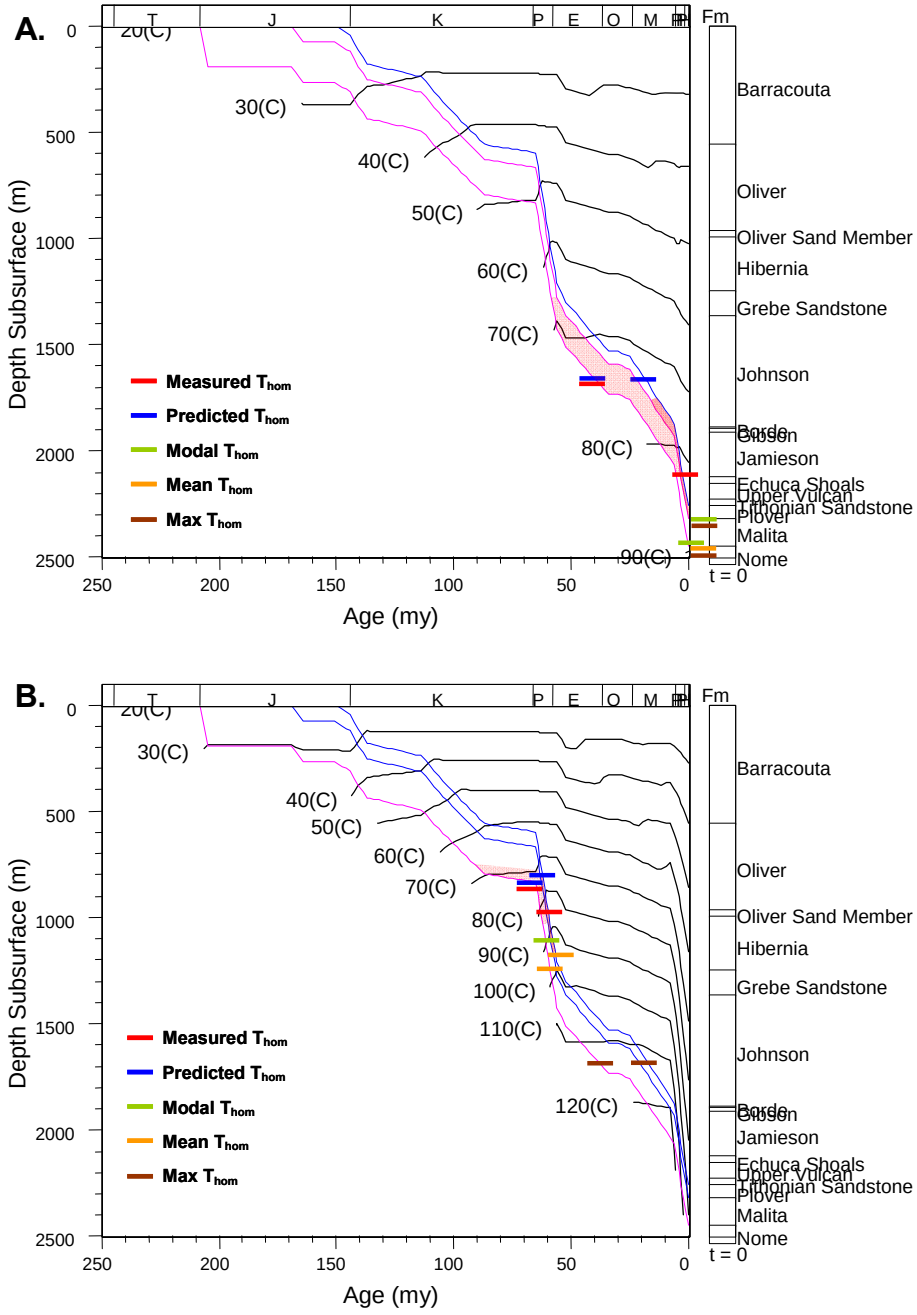

Figure 6-25: Basin models for the Douglas-1 well.

Burial history plots for the Triassic Pollard and Challis formations are shown with calculated isotherms overlain. The minimum T_{hom} value recorded in samples from the Douglas-1 well of 83°C in the Tithonian sandstone and 74°C in the Plover Formation is shown as the solid red lines, whilst the red shaded area represents a sensitivity envelope based on a ±10% variation in the recorded temperature. The other coloured lines are described in the legend and lines that plot to outside the main diagram represent values that exceed the maximum temperatures predicted by the model.

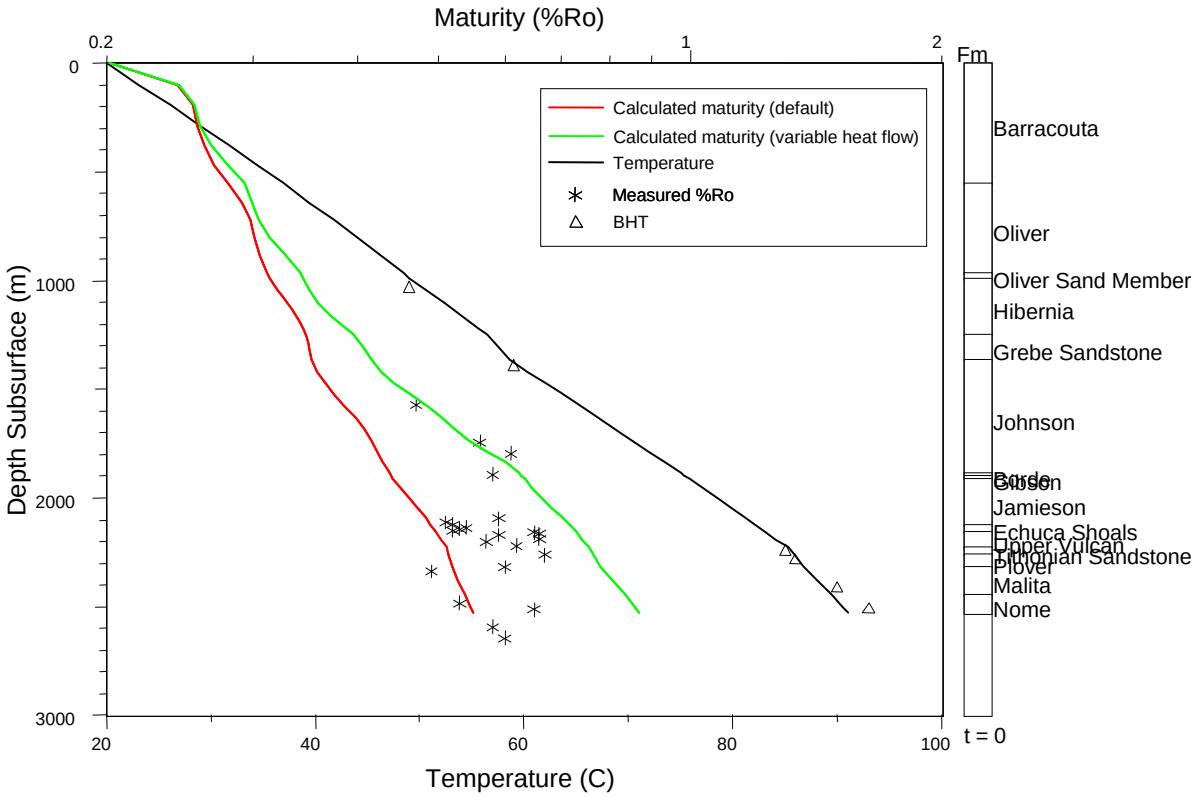

Figure 6-26: Calculated maturity compared with measured maturity data, Douglas-1.

Graph showing measured vitrinite reflectance values (%Ro) and temperature data as well as calculated profiles for temperature and two alternate calculated maturity profiles, one for a default thermal model and one for a variable heat flow model.

The second alterative model constructed invokes palaeo-heat flows that are about 50% higher than at present and requires these higher heat flows to be maintained into the Late Tertiary. This model produces a good match with the measured vitrinite reflectances in the mid-Cretaceous section but overestimates maturity values seen in the deeper section. The predicted onset of fluid inclusion entrapment is also earlier than for the default model, ranging from Late Cretaceous to Late Paleocene.

6.6.6 East Swan-2, Basin Modelling Results

The default 1D basin model utilised for the East Swan-2 well fails to produce formation temperatures in the Tertiary that exceed the minimum temperature measured from the fluid inclusions (Figure 6–27A). The calculated maturity profile shows excellent agreement with the measured vitrinite reflectance data within the Lower Jurassic Plover Formation but is consistently higher than measured values in the Upper Jurassic and basal Lower Cretaceous sections (Figure 6–28). These differences could reflect suppression of vitrinite reflectance, which is likely to be more pronounced in the more marine Upper Jurassic section and the FAMM data available for this well supports the presence of significant suppression effects.

Two alternative thermal history models were constructed to produce a better match with the majority of the measured data from the vitrinite reflectance and FAMM datasets. The first of these assumes that the measured BHT values have not been fully corrected to remove the temperature effects of drilling fluid circulation during the period that logging was conducted. To produce a relatively good match with the measured FAMM values the corrected BHT would need to underestimate the true formation temperature by about 40%, which seems unlikely. Typically, the thermal impact introduced as a result of residual circulation effects may produce a 10-20% cooling effect on the measured temperatures (Waples et. al., 2004) so differences greater than this are unlikely to be caused by this mechanism.

A second simulation employs a variable heat flow model that uses palaeo-heat flows that are about 50% higher than at present and requires these higher heat flow levels to be maintained into the Late Tertiary (Figure 6–27B). This approach produces a reasonable match with the measured FAMM results (Figure 6–28).

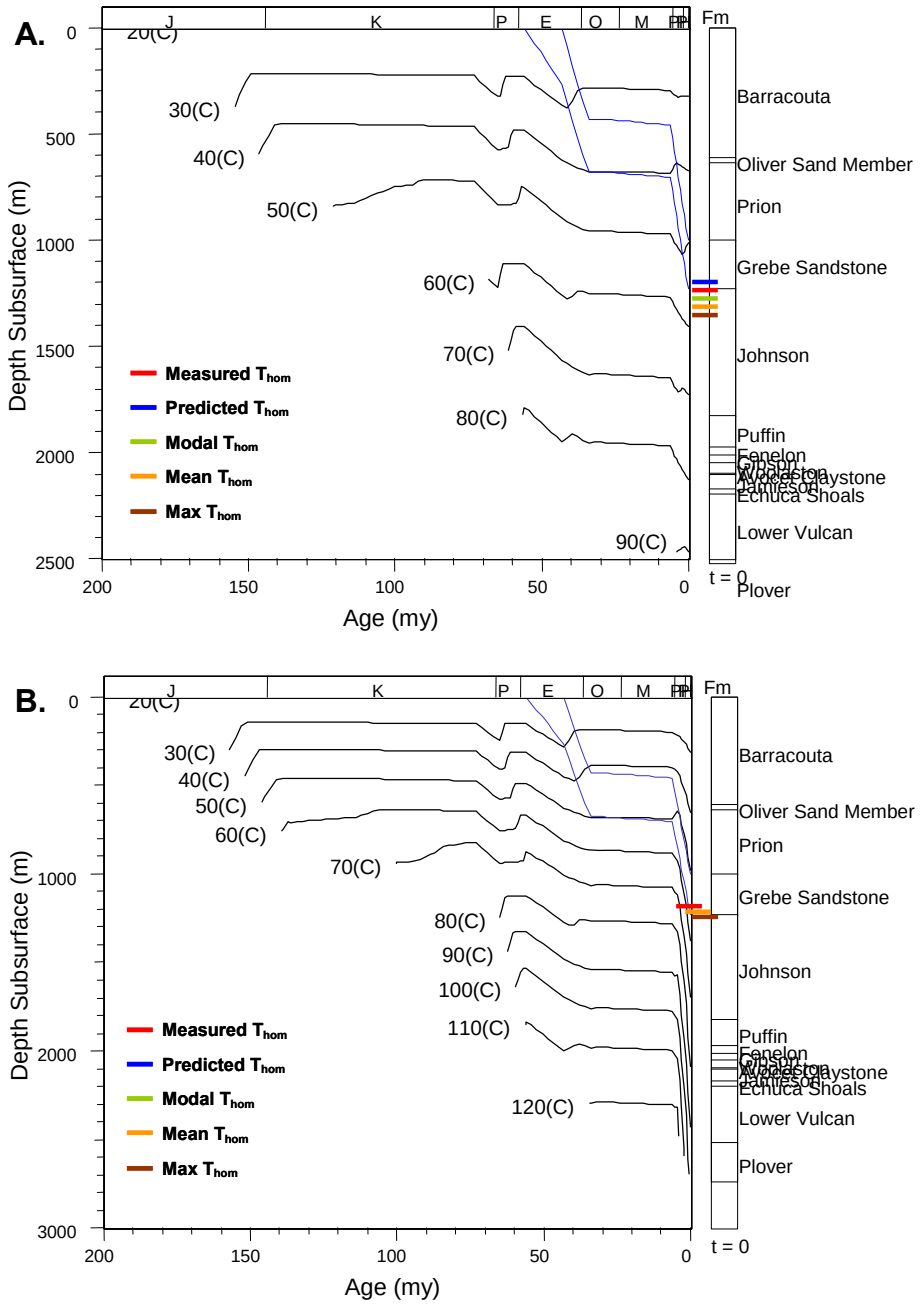

Figure 6-27: Basin models for the East Swan-2 well.

Burial history plots for the Tertiary Grebe Sandstone (blue lines) are shown with calculated isotherms overlain. The minimum T_{hom} value recorded in samples from the East Swan-2 well of 58°C is shown as the solid red line. The other coloured lines are described in the legend and lines that plot to outside the main diagram represent values that exceed the maximum temperatures predicted by the model.

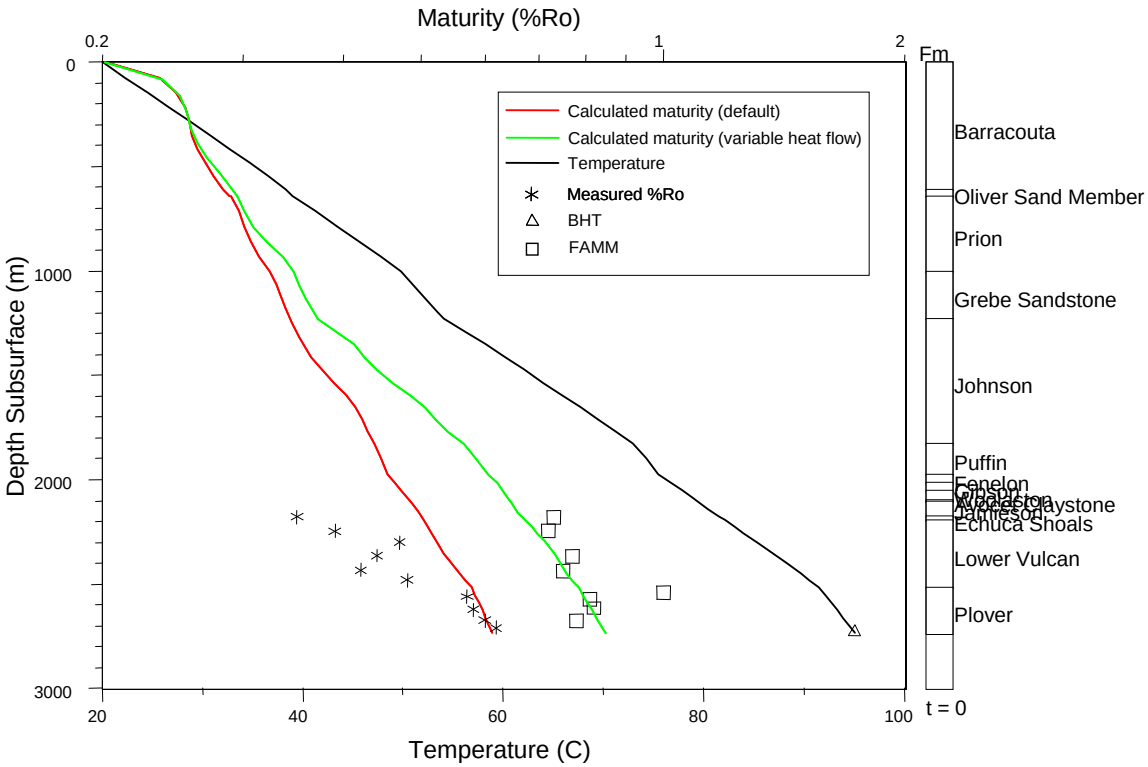

Figure 6-28: Calculated maturity compared with measured maturity data, East Swan-2.

Graph showing measured vitrinite reflectance values (%Ro) and temperature data as well as calculated profiles for temperature and two alternate calculated maturity profiles, one for a default thermal model and one for a variable heat flow model.

The variable heat flow model also results in calculated formation temperatures for the Grebe Sandstone that exceed the minimum fluid inclusion temperature recorded in samples from that interval by the Pleistocene. Consequently the model predicts the onset of fluid inclusion entrapment to be an extremely recent event (Figure 6–27B).

6.6.7 Eclipse-1, Basin Modelling Results

The default 1D basin model utilised for the Eclipse-1 well produces a timing estimate for the onset of trapping of fluid inclusions by quartz overgrowths of the Early Eocene, but this prediction is relatively sensitive to the accuracy of the minimum temperature estimate (Minimum T_{hom} = 99°C). Modifying this recorded temperature by ±10°C results in a relatively wide range in predicted timings that vary from Early Eocene to Pleistocene time (Figure 6–29A).

Calculated maturity profiles produced by the default model (Figure 6–30), however, consistently overestimate the measured vitrinite reflectance data and, unlike earlier models, suggest palaeo-heat flows may have been lower in the past or that the BHT is anomalously high (Figure 6–30). The consistency of the measured profile of vitrinite reflectance data makes it unlikely that cavings from higher in the section could explain the apparently low values.

An alternative thermal model (Figure 6–29B) that invokes much lower palaeo-heat flow throughout the Tertiary produces an excellent match with the measured vitrinite reflectance data (Figure 6–30). However, this alternative model requires a reduction in heat flow for this period relative to the current day of about 50%, and it is difficult to envisage a process that could provide such a large reduction in this type of geological setting.

Timing predictions that are derived from this alternate model for the onset of trapping of fluid inclusions by the crystallisation of quartz overgrowths are later than indicated for the default model (Figure 6–29A), with a Pleistocene timing being the result (Figure 6–29B).

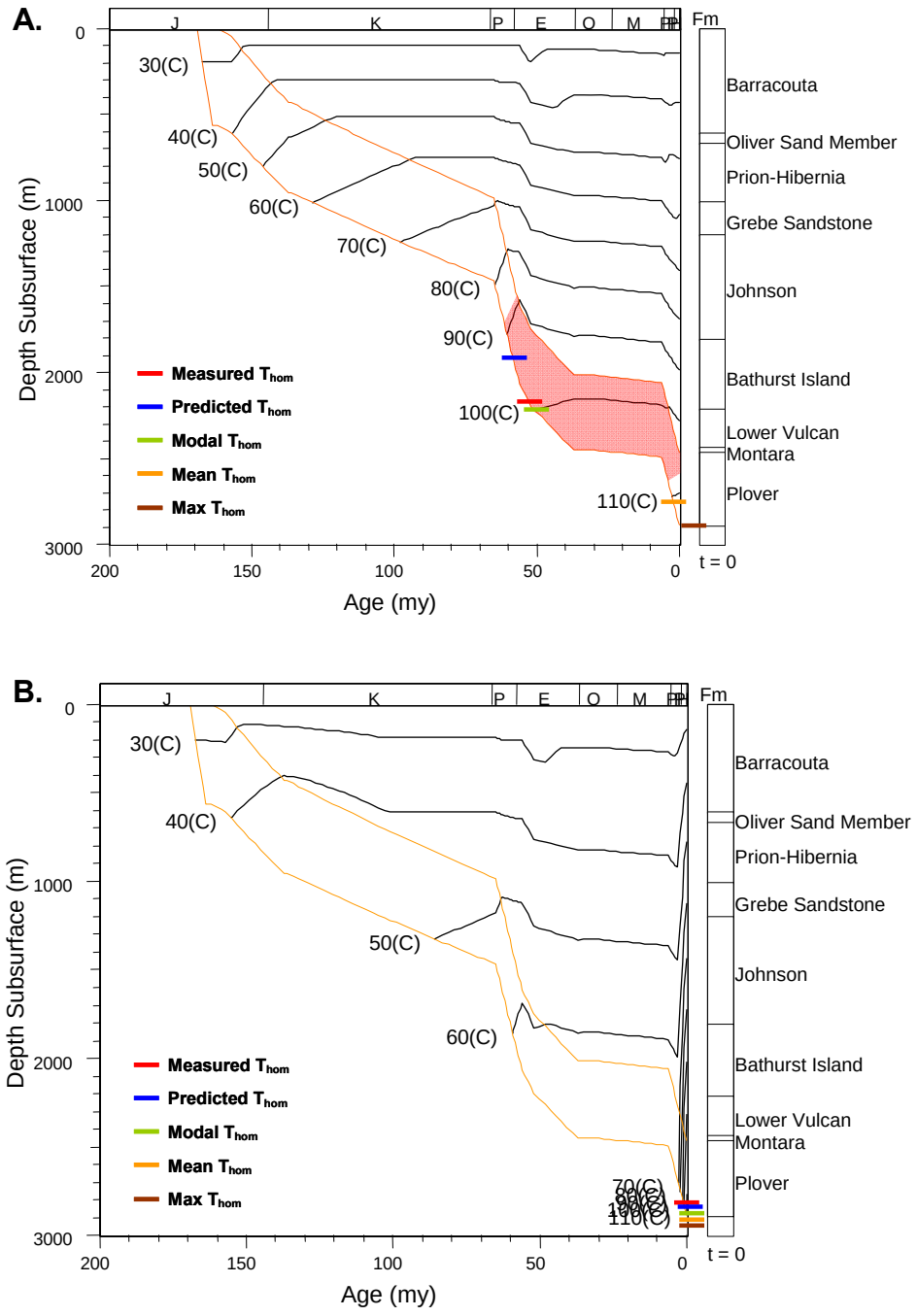

Figure 6-29: Basin models for the Eclipse-1 well.

Burial history plots for the Jurassic Plover Formation (red lines) are shown with calculated isotherms overlain. The minimum T_{hom} value recorded in samples from the Eclipse-1 well of 99°C is shown as the solid red line, whilst the red shading represents a sensitivity envelope based on a ±10% variation in the lowest T_{hom} value. The coloured lines are described in the legend and lines that plot to outside the main diagram represent values that exceed the maximum temperatures predicted by the model.

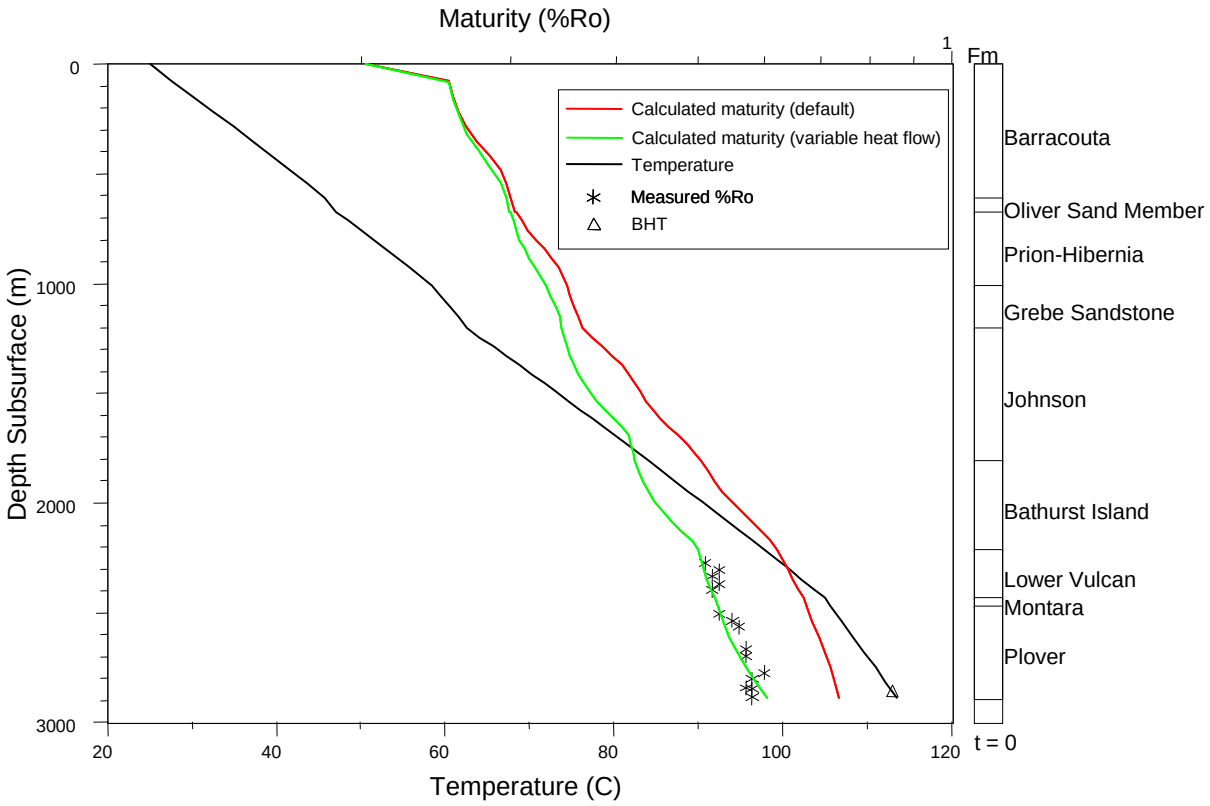

Figure 6-30: Calculated maturity compared with measured maturity data, Eclipse-1.

Graph showing measured vitrinite reflectance values (%Ro) and temperature data as well as calculated profiles for temperature and two alternate calculated maturity profiles, one for a default thermal model and one for a variable heat flow model.

6.6.8 Hadrian-1, Basin Modelling Results

The default 1D basin model that has been utilised for the Hadrian-1 well produces a timing estimate for the onset of trapping of fluid inclusions by quartz overgrowths of Early Oligocene time (Figure 6–31A), but this prediction is relatively sensitive to the accuracy of the minimum temperature estimate used (Minimum T_{hom} = 104°C). Modifying this temperature by ±10°C results in wider range in predicted timings that vary from Early Eocene to Early Miocene time.

The maturity profile that is calculated by the default model is slightly higher the measured vitrinite reflectance data but probably reflects some suppression effects and alternative models have not been extensively considered (Figure 6–32). A slightly lower palaeo-heat flow profile does result in an improved fit with the measured vitrinite reflectances and if adopted would result in a slightly more recent timing for the entrapment of fluid inclusions by the crystallisation of quartz overgrowths (Figure 6–31B).

6.6.9 Jabiru-1A, Basin Modelling Results

The default 1D basin model that was utilised for the Jabiru-1A well produces a timing estimate for the onset of trapping of fluid inclusions within quartz overgrowths of the Pleistocene and this prediction is relatively insensitive to the accuracy of the minimum temperature estimate (Figure 6–33A). The calculated maturity profiles, however, consistently underestimate the measured vitrinite reflectance data and this suggests that the palaeo-heat flow could have been higher in the geological past (Figure 6–34).

The default thermal model utilises measured formation temperatures estimates that were Horner plot extrapolated and the effects of fluid circulation may not have been fully removed. An alternate model was constructed using the temperature data recorded during extended production tests that are likely to more accurately measure the current reservoir temperature, but this change makes only a minimal difference to the maturity values calculated by the model (Figure 6–34).

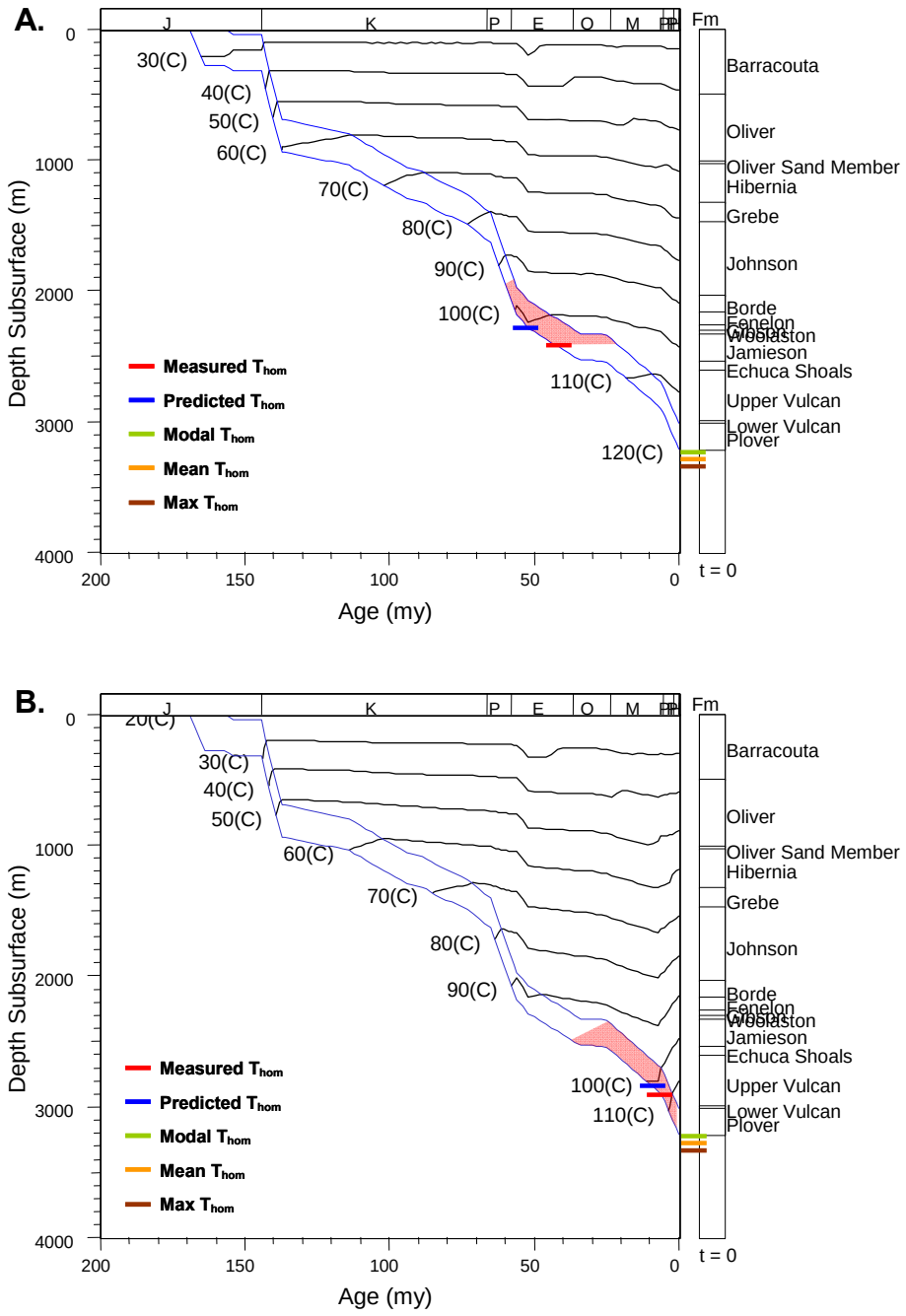

Figure 6-31: Basin models for the Hadrian-1 well.

Burial history plots for the Jurassic Plover Formation are shown with calculated isotherms overlain. The minimum T_{hom} value recorded in samples from the Hadrian-1 well of 104°C is shown as the solid red line, whilst the red shading represents a sensitivity envelope based on a ±10% variation in the lowest T_{hom} value. The other coloured lines are described in the legend and lines that plot to outside the main diagram represent values that exceed the maximum temperatures predicted by the model.

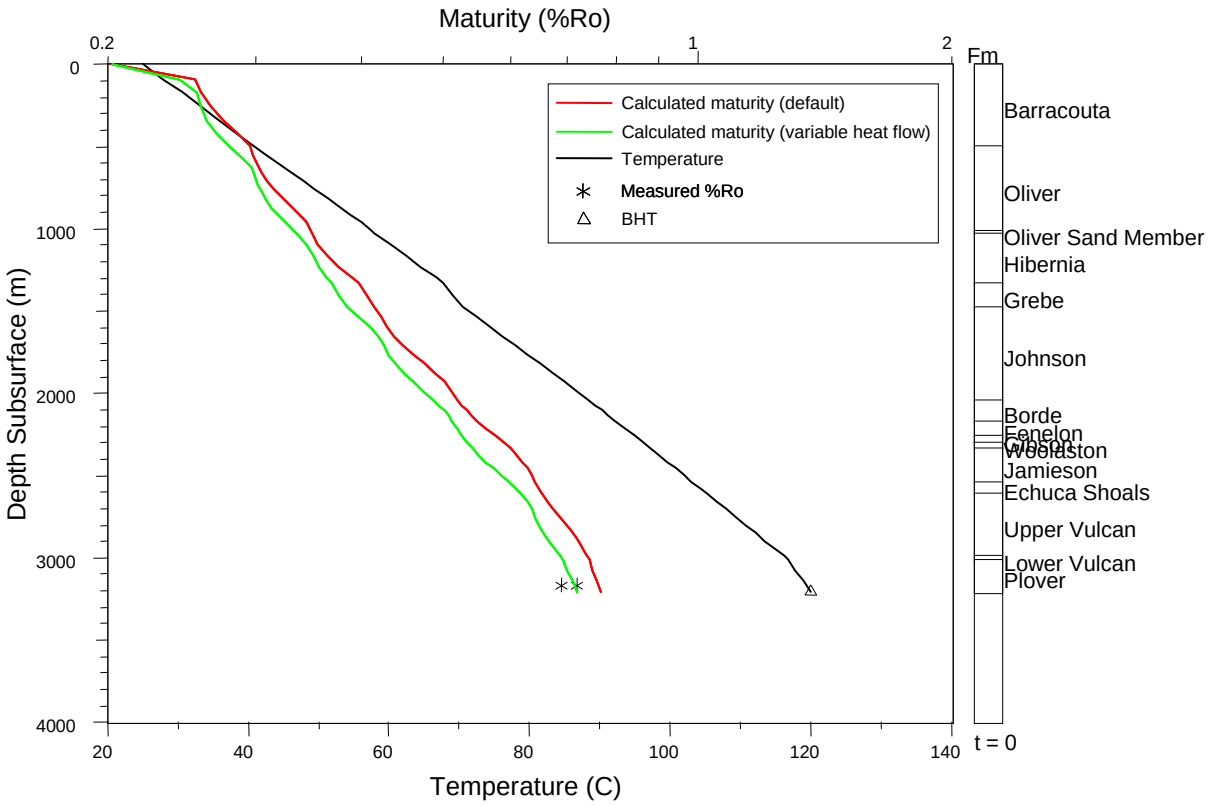

Figure 6-32: Calculated maturity compared with measured maturity data, Hadrian-1

Graph showing measured vitrinite reflectance values (%Ro) and temperature data as well as calculated profiles for temperature and two alternate calculated maturity profiles, one for a default thermal model and one for a variable heat flow model.

This variable heat flow model requires palaeo-heat flows to be about 50% higher than present and needs these higher heat flows to be maintained into the Late Tertiary in order to produce a calculated maturity profile that matches the measured vitrinite reflectance values. The predicted onset of fluid inclusion entrapment is earlier for this model than in the previous default model, ranging from Late-Miocene to Pliocene (Figure 6–33B).

6.6.10 Jabiru-2 Basin Modelling Results

The default 1D basin model utilised for the Jabiru-2 well produces a timing estimate for the onset of trapping of fluid inclusions by the crystallisation of quartz overgrowths of Late Eocene time for the Plover Formation (Figure 6–35) but this prediction is relatively sensitive to the accuracy of the minimum temperature estimate provided from the fluid inclusions (Minimum T_{hom} value = 64°C).

Modifying this temperature estimate by ±10°C results in a relatively wide range in predicted timings that vary from about Paleocene to Pleistocene time. The temperatures predicted by the default thermal model at the Eocene Grebe sandstone level never exceed the minimum T_{hom} value that was recorded on the fluid inclusions that were measured in this sample (Figure 6–35).

In the absence of any measured maturity data for the Jabiru-2 well the veracity of this thermal model is constrained only by the current formation temperatures (Figure 6–35). Comparison of this model with the one for the nearby Jabiru-1A well (Figure 6–34) would suggest that higher palaeo-heat flow values are probably justified given the poor match between the calculated maturity and measured maturity values in that well when using the default thermal model.

However, for the sample taken from Jabiru-2 that comes from the relatively shallow buried Tertiary section (Eocene Grebe Sandstone), this sample will be unaffected by heat flow variations that occurred in the distant geological past. Similarly, any more recent heat flow changes that may have occurred are likely to have limited impact given the lack of significant burial present at that time.

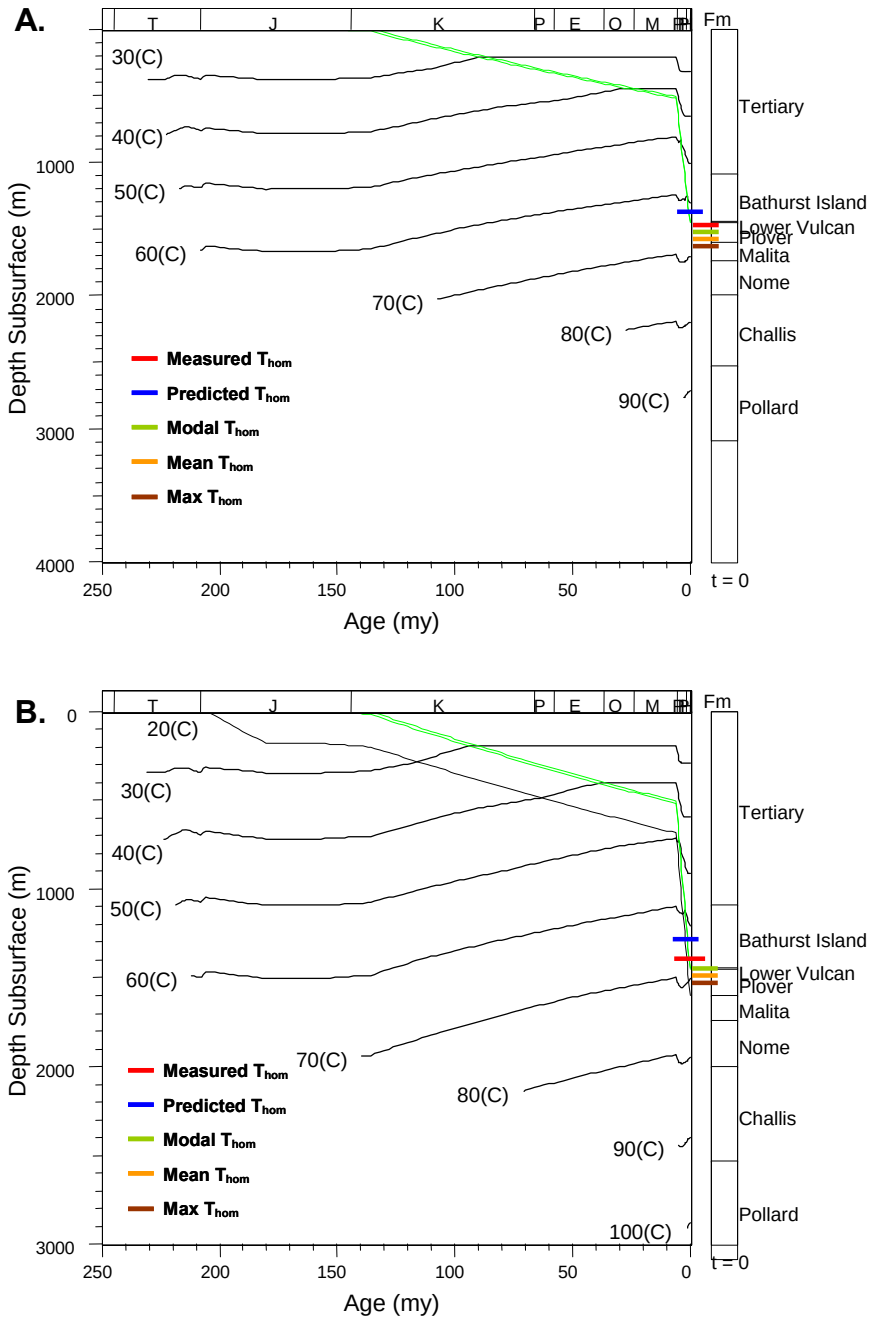

Figure 6-33: Basin models for the Jabiru-1A well.

Burial history plots for the Jurassic Plover Formation are shown with calculated isotherms overlain. The minimum T_{hom} value recorded in samples from the Jabiru-1A well of 67°C is shown as the solid red line, whilst the red shading represents a sensitivity envelope based on a ±10% variation in the lowest T_{hom} value. The other coloured lines are described in the legend and lines that plot to outside the main diagram represent values that exceed the maximum temperatures predicted by the model.

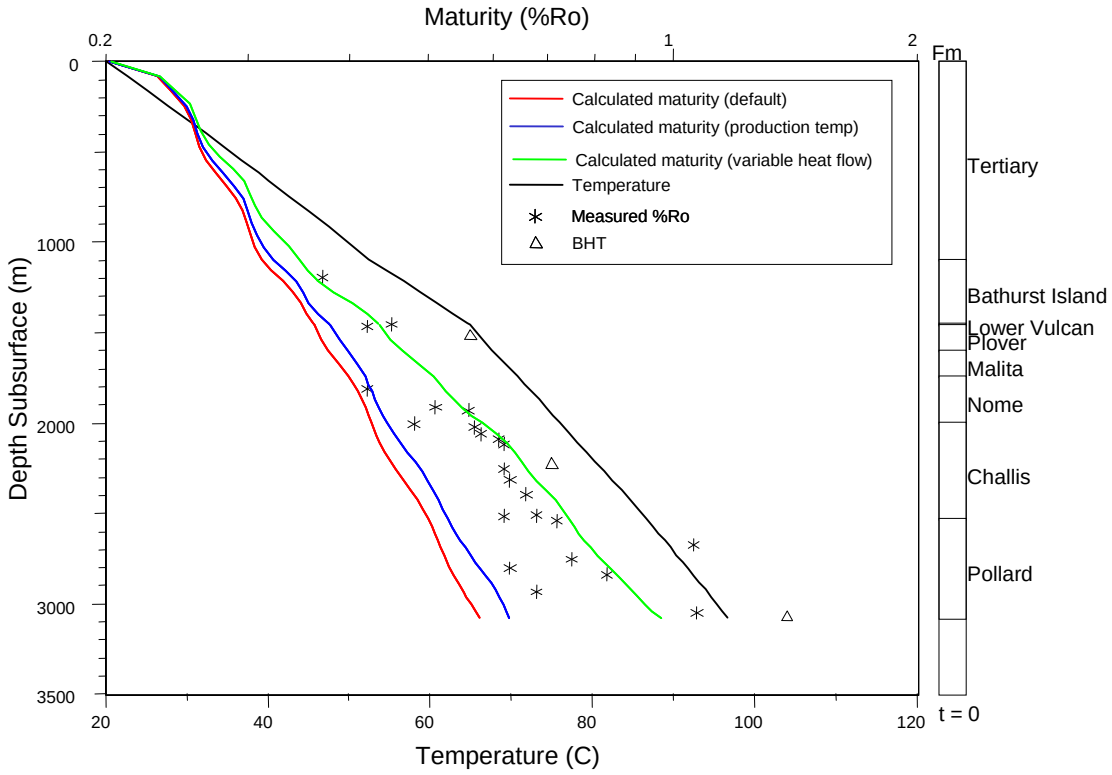

Figure 6-34: Calculated maturity compared with measured maturity data, Jabiru-1A

Graph showing measured vitrinite reflectance values (%Ro) and temperature data as well as calculated profiles for temperature and two alternate calculated maturity profiles, one for a default thermal model and one for a variable heat flow model.

6.6.11 Keeling-1, Basin Modelling Results

The default model utilised for the Keeling-1 well produces a timing estimate for the onset of trapping of fluid inclusions by quartz overgrowths of Early Eocene time (Figure 6–37), but this prediction is relatively sensitive to the accuracy of the minimum temperature estimate (Minimum T_{hom} value = 90°C).

Modifying this temperature by ±10°C results in a relatively wide range in predicted timings that vary from Early Paleocene to Late Miocene time (Figure 6–37). The default model results in quite good agreement with most of the measured vitrinite reflectance data except for a couple of outliers in the Tertiary section (Figure 6–38). The outlier values cannot be adequately modelled by considering conductive heat transfer alone and may represent reworked vitrinite.

Alternatively if all of the measured data points are taken as being representative then the near vertical profile implies that heat transfer by convection rather than conduction. Large cross formation flow of formation water would be one way of producing such a profile.

6.6.12 Octavius-2, Basin Modelling Results

The default basin model utilised for the Octavius-2 well produces a timing estimate for the onset of trapping of fluid inclusions by the crystallisation of quartz overgrowths in the Tithonian Sandstone of Mid-Eocene time (Figure 6–39A) and this prediction is relatively sensitive to the accuracy of the minimum temperature estimate used (Minimum T_{hom} value = 105°C). Modifying this minimum temperature value by ±10°C results in a relatively wide range in predicted timings that vary from Early Paleocene time to the current day (Figure 6–39A).

The minimum T_{hom} value (128°C) measured on fluid inclusions from the Plover Formation sample exceeds the maximum temperatures predicted by the 1D basin model and this sample cannot be reconciled by a simple conductive heat transfer model if the default model is accepted.

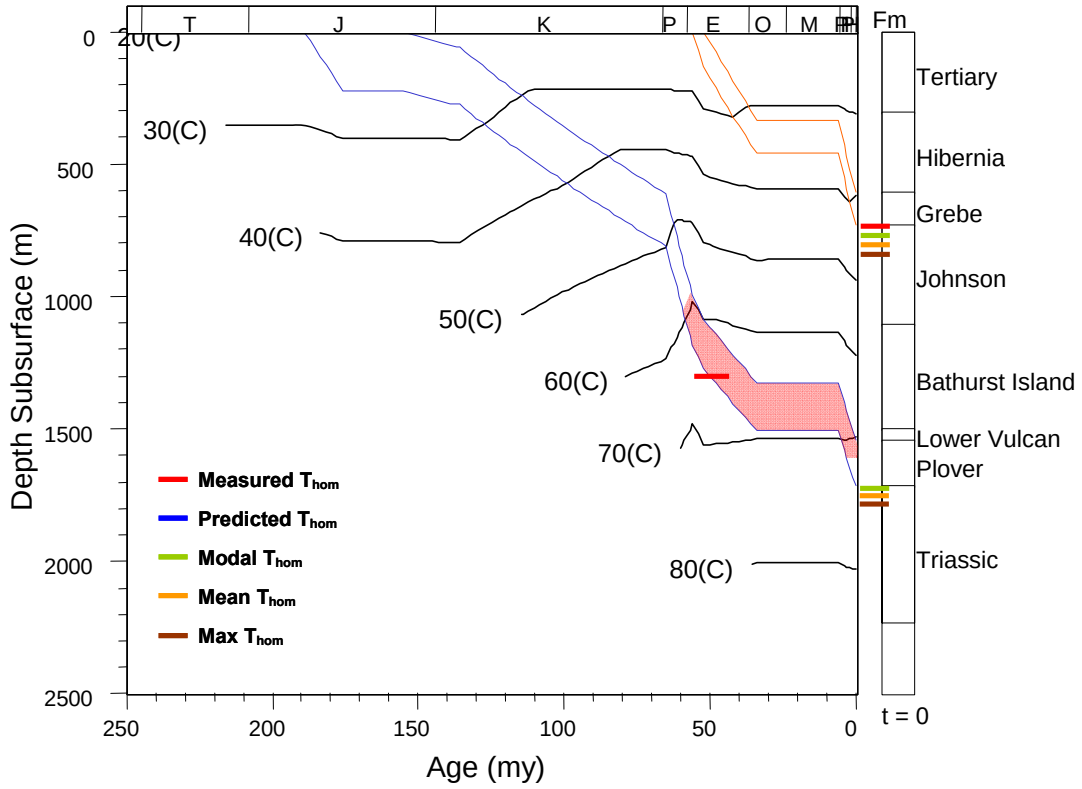

Figure 6-35: Basin models for the Jabiru-2 well.

Burial history plots for the Tertiary Grebe Sandstone (orange lines) and Plover Formation (blue lines) are shown with calculated isotherms overlain. The minimum T_{hom} value recorded in samples from the Jabiru-2 well of 83°C in the Grebe Sandstone and 64°C in the Plover are shown as the solid red lines, whilst the red shading represents a sensitivity envelope based on a ±10% variation in the lowest T_{hom} value. The other coloured lines are described in the legend and lines that plot to outside the main diagram represent values that exceed the maximum temperatures predicted by the model.

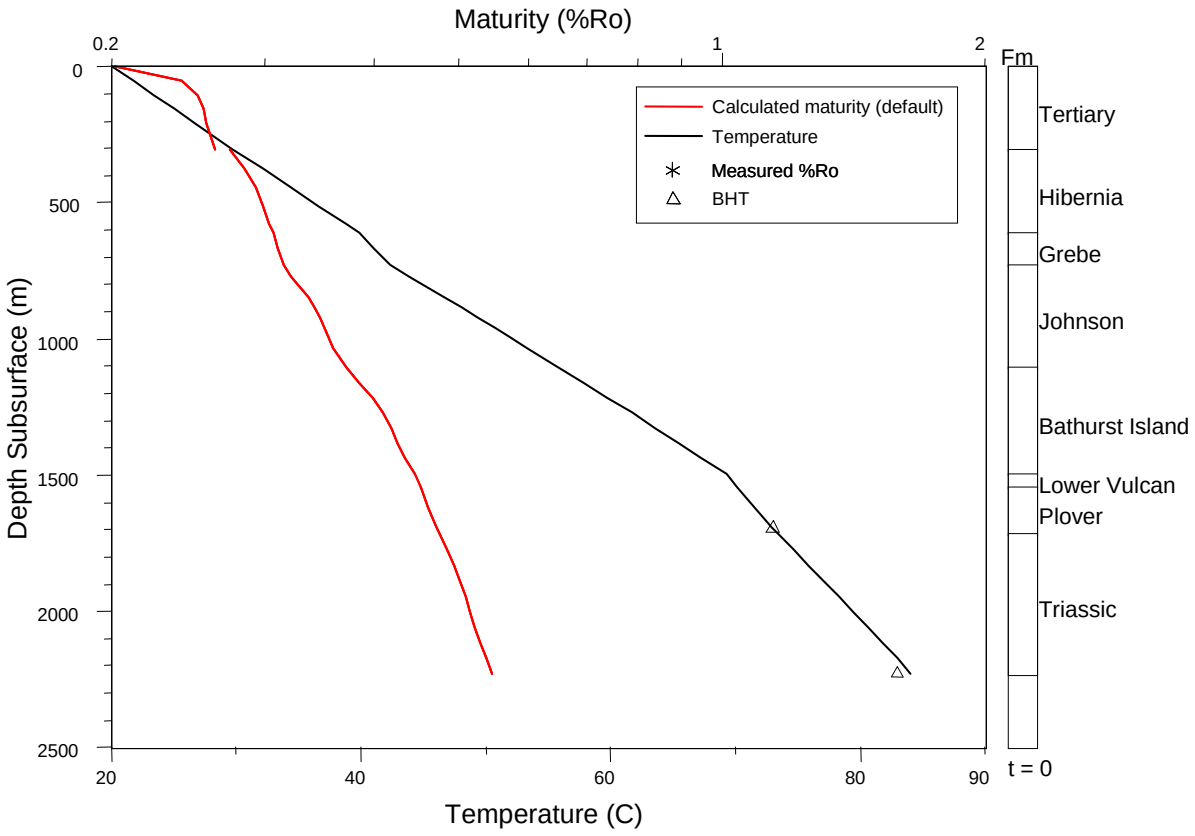

Figure 6-36: Calculated maturity compared with measured maturity data, Jabiru-2

Graph showing temperature data as well as calculated profiles for temperature and maturity.

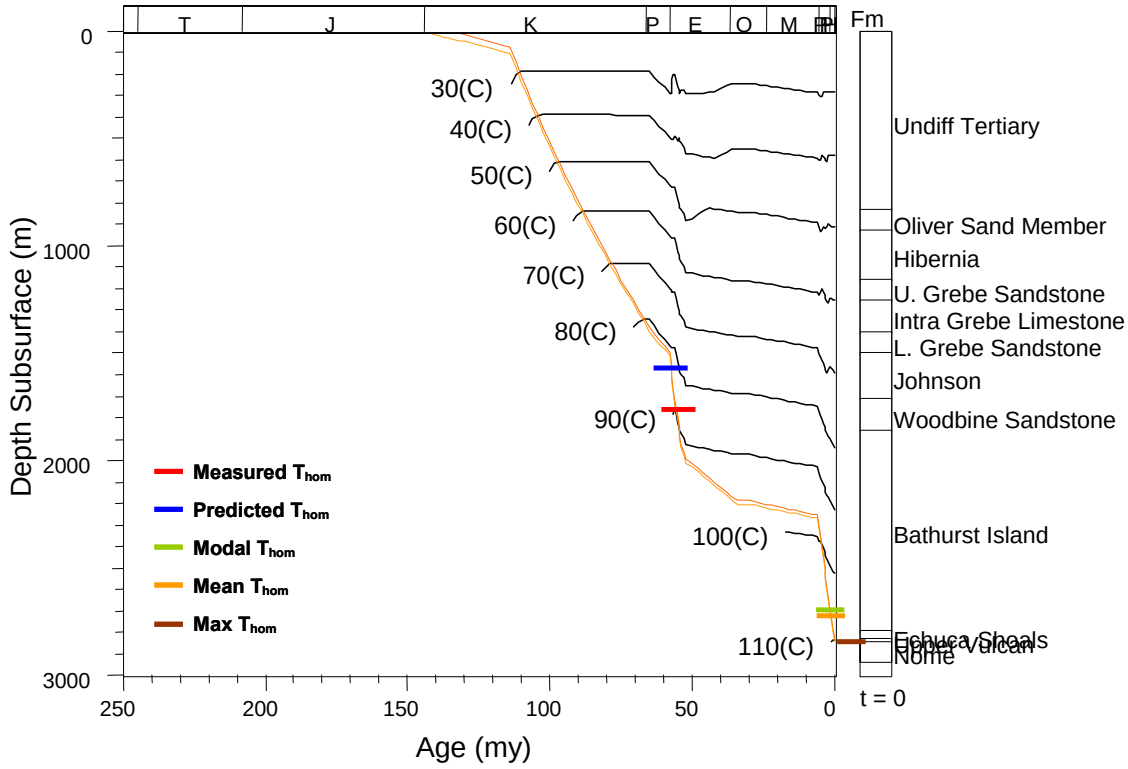

Figure 6-37: Basin models for the Keeling-1 well.

Burial history plots for the Tertiary Grebe Sandstone are shown with calculated isotherms overlain. The minimum T_{hom} value recorded in samples from the Keeling-1 well of 90°C is shown as the solid red line, whilst the other coloured lines are described in the legend.

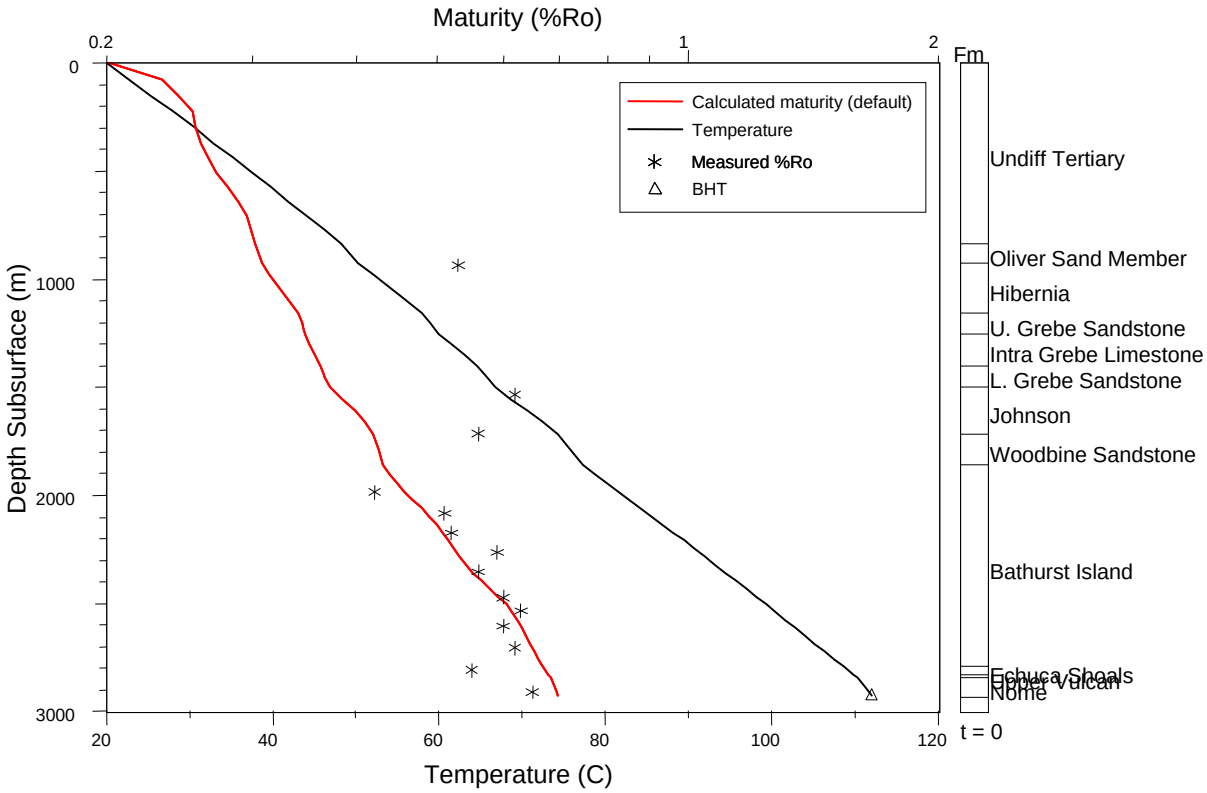

Figure 6-38: Calculated maturity compared with measured maturity data, Keeling-1

Graph showing measured vitrinite reflectance values (%Ro) and temperature data as well as calculated profiles for temperature and maturity.

Calculated maturity profiles, however, consistently falls between the measured vitrinite reflectance data and the FAMM data available for this well (Figure 6–40). If the FAMM data are preferred then palaeo-heat flows may have been higher in the past or the corrected BHT has not fully removed the circulation effects.

An alternative thermal model that employs a 10% increase on the recorded BHT provides a good match with the FAMM data and produces very similar timing estimates to the default model for the Tithonian sandstone and enables the minimum T_{hom} recorded in the Plover Formation sample to be reconciled (Figure 6–39B).

6.6.13 Oliver-1, Basin Modelling Results

The default 1D basin model utilised for the Oliver-1 well produces a timing estimate for the onset of trapping of fluid inclusions by quartz overgrowths of Mid Eocene time (Figure 6–41A) but this prediction is sensitive to the accuracy of the minimum temperature estimate from the fluid inclusion data (Minimum T_{hom} value = 100°C). Modifying this temperature by ±10°C results in predicted timings that vary from Paleocene to Pliocene time (Figure 6–41A).

The maturity profile calculated for this default model, however, consistently falls between the measured vitrinite reflectance data and the FAMM data available for this well (Figure 6–42). If the FAMM data are used then palaeo-heat flows may have been higher in the past or the corrected BHT has not fully removed the effects of circulation. The marine nature of the section increases the likelihood that the vitrinite data has been suppressed and in this setting the FAMM data are preferred.

Two alternative models were constructed in an attempt to produce a better match with the majority of the measured vitrinite reflectance data and the calculated maturity profile. The first of these assumes the measured BHT values have not been fully corrected to remove the effects of circulation during logging. To produce a relatively good match with the FAMM values the corrected BHT would need to underestimate the true formation temperature by about 20%.

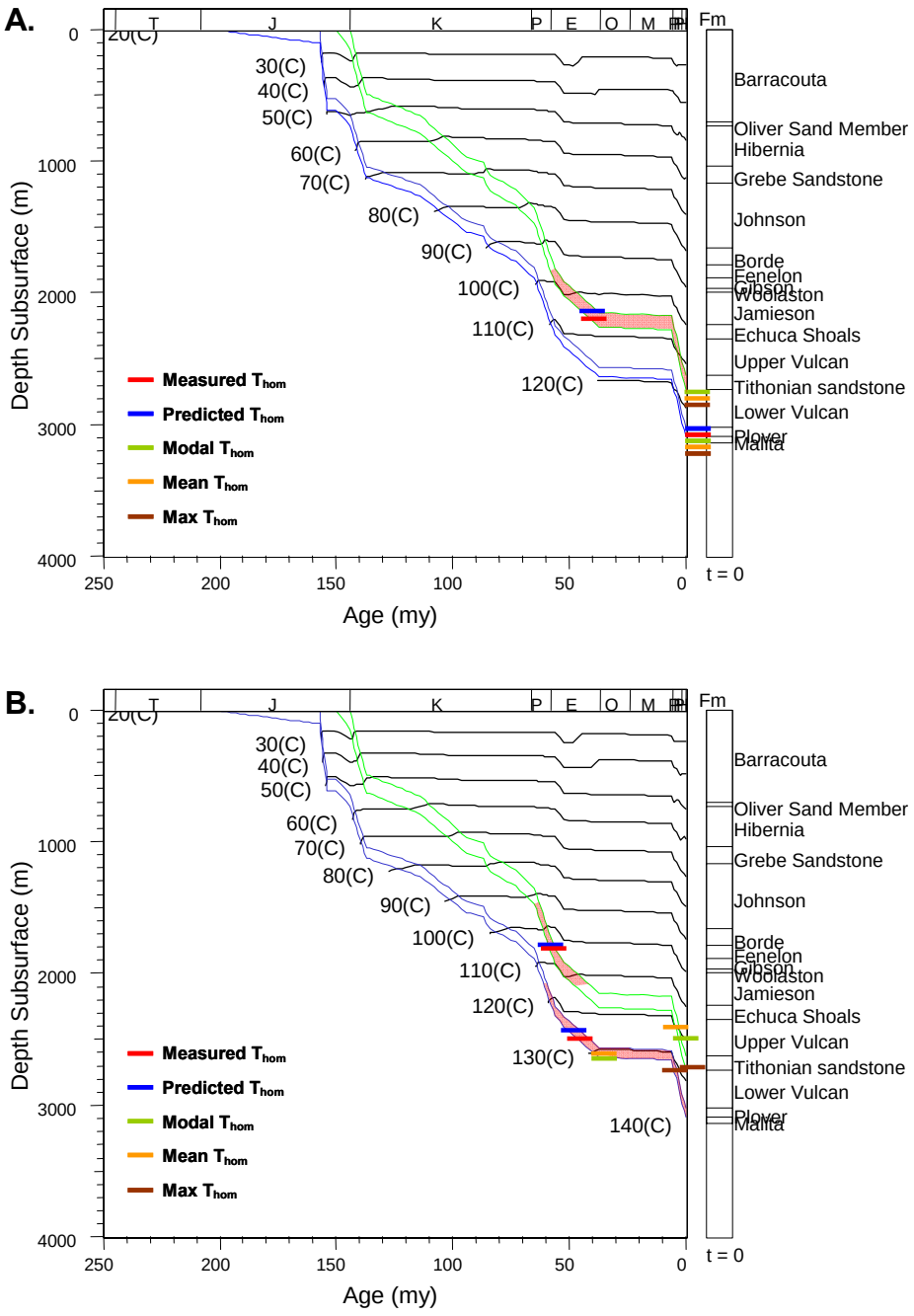

Figure 6-39: Basin models for the Octavius-2 well.

Burial history plots for the Jurassic Plover Formation and the Tithonian sandstone are shown with calculated isotherms overlain. The minimum T_{hom} value recorded in samples from the Octavius-2 well of 107°C for the Tithonian and 128°C are shown as the solid red lines, whilst the red shading represents a sensitivity envelope based on a ±10% variation in the lowest T_{hom} value. The other coloured lines are described in the legend and lines that plot to outside the main diagram represent values that exceed the maximum temperatures predicted by the model.

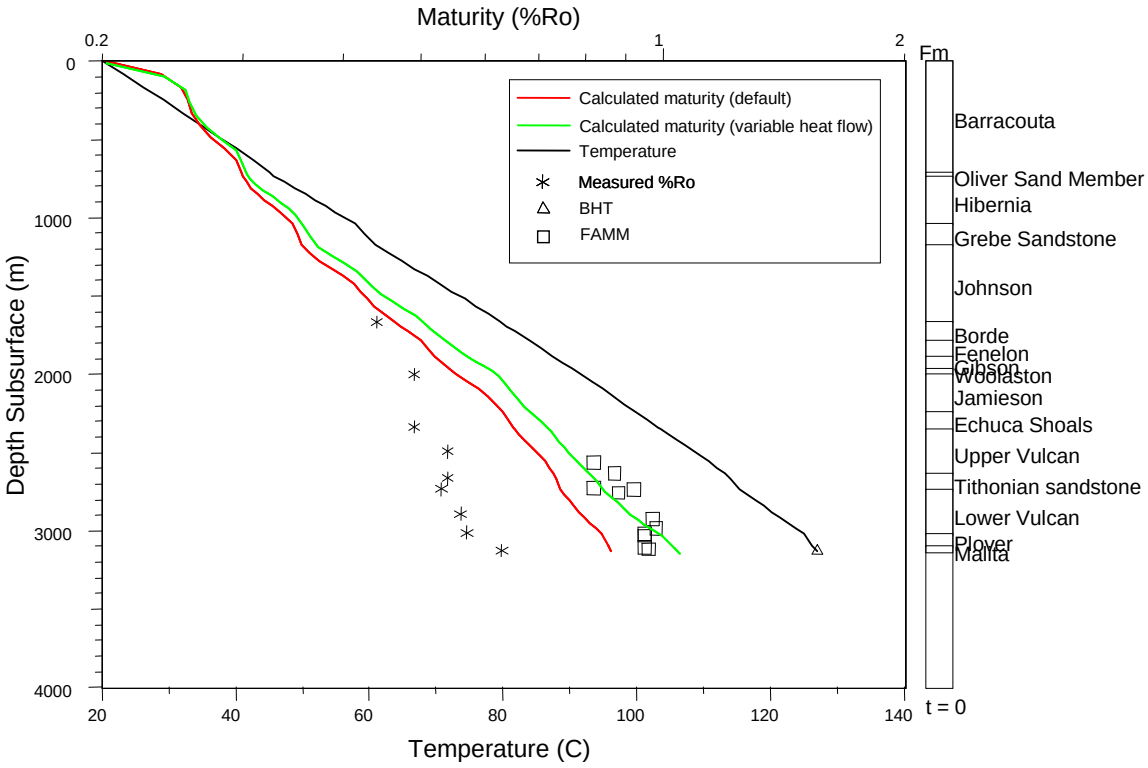

Figure 6-40: Calculated maturity compared with measured maturity data, Octavius-2

Graph showing measured vitrinite reflectance values (%Ro) and temperature data as well as calculated profiles for temperature and two alternate calculated maturity profiles, one for a default thermal model and one for a variable heat flow model.

The impact on the predicted timing for the onset of trapping of fluid inclusions using this model is slight, so has not been shown diagrammatically.

An alternative model that employs a variable heat flow history incorporating palaeo-heat flows that are about 50% higher than at present and requiring these higher heat flows to be sustained into the Tertiary produces a reasonable match with measured FAMM data (Figure 6–42). This model results in an earlier predicted onset of fluid inclusion entrapment with Late Cretaceous to Early Paleocene timing being indicated from this model (Figure 6–41B).

6.6.14 Parry-1, Basin Modelling Results

A lack of measured maturity data and BHT values for the Parry-1 well makes any produced model unconstrained (Figure 6–43, Figure 6–44). Using a simple default basin model produces a timing estimate for the onset of trapping of fluid inclusions by quartz overgrowths of Mid-Eocene time and this prediction is relatively insensitive to the accuracy of the minimum temperature estimate (Minimum T_{hom} value = 65°C). Modifying this temperature by ±10°C results in predicted timings that vary from Early Eocene to Early Miocene time (Figure 6–43).

In light of the other results presented in this section, where the default model rarely produces a good match with available vitrinite reflectance data the value of models that lack these constraints is questionable and consistency with other nearby wells is likely to be a better guide to the validity of the unconstrained models.

6.6.15 Skua-3, Basin Modelling Results

The default 1D basin model constructed for the Skua-3 well produces a timing estimate for the onset of trapping of fluid inclusions by the crystallisation of quartz overgrowths of about Mid-Eocene time (Figure 6–45), but this timing prediction is relatively sensitive to the accuracy of the minimum temperature estimate provided by the fluid inclusion data (Minimum T_{hom} value = 78°C).

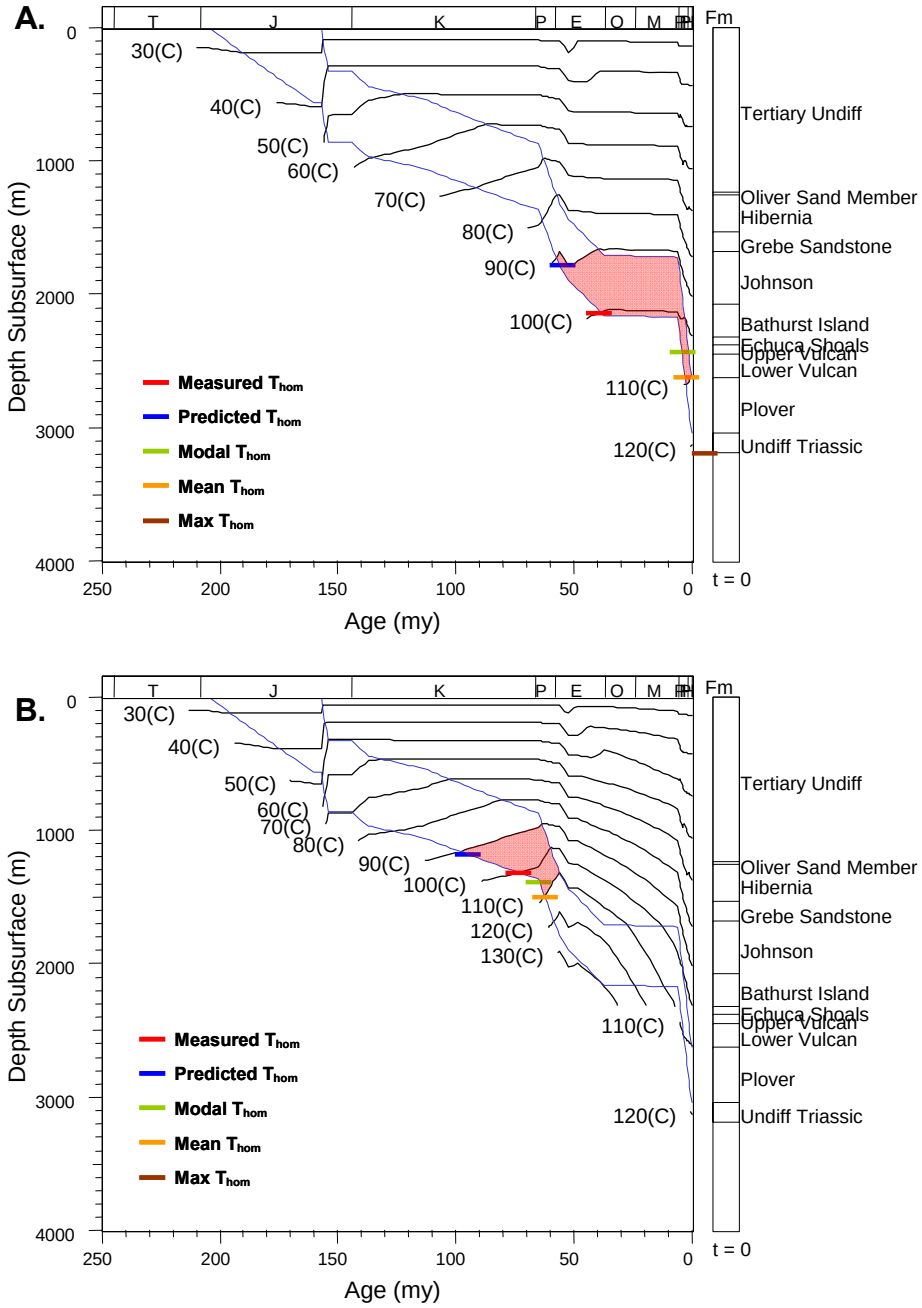

Figure 6-41: Basin models for the Oliver-1 well.

Burial history plots for the Jurassic Plover Formation are shown with calculated isotherms overlain. The minimum T_{hom} value recorded in samples from the Oliver-1 well of 100°C is shown as the solid red line, whilst the red shading represents a sensitivity envelope based on a ±10% variation in the lowest T_{hom} value. The other coloured lines are described in the legend and lines that plot to outside the main diagram represent values that exceed the maximum temperatures predicted by the model.

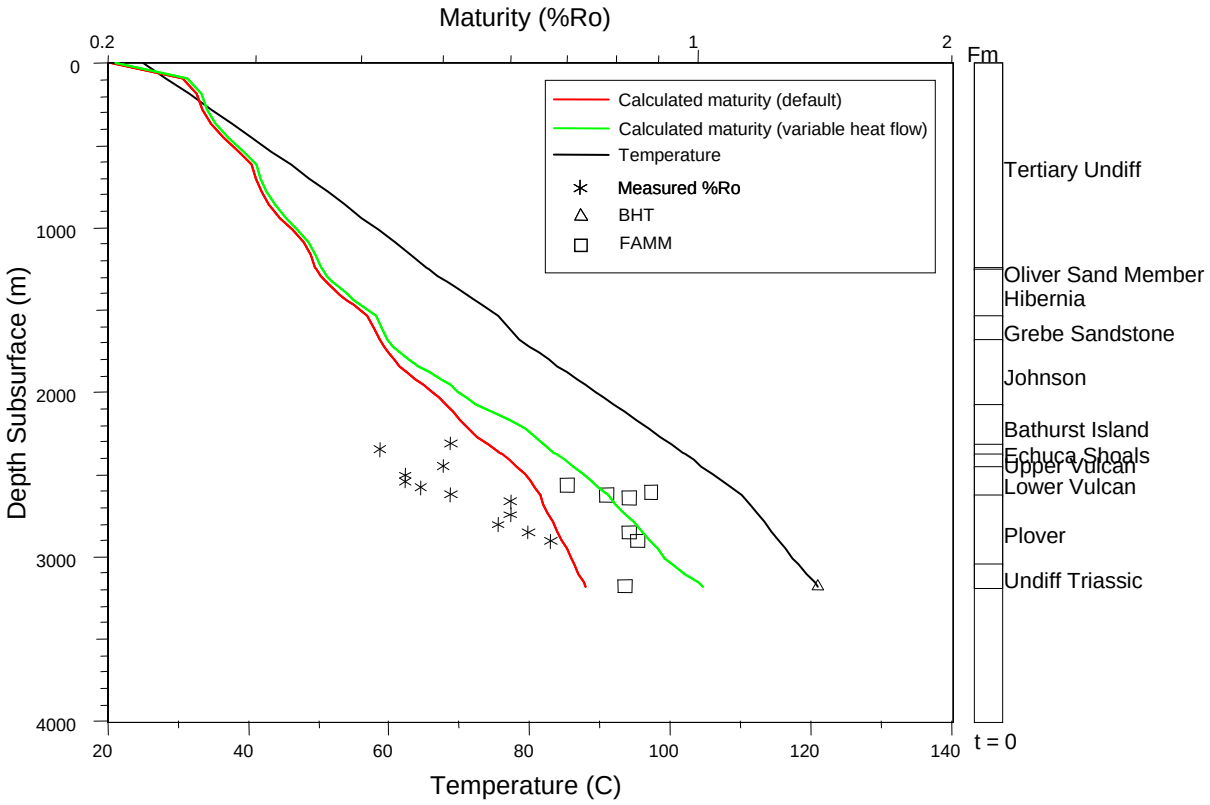

Figure 6-42: Calculated maturity compared with measured maturity data, Oliver-1.

Graph showing measured vitrinite reflectance values (%Ro) and temperature data as well as calculated profiles for temperature and two alternate calculated maturity profiles, one for a default thermal model and one for a variable heat flow model.

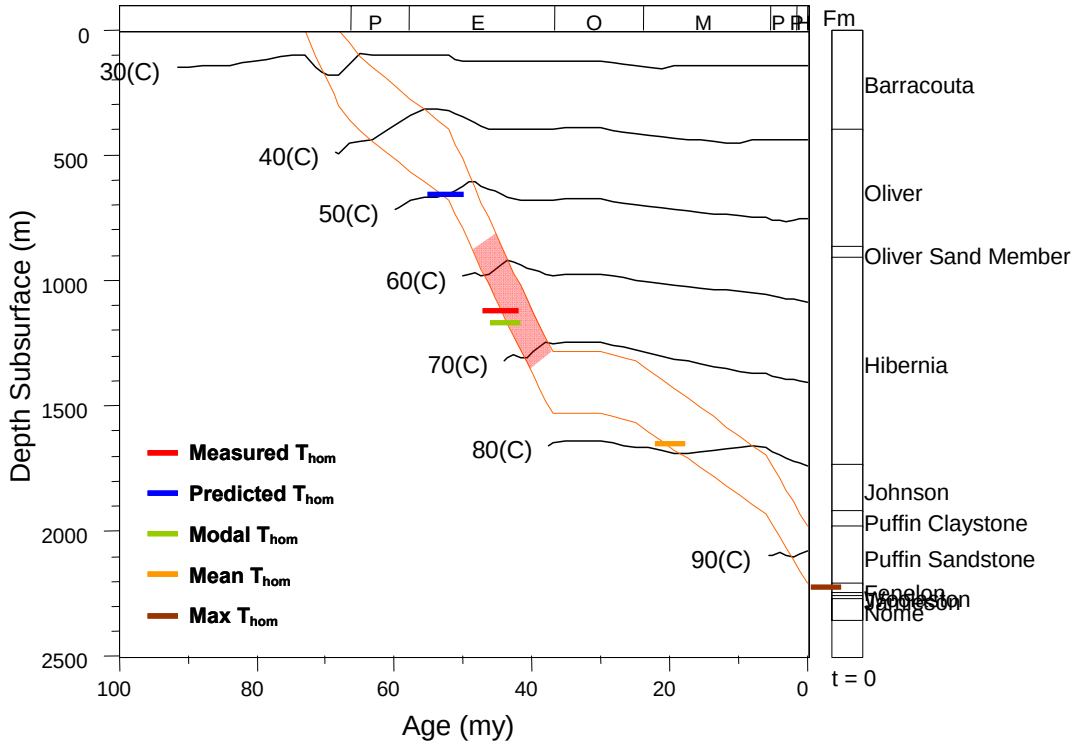

Figure 6-43: Basin models for the Parry-1 well.

Burial history plots for the Cretaceous Puffin sandstone are shown with calculated isotherms overlain. The minimum T_{hom} value recorded in samples from the Parry-1 well of 65°C is shown as the solid red line, whilst the red shading represents a sensitivity envelope based on a ±10% variation in the lowest T_{hom} value. The other coloured lines are described in the legend and lines that plot to outside the main diagram represent values that exceed the maximum temperatures predicted by the model.

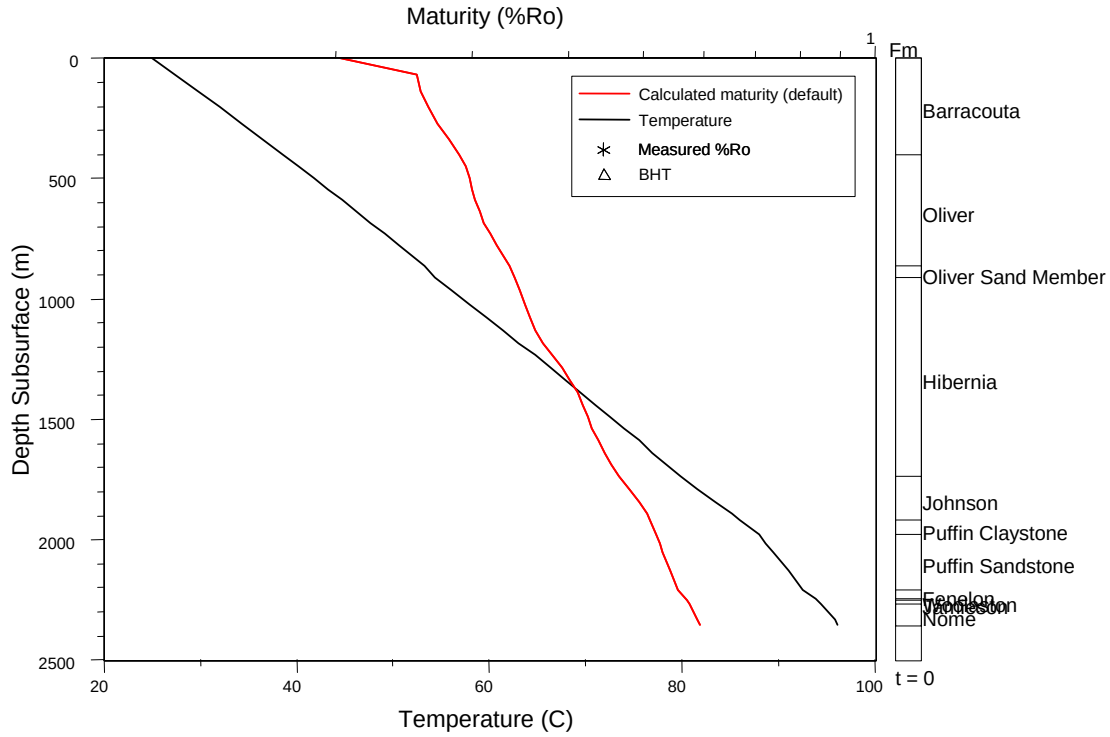

Figure 6-44: Calculated maturity compared with measured maturity data, Parry-1.

Graph showing calculated profiles for temperature and maturity. No current formation temperature or measured maturity data was available for this well.

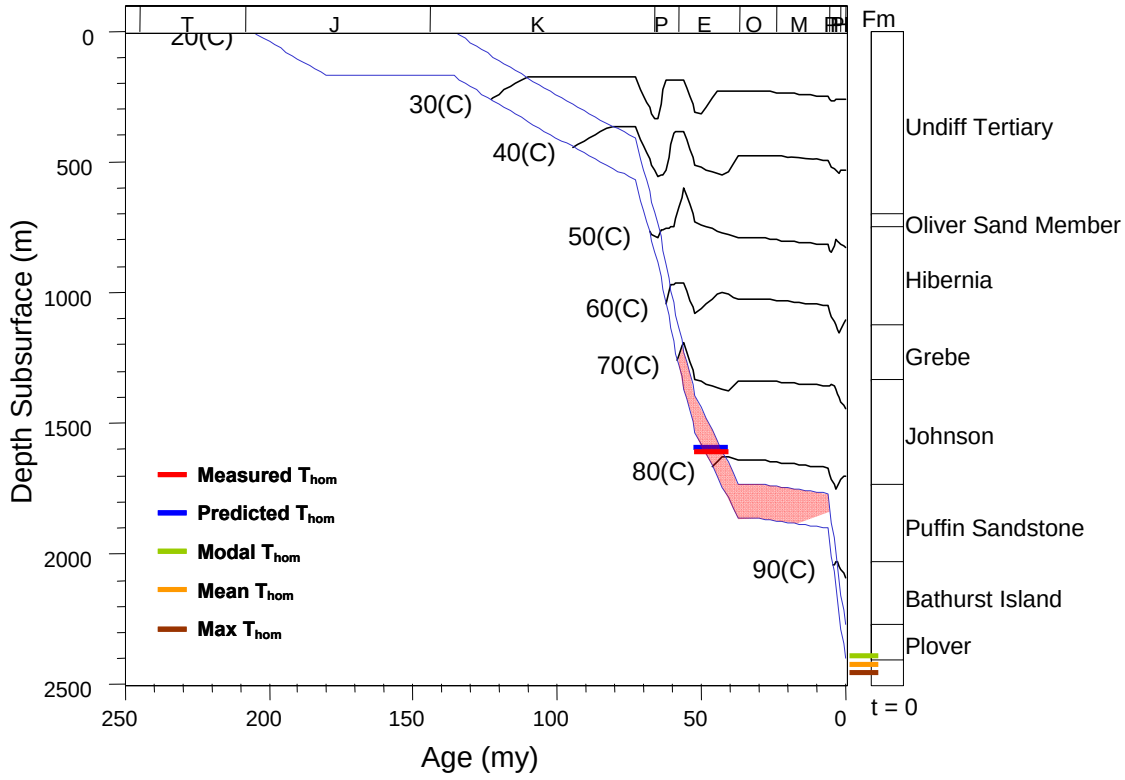

Figure 6-45: Basin models for the Skua-3 well.

Burial history plots for the Jurassic Plover Formation are shown with calculated isotherms overlain. The minimum T_{hom} value recorded in samples from the Skua-3 well of 78°C is shown as the solid red line, whilst the red shading represents a sensitivity envelope based on a ±10% variation in the lowest T_{hom} value. The other coloured lines are described in the legend and lines that plot to outside the main diagram represent values that exceed the maximum temperatures predicted by the model.

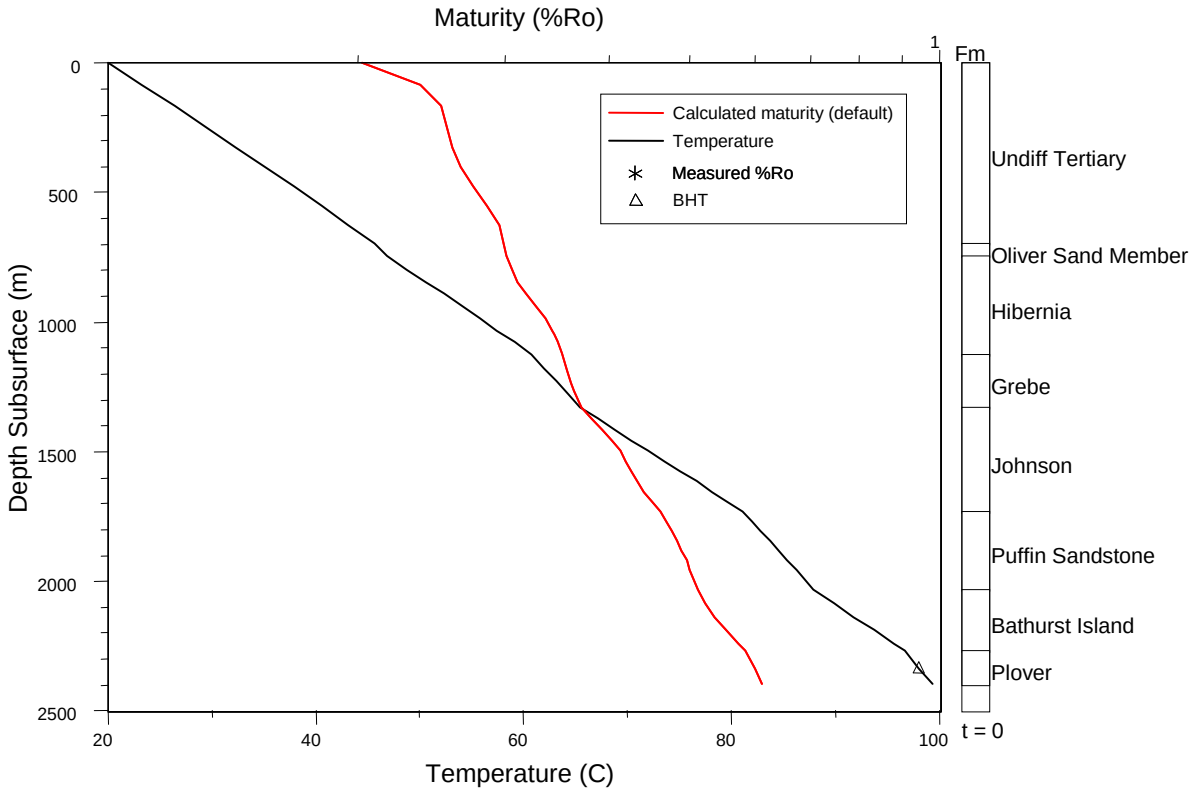

Figure 6-46: Calculated maturity profile, Skua-3.

Graph showing temperature data as well as calculated profiles for temperature and maturity.

Modifying this temperature by ±10°C results in a relatively wide range in predicted timings that vary from Paleocene to Late Miocene time (Figure 6–45). In the absence of measured maturity data this model relies purely on the current formation temperature as the only constraint on the model (Figure 6–46).

6.6.16 Geological Consistency of Absolute Timing Estimates

Many of the models generated in this study represent non-unique solutions and other combinations of heat flow, surface temperature and amount of section eroded at unconformities could satisfy the maturity constraints. In addition, the models only consider conductive heat transfer and perturbation of this background by convective heat transfer generated through fluid-flow could also provide an alternative solution to account for the inconsistencies in some of the examples shown.

In general, the use of default models produces the most consistent range in predicted timings with Eocene timing indicated in most cases (Figure 6–47). Significantly, this timing estimate immediately follows a period of increased regional subsidence in the Paleocene, which is likely to have promoted oil generation within source kitchens. A rapid increase in subsidence is also noted from the Pliocene to the current day and whilst this event has undoubtedly promoted hydrocarbon generation it generally post dates the most likely migration timing indicated from the basin models.

The use of the default model may generate a regionally and geologically consistent pattern in predicted charge timing; however, in many wells these default settings fail to adequately produce a calculated maturity profile that resembles the measured vitrinite reflectance values. Use of a variable heat flow model does enable closer matches to be obtained in individual models but results in a less consistent, and generally earlier, range of timings for the models as a whole.

These variable heat flow models also require much higher palaeo-heat flows to persist well into the Tertiary before falling sharply to accommodate the constraint provided by the current formation temperatures and the geological mechanism for this implausible change is unclear.

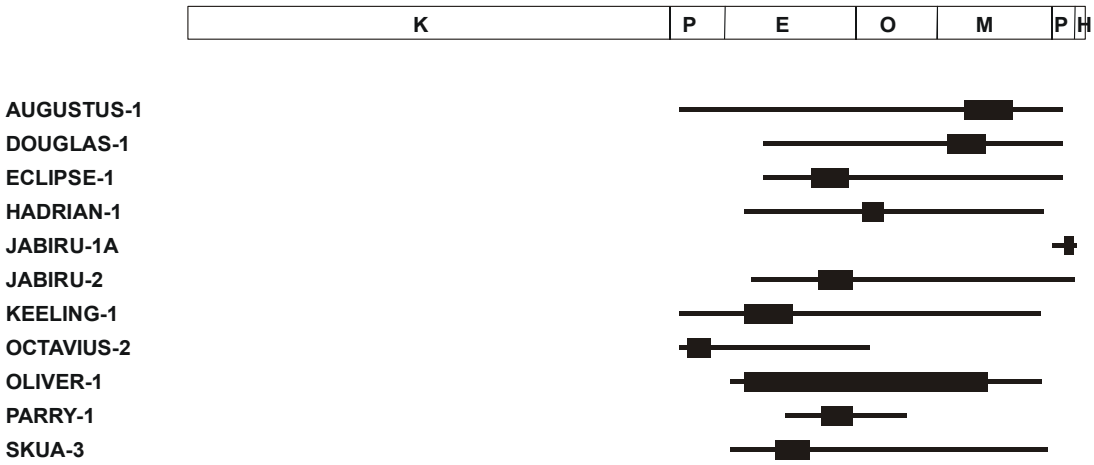

Figure 6-47: Summary of timings predicted from palaeotemperature data

Timings for the onset of fluid inclusion entrapment by the crystallization of quartz overgrowths are based on the preferred basin model that was adopted for each well, with the thicker lines indicating the range associated with the ±10% sensitivity factor. The thinner lines show the ranges that cover all of the models considered.

Mechanisms to explain such conditions in a geologically plausible manner are difficult to support, particularly given that this type of thermal history is only needed in certain wells and hence does not represent a regional background thermal state. The preferred alternative is to use the default model for assessing the timing of fluid inclusion entrapment solely because it results in predictions that are regionally consistent and geologically more plausible.

As mentioned previously, the use of minimum T_{hom} values to constrain the onset of fluid inclusion entrapment is not the most common method for the interpretation of homogenisation temperature data. Many workers utilise mean T_{hom} values to constrain the period of greatest diagenesis and in these instances it would normally be appropriate to also apply a pressure correction to the data as would theoretically be required. However, this approach is not appropriate where evidence of heterogeneous two-phase trapping is observed as some T_{hom} values are invariability non-geological caused by the trapping of a second phase.

Figure 6–48 shows the inferred trapping predictions that are derived when mean T_{hom} values are used for each sample and the consistency of predictions is poorer overall and many samples the mean values exceed the highest formation temperatures predicted by the basin models. This observation further demonstrates the value in using minimum T_{hom} values as a guide to constrain the onset of crystallisation and avoid or minimise the risk of two-phase trapping impacting on the geological application of the thermometric data.

6.7 SUMMARY

Fluid inclusion palaeotemperature (thermometric) data can be accurately determined where high quality, well calibrated, equipment is used and if a careful analytical procedure is adopted. An important consideration when interpreting the data produced by this approach is the recognition that the measurements of homogenisation temperature constitute a phase-change event that in isolation has little geological relevance unless a range of certain criteria are met.

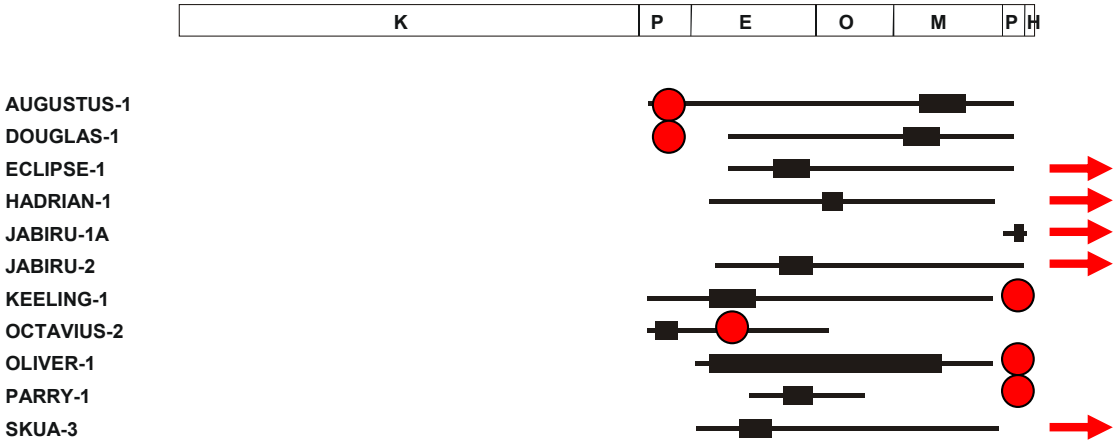

Figure 6-48: Timings based on use of mean T_{hom} values.

Modified version of Figure 6–47 showing the predicted timing of fluid inclusion entrapment if the mean (red points) rather than minimum T_{hom} values are adopted (red arrows show that mean temperature was not reached by any of the models run.

However, where these careful criteria are recognised then the results can be reliably interpreted and provide a valuable method to directly measure the palaeo-reservoir temperature. In this regard they provide a key constraint on the validity of basin modelling simulations that can augment the more traditionally used thermal maturity indicators such as vitrinite reflectance.

The wide range in measured T_{hom} in nearly all samples together with variable liquid vapour ratios within discrete fluid inclusion assemblages indicate that heterogeneously trapped inclusions make up a significant proportion of the measurements made in this study. Widespread heterogeneous trapping is also reflected in the distribution of measurements from each sample with most samples conforming to an exponential probability function that is predicted for heterogeneous trapping of two-phases. Whether this represents the influence of a more gas-rich petroleum system operating in the Vulcan Sub-basin or is indeed a reality of thermometric analyses of samples from sedimentary basins more widely is uncertain but requires careful protocols to be followed if geologically sensible interpretations are to be made.

Preferential selection of inclusions with a low liquid-vapour ratio was utilised to avoid or minimise the impact of heterogeneous two-phase trapping, but whilst this approach has been helpful in limiting the addition of heterogeneously trapped inclusions to the dataset the results obtained in this study demonstrate that such a method is not robust enough to avoid this unwanted outcome. This is clearly demonstrated in nearly every sample where at least some measurements lie above the maximum reservoir temperatures indicated by independent thermal maturity data (Vitrinite Reflectances). These most likely reflect the measurement of inclusions that trapped both water and gas in the same inclusion leading to an artificial increase in the measured homogenisation temperatures.

To avoid any spurious data from influencing the geological application of these data preference has been given to use of the minimum temperatures to indicate the onset of inclusion entrapment by the crystallisation of quartz overgrowths, recognising that heterogeneous entrapment of more than one phase acts to progressively increase the measured T_{hom} values above geologically meaningful values. This approach is unlike

the majority of other published studies that employ a reference to heterogeneous trapping to indicate that inclusions were trapped on the bubble point curve and do not require pressure correction. Using that approach, however, fails to recognise this condition is only true for those specific inclusions that trap an infinitesimally small amount of the second phase that in reality is impossible to identify these inclusions unless the methane concentration in each inclusion is measured.

The addition of any more only acts to progressively increase the recorded homogenisation temperature to levels above true geological levels. Consequently the use of minimum T_{hom} values rather than mean or modal values is crucial if inappropriate conclusions are to be drawn from the interpretation of this type of data.

When minimum T_{hom} values of this type, that have been collected on wells from across the VSB, are integrated with basic thermal models, they produce a fairly common prediction of the timing of fluid inclusion entrapment, with trapping in the Eocene indicated for most reservoirs. This agrees well with subsidence curves, which show a period of increased subsidence in the Paleocene that is likely to have promoted oil generation and created the start of oil migration from source kitchen to carrier bed and ultimately to the trap at the end of the migration path. Conversely, if mean or modal values are used then more variable timing estimates are produced that are difficult to interpret in a regionally sensible fashion.

These models, however, are not intended to represent a unique solution and other models that utilise variable heat flow often result in calculated maturity profiles that more closely match the measured temperature and maturity data. These alternatives, however, are less attractive as they are difficult to explain in the geologically sensible manner and such models result in a wider range in predicted timings than is produced by the default models.

7. PALAEO-HYDROLOGY

7.1 INTRODUCTION

The careful evaluation of formation waters can yield important in-sights into the hydrology of petroliferous basins, which can have significant implications for evaluating the hydrocarbon migration, entrapment and retention. Formation waters trapped as fluid inclusions within authigenic mineral cements provide critical constraints on the palaeo-hydrology. In combination with information on the current pore water composition either directly from downhole sampling or indirectly by wireline log analysis these data can highlight important basin processes and address key risks controlling hydrocarbon prospectivity.

Understanding the evolution of the formation water system is frequently overlooked in most basin studies. Water samples are rarely taken during exploration drilling or are of poor quality due to contamination by water-based drilling fluids. Formation water chemistry is addressed in a more fundamental way during field development, where the salinity of the water is a critical constraint on determining formation water resistivity as an input into hydrocarbon saturation calculations (Kuttan et al., 1986). Water composition can also play a role in facilities planning and can be particularly important for planning the efficient and safe disposal of any produced water.

Water pressure data, collected during downhole sampling with RFT or MDT tools provides a further insight into basin hydrology but are generally only acquired when a discovery has been made. Pressure data to establish water gradients can in combination with pressure data from hydrocarbon zones be used to locate hydrocarbon-water contacts where these gradients intersect. If the composition of the water is known, or can be estimated, then the water pressure data can be converted into values of hydraulic head that in turn can be used to ascertain flow directions (Otto el al., 2001) either laterally within individual aquifers, vertically across recognised aquitards via faults (Yassir and Otto, 1997).

7.2 PALAEO-FORMATION WATER SALINITY

Aqueous fluid inclusions represent formation water samples from which the host cement crystallised so provide detailed information on fluid compositions prevailing at that time. The palaeo-formation waters sealed within fluid inclusions are isolated from the pore network, so they remain untainted by subsequent modifications to pore fluid composition, or by contamination associated with drilling. Consequently they provide pristine examples of the formation water extant at different points in the geological past. Determination of salinity represents the most commonly derived information but insights into the more detailed chemistry of the contained fluids can be obtained using methods like Laser Raman spectroscopy (Dubessy et. al., 2001).

7.2.1 Method

The salinity of water contained in fluid inclusions is not directly measured but can be derived from an ice-melting temperature that is observed visually. For ice melting temperatures the phase change involves a solid-liquid-vapour triple point (Figure 7–1). The relationship between ice-melting temperature and salinity is well constrained by physical chemistry experiments that relate the depression of freezing point with variation in the amounts of total dissolved solids (Potter et al., 1978).

The salinity of water within aqueous inclusions was estimated from final ice melting temperatures using the expression:

$$salinity\left(ppm\right) = \left(-1.76T_{ice} - 0.041T_{ice}^{2} - 0.00037T_{ice}^{3}\right) \times 10000$$

This equation is modified after a regression on the NaCl-H2O system (Hall et al., 1988) to give approximate agreement with the CaCl2-H2O system (Oakes et al., 1990) at melting points below the eutectic temperature (-21°C) of a purely NaCl-H_2O solution (Krieger et al., 1996). In practical terms the involvement of calcium rich brines is rare in most sedimentary environments.

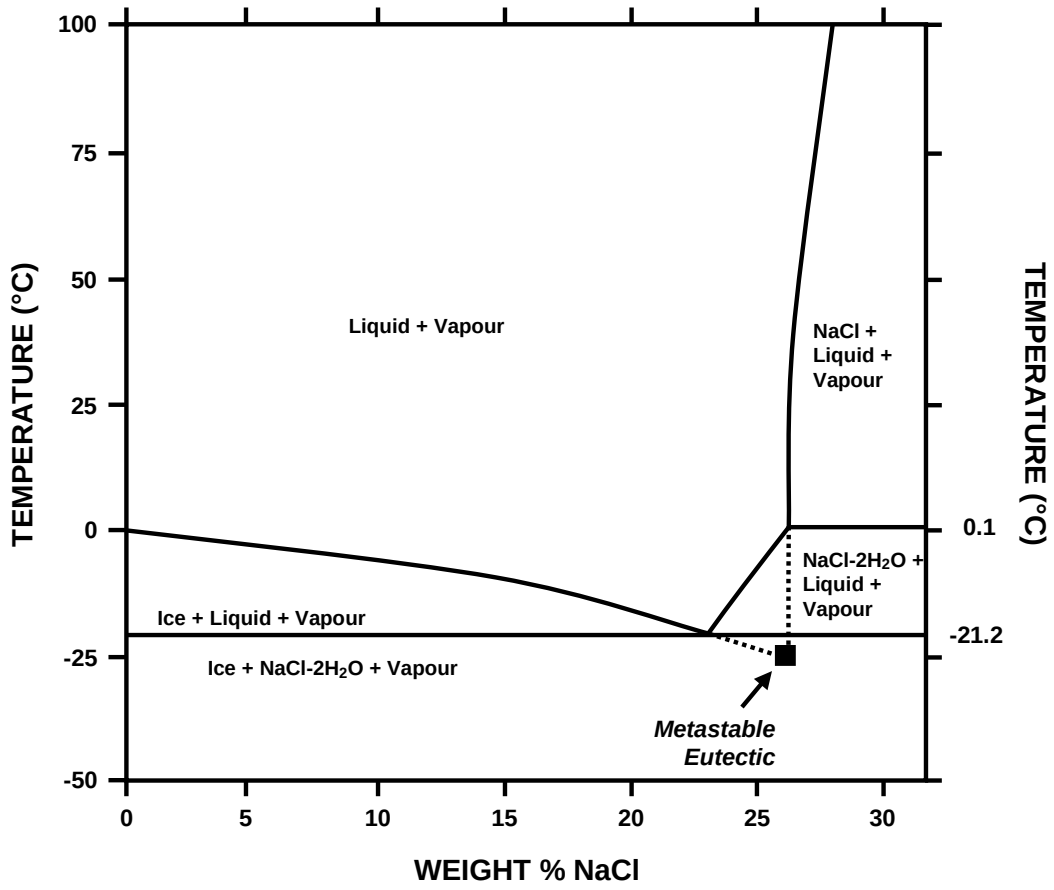

Figure 7-1: Phase diagram for water + ice + NaCl.

A plot of temperature against salt content for the system H_2O-NaCl (from Goldstein and Reynolds, 1994). The diagram illustrates the progressive lowering of ice melting temperature with increasing content of NaCl salts in solution down to a eutectic composition of -21.2°C (23.2 wt% NaCl). First melting (Eutectic melting) consistently occurs at -21.2°C irrespective of NaCl salt content with a mixture of Ice + Liquid + Vapour persisting until final melting occurs (Liquid + Vapour), the latter temperature being directly determined by the NaCl salt content.

Initially the temperature is lowered rapidly (35-50°C per minute) until the contents of the inclusion freeze (Figure 7–2). Typically the freezing is accompanied by a visual change in the refractive index of the internal part of the inclusion and the deformation or complete loss of the vapour bubble due to ice expansion on freezing.

A general relationship exists between the freezing temperature and the salinity of the water, with lower freezing temperatures for more saline inclusions. Although this relationship is not robust enough to accurately determine salinity it provides a guide to the likely ice melting temperature and is useful in determining the temperature range where the heating rate should be slowed in anticipation of final ice melting. At this point heating rates are progressively slowed to between 1-5°C per minute. In some inclusions the formation of the first melt can be observed by a slight twitch and this temperature is referred to as the eutectic temperature and is related to the cations present in the water. For typical oil-field brines that are dominated by NaCl ions the eutectic temperature occurs at -21.2°C, whilst brines that are calcium rich show a lower eutectic temperature at -49.8°C (Figure 7–3). In practice observation of first melting is difficult for the small inclusions typically encountered in the low temperature diagenetic realm and was not routinely measured in this study.

Once melting begins the proportion of liquid to ice progressively increases as the temperature is increased (Figure 7–1) and often ice crystals can be seen to float within the inclusion, firstly as small aggregates and the re-organising into larger fragments as melting proceeds (Figure 7–2). Eventually all of the ice melts to liquid and this final transition is known as the final ice melting temperature (T_{ice}).

As with the previously described determination of homogenisation temperatures, reproducible ice melting temperatures were obtained by using a temperature cycling method (Figure 7–2). The cycling method used (Goldstein and Reynolds, 1994) is an ascending plateau method, testing for the disappearance of ice at each temperature plateau. The temperature plateau is a 15 second pause to allow any temperature gradients that have developed within the heating stage to reach equilibrium, ensuring an accurate measurement is obtained.

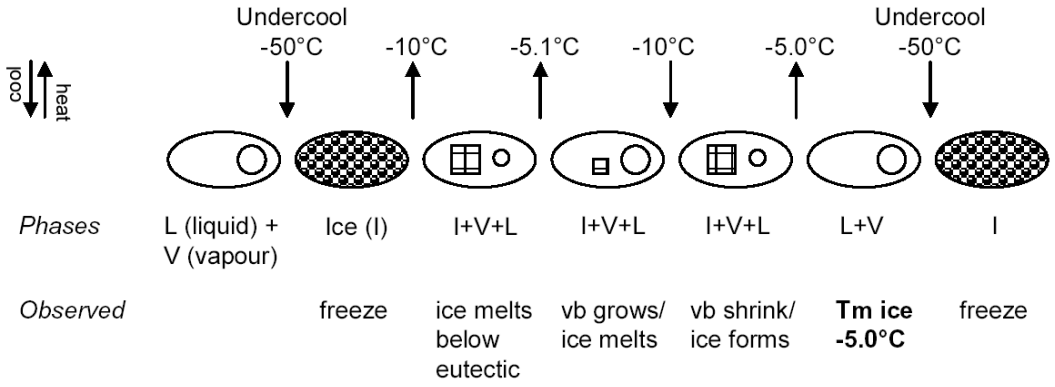

Figure 7-2: Measurement of ice melting temperatures.

Schematic representation of the "cycling" technique used for determining the final melting point of ice (T_m) for constraining the depression of freezing point in salt solutions (Goldstein and Reynolds, 1994). The example refers to determination of a -5.0°C ice melting temperature for a two-phase inclusion. L = liquid V = vapour, I = ice and vb refers to vapour bubble.

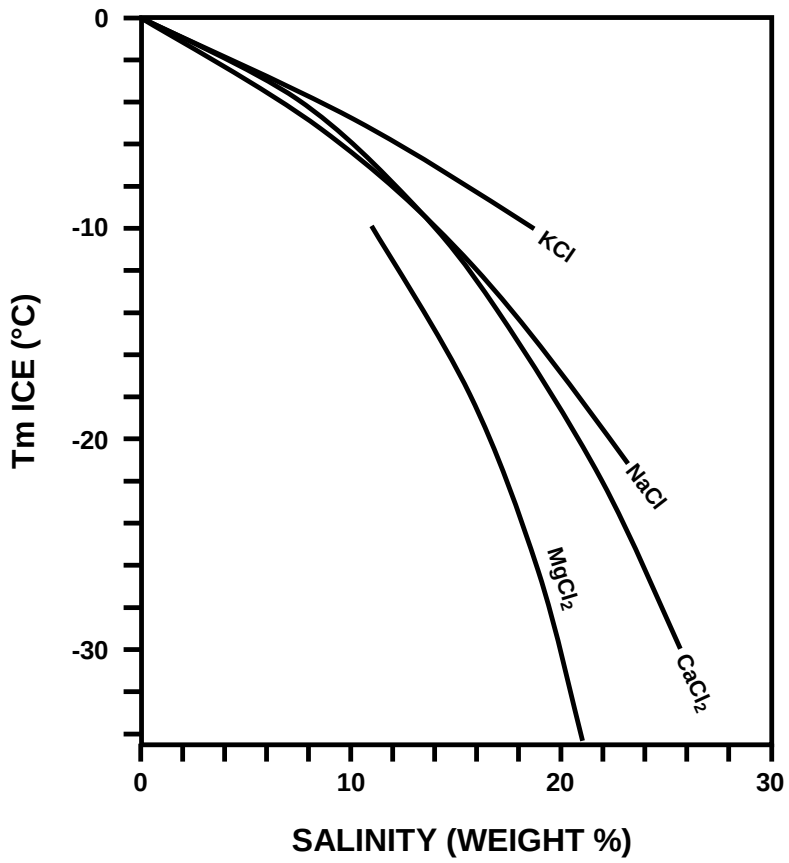

Figure 7-3: Final ice melting temperatures of ice for different salts in solution.

Cross plot of final melting of ice (T_m) against salinity showing the impact on final ice-melting of different pure salts within the solution (Modified from Goldstein and Reynolds, 1994).

The test for ice is made by lowering the temperature from this plateau and visually looking for immediate re-growth of ice crystals. Re-growth of ice crystals indicates some ice was still present within the inclusion at that temperature, as the remaining ice provides a nucleation site needed to allow new ice crystals to grow. Cooling from temperatures above this phase change (i.e. complete melting) requires a more substantial temperature reduction and typically temperatures of –20 to –40 °C are required to re-freeze the inclusion. With repeated cycles the ice melting temperature can be bracketed with increasing precision and accuracy. Ice melting temperatures derived using these methods are accurate to at least ±0.5°C, with precision of ±0.1°C.

Occasionally some inclusions will exhibit apparent final melting (typically instantaneous bubble return) at temperatures above the ice melting temperature, which precludes cycling and the demonstration of reversible phase change. Most inclusions with positive ice melting temperatures are attributed to metastability in re-nucleating a vapour bubble until after the melting of ice. In these instances the recorded temperature is not a true final melting; rather metastability of the liquid and vapour phases allows a single phase to persist where two phases would be predicted.

7.3 FORMATION WATER SALINITIES IN THE VULCAN SUB-BASIN

The interpretation of salinity data requires consideration of the types of formation water that can be expected in a sedimentary environment. Normal marine waters have salinities of about 35,000 ppm (Hanor, 1994a, b) and are the expected depositional water for marine sediments. For the fluvio-deltaic sediments of the Plover Formation the degree of marine incursion will have controlled salinity but the salinity of connate waters in this area is likely to have ranged from fresh to brackish compositions. Additionally, ingress of meteoric waters may have occurred in the VSB during periods of sub-aerial exposure associated with the Callovian and Intra-Valanginian Unconformities (Pattillo and Nicholls, 1990). Inundation of the margin in response to post-rift thermal subsidence led to the establishment of marine depositional environments in the Upper Jurassic that have largely persisted until the current day. The emplacement of salt by Tertiary diapirism provided the opportunity for hypersaline formation waters derived from the dissolution of these salt diapirs.

Original waters present during deposition will change through time with salinities generally rising with increased burial due to accelerated diagenesis with depth (Hanor, 1994a). A salinity increase through diagenesis occurs in response to the alteration of chloride-bearing minerals such as feldspar. The exact increase in salinity achieved by these processes is poorly understood, although prima facie evidence from analyses of formation waters in closed-system basins indicates that values of up to about 100,000 ppm are possible. The release of low salinity waters from the dehydration of clay minerals is one mechanism through which a reduction in salinity can occur during diagenesis (Morton and Land, 1987), although there is considerable debate regarding whether this process could significantly affect the overall formation water salinity.

7.3.1 Fluid Inclusion Palaeo-salinities

Thirty-two samples, taken from 15 wells across the VSB, have been analysed (Figure 7–4) for palaeo-salinity determination, including 7 from current hydrocarbon columns, 4 from interpreted palaeo-oil columns and 4 from water-wet wells. The analyses represent a combination of new data, existing CSIRO data (Eadington et al, 1991, 1992; Hamilton et al, 1991; Lisk et al, 1992; O'Brien et al, 1996a, 1998a) and a small number of analyses from an unpublished study (Bone, 1990). Results generated in this study are presented individually and then combined with the pre-existing data to investigate regional trends within the main aquifer horizons.

The samples are mostly from Jurassic or Triassic reservoir units encountered immediately below the Callovian Unconformity (Pre and Syn Rift section), with a few samples from Cretaceous and Tertiary sandstones, within the Post Rift section. Recorded ice-melting temperatures for aqueous inclusions within quartz overgrowths show a wide range varying from –0.1°C to –37.0°C. Equivalent salinities, derived using the equations of Hall et al. (1988), range from 2,000 ppm to 277,300 ppm NaCl equivalent (Figure 7–5).

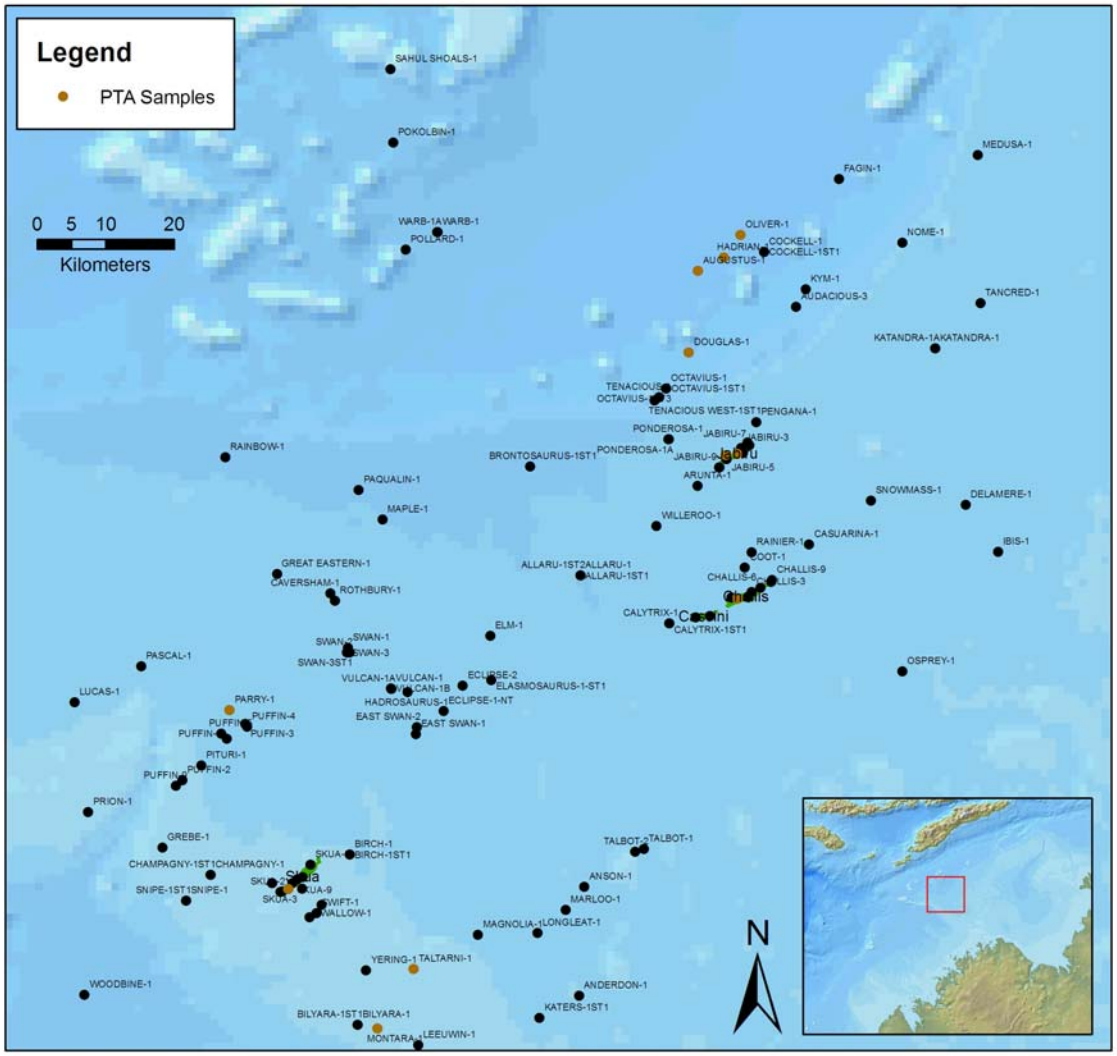

Figure 7-4: Location of wells with palaeo-salinity data.

The map shows the location of samples used for palaeo-thermometric analysis (PTA) that includes determination of ice melting temperatures. Samples have been taken from across the VSB and include a number of different interpreted fluid zones including current and palaeo-hydrocarbon zones and wells which are interpreted to have always been water-wet.

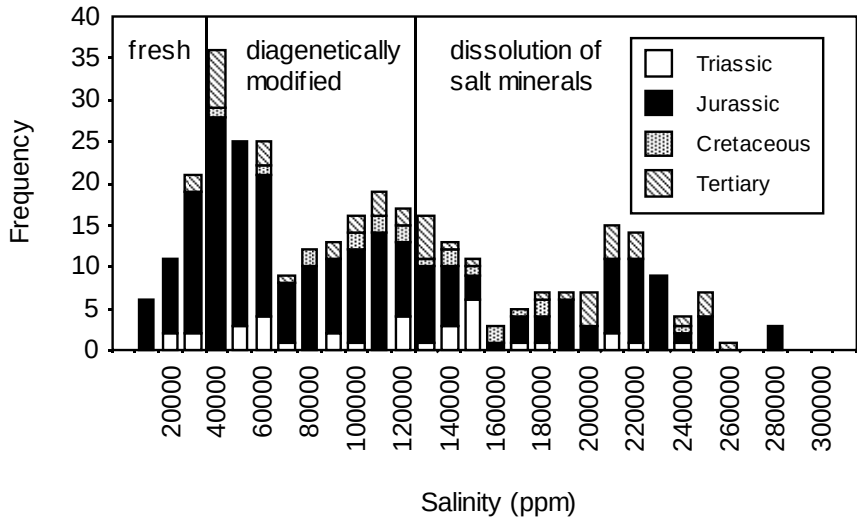

Figure 7-5: Histogram of palaeo-salinities from the VSB.

Summary of fluid inclusion salinity determinations for samples from the VSB split by stratigraphic level. A tri-modal distribution is apparent that implies contribution of fluids with a different origin. At the high salinity end the data indicate a contribution from the dissolution of salt minerals, whilst two discrete populations occur at lower salinity, one indicating the trapping of relatively fresh waters, the other more likely to reflect diagenetic modification of original connate water.

7.3.1.1 Ice Melting Temperatures, Eclipse-1

Thermometric measurements were made on inclusions from a single cuttings sample from within the recognised palaeo-oil column at 2679-82 mRT. The measured inclusions are from a single fluid inclusion assemblage, primary two-phase aqueous inclusions located at the quartz overgrowth boundary (n = 11, where n = number of inclusions measured). Measured ice melting temperatures for these inclusions range from –1.0 to –15.5°C, corresponding to calculated salinity values of between 17,000 and 188,000 ppm (Table 7–1), using the modified equations of Hall et al. (1998).

7.3.1.2 Ice Melting Temperatures, Jabiru-2

Thermometric measurements have been made on fluid inclusions from two cuttings samples, one from Tertiary sandstones at 790-800 mRT (Grebe sandstone) and one from the palaeo-oil column in the Middle Jurassic Plover Formation (1661-64 mRT).

In the Tertiary sample (790-800mRT) all of the inclusions measured are two-phase primary aqueous inclusions located on the quartz overgrowth boundary (n = 16, where n = number of inclusions measured). Measured ice melting temperatures range from –4.0 to –29.0°C, representing calculated salinities of between 64,000 and 256,000 ppm (Table 7–2), using the modified equations of Hall et al. (1998).

In the deeper sample (1661-64mRT) ice melting temperatures were measured on inclusions from two fluid inclusion assemblages. Primary aqueous inclusions from the quartz overgrowth boundary have ice melting temperatures that range from –4.4 to –20.5°C, corresponding to calculated salinities of between 70,000 and 220,000 ppm (Table 7–2), using the modified equations of Hall et al. (1998). Secondary aqueous inclusions on fractures cutting quartz overgrowths have ice melting temperatures ranging from –12.0 to –27.0°C, corresponding to calculated NaCl equivalent salinities of between 159,000 and 249,000 ppm (Table 7–2).

Table 7-1: Eclipse-1, fluid inclusion salinity results.

In all tables QOB refers to Quartz Overgrowth Boundary and FCO refers to Fracture Cutting the quartz Overgrowth.

Well Name	Start Depth (mRT)	End Depth (mRT)	CSIRO Number	Sample Type	Mineral Type	Inclusion Type	Location	Tm (°C)	Salinity (ppm)
Eclipse-1	2679	2682	123347	cuttings	quartz	aqueous	QOB	-2.1	35000
Eclipse-1	2679	2682	123347	cuttings	quartz	aqueous	QOB	-1.4	24000
Eclipse-1	2679	2682	123347	cuttings	quartz	aqueous	QOB	-1.7	29000
Eclipse-1	2679	2682	123347	cuttings	quartz	aqueous	QOB	-1	17000
Eclipse-1	2679	2682	123347	cuttings	quartz	aqueous	QOB	-3.5	57000
Eclipse-1	2679	2682	123347	cuttings	quartz	aqueous	QOB	-3.2	52000
Eclipse-1	2679	2682	123347	cuttings	quartz	aqueous	QOB	-3.3	54000
Eclipse-1	2679	2682	123347	cuttings	quartz	aqueous	QOB	-14.6	181000
Eclipse-1	2679	2682	123347	cuttings	quartz	aqueous	QOB	-15.4	187000
Eclipse-1	2679	2682	123347	cuttings	quartz	aqueous	QOB	-15.5	188000
Eclipse-1	2679	2682	123347	cuttings	quartz	aqueous	QOB	-15.3	187000

Table 7-2: Jabiru-2, fluid inclusion salinity results.

Well Name	Start Depth (mRT)	End Depth (mRT)	CSIRO Number	Sample Type	Mineral Type	Inclusion Type	Location	Tm (°C)	Salinity (ppm)
Jabiru-2	790	800	122399	cuttings	quartz	aqueous	QOB	-4	64000
Jabiru-2	790	800	122399	cuttings	quartz	aqueous	QOB	-5.5	85000
Jabiru-2	790	800	122399	cuttings	quartz	aqueous	QOB	-5.9	90000
Jabiru-2	790	800	122399	cuttings	quartz	aqueous	QOB	-6.8	102000
Jabiru-2	790	800	122399	cuttings	quartz	aqueous	QOB	-7.2	107000
Jabiru-2	790	800	122399	cuttings	quartz	aqueous	QOB	-7.2	107000
Jabiru-2	790	800	122399	cuttings	quartz	aqueous	QOB	-8.6	123000
Jabiru-2	790	800	122399	cuttings	quartz	aqueous	QOB	-8.6	123000
Jabiru-2	790	800	122399	cuttings	quartz	aqueous	QOB	-9	128000
Jabiru-2	790	800	122399	cuttings	quartz	aqueous	QOB	-9	128000
Jabiru-2	790	800	122399	cuttings	quartz	aqueous	QOB	-10.5	144000
Jabiru-2	790	800	122399	cuttings	quartz	aqueous	QOB	-18	206000
Jabiru-2	790	800	122399	cuttings	quartz	aqueous	QOB	-19	212000
Jabiru-2	790	800	122399	cuttings	quartz	aqueous	QOB	-25	242000
Jabiru-2	790	800	122399	cuttings	quartz	aqueous	QOB	-27	249000
Jabiru-2	790	800	122399	cuttings	quartz	aqueous	QOB	-29	256000
Jabiru-2	1661	1664	122352	cuttings	quartz	aqueous	FCO	-12	159000
Jabiru-2	1661	1664	122352	cuttings	quartz	aqueous	FCO	-13	168000
Jabiru-2	1661	1664	122352	cuttings	quartz	aqueous	FCO	-16	192000
Jabiru-2	1661	1664	122352	cuttings	quartz	aqueous	FCO	-17.5	202000
Jabiru-2	1661	1664	122352	cuttings	quartz	aqueous	FCO	-18	206000
Jabiru-2	1661	1664	122352	cuttings	quartz	aqueous	FCO	-18	206000
Jabiru-2	1661	1664	122352	cuttings	quartz	aqueous	FCO	-19.5	215000
Jabiru-2	1661	1664	122352	cuttings	quartz	aqueous	FCO	-20	218000
Jabiru-2	1661	1664	122352	cuttings	quartz	aqueous	FCO	-20.1	218000
Jabiru-2	1661	1664	122352	cuttings	quartz	aqueous	FCO	-20.5	220000
Jabiru-2	1661	1664	122352	cuttings	quartz	aqueous	FCO	-20.5	220000
Jabiru-2	1661	1664	122352	cuttings	quartz	aqueous	FCO	-20.5	220000
Jabiru-2	1661	1664	122352	cuttings	quartz	aqueous	FCO	-22	228000
Jabiru-2	1661	1664	122352	cuttings	quartz	aqueous	FCO	-22.5	231000
Jabiru-2	1661	1664	122352	cuttings	quartz	aqueous	FCO	-25	242000
Jabiru-2	1661	1664	122352	cuttings	quartz	aqueous	FCO	-26	245000
Jabiru-2	1661	1664	122352	cuttings	quartz	aqueous	FCO	-27	249000
Jabiru-2	1661	1664	122352	cuttings	quartz	aqueous	QOB	-4.4	70000
Jabiru-2	1661	1664	122352	cuttings	quartz	aqueous	QOB	-4.5	71000
Jabiru-2	1661	1664	122352	cuttings	quartz	aqueous	QOB	-4.6	73000
Jabiru-2	1661	1664	122352	cuttings	quartz	aqueous	QOB	-4.7	74000
Jabiru-2	1661	1664	122352	cuttings	quartz	aqueous	QOB	-5.3	82000
Jabiru-2	1661	1664	122352	cuttings	quartz	aqueous	QOB	-10	139000
Jabiru-2	1661	1664	122352	cuttings	quartz	aqueous	QOB	-12.5	163000
Jabiru-2	1661	1664	122352	cuttings	quartz	aqueous	QOB	-13	168000
Jabiru-2	1661	1664	122352	cuttings	quartz	aqueous	QOB	-13.5	172000
Jabiru-2	1661	1664	122352	cuttings	quartz	aqueous	QOB	-16	192000
Jabiru-2	1661	1664	122352	cuttings	quartz	aqueous	QOB	-17.5	202000
Jabiru-2	1661	1664	122352	cuttings	quartz	aqueous	QOB	-18	206000
Jabiru-2	1661	1664	122352	cuttings	quartz	aqueous	QOB	-18	206000
Jabiru-2	1661	1664	122352	cuttings	quartz	aqueous	QOB	-20.5	220000

7.3.1.3 Ice Melting Temperatures, Keeling-1

Thermometric measurements were made on a single cuttings sample from within Triassic sandstones at 3039-42 mRT that comes from the interpreted palaeo-oil column. The inclusions measured comprise a single fluid inclusion assemblage, consisting of primary aqueous inclusions from the quartz overgrowth boundary (n = 21, where n = number of inclusions measured). The measured ice melting temperatures range from –3.3 to –19.3°C, corresponding to calculated salinity values of between 58,000 ppm and 214,000 ppm NaCl equivalent (Table 7–3).

7.3.1.4 Ice Melting Temperatures, Oliver-1

Thermometric measurements were made on one core sample from the interpreted palaeo-oil column within presently gas saturated Jurassic sandstones at 2774.38 mRT (Plover Formation). The inclusions form a single fluid inclusion assemblage, consisting of primary aqueous inclusions on the quartz overgrowth boundary (n = 19, where n = number of inclusions measured). Measured ice melting temperatures for these inclusions range from –1.9 to –7.8°C, corresponding to calculated salinities of between 32,000 and 114,000 ppm NaCl equivalent (Table 7–4).

7.3.1.5 Ice Melting Temperatures, Parry-1

Thermometric measurements have been made on a single cuttings sample that was taken from the interpreted a palaeo-oil column in currently water-wet Maastrichtian sandstones at 2094-97 mRT (Puffin sandstone). The inclusions measured all come from a single fluid inclusion assemblage, that consists of primary aqueous inclusions at the quartz overgrowth boundary (n = 20, where n = number of inclusions measured). The ice melting temperatures measured for these inclusions vary widely, ranging from –2.2°C to –23.4°C, corresponding to calculated equivalent salinities of between about 37,000 ppm and 235,000 ppm NaCl equivalent (Table 7–5).

Table 7-3: Keeling-1, fluid inclusion salinity results.

QOB refers to Quartz Overgrowth Boundary.

Well Name	Start Depth (mRT)	End Depth (mRT)	CSIRO Number	Sample Type	Mineral Type	Inclusion Type	Location	Tm (°C)	Salinity (ppm)
Keeling-1	3039	3042	122385	cuttings	quartz	aqueous	QOB	-3.6	58000
Keeling-1	3039	3042	122385	cuttings	quartz	aqueous	QOB	-4.4	70000
Keeling-1	3039	3042	122385	cuttings	quartz	aqueous	QOB	-5.3	82000
Keeling-1	3039	3042	122385	cuttings	quartz	aqueous	QOB	-7.6	112000
Keeling-1	3039	3042	122385	cuttings	quartz	aqueous	QOB	-7.7	113000
Keeling-1	3039	3042	122385	cuttings	quartz	aqueous	QOB	-7.8	114000
Keeling-1	3039	3042	122385	cuttings	quartz	aqueous	QOB	-7.8	114000
Keeling-1	3039	3042	122385	cuttings	quartz	aqueous	QOB	-8.6	123000
Keeling-1	3039	3042	122385	cuttings	quartz	aqueous	QOB	-9.2	130000
Keeling-1	3039	3042	122385	cuttings	quartz	aqueous	QOB	-10	139000
Keeling-1	3039	3042	122385	cuttings	quartz	aqueous	QOB	-10.4	143000
Keeling-1	3039	3042	122385	cuttings	quartz	aqueous	QOB	-10.8	147000
Keeling-1	3039	3042	122385	cuttings	quartz	aqueous	QOB	-10.8	147000
Keeling-1	3039	3042	122385	cuttings	quartz	aqueous	QOB	-11	149000
Keeling-1	3039	3042	122385	cuttings	quartz	aqueous	QOB	-11	149000
Keeling-1	3039	3042	122385	cuttings	quartz	aqueous	QOB	-11.1	150000
Keeling-1	3039	3042	122385	cuttings	quartz	aqueous	QOB	-12.2	160000
Keeling-1	3039	3042	122385	cuttings	quartz	aqueous	QOB	-14.3	179000
Keeling-1	3039	3042	122385	cuttings	quartz	aqueous	QOB	-17.9	205000
Keeling-1	3039	3042	122385	cuttings	quartz	aqueous	QOB	-18	206000
Keeling-1	3039	3042	122385	cuttings	quartz	aqueous	QOB	-19.3	214000

Table 7-4: Oliver-1, fluid inclusion salinity results.

QOB refers to Quartz Overgrowth Boundary.

Well Name	Start Depth (mRT)	End Depth (mRT)	CSIRO Number	Sample Type	Mineral Type	Inclusion Type	Location	Tm (°C)	Salinity (ppm)
Oliver-1	2974		75959	core	quartz	aqueous	QOB	-4.2	67,000
Oliver-1	2974		75959	core	quartz	aqueous	QOB	-5.5	85,000
Oliver-1	2974		75959	core	quartz	aqueous	QOB	-3.4	55,000
Oliver-1	2974		75959	core	quartz	aqueous	QOB	-2.1	35,000
Oliver-1	2974		75959	core	quartz	aqueous	QOB	-3.3	54,000
Oliver-1	2974		75959	core	quartz	aqueous	QOB	-5.7	88,000
Oliver-1	2974		75959	core	quartz	aqueous	QOB	-6.5	98,000
Oliver-1	2974		75959	core	quartz	aqueous	QOB	-6.5	98,000
Oliver-1	2974		75959	core	quartz	aqueous	QOB	-2.4	40,000
Oliver-1	2974		75959	core	quartz	aqueous	QOB	-6.5	nd
Oliver-1	2974		75959	core	quartz	aqueous	QOB	-7.8	114,000
Oliver-1	2974		75959	core	quartz	aqueous	QOB	-6.9	103,000
Oliver-1	2974		75959	core	quartz	aqueous	QOB	-7	104,000
Oliver-1	2974		75959	core	quartz	aqueous	QOB	-6.8	102,000
Oliver-1	2974		75959	core	quartz	aqueous	QOB	-6.4	97,000
Oliver-1	2974		75959	core	quartz	aqueous	QOB	-7	104,000
Oliver-1	2974		75959	core	quartz	aqueous	QOB	-1.9	32,000
Oliver-1	2974		75959	core	quartz	aqueous	QOB	-4.2	67,000
Oliver-1	2974		75959	core	quartz	aqueous	QOB	nd	nd
Oliver-1	2974		75959	core	quartz	aqueous	QOB	-7.3	108,000

7.3.1.6 Ice Melting Temperatures, Skua-3

Thermometric measurements have been made on two cuttings samples from Skua-3, one taken from within the current oil column at 2425-2428 mRT and one taken from the interpreted palaeo-oil column at 2434-37 mRT within the currently water-wet sandstones below the current oil zone. In each cuttings sample the measured ice melting temperatures were determined for two-phase aqueous inclusions that come from two discrete fluid inclusion assemblages:

1. Primary aqueous fluid inclusions located on the quartz overgrowth boundary, 2425-28 mRT sample (n = 16, where n = number of inclusions measured). Measured ice melting temperatures range from –0.6 to –4.2°C, corresponding to calculated salinities of between 10,000 and 67,000 ppm NaCl equivalent (Table 7–6).

2. Secondary aqueous inclusions located within healed fractures cutting the quartz overgrowths, 2425-28 mRT sample (n = 3, where n = number of inclusions measured). The measured ice melting temperatures range from –9.3 to –10.8°C, corresponding to calculated salinities of between 131,000 and 147,000 ppm NaCl equivalent (Table 7–6).

3. Primary aqueous inclusions located on the quartz overgrowth boundary, 2434-37 mRT sample (n = 27, where n = number of inclusions measured). Measured ice melting temperatures range from –1.5 to –21.5°C, corresponding to calculated salinities of between 25,000 and 226,000 ppm NaCl equivalent (Table 7–6).

4. Secondary aqueous inclusions located on healed fractures cutting quartz overgrowths, 2434-37 mRT sample (n = 4, where n = number of inclusions measured). Measured ice melting temperatures range from –1.5 to –4.9°C, corresponding to calculated salinities of between 25,000 and 77,000 ppm NaCl equivalent (Table 7–6).

Table 7-5: Parry-1, fluid inclusion salinity results.

QOB refers to Quartz Overgrowth Boundary.

Well Name	Start Depth (mRT)	End Depth (mRT)	CSIRO Number	Sample Type	Mineral Type	Inclusion Type	Location	Tm (°C)	Salinity (ppm)
Parry-1	2094	2097	123481	cuttings	quartz	aqueous	QOB	-2.2	37000
Parry-1	2094	2097	123481	cuttings	quartz	aqueous	QOB	-3.7	60000
Parry-1	2094	2097	123481	cuttings	quartz	aqueous	QOB	-4.7	74000
Parry-1	2094	2097	123481	cuttings	quartz	aqueous	QOB	-4.8	75000
Parry-1	2094	2097	123481	cuttings	quartz	aqueous	QOB	-6.6	99000
Parry-1	2094	2097	123481	cuttings	quartz	aqueous	QOB	-6.6	99000
Parry-1	2094	2097	123481	cuttings	quartz	aqueous	QOB	-7.1	106000
Parry-1	2094	2097	123481	cuttings	quartz	aqueous	QOB	-7.4	109000
Parry-1	2094	2097	123481	cuttings	quartz	aqueous	QOB	-7.8	114000
Parry-1	2094	2097	123481	cuttings	quartz	aqueous	QOB	-8.3	120000
Parry-1	2094	2097	123481	cuttings	quartz	aqueous	QOB	-9	128000
Parry-1	2094	2097	123481	cuttings	quartz	aqueous	QOB	-9.9	138000
Parry-1	2094	2097	123481	cuttings	quartz	aqueous	QOB	-10.1	140000
Parry-1	2094	2097	123481	cuttings	quartz	aqueous	QOB	-10.4	143000
Parry-1	2094	2097	123481	cuttings	quartz	aqueous	QOB	-11.2	151000
Parry-1	2094	2097	123481	cuttings	quartz	aqueous	QOB	-11.7	156000
Parry-1	2094	2097	123481	cuttings	quartz	aqueous	QOB	-12.4	162000
Parry-1	2094	2097	123481	cuttings	quartz	aqueous	QOB	-13.4	171000
Parry-1	2094	2097	123481	cuttings	quartz	aqueous	QOB	-14.4	180000
Parry-1	2094	2097	123481	cuttings	quartz	aqueous	QOB	-23.4	235000

Table 7-6: Skua-3, fluid inclusion salinity results.

QOB refers to Quartz Overgrowth Boundary and FCO refers to Fracture Cutting Overgrowth.

Well Name	Start Depth (mRT)	End Depth (mRT)	CSIRO Number	Sample Type	Mineral Type	Inclusion Type	Location	Tm (°C)	Salinity (ppm)
Skua-3	2425	2428	122423	cuttings	quartz	aqueous	FCO	-9.3	131000
Skua-3	2425	2428	122423	cuttings	quartz	aqueous	FCO	-10.1	140000
Skua-3	2425	2428	122423	cuttings	quartz	aqueous	FCO	-10.8	147000
Skua-3	2425	2428	122423	cuttings	quartz	aqueous	QOB	-0.6	10000
Skua-3	2425	2428	122423	cuttings	quartz	aqueous	QOB	-1.2	21000
Skua-3	2425	2428	122423	cuttings	quartz	aqueous	QOB	-1.2	21000
Skua-3	2425	2428	122423	cuttings	quartz	aqueous	QOB	-1.3	22000
Skua-3	2425	2428	122423	cuttings	quartz	aqueous	QOB	-1.7	29000
Skua-3	2425	2428	122423	cuttings	quartz	aqueous	QOB	-2	34000
Skua-3	2425	2428	122423	cuttings	quartz	aqueous	QOB	-2.1	35000
Skua-3	2425	2428	122423	cuttings	quartz	aqueous	QOB	-2.2	37000
Skua-3	2425	2428	122423	cuttings	quartz	aqueous	QOB	-2.2	37000
Skua-3	2425	2428	122423	cuttings	quartz	aqueous	QOB	-2.3	38000
Skua-3	2425	2428	122423	cuttings	quartz	aqueous	QOB	-2.5	42000
Skua-3	2425	2428	122423	cuttings	quartz	aqueous	QOB	-2.9	48000
Skua-3	2425	2428	122423	cuttings	quartz	aqueous	QOB	-3	49000
Skua-3	2425	2428	122423	cuttings	quartz	aqueous	QOB	-3.4	55000
Skua-3	2425	2428	122423	cuttings	quartz	aqueous	QOB	-3.5	57000
Skua-3	2425	2428	122423	cuttings	quartz	aqueous	QOB	-4.2	67000
Skua-3	2434	2437	122424	cuttings	quartz	aqueous	FCO	-1.5	25000
Skua-3	2434	2437	122424	cuttings	quartz	aqueous	FCO	-1.8	30000
Skua-3	2434	2437	122424	cuttings	quartz	aqueous	FCO	-2.5	42000
Skua-3	2434	2437	122424	cuttings	quartz	aqueous	FCO	-4.9	77000
Skua-3	2434	2437	122424	cuttings	quartz	aqueous	QOB	-1.5	25000
Skua-3	2434	2437	122424	cuttings	quartz	aqueous	QOB	-1.8	30000
Skua-3	2434	2437	122424	cuttings	quartz	aqueous	QOB	-1.8	30000
Skua-3	2434	2437	122424	cuttings	quartz	aqueous	QOB	-2	34000
Skua-3	2434	2437	122424	cuttings	quartz	aqueous	QOB	-2.5	42000
Skua-3	2434	2437	122424	cuttings	quartz	aqueous	QOB	-3.3	54000
Skua-3	2434	2437	122424	cuttings	quartz	aqueous	QOB	-4	64000
Skua-3	2434	2437	122424	cuttings	quartz	aqueous	QOB	-4.7	74000
Skua-3	2434	2437	122424	cuttings	quartz	aqueous	QOB	-4.8	75000
Skua-3	2434	2437	122424	cuttings	quartz	aqueous	QOB	-5	78000
Skua-3	2434	2437	122424	cuttings	quartz	aqueous	QOB	-7.1	106000
Skua-3	2434	2437	122424	cuttings	quartz	aqueous	QOB	-7.5	111000
Skua-3	2434	2437	122424	cuttings	quartz	aqueous	QOB	-10	139000
Skua-3	2434	2437	122424	cuttings	quartz	aqueous	QOB	-14.2	178000
Skua-3	2434	2437	122424	cuttings	quartz	aqueous	QOB	-15	184000
Skua-3	2434	2437	122424	cuttings	quartz	aqueous	QOB	-15	184000
Skua-3	2434	2437	122424	cuttings	quartz	aqueous	QOB	-17.5	202000
Skua-3	2434	2437	122424	cuttings	quartz	aqueous	QOB	-18.5	209000
Skua-3	2434	2437	122424	cuttings	quartz	aqueous	QOB	-19	212000
Skua-3	2434	2437	122424	cuttings	quartz	aqueous	QOB	-19	212000
Skua-3	2434	2437	122424	cuttings	quartz	aqueous	QOB	-19.3	214000
Skua-3	2434	2437	122424	cuttings	quartz	aqueous	QOB	-20	218000
Skua-3	2434	2437	122424	cuttings	quartz	aqueous	QOB	-20	218000
Skua-3	2434	2437	122424	cuttings	quartz	aqueous	QOB	-20	218000
Skua-3	2434	2437	122424	cuttings	quartz	aqueous	QOB	-20.5	220000
Skua-3	2434	2437	122424	cuttings	quartz	aqueous	QOB	-21	223000
Skua-3	2434	2437	122424	cuttings	quartz	aqueous	QOB	-21.5	226000

7.3.2 Composition of Current Formation Waters

Reliable estimates of current formation water salinities in the VSB are limited by the lack of samples or where samples exist contamination by drilling fluids. Salinities derived from electric log interpretation and water samples obtained by Repeat Formation Tester (RFT) represent the most commonly available data. Heavy mud filtrate contamination is indicated where chemical analyses are available with the majority of RFT samples from the VSB unlikely to be representative of the virgin formation water (Underschultz et al., 2002).

RFT data using a Tritium tracer allow the salinity of formation water to be ascertained with greater confidence. Tritiated water differs from normal water in that one of the hydrogen atoms in the molecule is replaced with an atom of tritium, the heavy isotope of hydrogen. Chemical tracers such as Tritium that are foreign to the sub-surface environment are added to the drilling fluid to assess the degree of drilling fluid contamination (Bennion et al., 2001).

In this study, salinity estimates that have been derived from electric log (resistivity or spontaneous potential logs) analysis have been used preferentially, although it is recognised that these data may also be prone to significant error based on the validity of the input parameters and associated assumptions. Nevertheless, these data represent the only widely available estimates of current salinity values and provide an opportunity, albeit cautiously, to investigate the regional salinity trends from the VSB. To augment the data collated in this study other published salinity data-sets for the VSB have also been utilised that include data from analysis of formation pressures (Underschultz et al., 2002).

Estimates of present day salinity range from about 20,000 ppm to more than 150,000 ppm (Figure 7–6). Salinities are consistently lower at the basin margin and increase markedly into the deepest parts of the basin (Figure 7–6). Salinities generally increase with depth, a trend that would be consistent with an expected increase in diagenesis with increasing burial depth (Figure 7–7, Hanor, 1994a).

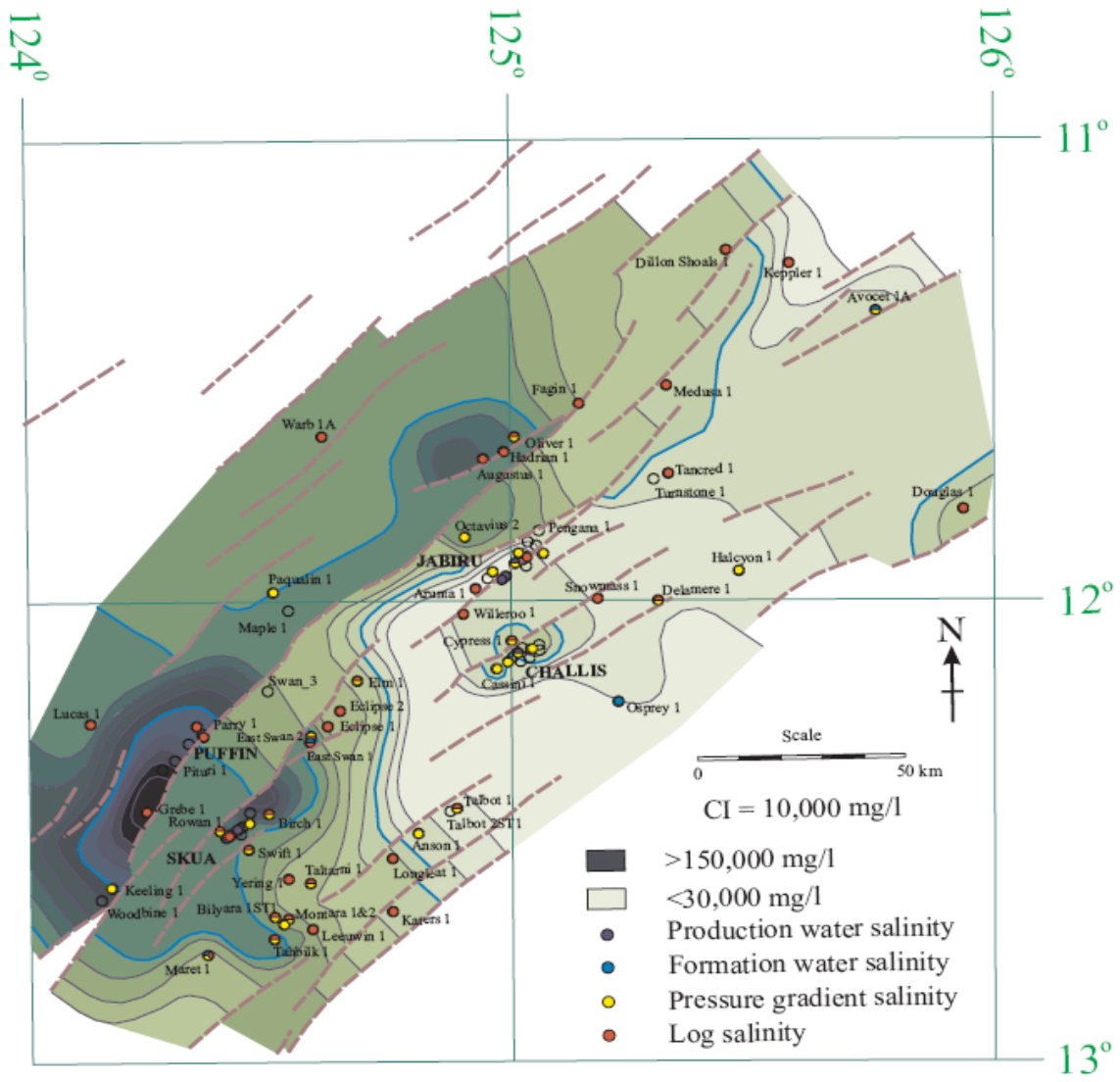

Figure 7-6: Current salinity values for the VSB

Contour map (from Underschultz et al., 2002) showing salinity (mg/litre) distribution for the Plover Formation aquifer across the VSB relative to the major structural elements (dashed lines represent major faults. Data are derived from recovered water sample, electric log and wireline pressure data. Salinity values decrease towards the basin margin in the east where there is potential for meteoric water recharge. The highest salinity values occur in wells located near the main depocentres (Swan Graben, Skua Trough and Cartier Trough) suggesting that increased diagenesis at greater burial depth is a key control on formation water salinity.

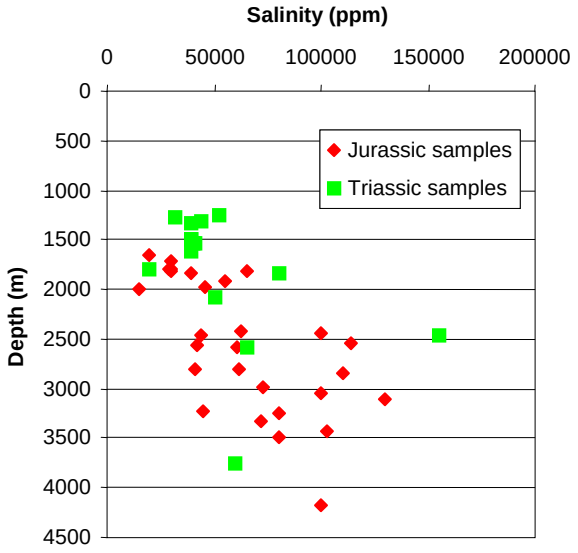

Figure 7-7: Salinity-depth trends for current formation waters

Graph of measured or calculated salinity derived from RFT recoveries or wireline log analysis against depth for the Triassic and Jurassic reservoirs in wells from the VSB. Data come from available well completion reports and have not been quality controlled. An overall increase in salinity with increasing depth of burial is observed at both levels and probably reflects increasing diagenesis and connate water modification at depth and is consistent with the geographic distribution of salinities (see map shown in Figure 7–6).

A few wells have current salinities that are higher than would be anticipated purely through diagenetic modification of connate waters but these outliers could be contaminated where hypersaline drilling fluids were used.

Formation waters with salinities below that of seawater (35,000 ppm) are rare in VSB wells and are restricted to relatively shallow buried reservoirs (Figure 7–6; Figure 7–7). The shallow depth does not support a clay-dehydration origin for these waters and infers meteoric water ingress if these are representative water samples.

7.3.3 Composition of Palaeo-formation Waters

In contrast to the present day formation waters, the fluid inclusion salinities show a wider range that indicates derivation of fluids from different sources (Figure 7–8). As waters with different salinity are miscible fluids, these variations can be taken to reflect changes in hydrology over time. Many of the fluid inclusion measurements can be attributed to change in salinity that is expected to occur during normal diagenesis that accompanies increasing burial. However, the maximum fluid inclusion salinities from many wells exceed 200,000 ppm (Figure 7–8) and are too high to reflect the modification of connate waters by diagenetic processes. Salinities of this magnitude are recorded on formation waters from basins with evaporite strata, either as salt beds, salt diapirs or related sabkha-type environments (Hanor, 1994b).

7.3.4 Source of the Hyper-saline Brines

The very saline fluids trapped in fluid inclusions are almost certainly derived from the dissolution of evaporite minerals by interaction with under-saturated formation waters. However, such evaporitic sediments have not been widely recognised within the Mesozoic section of the Vulcan Sub-basin, where the relatively high palaeo-latitudes that prevailed during Jurassic sedimentation are unlikely to have allowed the high evaporation rates that would be suitable for widespread salt formation.

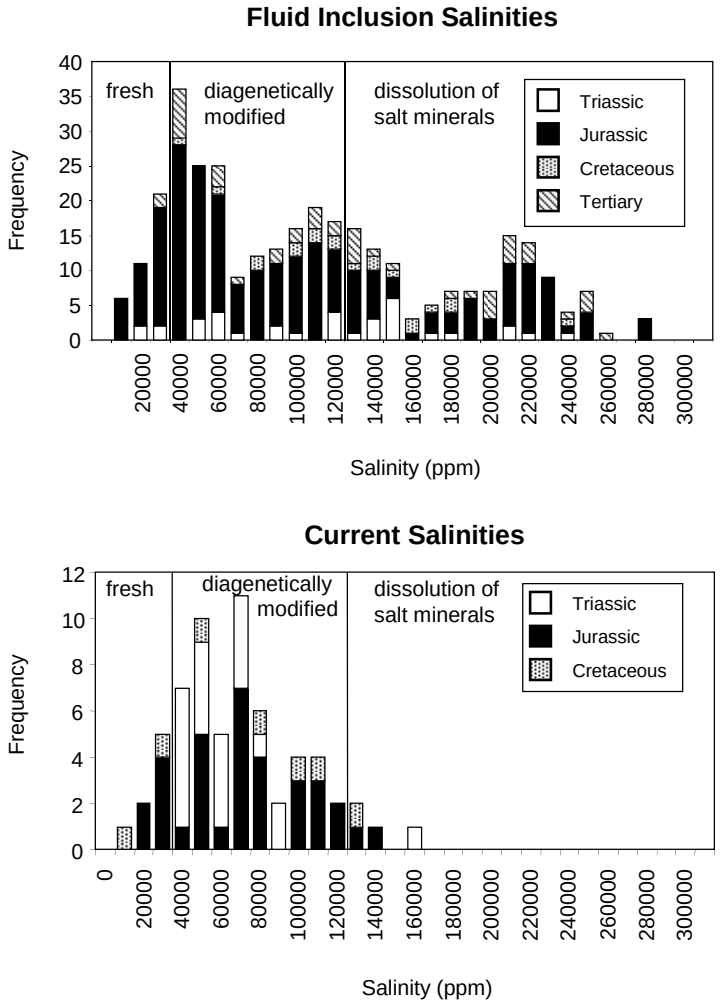

Figure 7-8: Comparison of current salinity versus fluid inclusion salinity.

Histograms of measured fluid inclusion salinity (upper) and formation water salinity (lower) split by stratigraphic location. The position of boundaries separating fresh water from diagenetically modified and waters derived from the dissolution of salt minerals are approximate and broadly consistent with ranges described in Hanor (1994a, b). The miscible nature of formation waters of different salinity indicates formation water salinity has changed through time, with at least three discrete end-member processes recognised.

The most obvious source of the brine seen in fluid inclusions from the VSB is the same sequence that sourced the drilled Paqualin and geophysically inferred Swan salt diapirs within the Paqualin Graben which pierce through the Mesozoic and Tertiary sequence as high as Miocene sediments (Smith and Sutherland, 1991; Woods, 1994).

The age of this salt (by analogy with the Carribuddy Group in the onshore Canning Basin) has been inferred to be Silurian-Devonian (Mory, 1988; O'Brien et al, 1996b), an age supported by recent strontium isotope determinations (O'Brien et al, 1998a).

It should be recognised, however, that definitive evidence for either the age, or the exact distribution, of evaporites in the VSB is lacking, a problem exacerbated by the generally poor seismic resolution below the Near Top Permian seismic marker that precludes definitive salt identification. Some workers (e.g. Woods, 1992) have, proposed that a Palaeozoic salt layer is widespread across the Timor Sea and may have acted as a detachment surface on which the subsequent Mesozoic and Tertiary fault systems developed.

7.3.5 Mechanisms for Brine Migration

The dissolution of the Paqualin and Swan salt diapirs (Figure 7–9) represents one opportunity for hyper-saline fluids to access juxtaposed Mesozoic sandstones. Formation waters dissolving salt from the flanks of these salt diapirs will flow down-dip given the significant density difference between these fluids and the much lower salinity of existing connate waters.

A simplified depth-structure map for the Base Cretaceous surface based on constraints from well penetrations alone (Figure 7–10) demonstrates that the migration of brine from the dissolution of these salt diapirs alone cannot account for the observed distribution of high salinities with most samples located in wells that are up-dip from the Swan and Paqualin wells. Instead, the widely spaced distribution of samples with high-salinity fluid inclusions (Figure 7–11) is more consistent with a geographically extensive salt layer, with faults providing the vertical conduits for flow into the shallow section.

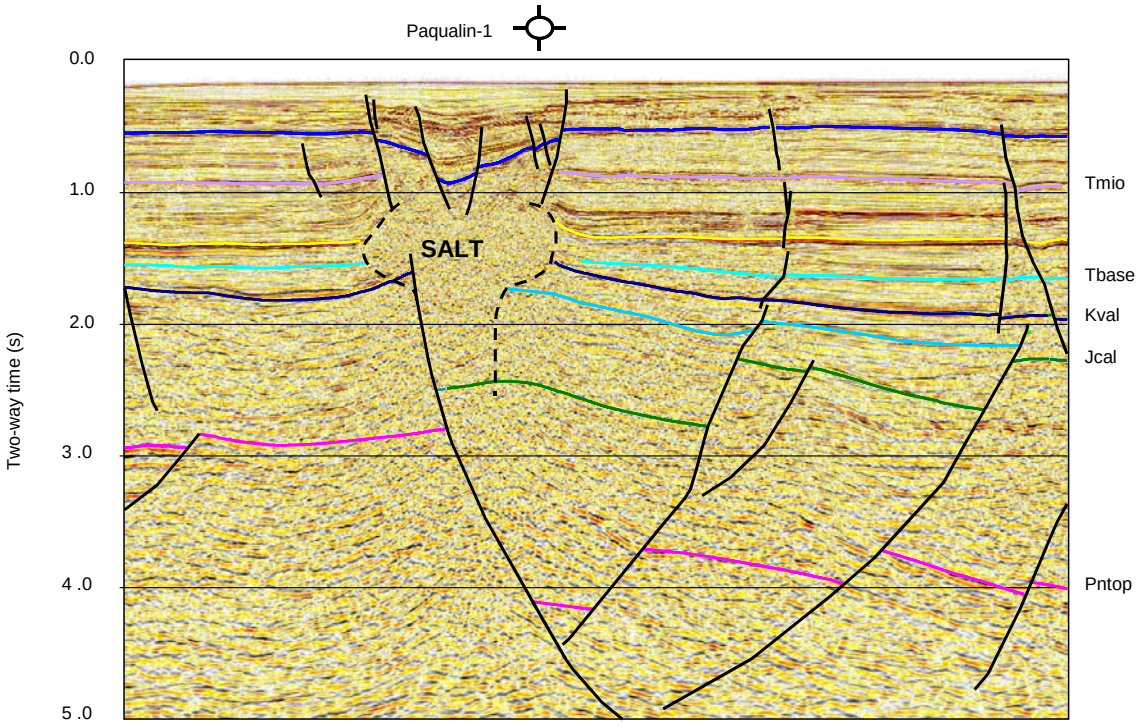

Figure 7-9: Seismic line through the Paqualin Salt Diapir.

Interpreted 2D seismic line (VTT 163-10) seconds in two way time across the Paqualin salt diapir penetrated by the Paqualin-1 well. Horizons referred to include Top Miocene (Tmio), Base Tertiary (Tbase), Valanginian (Kval), Callovian (Jcal) and top Permian (Pntop). Note the extensional faults that occur across the crest of the salt diapir and represent collapse related to salt dissolution (Modified from Lisk et al., 1999 and O'Brien et al., 1996c).

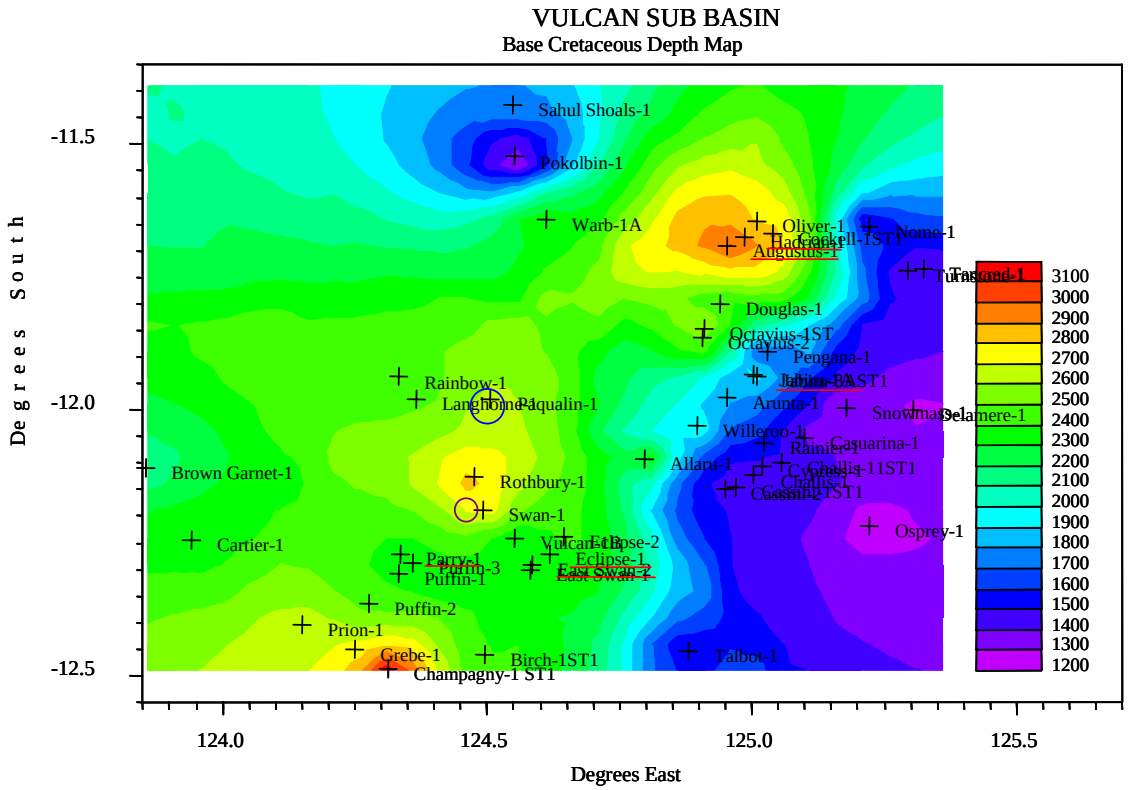

Figure 7-10: Base Cretaceous depth map.

Simplified Base Cretaceous surface derived from gridding (by interpolation) of well stratigraphy data. Whilst not as detailed as an interpreted seismic horizon the key highs that flank the VSB (Ashmore Platform to the west and Londonderry High to the east) and the major depocentres of the Cartier and Paqualin troughs and the northern edge of the Swan Graben can be recognised. Flow of brine derived from the Paqualin (blue circle) or Swan (purple circle) salt features is likely to flow down-dip due to density contrasts into the adjacent Paqualin Graben and hence is unlikely to be the source of all of the high salinity fluids that are trapped within fluid inclusions (wells shown underlined in red).

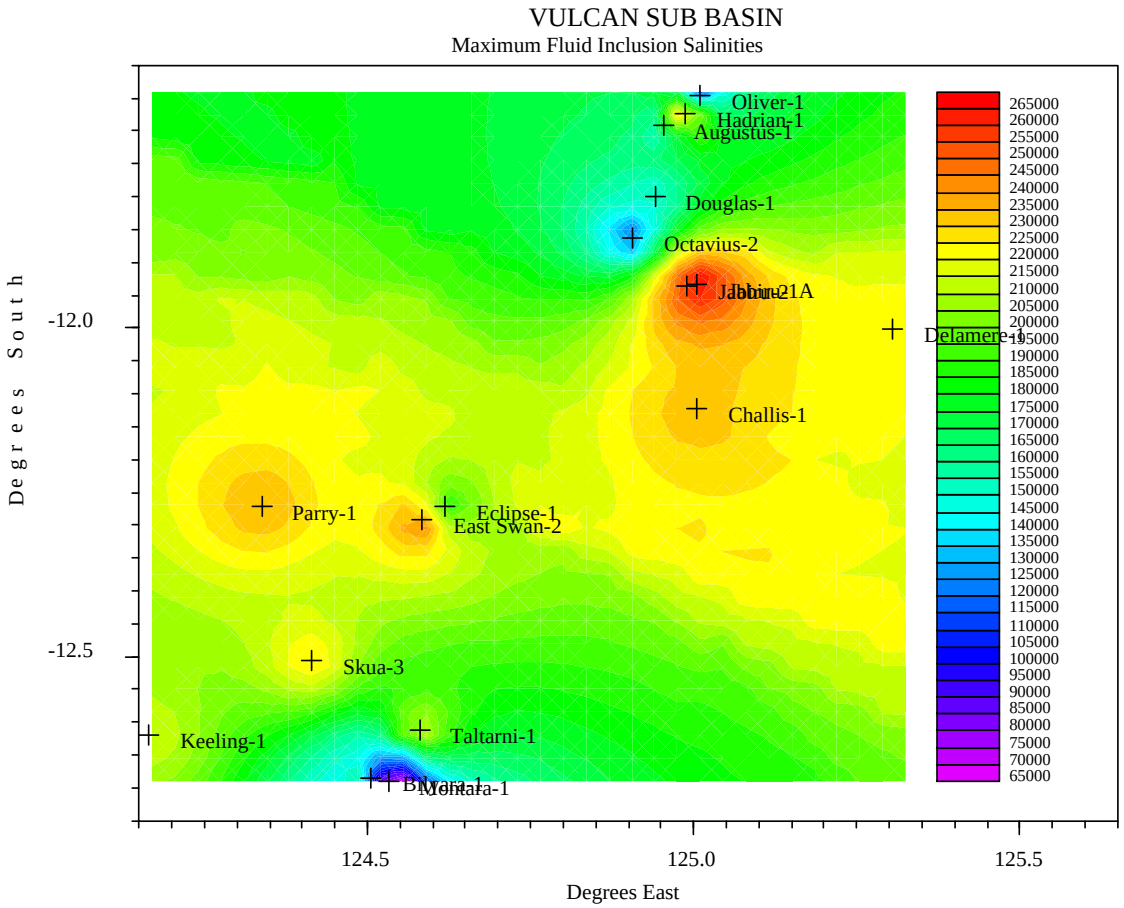

Figure 7-11: Distribution of maximum salinity values indicated from fluid inclusion results.

Contour map based on maximum salinity (in ppm) values recorded in fluid inclusions from samples in each of the wells shown. The highest values recorded occur in wells located on the structurally high parts of the basin (compare with Figure 7–10) and this distribution is not consistent with the expected accumulation of dense brine in structural lows.

The migration of hypersaline fluids was probably facilitated by the reactivation of fault systems into the Mesozoic and Tertiary section during margin scale tectonism/foreland development associated with plate convergence and increased burial in the Mio-Pliocene (O'Brien et al, 1998a,b). Fluid-flow may also have been driven by the release of significant sub-salt overpressure deep in the section by fault reactivation at this time (see O'Brien and Woods, 1995; O'Brien et al, 1996a).

The absence of ultra-high salinities in the current formation waters indicates that the flow of brine has ceased and that high salinity fluids have been diluted or have subsided into the deeper parts of the basin due to density contrasts with the surrounding connate water. Brine flow driven by the release of sub-salt overpressure is likely to have been short-lived with fault breaching allowing a rapid return to hydrostatic conditions and an associated loss of hydraulic head needed to support upwards migration of a dense brine plume.

7.4 SIGNIFICANCE OF OBSERVED PALAEO-SALINITY VARIATIONS

The recognition of large salinity variations in the VSB is more significant for hydrocarbon exploration than it may initially appear. Aside from indicating a dynamic basin history and revealing a potential link with regional fault reactivation the distribution of high salinities reveals a more direct link with distribution of hydrocarbon fluids. Closer examination of the fluid inclusion salinity data reveals an important pattern in the distribution of samples with high salinities.

7.4.1 Salinity Distribution in Current Hydrocarbon Fields

Fluid inclusions in samples from current hydrocarbon zones generally show a more restricted range in salinity than is observed in samples taken from below the current oil water contact (OWC, Figure 7–12). In samples taken from within six of the seven current, intact, hydrocarbon columns studied, the fluid inclusion salinities range between about 12,000 ppm and 131,000 ppm NaCl equivalent (Figure 7–13). This salinity range is generally consistent with that expected for diagenetically modified marine connate water under a closed system environment.

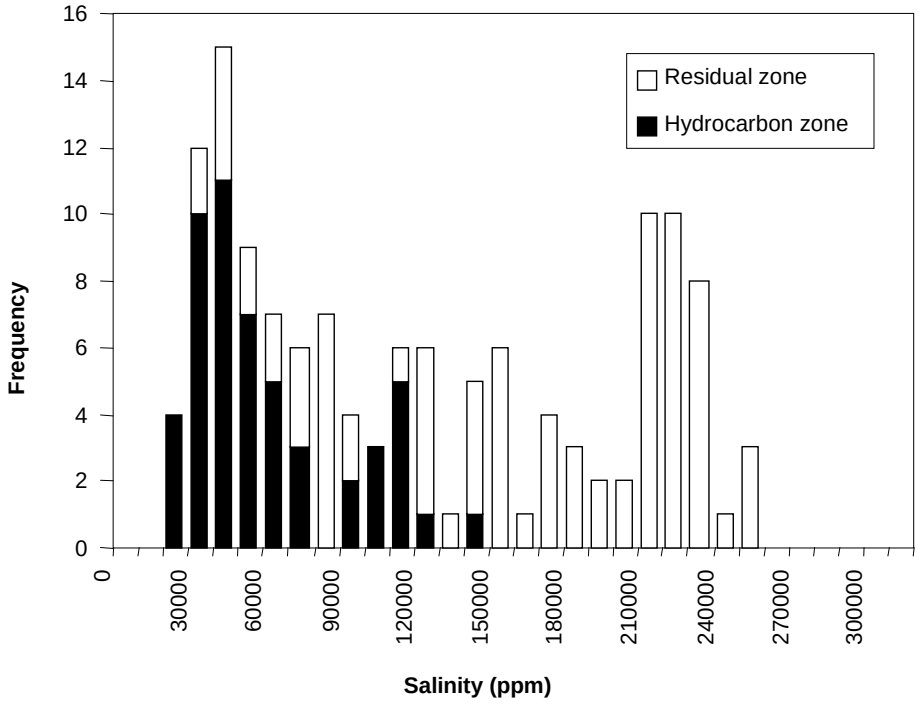

Figure 7-12: Fluid inclusion salinity data from intact versus breached traps.

Histogram of salinity values inferred from ice melting temperatures recorded on fluid inclusions from samples taken within currently hydrocarbon bearing reservoirs compared against values recorded on samples from residual zones interpreted below the current OWC. A more restricted salinity range observed in samples from the current hydrocarbon zones implies access of high salinity fluids was prevented by the presence of hydrocarbons (due to low relative permeability to water), in turn suggesting that brine flow post-dated the accumulation of hydrocarbons.

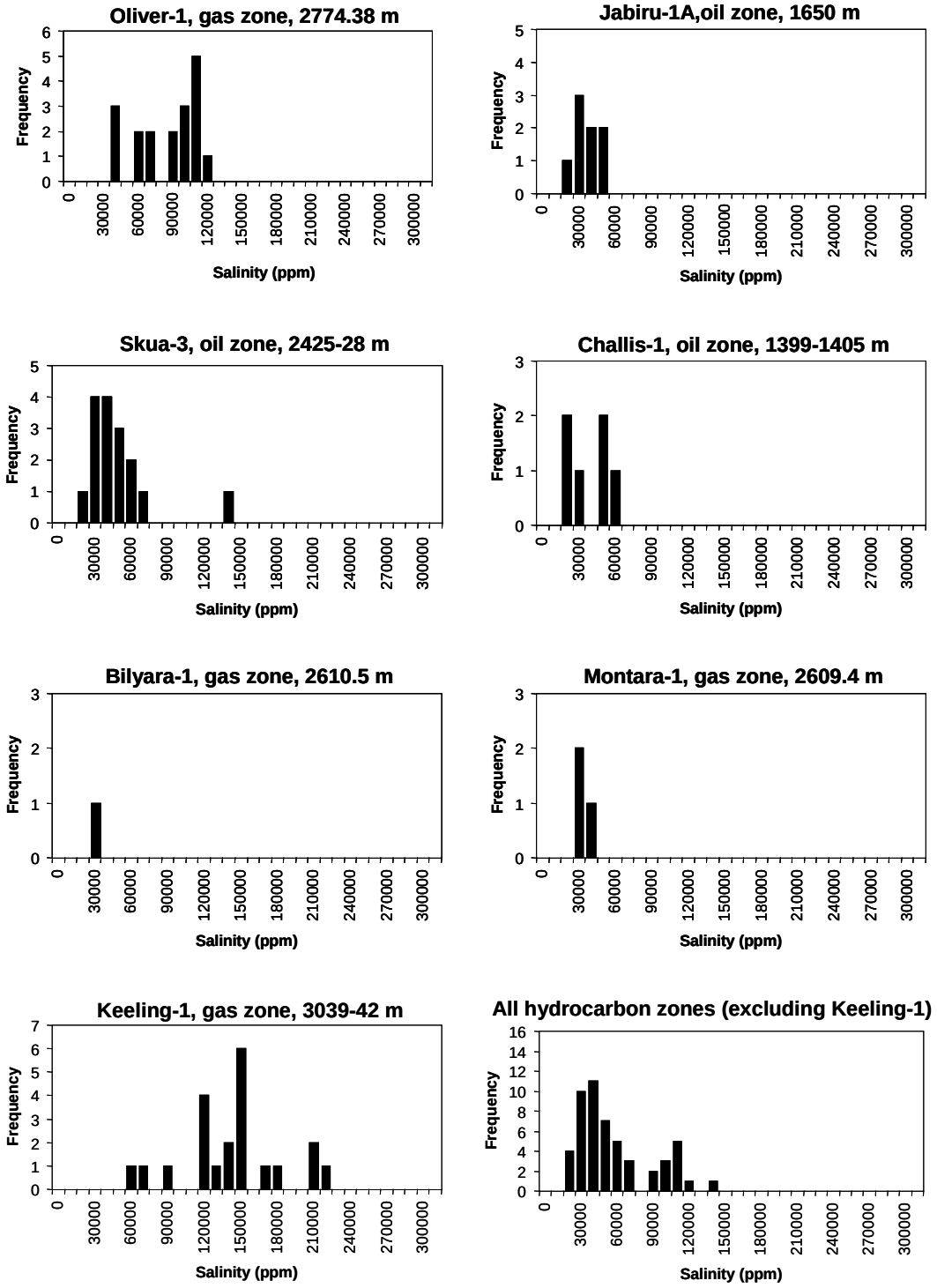

Figure 7-13: Fluid inclusion salinity results from intact hydrocarbon zones.

Histograms of fluid inclusion salinity results for samples from currently hydrocarbon bearing rocks that collectively make up the "hydrocarbon zone" series in Figure 7–13.

In contrast, samples taken from below the current OWC, where maximum salinity values recorded in the fluid inclusions generally peak above 200,000 ppm (Figure 7–12, Figure 7–14), are too high to be achieved by normal diagenesis and infer ingress of fluids that are derived from the dissolution of evaporites.

The observed salinity distribution suggests migration of the most saline fluids post-dated the accumulation of hydrocarbons, with high saturation with oil or gas acting to isolate these zones from hydrologic changes occurring in the underlying water-leg (Figure 7–15) due to low relative permeability to water.

The Keeling-1 gas discovery is the only example where high-salinity fluid inclusions have been recorded in a current hydrocarbon zone (Figure 7–13). In contrast to the other hydrocarbon zones studied, the presence of high-salinity fluid inclusions in the Keeling-1 gas zone suggests brine migration occurred prior to gas charge.

7.4.2 Salinity Distribution in Water-wet Wells

Results from wells that are currently water-saturated can be grouped into two categories based on the interpreted hydrocarbon charge history, those that once contained a hydrocarbon column (palaeo-hydrocarbon columns) and those that have never experienced high hydrocarbon saturation.

7.4.2.1 Palaeo-hydrocarbon Columns

Fluid inclusion salinities measured on samples from three of the four palaeo-oil columns investigated have similar variations to those observed in the residual and water zone samples from the aforementioned hydrocarbon fields (Figure 7–16). These observations are consistent with loss of oil from these traps also being caused by fault breach with the injection of brines from depth and the attendant vertical leakage of hydrocarbons either into the shallower section or through complete loss into the water column.

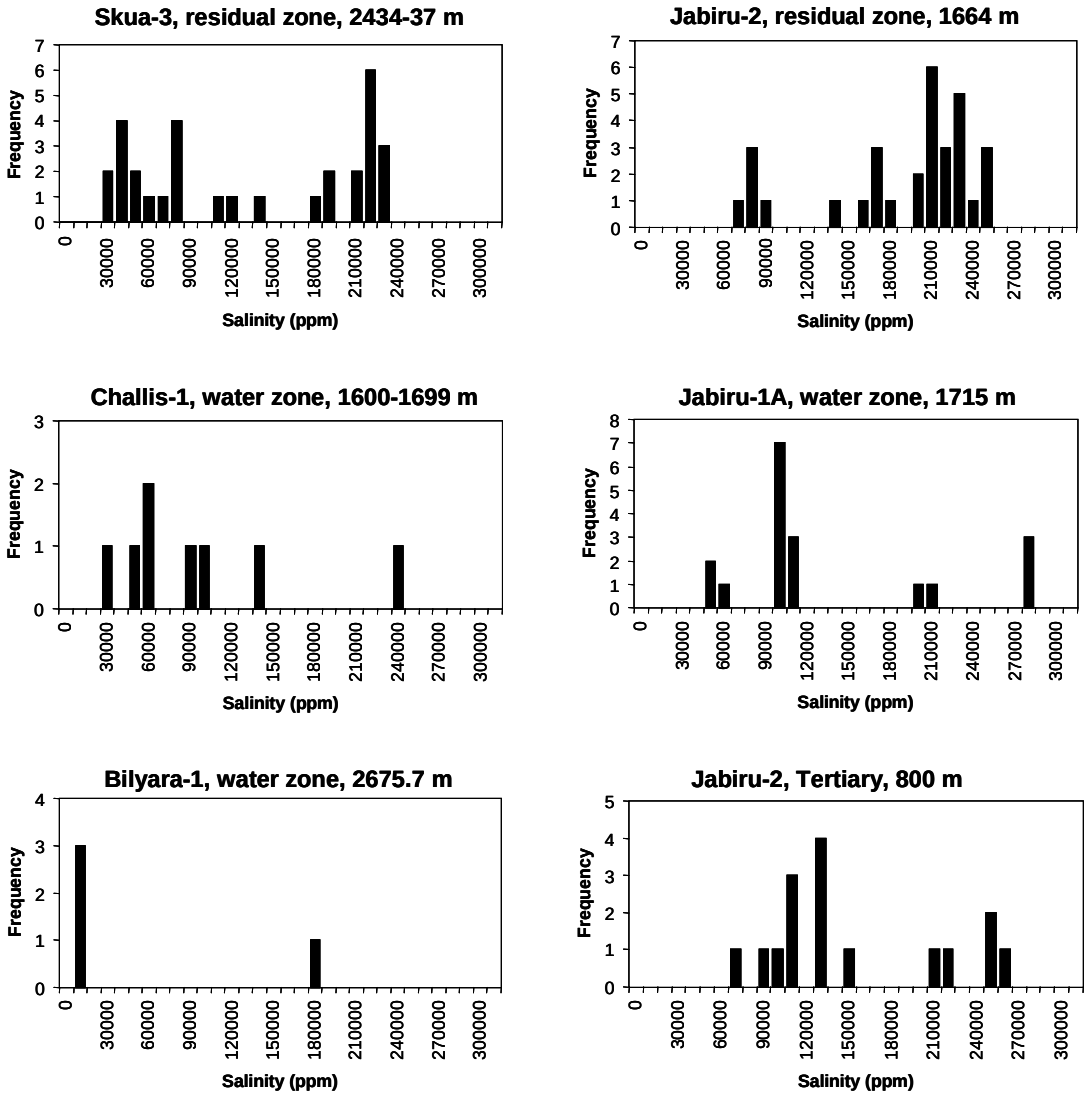

Figure 7-14: Fluid inclusion salinity data from residual and water zones.

Histograms of fluid inclusion salinity results for samples from currently water bearing rocks that collectively make up the "residual zone" series in Figure 7–13.

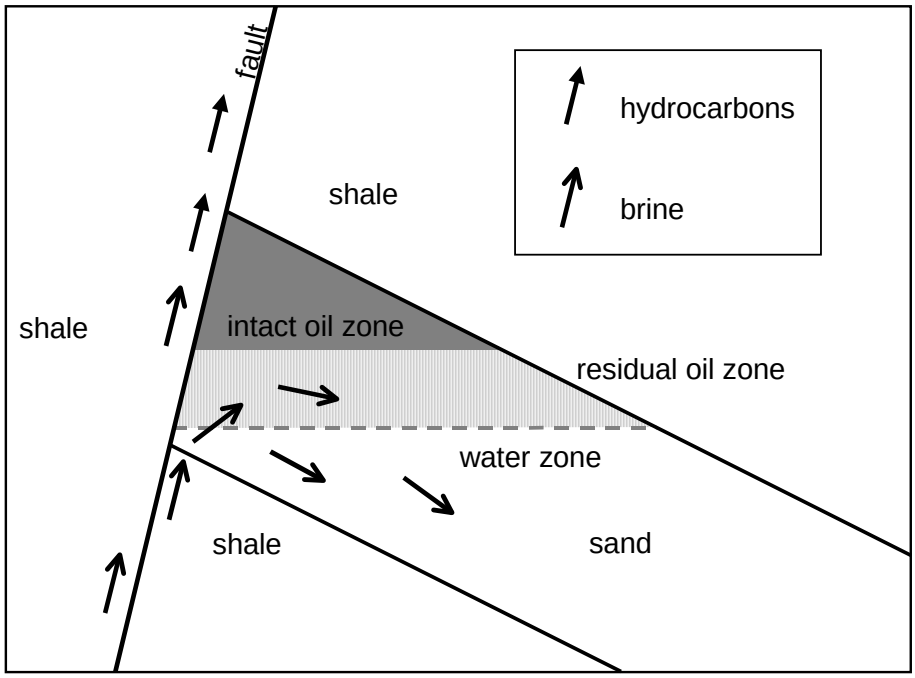

Figure 7-15: Cartoon showing brine flow pathways into partially breached oil column.

Example of fluid migration pathways for hydrocarbons (solid arrows) and formation water (open arrows) during reactivation of the bounding fault of a tilted fault block trap. Hypersaline formation water derived from depth flows within the fault whilst the fault zone permeability is greater than the host rock and into the formation where the formation permeability exceeds the fault zone permeability. Leakage of hydrocarbons allows hypersaline water to access the residual zone as well as the water-leg but continued high hydrocarbon saturation in the intact oil zone continues to prevent ingress of high salinity brine.

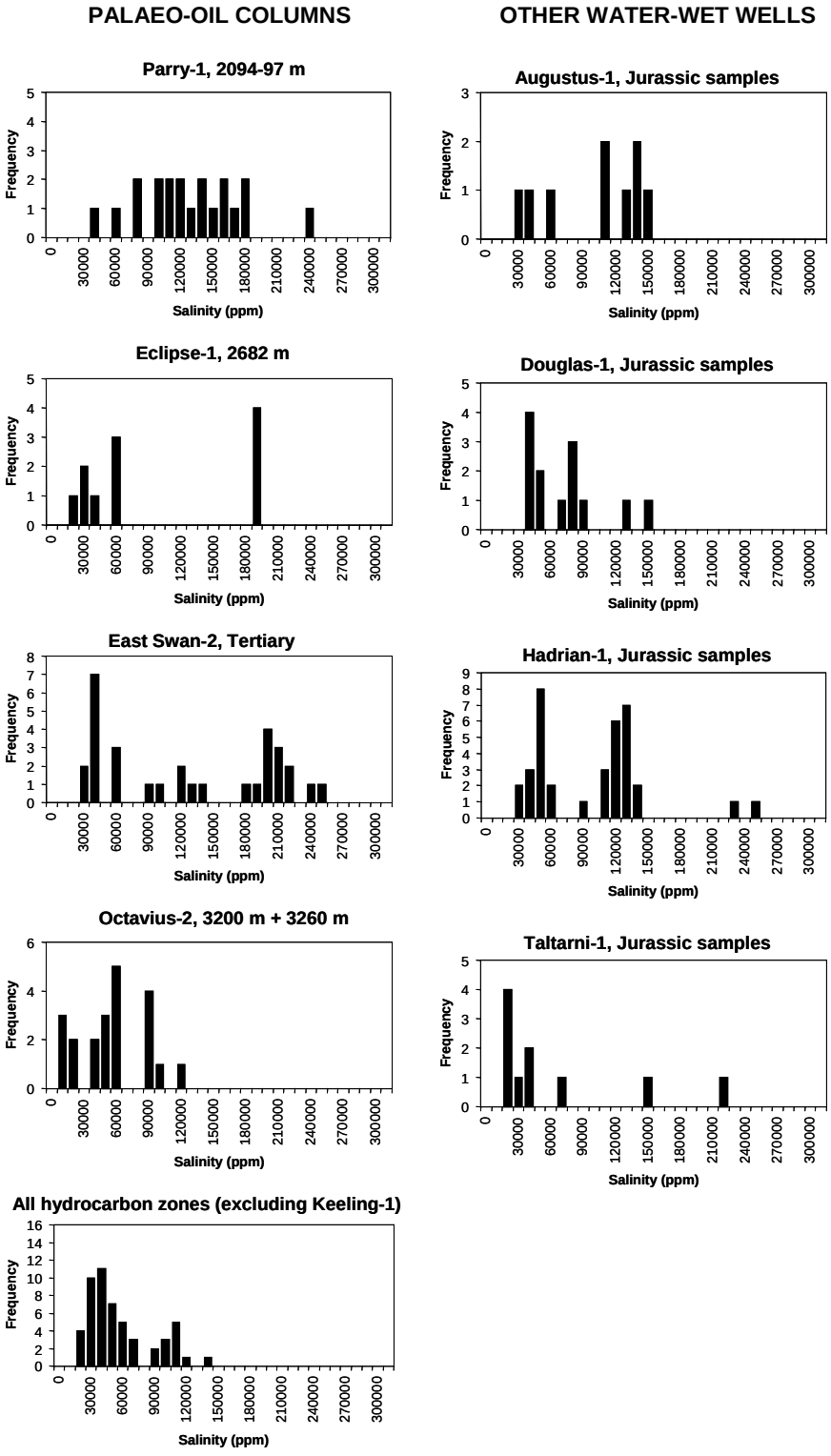

Figure 7-16: Fluid inclusion salinity data from currently water-wet wells.

Histograms for wells where a palaeo-oil column has been detected (left) compared with wells that are interpreted to have always been water-wet (right). High salinity values are prevalent in 3 of the 4 palaeo-oil zones sampled suggesting that trap breach and brine flow are associated events.

In contrast, the fluid inclusion salinities recorded in the Octavius-2 palaeo-oil column (Figure 7–16) are more similar to the range recorded in current hydrocarbon columns (Figure 7–16) and in this instance fault breach is not inferred. This observation highlights the potential value of palaeo-salinity data as a tool to ascertain the likelihood of trap breach and could in this instance suggest that processes other than catastrophic trap breach have been responsible for the loss of oil.

7.4.2.2 Palaeo-migration Pathways

Samples taken from the four wells examined in this study with no evidence of prior oil accumulation also have some fluid inclusions that contain high-salinity brine (Figure 7–16), suggesting that these traps have also been affected by Neogene fault reactivation but were not hydrocarbon bearing previously.

All traps where high salinity fluids have been recognised have experienced some degree of reactivation and together with the absence of hypersaline brines in nearly all current hydrocarbon zones a causal effect is inferred. However, it is also conceivable that the high-salinity fluids may have had entry points to Mesozoic reservoirs, which are remote from the well location. Downward flow of brine, driven by density contrasts with the resident connate waters, could allow brine to flow past well intersections that are distal from the point of injection. Entry points for brine flow are likely to be focused along the flanks of the basin where the degree of fault reactivation was more intense, thus allowing the current basin depocentres to act as ‘sinks’ for these more dense fluids.

7.5 THERMAL IMPACT OF BRINE FLOW

Aside from the potential dissolution of salt diapirs the majority of brines trapped within fluid inclusions in samples from the Mesozoic and Tertiary section are most likely derived from Palaeozoic evaporite beds deeper in the VSB. Whilst these beds have not been drilled features on seismic data interpreted to be salt pillows (Figure 7–17) are present at about 7 seconds two-way-time (TWT), corresponding to depths of about 9km (Woods, 1994).

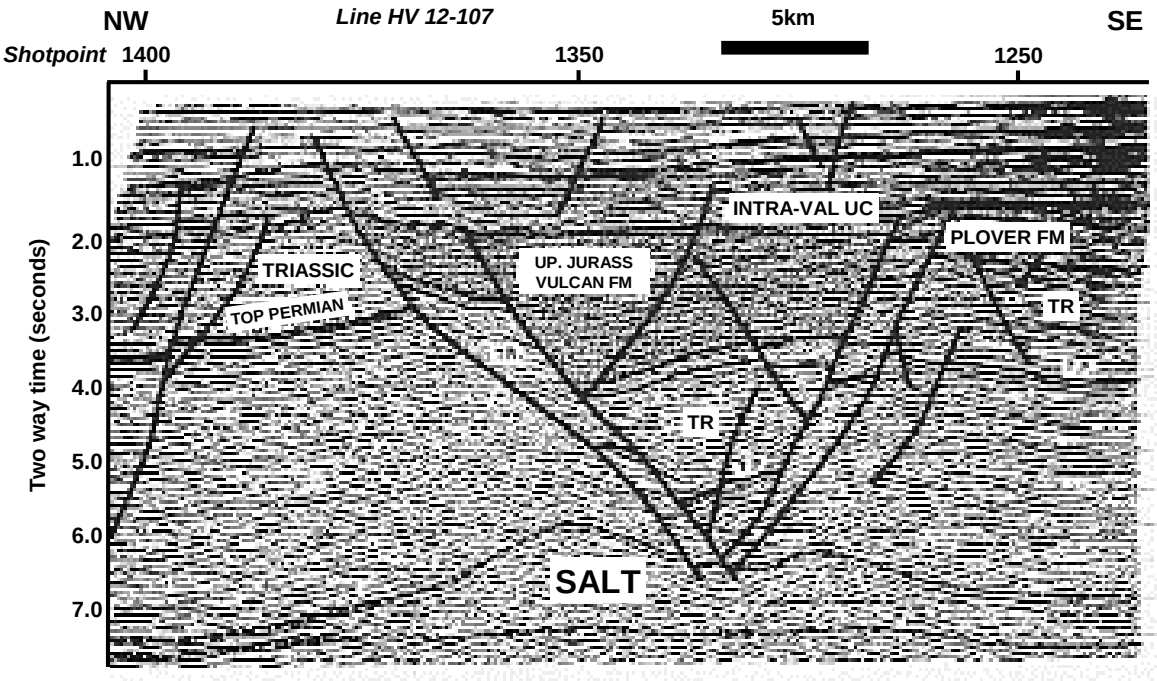

Figure 7-17: Seismic image showing interpreted salt pillows.

Interpreted 2D seismic line (HV12-107) from the Vulcan Sub-basin showing mounded features below about 6 seconds two way time that have been interpreted as possible salt pillows (From Woods, 1994).

Hypersaline brine derived from these salt beds are likely to be hot given the burial depth of the inferred source. Using an average geothermal gradient of 30°C/km for the VSB temperatures can be estimated to have been about 250–300°C at source and the migration of these fluids into the shallow section may have imparted a significant convective heat transfer effect associated with rapid fluid-flow.

The potential for hydrothermal distortion related to fluid flow has been widely documented in numerical modelling studies (Roberts, 2001; Roberts and Nunn, 1995; Smith and Chapman, 1983; Person and Garvin, 1992) but published well calibrated field examples are more restricted.

7.5.1 Impact on Palaeo-temperature Indicators

The timing of brine flow is most likely related to intense Neogene fault reactivation. O'Brien et al. (1998) modelled fission track decay to demonstrate that any convective thermal effect associated with brine flow would be relatively short lived and consequently it is more likely that evidence of thermal perturbation associated with brine flow will be most evident in palaeo-temperature indicators. These indicators could include techniques that measure accumulated thermal stress such as vitrinite reflectance and apatite fission track data or direct measurement of palaeo-formation temperature provided by fluid inclusion thermometric measurements. Other indirect observations such as illite-smectite transformations (Xie et al., 2001) or a range of geochemical maturation parameters (Whelan et al., 1994) could also be used to recognise transient heating events.

7.5.1.1 Measured Palaeo-temperatures

Fluid inclusion palaeo-temperatures from some breached palaeo-oil columns appear to define higher temperatures for inclusions that contain high-salinity fluids. Cross-plots of calculated salinity against measured homogenisation temperature for aqueous inclusions are shown in Figure 7–18 and whilst some positive correlations are shown there is also considerable variability.

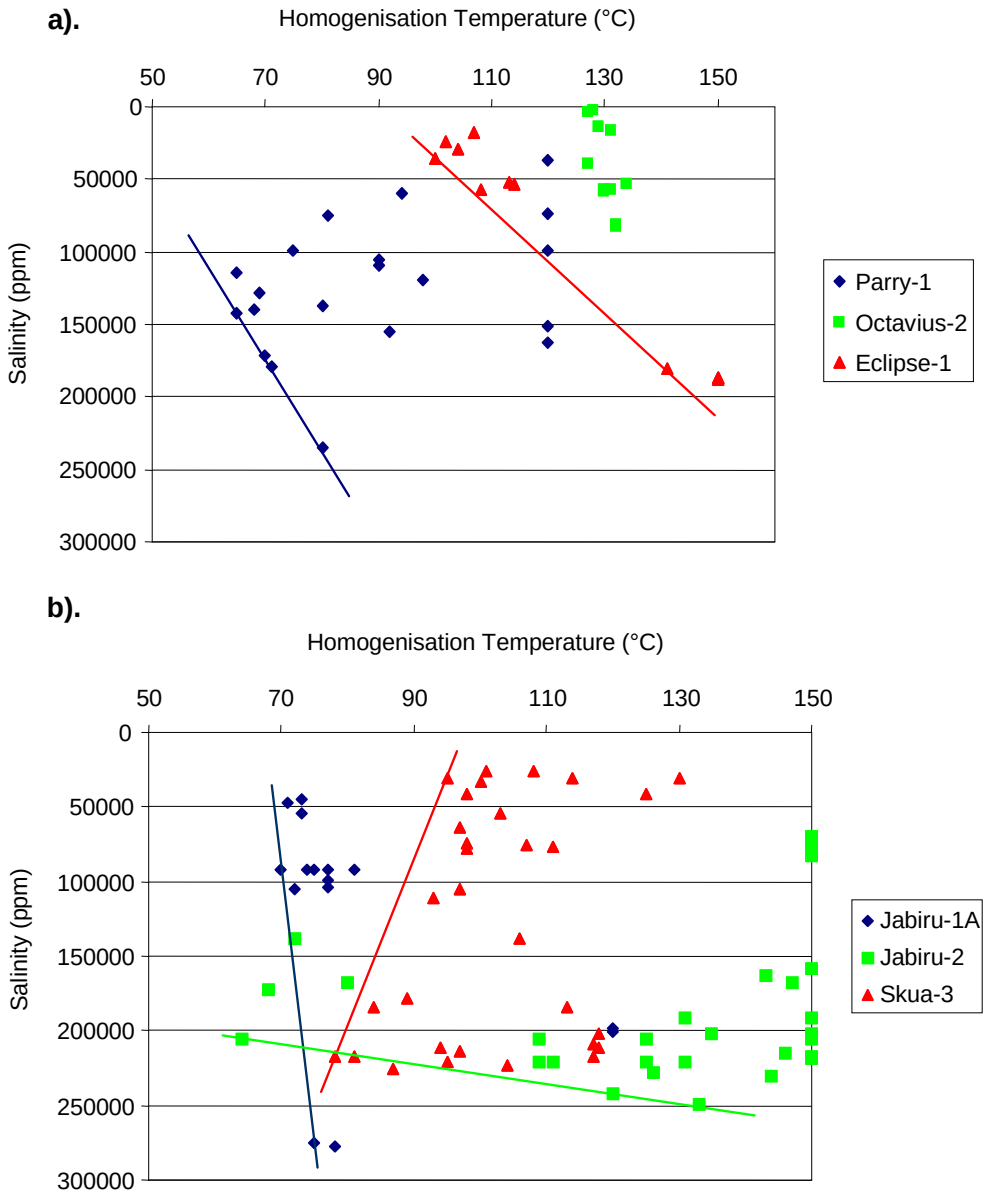

Figure 7-18: Cross plots of homogenisation temperature against salinity

Fluid inclusion homogenisation temperatures are plotted against fluid inclusion salinity measurements for wells investigated from the Vulcan Sub-basin. a). Selected wells where there appears to be a positive relationship between minimum homogenisation temperatures and measured salinity with higher salinities associated with higher temperatures. Temperatures that plot to the right of the trend line are interpreted to be affected by heterogeneous trapping and are unlikely to be geologically valid temperatures. b). Data from selected oil field residual zones showing more variable relationships including both positive and negative correlations between temperature and salinity.

In evaluating these data, the minimum fluid inclusion homogenisation temperatures are used to lessen the influence of inclusions that have trapped mixtures of pore water and gas, as this produces erroneously high temperatures. In currently water-wet traps where a palaeo-oil column has been interpreted these cross plots show trends of increasing salinity with higher minimum homogenisation temperature consistent with higher temperatures during brine migration (Figure 7–18).

Similar plots from reactivated oilfields, however, show a more chaotic pattern (Figure 7–18) and clear evidence of heating cannot be strongly demonstrated from the fluid inclusion data alone.

7.5.1.2 Apatite Fission Track Analysis Data

Apatite Fission Track Analysis (AFTA) provides a powerful tool to constrain thermal history. The technique relies on the gradual annealing of detrital apatite grains during heating, allowing both the magnitude and timing of thermal events to be determined (Gleadow and Duddy, 1981; Gleadow et al., 1983; Green et al., 1989).

O'Brien et al. (1996a) cited Apatite Fission Track Analysis (AFTA) data to support localised heating in sediments from oil fields in the VSB that are leaking at the present day. In Challis-1 for example the distribution of fission track lengths and the progressively increasing apatite ages (Figure 7–19) point to palaeo-temperatures of up to 60°C hotter than the current reservoir temperature. The AFTA profiles cannot be explained by higher heat flow or burial and instead a convective heating event is interpreted (O'Brien et al., 1996a). In contrast, in inferred high integrity structures, such as the Oliver-1 well, the AFTA data reconcile closely with the current reservoir temperatures (Figure 7–19) and can be explained using conductive heat transfer.

7.5.1.3 Vitrinite Reflectance Data

Vitrinite reflectance data provide a measure of the accumulated thermal stress, being sensitive to the maximum temperatures experienced during the entire burial history.

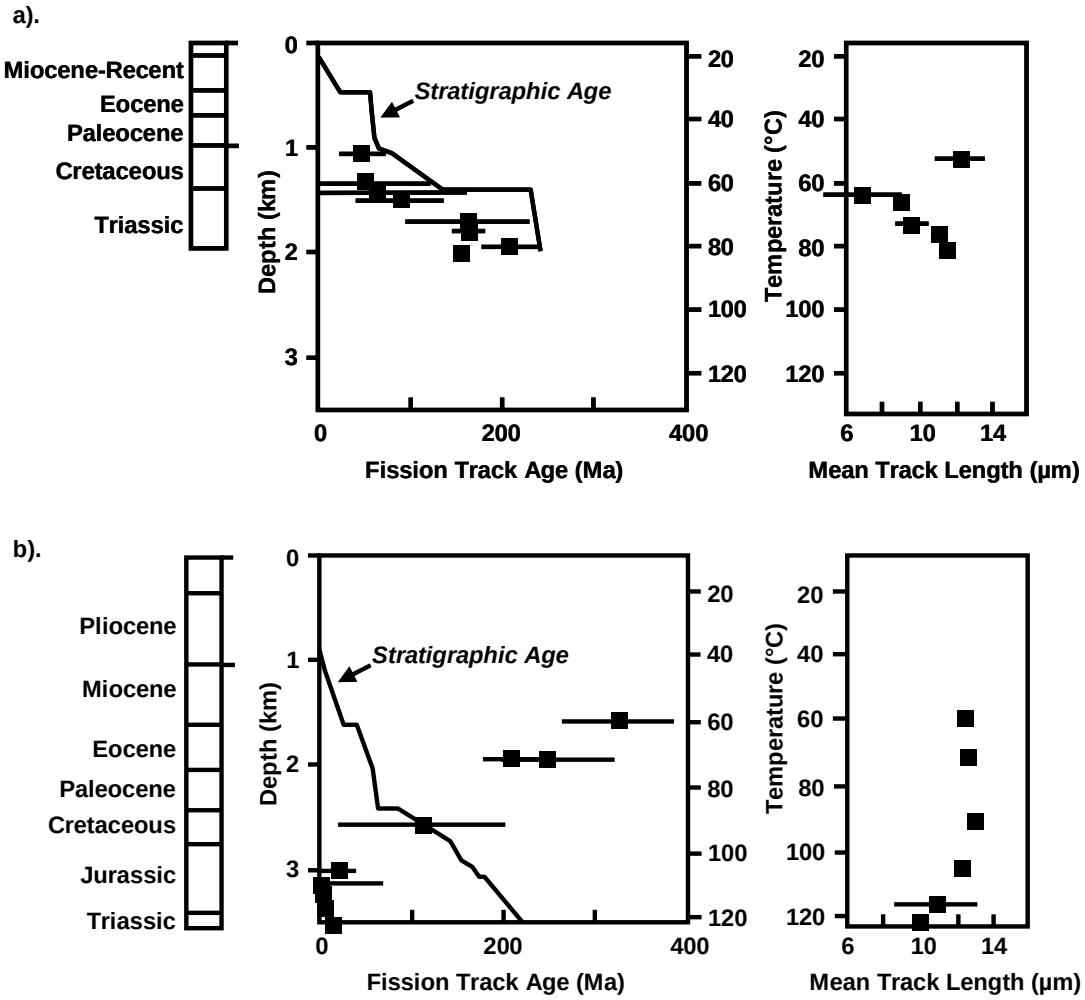

Figure 7-19: AFTA results from the Challis-1 and Oliver-1 wells.

AFTA parameters of track length and apatite age plotted against sample depth and present temperature for samples from a). Challis-1 and b). Oliver-1 wells. The variation of stratigraphic age is also shown as the solid line in the middle panel. In Challis-1 the apatite age and mean track length both increase down the well pointing to anomalously high temperatures in the geological past. In contrast the profiles shown by the Oliver-1 samples the apatite age and the mean track length decrease down hole and are consistent with the observed current reservoir temperature being the maximum.

Vitrinite reflectance measurements are principally obtained from shales that contain suitable organic matter. Sampling of shales also reduces the impact of oxidation that can affect vitrinite particles within rocks with more dispersed organic matter such as shaly sandstones. However, heat transfer by convection related to fluid flow will be the greatest within sandstones where the rock permeability is likely to exceed the permeability of the fault plane allowing brine flow into the formation.

Impermeable shales are less likely to experience the effects of convective heating where low permeability will have focused brine flow within the fault plane, restricting the extent of any thermal aureole (Figure 7–20). Only shales immediately adjacent to aquifer units or intercalated with the sandstones are likely to experience localised heating in a similar manner to the alteration of country rock that accompanies contact metamorphism (Figure 7–20). In most wells the existing vitrinite reflectance data are widely spaced and are not in an optimal position to detect localised heating.

A compilation of vitrinite reflectance (VR) data from wells in the Vulcan Sub-basin, with interpolation used to estimate thermal maturity immediately above the Callovian unconformity (Figure 7–21), shows no clear evidence of advanced maturation by localised convective heating. Rather the measured maturity levels appear to be varying primarily in response to the burial depth (Figure 7–22).

7.5.1.4 Fluorescence Alteration of Multiple Macerals (FAMM)

In an effort to address the sample location problems encountered with the existing vitrinite reflectance data a small suite of conventionally measured Vitrinite Reflectance (VR) data and FAMM (Fluorescence Alteration of Multiple Macerals) data were acquired from a key well to test the convective heating concept.

Samples for this experiment were preferentially sought directly adjacent to potential high permeability aquifers where the thermal impact of hot brine migration is likely to have been greatest (Lisk et al., 2000b).

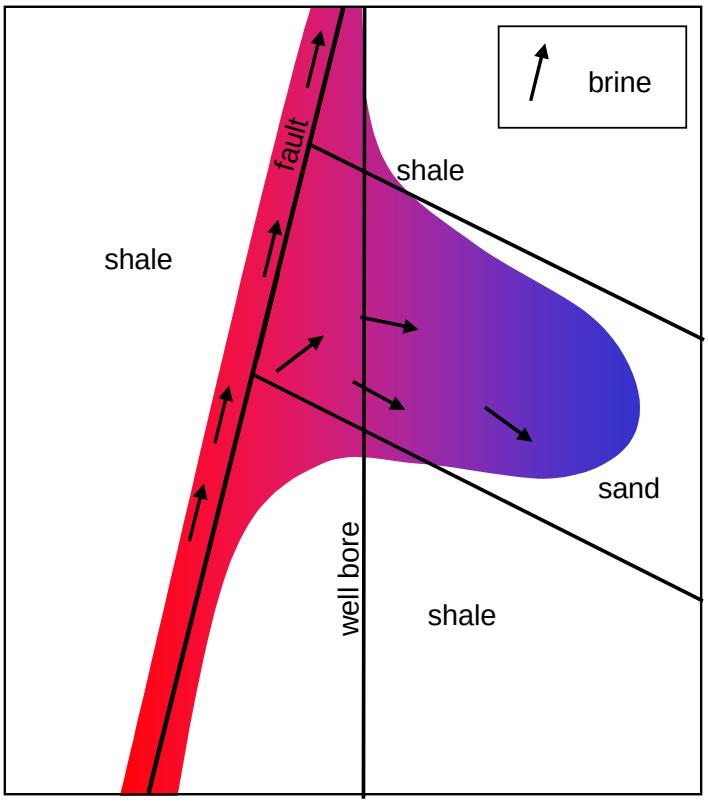

Figure 7-20: Cartoon showing probable thermal effect of brine flow.

Vertical flow of brine along the fault plane enclosed by low permeability shale is likely to impart only a limited convective heating affect whereas intersections with high permeability sandstones will allow flow of brine out of the fault plane into the formation thereby enlarging the extent of localised heating.

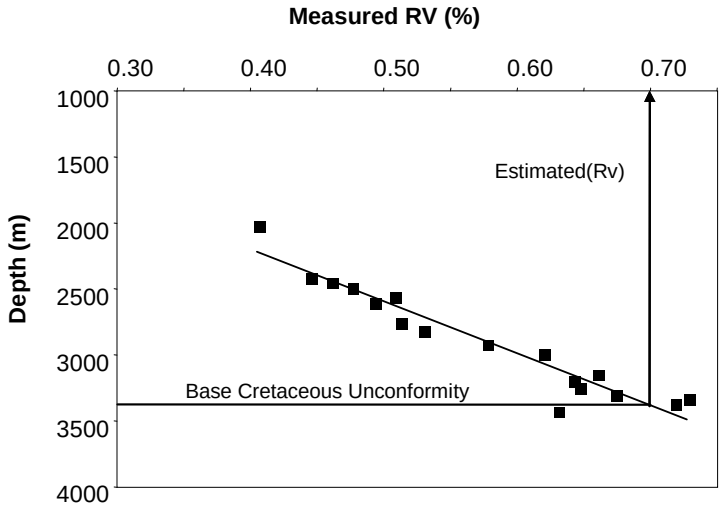

Figure 7-21: Method used to define thermal maturity at the Callovian Unconformity.

A schematic example showing a profile of measured vitrinite reflectance (R_v) measurement against depth with the Base Cretaceous Unconformity corresponding to an interpolated R_v of about 0.7%.

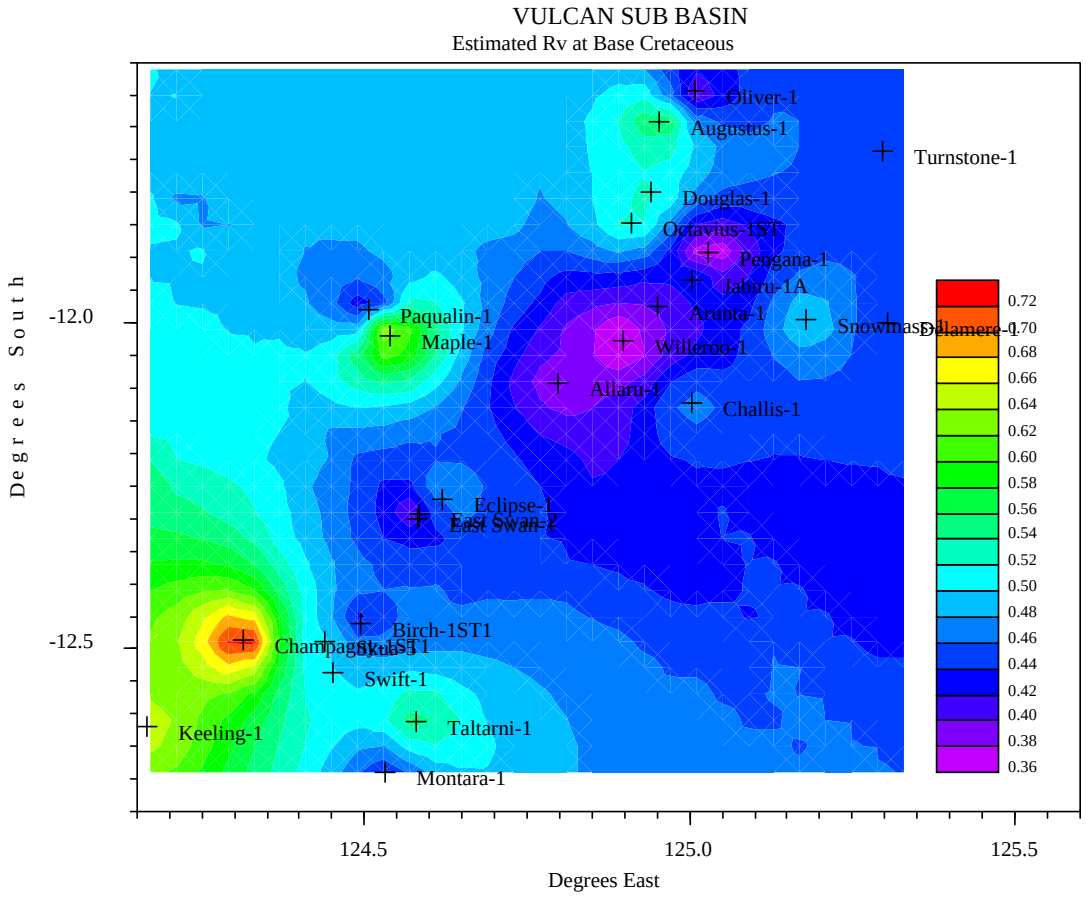

Figure 7-22: Vitrinite reflectance levels at the Base Cretaceous Unconformity

Contour map showing maturity variation at base Cretaceous level estimated by interpolating measured vitrinite reflectances as shown in Figure 7–17.

Unfortunately, many of the intervals sampled were so lean in suitable organic material, the reliable determination of both conventional and FAMM derived maturity estimates was not possible in most cases.

The scarcity of suitable organic matter in these samples may reflect the influx of brine, as these fluids were probably in chemical disequilibrium and reactive with the surrounding rocks, causing oxidation of the organic matter. The AFTA study may have been similarly affected with low yields of apatite grains attributed to the dissolution by acidic brines (O'Brien et al., 1996a). Despite these problems data collected on the East Swan-2 well (a breached palaeo-oil column) did provide a suite of both reliable FAMM and conventional VR data.

Significant vitrinite suppression typical of marine shales from the North West Shelf (Wilkins et al., 1992) was observed with conventional VR values suppressed by up to 0.2% (Figure 7–23). However, both datasets appear to show a significant maturity increase in the sample from immediately below the Callovian Unconformity (Figure 7–23) that is consistent with localised heating of organic matter immediately adjacent to the main aquifer.

This observation contrasts the observations of O'Brien et al. (1996a), who noted no strong evidence of heating in AFTA data from traps such as East Swan. As such, VR or FAMM data are considered to be somewhat more sensitive indicators of short-term heating effects than AFTA data. O'Brien et al. (1998) modelled AFTA response to heating over different time periods to demonstrate that short lived (<100,000 years) transient heat pulses had little impact and that at least 1 million years was required to produce a clear AFTA response. They attributed the absence of a transient signature in the East Swan AFTA data to catastrophic trap breach leading to a rapid, but short lived heating event whereas partially breached traps leak over a longer time period.

It should also be noted, however, that samples taken in the current study were specifically selected to recognise heating events that are concentrated in shales adjacent to aquifer units and this could also explain the apparent disparity.

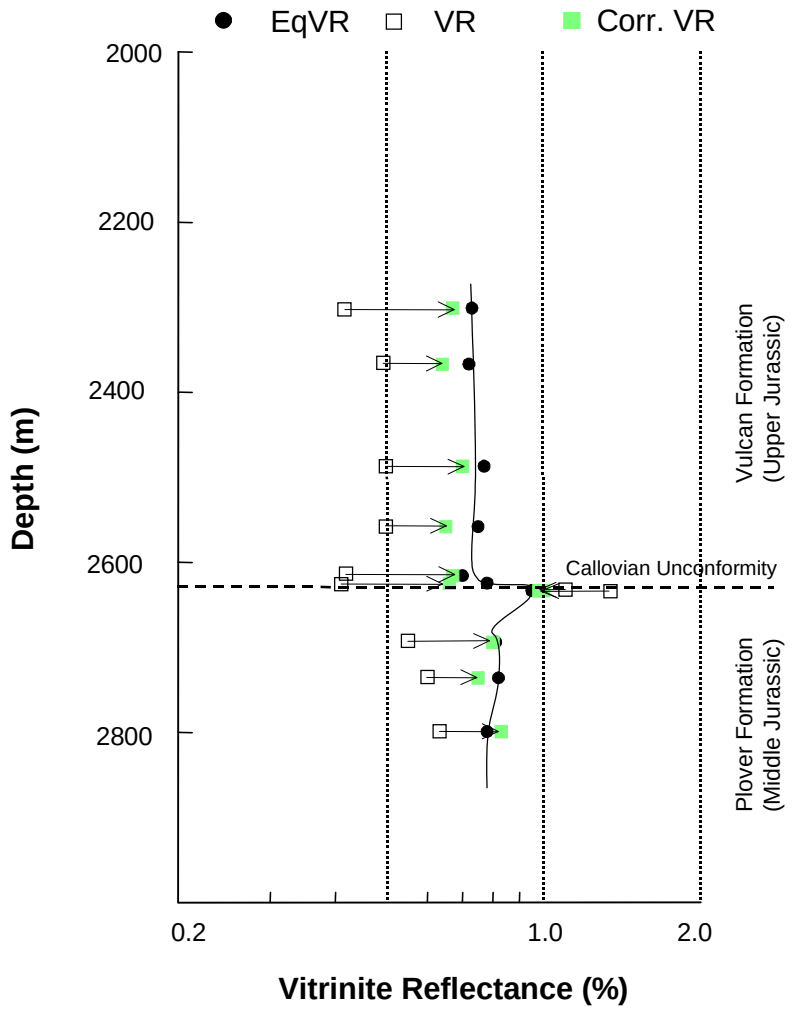

Figure 7-23: Vitrinite reflectance and FAMM results from East Swan-2.

Plot of maturity data against depth showing conventional vitrinite reflectance data (VR) and equivalent vitrinite reflectance data (EqVR) derived from the FAMM technique. Also plotted are the corrected VR data that have been adjusted to account for the degree of suppression related to the perhydrous nature of the virtinites from the marine Vulcan and mixed marine/terrestrial Plover formations. A significant increase in VR and equivalent VR from FAMM is noted at the Callovian unconformity where porous sandstones of the Plover Formation lie beneath shales of the Upper Jurassic Vulcan Formation.

Perturbations of organic maturity profiles attributed to convective thermal effects caused by transient fluid flow have been widely reported in the literature with examples of both convective heating (Xie et al., 2001) and cooling (Lampe et al., 2002) being documented for sedimentary basins.

7.5.2 Impact on Present Day Temperatures

Temperature gradients derived from extrapolated bottom hole temperatures, recorded in 48 wells, fail to record unusually high temperatures. A maximum variation of less than 10°C/km from the average (30°C/km) is observed with most wells varying by no more than 5°C/km (Figure 7–24).

The absence of significant thermal perturbation in current formation temperatures suggests there has been a cessation of brine flow, which is in agreement with both the generally low salinities of formation waters at the current day and the integrated findings of O'Brien et al. (1996a).

7.5.3 Numerical Modelling of Brine Flow

Numerical simulation techniques, using the finite element code RIFT2D (Person et al., 2000), have been used to validate the fluid flow model interpreted from the empirical palaeo-salinity data. These models provide outcomes which are broadly consistent with expectations but did require the use of specific combinations of input data in order to produce results that accommodate the measured data (Lisk et al., 2000b; Bekele et al., 2001).

These input parameters included a rigorous evaluation of available rock permeability data to obtain realistic input values for faults and the adjacent stratigraphy as well as a gradual accumulation of overburden if the timing and amount of overpressure needed to drive the model were to be achieved.

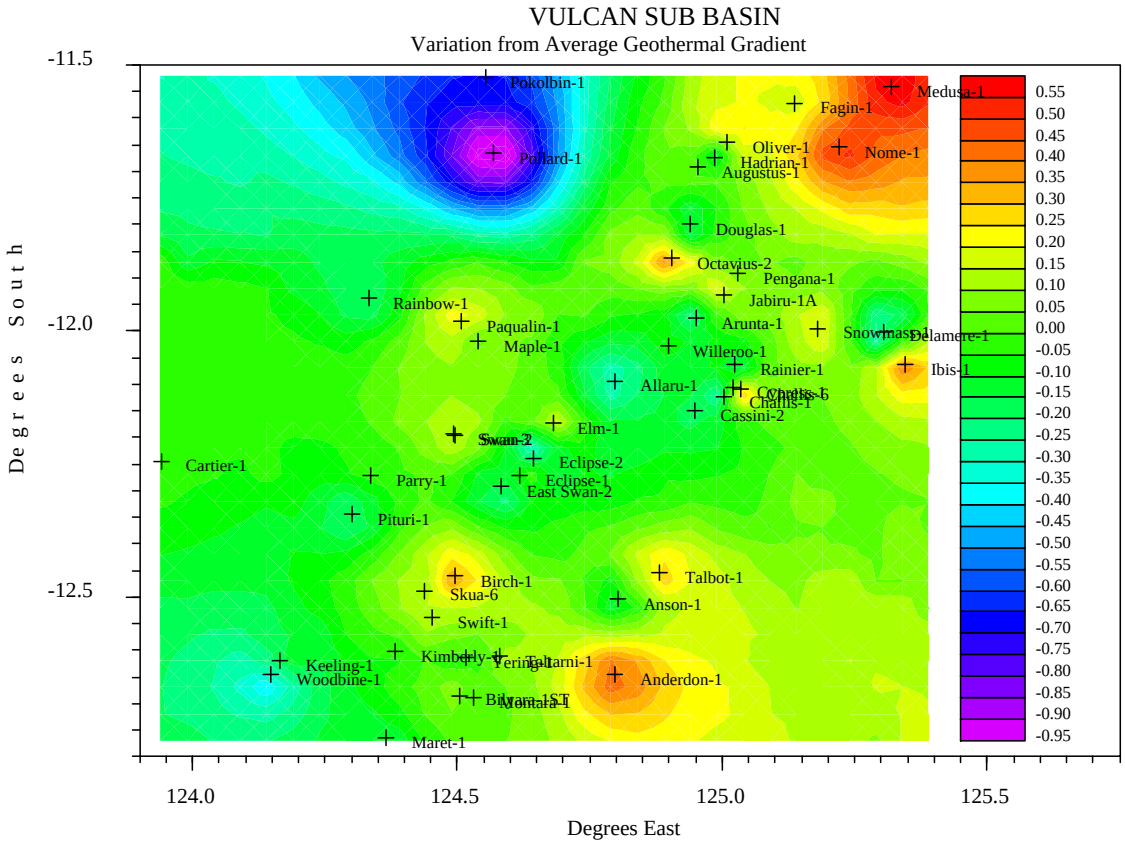

Figure 7-24: Map showing variation from the average VSB geothermal gradient.

Difference map showing the variation away from average geothermal gradient for the VSB (30°C/km). Across much of the basin there is only limited variation except in the NE where geothermal gradients are significantly higher and across the northern part Ashmore Platform where geothermal gradients are abnormally lower than the basin average (input data taken from well completion reports).

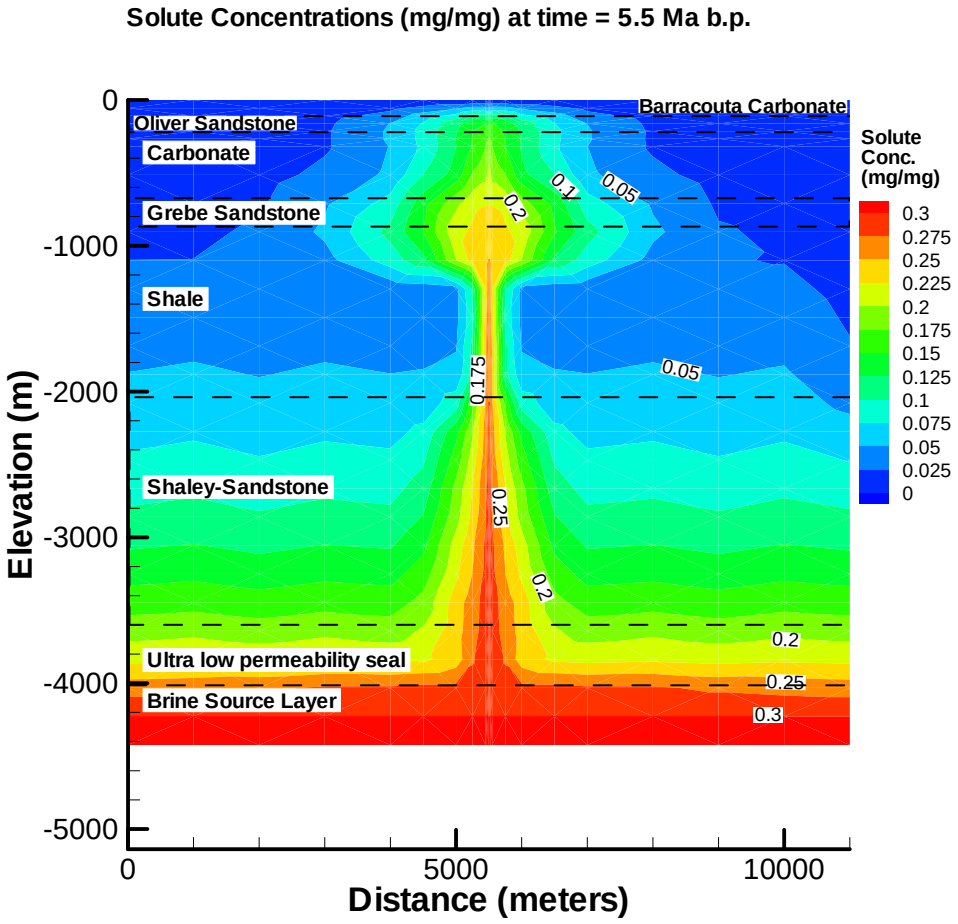

Figure 7-25: Simulated solute concentrations for modelled brine flow.

Output from a numerical modelling package (RIFT2D, Person et al., 2000) showing the development of a significant brine plume in the Tertiary Grebe sandstone immediately following trap breach at about 5.5Ma. Solute concentrations of up to 250,000ppm are predicted that closely match measured fluid inclusion salinity values in the East Swan-2 well, the trap which provided the basis for the design of this model.

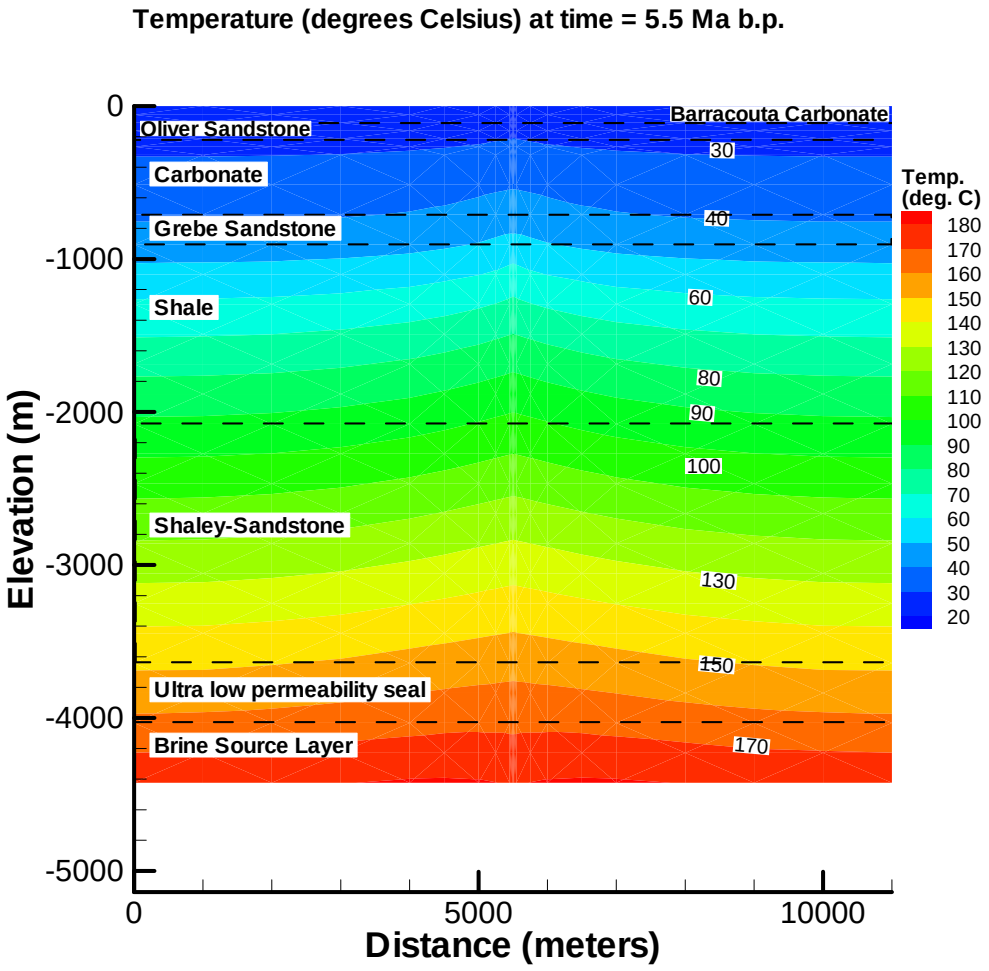

Figure 7-26: Predicted temperature anomalies associated with brine flow.

Output from a numerical modelling package (RIFT2D) showing the predicted temperatures associated with vertical brine flow immediately following trap breach at about 5.5Ma. The perturbation of the temperatures is much less than is indicated by the AFTA and fluid inclusion results and indicates that the model requires further modification to be predictive but the results confirm temperature anomaly associated with brine flow into the shallow section.

Using these inputs vertical flow within the reactivated fault when enclosed by shale and lateral ingress of highly saline fluid (200,000k ppm) when the fault crosses permeable aquifer units can be simulated (Figure 7–25). These simulations also show good agreement with the magnitude of salinities recorded from aqueous fluid inclusions in the Jurassic residual oil zones and the shallow Tertiary aquifer units overlying reactivated traps.

The temperature profiles produced by the simulation (Figure 7–26), however, do not show the magnitude of heating that is indicated by the thermal maturity data and further manipulation of the input data is needed to obtain a closer match with the observed temperature data.

7.6 SUMMARY

Fluid inclusion palaeo-salinity data have been used to identify a regionally extensive fluid-flow event in the VSB, involving vertical, cross formation, transfer of highly saline brine. These pore waters, with maximum salinities in excess of 200,000 ppm, record the migration of high-salinity brines through sandstones in the Mesozoic and Tertiary sequences. Mio-Pliocene fault reactivation is considered the most likely cause of this transient fluid flow event, providing the vertical permeability conduits for brine flow. Hyper-saline fluids are not recorded in samples taken from intact hydrocarbon columns indicating the flow of brine occurred subsequent to hydrocarbon charge, with high hydrocarbon saturations acting to prevent the ingress of these fluids. Further, the presence of high salinities in samples from recognised residual oil zones suggests that breaching of these traps facilitated the ingress of high-salinity brines, thus making the brines a regional marker for fault reactivation. Fault controlled injection of brine from bedded Palaeozoic salt at depths of up to 10 km is considered to be the main source for brine migration, with release of overpressure seen as the most likely impelling force. Numerical simulations, utilised to test this hypothesis, produce outcomes, which broadly match the observed vertical distribution of samples with high salinity fluid inclusions. Additionally partial or complete dissolution of salt diapirs provided an additional source of brine but these

appear to be too geographically restricted to explain the broad distribution of wells with a brine signature.

Flow of saline brines from deep Palaeozoic strata may have produced a convective overprint of the conductive thermal background. The current geothermal conditions reveal no perturbation, as these events are palaeo- rather than contemporary in nature. Apatite Fission Track Analysis data afford evidence for transient heating events in the recent geological past as do thermal maturity data provided by vitrinite reflectance data. Localised heating of sediments located immediately adjacent to faults bounding breached oil columns is attributed to the flow of brine from faults into more permeable reservoir sections to create deviations in thermal maturity profiles. Inadvertent use of these anomalous maturity data as inputs to an appraisal of regional hydrocarbon generation could lead to spurious conclusions if the restricted spatial extent of these convective effects is not recognised. The significant thermal anomalies that appear to accompany brine flow together with the highly saline nature of the fluids and absence of a shallow salt source all lend support to derivation from deeply buried Palaeozoic evaporites.

appear to be too geographically restricted to explain the broad distribution of wells with a brine signature.

Flow of saline brines from deep Palaeozoic strata may have produced a convective overprint of the conductive thermal background. The current geothermal conditions reveal no perturbation, as these events are palaeo- rather than contemporary in nature. Apatite Fission Track Analysis data afford evidence for transient heating events in the recent geological past as do thermal maturity data provided by vitrinite reflectance data. Localised heating of sediments located immediately adjacent to faults bounding breached oil columns is attributed to the flow of brine from faults into more permeable reservoir sections to create deviations in thermal maturity profiles. Inadvertent use of these anomalous maturity data as inputs to an appraisal of regional hydrocarbon generation could lead to spurious conclusions if the restricted spatial extent of these convective effects is not recognised. The significant thermal anomalies that appear to accompany brine flow together with the highly saline nature of the fluids and absence of a shallow salt source all lend support to derivation from deeply buried Palaeozoic evaporites.

8. HYDROCARBON/PORE WATER FLUID FLOW HISTORY

8.1 INTRODUCTION

The integration of information on the different fluid phases characterised in this study allows a coupled hydrocarbon-formation water model to be constructed for the Vulcan Sub-basin. Five discrete fluid phases are recognised, including at least three hydrocarbon phases (H1 to H3) and at least two important fluid flow events involving different types of formation water (W1 and W2). Collectively these events can be related to five key steps in the fluid flow history that can be directly linked to the tectonic and subsidence history of the region. These five phases include:

1. Compaction phase (W1)

2. Early gas charge (H1)

3. Main oil charge (H2)

4. Trap Breach (W2)

5. Late gas charge (H3)

This integrated fluid history model provides a regionally extensive platform to more comprehensively evaluate the operation and the effectiveness of the recognised Jurassic Vulcan-Plover (!) petroleum system (Figure 8–1) across the VSB.

This newly created data resource provides a unique opportunity to assess the effectiveness and reliability of existing and future predictive methodologies for assessing charge and trap integrity risks associated with this petroleum system by enabling the predicted outcomes to be validated against a well constrained regional understanding of the hydrocarbon charge history.

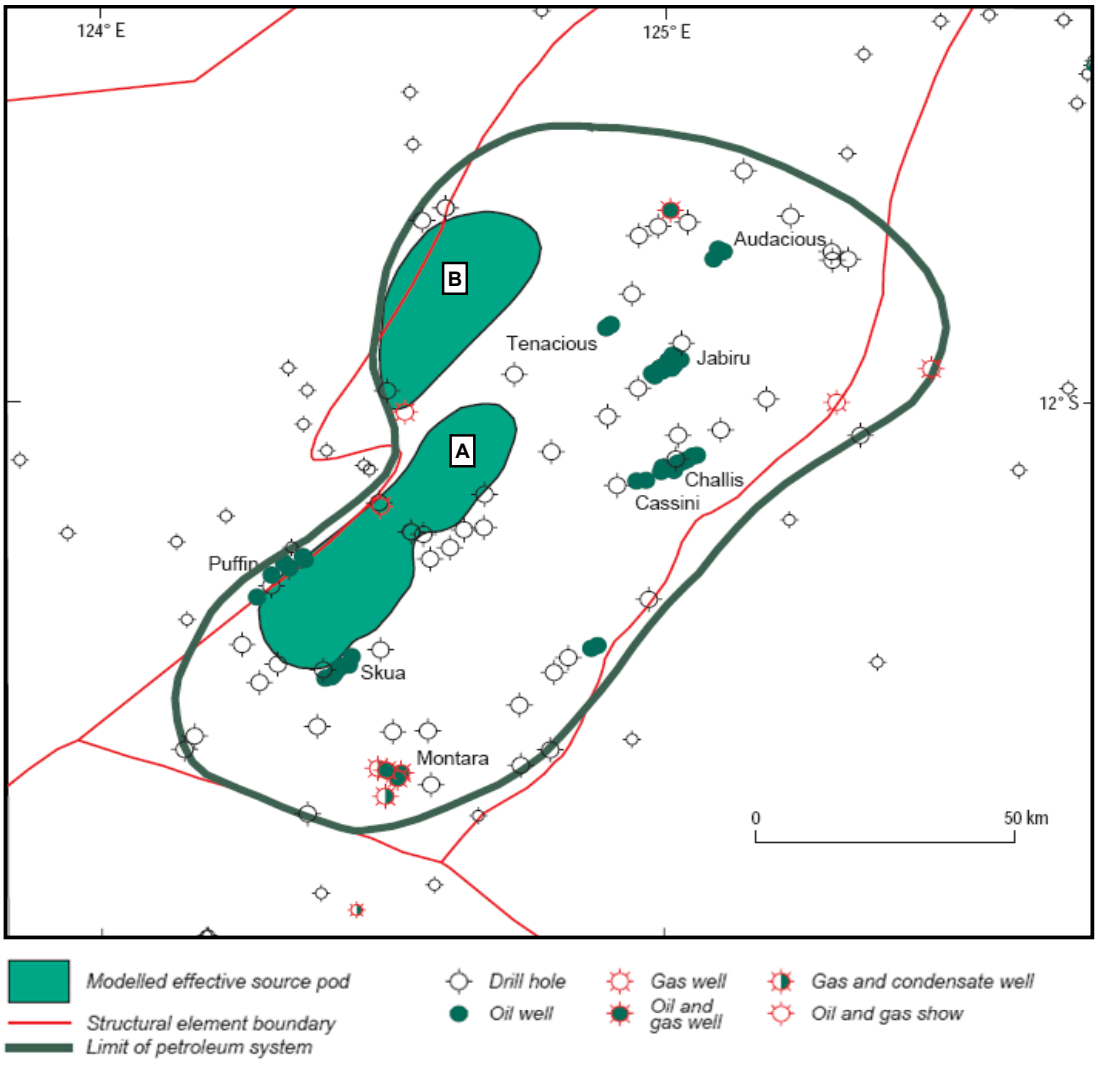

Figure 8-1: Extent of the recognised Jurassic Vulcan-Plover (!) Petroleum System

Map shows the approximate geographic extent of wells covered by the combined Vulcan-Plover Petroleum System, with the limit of active generation from the key source kitchens of the Swan (A) and Paqualin (B) grabens shown by the green shading (from Barrett et al., 2004). Note that most of the fields are located well away from these recognised kitchens indicating that a significant component of lateral migration is required to produce hydrocarbon charge to these fields.

8.2 COMPACTION PHASE (W1)

Deposition of the Post-rift Megasequence from the Early Cretaceous produced the first major change to the fluid history of the Vulcan Sub-basin. Thermal subsidence associated with the cessation of rifting produced increased accommodation space and led to the deposition of the regional seal, effectively creating a closed system where connate waters trapped within the key Mesozoic reservoir horizons at the time of deposition began to be modified by diagenesis.

Prior to this event the salinity of Jurassic connate waters in the VSB is likely to have been controlled by the prevailing depositional environment ranging from meteoric water compositions associated with fluvial sedimentation through brackish waters in the fluvio-deltaic section to fully marine water salinities (circa 35,000ppm) in the more marine dominated upper part of the Plover Formation.

Ingress of meteoric waters due to emergent topography associated with rifting at that time was also likely (Figure 8–2). Footwall erosion of fault blocks is noted across the VSB (Baxter et. al., 1999), related to thermally driven rift related uplift (Wernicke and Axen, 1988), and indicates periods of sub-aerial exposure. Topographically driven groundwater flow allowing ingress of meteoric waters in these points of sub-aerial exposure is likely to have been countered by compaction driven flow from the subsiding basin centre creating a mixing zone where these fluids interact.

The mineral phases produced during early diagenesis allow the composition of extant formation waters to be further constrained. Stable isotope analyses are particularly useful in this regard, allowing the oxygen isotopic composition of many common authigenic minerals to be translated into their parental water compositions. Meteoric waters have oxygen isotope compositions that are strongly correlated with latitude, altitude and distance from the coastline and reflect differences in the mean annual air temperature (Dansgaard, 1964; Yurtsever and Gat, 1981). Meteoric waters have negative (depleted) $\delta^{18}O$ compositions that become progressively more depleted with increasing latitude (Yurtsever and Gat, 1981).

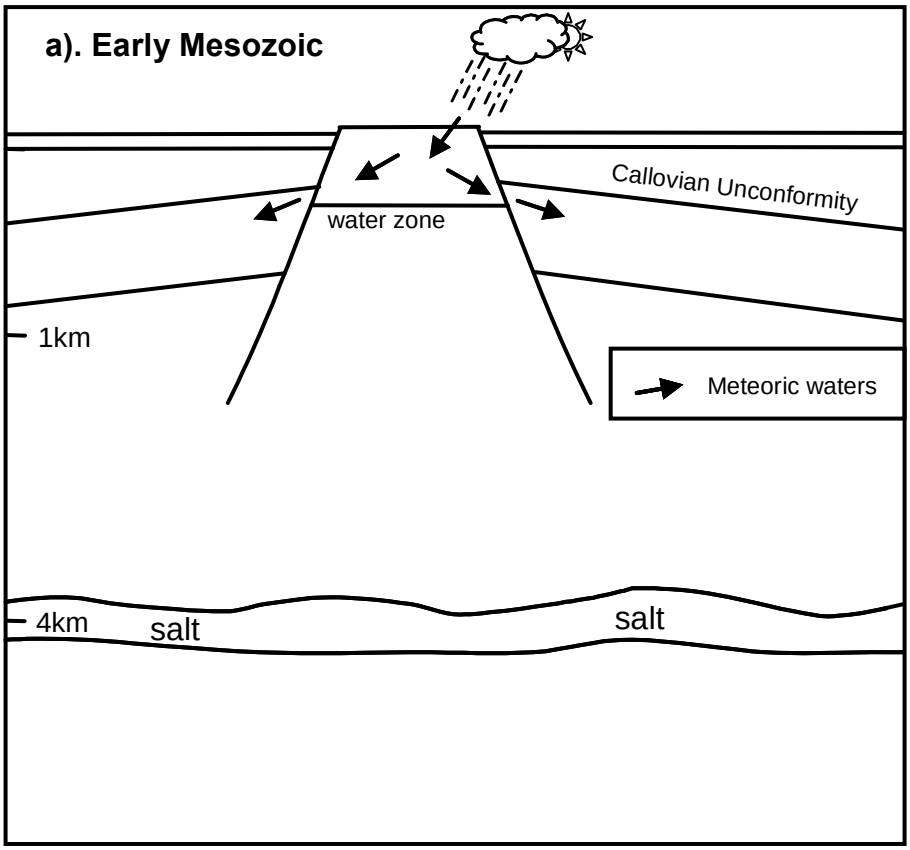

Figure 8-2: Cartoon showing fluid flow during an early compaction phase

Diagram shows the VSB in early Mesozoic times with deposition of sediments into a faulted topography with active rifting producing significant topography with erosion of exposed horst and tilted fault block structures and associated sedimentary growth in grabens adjacent to these high blocks. Sub-aerial exposure is indicated by eroded footwall highs on seismic data and by the isotopic composition of early diagenetic cements that show depleted $\delta^{18}O$ values that are consistent with the involvement of meteoric waters. The interaction of topographically driven meteoric water ingress with compaction driven flow from the subsiding depocentres produced a range in formation water salinity ranging mostly from marine to brackish composition. Deep Palaeozoic salt beds have insufficient burial to produce diapirism and exist as rheologically stable bedded salt deposited in earlier rift basins that underlie the Mesozoic stratigraphy.

During the Middle to Late Jurassic period the VSB lay at high latitude (50°S from Veevers, 1984) and the isotopic composition of meteoric waters from current variations with latitude (Yurtsever and Gat, 1981) is calculated to have been about -7‰ (per mille, or one part per thousand) referenced against $\delta^{18}O$ SMOW (Standard Marine Ocean Water). In contrast, marine waters exhibit constant $\delta^{18}O$ compositions and remain close to 0‰ irrespective of the climate or other factors.

Stable isotope analyses of early formed siderite cements (Figure 8–3) have been reported for the Plover Formation in Delamere-1, with oxygen isotope compositions that, under likely depositional temperatures, yield calculated parental pore water compositions that are influenced by meteoric waters (Hamilton et al., 1991). However, whilst slightly depleted the estimated composition of water parental to these cements is not depleted enough to be derived from purely Jurassic meteoric water and some mixing with connate sea water is implied (Figure 8–3). Involvement of fresh water, that is likely to have been slightly acidic, probably promoted dissolution of fossiliferous material that was subsequently recrystallised as these early-formed carbonate minerals that are seen in many samples.

Kaolinite crystallisation is the first major diagenetic event to cause significant degradation of reservoir quality in the VSB. Increased diagenesis due to rising formation temperatures is likely to have caused an overall increase in the salinity of associated formation waters (W1) reflecting the dissolution of chloride bearing detrital minerals. Reported stable isotope data for widespread kaolinite cements in a collection of VSB wells (Figure 8–3) indicate a persistence of meteoric water involvement even after regional drowning of the margin in Early Cretaceous time. At likely temperatures of crystallisation, in some instances constrained by minimum fluid inclusion homogenisation temperatures for later formed quartz overgrowths, water parental to kaolinite remain depleted relative to sea-water (Figure 8–3; Eadington et al., 1990a, b; Hamilton et al., 1991; Lisk et al., 1992).

Carbonate minerals that postdate kaolinite but precede quartz overgrowths have reported $\delta^{18}O$ values that yield estimated parental water compositions that are slightly enriched at likely temperatures of crystallisation and an end to meteoric water involvement by this time (Figure 8–3; Eadington et al., 1992).

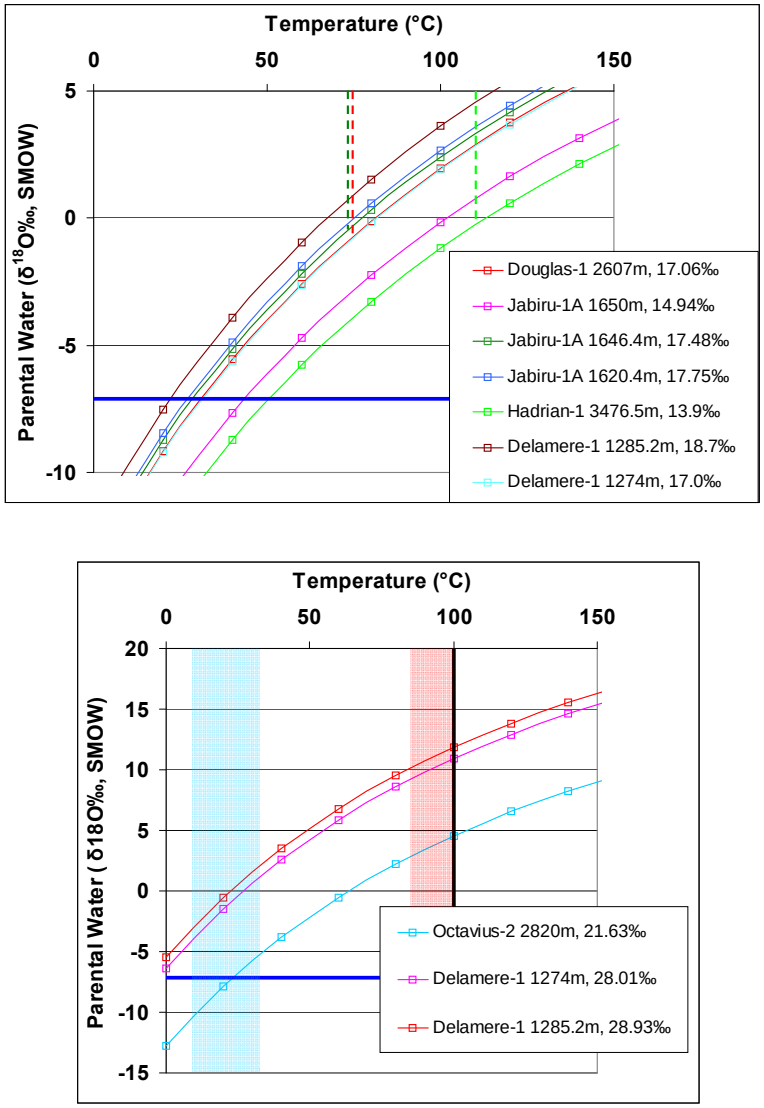

Figure 8-3: Summary of stable isotope data from authigenic cements in the VSB.

The two plots show temperature dependant fractionation curves for kaolinite cements (upper diagram) and carbonate minerals (lower diagram). Oxygen isotope values measured on these cements are related by a relevant fractionation equation (Land and Dutton, 1978 for kaolinite; O'Neil et al., 1969 for siderite and ankerite) to estimate the isotopic composition of waters that are parental to each cement phase. For kaolinite cement available fluid inclusion temperatures for later quartz overgrowths (vertical dashed lines in equivalent colour) place an upper constraint on the temperature of kaolinite formation and indicate that all samples analysed were derived from waters with some meteoric water contribution. Parental waters are not depleted enough to equate with estimated compositions of Jurassic meteoric water (blue horizontal line) and imply partial mixing with sea-water. For the carbonate minerals (lower diagram) the early formed siderite in Delamere-1 is depleted relative to sea-water assuming low temperatures of formation for these early formed cements (shaded blue zone). In contrast, ankerite cement in samples from Octavius-2 post-date kaolinite and are enriched relative to sea-water across the range of likely crystallisation temperatures (pink zone), the upper limit (vertical black line) representing current conditions estimated from bottom hole temperatures.

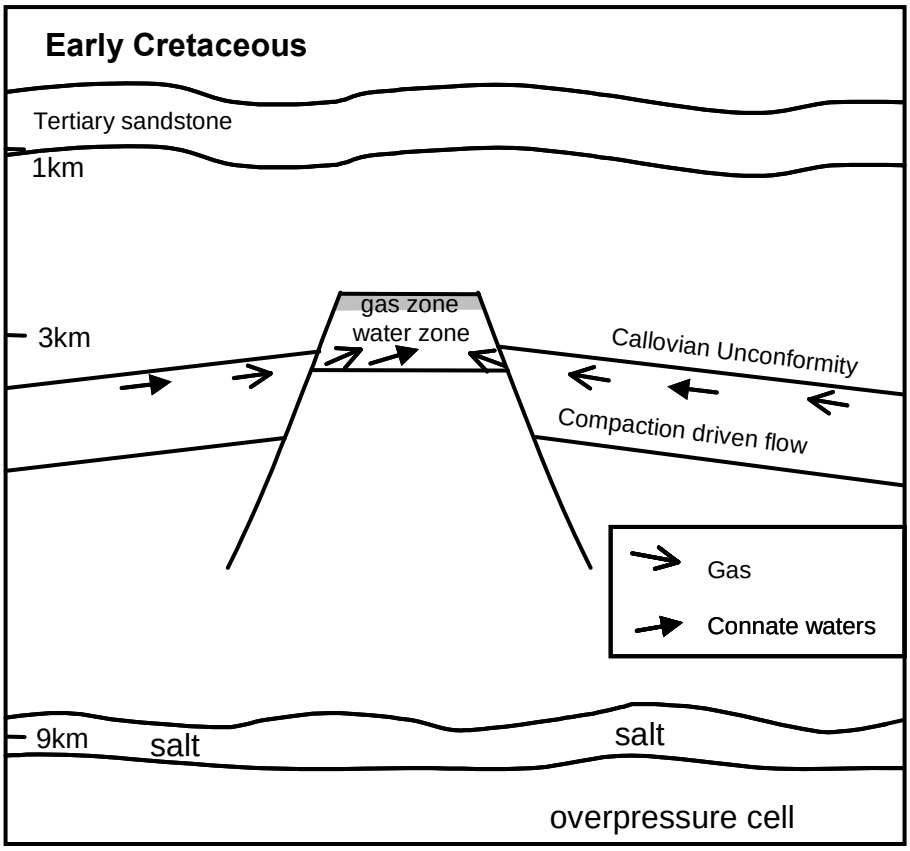

Figure 8-4: Cartoon showing VSB during early gas charge.

Diagram showing schematic representation of the VSB by the Early Cretaceous as high heat flows established during rifting coupled with rapid burial in the Late Jurassic and Early Cretaceous produced expulsion of early generated gas from terrestrially dominated source rocks. Previously water-wet structures are filled with gas but low expelled volumes coupled with poor seal capacity of these shallow buried traps probably limited the size of columns and few structures are filled to spill. In some instances where trap capacity was small (Delamere-1, Pengana-1) gas charge completely filled these structures and this early charge prevented the access of the later and volumetrically larger main oil charge. Groundwater flow is dominated by compaction driven flow as open oceanic circulation is established due to post rift thermal subsidence and previously exposed structural high are buried beneath a blanket of Cretaceous shales and marls thus preventing further ingress of meteoric water. Increased formation temperatures coupled with changing groundwater chemistry combine to begin alteration of labile detrital minerals such as feldspar which are progressively converted into authigenic clay minerals, mostly kaolinite clays. Burial remains insufficient to mobilise deep salt beds and major faulting ceases as the VSB develops into a tectonically quiescent passive margin.

8.3 EARLY GAS CHARGE (H1)

An early hydrocarbon pulse, probably derived from terrestrial, gas prone, source rocks within the Early Jurassic Plover Formation was generated in response to high heat-flow during rifting. This resulted in gas charge (H1) to structural closures that existed throughout the basin at the cessation of rifting (Figure 8–4).

Remnants of this early gas charge appear to be preserved as intact gas-legs within the Skua, Bilyara, Delamere and Pengana traps and as palaeo-gas caps within the Cassini, Jabiru and East Swan structures. In some instances, such as Pengana-1 and possibly Delamere-1, this hydrocarbon charge totally filled the available closure, thus preventing such traps from receiving a later oil charge.

In all other cases, such as in the Bilyara-1 and East Swan-2 wells, this early gas charge appears to have only partially filled available closure, although it is unclear if this reflected a restricted charge or if the palaeo-structures had less capacity at that time. Reduced trap capacity could reflect the presence of smaller structural closures or may indicate that the degree of trap fill by the early gas charge was controlled by the seal capacity of overlying shales. The limited burial by this time would make palaeo-traps more prone to capillary failure and dynamic leakage during the early burial history thus limiting the column heights that could be retained.

The absolute timing of the early phase of gas migration not well constrained by the results of the current study other than to say it preceded the main phase of oil charge (H2). Regional basin modelling completed in the Vulcan Sub-basin (Kennard et. al., 1999) attributes this initial hydrocarbon charge to early gas generation from Lower Jurassic coaly source rocks. Their modelling identifies the timing of this event as Late Jurassic to Early Cretaceous. Generation of both oil and gas is predicted in their models, but expulsion is predicted to be limited to gas due to different expulsion efficiencies used for oil versus gas prone kerogen (Kennard et al,. 1999).

8.4 MAIN OIL CHARGE (H2)

The principal phase of oil migration in the basin is predicted to have occurred in the Mid- to Late Tertiary (Kennard et al,. 1999) and resulted in widespread oil charge (H2) to traps sub-cropping the Callovian Unconformity and within the Syn-rift Megasequence (Figure 8–5). This produced many large oil accumulations, with column heights controlled by available structural closure rather than the generative potential of the source interval.

Results from the current study also indicate a Mid-Late Tertiary timing of the main oil charge in the Vulcan Sub-basin. Fluid inclusion palaeo-temperatures, when combined with temperature predictions from 1-D basin modelling, indicate the earliest onset of oil migration occurred in Paleocene to Eocene time (Figure 8–6). This was when quartz overgrowths first began to trap oil inclusions, so does not directly preclude earlier charge.

More sophisticated regional 2D and 3D basin modelling studies (Chen et al., 2002; Fujii, (2007) broadly concur with the simple models produced in the current study and previously by Kennard et al. (1999), but predict an earlier onset (Cretaceous) of expulsion from within the main depocentres. Predicted oil and gas generation was also more widespread than was indicated by Kennard et al. (1999), largely reflecting the inclusion in the later models of the Plover Formation as a significant source rock.

Fujii et al. (2004) and Fujii (2007) predict oil expulsion from the Late Jurassic Lower Vulcan Formation within the Swan Graben was active from the Early Cretaceous to the present day, but results for the Cartier Trough concur with Kennard et al. (1999) where expulsion thresholds are not predicted to be reached until the Late Tertiary.

The differences in predictions related to the timing of oil expulsion between the different models are based largely on the use of different expulsion thresholds that are not well constrained for VSB source rocks by any direct measurements, rather they rely on published work from elsewhere. In addition, Fujii et al. (2004) also utilise a single palaeo-heat flow history for their model that falls at the upper end of the spatially variable palaeo-heat flow models employed by Kennard et al. (1999).

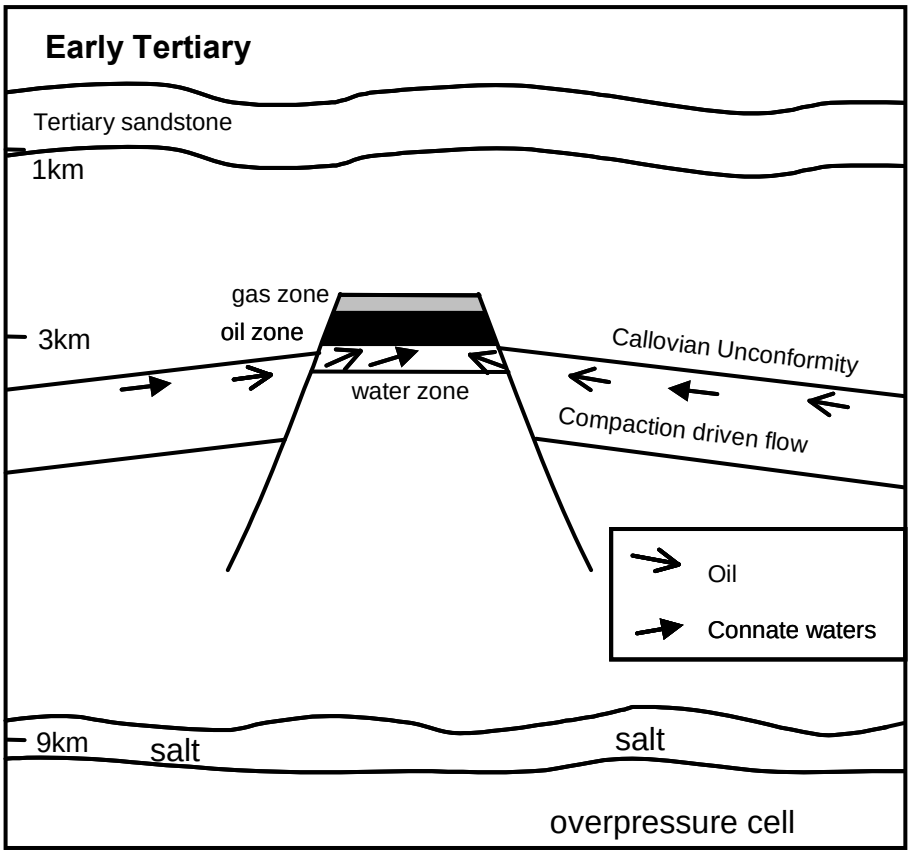

Figure 8-5: Cartoon showing VSB during early the main phase of oil charge.

Schematic representation of the VSB during the onset of the main hydrocarbon charge (H2) in Early Tertiary time showing lateral and vertical migration of hydrocarbons with oil charge likely derived from mature Upper Jurassic source rocks immediately overlying the main Plover Formation reservoir. As a tectonically quiescent passive margin blanketed by regionally extensive shales the basin architecture established during the syn-rift phase created an efficient petroleum system where a high proportion of valid structures were filled with oil and gas. Burial depths still remain insufficient to mobilise deep salt beds, but likely contribute to growing inflationary overpressures below the impermeable salt layer.

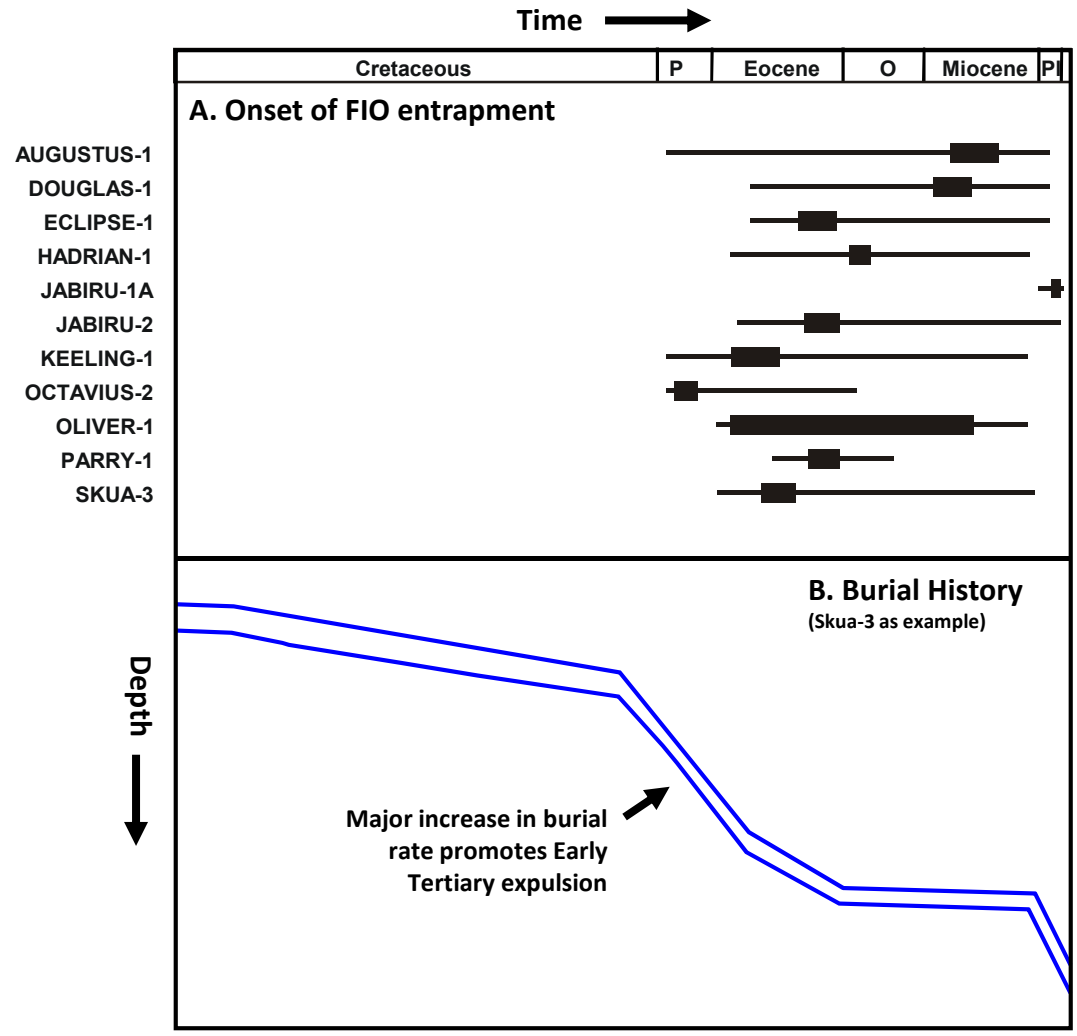

Figure 8-6: Timing of hydrocarbon charge indicated by fluid inclusion palaeotemperatures.

(A.) Inferred earliest trapping of fluid inclusions by the crystallisation of quartz overgrowths determined from minimum homogenisation temperatures measured on aqueous inclusions that have been converted into time estimates through integration with formation temperature history derived from separate 1-D basin models for each of the wells listed. Observations of coeval oil inclusions indicate oil was also being trapped at this time with major increased burial in the Early Tertiary (B.) contributing to the onset of oil generation and expulsion. The burial curves shown (B) are a composite of the wells modelled and reflects the path of Lower Vulcan Formation source rocks with time. Letters on timescale correspond to P for Paleocene, O for Oligocene and Pl for Pliocene.

This assumption about heat flow history in the Fujii et al. (2004) model also contributes to the earlier timing estimates, but relies on implied (i.e. not defined by techniques such as FAMM) vitrinite suppression to explain a relatively poor match between modelled maturity levels and vitrinite reflectances measured in the wells.

The current study considers impact of these assumptions to be significant and whilst earlier oil charge is not inconsistent with the fluid inclusion data presented herein, models that more accurately concur with the observational data are deemed to yield a more consistent outcome. Consequently the timing predictions from the more simplistic model 1D basin models of this study and that of Kennard et al. (1999) are preferred over those derived from the more complex but ultimately no better constrained 2D and 3D models.

The published basin modelling studies (Kennard et al., 1999; Chen et al., 2002; Fujii et al., 2004) coupled with constraints provided by geochemical analysis of recovered hydrocarbons (Edwards et al., 2004) all indicate that at least three discrete charge kitchens contributed to the hydrocarbon fill of traps within the VSB, namely the Swan and Paqualin grabens and the Cartier Trough, but each study varies somewhat in regard to the degree of contribution from the Cartier Trough kitchen.

The nature of these kitchens and the source rock intervals within the Lower Vulcan and Plover formations contained therein contributed geochemically distinct products that were strongly controlled by the structural history of the VSB that has produced varying source rock depositional environments and different subsidence histories.

8.4.1 Swan Graben Kitchen

Maps showing thermal evolution of the key source kitchens within the VSB (Figure 8–7; from Chen et al., 2001) demonstrate the importance of the Swan Graben (and associated Paqualin Graben immediately to the north) as prolific source kitchens. The large throw rift faults that flank the Swan Graben produced major Upper Jurassic sedimentary growth sections that provided the ideal conditions for deposition and preservation of rich oil-prone source rocks within the Lower Vulcan Formation.

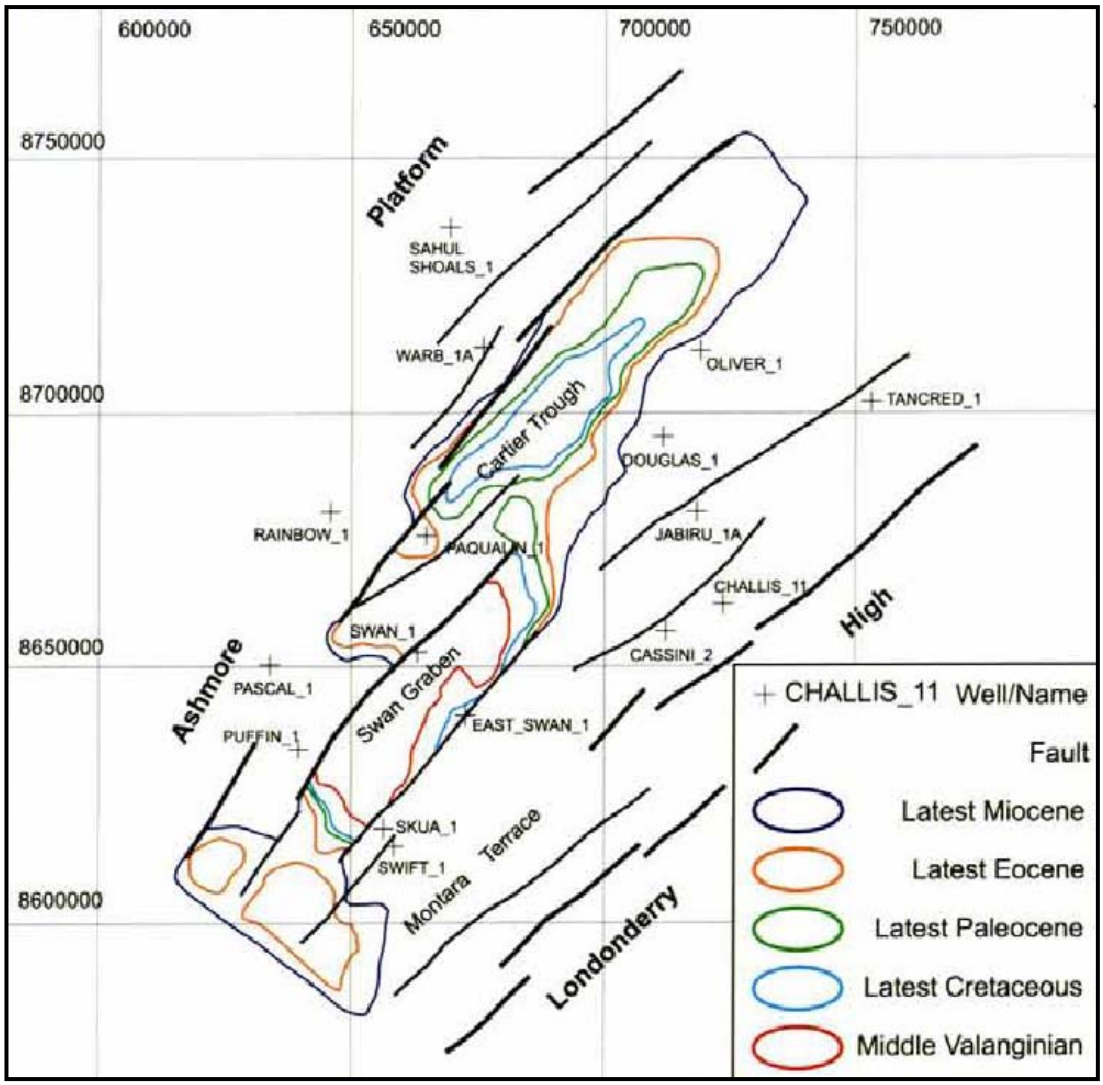

Figure 8-7: Evolution of mature source kitchens in the VSB through time.

Map showing the geographic extent of the key source kitchens in the VSB with time as indicated from the results of 2D-3D basin modelling (From Chen et al., 2001). These are overlain on a simplified regional fault map with location of wells also shown. Large syn-rift throws on the faults bounding the Swan Graben contributed to rapid maturation during the Jurassic rifting event where high heat-flows prevailed and relatively little burial was required to reach generative temperature levels. In contrast much of the burial in the Cartier Trough resulted from increased Late Tertiary subsidence and as a consequence charge onset is much more recent than seen in the Swan and Paqualin grabens.

The growth associated with syn-depositional faults promoted maturation of source rocks deposited into the developing accommodation space by rapidly increasing burial that in conjunction with high heat flow during and immediately following rifting boosted formation temperatures into the hydrocarbon generation window.

A striking feature of the source rock maturity map is that nearly all of the discoveries lie outside the extent of mature source rock (Figure 8–7) and therefore rely on a component of lateral migration for charge. Migration distances of more than 50 kilometres are needed for the most distant fields, including the major Jabiru and Challis-Cassini oil fields.

Migration pathway analysis confirms intuitive expectations with migration away from the key Swan Graben source kitchen strongly controlled by the prevailing NE-SW structural grain (Figure 8–8) established during episodes of Jurassic rifting. Typically petroleum systems relying on significant lateral migration are considered higher risk but in the VSB the fault relay ramps set up by the *en echelon* arrangement of rift faults allow focusing of the migration pathways and enable long migration distances to be achieved.

A distinct advantage of having traps remote from the mature source kitchen is better reservoir properties than would be associated with more deeply buried traps that lie closer to or within the pod of active source rock. In the VSB this resulted in excellent reservoir quality being a feature of the main oil fields with only limited alteration by diagenesis, enabling these fields to display high productivity.

Shorter distance hydrocarbon migration paths for oil derived from the Swan Graben kitchen (Figure 8–8) were equally effective, allowing oil charge to the Skua and probably Swift oil fields and producing the substantial palaeo-oil accumulations at Eclipse-1, Eclipse-2, East Swan-2 and Paqualin-1.

Deeper burial associated with these more proximal traps typically results in reduced reservoir quality due to more advanced diagenesis, although generally this has not advanced sufficiently to become a critical factor in determining the viability of these intervals as productive hydrocarbon reservoirs.

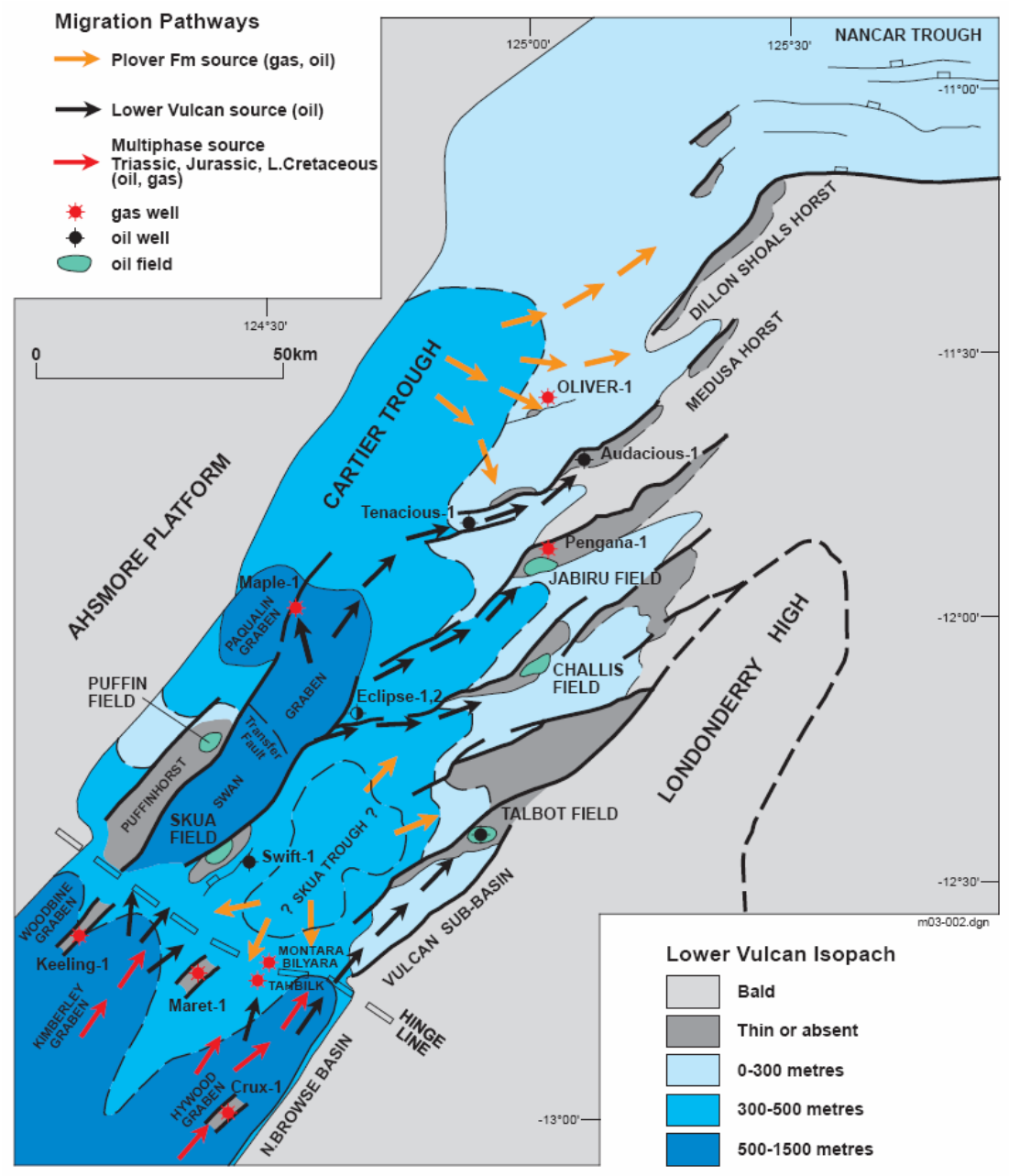

Figure 8-8: Simplified migration pathways for the VSB.

Map shows the location of major oil-prone source kitchens based on the thickness of the Upper Jurassic (Lower Vulcan Formation) isopach as well as inferred migration pathways for hydrocarbons derived from different source rocks levels. The rift controlled NE-SW structural grain plays an important role in enabling long distance migration to charge the main oil fields of Jabiru and Challis. A possible contribution from the adjacent Browse Basin (suggested by Kennard et al., 1999) is also indicated, in part to deal with the speculative nature of the implied Skua Trough kitchen.

Porosity reduction in the more deeply buried traps is driven by compaction and the widespread crystallisation of authigenic quartz overgrowths as well variable amounts of kaolinite clay related largely to the alteration of limited amounts of detrital feldspar in these quartz arenite sandstones.

The Swan Graben kitchen may have provided the oil charge to the presently gas-bearing Keeling structure to the southwest, although currently this structure lies outside the demonstrable fetch area of the Swan Graben kitchen and would rely on a different basin configuration in the past to achieve charge from this kitchen. Current migration directions towards the Keeling trap (Figure 8–8) favour an input from the adjacent Browse Basin further to the southwest, but perhaps this is the source of the later gas that subsequently replaced the earlier formed palaeo-oil accumulation.

Detailed oil and source rock geochemistry indicates that the oil produced from Upper Jurassic mudstones within the Swan Graben (Lower Vulcan Formation) can be assigned to a single oil family (Group A oils from Edwards et al., 2004). Coupling the crude oil geochemistry with similar analyses conducted on the fluid inclusion oils helps to broaden the footprint collectively enabling a clear oil-source correlation to be demonstrated with the Lower Vulcan Formation for both the proximal and distal products of this prolific source kitchen (Figure 8–9).

Fields located away from the clearly defined migration fetch area for the Swan Graben kitchen indicate that other source kitchens must also have contributed to hydrocarbon charge. These include accumulations that border the Cartier Trough to the north east such as the Oliver oil and gas field as well as fields such as Montara, Tahbilk and Talbot that are located on the southern and eastern margins of the Skua Trough. The Jurassic Plover Formation is typically viewed to be the most likely source of hydrocarbons not linked to the Swan Graben kitchen (Edwards et al., 2004) and is expected to be more gas-prone reflecting the greater involvement of terrestrial organic matter. The gas rich composition of the hydrocarbon fill in these fields, together with geochemical analysis of the recovered hydrocarbons, confirms the involvement of a compositionally discrete family of hydrocarbon fluids, mostly assigned as Group B oils using the classification of Edwards et al. (2004).

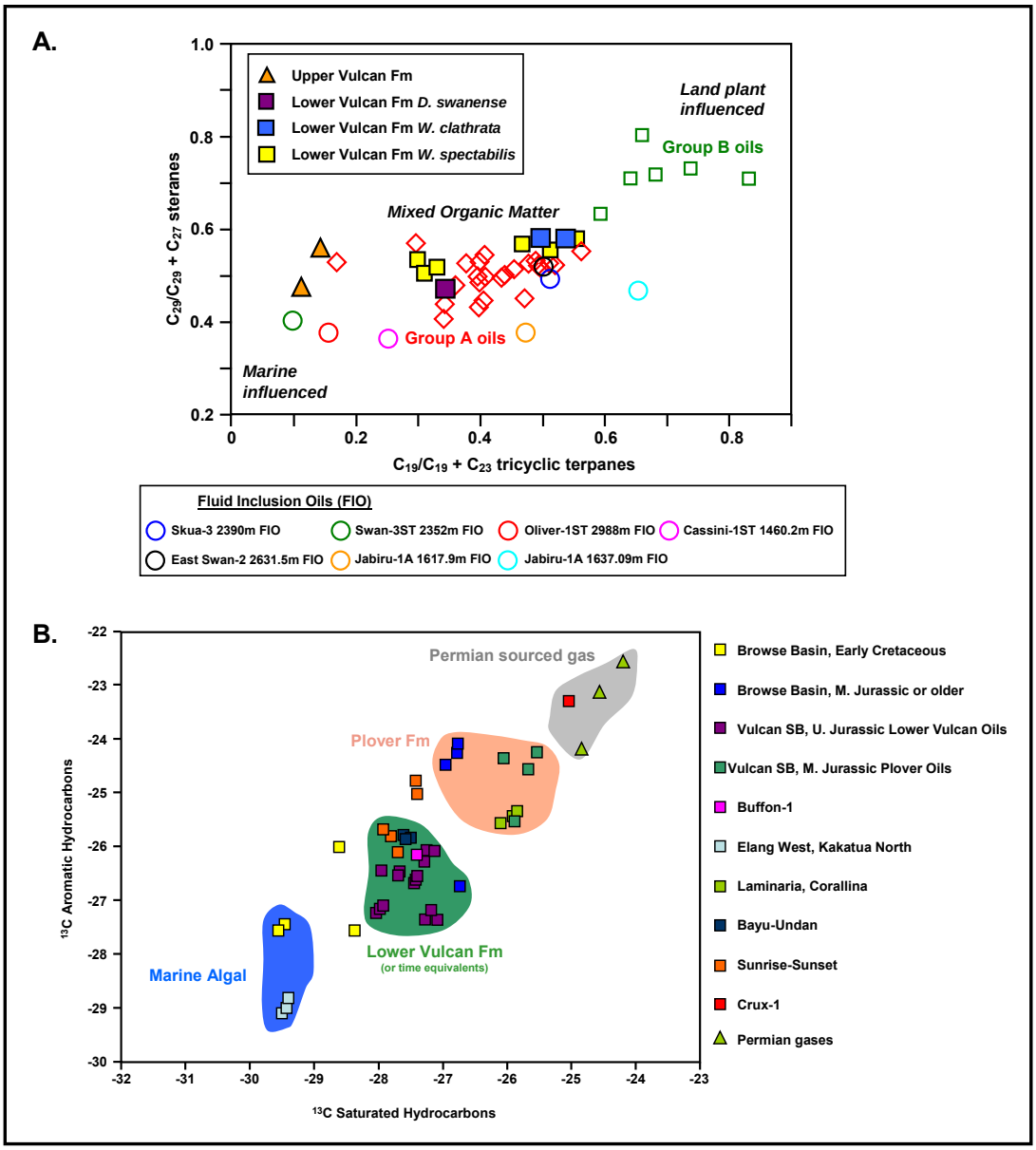

Figure 8-9: Oil-source correlations for hydrocarbons fields from Northern Australia

A. Sterane versus tricyclic terpane cross plot showing crude oils and fluid inclusion oils relative to source rock analyses from the Lower Vulcan Formation. All FIOs show a clearer association with the mixed organic matter facies of the Upper Jurassic Lower Vulcan Formation with Group B crude oils interpreted to be derived from source rocks with a greater land plant influence and most probably sourced from the fluvio-deltaic Plover Formation (modified from Edwards et al., 2004). **B.** Plot of the carbon isotopes for aromatic against saturated hydrocarbons with a selection of key fields shown and inferred source interval. A clear distinction can be made between those VSB oils sourced from Upper Jurassic source rocks of the Lower Vulcan Formation compared against those derived from the Middle-Lower Jurassic Plover Formation (Modified from Kaouru et al., 2004).

8.4.2 Cartier Trough

A clear contribution from the Cartier Trough kitchen can be demonstrated by the Oliver Field that can only be fetch hydrocarbons from that depocentre (Figure 8–8). The gas dominated charge in the Oliver Field together with the generally less oil prone nature of source rocks in the principal depocentre, the Cartier Trough has led to a perception that traps in this area have a higher tendency for gas-rich charge.

The FIO data from Oliver-1 define a much larger oil column than is currently present that together with more recent oil discoveries made at Tenacious (Woods and Maxwell, 2004) and Audacious (Maxwell et al., 2004) and evidence from the GOI results for a substantial oil charge to the presently water-wet Octavius-2 well indicate that the perceived gas risk may mask what was, at least initially, a liquids prone charge system where large palaeo-oil columns were able to accumulate.

The Oliver-1 hydrocarbons are, however, enigmatic with respect to the recognised oil-source correlations. The waxy nature of the oil has previously been used to imply derivation from the terrestrially dominated Plover Formation (Group B, Figure 8–9) with the lack of a defined depocentre in Jurassic times limiting the opportunity for deposition of organically rich Upper Jurassic mudstones that typify the Swan Graben kitchen (Group A).

However, the fluid inclusion oil geochemistry from Oliver-1 indicates a putative source rock, apparently unrelated to either the Plover or Lower Vulcan source rocks. The FIO shows a clear marine signature (Figure 8–9) for the parental source rock with only a limited involvement of higher plants. The current hydrocarbon composition is suggested to be achieved by mixing of an early oil charge, derived from a marine source rock that has subsequently mixed with gas derived from the Plover Formation within a rapidly subsiding Cartier Trough. What remains unclear is whether Upper Jurassic source rocks in the Cartier Trough exhibit a more marine composition than those represented in the Swan Graben or if a totally different source rock was responsible for generating this particular oil.

Potentially this fluid represents a parental end-member of the Group A oils (Figure 8–9), which are themselves a mixture of a marine oil derived from more oil-prone kerogen within the Lower Vulcan Formation together with a contribution from the more terrestrially derived organic matter either associated with facies changes in the Upper Jurassic or reflecting a contribution from the underlying Plover Formation. Indeed it seems unlikely that thermally mature Plover Formation would not have contributed to the charge given the deeper stratigraphic position of this unit. Furthermore whilst older rocks might be expected to provide the earlier charge, the broader activation energies needed to achieve generation and expulsion from such terrestrial (Type III organic matter) source rocks facies (Tissot et al., 1987; Horsfield and Rullkötter, 1994) provides a mechanism to delay the arrival of these hydrocarbons until after charge derived from the thermally more labile shales (higher proportion of Type II organic matter) of the Upper Vulcan Formation.

A significant observation with important implications for future exploration opportunities in the Cartier Trough is that most wells have failed to test a valid closure. Indeed the only valid traps tested in this part of the basin all show evidence of having received oil charge and produced oil columns. On this basis the oil charge rate is placed at 100% (Lisk et al., 1998b) and whilst this is observation is constrained by only a limited number of traps it seems highly likely that any other valid traps will likely also have been oil charged. Additionally, the onset of generation and expulsion from the Cartier Trough in the north eastern VSB is demonstrably much more recent, being driven by increased Late Tertiary subsidence associated with Neogene plate collision. A key implication of the difference in charge timing is that late formed traps can capture oils produced from the Cartier Trough kitchen later in the charge history than predicted from the other source kitchens.

8.4.3 Skua Trough

Traps potentially relying on sourcing of oil from the Skua Trough have previously been considered to include the oil and gas fields of Montara, Tahbilk, Bilyara, and Talbot. Across the Skua Trough the absence of thick Upper Jurassic source rocks coupled with insufficient thermal maturity at this level (Figure 8–7) suggests

hydrocarbons are being derived from fluvio-deltaic facies of the older and more thermally mature Plover Formation. A likely oil-source correlation with the Plover Formation has been defined for these oils (Group B in Edwards et al., 2004), but the dispersed and variable nature of source rocks from this type of depositional setting makes accurate correlations difficult.

Some workers have challenged the role of the Skua Trough as a viable source kitchen with Kennard et al. (1999) suggesting that the Talbot oil field was charged from the Swan Graben and that the Bilyara, Montara and Tahbilk oils were probably sourced from depocentres in the adjacent Browse Basin (Figure 8–8). Irrespective of which source kitchen was responsible for these fields an overall greater propensity for gas indicates a more complicated charge history involving contribution from a mix of different source facies.

Samples taken from these fields have more variable fluid inclusion distributions, typically not showing elevated GOI numbers despite the presence of high oil saturation at the current day. The geochemical composition of the currently reservoired oils provides a possible explanation for this observation, suggesting these oils may be the product of evaporative fractionation. Under this scenario charge to these fields would initially have been single-phase wet gas that converted to a discrete oil leg overlain by gas due to a fall in reservoir pressure after initial charge. Partial trap breach is implied as the mechanism for the required drop in reservoir pressure. In this instance the paucity of oil inclusions reflects the dominant phase of hydrocarbon with gas rather than oil first filling these structures.

8.4.4 Formation Waters during the Passive Margin Stage

Formation waters in the VSB underwent burial related modification throughout the passive margin stage that postdated the end of rifting. The basin became isolated from meteoric water input due to a major marine transgression in the Cretaceous, whilst increasing burial allowed compaction driven flow to become the dominate control on formation water movement.

Current formation waters within the Plover Formation based on hydraulic head values show a dominant flow vector from the south western end of the VSB towards the north east (Figure 8–10) that is inconsistent with radial compaction driven flow away from the discrete depocentres and is most likely reflecting the impact of more recent Neogene plate collision.

Fluid inclusion salinities from samples taken within intact hydrocarbon columns show that formation waters present during the main phase of oil charge were mostly low salinity, ranging from slightly brackish salinities to just above 100kppm (Figure 8–11). These values are consistent with the likely increases in connate water salinity that are produced in closed system diagenesis and derived from basinal fluids being expelled from depocentres by compaction-driven flow. The latter process could explain the bimodal distribution (Figure 8–11) with in situ connate waters mixing with basinal derived waters expelled as burial depths increased in the depocentres.

Stable isotope analyses of carbonate cement that precede quartz overgrowths confirm diagenetically modified water as the most likely parental pore water by this time (Figure 8–3). At likely temperatures of precipitation, oxygen isotopic composition ($\delta^{18}O$) of these waters is calculated to be greater than about 0‰ and possibly as high as 5‰ (Figure 8–3). Marine waters would be expected to have $\delta^{18}O$ values of 0‰ with diagenesis acting to makes these fluids more isotopically enriched (positive $\delta^{18}O$ values); hence the parental waters are likely to represent modified sea-water.

The position of the VSB at higher latitudes during deposition in the Middle to Late Jurassic period suggests that the calculated connate water isotopic composition is likely to have varied from about -7‰ for $\delta^{18}O$ SMOW had meteoric waters been involved up to 0‰ for entirely marine connate waters.

Anticipated increases in $\delta^{18}O$ values for connate waters through time due to increasing burial could easily have produced parental waters with isotopic compositions in excess of 0‰ for the crystallisation of late stage cements.

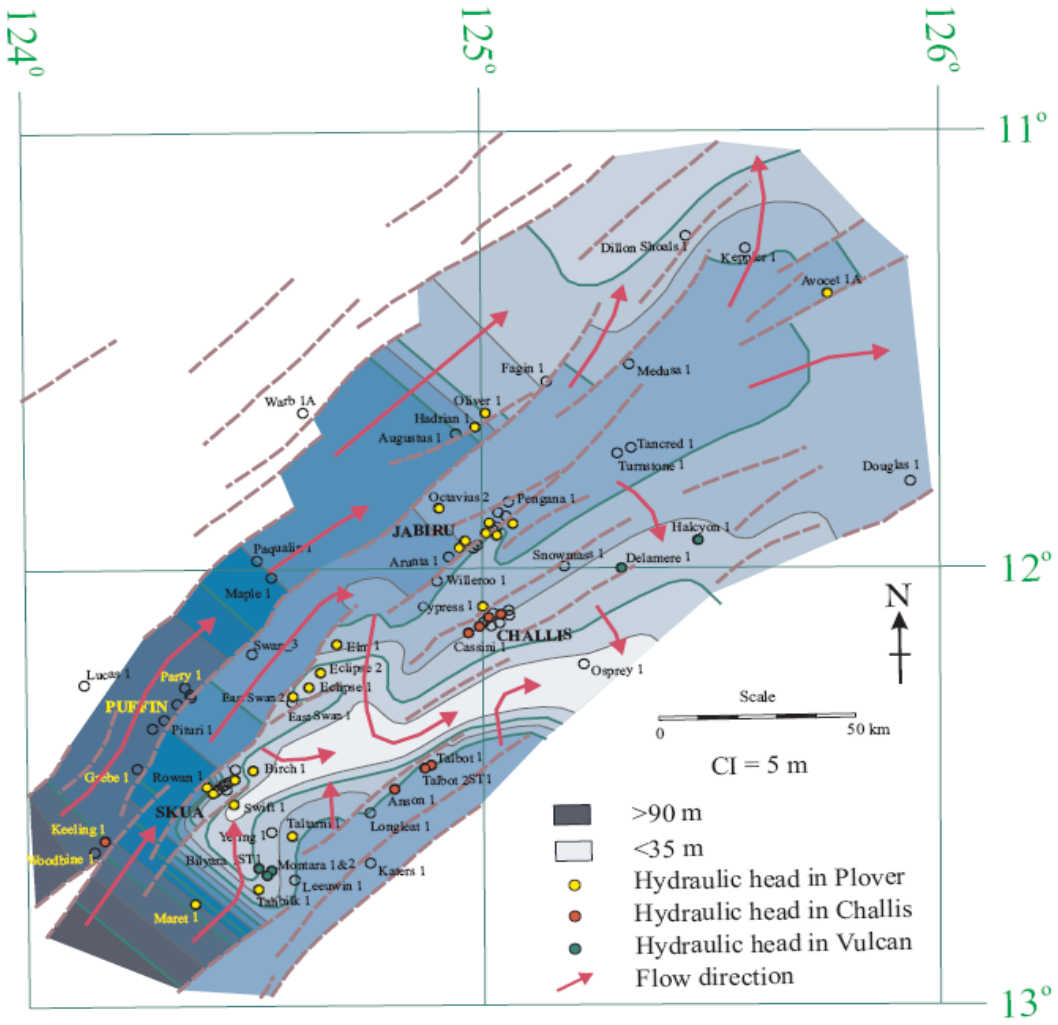

Figure 8-10: Fresh water hydraulic head distribution for the Plover aquifer in the VSB

Map showing hydraulic head values for wells shown in yellow contoured up to illustrate current flow directions for formation waters in the Plover aquifer. A strong gradient in measured hydraulic head indicates water movement is dominated by flow from the southwest to the northeast.

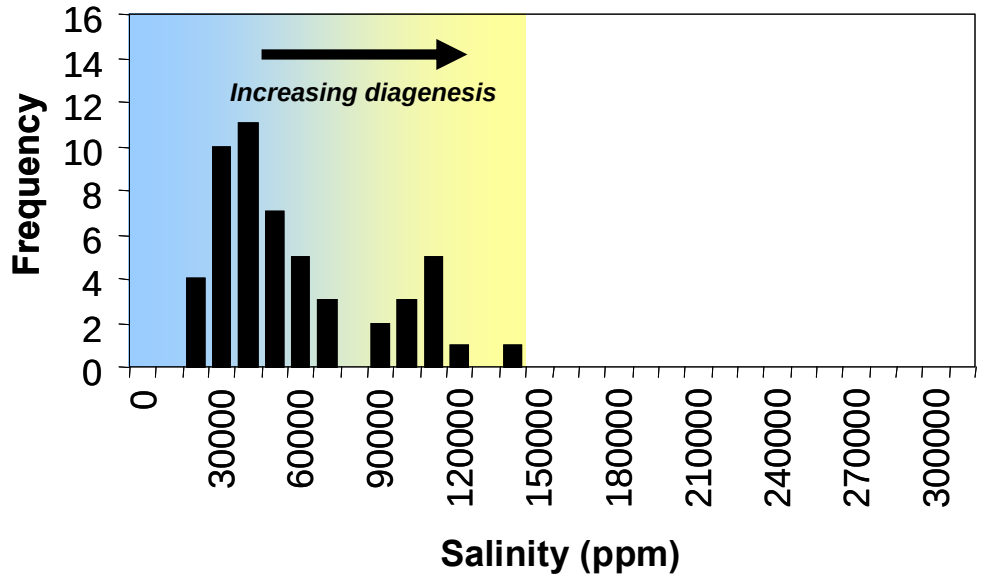

Figure 8-11: Summary of fluid inclusion salinities from current hydrocarbon zones

Salinity measurements made on aqueous fluid inclusions trapped within quartz overgrowths are taken as a proxy for the likely formation water salinities prevailing during hydrocarbon charge. The emplacement of hydrocarbons acts to close these fluids off from the water-leg due to low relative permeability for water (irreducible phase) thus making it unlikely that these samples have been exposed to later "open system" changes to formation water salinity. Instead they reflect ongoing diagenetic modification of original connate waters in a closed system environment and range from values similar to expected depositional conditions up to about 100,000ppm where traps have access to waters expelled from deeper parts of the basin. The bimodal nature of the distribution could reflect inflow of these diagenetically altered waters prior to hydrocarbon charge.

Indeed the relatively modest enrichment (increase in inferred isotopic composition) of formation waters considered parental to these late cements relative to the composition of sea-water indicates original connate waters are likely to have been brackish in nature. This proposition is entirely consistent with the isotopically depleted nature of waters parental to the early diagenetic cements (i.e. derived from meteoric waters) and the fluvio-deltaic depositional environments of the Plover Formation and overlying Lower Vulcan Formation, where mixed marine and non-marine waters would have prevailed as the connate waters.

8.4.5 The Vulcan-Plover (!) Petroleum System by Mid Tertiary Time

Collectively the evidence for the nature of the hydrocarbons and formation waters provided by the fluid inclusion data point to a typical passive margin setting where the Vulcan-Plover (!) Petroleum Systems had developed in a predictable way. By this point in time, somewhere in the Middle Tertiary, a highly effective petroleum system had been created where prolific generation and expulsion of hydrocarbons had produced widespread oil and gas charge derived from at least three discrete source kitchens (Figure 8–12).

Fault dependant traps created or augmented during episodes of Jurassic rifting and blanketed by thick ductile, low permeability, shales provided highly effective trapping configurations allowing most traps to fill with hydrocarbons to the full extent of their available structural closure. Similarities with more productive rift basins such as the Carnarvon Basin (i.e. Kopsen and McGann, 1985; Woodside, 1988; McClure et al., 1998; Tindale et al., 1998) in Australia or the North Sea (Johnson and Fisher, 1998; Gluyas, 2003) would have been striking at this point in time, both in respect to the frequency of charge and the volumetric size of the accumulations at least in the Carnarvon Basin. Furthermore, burial depths across most of the basin remained relatively shallow by this time, with the principal reservoirs maintaining good porosity and permeability. Mud-rich facies deposited locally during the late syn-rift and more regionally during post-rift basin-wide transgression provided traps with excellent seals that were largely unfaulted and had capillary properties capable of retaining closure heights well in excess of most, if not all, maximum structural closure heights.

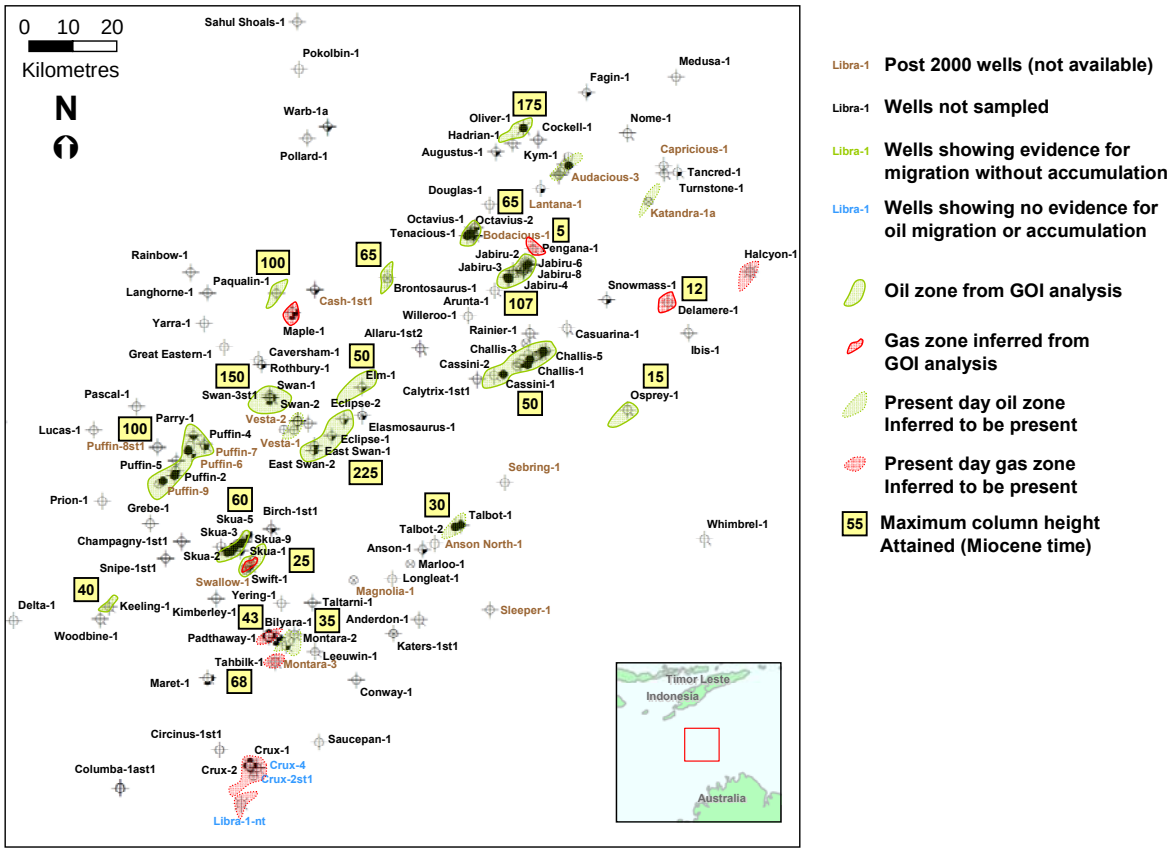

Figure 8-12: Distribution of hydrocarbon accumulations prior to Neogene Collision.

Summary of spatial distribution, interpreted column heights and hydrocarbon phase contained in VSB traps in Miocene time. Also shown is a breakdown of wells by drilling date to show which wells existed at the start of the current study (i.e. pre 2000). Hydrocarbon zones that exist at the current day but have no GOI data available to assess the palaeo-fill history are shown with dashed outlines except where other evidence is available to show they were not charged until after Neogene reactivation. The Tenacious Field is omitted for example because the structure formed as a product of post Miocene fault reactivation and hence charge must post-date reactivation.

Prograding Cretaceous and Tertiary sediments produced some modification of traps through regional tilting induced by differential loading and compaction. This resulted in subtle trap geometry changes that modified spill points and allowed redistribution within traps and remigration of some of these oils across the revised spill-points. The only impediment to traps being filled to spill appears to have been zones of pre-existing structural weakness caused by the intersection of Proterozoic Basement faults with Jurassic rift faults that were initially re-activated in the Early Tertiary, immediately prior to the onset of oil charge.

Gartrell et al. (2002, 2004) described the role of these fault intersections in controlling the fill capacity of the Skua Oilfield in the southwestern part of the VSB. Reported seepage data (O'Brien et al., 1996; 1998) including hydrocarbon slicks floating on the water and seismically inferred Hydrocarbon Related Diagenetic Zones (HRDZ) described by O'Brien and Woods (1995) cluster above these fault intersections (Cowley and O'Brien, 2000; Figure 8–13). These intersection zones were created by fault reactivation pre-dating the main phase of Neogene reactivation. Gartrell et al. (2004) attribute these to far field effects probably initiated by the collision of Greater India with Asia sometime in the middle Eocene (40–45 Ma; Veevers et al., 1991) and augmented by early Miocene deformation related to the onset of collision along the northern Australian passive margin (Etheridge et al., 1991). These structural weaknesses preceded hydrocarbon migration into the Skua area and provided passive leak points on the flanks of the Skua Field that appear to have limited the size of the accumulation (Gartrell et al., 2004).

The broader role of similar fault intersection zones in controlling trap integrity remains to be demonstrated for the VSB, but the clearly defined intersection of different rift fault sets together with the distribution of inferred Proterozoic lineaments across the VSB and adjacent Browse Basin (O'Brien et al., 1993; Figure 8–13) makes it unlikely that the observations made at the Skua Field represent an isolated example.

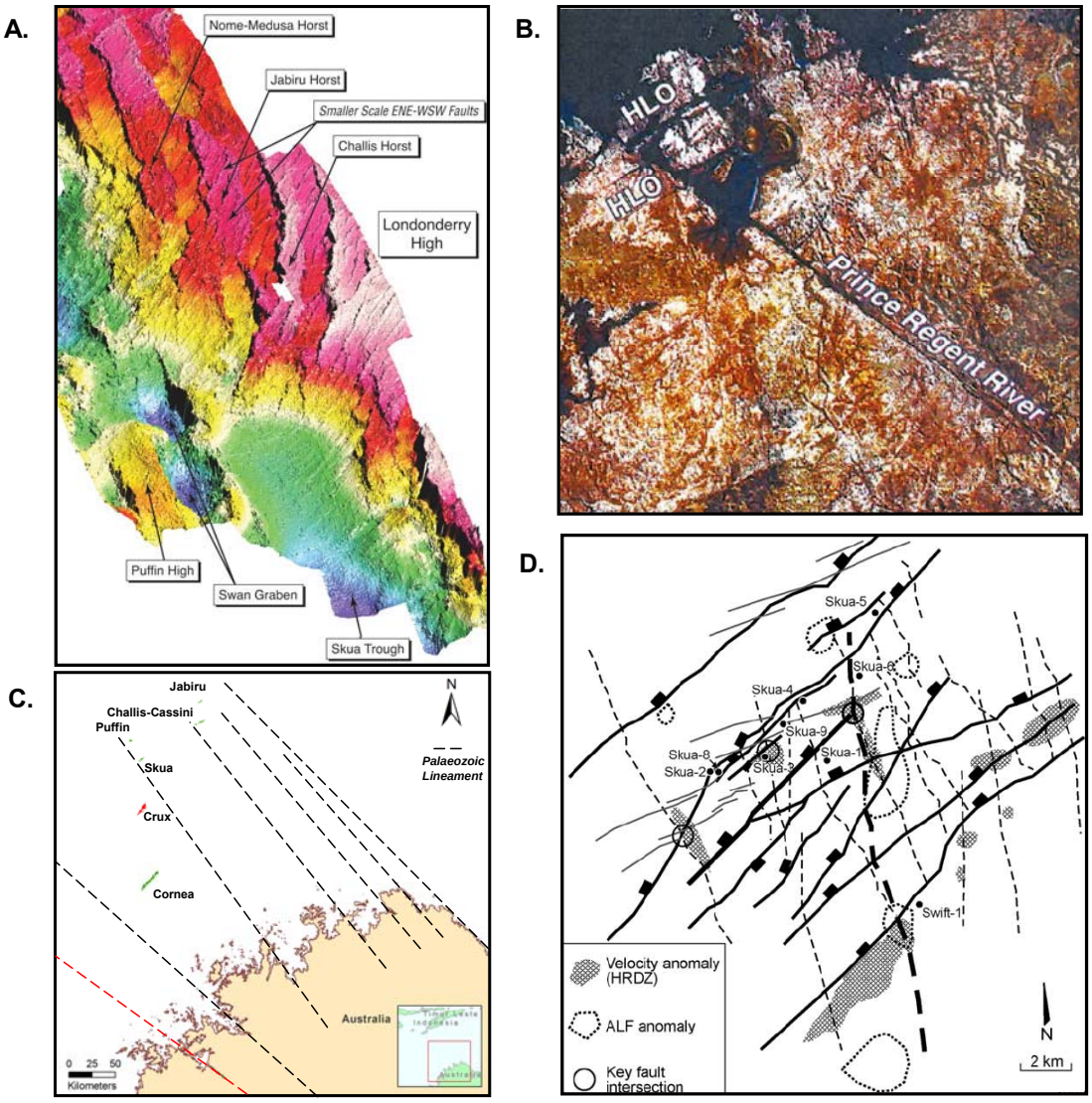

Figure 8-13: Role of basement faults in controlling initial trap fill.

Faults seen at the Top Permian surface (A.) clearly indicate intersecting fault trends with a dominant NE-SW set overprinted by a more N-S orientated population. Major NW-SE trending lineaments cross the current Kimberly cratonic block (B.) and the reentrants in the present coastline are considered to be the result of similar long-lived Proterozoic lineaments (C.). Gartrell et al., (2002) described a relationship between these lineaments and subsequent Jurassic rift and Tertiary reactivation faults near the Skua Field showing a strong focusing of vertical leakage indicators (HRDZs and ALF anomalies) where these fault trends intersect (D.).

8.5 NEOGENE COLLISION (W2)

The relatively minor fault reactivation noted in the Early Tertiary represents the first indication that plate tectonic collision initiated by episodes of Jurassic rifting along the North West Shelf and Cretaceous rifting from Antarctica along the Australian southern margin would transmit an increasingly destructive impact on the Timor Sea petroleum systems. These early signs, probably reflecting the indentation of Greater India with Asia at about 45Ma (Veevers et al., 1991; Hall, 1996, 2003) were dramatically increased when the northwards moving Australian Plate began to collide with the predominantly east-west orientated S.E. Asian plates to the north.

Initial collision occurred away to the east with a promontory of Australian crust reaching the area near the current position of New Guinea Island at about 25Ma (Figure 8–14), resulting in terrane accretion and widespread uplift along the entire New Guinea Fold Belt (Hill and Hall, 2003; Keep et al., 2002). Aside from some minor neo-formed faulting and limited rift fault reactivation the VSB likely remained relatively unaffected by the far field effects experienced at this time. With the Australian continent pinned near New Guinea strain associated with the ongoing northwards drift of the Australian Continent was increasingly accommodated both by shortening at the pin point (i.e. compression) and by the consumption, through subduction, of oceanic crust lying to the south of Sumba and outboard of the Bonaparte and Browse basins (Pigram et al., 1991) since 25Ma (Muller et al., 1998; Keep et al., 2002; Figure 8–14).

A series of more dramatic impacts stemming from these events occurred in two distinct stages that were initiated in the Late Miocene as convergence and collision between the Australian continental plate and the Banda Island Arc began (Woods, 1994). The two main stages of Neogene collision are recognised from observations on Timor Island (Charlton et al., 1991; Woods 1994) where the timing of the main tectonic events can be discerned. The first stage is inferred to have occurred in the late Miocene (~8Ma) when the transitional Australian continental crust first reached the subduction system, whilst the second stage was initiated when true Australian continental crust entered the subduction system in the middle Pliocene (3Ma).

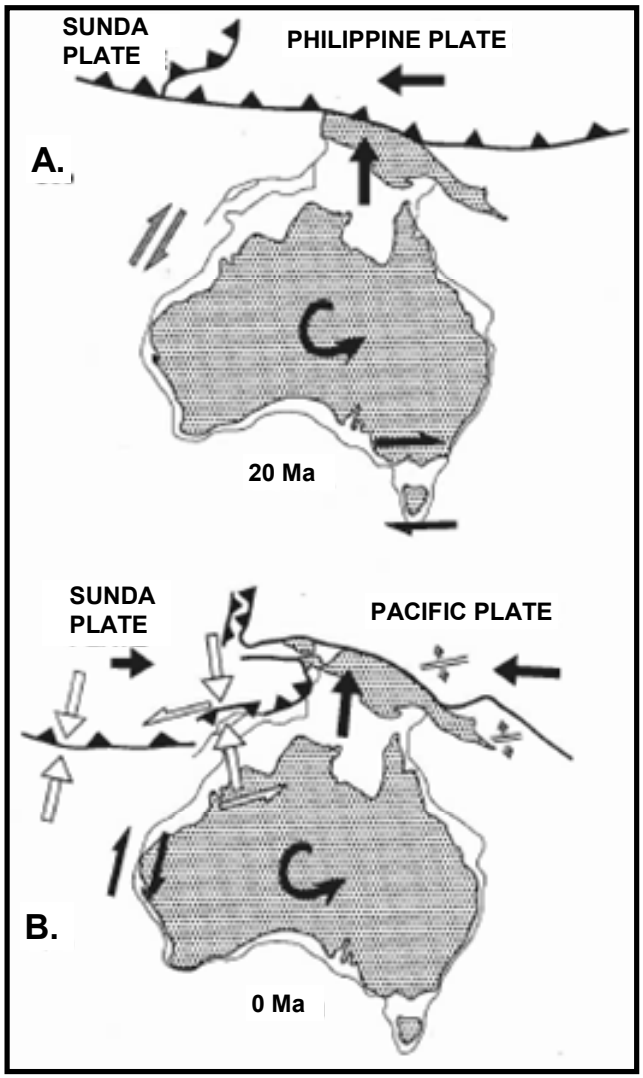

Figure 8-14: Interpreted strain regimes across Northern Australia through the Tertiary.
Interpreted plate margin orientation and vectors shown for the plate margin at A). 25-20 Ma and B). 5Ma to present (from Keep et al., 2002). Interaction of the westward moving Philippine Plate with the Australian Plate from 25-20Ma produced sinistral rotation of the Australian Continental lithosphere during this time. From 5Ma until the present the leading edge of Australia moved more than 1000km north of the former zone of oceanic plate subduction extending east from the southern margin of Sundaland, with continued sinistral rotation along the northern New Guinea margin coupled with dramatic shortening associated with oblique convergence between the Sunda and Australian plates. Barbed lines = plate boundaries; shaded areas = continental crust; solid black arrows = absolute plate motion vectors; white arrows = relative plate motion vectors; grey arrows = local deformation regimes; small opposing arrows and parallel lines = spreading centres.

The introduction of buoyant Australian Continental crust had the effect of blocking the subduction zone in the Timor region that in turn caused the Banda Arc and associated accretionary complex to be thrust northwards over the floor of the Banda Sea (Snyder and Barber, 1997), resulting in the rapid uplift of the island of Timor.

Northwards movement of the Australian Plate continues at the current day at about 8 cm/y (Veevers at al., 1991) with Global Positioning System (GPS) geodetic measurements showing that Timor Island and the inner Banda arc are moving northward at the same rate as the Australian Continent (Genrich et al., 1996). This suggests that ongoing convergence is no longer being accommodated by movement on the Timor thrust to the north, rather continued convergence is thought to be taken up by a combination of back arc thrust faulting and strike slip cross arc faulting across the Wetar back arc thrust zone immediately to the north of Timor Island (Snyder and Barber, 1997).

Pronounced flexural bending of the leading edge of the Australian Plate margin and creation of the deepening Timor Trough during the early Miocene (Patillo and Nicholls, 1990; O'Brien et al., 1993) produced a sharp increase in sedimentation and initiated the widespread reactivation of pre-existing Precambrian to Mesozoic faults (Nelson, 1993; Shuster et al., 1998) as well as formation of associated arrays of neoformed faults. Fault movement started at about 8–10 Ma, with a distinct growth pulse occurring at 3–5 Ma in some areas (Gartrell et al., 2006). The highly effective petroleum system that existed in the VSB prior to the Early Miocene was dramatically and irrevocably diminished by this phase of intense fault reactivation, which led to the widespread breaching of hydrocarbon columns across the Vulcan Sub-basin (Patillo and Nicholls, 1990; Lisk et al., 1998a) and broader Bonaparte Basin (Castillo et al., 2000; de Ruig et al., 2000; Brincat et al., 2001).

Many workers attempt to explain the nature of fault reactivation in the Timor Sea region with reference to the contemporary stress field (Hillis, 1998; Castillo et al., 1998; Castillo et al., 2000; de Ruig et al., 2000). Contemporary stress measurements, based on borehole information, generally indicate that strike-slip or mixed strike-slip and extensional (transtensional) mode stress regimes currently exist across the region with $\sigma 1$ being horizontal (Sh_{max}) and oriented approximately 55–65° (Hillis, 1998).

These studies consider that in a population of pre-existing fractures, those that are critically stressed with respect to the in-situ stress tensor are more likely fail and could provide suitable permeable conduits for vertical fluid leakage (Jones et al., 2002). The parallel orientation of fault trends with the direction of Sh_{max} (Figure 8–15) indicates that a majority of traps in the VSB are prone to fault reactivation under the prevailing stress field.

A principal assumption associated with these predictions is that the stress field has remained unchanged. Hillis (1998) notes that the high differential stress ($\sigma 1 - \sigma 3$) that currently exists across the Timor Sea region promotes fracturing by shear failure and that tensile failure is not possible in this setting. The presence of extensional faults, however, that are apparently unrelated to older faults demonstrates that not all of the deformation can be explained by a transtensional stress field as the development of these neoformed normal faults is difficult to explain in the current stress field (i.e. when $\sigma 1$ is horizontal; Gartrell and Lisk, 2005).

The concept of a constant stress field is difficult to accept in light of the complex Neogene tectonic history and O'Brien et al. (1999a) suggest a significant change in the regional stress regime occurred at approximately 2.5 Ma, when volcanism and thrusting on Timor stopped, and convergence between Timor and the Australian mainland apparently ceased. A notable decrease in fault displacements to the in the Timor Sea since that time supports this proposition (e.g., Meyer et al., 2002).

In order to gain a more direct estimate of the palaeo-stress field operating in the VSB Gartrell and Lisk (2005) used a fault slip inversion method to evaluate the palaeo-stress conditions operating in the Miocene in the vicinity of the Skua oil field. This work contributes a geomechanical explanation of the observed fault patterns that is consistent with the regional tectonic evolution over the Miocene to recent time period. In contrast to the contemporary stress field where mixed strike-slip and extensional mode stress regimes prevail, the work by Gartrell and Lisk (2005) demonstrates that a principally extensional stress regime existed in the VSB at Late Miocene time, with $\sigma 1$ oriented vertically.

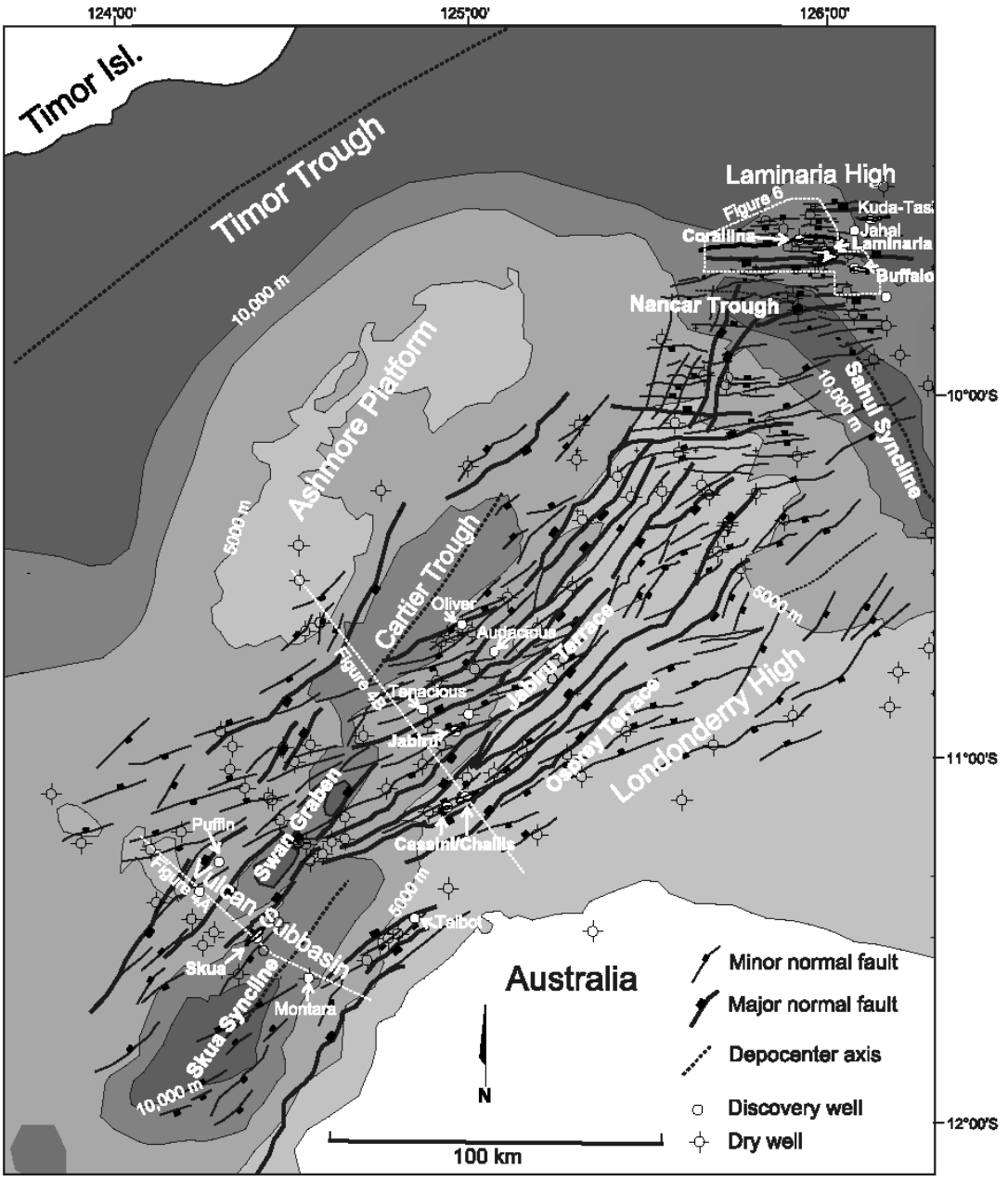

Figure 8-15: Regional fault map at the top Permian seismic marker level for the Timor Sea.

Taken from Gartrell et al. (2006) the map compiles fault information taken from Woods, 1992; Shuster et al., 1998; de Ruig et al., 2000 and Edwards et al., 2005 and demonstrates the prevailing NE-SW orientation of faults in the Vulcan Sub-basin with a E-W orientation dominant across the Laminaria High and Nancar Trough to the northeast.

Mohr circle constructions presented by Gartrell and Lisk (2005) demonstrate the practical importance of concluding that the stress field has recently changed (Figure 8–16). Prior to the Miocene the VSB existed as a passive margin where the impact of accumulating burial would be expected to produce a maximum stress ($\sigma 1$) that is vertically orientated. Existing faults and fractures formed during the main Jurassic rift phase mostly persisted as tectonically inactive features at this time (Figure 8–16).

The impact of sharply increased subsidence associated with early plate collision was a dramatic acceleration in the rate of burial, causing vertical stresses to climb and leading to an overall higher maximum stress ($\sigma 1$). A higher value for $\sigma 1$ produced a larger differential stress (i.e. $\sigma 1$-$\sigma 3$); enlarging the size of the failure envelope and causing existing faults to be reactivated (Figure 8–16). Comparison with inverted fault slip data from the Skua oil field allowed this theoretical prediction to be validated (Figure 8–16) at least at the field scale (Gartrell and Lisk, 2005).

Reactivated Jurassic rift faults pierced through the Cretaceous regional seal (Figure 8–17) and together with shallow arrays of neoformed faults that formed concomitantly created pathways of linked structural permeability (Sibson, 1996) that allowed vertical fluid flow into the shallow section from underlying Jurassic reservoirs (Figure 8–18).

Observational evidence from the Timor Sea region based on mapping the frequency and displacement profiles of reactivated faults demonstrate that within a given fault population, strain tends to progressively localise onto the largest faults over time (Meyer et al., 2002). Large faults grow at the expense of smaller faults and display higher growth rates (Gartrell et al., 2006). This process of strain localization is characteristic of fault systems in general and has been demonstrated at a range of scales, using a variety of techniques (e.g., Cowie 1998; Walsh et al., 2001).

In general the impact of strain localisation processes in the VSB was deleterious to the preservation of large hydrocarbons columns as these typically would occur in the biggest fault bound traps, which provide the greatest area of closure and often represent regional structural highs that in turn act as focal points for the largest hydrocarbon migration fetch areas.

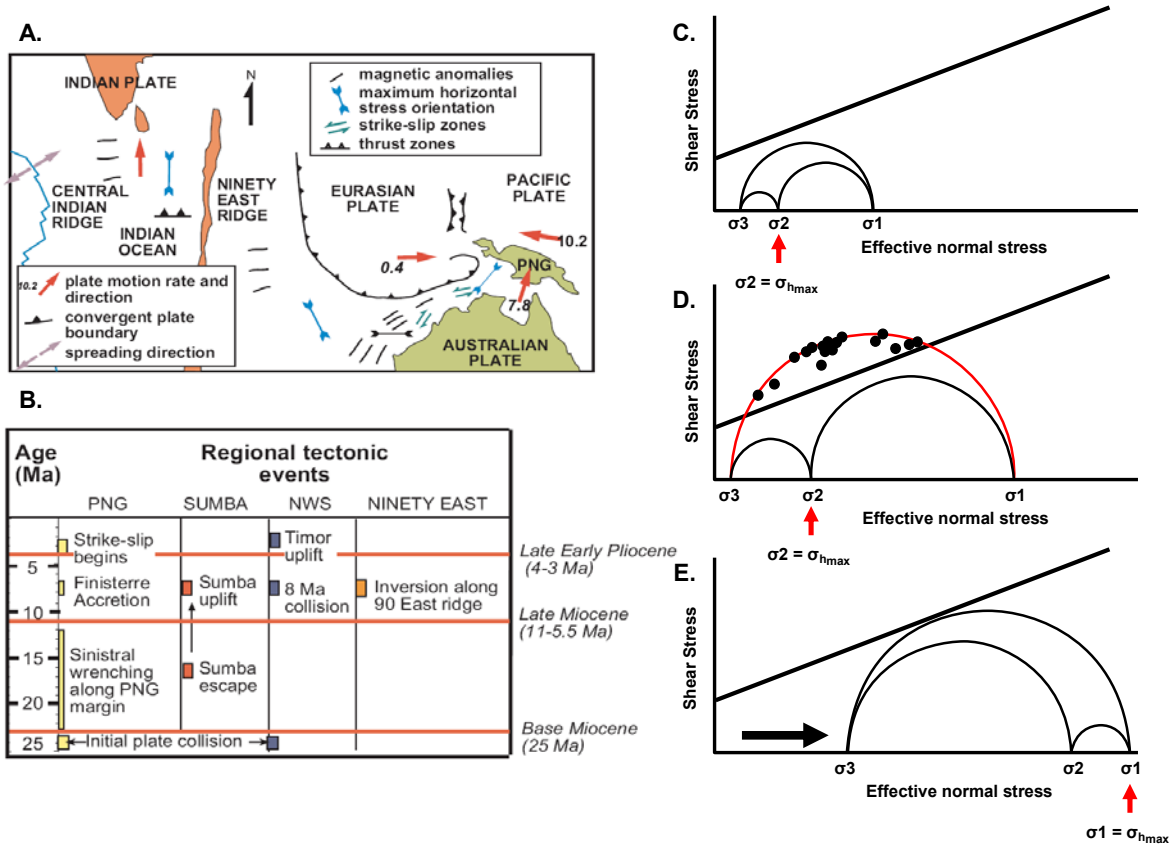

Figure 8-16: Tectonic evolution of the VSB during the Tertiary.

Composite diagram taken from Keep et al. (2002) and Gartrell and Lisk (2005) showing A., the relative direction and rate of plate margins at the current day together with B., a summary of the key regional tectonic events. C-E shows indicative Mohr Circles and failure envelopes for fault rocks that have an implied degree of cohesive strength. Stress conditions be the early Miocene are less than required to reactivate existing faults (C.) but a dramatic increase in vertical stress (σ1) caused by rapid Tertiary burial enlarges the Mohr circle placing existing faults above the failure envelope and resulting in reactivation of existing faults and propagation of new ones (D.). The black dots represent the orientations of activated fault planes determined from the inversion of fault slip data from the Skua Field (Gartrell and Lisk, 2005). Jamming of the subduction zone by introduction of Australian Continental crust by Late Miocene time produces a rapid increase in both vertical and horizontal stresses so that the higher magnitudes for all the principal stresses (i.e., higher mean stress) causes the Mohr circle for the present-day stress tensor is shifted to the right, away from the failure envelope (E). This concurs with the observed reduction in the amount of reactivation seen on regional seismic data.

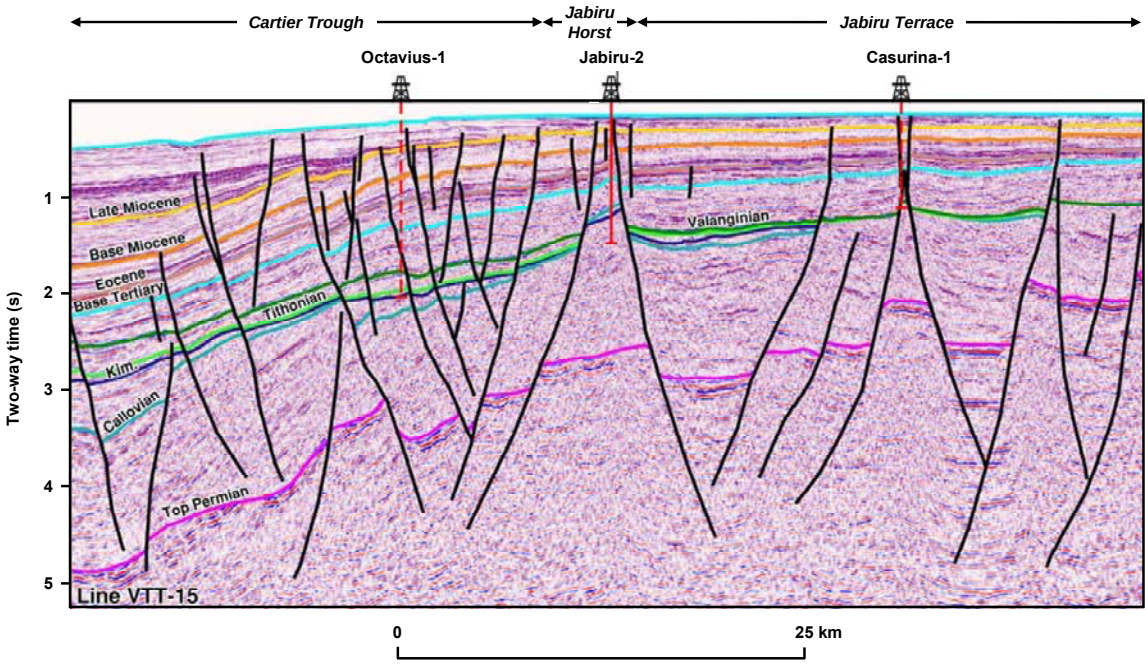

Figure 8-17: Seismic examples of fault reactivation in the VSB

A section of the 2D seismic line VTT-15 (from Geoscience Australia, 2008) showing typical examples of fault reactivation that is widespread across the VSB. A comparison of fault offset between the Base Miocene and Callovian horizons can be used to assess the magnitude of reactivation and shows how trap configurations at the Jurassic level can be altered significantly as a result of Neogene reactivation. Also note the lack of sea-floor offset as well as the reducing fault throws at the Late Miocene horizon compared with the Base Miocene horizon and the general reduction in the amount of faulting. All of these observations point to a system where the intensity of reactivation is decreasing from a maximum experienced in the Early Miocene.

Additionally these large structures are likely to be the most prominent features that are normally recognised earlier in the exploration history of a basin and are preferentially targeted by exploration drilling, typically in order of decreasing size.

The widespread reactivation of faults during this major tectonic episode and the accompanying creation of linked vertical permeability pathways have resulted in two equally widespread and interlinked fluid-flow events.

1. Hydrocarbon leakage from reactivated fault dependant traps

2. Flow of highly saline brine probably released from deep overpressured salt beds

Widespread trap breaching and the associated leakage of hydrocarbons is recognised from the identification of numerous residual (from conventional oil show data) or palaeo-oil columns (from fluid inclusion data) at the Jurassic reservoir levels (Lisk et al., 1998b) and through the detection of hydrocarbon seepage into the shallow overburden section and the overlying water column (Lisk et al., 1998b; O'Brien et al., 1996a; 1998; O'Brien and Woods, 1995).

Fault reactivation demonstrably compromised seal integrity of Mesozoic traps, with partial or complete breach of more than 10 oilfields (Lisk et al, 1998b) and attendant loss of substantial hydrocarbon volumes. O'Brien et al. (1996a) estimated that more than 400 million barrels of oil leaked from the Jabiru and Skua fields alone.

The vertical migration of oil and gas across the intervening Cretaceous regional seal via newly formed fault pathways enabled Jurassic derived hydrocarbons to access high permeability sandstones in the Cretaceous Puffin Formation, probably allowing charge to the Puffin (oil) and Swan (gas) fields that are reservoired at this level (Figure 8–18). Where these sandstones were absent or poorly developed vertical hydrocarbon leakage continued upwards into the Tertiary section. Porous potential reservoirs are represented by the Grebe and Oliver sandstones typically lack viable seals with a combination of high primary porosity of the Barracouta Formation calcarenites and the intense faulting probably allowed most of oil and gas to seep directly into the water column (Figure 8–18).

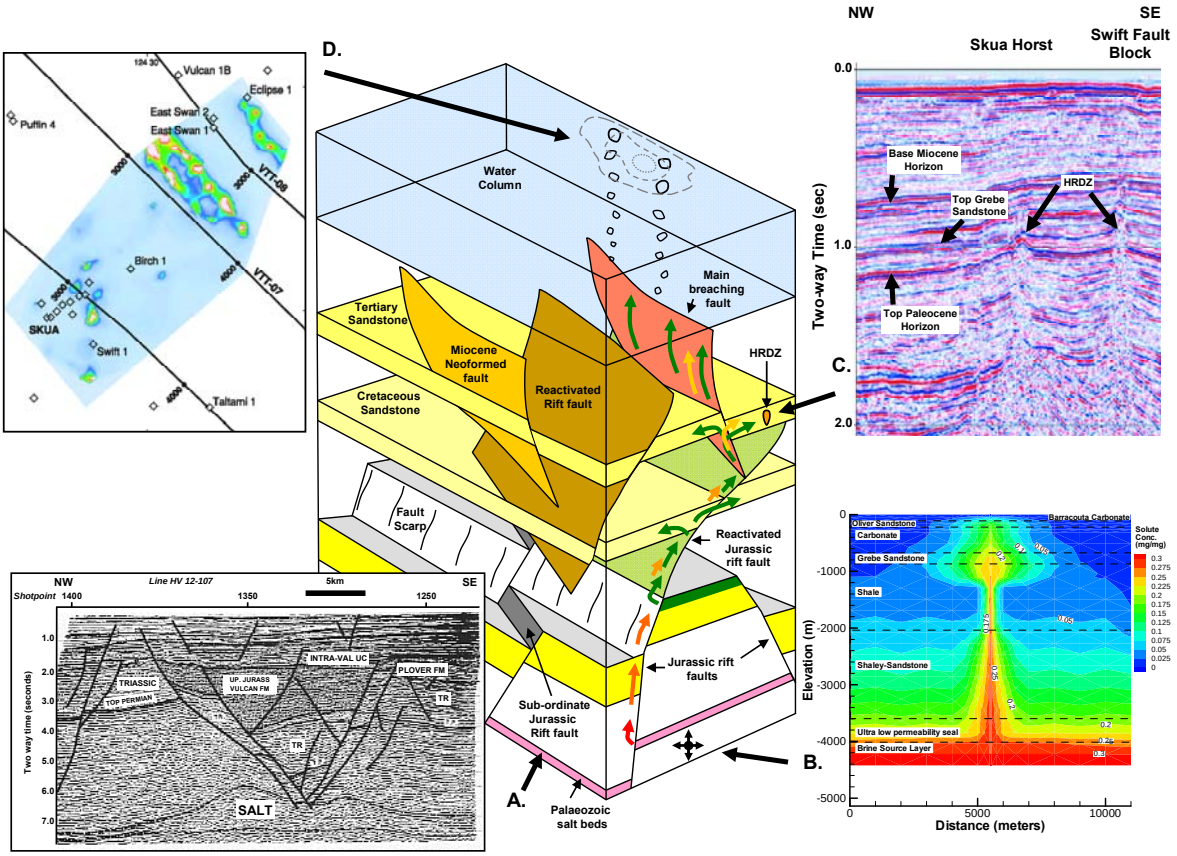

Figure 8-18: Schematic cartoon showing impact of fault breaching on fluid distribution.

The key components contributing to the observed palaeo and present day fluid distribution are shown relative to a block diagram illustrating the position of each feature in a simplified composite diagram. Deep salt beds (A) not penetrated by wells but inferred from seismic observations (from Woods, 1994) provide an impermeable layer that allow overpressure to build that probably plays a key role in driving fault reactivation. Reactivation of major rift faults breaches the overpressured sub-salt section and allows a hot brine plume (B) to flow vertically up faults and into Mesozoic and Tertiary strata (Lisk et al., 2000b). Hydrocarbon filled traps in the Jurassic section are compromised by fault reactivation with attendant vertical leakage of hydrocarbons into the shallow section to provide a remigrated charge into Cretaceous sandstones or leakage into the Tertiary section where degradation of hydrocarbons results in the formation of hydrocarbon related diagenetic zones (C; HRDZs; O'Brien and Woods, 1995). Where faults extend near to the surface increased matrix porosity or structural damage zones associated with reactivation allow seepage directly into the water column to be detected by remote sensing techniques or direct sampling of the water column (D; O'Brien et al., 1998).

Remnants of the hydrocarbons that have leaked from deeper reservoirs remain in the shallow section, sometimes reported as residual oil staining but more widely as features referred to as hydrocarbon related diagenetic zones (HRDZs, Figure 8–18). HRDZs (O'Brien and Woods, 1995) are commonly observed in the shallow section across the Timor Sea region (Cowley and O'Brien, 2000) and are attributed to the degradation of hydrocarbons leaking from the underlying Mesozoic traps. The hydrocarbon link comes from carbon isotope analyses on rock samples taken from HRDZs that have been drilled, with strongly depleted isotopic compositions measured on pervasive calcite cements being ascribed to low temperature biological oxidation of leaking hydrocarbons (O'Brien and Woods, 1995; Boetius et al., 2000).

Abundant CO_2 produced by this process resulted in zones of intense, but localised, carbonate cementation (O'Brien and Woods, 1995; O'Brien et al., 1998) within these sandstones that in turn produce sufficient acoustic impedance contrast to cause a strong seismic response (Figure 8–19), allowing the HRDZs to be easily mapped on seismic data (Cowley and O'Brien, 2000).

The HRDZs show a strong association with through-going reactivated faults often clustering above such features (Figure 8–19) and are larger where observed over breached oil columns such as East Swan compared with HRDZs recorded over intact oil fields (O'Brien et al., 1996a; 2002b). Above the partially breached Jabiru Field where GOI data define a thick palaeo-oil zone beneath the current OWC the observed HRDZs cluster above faults that transect the Jurassic reservoir section above the palaeo-OWC but down-dip from the present OWC. This distribution suggests leakage from the Jabiru Field was focused on faults at the edges of the field with more crestal faults being shielded from reactivation and thereby remaining effective seals (Figure 8–18).

Aside from the remigration of hydrocarbons during fault reactivation fluid inclusion salinity data indicate highly saline formation waters, probably derived from deep overpressured Palaeozoic salt beds, migrated vertically at the same time. This brine flow event is equally widespread and is likely to have had a significant impact on the rocks it flowed past and the composition of the formation waters left behind.

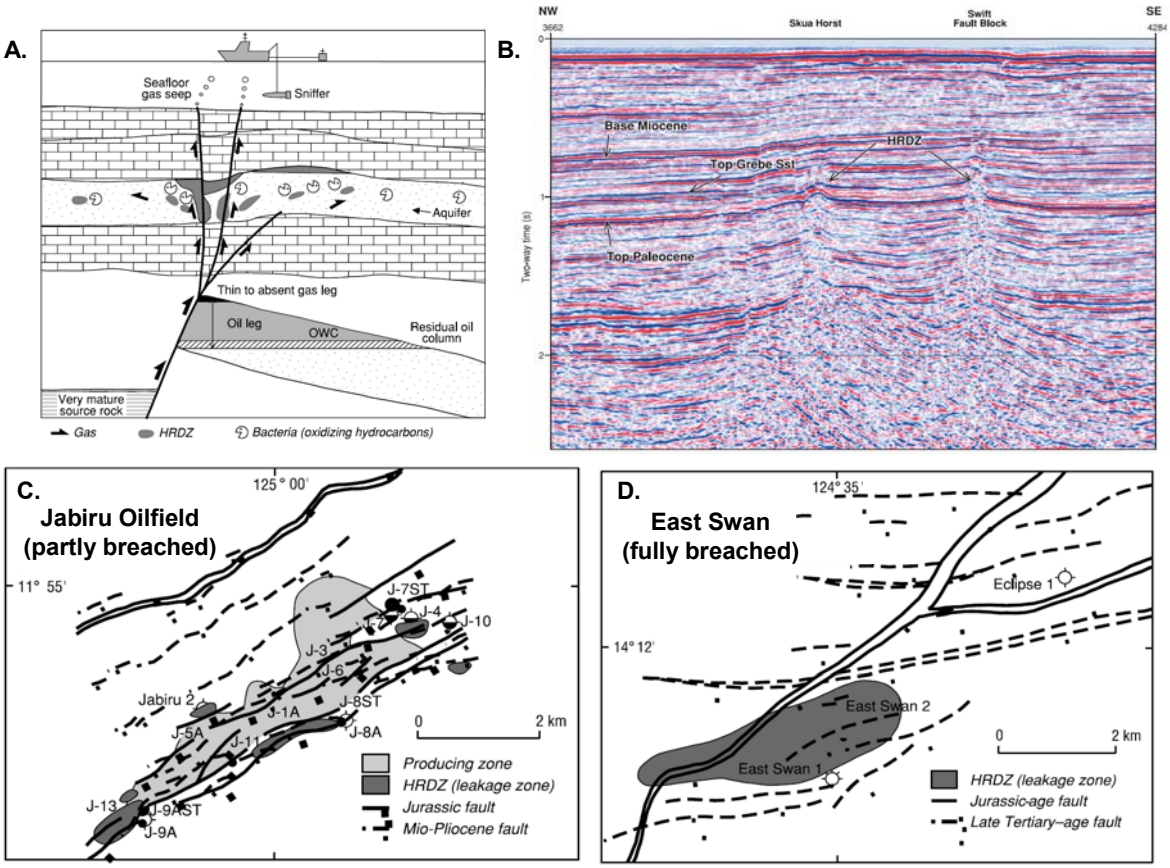

Figure 8-19: Formation of Hydrocarbon Related Diagenetic Zones (HRDZ)

A composite diagram describing the key features that characterise the many HRDZs seen in the Tertiary section from across the VSB (taken from O'Brien and Woods, 1995 and O'Brien et al., 1996a). A. The process of HRDZ formation is illustrated with leaking hydrocarbons being consumed by methanogenic microbes within shallow aquifers with the resultant excess CO_2 being buffered by the crystallisation of localised carbonate cements. B. Seismic distortion in two-way-time being produced by velocity anomalies associated with the HRDZs across the Skua-Swift fields. C. The distribution of HRDZs around the margins of the partially breached Jabiru oil-field consistent with the shrinkage of the oil zone due to vertical hydrocarbon loss. D. A contrasting much larger HRDZ associated with the fully breached East Swan palaeo-oil column that is characterised by high-angle fault intersections.

Whilst the flow of saline brine may have been simply a consequence of the widespread fault reactivation it seems possible that these deep salt beds may have played an important role in driving the process, initially as décollement surfaces (Woods, 1994), but then through the release of major overpressure trapped beneath previously impermeable salt beds (Figure 8–20) acting as a key impelling force (Sibson, 1987; 1996) in propagating fault failure. Furthermore, the hot and chemically reactivate brines probably contributed to the maintenance of fault zone permeability after fault movement abated.

The timing of brine flow can be discerned from the distribution of high salinity fluid inclusions that are restricted to samples from residual hydrocarbon zones or current water-legs (Figure 8–20). Highly saline brines flowed into the reservoirs where faults intersected sandstone aquifers, except where continued high hydrocarbon saturations provided zones with low permeability to water that acted to isolate the hydrocarbon zone and prevent ingress of high-salinity fluids (Figure 8–20). This places brine flow after initial hydrocarbon charge, with Neogene fault reactivation providing the driving mechanism for flow to occur.

Significant localised convective heating associated with brine flow affected maturation levels in traps located close to these brine injection points (Figure 7–23), but does not appear to have influenced regional maturity levels (Figure 7–24). Examples of convective heating associated with fluid flow along faults are becoming more widely recognised in sedimentary basins (Xie et al., 2001; Lampe et al., 2002). Following entry to the aquifer, down-dip migration of brines was promoted by the significant density contrast between the dense brine and the resident, relatively low salinity, low density connate water. The heat transfer potential of groundwater flow is well documented (e.g. Bethke, 1985) and traps located away from the point of brine entry may have experienced a relative cooling effect with downward flowing brine acting as a heat sink.

Brine flow waned as the excess fluid pressure created by the release of overpressure was bled off causing a return to static conditions, with a residual salinity anomaly only present in areas where leakage is ongoing and in the deeper parts of the basin where these denser fluids would have been collecting due to the density contrast.

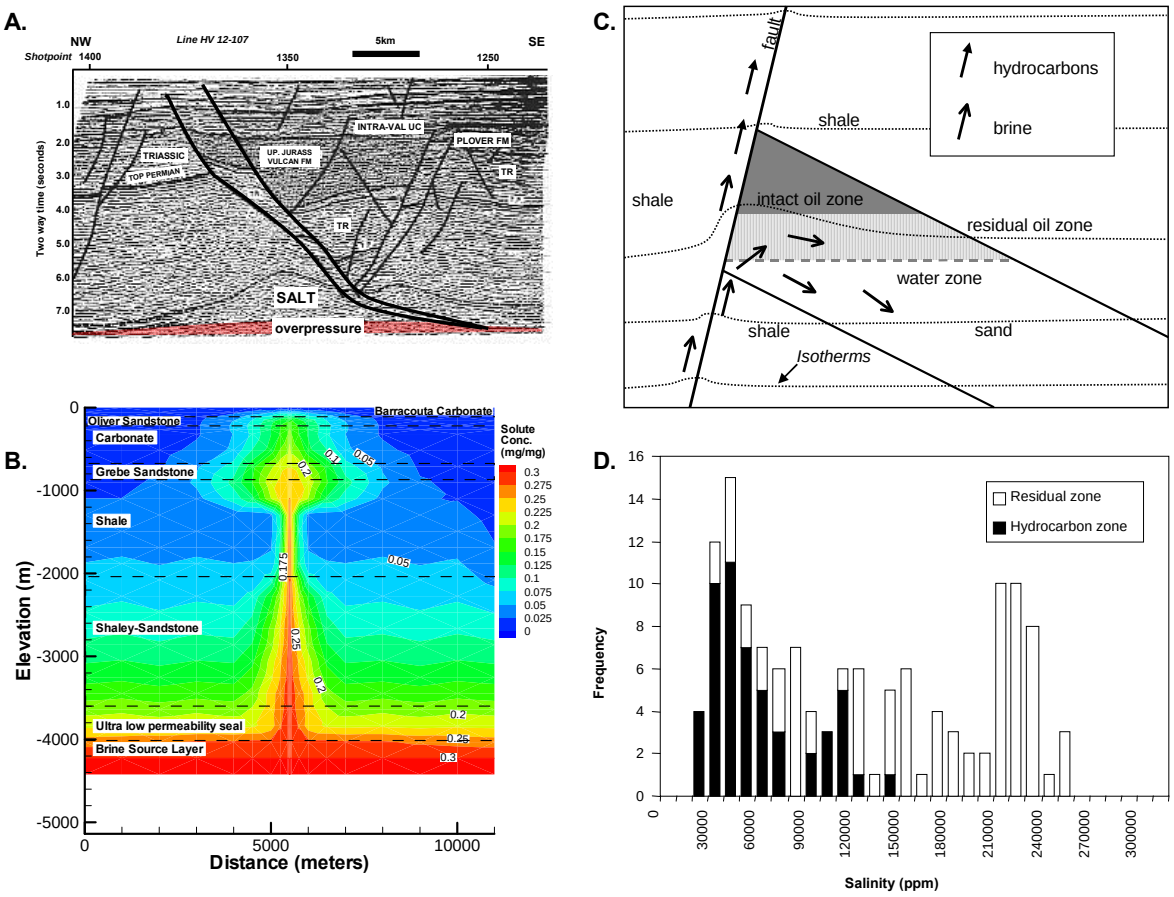

Figure 8-20: Role of regional brine flow in the VSB.

Summary of the key elements associated with the flow of saline brine. A. 2D seismic line (HV12-107) showing interpreted salt pillows (From Woods, 1994) with an implied overpressure cell trapped beneath ultra-low permeability salt beds. B. Output from a numerical modelling package (RIFT2D) showing the development of a significant brine plume in the Tertiary Grebe sandstone developed as a result of trap breach at about 5.5Ma (from Lisk et al., 2000b). C. Cartoon showing brine flow pathways into a partially breached oil column. Isotherms show the increased thermal impact of associated convective heat transfer on permeable reservoir layers compared with sections of the fault encased in low permeability shales. D. Histogram showing fluid inclusion salinity data from intact hydrocarbon zones versus breached traps, with high ongoing oil saturation preventing access of saline brine into hydrocarbon zones, thereby constraining brine flow to postdate initial hydrocarbon charge.

In addition to the breaching of hydrocarbon traps this tectonic activity triggered a renewed phase of salt-controlled tectonism, being manifest as salt diapirs in the Swan Graben (Smith and Sutherland, 1991). Salt diapirism may have been more widespread across the VSB with removal of shallow salt features through dissolution due to formation waters being under-saturated with respect to salt.

8.6 POST BREACH CONSOLIDATION

The dramatic impact of Neogene fault reactivation severely compromised the effectiveness of the petroleum systems that have operated in the VSB. From an initially catastrophic impact a series of post-breach effects were to continue to influence the Jurassic Vulcan-Plover (!) petroleum system, both in a detrimental way but also with some positive benefits.

Seismic data from the VSB show that few faults actually offset the sea-floor (Figure 8–17) suggesting that the frequency of fault reactivation since the main phase of Miocene reactivation has diminished. Measured displacement rates after about 3 Ma decrease significantly (Gartrell et al., 2006) and it follows that the leakage of hydrocarbons, because of fault reactivation, would also be likely to decrease to the present day (Gartrell and Lisk, 2005).

A shift from an extensional stress regime (where σ1 is dominantly vertical) to one with a significant component of oblique slip in a more transtensional environment (where σ1 is horizontal and increasing in magnitude due to locking of the subduction zone to the north) has important implications for the role fault reactivation plays in determining the relative level of trap integrity in the VSB and across the region more broadly. In a prevailing stress regime where σ1 is horizontal (i.e. the present-day configuration) Tertiary extensional faults that are apparently unrelated to older faults (i.e. reactivated faults) are difficult to explain (Gartrell et al., 2006) so a reduction in the frequency of such faults is entirely consistent with the observations.

Estimation of the magnitudes of the principal stresses indicate that the differential stress (σ1- σ3) in the late Miocene was similar to the present, but that greater mean stress in the present-day stress state pushed the predicted Mohr circle away from the

failure envelope resulting in reducing reactivation risk with time (Gartrell and Lisk, 2005; Figure 8–15).

The onset of a regional stress regime where σ1 corresponds to sh_{max} and where the margin is strike-slip will influence the propensity for traps to continue to be breached and could contribute to an overall improvement in trap integrity in some cases. At the scale of individual traps it is not uncommon to see elements of both transpression and transtension with coupled releasing bends and restraining bends a feature of individual faults or paired faults that define individual relay ramps (Figure 8–21A; Gartrell et al., 2006). The orientation of the maximum horizontal stress (σH_{max}) relative to the detailed fault geometry will strongly influence the degree of transpression or transtension that is experienced within the fault bend region (Tikoff and Teyssier 1994).

Releasing bends along faults are typically sites of enhanced dilation and high fluid flow (Cunningham and Mann, 2007), promoting vertical transmission of fluids due to increased structural permeability, with the corresponding restraining bend likely to be relatively more sealing (Figure 8–21A). The position of the structural crest relative to location of releasing bends is likely to be a critical control on whether partial or complete leakage occurs from an individual trap.

Many world-class mineral deposits are considered have formed where fluid flow is focused in dilational sites along releasing fault bends (Sibson, 2001; Cox, 2001). In contrast, pop-up structures (Figure 8–21B,C) associated with restraining bends offer attractive petroleum exploration targets that have been highly successful in other basins around the world (Harding, 1985), testament to the generally high trap integrity characteristics of such structures.

Collectively the observations made from the VSB and the models derived from those observations suggest that the intensity of fault reactivation peaked in the late Tertiary before progressively decreasing to the present day. The reduction in faulting produced an associated reduction in the rate of leakage and in some cases led to an improvement in the integrity of some traps including those displaying trap configurations considered to be at a high risk of breaching.

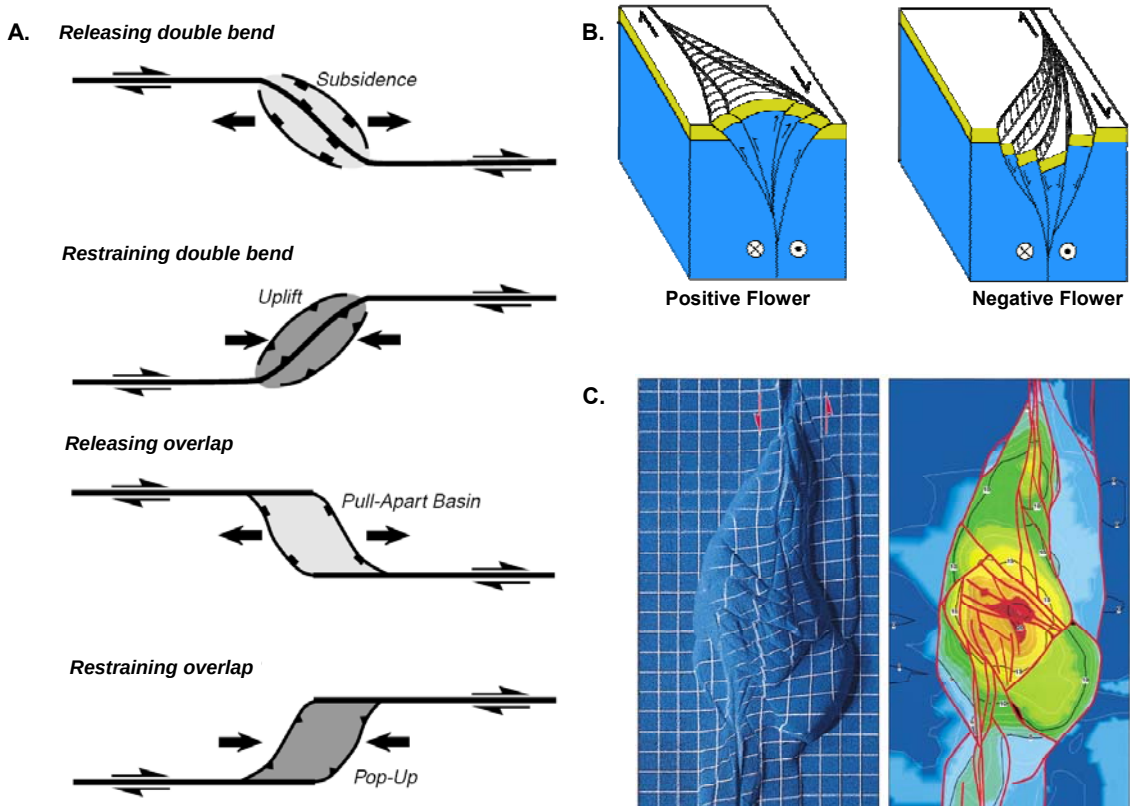

Figure 8-21: Geometries of strike-slip faults in plan and map view.

A. - schematic cartoons illustrating the characteristics of bends in faults produce that produce localised zones of transtension (releasing double bend) resulting in extension and subsidence and transpression (restraining double bend) that results in compression and uplift. At larger scales the zones of overlap between two offset fault systems produce either pull-apart basins under transtension or pop-ups under transpression that with increased strike-slip offset can produce more rhombic shaped features (Mann et al. 2007). **B.** - Block diagrams illustrating positive and negative flower structures developed along minor restraining and releasing bends on a dextral (right-lateral) strike-slip fault. Symbols indicate movement direction with crosses indicating movement into the page. **C.** Results of a sandbox analogue model showing an inverted pop-up structure produced in a transtensional environment with a contoured map derived from the model used to demonstrate the structural similarity with real traps. (Figures A. and C. taken from McClay and Bonora, 2001).

The degree of structural complexity of many structures across the VSB, coupled with the different sealing behaviour that can be expected under different stress and strain regimes suggests that careful structural analysis is a requisite to properly assess the likelihood of faults compromising the structural integrity of any particular trap.

A benefit of recognising the impact of these collective processes can be demonstrated by the improvements in the interpretation of the various indicators of hydrocarbon seepage that have been employed in the VSB to address this key risk. Combined seepage data, collected across the south western VSB and integrated with leakage indicators on seismic (HRDZs) and detailed fault mapping (O'Brien et al., 2002b) enables the data to be integrated with fewer discrepancies. Where traps have been fully reactivated and now exhibit low trap integrity seepage tends to be dispersed and dominated by an increased methane response (Figure 8–22). In contrast, where traps have been partially reactivated and have been able to retain some of the original hydrocarbons contemporary seepage tends to be more point sourced (Figure 8–22) and dominated by wetter hydrocarbon compositions. This probably reflects a seepage response that is being actively fed by the hydrocarbons still preserved in the trap at depth (O'Brien et al., 2002b).

The proposition that some traps may have been enhanced by the recent change in the prevailing stress-field can be demonstrated by recent oil discoveries made in the VSB. The Tenacious oil field, discovered in 1997, defined a new play in the VSB, finding oil in the Tithonian-aged sandstone of the Upper Vulcan Formation but was also significant by demonstrating the retention of oil charge in traps that were charged after the main episode of fault breach (Woods and Maxwell, 2004).

The main fault bounding the closure at the Tithonian sandstone level in Tenacious formed during Neogene structuring, as a reactivation of a deeper Kimmeridgian–early Tithonian fault (Woods and Maxwell, 2004). The significance of the Tenacious discovery is notable as it indicates that even heavily reactivated structures can be prospective if oil charge post-dates the Miocene reactivation event. Coupled with late stage maturation of Jurassic source rocks in the Cartier Trough these observations high grade the potential of similar trap types in the northeastern Vulcan Sub-basin.

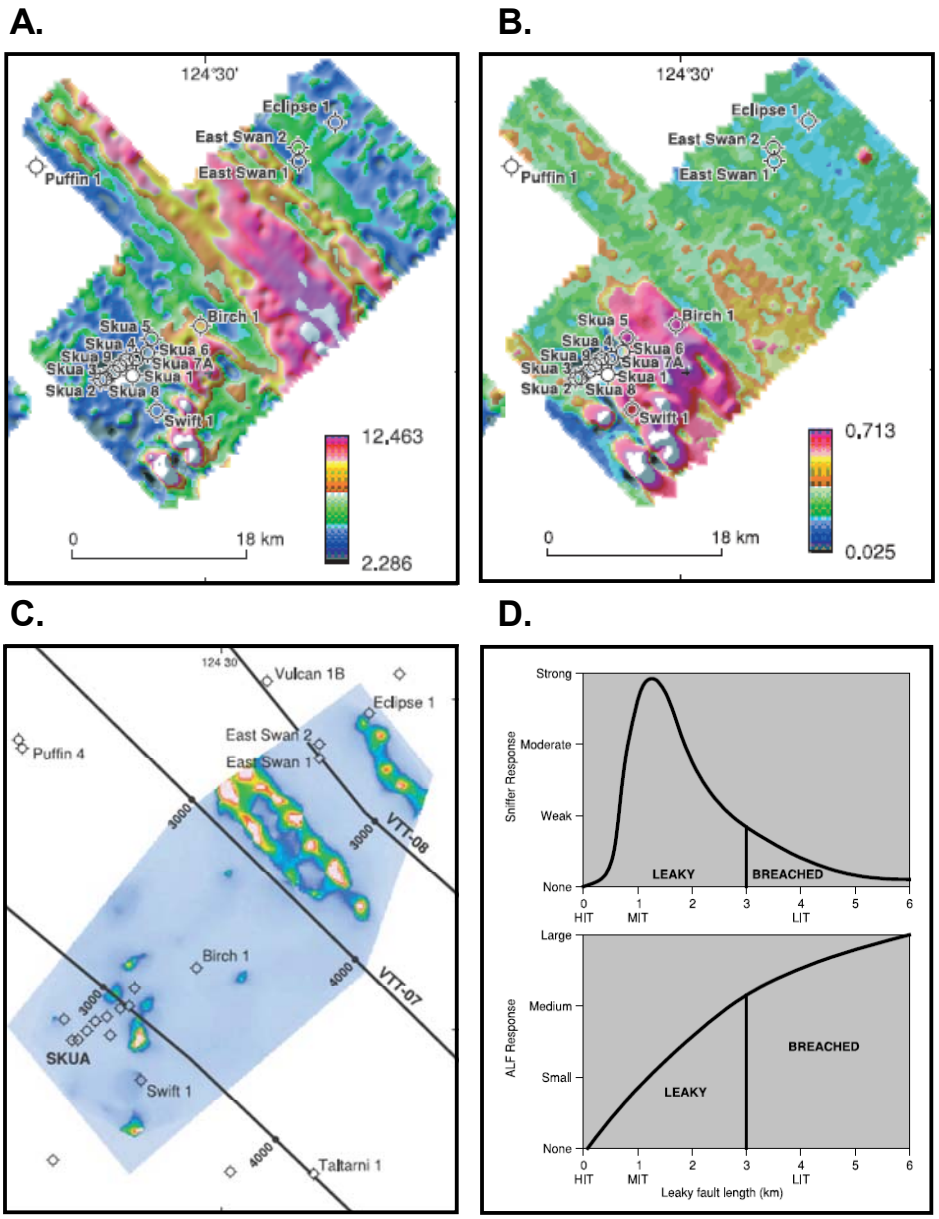

Figure 8-22: Examples of conventional hydrocarbon seepage from the VSB.

Geochemical sniffer results from the Vulcan Sub-basin showing A. water bottom methane concentrations and B. ethane concentrations plotted on logarithmic scales to enhance relatively small anomalies. Methane anomalies are associated with the breached East Swan and Eclipse traps, with the ethane response being more significant over the Skua oilfield. C. Examples of Airborne Laser Fluorosensor (ALF) acquired in the southern Vulcan Sub-basin showing major anomalies over the breached East Swan and Eclipse traps compared with more subtle features over the intact Skua oilfield. D. Schematics cartoon summarising the expected seepage response produced by traps with different levels of integrity (LIT = low integrity trap, MIT = moderate integrity trap and HIT = high integrity trap). All diagrams come from O'Brien et al., 2002b.

8.7 LATE GAS CHARGE (H3)

Dramatically increased subsidence in the Mio-Pliocene resulted in a transition from predominantly oil to widespread gas generation (H3) and allowed late gas-flushing of many of the oil columns that remained intact by this time (Figure 8–23). Ironically it was traps that most successfully retained high integrity during fault reactivation from 5Ma and 3Ma that were most negatively affected by late gas charge.

Areas that experienced rapidly increasing subsidence such as the Cartier Trough were the most affected. Examples such as the Oliver trap were ideally positioned to catch the late gas charge causing substantial oil volumes to be flushed from the Oliver trap, only to leave a currently sub-economic gas cap with a thin underlying oil rim (Lisk et al., 2002; Ambrose, 2004).

The timing of gas flushing is somewhat uncertain but it is placed after fault reactivation in order to accommodate the data available from the Swan Field. In this example, flushing of a pre-existing oil column by late gas charge requires the existence of effective migration pathways into the Cretaceous section and these are most likely to have been created by Neogene fault reactivation.

The impact of late gas charge is, however, difficult to characterise as not all oil fields have been flushed. Indeed fields like the Tenacious (Woods and Maxwell, 2004) and Audacious oil fields (Maxwell et al., 2004) located immediately along strike of the mostly gas filled Oliver field have not been affected. These high gravity oils are undersaturated with gas (Woods and Maxwell, 2004) and appear to have been shielded from any significant late gas phase, or perhaps the reduced trap integrity allowed preservation of oil through preferential soft bleed of the more buoyant gas.

Complex migration pathways could explain this observation as could interruption of the migration pathway by newly formed fault pathways. Cooper et al. (1998) considered this mechanism to have been responsible for a prominent ALF seepage anomaly noted on the north eastern side of the Cartier Trough (Figure 8–24) immediately down-dip of structures proven dry by previous exploration drilling.

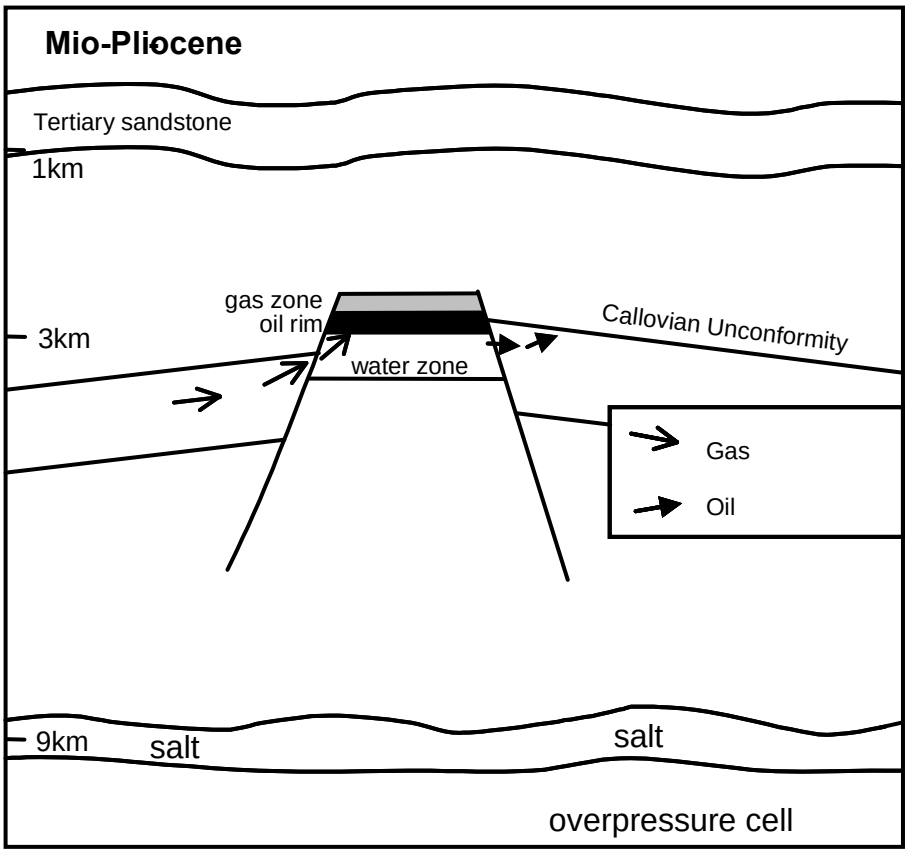

Figure 8-23: Late gas charge in the VSB.

Cartoon showing the arrival of a late gas charge into traps that retained intact oil columns after the widespread trap breach episode in the Miocene. Traps that currently contain gas are typically those that display high trap integrity where the input of late gas acts to displace the oil across the spill-point of the structure. Traps with lower trap integrity can also retain an earlier oil charge with preferential loss of later gas charge by a soft bleed mechanism related to differential buoyancy effects.

8.8 IMPACT ON REGIONAL PROSPECTIVITY ASSESSMENT

A noted aim of this investigation was the provision of data that would constitute an atlas of hydrocarbon charge for the Vulcan Sub-basin that could be used to help ground truth the predictions of existing and yet to be developed techniques for assessing trap integrity.

The VSB remains a prospective hydrocarbon province that has continued to yield a series of new discoveries since this study began and has attracted the ongoing attention of researchers looking to address the key factor restricting exploration, namely trap integrity prediction. As a consequence of numerous authors documenting the deleterious effects of fault reactivation across the VSB and Northern Bonaparte Basin a variety of tectonic models have been proposed to explain the mechanisms controlling fault reactivation.

Each of the proposed models aims to deliver an effective predictive tool to address hydrocarbon preservation potential pre-drill and to thereby contribute to increased exploration success into the future.

The first step of this process is an appreciation of how the results of the current study have impacted the understanding that prevailed at the onset of the study. This can then be integrated with the substantial body of additional work that has been contributed by other workers over the duration of this project to better evaluate the effectiveness of strategies or techniques developed to address the key risks.

8.8.1 Retrospective Risk Evaluation

Despite the risks associated with exploration in the VSB being largely recognised and relatively well documented at the onset of the current investigation, the outcomes of this study have enabled the relative importance of these key risks to be more definitely described. Petroleum exploration involves dealing with relative risks that are assessed from a dataset that is never complete, so there will always be a reliance on models to help improve the success rate of future drilling.

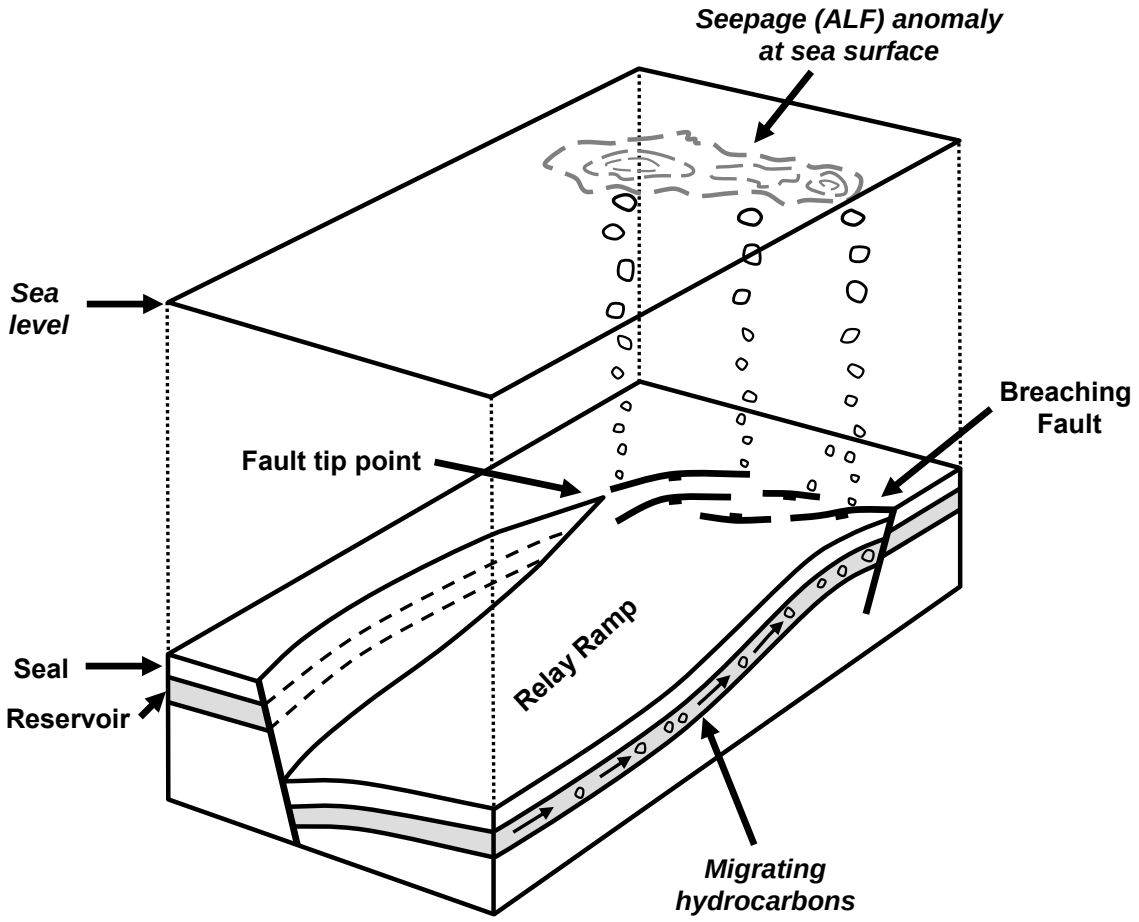

Figure 8-24: Interruption of migration pathways due to faults.

Block diagram modified from Cooper et al. (1998) showing the piercement of the top seal by a breached fault relay ramp providing a pathway for gas leakage from the hydrocarbon reservoir into the shallow section and ultimately into the water column where it could be recognised by seepage detection methods such as ALF. Traps located further up-dip on this migration pathway would potentially be shielded from late gas charge, but could still have been charged with oil prior to the breaching of the relay ramp.

By the year 2000 the drilling of about one hundred and fifty exploration wells across the greater Vulcan Sub-basin, had resulted in fifteen hydrocarbon discoveries; an encouraging, if not exceptional, technical success rate of one in ten. However, eight of these discoveries are mostly gas and remain too small to warrant development and when these are excluded the discovery rate falls to one in twenty one. Indeed, if only producing fields are included, then the commercial success rate is only one in fifty.

In the current study, the majority of wells evaluated come from the central part of the Vulcan Sub-basin, which has proved to be relatively more lucrative area for explorers than the adjacent Ashmore Platform and Londonderry High. For seventy-three wells drilled within this central zone, the technical success rate is about one in five for both oil and gas (one in nine for oil discoveries), but is less than one in twenty-four for discoveries that have been produced, are under production or considered likely to be commercial.

A review of all publicly available operating company well completion reports (public domain data from Geoscience Australia) was undertaken to identify the key geotechnical risks recognised in post-drill analyses. A qualitative approach to risk analysis has been adopted which allows various elements of the play concept to be characterised in a visual manner, allowing the perceived uncertainties and critical risks to be considered. Each spoke on the wheel represents a potential risk, with each spoke filled from the centre outwards depending on the results of drilled wells; the circumference represents limited perceived risk whereas the core represents a demonstrated critical risk (Figure 8–25). In some instances the well completion report did not specifically identify a reason for failure and a degree of interpretation was required to characterise some of the well results.

Figure 8–25 illustrates a summary of the key risks directly identified by the operating company in the post-drill review or inferred from a review of the well result by the author (Lisk et al., 1998b). An inability to correctly map structure pre-drill is the primary risk accounting for about 40% of the dry holes drilled in the VSB and principally relates to poor seismic data quality and depth-conversion uncertainties.

Relatively low risks are perceived for availability of reservoir and source rocks, while appropriate thermal maturity levels support widespread oil generation. In contrast, in many wells, the lack of substantial oil or gas shows has been taken to constitute a migration risk for hydrocarbons. Generally the reservoirs have well developed top seals that rarely are offset by faults and that have capillary properties are capable of retaining substantial hydrocarbon columns such that a low trap effectiveness could be implied. However, as most traps rely on faults to obtain closure the key control on trap effectiveness has been fault seal failure, although not always directly implicated.

The qualitative risk analysis diagram (Figure 8–25A), reworked to incorporate the results generated in this study, shows that the key risks facing explorers in the Vulcan Sub-basin are more restricted than was perceived when these wells were drilled (Figure 8–25B) and was generally appreciated at the onset of this study.

The presence of oil inclusions in all but one of the wells examined in this study suggests that most traps were connected to oil-prone source rocks and that the migration risk for the basin has been overestimated (Figure 8–25B). This is particularly the case given that a large number of wells lie outside the area of active generation (source pod) and rely on a component of lateral migration that precludes the possibility of the oil seen in the fluid inclusions being generated *in situ*. Further, the recognition of many palaeo-oil columns in both gas-filled and water-wet wells indicates a system dominated by liquids, confirming the widespread existence of oil-prone source rocks and viable migration pathways.

Late gas flushing is a clear risk to commercial success, although the evidence of prior oil charge to some gas fields indicates the potential created by the remigration of these oils that is yet to be fully appreciated. Complex fault reactivation plays a role in controlling which traps get gas flushed as opposed to those that are shielded from late gas charge by faults that disrupt the effectiveness of the migration pathways.

The retention of oil charge is a critical risk, highlighted by the presence of residual oil zones recognised below most of the oil fields and the eight palaeo-oil columns identified in presently water-wet traps.

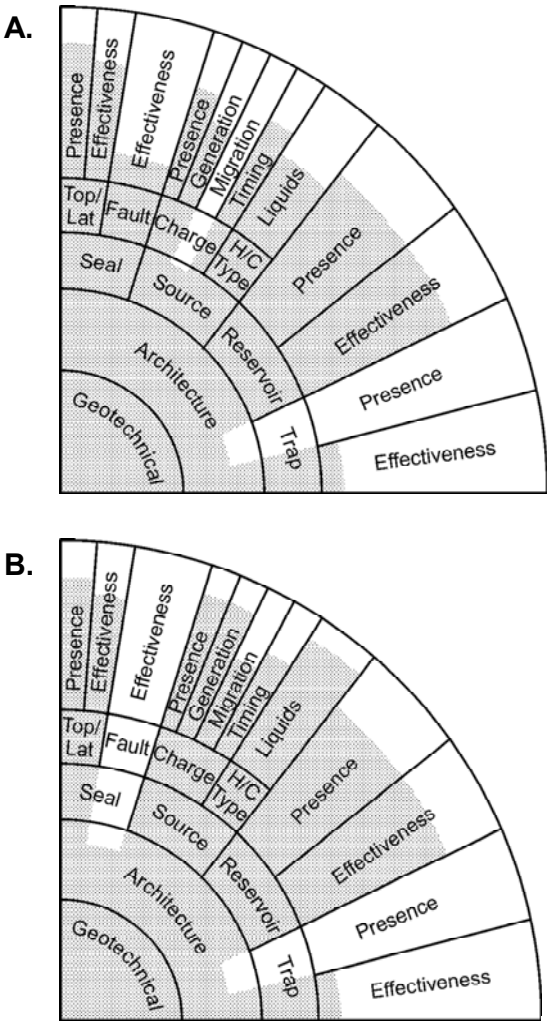

Figure 8-25: Retrospective risk analysis at the onset (A.) and completion (B.) of this study.

Diagrams describe the key elements that would constitute the basis of a typical petroleum system based assessment dealing with the four principal components of Seal, Source, Reservoir and Trap. At the onset of the current study (A.) the elements related to trap were recognised as major risks with poor seismic quality and structural complexity contributing to uncertainty in correctly delineating traps (trap presence), whilst breached traps had also been attributed to reactivation of faults (trap effectiveness). Overbalanced drilling practices contributed to significant uncertainty regarding the presence of effective migration pathways as many wells lacked reliable hydrocarbon shows. The key contribution of the current study has been to confirm that this aspect of the system has been too conservative and that rather than migration pathways being absent widespread oil migration and charge had been achieved. Correctly identifying traps remains difficult but is improving with the application of greater 3D seismic and improved seismic acquisition and processing techniques. Low trap integrity, primarily due to fault seal failure remains an unresolved risk from the fluid inclusion data alone, but the data provide a way to calibrate and test other methodologies.

Given that the majority of the traps rely on faults to achieve closure, the impact of late stage Neogene fault reactivation has generally been deleterious to the preservation of oil columns.

The high level of structural complexity coupled with (or because of) poor seismic imaging has contributed to inaccurate definition of structure and despite major improvements in seismic acquisition (Long and Ramsden, 2004) and processing (Maxwell et al., 2004) techniques this factor continues to adversely influence drilling success. The new approaches have played a demonstrable role in improving success, as shown by the Audacious oil discovery in 2003 where Pre-stack Depth Migration seismic processing techniques were employed (Maxwell et al., 2004).

8.8.2 Towards Predictive Trap Integrity Methods

The problems experienced by explorers in the VSB in terms of poor pre-drill trap integrity predictions has provided a fertile area for research and produced many different proposed solutions. These predictive methods intended to address the retention risk posed by poor trap integrity can be broadly grouped into several categories although ultimately each relies on an improved tectonic model and better integration of the key datasets. The main approaches are:

1. Direct seepage detection

2. Contemporary stress field evaluation

3. Kinematic structural models

Ultimately, these predictive approaches aim to address the critical question facing explorers of whether these events have irreparably diminished the wealth of this system, such that the opportunities to discover economic reserves of hydrocarbons are now too few compared with other like basins.

8.8.2.1 Direct Seepage Detection

The detection of hydrocarbon seepage has been used as a tool in offshore oil and gas exploration since the 1930s (Abrams and Segall, 2001). Seepage detection methods rely on interpreting indications of hydrocarbon leakage into the shallow section or to the surface. Hydrocarbon seeps in either near-surface sediments, on the seabed, or within the water column, may provide strong evidence of an active petroleum system (Abrams, 1992, 1996; Abrams and Segall, 2001).

Recognition of hydrocarbon seepage and related accumulations of shallow gas in the overburden section is also important as they may constitute a drilling geohazard in the form of unexpected drilling kicks (UK Offshore Operators Association, 2000).

A wide range of observations can be attributed to hydrocarbon seepage. Within the water column (Figure 8–26) indications of leaking hydrocarbons are mostly related to free gas that can be readily identified using side-scan sonar or echo sounders (Rollet et al., 2005; Etiope et al., 2006). Further investigation with a Remote Operated Vessel (ROV) can help to reveal the location of the actual seep (Etiope et al., 2006) and enable sampling to be completed, whilst arrival of gas bubbles at the surface or the formation of 'pancakes' on the sea-surface (Williams and Lawrence, 2002) provide further direct indications of seepage (Figure 8–26). Smoothing of the sea surface by oil can be used to detect such seeps using high resolution satellite systems such as Synthetic Aperture Radar (SAR; Williams and Lawrence, 2002).

On the seafloor gas leakage often results in the formation of clusters of reflective blocks, hard-grounds, pockmark fields, and mounds (Figure 8–27). Pockmarks form by fluid expulsion and are characteristically cone-shaped circular or elliptical depressions that typically range from 0.5–20 m deep and from 1 to 1000 m long (Hovland and Judd, 1988). Hardgrounds and mounds are often associated with authigenic methane-derived carbonates that provide a durable substrate that is readily colonised by chemosynthetic fauna (Figure 8–27) that could represent precursors of bioherms and carbonate reef formation (Hovland, 1990).

Within the sedimentary pile leakage indicators can include direct geophysical detection of hydrocarbon represented by gas chimneys or amplitude blooms defining

shallow gas accumulations. Often amplitude 'flags' form adjacent to faults suggesting the fault has acted as a migration conduit (Figure 8–27). Indirect evidence can be provided by hydrocarbon related diagenetic zones, palaeo-pock marks and hydrate formations that exhibit bottom simulating high amplitude reflectors (BSR).

Gas chimneys, namely features associated with the upward movement of fluids or free gas (Hovland and Judd, 1988) in the sediment pile, are readily visible in seismic data as columnar disturbances (Figure 8–28), where the continuity of reflectors is missing or degraded, and the reflection amplitudes are noticeably weaker than observed in the surrounding areas (Heggland, 1998, 2004). The presence of gas chimneys as indictors of hydrocarbon leakage pathways is a well established relationship and mapping of such chimneys by neural network techniques has been developed as an exploration tool (Meldahl et al., 2002; Heggland, 2004).

The remotely sensed nature of the aforementioned methods provides the opportunity to make pre-drill predictions at relatively low cost, but the complexity of hydrocarbon leakage and the type of seepage in a particular marine setting requires a detailed understanding of substrate features and related geochemical processes (Abrams and Segall, 2001) and the ability to successfully attribute different seepage signatures to specific trap types remains a key challenge. The complexity associated with relating near-surface hydrocarbon seepages to subsurface petroleum generation and entrapment (Schroot et al., 2005) requires the use of multiple parameters and integrated interpretation is needed (Gay et al., 2006; Figure 8–29).

Across the Timor Sea region seep detection methods have been widely applied. Extensive palaeo hydrocarbon leakage and contemporary hydrocarbon seepage has been inferred directly from remote sensing techniques including Synthetic Aperture Radar, Airborne Laser Fluorosensor (ALF) and water column hydrocarbon detection (O'Brien et al., 1998; 2002a; Cooper et al., 1998; Rollet et al., 2005) and indirectly through seismic DHIs (Avseth et al., 2005) including the mapping of Hydrocarbon Related Diagenetic Zones (HRDZs; O'Brien and Woods, 1995).

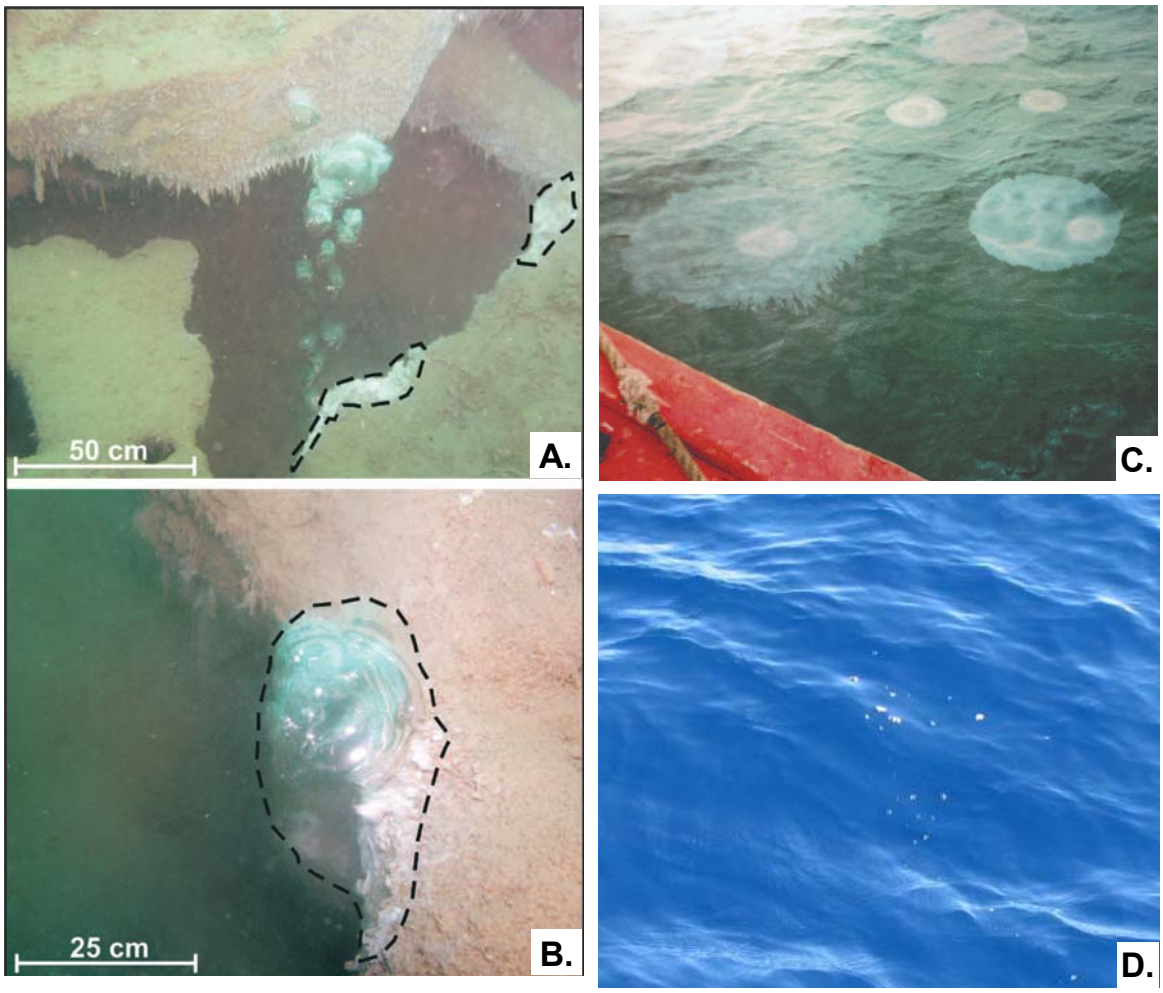

Figure 8-26: Examples of seepage into the water column

A., B. Gas bubbles and associated bacterial mat at the offshore Katakolo seeps on the Ionian coast of north western Peloponnesus, Greece (from Etiope et al., 2006). **C.** Surfacing oil bubbles forming pancakes on the sea surface, South Caspian Sea (from Williams and Lawrence, 2002). **D.** Gas bubbles that have risen to the sea surface from natural hydrocarbon seeps on the Yampi Shelf from the Browse Basin in northern Australia (from Jones et al., 2005b).

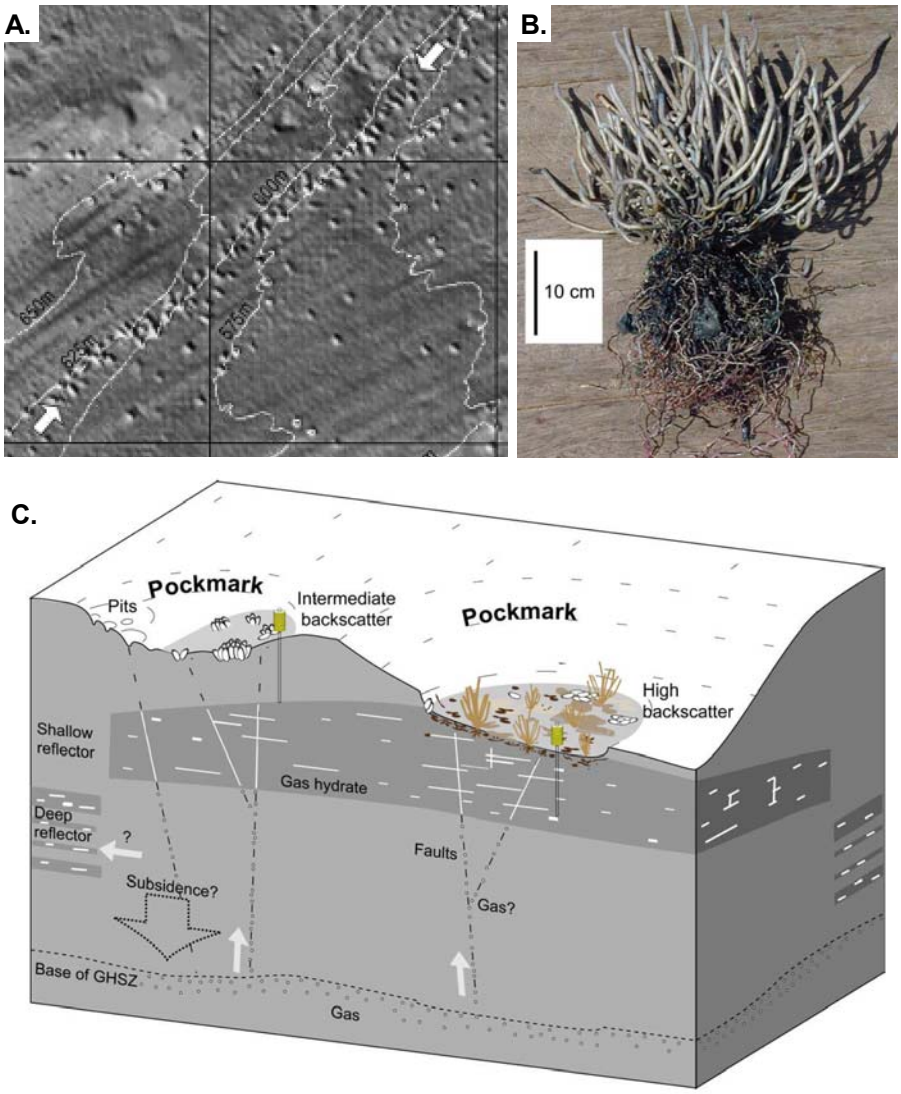

Figure 8-27: Examples of sea-bed features that can indicate seepage

A. Shaded relief image showing extensive pockmarks on the sea-floor from the Skagerrak region located between Norway, Sweden and Denmark with 25 m bathymetric contours also shown (from Rise et al., 1999). Note the concentration of pockmarks along a 10 km long lineament, reflecting the termination of a fault at the base of the Quaternary (marked with arrows). B. A small bush of living vestimentiferan tubeworms. The anterior tubes extended about 20 cm above the sediments; the posterior parts form a "root ball" of similar size in the sediments (from Sahling et al., 2008). C. A schematic model of pockmark (not to scale) formation based on an example from the Northern Congo Fan, SW Africa. Transient release of gas leads to the deposition of gas hydrate at shallow sediment depths, forming high-amplitude reflections in the echo-sounder records ("shallow reflector"). Free gas may horizontally migrate into low permeable reflectors forming hydrates ("deep reflector"). Colonisation of the seeps by marine fauna such as Vesicomyid clam clusters and vestimentiferan tube worms can also occur (from Sahling et al., 2008).

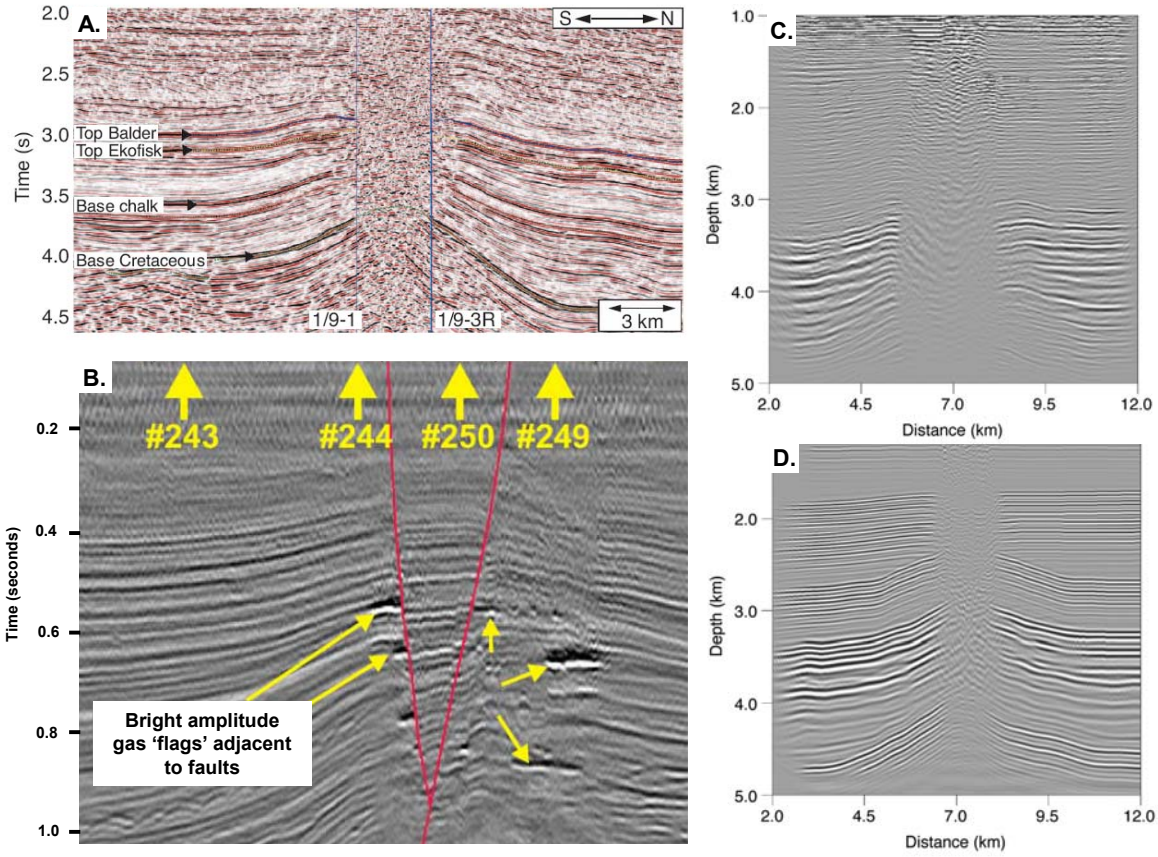

Figure 8-28: Examples of seismic gas chimneys

A. A prominent gas chimney above the Tommeliten Alpha gas field from the Central Graben region of the North Sea (from Granli et al., 1999) showing pronounced vertical zones of deteriorated seismic data quality is a classic feature of gas leakage from below. B. A Seismic profile inline from a 3D survey across a leaking fault system (Schroot et al., 2005) showing typical amplitude brightening in sands adjacent to a fault that appear as 'flags' on the footwall side. C. Raw prestack depth migration of a Statoil research line across the Tommeliten Alpha field showing a well developed vertical seismic chimney (Arntsen et al., 2007). D. A synthetic seismic line showing a modelled gas chimney (Arntsen et al., 2007).

Initially seepage detection in the VSB relied mostly on indirect methods with O'Brien and Woods (1995) describing zones of pervasive cementation that on seismic data present as localised velocity anomalies that can resemble gas chimneys (HRDZs, Figure 8–19), but relate to lithology rather than hydrocarbon effects.

Although HRDZs are different to genuine gas chimneys where the presence of free gas in the shallow section can be directly inferred the presence of an HRDZ can provide an indicator of palaeo-hydrocarbon leakage that may represent the only record of trap failure if the seepage has subsequently ceased.

The distribution of mapped HRDZs from the VSB, collated from descriptions described in O'Brien and Woods (1995), O'Brien et al., (1999a) and Cowley and O'Brien (2000) generally shows good agreement with the results of the current study. O'Brien and Woods (1995) show a positive correlation between the orientations of the Tertiary faults in comparison with the underlying Jurassic rift faults and the level of trap integrity. Traps where these faults show parallel orientations typically lack evidence for leakage and where hydrocarbon charged invariably have a gas cap or are fully gas filled. Examples include the Montara and Oliver accumulations and in these traps HRDZs are absent in the overburden. Paradoxically, these observations suggest that structures with high trap integrity do not represent the best prospects as they are likely to be gas-flushed and are too small to represent economically viable accumulations as gas fields (O'Brien and Woods, 1995; O'Brien et al., 1996a).

Conversely, traps that display more oblique fault orientations are generally associated with the presence of HRDZs in the overburden, indicating a degree of leakage. The greater the degree of fault obliquity the more prone the traps becomes to hydrocarbon loss and the larger the attendant HRDZs become. Those traps with less obliquity contain oil with residual zones below the OWC (i.e. Skua, Jabiru, Challis), whilst those where the Miocene faults show a significant rotation in orientation are completely dry (i.e. East Swan, Eclipse), but contain significant palaeo-oil columns and have large HRDZs (O'Brien et al., 1998). The spatial distribution of the HRDZs also appears to be diagnostic with partially breached trap showing a circumferential distribution forming a ring of small HRDZs around the periphery of the retained accumulation (Figure 8–30).

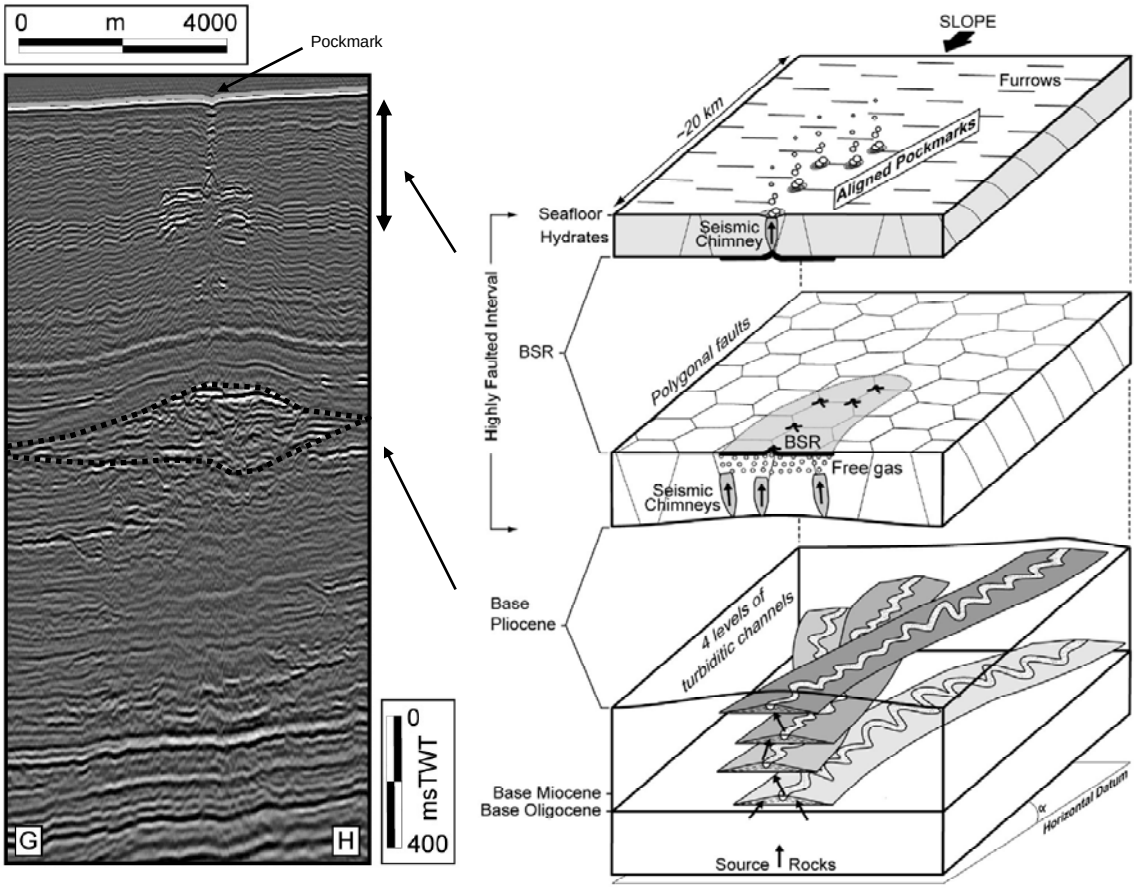

Figure 8-29: Example of integrated seep detection from the Lower Congo Basin.

A. Seismic profile GH across a single pockmark showing a chimney below the pockmark that is disrupted by a high-amplitude reflection parallel to the seafloor, which is interpreted as a hydrate layer. The gas is interpreted to be leaking from underlying Oligocene-Miocene turbiditic palaeo-channels (dashed outline) through a polygonal fault system in the top seal. B. Schematic block-diagram illustrating the likely relationship between the Oligocene-Miocene palaeo-channels, the seismic chimneys and hydrates, and the seafloor pockmarks (from Gay et al., 2006).

This anecdotal evidence suggests the mapping of HRDZs may be a powerful tool for the assessment of trap integrity where the fault orientations have been carefully mapped. However, the presence or absence of HRDZs is not a diagnostic indicator of trap integrity for all areas in the Timor Sea. For example, the Eclipse trap, located along strike from East Swan and relying on the same fault system for closure contains one of the largest palaeo-oil columns in a currently water-wet reservoir section, yet has no associated HRDZ. Similarly, on the Laminaria High, no convincing HRDZs are observed, although there is equally good evidence for hydrocarbon leakage in that area (Brincat et al., 2004; Gartrell et al., 2005).

Consideration of the factors needed to produce an HRDZ, such as shallow aquifers with suitable temperatures to promote microbial activity are likely to be critical in determining which traps would be expected to develop an HRDZ. In shallow parts of the basin where Tertiary burial is limited (i.e. the Challis/Cleghorn or Jabiru horsts) conditions for the formation of HRDZs are likely to be more favourable than in deeper parts of the basin (i.e. Paqualin Graben or Cartier Trough) where temperatures in the shallow aquifers are too high. This is a likely explanation for the lack of an HRDZ over the breached Eclipse trap with increasing fault throw to the NE resulting in a thicker post-rift section and leading to more deeply buried Tertiary horizons than at the East Swan structure. Consequently the mapping of HRDZs is unlikely to fully de-risk traps and requires integration with other datasets.

Recognising that an integrated solution would be more powerful, O'Brien and Woods (1995) combined their HRDZ observations with 2730km of Direct Hydrocarbon Detection (DHD or 'sniffer') water column geochemical data that was acquired in 1990 (O'Brien, 1992). These data show significant spikes in ethane concentration within the water column across the Skua Horst but much lower baseline levels are recorded over the intact Montara (gas and oil) structure and the breached (palaeo-oil column) East Swan structures (O'Brien and Woods, 1995).

These observations are consistent with the model that some traps have remained intact throughout Neogene tectonism allowing them to retain both oil and gas. O'Brien et al., 1996a; 1999a) attributed the absence of active seepage over the breached East Swan structure to reflect a reduction or cessation of seepage since this

trap was reactivated in the Miocene, implying that a retained column in the subsurface was needed to get a contemporary seepage response in the water column.

Encouraged by the evidence to support leakage of hydrocarbons into the shallow section, but conscious that local geological complexity precluded a unique single component solution a series of further surveys were commissioned throughout the early part of the last decade in an attempt to add support to the model through the detection of current hydrocarbon seepage. A variety of methods were employed across a region centered on the Skua oil field with the integration of further water column sniffer with new data derived from Airborne Laser fluorosensor (ALF) and Synthetic Aperture Radar (SAR) techniques together with the outcomes provided by the previous HRDZ identification (O'Brien et al, 1998; 1999a; 2002b).

Comparison of these data and those for the mapped HRDZs outlined in O'Brien and Woods (1995), O'Brien et al., (1996a) and Cowley and O'Brien (2000) has further refined the previously proposed integrated trap integrity solution (O'Brien et al., 1998). These new results largely confirmed the interpretation of the earlier water column geochemical data, showing elevated methane and ethane levels over the Skua Field. Seepage across the breached East Swan trap remained low with respect to ethane (Figure 8–22), but a broad low-level methane signature was noted to the south of this structure (Figure 8–22). O'Brien et al. (1998) suggesting ongoing low-level of contemporary seepage, with the composition of the hydrocarbons being detected now reflecting a now gas mature source kitchen.

The limited availability of equivalent data sets across a broader region largely limits further examination of these integrated studies against the charge history map produced by the current study, but it seems reasonable to conclude that the consistency in results from this area with those derived from the GOI results supports the application of these methods as a useful tool to de-risk trap integrity more widely.

However, it should also be noted that as remote sensing techniques are becoming widely applied more is being understood about the driving forces behind the observations that in some instances have revealed non-hydrocarbon related processes that could lead to erroneous interpretations. For example in an application of these

methods on the Yampi Shelf in the adjacent Browse Basin a series of slicks seen on SAR data and previously attributed to hydrocarbon seepage (O'Brien et al., 2002a) now appear more likely to be the result of bathymetric controlled current flow and perhaps periodic coral spawning events (Jones et al., 2005). Again the data point to the need for an integrated solution rather than relying on a single parameter to define a unique solution to an issue that is clearly complex and multi-parameter in nature.

8.8.2.2 Contemporary Stress Field Evaluation

A widely applied approach to the prediction of trap integrity across the VSB and northern Bonaparte Basin has centered on the role of the contemporary stress field in controlling the propensity for traps to be breached (Mildren, 1994; Hillis, 1998; de Ruig et al., 2001; Castillo et al., 2000; Mildren et al., 2002). These methods consider scenarios where a static stress regime is perturbed by a change in pore pressure leading to fault reactivation.

An understanding of the stress field augments the more traditional fault seal methods based on juxtaposition and fault deformation processes (Allan, 1989; Knipe, 1997; Yielding et al., 1997; Bretan et al., 2003) that can define the sealing potential of faults that have been inactive since hydrocarbon charge, but ignore the potential for seal breach due to fault reactivation subsequent to charge. Juxtaposition or deformation process (clay smear or gouge) seals may be breached if the fault is reactivated subsequent to hydrocarbons charging the trap so addressing the impact of reactivation is necessary in tectonically active basins.

Despite the wide application of these methods the purpose of conducting such analyses is commonly misrepresented. Many of the papers on this topic propose that any fault that is critically stressed, with respect to the present-day stress field, has a high likelihood of being reactivated, thereby re-creating fault zone permeability that enables hydrocarbons to leak. Whilst this is applicable where future predictions are required, such as estimating the likelihood of reactivating a fault due to pressure depletion during production, the clear presence of reactivated faults on seismic already provides evidence that the faults have been reactivated and an understanding of the contemporary stress field is not required to reach this conclusion.

If avoiding traps that have been reactivated was required to mitigate risk then very few traps in the region would have been drilled as fault reactivation is so pervasive. Clearly fault reactivation is not purely synonymous with hydrocarbon leakage otherwise the intact fields across the VSB, all of which are reactivated to some degree, would be difficult to explain.

The more pertinent implication of defining faults that are critically stressed is in fact related to the propensity for these segments of a reactivated fault to be prone to act as conduits for fluid flow (Barton et al., 1995; Sibson, 1994; Mildren et al., 2002).

Published workflows typically seek to combine knowledge of the prevailing stress field with mapped fault geometries, pore pressure, and the failure envelope for the fault rocks to assess which faults could be critically stressed in the in-situ stress field. The orientation and magnitude of the prevailing stress field are determined from a variety of well bore geomechanical techniques (Mildren et al., 1994; Castillo et al., 2000). The orientation of the horizontal stresses (the in-situ stress tensor) comes from an evaluation of borehole breakouts and drilling-induced tensile fractures, typically obtained from well bore image logs. Density and check-shot velocity data yield the level of vertical stress, whilst leak-off and extended leak-off tests yield the magnitude of the minimum horizontal stress. The magnitude of the maximum horizontal stress ($\sigma Hmax$) is typically the most difficult component of the stress tensor to quantify, relying on the nature of breakouts and drilling-induced tensile fractures and an estimate of rock strength.

Fault orientation (dip and strike) is determined from depth-converted seismic interpretations, whilst estimated pore pressure comes from downhole measurements, usually RFT pressures. Knowledge of the fault failure envelope is rarely available, but can be determined from laboratory testing of intact fault rocks (Handin and Jaeger, 1957; Handin, 1969; Jaeger and Cook, 1976; Dewhurst and Jones, 2002).

Collectively these inputs enable the shear and normal stresses acting over a mapped fault surface to be calculated for the in situ stress regime and the magnitudes of the resolved stresses to be compared with a Coulomb slip criterion to determine how close different points on the fault(s) surface are to reaching the failure envelope

given a change in pore fluid pressure (e.g. Zoback et al. 2002, Streit and Hillis 2004, Chiaramonte et al. 2008; Figure 8–30). The likelihood of fault reactivation is expressed by the increase in pore pressure (ΔP) necessary to reach the failure envelope and cause the fault to slip (Mildren et al., 1994). The mode of failure will depend on the differential stress as well as the shape of the failure envelope that reflects the inherent strength of both the fault and host rocks prior to the fault being reactivated (Figure 8–30).

The application of stress based methods has become widespread across the Timor Sea region, both to risk trap integrity and to address wellbore stability problems commonly encountered during drilling. From an initial proposition that the in situ stress field could be controlling trap integrity in the Timor Sea (Mildren et al., 1994) further application of this approach for trap integrity assessment yielded a number of convincing examples that highlighted the utility of this approach.

In the Northern Bonaparte Basin exploration drilling results provided anecdotal evidence that traps with bounding faults that were east-west orientated were more successful than those with bounding faults striking in a more NE-SW orientation. The determination of in situ stress tensors for these wells showed that NE-SW oriented faults were aligned parallel the direction of σHmax whereas the more successful E-W oriented traps were at a high angle to σHmax (Castillo et al., 1998, 2000; de Ruig et al., 2000; Figure 8–31).

Subsequent work by Brincat et al. (2001) demonstrated the presence of palaeo-oil columns in numerous traps where the bounding faults lay parallel with the direction of σHmax (Figure 8–31). At a trap scale in the same region Castillo et al. (2000) showed examples where low calculated ΔP values characterised the bounding fault of the currently water-wet Ludmilla structure that contains evidence for a palaeo-oil accumulation (Figure 8–32).

However, the work of Brincat et al. (2001) and more recent studies (George et al., 2004a; Gartrell et al., 2006) also describe significant palaeo-oil zones below hydrocarbon zones in traps from the Northern Bonaparte basin with E-W orientated bounding faults, indicating that these traps experienced substantial leakage.

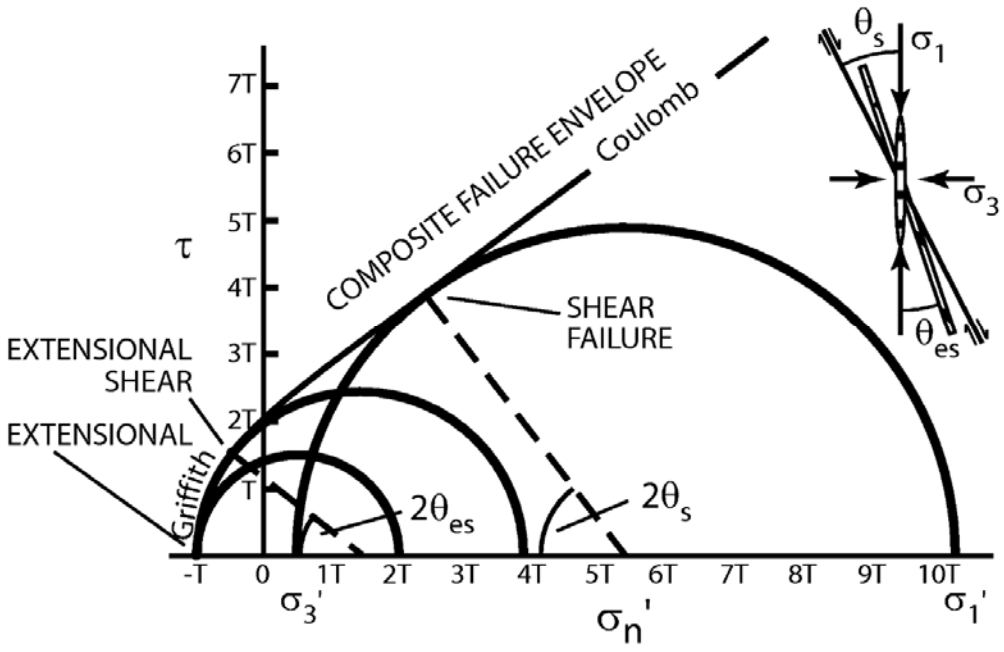

Figure 8-30: The basis of the Coulomb slip criterion

A Mohr diagram with composite failure envelope for intact rock with tensile strength, T, illustrating the stress conditions and orientations with respect to the stress field of extensional (tensile), shear and mixed-mode (extensional-shear) failure (Sibson, 1994). The magnitude of the differential stress (σ1-σ3) determines the size of the Mohr circle and together with the strength of the rocks controls the type of failure that can be anticipated under different stress fields.

Consequently, whilst traps with E-W orientated bounding faults may statistically have been more successful the fault orientation is clearly not the primary control on the level of trap integrity.

Aside from the Laminaria High region the maximum horizontal stress orientation (σHmax) is considered to be relatively consistent across the Bonaparte Basin with a mean σHmax orientation of 055° for the Timor Sea area obtained from the Australian Stress Map (Hillis and Reynolds, 2000; Mildren et al., 2004).

The fairly parallel alignment of σHmax and the principal faults trends in the VSB doesn't bode well for the maintenance of high trap integrity across the region. Indeed this concern is consistent with the results of the current study that highlight numerous palaeo-hydrocarbon columns. However, the fact that many of the intact hydrocarbon fields from the region also show similar fault orientations to the measured σHmax direction (Hillis, 1998) implies that processes other than the in situ stress field need also to be considered as possible controlling factors on trap integrity.

An attempt to calibrate the application of contemporary stress field analysis (Figure 8–33) as a tool to predict fault seal, Mildren et al. (2002) compared stress based predictions against well results from the VSB and reported a good agreement with known fields and reported palaeo-hydrocarbon columns. These authors used a generalised contemporary stress field for the Timor Sea region derived from previous studies (stress tensor in the Timor Sea area; Hillis and Williams, 1993; Mildren et al., 1994; Hillis et al., 1997a; Hillis et al., 1997b; Castillo et al., 1998 and Hillis, 1998) together with cohesive strength of existing faults that is assumed to be 5 MPa and a coefficient of friction assumed to be 0.7. A lack of geomechanical data for Timor Sea fault rocks, reflecting a paucity of cored faults in the region, required the use of experimental data from geomechanical testing of faults from the Otway Basin in southeastern Australia (Dewhurst et al., 2002; Streit, 1999).

Mildren et al. (2002) also quantified the degree of pore pressure change needed to induce seal breach using trap assignments based on the tripartite trap classification scheme of O'Brien et al. (1996a).

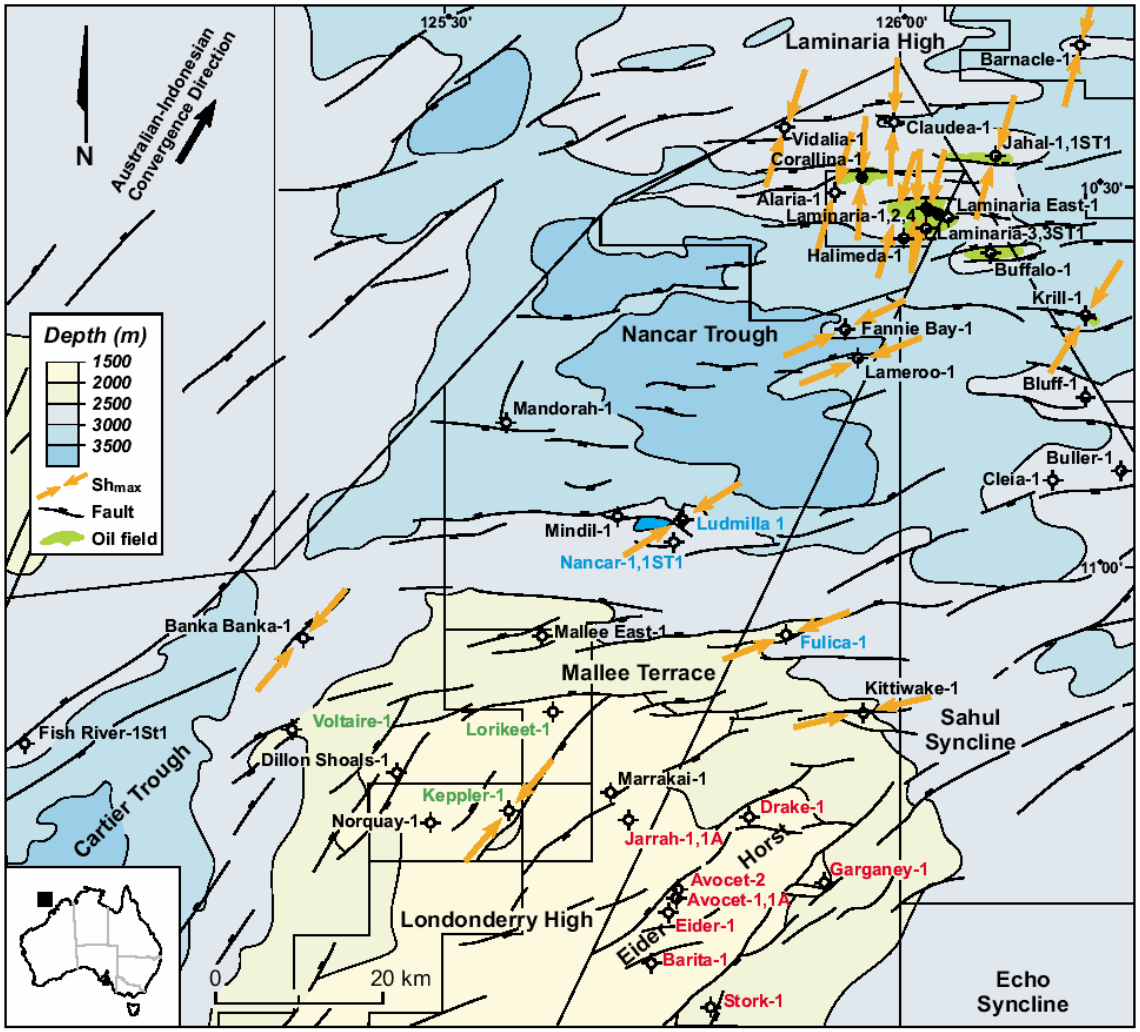

Figure 8-31: Application of stress field analysis to the Northern Bonaparte Basin

Regional tectonic elements map for the Northern Londonderry high area at the top Flamingo Formation level, with arrows indicating the direction of σHmax in the in situ stress field (Modified from de Ruig et. al., 2000). Intact oil fields on the Laminaria High have east-west orientated bounding faults that strike at a high angle to σHmax, whilst many of the dry holes have faults that are more parallel with the direction of σHmax. Brincat et al. (2001) described the presence of palaeo-oil columns in the Avocet-1A, Avocet-2, Drake-1, Eider-1, Garganey-1, Ludmilla-1, all of which have fault orientations that parallel the regionally defined σHmax direction.

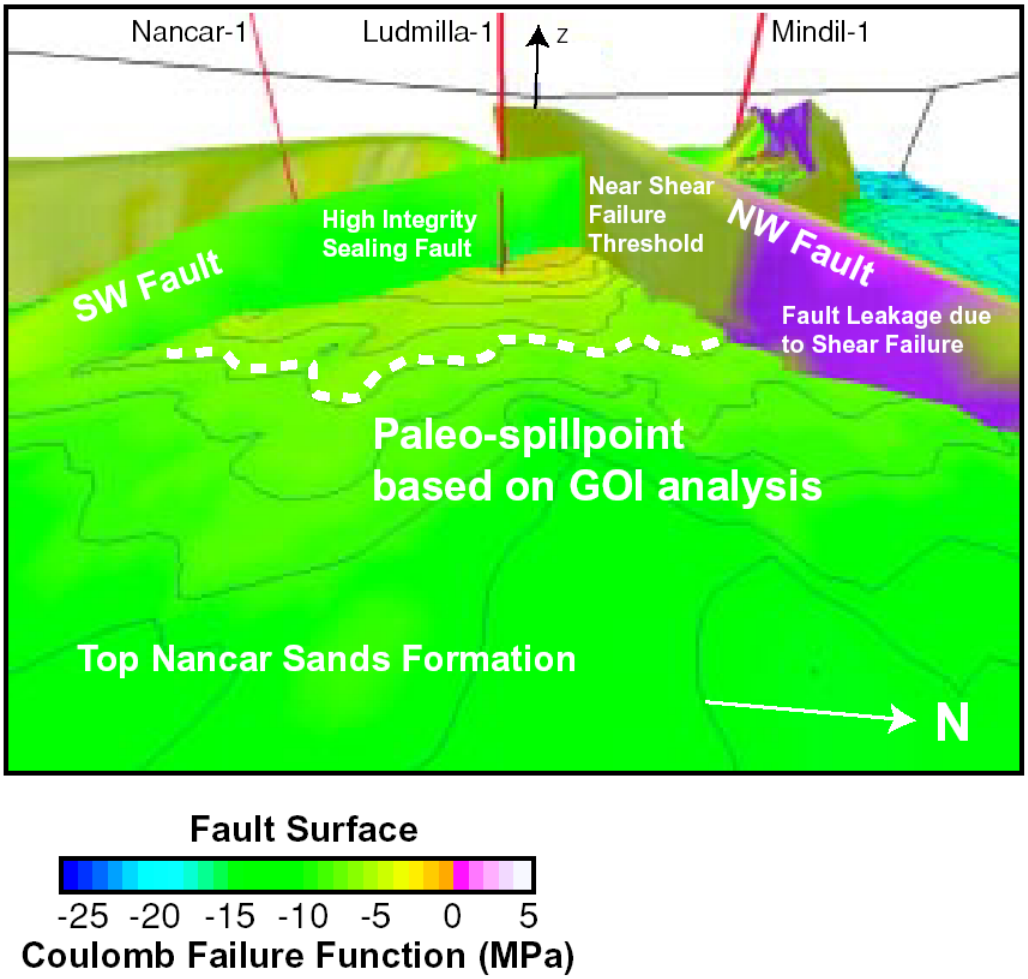

Figure 8-32: Example of the application of stress field analysis to the Ludmilla Structure

3D perspective view of the Ludmilla-1 structure showing the approximate location of the palaeo-oil-water-contact inferred from GOI analysis in Ludmilla-1 (from Castillo et al., 2000). This palaeo-contact coincides with sections of the fault with low ΔP values with the entire NW fault being close to becoming critically-stressed for shear failure using the calculated Coulomb Failure Function and therefore, less likely to behave as an adequate fault seal for trap integrity. Refer to Figure 8–33 for the location of the well.

Low integrity traps are suggested to have ΔP values less than 10 MPa, moderate integrity traps correspond with values between 10 and 15 MPa and high integrity traps correspond with values greater than 15 MPa (Figure 8–34). Faults with dips greater than 60° in the Timor Sea area were also recognised as being more likely to be prone to reactivation, with shear failure the most likely mode of reactivation.

In broad terms the results from Mildren et al. (2002) show significant differences in the predicted fault reactivation risk between the inferred high integrity Oliver trap and the lower trap integrity that is implied for the breached East Swan trap or the partially breached Challis and Skua traps (Figure 8–34). However, the differences between the breached trap at East Swan and the partially intact Challis and Skua oil fields is much less convincing and only minor differences recorded for ΔP that could easily be attributed to coincidence, particularly given the significant uncertainties associated with the various input data used.

The difficulty in confidently distinguishing between a moderate and low integrity trap is highly significant as it is the moderate integrity trap that is most likely to have the greatest chance of retaining an economic accumulation where the fill is predominantly oil. In contrast, the high integrity trap is likely to contain predominantly or exclusively gas and therefore is likely to be no more economic in the current environment than a low integrity breached trap.

Closer examination of the individual traps, where colour-coded fault segments plotted on a map have been used to display the calculated ΔP values (Figure 8–34) is more revealing about the strength of the predictions made in the Mildren et al. (2002) paper. The East Swan 'low integrity' structure for example is characterised by changing ΔP values along the length of the fault, ranging from more than 15MPa at the southwestern end to less than 10Mpa at the northeastern end.

Whilst changing values are not unexpected, especially where significant changes in fault orientation and/or dip are observed, the results suggest that the most crestal part of the structure is characterised by relatively high ΔP values. Failure of the fault may still be occurring along strike of the fault, but the retention of some hydrocarbons would be expected at the crest.

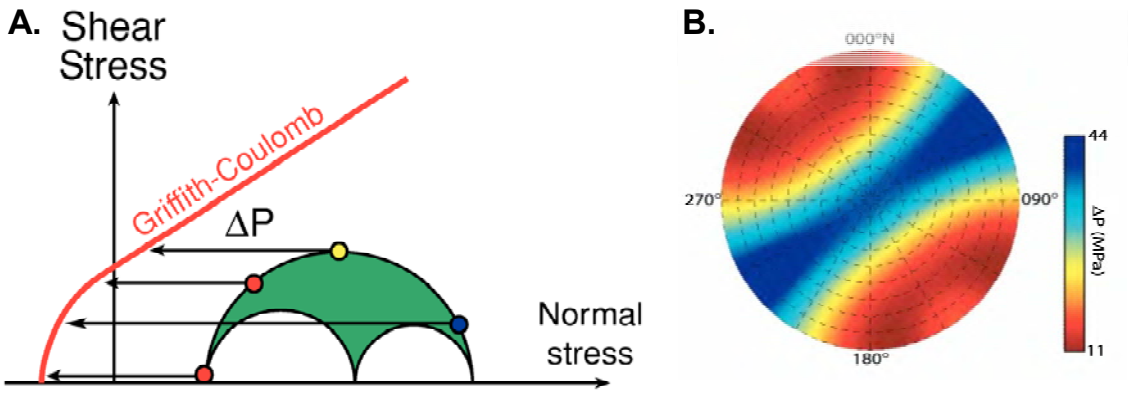

Figure 8-33: Risk of reactivation determined by stress field analysis

A schematic cartoon describing how the risk of failure varies in response to pore pressure changes needed to induce failure and a projection showing the risk defined for the Timor Sea generalised contemporary stress field and assuming a constant failure envelope (diagrams all from Mildren et al., 2002). **A.** Three-dimensional Mohr diagram with composite Griffith-Coulomb failure envelope. All possible orientations of planes lie within the green shaded area. The horizontal distance between any fault orientation and the failure envelope (which may be thought of as the increase in pore pressure (ΔP), required to cause failure) is used to assess the propensity of a fault plane to fail. B. When displayed on an equal angle, lower hemisphere stereographic projection of poles to planes the likelihood of a fault/fracture plane being at a critical stress condition can be evaluated. Numerical values on scale refer to increase in fluid pressure required to cause reactivation (ΔP). High ΔP implies low risk (blue) and low ΔP implies high risk (red).

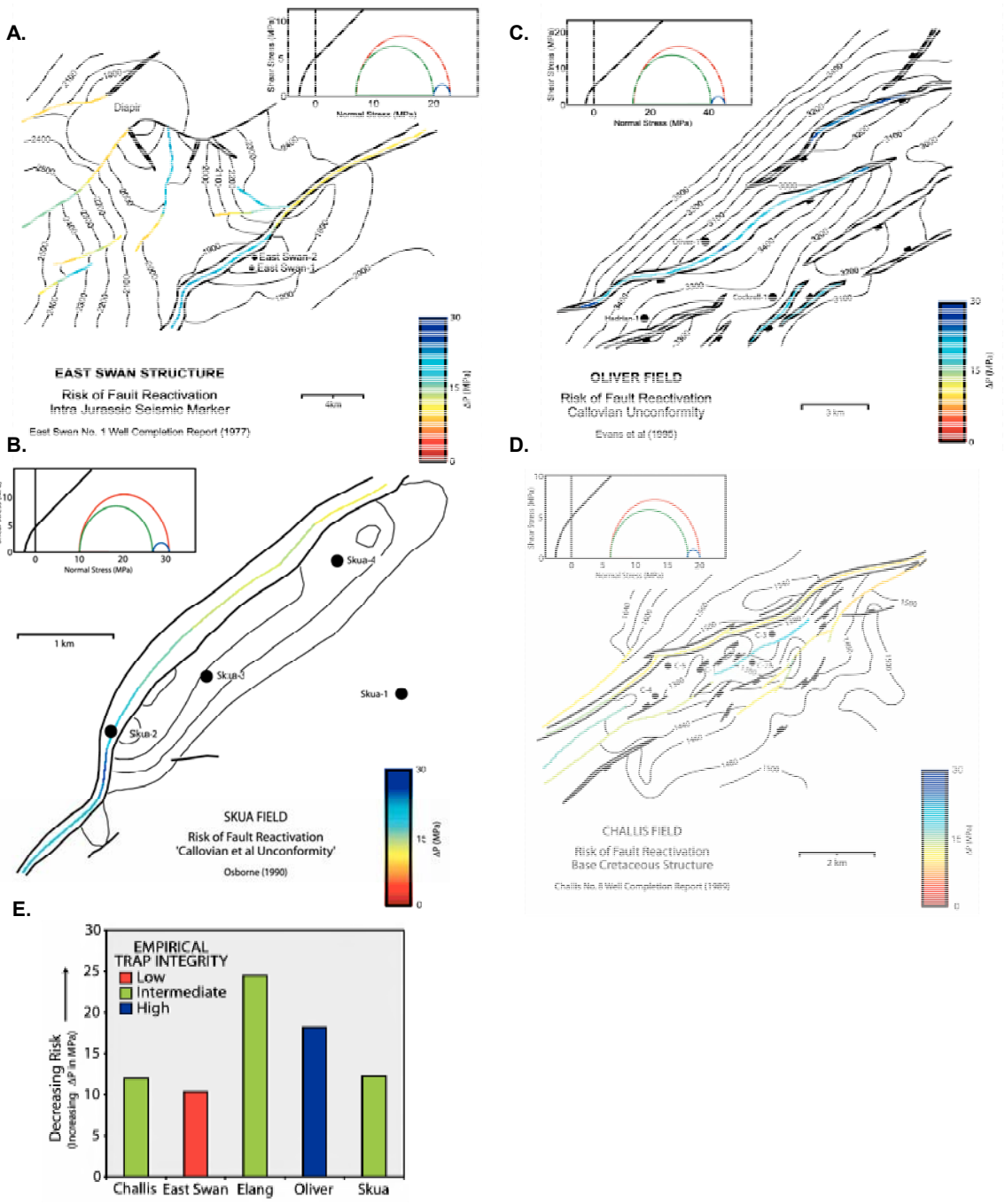

Figure 8-34: Trap ranking using the contemporary stress field.

Predicted risk of fault reactivation for selected traps from the VSB measured by ΔP in MPa and projected on a three-dimensional Mohr circle construction using a generalised Timor Sea stress tensor. Fault segments for A. the East Swan trap stress environment at 1750m depth, B. the Oliver Field stress environment at 3300 m depth, C. the Skua Field stress environment at 2300 m depth and D., the Challis Field stress environment at 1500 m depth. E. Comparison of empirical trap integrity with predicted fault reactivation risk. Fault reactivation risk is given as an average of the maximum risk for each individual bounding fault of a trap.

Similarly, faults bounding the implied 'moderate' integrity Challis oil field show a range of ΔP values that are consistently less than 15MPa along the entire length of the northern main bounding fault (Figure 8–35). This observation used independently would lead to a conclusion that the trap was riskier than the breached East Swan trap.

Mildren et al. (2002) explicitly acknowledge that there may be a relatively minor difference between conditions required to produce a low integrity trap with those needed to produce a moderate integrity trap, yet still conclude that that a good correlation exists between observed fault trap integrity and fault reactivation predictions made using their methodology. This is clearly not the case if only the moderate integrity traps represent the economic oil accumulations.

The significant role that fault dip plays is also recognised with an acceptance that the fault strike can vary by as much as 60° and still maintain relatively low ΔP values (high risk), whilst ΔP can alter by as much as 15 MPa with only a relatively minor change in dip magnitude of less than 10°.

Even on good quality 3D seismic data accurate determination of fault dip can easily exceed 10°, particularly if care is not taken to pick the fault surface accurately or the data quality is poor. On 2D seismic data additional difficulties arising from fault aliasing effects between even closely spaced lines can easily introduce variability of this magnitude in the interpreted dip values.

In addition to issues related to accurate mapping of fault surfaces a number of other factors are likely to significantly influence the predictions that are derived from this type of trap integrity analysis. These include the significant potential for localised perturbations to the in situ stress field that can make predictions that are based on a regionally defined stress field invalid for trap scale applications.

Assumptions that are also made regarding the inherent strength of fault rocks, including assuming that all faults lack cohesion (Figure 8–35), are demonstrably incorrect (i.e. Dewhurst and Jones, 2002), but are commonly used due to the lack of suitable geomechanical analyses or considerations that fault strength in a less unimportant factor (Castillo et al., 2000).

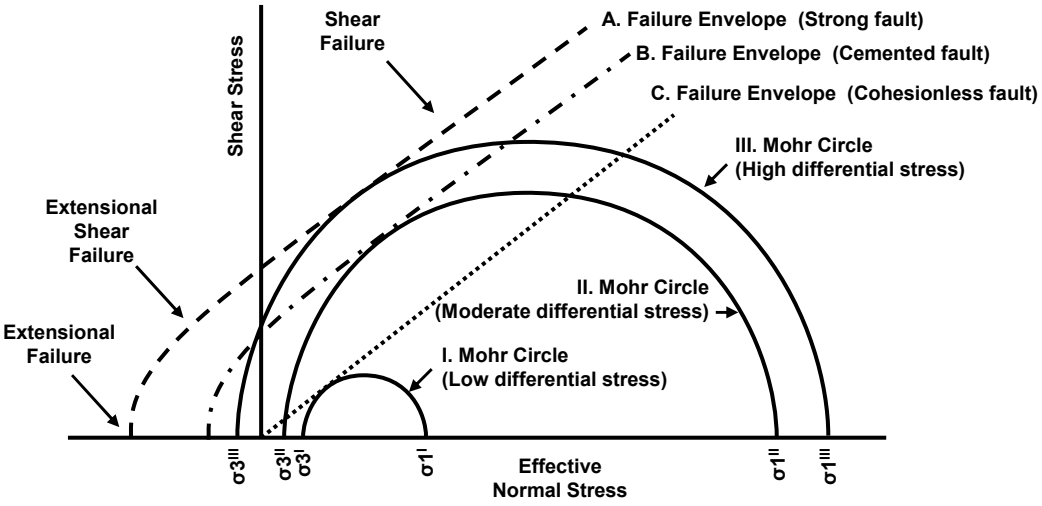

Figure 8-35: Impact of changing input parameters on fault reactivation predictions.

Simplified Mohr Circle construction showing the impact of changes produced to the failure envelope by applying different fault rock strengths or changes to the Mohr Circle through varying differential stress (σ1-σ3). For faults lacking cohesion failure of pre-existing faults can be by shear failure only (Coulomb Failure Function used by Castillo et al., 2000). However, if fault rocks are given inherent strength (Mildren et al., 2002, 2005) then both the propensity for failure and the mode of failure can be altered significantly. Increased fault rock strength increases the level of ΔP needed to produce a critically stressed fault segment and allows for extension or mixed mode (extensional shear) failure to occur at higher differential stress or higher stress magnitudes than would be expected if weaker fault rocks are assumed.

The Mildren et al. (2002) study recognises these issues and opt for a constant cohesive strength (5 MPa) for existing faults, despite acknowledging analyses with variations of 4-14 MPa (Streit, 1999) and other published values showing similar ranges (i.e. 9-15 MPa for Otway Basin fault rocks reported by Dewhurst et al., 2005).

The use of a cohesion intercept to reflect the inherent strength of the existing fault rocks not only changes the predicted ΔP values (Figure 8–35) required to produce fault reactivation but the greater fault rock strength also increases the opportunity for tensile rather than shear failure (Figure 8–35) under the same stress field. Incorrect predictions of the type of anticipated mode of failure could lead to erroneous conclusions about the degree of fault zone permeability that is created by the process of fault reactivation that in turn could lead to an erroneous trap integrity prediction.

Mildren et al. (2005) recognise the impact of these uncertainties together with the impracticality of completing sufficient experimental work to cover this risk. Indeed as with any rock based analysis there remains major uncertainty about the representativeness of a small numbers of geomechanical analyses and in the absence of sufficient numbers of analyses there is no way to ascertain the ranges that should be applied to account for natural variability. To address these issues Mildren et al. (2005) recommend the use of sensitivity analysis, ideally using probabilistic 'Monte Carlo' type methods to explore the impact of these variables on the predictions.

When this type of sensitivity analysis was applied to their Otway Basin example Mildren et al. (2005) demonstrated significant differences in predicted ΔP values when different cohesive fault rock strengths or σHmax stress magnitudes are applied (Figure 8–36). Much higher pore pressures were needed to reactivate even optimally oriented faults in the lower σHmax and strong fault cases (Figure 8–36).

The application of contemporary stress field analysis to trap integrity predictions also assumes that where a Mohr–Coulomb failure occurs, permeability along the fault is always increased and hence the chance of leakage is notably higher for the faults that are shown to be critically stressed.

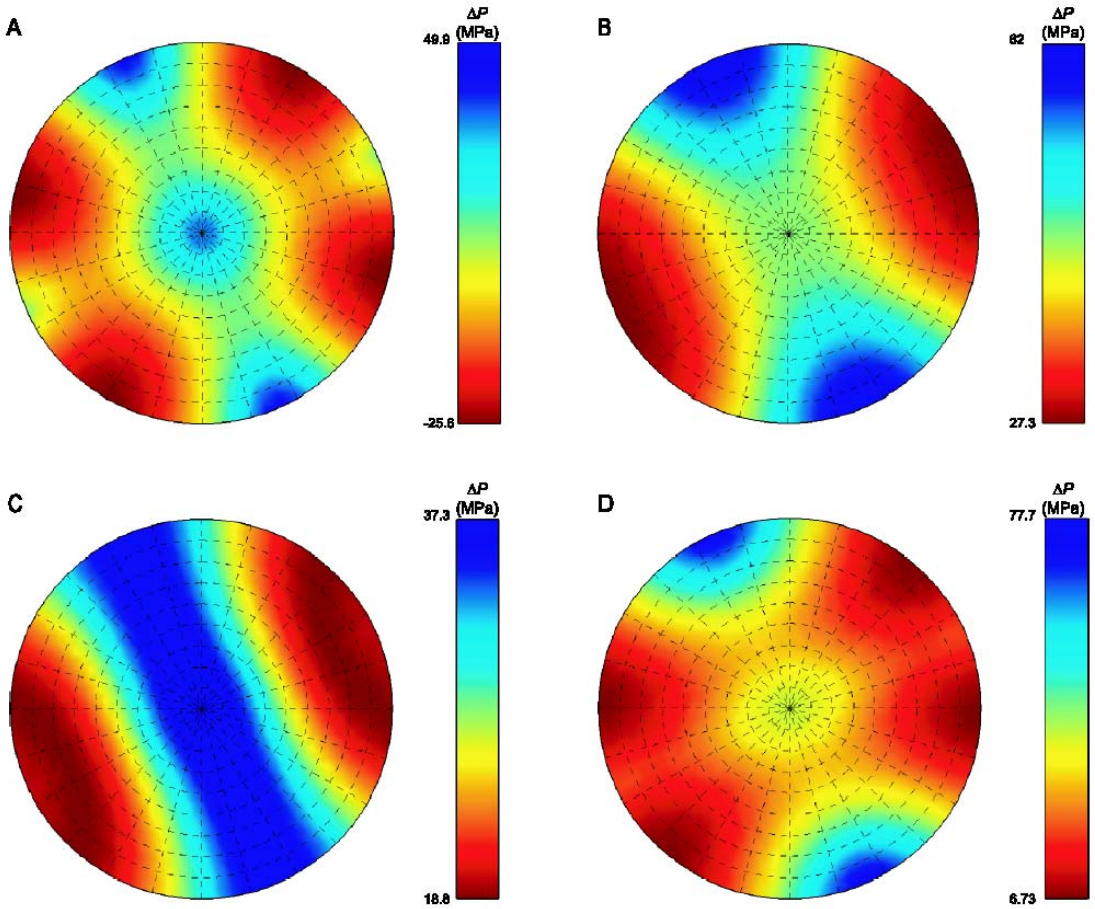

Figure 8-36: Sensitivity analysis applied to trap integrity predictions.

The likelihood of fault reactivation as assessed by analysis of the contemporary stress field in the Otway Basin conditioned to account for possible ranges in fault rock strength including (A) Weak fault rocks and (B) strong fault rocks as well as the impact of changing σHmax values between lower (C) and higher limits. Plots are polar diagrams of normal to planes colored by σP values to reflect proximity to failure due to a change in pore pressure (from Mildren et al., 2005).

Whilst it seems intuitively probable that the likelihood of faults becoming fluid conduits due to reactivation and fluid flow associated with earthquakes is well documented (e.g. Sibson, 1981; Rojstaczer and Wolf, 1992) there is little published data that addresses the empirical probability of this outcome at the trap scale. General rules may be applicable with King and Muir-Wood (1994) suggesting the style of fault displacement plays a dominant role on the likelihood of fluid flow with normal faults being more conductive than is seen with reverse faults.

Irrespective of the theoretical considerations, several examples of preserved hydrocarbon columns in the VSB exist (e.g., Skua, Jabiru, Challis, Talbot, Oliver, Tenacious, Audacious) in heavily reactivated structures where σHmax (approximately northeast-southwest) is oriented at low angles to the trap-bounding fault(s). The retention of hydrocarbons in these structures shows that an assumption that fault reactivation leads to complete loss of accumulated hydrocarbons is clearly an invalid supposition.

The application of stress based methods to the prediction of future fault slip events, such as those induced by pressure changes during drilling or production or to address questions increasingly being posed by geosequestration studies that utilise a structural trapping configuration is clearly highly useful. In contrast predictions about the loss of hydrocarbon columns by fault reactivation that occurs under different stress regimes remains open to considerable debate. Even the very use of the "contemporary stress field" itself introduces a major assumption that stress fields have not changed through time, an assumption that is difficult to accept for most basins, let alone one like the VSB that has been severely impacted by multiple episodes of major regional plate reorganisation.

The most useful application of contemporary stress field assessment in the VSB may in fact be in the interpretation of contemporary hydrocarbon seepage that currently lacks a robust understanding of the mechanisms controlling the rate of fluid flux. In this application the factor being considered by the analysis, namely an increase in fluid permeability for faults that are critically stressed could be tested and enable more robust interpretation of seeps data.

8.8.2.3 Kinematic Structural Models

The considerable uncertainty associated with the exact role that reactivated faults play in controlling trap integrity and the bearing this has on the application of the stress or seepage based techniques discussed in the preceding sections has encouraged other workers to undertake a more detailed assessment of the fault architecture associated with hydrocarbon traps in the VSB.

Whilst much work has been done at the plate margin and basinwide scales (Warris, 1973; Woods, 1992, 2004; O'Brien, 1993; O'Brien et al., 1999a; Baxter et al., 1997; Keep et al., 1998, 2002; Muller et al., 1998; Upton et al., 1998) initial trap specific studies aimed to define the local structural style rather than address the impact of fault reactivation on hydrocarbon preservation potential (Woods, 1988; Nelson, 1989; Fittall and Cowley, 1992). As the role of fault reactivation in controlling trap integrity risk was recognised more recent studies have examined the fault systems in more detail to better understand this key risk. Aside from simple observations such as faults that terminate at the current sea-bed being higher risk or a greater propensity for reactivation of traps that were bounded by large displacement faults no effective predictive models had been developed until relatively recently.

O'Brien and Woods (1995) observed that traps with greater obliquity between the Jurassic rift faults and the overlying Miocene fault trends tended to be breached whilst those with more parallel orientations retained better trap integrity. They speculated that oblique reactivation produced pairs of restraining and releasing bends in response to a component of strike slip with the releasing bends acting as fluid-flow conduits. However, more recent observations from the Laminaria High contrast these empirical observations where post rift faults above intact oil columns strike at high angles relative to the orientation of the underlying rift faults (Gartrell et al., 2006).

Partly in response to the acquisition of regional 3D seismic surveys across the VSB in recent times and through improved imaging attained by better acquisition and processing workflows and partly due to the limited success attributed to other methods this gap has been addressed by a number of more comprehensive studies of fault populations (Meyer et al., 2002; Peresson et al., 2004; Gartrell et al., 2005).

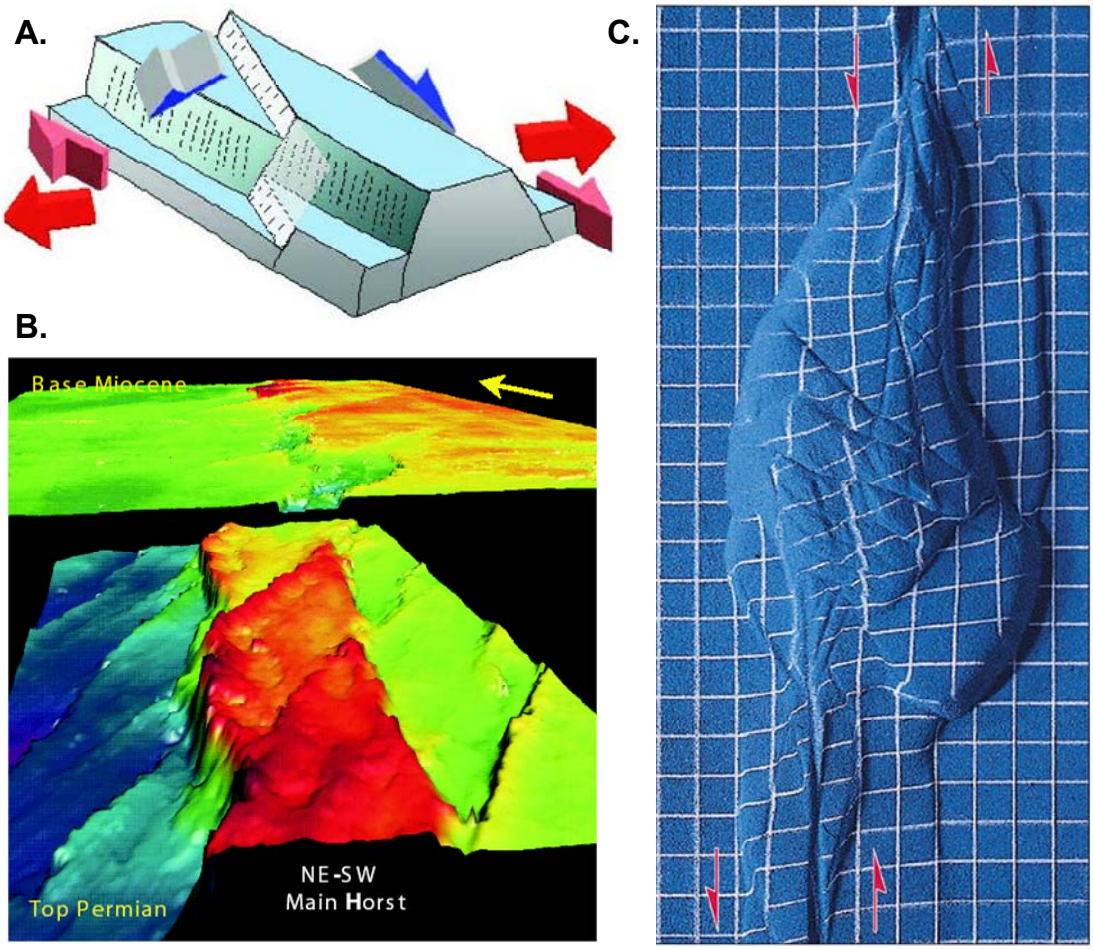

Figure 8-37: Role of complex faulting in producing sub-traps

A schematic cartoon fault block model **(A)** showing the segmentation of a horst block formed during initial rifting by an oblique set of faults that cross-cuts the main horsts and define a series of structurally higher sub-horsts **(B)**. Unlike the earlier formed main horst faults the cross-cutting faults indicate a component of oblique-normal slip with a small right-lateral component producing an *en echelon* pattern (A and B from Peresson et al., 2004). In sandbox modelling **(C)** this type of faulting produces pop-up structures that can occur along the length of the pre-existing fault where there is a component of transpression.

Building on previous studies, Peresson et al. (2004) noted that oblique fault reactivation in the VSB frequently produced a series of *en echelon* oversteps where the breaching of overlapping relay ramps segmented existing horst blocks (Figure 8–38), giving rise to rhombic-shaped fault blocks in map view (de Ruig et al., 2000). The style of faulting remains normal, but there are indications that the sense of shear along the faults has a left-lateral oblique component (Peresson et al., 2004).

Whilst this fault style had been noted previously for a variety of VSB structures (Nelson, 1993) Peresson et al. (2004) recognised the role that this process played in creating new traps (Figure 8–38). These workers surmised that in locations away from the crests of these newly formed structures these new faults could produce potential fluid leak points where they intersected the pre-existing large offset faults that define the main horst block.

Although the work of Peresson et al. (2004) was beginning to associate the complex interplay of fault orientations with leakage potential the idea of these sub-structures could also act to shield traps from breach was not fully appreciated. The concept of protected structures was first described in the Northern Bonaparte Basin by Gartrell et al. (2005) drawing on work by Meyer et al. (2002) dealing with the progressive localisation of strain that occurs during the evolution of a normal fault population. Large faults grow at the expense of smaller faults, which display slower growth rates and may eventually become dormant, a process referred to as strain localisation (e.g., Cowie 1998; Walsh et al., 2001).

Gartrell et al. (2005) noted that whilst most rift faults in the region have experienced some degree of reactivation the accommodated strain was heterogeneously distributed, with the larger (longest and greater displacements) Jurassic rift faults showing higher displacement rates, greater accumulated post-rift displacements and more prolonged sedimentary growth than smaller rift faults in the population.

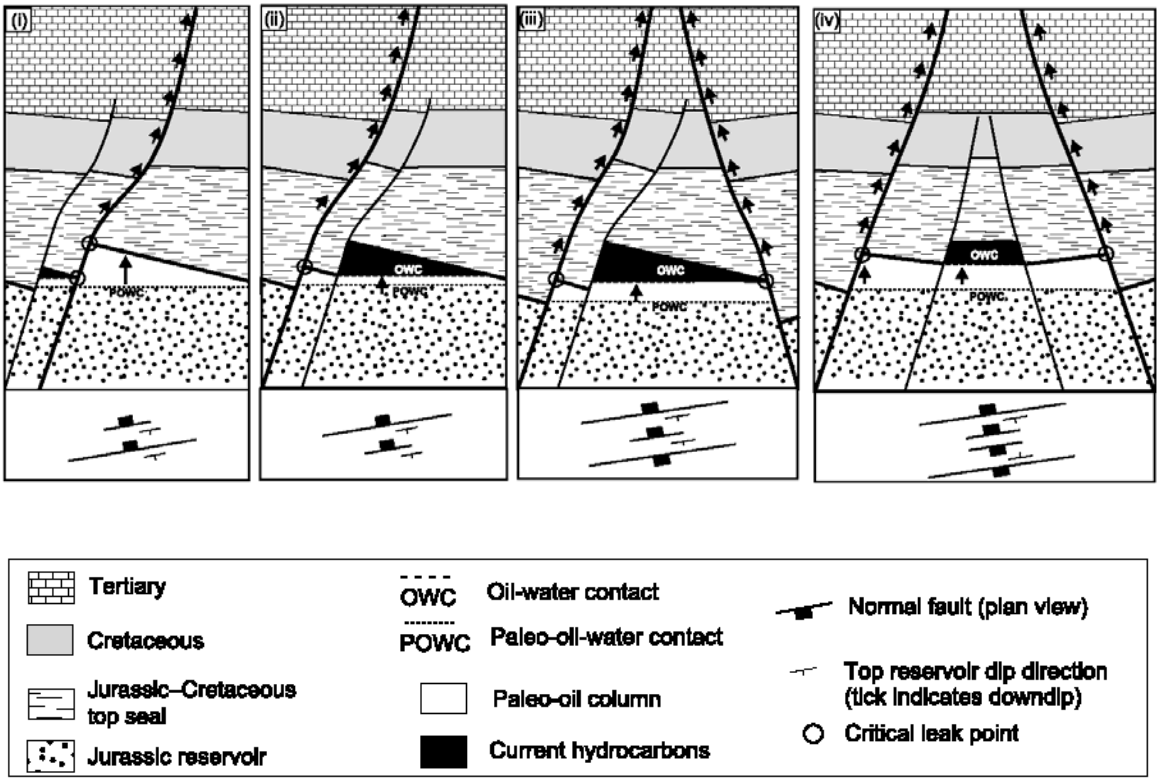

Figure 8-38: Trap integrity model for reactivated fault-bound traps

A series of characteristic cross sections through reactivated fault-bound traps showing the predicted relationships of present and palaeo-oil columns relative to the location of key leak points (from Gartrell et al., 2005; 2006). Large faults will accumulate more strain than the smaller faults making them more prone to increased vertical transmissibility and leakage. Where large faults provide the principal closure (i) the accumulation of strain during reactivation makes such faults less likely to be sealing. In contrast, faults that are shielded from these high strain faults are more likely to preserve hydrocarbons and a variety of geometric scenarios can be envisaged (i.e. ii, iii and iv).

A simple geometric model, which indicates various trap integrity risks and hydrocarbon preservation scenarios for different fault associations, was constructed from these observations (Figure 8–39). The position of the structural crest relative to the point where the high displacement faults intersect the reservoir section controls the level of implied trap integrity.

Traps where high displacement faults act as the main trap bounding fault suffer complete loss of hydrocarbons whereas partial preservation is achieved where the high displacement fault plays a subsidiary role in controlling trap size (Figure 8–39). Somewhat paradoxically regions with relatively high structural complexity are more likely to provide areas with enhanced opportunity for traps with low-risk geometries to occur (Gartrell et al., 2006), albeit with smaller volumetric capacity. As recognised by Peresson et al. (2003), Gartrell et al. (2005) suggests that high-quality 3-D seismic data capable of allowing more accurate characterisation of these subtle structural configurations is needed to reduce this critical risk.

A key difference with the approach adopted by Gartrell et al. (2005) was the integration of the detailed structural analysis with information on the palaeo-distribution of hydrocarbons derived from fluid inclusion data contained in associated studies (Brincat et al., 2001; George et al., 2004a).

Examples from wells across the Laminaria High demonstrated a good correlation between the extent of palaeo-oil zone inferred from conventional shows and the fluid inclusion methods and the depth of intersection at top reservoir level of the high-strain faults (Gartrell et al., 2005; 2006).

The greater Buffalo structure represented one of several compelling examples with a retained oil column (the Buffalo oil field) located within a central sub-horst formed by smaller faults that is flanked by larger faults. A greater proportion of the total strain has accumulated on these large faults acting to shield the internal sub-horst and prevent total loss of hydrocarbons (Figure 8–40). A significant palaeo-oil zone was detected below the current OWC indicating only partial preservation had occurred within the Buffalo trap (George et al., 2007).

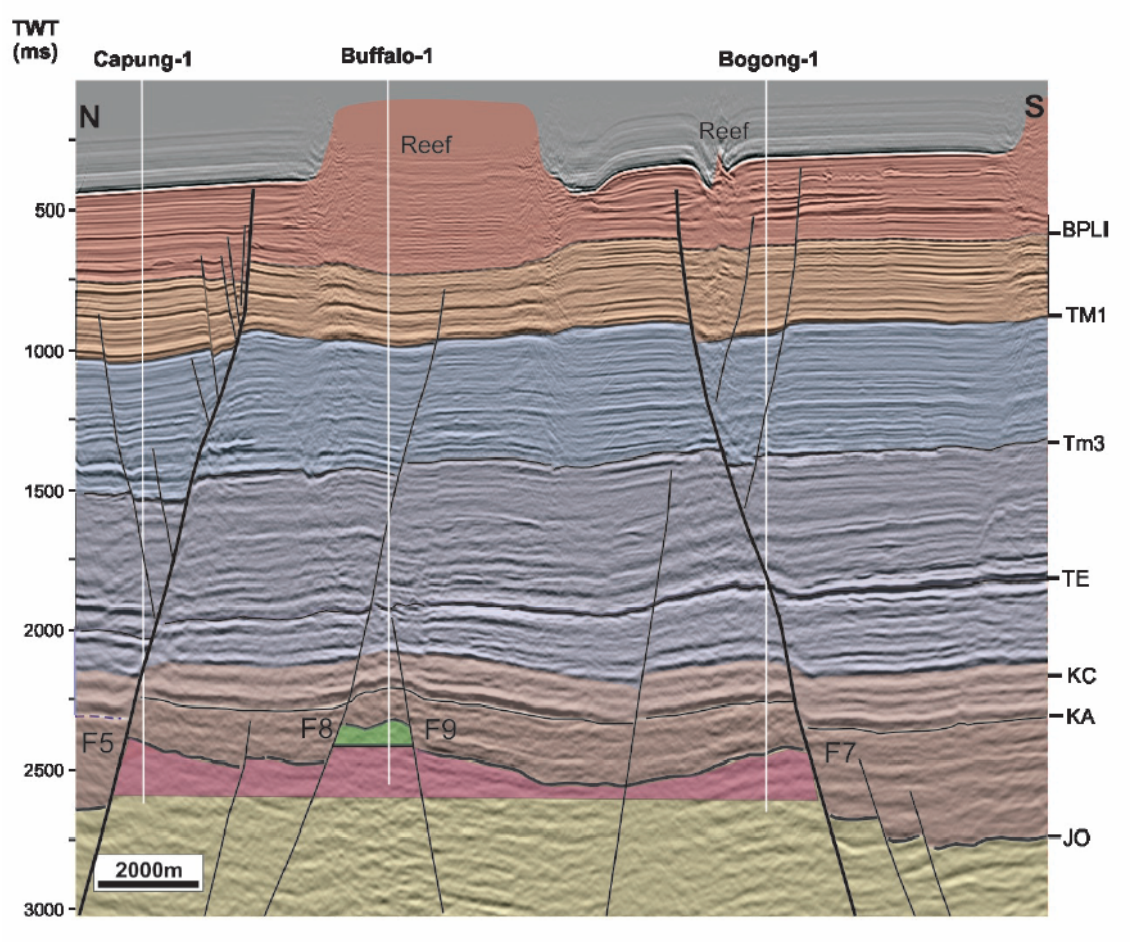

Figure 8-39: Application of the strain localisation model to the Buffalo oil field

Cross-section though the Capung (dry hole), Buffalo (intact oil zone) and Bogong (dry hole) structures. Buffalo is bound by low post-rift displacement faults and contains 50 m oil column, plus palaeo-oil column (defined by GOI analysis). The dry Capung and Bogong structures have high strain faults (F5 and F7) that intersect the top reservoir at the crest of the traps and both traps contain large palaeo-columns. Present day oil column shaded in green transparency. Palaeo-oil columns shaded in pink transparency. Thicker black lines denote faults with high post-rift strains and prolonged growth histories. Note: palaeo-oil water contact locations on figure are only approximate (Figure from Gartrell et al., 2005).

In contrast parts of the structure that are bound by the higher displacement faults were fully compromised, with palaeo-oil columns defined in the Capung-1A and Bogong-1 dry holes testament to a once much larger accumulation that subsequently leaked (Figure 8–40). Similar examples were also recognised for the greater structure containing the Laminaria and Corallina oilfields and the model was found to be applicable to both tilted fault block and horst block structures (Gartrell et al., 2005).

A subsequent application of this strain localisation model to the Vulcan Sub-basin was reported to be largely consistent with prediction when tested against a database of 69 drilled traps across the region (Gartrell et al., 2006). These case examples provide the opportunity to compare with the examples from the current study where a detailed charge history has been determined for a number of different trap types.

The characterisation of hydrocarbon traps in three dimensions is critical to be able to constrain the positions of leak points, spill points, and fluid contacts, which provide a basis to understand the likely controls on trap integrity using a strain localisation model. As a consequence the application of the model to areas such as the VSB was initially more difficult due to the lack of 3D seismic coverage. The acquisition of regional 3D seismic mega-surveys such as the Onnia survey (Edwards et al., 2005) aimed to address this need but poor data quality still limits the ability to image the structural complexity. Despite these limitations a number of key structures from the VSB still yielded valuable information that appear to support the predictions made by Gartrell et al. (2006).

The Challis and Cassini oil fields are located within a partially protected asymmetric hourglass structure, where strain has been strongly partitioned onto a major northwesterly dipping fault adjacent to the Ranier-1 well (Gartrell, et al., 2006; Figure 8–41). Post-rift fault displacements are relatively large on all observed faults but this largest fault has nearly twice the throw at the Miocene level (~85 m) compared to those observed on the faults that bound the Challis field (<40 m). The fluid inclusion (GOI) data collected in the current study demonstrates leakage from the Challis-Cassini field, involving the loss of an original gas cap to produce two accumulations separate oil columns within discrete structural culminations.

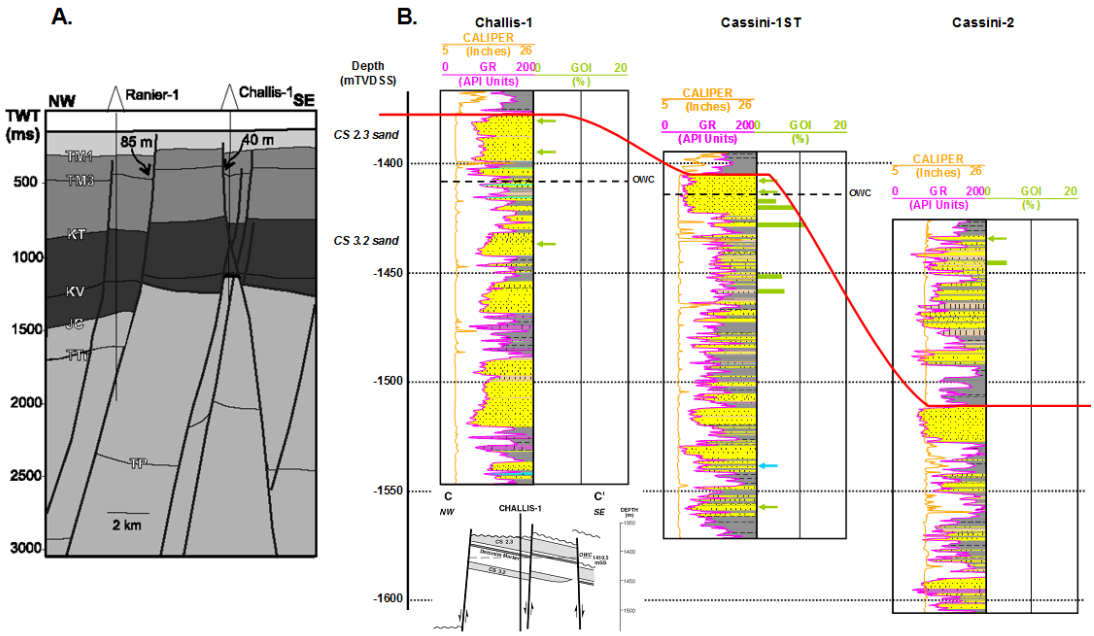

Figure 8-40: Application of the strain localisation model to the Challis-Cassini structure

A. Schematic diagram from Gartrell et al. (2006) showing the narrow Challis-Cassini horst flanked to the northwest by a significant reactivated fault with more than twice the displacement at TM3 time (Miocene) of the largest fault bounding the Challis trap. B. Fluid inclusion (GOI) data (note – green arrows refer to GOI values of <1% whilst the blue arrows indicate samples that are devoid of oil inclusions) from the Challis-1 and Cassini wells defines a larger palaeo-accumulation comprising a gas cap and underlying oil rim. Fluid loss has involved leakage of the original gas cap to leave the oil column seen at the current day. These data suggest that fault reactivation over the Challis horst has contributed to partial loss of hydrocarbons from this trap.

Evidence for leakage suggests that reactivation of the bounding faults was sufficient to partially breach the structure and appears contradictory to the model of Gartrell et al. (2006). In this instance the preferential loss of the original gas cap could indicate that fault reactivation reduced the trap integrity for gas (the more buoyant fluid) but remained sufficiently high to retain the oil-leg.

This could reflect differences in the degree of structural permeability created at the scale of the pore network with leakage being controlled by different capillary entry pressures for gas compared with oil. Progressive localisation of strain onto the larger fault may have prevented further damage to the seal by the trap bounding faults enabling the field to retain a less buoyant and overall smaller hydrocarbon column.

Gartrell et al. (2006) characterised the Skua oil field as a protected tilted fault block according to their trap integrity model, with increasing strain being progressively partitioned away from the main trap bounding fault of the Skua Field onto the larger adjacent Rowan fault. In contrast to the fault bounding the Skua Field the nearby Rowan fault displays a relatively higher post-rift displacement (~80m), extends to shallower levels, and exhibits prolonged sedimentary growth compared with the Skua fault over the length of the field (Figure 8–42). Whilst the GOI data collected on the Skua Field (Lisk et al., 1998a; Gartrell et al., 2002, 2004) defined palaeo-oil zones below the current OWC the distribution of these zones supports post-charge tilting rather than trap breach as the most probable mechanism to describe the observed results. Consequently, the assignment of the Skua trap as a protected fault block in the Gartrell et al. (2006) model may not directly test the model but their prediction is not inconsistent with the observation of palaeo-oil zones derived from the GOI data.

Other examples recognised by Gartrell et al. (2006) have only limited GOI data to assess the charge history (Talbot) or were drilled after the onset of the current study (Audacious, Vesta) and have not been examined. The Talbot field is seen as a partially protected structure with strain being partitioned onto the larger bounding fault that has more than twice the amount of post-rift displacement as the fault that penetrates the reservoir section down-dip of the crest (Figure 8–43A).

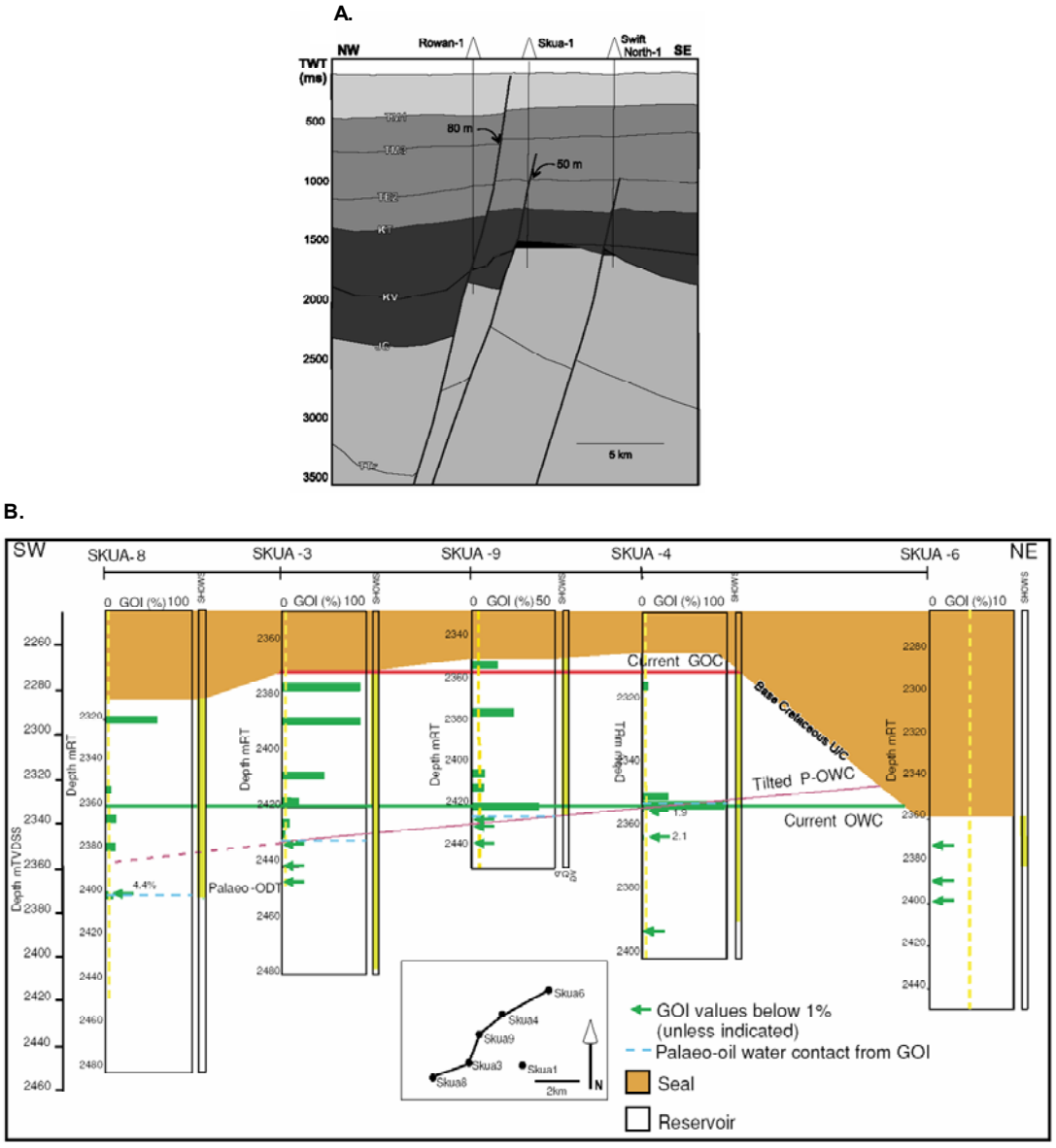

Figure 8-41: Application of the strain localisation model to the Skua field

A. Schematic diagram showing the shielding of the faults defining the Skua and Swift North oil accumulations by the larger Rowan fault (from Gartrell et al., 2006). B. GOI data from the Skua Field presented in Gartrell et al. (2004) showing an inclined palaeo-OWC defined by GOI data from multiple wells across the field. In this instance the palaeo-oil zone can be attributed to post-charge structural tilting rather than trap breach, a conclusion that supports the assignment of this trap as a shielded structure.

GOI data collected on the Talbot-1 well in the current study failed to provide evidence for high oil saturation despite the clearly defined and tested oil accumulation defined by the well. The unusual geochemical composition of the oil that suggested derivation from an initial gas phase (Edwards et al., 2004) was cited as a possible explanation for the low GOI values (Chapter five, section 5.5.2). Initial charge of the Talbot structure with single phase gas followed by partial breach and gas leakage could have resulted in a reduced column height, with the associated drop in pressure allowing the oil-phase to condense from the gas, allowing this phase change to not be represented in the fluid inclusion record. Dynamic seal behaviour influenced by a complex interplay between fluid pressures related to reducing column height and localised seal damage related to post-rift strain localisation may be controlling trap integrity of the Talbot horst.

In contrast, the Audacious oilfield discovered in 2001 (Maxwell et al., 2004) represents a typical example of a protected horst block with the post-rift strain being strongly localised onto the large faults that flank the trap below the current OWC (Figure 8–43B). The greater Audacious trap was first tested by the Kym-1 well, drilled in 1996, encountered a good quality, but water-wet reservoir section (Figure 8–44) and was plugged and abandoned as a dry hole. GOI analyses conducted on Kym-1 showed values <1% but provided confirmation that the well had penetrated a potential migration pathway (Cultus Timor Sea Ltd, 1998).

Further seismic reprocessing and velocity model refinement demonstrated up-dip potential remained on the greater Audacious horst, subsequently confirmed by new 3D seismic data (Maxwell et al., 2004). The revised closure relied on an increase in overburden velocities northeast of Kym-1 with improved fault imaging and clearer horizon interpretation aiding the interpretation (Figure 8–44).

The Audacious-1 well came in close to the pre-drill depth prognosis (±5m) and penetrated the reservoir significantly up-dip from the previous Kym-1. The delineated oil zone was restricted to the central horst block closure (Maxwell et al., 2004; Figure 8–43; 8–44) where the bounding faults have much less displacement than those of the greater structure.

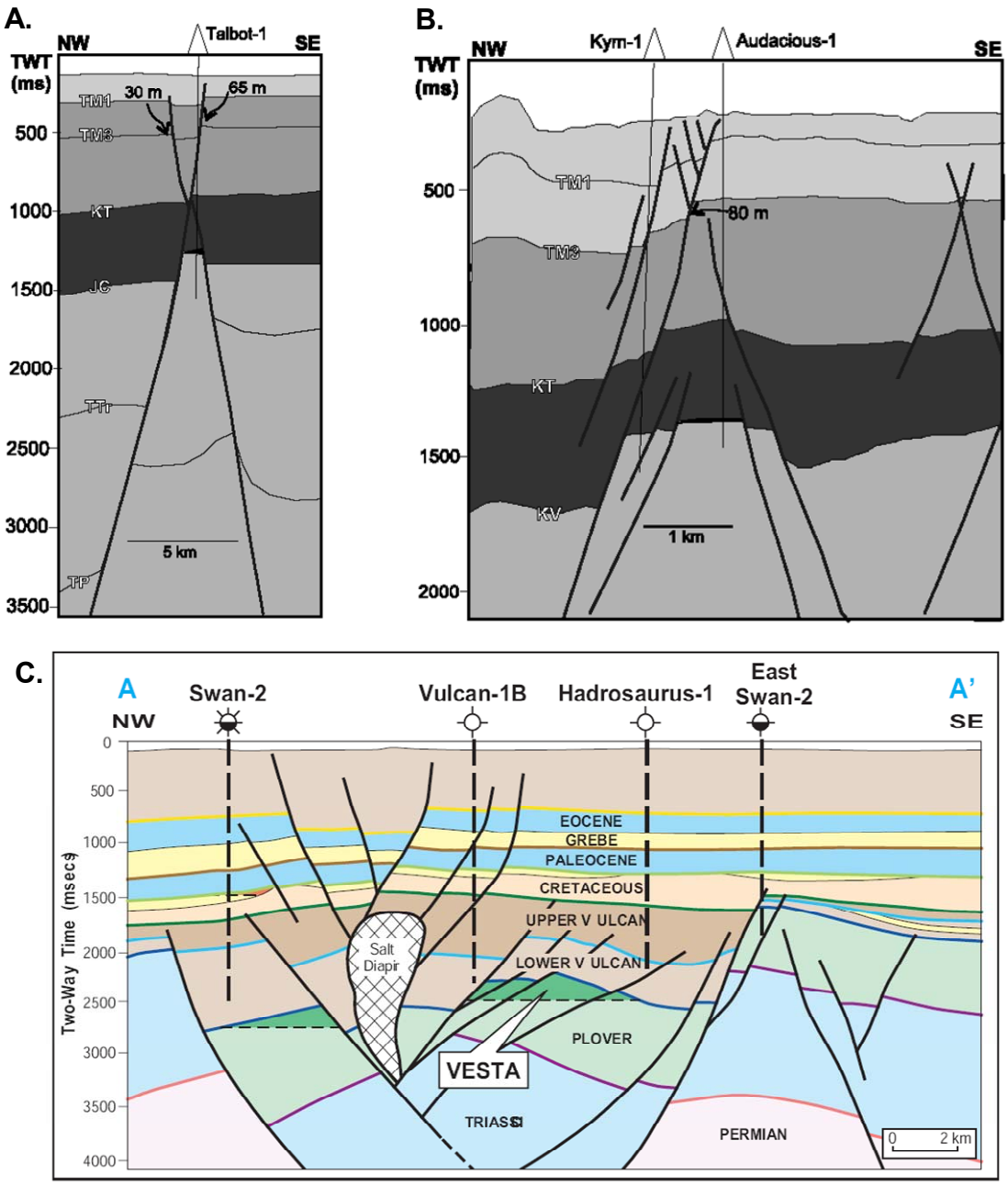

Figure 8-42: The strain localisation model applied to the Talbot, Audacious and Vesta fields.

A. The Talbot field shows a fault arrangement that represents a partially protected horst block with the column height constrained by a high-displacement NW dipping fault that intersects the reservoir close to the oil water contact. B. The 2001 Audacious-1 oil discovery represents a clear example of a protected horst block with the strain being strongly localised onto the large faults that flank the trap below the current OWC. C. The 2005 Vesta-1 oil discovery is another recent drilling result that appears consistent with the Gartrell et al. (2006) model being an intra-graben high with post-rift displacements being focused onto the large displacement graben margin faults that bound the East Swan and Eclipse palaeo-oil columns.

The 2005 Vesta-1 oil discovery provides a further example of the applicability of the strain localisation model of Gartrell et al. (2006), with the well being located on an intra-graben high within the Swan Graben (Figure 8–43). Limited information about this recent discovery has been released but the schematic cartoon shown in Figure 8–43 would be consistent with post-rift displacements being focused onto the large displacement faults that define the graben and that also bound the adjacent East Swan and Eclipse traps that both contain substantial palaeo-oil columns.

Overall Gartrell et al. (2006) studied the fault geometries of sixty nine traps across the Timor Sea region and considered 55 of these well results to be consistent with the model prediction based on their basic geometry. Where the prediction was inconsistent with the well result, five of these were categorised as high risk, but contained hydrocarbon columns.

Due to the relatively small hydrocarbon column height (15–35m) seen in some of these cases and taking into consideration the resolution of the seismic data at these reservoir depths, Gartrell et al. (2006) suggest that the preserved columns could be explained if these minor accumulations are trapped in small fault-independent closures that have not been recognised on seismic data.

Two distinct exceptions to the Gartrell et al. (2006) model that cannot be attributed to imaging uncertainties occur at the Jabiru oil field and the Oliver gas and oil field. The Jabiru trap is characterised as an internally faulted horst with some protected fault blocks (e.g. the Jabiru-1 sub-horst), but the greater oil-bearing structure relies on the main southern-bounding fault that offsets the sea floor, placing the structure in the high-risk category (Figure 8–45).

Gartrell et al. (2006) attribute this disparity to the fairly small post-rift displacements (a maximum of about 55m), presumably resulting in less fault related disruption of the top seal as well as greater accommodation of strain by ductile rather than brittle deformation. The relatively shallow reservoir depth (i.e. limited overburden) probably also controlled the ability of faults to propagate to the surface through such ductile sediments.

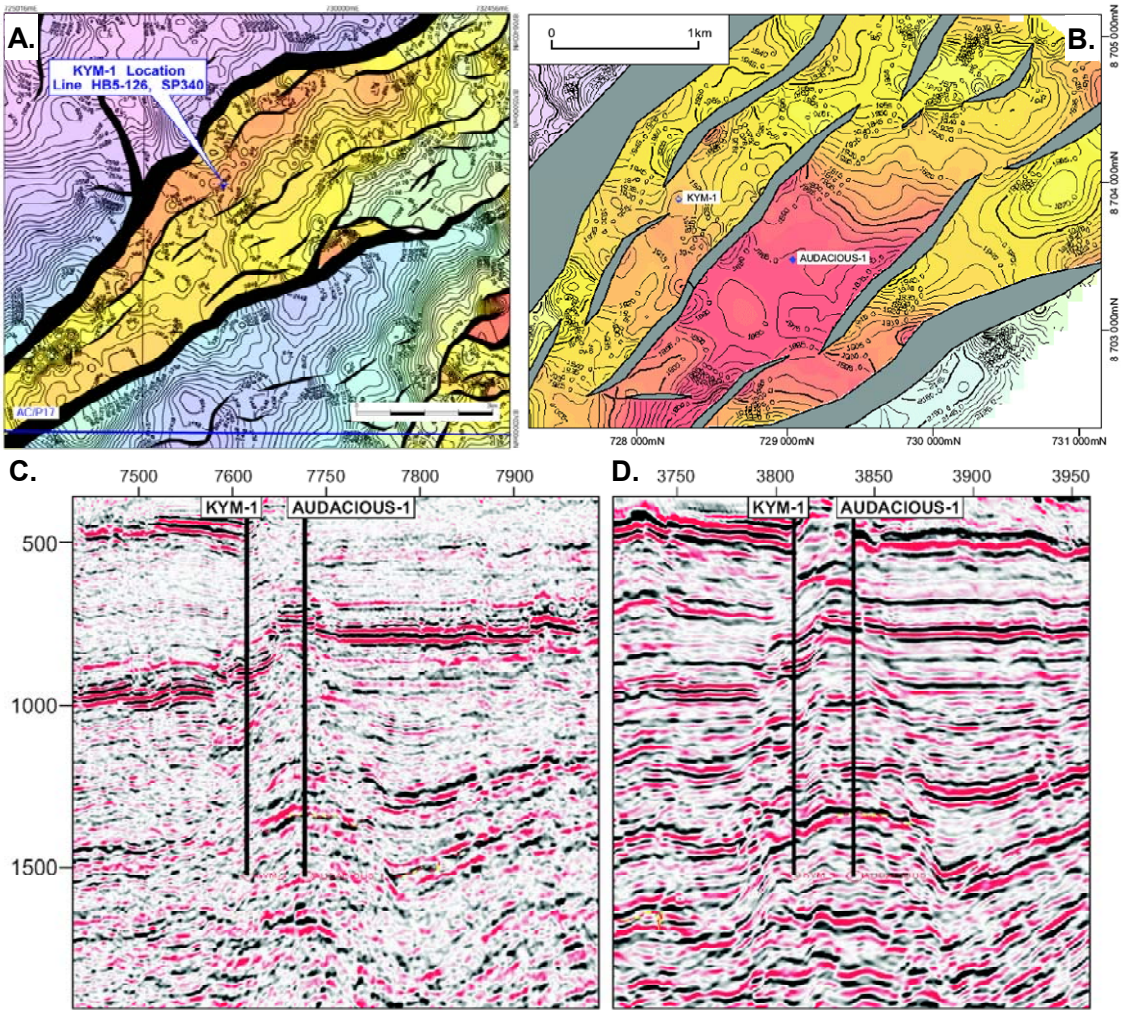

Figure 8-43: Importance of improved seismic imaging on the Audacious oil discovery.

A. Pre-drill (Kym-1) Callovian Unconformity depth map showing the crestal position of the well within a horst block defined by large displacement faults. Note the minor nature of the intra-horst faults with limited throws (contour interval is 10m). **B.** Post-well Callovian Unconformity depth structure map showing the position of the Audacious-1 discovery well within a protected horst. Maximum throw on the intra-horst faults is about 75m (contour interval is 5m). **C.** Phase-1 Pre-stack depth migration (PreSDM) seismic line showing relatively poor horizon and fault imaging compared to the more continuous reflectors and better imaged fault traces seen on the Phase-2 PreSDM (**D.**) processed data.

As with other predictive methodologies it seems likely that these disparities may be resolved by accepting that no one technique will provide accurate predictions in all settings. Rather it seems more likely that careful integration of techniques will be required to unravel the complex interplay between the structural and fluid histories.

Clearly, however, any proposed model that fails to successfully predict the largest and economically most significant oil accumulation in the basin limits the broader application as a pre-drill predictive tool until these apparent disparities are more clearly explained. Feasible options that might explain such apparent false negative outcomes could include an improved understanding of the palaeo- and contemporary stress field as well as consideration of dynamic seal behaviour related to column height considerations and differential seal capacity.

The second trap that appears unresolved by the strain partitioning model is the Oliver field that is considered to have a high-risk geometry as the bounding fault displays substantial post-rift displacement (~300 m), yet currently retains a large gas column (Figure 8–46). Fluid-inclusion data indicate the trap originally contained a 99m oil column with displacement of oil by later gas flushing considered the most likely explanation for the transition to the current fluid configuration (Lisk et al., 2002). The interpretation of the Oliver trap as a high integrity structure is supported by the interpretation of the contemporary stress field (Mildren et al., 2002) and the lack of any HRDZs in the shallow section.

Gartrell et al. (2006) suggested that the Oliver field could be dynamically leaking due to abundant late stage gas charge related to rapid subsidence of the Cartier Trough during the Miocene–Pliocene helping to exceed the capacity of the partially damaged top seal. Alternatively they suggested that the trap-bounding fault may have first leaked the original palaeo-oil column and been sufficiently resealed to allow the later gas charge to accumulate.

Evidence for vertical leakage of oil into the overburden is seen from fluorescence recorded in ditch cuttings (1976-2025m) from the shallower Eocene sandstones in the Oliver-1 well (BHP Petroleum Ltd, 1988d), so the loss of the original oil charge remains a viable alternate explanation.

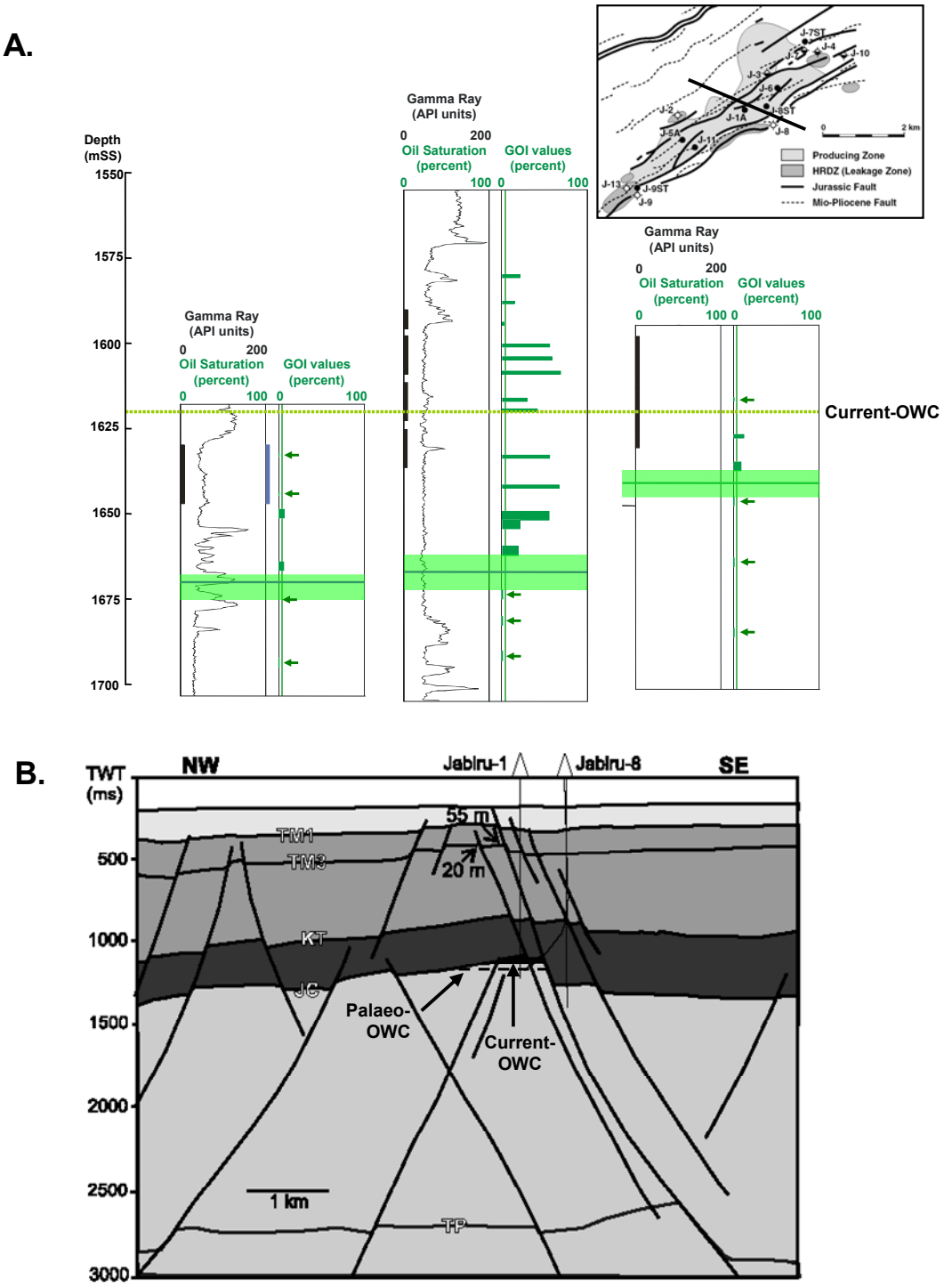

Figure 8-44: Application of the strain partitioning model to the Jabiru Field

A. GOI results from the Jabiru Field showing palaeo-oil zones (green shaded areas) below the current OWC that indicate partial breach of the field, supported by the circumferential distribution of HRDZ leakage indicators around the periphery of the field in map view (inset). **B.** In cross section (approximate line of section shown in the map) both the current and palaeo-OWCs rely on the largest fault for closure.

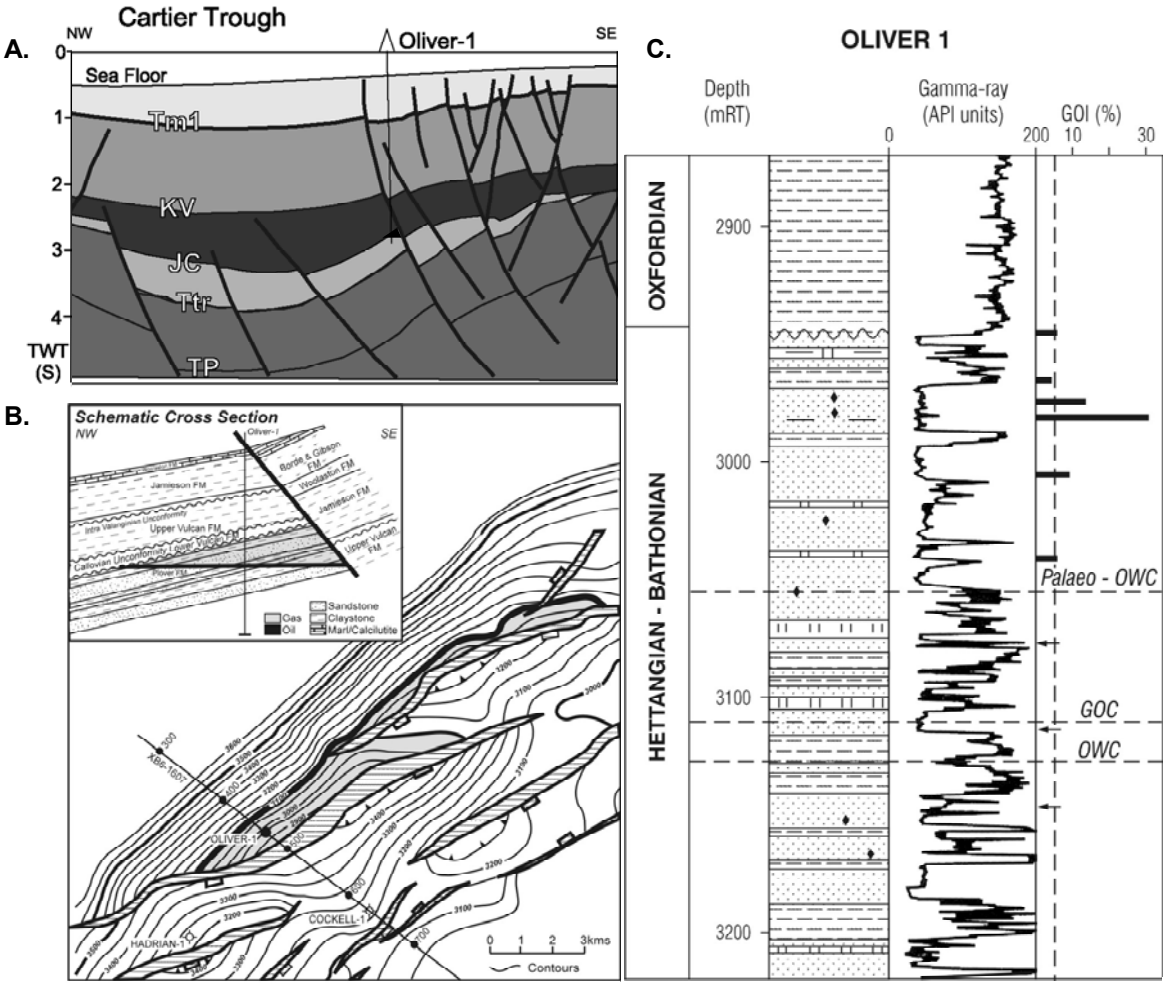

Figure 8-45: Application of the strain localisation model to the Oliver gas field.

The Oliver structure presents as a high risk trap due to the large displacement on the bounding fault that extends to seafloor (**A**) and the overlap of faults in a relay ramp setting (**B**). Despite these features the trap currently contains a thick gas column underlain by a thin oil column and shows evidence from GOI data for a substantial palaeo-oil column (**C**).

Formation temperatures for the Eocene level in Oliver-1, derived from a geothermal gradient of about 29°C/km and extrapolated from the measured bottom hole temperature assuming a 20°C sea-bed temperature, are about 75-80°C, high enough to sterilise the requisite methanogenic bacteria could be a viable explanation for the lack of an HRDZ at this level above the field.

The re-sealing of the fault zone after an initial phase of fault reactivation and associated trap breach is consistent with proposed models of the palaeo-stress field that have been described from the Skua Field (Gartrell and Lisk, 2005). As described earlier these models allow for fault reactivation and leakage under a dominantly extensional stress region at Miocene time with the current transtensional stress regime acting to reduce the intensity of reactivation. Although no fault slip inversion work has been completed over the Oliver trap the model proposed for Skua is likely to be a margin wide process across the Timor Sea region such data would provide an opportunity to assess the apparent disparity represented by the Oliver trap. Indeed such a study would be vital to properly assess the displaced oil-leg potential recognised in Lisk et al., 2002).

8.8.2.4 Combined Models

From the review of the different predictive techniques that have been applied to the VSB it is clear that none can fully explain the observational constraints provided by the current field distribution and the palaeo-charge record provided by the residual oil shows or the fluid inclusion defined palaeo-hydrocarbon columns. Each approach clearly has merit, with convincing examples available but these are plagued by an equal or greater number of exceptions. A common feature of the previous studies is a focus on different first order controls rather than to attempt to integrate all of the data to produce a rigorous model and as a consequence the success of the predictions is impaired. A number of factors contribute to this outcome, not least the scale and complexity of the solution that ultimately require regional studies of considerable breadth and magnitude. What is clear from many of the observations is that the system is a dynamic one, both temporally and spatially so the range of methods needed to define the system is likely to be varied.

On a more positive note it is clear that genuine progress in being made with more recent models (i.e. Gartrell et al., 2006) showing fewer exceptions than has been recorded for previously published predictive methods.

A thorough integration of results from the current study with the published predictive methods needed to produce an effective predictive capability is beyond the scope of the current investigation. Some general observations can be made that may help define the nature of future attempts to address the aim of developing effective predictive models in the VSB and indeed more widely.

1. Traps are more resilient to the effects of fault reactivation than previously recognised and maintain more effective seal where they have been shielded from intense modification due to the style or orientation of faults that bound the traps. Good seismic imaging these features is critical to correctly recognising the level of risk on a trap by trap basis.

2. Unique solutions probably don't exist or are limited to specific conditions. Methods that aim to probabilistically risk the likelihood of different outcomes are more likely to succeed than those that are overly deterministic.

3. Linking the structural and fluid histories is essential as somewhat paradoxically, the most robust traps rank almost as poorly as the most fragile traps due to the risk of being filled with non-economic gas. Dynamic controls on the petroleum system are clearly the least understood but probably the most important for addressing seal effectiveness risk.

4. The *in situ* conditions represent the sum of an accumulated history the individual parts that can only be resolved by considering the complex interplay between the movement of sub-surface fluids, the tectonic history and the rheological nature of the deforming sediment pile.

8.9 SUMMARY

A coupled model describing the evolution of hydrocarbon and formation waters has been produced that contributes to an improved understanding of the major petroleum system operating within the Vulcan Sub-basin. This integrated understanding can be placed within the existing tectono-stratigraphic models and serves as a significant data resource to constrain the validity of models that seek to determine regional prospectivity in a predictive sense.

At least two discrete formation water phases (W1 and W2) and three hydrocarbon phases (H1, H2, H3) are recognised within the VSB. The timing of these events can be linked to important phases in the evolution of the basin to produce a coupled fluid-flow history that directly constrains the retention risk faced by different trap types. Clastic reservoir sequences of Triassic and Jurassic age developed during successive periods of Jurassic rifting exist in numerous trapping configurations that have been regionally capped by effective seal facies within the overlying Cretaceous and Early Tertiary overburden section. Early diagenetic alteration of these fluvio-deltaic and marine sandstones appears to have been influenced by low salinity waters (W1) either as connate fluids or through the ingress of meteoric water during uplift associated with Jurassic rifting. Thermal collapse accompanied the end of rifting leading to isolation of the reservoir systems from the biosphere and an increasing dominance of waters controlled by closed system diagenesis (W2).

High heat flow persisted after rifting ceased (drift phase) and coupled with rapid sedimentation rates throughout the early post-rift phase resulted in maturation of non-marine gas-prone coaly source rocks in the thick Early Jurassic pre-rift section. These events combined to produce a pulse of early gas charge (H1) that was volumetrically unable to fill all available closure in all but the smallest structural closures. Exponential thermal decay and slowing burial rates related to the reduced accommodation space quickly quenched this early charge phase, probably limiting the volumetric output associated with H1.

The overlying oil prone source rocks that developed in the syn-rift sedimentary sequence contain highly generative Lower Jurassic source rocks, but low maturity

levels during the early post-rift phase limited generation to the Swan and Paqualin grabens and probably did not reach high enough levels to allow expulsion thresholds to be reached. Slow burial characterised the Cretaceous period and not until the middle Tertiary time did maturity levels return to sufficient levels to re-initiate oil generation. Increased subsidence related to the onset of plate margin collision near the island of New Guinea produced a rapid rise in maturity levels and a substantial liquid-rich hydrocarbon charge was produced in the Swan and Paqualin grabens. Pre-existing rift architecture in the form of en echelon orientated fault relay ramps allowed oil generated in these localised grabens to migrate long distances and as a consequence numerous oil columns accumulated in Jurassic reservoirs that had access to these syn-rift source rock facies. Only where the product of an early gas charge had previously filled available closure does oil appear to have been excluded from valid traps. Formation fluids trapped as irreducible waters by the oil charge were diagenetically modified versions of W2 that had salinity levels well above the original connate compositions and reached about 100,000ppm TDS in extreme cases.

Subsidence rates increased through the Tertiary as compression related to far field tectonic effects produced bending across the leading edge of the Australian Plate and the development of deep troughs ahead of the flexing slab. This allowed a new source kitchen to become active in the northeastern part of the VSB as the Tertiary aged Cartier Trough rapidly developed and led to late maturation of Jurassic source rocks. Initially oil was produced that migrated to fill traps across the southern edge of the developing trough but quickly gas became the dominant product as maturity levels rose sharply. Increased flexure coupled with rapid burial could no longer be accommodated by bending alone and widespread extensional failure produced an array of neoformed faults in the shallow section as well as reactivation of existing buried rift faults.

The dramatic increase in vertical permeability caused by Neogene faulting catastrophically impacted trap integrity and led to widespread trap breaching and the associated leakage of hydrocarbons from many traps. A complex interplay of multiple factors contributed to the way in which this increased strain was accommodated and together with the evolving stress field produced different responses for different trap configurations. The most heavily reactivated traps

typically failed completely being unable to deal with the magnitude of the event. The least reactivated traps may have been the most robust in terms of hydrocarbon retention but these quickly filled with gas from the now highly mature source rocks resulting in uneconomic gas accumulations. Traps with intermediate levels of fault reactivation were also compromised and many of these lost significant amounts of their initial hydrocarbon fill. However unlike the traps that experienced massive tectonic adjustment a combination of reduced column height due to partial leakage, preferential loss of gas and geometric considerations related to differential accommodation of strain resulted in a more dynamic response to these events. A proportion of these traps were able to retain partial hydrocarbon fill that was dominated by oil fill rather than gas.

An associated consequence of fault reactivation was the introduction of high saline formation waters (W3) with salinity levels in excess of 200,000 ppm. These brines thought to be derived from the release of deep overpressured fluid cells through fault reactivation or less commonly through the localised dissolution of salt diapirs that pierced through the stratigraphy. Sourced from considerable depth and probably released in a sudden pulse these fluids also carried a significant thermal anomaly that overprinted maturity levels immediately in the vicinity of the up-flow zones. Where high hydrocarbon saturation remained these fluids were denied entry and are restricted in their distribution to samples from residual or water-leg locations. Highly reactive in a thermal and compositional sense these fluids probably helped to maintain fault zone permeability and in combination with the inhibition of fault healing due to oil staining could have allowed extended periods of hydrocarbon leakage to occur.

Maturation levels in all key source kitchens continued to rise and in all cases hydrocarbon charge became dominated by gas (H3). However, unlike the conditions that existed during the main phase of oil expulsion the fault relay ramps that initially facilitated long distance migration had become heavily segmented by faults are no longer able to provide effective connection for traps located outside the area of active generation. Instead vertical permeability exceeds lateral permeability anywhere the migration path is impeded by fault offsets and upwards leakage lowers the effectiveness of lateral migration. Leakage of hydrocarbons into the shallow section

is mostly detrimental except where remigration into viable reservoir-seal couplets enables new accumulations to form, principally within the Cretaceous sandstones of the Puffin Sandstone.

Rapid subsidence invoked by compressional flexure of the plate margin continued unabated but increasingly the crustal shortening that accompanied the blocking of subduction zones to the north by buoyant Australian continental crust led to a sharp increase in the component of horizontal stress. These stress level inflated beyond the vertical stress component and assumed the role of the maximum stress leading to a change in the style of deformation from purely extensional to increasingly strike-slip. This introduced a further control on trap integrity with areas of transtension continuing to promote shallow leakage but areas of transpression associated with the restraining rather than releasing bends acting to prevent further leakage. The net effect of these two processes appears to have been a gradual improvement in trap integrity with time that in some cases traps regained sufficient capacity to trap the products of late stage expulsion.

Overall, however the petroleum system that operated in the VSB was irrevocably altered by the Neogene fault episode and represents only a remnant of its former self, with the majority of the original hydrocarbon fill lost into the water column or left as residual oil in predominantly water-saturated rocks.

The increasing knowledge that has been gained from a detailed examination of the processes that have controlled fault breach has enabled significant progress to be made in successfully predicting in a pre-drill sense the likely integrity of different trap styles. Too often, however, these methods have focused on one aspect as the first order control, whereas in reality the combination of factors is probably more significant than any one part. Integrated methods that consider the interplay between the key processes offer more potential to improve these predictions into the future.

9. CONCLUSIONS AND RECOMMENDATIONS

The regional breadth of the current investigation coupled with the application of new or improved techniques that produce novel types of information have delivered new insights into the evolution of hydrocarbon and pore water systems both in the Vulcan Sub-basin, regionally across the northern margin of Australia and more widely across sedimentary basins in general. Conclusions drawn from this work can be broadly divided into two principal categories, firstly those that relate to the techniques used in acquiring the data and secondly the impact of the data collected on the understanding of the petroleum geology of the Vulcan Sub-basin.

9.1 IMPROVEMENTS IN FLUID INCLUSION METHODOLOGY

The current study is the largest regional application of the Grains with Oil Inclusions (GOI) method to detect oil migration pathways and to evaluate the level of palaeo-oil saturation for more than 70 wells from across the Vulcan Sub-basin. The results demonstrate substantial variations in GOI values that can be attributed to changes in the level of oil saturation, where zones of continuously elevated GOI numbers are followed by zones of consistently low values. These sharp changes in GOI numbers occur where a transition to lower oil saturation is implied in response to the crossing of a palaeo-water or palaeo-gas contact. The data collected on samples from the discovered fields have provided a substantial contribution to the database of oil fields used to constrain the magnitude of response in circumstances where the oil saturation is demonstrably high. As a developing technique these data have provided a valuable contribution to enable confident application of the GOI technique to water wet or gas saturated reservoirs, where the level of oil saturation is uncertain. For the first time a calibration dataset has been compiled to demonstrate the reproducibility of the GOI analysis method by repeated analyses of the same sample with an extended time period between individual analyses. These results indicate that reliable measurements can be made where careful adherence to analytical protocols is followed with individual measurements repeatable to at least ±20% of the original GOI number (i.e. GOI number = 10%±2) across a range of GOI values.

The current study has pioneered the collection of GOI data on multiple wells from the same trap to demonstrate the consistent position of the palaeo-fluid contacts, an observation critical to demonstrating that these sharp reductions reflect genuine changes in the level of palaeo-oil saturation. Coupling the fluid history more directly with the trap configuration enables the role of the structural history in controlling the position of critical spill-points to be examined. This approach gives an enhanced and unique insight into the charge history of individual traps and allows a better appreciation of regional events controlling the observed fluid distribution.

Aside from the application of the GOI technique a comprehensive dataset of conventional fluid inclusion thermometric measurements have also been collected, representing one of the largest and most regionally extensive publically available data-sets obtained by a single study. Unlike most other published studies involving the diagenetic realm the collection of both homogenisation temperatures to constrain the temperature of entrapment and ice melting temperatures to derive the salinity of associated formation waters has yielded important insights into the fluid history of the basin. Sampling across a range of current hydrocarbon zones and underlying water zones has enabled the hydrocarbon charge history to be coupled with the evolution of formation water to reveal important insights into the geological evolution of the basin. A different path of interpretation has been taken to estimate temperatures of inclusion entrapment that recognises the important role that fully methane saturated formation water plays in controlling the trapping of discrete water and gas phases. An interpretation that recognises the minimum recorded temperatures as the sole valid temperature where heterogeneous trapping is implied rather than using mean values has produced a more regionally consistent constraint on the absolute timing of inclusion formation. To ascertain the reliability of the measured minimum temperature geostatistical methods have been applied to assess the probability that a true minimum homogenisation temperature has been measured that further enhances the this type of interpretation procedure.

9.2 GEOLOGICAL APPLICATION TO THE VULCAN SUB-BASIN

The Vulcan Sub-basin has provided an ideal natural laboratory for the current study. The key characteristics that usually define an excellent petroleum system are available, yet the system has failed to deliver the anticipated success. Good quality clastic reservoirs are capped by effective, regionally extensive, seal rocks, with source rocks that are organically rich and mature enough to allow expulsion of hydrocarbons directly into these reservoirs. Migration pathways, often utilising structural ramps related to the rift architecture demonstrably focus hydrocarbon flow over long distances allowing traps far removed from the area of the active source pod to accumulate hydrocarbon columns of significant size. In spite of these favourable conditions the true potential of the region has been irrevocably diminished by late stage fault reactivation that has adversely compromised the retention capacity of the major hydrocarbon-bearing structures.

Combining conventional data types derived during normal drilling practices with unique information provided by the various fluid inclusion methods employed in this study has dramatically widened the footprint of investigation. An understanding of the petroleum systems that have operated in this region through time is achieved that is more fully constrained than would be possible using either approach independently. The information derived from application of the fluid inclusion methods employed in this study have enabled detailed fluid histories to be determined for individual traps that collectively combine to define a coupled hydrocarbon-formation water model for the Vulcan Sub-basin. This model recognises five discrete fluid phases, including three discernible hydrocarbon phases (H1 to H3) and at least two flow events involving different types of formation water (W1 and W2). These different fluid events can be readily linked to the key geological events that have defined the basin history and serve to illustrate the close association shared by the structural and fluid histories.

9.2.1 Pre-hydrocarbon Phase (WI)

The products of early diagenetic processes reflect the original depositional environments of the large Jurassic Plover delta ranging from non-marine fluvial

systems of the Early Jurassic, the increasingly marine conditions prevalent towards the Upper Jurassic that were offset by fresh water ingress associated with sub-aerial emergence driven by rift-related footwall uplift and erosion. Dispersed glauconite and pyrite cement attest to the marine incursions across the delta plain that are clearly recorded by zones of intense bioturbation seen in cores from the Jurassic reservoir sections. Fully marine conditions prevailed across much of the basin by the end of the Jurassic yet indications from stable isotope compositions of early carbonate cements and later authigenic kaolinite clay suggest meteoric waters continued to be involved. Post-rift thermal collapse led to wide-spread transgression, blanketing the basin with shales that would provide the top seals to the horst and rotated fault blocks that constitute the principal hydrocarbon trap types.

9.2.2 Initial Hydrocarbon Charge (H1, H2)

The first of three discernible phases of hydrocarbons represents an early gas charge (H1) that appears to be widespread in the basin. A combination of rapid post rift burial and high basin heat flows associated with recently completed rifting produced a gas-rich charge, probably derived from gas-prone coals in the more deeply buried Lower Jurassic section of the Plover Formation. Clear examples of this phase are seen as current gas-fill in traps like those tested by Pengana-1 and Delamere-1, whilst current gas caps seen in traps like Skua and inferred from the fluid inclusion results recorded in the Challis field and dry holes such as East Swan-2 could also be examples of this early gas charge. The impact of the early gas charge is not particularly significant and the small column heights probably reflect a limited volumetric contribution from source rocks that barely reached maturity levels needed to promote expulsion. Early gas charge may have been deleterious to regional prospectivity by filling traps that would have been well positioned to receive later oil charge and making them uneconomic due to the small gas volumes.

Falling heat flow levels and waning sedimentation during the passive margin drift phase produced a net decrease in formation temperatures that effectively quenched the early phase of hydrocarbon generation and delayed a return to active generation until the Mid-Tertiary when burial rates increased due to far-field effects related to early collision of the Australian Plate at New Guinea Island. Higher maturity levels,

extending up to the more oil-prone source rocks in the Upper Jurassic section produced a regionally extensive oil charge (H2) that produced numerous, volumetrically significant, oil columns. Charge rates to structurally valid traps were high with at least one in every three traps examined in this study showing evidence of oil accumulation. Oil charge from Eocene time can be inferred from the fluid inclusion palaeotemperature results, which have been integrated with basic thermal models to produce this absolute timing constraint. This prediction agrees well with subsidence curves, which show a period of increased subsidence in the Paleocene that is likely to have increased maturity levels and promoted extensive oil generation. On the basis of these results an effective petroleum system can be demonstrated to have been produced by the middle Tertiary. This outcome equates very well with the fulfillment of the potential that the Plover-Vulcan (!) petroleum system clearly had based on the quality of its constituent parts.

9.2.3 Post Charge Modifications (W2, H1, H2)

A series of significant events have occurred since initial hydrocarbon charge, in many instances severely compromising the retention aspects of this petroleum system. Initially traps were modified by regional tilting, driven by widespread Tertiary carbonate progradation, causing a change in the position of spill-points and a redistribution of oil and gas. Modification to spill-points after initial oil charge is clearly apparent in the Skua Field where the original OWC is inclined, and is attributed to establishment of northwesterly tilting in the Late Tertiary. High angle fault intersections appear to have played a key role in controlling the fill history of some traps, acting as long-lived conduits for hydrocarbon leakage and could represent a more widespread issue than has previously been recognised. However, fault reactivation caused by oblique collision of the Australian Plate and the S.E. Asian Plate in the Neogene has had the most significant effect on trap integrity, producing reactivation of deeper rift fault systems, and the formation of extensive arrays of shallow Mio-Pliocene faults. Evolution of the stress field may have played a key role in controlling the style of fault reactivation, initially sharply increased burial rates caused by flexure along the plate margin led to purely extensional failure, but as collision preceded the increased horizontal stresses caused $\sigma 1$ to flip from vertical to horizontal leading to a change in reactivation style to more oblique-slip

deformation in a transtensional stress field. Collectively, the fault reactivation led to a dramatic increase in net-vertical structural permeability causing the breaching of hydrocarbon traps and the attendant leakage of oil and gas. Fluid inclusion results from thirteen hydrocarbon discoveries and evaluation of thirty-five plugged and abandoned wells using the GOI technique have revealed the presence of numerous palaeo-oil columns. The main oil fields in the region had significantly different palaeo-Oil Water Contacts (OWC) to those observed at the current day, with volumes of palaeo-oil in place as much as twice that presently reservoired. This information in essence represents a base map of charge history in the Vulcan Sub-basin that offers an opportunity to test the applicability of models proposed to predict the retention of hydrocarbons. The data in this study are integral to refining the predictive aspects of these models by clearly defining the charge history of different trap types. The rigorous integration of these data into numerical models of fault reactivation that describe the complex interplay between stress, fluid-flow and regional tectonics will contribute to a better understand the mechanisms controlling fault breach in this region.

This increase in structural permeability also facilitated another major regional fluid-flow event, with fluid inclusion palaeo-salinity data highlighting vertical, cross formation, transfer of highly saline brine. These pore waters, with maximum salinities in excess of 200,000 ppm, record the migration of high-salinity brines through sandstones in the Mesozoic and Tertiary sequences. Fault controlled injection of brine from bedded salt at depths of up to 10 km is considered to be the main source for brine migration. Salt diapirs may have contributed some of this hypersaline fluid, but these are too geographically restricted to reconcile the widespread distribution of these brines. The absence of these hyper-saline fluids in samples taken from intact hydrocarbon columns, places a significant temporal constraint on the timing of brine flow, suggesting that flow must have occurred subsequent to hydrocarbon charge. Further, the presence of high salinities in samples from recognised residual oil zones suggests that breaching of these traps facilitated the ingress of high-salinity brines, with brines providing a marker for fault reactivation. Numerical simulations, utilised to test this hypothesis, produce outcomes, which broadly match the observed vertical distribution of samples with high salinity fluid inclusions. The other major impact of brine flow from more deeply

buried Palaeozoic strata is the apparent convective overprint this fluid-flow event imparts on the conductive thermal background. This is not represented by the current geothermal conditions, as these events are palaeo- rather than contemporary in nature. However, thermal maturity data, recording accumulated thermal stress, does support localised heating of sediments located immediately adjacent to faults that bound breached oil columns. Inadvertent use of these anomalous maturity data as inputs to an appraisal of regional hydrocarbon generation based on conductive hear transfer could lead to spurious conclusions if the restricted spatial extent of these convective effects is not recognised.

9.2.4 Late Gas Charge (H3)

Flushing of traps by late gas (H3) occured throughout the Vulcan Sub-basin due to rapid subsidence caused by lithospheric flexure of the margin during Neogene plate collision. Many currently gas-bearing reservoirs previously contained oil columns and considerable potential exists in the Swan and Oliver fields for down-dip or displaced oil legs respectively. Detailed volumetric calculations based on the position of palaeo-OWCs derived from the GOI data allow volumes of initial oil in place to be determined, thus providing constraint on the size of any remigrated oil charge. Differentiation of this late charge (H3) from the early gas charge (H1), however, is important to avoid spurious prediction of displaced oil legs. This can be achieved by a combination of fluid inclusion (GOI) and conventional geochemical appraisal to confirm prior oil accumulation.

Another aspect of continuing hydrocarbon charge is the potential for previously breached traps or the new traps that have been created by the fault reactivation to trap these late stage charge products. The observed slow down in the frequency of fault reactivation that can be seen on seismic data and from sea-bed imaging that show a lack of faults offsetting the sea-floor points to a system that may be regaining improved trap integrity. Integration of these observations with stress field modelling offer a potential mechanism with which to explain these observations and the generally subdued nature of the contemporary seepage patterns.

9.3 RECOMMENDED FUTURE WORK

The ideas presented in this study, as with all geological investigations, represent a progress report. As future work is undertaken, the models developed for this region will be modified and hopefully improved. The work represents a data resource, which will contribute to other research programs and indeed the true practitioners, the explorers, by providing a set of hard data to validate current and future predictive models. These models are the critical element that will determine the future prospectivity of the region, but they will also provide concepts and methods that can be readily exported to other basins, particularly those at an earlier stage in the exploration cycle. Describing the trap integrity problem that faces the Vulcan Sub-basin represents an important piece of a highly complex puzzle, but truly effective predictions are yet to be achieved. Learning how to mitigate the key risks and more effectively predict the outcome of new drilling is always the ultimate aim, however elusive the goal. Specifically the following challenges need to be completed:

1. Greater integration of these data with the plethora of predictive methods already available to produce truly coupled tectono-fluid models that address both the cause and the effect.

2. Progress towards the development of more robust numerical models that truly couple the fluid-flow and tectonic elements of the system.

3. Development of new play concepts that target the massive volume of remigrated hydrocarbons, a proportion of which is likely to lie in shallow reservoirs that have not been fully explored.

Overall the significant advances that have been made in the quality of seismic imaging coupled with the great progress those complimentary studies addressing the trap integrity have achieved augers well for future exploration success in the Vulcan Sub-basin. Future discoveries will be smaller and more difficult to detect, but the frequency of these discoveries is likely to be increased as the controls on the system as a whole are more clearly understood.

10.REFERENCES

Aarssen, B.G.K. van, Alexander, R. and Kagi, R.I., 1996, The origin of Barrow Sub-Basin crude oils: A geochemical correlation using land-plant biomarkers, The APPEA Journal, 36 (1), 465-476.

Aarssen, B.G.K. van, Bastow, T.P., Alexander, R. and Kagi, R.I., 1999, Age determination of crude oils in the Barrow Sub-basin using palaeoclimate related variations in higher plant biomarkers. The APPEA Journal, 39(1), 399–406.

Abrams, M.A., 1992. Geophysical and geochemical evidence for subsurface hydrocarbon leakage in the Bering Sea, Alaska. Marine and Petroleum Geology Bulletin 9, 208–221.

Abrams, M.A., 1996. Distribution of subsurface hydrocarbon seepage in near-surface marine sediments. In: Schumacher, D., Abrams, M.A. (Eds.), Hydrocarbon Migration and its Near-Surface Expression, vol. 66. AAPG Memoir, pp. 1–14.

Abrams, M. A. and Segall, M. P., 2001. Best practices for detecting, Identifying and Characterizing Near-Surface Migration of Hydrocarbons within Marine Sediments. Offshore Technology Conference in Houston, Texas.

Aase, N. E., Bjorkum, P. A. and Nadeau, P. H., 1996, The effect of grain-coating microquartz on preservation of reservoir porosity, AAPG Bulletin, 80, 1654–1673.

AGSO North West Shelf Study Group, 1994, Deep Reflections on the North West Shelf: Changing Perceptions of Basin Formation, in Purcell, P.G. and Purcell, R.R., (Eds), 1994, The Sedimentary Basins of Western Australia: Proceedings of the Petroleum Exploration Society of Australia, Perth, 1994, 63-76.

Ajdukiewicz, J. M. and Lander, R. H., 2010, Sandstone reservoir quality prediction: The state of the art, AAPG Bulletin, 94, 1083-1091.

Al-Aasm, I.S., Scotchman, I.C. and Verweij, J. (eds) 2002. Marine and Petroleum Geology 19 (3). Thematic set on Origins, characterization and significance of fluids in sedimentary basins, 207-388.

Alexander, R., Larcher, A.V., Kagi, R.I. and Price, P.l., 1988, The use of plant derived biomarkers for correlation of oils with source rocks in the Cooper/Eromanga Basin System, Australia, The APPEA Journal 28(1), 310-324.

Allan, U. S., 1989, Model for hydrocarbon migration and entrapment within faulted structures. APPG Bulletin, v. 73, p. 803-811.

Allen, P.A., and Allen, J.R., 1990, Basin Analysis, Principles and Applications, Blackwell Science, Oxford, U.K., 451 p.

Allen, D., Flaum, C., Ramakrishnan, T., Bedford, J., Castelijns, K, Fairhurst, D., Gubelin, G., Heaton, N., Minh, C., Norville, M., Seim, M., Pritchard, T. and Ramamoorthy, R., 2000, Trends in NMR logging, Oilfield Review (2000), 2–20 Autumn.

Ambrose, G.J., 2004, Jurassic sedimentation in the Bonaparte and northern Browse basins: new models for reservoir-source rock development, hydrocarbon charge and entrapment. In: Ellis, G.K., Baillie, P.W. and Munson, T.J. (editors), Timor Sea Petroleum Geoscience, Proceedings of the Timor Sea Symposium, Darwin, 19-20 June 2003. Northern Territory Geological Survey, Special Publication 1, 125-142.

Aplin, A. C., Mcleod, G., Larter, S. R., Pedersen, K. S., Sorensen, H., and Booth, T., 1999, Combined use of confocal laser microscopy and PVT simulation for estimating the composition and physical properties of petroleum in fluid inclusions. Marine and Petroleum Geology, 16, 97–110.

Arco Australia Ltd., 1972, Osprey-1 well completion report (unpublished).

Arco Australia Ltd., 1973, Swan-1 well completion report (unpublished).

Arntsen, B., Wensaas, L., Løseth, H., and Hermanrud, C., 2007, Seismic modeling of gas chimneys, Geophysics, 72 (5), 251-259.

Arribas, A., Mas, R., Arribas, M.E., Ochoa, M., González, L., 2007, Sandstone petrofacies in the Northwestern sector of the Iberian Basin. Journal of Iberian Geology, 33(2), 191-206.

Audley-Charles, M.G., Ballantyne P.D. and Hall R., 1988, Mesozoic-Cenozoic rift-drift sequence of Asian fragments from Gondwanaland, Tectonophysics 155, 317-330.

Avseth, P., Mukerji, T and Mavko, G., 2005, Quantitative seismic interpretation, applying rock physics tools to reduce interpretation risk, Cambridge University Press, 359p.

Baillie, P.W., Powell, C.McA., Li, Z.X. and Ryall, A.M., 1994, The tectonic framework of Western Australia's Neoproterozoic to Recent Sedimentary Basins, in Purcell, P.G. and Purcell, R.R., (Eds), The Sedimentary Basins of Western Australia: Proceedings of the Petroleum Exploration Society of Australia, Perth, 1994, 45-62.

Baker, J. C., 2000, Petrology of Puffin-5 samples, unpublished report to AED International.

Baker Hughes INTEQ, 1993, Wellsite Geology, Reference Guide.

Bao, J., 1997, 25-norhopane series in the unbiodegraded oil and the source rocks Chinese Science Bulletin, 42 (16), 1388-91.

Ban, S. and Pitt, G., 2006, The Ichthys giant gas-condensate field. 2006 AAPG International Conference and Exhibition, 5-8 November, Perth, Australia, Abstract.

Barclay, S. A., Worden, R. H., Parnell, J., Hall, D. L. and Sterner, S. M., 2000. Assessment of Fluid Contacts and Compartmentalization in Sandstone Reservoirs Using Fluid Inclusions: An Example from the Magnus Oil Field, North Sea. AAPG Bulletin, 84, p. 489 – 504.

Barker, C. and Smith, M.P., 1986. Mass spectrometric determination of gases in individual fluid inclusions in natural minerals. Anal. Chem. 58, 1330–1333.

Barres, O., Burneau, A., Dubessy, J., and Pagel, M., 1987, Application of Micro-FT-IR Spectroscopy to Individual Hydrocarbon Fluid Inclusion Analysis. Applied Spectroscopy, 41 (6), 933-1082.

Barrett, A.G., Hinde, A.L. and Kennard, J.M., 2004, Undiscovered resource assessment methodologies and application to the Bonaparte Basin. In: Ellis, G.K., Baillie, P.W. and Munson, T.J. (editors), Timor Sea Petroleum Geoscience, Proceedings of the Timor Sea Symposium, Darwin, 19-20 June 2003. Northern Territory Geological Survey, Special Publication 1, 353-372.

Barton, C. A., M. D. Zoback, and D. Moos, 1995, Fluid flow along potentially active faults in crystalline rock: Geology, v. 23, p. 683–686.

Baxter, K., 1996, Flexural isostatic modelling. In: Colwell, J.B. and Kennard, J.M., Petrel Sub-basin study 1995-1996, Australian Geological Survey Organisation Record 1996/40, 68-77.

Baxter, K., Cooper, G.T., O'Brien, G.W., Hill, K.C. and Sturrock, S., 1997, Flexural isostatic modelling as a constraint on basin evolution, the development of sediment systems and palaeo-heat flow: application to the Vulcan Sub-basin, Timor Sea. APPEA Journal 37 (1), 136-53.

Baxter, K., Hill, K.C. and Cooper, G.T., 1998, Qualitative modelling of the Jurassic-Holocene subsidence history of the Vulcan Sub-basin, North West Shelf: constraints on lithosphere evolution during continental breakup. Australian Journal of Earth Sciences 45, 143-54.

Baxter, K., Cooper, G.T., Hill, K.C. and O'Brien, G.W., 1999, Late Jurassic subsidence and passive margin evolution in the Vulcan Sub-basin, north-west Australia: constraints from basin modelling. Basin Research, 11, 97–111.

Beardsmore, G.R. and Cull, J.P., 2001, Crustal heat flow: A guide to measurement and modelling. Cambridge University Press. 321pp.

Bekele, E.B., Lisk, M. and Otto, M., 2001, Palaeo-fluid flow along reactivated faults in the Vulcan Sub-basin, Timor Sea, CSIRO Land and Water Technical Report 2/01, 33p.

Bennion, D.B. Thomas, F.B. and Ma, T., 2001, Determination of Initial Fluid Saturations Using Traced Drilling Media, Journal of Canadian Petroleum Technology, 40 (1), 31-37.

Berner, R. A., 1984, Sedimentary pyrite formation: an update, Geochimica et Cosmochimica Acta 48, 605-615.
Bethke, C.M. 1985. A numerical model of compaction-driven groundwater flow and heat transfer and its application to the palaeohydrology of intracratonic sedimentary basins. Journal of Geophysical Research 90, B8, 6817-6828.
Bethke, C.M. 1986. Hydrologic constraints on the genesis of the Upper Mississippi Valley mineral district from Illinois basin brines. Economic Geology, 81, 233-249.
BHP Petroleum Ltd., 1983a, Jabiru-1A well completion report (unpublished).
BHP Petroleum Ltd., 1983b, Jabiru-2 well completion report (unpublished).
BHP Petroleum Ltd., 1984a, Jabiru-3 well completion report (unpublished).
BHP Petroleum Ltd., 1984b, Swift-1 well completion report (unpublished).
BHP Petroleum Ltd., 1984c, Eclipse-1 well completion report (unpublished).
BHP Petroleum Ltd., 1985, Challis-1 well completion report (unpublished).
BHP Petroleum Ltd., 1986, Eclipse-2 well completion report (unpublished).
BHP Petroleum Ltd., 1988a, Skua-3 well completion report (unpublished).
BHP Petroleum Ltd., 1988b, Skua-4 well completion report (unpublished).
BHP Petroleum Ltd., 1988c, Cassini-1ST well completion report (unpublished).
BHP Petroleum Ltd, 1988d, Oliver-1 well completion report, unpublished.
BHP Petroleum Ltd., 1988e, Bilyara-1 well completion report (unpublished).
BHP Petroleum Ltd., 1988f, Montara-1 well completion report (unpublished).
BHP Petroleum Ltd., 1988g, Pengana-1 well completion report (unpublished).
BHP Petroleum Ltd., 1988h, Parry-1 well completion report (unpublished).
BHP Petroleum Ltd., 1989a, Skua-6 well completion report (unpublished).
BHP Petroleum Ltd., 1989b, Cassini-2 well completion report (unpublished).
BHP Petroleum Ltd., 1989c, East Swan-2 well completion report (unpublished).
BHP Petroleum Ltd., 1989d, Paqualin-1 well completion report (unpublished).
BHP Petroleum Ltd., 1991, Tahbilk-1 well completion report (unpublished).
BHP Petroleum Ltd., 1992, Swan 3ST-1 well completion report (unpublished).
BHP Petroleum Ltd., 1994, Elm-1 well completion report (unpublished).
BHP Petroleum Ltd., 1995, Pituri-1 well completion report (unpublished).
Bhullar, A.G., Karlsen, D.A., LaCharpagne, J.C., and Holm, K., 1999, Reservoir screening using Iatroscan TLC-FID and identification of palaeo-oil zones, oil–water contacts, tar-mats and residual oil saturations in the Frøy and Rind petroleum accumulations. Journal of Petroleum Science and Engineering, 23 (1), p. 41-63.
Bint A.N., Fischer, M.W. and Oldham, A.C., 1998, 1998–1997 exploration review – the momentum builds. APPEA Journal 38 (2), 106-16.
Bishop, D.J. and O'Brien, 1998, A multi-disciplinary approach to definition and characterisation of carbonate shoals, shallow gas accumulations and related complex near surface sedimentary structures in the Timor Sea. APPEA Journal 38 (1), 93-114.
Bjørlykke, K., 1984, Formation of secondary porosity: How important is it? In: D. A. MacDonald and R. C. Surdam (Eds.), Clastic diagenesis, AAPG Memoir 37, 277–286.
Blamey, N.J.F. and Ryder A.G., 2007, Hydrocarbon Fluid Inclusion Fluorescence: A review, Reviews in Fluorescence 2007, Annual Volumes, 4, 299-334.
Blanc, Ph. and Connan, J., 1992, Origin and occurrence of 25-norhopanes: a statistical study, Organic Geochemistry 18 (6), 813-828.
Blevin, J.E., Struckmeyer, H.I.M., Cathro, D.L., Totterdell, J.M., Boreham, C.J., Romine, K.K., Loutit, T.S. and Sayers, J., 1998a, Tectonostratigraphic framework and petroleum systems of the Browse Basin, North West Shelf. In: Purcell, P.G. and R.R. (eds), The Sedimentary Basins of Western Australia 2: Proceedings of Petroleum Exploration Society of Australia Symposium, Perth, WA, 1998, 396-95.
Blevin, J.E., Boreham, C.J., Summons, R.E., Struckmeyer, H.I.M. and Loutit, T.S., 1998b, An effective Lower Cretaceous petroleum system on the North West Shelf: evidence from the Browse Basin. In: Purcell, P.G. and Purcell, R.R. (editors), The Sedimentary Basins of Western Australia 2: Proceedings of the Petroleum Exploration Society of Australia Symposium, Perth, 1998, 397-420.

Bloch S., 1991, Empirical prediction of porosity and permeability in sandstones, AAPG Bull. 75, 1145-1160.
Bloch, S., and Helmold, K. P., 1995, Approaches to predicting reservoir quality in sandstones, AAPG Bulletin, 79(1), 97-115.
Bloch, S., R. H. Lander, and L. M. Bonnell, 2002, Anomalously high porosity and permeability in deeply buried sandstone reservoirs: Origin and predictability, AAPG Bulletin, 86, 301–328.
Bodnar, R. J., 2003, Re-equilibration of fluid inclusions. In: Samson, I., Anderson, A. and Marshall, D., eds., Fluid Inclusions: Analysis and Interpretation. Mineral. Assoc. Canada, Short Course 32, 213-230.
Bodnar, R.J., Binns, P.R. and Hall, D.L., 1989, Synthetic fluid inclusions, VI., Quantitative evaluation of the decrepitation behavior of fluid inclusions in quartz at one atmosphere confining pressure. Journal of Metamorphic Geology, 7, 229-242.
Bodnar, R. J. and Binns, P.R., 1986, Decrepitation behaviour of fluid inclusions in quartz at one atmosphere confining pressure, [abs]: Am. Geophys. Union Trans., 67, 399.
Boetius, A., K. Ravenschlag, C. Schubert, D. Rickert, F. Widdel, A. Gieseke, R. Amann, B., Jørgensen, B., Witte, U., and Pfannkuche, O., 2000, A marine microbial consortium apparently mediating anaerobic oxidation of methane. Nature, 407, 623–626.
Bone, Y., 1990, Palaeotemperature analysis Timor Sea, Northern Australia. Report to BHP Petroleum Ltd., unpublished.
Bourne, J. D. and Faehrmann, P.A. 1991. The Talbot Oilfield, Vulcan Sub-basin: A Triassic Oil Discovery, APEA Journal, 31, 42-54.
Bradley, D. C. and Kidd, W.S.F., 1991, Flexural extension of the upper continental crust in collisional foredeeps, GSA Bulletin 103 (11), 1416-1438.
Bradshaw, M.T., Yeates, A.N., Beynon, R.M., Brakel, A.T., Langford, R.P., Totterdell, J.M. and Yeung, M., 1988, Palaeogeographic evolution of the North West Shelf region in Purcell, P.G. and Purcell, R.R., (Eds), The North West Shelf, Australia: Proceedings of the Petroleum Exploration Society of Australia, Perth, 1988, 29-54.
Bradshaw, M.T., Bradshaw, J., Murray, A.P., Needham, D.J., Spencer, L., Summons, R.E., Wilmot, J. and Winn, S, 1994, Petroleum systems in west Australian basins, in Purcell, P.G. and Purcell, R.R., (Eds), The Sedimentary Basins of Western Australia: Proceedings of the Petroleum Exploration Society of Australia, Perth, 1994, 93-118.
Bransden, S. J., and P. J. E. Matthews. 1992. Structural and stratigraphic evolution of the east Java Sea. Proceedings Indonesian Petroleum Association, 21st Annual Convention, 417 - 454.
Bredehoeft, J.D. and Norton D.L., 1990, Mass and energy transport in a deforming Earth's crust. In: The Role of Fluids in Crustal Processes, 27-41. Washington, DC: Natl. Acad.
Bretan, P., Yielding, G. and Jones, H., 2003, Using calibrated shale gouge ratio to estimate hydrocarbon column heights: AAPG Bulletin, 87, 397-413.
Brincat, M.P., O'Brien, G.W., Lisk, M., De Ruig, M.J., 2001. Hydrocarbon charge history of the Northern Londonderry High: Implications for trap integrity and future prospectivity. The APPEA Journal, 41 (1), 483-495.
Brincat, M.P. and Dutkiewicz, A., 1998, Fluid migration history of the Upper Vulcan A Formation of Tenacious-1 and Tenacious-1 ST, Permit AC/P17, Bonaparte Basin. CSIRO Petroleum Confidential Report for Cultus Timor Sea Ltd, unpublished.
Brooks, J.M., Kennicutt, M.C., Barnard, L.A., Denoux, G.J. and Carey, B.D., 1983. Applications of total scanning fluorescence to exploration geochemistry: Proceedings, 15th Offshore Technology Conference, Houston, Texas, 3, 393–400.
Brooks, D.M., Goody, A.K., O'Reilly, J.B. and McCarty, K.L., 1996, Bayu/Undan gas condensate discovery: Western Timor Gap zone of cooperation, Area A. The APPEA Journal, 36(1), 142–160.
Bureau of Transport and Regional Economics (BTRE), 2005. Is the world running out of oil? A review of the debate. Working Paper 61, 54p.
Burke, E. A. J., 2001, Raman microspectrometry of fluid inclusions. Lithos 55:139–158.

Burley, S.D., Mullis, J. and Matter, A., 1989, Timing diagenesis in the Tartan Reservoir (UK North Sea): constraints from combined cathodoluminescence microscopy and fluid inclusion studies, Marine and Petroleum Geology, Volume 6 (2), 98-104.

Burley, S.D. and Worden, R.H., 2003, Clastic diagenesis: recent and ancient, Reprint Series of the International Association of Sedimentologists, 4, Blackwells, Oxford.

Burruss, R.C., 1981. Hydrocarbon fluid inclusions in studies of sedimentary diagenesis In: L. S. Hollister and M. L. Crawford (Eds.). Short Course in Fluid Inclusions: Applications to Petrology, Mineral. Assoc. Can. Short Course Handbook, Vol. 6. pp. 138–156.

Burruss, R.C., 1992, Phase behaviour in petroleum-water (brine) systems applied to fluid inclusions, in proceedings, Fourth Biennial Pan-American Conference on Research on Fluid Inclusions (PACROFI IV), 116-118.

Cadman, S.J. and Temple, P.R., 2003. Bonaparte Basin, NT, WA, AC and JPDA, Australian Petroleum Accumulations Report 5, 2nd Edition, Geoscience Australia, Canberra.

Caenn, R. and Chillingar, G. V., 1996, Drilling fluids: State of the art, Journal of Petroleum Science and Engineering 14(3-4), 221-230.

Campbell, C.J. and LaHerrere, J.H., 1998. The end of cheap oil. Scientific American, 78-83.

Carruthers, D. J., 2003, Modeling of secondary petroleum migration using invasion percolation techniques, in S. Duppenbecker and R. Marzi, eds., Multidimensional basin modeling, AAPG/Datapages Discovery Series No. 7, 21–37.

Carruthers, D. and Ringrose, P., 1997, Oil-rock contact volumes during secondary oil migration, in: Hendry, J., Carey, P., Parnell, J., Ruffell, A. and Worden, R. (Eds), Geofluids II: Contributions to the second international conference on fluid evolution, migration and interaction in sedimentary basins and orogenic belts, Belfast, UK, 6-9.

Carruthers, D., Ringrose, J., 1998, Secondary oil migration: oil rock contact volumes, flow behaviour and rates, In: Parnell, J. (Ed.), Dating and Duration of Fluid Flow and Fluid Rock Interaction. Geological Society Special Publication, vol. 144, The Geological Society Publishing House, London, 205-220.

Castillo, D. A., Hillis, R. R., Asquith, K., and Fischer, M., 1998: State of Stress in the Timor Sea Area, Based on Deep Wellbore Observations and Frictional Failure Criteria: Application to Fault Trap Integrity; in the Sedimentary Basins of Western Australia 2, eds. Purcell, P. G. and Purcell, R. R. Proceedings West Australian Basins Symposium, Perth, Western Australia, 325-341.

Castillo, D.A., Bishop, D.J., Donaldson, I., Kuek, D., De Ruig, M., Trupp, M. and Shuster, M.W., 2000, Trap integrity in the Laminaria High-Nancar Trough Region, Timor Sea: Prediction of fault seal failure using well-constrained stress tensors and fault surfaces interpreted from 3D seismic. The APPEA Journal, 40(1), 151-173.

Cathles, L.M., 1981, Fluid flow and hydrothermal ore deposits. Econ. Geol. 75, 424-57.

Catlan, L., Xiaowen, I., Dullien, E.A., 1992, An experimental study of secondary migration, AAPG Bulletin 76, 638-650.

Charlton, T.R., 2000, Tertiary evolution of the eastern Indonesia collision complex, Journal of Asian Earth Sciences, 18, 603-631.

Charlton, T.R., A.J. Barber and S.T. Barkham, 1991, The structural evolution of the Timor collision complex, eastern Indonesia, Journal of Structural Geology, 13, 489-500.

Chaudhry A. U., 2003, Gas Well Testing Handbook. Elsevier Inc. USA. 2003.

Chen, G., Hill, K.C. and Hoffman, N., 2002, 3D structural analysis of hydrocarbon migration in the Vulcan Sub-basin, Timor Sea. In: Keep, M. and Moss, S.J. (editors), The Sedimentary Basins of Western Australia 3, Proceedings of the Petroleum Exploration Society of Australia Symposium, Perth, 2002, 377-388.

Chen, G., Hill, K.C., Hoffman, N. and O'Brien, G.W., 2001, 3D Palaeo-Migration Pathway Analysis: An Example from Timor Sea. In: Hill, K.C. and Bernecker, T., (eds), A refocused energy perspective for the future: Proceedings, PESA, Special Publication, 629-36.

Chiaramonte, L., Zoback, M.D., Friedmann, J. and Stamp, V., 2008, Seal integrity and feasibility of CO2 sequestration in the Teapot Dome EOR pilot: geomechanical site characterization, Environ Geol, 54, 1667-1675.

CIE (1932). Commission internationale de l'Eclairage proceedings, 1931. Cambridge University Press, Cambridge.
Citco Australia Petroleum Ltd., 1980, Swan-2 well completion report (unpublished).
Civan, F., 2007, Reservoir Formation Damage- Fundamentals, Modeling, Assessment, and Mitigation, Second Edition, Elsevier, Gulf Professional Pub., Burlington, MA, 1114p.
Clews, P., 2000, Crux-1, petrography of 15 CST samples from the interval 2657.3 - 3903.6m, unpublished report to Nippon Oil Exploration Pty. Ltd.
Cloud, P. E., Jr., 1955, Physical limits of glauconite formation: AAPG. Bull. 39, 484-492.
Coblentz, D.D., S. Zhou, R.R. Hillis, R.M. Richardson and M. Sandiford, 1998, Topography, boundary forces, and the Indo-Australian intraplate stress field, Journal of Geophysical Research, 103, 919-931.
Colwell, J.B. and Kennard, J.M., 1996, Petrel Sub-basin study 1995-1996, Australian Geological Survey Organisation Record 1996/40, 122p. Record 1996/40.
Conliffe, J., Blamey, N. F., Feely, M., Parnell, J. and Ryder, A. G., 2010, Hydrocarbon migration in the Porcupine Basin, offshore Ireland: evidence from fluid inclusion studies, Petroleum Geoscience, 16, 67-76.
Connan, J., 1984, Biodegradation of crude oils in reservoirs, in Brooke, J. and Welte, D.H. (eds), Advances in Petroleum Geochemistry Vol. 1, Academic Press, New York, 299-336.
Cooper, G. T., C. R. Barnes, J. D. Bourne, and G. J. Channon, 1998, Hydrocarbon leakage on the North West Shelf: New information from the integration of airborne laser fluorosensor (ALF) and structural data, in P. G. Purcell and R. R Purcell, eds., The sedimentary basins of Western Australia 2: Proceedings of the Petroleum Exploration Society of Australia Symposium, p. 255– 271.
Cowley, R. and O'Brien, G.W., 2000, Identification and interpretation of leaking hydrocarbons using seismic data: a comparative montage of examples from the major fields of Australia's north west shelf and Gippsland Basin, The APPEA Journal, 40 (1), 121-150.
Cowie, P. A., 1998, A healing-reloading feedback control on the growth rate of seismogenic faults: Journal of Structural Geology, 20, 1075-1087.
Cox, S. F., M. A. Knackstedt, and J. Braun, 2001, Principles of structural control on permeability and fluid flow in hydrothermal systems: Society of Economic Geologists Reviews, 14, 1–24.
Cuevas-Cubria, C. and Riwoe, D. 2006, Australian Energy: National and State Projections to 2029-30, ABARE Research Report 06.26 Prepared for the Australian Government Department of Industry, Tourism and Resources, Canberra, December.
Cultus Timor Sea ltd., 1997, Tenacious-1ST1 well completion report, unpublished.
Cultus Timor Sea ltd., 1998, Kym-1 well completion report, unpublished.
Cunningham, W. D. and Mann, P., 2007, Tectonics of strike-slip restraining and releasing bends Geological Society London, Special Publications, 290, 1-12.
Dake, L.P., 2001, Practice of Reservoir Engineering, Elsevier, 570p.
Dake, L.P., 1978, Fundamentals of Reservoir Engineering. Elsevier, 437p.
Dandekar, A.Y., 2006, Petroleum Reservoir Rock and Fluid Properties, Taylor and Frencis, 460p.
Dansgaard, W., 1964, Stable isotopes in precipitation. Tellus, 16, 436-468.
Darley, H. C. H. and Gray, G. R., 1988, Composition and properties of drilling and completion fluids, Fifth Edition, Gulf, Houston, TX, p. 630.
Dawson, D., Grice, K., Alexander, R. and Edwards, D. 2007. The effect of source and maturity on the stable isotopic compositions of individual hydrocarbons in sediments and crude oils from the Vulcan Sub-basin Timor Sea, Northern Australia. Organic Geochemistry, 38, 1015-1038.
De Boer, R., 2004, The Puffin Sandstone, Timor Sea, Australia: Anatomy of a sub-marine fan. In: Ellis, G.K., Baillie, P.W. and Munson, T.J. (eds), Timor Sea Petroleum Geoscience, Proceedings of the Timor Sea Symposium, Darwin Northern Territory,

19-20 June 2003, 373-390. Northern Territory Geological Survey, Special Publication 1.

Dembicki, H., Jr., 2009, Three common source rock evaluation errors made by geologists during prospect or play appraisals, AAPG Bulletin 93 (3), 341-356.

Dembicki, H. and Anderson, M.J., 1989, Secondary migration of oil; experiments supporting efficient movement of separate, buoyant oil phase along limited conduits, AAPG Bulletin 73 (8), 1018-1021.

Dewhurst, D. N., and Jones, R. M., 2002, Geomechanical, Microstructural, and Petrophysical Evolution in Experimentally Reactivated Cataclasites: Applications to Fault Seal Prediction, AAPG Bulletin, 86 (8), 383-1405.

Dewhurst, D.N., Boult, P.J., Jones, R.M. and Barclay, S.A., 2005, Fault healing and fault sealing in impure sandstones. In: Boult, P. and Kaldi, J. (eds). Evaluating fault and cap rock seals, AAPG Hedberg Series 2, 37–56.

Dubessy, J., Buschaert, S., Lamb, L., Pironon, J., and Thiéry, R., 2001, Methane-bearing aqueous fluid inclusions: Raman analysis, thermodynamic modelling and application to petroleum basins. Chemical Geology, 173, 193–205.

Duppenbecker S. J. and Iliffe J. E., Basin Modelling: Practice and Progress, Geological Society Special Publication, (1998).

De Ruig, M.J., Trupp, M., Bishop, D.J., Kuek, D. and Castillo, D.A., 2000, Fault architecture and the mechanics of fault reactivation in the Nancar Trough/Laminaria area of the Timor Sea, The APPEA Journal, 40 (1), 174-193.

Dutkiewicz, A., Volk, H., Ridley, J. and George, S., 2003. Biomarkers, brines, and oil in the Mesoproterozoic, Roper Superbasin, Australia, Geology, 2003; 31(11), 981-984.

Eadington, P.J., Lisk, M. and Hamilton, P.J., 1990, Fluid History Analysis of samples from Augustus-1, Douglas-1, Challis-1 and Jabiru-1A, Timor Sea, CSIRO Restricted Report 257, unpublished, 148p.

Eadington, P.J. and Hamilton, P.J., 1990, Fluid migration history and thermal history of Tithonian sandstones, Lower Swan Formation, Octavius-1 borehole, Timor Sea, CSIRO Restricted Report 188R, unpublished, 49p.

Eadington, P.J., Hamilton, P.J. and Bai, G.P., 1991a. Fluid history analysis – a new concept for prospect evaluation. APEA Journal 31 (1), 282–294.

Eadington P.J., Hamilton P.J., and Lisk, M., 1992, Fluid history investigation of sandstones in the Vulcan and Plover formations in Octavius-2. CSIRO Restricted Report 319, unpublished.

Eadington, P. J., Lisk, M. and Krieger, F. W., 1996, Identifying oil well sites, United States Patent No. 5,543,616.

Eadington, P. J. and Kempton, R., 2008. New developments in constraining models of oil generation and migration using data from fluid inclusions, APPEA Journal, 48 (1).

Edwards, D. S., Summons, R. E., Kennard, J. M., Nicoll, J., Bradshaw, M. Foster, C. B., O'Brien, G. W., and Zumberge, J. F., 1997, Geochemical Characteristics of Palaeozoic Petroleum Systems in Northwestern Australia, The APPEA Journal, 37 (1), 351-79.

Edwards, D.S., Preston, J.C., Kennard, J.M., Boreham, C.J., van Aarssen, B.G.K., Summons, R.E. and Zumberge, J.E., 2004, Geochemical characteristics of hydrocarbons from the Vulcan Sub-basin, western Bonaparte Basin, Australia. In: Ellis, G.K., Baillie, P.W. and Munson, T.J. (editors), Timor Sea Petroleum Geoscience, Proceedings of the Timor Sea Symposium, Darwin, 19-20 June 2003. Northern Territory Geological Survey, Special Publication 1, 169-201.

Edwards, H., Crosby, J., David, N, Loader, C. and Westlake, S., 2005, Australian Megasurveys – The Key To New Discoveries In Maturing Areas? The APPEA Journal, 45 (1), 407-19.

Ehrenberg, S. N., 1993, Preservation of anomalously high porosity in deeply buried sandstones by grain-coating chlorite, Examples from the Norwegian continental shelf: AAPG Bulletin, 77, 1260–1286.

England, W.A., Mackenzie, A.S., Mann, D.M. and Quigley, T.M., 1987, The movement and entrapment of petroleum fluids in the subsurface. Journal of the Geological Society of London, 144, 327–347.

England, W.A., 1993, Petroleum migration. In: Parnell, J., Ruffell, A.H., Moles, N.R. (Eds.), Geofluid'93. Contribution to an International Conference on Fluid Evolution, Migration and Interaction in Rocks. Queen's University, Belfast, 54-55.

Etgen, J., Gray, S.H. and Zhang, Y., 2009, An overview of depth imaging in exploration geophysics, Geophysics 74 (6).

Etheridge, M. A., McQueen, H., and Lambeck, K., 1991, The role of intraplate stress Tertiary (and Mesozoic) deformation of the Australian continent and its margins: a key factor in petroleum trap formation, Exploration Geophysics, 22, 123–128.

Etheridge, M.A. and O'Brien, G.W., 1994, Structural and tectonic evolution of the Western Australian margin basin system. PESA Journal, 22, 45-63.

Etiope, G., Papatheodorou, G, Christodoulou, D.P., Ferentinos, G., Sokos, E., and Favali, P., 2006, Methane and hydrogen sulfide seepage in the northwest Peloponnesus petroliferous basin (Greece): Origin and geohazard, AAPG Bulletin, 90 (5), 701–713.

Evans, B.J., Oke, B.F., Urosevic, M., Chakraborty, K., 1995, A comparison of physical model with field data over Oliver Field, Vulcan Graben, APEA Journal, 35(1), 26-43.

Folk, R.L., 1974, The petrology of sedimentary rocks: Austin, Tx, Hemphill Publishing Co., 182 p.

Forman, D.J and Wales, D.W., 1981, Geological evolution of the Canning Basin, Western Australia, Bureau of Mineral Resources, Geology and Geophysics Bulletin, 210, 91p.

Fittall A.M. and Cowley R.G. 1992. The HV11 3-D seismic survey: Skua-Swift area geology revealed. The APEA Journal, 32, 159-170.

Freedman, R. and Heaton, N., 2004, Fluid Characterization using Nuclear Magnetic Resonance Logging, Petrophysics 45, Number 3, 241–250.

Fujii, T., O'Brien, G.W., Tingate, P and Chen, G., 2004, Using 2D and 3D basin modelling to investigate controls on hydrocarbon migration and accumulation in the Vulcan Sub-basin, Timor Sea, northwestern Australia. The APPEA Journal 44(1), 93-122.

Fujii, T., 2007, Using 2D and 3D basin modelling and seismic seepage indicators to investigate controls on hydrocarbon migration and accumulation in the Vulcan Sub-basin, Timor Sea, North-western Australia. Unpublished M.Sc. Thesis, Australian School of Petroleum, 2007.

Fujisawa, G. and Mullins, O.C., 2007, Live Oil Sample Acquisition and Downhole Fluid Analysis, in Mullins, O.C., Sheu, E. Y., Hammami, A. and Marshall, A.G. (eds), Asphaltenes, Heavy Oils, and Petroleomics, Springer New York, 589-616.

Gartrell, A., M. Lisk, and J. Underschultz, 2002, Controls on trap integrity of the Skua oil field, Timor Sea, in M. Keep and S. J. Moss, eds., The sedimentary basins of Western Australia 3: Proceedings of Petroleum Exploration Society of Australia Symposium, Perth, Western Australia, 2002, p. 389–407.

Gartrell, A., Y. Zhang, M. Lisk, and D. Dewhurst, 2004, Fault intersections as critical hydrocarbon leakage zones: Numerical modeling of an example from the Timor Sea, Australia: Marine and Petroleum Geology, v. 21, 1165–1179.

Gartrell, A. P., and M. Lisk, 2005, Potential new method for palaeostress estimation by combining 3D fault restoration and fault slip inversion techniques: First test on the Skua field, Timor Sea, in P. Boult and J. K. Kaldi, eds., Evaluating fault and cap rock seals: AAPG Hedberg Series, no. 2, p. 23–36.

Gartrell, A. P., Bailey, W. R. and Brincat, M. P., 2005, Strain localisation and trap geometry as key controls on hydrocarbon preservation in the Laminaria High area: APPEA Journal (Australian Petroleum Production and Exploration Association), 45, 477–492.

Gartrell, A. P., Bailey, W. R. and Brincat, M. P., 2006, A new model for assessing trap integrity and oil preservation risks associated with post-rift fault reactivation in the Timor Sea, AAPG Bulletin, 90 (12), 1921–1944.

Gartrell, A.P., 2000, Rheological controls on extensional styles and the structural evolution of the Northern Carnarvon Basin, North West Shelf, Australia. Australian Journal of Earth Sciences 47, 231 – 244.

Garven, G. 1995, Continental-scale groundwater flow and geologic processes. Annual Review of Earth Planetary Sciences 23, 89-117.

Garven, G., 1989, A hydrogeologic model for the formation of the giant oil sands deposits of the Western Canada sedimentary basin Am. J. Sci. 289, 105-166.

Gay, A., Lopez, M., Cochonat, P. Levache´, D., Sermondadaz, G., and Seranne, M., 2006, Evidences of early to late fluid migration from an upper Miocene turbiditic channel revealed by 3D seismic coupled to geochemical sampling within seafloor pockmarks, Lower Congo Basin, Marine and Petroleum Geology, 23, 387–399.

Genrich, J.F., Bock, Y., McCaffrey, R., Calais, E., Stevens, C.W., and Subarya, C., 1996, Accretion of the southern Banda arc to the Australian plate margin determined by Global Positioning System measurements, Tectonics, 15, 288-295.

George, S.C, Volk, H., Dutkiewicz, A., Ridley, J. and Buick, R., 2008, Preservation of hydrocarbons and biomarkers in oil trapped inside fluid inclusions for >2 billion years. Geochimica et Cosmochimica Acta 72, 844–870.

George, S. C., Lisk, M., Eadington, P. J., Quezada, R. A., Krieger, F. W., Greenwood, P. F. and Wilson, M. A., 1996, Comparison of palaeo oil charges with currently reservoired hydrocarbons using the geochemistry of oil-bearing fluid inclusions. SPE paper 36980, Society of Petroleum Engineers, Asia Pacific Oil and Gas Conference, 28-31 October 1996 Adelaide, Australia, pp. 159-171.

George, S. C., Greenwood, P. F., Logan, G. A. Quezada, R. A., Pang, L. S. K., Lisk, M., Krieger, F. K. and Eadington, P. J., 1997, Comparison of palaeo-oil charges with currently reservoired hydrocarbons using molecular and isotopic analyses of oil bearing fluid inclusions, Jabiru Oilfield, The APPEA Journal, 37 (1), 490-504.

George, S.C., Lisk, M., Eadington, P.J. and Quezada, R.A., 1998, Geochemistry of a palaeo-oil column, Octavius 2, Vulcan Sub-basin. In: Purcell P.G. and R.R. (Eds), 1998, The Sedimentary Basins of Western Australia 2: Proceedings of the Petroleum Exploration Society of Australia Symposium, Perth, WA, 1998, 195–210.

George, S.C., Ruble, T.E. and Dutkiewicz, A., 2001. The use and abuse of fluorescence colours as maturity indicators of oil in inclusions from Australian petroleum systems. The APPEA Journal, 41(1), 505-522.

George, S., Volk, H., Ruble, T., Lisk, M., Ahmed, M., Liu, K., Quezada, R., Dutkiewicz, A., Brincat, M., Smart, S., Horsfield, B., 2001. Extracting oil from fluid inclusions for geochemical analyses: size matters! Abstracts of the 20th International Meeting on Organic Geochemistry, 10–14 September 2001, Nancy, France, P/TUE1/37, pp. 467–468.

George, S.C., Ruble, T.E., Dutkiewicz, A. and Eadington, P.J., 2001, Assessing the maturity of oil trapped in fluid inclusions using molecular geochemistry data and visually-determined fluorescence colours. Applied Geochemistry, 16, 451–473.

George, S. C., Lisk, M., Eadington, P. J., and Quezada, R. A., 2002, Evidence for an early, marine-sourced oil charge prior to gas-condensate migration, Bayu-1, Timor Sea. In The Sedimentary Basins of Western Australia 3, eds Keep, M. and Moss, S. J., pp. 465-474. Proceedings of the Petroleum Exploration Society of Australia Symposium, Perth, WA, 2002.

George , S. C. , Lisk, M., and Eadington, P. J., 2004a, Fluid inclusion evidence for an early, marine-sourced oil charge prior to gas-condensate migration, Bayu-1, Timor Sea, Australia. Marine and Petroleum Geology 21, 1107-1128.

George, S.C., Ahmed, M., Liu, K., Volk, H., 2004b. The analysis of oil trapped during secondary migration. Org. Geochem. 35, 1489–1511.

George, S. C., Volk, H. and Ahmed, M., 2007, Geochemical analysis techniques and geological applications of oil-bearing fluid inclusions, with some Australian case studies. Journal of Petroleum Science and Engineering, 57, 119-138.

Geoscience Australia, 2006a, Oil and Gas Resources of Australia 2004. Geoscience Australia, Canberra.

Geoscience Australia, 2006b, Release of offshore petroleum exploration areas, AC06-1 Vulcan Sub-basin, Bonaparte Basin, Territory of Ashmore and Cartier Islands.

Geoscience Australia, 2008, Explore Australia, Vulcan Sub-basin, Bonaparte Basin, Territory of Ashmore and Cartier Islands, Release Areas AC08-4, AC08-5 and AC08-6, 2008 Release of Offshore Petroleum Exploration Areas.

Giles, M. R., and Marshall, J. D., 1986, Constraints on the development of secondary porosity in the subsurface, Re-evaluation of processes, Marine and Petroleum Geology, 3, 243–255.

Girard, J.P., Munz, I. A., Johansen, H., Hill, S., and Canham, A., 2001, Conditions of quartz cementation in Brent reservoirs, Hild Field, North Sea: Constraints from fluid inclusions and SIMS oxygen isotope microanalysis. Chemical Geology, 176 (1-4), 73–92.

Gleadow, A.J.W., and Duddy, I.R., 1981, A natural long-term track annealing experiment for apatite. Nuclear Tracks, 5, 169-174.

Gleadow, A.J.W., Duddy, I.R., and Lovering, J.F., 1983, Fission Track Analysis: A New Tool for the Evaluation of Thermal Histories and Hydrocarbon Potential. APEA Journal. 23, 93-102.

Gluyas, J.G. and Hichens, H.M. (eds.) 2003, United Kingdom Oil and Gas Fields, Commemorative Millennium Volume, Geological Society of London, Memoir 20.

Goldstein, R. H., 2001, Fluid inclusions in sedimentary and diagenetic systems, Lithos, 55 (1-4), pp. 159-193.

Goldstein, R.H. and Reynolds, T.J., 1994, Systematics of fluid inclusions in diagenetic minerals. Society of economic palaeontologists and mineralogists. Short Course 31.

Gorman, I. G. D., 1990, The role of reservoir simulation in the development of the Challis and Cassini fields. The APEA Journal, 1990, 212-221.

Granli, J. R., Arnsten, B., Anders, S. and Hilde, E. 1999, Imaging through gas-filled sediments using marine shear-wave data: Geophysics, 64, 668-677.

Green, P.F., Duddy, I.R., Gleadow, A.J.W., and Lovering, J.F., 1989, Apatite Fission Track Analysis as a Paleotemperature Indicator for Hydrocarbon Exploration. In: Naeser, N.D. and McCulloh, T. (eds). Thermal History of Sedimentary Basins - Methods and Case Histories, Springer-Verlag, New York, 181-195.

Greenwood, P. F., George, S. C. and Hall, K., 1998, Applications of laser micropyrolysis-gas chromatography-mass spectrometry. Organic Geochemistry 29, 1075-1089.

Guilhaumou, N., Cordon, S., Durand, C., Sommer, F., 1998. P-T conditions of sandstones silicification from the Brent Group (Dunbar, North Sea), Eur. J. Mineral. 10, 355–366.

Gunn, P.J., 1988. Bonaparte Basin: Evolution and structural framework, in Purcell, P.G. and Purcell, R.R., (Eds), The sedimentary basins of Western Australia: Proceedings of Petroleum Exploration Society of Australia symposium, p. 275-287.

Gussow, W. C., 1954, Differential entrapment of oil and gas: A fundamental principle; AAPG Bulletin, 38 (5), 816-853.

Hagemann, H. W. and Hollerbach, A., 1985, The fluorescence behaviour of crude oils with respect to their thermal maturation and degradation. Organic Geochemistry 10, 473-80.

Hall, D.L, Sterner, S.M., and Bodnar, R.J., 1988, Freezing Point Depression of NaCl - KCl - H20 solutions. Economic Geology, 83, 197-203.

Hall, D.L., Shentwu, W., Sterner, S.M. and Wagner, P.D., 1997, Using Fluid Inclusions to Explore for Oil and Gas, Hart's Petroleum Engineer International, No. 11, p. 29-34.

Hall, R., 2002. Cenozoic geological and plate tectonic evolution of Southeast Asia and the southwest Pacific: computer-based reconstructions, models and animations. Journal of Asian Earth Sciences, 20, 353-431.

Hall, R., 1996. Reconstructing Cenozoic SE Asia. In R. Hall and D.J. Blundell (Eds.), Tectonic Evolution of Southeast Asia. Geological Society of America Special Publication 106, 153–184.

Hamilton P.J., Eadington, P.J., and Lisk, M., 1991, Fluid history analysis of Upper Vulcan Formation core from Delamere- 1. CSIRO Restricted Report 212R, unpublished, 71p.
Handin, J., 1969, On the Coulomb-Mohr Failure Criterion, Journal of Geophysical Research, 74, 5343-5348.
Handin, J., and Jaeger, R. V., 1957, Experimental deformation of sedimentary rocks under confining pressure: Tests at room temperature on dry samples, AAPG Bulletin, 41, 1–50.
Hanor, J.S., 1994, Origin of saline fluids in sedimentary basins. In: Parnell, J. (ed.) Geofluids: Origin, Migration and Evolution of Fluids in Sedimentary Basins, Geological Society Special Publication 78, 151-174.
Hanor J. S., 1994b, Physical and chemical controls on the composition of waters in sedimentary basins, Mar. Petrol. Geol., 11 (1), 31–45.
Hanor, J. S., 1980, Dissolved methane in sedimentary brines: potential effect on the PVT properties of fluid inclusions. Econ. Geol. 75, 603-617.
Hanor, J. S. 1979. The sedimentary genesis of hydrothermal fluids. In Geochemistry of Hydrothermal Ore Deposits, ed. HL Barnes, pp. 137-72. New York: Wiley. 2nd ed.
Hantschel, T and Kauerauf, A. I., 2009, Fundamentals of Basin and Petroleum Systems Modeling, Springer-Verlag, 476 p.
Haq, B. U., J. Hardenbol, and P. R. Vail, 1987, Chronology of fluctuating sea levels since the Triassic: Science, 235, 1156–1167.
Hart, G.A. and Fisher, S.J., 1998, Petroleum geochemistry of crude oil contaminated with NovaPlus. PESA Journal, 26, 40–51.
Harding, T.P., 1985. Seismic characteristics and identification of negative flower structures, positive flower structures, and positive structural inversion. American Association of Petroleum Geologists Bulletin 69 (4), 582–600.
Haszeldine, R. S. and Osborne, M., 1993, Fluid inclusions temperatures in diagenetic quartz reset by burial: implication for oil field cementation, in A. D. Horburyand A. G. Robinson, eds., Diagenesis and basin development: AAPG Studies in Geology 36, 35–46.
Heggland, R., 1998, Gas seepage as indicator of deeper prospective reservoirs: a study based on exploration 3D seismic data. Marine and Petroleum Geology, 15, 1-9.
Heggland, R., 2004, Using gas chimneys in seal integrity analysis: A discussion based on case histories, in P. Boult and J. Kaldi, eds., Evaluating fault and caprock seals, AAPG Hedberg Series, 237–245.
Heine, C. and Müller, R.D., 2005, Late Jurassic rifting along the Australian North West Shelf: margin geometry and spreading ridge configuration, Australian Journal of Earth Sciences 52, 27-39.
Hermanrud, C., Cao, S., and Lerche, I., 1990, Estimates of virgin rock temperature derived from BHT measurements: bias and error. Geophysics 55, 924-931.
Hill, K.C. and Raza, A., 1999, Arc-continent collision in Papua Guinea: Constraints from fission track thermochronology, Tectonics, 18, 950-966.
Hill, K.C. and Hall, R., 2003, Mesozoic-Cainozoic Evolution of Australia's New Guinea Margin in a West Pacific Context, GSA Special Papers 2003, 372, 265-290.
Hillis, R. R. and Williams, A. F., 1993, The stress field of the Northwest Shelf and wellbore stability, The APPEA Journal, 33 (1), 373-386.
Hillis, R.R., Mildren, S.D., Pigram, C.J. and Willoughby, D.R., 1997. Rotation of horizontal stresses in the Australian North West Continental Shelf due to the collision of the Indo-Australian and Eurasian Plates. Tectonics, 16, 323-335.
Hillis, R. R., 1998, Mechanisms of dynamic seal failure in the Timor Sea and Central North Sea basins, in P. G. Purcell and R. R. Purcell, eds., The sedimentary basins of Western Australia 2: Proceedings of the Petroleum Exploration Society of Australia Symposium, 313– 324.
Hillis, R.R. and Reynolds, S.D., 2000. The Australian Stress Map. Journal of the Geological Society, London, 157, 915-921

Hirsch, L. M. and Thompson, A. H., 1995, Minimum saturations and buoyancy in secondary migration, American Association of Petroleum Geologists Bulletin 79 (5), 676-710.
Hode, T., Zebühr Y. and Broman, C., 2006, Towards biomarker analysis of hydrocarbons trapped in individual fluid inclusions: first extraction by ErYAG laser. Planetary and Space Science 54, 1575–1583.
Horbury, A. and Robinson, A. (Eds.), 1993, Diagenesis and basin development. Am. Assoc. Petrol Geol Studies in Geology 36, 274 p.
Horner, D. R., 1951, Pressure buildup in wells: Proc. Third World Petr. Cong., The Hague, 2, 503-521.
Horsfield, B. and Mclimans, R.K., 1984, Geothermometry and geo-chemistry of aqueous and oil-bearing fluid inclusions from Fateh Field, Dubai. Organic Geochemistry, 6, 733-740.
Horsfield, B. and Rullkötter, J. 1994, Diagenesis, catagenesis, and metagenesis of organic matter, In: Magoon, L.B. and W.G. Dow (eds), The petroleum system – from source to trap. AAPG Memoir 60: The American Association of Petroleum Geologists, Tulsa, USA, 189-199.
Horstad, I., Larter, S.R., Mills, N., 1995. Migration of hydrocarbons in Tampun Spur area, Norwegian North Sea: a reservoir geochemical evaluation. In: Cubitt, J.M., England, W.A. Eds: The Geochemistry of Reservoirs. Geological Society Special Publication, 86, 159–183.
Houseknecht, D. W., 1984, Influence of grain size and temperature on intergranular pressure solution, quartz cementation, and porosity in a quartzose sandstone, Jour. Seal. Petrology, 54, 348-361.
Hovland, M., and A. Judd, 1988, Seabed pockmarks and seepages. Impact on geology, biology and the marine environment: London, Graham and Trotman, 293 p.
Hovland, M., 1990. Do carbonate reefs form due to fluid seepage? Terra Nova, 2, 8-18.
Hovland, M., Crockwer, P.F. and Martin, M., 1994, Faults-associated seabed mounds (carbonate knolls?) off western Ireland and north-west Australia, Marine and Petroleum Geology, 11, 232-246.
Hubbert, M.K., 1953, Entrapment of petroleum under hydrodynamic conditions. Am. Assoc. Petrol. Geol. Bull. 37, 1954-2026.
Ingram, G.M., Eaton, S. and Regtien, J.M.M., 2000, Cornea case study: lessons for the future, The APPEA Journal, 40(1), 56–65.
IPCC, 2007. Climate Change 2007: The Physical Science Basis. Contribution of Working Group I to the Fourth Assessment Report of the Intergovernmental Panel on Climate Change [Soloman, S., Qin, D., Manning, M., Chen, Z., Marquis, M., Avery, K.B., Tignor, M. and Miller, H.L. (eds.)]. Cambridge University Press, Cambridge, United Kingdom and New York, NY, USA, 996pp.
Isaklsen, G. H., Pottorf, R. J. and Jenssen, A. I., 1998, Correlation of fluid inclusions and reservoired oils to infer trap fill history in the South Viking Graben, North Sea, Petroleum Geoscience, 4, 41-55.
Jablonski, D. and Saitta, A.J., 2004, Permian to Lower Cretaceous Plate Tectonics and its impact on the Tectono-stratigraphic development of the Western Australian Margin, APPEA Journal 44(1), 287-327.
Jaeger, J. C., and Cook, N. G. W., 1976, Fundamentals of Rock Mechanics, John Wiley, New York, 585 pp.
Johnson, H.D. and Fisher, M.J., 1998, North Sea Plays: Geological Controls on Hydrocarbon distribution, In: Glennie, K.W., (ed), Petroleum Geology of the North Sea, basic concepts and recent advances, 4th Edition, London, Blackwell Science Ltd, 463-547.
Jones, B. G., 1988a, Petrology Analysis Report - Jabiru-10, Timor Sea, unpublished report to BHP Petroleum Ltd.
Jones, B. G., 1988b, Petrology Analysis Report - Oliver-1 well, Timor Sea, unpublished report to BHP Petroleum Ltd.
Jones, B. G., 1989a, A sedimentological and petrological appraisal of the Taltarni-1 well, Timor Sea, N.T., Australia, unpublished report to BHP Petroleum Ltd.

Jones, B. G., 1989b, Petrology Report - Cockell-1, Timor Sea, unpublished report to BHP Petroleum Ltd.

Jones, B. G., and Phillips, S.E., 1990, Petrology Report, East Swan-2, Timor Sea, unpublished report to BHP Petroleum Ltd.

Jones, R.M., D.N. Dewhurst, R.R. Hillis and S.D. Mildren, 2002, Geomechanical fault characterisation: impact on quantitative fault seal risking, SPE/ISRM paper 78213.

Jones, A.T., Logan, G.A., Kennard, J.M. and Rollet, N., 2005, Reassessing potential origins of synthetic aperture radar (SAR) slicks from the Timor Sea region of the North West Shelf on the basis of field and ancillary data. APPEA Journal, 45, 311-331.

Karlsen, D.A. and Larter S.R., 1989. A rapid correlation method for petroleum population mapping within individual petroleum reservoirs: applications to petroleum reservoir description. In: Haresnape, J. Ed., Correlation in Hydrocarbon Exploration. Graham and Trotman, London, p. 77–85.

Karlsen, D.A., and Larter, S.R., 1991. Analysis of petroleum fractions by TLC-FID: applications to petroleum reservoir description. Organic Geochemistry, 17, 603–617.

Karlsen, D.A., Nedkvitne, T., Larter, S.R., Bjørlykke, K., 1993. Hydrocarbon composition of authigenic inclusions: application to elucidation of petroleum reservoir filling history. Geochim. Cosmochim. Acta 57, 3641–3659.

Kaoru, M., Kurata, Y., Christiansen, D.J. and Scott, J., 2004, The Crux gas-condensate discovery, northern Browse Basin, Australia. In: Ellis, G.K., Baillie, P.W. and Munson, T.J. (editors), Timor Sea Petroleum Geoscience. Proceedings of the Timor Sea Symposium, Darwin, 19–20 June 2003. Northern Territory Geological Survey, Special Publication 1, 67–79.

Keene, J.B., 1988a, Petrology report, Pengana-1, Timor Sea, unpublished report to BHP Petroleum Ltd.

Keene, J.B., 1988b, Petrology analysis report, Rainier-1 well, Timor Sea, unpublished report to BHP Petroleum Ltd.

Keep, M., Powell, C. McA. and Baillie, P.W., 1998. Neogene deformation of the North West Shelf, Australia. IN: Purcell, P.G. and Purcell, R.R. (Editors), The sedimentary basins of Western Australia 2: Proceedings of the Petroleum Exploration Society of Australia Symposium, Perth, 1998, 81-91.

Keep, M. and Moss, S., (Eds), 2002. The Sedimentary Basins of Western Australia 3: Proceedings of the Petroleum Exploration Society of Australia Symposium, Perth, 2002.

Keep, M., Clough, M. and Langhi, L., 2002. Neogene tectonic and structural evolution of the Timor Sea region, NW Australia. In: Keep, M. and MOSS, S., (Eds), The Sedimentary Basins of Western Australia 3: Proceedings of the Petroleum Exploration Society of Australia, Perth, 2002, 341-353.

Kennard J.M. Deighton I., Edwards D.S. Colwell J.B. O'Brien, G.W. and Boreham, C.J., 1999, Thermal history modeling and transient heat pulses: new insights into hydrocarbon expulsion and 'hot flushes' in the Vulcan Sub-basin, Timor Sea. The APPEA Journal, 39, 177-207.

Kihle, J., 1996, Adaptation of fluorescence excitation-emission microspectroscopy for characterization of single hydrocarbon fluid inclusions. Organic Geochemistry, 23, 1029–1042.

King, G.C.P., and Muir-Wood, R., 2004, The impact of earthquakes on fluids in the crust, Annali Di Geofisica, XXXVII (6), 1453-1460.

Kivior, T., Kaldi, J.G. and Lang, S.C., 2002, Seal Potential in Cretaceous and Late Jurassic Rocks of the Vulcan Sub-basin, Northwest Shelf Australia. The APPEA Journal, 42 (1), 203-224.

Knipe, R. J., 1997, Juxtaposition/ seal diagrams to facilitate fault seal analysis of hydrocarbons. APPG Bulletin, 81 (2), 187-195.

Koning, T., 2003, Oil and gas production from basement reservoirs, Geological Society of London, Special Publication 214, Titled "Hydrocarbons in Crystalline Rocks".

Kopsen, E. and McGann, G., 1985, A review of the hydrocarbon habitat of the eastern and central Barrow-Dampier Sub-basin, Western Australia. The APEA Journal 25 (1), 154-176.

Krieger, F. W., Eadington. P. J. and Lisk, M., 1996, Fluid inclusion data for R_w in reserves estimation. SPE paper 36975, Society of Petroleum Engineers, Asia Pacific Oil and Gas Conference, 28–31 October 1996 Adelaide, Australia, 137-141.

Kuttan, K., Kulla, J.B. and Neumann, R.G., 1986, Freshwater influx in the Gippsland Basin: impact on formation evaluation, hydrocarbon volumes and hydrocarbon migration, The APEA Journal 26 (1), 242-249.

LaFargue, E. and Barker, C., 1988, Effect of water-washing on crude oil compositions, AAPG Bulletin 72, 263-76.

Lampe, C. and Person. M., 2002, Advective cooling within sedimentary rift basins – Applications to the Upper Rhine graben (Germany), Marine and Petroleum Geology, 19, 361-375.

Lampe, C, Person, M., Nöth, S. and Ricken, W., 2001, Episodic fluid flow within continental rift basins: some insights from field data and mathematical models of the Rhinegraben, Geofluids 1, 42-52.

Land L. S. and Dutton S. P., 1978, Cementation of a Pennsylvanian deltaic sandstone: Isotopic data. J. Sediment. Petrol. 48, 1167- 1176.

Larsen, G. and Chillinger, G.V., 1979, Diagenesis in Sediments and Sedimentary Rocks (Developments in Sedimentology 25A), Elsevier Publ. Co., 289 p.

Lemon, N.M., 1990, Petrographic analysis report, Talbot-2, unpublished report to Santos Ltd.

Li, B. and Mai, B., 1992. The application of fluorescence spectrum of organic inclusions to studying evolution and migration of hydrocarbons. In: Proceedings of Fourth Biennial Pan-American Conference on Research on Fluid Inclusions (PACROFI IV), 53.

Lisk, M., Hamilton P.J. and Eadington, P.J., 1992, Fluid History Analysis of samples from Hadrian-1, Timor Sea. CSIRO Restricted Report 283, unpublished, 100p.

Lisk, M., Eadington, P. J. and Kotaka, T., 1993, Hydrocarbon and pore water migration history in relation to diagenesis in the Toro and Iagifu sandstones, S.E. Gobe-2. in: Carman, G. J. and Z. (Eds) Petroleum Exploration and Development in Papua New Guinea, Proceedings of the 2nd PNG Petroleum Convention, Port Moresby, 477-88.

Lisk, M. and Eadington, P.J., 1994. Oil migration in the Cartier Trough, Vulcan Sub-basin. In: Purcell, P.G. and R.R. (Eds.), The Sedimentary Basins of Western Australia: Proceedings of the West Australian Basins Symposium, Perth, 301-12.

Lisk, M., George., S. C., Summons R. E., Quezada, R. A., and O'Brien, G. W., 1996a, Mapping hydrocarbon charge histories: detailed characterisation of the South Pepper oil field, Carnarvon Basin, The APPEA Journal, 36 (1), 445-464.

Lisk, M., O'Brien, G. W., and Eadington, P. J. 1996b, Insights into trap integrity via the reconstruction of charge histories in the Timor Sea, in: The importance of faulting on the North West Shelf of Australia - controls on fault distribution, orientation and sealing potential, Formation Evaluation Society of Western Australia (FESWA) Seminar, Perth.

Lisk, M., O'Brien, G. W., and Brincat, M. P., 1997, Gas displacement: An important control on oil and gas distribution in the Timor Sea? The APPEA Journal, 37 (1), 259-271.

Lisk, M., Brincat, M.P., Eadington, P.J. and O'Brien, G.W., 1998. Hydrocarbon charge in the Vulcan Sub-basin. In: Purcell, P.G. and R.R. (Eds.), The Sedimentary Basins of Western Australia 2. Proceedings of the West Australian Basins Symposium, Perth, 287-305.

Lisk, M., Eadington, P.J. and O'Brien, G.W., 1998, Unravelling complex filling histories by constraining the timing of events which modify oil fields after initial charge. In: Parnell, J. (ed.) Dating and Duration of Fluid Flow and Fluid Rock Interaction. Geological Society, London, Special Publications, 144, 189-203.

Lisk, M., Brincat, M.P., O'Brien, G.W., Eadington, P.J. and Faiz. M., 1999. Palaeohydrology of the Vulcan Sub-basin: Implications for trap integrity. The APEA Journal 39 (1), 208-226.

Lisk, M., 2000, The impact of oil emplacement on diagenesis: A novel solution from fluid inclusion observations. AAPG Meeting, Bali, November 2000. Am. Assoc. Pet. Geol. Bull. (Abstract).

Lisk, M., Faiz, M. M., Bekele, E. B. and Ruble, T. E., 2000, Transient fluid flow in the Timor Sea, Australia: implications for prediction of fault seal integrity. Journal of Exploration Technology, 40 (2), 27-43.

Lisk, M., O'Brien, G. W. and Eadington, P. J., 2002, Quantitative evaluation of the oil leg potential in the Oliver gas field, Timor Sea, Australia. American Association of Petroleum Geologists Bulletin, 86, 1531-1542.

Lisk, M., Gartrell A., Bailey, W.R., Underschultz, J., Brincat, M.P. and Johnson, L., 2005, Integrating structural and fluid-flow histories: A TEAM approach to addressing hydrocarbon charge and preservation, APPEA Conference 2005, Perth 2005, Poster presentation.

Liu, K., George, S. and Eadington, P.J., 2003, Predicting abundances and n-alkane profiles of oil inclusions from bulk fluorescence spectrophotometry. 21st Meeting of Organic Geochemistry, Krakow, Poland.

Liu, K. and Eadington, P., 2003, A new method for identifying secondary oil migration pathways, Journal of Geochemical Exploration 78-79, 389 394.

Liu, K., Eadington, P.J., Kennard, J.M., Middleton, H.A., George, S.C., Ahmed, M., Cope, P., 2004. Oil migration in the Vulcan Sub-basin, Timor Sea, investigated using GOI and FIS Data. In: Ellis, G.K., Baillie, P.W., Munson, T.J. (Eds.), Timor Sea Petroleum Geoscience, Proceedings Of The Timor Sea Symposium, Darwin, Northern Territory, 19–20 June 2003. Northern Territory Geological Survey, Special Publication, vol. 1, pp. 333–351.

Liu, K. and Eadington, P., 2005a. Quantitative fluorescence techniques for detecting residual oils and reconstructing hydrocarbon charge history. Org. Geochem. 36, 1023–1036.

Liu, K., Fenton, S., Bastow, T., Van Aarssen, B. and Eadington, P., 2005b, Geochemical evidence of multiple hydrocarbon charges and long distance oil migration in the Vulcan Sub-basin, Timor Sea. The APPEA Journal 45(1), 493-509.

Long, A.S. and Ramsden, C.R.T., 2004, Optimal 3D seismic acquisition in the Timor Sea: High-density 3D, In: Ellis, G.K., Baillie, P.W. and Munson, T.J. (eds), Timor Sea Petroleum Geoscience, Proceedings of the Timor Sea Symposium, Darwin, 19-20 June 2003. Northern Territory Geological Survey, Special Publication 1, 313-321.

Long, A., 2010, An overview of seismic azimuth for towed streamers, The Leading Edge 29, 512 - 523.

Longley, I.M., Beussenschuett, C., Clydesdale, L.,Cubitt, C.J., Davis, R.C., Johnson, M.K.,Marshall, N.M., Murray, A.P., Somerville, R.,Spry, T.B. and Thompson, N.B., 2002, The North West Shelf of Australia - a Woodside perspective. In: Keep, M. and Moss, S.J. (Eds), 2002, The Sedimentary Basins of Western Australia 3: Proceedings of the Petroleum Exploration Society of Australia Symposium, Perth, WA, 2002, 27–88.

Ludden J. N. 1992. Radiometric age determinations for basement from Sites 765 and 766, Argo Abyssal Plain, Northwest Australian margin. Proceedings of the Ocean Drilling Program Scientific Results 123, 557 – 559.

Loucks, R.R., Precise Geothermometry on fluid inclusion populations that trapped mixtures of immiscible fluids, 2000, American Journal of Science, 300, 23–59.

McAuliffe, C. D., 1979, Oil and gas migration: Chemical and physical constraints. American Association of Petroleum Geologists Bulletin, 63(5), 761–778.

McCaffrey, R., 1996, Slip partitioning at convergent plate boundaries of SE Asia, in Hall, R. and Blundell, D., (Eds), Tectonic Evolution of Southeast Asia: Geological Society Special Publication, 106, 3-18.

McClay, K. and Bonora, M., 2001, Analogue models of restraining stepovers in strike-slip fault systems, AAPG Bulletin 85, 233-260.

Macleod, G., Larter, S.R., Aplin, A.C., Pedersen, K.S., Booth, T.A., 1996, Determination of the e ective composition of single petroleum inclusions using confocal scanning laser microscopy and PVT simulation, In: Brown, P.E., Hage-mann, S.G. (Eds.), Proceedings of the Sixth Biennial Pan-American Conference on Research on Fluid Inclusions, (PACROFI VI). Madison, Wisconsin, USA, 81-82.

McClure, I.M., Smoth, D.N., Williams, A.F., Clegg, L.J. and Ford, C.C., 1988, Oil and Gas Fields in the Barrow sub-basin, in Purcell, P.G. and Purcell, R.R., (Eds), The North West Shelf, Australia: Proceedings of the Petroleum Exploration Society of Australia, Perth, 1988, 372-390.

McConachie, B.A., Bradshaw, M.T. and Bradshaw, J., 1996, Petroleum systems of the Petrel Sub-basin - an integrated approach to basin analysis and identification of hydrocarbon exploration opportunities. The APPEA Journal, 36(1), 248-268.

MacDaniel, R.P. 1988. Jabiru Oilfield. In Purcell, P.G. and R.P., (Eds), The North West Shelf, Australia: Proceedings of Petroleum Exploration Society Australia Symposium, Perth, 1988. 439-440.

McLimans, R. K., 1987, The application of fluid inclusions to migration of oil and diagenesis in petroleum reservoirs, Applied Geochemistry 2, 585-603.

Magoon, L.B., 1987, The petroleum system - A classification scheme for research, resource assessment and exploration [abs.]: American Association of Petroleum Geologists Bulletin, 71 (5), p. 587.

Magoon L.B., and Dow, W.G., 1994, The petroleum system – from source to trap, American Association of Petroleum Geologists Bulletin, 75, 3-25.

Mann, P., 2007, Global catalogue, classification and tectonic origins of restraining- and releasing bends on active and ancient strike-slip fault systems: in Cunningham, W.D. and Mann, P., eds., Tectonics of Strike-Slip Restraining and Releasing Bends: Geological Society (London) Special Publication 290, 13-142.

Marshall, J. D., (Ed.), 1987, Diagenesis of sedimentary sequences, Geological Society Sp. Pub. 36, Blackwell Sci. Pub., 360 p

Martin, K., 1987, Diagenesis and reservoir quality in the Challis Field, Browse Basin, Northern Territory. Unpublished report to BHP Petroleum Ltd.

Martin, K., 1991, Petrography of core samples from Delamere-1, AC/P 4, Northern Territory. Unpublished report to BHP Petroleum Ltd.

Martin, K., 1991, Petrography of sidewall core samples from the Plover Formation in Octavius No. 2, AC/P 11, Northern Territory. Unpublished report to Western Mining Corporation Ltd.

Martin, K., 1991, Petrography of sidewall core samples from the Plover Formation in Hadrian No. 1, AC/P 11, Northern Territory. Unpublished report to Western Mining Corporation Ltd.

Maxwell, A., Vincent, L. and Woods, E.P., 2004, The Audacious discovery, Timor Sea and the role of Pre-Stack Depth Migration seismic processing. In: Ellis, G.K., Baillie, P.W. and Munson, T.J. (editors), Timor Sea Petroleum Geoscience, Proceedings of the Timor Sea Symposium, Darwin, 19-20 June 2003. Northern Territory Geological Survey, Special Publication 1, 53-65.

Meldahl, P., R., Bril, H. R., de Groot, P. and Aminzadeh, F., 2002, Identifying seismic objects by their texture, orientation and size: A new interpretation tool, paper presented at the AAPG Annual Meeting, Houston, Texas, March 1-3, 2002.

Metcalfe, I., 1999, Gondwana dispersion and Asian accretion: An overview, in Metcalfe, I., (Ed), Gondwana Dispersion and Asian Accretion: IGCP 321 Final Results Volume, A.A. Balkema, Rotterdam, 9-28.

Meyer, V., A. Nicol, C. Childs, J. J. Walsh, and J. Watterson, 2002, Progressive localisation of strain during the evolution of a normal fault population: Journal of Structural Geology, v. 24, p. 1215–1231.

Mihut, D. and Müller, R.D, 1998, Revised seafloor spreading history of the Argo Abyssal Plain, In: Purcell, P.G. and R.R. (eds), The Sedimentary Basins of Western Australia 2: Proceedings Petroleum Exploration Society of Australia Symposium, Perth, 73-80.

Mildren, S. D., Hillis, R. R., Fett, T. and Robonson, P. H., 1994, Contemporary Stresses in the Timor Sea: Implications for Fault Trap Integrity, in: Purcell, P.G. and R.R. (Eds) The Sedimentary Basins of Western Australia: Proceedings of the West Australian Basins Symposium, Perth, 291-300.

Mildren, S.D., Hillis, R.R. and Kaldi, J., 2002, Calibrating predictions of fault seal reactivation in the Timor Sea. Australian Petroleum Production and Exploration Association Journal, 42 (1), 187-202.

Mildren, S.D., Hillis, R.R., Kivior, T. and Kaldi, J.G., 2004, Integrated seal assessment and geologic risk with application to the Skua Field, Timor Sea, Australia. In: Ellis, G.K., Baillie, P.W. and Munson, T.J. (editors), Timor Sea Petroleum Geoscience, Proceedings of the Timor Sea Symposium, Darwin, Northern Territory, 19-20 June 2003, Northern Territory Geological Survey, Special Publication 1, 275-294.

Mildren, S.D., Hillis, R.R., Dewhurst, D.N., Lyon, P.J., Meyer, J.J. and Boult, P.J., 2005, FAST: A New Technique for Geomechanical Assessment of the Risk of Reactivation-Related Breach of Fault Seals. In: Boult, P. and Kaldi, J. (eds). Evaluating fault and cap rock seals, AAPG Hedberg Series 2, 73–85.

Moldowan, J.M., Huizinga, B.J., Dahl, J.E., Fago, F.J., Taylor, D.W. and Hickey, L.J., 1994, The molecular fossil record of oleanane and its relationship to angiosperms. Science, 265, 768-771.

Monicard, R. P., 1980, Properties of reservoir rocks: core analysis, Houston, Gulf Publishing Co., 34p.

Morton, J. P. and Long, L. E., 1984, Rb-Sr ages of glauconite recrystallisation: Dating times of regional emergence above sea level. J. Sed. Petrol. 54, 495-506.

Morton R. A. and Land L. S., 1987, Regional variations in formation water chemistry, Frio Formation (Oligocene) Texas Gulf Coast, AAPG Bulletin, 71, p. 191.

Mory, A.J., 1988, Regional geology of the offshore Bonaparte Basin. In: Purcell, P.G. and R.R. (eds) The North West Shelf, Australia. Proceedings of the PESA Symposium, Perth, 287-309.

Müller, R.D., Mihut, D. and Baldwin, S., 1998, A new kinematic model for the formation and evolution of the west and northwest Australian margin. In: Purcell, P.G. and R.R. (eds), The Sedimentary Basins of Western Australia 2: Proceedings of Petroleum Exploration Society of Australia Symposium, Perth, WA, 1998, 55-71.

Munz, I.A., Wangen, M., Girard, J., Lacharpagne, J., and Johansen, H., 2004, Pressure–temperature–time–composition (P–T–t–X) constraints of multiple petroleum charges in the Hild field, Norwegian North Sea, Marine and Petroleum Geology 21, 1043–1060.

Murray, R.C., 1957, Hydrocarbon fluid inclusions in quartz, American Association of Petroleum Geologists Bulletin 41, 950-956.

Nedkvitne, T., Karlsen, D. A., Bjørlykke, K. and Larter, S. R., 1993, The relationship between diagenetic evolution and petroleum emplacement in the Ula Field, North Sea, Marine and Petroleum Geology, 10, 255-270.

Nelson, A.W., 1989, Jabiru Field - horst, sub-horst or inverted graben? The APEA Journal, 29 (1), 176-194.

Nelson, A., 1993, Wrench and inversion structures in the Timor Sea region: PESA Journal, 21, 3-30.

Nelson , P.H., 2000, Evolution of permeability - porosity trends in sandstones. SPWLA 41st Annual Logging Symposium, June 4-7, 14 p.

Newell, N.A., 1999, Water-washing in the Northern Bonaparte Basin. The APPEA Journal, 39 (1), 227-247.

Nicoll, R.S. and Foster, C.B., 1994, Late Triassic conodont and palynomorph biostratigraphy and conodont thermal maturation, North West Shelf, Australia, AGSO Journal of Australian Geology and Geophysics, 15, 101-118.

Nippon Oil Exploration (Vulcan) Pty Ltd, 2001, Crux 1 Final Geological Report, Volume 1, unpublished.

Noble, R. A., R. Alexander, R. I. Kagi, and J. Knox, 1985, Tetracyclic deterpenoid hydrocarbons in some Australian coals, sediments and crude oils: Geochimica et Cosmochimica Acta, 49, 2141-2147.

Norcen Ltd., 1990, Keeling-1 well completion report (unpublished).

Northern Territory Department of Regional Development, Primary Industry, Fisheries and Resources, 2009, Northern Territory Oil and Gas 2008, 36 p.

Oakes C.S., Bodnar R.J., Simonson J.M. 1990, the system NaCl - CaCl2-H2O. I. The hosts liquids at 1 atm total pressure. Geochimica et Cosmochimica Acta, 54: 603-610.

O'Brien, G.W., 1992, Light hydrocarbon geochemistry of the Vulcan Sub-Basin, Timor Sea: Rig Seismic Survey 97: Project 121.19. Geoscience Australia Publication-Record 1992/062.

O'Brien, G.W., Etheridge, M.A., Willcox, J.B., Morse, M., Symonds, P., Norman, C. and Needham, D.J., 1993, The structural architecture of the Timor Sea, north-western Australia: implications for basin development and hydrocarbon exploration. The APEA Journal, 33(1), 258-278.

O'Brien, G.W. and Woods, E.P., 1995, Hydrocarbon-related diagenetic zones (HRDZs) in the Vulcan Sub-basin, Timor Sea: recognition and exploration implications. The APEA Journal 35(1), 220-52.

O'Brien, G.W., Lisk, M., Duddy, I.R., Eadington, P.J., Cadman, S. and Fellows, M., 1996a, Late Tertiary fluid migration in the Timor Sea: A key control on thermal and diagenetic histories? The APPEA Journal 36(1), 399-427.

O'Brien, G.W., Higgins, R., Symonds, P., Quaife, P., Colwell , J., and Blevin, J., 1996b, Basement control on the development of extensional systems in Australia's Timor Sea: An example of hybrid hard linked/soft linked faulting? The APPEA Journal 36(1), 161-201.

O'Brien, G. W., Sturrock, S., Barber, P., Martin, M., Woollard, K. and Wilson, D., 1996c, Vulcan Tertiary Tie (VTT) Basin Study, Vulcan Sub-basin, Timor Sea, North-western Australia, AGSO Record 1996/61.

O'Brien, G.W., Quaife, P., Cowley, R., Morse, M., Wilson, D., Fellows, M. and Lisk, M., 1998, Evaluating trap integrity in the Vulcan Sub-basin, Timor Sea, Australia, using integrated remote sensing geochemical technologies. In: Purcell, P.G. and R.R. (eds), Sedimentary Basins of Western Australia 2. Petroleum Exploration Society of Australia Symposium, Perth, 237-254.

O'Brien, G. W., Lisk, M., Duddy, I. R., Hamilton, P. J., Woods, P. and Cowley, R., 1999, Plate convergence, foreland development and fault reactivation: primary controls on brine migration, thermal histories and trap breach in the Timor Sea Australia. Marine and Petroleum Geology 16 (6), 533-560.

O'Brien, G.W., Morse, M., Wilson, D., Quaife, P., Colwell, J., Higgins, R. and Foster, C.B., 1999b – Margin-scale, basement-involved compartmentalisation of Australia's North-West Shelf: a primary control on basin scale rift, depositional and reactivation histories. The APPEA Journal, 39(1), 40-63.

O'Brien, G.W., Lawrence, G., Williams, A., Webster, M., Wilson, D., Burns, S., 2000. Using integrated remote sensing technologies to evaluate and characterise hydrocarbon migration and charge characteristics on the Yampi Shelf, north-western Australia: a methodological study. APPEA Journal, 40(1), 230-255.

O'Brien, G.W., Glenn, K., Lawrence, G., Williams, A.K., Webster, M., Burns, S. and Cowley, R., 2002a, Influence of Hydrocarbon migration and seepage on benthic communities in the Timor sea, Australia, The APPEA Journal, 42 (1), 225-239.

O'Brien, G. W., Cowley, R., Quaife, P. and Morse, M., 2002b, Characterizing hydrocarbon migration and fault-seal integrity in Australia's Timor Sea via multiple, integrated remote sensing technologies, in Surface exploration case histories: Applications of geochemistry, magnetics, and remote sensing, D. Schumacher and L. A. LeSchack,

eds., AAPG Studies in Geology No. 48 and SEG Geophysical References Series No. 11, p. 393–413.
O'Brien, G.W., 1993, Some ideas on the rifting history of the Timor Sea from the integration of deep crustal seismic and other data. PESA Journal, 21, 95-113.
O'Grady, M. R., Bodnar, R. J., Hellgeth, J. W., Conroy, C. M., Taylor, L. T. and Knight, C. L., 1989, Fourier transform infrared microprobe (FTIRM) analysis of individual petroleum fluid inclusions in geologic samples: In *Microbeam Analysis*–1989, P. E. Russell (ed.). San Francisco Press, 579–582.
OMV Australia Ltd., 2000, Tenacious West-1 ST1 well completion report (unpublished).
O'Neil, J.R., Clayton, R.N., and Mayeda, T.K., 1969. Oxygen isotope fractionation in divalent metal carbonates. J.Chem. Phys., 51, 5547-5558.
Osborne, D.G., 1994, Nebo Oil discovery, Beagle Sub-basin. In: Purcell, P.G. and Purcell, R.R. (editors), The Sedimentary Basins of Western Australia 2: Proceedings of Petroleum Exploration Society of Australia Symposium, Perth, WA, 1998, p 653
Osborne, M.I., 1990. The Exploration and Appraisal History of the Skua Field, AC/P2 - Timor Sea, The APEA Journal, 30 (1), 197-201.
Osborne, M. and Haszeldine, R.S., 1993, Evidence for resetting fluid inclusion temperatures from quartz cements in oilfields: Marine and Petroleum Geology, 10, 271–278.
Otis, R.M. and Schneidermann, N., 1997, A Process for Evaluating Exploration Prospects, AAPG Bulletin, 81 (7), 1087–1109.
Otto, C., Underschultz, A.L. and Roy, V., 2001. Hydrodynamic analysis of flow systems and fault seal integrity in the Northwest Shelf of Australia. The APPEA Journal, 41 (1), 347-365.
Oxtoby, N. H., Mitchell, A. W. and Gluyas, J. G., 1995, The filling and emptying of the Ula Oilfield: fluid inclusion constraints. in: Cubitt, J. M. and England, W.A. (Eds), The Geochemistry of Reservoirs, Geological Society Special Publication No. 86, 141-57.
P'an, Ch.-H., 1982, Petroleum in Basement Rocks, AAPG Bulletin, 66, 1597-1643.
Parnell, J. (ed.) 1994. Geofluids: Origin, migration and evolution of fluids in sedimentary basins. Geological Society, London, Special Publication 78, 372 p.
Parnell, J. (ed.) 1998. Dating and duration of fluid flow and fluid-rock interaction. Geological Society, London, Special Publication 144, 284 p.
Parnell, J., Middleton, D., Honghan, C. and Hall, D. 2001, The use of integrated fluid inclusion studies in constraining oil charge history and reservoir compartmentalisation: examples from the Jeanne d'Arc Basin, offshore Newfoundland. Marine and Petroleum Geology, 18(5), 535–549.
Pattillo, J. and Nicholls, P.J., 1990, A Tectono-stratigraphic Framework for the Vulcan Graben, Timor Sea Region. The APEA Journal, 30(1), 27-50.
Peresson, H., Woods, E.P. and Fink, P., 2004, Fault architecture along the southeastern margin of the Cartier Trough, Vulcan Sub-basin, North West Shelf, Australia; implications for hydrocarbon exploration. In: Ellis, G.K., Baillie, P.W. and Munson, T.J. (editors), Timor Sea Petroleum Geoscience, Proceedings of the Timor Sea Symposium, Darwin, Northern Territory, 19-20 June 2003, Northern Territory Geological Survey, Special Publication 1, 156-167.
Person, M., Neuzil, C., Hseih, P., Mailloux, B., Bekele, E., Swenson, J., Eadington, P.J., 2000, Rift2D: a finite element model for simulating two-dimensional ground water flow, heat, solute-mass transport, and petroleum generation within evolving sedimentary basins (user guide), Minneapolis, University of Minnesota, Department of Geology and Geophysics, 210 p.
Person, M. and Garven, G., 1992, Hydrologic constraints on petroleum generation within continental rift basins: Theory and application to the Rhine Graben, American Association of Petroleum Geologists Bulletin, 76, 468–488.
Person, M., and Baumgartner, L., 1995, New evidence for long-distance fluid migration within the Earth's crust, Rev. Geophys., 33(S1), 1083–1092.
Peters, K. E., and Moldowan, J. M., 1993, The Biomarker Guide, Interpreting molecular fossils in petroleum and ancient sediments, Prentice Hall, 363 p.

Pettijohn F.J., Potter, P.E. and Siever R., 1987, Sand and Sandstone, Springer, New York, 553 p

Phillips, S.E., 1998, Petrology report, Tenacious West-1, Vulcan Sub-basin, unpublished report to Woodside Energy Ltd

Pichavant, M., Ramboz, C., and Weisbrod, A., 1982, Fluid immiscibility in natural processes: Use and misuse of fluid inclusion data I. Phase equilibria analysis – A theoretical and geometrical approach, Chemical Geology, v.37, 1-27.

Pigram C. J. and Symonds P. A. 1991. A review of the timing of the major tectonic events in the New Guinea Orogen. Journal of Asian Earth Sciences 6, 307-318.

Pironon, J., Sawatzki, J., Dubessy, J., 1992. NIR FT-Raman microspectroscopy of fluid inclusions: comparisons with VIS Raman and FT-IR microspectroscopies. Geochim. Cosmochim. Acta 55, 3885–3891.

Pironon, J., Canals, M., Dubessy, J., Walgenwitz, F., Laplace-Builhe, C., 1998. Volumetric reconstruction of individual oil inclusions by confocal scanning laser microscopy, Eur. J. Mineral. 10, 1143–1150.

Platte River Associates, 1995. BasinMod 1-D for Windows Basin Modelling System Version 5.0. Platte River Associates, Inc., Denver, Colorado, USA, October 1995 (two volume user manual).

Playford, P., 2002, Palaeokarst, pseudokarst, and sequence stratigraphy in Devonian reef complexes of the Canning Basin, Western Australia, in Keep, M. and Moss, S.J. (Eds), 2002, The Sedimentary Basins of Western Australia 3: Proceedings of the Petroleum Exploration Society of Australia, Perth, 1994, 63-76.

Pockalny, R.A., Fox, P.J., Fornari, D.J., MacDonald, K.C. and Perfit, M.R., 1997. Tectonic reconstruction of the Clipperton and Siqueiros Fracture Zones: Evidence and consequences of plate motion change for the last 3 Myr, Journal of Geophysical Research, 102, 3167-3181.

Pontifex, I., 1997, Mineralogical Report No. 7412 - Tenacious-1, unpublished report to Cultus Petroleum Ltd.

Potter, R. W., Clynne, M. A., and Brown, D. L., 1978 Freezing point depression of aqueous sodium chloride solutions: Economic Geology, v. 73, 284–285.

Powell, T.G., 2001, Understanding Australia's Petroleum Resources, Future production trends and the role of the frontiers, The APPEA Journal, 41 (1), 273-287.

Preston, J.C. and Edwards, D.S., 2000, The petroleum geochemistry of oils and source rocks from the Northern Bonaparte Basin, offshore Northern Australia, The APPEA Journal, 40 (1), 257 – 281.

Prezbindowski, D.R. and Larese, R.E., 1987, Experimental stretching of fluid inclusions in calcite – implications for diagenetic studies, Geology, 15, 333-336.

Price, L.C., 1976. Aqueous solubility of petroleum as applied to its origin and primary migration. AAPG Bulletin, 60, 213–244.

Purcell, P.G. and Purcell, R.R, 1988, The North West Shelf, Australia - An Introduction, in Purcell, P.G. and Purcell, R.R., (Eds), The North West Shelf, Australia: Proceedings of the Petroleum Exploration Society of Australia, Perth, 1988, 3-15,

Purcell, P.G. and Purcell, R.R., (Eds), 1994, The Sedimentary Basins of Western Australia: Proceedings of the Petroleum Exploration Society of Australia, Perth, 1994, 1-15.

Purcell, P.G. and Purcell, R.R., (Eds), 1998, The Sedimentary Basins of Western Australia 2: Proceedings of the Petroleum Exploration Society of Australia, Perth, 1998.

Quarles van Ufford, A. and Cloos, M., 2004, Cenozoic tectonics of New Guinea, AAPG Bulletin, 89 (1), 119–140.

Radke, M and Welte, D.H., 1983, The methyl phenanthrene index (MPI); a maturity parameter based on aromatic hydrocarbons, in Bjorøy, M. et al. (eds), Advances in Organic Geochemistry 1981, Wiley, Chichester, 504-512.

Radke, M, Leythaeuser, D. and Teichmuller, M., 1984, Relationship between rank and composition of aromatic hydrocarbons for coals of different origins, Organic Geochemistry 6, 423-30.

Ramboz, C., Pichavant, M., and Weisbrod, A., 1982, Fluid immiscibility in natural processes: Use and misuse of fluid inclusion data II. Interpretation of fluid inclusion data in terms of immiscibility, Chemical Geology, v.37, 29-48.
Ramm, M. and Bjørlykke, K., 1994, Porosity/depth trends in reservoir sandstones; assessing the quantitative effects of varying pore-pressure, temperature history and mineralogy, Norwegian Shelf data, Clay Minerals 29(4), 475-490.
Reeckman, S.A., and Mebberson, A.J., 1984, Igneous intrusions in the northwest Canning Basin and their impact on oil exploration, in Purcell, P.G. (Ed) The Canning Basin, WA, Proceedings, GSA/PESA Canning Basin Symposium, Perth, 389-400.
Rider, M., 1996, The geological interpretation of well logs, Whittles Publishing, 280 p.
Rise, L., Sættemb, R., Fanavoll, S., Thorsnes, T, Ottesen, D., and BøE, R., 1999, Sea-bed pockmarks related to fluid migration from Mesozoic bedrock strata in the Skagerrak offshore Norway, Marine and Petroleum Geology 16, 619-631.
Roberts, S., 2001, Fluid flow in the south Eugene Island area, Offshore Louisiana: Results of numerical simulations, Marine and Petroleum Geology 18, 799-805.
Roberts, S.J. and Nunn, J.A., 1995, Episodic fluid expulsion from geopressured sediments. Marine and Petroleum Geology, 12, 195-204.
Robinson, A., Grant, S. and Oxtoby, N., 1992, Evidence against natural deformation of fluid inclusions in diagenetic quartz, Marine and Petroleum Geology, 9 (5), 568-572.
Robinson, A. and Gluyas, J., 1992, Duration of quartz cementation in sandstones, North Sea and Haltenbanken Basins, Marine and Petroleum Geology, 9 (3), 324-327.
Roedder, E., 1981. In: Origin of fluid inclusions and changes that occur after trapping: Mineralogical Association of Canada, Short Course in Fluid Inclusions: Applications to Geology, 101-129.
Roedder, E., 1984. Fluid Inclusions, Mineralogical Society of America, Reviews in Mineralogy 12, Washington, D.C., 644pp.
Rojstaczer, S. and Wolf, S., 1992, Hydrologic changes associated with the Loma Prieta earthquake in the San Lorenzo and Pescadero drainage basins, Geology, 20 (3), 211-214.
Rollet, N., Logan, G. A., Kennard, J. M., O'-Brien, P. E., Jones, A. T., Sexton, M ., 2006, Characterisation and correlation of active hydrocarbon seepage using geophysical data sets: An example from the tropical, carbonate Yampi Shelf, Northwest Australia: Paleooceanography - Marine and petroleum geology , 23 (2), 145-164.
Rose, P. R., 1987, Dealing with risk and uncertainty in exploration: How can we improve? AAPG Bulletin, 71, 1-16.
Rose, P.R., 1999, Risk Behaviour in Petroleum Exploration; The adoption of systematic risk analysis by international corporations during the 1990s., The Leading Edge, 192-199.
Ruble, T.E., George, S.C., Lisk, M., Quezada, R.A., 1998. Organic compounds trapped in aqueous fluid inclusions. Org. Geochem. 29, 195–205.
Ryder, A.G., 2004, Time resolved fluorescence spectroscopic study of crude petroleum oils: influence of chemical composition, Applied Spectroscopy 58(5), 613-623.
Ryder, A.G., 2005, Analysis of crude petroleum oils using fluorescence spectroscopy, Reviews in Fluorescence 2005, Annual Volumes, 2, 169-198.
Sahling, H., Bohrmanna, G., Spiessa, V., Bialasb, J., Breitzkec, M., Ivanovd, M., Kastenc, S., Krastela, S. and Schneider, R., 2008, Pockmarks in the Northern Congo Fan area, SW Africa: Complex seafloor features shaped by fluid flow, Marine Geology, 249, 3-4, 206-225.
Santos Ltd, 1990a, Talbot-1 Well Completion Report, unpublished Santos Ltd report.
Santos Ltd, 1990b, Anson-1 Well Completion Report, unpublished Santos Ltd report.
Sava, P., 2006, Subsalt Exploration and Development: Imaging, Interpretation, and Drilling—What have we learned? 2006 SEG/EAGE Summer Research Workshop, The Leading Edge 25, 1370-1376.
Schmid, S., Worden, R.H. and Fisher, Q.J., 2004, Diagenesis and reservoir quality of the Sherwood Sandstone (Triassic), Corrib Field, Slyne Basin, west of Ireland, Marine and Petroleum Geology 21 (3), 299–315.

Scholle, P. A. and Schluger, P. R., (Eds.), 1979, Aspects of Diagenesis: Tulsa, OK, SEPM Special Publication 26, 443 p.

Schowalter, T.T., 1979, Mechanics of Secondary Hydrocarbon Migration and Entrapment, AAPG Bulletin, 63 (5), 723-760.

Schowalter, T.T. and Hess, P.D., 1982, Interpretation of Subsurface Hydrocarbon Shows, AAPG Bulletin, 66 (9), 1302-1327.

Schroot, B. M., Klaver, G. T., and Schuttenhelm, R. T. E., 2005, Surface and subsurface expression of gas seepage to the seabed-examples from the southern North Sea, Marine and Petroleum Geology, 22(3), 499–515.

Schwark, L., Stoddart, D., Keuser, C., Spitthoff, B. and Leythaeuser, D., 1997. A novel sequential extraction system for whole core plug extraction in a solvent flow-through cell-application to extraction of residual petroleum from an intact pore-system in secondary migration studies. Org. Geochem. 26, ½, p. 19-31.

Selle, O.M., Jensen, J.I., Sylta, Ø., Andersen, T., Nyland, B., Broks, T.M., 1993, Experimental verification of low-dip, low rate two-phase secondary migration by means of gamma-ray absorption, In: Parnell, J., Ruffell, A.H. and Moles, N.R. (Eds.), Geofluid'93, Contribution to an International Conference on fluid evolution, migration and interaction in rocks, 72–75.

Sentftle, J. T. and Landis, C. R., 1991, Vitrinite Reflectance as a tool to assess thermal maturity, in Merrill (Ed), Source and migration processes and evaluation techniques, AAPG Treatise of Petroleum Geology, Handbook of Petroleum Geology, 119-125.

Shuster, M. W., Eaton, S., Wakefield L. L. and Kloosterman, H. J., 1998, Neogene Tectonics, Greater Timor Sea, Offshore Australia: Implications for trap risk. The APPEA Journal 38 (1), 351-379.

Sibson, R. H. 2001, Seismogenic framework for hydrothermal transport and ore deposition. Reviews in Economic Geology, 14, 25–50.

Sibson, R. H., 1996, Structural Permeability of fluid-driven fault-fracture meshes. Journal of Structural Geology, 18 (8), 1031–1042.

Sibson, R. H., 1994, Crustal stress, faulting and Fluid-flow, In: Parnell, J., Geofluids: origin, migration and evolution of fluids in sedimentary basins. The Geological Society Special Publication. 78, 69-84.

Sibson, R. H., 1987, Earthquake rupturing as a mineralizing agent in hydrothermal systems: Geology, v. 15, p. 701– 704.

Sibson, R. H., 1981, Fluid flow accompanying faulting: field evidence and models. In: Simpson, D.W. and Richards, P.G. (eds) Earthquake Prediction: an International Review. American Geophysical Union, Maurice Ewing Series, 4, 593-603.

Siljestrom, S., Lausmaa, J., Sjovall, P., Broman, C., Thiel, V. and Hode, T., 2010, Analysis of hopanes and steranes in single oil-bearing fluid inclusions using time-of-flight secondary ion mass spectrometry (ToF-SIMS), Geobiology 8, 37–44.

Smith, L. and Chapman, D.S., 1983, On the thermal effects of groundwater flow, 1. Regional scale systems, Journal of Geophysical Research, 88, 593-608.

Smith, P.M. and Sutherand, N.D., 1991, Discovery of salt in the Vulcan Graben: a geophysical and geological evaluation. The APEA Journal, 31(1), 229-243.

Smith, G.C., Tilbury, L.A., Chatfield, A., Senycia, P. and Thompson, N.B., 1996, Laminaria: a new Timor Sea discovery, The APPEA Journal, 36 (1), 12-29.

Snyder, D.B., and Barber, A. J., 1997. Australia-Banda Arc collision as an analogue for early stages in Iapetus closure. Journal of the Geological Society of London, 154, 589-592.

Spry, T.B. and Ward, I., 1997, The Gwydion discovery: a new play fairway in the Browse Basin. The APPEA Journal, 37(1), 87–104.

Stagg H. M. J., Wilcox J. B., Symonds P. A., O'Brien G. W., Colwell J. B., Hill P. J. A., Lee C-S., Moore A. M. G. and Struckmeyer H. I. M. 1999. Architecture and evolution of the Australian continental margin. AGSO Journal of Australian Geology and Geophysics 17, 17 – 33.

Stasiuk, L.D., Snowdon, L.R., 1997. Fluorescence micro-spectrometry of synthetic and natural hydrocarbon fluid inclusions: crude oil chemistry, density and application to petroleum migration. Applied Geochemistry 12 (3), 229–241.

Stein, A., Myers, K., Lewis, C., Cruse, T. and Winstanley, S., 1998, Basement control and geoscientific definition of the Cornea discovery, Browse Basin, Western Australia. In: Purcell, P.G. and Purcell, R.R. (editors), The Sedimentary Basins of Western Australia 2: Proceedings of the Petroleum Exploration Society of Australia Symposium, Perth, 1998, 421–431.

Streit, J. E., 1999, Conditions for earthquake surface rupture along the San Andreas fault system, California, J. Geophys. Res., 104(B8), 17,929–17,939.

Streit, J.E. and Hillis, R. R., 2004, Estimating fault stability and sustainable fluid pressures for underground storage of CO2 in porous rock, Energy, 29/9-10, 1445-1456.

Struckmeyer, H.I.M, Blevin, J.E., Sayers, J., Totterell, J.M., Baxter, K. and Cathro, D., 1998, Structural Evolution of the Browse basin, North West Shelf: New Concepts from deep seismic data, in Purcell, P.G. and Purcell, R.R., (Eds), The Sedimentary Basins of Western Australia 2: Proceedings of the Petroleum Exploration Society of Australia, Perth, 1998, 345-367.

Summons, R.E., Bradshaw, M., Crowley, J., Edwards, D.S., George, S.C. and Zumberge, J.E., 1998, Vagrant oils: geochemical signposts to unrecognised petroleum systems, in Purcell, P.G. and Purcell, R.R., (Eds), The Sedimentary Basins of Western Australia 2: Proceedings of the Petroleum Exploration Society of Australia, Perth, 1998, 169-184.

Supernaw, I.R., 1988. US patent 201729, Method for detecting oil content of an underground formation.

Sylta, Ø., Pedersen, J. I. and Hamborg, M., 1997. On the vertical and lateral distribution of hydrocarbon migration velocities during secondary migration. in: Hendry, J., Carey, P., Parnell, J., Ruffell, A. and Worden, R. (Eds), Geofluids II: Contributions to the second international conference on fluid evolution, migration and interaction in sedimentary basins and orogenic belts, Belfast, UK, 55-58.

Sylta, Ø., 2008, Quantifying secondary migration efficiencies, Geofluids 2 (4), 285–298.

Taylor, J.R., 1997, An Introduction to Error Analysis: The Study of Uncertainties in Physical Measurements, University Science Books, 333 p.

Taylor, T. R., Giles, M. R., Hathon, L.N., Diggs, T.N., Braunsdorf, N.R., Birbiglia, G.V., Kittridge, M.G., Macaulay, C.I. and Espejo, I.S., 2010, Sandstone diagenesis and reservoir quality prediction: Models, myths, and reality, AAPG Bulletin 94(8), 1093-1132.

Teinturier, S., Pironon, J., Walgenwitz, F., 2002. Fluid inclusions and PVTX modelling: examples from the Garn Formation in well 6507/2-2, Haltenbanken, Mid-Norway. Marine and Petroleum Geology, 19, 755–765.

ten Haven, H.L., Arbin, P., Simon, B., Collo, G., le Cann, J.P. and Mulero, P., 2006, Applications and Limitations of Mud Logging Gas Data in the Detection of Formation Fluids and overpressure: Examples from South-East Asia, IPA, 2006 - Proceedings of an International Conference on Gas Habitats of SE Asia and Australasia, 1999.

Thiery, R., Pironon, J., Walgenwitz, F. and Montel, F., 2002, Individual characterization of petroleum fluid inclusions (composition and P-T trapping conditions) by microthermometry and confocal scanning laser microscopy: Inferences from applied thermodynamics of oils: Marine and Petroleum Geology 19 (7), 847– 859.

Thomas, A.P., 1992, Petrology report, Montara-2, Timor Sea, unpublished report to BHP Petroleum Ltd.

Thomas, A.P., 1992, Petrology report, Leeuwin-1, Timor Sea, unpublished report to BHP Petroleum Ltd.

Thomas, M. M. and Clouse, J. A., 1995, Scaled physical model of secondary migration: American Association of Petroleum Geologists Bulletin, 79 (1), p. 19-29.

Thompson, K.F.M., 1987, Fractionated aromatic petroleums and the generation of gas-condensates. Organic Geochemistry, 11(6), 573–590.

Thompson, K.F.M., 1988, Gas-condensate migration and oil fractionation in deltaic systems. Marine and Petroleum Geology, 5, 237–246.

Tikoff, B. and Teyssier, C. 1994. Strain modelling of displacement-field partitioning in transpressional orogens. Journal of Structural Geology, 16, 1575-1588.

Tindale, K., Newell, N., Keall, J. and Smith, N., 1998, Structural evolution and charge history of the Exmouth Sub-basin, northern Carnarvon Basin, western Australia, in Purcell, P.G. and Purcell, R.R., (Eds), The Sedimentary Basins of Western Australia 2: Proceedings of the Petroleum Exploration Society of Australia, Perth, 1998, 447-472.

Tissot, B.P., Pelet, R. and Ungerer, P., 1987, Thermal history of sedimentary basins, maturation indices and kinetics of oil and gas generation, AAPG Bulletin, 71, 1445-1466.

Torgerson, T. 1990. Crustal-scale fluid transport: magnitude and mechanisms. EOS, Transactions of the American Geophysical Union, 71, l, 4, 13.

Trewin, N.H., 1983, Petrology, diagenesis and depositional environment of reservoir sandstones in Jabiru-1A, unpublished report to BHP Petroleum Ltd.

Tseng, H. and Pottorf, R. J., 2002, Fluid inclusion constraints on petroleum PVT and compositional history of the Greater Alwyn-South Brent petroleum system, northern North sea, Marine and Petroleum Geology, 19 (7), 797-809.

Tsui, T. K., 1990, Characterising fluid inclusion oils via UV fluorescence microspectrophotometry - A method for projecting oil quality and constraining oil migration history. American Association of Petroleum Geologists Bulletin 74, 781.

Tucker, M.E., 2001, Sedimentary Petrology (Third Edition), Blackwell Science Ltd., 262p.

UK Offshore Operators Association, 2000, Guidelines for the conduct of mobile drilling rig site investigations in deep water, July 2000, version 1.0, 21p.

Underschultz, J.R., Ellis, G.K., Hennig, A., Bekele, E., and Otto, C., 2002, Estimating Formation Water Salinity from Wireline Pressure Data: Case Study in the Vulcan Sub-basin, In: Keep, M. and Moss, S.J. (Eds), 2002, The Sedimentary Basins of Western Australia 3: Proceedings of the Petroleum Exploration Society of Australia Symposium, Perth, WA, 2002, 285-303.

Upton, P., Baxter, K. and O'Brien, G.W., 1998, Coupled Mechanical/Fluid Flow Models of Trap Integrity and Fault Reactivation: Application to the North West Shelf of Australia. The APPEA Journal, 38(1), 488-499.

Veevers, J.J.,1984. Phanerozoic earth history of Australia. Oxford Goelogical Science No.2, Claredon Press, Oxford, p.418.

Veevers J. J., Powell C. MCA. and Roots S. R. 1991. Review of seafloor spreading around Australia. I. Synthesis of the patterns of spreading, Australian Journal of Earth Sciences, 38, 373 – 389.

Veevers J. J. 1988. Morphotectonics of Australia's northwestern margin – a review, In: Purcell P.G. and Purcell R.R. eds. The North West Shelf Australia: Proceedings of Petroleum Exploration Society of Australia Symposium. Perth, 19-27.

Vincent, P. and Tilbury, L., 1988, Gas and oil fields of the Rankin Trend and northern Barrow-Dampier Sub-basin, in Purcell, P.G. and Purcell, R.R., (Eds), The North West Shelf, Australia: Proceedings of the Petroleum Exploration Society of Australia, Perth, 1988, 341-369.

Volk, H., George, S.C., Lisk, M., Killops, S.D., Ahmed, M., Quezada, R.A., 2001. Charge histories of petroleum reservoirs in the Gippsland and Taranaki Basins — evidence from the analysis of oil inclusions and crude oils. In: Hill, K.C., Bernecker, T. (eds.), Eastern Australasian Basins Symposium, A Refocused Energy Perspective for the Future. Petroleum Exploration Society of Australia, Special Publication, 413–422.

Volk, H., Fuentes, D., Fuerbach, A., Miese, C., Koehler, W., Bärsch N. and Barcikowski, S., 2010, First on-line analysis of petroleum from single inclusion using ultrafast laser ablation. Organic Geochemistry, 41 (2), 74-77.

Volkman, J.K., Alexander, R., Kagi, R.I., Noble R.A. and Woodhouse, G.W., 1983, A geochemical reconstruction of oil generation in the Barrow Sub-Basin of Western Australia, Geochemical et Cosmochima Acta, 47, 2091-2105.

Wallace, T.D., and Balnaves, C., 1988, Jabiru Field simulation: a case history, Proceedings SPE International Meeting on Petroleum Engineering, Tianjin, China, p. 525-538: SPE Pper 17602.

Walsh, J. J., et al., 2001, Geometric controls on the evolution of normal fault systems, in R. E. Holdsworth, R. A. Strachan, J. F. Magloughlin, and R. J. Knipe, eds., The nature and tectonic significance of fault zone weakening: Geological Society (London) Special Publication 186, 157–170.

Waples, D. W., Pacheco, J. and Vera., A., 2004, method for correcting log-derived temperatures in deep wells, calibrated in the Gulf of Mexico Petroleum Geoscience, 2004; 10(3), 239-245.

Warris, B. J., 1973, Plate tectonics and the evolution of the Timor Sea, north west Australia, APEA Journal, 13(1), 13-18.

Weltje, G.J. and von Eynatten, H., 2004, Quantitative provenance analysis of sediments: review and outlook, Sedimentary Geology, 171, 1-11.

Wentworth, C.K., 1922, A scale of grade and class terms for clastic sediments. Journal of Geology 30, 377-392.

Wernicke, B.P. and Axen, G.J., 1988, On the role of isostasy in the evolution of normal fault systems. Geology, 16(9), 848–851.

Whelhan, J. K.; Kennicutt M. C.; Brooks J. M.; Schumacher D.; and Eglington, L. B., Organic geochemical indicators of dynamic fluid flow processes in petroleum basins, 1994, Organic geochemistry 22, 587-615.

Whibley, M. and Jacobson, T., 1990, Exploration in the northern Bonaparte Basin, Timor Sea - WA-199-P. The APEA Journal, 30(1), 7-25.

Wilhems, A., Horstad, I. and Karlsen, D, 1996. Sequential extraction-a useful tool for reservoir geochemistry? Org. Geochem. 24 (12), p. 1157-1172.

Wilkins, R.W.T., Wilmshurst, J.R., Hladky, G., Ellacott, M.V., Buckingham, C.P., 1992., Fluorescence alteration and the suppression of vitrinite reflectance Organic Geochemistry, 18, 629-640.

Wilkins, R.W.T., Buckingham, C.P., Sherwood, N., Russell, N.J., Faiz, M. and Kurusingal, J., 1998. The current status of the FAMM thermal maturity technique for petroleum exploration in Australia. The APPEA Journal 38 (1), 421-437.

Wilkinson, M., Haszeldine, R.S., Ellam, R.M. and Fallick, A., 2004, Hydrocarbon filling history from diagenetic evidence: Brent Group, UK North Sea, Marine and Petroleum Geology 21(4), 443–455.

Williams, A. and Lawrence, G., 2002, The role of satellite seep detection in exploring the South Atlantic's ultra-deep water. Surface Exploration Case Histories: Applications of Geochemistry, Magnetics, and Remote Sensing, pp. 327-344. American Association of Petroleum Geologists, Tulsa, OK.

Williams, A. K., A. Kloster, R. Duckworth, and N. Piggott, 1995, The role of the airborne laser fluorosensor (ALF) and other seepage detection techniques in exploring frontier basins, in S. Hanslein, ed., Petroleum exploration and exploitation in Norway: Norwegian Petroleum Society Special Publication 4, p. 421–431.

WMC Petroleum Ltd., 1990, Octavius-1 well completion report (unpublished).

WMC Petroleum Ltd., 1992, Octavius-2 well completion report (unpublished).

Woods, E.P., 1992, Vulcan Sub-basin fault styles – implications for hydrocarbon migration and entrapment. The APEA Journal, 32(1), 138-158.

Woods, E.P., 1994, A salt related detachment model for the development of the Vulcan Sub-basin. In: Purcell, P.G. and R.R. (eds) The Sedimentary Basins of Western Australia. Proceedings of the Petroleum Exploration Society of Australia Symposium, Perth, 259-274.

Woods, E.P., 2004, Twenty years of Vulcan Sub-basin exploration since Jabiru - what lessons have been learnt? IN: Ellis, G.K., Baillie, P.W. and Munson, T.J. (Editors), Timor Sea Petroleum Geoscience: Proceedings of the Timor Sea Symposium, Darwin, Northern Territory, 2003. Northern Territory Geological Survey, Special Publication 1.

Woods, E.P. and Maxwell, A.J., 2004, The significance of the Tenacious oil discovery, Vulcan Sub-basin, Australia. In: Ellis, G.K., Baillie, P.W. and Munson, T.J. (editors), Timor Sea Petroleum Geoscience. Proceedings of the Timor Sea Symposium, Darwin, 19-20 June 2003. Northern Territory Geological Survey, Special Publication 1, 471-482.

Woodside 1988, Petroleum geology and hydrocarbon potential of the Barrow-Dampier Sub-basin and environs. Petroleum in Australia: the first century. Sydney: Australian Petroleum Exploration Association, 213-231.

Worden R.H., Warren E.A., Smalley P.C., Primmer T.J. and Oxtoby N.H., 1995, Discussion of 'Evidence for resetting of fluid inclusion temperatures from quartz cements in oilfields' by Osborne and Haszeldine, 1993, Marine and Petroleum Geology, 12, 566-570.

Wormald G.B. 1988. The geology of the Challis Oilfield, Timor Sea, Australia. Proceedings of Petroleum Exploration Society Australia Symposium, Perth, 1988, 425-437.

Wycherley, L., Parnell, J., Watt, G. R., Chen, H. and Boyce, A. J., 2003, Indicators of hot fluid migration in sedimentary basins: evidence from the UK Atlantic Margin, Petroleum Geoscience, 9, 357-374.

Xie, X, Li, S, Dong, W., and Hu, Z., 2001, Evidence for hot fluid flow along faults near diapiric structure of the Yinggehai basin, South China Sea, Marine and Petroleum Geology, 18(6), 715-728.

Yassir, N., and Otto, C. J., 1997, Hydrodynamics and Fault Seal Assessment in the Vulcan Sub-basin, Timor Sea, The APPEA Journal, 37 (1), 380-414.

Yeates, A.N., Bradshaw, M.T., Dickins, J.M., Brakel, A.T., Exon, N.F., Lanford, R.P., Mulholland, S.M., Totterdell, J.M. and Yeung, M., 1987, The Westralian Superbasin, an Australian link with Tethys, in McKenzie, K.G., (Ed), Shallow Tethys 2: International Symposium on Shallow Tethys 2, Wagga Wagga, 1987, 199-213.

Yielding, G., Freeman, B., and Needham, T., 1997, Quantitative fault seal prediction. APPG Bulletin, 81 (6), 897-971.

Young, I., Schmedje, T.M. and Muir, W.F., 1995, The Elang oil discovery establishes new oil province in the Eastern Timor Sea (Timor Gap Zone of Cooperation, The APEA Journal 35 (1), 44-64.

Yurtsever, Y., and Gat, J.R., 1981, Atmospheric waters, in Gat, J.R., and Gonfiantini, R., (eds.), Stable Isotope Hydrology: Deuterium and Oxygen-18 in the Water Cycle. IAEA Vienna, 103-142.

Zierfuss, H., and Coumou, D.J., 1956, The Use of Qualitative Fluorescence Measurements in Drilling Operations: AAPG Bulletin, 40, p. 2724-2734.

Zoback, M.L., 1992. First- and second-order patterns of stress in the lithosphere: the world stress map project. Journal of Geophysical Research, 97, 11703-11728.

APPENDIX A – SAMPLE CATALOGUE

This appendix provides a list of samples prepared for this study and the types of analyses that were undertaken. Items shown in italics represent samples that were not analysed by the author but make an important contribution to the discussion.

Well Name	Sample Depth (mRT)	Sample Number	Sample Type	GOI Analysis	Thermometric Analysis	MCI Analysis	Stable Isotope Analyses
Allaru-1	2376	124137	cuttings	Yes	No	No	No
Allaru-1	2388	124138	cuttings	Yes	No	No	No
Allaru-1	2547	124140	cuttings	Yes	No	No	No
Allaru-1	2892	124141	cuttings	Yes	No	No	No
Allaru-1	2931	124142	cuttings	Yes	No	No	No
Allaru-1ST2	2538	124143	cuttings	Yes	No	No	No
Allaru-1ST2	2871	124144	cuttings	Yes	No	No	No
Allaru-1ST2	2910	124145	cuttings	Yes	No	No	No
Allaru-1ST2	2955	124146	cuttings	Yes	No	No	No
Anson-1	1707	123354	cuttings	Yes	No	No	No
Anson-1	1716	123355	cuttings	Yes	No	No	No
Anson-1	1725	123356	cuttings	Yes	No	No	No
Augustus-1	3485	75874	cuttings	No	Yes	No	No
Augustus-1	3500	75874	cuttings	Yes	Yes	No	No
Augustus-1	3515	75876	cuttings	Yes	No	No	No
Bilyara-1	2608.4	123282	core	Yes	No	No	No
Bilyara-1	*2610.5*	*n/a*	*core*	*No*	*Yes*	No	No
Bilyara-1	2619.8	123279	core	Yes	No	No	No
Bilyara-1	*2631.6*	*n/a*	*core*	*No*	*Yes*	No	No
Bilyara-1	2635.6	123280	core	Yes	No	No	No
Bilyara-1	2642.1	123468	core	Yes	No	No	No
Bilyara-1	2643.2	123469	core	Yes	No	No	No
Bilyara-1	2651.9	123281	core	Yes	No	No	No
Bilyara-1	*2675.7*	*n/a*	*core*	*No*	*Yes*	No	No
Bilyara-1	2694	123283	cuttings	Yes	No	No	No
Bilyara-1	2703	123284	cuttings	Yes	No	No	No
Bilyara-1	2712	123285	cuttings	Yes	No	No	No
Calytrix-1	1565	124159	cuttings	Yes	No	No	No
Calytrix-1	1570	124160	cuttings	Yes	No	No	No
Calytrix-1	1575	124161	cuttings	Yes	No	No	No
Calytrix-1	1580	124162	cuttings	Yes	No	No	No
Calytrix-1	1585	124163	cuttings	Yes	No	No	No
Calytrix-1	1590	124164	cuttings	Yes	No	No	No
Cassini-1ST	1434	123138	cuttings	Yes	No	No	No
Cassini-1ST	1439.43	123134	core	Yes	No	No	No
Cassini-1ST	1443.9	123135	core	Yes	No	No	No
Cassini-1ST	1447.45	123136	core	Yes	No	No	No
Cassini-1ST	1460.25	123137	core	Yes	No	*Yes*	No
Cassini-1ST	1476	123140	cuttings	Yes	No	No	No
Cassini-1ST	1485	123286	cuttings	Yes	No	No	No
Cassini-1ST	1566	123542	cuttings	Yes	No	No	No
Cassini-1ST	1581	123543	cuttings	Yes	No	No	No
Cassini-1ST	1596	123544	cuttings	Yes	No	No	No
Cassini-2	1464	123290	cuttings	Yes	No	No	No
Cassini-2	1470	123291	cuttings	Yes	No	No	No

Well Name	Sample Depth (mRT)	Sample Number	Sample Type	GOI Analysis	Thermometric Analysis	MCI Analysis	Stable Isotope Analyses
Challis-1	1399.2	122502	core	Yes	Yes	No	No
Challis-1	1405.05	122503	core	Yes	No	No	No
Challis-1	1447.15	122504	core	Yes	No	No	No
Challis-1	1600	75865	cuttings	No	Yes	No	No
Challis-1	1861	75866	cuttings	No	Yes	No	No
Champagny-1	3210	123409	cuttings	Yes	No	No	No
Champagny-1	3225	123410	cuttings	Yes	No	No	No
Champagny-1	3350	123411	cuttings	Yes	No	No	No
Champagny-1	3402	123412	cuttings	Yes	No	No	No
Delamere-1	1274.1	123770	core	Yes	No	No	Yes
Delamere-1	1285.2	123771	core	Yes	No	No	Yes
Douglas-1	2455	75871	cuttings	No	Yes	No	No
Douglas-1	2515	75872	cuttings	Yes	Yes	No	No
Douglas-1	2602	75873	cuttings	No	Yes	No	No
Douglas-1	*2607*	*n/a*	*sidewall core*	*No*	*No*	*No*	*Yes*
East Swan-1	2726	124130	cuttings	Yes	No	No	No
East Swan-1	2750	124131	cuttings	Yes	No	No	No
East Swan-1	2765	124132	cuttings	Yes	No	No	No
East Swan-1	2814	124135	cuttings	Yes	No	No	No
East Swan-2	1125	75910	cuttings	No	Yes	No	No
East Swan-2	1215	75911	cuttings	No	Yes	No	No
East Swan-2	1285	75912	cuttings	No	Yes	No	No
East Swan-2	2609.4	122408	core	Yes	No	No	No
East Swan-2	2620.7	122366	core	Yes	No	No	No
East Swan-2	2630.08	122409	core	Yes	No	No	No
East Swan-2	*2631.5*	*n/a*	*core*	*No*	*No*	*Yes*	No
East Swan-2	2658	122339	cuttings	Yes	No	No	No
East Swan-2	2679	122340	cuttings	Yes	No	No	No
East Swan-2	2700	122341	cuttings	Yes	No	No	No
East Swan-2	2718	122342	cuttings	Yes	No	No	No
East Swan-2	2751	122343	cuttings	Yes	No	No	No
East Swan-2	2778	122344	cuttings	Yes	No	No	No
Eclipse-1	2547.9	122459	core	Yes	No	No	No
Eclipse-1	2554.5	122460	core	Yes	No	No	No
Eclipse-1	2565	122491	cuttings	Yes	No	No	No
Eclipse-1	2574	122492	cuttings	Yes	No	No	No
Eclipse-1	2586	122856	cuttings	Yes	No	No	No
Eclipse-1	2604	122857	cuttings	Yes	No	No	No
Eclipse-1	2607	122494	cuttings	Yes	No	No	No
Eclipse-1	2616	122858	cuttings	Yes	No	No	No
Eclipse-1	2622	123104	cuttings	Yes	No	No	No
Eclipse-1	2634	123105	cuttings	Yes	No	No	No
Eclipse-1	2649	123106	cuttings	Yes	No	No	No
Eclipse-1	2679	123347	cuttings	Yes	Yes	No	No
Eclipse-1	2690	123348	cuttings	Yes	No	No	No
Eclipse-1	2703	123349	cuttings	Yes	No	No	No
Eclipse-1	2733	123350	cuttings	Yes	No	No	No
Eclipse-1	2760	123487	cuttings	Yes	No	No	No
Eclipse-1	2787	123488	cuttings	Yes	No	No	No
Eclipse-1	2808	123489	cuttings	Yes	No	No	No
Eclipse-2	2454	123351	cuttings	Yes	No	No	No
Eclipse-2	2781	123491	cuttings	Yes	No	No	No
Eclipse-2	2784	123107	cuttings	Yes	No	No	No
Eclipse-2	2793	123108	cuttings	Yes	No	No	No
Eclipse-2	2805	123109	cuttings	Yes	No	No	No
Eclipse-2	2823	123110	cuttings	Yes	No	No	No
Eclipse-2	2838	123111	cuttings	Yes	No	No	No
Eclipse-2	2871	123112	cuttings	Yes	No	No	No

Well Name	Sample Depth (mRT)	Sample Number	Sample Type	GOI Analysis	Thermometric Analysis	MCI Analysis	Stable Isotope Analyses
Elm-1	2778	124150	cuttings	Yes	No	No	No
Elm-1	2793	124151	cuttings	Yes	No	No	No
Elm-1	2829	124152	cuttings	Yes	No	No	No
Elm-1	2838	124148	cuttings	Yes	No	No	No
Elm-1	2946	124153	cuttings	Yes	No	No	No
Elm-1	2970	124154	cuttings	Yes	No	No	No
Elm-1	2991	124155	cuttings	Yes	No	No	No
Elm-1	2997	124156	cuttings	Yes	No	No	No
Elm-1	3009	124157	cuttings	Yes	No	No	No
Elm-1	3018	124158	cuttings	Yes	No	No	No
Hadrian-1	3110	75884	cuttings	No	Yes	No	No
Hadrian-1	3476.5	75882	core	Yes	Yes	No	*Yes*
Hadrian-1	3507	75883	cuttings	No	Yes	No	No
Ibis-1	1275	123457	cuttings	Yes	No	No	No
Ibis-1	1285	123458	cuttings	Yes	No	No	No
Ibis-1	1300	123459	cuttings	Yes	No	No	No
Ibis-1	1350	123460	cuttings	Yes	No	No	No
Jabiru-1A	1604	122400	cuttings	Yes	No	No	No
Jabiru-1A	1613	122401	cuttings	Yes	No	No	No
Jabiru-1A	*1617.9*	*n/a*	*core*	*No*	*No*	*Yes*	No
Jabiru-1A	1620.4	75867	core	Yes	No	No	*Yes*
Jabiru-1A	1627.7	122192	core	Yes	No	No	No
Jabiru-1A	1632.2	122218	core	Yes	No	No	No
Jabiru-1A	1637.1	122219	core	Yes	No	*Yes*	No
Jabiru-1A	1646.4	75868	core	Yes	Yes	No	*Yes*
Jabiru-1A	1650	75869	core	Yes	Yes	No	*Yes*
Jabiru-1A	1665.9	122220	core	Yes	No	No	No
Jabiru-1A	1676	122221	core	Yes	No	No	No
Jabiru-1A	1685	123173	cuttings	Yes	No	No	No
Jabiru-1A	1688	122332	cuttings	Yes	No	*Yes*	No
Jabiru-1A	1688	122222	cuttings	Yes	No	No	No
Jabiru-1A	1697	122402	cuttings	Yes	No	No	No
Jabiru-1A	1712	122403	cuttings	Yes	Yes	No	No
Jabiru-1A	1712	122418	cuttings	Yes	No	No	No
Jabiru-1A	1721	122333	cuttings	Yes	No	No	No
Jabiru-1A	1733	122419	cuttings	Yes	No	No	No
Jabiru-2	790	122399	cuttings	Yes	Yes	No	No
Jabiru-2	1642	122361	core	Yes	No	No	No
Jabiru-2	1655.21	122362	core	Yes	No	No	No
Jabiru-2	1661	122352	cuttings	Yes	Yes	No	No
Jabiru-2	1679	122353	cuttings	Yes	No	No	No
Jabiru-2	1689	122354	cuttings	Yes	No	No	No
Jabiru-2	1712	122355	cuttings	Yes	No	No	No
Jabiru-3	1625	123132	core	Yes	No	No	No
Jabiru-3	1637.7	123133	core	Yes	No	No	No
Jabiru-3	1647	123100	cuttings	Yes	No	No	No
Jabiru-3	1659	123244	cuttings	Yes	No	No	No
Jabiru-3	1662	123101	cuttings	Yes	No	No	No
Jabiru-3	1680	123102	cuttings	Yes	No	No	No
Jabiru-3	1704	123103	cuttings	Yes	No	No	No
Keeling-1	3033	111286	cuttings	Yes	No	No	No
Keeling-1	3039	111290	cuttings	Yes	Yes	No	No
Keeling-1	3039	122385	cuttings	Yes	No	No	No
Keeling-1	3057	111287	cuttings	Yes	No	No	No
Keeling-1	3060	111288	cuttings	Yes	No	No	No
Keeling-1	3063	122359	cuttings	Yes	No	No	No
Keeling-1	3069	122406	cuttings	Yes	No	No	No

Well Name	Sample Depth (mRT)	Sample Number	Sample Type	GOI Analysis	Thermometric Analysis	MCI Analysis	Stable Isotope Analyses
Keeling-1	3072	111289	cuttings	Yes	No	No	No
Keeling-1	3084	122360	cuttings	Yes	No	No	No
Langhorne-1	2511	124971	cuttings	Yes	No	No	No
Langhorne-1	2526	124972	cuttings	Yes	No	No	No
Langhorne-1	2541	124973	cuttings	Yes	No	No	No
Leeuwin-1	1653	123508	cuttings	Yes	No	No	No
Leeuwin-1	1674	123510	cuttings	Yes	No	No	No
Leeuwin-1	1749	123511	cuttings	Yes	No	No	No
Leeuwin-1	1761	123512	cuttings	Yes	No	No	No
Leeuwin-1	1869	123513	cuttings	Yes	No	No	No
Leeuwin-1	2469	123515	cuttings	Yes	No	No	No
Longleat-1	1938	124974	cuttings	Yes	No	No	No
Longleat-1	1974	124975	cuttings	Yes	No	No	No
Longleat-1	2016	124976	cuttings	Yes	No	No	No
Longleat-1	2064	124977	cuttings	Yes	No	No	No
Longleat-1	2115	124978	cuttings	Yes	No	No	No
Longleat-1	2154	124979	cuttings	Yes	No	No	No
Maple-1	3666	124980	cuttings	Yes	No	No	No
Maple-1	3681	124981	cuttings	Yes	No	No	No
Maple-1	3684	124983	cuttings	Yes	No	No	No
Maple-1	3720	124982	cuttings	Yes	No	No	No
Maple-1	3903	124985	cuttings	Yes	No	No	No
Maple-1	3975	124986	cuttings	Yes	No	No	No
Maple-1	4101	124987	cuttings	Yes	No	No	No
Montara-1	2604.4	122410	core	Yes	No	No	No
Montara-1	*2606.1*	*n/a*	*core*	*No*	*Yes*	No	No
Montara-1	*2609.4*	*n/a*	*core*	*No*	*Yes*	No	No
Montara-1	2610.05	122411	core	Yes	No	No	No
Montara-1	2616	122412	cuttings	Yes	No	No	No
Montara-1	2622	122413	cuttings	Yes	No	No	No
Montara-1	2625	123357	cuttings	Yes	No	No	No
Montara-1	2628	123358	cuttings	Yes	No	No	No
Montara-1	2631	122414	cuttings	Yes	No	No	No
Montara-1	2634	123359	cuttings	Yes	No	No	No
Montara-1	2640	122415	cuttings	Yes	No	No	No
Montara-1	2643	122416	cuttings	Yes	No	No	No
Montara-1	2649	122417	cuttings	Yes	No	No	No
Octavius-2	*2820*	*n/a*	*sidewall core*	*No*	*No*	*No*	*Yes*
Octavius-2	3195	75907	cuttings	Yes	Yes	*Yes*	No
Octavius-2	3245	125564	cuttings	Yes	No	No	No
Octavius-2	3260	75909	swc	Yes	Yes	No	No
Oliver-1	2946	122223	cuttings	Yes	No	No	No
Oliver-1	2967	122224	cuttings	Yes	No	No	No
Oliver-1	2974.38	122407	core	Yes	Yes	No	No
Oliver-1	2982	122225	cuttings	Yes	No	*Yes*	No
Oliver-1	3006	122226	cuttings	Yes	No	No	No
Oliver-1	3042	122227	cuttings	Yes	No	No	No
Oliver-1	3078	122228	cuttings	Yes	No	No	No
Oliver-1	3114	122229	cuttings	Yes	No	No	No
Oliver-1	3147	122230	cuttings	Yes	No	No	No
Osprey-1	2476	75964	cuttings	Yes	No	No	No
Osprey-1	2482	75966	cuttings	Yes	No	*Yes*	No
Osprey-1	2488	75968	cuttings	Yes	No	No	No
Osprey-1	2491	75969	cuttings	Yes	No	No	No
Paqualin-1	2067	124988	cuttings	Yes	No	No	No
Paqualin-1	2835	124990	cuttings	Yes	No	No	No
Paqualin-1	2844	124991	cuttings	Yes	No	No	No

Well Name	Sample Depth (mRT)	Sample Number	Sample Type	GOI Analysis	Thermometric Analysis	MCI Analysis	Stable Isotope Analyses
Paqualin-1	2877	124992	cuttings	Yes	No	No	No
Paqualin-1	2880	124993	cuttings	Yes	No	No	No
Paqualin-1	4137	124994	cuttings	Yes	No	No	No
Paqualin-1	4143	124995	cuttings	Yes	No	No	No
Paqualin-1	4164	124996	cuttings	Yes	No	No	No
Paqualin-1	4176	124997	cuttings	Yes	No	No	No
Parry-1	2097	123482	cuttings	Yes	Yes	No	No
Parry-1	2103	123483	cuttings	Yes	No	No	No
Parry-1	2119	123294	cuttings	Yes	No	No	No
Pengana-1	1641.15	122461	core	Yes	No	No	No
Pengana-1	1651.09	122462	core	Yes	No	No	No
Pituri-1	1708	123318	cuttings	Yes	No	No	No
Pituri-1	1720	123319	cuttings	Yes	No	No	No
Pollard-1	2040	124998	cuttings	Yes	No	No	No
Pollard-1	2048	124999	cuttings	Yes	No	No	No
Pollard-1	2100	125000	cuttings	Yes	No	No	No
Rainbow-1	2573	125001	cuttings	Yes	No	No	No
Rainbow-1	2591	125002	cuttings	Yes	No	No	No
Rainbow-1	2621	125003	cuttings	Yes	No	No	No
Skua-3	2378.1	122334	core	Yes	No	No	No
Skua-3	2389.9	122335	core	Yes	No	*Yes*	No
Skua-3	2409.2	122336	core	Yes	No	No	No
Skua-3	2416	122422	cuttings	Yes	No	No	No
Skua-3	2416	122337	cuttings	Yes	No	No	No
Skua-3	2425	122423	cuttings	Yes	Yes	No	No
Skua-3	2434	122424	cuttings	Yes	Yes	No	No
Skua-3	2440	122425	cuttings	Yes	No	No	No
Skua-3	2449	122426	cuttings	Yes	No	No	No
Skua-4	2349.8	123117	core	Yes	No	No	No
Skua-4	2353	123118	cuttings	Yes	No	No	No
Skua-4	2361	123119	cuttings	Yes	No	No	No
Skua-4	2391	123120	cuttings	Yes	No	No	No
Skua-6	1875	123121	cuttings	Yes	No	No	No
Skua-6	2388	123123	cuttings	Yes	No	No	No
Skua-6	2394	123124	cuttings	Yes	No	No	No
Skua-6	2706	123125	cuttings	Yes	No	No	No
Snowmass-1	1294	122477	cuttings	Yes	No	No	No
Snowmass-1	1318	122478	cuttings	Yes	No	No	No
Snowmass-1	1345	122479	cuttings	Yes	No	No	No
Snowmass-1	1417	122480	cuttings	Yes	No	No	No
Swan-1	2359	123325	cuttings	Yes	No	No	No
Swan-1	2396	123326	cuttings	Yes	No	No	No
Swan-1	2402	123327	cuttings	Yes	No	No	No
Swan-2	2253	123360	cuttings	Yes	No	No	No
Swan-2	2265	123328	cuttings	Yes	No	No	No
Swan-2	2277	123329	cuttings	Yes	No	No	No
Swan-2	2316	123548	cuttings	Yes	No	No	No
Swan-2	2319	123549	cuttings	Yes	No	No	No
Swan-2	2325	123330	cuttings	Yes	No	No	No
Swan-2	2328	123550	cuttings	Yes	No	No	No
Swan-2	2337	123551	cuttings	Yes	No	No	No
Swan-3	2312.1	123141	core	Yes	No	No	No
Swan-3	2325.35	123142	core	Yes	No	No	No
Swan-3	2415	123143	cuttings	Yes	No	No	No
Swan-3ST1	2340	123144	cuttings	Yes	No	No	No
Swan-3ST1	*2346*	*n/a*	*cuttings*	*No*	*No*	*Yes*	No
Swan-3ST1	2349	123465	cuttings	Yes	No	No	No

Well Name	Sample Depth (mRT)	Sample Number	Sample Type	GOI Analysis	Thermometric Analysis	MCI Analysis	Stable Isotope Analyses
Swan-3ST1	2355	123130	cuttings	Yes	No	No	No
Swan-3ST1	2370	123131	cuttings	Yes	No	No	No
Swan-3ST1	2445	123145	cuttings	Yes	No	No	No
Swift-1	2402.5	123470	core	Yes	No	No	No
Swift-1	2417.65	123471	core	Yes	No	No	No
Swift-1	2431.6	123472	core	Yes	No	No	No
Swift-1	2441	123473	cuttings	Yes	No	No	No
Talbot-1	1507	123126	cuttings	Yes	No	No	No
Talbot-1	1525	123127	cuttings	Yes	No	No	No
Talbot-1	1540	123361	cuttings	Yes	No	No	No
Talbot-1	1558	123128	cuttings	Yes	No	No	No
Talbot-1	1597	123129	cuttings	Yes	No	No	No
Taltarni-1	2853.9	123413	core	Yes	No	No	No
Taltarni-1	*2854.5*	*n/a*	*core*	*No*	*Yes*	No	No
Taltarni-1	*2862.9*	*n/a*	*core*	*No*	*Yes*	No	No
Taltarni-1	2865.1	123414	core	Yes	No	No	No
Taltarni-1	2870	123415	core	Yes	*Yes*	No	No
Taltarni-1	3009	123416	cuttings	Yes	No	No	No
Tancred-1	1344	123484	cuttings	Yes	No	No	No
Tancred-1	1365	122471	cuttings	Yes	No	No	No
Tancred-1	1386	122472	cuttings	Yes	No	No	No
Tancred-1	1419	122473	cuttings	Yes	No	No	No
Tancred-1	1455	122474	cuttings	Yes	No	No	No
Tancred-1	1479	122475	cuttings	Yes	No	No	No
Turnstone-1	1521	122483	cuttings	Yes	No	No	No
Turnstone-1	1530	122484	cuttings	Yes	No	No	No
Turnstone-1	1542	122485	cuttings	Yes	No	No	No
Turnstone-1	1558	122486	cuttings	Yes	No	No	No
Turnstone-1	1573	122487	cuttings	Yes	No	No	No
Turnstone-1	1588	122488	cuttings	Yes	No	No	No
Turnstone-1	1618	122489	cuttings	Yes	No	No	No
Warb-1	1205	125004	cuttings	Yes	No	No	No
Warb-1	1735	125005	cuttings	Yes	No	No	No
Warb-1	2365	125006	cuttings	Yes	No	No	No
Warb-1	2380	125007	cuttings	Yes	No	No	No
Warb-1	2400	125008	cuttings	Yes	No	No	No
Warb-1	2405	125009	cuttings	Yes	No	No	No
Warb-1	2430	125010	cuttings	Yes	No	No	No
Yarra-1	2557	125011	cuttings	Yes	No	No	No
Yarra-1	2638	125013	cuttings	Yes	No	No	No
Yarra-1	2698	125014	cuttings	Yes	No	No	No
Yarra-1	2812	125015	cuttings	Yes	No	No	No
Yering-1	2812	123406	cuttings	Yes	No	No	No
Yering-1	2923	123407	cuttings	Yes	No	No	No
Yering-1	2959	123408	cuttings	Yes	No	No	No

APPENDIX B – UNITS AND GLOSSARY OF TERMS

Units

API degrees = American Petroleum Institute measure of fluid gravity
Bbbl billion barrels = 10^9 barrels
BCF billion cubic feet = 10^9 cubic feet
BCM billion cubic metres = 10^9 m^3
Bscf billions of standard cubic feet
GL gigalitre = 10^6 cubic metres = 6.28981 million barrels
kbbl thousand barrels
kcm thousand cubic metres
kL kilolitre
kPa kilopascals, a unit of pressure
m^3 cubic metre
ML megalitre = million litres
MMbbl million barrels
Millidarcy (md) – 1/1000 of a Darcy, a unit of measurement used to describe permeability
PJ petajoule = 10^{15} joules
Tcf trillion cubic feet = 10^{12} cubic feet
TJ terajoule = 10^{12} joules

Conversion factors (approximate)

1 kilolitre = 6.2898 barrels
1 cubic metre = 1 kilolitre = 35.315 cubic feet
1 barrel = 0.159 kilolitres
1 cubic foot = 0.0283 cubic metres
Throughout the text one thousand million (10^9) is referred to as one billion, and one million million (10^{12}) as one trillion.

Abbreviations and Terminology

Air gun – The most common acoustic source used for seismic surveying offshore that utilises compressed air released from a chamber.
Annulus – Space between the drill pipe and the wall of the wellbore
Associated gas – natural gas produced with crude oil from the same reservoir
AVO – Amplitude Versus Offset, a geophysical analysis technique that uses variation in seismic reflection amplitude with change in distance between the shotpoint and receiver to determine thickness, porosity, density, velocity, lithology and fluid content of rocks.
Bad Hole – A borehole that is out of gauge or is rugose due to wash-outs or break-outs.
Barrel (bbl) – a unit of measure for oil and petroleum products that is equivalent to 42 U.S. gallons.
BHT – Bottom Hole Temperature.
Blowout – the uncontrolled flow of gas, oil or other fluids from a well.
Blowout preventer (BOP) – the equipment installed at the wellhead to control pressures in the annular space between the casing and drill pipe or tubing during drilling, completion, and workover operations.
BOPD – Barrels of Oil Per Day
BRS – Bureau of Resource Sciences
Casing – metal pipe inserted into a wellbore and cemented in place to protect both subsurface formations (such as groundwater) and the wellbore.
Cased hole – A wellbore in which casing has been run.

Casing point – The depth in a well at which casing is set, generally the depth at which the casing shoe rests.

Circulation – Continuous pumping of drilling mud down through drill-string and back up the annulus to the drilling rig during rotary drilling used to cool the drill bit and to bring drill cuttings from bottom of well bore to surface.

Closure – The area enclosed by the lowest closing contour that defines a trap.

Completion – Processes which takes place immediately after the drilling operation is completed, normally to prepare the well for testing or production.

Core sample – A cylindrical section of rock recovered through conventional coring.

Crude Oil – Raw, liquid petroleum as it comes out of the ground as distinguished from refined oils manufactured from it.

Cut Fluorescence – Fluorescence observed when solvent is added to a sample

Darcy – A unit of rock permeability in which fluid centipoise viscosity will flow at a velocity of one centimeter.

Development well – a well drilled within the proved area of an oil or gas reservoir to the depth of a stratigraphic horizon known to be productive; a well drilled in a proven field for the purpose of completing the desired spacing pattern of production.

Direct Fluorescence – Fluorescence observed when samples are viewed under UV light without the addition of a solvent

Directional drilling – Intentional deviation of a wellbore from the vertical.

Drilling Mud, Drilling Fluid – Fluid used to lubricate the drill string, line, the walls of a well, flush cuttings to the surface and create enough hydrostatic weight to prevent blowouts.

Drill cuttings – the small pieces of rock created as a drill bit cuts through underground formations while drilling.

Drill string – A connected column (string) of steel pipe that transmits drilling fluid (via the mud pumps) and torque (via the top drive) to the drill bit.

Drill bit – Located at end of drill-string cutting head is generally designed with three cone-shaped wheels tipped with hardened teeth. Drill bits used for extra-hard rock are studded with thousands of tiny industrial diamonds.

Drill collars – Heavy pipe-sections that put weight on drill bit.

Drill Pipe – Heavy, thick-walled steel pipe used in rotary drilling to turn the drill bit and to provide a conduit for the drilling mud. Joints of drill pipe are about 30 feet long.

Dry hole – any exploratory or development well that does not find commercial quantities of hydrocarbons.

Dry Gas – Natural gas that does not have a significant amount of liquid hydrocarbons or water vapor.

DST – Drill Stem Test

Electric Log – A subsurface recording that indicates a well's rock formation characteristics by illustrating its responses to an electrical current.

Enhanced oil recovery (EOR) – refers to a variety of processes to increase the amount of oil removed from a reservoir, typically by injecting a liquid (e.g., water, surfactant) or gas (e.g., nitrogen, carbon dioxide).

EUR – Estimated Ultimate Recovery

Exploration well – a hole drilled: a) to find and produce oil or gas in an area previously considered unproductive area; b) to find a new reservoir in a known field, i.e., one previously producing oil and gas from another reservoir, or c) to extend the limit of a known oil or gas reservoir.

Field – A subsurface accumulation of hydrocarbons.

Fish – To retrieve object that has been unintentionally dropped down the wellbore or to free equipment that has become stuck down the hole.

Formation – A formal term used to reference a genetically related rock unit.

Formation damage – the reduction in permeability in reservoir rock due to the infiltration of drilling or treating fluids into the area adjacent to the wellbore.

FPSO – Floating Production, Storage and Offloading

Gas Oil Ratio (GOR) – Number of cubic feet of gas produced per barrel of oil.

Gas Show – A significant increase in gas detector response from an increasing concentration of natural gas in the mud system of a drilling well.

Hydrocarbons – A compound of the elements hydrogen and carbon, in either liquid or gaseous form. Natural gas and petroleum are mixtures of hydrocarbons.

Horizon – A term describing a layer of rock, most typically associated with a mapped seismic reflection.

Horner plot – a semi-log plot produced during pressure buildup analysis.

Kick – An unexpected intrusion of formation fluid (typically gas) into the wellbore that causes drilling fluid to be displaced. It can be the precursor to a blowout.

Killing a well – Adding heavy drilling mud to stop control or stop the flow of oil or gas.

Lag time – The time taken for drill cuttings to reach the surface from the drill-bit.

LCM – Loss Control Material, a collective term for substances added to lighten drilling fluids when drilling fluids are being lost to the formation down-hole.

Leak-off test – A test to determine the strength or fracture pressure of the open formation, usually conducted immediately after drilling below a new casing shoe.

LNG – Liquefied Natural Gas

Lost Circulation – Mud lost to a formation, usually in cavernous, pressured, or coarsely permeable beds.

LPG – Liquefied Petroleum Gas

MDT (Modular formation dynamics tester) – Measures fluid pressures down-hole and enables small fluid samples to be collected.

mRT – metres below Rotary Table

Mudlogging – The recording of information derived from examination and analysis of formation cuttings made by the bit and of mud circulated out of the hole.

Non-associated gas – natural gas produced from a reservoir that does not contain significant quantities of crude oil.

Operator – A company or individual, acting for himself or as an agent for others who has primary responsibility for undertaking work commitments and complying with regulatory requirements for a permit.

OOIP or OGIP – Original Oil/Gas in Place is an estimate of the amount of oil or gas contained in the reservoir based on physical features of the reservoir.

P&A (plugged and abandoned) – a depleted well or dry hole that has been (typically) filled with cement and marked, with all surface equipment removed.

Pay – A reservoir or portion of a reservoir containing hydrocarbons that can be economically produced, also referred to as "pay sand" or the "pay zone".

Perforations – Holes within and through casing and cement into a productive formation.

Play – A set of oil or gas accumulations sharing similar geological properties, such as source rock, hydrocarbon type, and migration pathways.

Possible Reserves – Possible reserves are less certain than Probable reserves and can be estimated with a lower degree of certainty.

Probable Reserves – Probable reserves are less certain than Proved reserves and can be estimated with a degree of certainty sufficient to indicate that they are more likely to be recovered than not.

Produced water – the water extracted from the subsurface with oil and gas. It may include water from the reservoir, water that has been injected into the formation, and any chemicals added during the production/treatment process.

Prospect – An undrilled, untested, and unproven, hydrocarbon trap.

Proven Reserves – Estimated quantities of hydrocarbons that geological and engineering data demonstrate will be recoverable from known oil and natural gas reservoirs under existing economic and operating conditions.

Reservoir – A porous rock unit capable of containing recoverable hydrocarbons.

RFT – Repeat Formation Test, used to measure reservoir pressure and recovery small fluid samples.

ROP – Rate of penetration (ROP) is a measure of the speed at which the bit drills through the formation.

Rotary Table (RT) – Turning device on derrick floor in which drill-string is held and rotated.

Scf – standard cubic feet (cubic feet at standard atmospheric temperature and pressure).

Shale shaker – Large vibrating screen for sifting out rock cuttings from the drilling mud to be examined and described by the wellsite geologist.

Show – An indication while drilling that hydrocarbons are present in the well.

Sidetrack – A remedial drilling operation that results in creation of a new section of well bore for purpose of detouring around "junk", re-drilling a lost hole or straightening crooked holes.

SWC – Sidewall Core Sample, a small sample taken on wireline tools that can be percussive or rotary in nature.

Solution Gas – Gas that is present in the formation water.

Sour crude oil – oil containing free sulfur or other sulfur compounds whose total sulfur content is in excess of 1 percent.

Sour gas – natural gas containing hydrogen sulfide.

Source Rock – An organic rich rock (typically shale or deepwater carbonate) capable of generating hydrocarbons under certain conditions of temperature and pressure.

Swab, Swabbing – The process of mechanically pulling (or lifting) liquids from a well bore.

Sweet Gas – Natural gas not containing hydrogen sulfide.

Spud – Commencement of drilling operations.

Suspended discovery – An oil or gas field identified by a discovery well but not presently being produced or developed.

2D seismic Data – A two-dimensional picture of the subsurface. It generates a seismic section, which is a two-dimensional slice from the surface of the earth downward.

3D Seismic Data – Seismic data that is recorded, processed and interpreted in a three-dimensional volume instead of individual two-dimensional lines.

Trap – A structure capable of retaining hydrocarbons.

Trip – Insertion or removal of the drill-string

Trip Gas – Gas entrained in the drilling fluid during a pipe trip, which typically results in a significant increase in gas that is circulated to surface

Underbalanced drilling – drilling under conditions where the pressure being exerted inside the wellbore (from the drilling fluids) is less than the pressure of the oil or gas in the formation.

Wellhead – the equipment at the surface of a well used to control the pressure; the point at which the hydrocarbons and water exit the ground

Wet gas – natural gas containing significant amounts of liquefiable hydrocarbons.

Wildcat well – a well drilled in an area where no current oil or gas production exists.

Wireline logs – Logging tools lowered on a wire and conductor line into the completed well.

APPENDIX C – ADDITIONAL GOI LOGS

This appendix provides GOI logs for wells where only low GOI values have been recorded and that consequently lack evidence of prior oil accumulation. The primary application of the GOI method in this study has been as a tool to recognise palaeo-oil zones rather than map migration pathways on a basin scale. Nevertheless the wells with exclusively low GOI values still provide useful information so the critical elements pertinent to the interpretation of these results, in contrast to high GOI values, are reviewed.

In simplest terms the wells that recorded exclusively low GOI values can be interpreted as providing positive evidence for oil having been present in the pore space providing that the chance of reworking from a previous sedimentary environment can be excluded. The observation of oil inclusions within authigenic minerals that retain well developed crystal faces provides a clear indication that the oil inclusions have not been inherited. However in samples where oil inclusions occur solely on fractures within detrital minerals reworking is impossible to rule out, but the likelihood of such an outcome is improbable when one considers the cumulative probability of producing the series of events needed to deliver such an outcome. Firstly the reworked sediment needs to have been exposed to a petroleum system and to migration or accumulation of oil at that time. Quartz grains eroded from the host need to be transported and deposited in a suitable location that is subsequently modified to produce a valid structure that attracts drilling and finally sampled at an optimum position.

The likelihood of this occurring becomes even more remote when the processes that control the migration of oil in the sub-surface are taken into account. The mechanism for secondary oil migration through porous reservoir rocks (Schowalter, 1979) relies on buoyancy pressure (*Pb*) of oil in water being the main driving force and capillary entry pressure (*Pc*) of the pore spaces within the carrier bed acting as the main resistant force. Wettability will also play an important role but can be largely ignored for clastic reservoirs that are rarely oil-wet rather than water-wet.

The buoyancy pressure (*Pb*) is determined by the density difference between the hydrocarbon phase and the formation water and can be calculated using:

$$Pb = Pc = (\rho w - \rho o)gh = \Delta \rho gh$$

Where ρw and ρo are densities of formation water and the migrating oil, g is the gravitational constant and h is the height of continuous oil phase.

The level of resistance to flow relates to the capillary pressure (*Pc*) of pore network within the carrier bed, a factor that is determined by the equation:

$$Pc = 2\sigma \cos \Theta / R$$

where R is the radius of the pore throats of the rock, the hydrocarbon-water interfacial tension (σ), and the contact angle between oil/water interface and the rock or wettability (Θ) (Berg, 1975).

Various investigations point to oil migration pathways being confined to a narrow zone immediately below a capillary barrier, with the migrating front rarely more than a few metres in height and occupying a stringer of interconnected pore spaces (Dembicki and Anderson, 1989; Catlan et al., 1992; Selle et al., 1993; Sylta et al., 1997). This focusing provides an effective mechanism to transmit large volumes of hydrocarbons with relatively limited losses along the migration path, but also means that very little of the total pore network is ever exposed to oil. Laboratory experiments (Dembicki and Anderson, 1989; Catlan et al., 1992) and computer modelling (Carruthers and Ring-rose, 1998; Sylta et al., 2008) suggest only a few percent of loss occurs along the migration path. As a consequence only a very small proportion of suitable reservoir rocks ever come into contact with a migration oil phase, making the chance of reworking from a previous sedimentary cycle statistically remote.

If reworking is considered unlikely then a conclusion about oil migration can be reached if *in situ* generation the oil can be excluded as a mechanism to explain the presence of oil contained within fluid inclusions. Typically oil generation requires temperatures of greater than about 80°C or equivalent vitrinite reflectance values of

0.6% so an initial screening allows samples with potential migrated oil to be discerned from those that had the potential to have been locally generated.

Whilst the methods described above could be utilised to discriminate oil inclusions that have been inherited or indigenous from migrated hydrocarbons a more robust approach for interpreting the significance of low GOI values involves consideration of the theory of two-phase flow through porous media that describes the vector of the impelling and resistive forces provided by buoyancy and capillarity respectively.

Although more sophisticated techniques for detecting potential migration pathways through calculation of this migration vector are available (e.g. OMI technique of Liu and Eadington, 2003) the same outcome can be achieved in most cases simply by inspecting the shape of the profile of GOI values relative to the position of obvious capillary barriers. Migration profiles anticipated for sandstones with sharp tops will be relatively thin (less than a few metres), whereas sandstones with gradually fining upwards sequences will potentially have much broader migration zones.

Sample selection procedures for GOI analysis seek to exploit these forces by preferentially favouring samples from below obvious capillary barriers, such as shales, that act to focus migrating hydrocarbons. In sandstones with well defined sharp tops the number of samples needed to evaluate each discrete bed is small and this approach is satisfactory, However, sandstone sections with gradually fining upwards sequences or strongly intercalated sand-shale sequences present difficulties in choosing where the reservoir ends and where the capillary barrier begins, requiring a large number of samples to correctly evaluate the interval of interest.

The requirement for large numbers of samples needed to address oil migration pathway severely impedes the applicability of operator intensive point-counting petrographic techniques such as GOI by preventing the collection of datasets of sufficient size to meaningfully interpret the results in terms of predicted migration profiles. In this instance the theoretical considerations are used to validate the significance of samples containing oil inclusions rather than to draw rigorous conclusions about regional oil migration.

Rather than over interpret the significance of the low GOI values, the preferred approach in wells with exclusively low GOI values is to consider the samples with GOI values above zero to be permissive of oil migration. Similarly, for the samples that lack oil inclusions deem it possible that the well may have been in a migration shadow. Integration of GOI data with other indicators of oil migration such as conventional oil shows is an essential part of the evaluation process. Ultimately, the validity of other possibilities should be tested against other geological data, but great caution should be displayed when interpreting low GOI values in isolation to avoid arriving at erroneous conclusions.

Figure C1: GOI results from Allaru-1

In this and in all subsequent GOI logs contained in this appendix the recorded GOI results are displayed against to the gamma ray log. On the GOI log the width of the horizontal green lines showing the position and magnitude of the recorded GOI value (actual values shown to the right). Samples with low or zero GOI values are marked with an arrow. The depth axis is given in metres below the rotary table (mRT).

In samples from Allaru-1 the presence of oil inclusions in several samples is permissive of oil migration, but the lack of gamma ray logs precludes greater consideration about the significance of these results. The oil inclusion all occur on fractures through detrital minerals so the potential for reworking from a previous sedimentary cycle cannot be excluded. The recorded reservoir temperature of 84°C at 2400m coupled with vitrinite reflectance values of 0.45% (Allaru-1 well completion report) make generation *in situ* unlikely.

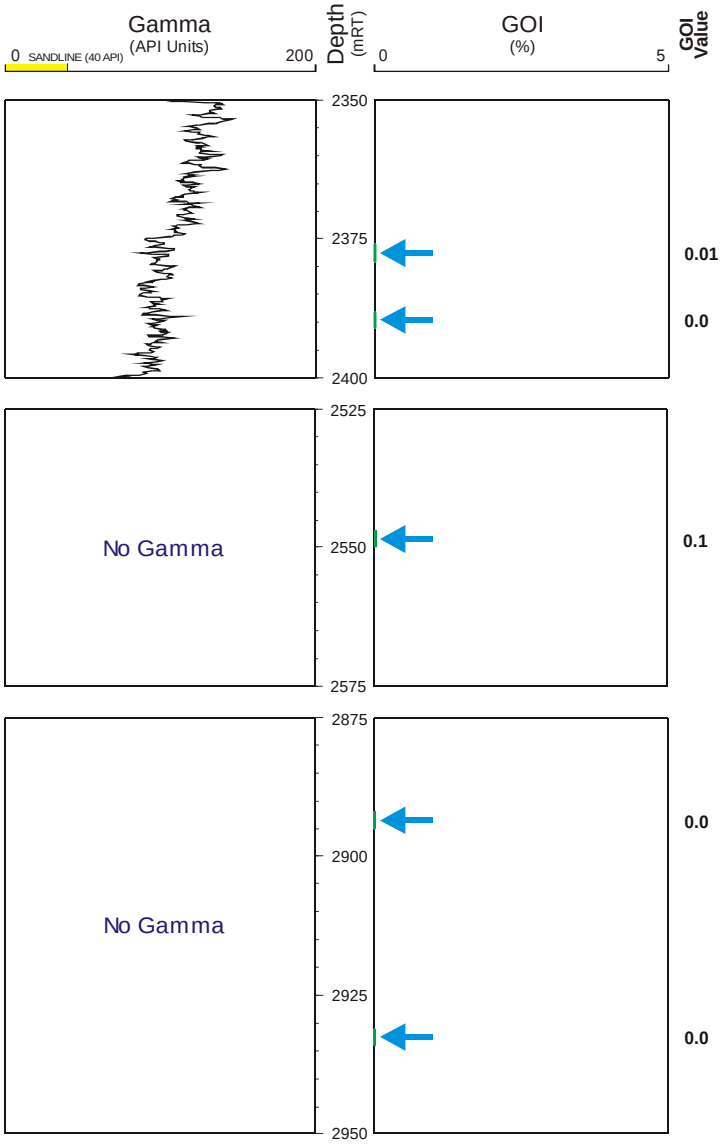

Figure C2: GOI results from Allaru-1ST1

In samples from Allaru-1ST1 the presence of oil inclusions in a single sample is permissive of oil migration, but the lack of gamma ray logs precludes greater consideration about the significance of these results. The oil inclusions all occur on fractures through detrital minerals so the potential for reworking from a previous sedimentary cycle cannot be excluded. Refer to Figure A1 caption for a description of the layout used.

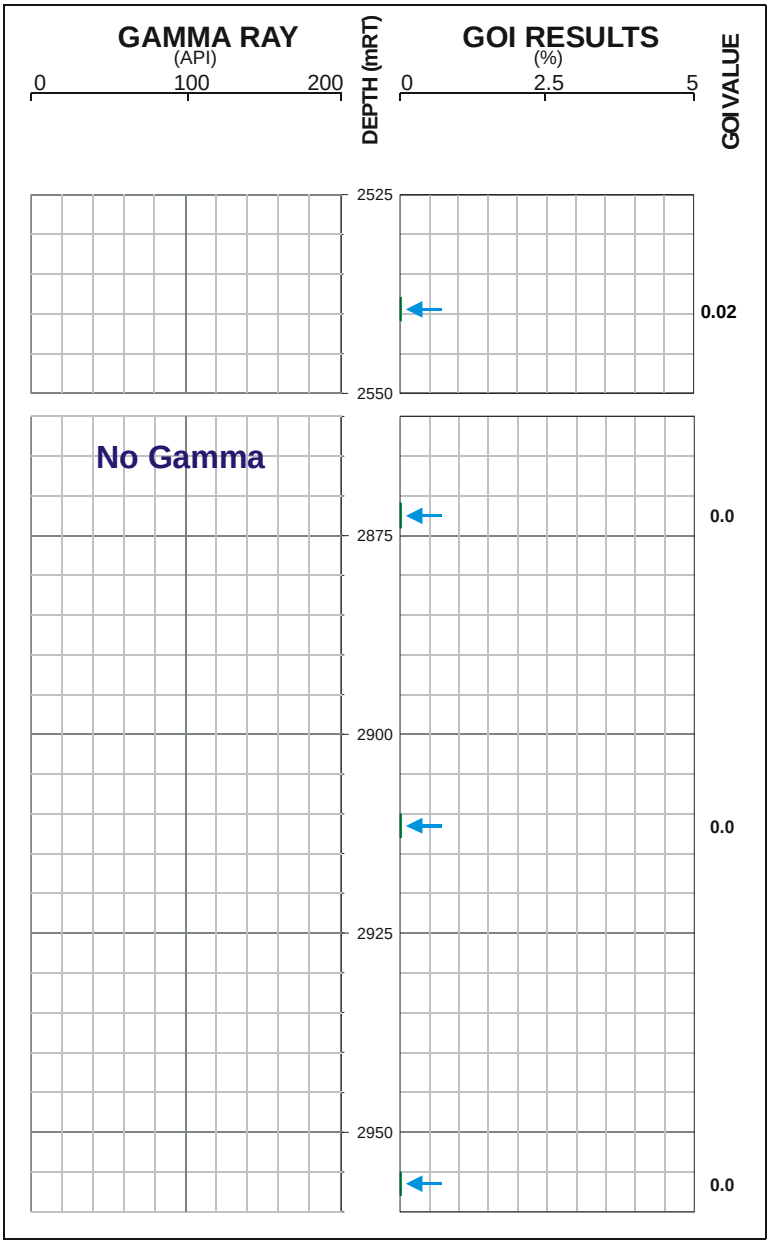

Figure C3: GOI results from Anson-1

GOI results of ≤ 0.1% are permissive of oil migration given that the samples lack burial depths to support local generation. Spore coloration data reported in the Anson-1 well completion report suggest the sampled section is immature to only marginally mature and generation *in situ* is unlikely. However, the oil inclusions all occur on fractures through detrital minerals so the potential for reworking from a previous sedimentary cycle cannot be excluded. Refer to Figure A1 caption for a description of the layout used.

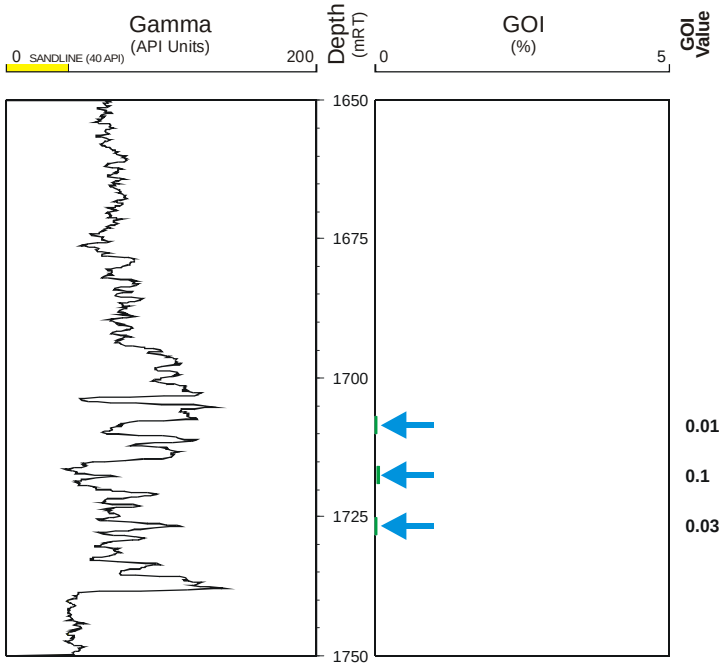

Figure C4: GOI results from Augustus-1

GOI results of ≤ 1.0% are permissive of oil migration given that the section is immature for *in situ* generation (Augustus-1 well completion report) but the oil inclusions all occur on fractures through detrital minerals so the potential for reworking from a previous sedimentary cycle cannot be excluded. Refer to Figure A1 caption for a description of the layout used.

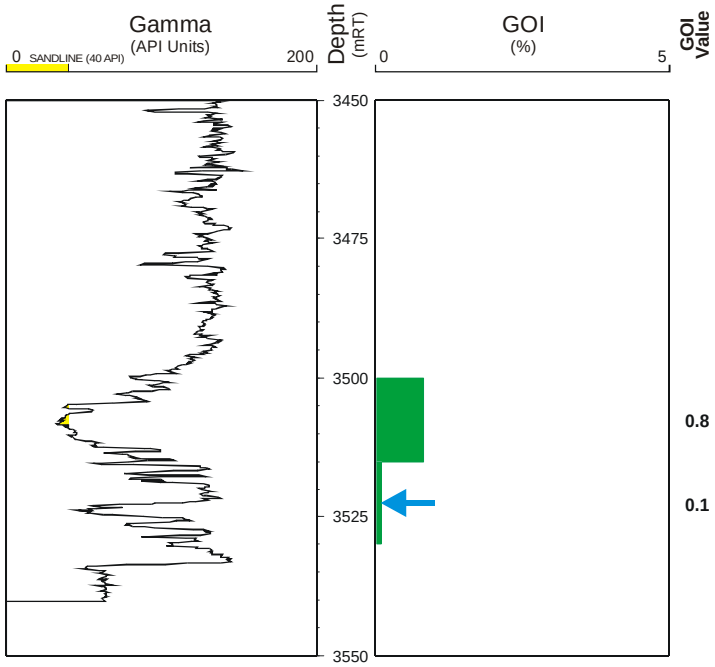

Figure C5: GOI results from Calytrix-1

A GOI value of 0.4% recorded in the first sand is permissive of oil migration given that the samples lack burial depths to support local generation and current reservoir temperatures are <75°C (Calytrix-1 well completion report). However, the oil inclusions all occur on fractures through detrital minerals so the potential for reworking from a previous sedimentary cycle cannot be excluded. The lowermost sample could represent an oil migration pathway or given that it is a cuttings sample could represent caving from higher in the well. Refer to Figure A1 caption for a description of the layout used.

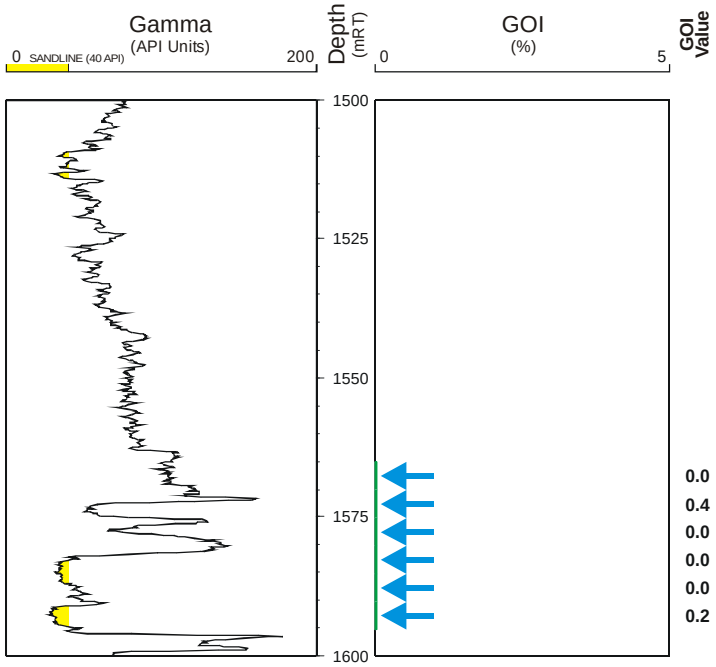

Figure C6: GOI results from Champagny-1

GOI results of ≤ 0.4% are permissive of oil migration given that oil inclusions in some samples occur within authigenic quartz overgrowths and hence have not been inherited from a previous sedimentary cycle. However, vitrinite reflectances measured over the sampled interval range from 0.65 to 0.75% (Champagny-1 well completion report) and indicate that the section marginally mature for local oil generation making it possible that the oil seen in fluid inclusions is not a product of regional oil migration. Refer to Figure A1 caption for a description of the layout used.

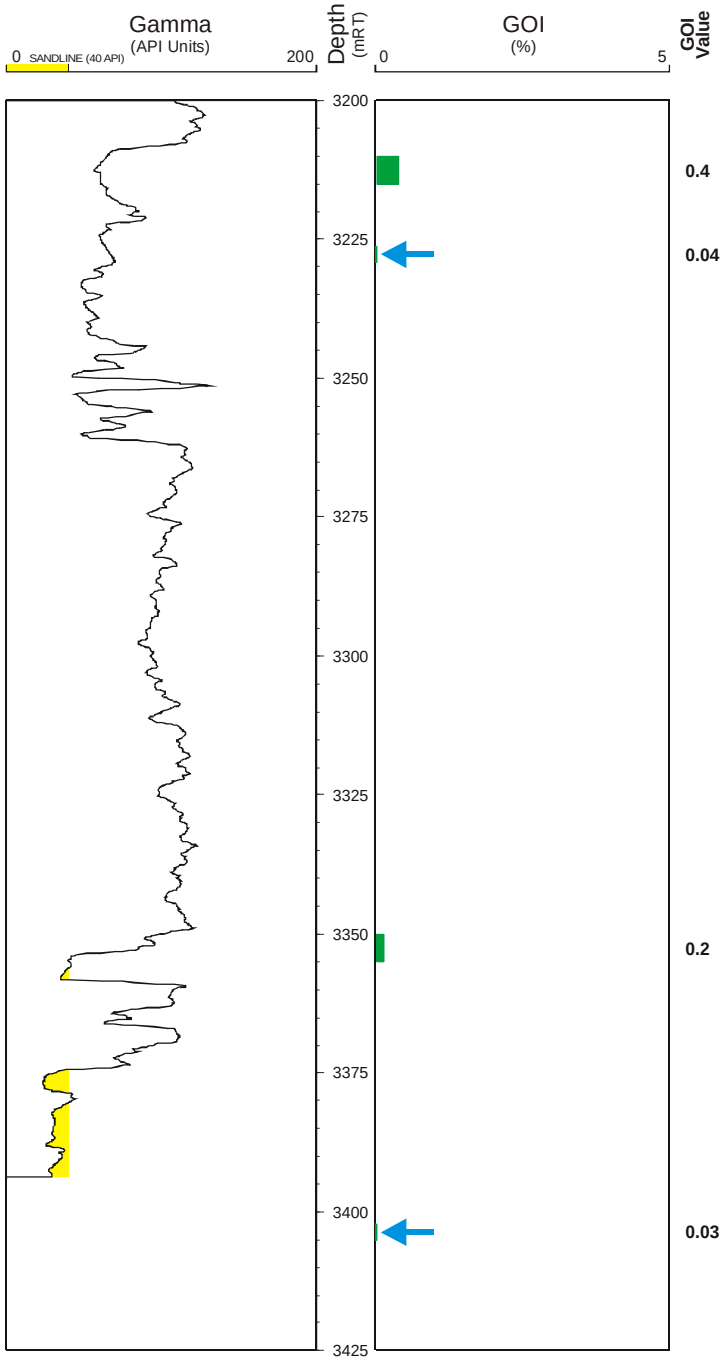

Figure C7: GOI results from Douglas-1

A GOI result of 0.2% is permissive of oil migration but available vitrinite reflectance data shows the sampled section is marginally mature for hydrocarbon generation (Douglas-1 well completion report). The position of the sample well below any obvious capillary barriers is not consistent with an anticipated buoyancy profile, but as this is a cuttings sample caving from the higher section could account for this observation. In addition, the oil inclusions all occur on fractures through detrital minerals so the potential for reworking from a previous sedimentary cycle cannot be excluded. Refer to Figure A1 caption for a description of the layout used.

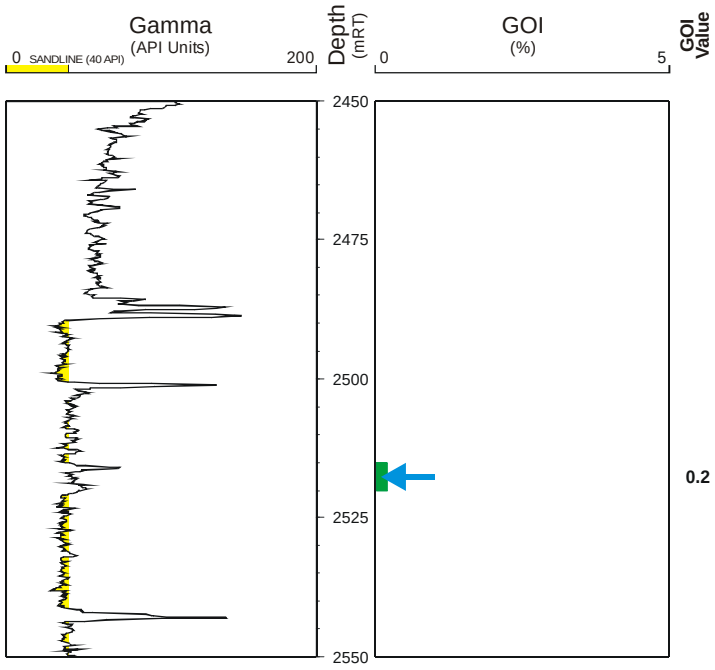

Figure C8: GOI results from East Swan-1

A lone GOI result of 0.2% is permissive of oil migration given that the available vitrinite reflectance data (East Swan-1 well completion report) indicate the section is immature for *in situ* hydrocarbon generation. However, the oil inclusions all occur on fractures through detrital minerals so the potential for reworking from a previous sedimentary cycle cannot be excluded. Refer to Figure A1 caption for a description of the layout used.

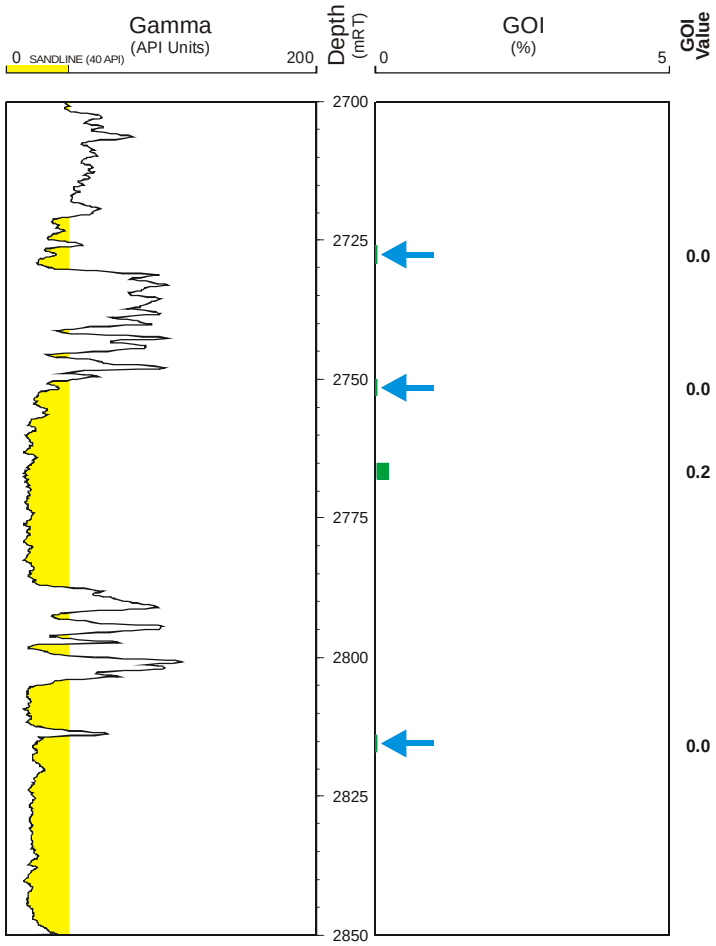

Figure C9: GOI results from Hadrian-1

The GOI result of 0.4% is permissive of oil migration given the proximity to a significant capillary barrier but vitrinite reflectances recorded in the adjacent section is marginally mature for oil generation (Hadrian-1 well completion report) and the oil seen in inclusions may have been locally generated. In addition, the oil inclusions all occur on fractures through detrital minerals so the potential for reworking from a previous sedimentary cycle cannot be excluded. Refer to Figure A1 caption for a description of the layout used.

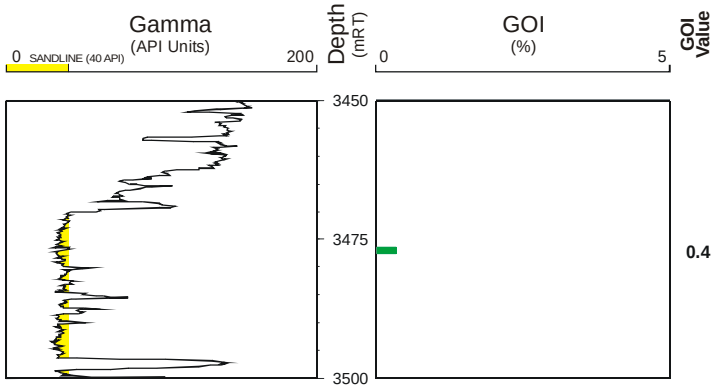

Figure C10: GOI results from Ibis-1

GOI results of ≤ 0.1% are permissive of oil migration given that the samples lack burial depths to support local generation. Vitrinite reflectance data from the Ibis-1 well completion report confirms that the sampled section is immature for hydrocarbon generation. The presence of oil inclusions all within quartz overgrowths in the deepest sample also makes it unlikely there has been reworking from a previous sedimentary cycle. Refer to Figure C1 caption for a description of the layout used.

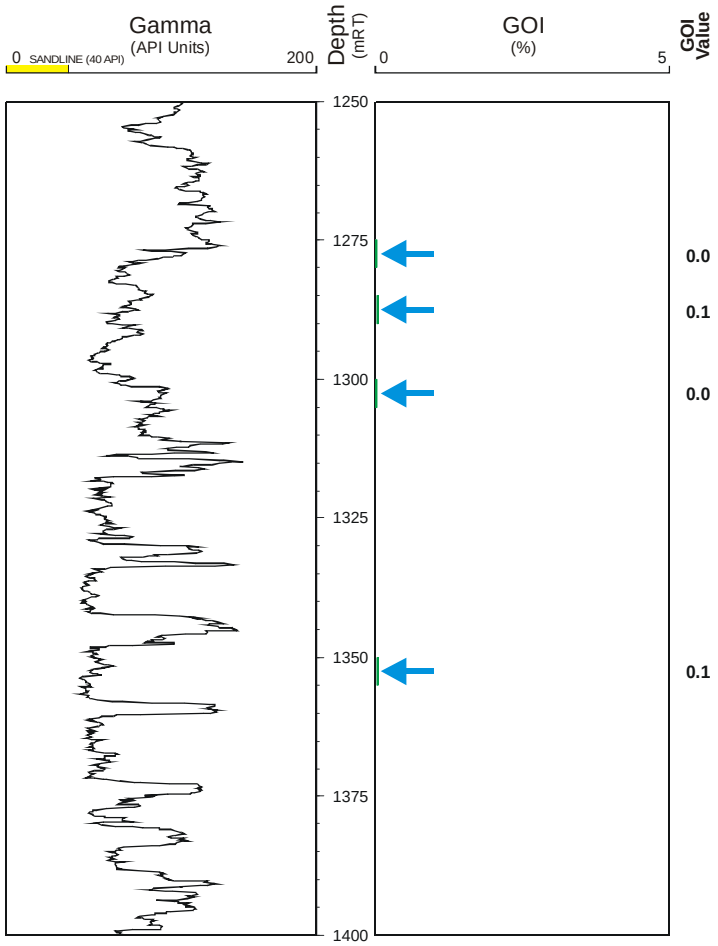

Figure C11: GOI results from Langhorne-1

The lack of oil inclusions in all samples provides no evidence to support oil migration over the interval sampled in the Langhorne-1 well. Refer to Figure C1 caption for a full description of the layout used.

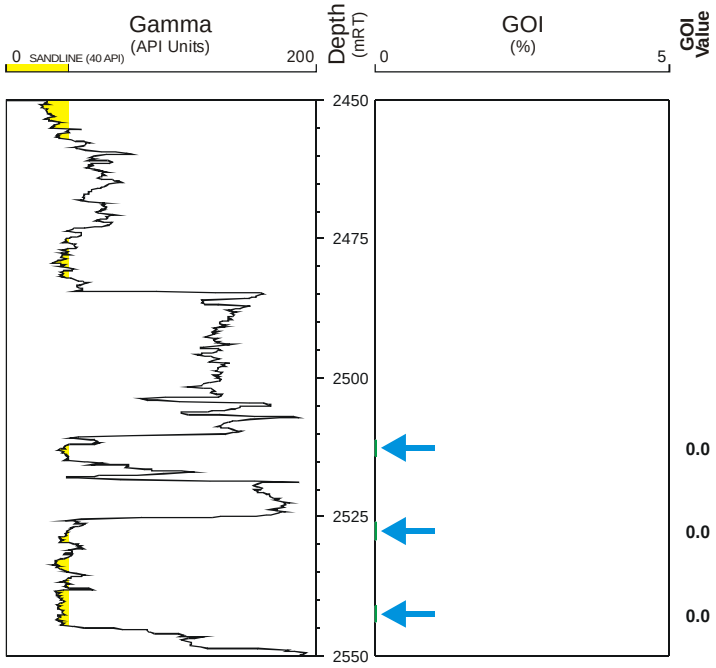

Figure C12: GOI results from Leeuwin-1

GOI results of ≤ 0.1% are permissive of oil migration given that the samples lack burial depths to support local generation. Vitrinite reflectance data reported in the Leeuwin-1 well completion report confirm the sampled section is not thermally mature for hydrocarbon generation. However, the oil inclusions all occur on fractures through detrital minerals so the potential for reworking from a previous sedimentary cycle cannot be excluded. Refer to Figure C1 caption for a description of the layout used.

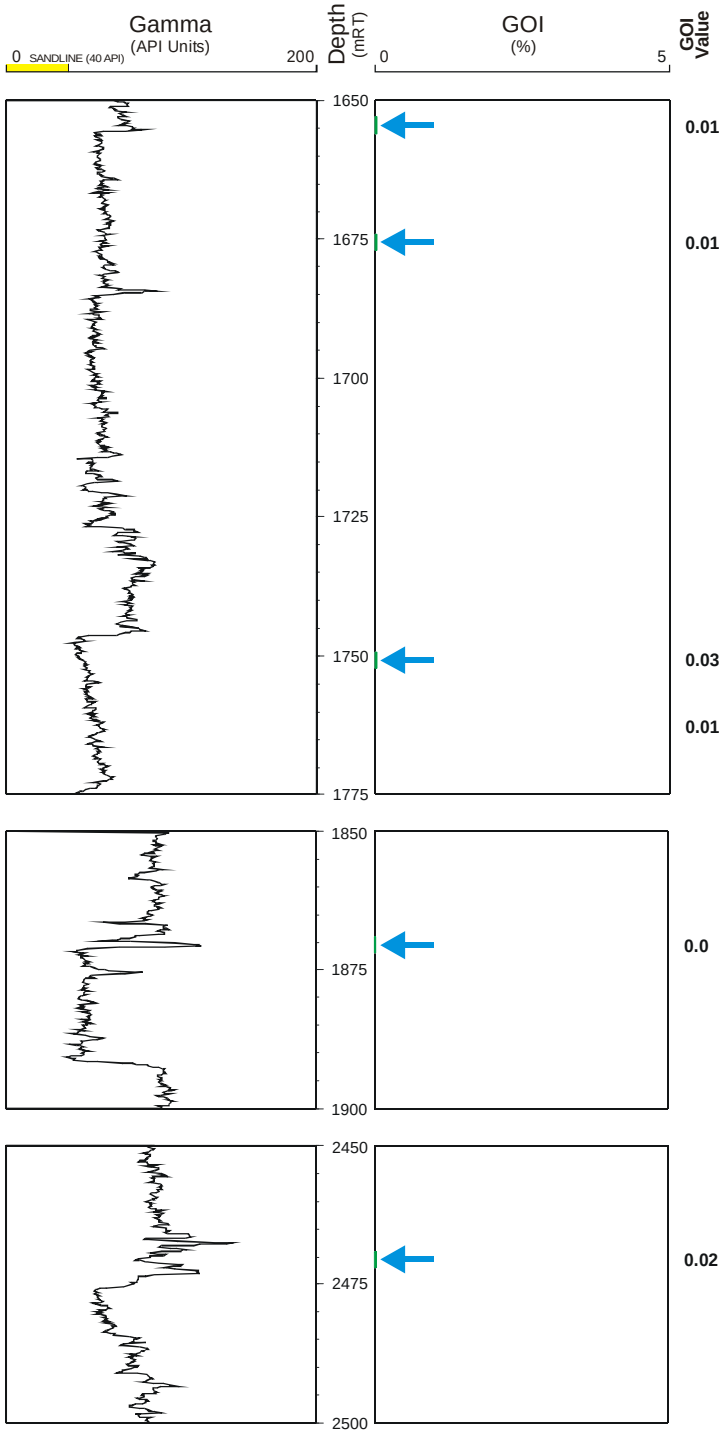

Figure C13: GOI results from Longleat-1

GOI results of ≤ 0.1% are permissive of oil migration given that the samples lack burial depths to support local generation. Vitrinite reflectance data from the Longleat-1 well completion report confirm that the sampled section is immature for oil generation. However, the oil inclusions all occur on fractures through detrital minerals so the potential for reworking from a previous sedimentary cycle cannot be excluded. Refer to Figure C1 caption for a description of the layout used.

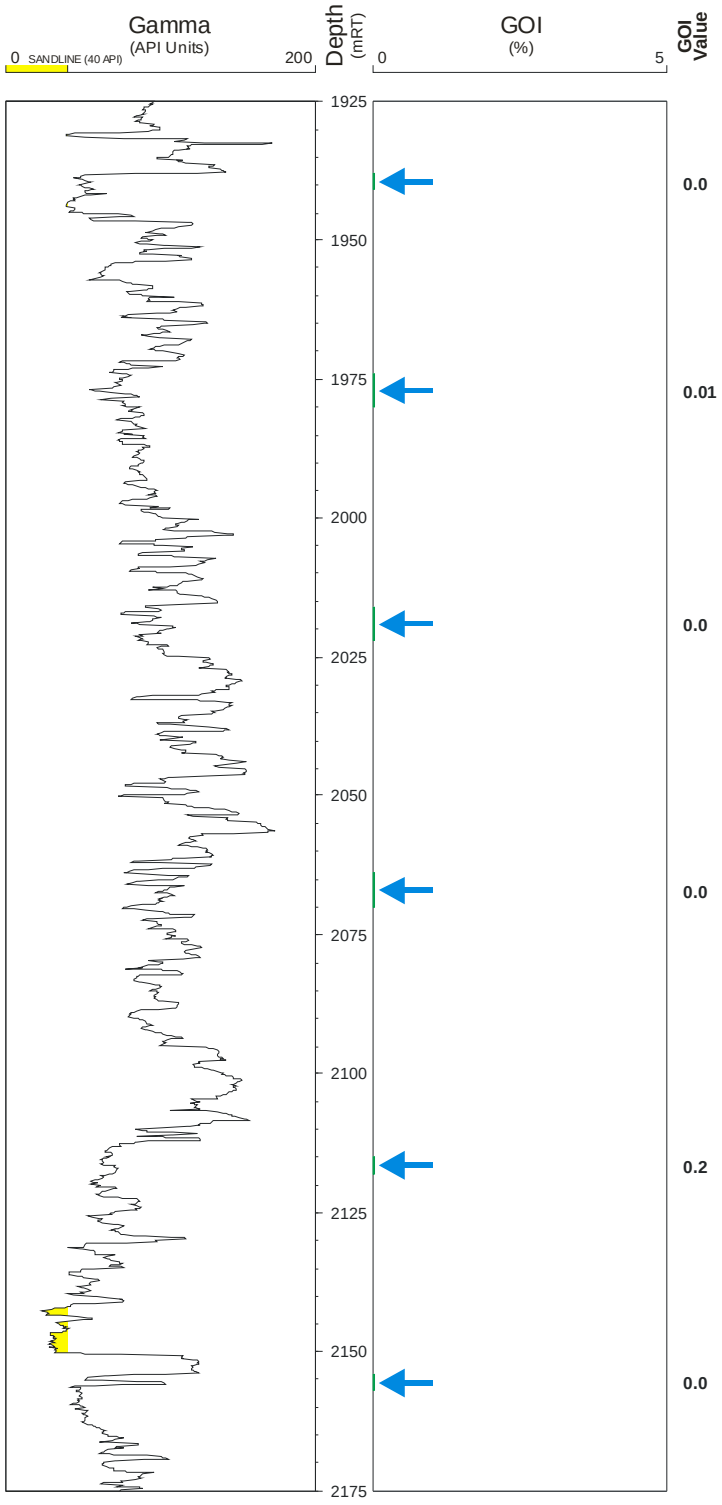

Figure C14: GOI results from Maple-1

The GOI results in all but one sample are ≤ 0.1% and are permissive of oil migration given that available vitrinite reflectance data indicate the section is immature (Maple-1 well completion report). The elevated GOI value recorded in the 3684-87m sample is below the threshold for oil accumulation (5%) but considerably above the values normally recorded on migration pathways where GOI values rarely exceed 1%. Significant gas saturations are interpreted from log analysis (Maple-1 well completion report) over the sampled section and an accumulation of gas is inferred. The GOI data indicate significant oil migration likely preceded gas charge. Refer to Figure C1 caption for a description of the layout used.

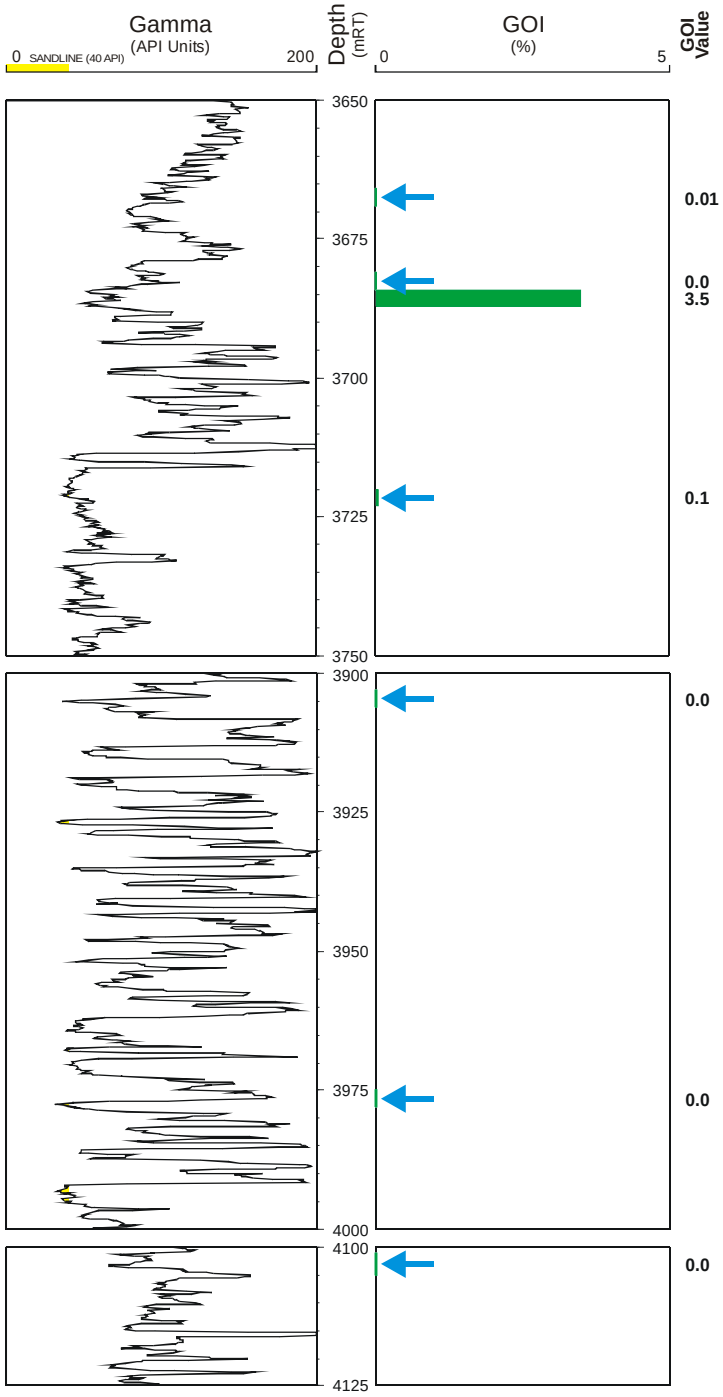

Figure C15: GOI results from Pollard-1

In samples from Pollard-1 the presence of oil inclusions in a single sample is permissive of oil migration given local generation is precluded by shallow burial and low measured vitrinite reflectances (Pollard-1 well completion report). The oil inclusions all occur on fractures through detrital minerals so the potential for reworking from a previous sedimentary cycle cannot be excluded. Refer to Figure C1 caption for a description of the layout used.

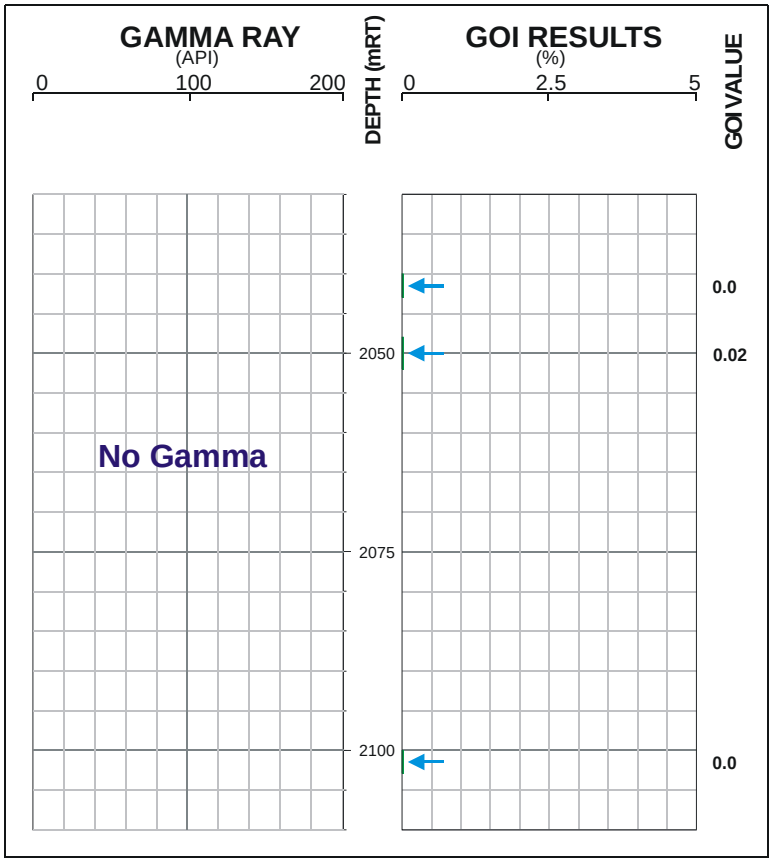

Figure C16: GOI results from Rainbow-1

In samples from Rainbow-1 the presence of oil inclusions in a single sample is permissive of oil migration through the uppermost sand of the reservoir section given that the section is immature for *in situ* oil generation (Rainbow-1 well completion report). The oil inclusions all occur on fractures through detrital minerals so the potential for reworking from a previous sedimentary cycle cannot be excluded. Refer to Figure C1 caption for a description of the layout used.

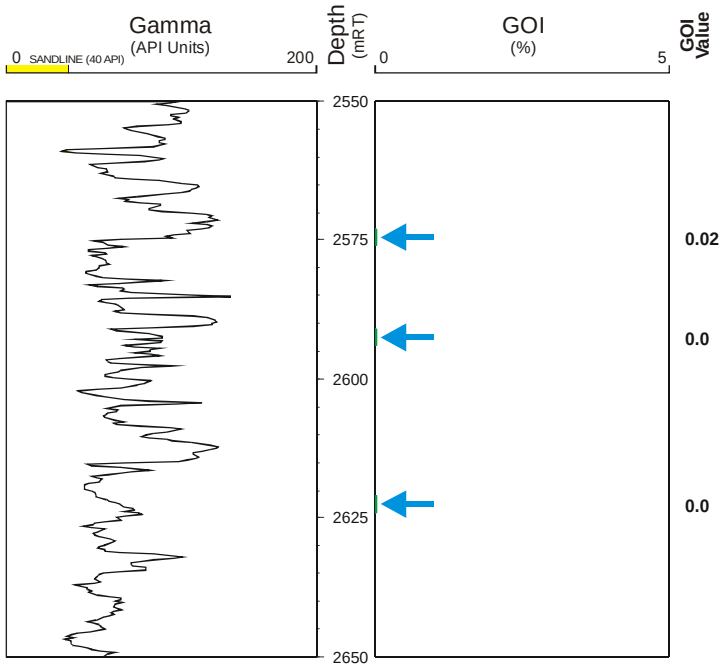

Figure C17: GOI results from Snowmass-1

In samples from Snowmass-1 the presence of oil inclusions in a single sample is permissive of oil migration, given that local oil generation is unlikely at these shallow burial depths and this is confirmed by low vitrinite reflectances (Snowmass-1 well completion report). The oil inclusions all occur on fractures through detrital minerals so the potential for reworking from a previous sedimentary cycle cannot be excluded. Refer to Figure C1 caption for a description of the layout used.

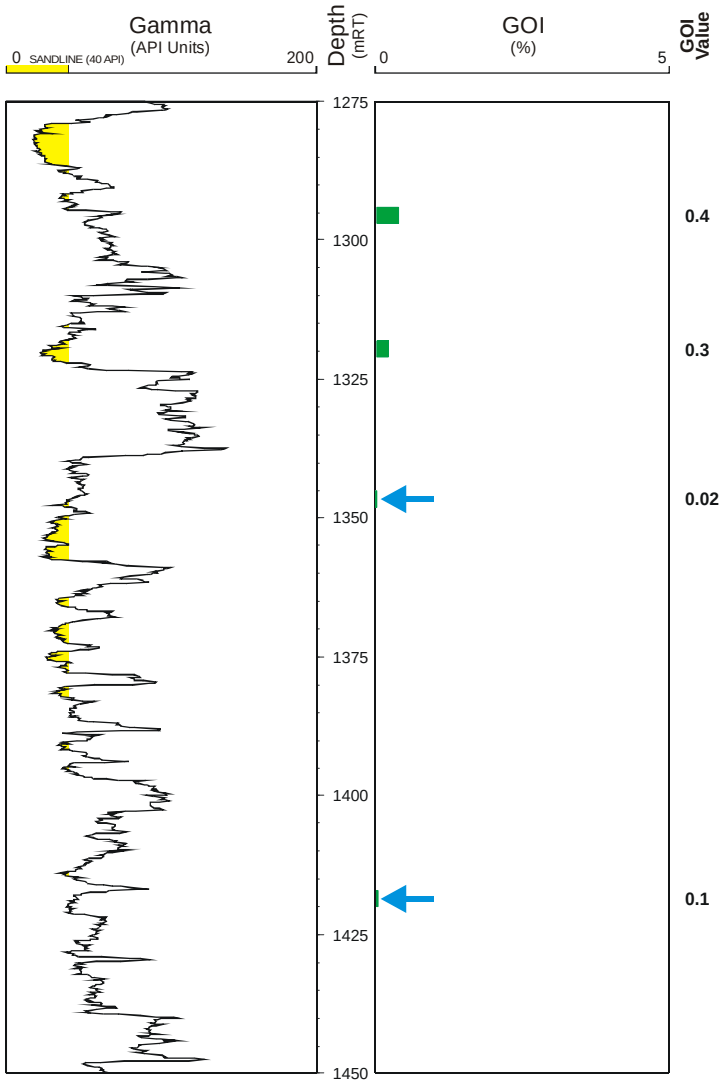

Figure C18: GOI results from Taltarni-1

In samples from Taltarni-1 the presence of oil inclusions in a single sample is permissive of oil migration, and although not positioned below the obvious seal the sample is a cuttings interval that could contain caving. Vitrinite reflectance data demonstrates that the interval is immature for in situ oil generation (Taltarni-1 well completion report) adding support to a conclusion of oil migration. The oil inclusions all occur on fractures through detrital minerals so the potential for reworking from a previous sedimentary cycle cannot be excluded. Refer to Figure C1 caption for a description of the layout used.

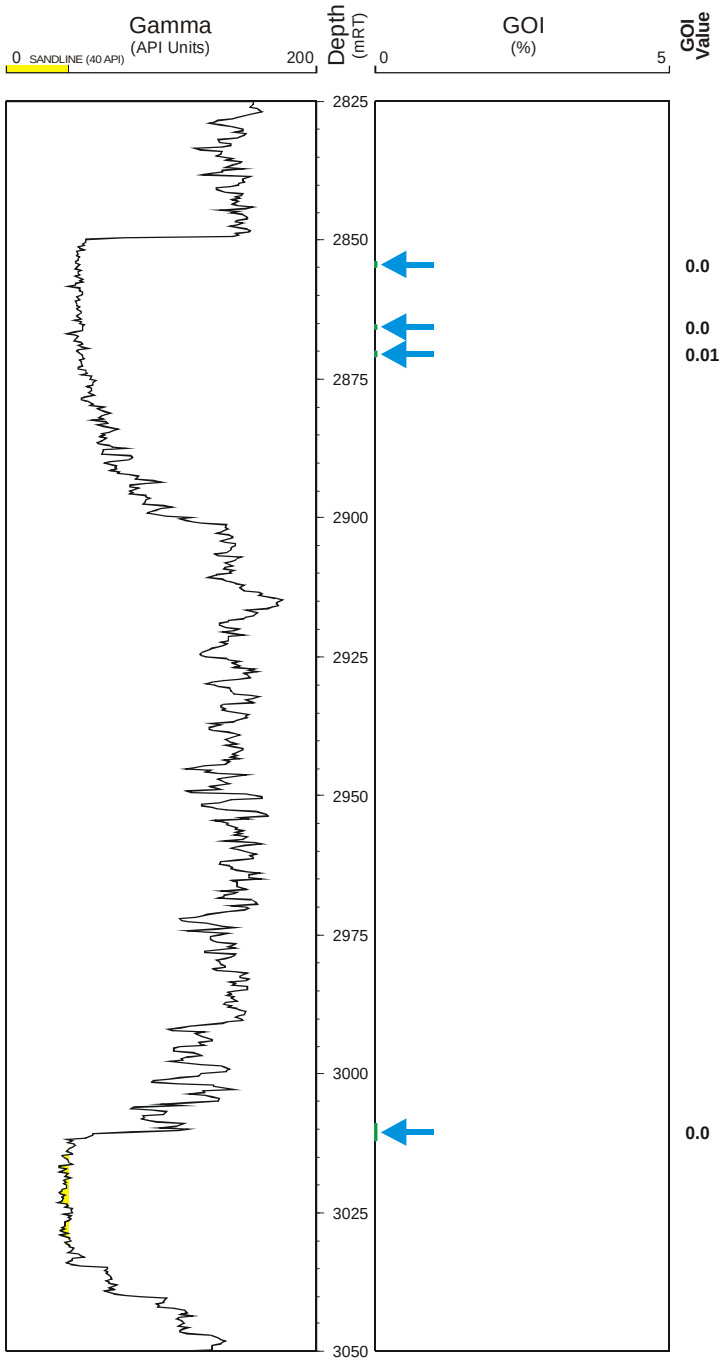

Figure C19: GOI results from Tancred-1

Low to moderate GOI values in multiple samples from Tancred-are permissive of oil migration in the uppermost sands and the shallow burial depths suggest local oil generation is unlikely. The presence of oil inclusions within authigenic quartz overgrowths in the upper most sample precludes reworking from a previous sedimentary cycle. Refer to Figure C1 caption for a description of the layout used.

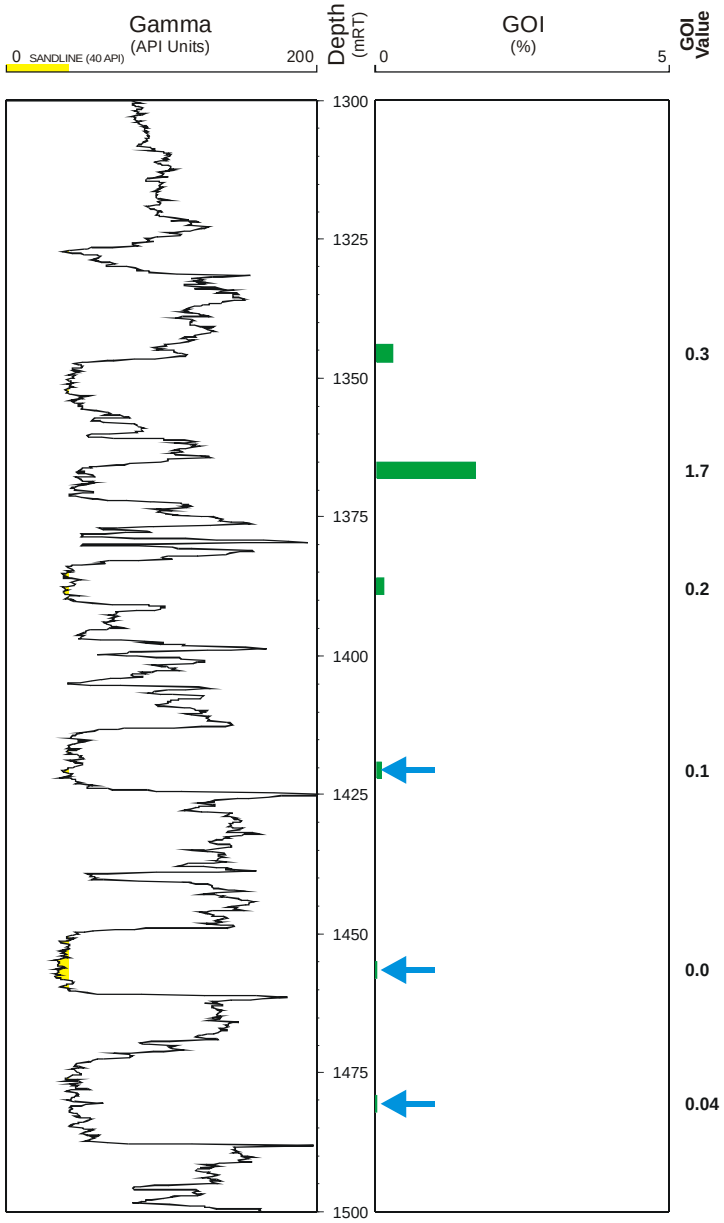

Figure C20: GOI results from Warb-1

In samples from Warb-1 the presence of oil inclusions in a multiple samples from the deeper Triassic Challis Formation section is permissive of oil migration, but geochemical extract analysis suggests the presence of *in situ* generated oil (Warb-1 well completion report) so the oil in the inclusions might not represent a migrated phase of hydrocarbons. The oil inclusions all occur on fractures through detrital minerals so the potential for reworking from a previous sedimentary cycle cannot be excluded. Refer to Figure C1 caption for a description of the layout used.

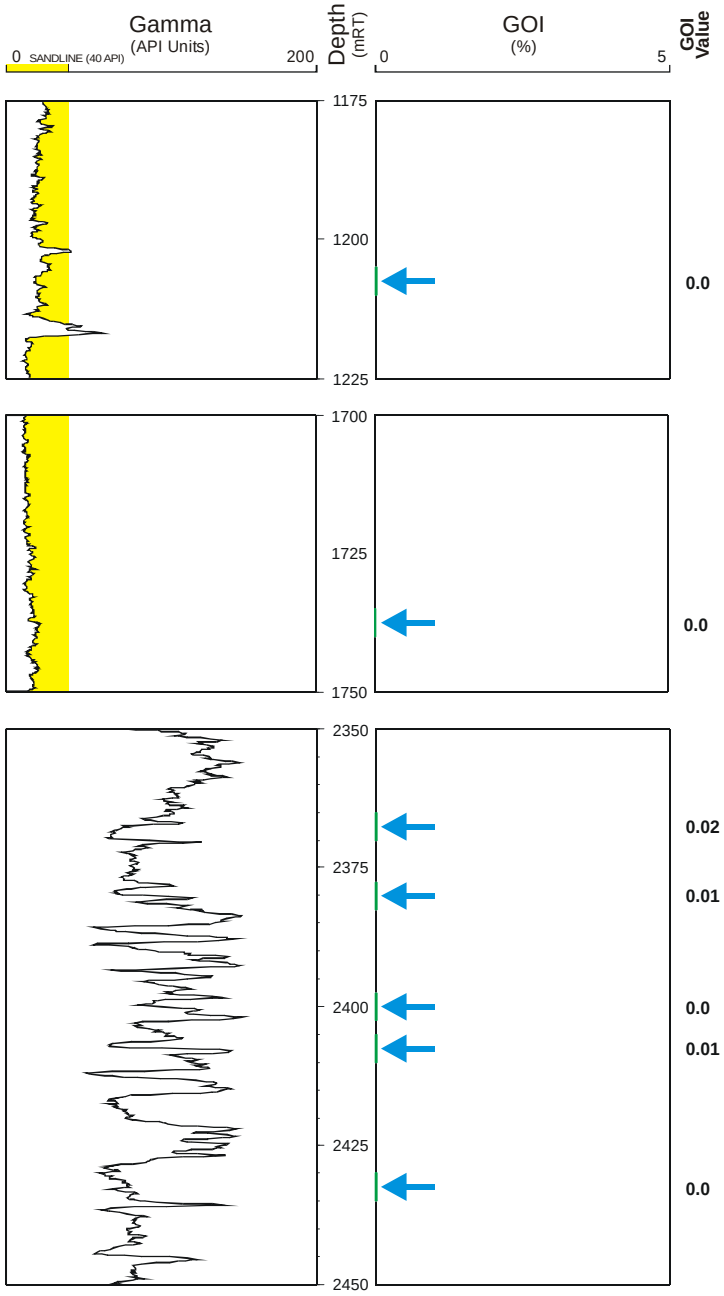

Figure C21: GOI results from Yarra-1

In samples from Yarra-1 the presence of oil inclusions in a single sample is permissive of oil migration and the low vitrinite reflectance values reported in the Yarra-1 well completion report preclude local oil generation. The oil inclusions all occur on fractures through detrital minerals so the potential for reworking from a previous sedimentary cycle cannot be excluded. Refer to Figure C1 caption for a description of the layout used.

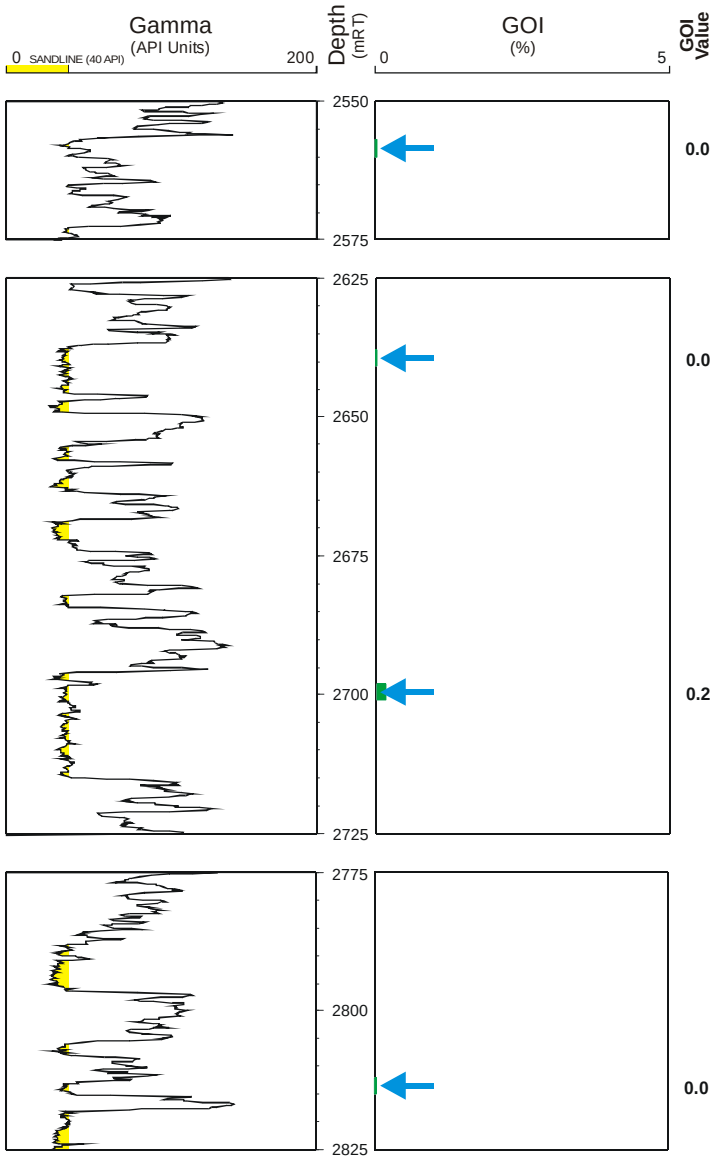

Figure C22: GOI results from Yering-1

In samples from Yering-1 the presence of oil inclusions in two samples is permissive of oil migration and low vitrinite reflectance values reported in the Yering-1 well completion report preclude local oil generation. The oil inclusions all occur on fractures through detrital minerals so the potential for reworking from a previous sedimentary cycle cannot be excluded. Refer to Figure C1 caption for a description of the layout used.